SHOUT
SHARE
IT

MBL

THE
BIOLOGICAL BULLETIN
AUGUST 1999

Editor	Michael J. Greenberg	The Whitney Laboratory, University of Florida
Associate Editors	Louis E. Burnett	Grice Marine Biological Laboratory, College of Charleston
	R. Andrew Cameron	California Institute of Technology
	Charles D. Derby	Georgia State University
	Michael LaBarbera	University of Chicago
Section Editor	Shinya Inoué, *Imaging and Microscopy*	Marine Biological Laboratory
Online Editors	James A. Blake, *Keys to Marine Invertebrates of the Woods Hole Region*	ENSR Marine & Coastal Center, Woods Hole
	William D. Cohen, *Marine Models Electronic Record and Compendia*	Hunter College, City University of New York
Editorial Board	Peter B. Armstrong	University of California, Davis
	Ernest S. Chang	Bodega Marine Lab., University of California, Davis
	Thomas H. Dietz	Louisiana State University
	Richard B. Emlet	Oregon Institute of Marine Biology, Univ. of Oregon
	David Epel	Hopkins Marine Station, Stanford University
	Gregory Hinkle	Cereon Genomics, Cambridge, Massachusetts
	Makoto Kobayashi	Hiroshima University of Economics, Japan
	Donal T. Manahan	University of Southern California
	Margaret McFall-Ngai	Kewalo Marine Laboratory, University of Hawaii
	Mark W. Miller	Institute of Neurobiology, University of Puerto Rico
	Tatsuo Motokawa	Tokyo Institute of Technology, Japan
	Yoshitaka Nagahama	National Institute for Basic Biology, Japan
	Sherry D. Painter	Marine Biomed. Inst., Univ. of Texas Medical Branch
	J. Herbert Waite	University of California, Santa Barbara
	Richard K. Zimmer	University of California, Los Angeles
Editorial Office	Pamela Clapp Hinkle	Managing Editor
	Victoria R. Gibson	Staff Editor
	Carol Schachinger	Editorial Assistant
	Patricia Burns	Subscription & Advertising Secretary

Published by
Marine Biological Laboratory
Woods Hole, Massachusetts

Cover

The ascoglossan sea slug, *Elysia chlorotica* (Gould), shown on the cover (photograph by S. K. Pierce), seeks out and specifically eats a chromophytic alga, *Vaucheria litorea.* Like certain other species of sea slugs, *E. chlorotica* has developed the ability to acquire the chloroplasts from its algal foodstuff and to utilize them for nutrition. The plastids are usually engulfed by particular epithelial cells in the digestive gland where they photosynthesize and, in some species, provide sufficient nutrients to sustain life and reproduction—even when no other food is available.

In *E. chlorotica,* the function of the captured chloroplasts is maintained for up to 8 months—a surprisingly long period, surpassing similar chloroplast symbioses by many months. Throughout this period, furthermore, plastid proteins are continuously synthesized, and some of the proteins appear to be encoded by the slug genome. Another remarkable feature of these slug populations is the abrupt end of the annual life cycle—all of the animals dying synchronously, whether in the laboratory or in the field.

In this issue, Skip Pierce and his colleagues (p. 1) report a widespread viral infection of the slug population; this phenomenon also occurs annually and is coincident with the mass mortality. The viruses (see inset) seem to be endogenous and have many characteristics in common with retroviruses. The report suggests that the viruses may not only be involved in the regulation of the slug's life cycle, but may be the means by which algal genes are transferred to the slug genome.

CONTENTS

Volume 197, No 1: August 1999

RESEARCH NOTES

Pierce, Sidney K., Timothy K. Maugel, Mary E. Rumpho, Jeffrey J. Hanten, and William L. Mondy
Annual viral expression in a sea slug population: life cycle control and symbiotic chloroplast maintenance . 1

Thomas, Florence I.M., Kristen A. Edwards, Toby F. Bolton, Mary A. Sewell, and Jill M. Zande
Mechanical resistance to shear stress: the role of echinoderm egg extracellular layers 7

Rinkevich, B., S. Ben-Yakir, and R. Ben-Yakir
Regeneration of amputated avian bone by a coral skeletal implant 11

ECOLOGY AND EVOLUTION

Miner, Benjamin G., Eric Sanford, Richard R. Strathmann, Bruno Pernet, and Richard B. Emlet
Functional and evolutionary implications of opposed bands, big mouths, and extensive oral ciliation in larval opheliids and echiurids (Annelida). 14

Johnsen, Sönke, Elizabeth J. Balser, Erin C. Fisher, and Edith A. Widder
Bioluminescence in the deep-sea cirrate octopod *Stauroteuthis syrtensis* Verrill (Mollusca: Cephalopoda) . 26

NEUROBIOLOGY AND BEHAVIOR

Ganter, Geoffrey K., Ralf Heinrich, Richard P. Bunge, and Edward A. Kravitz
Long-term culture of lobster central ganglia; expression of foreign genes in identified neurons 40

Hanlon, Roger T., Michael R. Maxwell, Nadav Shashar, Ellis R. Loew, and Kim-Laura Boyle
An ethogram of body patterning behavior in the biomedically and commercially valuable squid *Loligo pealei* off Cape Cod, Massachusetts 49

Bushmann, Paul J.
Concurrent signals and behavioral plasticity in blue crab (*Callinectes sapidus* Rathbun) courtship 63

PHYSIOLOGY

Engebretson, Hilary P., and Gisèle Muller-Parker
Translocation of photosynthetic carbon from two algal symbionts to the sea anemone *Anthopleura elegantissima* 72

DEVELOPMENT AND REPRODUCTION

Grabowski, Gregory M., John G. Blackburn, and Eric R. Lacy
Morphology and epithelial ion transport of the alkaline gland in the Atlantic stingray (*Dasyatis sabina*) . . . 82

Krug, Patrick J., and Adriana E. Manzi
Waterborne and surface-associated carbohydrates as settlement cues for larvae of the specialist marine herbivore *Alderia modesta* 94

Chaparro, O.R., R.J. Thompson, and C.J. Emerson
The velar ciliature in the brooded larva of the Chilean oyster *Ostrea chilensis* (Philippi, 1845). 104

* * *

Annual Report of the Marine Biological Laboratory R1

THE BIOLOGICAL BULLETIN

THE BIOLOGICAL BULLETIN is published six times a year by the Marine Biological Laboratory, 7 MBL Street, Woods Hole, Massachusetts 02543.

Subscriptions and similar matter should be addressed to Subscription Manager, THE BIOLOGICAL BULLETIN, Marine Biological Laboratory, 7 MBL Street, Woods Hole, Massachusetts 02543. Subscription per year (six issues, two volumes): $205 for libraries; $95 for individuals. Subscription per volume (three issues): $102.50 for libraries; $47.50 for individuals. Back and single issues (subject to availability): $40 for libraries; $20 for individuals.

Communications relative to manuscripts should be sent to Michael J. Greenberg, Editor-in-Chief, or Pamela Clapp Hinkle, Managing Editor, at the Marine Biological Laboratory, 7 MBL Street, Woods Hole, Massachusetts 02543. Telephone: (508) 289-7428. FAX: 508-457-1924. E-mail: pclapp@mbl.edu.

http://www.mbl.edu/BiologicalBulletin/

The home page for the electronic companion to THE BIOLOGICAL BULLETIN—*the Marine Models Electronic Record*—and other BIOLOGICAL BULLETIN publications is available on the World Wide Web at the address shown above.

THE BIOLOGICAL BULLETIN is indexed in bibliographic services including *Index Medicus* and MEDLINE, *Chemical Abstracts, Current Contents, Elsevier BIOBASE/Current Awareness in Biological Sciences,* and *Geo Abstracts.*

Printed on acid free paper,
effective with Volume 180, Issue 1, 1991.

POSTMASTER: Send address changes to THE BIOLOGICAL BULLETIN, Marine Biological Laboratory,
7 MBL Street, Woods Hole, MA 02543.

Copyright © 1999, by the Marine Biological Laboratory

Periodicals postage paid at Woods Hole, MA, and additional mailing offices.
ISSN 0006-3185

INSTRUCTIONS TO AUTHORS

The Biological Bulletin accepts outstanding original research reports of general interest to biologists throughout the world. Papers are usually of intermediate length (10–40 manuscript pages). A limited number of solicited review papers may be accepted after formal review. A paper will usually appear within four months after its acceptance.

Very short, especially topical papers (less than 9 manuscript pages including tables, figures, and bibliography) will be published in a separate section entitled "Research Notes." A Research Note in *The Biological Bulletin* follows the format of similar notes in *Nature.* It should open with a summary paragraph of 150 to 200 words comprising the introduction and the conclusions. The rest of the text should continue on without subheadings, and there should be no more than 30 references. References should be referred to in the text by number, and listed in the Literature Cited section in the order that they appear in the text. Unlike references in *Nature,* references in the Research Notes section should conform in punctuation and arrangement to the style of recent issues of *The Biological Bulletin.* Materials and Methods should be incorporated into appropriate figure legends. See the article by Lohmann *et al.* (October 1990, Vol. **179:** 214–218) for sample style. A Research Note will usually appear within two months after its acceptance.

The Editorial Board requests that regular manuscripts conform to the requirements set below; those manuscripts that do not conform will be returned to authors for correction before review.

1. ***Manuscripts.*** Manuscripts, including figures, should be submitted in quadruplicate, with the originals clearly marked. (Xerox copies of photographs are not acceptable for review purposes.) The submission letter accompanying the manuscript should include a telephone number, a FAX number, and (if possible) an E-mail address for the corresponding author. The original manuscript must be typed in no smaller than 12 pitch or 10 point, using double spacing (*including* figure legends, footnotes, bibliography, etc.) on one side of 16- or 20-lb. bond paper, 8 by 11 inches. Please, no right justification. Manuscripts should be proofread carefully and errors corrected legibly in black ink. Pages should be numbered consecutively. Margins on all sides should be at least 1 inch (2.5 cm). Manuscripts should conform to the *Council of Biology Editors Style Manual,* 5th Edition (Council of Biology Editors, 1983) and to American spelling. Unusual abbreviations should be kept to a minimum and should be spelled out on first reference as well as defined in a footnote on the title page. Manuscripts should be divided into the following components: Title page, Abstract (of no more than 200 words), Introduction, Materials and Methods, Results, Discussion, Acknowledgments, Literature Cited, Tables, and Figure Legends. In addition, authors should supply a list of words and phrases under which the article should be indexed.

2. ***Title page.*** The title page consists of a condensed title or running head of no more than 35 letters and spaces, the manuscript title, authors' names and appropriate addresses, and footnotes listing present addresses, acknowledgments or contribution numbers, and explanation of unusual abbreviations.

3. ***Figures.*** The dimensions of the printed page, 7 by 9 inches, should be kept in mind in preparing figures for publication. We recommend that figures be about 1 times the linear dimensions of the final printing desired, and that the ratio of the largest to the smallest letter or number and of the thickest to the thinnest line not exceed 1:1.5. Explanatory matter generally should be included in legends, although axes should always be identified on the illustration itself. Figures should be prepared for reproduction as either line cuts or halftones. Figures to be reproduced as line cuts should be unmounted glossy photographic reproductions or drawn in black ink on white paper, good-quality tracing cloth or plastic, or blue-lined coordinate paper. Those to be reproduced as halftones should be mounted on board, with both designating numbers or letters and scale bars affixed directly to the figures. All figures should be numbered in consecutive order, with no distinction between text and plate figures and cited, in order, in the text. The author's name and an arrow indicating orientation should appear on the reverse side of all figures.

Color: The Biological Bulletin will publish color figures and plates, but must bill authors for the actual additional cost of printing in color. The process is expensive, so authors with more than one color image should—consistent with editorial concerns, especially citation of figures in order—combine them into a single plate to reduce the expense. On request, when supplied with a copy of a color illustration, the editorial staff will provide a pre-publication estimate of the printing cost.

4. ***Tables, footnotes, figure legends, etc.*** Authors should follow the style in a recent issue of *The Biological Bulletin* in preparing table headings, figure legends, and the like. Because of the high cost of setting tabular material in type, authors are asked to limit such material as much as possible. Tables, with their headings and footnotes, should be typed on separate sheets, numbered with consecutive Roman numerals, and placed after the Literature Cited. Figure legends should contain enough information to make the figure intelligible separate from the text. Legends should be typed double spaced, with consecutive Arabic numbers, on a separate sheet at the end of the paper. Footnotes should be limited to authors' current addresses, acknowledgments or contribution numbers, and explanation of unusual abbreviations. All such footnotes should appear on the title page. Footnotes are not normally permitted in the body of the text.

5. ***Literature cited.*** In the text, literature should be cited by the Harvard system, with papers by more than two authors cited as Jones *et al.*, 1980. Personal communications and material in preparation or in press should be cited in the text only, with author's initials and institutions, unless the material has been formally accepted and a volume number can be supplied. The list of references following the text should be headed Literature Cited, and must be typed double spaced on separate pages, conforming in punctuation and arrangement to the style of recent issues of *The Biological Bulletin*. Citations should include complete titles and inclusive pagination. Journal abbreviations should normally follow those of the U. S. A. Standards Institute (USASI), as adopted by BIOLOGICAL ABSTRACTS and CHEMICAL ABSTRACTS, with the minor differences set out below. The most generally useful list of biological journal titles is that published each year by BIOLOGICAL ABSTRACTS (BIOSIS List of Serials; the most recent issue). Foreign authors, and others who are accustomed to using THE WORLD LIST OF SCIENTIFIC PERIODICALS, may find a booklet published by the Biological Council of the U.K. (obtainable from the Institute of Biology, 41 Queen's Gate, London, S.W.7, England, U.K.) useful, since it sets out the WORLD LIST abbreviations for most biological journals with notes of the USASI abbreviations where these differ. CHEMICAL ABSTRACTS publishes quarterly supplements of additional abbreviations. The following points of reference style for THE BIOLOGICAL BULLETIN differ from USASI (or modified WORLD LIST) usage:

A. Journal abbreviations, and book titles, all underlined (for *italics*)

B. All components of abbreviations with initial capitals (not as European usage in WORLD LIST *e.g., J. Cell. Comp. Physiol.* NOT *J. cell. comp. Physiol.*)

C. *All* abbreviated components must be followed by a period, whole word components *must not* (*i.e., J. Cancer Res.*)

D. Space between all components (*e.g., J. Cell. Comp. Physiol.*, not *J.Cell.Comp.Physiol.*)

E. Unusual words in journal titles should be spelled out in full, rather than employing new abbreviations invented by the author. For example, use *Rit Vísindafjélags Islendinga* without abbreviation.

F. All single word journal titles in full (*e.g., Veliger, Ecology, Brain*).

G. The order of abbreviated components should be the same as the word order of the complete title (*i.e., Proc.* and *Trans.* placed where they appear, not transposed as in some BIOLOGICAL ABSTRACTS listings).

H. A few well-known international journals in their preferred forms rather than WORLD LIST or USASI usage (*e.g., Nature, Science, Evolution* NOT *Nature, Lond., Science, N.Y.; Evolution, Lancaster, Pa.*)

6. ***Reprints, page proofs, and charges.*** Authors of articles in black and white (no color figures) receive their first 50 reprints (without covers) free of charge. Color reprints and additional black-and-white reprints may be purchased; authors will receive order forms. Reprints normally will be delivered about 2 to 3 months after the issue date. Authors (or delegates for foreign authors) will receive page proofs of articles shortly before publication. They will be charged the current cost of printers' time for corrections to these (other than corrections of printers' or editors' errors). Other than these charges for authors' alterations, *The Biological Bulletin* does not have page charges.

Reference: *Biol. Bull.* **197:** 1–6. (August 1999)

Annual Viral Expression in a Sea Slug Population: Life Cycle Control and Symbiotic Chloroplast Maintenance

SIDNEY K. PIERCE[1,*], TIMOTHY K. MAUGEL[1], MARY E. RUMPHO[2], JEFFREY J. HANTEN[1], AND WILLIAM L. MONDY[1]

[1]*Department of Biology, University of Maryland, College Park, Maryland 20742; and* [2]*Department of Horticultural Sciences, Texas A & M University, College Station, Texas 77843*

In a few well-known cases, animal population dynamics are regulated by cyclical infections of protists, bacteria, or viruses. In most of these cases, the pathogen persists in the environment, where it continues to infect some percentage of successive generations of the host organism. This persistent re-infection causes a long-lived decline, in either population size or cycle, to a level that depends upon pathogen density and infection level (1–4). We have discovered, on the basis of 9 years of observation, an annual viral expression in Elysia chlorotica, *an ascoglossan sea slug, that coincides with the yearly, synchronized death of all the adults in the population. This coincidence of viral expression and mass death is ubiquitous, and it occurs in the laboratory as well as in the field. Our evidence also suggests that the viruses do not re-infect subsequent generations from an external pathogen pool, but are endogenous to the slug. We are led, finally, to the hypothesis that the viruses may be involved in the maintenance of symbiotic chloroplasts within the molluscan cells.*

Populations of the ascoglossan sea slug *Elysia chlorotica* occur in salt marshes from the Chesapeake Bay to Nova Scotia. The life cycle of the slug lasts about 10 months. The hermaphroditic adults lay egg masses in the spring of each year, and all of the adults die shortly afterward (5, 6). A week or so after the egg deposition, veliger larvae hatch. These larvae spend a few weeks in the plankton and, if filaments of the chromophytic alga *Vaucheria litorea* are present, each veliger homes in on one of them and attaches to it. During the next 24 h, the larva metamorphoses into a juvenile slug while still attached to the algal filament. If the algal filaments are not present, metamorphosis rarely occurs, at least not in laboratory cultures (5, 6). *Vaucheria* is the only alga that *E. chlorotica* eats, and it is the source of the symbiotic chloroplasts that are acquired during feeding. The juvenile slug immediately begins eating the algal filaments and taking on its first load of chloroplasts, which are sequestered by specialized cells in the epithelium lining the digestive diverticula (5, 6). During the next several months, the slugs continue to eat *Vaucheria* and grow, until winter temperatures cause them to become inactive. As the salt marshes warm in the spring, the slugs become active again, begin laying egg masses, and then die. By the time the egg masses have hatched in May, all the adults are gone. This mass mortality occurs synchronously in the laboratory as well as in the field and regardless of the time of year that the slugs were collected.

Symbioses in which chloroplasts—usually from a particular species of alga—are taken up and retained within the cytoplasm of an animal cell occur in several phyla, but they are most commonly encountered in molluscan sea slugs, particularly in the order Ascoglossa (=Sacoglossa) (Opisthobranchia). Certain of the molluscan cells can capture chloroplasts from algal food (usually from a specific species of either Rhodophyceae or Chlorophyceae), and these organelles retain some degree of photosynthetic function for a time (*e.g.*, 7, 8, 9). Whether this intracellular association is a symbiosis in the strict sense is debatable; some authors prefer terms like chloroplast symbiosis, chloroplast retention, or kleptoplasty (7, 9, 11, 12, 13), which indicate that the benefit of the association is entirely to the animal.

The duration of the association between the molluscan cell and the algal plastid varies from species to species.

Received 1 June 1999; accepted 17 June 1999.

[*] To whom correspondence should be addressed: E-mail: sp30@umail.umd.edu

Some associations last less than a week [*e.g.*, *Hermaea bifida* and *Elysia hedgpethi* (see 14)]; and although the plastids are initially functional, photosynthesis stops or is greatly reduced after a week of starvation. In contrast, plastid function continues for more than a week in starved specimens of several species, most belonging to the ascoglossan family Elysiidae (*e.g.*, 7, 10, 15, 16). In the species with the longer duration symbioses, the algal chloroplasts within the molluscan cells fix $^{14}CO_2$, and the ^{14}C appears in a variety of compounds in the animal tissues (15, 17, 18, 19, 20, 21). Thus, there is no doubt that the captured chloroplasts are photosynthetically active within the molluscan cell cytoplasm, and that the products of the synthesis are utilized by the host animal. Indeed, once the symbiosis is established, the species with the longer-lived chloroplast associations can be starved and, as long as light is provided, will maintain or actually gain body weight until the chloroplast function finally fails (7).

In plant cells, continued photosynthetic activity requires continuous synthesis of chloroplast proteins because several proteins, including those used in light harvesting, are rapidly turned-over during the process and must be replaced (22, 23, 24). But, several of these photosynthetic proteins (or their subunits) are encoded in the nucleus, so plastid protein synthesis requires the integration of two distinct genomes, that of the chloroplast and that of the plant cell nucleus (reviewed in 25). Because normal plastid photosynthetic function is dependent upon major nuclear and cytoplasmic support, the ultimate failure of photosynthesis by the symbiotic chloroplasts within the molluscan cells is not surprising. But the symbiotic plastids of *E. chlorotica* stay photosynthetically functional for 8–9 months (5, 26)—many months longer than those of any other species yet described. This remarkable persistence of chloroplast function during starvation indicates that replacement of at least the essential photosynthetic proteins must be occurring within the plastid while it is housed in the molluscan cytoplasm; and indeed, synthesis of plastid proteins, primarily those associated with photosynthesis, occurs in the *E. chlorotica* plastids (26, 27, 28).

The plastid proteins synthesized within the cells of *E. chlorotica* are of two pharmacologically distinguishable sorts: those whose synthesis is blocked by chloramphenicol, and those blocked by cycloheximide (26). Protein synthesis on *plastid* ribosomes is blocked by chloramphenicol, whereas synthesis on *cytoplasmic* ribosomes, usually directed by nuclear genes, is blocked by cycloheximide. These results suggest strongly that some plastid proteins are synthesized upon slug cell ribosomes (26). If this is the case, the genetic information coding for these proteins must somehow be present in the molluscan DNA or must be acquired by all the slugs from the alga in every generation. Our findings presented below suggest a vehicle for this transfer of genetic information from the alga to the slug.

In 1990, as part of an ongoing ultrastructural study of morphological changes in the fine structure of the dying slugs from a population on Martha's Vineyard, Massachusetts, we discovered viruses in digestive cells and hemocytes (29; also Fig. 1). Every year since then, every animal examined near the end of the life cycle has had viruses present, whether it was fixed within hours of collection from the field or maintained for months in our aquarium. No evidence of viruses has been found in any slug earlier in the year, except occasionally within the confines of the plastid (Fig. 1E, see below).

Viruses in the spring slugs are present in the nucleus and cytoplasm of several cell types. They appear to be assembled in the nucleus, then move into the cytoplasm, and finally bud out either into the extracellular space or into a vacuole (Fig. 1A). The diameters of the icosahedral viral capsids in the nuclei average 89 nm (±1.0); but in the cytoplasm, after they have picked up an envelope, they are 109 nm (±1.6) (Fig. 1B). The shapes and sizes of the capsids and envelopes are very similar to those in the Retroviridae, but other viral types have similar dimensions, and known retroviruses are not assembled in the nucleus (30, 31). In addition to these larger viruses, some chloroplasts within the cells of spring slugs contain structures (diameter = 20 nm ± 0.4) that could either be smaller viruses or viral cores. These particles occur loosely collected in areas between the plastid membranes (Fig. 1C). They also occur as particle clumps in the cytoplasm (Fig. 1D), sometimes near material that could be the remnants of chloroplasts. In some instances, in a few fall animals, these particles are present in crystalline arrays (Fig. 1E). Ribulose-1,5-bisphosphate-carboxylase oxygenase (RuBisCO) occurs in crystalline form in some plant plastids fixed under hyperosmotic conditions (32, 33). However, the particles in such RuBisCO crystals are much smaller and usually lack a visual substructure (32, 33), whereas the array particles in the symbiotic plastids in *Elysia* clearly have a substructure (Fig. 1E). The particle arrays in the *E. chlorotica* plastids are more reminiscent of mosaic viruses in plants (34), although almost nothing is known about such crystals in the viruses and plastids of algae. In summary, the morphology suggests that either more than one viral type is present in the slug cell and captured plastids, or we have found several stages of a single viral type.

In addition to the morphology, we have some biochemical information about the identity of the viruses. Using differential and sucrose-gradient centrifugation, we have isolated a fraction from slug homogenates at a density of 1.18 g/ml that has reverse transcriptase (RT) activity. This activity, which is considered diagnostic for retroviruses, is two orders of magnitude higher in spring slugs than in slugs tested in the fall (Fig. 2). In addition, the RT activity of fall animals, but not spring animals, is inhibited by rifampicin (Fig. 3). This inhibition indicates that the activity measured

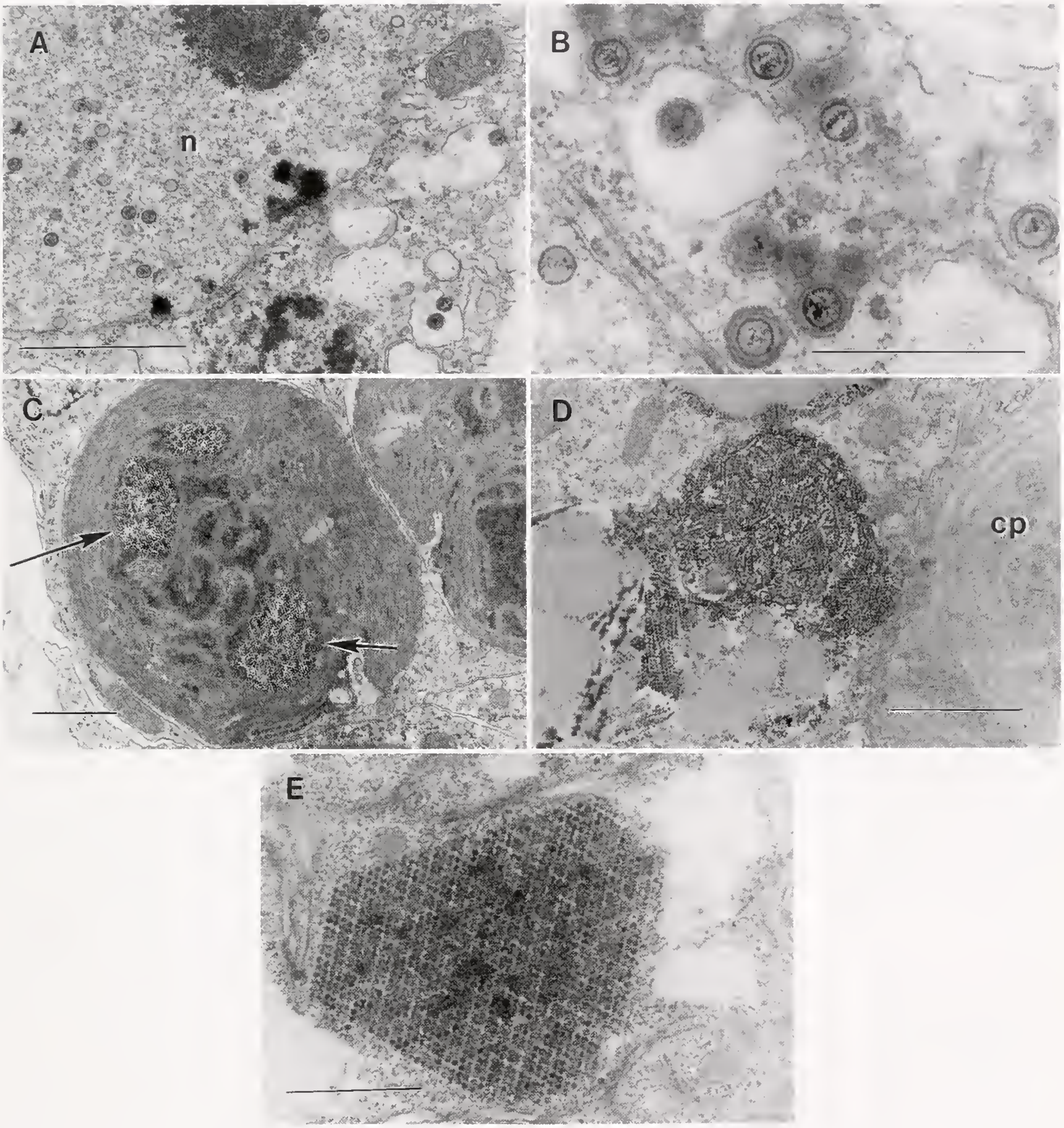

Figure 1. Electron micrographs of viruses in *Elysia chlorotica*. (A) Viral particles in various stages of maturation are present in the nucleus (n) and cytoplasm of a hemocyte from a dying slug (magnification = 33,750×, scale bar = 1 μm). (B) Higher magnification (85,000×, scale bar = 0.5 μm) of viruses budding into cytoplasmic vacuoles. Icosahedral shape and double envelopes of the mature virus are apparent. (C) Viral aggregates (arrows) within the symbiotic chloroplast of a spring *Elysia* (magnification = 16,880, scale bar = 1.0 μm). (D) Viral particles very similar in appearance to those in (C) located in the cytoplasm of a chloroplast (cp)-containing digestive cell of a spring slug. The diffuse, gray areas in the cytoplasm are lipid produced by the plastid (magnification = 27,000, scale bar = 1.0 μm). (E) Viral crystal contained in a symbiotic chloroplast from a fall slug (magnification = 54,000, scale bar = 0.5 μm).

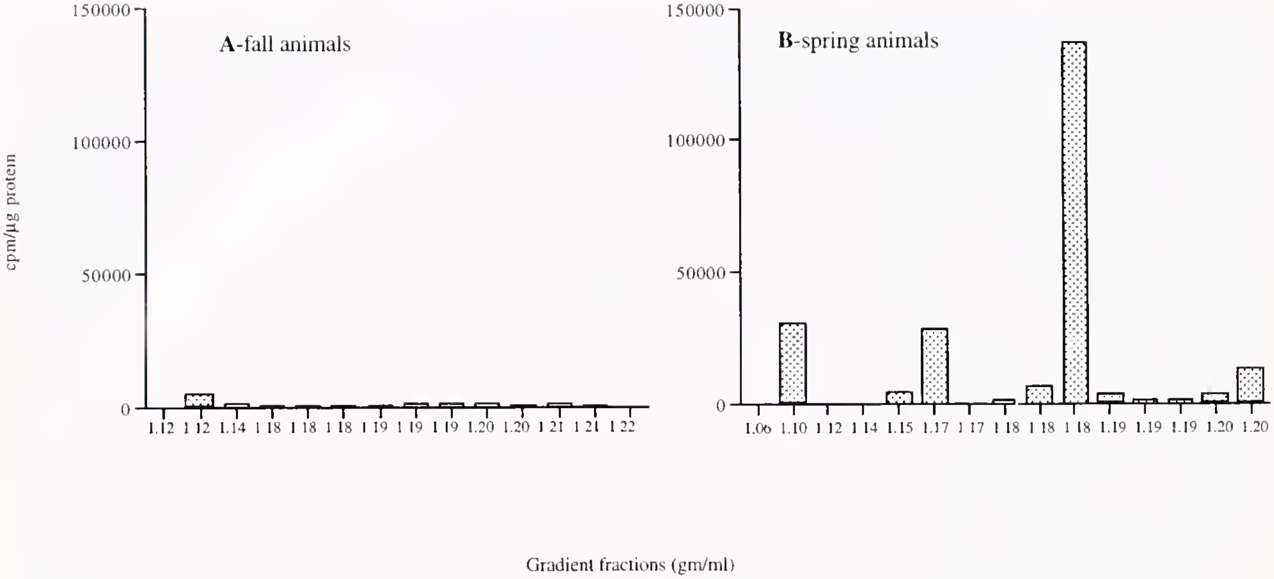

Figure 2. Comparison of reverse transcriptase activity in sucrose-gradient fractions from a typical extract of fall slugs (A) and spring slugs (B). The results are essentially the same whether the animals were freshly collected in the spring or collected in the fall and overwintered in aquaria.

in the fall animals is due to DNA dependent-RNA polymerase (which utilizes the same substrates in the RT assay) rather than RT, and confirms the absence of viruses in the fall animals. Taken together, the morphology, the buoyancy, and the presence of RT all suggest that a retro-like virus is present in the cells of the dying slugs.

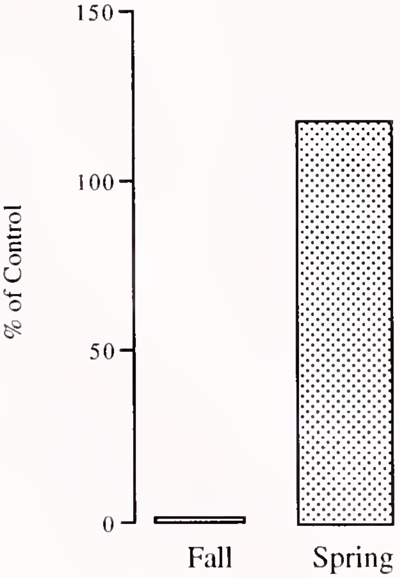

Figure 3. Rifampicin inhibits reverse transcriptase activity. Enzyme activity was assayed in pooled gradient fractions with densities from 1.16 to 1.18 g/ml prepared from fall and spring slugs. The effect of the inhibitor is expressed as a percentage of control values.

The relationships between the nuclear, cytoplasmic, and plastid viruses are not known at present. However, for the last 9 years, the viruses have been found in every dying slug examined. Since some of the slugs had been maintained in the laboratory, in aquaria containing artificial seawater and with no access to *Vaucheria* for 8 months before the viruses appeared, the infection is unlikely to have been opportunistic. Instead, the results suggest either that the demise of the entire population is caused by an endogenous virus or that the virus can be expressed only as the defense systems of the aging animals begin to fail. Furthermore, if the effect on the life cycle is due to a retrovirus, as our data suggest, then the viral genome is probably transmitted to the next generation of slugs in the molluscan DNA. Infection of germ cells by retroviruses produces endogenous proviruses that are inherited as Mendelian genes (33). Alternatively, the viruses might enter all of the slugs *via* the sequestered chloroplasts, either as part of the plastid genome or as constituted viral particles. In either case, viral expression is coincident with increases in environmental temperature, at least in the field slugs. Both the onset of egg laying and the death of the population are associated with the rise of water temperatures in the spring. We can delay the demise of the slugs by maintaining them at very cold temperatures (2°–5°C), but eventually—6–8 weeks after the warmer-maintained slugs have died—the cooled slugs also die with viruses in their cells, indicating that temperature is not the only expression stimulus.

It will take some time to sort out both the types of viruses involved here and the molecular relationships between the slugs, the algae, the plastids, and the viruses. Nevertheless, the nine-year, annual occurrence of the association between population demise and viral expression at the end of the *E. chlorotica* life cycle strongly suggests that the virus has a role in regulating this coincidence. Indeed, we speculate that the viral infection may have caused the transfer, from the alga to the slug, of algal genes that allow the molluscan cells to assist in plastid maintenance. Although the transfer, integration, and expression of such a group of genes between species should succeed only rarely, those successes that did occur should have profound, immediate, heritable effects on the phenotype of the infected species. Such heritable effects must certainly be associated with the mechanism of the widely accepted endosymbiotic origin of intracellular organelles such as mitochondria and chloroplasts; a variety of genes must have been transferred from the symbiont into the host cell nucleus to consummate such a relationship. In addition, a retrovirus as a gene transmission vehicle might have merit as a hypothesis to explain genetic similarities between distantly related or unrelated species (*e.g.*, 35) and is the basis of some genetic therapies (36). If a successful interspecies gene transfer between an alga and a slug mediated by an endogenous virus could be demonstrated in the case of *E. chlorotica*, then an exemplary mechanism for this process would have been provided.

Methods

Viral isolation

The fractionation procedure was carried out using autoclaved equipment. All reagents were molecular biological grade (DNAase-, RNAase-, and protease-free; from Sigma Chemicals, unless otherwise noted) and filtered (0.2 μm pore). Approximately 3.0 g of *E. chlorotica* was homogenized in an ice-cold buffer (450 m*M* NaCl, 1.0 m*M* EDTA, 5.0 m*M* 3-[*N*-morpholino]propane-sulfonic acid (MOPS), 2.3 μM leupeptin, 1.0 m*M* dithiothreitol (DTT), 500 μM phenylmethylsulfonyl fluoride (PMSF), pH 7.5) containing the mucolytic agent *n*-acetyl cysteine (500 m*M*), which is necessary to disperse the copious mucus produced by the slug (26). The homogenate was filtered through six layers of cheesecloth, then through one layer of Miracloth (Calbiochem), and finally through two layers of Miracloth. The filtrate was centrifuged for 5 min at 4300 × *g* (4°C), and the supernatant was centrifuged at 20,000 × *g* for 30 min (4°C). The supernatant from the second spin was layered over a 20% sucrose cushion and centrifuged at 180,000 × *g* for 2 h (4°C) in a swinging bucket rotor. The supernatant was discarded, and the pellet was resuspended in ice-cold homogenization buffer (without *n*-acetyl cysteine). This suspension was layered on the top of a 15%–50% continuous sucrose gradient and centrifuged at 180,000 × *g* for 43 h (4°C).

The gradients were then fractionated by piercing the bottom of the centrifuge tube and raising the gradient out of the tube with 65% sucrose. Twenty 600-μl fractions were collected, and the density of each was determined by weighing 50 μl with an analytical balance. The sucrose in each fraction was then diluted with homogenization buffer (without *n*-acetyl cysteine), and each fraction was centrifuged a final time at 180,000 × *g* for 2 h. The supernatants from this last spin were discarded, and RT assays (see below) and protein assays (37) were run on the pellets.

Reverse transcriptase assay

The final pellets (above) were treated with a detergent buffer (50 m*M* Tris-HCl, 5 m*M* KCl, 0.2 m*M* EDTA, and 0.02% Triton X-100, pH 8.2). Fifteen-microliter aliquots of this digest were added last to 50 μl of buffer (100 m*M* Tris-HCl, 200 m*M* KCl, 10 m*M* $MgCl_2$, pH 8.2), 6 μl 100 m*M* DTT, 9.75 μl 100 m*M* thymidine triphosphate (TTP), 1.25 μl RNA-guard (Pharmacia), 1.0 μl poly(rA)-p(dT) (Pharmacia), and 10 μCi of ^{32}P-TTP (ICN, 10 μCi/μl). The final volume was adjusted to 100 μl with buffer, as necessary, to compensate for ^{32}P half life. This solution was mixed and incubated at 37°C for 65 min on a shaker table. The reaction was terminated by adding 30 μl of 10 m*M* EDTA in 5% TCA and placing the reaction mixture on ice for 20 min. DNA was then precipitated by the addition of 9 μl of 72% TCA, and the precipitate was pelleted by centrifugation at 6610 × *g* for 10 min. The pellet was washed three times in 5% TCA, the final pellet dissolved in 0.1 *N* NaOH, and the radioactivity determined by scintillation counting. The protein concentration of a separate aliquot was determined, and RT activity was expressed as counts per minute per microgram (cpm/μg) protein (38).

Electron microscopy

Small pieces of tissue were prepared for microscopy by fixation in 2% glutaraldehyde in 0.15 *M* cacodylate-0.58 *M* sucrose buffer (pH 7.3) at 900 mosm. The tissue pieces were post-fixed in 1.0% OsO_4 in the same buffer followed by 2.0% aqueous uranyl acetate. The fixed tissue was dehydrated in an ethanol series, infiltrated with propylene oxide, and embedded in Spurr's medium. Silver sections were cut with an ultramicrotome (Reichert), mounted on 75 × 300 mesh copper grids, and stained with uranyl acetate and lead citrate. The sections were viewed and photographed with a transmission electron microscope (Zeiss EM 10).

Acknowledgments

This work was supported by an NSF grant to SKP and MER. We thank Margaret Palmer, Ulrich Mueller, and Jeffery DeStefano for critically reading early versions of this paper. Contribution #91 from the Laboratory of Biological Ultrastructure.

Literature Cited

1. **D'Amico, V., J. S. Elkington, G. Dwyer, R. B. Willis, and M. E. Montgomery. 1998.** Foliage damage does not affect within-season transmission of an insect virus. *Ecology* **79:** 1104–1110.
2. **Hawkins, B. A., H. V. Cornell, and M. E. Hochburg. 1997.** Predators, parasitoids and pathogens as mortality agents in phytophagous insect populations. *Ecology* **78:** 2145–2152.
3. **Kohler, S. L., and M. L. Wiley. 1997.** Pathogen outbreaks reveal large-scale effects of competition in stream communities. *Ecology* **78:** 2164–2176.
4. **Rothman, L. D. 1997.** Immediate and delayed effects of a viral pathogen and density on tent caterpillar performance. *Ecology* **78:** 1481–1493.
5. **West, H. H. 1979.** Chloroplast symbiosis and development of the ascoglossan opisthobranch *Elysia chlorotica.* Ph.D. dissertation, Northeastern University, Boston. 161 pp.
6. **West, H. H., J. F. Harrigan, and S. K. Pierce. 1984.** Hybridization of two populations of a marine opisthobranch with different developmental patterns. *Veliger* **26:** 199–206.
7. **Hinde, R., and D. C. Smith. 1974.** "Chloroplast symbiosis" and the extent to which it occurs in Sacoglossa (Gastropoda: Mollusca). *Biol. J. Linn. Soc.* **6:** 349–356.
8. **Clark, K. B., and M. Busacca. 1978.** Feeding specificity and chloroplast retention in four tropical Ascoglossa, with a discussion of the extent of chloroplast symbiosis and the evolution of the order. *J. Molluscan Stud.* **44:** 272–282.
9. **Clark, K. B., K. R. Jensen, and H. M. Strits. 1990.** Survey for functional kleptoplasty among West Atlantic Ascoglossa (=Sacoglossa) (Mollusca: Opisthobranchia). *Veliger* **33:** 339–345.
10. **Clark, K. B., K. R. Jensen, H. M. Strits, and C. Fermin. 1991.** Chloroplast symbiosis in a non-elysiid mollusc, *Costasiella lilianae* Marcus (Hermaeidae: Ascoglossa (=Sacoglossa): effects of temperature, light intensity and starvation on carbon fixation rate. *Biol. Bull.* **160:** 43–54.
11. **Taylor, D. L. 1970.** Chloroplasts as symbiotic organelles. *Int. Rev. Cytol.* **27:** 29–64.
12. **Gilyarov, M. S. 1983.** Appropriation of functioning organelles of food organisms by phytophagous and predatory opisthobranch mollusks as a specific category of food utilization. *Zh. Obshch. Biol.* **44:** 614–620.
13. **Waugh, G. R., and K. B. Clark. 1986.** Seasonal and geographic variation in chlorophyll level of *Elysia tuca* (Ascoglossa: Opisthobranchia). *Mar. Biol.* **92:** 483–488.
14. **Greene, R. W. 1970.** Symbiosis in sacoglossan opisthobranchs: functional capacity of symbiotic chloroplasts. *Mar. Biol.* **7:** 138–142.
15. **Greene, R. W., and L. Muscatine. 1972.** Symbiosis in sacoglossan opisthobranchs: photosynthetic products of animal-chloroplast associations. *Mar. Biol.* **14:** 253–259.
16. **Graves, D. A., M. A. Gibson, and J. S. Bleakney. 1979.** The digestive diverticula of *Alderia modesta* and *Elysia chlorotica. Veliger* **21:** 415–422.
17. **Trench, R. K. 1969.** Chloroplasts as functional endosymbionts in the mollusc *Tridachia crispata* (Bergh), (Opisthobranchia, Sacoglossa). *Nature* **222:** 1071–1072.
18. **Trench, M. E., R. K. Trench, and L. Muscatine. 1970.** Utilization of photosynthetic products of symbiotic chloroplasts in mucous synthesis by *Placobranchus ianthobapsus* (Gould), Opisthobranchia, Sacoglossa. *Comp. Biochem. Physiol.* **37:** 113–117.
19. **Greene, R. W. 1970.** Symbiosis in sacoglossan opisthobranchs: translocation of photosynthetic products from chloroplast to host tissue. *Malacologia* **10:** 360–380.
20. **Trench, R. K., J. E. Boyle, and D. C. Smith. 1973.** The association between chloroplasts of *Codium fragile* and the mollusc, *Elysia viridis* II. Chloroplast ultrastructure and photosynthetic carbon fixation in *E. viridis. Proc. R. Soc. Lond. B.* **184:** 63–81.
21. **Trench, R. K. 1975.** Of "Leaves That Crawl": functional chloroplasts in animal cells. *Soc. Exp. Biol. Cambridge Symp.* **29:** 229–266.
22. **Greenberg, B. M., V. Gaba, O. Cananni, S. Malkin, A. T. Matoo, and M. Edelman. 1989.** Separate photosensitizers mediate degradation of the 32 kDa photosystem II reaction center protein in the visible and UV spectral regions. *Proc. Natl. Acad. Sci. USA* **86:** 6617–6620.
23. **Matoo, A. K., J. B. Marder, and M. Edelman. 1989.** Dynamics of the photosystem II reaction center. *Cell* **56:** 241–246.
24. **Barber, J., and B. Andersson. 1992.** Too much of a good thing: Light can be bad for photosynthesis. *Trends Biochem. Sci.* **17:** 61–66.
25. **Berry-Lowe, S. L., and G. W. Schmidt. 1991.** Chloroplast protein transport. Pp. 257–302 in *The Molecular Biology of Plastids: Cell Culture and Somatic Cell Genetics of Plants* Vol. 7A. L. Bogorad and I. K. Vasil, eds. Academic Press, New York.
26. **Pierce, S. K., R. W. Biron, and M. E. Rumpho. 1996.** Endosymbiotic chloroplasts in molluscan cells contain proteins synthesized after plastid capture. *J. Exp. Biol.* **199:** 2323–2330.
27. **Mujer, C. V., D. L. Andrews, J. R. Manhart, S. K. Pierce, and M. E. Rumpho. 1996.** Chloroplast genes are expressed during intracellular symbiotic association of *Vaucheria litorea* plastids with the sea slug *Elysia chlorotica. Proc. Natl. Acad. Sci. USA* **93:** 12333–12338.
28. **Green, Brian J., W-y Li, J. R. Manhart, T. C. Fox, R. A. Kennedy, S. K. Pierce, and M. E. Rumpho. 1999.** Mollusc-algal chloroplast endosymbiosis: chloroplast gene expression, thylakoid protein maintenance and synthesis, and photosynthetic activity continue for many months in the absence of the algal nucleus. *Plant Physiol.* (in press).
29. **Maugel, T. K., and S. K. Pierce. 1994.** Is the life cycle of *Elysia chlorotica* ended by disease? *Proc. 52nd Ann. Meeting Microsc. Soc. Am.* 266–267.
30. **Murphy, F. A., C. M. Fauquet, D. H. L. Bishop, S. A. Ghabrial, A. W. Jarvis, G. P. Martelli, M. A. Mayo, and M. D. Summers. 1995.** Virus taxonomy. *Arch. Virol. Suppl. 10,* 586 pp.
31. **Goto, T., M. Nakai, and K. Ikuta. 1998.** The life-cycle of human immunodeficiency virus type 1. *Micron* **29:** 123–138.
32. **Baker, T. S., S. W. Suh, and D. Eisenberg. 1977.** Structure of ribulose-1,5-bisphosphate carboxylase-oxygenase: Form III crystals. *Proc. Natl. Acad. Sci. USA* **74:** 1037–1041.
33. **Shumway, L. K., T. E. Weier, and C. R. Stocking. 1967.** Crystalline structures in *Vicia faba* chloroplasts. *Planta* **76:** 182–189.
34. **Francki, R. I. B., R. G. Milne, and T. Hatta. 1985.** *Atlas of Plant Viruses,* Vol. I and II, CRC Press, Boca Raton, FL.
35. **Pennisi, E. 1999.** Is it time to uproot the tree of life? *Science* **284:** 1305–1307.
36. **Sikorski, R., and R. Peters. 1998.** Treating with HIV. *Science* **282:** 1438.
37. **Peterson, G. L. 1977.** A simplification of the protein assay method of Lowry, *et al.,* which is more generally applicable. *Anal. Biochem.* **83:** 346–356.
38. **Adolph, K. W. 1996.** *Viral Genome Methods.* CRC Press, Boca Raton, FL. p. 122.

Reference: *Biol. Bull.* **197:** 7–10. (August 1999)

Mechanical Resistance to Shear Stress: The Role of Echinoderm Egg Extracellular Layers

FLORENCE I. M. THOMAS[1,2,*,†], KRISTEN A. EDWARDS[1,2], TOBY F. BOLTON[1,2,*],
MARY A. SEWELL[3], AND JILL M. ZANDE[1]

[1] *The Marine Environmental Sciences Consortium, Dauphin Island Sea Lab, Dauphin Island, Alabama;*
[2] *The Department of Marine Sciences, The University of South Alabama, Mobile, Alabama; and*
[3] *The Department of Biology, University of Southern California, Los Angeles, California*

Extracellular layers (jelly coats) on echinoderm eggs are composed of a fibrous network imbedded in a gelatinous material. This type of fibrous network has the potential to protect eggs from mechanical stress. To determine the effects of shear stress and the role of jelly coats in protecting eggs from these stresses, eggs of the sea urchin Lytechinus variegatus, *both with and without intact jelly coats, were exposed to shear stresses ranging from 0.3 to 2 Pa in a cone and plate viscometer. The percentage of eggs remaining intact after exposure to the shear stress was assessed. The results indicate that shear stress can damage eggs and that jelly coats may play a role in decreasing the effects of these stresses. Eggs with jelly coats remained intact and fertilizable at greater shear stresses than those with the coats removed. This is the first evidence that extracellular layers on invertebrate eggs can provide protection from mechanical forces.*

In free-spawning invertebrates, the eggs and sperm, having passed through a gonoduct and gonopore, are released directly into the water column. During the spawning process, gametes are exposed to shear stresses (force per area) in the gonoduct and in the external environment. If gametes are harmed by shear stress before fertilization, irreversible damage will effectively lower the probability of fertilization by decreasing the number of viable gametes in a volume of seawater. Moreover, if gametes are damaged by shear stress, they may survive and be fertilized, but the resultant embryos may not develop normally. Therefore, the number of larvae produced by a given number of eggs may be reduced by exposure to shear stress.

Eggs are first exposed to shear stresses as they traverse the gonoduct on their way to the gonopore. As fluid moves down a tube such as the oviduct, a shear gradient develops in the fluid and imposes a shear stress on the fluid and eggs within the duct. Estimates of shear stresses in the oviduct of one species of sea urchin, *Arbacia punctulata,* ranged from near zero at the center of the duct to over 41 Pa near the wall of the duct (1). This magnitude of shear stress exceeds that estimated to occur in the external environment (2), where gametes meet their second challenge from shear stress after they are released from the gonopore. After eggs are released, they encounter shear stress produced by the interaction of eddies within the water column or within the momentum boundary layer at the surface of the spawning adult. The effects of such shear stress on fertilization and development have only recently been addressed in a hydrodynamic study of fertilization in the purple sea urchin *Strongylocentrotus purpuratus* (2). High shear stress produced experimentally in a Couette cell resulted in low fertilization success and abnormal embryo development. Mead and Denny (2) postulate that high shear stress, as produced in turbulent environments, might reduce the encounter rates of gametes during fertilization, decrease the ability of sperm to remain attached to the egg after contact, and damage eggs prior to fertilization and embryos after fertilization.

Given the two sources of shear stress that eggs experience prior to fertilization, it is possible that there has been selection for egg properties that could reduce the damage caused by these stresses. This idea is supported by the fact that at least one property of echinoid eggs, their viscosity, is positively correlated to wave exposure in three species (3). One

---

Received 16 April 1998; accepted 2 June 1999.

* Present address: Department of Biology, University of South Florida, Tampa, Florida 33620-5150

† To whom correspondence should be addressed. E-mail: fthomas@chuma1.cas.usf.edu

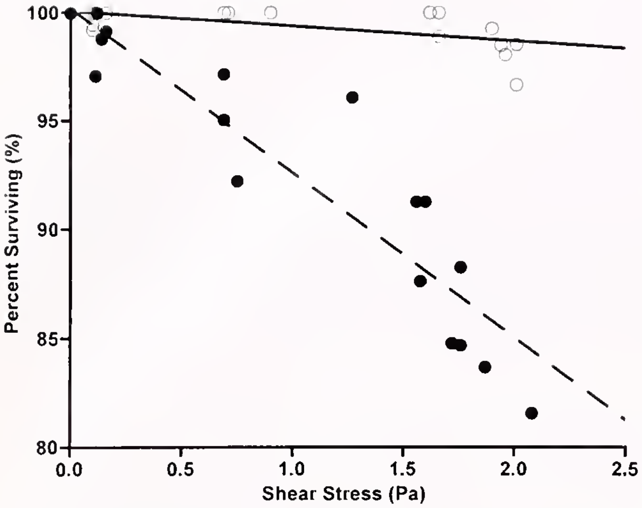

Figure 1. Percentage of *Lytechinus variegatus* eggs remaining intact after exposure to shear stresses. Sea urchins were collected from St. Joseph's Bay, Florida, transported to the Dauphin Island Sea Lab, Alabama, and maintained in laboratory aquaria. Additional animals were obtained from the Carolina Biological Supply Company. Urchins were maintained in seawater collected from St. Joseph Bay (salinity 29–30 ppt), aerated continuously, and fed either spinach or lettuce. We obtained eggs by injecting urchins with 0.5 M KCl. Eggs were used immediately after spawning. Paired samples of eggs with and without jelly coats from each of five females were prepared by removing the jelly coats from half of the eggs collected from a female. The coats were removed using a technique commonly employed in embryology (19). Eggs were poured through a plankton screen (Nytex) with 202-μm-diameter pores. To determine whether the jelly coats had been removed from these eggs, a 200-μl aliquot was pipetted onto a depression slide and Sumi ink was used to visualize the edges of the jelly coats under a compound microscope at 100 × magnification (20). To minimize the probability of damaging the eggs by subjecting them to unnecessary passes through the plankton screen, the eggs were checked for the presence of jelly coats after every two pours.

To assess the effects of shear stress and the potential effect of jelly coats on egg survival, eggs were exposed to a range of shear stresses in a cone and plate viscometer (Brookfield Digital Viscometer, DV-II) attached to a constant temperature bath (Neslab RTE-8). Shear stress was changed by adjusting the shear rate and the viscosity of the fluid (μ). The viscosity was altered by adding hydroxyethyl cellulose (Proto-slo) to filtered seawater. Eight viscous fluids were tested: KY jelly (chlorhexidine gluconate); hydroxyethyl cellulose; polyvinylpyrrolidone; polyvinylpolypyrrolidone; Percoll; methylcellulose; Dextran; and egg homogentate. Two criteria were used to select a fluid: (1) after exposure to the fluid, eggs both with and without jelly coats remained viable; and (2) no cell leakage was detected with visual inspection. Hydroxyethyl cellulose was the only fluid that met both criteria, so it was chosen for use in the experiment. Experiments at shear stresses up to 1.5 Pa were also conducted in seawater only, and the results indicated that use of the hydroxyethyl cellulose could not account for all of the egg loss.

A known number of eggs in 0.5 ml filtered seawater were exposed to a given shear stress for 2 min. The shear stress significantly affected the survival of eggs with (open circles: arcsine % intact = 1.57–0.07* shear stress, $r^2 = 0.48$, $P < 0.001$; 95% confidence limits for the slope are 0.04 to 0.10) and without jelly coats (closed circles: arcsine % intact = 1.53–0.28* shear stress, $r^2 = 0.91$, $P < 0.0001$, 95% confidence limits for the slope are 0.24 to 0.32). For those with jelly coats, there was little effect of shear stress: percent survival ranged from 100% to 96.7% over the entire range of shear stresses. For those without jelly coats, the effect of shear stress was more apparent: percent survival ranged from 100% to 82.0%.

property of eggs that has the potential to decrease the effects of shear stress is the extracellular layer, or jelly coat, that encapsulates the eggs of echinoderms (4). These coats are composed of a fibrous network imbedded in globular glycoprotein (5) and can account for a significant portion of the maternal energy invested in an egg (Bolton and Thomas, unpubl. data). Jelly coats are described for both echinoids and asteroids and consist of several concentric layers of complex fibrous networks (5–10) that are reminiscent of engineering materials designed to withstand shear stresses (11, 12). Although the jelly coat in echinoderms is involved in many parts of the fertilization process (13–18), it seems unlikely that this complex network is required for any of these functions. Thus it is possible that the structure of jelly coats plays a role in protecting eggs from shear stresses experienced in the external environment after spawning, in the oviduct during spawning, or both. The purpose of the research presented here is to explore whether jelly coats can provide this protection in the sea urchin *Lytechinus variegatus*.

To examine the potential role of jelly coats in resisting shear stress, we exposed eggs with and without jelly coats to shear stresses in a cone and plate viscometer and determined the percentage of those eggs that remained intact and fertilizable. A greater percentage of eggs with jelly coats remained intact after exposure to shear stress than did those with jelly coats removed (Fig. 1, Table I). A test for homogeneity of slopes indicated that shear stress affected eggs with jelly coats differently than eggs with coats removed. Eggs with jelly coats suffered a maximum loss of less than 4% as shear stresses approached 2 Pa. No eggs were damaged until shear stresses in excess of 1.7 Pa were reached. For eggs without jelly coats, damage occurred at lower shear stresses than for those with coats, and maximum loss reached nearly 20% as shear stress approached 2 Pa.

The fertilization success of eggs exposed to shear decreased with increasing shear stress both for eggs with jelly coats and for those without (Fig. 2). For both egg types, fertilization success was near 85% with no shear (the de-

Table I

Effect of shear stress on percentage of eggs remaining intact

Source	*F*	*P*
With/without coats (same intercepts)	1.99	0.165
Shear stress (slope = 0)	0.20	<0.001
Interaction (same slopes)	0.75	<0.001

Results from a test for homogeneity of slopes (1 degree of freedom) performed on the arcsine-transformed percentage of eggs intact after exposure to shear stress *versus* the magnitude of shear stress for eggs with and without jelly coats. There was a significant effect of shear stress on eggs remaining intact (slope is significantly different from 0). Eggs with and without jelly coats were affected by shear stress to a different degree (significant interaction between shear stress and jelly coat presence).

sired initial fertilization success). As shear increased, fertilization success dropped from 85% to 68% for eggs with coats and from 85% to 59% for eggs without coats. A test for homogeneity of slopes indicated that the shear stress affected fertilization differently for eggs without intact coats than for those with coats present (Fig. 2, Table II). The slope of the regression of fertilization *versus* shear stress was steeper for eggs with jelly coats removed than for those with intact coats (Fig. 2). After fertilization, developing embryos were assessed for developmental stage and normal development up to the pleuleus stage. Development was assessed throughout this period. All fertilized eggs, regardless of whether they had jelly coats or not, developed normally. This result indicates that if eggs are damaged by shear stress they are not fertilizable, but if they survive they apparently have not sustained any damage that limits normal development.

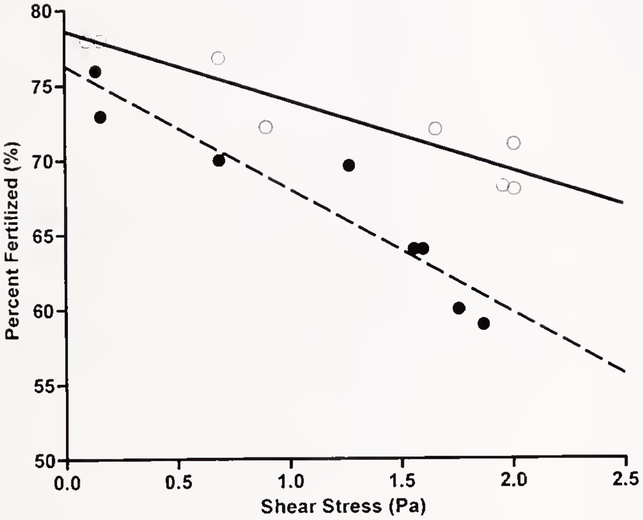

Figure 2. Percentage of eggs successfully fertilized after exposure to shear stress. The fertilizability of eggs with and without intact jelly coats was determined after eggs were exposed to a given shear for 2 min. Gametes for all experiments were obtained by injecting urchins with 0.5 *M* KCl. Females were allowed to spawn into filtered seawater; males spawned into a dry petri dish. Sperm were stored undiluted in a scintillation vial over ice until being used in the experiments. Eggs were used immediately after spawning and sperm within 1 h after spawning. The concentration of sperm yielding 80%–85% successful fertilization (10^4 dilution of dry spawned sperm in seawater) was determined from serial dilution experiments. We used this sperm dilution in all fertilization experiments to ensure that any fertilization decrease caused by egg damage would not be concealed by an overabundance of sperm (2). After exposure to shear, the eggs were added to 100 ml of seawater with the sperm solution. Un-sheared eggs were also fertilized as a control. A sample of approximately 60–100 eggs was examined for fertilization success. Fertilization was assessed at the four-cell stage of development, and normal development was determined after embryos reached the early pluteus stage.

There was a negative relationship between fertilization success and exposure to shear stress, both for eggs with jelly coats (open circles: arcsine % fertilized = 0.92–0.07* shear stress, r^2 = 0.88, $P < 0.001$, 95% confidence limits for the slope are −0.04 to −0.09) and for those without (closed circles: arcsine % fertilized = 0.87–0.11* shear stress, r^2 = 0.90, $P < 0.001$, 95% confidence limits for the slope are −0.08 to −0.15). Only eggs exposed to shear in the viscometer were used in these analyses. Results of a test for homogeneity of slopes indicates that shear stress affects fertilization success of eggs with jelly coats less than that of those without jelly coats (Table II).

Table II

Effect of shear stress on fertilization

Source	*F*	*P*
With/without coats (same intercepts)	2.6	0.13
Shear stress (slope = 0)	0.001	<0.001
Interaction (same slopes)	5.90	0.032

Results from a test for homogeneity of slopes (1 degree of freedom) performed on the arcsine-transformed percentage of eggs fertilized after exposure to shear stress *versus* the magnitude of shear stress for eggs with and without jelly coats. There was a significant effect of shear stress on fertilization (slope is significantly different from 0). Eggs with and without jelly coats were affected by shear stress to a different degree (significant interaction between shear stress and jelly coat presence).

The results of these experiments indicate that eggs can be damaged by shear stress and that the jelly coats on echinoderm eggs can provide mechanical strength, reducing the negative effects of shear stress on free-spawned eggs. If jelly coats are absent, survivorship (Fig. 1) and fertilization success (Fig. 2) are significantly less than when coats are present.

The shear regime experienced in the viscometer most closely approximates that seen in the gonoduct. The experimental shear is unidirectional, constant, and well within the range estimated to occur in the gonoduct during spawning (1). In contrast, the shear stresses imposed in the external environment not only are lower (2) than those used in these experiments, but are not constant and are unlikely to be unidirectional for sustained periods of time. Thus, the data presented here indicate strongly that eggs are susceptible to shear stress and can be damaged at stress levels in the range experienced during egg release. Therefore, the data show that jelly coats on echinoderm eggs do protect eggs from damage caused by shear stress. This result is significant because it is the first evidence that extracellular layers on invertebrate eggs can protect eggs from physical stress and may provide mechanical strength to eggs.

Acknowledgments

Research support was provided by a National Science Foundation (NSF) grant (IBN-9723770) and an NSF PECASE award to F. I. M. Thomas (OCE-9701434). Kristen Edwards initiated the research while participating in a research experience for undergraduate program funded by a NSF Grantto Judy Stout (REU, OCE-9619862). We also thank three anonymous reviewers for helpful suggestions. This is DISL contribution 309.

Literature Cited

1. **Thomas, F. I. M., and T. F. Bolton. In Press.** Shear stress experienced by echinoderm eggs in the oviduct during spawning: potential role in the evolution of egg properties. *J. Exp. Biol.*
2. **Mead, K. S., and M. W. Denny. 1995.** The effects of hydrodynamic shear stress on fertilization and early development of the purple sea urchin *Strongylocentrotus purpuratus*. *Biol. Bull.* **188:** 46–56.
3. **Thomas, F. I. M. 1994.** Physical properties of gametes in three sea urchin species. *J. Exp. Biol.* **194:** 263–284.
4. **Hoshi, M. 1985.** Lysins. Pp. 431–462 in *Biology of Fertilization*, Vol. 2. C. B. Metz and A. Monroy, eds. Academic Press, Orlando, FL.
5. **Bonnell, B. S., S. H. Keller, V. D. Vacquier, and D. E. Chandler. 1994.** The sea urchin jelly coat consists of globular glycoproteins bound to a fibrous fucan superstructure. *Dev. Biol.* **162:** 313–324.
6. **Kidd, P. 1978.** The jelly and vitelline coats of the sea urchin egg: new ultrastructural features. *J. Ultrastruct. Res.* **64:** 204–215.
7. **Holland, N. D. 1980.** Electron microscopic study of the cortical reaction in eggs of the starfish (*Patiria miniata*). *Cell Tissue Res.* **205:** 67–76.
8. **Crawford, B., and M. Abed. 1986.** Ultrastructural aspects of the surface coatings of eggs and larvae of the starfish, *Pisaster ochraceus*, revealed by Alcian Blue. *J. Morphol.* **187:** 29–37.
9. **Sousa, M., R. Pinto, P. Moradas-Ferreira, and C. Azevedo. 1993.** Histochemical studies of jelly coat of *Marthasterias glacialis* (Echinodermata, Asteroidea) oocytes. *Biol. Bull.* **185:** 215–224.
10. **Bonnell, B. S., C. Larabell, and D. E. Chandler. 1993.** The sea urchin egg jelly coat is a three-dimensional fibrous network as seen by intermediate voltage electron microscopy and deep etching analysis. *Mol. Reprod. Dev.* **35(2):** 181–188.
11. **Sastry, A. M., S. L. Phoenix, and P. Schwartz. 1993.** Analysis of interfacial failure in a composite microbundle pull-out experiment. *Composite Sciences and Technology.* **48:** 237–251.
12. **Sastry, A. M., X. Cheng, and C. W. Wang. 1998.** Mechanics of stochastic fibrous networks. *J. Thermoplastic Composite Materials. Vol. II.* 288–296.
13. **Vaquier, V. D., and G. W. Moy. 1977.** Isolation of bindin: the protein responsible for adhesion of sperm to sea urchin eggs. *Proc. Natl. Acad. Sci. USA* **74:** 2456–2460.
14. **Tilney, L. G., D. P. Kiehart, C. Sardet, and M. Tilney. 1978.** Polymerization of actin IV. Role of $Ca2^+$ and H^+ in the assembly of actin and in membrane fusion in the acrosomal reaction of echinoderm sperm. *J. Cell Biol.* **77:** 536–550.
15. **SeGall, G. K., and W. J. Lennarz. 1981.** Jelly coat and induction of the acrosome reaction in echinoid sperm. *Dev. Biol.* **86:** 87–93.
16. **Garbers, D. L., and G. S. Kopf. 1980.** The regulation of spermatazoa by calcium and cyclic nucleotides. *Adv. Cyclic Nucleotide Res.* **13:** 251–306.
17. **Nomura, K., and S. Isaka. 1985.** Synthetic study of the structure-activity relationship of sperm-activating peptides from the jelly coat of sea urchin eggs. *Biochem. Biophys. Res. Commun.* **126:** 974–982.
18. **Miller, R. L. 1985.** Sperm chemo-orientation in the Metazoa. Pp. 276–337 in *Biology of Fertilization*, Vol. 2. C. B. Metz and A. Monroy, eds. Academic Press, Orlando, FL.
19. **Hinegardner, R. 1975.** Care and handling of sea urchin eggs, embryos, and adults (principally North American species). Pp. 10–41 in *The Sea Urchin Embryo—Biochemistry and Morphogenesis*. G. Czihak, ed. Springer-Verlag, New York.
20. **Strathmann, M. F. 1987.** *Reproduction and Development of Marine Invertebrates of the Northern Pacific Coast.* University of Washington Press, Seattle. 670 pp.

Reference: *Biol. Bull.* **197:** 11–13. (August 1999)

Regeneration of Amputated Avian Bone by a Coral Skeletal Implant

B. RINKEVICH[1], S. BEN-YAKIR[2], AND R. BEN-YAKIR[2]

[1] *National Institute of Oceanography, Tel Shikmona, P.O.B. 8030, Haifa 31080, Israel; and*
[2] *Hod-Hasharon Veterinary Clinic, 17 Gordon Street, Hod Hasharon, Israel*

Bone fractures are common in both wild and captive birds (1, 2). Avian bones are thin and brittle and tend to break into fragments or shatter upon a variety of natural events (midair collisions, fights with other animals; ref. 2) or anthropogenic experiences (wounding by gunfire, collisions with cars or fences, encounters with traps, attacks by dogs or cats, etc.; ref. 1). The prospect of full recovery following repair of avian bone fracture is often poor, and the complication rate is high (3). For wild birds, anything less than complete normal function cannot be regarded as successful, and slight malunion or a change in a few degrees of rotation can produce a severe loss of flight function (4). Furthermore, in nomadic species, time is critical because long periods of rehabilitation may prevent the birds from reuniting with their flocks. In experiments with implantation of fragments of skeleton from the coral Stylophora pistillata, *we found the implants to be avian osteo-conductive biomaterial, acting as a scaffold for a direct osteoblastic deposition. In the case study presented here, the bird regained complete flight activity within 2 weeks after surgery, with full regeneration of the amputated ulna.*

The general principles for treating fractures in birds are similar to those established for mammals and include rigid stabilization (primary bone healing does not occur if there is a gap or motion at the fracture site; ref. 4). However, treatment such as external coaptation (slings, bandages, casts, splints, etc.), intramedullary pins or rods, bone plate fixation, or modifications of any of the traditional means of external skeleton fixation (3–5) not only fails for rehabilitating wild birds, but also involves prolonged hospitalization of avian patients. Internal fixation is one of the best procedures for fracture management, but the brittle nature of avian bones (3–5) results in problems that are not encountered in mammals.

We recently investigated the use of coral skeleton as a natural intramedullary fixation device for fractures of bird bone and found that fractured avian bones can be rehabilitated following the internal implantation of coral skeletal pins (unpubl. data). This investigation was based on studies with mammals (including humans) documenting that coral skeletons may be employed as osseous substitutes, as scaffolds for direct osteoblastic application, or as an artificial bone filler for repairing bone defects (6, 7). The coral tested here was of the branching species *Stylophora pistillata*, one of the most abundant coral species in the Gulf of Eilat (8).

Mature domestic pigeons (*Columba livia domestica*) were randomly assigned to a variety of treatment groups (in preparation). For all radiographic and surgical procedures, the birds were given Halothane as a general anesthetic. The skin was prepared for aseptic surgery using a septal scrub followed by a povidone-iodine wash. Whenever possible, flight feathers were not removed or clipped; others were plucked over the intended incision. Reflexes and cardiac and respiratory activities were monitored. Birds were placed on their backs and a limited ventral approach to the ulna was performed. Two of the same bones from the wings of two birds were used as experimental and control bones (bandaged in the traditional manner; ref. 5). Small processed coral pins were obtained from SagivCoral, P.O. Box 3337, Ramot Hashavim 45930, Israel. Postoperative radiographs were taken to evaluate fracture repair and to document the status of the coral implant. Pigeons were housed in the flypen system and fed with a commercial pigeon food supplemented with vitamin D and oyster shell as a calcium source.

In one of the experiments, which is detailed in this communication, the proximal half of the ulna (which pro-

Received 26 January 1999; accepted 23 April 1999.
E-mail: buki@ocean.org.il

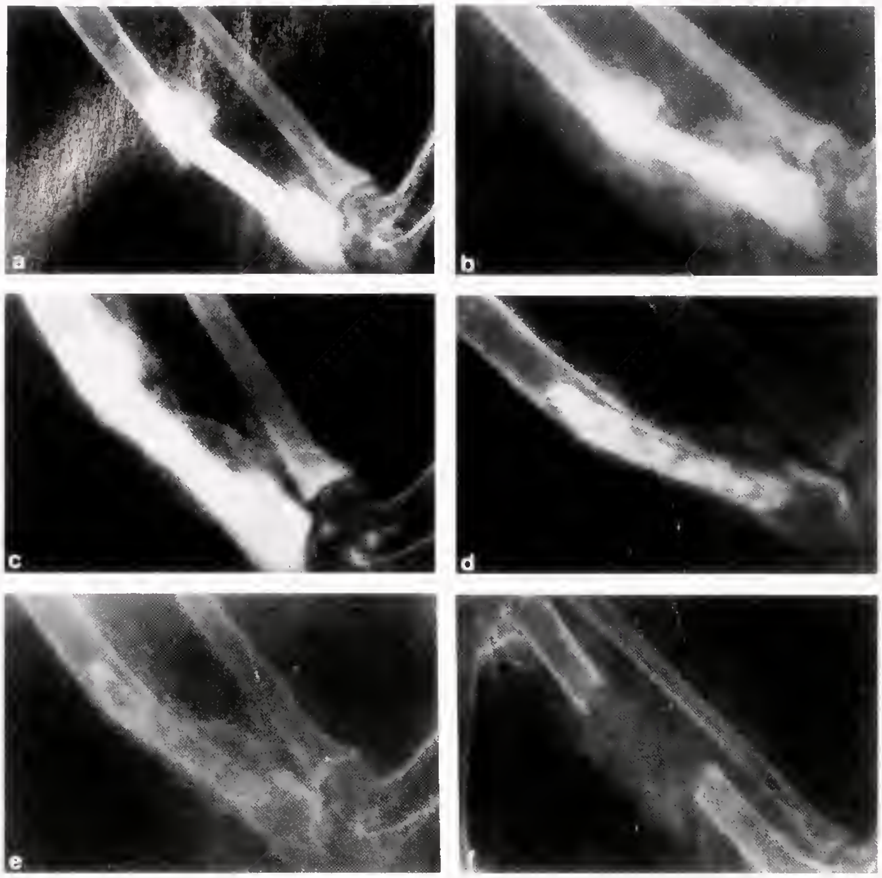

Figure 1. Progressive repair of ulna fracture treated by implantation of an intramedullary coral pin (a–e), compared to control, an untreated amputated ulna (f). Weeks after operation: a = 2, b = 4, c = 6, d = 8, e, f = 12.

vides primary support for the wing) was accidentally comminuted during surgery. Full rehabilitation of this amputation bone by the use of coral skeleton implant is described here.

In the case of the accidentally comminuted ulna, all brittle fragments were immediately removed and a small coral pin (24 mm length, 4 mm diameter) was first passed distally and then retrogradely until resistance was met at the proximal side of the ulna. The coral pin was then firmly wedged in place, forming an inert calcium carbonate milieu between the two separated parts, replacing the amputated portion of the ulna. This pigeon used the treated wing freely 14 days after the operation, alleviating ankylosis resulting from joint immobilization. In the control bird, the entire segment of proximal ulnar bone (cortex and medulla) was removed using Gilgi wire.

Two weeks after the operation, the coral pin was encapsulated firmly at both ends by overgrown calcium deposits and callus formation along the pin shaft, providing rotational stability (Fig. 1a). After 4 weeks (Fig. 1b), the coral implant was already overgrown by deposited material. By 6 weeks (Fig. 1c), deposited material surrounded the implant in layers and the first sign of coral resorption was evident. During resorption, which was significantly advanced at 8 and 12 weeks (Fig. 1d, e), radiography showed that the area between the two ends of the broken ulna was being filled with accumulated new bone, replacing the degradable pin. *Stylophora pistillata* skeleton (although its mechanical and biological properties were not yet evaluated) was thus found to be avian osteo-conductive biomaterial, acting as a scaffold for direct osteoblastic deposition. The bird regained full flight activities 2 weeks after surgery, and the coral pin activated skeletal regeneration (compare with the control; Fig. 1f). This process ended in complete regeneration of the amputated area.

This case of regeneration of an amputated bone and our study (in prep.) demonstrate the value of coral skeletal implants for avian bone repair. Coral material (calcium carbonate) is well tolerated by bird tissue. The pin matrix is porous enough to be colonized by the birds' bony cells, is biodegradable, and is easily adjustable in size and shape to the osseous site of grafting. Previous studies employing coral implants for bone repair in mammals have shown that coral resorption rates varied with porosity of the coral species used and with host reaction (9). We used natural fragments of *S. pistillata* skeletons, the first pocilloporid coral used in vertebrate skeleton rehabilitation. Each year, around the globe, veterinarians tend an ever-increasing number of wild and domestic birds with broken bones; unfortunately, at present the prognosis for many of these birds is poor. The approach described here may provide a fast and dependable method for rehabilitation of avian fractures, increasing the survival rate of birds treated for bone injuries.

Acknowledgments

This study was supported by the Minerva Center for Marine Invertebrate Immunology and Developmental Biology. Animal surgeries and treatments were conducted in conformance with the guidelines of the Canadian Council on Animal Care.

Literature Cited

1. **Fix, A. S., and S. Z. Barrows. 1990.** Raptors rehabilitated in Iowa during 1986 and 1987: a retrospective study. *J. Wildl. Dis.* **26:** 18–21.
2. **Houston, D. C. 1993.** The incidence of healed fractures to wing bones of White-backed and Ruppell's Griffon Vultures *Gyps africanus* and *G. rueppellii* and other birds. *Ibis* **135:** 468–475.
3. **Mathews, K. G., L. J. Wallace, P. T. Redig, J. E. Bechtold, R. R. Pool, and V. L. King. 1994.** Avian fracture healing following stabilization with intramedullary polyglycolic acid rods and cyanoacrylate adhesive *vs.* polypropylene rods and polymethylmethacrylate. *Vet. Comp. Orthop. Trauma* **7:** 158–169.
4. **Bennett, R. A., and A. B. Kuzma. 1992.** Fracture management in birds. *J. Zoo. Wildl. Med.* **23:** 5–38.
5. **MacCoy, D. M. 1992.** Treatment of fractures in avian species. *Vet. Clin. North Am. Small Anim. Pract.* **22:** 225–238.
6. **Kehr, P. H., A. G. Graftiaux, F. Gosset, I. Bogorin, and K. Bencheikh. 1993.** Coral as a graft in cervical spine surgery. *Orthop. Traumatol.* **3:** 287–293.
7. **Guillemin, G., J-L. Patat, and A. Meunier. 1995.** Natural corals used as bone graft substitutes. *Bull. Inst. Oceanogr. (Monaco)* **14:** 67–77.
8. **Loya, Y. 1976.** The Red Sea coral *Stylophora pistillata* is an r strategist. *Nature (Lond.)* **259:** 478–480.
9. **Roudier, M., C. Bouchon, J. L. Rouvillain, J. Amédée, R. Bareille, F. Rouais, J. Ch. Fricain, B. Dupay, P. Kien, R. Jeandot, and B. Basse-Cathalinat. 1995.** The resorption of bone-implanted corals varies with porosity but also with the host reaction. *J. Biomed. Mater. Res.* **29:** 909–915.

Reference: *Biol. Bull.* **197:** 14–25. (August 1999)

Functional and Evolutionary Implications of Opposed Bands, Big Mouths, and Extensive Oral Ciliation in Larval Opheliids and Echiurids (Annelida)

BENJAMIN G. MINER[1], ERIC SANFORD[2], RICHARD R. STRATHMANN[3], BRUNO PERNET[3], AND RICHARD B. EMLET[4]

[1]*Department of Zoology, University of Florida, 223 Bartram Hall, Gainesville, Florida 32611;*
[2]*Department of Zoology, Cordley Hall 3029, Oregon State University, Corvallis, Oregon 97331;*
[3]*Friday Harbor Laboratories and Department of Zoology, University of Washington, 620 University Road, Friday Harbor, Washington 98250; and* [4]*Department of Biology and Oregon Institute of Marine Biology, University of Oregon, P.O. Box 5389, Charleston, Oregon 97420*

Abstract. Larvae of two annelids, the opheliid *Armandia brevis* and the echiurid *Urechis caupo*, captured small particles between opposed prototrochal and metatrochal ciliary bands and also captured large particles with wide ciliated mouths. The body volume of larval *A. brevis* increased more rapidly than the estimated maximum clearance rate as segments were added. Capture of larger particles by late-stage larvae may compensate for this potentially unfavorable allometry. The existence of larvae that use two feeding mechanisms at once, not previously known in annelids, suggests possible evolutionary routes between larval forms that feed only with opposed bands (*e.g.*, serpulids and oweniids) and those that use complex oral ciliature to feed primarily on large particles (*e.g.*, polynoids and nephtyids). In particular, the metatroch and food groove of opposed-band feeders may have arisen as expansions of oral ciliation in ancestral large-particle feeders; alternatively, extensive oral ciliation in large-particle feeders may have originated as a modification of metatroch and food-groove cilia in ancestral opposed-band feeders.

Introduction

The trochophore is a larval form of several phyla: Annelida, Sipuncula, Mollusca, and Entoprocta (Nielsen, 1995). It is largely defined by the presence of the prototroch, a preoral ciliary band with a well-defined cell lineage. Despite this and other embryological similarities, trochophores are structurally and functionally diverse. Much of this diversity is found among the approximately 70 families of annelids in which larvae occur. Annelid larvae vary in the number and position of ciliary bands (though almost all possess a prototroch), and in whether or not they feed. Among annelid larvae that feed, mechanisms of capturing suspended particles have been described in only a few species (Strathmann, 1987).

One of these feeding mechanisms involves capturing and transporting particles with the prototroch and several postoral ciliary bands. The prototroch beats with an anterior-to-posterior effective stroke. A postoral band, the metatroch, parallels the prototroch and beats in opposition to it, with effective strokes from posterior to anterior. Particles small enough to fit between the prototroch and metatroch are captured between these two ciliary bands and transported to the mouth by a band of shorter cilia, the food groove. Particle capture by opposed bands has been described in larvae of two annelid families, the serpulids and the oweniids (Strathmann *et al.*, 1972; Emlet and Strathmann, 1994), and larvae of several other families possess the ciliary bands necessary to feed in this way.

Another feeding mechanism known in annelid larvae involves active responses to individual food particles. For example, polynoid larvae lack an opposing metatroch and a ciliated food groove. These larvae swim forward until they encounter relatively large particles, then manipulate each particle individually into the mouth with a tuft of long compound cilia (Phillips and Pernet, 1996). Larvae belong-

Received 16 December 1998; accepted 8 April 1999.
E-mail: miner@zoo.ufl.edu

ing to related families (*e.g.*, phyllodocids and nephtyids: Rouse and Fauchald, 1997) also lack a metatroch and a food groove (Bhaud and Cazaux, 1987), and are able to capture particles as large as bivalve larvae, but how they do this is not known. Additional feeding mechanisms are known or suspected from larvae of other annelid families (Strathmann, 1987; Nielsen, 1998).

The structural and functional variety of trochophores in annelids and related phyla has raised questions about their evolution (Strathmann, 1993; McHugh and Rouse, 1998). There is no consensus as to whether feeding or nonfeeding larvae are ancestral, or on which feeding mechanisms are primitive (Strathmann and Eernisse, 1994). Given uncertainties about such key issues as the distribution of traits among clades, the functional requirements for capturing particles, and the phylogeny of annelids, inferences about ancestral character states are weak.

Our study describes ciliation and mechanisms of particle capture in larvae of two families of annelids, the Opheliidae and the Echiuridae. We use these observations to compare the feeding capabilities of different annelid larvae and to suggest possible evolutionary transitions among annelid larval forms. These data also augment the number of informative characters available for phylogenetic inferences.

Hermans (1978) showed that larvae of the opheliid *Armandia brevis* possess prototrochal and metatrochal ciliary bands. Although the feeding mechanism was not described, these observations suggest that opposed-band feeding may occur. He also noted that late-stage *A. brevis* larvae are able to ingest large particles. A larva with 15 segments had ingested a tintinnid 80 μm in diameter and a diatom 35 μm in diameter and 260 μm long (Hermans, 1964). This implies that these larvae were using a different feeding mechanism, since other work on annelid and mollusc larvae indicates that opposed-band feeding is limited to particles that fit between the prototroch and metatroch (typically spaced <30 μm apart: Strathmann *et al.*, 1972; Strathmann and Leise, 1979).

Thus, limited observations suggested that *A. brevis* larvae might use several feeding mechanisms to capture particles of a broad range of sizes. Alternative mechanisms for the capture of larger particles by later stage larvae might supplement the opposed-band feeding mechanism. Such versatility might be particularly advantageous to later stage larvae if unfavorable allometric relationships reduce the profitability of opposed-band feeding as development progresses. An unfavorable allometry might occur if body volume and metabolic demands increase more rapidly than ciliary band area and maximum clearance rates as segments are added during development. Therefore, in addition to observing particle captures, we examined the relationship between clearance rates and body volume.

Echiurids have sometimes been placed in the phylum Annelida and sometimes in their own phylum, the Echiura, which is distinguished from the annelids by an apparent lack of segmentation (Nielsen, 1995). McHugh's (1997) molecular evidence shows that they are derived annelids, and she suggests that they should be placed in the annelid family Echiuridae. Larvae of the echiurid *Urechis caupo* bear prototrochal, metatrochal, and food-groove cilia (Newby, 1940; Suer, 1982), but how they capture particles has been unknown. We observed larval feeding in *U. caupo* to confirm use of the opposed-band feeding mechanism in the Echiuridae; to our surprise, we also obtained evidence that larger particles are captured at the mouth.

Our observations demonstrate that larvae in the annelid families Opheliidae and Echiuridae are able to capture particles both with opposed bands and directly at the mouth. This previously unrecognized combination of feeding mechanisms suggests hypotheses for evolutionary transitions among the diverse feeding larval forms of the Annelida.

Materials and Methods

Larval cultures

Reproductive adults of the opheliid *Armandia brevis* were collected in April and May 1998 in front of the Friday Harbor Laboratories, San Juan Island, Washington. Some animals were taken from beneath cobbles in the mid-intertidal zone and others from the plankton swarming at night to a light suspended from the laboratory dock. We isolated adults in finger bowls containing bag-filtered seawater (mesh size $\leq$ 10 μm) until gametes were released. Eggs were fertilized by the addition of sperm and then rinsed with filtered seawater. Fertilized eggs were placed in 450-ml beakers that held filtered seawater and were partially submerged in a seawater table at 11°–13°C. Larvae were fed a mixture of the algae *Isochrysis galbana* and *Chaetoceros gracilis*.

Adults of the echiurid *Urechis caupo* were dug in intertidal mudflats in Bodega Harbor, California, in June of 1995 and held in aquaria at the Bodega Marine Laboratory for use throughout the summer. Methods described by Gould (1967) were used for obtaining gametes and fertilizing eggs. We reared larvae in 800-ml beakers cooled in aquaria at 10° to 16°C (median 13.3°C), approximately the temperature of the coastal seawater. The seawater was filtered through meshes of 30 or 70 μm and larvae were fed the alga *Rhodomonas* sp. and occasionally *Isochrysis galbana* in addition to whatever food entered with the filtered seawater.

Ciliary bands

Light microscopy provided information about the ciliation of both opheliid and echiurid larvae. Larvae were viewed with differential interference contrast (DIC) optics for an optical section through the prototroch, food groove, and metatroch.

Scanning electron microscopy provided additional information about the ciliation of *Armandia brevis*. Larvae were relaxed in a 1:1 mixture of 7.5% $MgCl_2$ and seawater for 30 min and fixed in 1% OsO_4 in seawater. After a rinse in seawater, fixed larvae were dehydrated in ethanol, infiltrated with hexamethyldisilazane for 30 min, and air-dried. They were mounted on stubs with double-sided tape and sputter-coated with gold-palladium before viewing.

Analysis of particle capture

To record larval feeding, we used video cameras mounted on compound and dissecting microscopes. A time-date generator indicated intervals between video images to the nearest 0.01 s. Larvae of *Armandia brevis* were presented with small and large particles in separate trials, and feeding activity was recorded at room temperature (22°C) onto VHS tape. We observed capture of small particles by placing several larvae on a slide with polystyrene-divinylbenzene spheres (Duke Scientific) of 5 and 12 μm diameter (one size per slide), adding a raised coverslip, and viewing the larvae with a 20× objective and DIC optics. Larvae that had tethered themselves with mucous strands and were actively feeding (indicated by beating of both the prototroch and metatroch) were videotaped for about 10 min. We observed capture of large particles by placing larvae in a small petri dish onto a dissecting microscope and adding Sephadex beads ranging from 20 to 80 μm in diameter. Larvae were videotaped as they swam and fed.

For *Urechis caupo* larvae, feeding was observed at 15° to 20°C and recorded onto 8-mm tape. Larvae were confined within the spaces of a nylon mesh placed on a slide topped with a coverslip; they were free to rotate and change orientation but not to move forward continuously. We presented the larvae with three types of particles: the dinoflagellate *Prorocentrum micans* (length about 20 μm), polystyrene-divinylbenzene spheres (diameter 5 to 29 μm), and Sephadex beads (diameter 20 to 80 μm).

The size of particles captured and ingested by *U. caupo* was analyzed by inspecting the gut contents of particle-fed larvae. Larvae and suspensions of particles of several sizes were placed in vials that were rotated at 15 rpm. After 5 min, the larvae were fixed with formaldehyde for gut-content examination.

Scaling of clearance rate and body volume

The relationship of maximum clearance rate to body volume was estimated for larvae of *Armandia brevis* with 6 to 16 setigerous segments. We counted the number of seti-

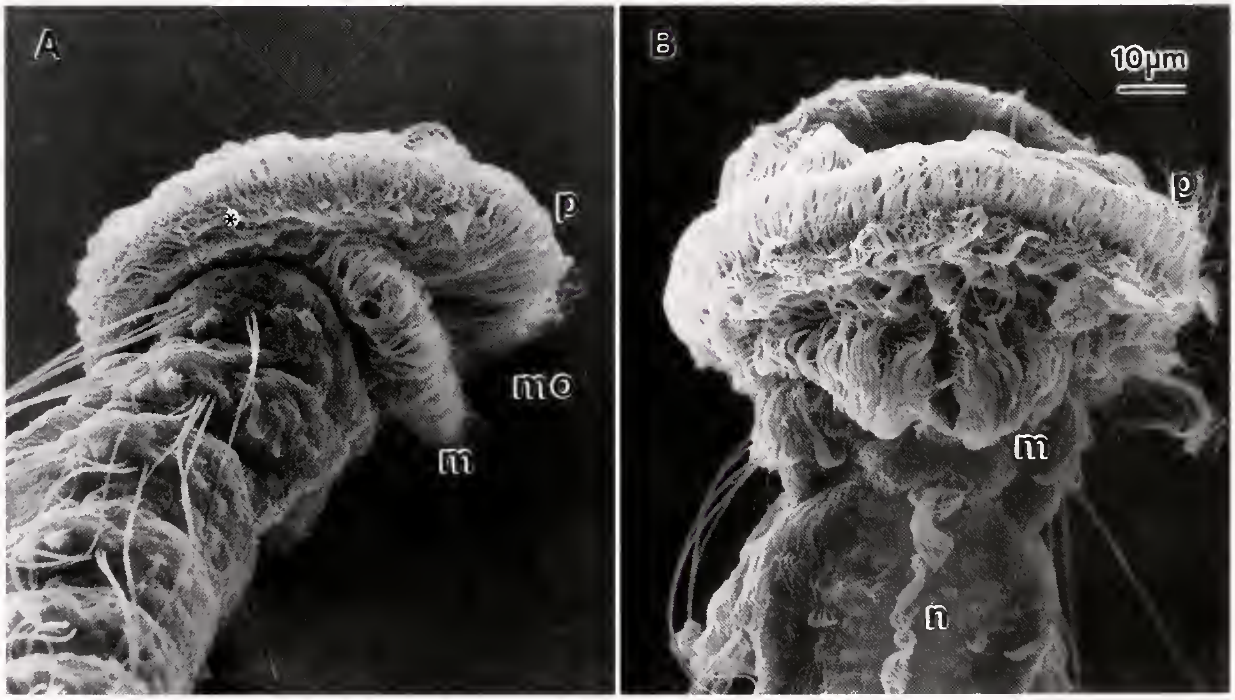

Figure 1. Scanning electron micrographs of larvae of *Armandia brevis*. (A) Posterolateral view of the anterior end of an 18-setiger larva. The food groove (*) is the region between the long compound cilia of the prototrochal (p) and metatrochal (m) ciliary bands. The inner surfaces of the mouth (mo) are heavily ciliated. (B) Ventral view of the anterior end of an 18-setiger larva, showing the long compound cilia of the metatroch (m) on the lower lip, the prototroch (p), and the short neurotroch (n). Both photos are to the same scale.

gers and measured body length (for the entire larva), width (at the middle segment), and prototroch diameter of live larvae (n = 36) under a compound microscope with 4× objective. A video camera and image analysis program (NIH Image 1.61; available free at http://rsb.info.nih.gov/nih-image) were used for these measurements. We estimated larval volume as a cylinder by the equation:

$$\text{larval volume} = \pi(D/2)^2(L)$$

where D is body width and L is body length.

Maximum clearance rates were estimated as the volume of water passing through the prototroch per unit of time. To calculate these rates, we measured particle velocities and particle distances to the base of the prototroch from videotaped sequences of three larvae in each of three size classes (6–7, 11–12, and 15–16 setigers). We observed larvae and 5-μm particles on a compound microscope with DIC optics and 20× objective lens, as described above. The larvae tethered themselves by mucous strands and were recorded for several minutes. The distances traveled by particles per unit of time and their distances to the base of the prototroch were measured from videorecorded sequences. Particles were measured as they passed within the direct influence of the cilia where velocities are negligibly affected by the slide or coverslip (Emlet, 1990).

We fitted binomial regressions from the origin through the plot of particle velocity versus particle distance from the cilium base. The rationale for fitting curvilinear lines to these data was both theoretical (Sleigh, 1984) and empirical (Strathmann and Leise, 1979). The studies in both areas suggest that velocity should increase from zero near the larval body surface to a maximum near the full length of the cilia; it should then decrease beyond the tips of the cilia. Since these curves included some particles that presumably passed beyond the tips of the cilia, it was necessary to estimate the lengths of the cilia for larvae of each of the three size classes. We measured cilium lengths (15 cilia per larva) with NIH Image from videotaped, live larvae with 0–17 setigers (n = 22 larvae). The binomial regression equations relating particle velocity to particle distance from the cilium base were then integrated from the origin (the base of the prototroch) to the estimated cilium length for that size class. The resulting areas represent estimates of the area of water that, in one unit of time, passes through one optical section of the prototroch in the plane of ciliary beat.

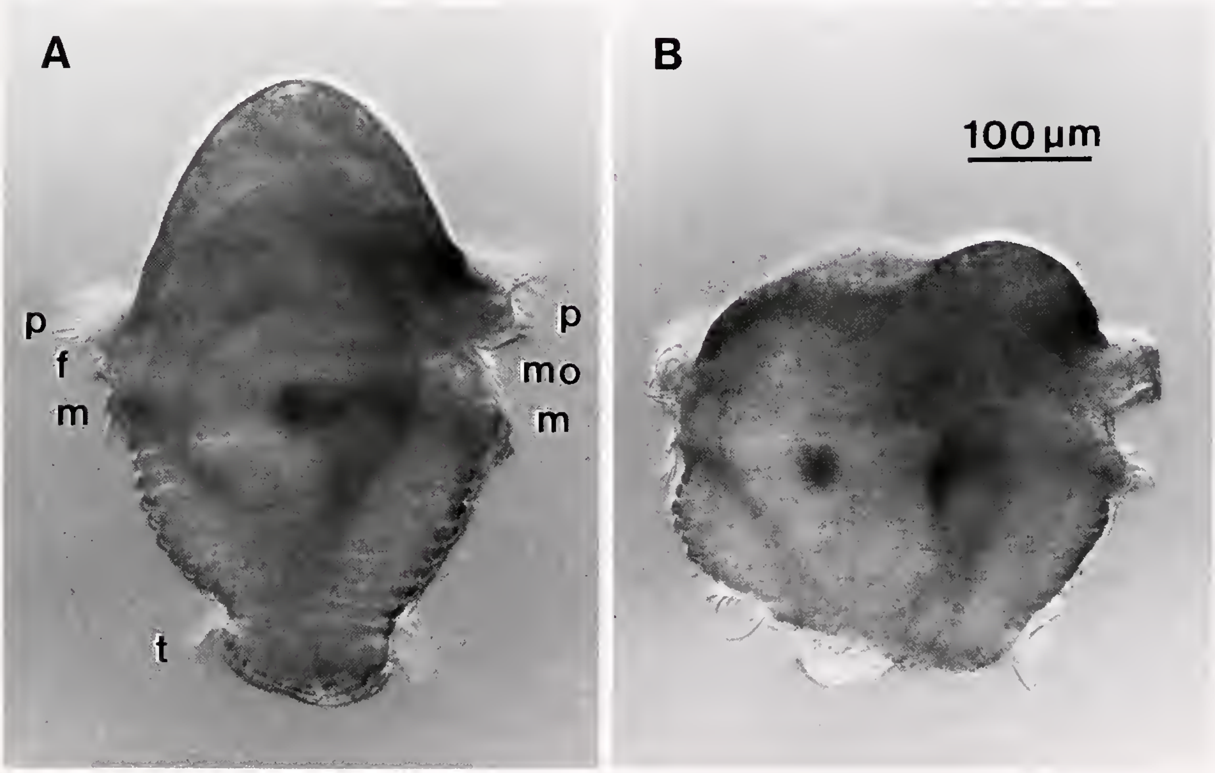

Figure 2. Light micrographs of larvae of *Urechis caupo*. (A) Lateral view with plane of focus through the prototroch (p), food groove (f), metatroch (m), and telotroch (t), dorsally. Ventrally, the plane of focus passes through the prototroch (p), mouth (mo), and metatroch (m). The neurotroch is not visible. The dark spot near the center is a particle in the gut. (B) The same larva when contracted. Both photos are to the same scale.

We then estimated maximum clearance rates for each size class by multiplying that value by the circumference of the prototroch halfway between the base of the cilium and its tip (midpoint prototroch circumference). Finally, to determine whether maximum clearance rate scaled proportionately to body size during larval growth, we divided the maximum clearance rate for a given size class by the average body volume for that size class.

Results

Ciliary bands

Scanning electron micrographs clearly show the prototrochal and metatrochal cilia of *Armandia brevis.* The prototroch is made up of several rows of compound cilia that completely encircle the larval body anterior to the mouth (Fig. 1). The metatroch is a postoral band of compound cilia that extends laterally from the lower lip of the mouth around the larval body to a dorsal position (Fig. 1A). The metatrochal cilia on the lower lip are longer than the other metatrochal cilia (Fig. 1A, B). The prototroch and metatroch define the boundaries of a cilia-lined food groove. The width of the food groove lateral to the mouth was estimated from a scanning electron micrograph to be 10 μm (SEM not shown). Dorsally, the food groove narrows. The mouth is large (about 50 μm wide in the 18-setiger larva shown in Fig. 1B) and both its upper and lower surfaces are heavily ciliated (Fig. 1A, B). A band of neurotrochal cilia runs along the ventral surface of the larva from just behind the mouth to the third setigerous segment (Fig. 1B).

Larvae of *Urechis caupo* also possess prototrochal and metatrochal ciliary bands (Fig. 2). The prototrochal cilia are longer than the metatrochal cilia. Again, these two ciliary bands define the boundaries of a food groove lined with simple cilia. Larvae also bear a midventral neurotroch, posterior to the mouth, and a telotroch.

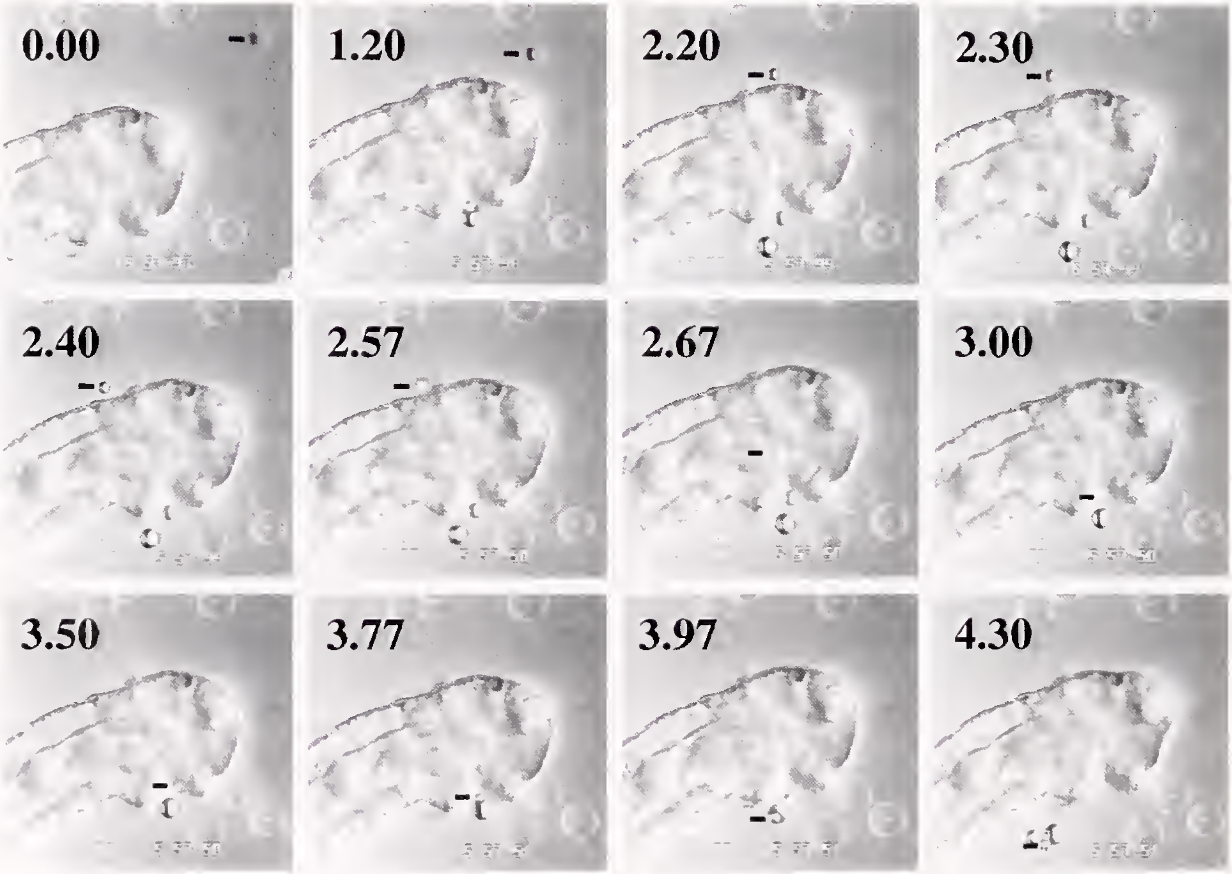

Figure 3. Videorecorded capture of a 5-μm sphere by opposed bands, and particle rejection by a self-tethered *Armandia brevis* larva. Time in seconds is in the upper left-hand corner. All images are at the same magnification. The larva is oriented with its dorsal side toward the top of the page. The sequence shows a particle, indicated by the black line, approach the dorsal part of the metatroch where it is captured and then transported along the food groove and deposited in the mouth. The particle is then rejected. During rejection the metatroch on the lower lip ceases to beat. At 0 s the larva is 120 μm in diameter at the base of the prototrochal cilia.

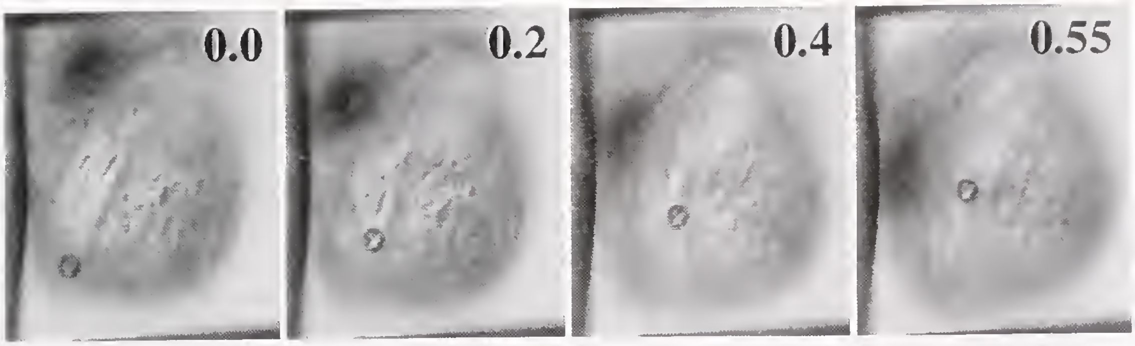

Figure 4. Videorecorded capture of a 13-μm sphere by a *Urechis caupo* larva. Time is in seconds in the upper right-hand corner. The particle has entered a dorsolateral part of the food groove at 0 s, moves along the food groove toward the mouth at 0.2 and 0.4 s, and enters the side of the mouth at 0.55 s. Rotation of the larva moves the mouth from upper right at 0 s to center at 0.55 s. The anterior end of the larva is toward the upper left. At 0 s the larva is 175-μm wide at the base of the prototrochal cilia.

Capture by opposed ciliary bands

In larvae of *Armandia brevis* and *Urechis caupo*, the movements of particles and the directions of recovery strokes of cilia indicated that the effective strokes of the prototrochal cilia were from anterior to posterior, and those of the metatrochal cilia were from posterior to anterior. For larvae of each species, we observed captures of more than 50 particles of 5 and 12 μm in diameter; particles that came within reach of the prototroch were transported into the food groove between the prototroch and metatroch and moved to the mouth *via* the food groove, presumably by the food-groove cilia (Figs. 3–5). Particles were captured between prototroch and metatroch on the lateral and dorsal surfaces of the larva. Particles in the food groove moved around to the mouth from both the left and the right sides and both with and against the direction of rotation of the larval body. These particle paths indicate an opposed-band feeding mechanism.

Capture of large particles

Larvae of both species also captured particles at the mouth, without transport in the food groove. A late-stage larva of *Armandia brevis* (with > 14 setigers) captured two large particles (50 μm in diameter) while videorecorded through a dissecting microscope (Fig. 6). When the swimming larva contacted a large particle in the vicinity of the mouth, the larva slowed and rotated so that the lower lip was aligned with the particle. The larva opened its mouth and ingested the particle, presumably using oral cilia or musculature.

Swimming *Urechis caupo* larvae used the mouth for direct capture of particles that passed over the episphere. Such captures occurred simultaneously with opposed-band particle captures (Fig. 5). Many of the particles caught directly by the mouth were too large to fit between opposed prototroch and metatroch, as illustrated by the gut contents in Figure 7 and the particles being rejected in Figure 8. In some cases the mouth gaped to admit a large particle. The 9-day-old larva in Figure 4 opened its mouth to a gape of about 35 μm with a width of 95 μm. The 17-day-old larva in Figure 8 opened its mouth to 70 to 95 μm, and the mouth's width when closed was about 125 μm. Cilia on the mouth's lower lip (anterior to the shorter cilia of the neurotroch) appeared to aid the movement of large particles into the mouth. These cilia seemed to be continuous with the metatrochal band, which would account for the posterior-

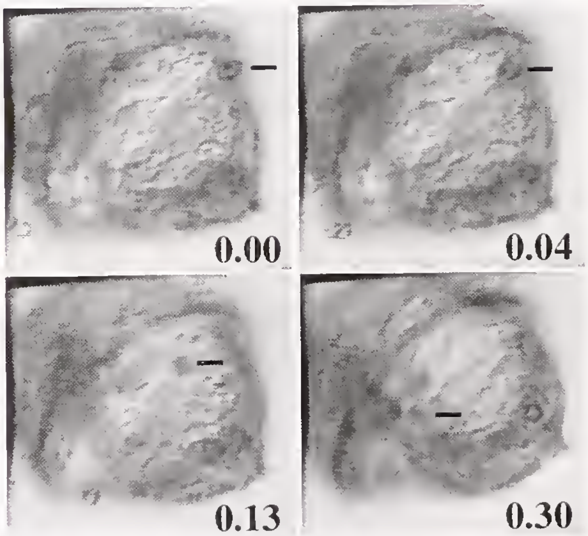

Figure 5. Videorecorded capture of two 12-μm spheres by a *Urechis caupo* larva. Time is in seconds in the lower right-hand corner. The particle marked by an adjacent black bar has entered a dorsolateral part of the food groove at 0 s, moves along the food groove toward the mouth at 0.04 and 0.13 s, and is near the side of the mouth at 0.30 s. The second particle passes over the prototroch directly into the mouth. It is near the prototrochal cilia at 0 s, passes over the anterior edge of the mouth at 0.04 and 0.13 s, and has entered the mouth at 0.30 s. The mouth is at the lower left; the anterior end toward the upper left. At 0 s the larva is 170-μm wide at the base of the prototrochal cilia.

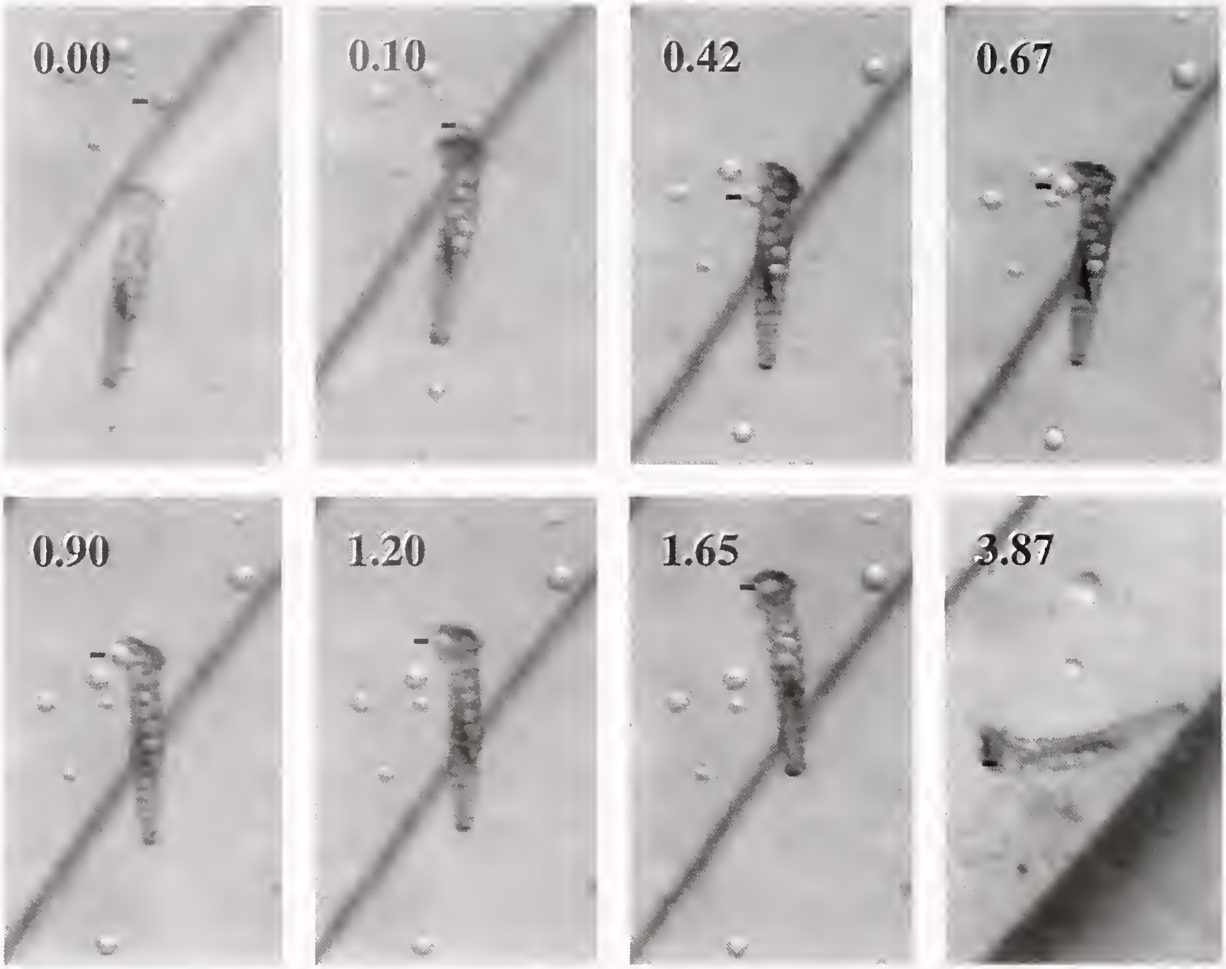

Figure 6. Videorecorded capture of a 50-μm sphere by a free swimming *Armandia brevis* larva under a dissecting microscope. Time in seconds is in the upper left-hand corner. All images are at the same magnification. A black line indicates the particle. The larva approaches the particle and then orients its mouth towards the particle, which is on the bottom of the dish. The particle is captured at the larva's mouth, presumably moved by the large oral compound cilia, and swallowed. At 0 s the larva is 85-μm wide at the center of the body.

to-anterior current past these cilia. In some cases a particle was brought into the mouth over the lower lip (Fig. 7).

Larvae of *U. caupo* captured large particles from an early stage. Small 4-day-old larvae ingested Sephadex spheres almost as large as those ingested by 16-day-old larvae (Table I). Even a 3-day-old larva ingested a 42-by-35-μm mineral grain. Larger larvae did capture larger spheres, however. When early and later stage larvae were fed the same suspension, as in the last two lines of Table I, the median sizes and the largest sizes of ingested spheres were significantly greater for larger, older larvae (Mann-Whitney *U* tests, $n_1 = 10$, $n_2 = 5$, $P < 0.05$). Objects larger than the spheres offered can be ingested. For example, a 49-day-old larva, 375 μm wide, ingested an unidentified object 366 μm long by 40 μm wide.

When larvae of *U. caupo* of different ages and sizes were offered smaller plastic spheres, all 10 of the small, 3-day-old larvae caught fewer spheres of 29-μm than of 12-μm, and all 4 of the larger, 48-day-old larvae ingested more of the 29-μm spheres than of the 12-μm spheres (Table II). Small, early-stage larvae did ingest 5- and 20-μm spheres in about the same ratio as ingested by larger larvae (Table II). Estimates of the width of the food groove of a single 5-day-old larva ranged from 22 to 34 μm, but the width of the food groove varies with contraction of the larva. The upper limit on the sizes of particles that could be transported in the food groove was not determined.

Rejection of particles

Larvae could actively reject particles. Particle rejection often occurred after a particle had been transported to the mouth and entered the esophagus. When a larva of *Armandia brevis* expelled a particle, the metatrochal cilia around

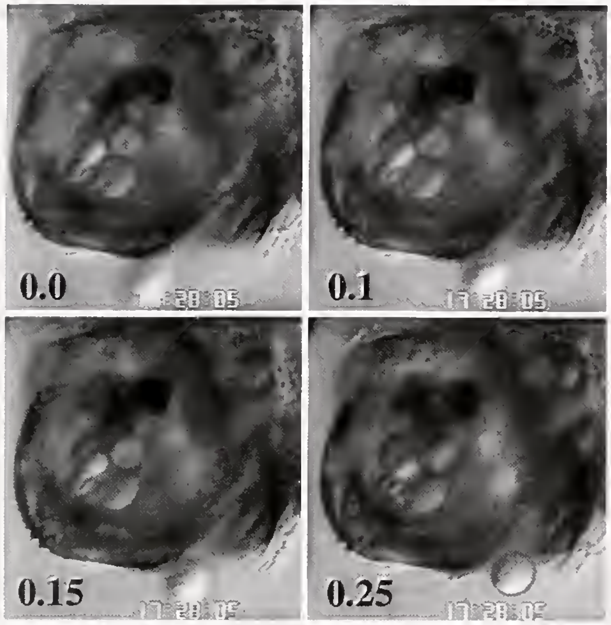

Figure 7. Videorecorded capture of a 40-μm sphere by a *Urechis caupo* larva. Time is in seconds in the lower left-hand corner. The sphere is near the metatrochal cilia at the posterior lip of the mouth at 0 s and moves over this band of cilia toward the mouth at 0.1 and 0.15 s. It is just entering the mouth at 0.25 s. The anterior end is toward the upper right. At 0 s the larva is 300-μm wide at the base of the prototrochal cilia.

the mouth stopped beating as the particle moved posteriorly down the body (Fig. 3). Metatrochal cilia at the mouth of larvae of *Urechis caupo* must also have altered beat during particle rejection, because large particles moved posteriorly over the lower lip and down the neurotroch during rejection (Fig. 8), in contrast to their posterior-to-anterior path over the lip during ingestion (Fig. 7).

Scaling of clearance rate and body volume

For larvae of *Armandia brevis*, prototroch circumference and prototrochal cilium length increased with number of setigerous segments (Fig. 9A, B). Larval volume increased exponentially with number of setigers (Fig. 9C).

Particle velocities increased slightly with number of setigers for larvae of *A. brevis* with 6–7, 11–12, and 15–16 setigers ($n = 9$) (Fig. 10). Increased particle velocities and cilium lengths resulted in a 30% increase in the area of water per prototrochal slice moved per second between larvae with 6–7 and 11–12 setigers and a 22% increase between larvae with 11–12 and 15–16 setigers (Table III). Maximum particle velocities were within the distal third of the cilium length (estimated for each size class from Fig. 9B), consistent with our expectations (Emlet and Strathmann, 1994). Although Strathmann *et al.* (1993) suggested that cilium lengths might be underestimated from videorecordings, our results indicate that this was not the case. In addition, our measurements agree with the cilium length of approximately 35 μm reported by Hermans (1964) for a larva with an unspecified number of setigers.

Although estimated maximum clearance rates increased with number of setigers, they did not increase proportionately to body volume (Table III). Late-stage larvae (15–16 setigers) had a maximum ratio of clearance to body volume that was less than half of that achieved earlier in development (6–7 setigers; Table III).

Prototrochal circumference and cilium length both increased with larval growth to a greater extent for larvae of *U. caupo* than for larvae of *A. brevis*, over the stages measured (Tables I–III). The relative increase in body length was much less for *U. caupo*. Early-stage larvae were nearly spherical and elongated to the shape shown in Figure 2A at later stages. Data for particle velocities are lacking for

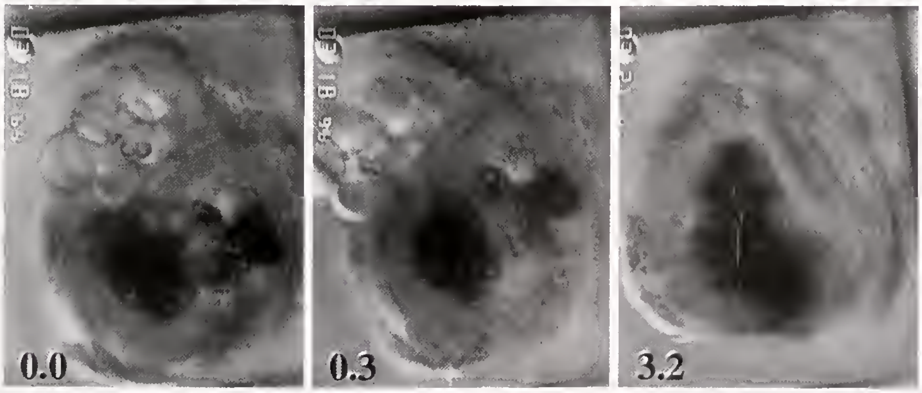

Figure 8. Videorecorded rejection of previously ingested spheres up to 50 μm in diameter by a *Urechis caupo* larva. Time is in seconds in the lower left-hand corner. At 0 and 0.3 s the mouth gapes at least 100-μm wide, and the clump of spheres moves over the posterior lip of the mouth and down the midventral neurotroch. The larva in the last frame is 295-μm wide at the base of the prototrochal cilia, and the mouth, now rotated toward the viewer, is closed and approximately 120-μm wide.

Table I

Sizes of Sephadex spheres ingested by larvae of Urechis caupo *differing in size and age*

Age (days)	Prototrochal diameter (μm)*	Cilium length (μm)	Particle diameter (μm)†		Number of larvae
			In suspension	Ingested	
4	159	45	45, 26–73 (50)	36, 19–53 (51)	12
5	165	44	44, 30–74 (50)	36, 19–60 (34)	10
16	318	65	44, 30–74 (50)	38, 21–73 (104)	5

* Diameter of the prototrochal band is diameter at the base of the prototrochal cilia.

† Values are median, range, and (in parentheses) number of particles.

U. caupo, but the increase in prototrochal area (cilium length times prototrochal circumference) relative to body volume was greater for this species than for *A. brevis.*

Discussion

Our observations add the Opheliidae and Echiuridae to those annelid families known to possess larvae with opposed-band feeding. As in other opposed-band feeders, larvae of both *Armandia brevis* and *Urechis caupo* possess a ciliated food groove between two parallel ciliary bands, a postoral metatroch and a prototroch. Direct observations confirm that particles are captured in the food groove (Figs. 3–5), probably through the combined action of long compound cilia in the prototroch (which beat anterior to posterior) and shorter compound cilia in the metatroch (which beat posterior to anterior). Simple cilia of the food groove may aid in retention of particles as well as in transport. This system is very effective in capturing relatively small particles (5–12 μm), regardless of which part of the prototrochal circumference is contacted (ventral, lateral, or dorsal). How common this feeding method is in larvae of other opheliids or echiurids is not known, but larvae of at least one other echiurid bear opposed bands of cilia (Salensky, 1876; Hatschek, 1880).

Larvae of both *A. brevis* and *U. caupo* also ingested particles larger than the space between prototrochal and metatrochal bands. For *A. brevis,* it was later stage (14–17 setiger) larvae that ingested large (50-μm) particles. These larvae approached large particles so that contact was directly at the mouth. This behavior was not observed in larvae at earlier stages. In contrast, larvae of *U. caupo* ingested particles greater than 50 μm at early stages. Larvae of *U. caupo* did not appear to change orientation as they approached large particles; however, their movements were constrained by mesh cages. Particles that were captured directly at the mouth entered either over the episphere and prototroch or over the extension of the metatroch on the lower lip. In both species the mouths were large, could be opened to a wide gape, and were heavily ciliated. The cilia bordering the lower lip of the mouth appear to be a continuation of the metatroch. The oral cilia of *A. brevis* may include additional compound cilia (Fig. 1). For both A. brevis and *U. caupo,* the large ciliated oral field and the large mouth aid in the capture of large particles.

The combination of two ciliary feeding mechanisms in individual larvae suggests hypotheses for evolutionary transitions among the feeding larvae of annelids. Some larvae, such as those of serpulids, appear to be restricted to capturing small particles between opposed bands; other larvae, like those of polynoids, lack opposed bands and appear to capture mostly large particles one by one, using complex oral ciliature (Phillips and Pernet, 1996). Our results dem-

Table II

Sizes of plastic spheres ingested by larvae of Urechis caupo *differing in size and age*

Age (days)	Prototrochal diameter (μm)*	Cilium length (μm)	Particle diameter		Number of larvae
			Ratio in suspension (29:12 μm)	Ratio ingested (29:12 μm)	
3	151	46	1.43:1	39/146 = 0.27	10
48	347	76	1.43:1	206/112 = 1.84	4
			(20:5 μm)	(20:5 μm)	
4	161	45	1:1	146/30 = 4.9	8
15	310	67	1:1	99/37 = 2.7	8

* Diameter of the prototrochal band is diameter at the base of the prototrochal cilia.

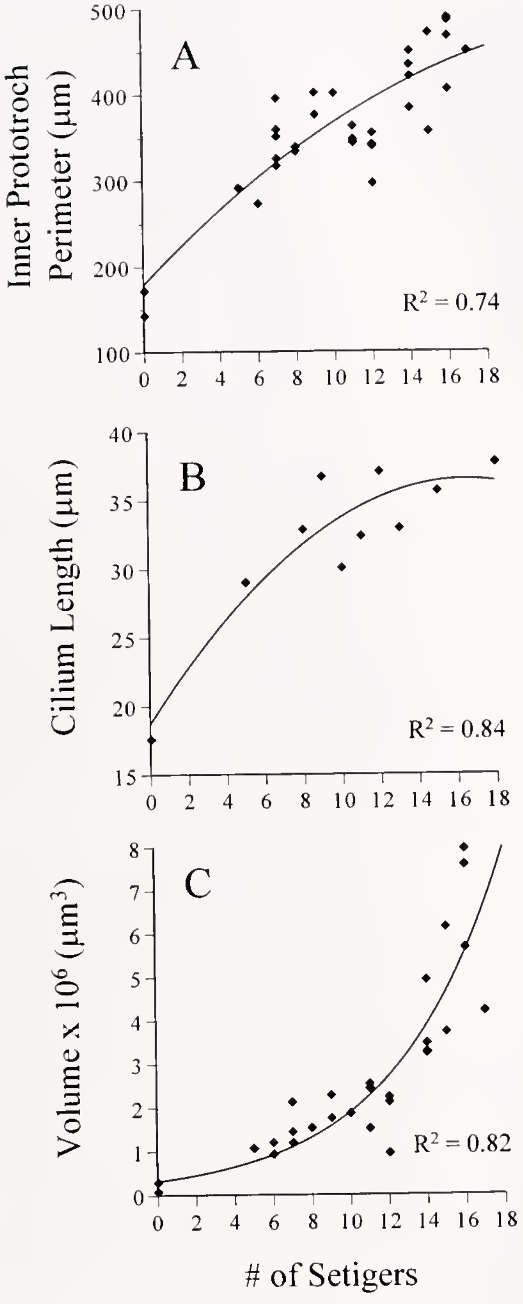

Figure 9. Binomial regression of various larval parameters *vs.* number of setigers for *Armandia brevis*. For all equations, X = number of setigers. The R^2 value is reported in the lower right-hand corner of each plot. (A) Inner prototroch perimeter (n = 36 larvae); larval circumference = $178.36 + 23.24x - 0.44x^2$. (B) Cilium length ($n$ = 22 larvae); cilium length = $18.67 + 2.16x - 0.07x^2$. (C) Larval volume (n = 36 larvae); larval volume = $10^{5.48 + 0.08x}$.

onstrate that in at least two families of annelids, both types of mechanisms can be employed simultaneously by the same larva. In addition, it appears that the oral ciliature of *A. brevis* and *U. caupo,* which is responsible for the capture of large particles, is continuous with the lateral and dorsal extensions of the metatroch and food groove. As an evolutionary transition, expansion of oral ciliation might result in a food groove and metatroch paralleling the whole length of the prototroch to produce an opposed-band system. Alternatively, enlargement of the mouth and elaboration of oral ciliation (with loss of the lateral and dorsal parts of the opposed-band system) could produce the variety of oral

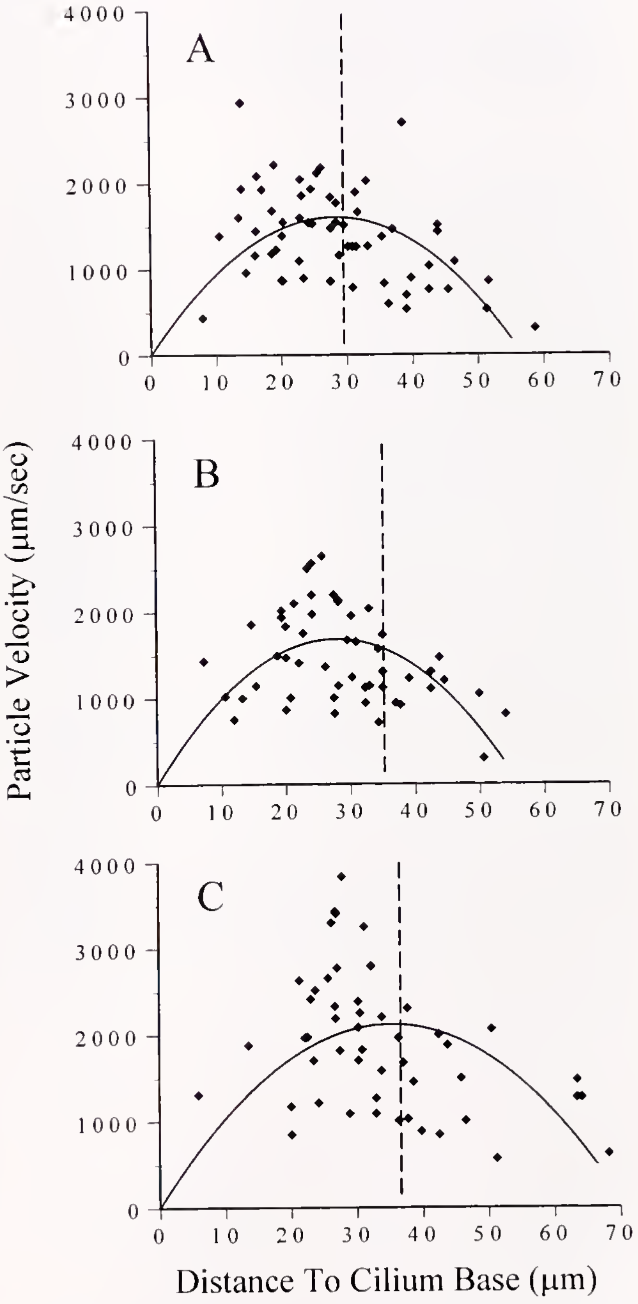

Figure 10. Particle velocity *vs.* distance of particle from the base of the prototroch for *Armandia brevis* larvae with (A) 6–7, (B) 11–12, and (C) 15–16 setigers. The vertical dotted line shows the estimated cilium length taken from the binomial regression of Figure 9B.

Table III

Estimated clearance rate and clearance rate per larval volume for three size classes of larvae of Armandia brevis

# of Setigers	Cilium length (μm)*	Water area per prototroch slice per unit time† (μm^2/s)	Midpoint prototrochal circumference (μm)	Max. clearance rate (μm^3/s)$\times 10^6$	Larval volume (μm^3)‡	Clearance rate/volume (1/s)
6–7	29.9	32846	422	13.9	998309	13.9
11–12	34.8	42602	549	23.4	2526475	9.3
15–16	36.4	51949	642	33.4	5310250	6.3

* Calculated from the binomial regression in Fig. 10B.

† Calculated from the areas under the curves in Fig. 11, bound by the origin and the estimated cilium length for that size class.

‡ Estimated from the binomial regression in Fig. 10C.

ciliature found in the diverse feeding larvae of annelids. Continued modification of such cilia might result in such unusual and functionally important structures as the group of long compound cilia on the left side of the mouth of polynoid larvae.

Estimated maximum clearance rates did not scale isometrically with body volume among the three size classes of *A. brevis.* Cilium length, prototroch circumference, and particle velocities through a prototrochal slice all increased as body volume increased, but not enough for maximum clearance rate to increase in proportion to body volume—thus the volume of water swept by cilia decreases relative to body volume as the larva adds segments. An analogous situation has been described for the cyphonautes larva of bryozoans, in which ciliated band length does not increase proportionately to body volume during growth and development (McEdward and Strathmann, 1987). This allometry is potentially unfavorable to larger larvae. In asteroid, echinoid, and bivalve larvae similar in size to *A. brevis* larvae, metabolic rates scale isometrically with body mass (Hoegh-Guldberg and Manahan, 1995). Further, in the larvae of an echinoid, metabolic demand scales isometrically with larval volume (McEdward, 1984). If these results can be generalized to larvae of *A. brevis,* and if we make the reasonable assumption that the masses of these larvae are proportional to their volume, then the maximum clearance rates of *A. brevis* larvae decline relative to metabolic demand as the larvae increase in size. However, larger larvae of *A. brevis* (>12 setigers) can supplement the amount of small particles captured by opposed-band feeding by capturing larger particles at the mouth. The increased size range of food may compensate, at least partly, for the decrease in clearance rate. This decrease in maximum clearance rate per larval volume may have selected for larvae that possess two types of feeding mechanisms.

Do other annelid larvae share this potentially unfavorable allometry of maximum clearance rate and body volume? Some annelid larvae resemble *A. brevis* in extreme elongation of a segmented body during the larval stage (Bhaud and Cazaux, 1987). Some of these larvae (*e.g.,* spionids) possess feeding mechanisms other than the opposed prototrochal and metatrochal bands. Thus, evolutionary changes in the size range of particles captured may have been favored in several groups of annelids as a result of a small head circumference and long larval body. Other possible solutions to this problem are opposed bands elongated on ciliated lobes, as reported for the rostraria larva of an annelid (Jägersten, 1972), or the sinuous opposed bands of mitraria larvae of oweniid annelids (Emlet and Strathmann, 1994).

The larvae of *U. caupo* and some other annelids probably do not face such an unfavorable allometry of maximum clearance rate to body volume, however. The larvae of *U. caupo* develop from nearly spherical trochophores (at 3 to 5 days) to forms with more elongate bodies (at several weeks), but the elongation is not as extreme (*cf.* Fig. 2 to Fig. 6). Also, these larvae capture relatively large particles from an early stage. Nevertheless, the circumferential ciliary bands are shorter, relative to body size, than similar bands that are extended on the velar lobes of many gastropod larvae (Richter and Thorson, 1975). Feeding on an extended size range of particles and extension of opposed, ciliary bands on lobes may be alternative ways of increasing ingestion rates.

Further analyses of larval feeding methods, as well as robust phylogenies, are required to understand the evolution and functional consequences of diverse larval feeding mechanisms in the Annelida. For example, why are opposed bands apparently used only in the capture of small particles? What functional constraints place an upper limit on the spacing of the prototroch and metatroch in opposed-band feeders? Such analyses may also reveal why some larvae (*e.g.,* serpulids) use restricted opposed bands to feed on small particles, and others (*e.g.,* polynoids) use complex oral ciliature to feed primarily on large particles instead of employing both methods, as do the opheliid and echiurid larvae described here.

Acknowledgments

NSF grant OCE9633193, the Robert Fernald Fellowship endowment, and the Friday Harbor Laboratories of the University of Washington supported the research on *Armandia brevis*. NSF grant OCE9301665 and the Bodega Marine Laboratory of the University of California at Davis supported the research on *Urechis caupo*. K. Uhlinger advised on collection of adults and culture of larvae of *U. caupo*. W. Borgeson provided algal medium and *Isochrysis galbana*. N. E. Phillips and C. Staude advised on analysis of videotapes of *U. caupo*. We thank J. Marcus for help in printing photographs, and J. Hoffman and two anonymous reviewers for useful comments on the manuscript.

Literature Cited

Bhaud, M., and C. Cazaux. 1987. Description and identification of polychaete larvae; their implications in current biological problems. *Oceanis* **13:** 595–753.

Emlet, R. B. 1990. Flow fields around ciliated larvae: the effects of natural and artificial tethers. *Mar. Ecol. Prog. Ser.* **63:** 211–225.

Emlet, R. B., and R. R. Strathmann. 1994. Functional consequences of simple cilia in the mitraria of oweniids (an anomalous larva of an anomalous polychaete) and comparisons with other larvae. Pp. 143–157 in *Reproduction and Development of Marine Invertebrates*, W. H. Wilson, Jr., S. A. Stricker, and G. L. Shinn, eds. Johns Hopkins University Press, Baltimore.

Gould, M. 1967. Echiurid worms: *Urechis*. Pp. 163–171 in *Methods in Developmental Biology*, F. H. Wilt and N. Wessels, eds. Crowell, New York.

Hatschek, B. 1880. Über die Entwicklungsgeschichte von *Echiurus* und die systematische Stellung der Echiuridae. *Arbeiten Zool. Inst. Wien* **3:** 45–78, plates 1–6.

Hermans, C. O. 1964. *The Reproductive and Developmental Biology of the Opheliid Polychaete*, Armandia brevis. M. S. Thesis, University of Washington. 131 pp.

Hermans, C. O. 1978. Metamorphosis in the opheliid polychaete *Armandia brevis*. Pp. 113–126 in *Settlement and Metamorphosis of Marine Invertebrate Larvae*, F.-S. Chia and M. E. R. Rice, eds. Elsevier, New York.

Hoegh-Guldberg, O., and D. T. Manahan. 1995. Coulometric measurement of oxygen consumption during development of marine invertebrate embryos and larvae. *J. Exp. Biol.* **198:** 19–30.

Jägersten, G. 1972. *Evolution of the Metazoan Life Cycle*. Academic Press, New York. 282 pp.

McEdward, L. R. 1984. Morphometric and metabolic analyses of the growth and form of an echinopluteus. *J. Exp. Mar. Biol. Ecol.* **82:** 259–287.

McEdward, L. R., and R. R. Strathmann. 1987. The body plan of the cyphonautes larva of bryozoans prevents high clearance rates: comparisons with the pluteus and a growth model. *Biol. Bull.* **172:** 30–45.

McHugh, D. 1997. Molecular evidence that echiurans and pogonophorans are derived annelids. *Proc. Natl. Acad. Sci. USA* **94:** 8006–8009.

McHugh, D., and G. W. Rouse. 1998. Life history evolution of marine invertebrates: new views from phylogenetic systematics. *Trends Ecol. Evol.* **13:** 182–186.

Newby, W. W. 1940. *The Embryology of the Echiuroid Worm* Urechis caupo. American Philosophical Society, Philadelphia. 219 pp.

Nielsen, C. 1995. *Animal Evolution*. Oxford University Press, Oxford. 467 pp.

Nielsen, C. 1998. Origin and evolution of animal life cycles. *Biol. Rev.* **73:** 125–155.

Phillips, N. E., and B. Pernet. 1996. Capture of large particles by suspension-feeding scaleworm larvae (Polychaeta: Polynoidae). *Biol. Bull.* **191:** 199–208.

Richter, G., and G. Thorson. 1975. Pelagische Prosobranchier-Larven des Golfes von Neapel. *Ophelia* **13:** 109–185.

Rouse, G. W., and K. Fauchald. 1997. Cladistics and polychaetes. *Zool. Scr.* **26:** 139–204.

Salensky, W. 1876. Über die Metamorphose des *Echiurus*. *Morphologisches Jahrbuch* **2:** 319–327.

Sleigh, M. A. 1984. The integrated activity of cilia: function and coordination. *J. Protozool.* **31:** 16–21.

Strathmann, R. R. 1987. Larval feeding. Pp. 465–550 in *Reproduction of Marine Invertebrates, Vol. 9. General Aspects: Seeking Unity in Diversity*, A. C. Giese, J. S. Pearse, and V. B. Pearse, eds. Blackwell, Palo Alto, CA.

Strathmann, R. R. 1993. Hypotheses on the origins of marine larvae. *Annu. Rev. Ecol. Syst.* **24:** 89–117.

Strathmann, R. R., and D. J. Eernisse. 1994. What molecular phylogenies tell us about the evolution of larval forms. *Am. Zool.* **34:** 502–512.

Strathmann, R. R., and E. Leise. 1979. On feeding mechanisms and clearance rates of molluscan veligers. *Biol. Bull.* **157:** 524–535.

Strathmann, R. R., T. L. Jahn, and J. R. C. Fonseca. 1972. Suspension feeding by marine invertebrate larvae: clearance of particles by ciliated bands of a rotifer, pluteus, and trochophore. *Biol. Bull.* **142:** 505–519.

Strathmann, R. R., L. Fenaux, A. T. Sewell, and M. F. Strathmann. 1993. Abundance of food affects relative size of larval and postlarval structures of a molluscan veliger. *Biol. Bull.* **185:** 232–239.

Suer, A. L. 1982. *Larval Settlement, Growth, and Reproduction of the Marine Echiuran* Urechis caupo. Ph.D. Thesis, University of California, Davis. 198 pp.

Reference: *Biol. Bull.* **197:** 26–39. (August 1999)

Bioluminescence in the Deep-Sea Cirrate Octopod *Stauroteuthis syrtensis* Verrill (Mollusca: Cephalopoda)

SÖNKE JOHNSEN[1], ELIZABETH J. BALSER[2], ERIN C. FISHER[1], AND EDITH A. WIDDER[1]

[1] *Marine Science Division, Harbor Branch Oceanographic Institution, Ft. Pierce, Florida; and*
[2] *Department of Biology, Illinois Wesleyan University, Bloomington, Illinois*

Abstract. The emission of blue-green bioluminescence (λ_{max} = 470 nm) was observed from sucker-like structures arranged along the length of the arms of the cirrate octopod *Stauroteuthis syrtensis.* Individual photophores either glowed dimly and continuously or flashed on and off more brightly with a period of 1–2 seconds. Examination of the anatomy and ultrastructure of the photophores confirmed that they are modified suckers. During handling, the photophores were unable to attach to surfaces, suggesting that, unlike typical octopod suckers, they have no adhesive function. The oral position of the photophores and the wavelength of peak emission, coupled with the animals' primary postures, suggests that bioluminescence in *S. syrtensis* may function as a light lure to attract prey.

Introduction

Bioluminescence is a common and complex characteristic in coleoid cephalopods. A large percentage of these animals are bioluminescent, many possessing complicated light organs utilizing lenses, reflectors, irises, interference filters, pigment screens, and shutters (Harvey, 1952; Herring, 1988). The diversity of the morphologies and anatomical distributions of cephalopod photophores is unparalleled among invertebrate phyla (Voss, 1967; Herring, 1988). However, despite this extraordinary radiation, bioluminescence appears to be rare among octopods. Although 63 of the 100 genera of squid and cuttlefish have bioluminescent species, only 2 of the 43 genera of octopods have species confirmed to be bioluminescent—the bolitaenids *Japetella* and *Eledonella* (Robison and Young, 1981; Herring *et al.*, 1987; Herring, 1988). In these genera, the light organs are found only in breeding females (Robison and Young, 1981) and are restricted to tissues associated with the oral ring and the base of the arms (Herring *et al.*, 1987). In the case of cirrate octopods, bioluminescence has been suggested but never confirmed (Aldred *et al.*, 1982, 1984; Vecchione, 1987).

This study provides the first description of bioluminescence in the cirrate octopod *Stauroteuthis syrtensis.* We also describe the anatomy and ultrastructure of the photophores in comparison with the morphology reported for cephalopod photophores (Herring *et al.*, 1987) and octopod suckers (Kier and Smith, 1990; Budelmann *et al.*, 1997). In addition, we present a hypothesis to explain how the presence of light organs relates to the feeding behavior postulated for these animals. A preliminary account of this research has been presented by Johnsen *et al.* (1999).

Materials and Methods

Source and maintenance of animals

Three specimens of *Stauroteuthis syrtensis* were obtained during a cruise of the R.V. *Edwin Link* to Oceanographer Canyon (on the southern rim of Georges Bank, USA) in August and September 1997. The animals were collected at depth using the research submersible *Johnson-Sea-Link* outfitted with acrylic collection cylinders (11-liter volume) with hydraulically activated, sliding lids. The three specimens were caught during daylight at depths of 755 m (225 m from bottom), 734 m (246 m from bottom), and 919 m (165 m from bottom) (dive numbers 2925 and 2927) and maintained for up to 2 days at 8°C in water collected at depth.

Received 16 March 1999; accepted 27 May 1999.

Address for correspondence: Dr. Sönke Johnsen, MS #33, Woods Hole Oceanographic Institution, Woods Hole, MA 02543-1049. E-mail: sjohnsen@whoi.edu

Video and photography

Specimens were videotaped in two situations. First, the behavior of two animals was recorded from the submersible. Second, the captured animals were filmed aboard ship in the dark by using an intensified video camera (Intevac's Nite-Mate 1305/1306 CCTV intensifier coupled to a Panasonic Charge Coupled Device). During shipboard filming, the animals were gently prodded to induce bioluminescence. Representative video frames were digitized (ITSCE capture board, Eyeview Software, Coreco Inc.). The animals were also placed in a plankton kreisel (Hamner, 1990) and photographed with a Nikon SLR camera with Kodak Elite 100 color film. Data from a previously recorded *in situ* video of a specimen of *S. syrtensis* from the slope waters near Cape Hatteras at 840 m (35 m from bottom; August 1996; R.V. *Edwin Link;* dive 2777) are also reported in this paper.

Spectrophotometry

Bioluminescent spectra were measured using an intensified optical multichannel analyzer (OMA-detector model 1420, detector interface model 1461, EG&G Princeton Applied Research) coupled to a 2-mm-diameter fiber optic cable. The detector was wavelength calibrated using a low-pressure mercury spectrum lamp (Model 6047, Oriel Inc.) and intensity calibrated using a NIST referenced low-intensity source (Model 310, Optronics Laboratories) intended for the calibration of detectors from 350 nm to 800 nm. For further details on the theory of operation and calibration of the OMA detector, see Widder *et al.* (1983). Three emission spectra were recorded from one animal, and an average spectrum was calculated.

Microscopy of photophores

The fixation, dehydration, and infiltration procedures were performed at room temperature aboard the R. V. *Edwin Link.* The animals were sacrificed by over-anesthesia with MS222 (Sigma Chemicals Inc.). One specimen was fixed in 10% formalin in seawater and dissected to confirm species identification. One arm of a different specimen was fixed in 2.5% glutaraldehyde in 0.2 *M* Millonig's buffer at pH 7.4, adjusted to an osmolarity of 1000 mOs with NaCl. After an initial 1-h fixation, several photophores were dissected from the arm and placed in fresh fixative for an additional 5.5 h. Postfixation of the dissected photophores in 1% osmium tetroxide in Millonig's buffer for 70 min was followed by dehydration through a graded series of ethyl alcohols. Over a period of 6 days, the specimens were slowly infiltrated with propylene oxide and Polybed 812 (Polysciences) and then embedded in Polybed 812.

Semithin (1 μm) and thin sections of embedded material were cut with a diamond knife (Diatome) and a Sorvall MT2 rotary ultramicrotome. Semithin sections were stained with 2% toluidine blue in 1% sodium borate and photographed with a Zeiss Photomicroscope II using Kodak Tmax 100 black-and-white film. Intact arms fixed in 10% formalin in seawater were photographed with a Tessovar photographic system. Thin sections for ultrastructural evaluation were stained with aqueous 3% uranyl acetate and 0.3% lead citrate. Stained sections were viewed and photographed with a Zeiss EM 9 transmission electron microscope.

For scanning electron microscopy, an arm with suckers was fixed in 2.5% gluteraldehyde (as described above), dehydrated with ethyl alcohol, infiltrated with hexamethyldisalizane (Pellco), and air-dried. Micrographs were obtained with a JEOL JSM 5800LV scanning electron microscope using Kodak Polapan 400 film.

Results

General description of animal and distribution of photophores

Figures 1A and 1B show the largest of the three captured specimens of *S. syrtensis.* The appearance of the specimen is typical for the species (Vecchione and Young, 1997). The mantle length is about 9 cm (mantle lengths of other two specimens ~ 6 cm), suggesting that all three animals were immature (Collins, unpubl. data). The measurements are highly approximate because the mantle in the living animal is easily deformed. The primary webbing extends for about three-quarters of the length of the arms. The arms are oral to the primary web and attached to it by a secondary web. The photophores are arranged in a single row along the oral surface of each arm, situated between successive pairs of cirri (Fig. 1B). Each arm supports about 40 photophores. The distance between photophores decreases from the base to the tip of the arm, with the greatest distance being 4 mm and the smallest less than 0.1 mm. The diameter and the degree of development of the photophores located at the tip are less than those located at the base of the arm. The fresh tissue of the entire animal had a gelatinous consistency typical of many deep-sea cephalopods (Voss, 1967). Although orange-red under the photo-floodlights, the color of the animal was closer to reddish-brown in daylight.

Bioluminescence

When mechanically stimulated, *S. syrtensis* emitted moderately bright, blue-green light (λ_{max} = 470 nm) from the sucker-like photophores along the length of each arm (Fig. 2). With continuous stimulation, these photophores produced light for up to 5 min, though the intensity of bioluminescence decreased over time. Individual photophores either glowed dimly and continuously or blinked on and off brightly at 0.5 to 1 Hz. The blinking photophores cycled asynchronously, producing a twinkling effect. All suckers

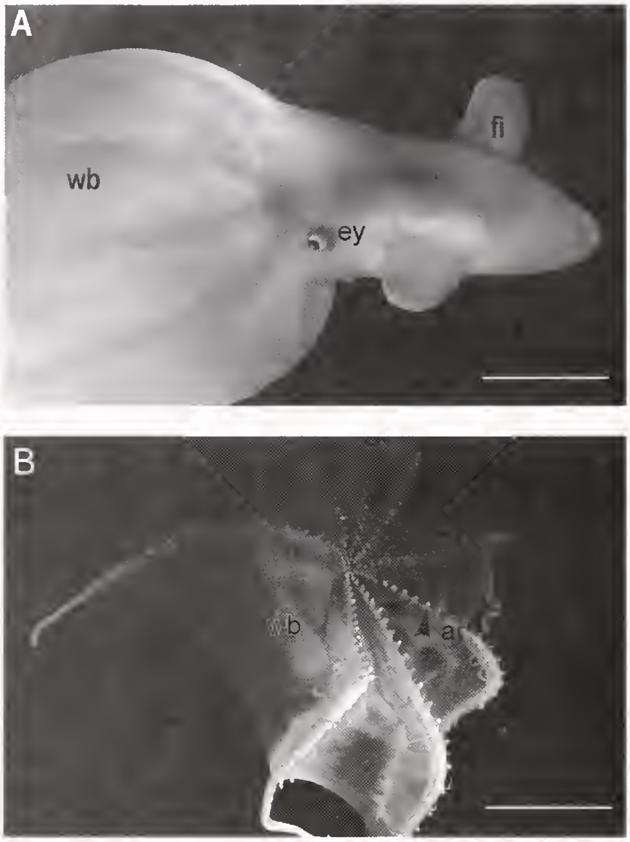

Figure 1. Photographs under artificial light of the deep-sea finned octopod *Stauroteuthis syrtensis* with the webbed arms in swimming posture (A) and spread (B) displaying the photophores/suckers (arrowheads) that appear as white spheres along the length of the inner surface of the arms. The posture shown in (B) may be one of extreme withdrawal intended to startle intruders with the sudden appearance of bioluminescent suckers. ar, arm; ey, eye; fi, fin; wb, webbing between arms. Scale bars = 4 cm.

(except possibly the very small ones at the tips of the arms) appeared capable of luminescence. No other portion of the body was observed to emit light.

Morphology of photophores

Each photophore is a raised papilla-like structure partially embedded in the connective tissue of the arm. The photophores are composed of three layers of cells: an outer epithelium modified to form a collar, infundibulum, and acetabulum; a capsule-like mass of muscle and neural tissue beneath the epithelium; and a thin layer separating the capsule from the dermis of the arm (Figs. 3, 4, 5). The collar epithelium is continuous with the epidermis and is folded inward, forming a rim around the central portion of the photophore (Figs. 3B, C; 4A). In both formalin- and glutaraldehyde-preserved specimens, the photophores appear to be either everted above (Fig. 3B) or retracted below (Fig. 3C) the outer edge of the collar.

Outer epithelium

The outer and inner folds of the collar epithelium are morphologically distinct and are different from the epidermis covering the arm (Figs. 5, 6). The epidermis of the arm is squamous to cuboidal in character and consists of epithelial cells possessing scattered apical microvilli (Fig. 6A). The outer edge of the collar is composed of columnar cells with apical microvilli, numerous electron-lucent and electron-dense vesicles, and large, apically placed, elongated nuclei (Fig. 6B). Like the epidermis, this region of the collar is not covered by a cuticle.

The inner edge of the collar is similar in cellular morphology to the outer collar epithelium except that the microvilli are more densely arranged and are covered by a cuticle (Figs. 6C, D). In this region, the cuticle is composed of at least three layers: an outer lamina 0.3 μm thick with irregular projections; a second electron-dense lamina, also 0.3 μm thick; and an inner layer approximately 1 μm thick consisting of amorphous material.

The epithelium and the overlying cuticle of the inner edge of the collar continue as the epithelium of a flat recessed region of the photophore corresponding to the infundibulum of typical octopod suckers (Figs. 3B; 4A; 5A, B). The outer edge of the infundibulum is ringed by hook-shaped denticles (Fig. 4B–D), which are elaborations of the cuticle (Fig. 6C, D). In addition to the presence of denticles, the cuticle covering the infundibular epithelium differs from that described for the inner part of the collar in that the outer layer contains more irregular projections and the innermost lamina is greatly expanded. The cuticle in this region is apparently secreted by the infundibulum and, as supported by Figure 6C and D, is periodically molted and replaced by a new, pre-formed cuticle. Subcuticular spaces were observed in association with what appear to be newly forming denticles.

Three cell types—gland cells, columnar epithelial cells, and multiciliated cells—were observed in the infundibular epithelium. Gland cells with narrow apical necks and a reduced number of apical microvilli are situated between columnar epithelial cells, which are characterized by a brush border of branched microvilli, rounded apical nuclei, apical endocytic vesicles, and mitochondria (Fig. 7A). Both columnar cells and gland cells have a fine granular cytoplasm replete with Golgi bodies and electron-dense and electron–lucent vesicles of varying sizes (Fig. 7B, C). Electron-dense granules, not bounded by a membrane, were observed between microvilli. These presumably originate from the infundibular cells and are incorporated into the cuticle (Fig. 7C). Multiciliated columnar cells were infrequently observed as part of the infundibulum. Cilia were not found in epidermal or collar cells. The cilia of the infundibular cells have two nearly parallel striated rootlets and appear to have reduced axonemes that do not project above the level of the

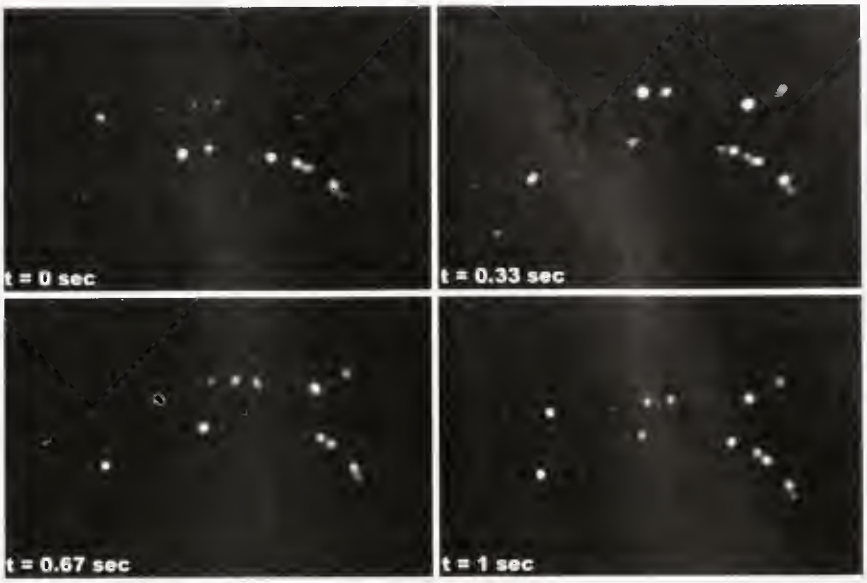

Figure 2. Digitized frames from a video sequence of light emission (white spots) from photophores/suckers taken from video of an animal filmed in the dark using an intensified video camera (Intevac's NiteMate 1305/1306 CCTV Intensifier coupled to a Panasonic CCD). Two arms are shown. For scale, their closest approach is approximately 1 cm.

microvilli (Fig. 7C). All three cell types are interconnected by apical adherens and subapical septate junctions (Fig. 7D).

At the center of the light organ, the infundibular epithelium invaginates to form the acetabulum, which is seen externally as an opening, or pore (Figs. 3B, 4A). This central opening continues internally as a blind canal (Fig. 5C). The acetabular cells differ from those of the infundibulum primarily in the basal position of the nuclei, the highly interdigitated lateral membranes, and the diminution of the outer two layers of the cuticle (Figs. 5C; 8A, B).

The infundibulum and the acetabulum rest on a basal lamina beneath which is located an expanded layer of connective tissue with a maximum thickness of 1.5 μm (Figs. 5C; 8C, D). Fibers, presumably collagen, although confirmation of this is not provided by the data, are arranged in alternating directions in multiple layers, giving the tissue a herringbone appearance. Occasional breaks, traversed by nerve axons, were observed in this otherwise continuous connective tissue sheath.

Muscle and neural tissue

Beneath the connective tissue underlying the epithelium of the infundibulum and acetabulum is a mass of tissue consisting of muscle and neural cells; this surrounds and encapsulates the outer epithelium (Figs. 5; 8A, E; 9). The myofilaments, which include thick filaments (25 and 50 nm in diameter) and thin filaments consistent with the size of myosin and actin, are oriented in three planes—circular, radial, and longitudinal with respect to the axis of the photophore. Although all sections were taken in the longitudinal plane of the photophore, the precise plane of each section for these transmission electron micrographs was not known. Thus, the differentiation of the fibers seen in Figure 8C (shown in cross-section) and Figure 9A (horizontal fibers shown in longitudinal section) as circular or radial cannot be determined.

Intermingled with the muscle cells are nerve cells characterized by electron-dense granules 0.1 μm in diameter. Nerve axons are located throughout the capsule and especially in the basal region closest to the dermis (Fig 9B). Although a direct connection was not documented, fluorescent images of the photophores indicate that axons originating from the large branchial nerve traverse the dermis and connect to the photophore.

The innermost layer of the photophores is an epithelium that separates the muscular capsule from the dermis of the arm. The cells of this layer have interdigitated lateral membranes and a cytoplasm that appears more granular than that of the outer epithelium. This layer is associated with extrinsic (to the photophore) muscle cells (Fig. 9A) and a blood vessel located in the dermis (Fig 9B).

In situ *behavior*

Animal 1 (from Cape Hatteras) was first seen in a bell posture with its fins sculling (Fig. 10A). It then moved away from the submersible, using a slow medusoid locomotion. After one contraction/expansion cycle, the animal closed its

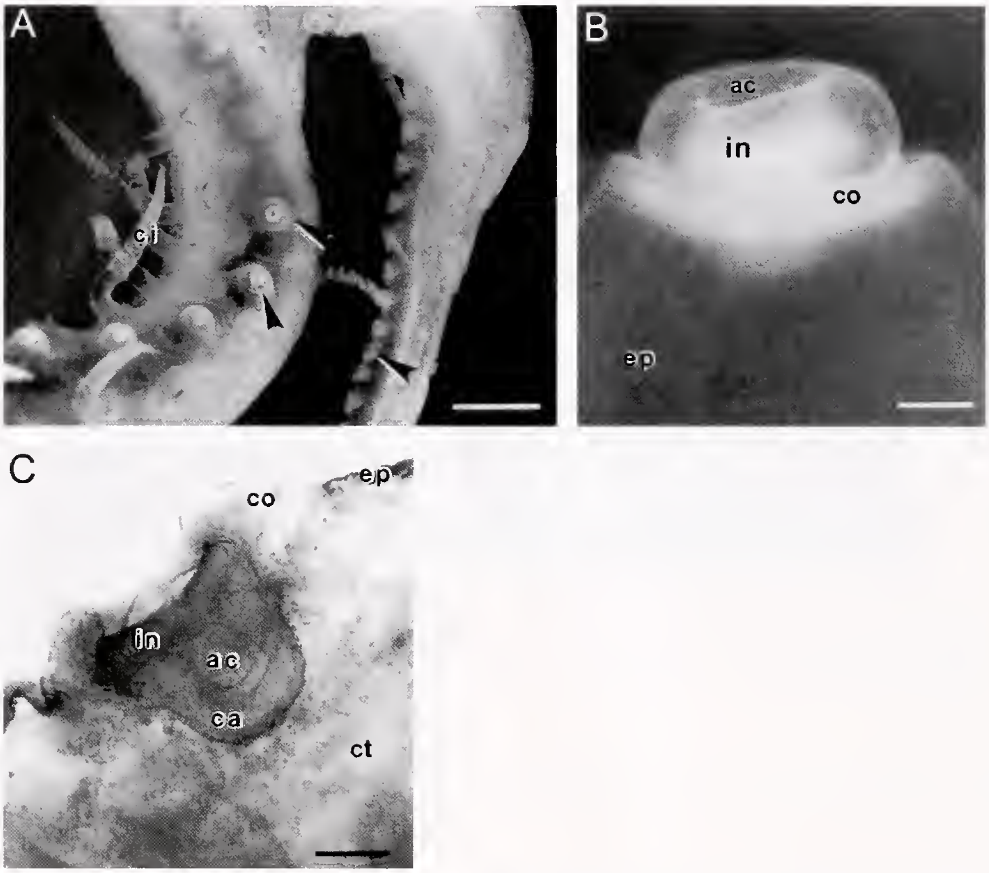

Figure 3. (A) Photograph of part of an arm of *Stauroteuthis syrtensis* with the webbing removed. Photophores (arrowheads) are arranged in a single row along the length of the arm and are unequally spaced with decreasing distance between light organs at the proximal tip of the arm. The positions of the photophores alternate with the positions of the cirri (ci). Scale bar = 0.5 cm. (B) Light micrograph of a fluorescent image of a single formalin-fixed photophore in the extended position. Like octopus suckers, the photophore is elevated above the epidermis (ep), is surrounded by a collar of epidermal cells (co), and consists of an infundibulum (in) and central acetabular canal (ac). (C) Light micrograph of a retracted photophore that has been bisected longitudinally. Internally, a capsule-like mass of tissue (ca) underlies the epithelium of the infundibulum and acetabulum. ct, dermal connective tissue of the arm. Scale bar for B and C = 0.1 mm.

web and assumed a highly distended balloon posture with motionless fins (Fig. 10B). After several minutes in this posture, the arms opened to a bell posture, and then closed to a considerably smaller balloon posture (Fig. 10C) referred to as the "pumpkin posture" by Vecchione (pers. comm.). After 2 min, the fins began sculling and the animal made one more medusoid contraction and then again closed its web to the pumpkin posture with fins sculling. After a minute, the animal made about seven more medusoid contractions and then closed to the pumpkin posture with fins sculling and head down.

Animal 2 (from Oceanographer Canyon) was first seen with its arms spread in the horizontal plane with the mouth oriented upwards (Fig. 10D). It underwent one medusoid contraction and then inflated to a highly distended balloon posture with fins motionless and cirri extended and pressed against the primary web. After several minutes, the fins began sculling and the animal simultaneously twisted its body and opened its arms (Fig. 10E).

Animal 3 (from Oceanographer Canyon) was first seen in a bell posture. Then, using slow medusoid locomotion, moved away from the submersible. During the escape, its fin sculled continuously and sometimes vigorously. During expansion of the primary web, the cirri could be seen and were extended perpendicular to the arms and pressed against the primary web.

Discussion

Morphology of photophores and homology with octopus suckers

Although the anatomical position and morphology of the light organs of *S. syrtensis* indicate their homology with octopod suckers, other aspects of their structure are consis-

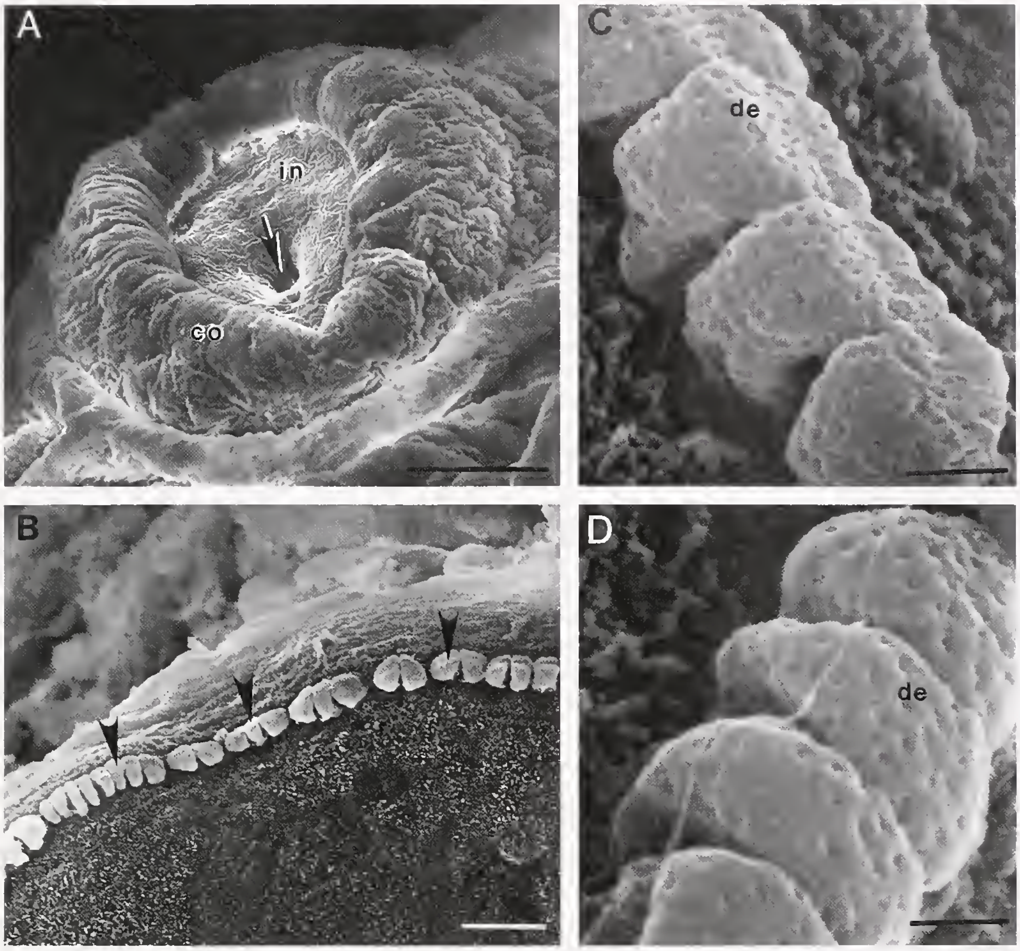

Figure 4. Scanning electron micrographs of photophores. (A) Externally, each photophore has three main recognizable parts: outer wall or collar (co), infundibulum (in), and acetabulum (arrow indicates the opening to the acetabular canal). Scale bar = 100 μm. (B) The junction between the infundibulum and the infolded collar is ringed by a row of denticles (arrowheads). Scale bar = 10 μm. (C–D) These hook-like denticles (de), which are atypical of octopod suckers, appear to be elaborations of the cuticle covering the infundibulum and acetabulum. Scale bars for C and D = 1 μm. A and B adapted from Johnsen *et al.* (1999), with permission from Nature, copyright 1999 Macmillan Magazines Ltd.

tent with those reported for simple photophores in other cephalopods (Young and Arnold, 1982; Herring *et al.*, 1987, 1994). Definitive structural characteristics of octopod suckers are given by Kier and Smith (1990) and Budelmann *et al.* (1997). Like the suckers of other cirrate octopods, the photophores of *S. syrtensis* are arranged in a single row along the oral surface of the arm with the largest, most developed organs located at the base of the arm, nearest the mouth. Suckers and these photophores both consist of three layers of tissue: an outer epithelium, an intrinsic muscular layer, and an extrinsic layer associated with muscle cells. The outer epithelium is covered by a cuticle that, as in suckers, appears to be periodically molted. Moreover, the epidermis associated with the photophore is modified to form the columnar epithelial cells of the recessed infundibulum and the invaginated acetabulum. The arrangement of myofilaments in the muscular capsule are consistent with the three-dimensional array of contractile fibers typical of suckers. Although this may be an artifact of fixation, the morphology and the arrangement of myofilaments would allow for the retraction and extension, as well as a change in the diameter, of the photophore and may be important in regulating the intensity of the emitted light.

Although denticles are not common in octopod suckers (Nixon and Dilly, 1977; Budelmann *et al.*, 1997), hooks and denticles of various sizes are found in decapod cephalopods. The functional significance, especially with the apparent loss of an adhesive function for the suckers, of the denticles on the photophores of *S. syrtensis* is unknown. They may, however, be vestigial structures indicating an evolutionary connection to the decapods.

Although definitive morphological characteristics are

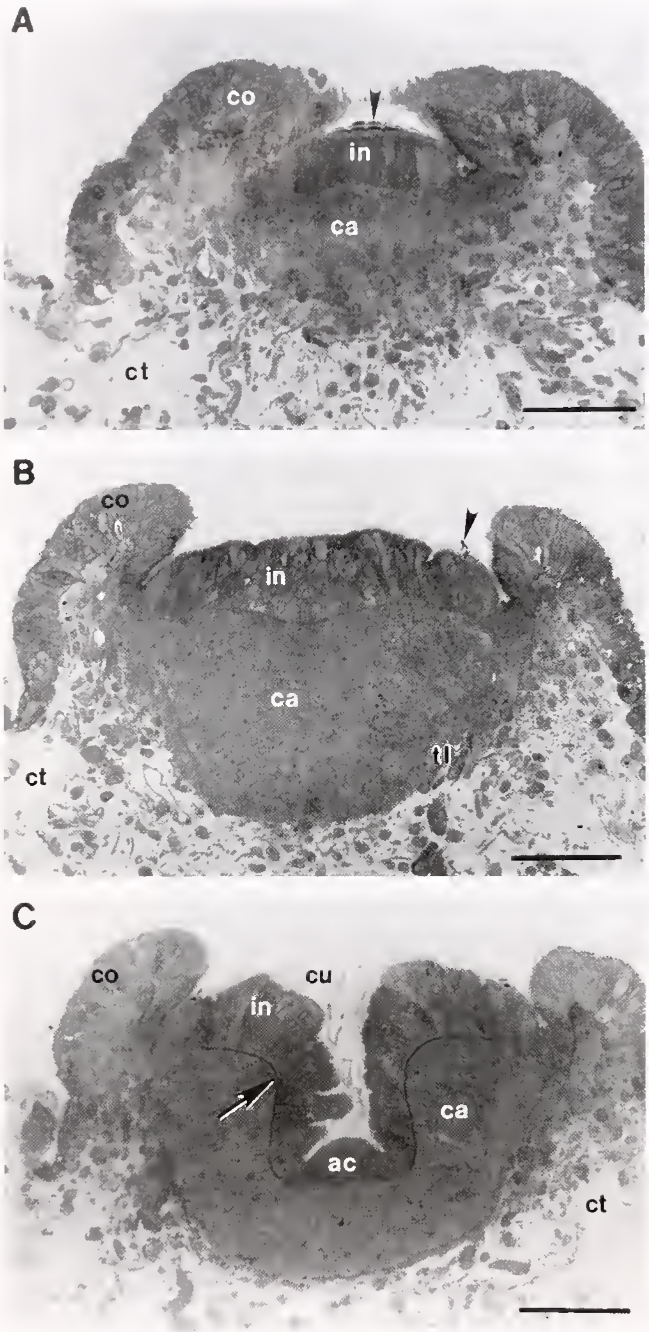

Figure 5. Light micrographs of a series of semithin sections from the outer edge of the infundibulum (A), through the middle region of the infundibulum (B), to the center of the acetabular canal (C). Each photophore consists of an outer epithelium that is recessed below the level of a supporting epidermal collar (co). This epithelium forms the infundibulum (in) and the acetabulum (ac) and is covered by a cuticle (cu). A capsule-like mass of tissue (ca) is located below the outer epithelium and is separated from the connective tissue (ct) of the arm by a third layer of cells (tl). Arrowheads, denticles; arrow, putative reflector. Scale bars = 0.2 mm.

lacking for photocytes in general (Herring, 1988), the epithelium of the acetabulum (and possibly of the infundibulum) is presumed to be the bioluminescent region of the photophores in *S. syrtensis.* Characteristics that identify photocytes in the octopod *Japetella diaphana* (Herring *et al.* 1987) and the squid *Abralia trigonura* (Young and Arnold, 1982) and are also found in the photophores of *S. syrtensis* include the presence of an amorphous, finely granular cytoplasmic ground substance containing numerous electron-dense vesicles, large basal nuclei, highly interdigitated lateral plasma membranes, ciliary rootlets, and abundant Golgi bodies. To some degree, this cellular morphology is found in the cells of both the infundibulum and the acetabulum. Since these ultrastructural traits are also typical of secretory epithelia, one hypothesis is that the infundibular epithelium secretes the cuticle, and the acetabular epithelium is involved in light production.

Reflectors in cephalopod photophores are typically composed of collagen fibers arranged in layers beneath the photocytes (Young and Arnold, 1982; Herring *et al.*, 1994). The layer of connective tissue separating the outer epithelium and the underlying capsule of muscle and nerve tissue in *S. syrtensis* conforms to this description. As in *J. diaphana* (Herring *et al.*, 1987), the fibrous layers appear concentric with respect to the axes of the photophore and alternate in orientation. In a longitudinal tangential section, this arrangement would produce the herringbone effect seen in the putative reflector of *S. syrtensis.*

The functional significance of bioluminescence

The replacement of adhesive suckers with photophores might have occurred during colonization of the pelagic deep sea from the shallow-water benthos. However, the significance of this transition and the function of the light emissions are, at present, unknown. One function of light emission common to almost all bioluminescent animals is defense (reviewed in Widder, 1999). The vast majority of bioluminescent animals emit light when disturbed, perhaps to startle predators or to attract larger animals that may prey upon the predator. Feeding experiments have shown that feeding rates of predators are diminished in the presence of bioluminescence (see Widder, 1999, for further details). Since *S. syrtensis* emitted light in response to physical disturbance, it is likely that defense is at least one function of its light emission.

The functions of bioluminescence in deep-sea animals are difficult to determine because these animals are seldom observed in their own environment, and then only under bright lights that both mask natural light emissions and affect behavior. Therefore, the following discussion is based on circumstantial rather than direct evidence and is necessarily speculative. On the basis of the anatomical distribution of the photophores, the optical characteristics of the emitted light, and the behavior of the animal, we propose two more functions for bioluminescence in *S. syrtensis:* sexual signaling and light luring. Visual communication is

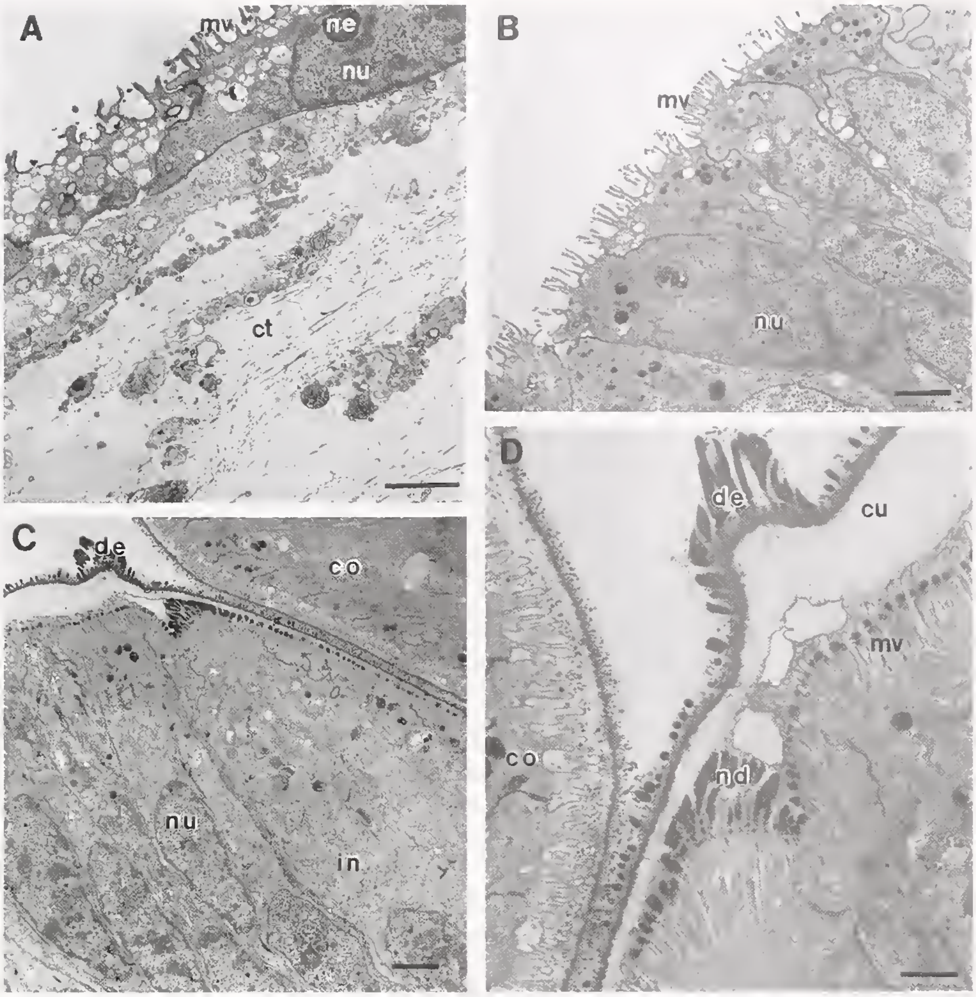

Figure 6. Transmission electron micrographs of tangential longitudinal sections through the epidermis (A), outer rim of the collar (B), and the inner rim of the collar and outer edge of the infundibulum (D and C). These, as do all TEM images, represent sections taken in the longitudinal axis of the photophore. The epidermis is composed of flat cells with scattered apical microvilli (mv). The inner rim of the collar (co) and the infundibulum (in) are covered externally by a cuticle (cu), which at the edge of the infundibulum is modified to form denticles (de). Like the cuticle of suckers, the photophore cuticle is apparently shed and replaced by a new pre-formed cuticle (nd). ct, dermal connective tissue of the arm; ne, nucleolus; nu, nucleus. Scale bars for A, B, and C = 1 μm. Scale bar for C = 3 μm.

extremely common among cephalopods (Hanlon and Messenger, 1996), and the suckers of certain shallow-water octopods have been implicated in (non-bioluminescent) sexual signaling (Packard, 1961). Indeed, sexual signaling is the proposed function of bioluminescence in the other bioluminescent genera of octopods (Robison and Young, 1981). In these animals, light organs are found only in mature breeding females. Males, immature females, and brooding females all lack this organ. In addition, Robison and Young (1981) noted that the emitted light is distinctly green (rather than the far more common blue-green) and suggested that the bioluminescence may be a private line of communication.

However, although the octoradial pattern of twinkling bioluminescence in *S. syrtensis* makes a highly species-specific signal, several factors contradict its use as a sexual signal. First, the photophores appear to be found in members of the species that, based on mantle length, are immature (Collins, unpubl. data). None of the three collected specimens were sexed by dissection. However, *S. syrtensis* can be externally sexed by a sexual dimorphism in suckers 9–22. In mature males, suckers 9–22 are considerably enlarged; in immature males, the enlargement is less noticeable (Collins, unpubl. data). By this method, two of the three animals were sexed as female; the sex of the third animal is unknown. All, including the animal observed from the submersible at Cape Hatteras, had the same characteristically reflective suckers. Second, the light organs' wave-

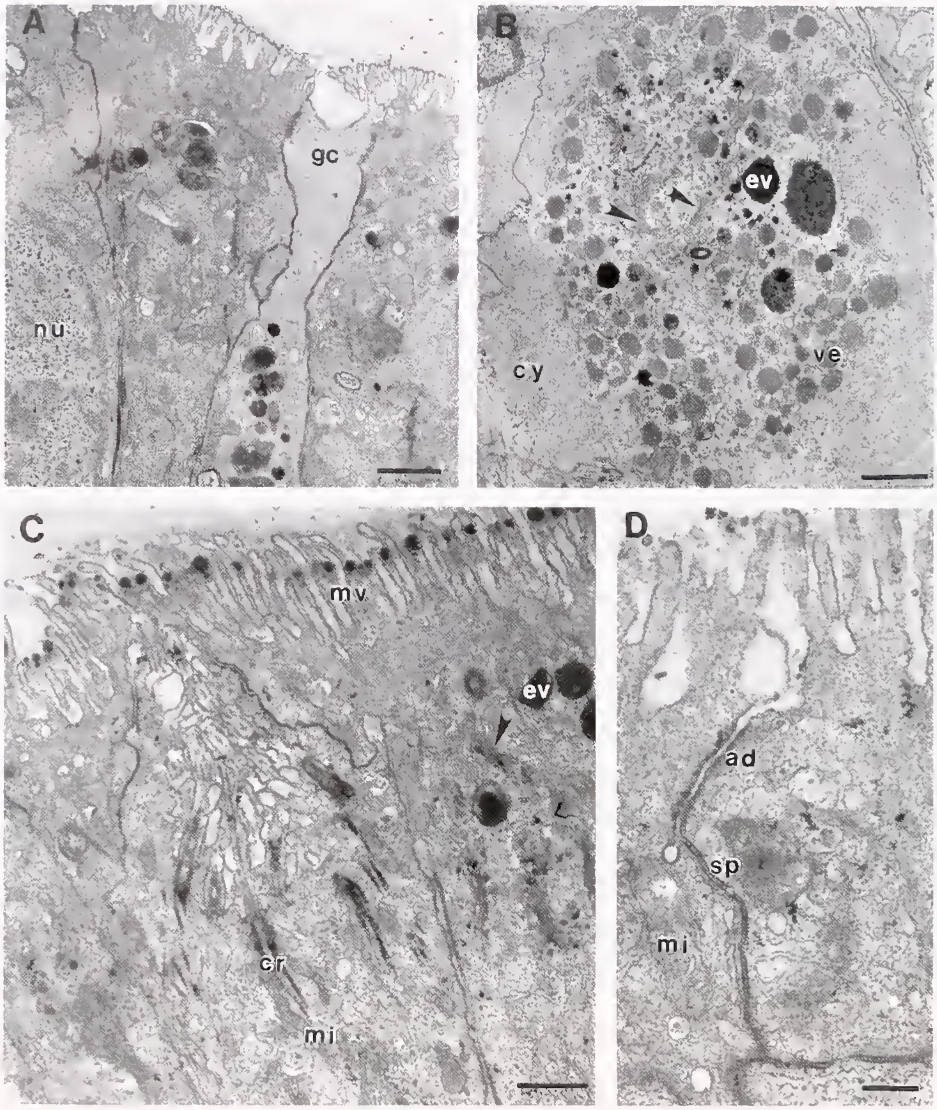

Figure 7. Transmission electron micrographs showing the details of the epithelial cells of the infundibulum. This epithelium contains gland cells (gc) and columnar epithelial cells (A) and multiciliated columnar cells (C). (A, B) Numerous electron-dense (ev) vesicles, vesicles that are less opaque (ve), and Golgi bodies (arrowheads) are found in finely granular cytoplasm (cy) of all cell types. Scale bars = 1 μm. (C) Both types of columnar epithelial cells are characterized by having mitochondria (mi) and a brush-border of branched microvilli (mv). A few multiciliated cells were identified by the presence of ciliary rootlets (cr) and short apical axonemes. Scale bar = 2μm. (D) Infundibular cells are interconnected by apicolateral adherens (ad) and subapical septate (sp) junctions. Scale bar = 0.5 μm. nu, nucleus.

length of peak emission closely approximates the wavelength of maximum light transmission in the ocean (475 nm) and the usual peak wavelengths of bioluminescence and visual sensitivity in deep-sea animals (Jerlov, 1976; Herring, 1983; Widder *et al.*, 1983; Frank and Case, 1988; Partridge *et al.*, 1992; Kirk, 1983). Therefore, though the bioluminescent signal would be visible at long distances to other members of *S. syrtensis*, it would also be visible at long distances to potential predators. In addition, since the octoradial pattern would be distorted by light scattering after a short distance underwater (Mertens, 1970), it would be difficult to distinguish from the many other bioluminescent signals of similar wavelength.

A more attractive hypothesis is that bioluminescence in *S. syrtensis* functions to lure potential prey. Voss (1967) has previously suggested that the photophores in some cephalopods function as light lures, and this function in *S. syrtensis* is supported by the following line of evidence. The cirrate genera *Stauroteuthis*, *Cirroteuthis*, and *Cirrothauma* feed on small planktonic crustaceans, and other researchers

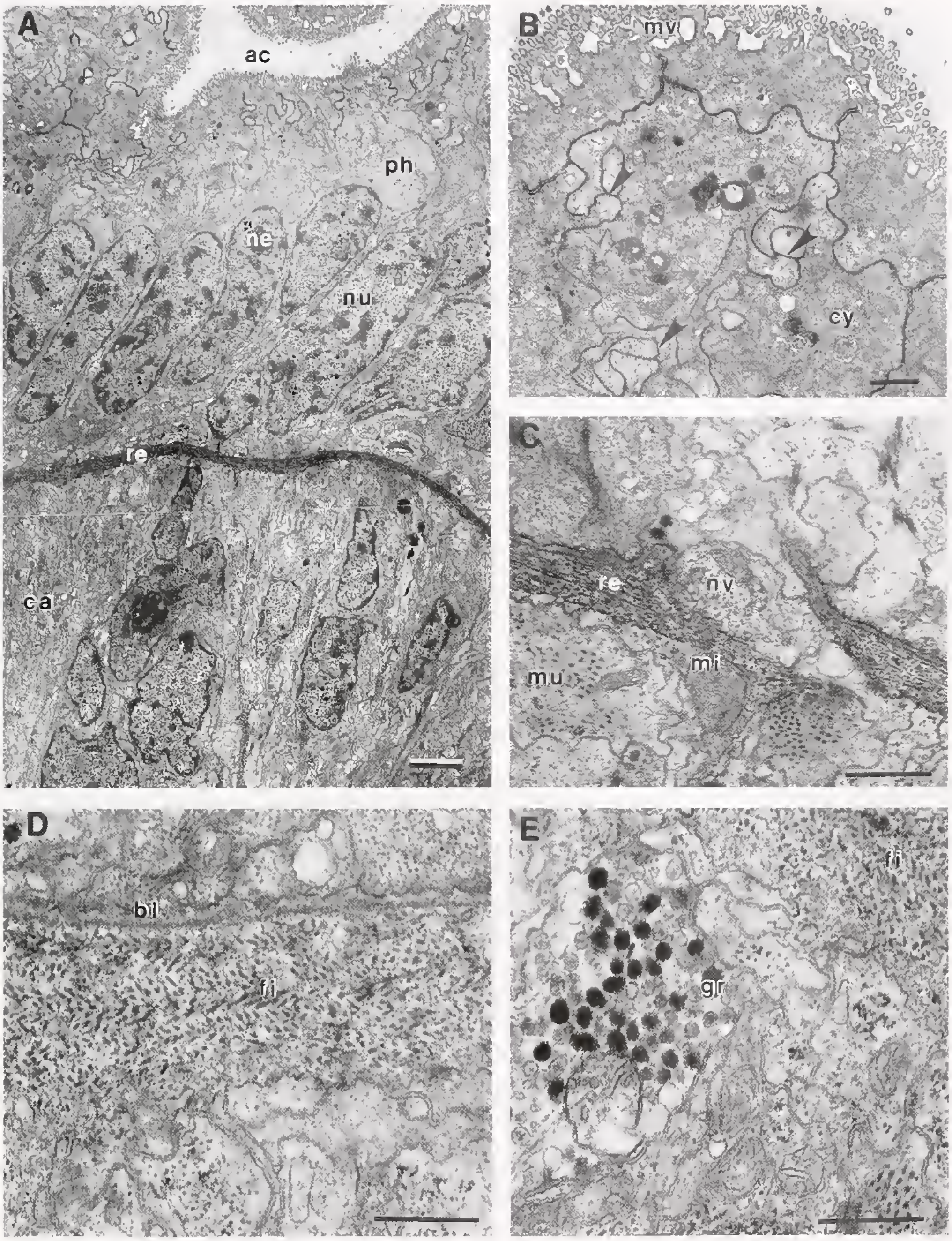

Figure 8. Transmission electron micrographs of the acetabular epithelium (A–C), the putative reflector (D), and distally positioned cells in the capsule of tissue beneath the outer epithelium (E). (A) A montage showing the presumptive photocytic epithelium (ph), reflector (re), and the underlying capsule (ca) of muscle and nerve cells. Scale bar = 3 μm. (B) Like photocytes of other cephalopods, the cells of the acetabulum have highly digitized lateral membranes (arrowheads) and a finely granular cytoplasm (cy). Scale bar = 0.5 μm. (C, D) A layer of connective tissue separates the acetabular epithelium from the underlying muscle (mu) and nerve cells. Breaks in the connective tissue layer are bridged by neurons (nv). Fibers (fi) in the connective tissue are arranged in layers with alternating orientation, giving the tissue a herringbone appearance. Scale bars = 0.5 μm. (E) Presumptive neurons with electron-dense granules (gr) are found throughout the capsule. Scale bar = 0.5 μm.

have suggested that these are trapped within a mucous web produced by buccal secretory glands and handled by the elongated cirri (Vecchione, 1987; Vecchione and Young, 1997). Since all three genera appear to have nonfunctional suckers (Aldred *et al.*, 1983; Voss and Pearcy, 1990), this method of feeding seems likely. In all three genera, the

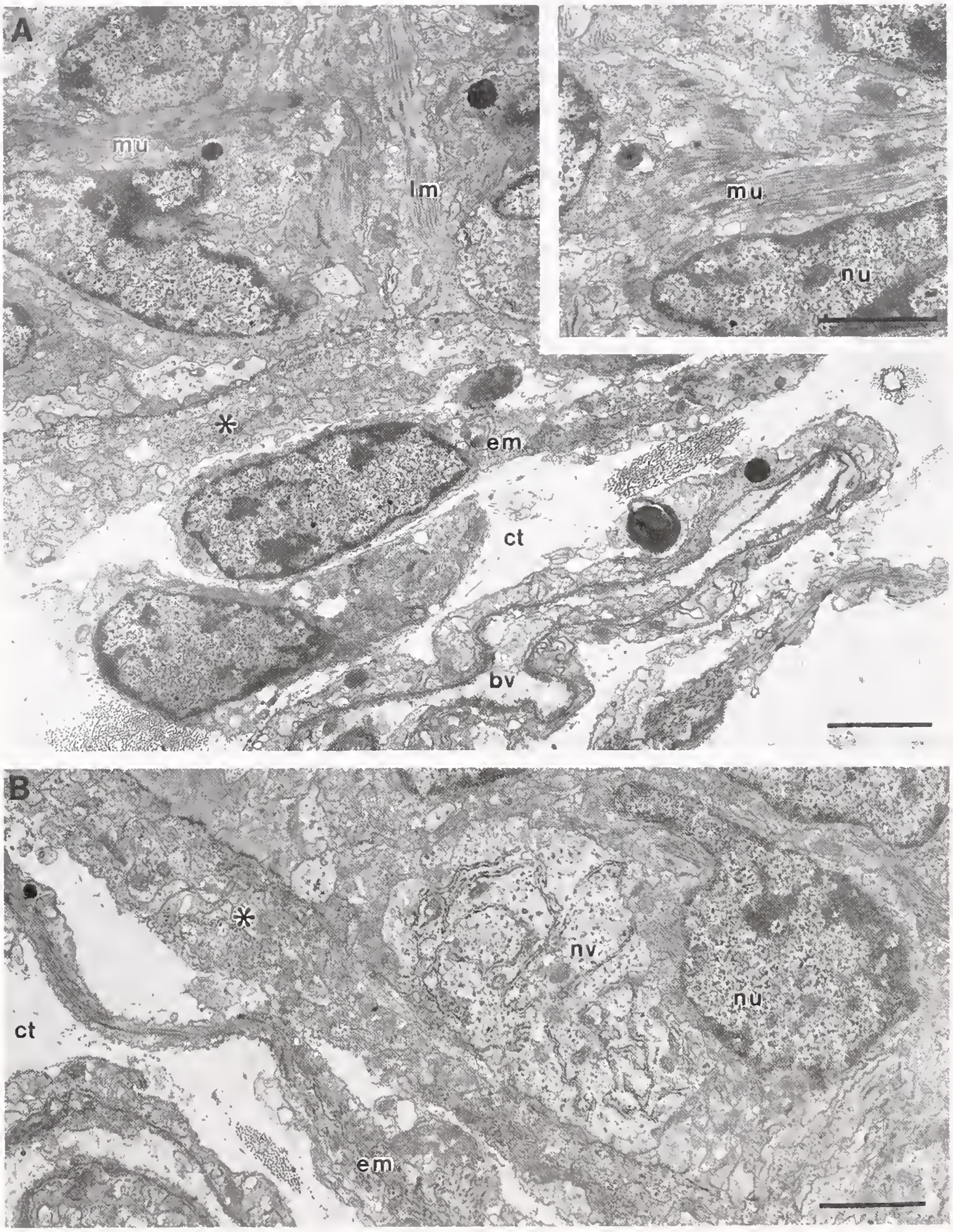

Figure 9. (A, B) Transmission electron micrographs of the medial region of the capsule and of the third innermost cell layer of the photophore. The capsule, like the intrinsic musculature of suckers, consists, in part, of cells with myofilaments arranged in three planes (also see inset). Longitudinal (lm) and horizontal fibers (mu) alternate throughout the capsule. Inset shows thick and thin filaments consistent with the size and appearance of myosin and actin. Neural axons (nv) are intermingled with muscle cells. The capsule is separated from the connective tissue of the arm (ct) by a third layer of cells (*), which is associated with extrinsic muscle cells (em). bv, lumen of a blood vessel; nu, nucleus. Scale bars = 1 μm.

shape of the primary web precludes any flow-through feeding current. Therefore, the prey cannot be filtered from the water column, but must somehow be attracted to the mucous web. Since many deep-sea crustaceans have well-developed, sensitive eyes and are attracted to light sources (Morin *et al.*, 1975), the photophores of *S. syrtensis* may provide the lure.

With the exception of the twisting behavior following ballooning (observed only once), the *in situ* behaviors of the three specimens of *S. syrtensis* reported here are similar to

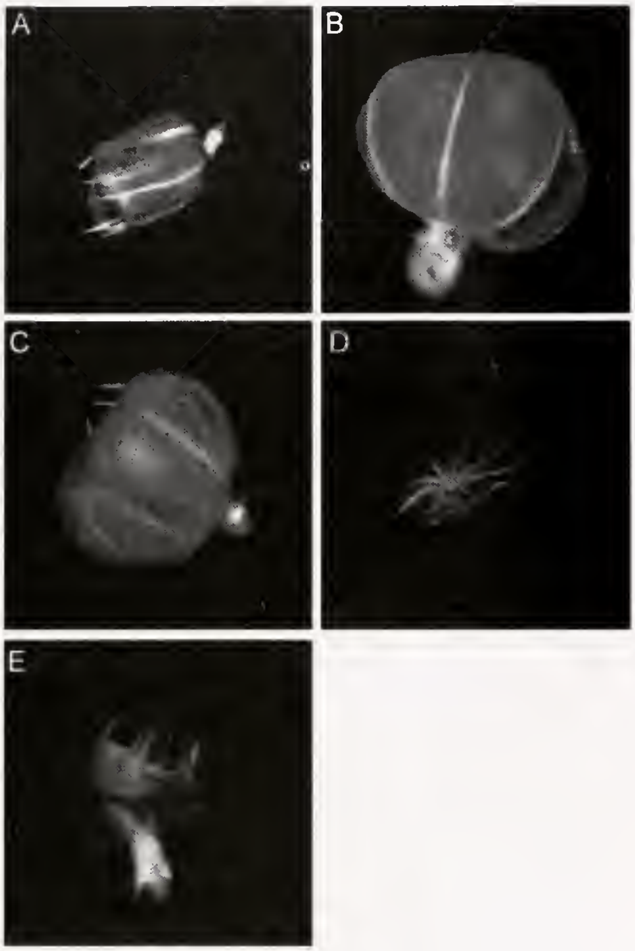

Figure 10. Digitized frames of *in situ* video of *Stauroteuthis syrtensis:* (A) bell posture; (B) distended balloon posture; (C) pumpkin posture (distinguished from the balloon posture by the fact the web is not fully inflated); (D) inverted umbrella posture; (E) animal twisting and opening its arms after ballooning. The highlights on the mantle in A, C, and E are reflections from the submersible lights.

those described from videos of two other specimens observed by Vecchione and Young (1997). When first approached, *S. syrtensis* is generally found with its arms spread in an umbrella or bell posture, with the mouth oriented either upwards or downwards (Roper and Brundage, 1972; Vecchione and Young, 1997; Villeneuva *et al.*, 1997). Since the animal almost certainly detects the relatively large and well-lit submersible well before itself being captured on video, it is difficult to know whether this is the natural posture or a defensive reaction. Given the assumption that the animals are in an undisturbed, non-withdrawal state when first filmed, their posture and the location of their photophores are consistent with the use of bioluminescence as a lure. As mentioned above, the wavelength of peak emission approximates the wavelength of maximum light transmission. This suggests that the emission spectrum of the photophores has been selected for maximum visibility. Finally, because the intensity of upwelling light is only a small percentage of that of downwelling light (Denton, 1990), animals bioluminescing in the mouth-up posture would be highly visible to potential prey in shallower depths. Collectively, these observations give credence to the idea that *S. syrtensis* uses photophores to attract prey.

Existence and evolution of photophores in octopods

Aside from the present study, the only other conclusive evidence of bioluminescence in octopods is restricted to the breeding females of the family Bolitaenidae (Herring, 1988). However, the existence of light organs within suckers (at the base of the peduncle) has been suggested in the cirrate octopod *C. murrayi* (Chun, 1910, 1913). As in the photophores of *S. syrtensis,* these organs have a bright white appearance due to reflection from a connective tissue layer and are found in suckers that have many reduced traits compared to typical octopod suckers (Aldred *et al.*, 1983). Unlike the photophores of *S. syrtensis,* the postulated light organs of *C. murrayi* are not found within the sucker itself. In addition, the connective tissue layer is situated such that the produced light would be reflected into the tissue of the arm. After a complex subsequent study (Aldred *et al.*, 1978, 1982, 1983), Aldred *et al.* (1984) tentatively interpreted the organs as unusual nerve ganglia (see also Vecchione, 1987).

Because photophores and photocytes have a bewildering variety of morphologies (Buck, 1978; Herring, 1988), conclusive determination of the presence or absence of light organs (which often emit only dim light) requires observation of a healthy specimen in near-total darkness by a thoroughly dark-adapted observer (*i.e.*, in near-total darkness for a minimum of 10 min) (Widder *et al.*, 1983). Owing to the bright lights of submersibles and remotely operated vehicles, bioluminescence is seldom observed *in situ*. In addition, since most bioluminescent animals produce light when disturbed, deep-sea cephalopods collected in nets generally have exhausted their light production by the time they reach the surface. Finally, observations of spontaneous luminescence are rare; most bioluminescent animals must be physically stimulated (often for a considerable period of time) before light is observed (Widder *et al.*, 1983).

The evolutionary history of photophores in any animal group is extremely difficult to determine because bioluminescence has no fossil record (Buck, 1978). The evolution of bioluminescence in the coleoid cephalopods is particularly intriguing because of the extraordinary diversity and complexity of photophores in deep-sea decapods and vampyromorphs and their apparent rarity and simplicity in deep-sea octopods (Herring, 1988). However, bioluminescence in the deep-sea octopods may not be as rare as previously assumed. For the reasons given in the previous paragraph, bioluminescence may be under-reported in the deep-sea octopods. *Cirrothauma murrayi* and *Cirroteuthis* are found at abyssal depths (except in polar regions, where they can be found at the surface) (Voss, 1988), making capture of healthy specimens extremely difficult. *Opistoteuthis* is found at shallower depths and has been maintained in aquaria (Pereyra, 1965), but it is not known whether it was observed under the specialized conditions necessary to detect bioluminescence. However, given that *Opistoteuthis* feeds on a variety of benthic prey that it apparently captures using functional suckers (Villaneuva and Guerra, 1991), if it is bioluminescent, its photophores are probably in a different site.

Octopod bioluminescence may exist only in *S. syrtensis* and the bolitaenids. A cladistic analysis of the Octopoda involving 66 morphological characters places the cirrates basal to the incirrates and the bolitaenids basal among the incirrates (Voight, 1997). This analysis also supports the monophyly of the bolitaenids and the two clades (Cirroteuthidae and Stauroteuthidae) composing the genera *Stauroteuthis, Cirrothauma,* and *Cirroteuthis.* The homology of the photophores in *S. syrtensis* and the bolitaenids is unlikely. The photophores of *S. syrtensis* appear to exhibit the rare trait of muscle derivation. The only other example of muscle-derived light organs has been found in the scopelarchid fish *Benthalbella infans* (Johnston and Herring, 1985). Although the luminous circumoral ring in the bolitaenid *Japetella diaphana* is initially a muscular band, the great increase in the size of the ring in adult females apparently requires *de novo* synthesis of luminous tissue (Herring *et al.,* 1987). In addition, the light organs differ in almost all other anatomical and morphological characteristics. Finally, only mature female bolitaenids have light organs, which appear to have a sexual function, whereas the light organs of *S. syrtensis* are found in immature animals and may be involved in feeding. Multiple independent evolutions of photophores are common in decapods, at least at taxonomic ranks of subfamily or higher (Young and Bennett, 1988; Herring *et al.,* 1992, 1994). Therefore, despite the close evolutionary relationship between the cirrates and the bolitaenids, photophores in these two groups seem to have evolved independently. However, the monophyly of *Stauroteuthis, Cirroteuthis,* and *Cirrothauma* and the fact that they all have suckers with reduced traits suggest the possibility of light production by modified suckers in the latter two genera.

Acknowledgments

We thank the captain and crew of the R.V. *Edwin Link* and the *Johnson-Sea-Link* pilots, Phil Santos and Scott Olsen, for assistance with all aspects of animal collection. We also thank Dr. Tamara Frank for a critical reading of the manuscript, Dr. Michael Vecchione for aid with identifying the specimens, Dr. Janet Voight for helpful discussions on octopod evolution, and Dr. Martin Collins for use of unpublished data. The authors are grateful to the Smithsonian Marine Station at Fort Pierce, Florida, for allowing the use of the photomicroscopes. Our thanks are also extended to Dr. William Jaeckle for his assistance with the scanning electron microscopy and to Julie Piriano for help with the transmission electron microscope. This work was funded by a grant from the National Oceanic and Atmospheric Administration (subgrant UCAP-95-02b, University of Connecticut, Award No. NA76RU0060) to Drs. Tamara Frank and EAW, a grant from the National Science Foundation (OCE-9313872) to Drs. Tamara Frank and EAW, and by a Harbor Branch Institution Postdoctoral Fellowship to SJ. This is Harbor Branch Contribution No. 1287 and Contribution No. 479 of the Smithsonian Station at Fort Pierce, Florida.

Literature Cited

Aldred, R. G., M. Nixon, and J. Z. Young. 1978. The blind octopus *Cirrothauma. Nature* **275:** 547–549.

Aldred, R. G., M. Nixon, and J. Z. Young. 1982. Possible light organs in finned octopods. *J. Molluscan Stud.* **48:** 100–101.

Aldred, R. G., M. Nixon, and J. Z. Young. 1983. *Cirrothauma murrayi* Chun, a finned octopod. *Philos. Trans. R. Soc. Lond. B* **301:** 1–54.

Aldred, R. G., M. Nixon, and J. Z. Young. 1984. Ganglia not light organs in the suckers of octopods. *J. Molluscan Stud.* **50:** 67–69.

Buck, J. 1978. Functions and evolutions of bioluminescence. Pp. 419–460 in *Bioluminescence in Action,* P. J. Herring, ed. Academic Press, London.

Budelmann, B. U., R. Schipp, and S. Boletzky. 1997. Cephalopoda. Pp. 119–414 in *Microscopic Anatomy of Invertebrates* Vol. 6A, F. W. Harrison and A. J. Kohn, eds. Wiley-Liss Publications, New York.

Chun, C. 1910. Die Cephalopoden. *Wiss. Ergebn. dt. Thiefsee-Exped. "Valdivia"* **18:** 1–552.

Chun, C. 1913. Cephalopoda. Pp. 1–21 in *Report on the Scientific Results of the "Michael Sars" North Atlantic Deep-Sea Expedition 1910* Vol. III, Part 1, J. Murray and J. Hjort, eds. The Trustees of the Bergen Museum, Bergen.

Denton, E. J. 1990. Light and vision at depths greater than 200 meters. Pp. 127–148 in *Light and Life in the Sea,* P. J. Herring, A. K. Campbell, M. Whitfield, and L. Maddock, eds. Cambridge University Press, New York.

Frank, T. M., and J. F. Case. 1988. Visual spectral sensitivities of bioluminescent deep-sea crustaceans. *Biol. Bull.* **175:** 261–273.

Hamner, W. M. 1990. Design developments in the planktonkreisel, a plankton aquarium for ships at sea. *J. Plankton Res.* **12:** 397–402.

Hanlon, R. T., and J. B. Messenger. 1996. *Cephalopod Behaviour.* Cambridge University Press, Cambridge.

Harvey, E. N. 1952. *Bioluminescence.* Academic Press, New York.

Herring, P. J. 1983. The spectral characteristics of luminous marine organisms. *Proc. R. Soc. Lond. B* **220:** 183–217.

Herring, P. J. 1988. Luminescent organs. Pp. 449–489 in *The Mollusca* Vol. 11, E. R. Trueman and M. R. Clarke, eds. Academic Press, New York.

Herring, P. J., P. N. Dilly, and C. Cope. 1987. The morphology of the bioluminescent tissue of the cephalopod *Japetella diaphana* (Cephalopoda: Bolitaenidae). *J. Zool. Lond.* **212:** 245–254.

Herring, P. J., P. N. Dilly, and C. Cope. 1992. Different types of photophore in the oceanic squids, *Octopoteuthis* and *Taningia* (Cephalopoda: Octopoteuthidae). *J. Zool. Lond.* **227:** 479–491.

Herring, P. J., P. N. Dilly, and C. Cope. 1994. The bioluminescent organs of the deep-sea cephalopod *Vampyroteuthis infernalis* (Cephalopoda: Vampyromorpha). *J. Zool. Lond.* **233:** 45–55.

Jerlov, N. G. 1976. *Marine Optics.* Elsevier Scientific Publishing, New York.

Johnsen, S., E. J. Balser, and E. A. Widder. 1999. Light-emitting suckers in an octopus. *Nature* **398:** 113–114.

Johnston, I. A., and P. J. Herring. 1985. The transformation of muscle into bioluminescent tissue in the fish *Benthalbella infans* Zugmayer. *Proc. R. Soc. Lond. B* **225:** 213–218.

Kier, W. M., and A. M. Smith. 1990. The morphology and mechanics of octopus suckers. *Biol. Bull.* **178:** 126–136.

Kirk, J. T. O. 1983. *Light and Photosynthesis in Aquatic Ecosystems.* Cambridge University Press, Cambridge.

Mertens, L. E. 1970. *In-water Photography: Theory and Practice.* Wiley Interscience, New York.

Morin, J. G., A. Harrington, K. Nealson, N. Krieger, T. O. Baldwin, and J. W. Hastings. 1975. Light for all reasons: versatility in the behavioral repertoire of the flashlight fish. *Science* **190:** 74–76.

Nixon, M., and P. N. Dilly. 1977. Sucker surfaces and prey capture. *Symp. Zool. Soc. Lond.* **38:** 447–511.

Packard, A. 1961. Sucker display of *Octopus vulgaris. Nature* **190:** 736–737.

Partridge, J. C., S. N. Archer, and J. Van Oostrum. 1992. Single and multiple visual pigments in deep-sea fishes. *J. Mar. Biol. Assoc. U.K.* **72:** 113–130.

Pereyra, W. T. 1965. New records and observations on the flapjack devilfish *Opistoteuthis californiana* Berry. *Pac. Sci.* **19:** 427–441.

Robison, B. H., and R. E. Young. 1981. Bioluminescence in pelagic octopods. *Pac. Sci.* **35:** 39–44.

Roper, C. F. E., and W. L. Brundage. 1972. Cirrate octopods with associated deep-sea organisms: new biological data based on deep benthic photographs (Cephalopoda). *Smithson. Contrib. Zool.* **121:** 1–45.

Vecchione, M. 1987. A multispecies aggregation of cirrate octopods trawled from north of the Bahamas. *Bull. Mar. Sci.* **40:** 78–84.

Vecchione, M., and R. E. Young. 1997. Aspects of the functional morphology of cirrate octopods: locomotion and feeding. *Vie Milieu* **47:** 101–110.

Villanueva, R., and A. Guerra. 1991. Food and prey detection in two deep-sea cephalopods: *Opisthoteuthis agassizi* and *O. vossi. Bull. Mar. Sci.* **49:** 288–299.

Villanueva, R., M. Segonzac, and A. Guerra. 1997. Locomotion modes of deep-sea cirrate octopods (Cephalopoda) based on observations from video recordings on the Mid-Atlantic Ridge. *Mar. Biol.* **129:** 113–122.

Voight, J. R. 1997. Cladistic analysis of the octopods based on anatomical characters. *J. Molluscan Stud.* **63:** 311–325.

Voss, G. L. 1967. The biology and bathymetric distribution of deep-sea cephalopods. *Stud. Trop. Oceanogr.* **5:** 511–535.

Voss, G. L. 1988. The biogeography of the deep-sea octopoda. *Malacologia* **29:** 295–307.

Voss, G. L., and W. G. Pearcy. 1990. Deep-water octopods (Mollusca: Cephalopoda) of the northeastern Pacific. *Proc. Calif. Acad. Sci.* **47:** 47–94.

Widder, E. A. 1999. Bioluminescence. Pp. 555–581 in *Adaptive Mechanisms in the Ecology of Vision,* S. N. Archer, M. B. A. Djamgoz, E. Loew, J. C. Partridge, and S. Vallerga, eds. Kluwer Academic Publishers, Dordrecht, The Netherlands.

Widder, E. A., M. I. Latz, and J. F. Case. 1983. Marine bioluminescence spectra measured with an optical multichannel detection system. *Biol. Bull.* **165:** 791–810.

Young, R. E., and J. M. Arnold. 1982. The functional morphology of a ventral photophore from the mesopelagic squid, *Abralia trigonura. Malacologia* **23(1):** 135–163.

Young, R. E., and T. M. Bennett. 1988. Photophore structure and evolution within the Enoploteuthidae (Cephalopoda). Pp. 241–251 in *The Mollusca* Vol. XII, E. R. Trueman and M. R. Clark eds. Academic Press, New York.

Reference: *Biol. Bull.* **197:** 40–48. (August 1999)

Long-Term Culture of Lobster Central Ganglia: Expression of Foreign Genes in Identified Neurons

GEOFFREY K. GANTER, RALF HEINRICH, RICHARD P. BUNGE[1,*],
AND EDWARD A. KRAVITZ†

Department of Neurobiology, Harvard Medical School, 220 Longwood Avenue, Boston, Massachusetts 02115; and [1] Miami Project to Cure Paralysis, University of Miami School of Medicine, Miami, Florida 33136

Abstract. The ventral nerve cords of lobsters (*Homarus americanus*) can be cultured *in vitro* for at least 7 weeks. Over this period, neurons maintain their normal electrophysiological features and continue, among other measures of neuronal health, to synthesize RNA and proteins. One application of this culture system is demonstrated: the manipulation of gene expression in identified neurons. After intracellular injection of complementary RNA (cRNA) encoding green fluorescent protein (GFP), the amount of protein product measured by fluorescent confocal microscopy increases for 4 days and then decreases to background by day 10. Thus, translation of the injected message must have increased for 4 days before declining. Moreover, after injection of cRNA encoding β-galactosidase, the levels of enzyme activity were measured using a fluorogenic substrate, revealing a peak of β-galactosidase activity at 6 to 9 days; this activity was still detectable for at least 10 days after injection.

Therefore, either GFP or β-galactosidase can be used as an injectable marker, allowing *in vivo* quantitation of expression in individual cells over time. We measured long-lasting expression of these proteins after a single injection, suggesting that it may be possible to manipulate the levels of expression of any gene of interest.

Introduction

The ventral nerve cord preparation has been a useful tool for exploring the physiology and pharmacology of central neurons in the lobster (see Otsuka *et al.*, 1967; Livingstone *et al.*, 1980; Ma and Weiger, 1993). The entire nerve cord, with the nerve roots sectioned, can be dissected from lobsters and maintained in oxygenated saline for up to 36 hours. After the ganglia have been desheathed, the large cell bodies of central neurons can be identified both by their positions and by their physiological properties as revealed in electrophysiological recordings.

In this study, we report an extension of this technique that allows experiments of at least 7 weeks duration to be carried out. Longer term experiments that become possible under these conditions include an exploration of the effects of manipulation of levels of gene expression. Since activation of a gene can take several days to affect cells, experiments of this type were not practical with the short-term preparations that are commonly used.

Genes from practically any source can be injected into *Xenopus* oocytes and the resulting heterologous expression analyzed (for review, see Dawid and Sargent, 1988). Use of this technique allows, for example, the effects of point mutations or deletions in genes to be examined. Although expression can be characterized in heterologous systems, the function of cloned genes might be more informatively explored if they could be expressed in cells of their native organism. Our studies show that this important option is

---

Received 16 December 1998; accepted 23 April 1999.

* This paper is dedicated to the memory of a good colleague and friend, Dr. Richard P. Bunge. Dick died on September 10, 1996, of esophageal cancer at the age of sixty-four. He was in the midst of an important project, that of rebuilding the Miami Project to Cure Paralysis, and in 1989 became the scientific director of that project. One of us (EAK) had the good fortune to work with Dick from 1968 to 1969 during his sabbatical visit to our laboratory in Boston. The organ culture system was developed at that time, and although these earlier experiments never were published, they are an important part of our present and future research activities. It is typical of Dick and his studies that they often were far ahead of their time. We are honored to include him as an author on this paper.

† To whom correspondence should be addressed. E-mail: edward_kravitz@hms.harvard.edu

now available for investigations of the roles of neuronal genes in the central neurons of the lobster. Moreover, we can use this technique to express proteins or peptides in neurons and investigate both the physiological responses of the neuron and the effectiveness of the introduced substance.

Injection of DNA or RNA into identified neurons can be a direct and effective means of altering gene expression in identified cells. Several investigators have used microinjection techniques to express genes in invertebrate neural systems; in particular, the effects of various proteins on synaptic transmission and electrical excitability of neurons have been determined. For example, Kaang and coworkers (1992) found that microinjection of DNA encoding an A-type Shaker potassium channel into *Aplysia* neurons shortened action potentials and thereby had a profound effect on transmitter release. Expression of a noninactivating potassium channel in another type of *Aplysia* neuron abolished spontaneous bursting activity (Zhao *et al.*, 1994). RNA encoding the leech homeobox protein Lox1, when injected into certain types of leech motoneurons, introduced active spike propagation to proximal neurites (Aisemberg *et al.*, 1997). In another system, Dearborn and coworkers (1998) injected rat synapsin IA1 into crayfish neurons and found an increase in transmitter release.

In this communication, we present an organ culture system that extends the time frame of nerve cord experimentation, allowing for such long-term experiments as the expression of foreign RNAs in lobster central neurons. We have induced the expression of green fluorescent protein (GFP) from the jellyfish *Aequoria victoria* (Prasher *et al.*, 1992; Chalfie *et al.*, 1994) and the enzyme β-galactosidase from the bacterium *Escherichia coli* (MacGregor *et al.*, 1987). Levels of both proteins were measured repeatedly in individual living cells over several days. Neither of these proteins interfered with the viability of the cells. These reagents can be injected either as continuous expression monitors or as fusion proteins linked with other proteins of interest (Lalumiere and Richardson, 1995; Gerdes and Kaether, 1996). This study confirms the effectiveness of the gene delivery system and our long-term organ culture system, a combination that promotes connections between the disciplines of molecular biology and physiology in the study of the lobster nervous system.

Materials and Methods

Dissection and neuron identification

Nerve cords were removed from ice-anesthetized adult lobsters and pinned out in lobster saline as previously described (Otsuka *et al.*, 1967; Harris-Warrick and Kravitz, 1984; Ma *et al.*, 1992). After desheathing the abdominal ganglia and removing the glial layers, we targeted two cell types for injections. These were identified according to criteria defined by Otsuka *et al.* (1967) and included large glutamate-containing motoneurons (M6/M7), with their axons projecting through ipsilateral 3rd roots, and GABA-containing neurons (I2), displaying prominent excitatory synaptic input and projecting through contralateral 3rd roots to the periphery.

Lobster organ culture system

After experimental manipulation, preparations were rinsed several times in sterile saline containing penicillin (50 μg/ml), streptomycin (50 μg/ml) and neomycin (100 μg/ml) (GIBCO/BRL). Nerve cords were rinsed twice in a modified Leibovitz's L-15 medium, pinned out in ethanol- and UV-sterilized Sylgard-coated (Dow Corning) petri dishes (60 mm diameter), and then incubated in the modified medium. The culture medium contained Leibovitz's L-15 medium with L-glutamine at 300 mg/l (GIBCO/BRL) and with the following additions made to bring the salt concentration to levels suitable for incubation of lobster tissues: NaCl was adjusted to 462 m*M;* KCl to 16 m*M;* $CaCl_2$ to 26 m*M;* $MgCl_2$ to 8 m*M;* and glucose to 11 m*M;* HEPES buffer (pH 7.4) at 10 m*M* (all salts from Sigma); fetal bovine serum (GIBCO/BRL) at a final concentration of 10%. Antibiotics and antifungal agents were added at the same concentrations specified above. Nerve cords were cultured at 16°C in an air incubator (Isotemp, Fisher) and the culture medium was changed twice weekly.

Lobster ganglion labeling and autoradiography

Labeling and autoradiography were carried out according to the method of Hendelman and Bunge (1969). Lobster ganglia were incubated in medium containing 10 μ*M* ^{3}H-uridine (RNA labeling) or 10 μ*M* ^{3}H-leucine (protein labeling) at high specific activity (New England Nuclear). Tissues were fixed in 2% osmium tetroxide buffered with veronal acetate (pH 7.4) with added $CaCl_2$ (0.05%) (all chemicals from Sigma). After several washes, ganglia were dehydrated in a graded ethanol series and embedded in a mixture of 10 parts Epon 812 (Structure Probe, Inc. (SPI)); 10 parts Aralidite 6005 (SPI); 24 parts DDSA (dodecenyl succinic anhydride, SPI); and 2% DMP-30 (2,4,6-tris(dimethylaminomethyl)phenol, Sigma). Sections of 1–1.5 μm were cut and autoradiographed at 4°C in Ilford L-4 emulsion (Ferranti-Dege). Slides were developed with D-19 (Kodak) and mounted in glycerin. Two experimental sets were examined in detail using this method. In one, pairs of ganglia were incubated in organ culture for 2 days or for 49 days, before incubation for 4 h in ^{3}H-leucine or ^{3}H-uridine, followed by 20 h of washout in nonradioactive medium, fixation and processing all as described above. In the second experimental set, ganglia were cultured for 30 and 45 days *in vitro* before labeling, fixation, and autoradiography.

GABA measurements

GABA in single cells was measured by the original assay method of Jakoby and Scott (1959). This method uses the enzymes GABA-glutamic transaminase and succinic semialdehyde dehydrogenase to generate spectrophotometrically detectable triphosphopyridine nucleotide (reduced) in direct proportion to the amount of GABA in a sample. Single-cell-body isolation, extraction, and enzyme measurements were carried out as described in Otsuka *et al.* (1967).

RNA reagents

Capped GFP cRNA was transcribed from Xho1-linearized pSEM/GFP (generously provided by Richard Dearborn, see Dearborn *et al.*, 1998) (enzyme from New England Biolabs) using the CapScribe SP6 kit (Boehringer Mannheim) and following the manufacturer's instructions. β-galactosidase-encoding cRNA was transcribed from pCMV-SPORT-β-gal (GIBCO/BRL, linearized with XmnI, New England Biolabs) by the same method. RNA quality and quantity were monitored by gel electrophoresis and UV spectrophotometry. The solutions used for injection contained cRNA at 0.5 to 1 μg/μl and included 0.1 U/μl of RNase inhibitor (RNasin, Promega).

RNA was introduced into the cytoplasm of lobster neurons by pressure injection through an intracellular recording electrode (pressure at compressor: 5–20 psi). Glass capillaries (Drummond Scientific Company) were baked overnight at 300°C to facilitate filling and to remove possible sources of RNase activity; microelectrodes were pulled (Narishige PE-2) and the tips were broken to less than 4 μm by tapping them against a fine glass rod under a compound microscope at 200× magnification. Electrodes were filled by first dipping their tips into 2 μl of the electrode solution (see below) on a small piece of Parafilm (American National Can). The remaining solution was picked up using a pipette tip and injected into the back of the electrode, where it quickly ran to the tip by capillarity. Electrodes were mounted in an electrode holder (MEH2RW, World Precision Instruments (WPI)) fitted with a silver wire long enough to make electrical contact with the solution in the tip of the electrode. The electrode wires were treated with RNaseZap! solution (Ambion), with care taken in loading the RNA solution to avoid RNase contamination. Potassium acetate was added to the RNA samples to a final concentration of 0.5 *M*, along with 0.05% phenol red (Sigma) for visualization. Control injections revealed that phenol red did not interfere with the fluorescence detection or the viability of the cells, and appeared to diffuse out of injected cells within a few hours. Cells were injected slowly with RNA solution until the somata appeared slightly red.

DNA reagents

Plasmid DNA was injected in the same way as was the RNA. Purified DNAs including the following constructs were injected at concentrations ranging from 0.1 to 5 μg/μl: (i) *Drosophila melanogaster* neuron-specific *elav* promoter (Yao and White, 1994) driving a β-galactosidase reporter gene (gift from Dr. Thomas Schwarz); (ii) human CMV immediate early enhancer/promoter (Thomsen *et al.*, 1984) driving a fusion of the human β-2 adrenergic receptor and the *Aequoria victoria* GFP (gift from Dr. Timothy McClintock); and (iii) *Drosophila melanogaster* heat-shock inducible promoter from *hsp70* (Pelham, 1982) driving GFP.

Physiological recordings

Intracellular recordings from neuronal somata were performed with glass microelectrodes filled with 1.0 *M* potassium acetate (12–25 MΩ resistance). For injections, this solution was replaced by a mixture of 0.5 *M* potassium acetate and the molecular constructs to be injected (3–5 MΩ resistance). Electrical signals were amplified with an Axoprobe 1A amplifier (Axon Instruments). The cells were physiologically identified by their synaptic input and antidromic stimulation of their axons in the 3rd roots following criteria defined by Otsuka and coworkers (1967). Nerve roots were stimulated by placing their cut ends into closely fitting suction electrodes. Electrical stimuli were generated and delivered by a Master-8 stimulus generator (A.M.P.I.) with built-in isolation units.

Detection of cRNA expression

Injected neurons were periodically monitored, using confocal fluorescence microscopy, for GFP expression or for β-galactosidase activity. Nerve cords were transferred from culture vessels to sterile, medium-filled, deep-well microscope slides that had a thin coat of Sylgard on their lower surfaces. The cords were pinned out, coverslipped, and observed with a scanning laser confocal microscope equipped with FITC filters (MRC 600, Bio-Rad). For β-galactosidase activity determinations, fluorescein di-(β-D-galactopyranoside)(Sigma) dissolved in dimethyl sulfoxide to make a final concentration of 0.67 mg/ml was added to the medium on ice after the preparation had been transferred to the slide.

For GFP measurements, 6.5-μm optical sections were taken through the cell body region of the injected cell and images recorded using the confocal microscope's photomultiplier tubes at various times after injection. For β-galactosidase measurements, a single section was scanned as quickly as possible after transferring the slide to the microscope, and the increase in fluorescence with time was measured over the next 35–40 min in periodic scans. Fluorescence was quantified by measuring average pixel intensity for comparable single sections using NIH Image software (Shareware by Wayne Rasband, National Institutes of Health). Following each imaging session, preparations were rinsed again in sterile saline and lobster L-15 and repinned in the culture dish; the culture was continued at 16°C.

Results

Survival of central neurons in long-term organ culture

The ventral nerve cord was removed from an adult lobster and maintained in a modified Leibovitz L-15 culture medium for at least 7 weeks. Over this period, identified neurons maintained features typical of their condition in the short-term preparation routinely used for physiological experiments (usually from 12 to 36 h).

Physiology of neurons. The positions of the somata of many neurons in the lobster ventral nerve cord have been mapped (Otsuka *et al.*, 1967; Beltz and Kravitz, 1983; Schwarz *et al.*, 1984; Schneider *et al.*, 1993). Cell bodies can be reliably and readily identified from preparation to preparation by their relative sizes, their position in a ganglion, their endogenous and nerve-evoked synaptic input, their spontaneous activity, and by backfiring their axons. To illustrate, 12, a large GABA-containing inhibitory motor neuron innervating the fast flexor muscles, was studied in a preparation maintained for 49 days in culture (Fig. 1). As shown in the schematic, an intracellular recording electrode was placed in the putative 12 cell in this ganglion, and stimulating electrodes were placed on the anterior connective (point 1) and contralateral 3rd root of the ganglion (point 2). Stimulation of the contralateral 3rd root led to the appearance in the cell body of small action potentials (action potentials do not invade these somata) that retained a constant amplitude with increasing intensities of stimulation. No other large cell bodies showing this property were seen in that location, hence the identification of the cell as 12 is highly likely and further supported by the demonstration that these neurons contain GABA. In contrast, with increasing levels of stimulation of the anterior connective (point 1, Fig. 1, left), excitatory postsynaptic potentials measured in 12 increased in amplitude, finally generating action potentials in these cells. This suggests that a progressive recruitment of presynaptic inputs to 12 is occurring, and that these inputs, too, have survived the long-term organ culture. When the connective between electrode 1 and the ganglion was crushed, excitation of 12 *via* this route was abolished (Fig. 1, top right), thereby assuring that the responses seen were not due to current spread from the stimulating electrode. Resting membrane potentials in 12 and other cells in this and in other experiments were within normal ranges (−50 to −65 mV, data not shown). GABA was detected in 12 cell somata dissected from organ-cultured ganglia at concentrations normally found in 12 cell bodies from freshly dissected preparations [fresh preparations—0.79 ± 1.75 × 10^{-10} moles/cell body (mean ± SD, $n = 14$) (Otsuka *et al.*, 1967); 6-week cultures—1.1 ± 7.11 × 10^{-10} moles/cell body (mean ± SD, $n = 4$)].

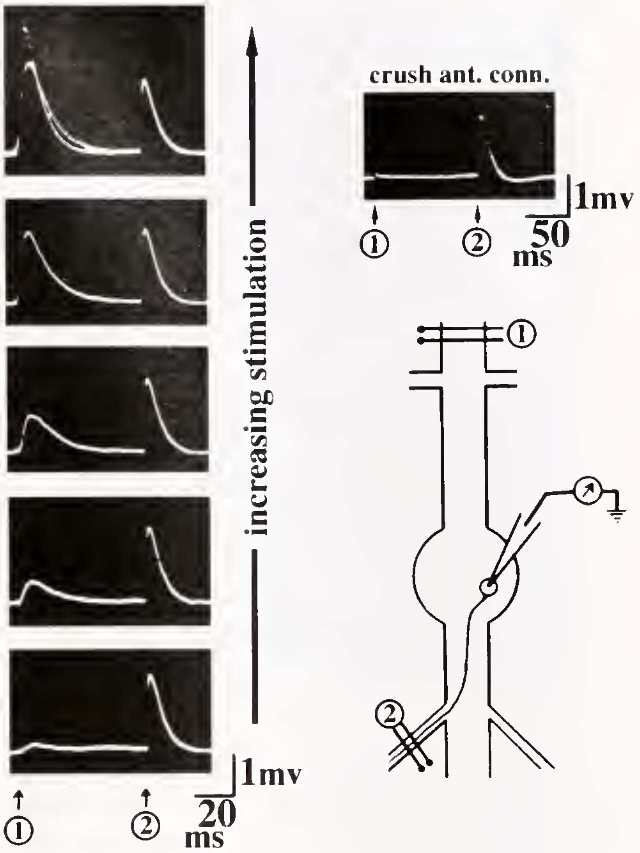

Figure 1. Normal activity in a lobster ganglion maintained in organ culture for 49 days. While recording intracellularly from an abdominal GABA-containing cell, 12, the preparation was stimulated from the anterior connective (point 1). Increasing stimulation intensity (left panel, bottom to top) elicited an increasing excitatory response in 12 (at point 1) that finally triggered an action potential. After the anterior connective was crushed between the stimulating electrode and the ganglion, the EPSPs in 12 disappeared (upper right). When the 3rd root was stimulated directly (point 2 at right), an antidromic action potential was triggered in 12 and recorded in the cell body. As expected, the action potential showed no size change with increasing stimulus intensity.

Evidence of RNA synthesis by neurons. RNA synthesis in cultured nerve cords was measured by radiolabeled precursor incorporation and autoradiography. In Figure 2, one example is presented. Lobster ganglia maintained in organ culture for 2 and 49 days were incubated in medium containing ^{3}H-uridine for 4 h, followed by a washout with unlabeled medium for 20 h. Ganglia were fixed, embedded, and sectioned, and autoradiography was performed. Silver grains are readily seen over the nuclei of neurons and glial cells (Fig. 2). These represent the location of newly synthesized RNA and demonstrate that neurons in long-term culture still actively transcribe RNA. Qualitatively, we saw

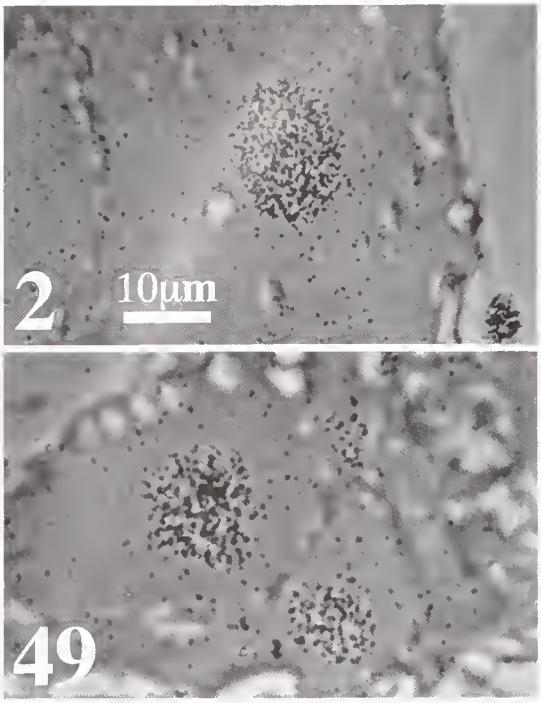

Figure 2. Autoradiography of newly synthesized RNA in lobster ganglia maintained for 2 and 49 days *in vitro*. Ganglia were treated with ^{3}H-uridine for 4 h, followed by a chase with unlabeled medium for 20 h. Following fixation, samples were embedded and sectioned, and autoradiography was performed. The resulting silver grains clustered primarily at the nuclei of cells cultured for 2 and 49 days indicate the presence of nascent RNA.

little difference in grain density between the 2-day and 49-day organ cultures.

Similar labeling experiments were performed after other times of incubation with both ^{3}H-uridine and ^{3}H-leucine. In the latter experiments, a cytoplasmic rather than nuclear distribution of silver grains was noted after autoradiography, indicating the synthesis of protein in the cultured ganglia (data not shown).

Cytology of ganglia. Some indication of overall health can be seen in the cytology of cultured ganglia. Cells of ganglia cultured for the longer time period appeared similar to cells of recently dissected ganglia, although the former usually had larger spaces between cells (not shown). Rarely, opaque or darkly colored cells were observed in cultured lobster ganglia, such as those shown in Figure 3 (bottom panel). These cells typically had low or no resting potentials and were likely to be dead or dying. Another feature of unhealthy cells is their slight autofluorescence (Fig. 3, top). The bright cell in Figure 3, top panel, is a GFP-expressing cell. As seen in bright-field illumination (Fig. 3, bottom panel), the GFP-expressing cell is transparent, whereas the two weakly fluorescent cells are opaque. The death of these two cells resulted from experimental DNA injection, described below. The numbers of spontaneously unhealthy cells was generally low throughout the culture period: most cells and their processes appeared morphologically undistinguishable from their counterparts in freshly dissected ganglia.

Expression of introduced RNAs in organ-cultured neurons

A single injection of cRNA for either GFP or β-galactosidase into central neurons in cultured ganglia led to the synthesis of these proteins. Their presence was detected with fluorescence and confocal microscopy, either directly in the case of GFP, or indirectly for β-galactosidase, by adding a fluorogenic substrate for the enzyme. Measurements were made by periodically locating the same injected cell in organ-cultured cords.

Induction of GFP expression. An identified cell, usually I2, M6, or M7, was pressure-injected with the cRNA for GFP and maintained in organ culture for periods of up to 10 days. At various time points the injected ganglia were imaged using a confocal fluorescence microscope to detect and measure GFP expression. GFP fluorescence in this cell was detected after one day, increased until day 4, then decreased to background

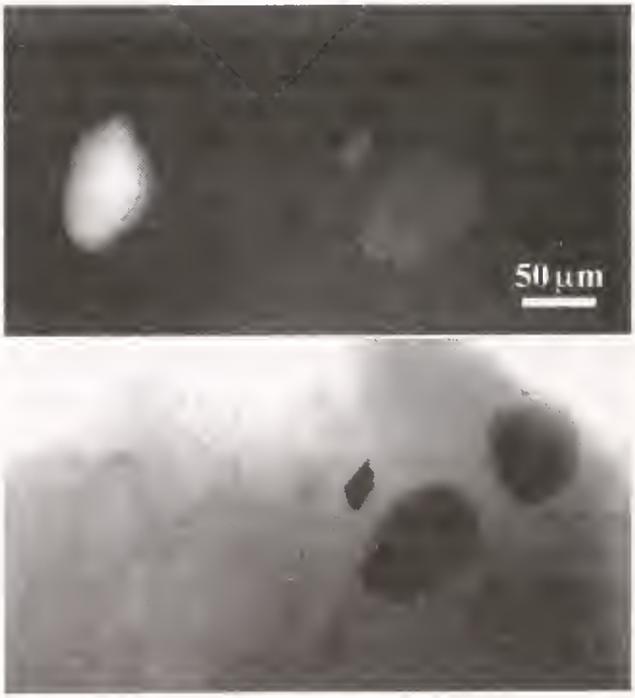

Figure 3. Comparison of a GFP-expressing neuron with two cells injected with high concentrations of plasmid DNA. The highly fluorescent cell seen with epifluorescent illumination (top panel) was injected with cRNA encoding green fluorescent protein (GFP). After 3 days of incubation, this cell appeared clear under bright-field illumination (bottom). In contrast, two cells injected with plasmid DNA fluoresced only weakly (top) and were opaque under bright-field illumination (bottom). These cells had poor (or no) resting membrane potentials and resembled untreated cells that occasionally died during prolonged organ culture.

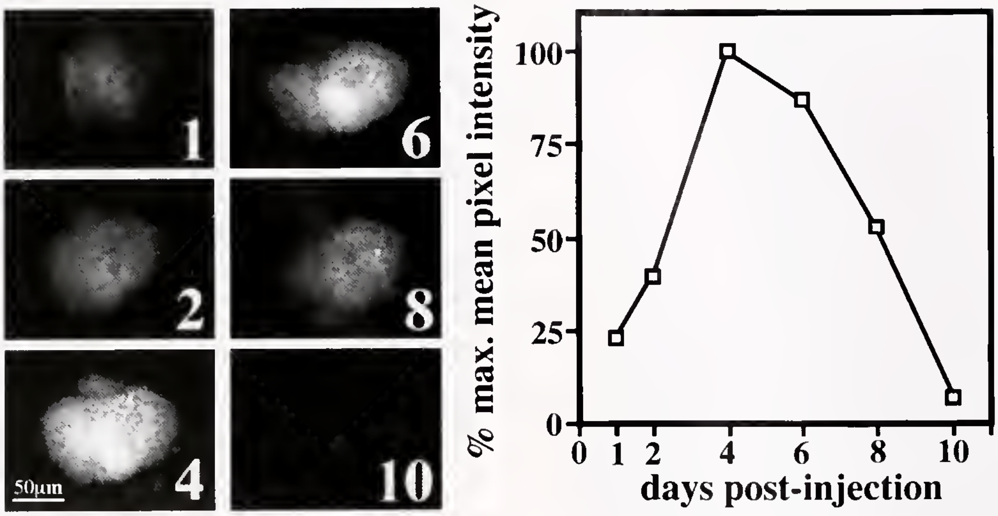

Figure 4. Time course of GFP expression after injection of cRNA. (Left) A single neuron injected with GFP-encoding cRNA was photographed, using a confocal fluorescent microscope, at various time points (in days) following injection. (Right) The intensity of fluorescence increased to a maximum at day 4, then declined to background at day 10.

by day 10 (Fig. 4). Other cells injected with this cRNA showed similar patterns of expression.

As the level of GFP fluorescence declined from its peak, its distribution in injected cells became patchy. In a few injections, GFP distribution was uniform in the cytoplasm but later became punctate, and the protein product appeared to be excluded from certain areas of the cytoplasm. In many cases, GFP fluorescence was seen in the primary neurite leaving the cell body (Fig. 5). However, we were unable to detect a GFP signal in deeper layers of the neuropil, in connectives, or in peripheral nerves.

Induction of β-galactosidase expression. Injection of the cRNA for β-galactosidase into cell somata resulted in enzyme activity detectable in cultured neurons within 2 days. Expression of this enzyme was determined by using the fluorogenic substrate fluorescein di-(β-D-galactopyranoside) to measure activity. Hence, we did not directly measure the amount of protein synthesized. Since enzyme activity probably was directly related to the amount of protein present, levels of expression of β-galactosidase apparently peaked between 6 and 9 days after injection. Strong β-galactosidase activity was still easily detectable in cultured ganglia 10 days after cRNA injection (Fig. 6). The fluorescence intensity increased rapidly and close to linearly in a β-galactosidase-expressing cell following addition of the fluorogenic substrate. Since the fluorescent cleavage product leaves the cells within a few hours, the same cells can be repeatedly tested for β-galactosidase activity on consecutive days.

Injection of DNA into lobster neurons

We attempted to induce reporter gene expression by the cytoplasmic microinjection of plasmid DNA. Identified cells were injected with DNA constructs containing three different promoters: the human CMV immediate early enhancer/promoter; *Drosophila melanogaster hsp70;* and *D. melanogaster elav* promoter driving either GFP or β-galactosidase. Injections of low concentrations of DNA (below 1 μg/μl in the electrode) had no detectable toxic effect on cells, whereas injections of DNA at concentrations above 1 μg/μl led to cell death. Most cells injected with higher levels of DNA became opaque and autofluorescent within 1 to 2 days (see Fig. 3), and all such cells showed low or no resting membrane potentials, indicating that they were dead or in the process of dying. In no case (low or high concentrations of DNA), however, did we observe any protein product expression.

Discussion

We have used an organ culture method to maintain the isolated central nerve cord of the lobster for up to 7 weeks, a significant extension beyond the 1 to 2 days previously possible. During this time RNA and protein synthesis, as well as physiological activity in identified neurons, appeared normal. This technique makes possible a range of long-term experiments, including study of the effects of pharmacological and hormonal treatment on the central nervous system, and the effects of manipulation of gene expression in central neurons.

Long-term culture of lobster ventral nerve cord

Ventral nerve cord preparations of crustaceans are valuable for exploring central circuitries because they allow absolute identification of neurons (see Otsuka *et al.*, 1967; Kennedy *et*

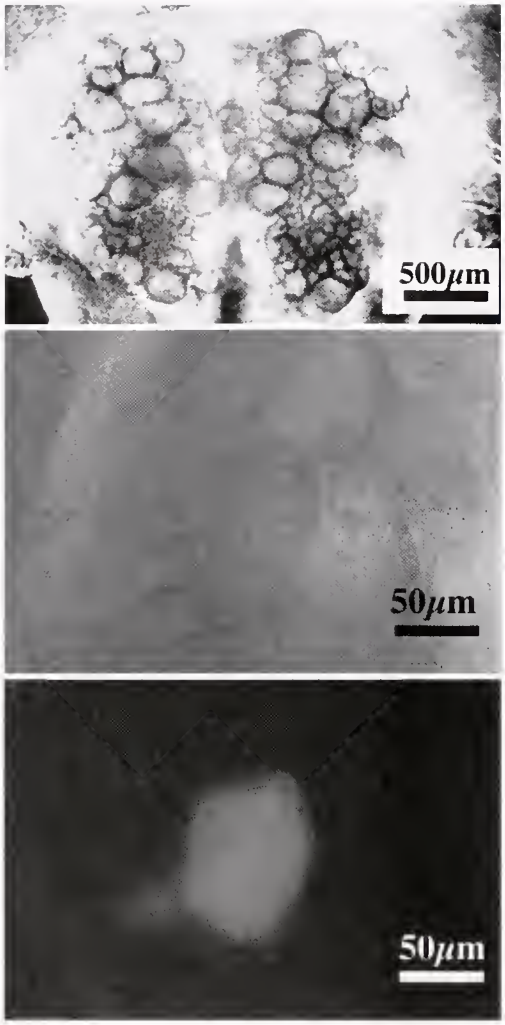

Figure 5. Lobster neuron injected with GFP cRNA. (Top) A desheathed lobster central ganglion at low magnification. (Middle) High-magnification view of an injected cell (center) under bright field illumination. (Bottom) The same view in dark field, showing fluorescent signal from the expressed GFP protein. The signal fills the injected soma and can be seen in the proximal section of the primary neurite as it descends into the neuropil.

al., 1969; Roberts *et al.*, 1982; Beltz and Kravitz, 1987; Ma *et al.*, 1992; Yeh *et al.*, 1996; Hörner *et al.*, 1997). Once exposed by removal of the connective tissue sheath, the somata of these neurons are easily visible and accessible to microelectrodes. Cells occur in predictable arrangements and can be unambiguously identified by their position, size, and activity, and by backfiring their axons from roots or connectives (Otsuka *et al.*, 1967). In our laboratory, preparations of this type have been used to explore the roles of amines in the neural networks involved in postural regulation (Harris-Warrick and Kravitz, 1984; Beltz and Kravitz, 1987; Ma *et al.*, 1992; Weiger and Ma, 1993). In crayfish, similar preparations have been used to define changes in synaptic properties accompanying changes in social status at particular synaptic sites (Yeh *et al.*, 1996).

In the organ culture system described here, we showed that neurons are suitable for electrophysiological experimentation for at least 7 weeks. We used only one example for illustration. In Figure 1 we showed that the large inhibitory motoneuron I2 could be activated by backfiring its axon at a distance of several centimeters from the cell body, and that interneurons upstream of I2 still could relay signals *via* the release of transmitters. Moreover, in single I2 cells dissected from long-term organ cultures of ganglia, the intracellular levels of GABA were comparable to those found in cells dissected from fresh preparations.

The autoradiographic studies demonstrated that neurons in ganglia cultured for 49 days still synthesized RNA (Fig. 2) and protein (data not shown). In addition, at a light microscopic level, the cytology of cultured neurons appeared normal, except for a somewhat more frequent vacuolar appearance of cell somata, and for larger spaces between cells and neuropil processes. These differences may result from looser cell packing in the excised and desheathed ganglia, from degeneration of sensory fibers from the periphery (Barker *et al.*, 1972), or both.

Cells that do not survive in organ culture appear dark with light microscopy and their autofluorescence is weak, making them easy to distinguish from surviving cells. Autofluorescence of unhealthy or dead cells has been reported elsewhere (Linnik *et al.*, 1993; Kosslak *et al.*, 1997), and is a useful way to prevent making comparisons between these cells and healthy cells in the cultures (O'Brien *et al.*, 1995). It is important to identify such cells so that their fluorescence is not confused with that of experimental markers like GFP.

GFP and LacZ *are suitable expression markers in lobster neurons*

GFP and *LacZ* (the gene encoding β-galactosidase) have been used as reporter and marker genes in studies involving a wide variety of organisms (see Chalfie, 1995). Lobsters and crayfish (see Dearborn *et al.*, 1998) now can be added to the list of organisms capable of expressing these proteins. The studies presented here, and those reported by Dearborn *et al.* (1998), suggest that it may be possible to use GFP and β-galactosidase as injection markers, as reporters for transcriptional studies, and as tags that can be fused to proteins under study in crustacean systems. To illustrate the latter, in preliminary studies (G. Ganter, unpubl. obs.), we have found that intracellular injections of cRNAs encoding a human β-2 adrenergic receptor/GFP fusion and a lobster amine receptor/GFP fusion result in fluorescent signals. Although different cRNAs might show differences in their rates of translation, thus far all cRNAs that we have injected have been expressed. Indeed, the different times we noted for peak detection of β-galactosidase and GFP could be due to differences in the translation rates of these two transcripts.

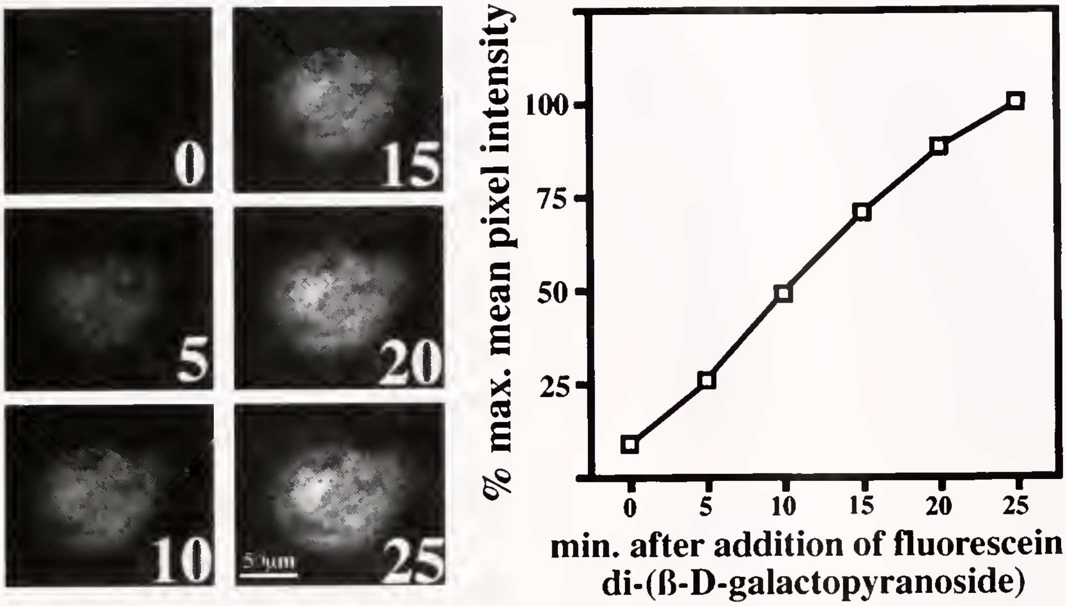

Figure 6. β-galactosidase activity in a lobster neuron maintained 10 days in organ culture after injection with *LacZ* cRNA. β-galactosidase activity was detected in a living injected cell by addition of a fluorogenic substrate, fluorescein di-(β-D-galactopyranoside). (Left) The cell was photographed, using a confocal fluorescent microscope, at various time points (in minutes) following addition of the substrate. (Right) The intensity of fluorescence increased almost linearly.

Future uses of the organ culture method

Long-term organ culture offers a controlled environment in which to perform experiments that were difficult to carry out in short-term studies using isolated nerve cords. This should allow us to explore the consequences of applying test substances to central ganglia in more biologically relevant time frames. For example, the lobster molting hormone, 20-hydroxyecdysone, is likely to have actions at both membrane and genomic levels (see Zakon, 1998). The genomic effects may take days to bring about observable changes at synaptic or circuit levels. The organ culture system offers enough time for such changes to be seen, in an environment in which tissues will continue to synthesize the RNA and protein required to trigger the changes. Long-term drug effects relating to aminergic function also can be examined in the cultured ganglia. At present we are particularly interested in chronic exposure of ganglia to Prozac (fluoxetine). In behavioral studies, acute exposure to Prozac has little effect on agonistic behavior in lobsters (Huber *et al.*, 1997); in contrast, chronic exposure increases the amount of time that animals are willing to fight (A. Delago, unpubl. obs.).

Another exciting application of the organ culture method is in the experimental manipulation of gene expression in identified neurons. The extended time frame makes it possible to examine the effects of gene expression on the physiology of cRNA-injected neurons and to analyze cloned genes in their native environment. For example, the serotonin-containing neurosecretory neurons of lobster appear to lack the mRNA for the *shab* form of the potassium channel (H. Schneider, unpubl. obs.). It would be interesting to express *shab* in these neurons, and then examine the consequences of this manipulation on the intrinsic properties of the injected cell and on the network in which it functions. Other applications could include injections of sense, antisense, or double-stranded RNAs coding for particular proteins into cells to ask how such manipulations alter function. These and other applications await further exploitation of this important system.

Summary and conclusions

We describe an organ culture method that maintains isolated lobster ganglia in viable states for up to 7 weeks. We have validated the method, showing that evidence of gene expression and electrophysiological activity persist throughout the culture period. Applications include long-term experiments to examine the consequences of chronic treatment with pharmacological or hormonal reagents and of changes to the levels of expression of particular genes in single neurons and in networks of neurons. The ability to introduce genes into lobster nerve cells should allow analysis of the function of these genes in their native environment, narrowing the gap between molecular methods and the study of physiology in this important system.

Acknowledgments

We acknowledge Dr. Gary N. Cherr, Dr. Frederick J. Griffen, and Ms. Carol Vines for help with confocal microscopy; the staff of the Bodega Marine Laboratory, Dr. Ernest S. Chang, and Ms. Sharon Chang for providing technical support, and a rich environment; and the University of California, Davis, for the fellowship support that funded these studies. We also thank Drs. Margaret Bradley and Stuart Cromarty for their ideas about the project and their helpful comments on the manuscript. This research was supported by a grant from the National Science Foundation (to EAK) and by a post-doctoral fellowship from the Alexander von Humboldt Foundation (to RH).

Literature Cited

Aisemberg, G. O., T. R. Gershon, and E. R. Macagno. 1997. New electrical properties of neurons induced by a homeoprotein. *J. Neurobiol.* **33:** 11–17.

Barker, D. L., E. Herbert, J. G. Hildebrand, and E. A. Kravitz. 1972. Acetylcholine and lobster sensory neurons. *J. Physiol.* **226:** 205–229.

Beltz, B. S., and E. A. Kravitz. 1983. Mapping of serotonin-like immunoreactivity in the lobster nervous system. *J. Neurosci.* **3:** 585–602.

Beltz, B. S., and E. A. Kravitz. 1987. Physiological identification, morphological analysis and development of identified serotonin-proctolin containing neurons in the lobster ventral nerve cord. *J. Neurosci.* **7:** 533–546.

Chalfie, M. 1995. Green fluorescent protein. *Photochem. Photobiol.* **62:** 651–6.

Chalfie, M., Y. Tu, G. Euskirchen, W. W. Ward, and D. C. Prasher. 1994. Green fluorescent protein as a marker for gene expression. *Science* **263:** 802–804.

Dawid, I. B., and T. D. Sargent. 1988. *Xenopus laevis* in developmental and molecular biology. *Science* **240:** 1443–1448.

Dearborn, R. E., Jr., B. G. Szaro, and G. A. Lnenicka. 1998. Microinjection of mRNA encoding rat synapsin Ia alters synaptic physiology in identified motoneurons of the crayfish, *Procambarus clarkii. J. Neurobiol.* **37:** 224–236.

Gerdes, H. H., and C. Kaether. 1996. Green fluorescent protein: applications in cell biology. *FEBS Lett.* **389:** 44–47.

Harris-Warrick, R. M., and E. A. Kravitz. 1984. Cellular mechanisms for modulation of posture by octopamine and serotonin in the lobster. *J. Neurosci.* **4:** 1976–1993.

Hendelman, W. J., and R. P. Bunge. 1969. Radioautographic studies of choline incorporation into peripheral nerve myelin. *J. Cell Biol.* **40:** 190–208.

Hörner, M., W. A. Weiger, D. H. Edwards, and E. A. Kravitz. 1997. Excitation of identified serotonergic neurons by escape command neurons in lobsters. *J. Exp. Biol.* **200:** 2017–2033.

Huber, R., K. Smith, A. Delago, K. Isaksson, and E. A. Kravitz. 1997. Serotonin and aggressive motivation in crustaceans: altering the decision to retreat. *Proc. Natl. Acad. Sci. USA* **94:** 5939–5942.

Jakoby, W. B., and E. M. Scott. 1959. Aldehyde oxidation. III. Succinic semialdehyde dehydrogenase. *J. Biol. Chem.* **234:** 937–940.

Kaang, B.-K., P. J. Pfaffinger, S. G. N. Grant, and E. R. Kandel. 1992. Overexpression of an *Aplysia* Shaker K^+ channel gene modifies the electrical properties and synaptic efficacy of identified *Aplysia* neurons. *Proc. Natl. Acad. Sci. USA* **89:** 1133–1137.

Kennedy, D., A. I. Selverston, and M. P. Remler. 1969. Analysis of restricted neural networks. *Science* **164:** 1488–1496.

Kosslak, R. M., M. A. Chamberlin, R. G. Palmer, and B. A. Bowen. 1997. Programmed cell death in the root cortex of soybean root necrosis mutants. *Plant J.* **11:** 729–745.

Lalumiere, M., and C. D. Richardson. 1995. Production of recombinant baculoviruses using rapid screening vectors that contain the gene for beta-galactosidase. *Meth. Mol. Biol.* **39:** 161–177.

Linnik, M. D., M. D. Hatfield, M. D. Swope, and N. K. Ahmed. 1993. Induction of programmed cell death in a dorsal root ganglia X neuroblastoma cell line. *J. Neurobiol.* **24:** 433–446.

Livingstone, M. S., R. M. Harris-Warrick, and E. A. Kravitz. 1980. Serotonin and octopamine produce opposite postures in lobsters. *Science* **208:** 76–79.

Ma, P. M., and W. A. Weiger. 1993. Serotonin-containing neurons in lobsters: the actions of γ-aminobutyric acid, octopamine, serotonin, and proctolin on activity of a pair of identified neurons in the first abdominal ganglion. *J. Neurophysiol.* **69:** 2015–2029.

Ma, P. M., B. S. Beltz, and E. A. Kravitz. 1992. Serotonin-containing neurons in lobsters: their role as "gain-setters" in postural control mechanisms. *J. Neurophysiol.* **68:** 36–54.

MacGregor, G. R., A. E. Mogg, J. F. Burke, and C. T. Caskey. 1987. Histochemical staining of clonal mammalian cell lines expressing *E. coli* beta-galactosidase indicates heterogeneous expression of the bacterial gene. *Somatic Cell Mol. Genet.* **13:** 253–265.

O'Brien, M. C., and W. E. Bolton. 1995. Comparison of cell viability probes compatible with fixation and permeabilization for combined surface and intracellular staining in flow cytometry. *Cytometry* **19:** 243–255.

Otsuka, M., E. A. Kravitz, and D. D. Potter. 1967. The physiological and chemical architecture of a lobster ganglion with particular reference to gamma-aminobutyrate and glutamate. *J. Neurophysiol.* **30:** 725–752.

Pelham, H. R. 1982. A regulatory upstream promoter element in the *Drosophila hsp70* heat-shock gene. *Cell* **30:** 517–528.

Prasher, D. C., V. K. Eckenrode, W. W. Ward, F. G. Prendergast, and M. J. Cormier. 1992. Primary structure of the *Acquoria victoria* green-fluorescent protein. *Gene* **111:** 229.

Roberts, A., F. B. Krasne, G. Hagiwara, J. J. Wine, and A. P. Kramer. 1982. Segmental giant: evidence for a driver neuron interposed between command and motor neurons in the crayfish escape system. *J. Neurophysiol.* **47:** 761–781.

Schneider, H., B. Trimmer, J. Rapus, M. Eckert, D. Valentine, and E. A. Kravitz. 1993. Mapping of octopamine-immunoreactive neurons in the central nervous system of the lobster. *J. Comp. Neurol.* **329:** 129–142.

Schwarz, T. L., G. M.-H. Lee, K. K. Siwicki, D. G. Standaert, and E. A. Kravitz. 1984. Proctolin in the lobster: the distribution, release, and chemical characterization of a likely neurohormone. *J. Neurosci.* **4:** 1300–1311.

Thomsen, D. R., R. M. Stenberg, W. F. Goins, and M. F. Stinski. 1984. Promoter-regulatory region of the major immediate early gene of human cytomegalovirus. *Proc. Natl. Acad. Sci. USA* **81:** 659–663.

Weiger, W. A., and P. M. Ma. 1993. Serotonin-containing neurons in lobsters: the actions of gamma-aminobutyric acid, octopamine, serotonin and proctolin on neuronal activity. *J. Neurophysiol.* **69:** 2015–2029.

Yao, K.-M., and K. White. 1994. Neural specificity of *elav* expression: defining a *Drosophila* promoter for directing expression to the nervous system. *J. Neurochem.* **63:** 41–51.

Yeh, S., R. Fricke, and D. Edwards. 1996. The effect of social experience on serotonergic modulation of the escape circuit of crayfish. *Science* **271:** 366–369.

Zakon, H. H. 1998. The effects of steroid hormones on electrical activity of excitable cells. *Trends Neurosci.* **21:** 202–207.

Zhao, B., F. Rassendren, B.-K. Kaang, Y. Furukawa, T. Kubo, and E. R. Kandel. 1994. A new class of noninactivating K^+ channels from *Aplysia* capable of contributing to the resting potential and firing patterns of neurons. *Neuron* **13:** 1205–1213.

Reference: *Biol. Bull.* **197:** 49–62. (August 1999)

An Ethogram of Body Patterning Behavior in the Biomedically and Commercially Valuable Squid *Loligo pealei* off Cape Cod, Massachusetts

ROGER T. HANLON, MICHAEL R. MAXWELL, NADAV SHASHAR, ELLIS R. LOEW[1], AND KIM-LAURA BOYLE

Marine Resources Center, Marine Biological Laboratory, Woods Hole, Massachusetts 02543; and
[1] *Department of Biomedical Sciences, Cornell University, Ithaca, New York 14853*

Abstract. Squids have a wide repertoire of body patterns; these patterns contain visual signals assembled from a highly diverse inventory of chromatic, postural, and locomotor components. The chromatic components reflect the activity of dermal chromatophore organs that, like the postural and locomotor muscles, are controlled directly from the central nervous system. Because a thorough knowledge of body patterns is fundamental to an understanding of squid behavior, we have compiled and described an ethogram (a catalog of body patterns and associated behaviors) for *Loligo pealei*. Observations of this species were made over a period of three years (≥440 h) and under a variety of behavioral circumstances. The natural behavior of the squid was filmed on spawning grounds off Cape Cod (northwestern Atlantic), and behavioral trials in the laboratory were run in large tanks. The body pattern components—34 chromatic (including 4 polarization components), 5 postural, and 12 locomotor—are each described in detail. Eleven of the most common body patterns are also described. Four of them are chronic, or long-lasting, patterns for crypsis; an example is Banded Bottom Sitting, which produces disruptive coloration against the substrate. The remaining seven patterns are acute; they are mostly used in intraspecific communication among spawning squids. Two of these acute patterns—Lateral Display and Mate Guarding Pattern—are used during agonistic bouts and mate guarding; they are visually bright and conspicuous, which may subject the squids to predation; but we hypothesize that schooling and diurnal activity may offset the disadvantage presented by increased visibility to predators. The rapid changeability and the diversity of body patterns used for crypsis and communication are discussed in the context of the behavioral ecology of this species.

Introduction

Cephalopods have a highly developed system of visual communication that is expressed mainly through the skin. The distinguishing features of this remarkable chromatophore system are its speed of change and the diversity of body patterns that each individual uses for either crypsis or communication (Hanlon and Messenger, 1996). A body pattern is defined as the total appearance of the animal at any given time, and includes the expression of the full complement of *chromatic* (*i.e.*, color or visual), *textural, postural,* and *locomotor* components (see Packard and Hochberg, 1977; Hanlon and Messenger, 1996). Among the components of the body pattern, the most conspicuous are chromatic, although squids probably perceive intraspecific signals monochromatically because cephalopods are thought to be color blind (Hanlon and Messenger, 1996). These chromatic components are produced primarily by chromatophore organs and various reflective cells in the dermis, and they are discrete neural entities (just as postural, textural, and locomotor components are) because the chromatophore organs are controlled by radial muscles under the direct control of the posterior chromatophore lobes in the brain (*e.g.*, Dubas *et al.*, 1986). Most of the reflective cells are also controlled by the squid (Cooper *et al.*, 1990). This neural control enables the cephalopod to change its appear-

Received 1 February 1999; accepted 20 April 1999.

E-mail: rhanlon@mbl.edu

ance in a fraction of a second, depending upon the visual sensory input it receives during behavioral interactions. Few, if any, animals can match the speed of change and diversity of cephalopod signals, and the body patterns are used in most behavioral interactions, whether they be for competition for resources or mates, or interactions between predators and prey. We are documenting these diverse body patterns, focusing primarily on adult squids during their inshore migration every year.

Squids, like other cephalopods, are sensitive to the partial polarization characteristics of light (Saidel *et al.*, 1983; Hanlon and Messenger, 1996; for a description of polarized light see Kattawar, 1994; Wolff and Andreou, 1995). Shashar and Hanlon (1997) described a few specific polarization components of squid and correlated these patterns with the distribution of iridophore cells in the animals' skin. In cuttlefish, partial polarization patterns have been associated with communication (Shashar *et al.*, 1996). Since squids may use polarization patterns for intraspecific communication, and since polarization-sensitive predators may be looking for polarization contrasts to locate squid prey, we also document here some polarization components presented by the squid.

The long-finned squid *Loligo pealei* Lesueur, 1821, is a renowned model in neuroscience research. The third-order giant axon, its attendant giant synapse, the complex eye, and several other organ systems in *L. pealei* have been studied in detail for over 50 years at the Marine Biological Laboratory (MBL) in Woods Hole (see Gilbert *et al.*, 1990). Although a great deal is known about the peripheral nervous system of *L. pealei*, little is known about the behaviors of this squid, which like most cephalopods, has an enormous brain relative to its body size. *Loligo pealei* is also a valuable commercial resource in the northeastern United States—worth about $30 million annually (McKiernan and Pierce, 1995; NEFSC, 1995). Curiously, little is known about the ecology, life history, and behavior of this species (*e.g.*, Verrill, 1880; Drew, 1911; Stevenson, 1934; Griswold and Prezioso, 1981; Summers, 1983; Gilbert *et al.*, 1990; Brodziak and Macy, 1996). The present report is part of a broad-based study that focuses on sexual selection processes in *L. pealei* from two perspectives: as a test of sexual selection theory (*e.g.*, Hanlon, 1996; Hanlon *et al.*, 1997) and as a study of the role that reproductive behavior plays in the life history and population dynamics of the species (Hanlon, 1998).

Materials and Methods

The behavior of *Loligo pealei* can be observed both in a natural setting and in the laboratory because the squids habituate quickly to divers and to laboratory surroundings. Overall, 27.5 h of videotape were analyzed for body patterning and behavior.

During the months of May 1996, May 1997, and May 1998, 103 scuba dives were made on squid spawning grounds by RTH and NS off the southern arm of Cape Cod, Massachusetts. Depths ranged from 3–10 m and most sites were within 2 km of shore between Hyannis and Chatham. Spawning squids were found mostly in or near commercial weir traps whose inner pocket dimensions (or capture arena) were roughly 20 m^2; often there were many thousands of squids in these traps, with a proportion of them actively engaged in reproductive behavior. Water temperatures ranged from about 4° to 13°C, currents were often strong, and visibility was usually poor. On about one-third of the dives, conditions were suitable for video. In total, 16.5 h of dive video were recorded, using video cameras (either analog or digital) in underwater housings, and analyzed, with multi-motion playback machines and high-resolution monitors.

Laboratory trials of mating behavior were performed from May through October in 1996, 1997, and 1998 in the Marine Resources Center of the MBL. Three large tanks were used, each measuring 3 m (diameter) by 1 m (height) and containing about 28,000 l of seawater. Each tank had a substrate of mixed gravel and sand, and a continuous supply of ambient seawater. Animals were acquired by squid jigging (both at night and during the day) off the MBL research vessel *Gemma* in Vineyard and Nantucket Sounds. This method minimizes skin damage for maximal survival in captivity (see Hanlon *et al.*, 1983). Squids were fed live fish (*Fundulus* sp.) daily. Trials involved from three to eight squids in various combinations of males and females. One set of trials was performed in an outdoor pond, 20 m × 20 m × 1 m deep, at the Environmental Systems Laboratory of the Woods Hole Oceanographic Institution. The squids were observed for 440 h in captivity, 11 of which were recorded on video.

All videos were reviewed multiple times, each time looking for only one category of component (*i.e.*, first viewing for chromatic components, second viewing for postural components, third viewing for locomotor components). In the laboratory, chromatic, postural, and locomotor components were recorded on separate data sheets each time they were seen. A chromatic component was recorded if it was expressed for at least 2 s; locomotor and postural components were recorded if they were performed for at least 3 s. All chromatic components were illustrated using a computer graphics program.

Polarization components were recorded using a video polarimeter based on a standard three-tube ENG camera (JVC BY-110) that uses a dichroic prism block for color separation. The dichroic prism has been replaced with a custom-made neutral prismatic splitter (Richter Enterprises, Manhattan Beach, CA) such that each of the three video channels receives 1/3 of the broad-spectrum image input. Since this assembly lacks the color-trimming filters cemented to the original dichroic prism, magnification errors due to pathlength differences were corrected with small quartz discs of appropriate thickness. A small disc of sheet polarizer (Polaroid, HNP'B) was placed immediately in front of each camera tube to impart polarization sensitivity to the channels. The orientation of the polarizers was adjusted so that the color channels now encoded 0°, 45°, and 90° polarization images. The camera electronics encode the three polarization channels as if they were color, making it possible to store all the data on a regular portable videocassette recorder and allowing for immediate viewing of a pseudocolor polarization image on a color monitor. Nonpolarizing elements of the scene have no color, whereas polarizing elements do. The signal in all three channels is identical, and the output of the tubes was adjusted to give white for a saturating faceplate intensity. A polarizer placed in front of the lens such that horizontally polarized light is freely transmitted produces the following normalized signals in the three "color" channels: the R channel signal is 1, the G channel is 0.707, and the B channel is 0. Monochromatic images of the same scene, taken from the three channels separately, were transferred through a frame grabber into the computer and their linear polarization characteristics were analyzed following procedures in Cronin *et al.* (1994). This camera is better suited than previously described polarimeters (Cronin *et al.*, 1994; Wolff and Andreou, 1995; Horvath and Varju, 1997) for recording the polarization patterns of moving animals, because it provides true instantaneous measurements. Technological limitations made it impossible to get the camera in an underwater housing; thus measurements were limited to the laboratory. Furthermore, the light conditions during measurements had to be precisely controlled, thereby allowing only 3 h of recorded footage. During these periods, the squids exhibited only a few behaviors that included fighting, mate guarding, and egg laying.

Ethogram

We constructed an ethogram for *Loligo pealei* on the basis of our field and laboratory observations. The components and body patterns identified (Table I) represent a segment of all behaviors, especially those related to reproduction. In fact, because of the size of the sample, most of the patterning components of the species were probably identified. The more than 440 h of observation far exceed the observation periods in other published accounts of *Loligo* spp. (*e.g.*, Hanlon, 1982, 1988; Hanlon *et al.*, 1983, 1994; Porteiro *et al.*, 1990).

The chromatic components of the ethogram are illustrated in Figures 1 and 3, and some of the postural components are shown in Figure 2. Unlike octopuses and cuttlefishes, loliginid squids do not show textural components in the skin. Table I, which lists all components, includes the number of times that we counted a component on videotape or from observation notes, giving an impression of how commonly it occurs. Unless otherwise indicated, all components and body patterns were shown by both sexes.

Light chromatic components

Chromatic components are produced mainly by the action of dermal chromatophore organs, which number in the hundreds of thousands in an adult squid. *Loligo pealei* has three color classes of chromatophores: yellow, red, and brown. Expansion of the chromatophores darks the skin, while retraction of the chromatophores (and the resultant expression of underlying iridophores) produces a lightening or even brightening effect. Intense darkness produced by maximal expansion and intense brightness produced by maximal retraction mark two ends of a chromatic continuum, and thus it is somewhat arbitrary to assign a component to light or dark. Some of these components are common to other *Loligo* spp., as described by Hanlon (1982) for *Loligo plei*, by Porteiro *et al.* (1990) for *Loligo forbesi*, and by Hanlon *et al.* (1994) for *Loligo vulgaris reynaudii*.

Clear is retraction of all or most chromatophores, thus rendering the animal *translucent* in clear water or white in murky water. In clear water, when viewed against a sand bottom or laterally against the aquatic background (Fig. 2B), the translucence renders the squid cryptic, or camouflaged, and often the Dorsal iridophore splotches are expressed simultaneously. Internal organs, such as the red accessory nidamental gland in females, are often visible. In murky water, Clear appears bright white in most lighting circumstances (*i.e.*, the brightness surpasses the albedo of the greenish water, producing a whitish color). In the immediate vicinity of egg beds, the white form of Clear seems to function as an intraspecific signal to repel other squids; a squid displaying this component is almost always engaged in mate guarding, egg laying, or agonistic bouts (see Fig. 2C). **White arms/head** results from variable retraction of chromatophores on the head and arms (three variations are illustrated in Fig. 1). This component sometimes preceded all white (or clear) in intraspecific encounters; thus, it appears to be a milder signal of alarm or repellent to approaching squids (Fig. 2G). White head/arms is most common in paired females near eggs and is seen when unpaired males approach. **White dorsal stripe** is retraction of chromatophores along a dorsal mantle that is otherwise dark; the stripe may be short or long (Fig. 1). It has been seen in

Table 1

Body patterns and their components in the squid Loligo pealei; *compare Figure 1*

BODY PATTERNS

Chronic (min to hours)	Acute (seconds)
1. Basic Amber Pattern	1. Very Dark
2. Clear Body Pattern	2. Blanch-Ink-Jet Maneuver
3. Countershading	3. Lateral Display
4. Chronic All Dark	4. Mate Guarding Pattern
5. Banded Bottom Sitting	5. Accentuated Testis
6. Chronic Bright White Pattern	

COMPONENTS*

Chromatic

Light:		Dark:	
1. Clear	(861)	1. All dark	(1440)
2. White arms/head	(769)	2. Dark arms/head	(133)
3. White dorsal stripe	(194)	3. Dark head	(853)
4. Accentuated testis (m)	(1179)	4. Dark dorsal stripe	(47)
5. Accentuated oviducal gland (f)	(183)	5. Ventral mantle stripe	(369)
Iridescent:		6. Mantle margin stripe	(283)
6. Dorsal mantle collar iridophores	(≥1000)	7. Dark arm stripes	(38)
7. Iridescent sclera	(167)	8. Fin spots	(195)
8. Dorsal iridophore splotches	(500)	9. Arm spots	(672)
9. Iridescent arm stripes	(338)	10. Infraocular spot	(129)
10. Dorsal iridophore sheen	(32)	11. Bands	(153)
		12. Shaded eye	(190)
Light polarization components:		13. Dark fins	(31)
1. Polarized arms		14. Dark posterior mantle	(42)
2. Skin surface polarization		15. Shaded testis (m)	(11)
3. Polarized eyes		16. Shaded oviducal gland (f)	(16)
4. Polarized dorsal sheen		17. Red accessory nidamental gland (f)	(≈200)
		18. Lateral mantle spot (f)	(147)
		19. Lateral blush (f)	(88)
		20. Weak lateral flame (m)	(13)

Locomotor

1. Inking	(12)
2. Jetting/fleeing	(336)
3. Chasing	(17)
4. Bottom sitting	(45)
5. Egg touching	(120)
6. Parallel positioning	(435)
7. Jockeying and parrying (m)	(62)
8. Fin beating (m)	(93)
9. Forward lunge/grab (m)	(206)
10. Male-parallel mating	(59)
11. Head-to-head mating	(24)
12. Oviposition	(≈300)

Postural

1. Raised arms	(1065)
2. Splayed arms	(667)
3. Drooping arms	(54)
4. Raised & splayed arms	(560)
5. Flared arms	(30)

* Letters in parentheses indicate that the component is sex-specific: f = female; m = male. Numbers indicate how many times each component was observed on video or in laboratory trials.

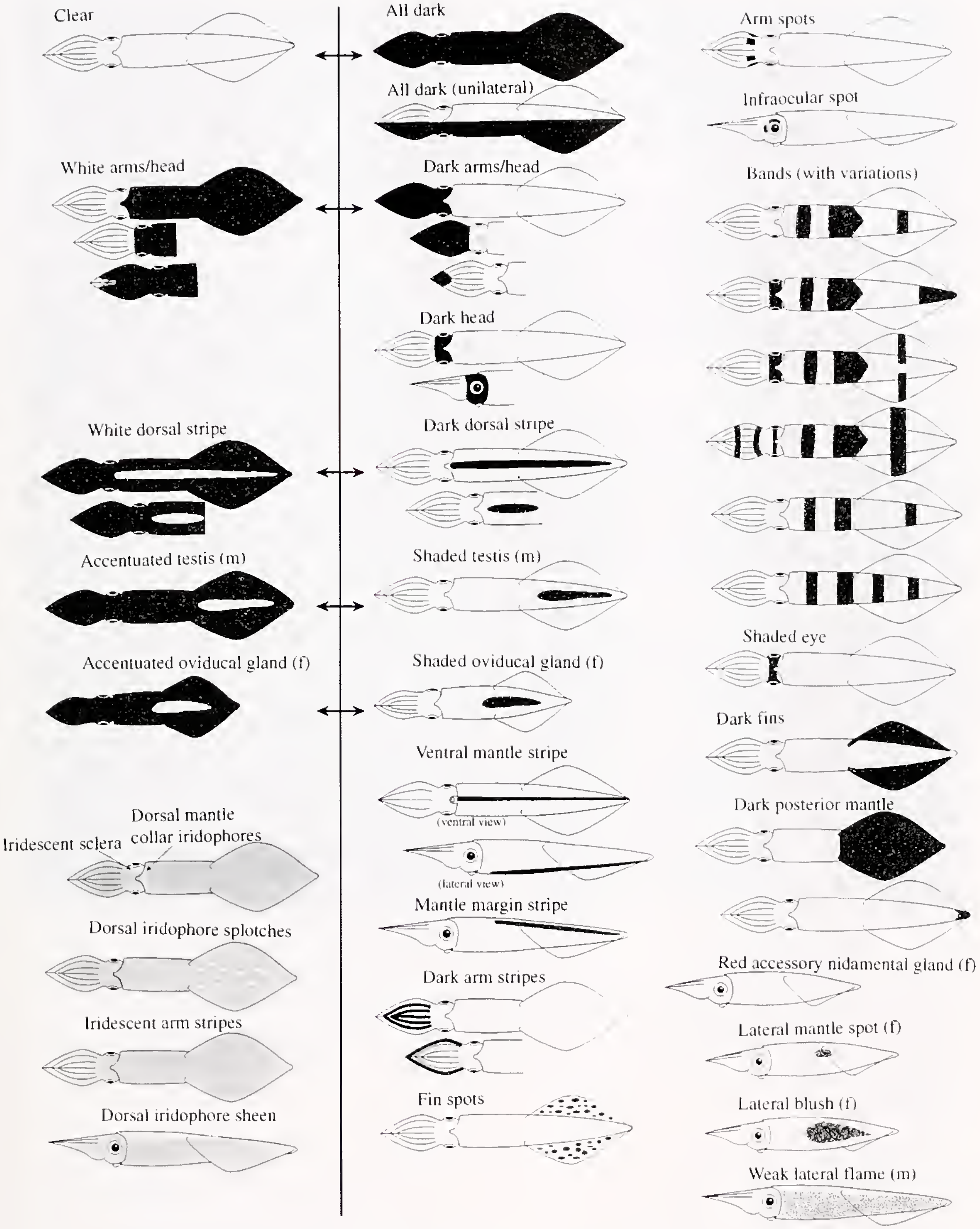
Clear
White arms/head
White dorsal stripe
Accentuated testis (m)
Accentuated oviducal gland (f)
Dorsal mantle collar iridophores
Iridescent sclera
Dorsal iridophore splotches
Iridescent arm stripes
Dorsal iridophore sheen
All dark
All dark (unilateral)
Dark arms/head
Dark head
Dark dorsal stripe
Shaded testis (m)
Shaded oviducal gland (f)
Ventral mantle stripe
(ventral view)
(lateral view)
Mantle margin stripe
Dark arm stripes
Fin spots
Arm spots
Infraocular spot
Bands (with variations)
Shaded eye
Dark fins
Dark posterior mantle
Red accessory nidamental gland (f)
Lateral mantle spot (f)
Lateral blush (f)
Weak lateral flame (m)

Figure 1. Chromatic components of body patterning in the squid *Loligo pealei*. The arrangement generally follows Table I and the text.

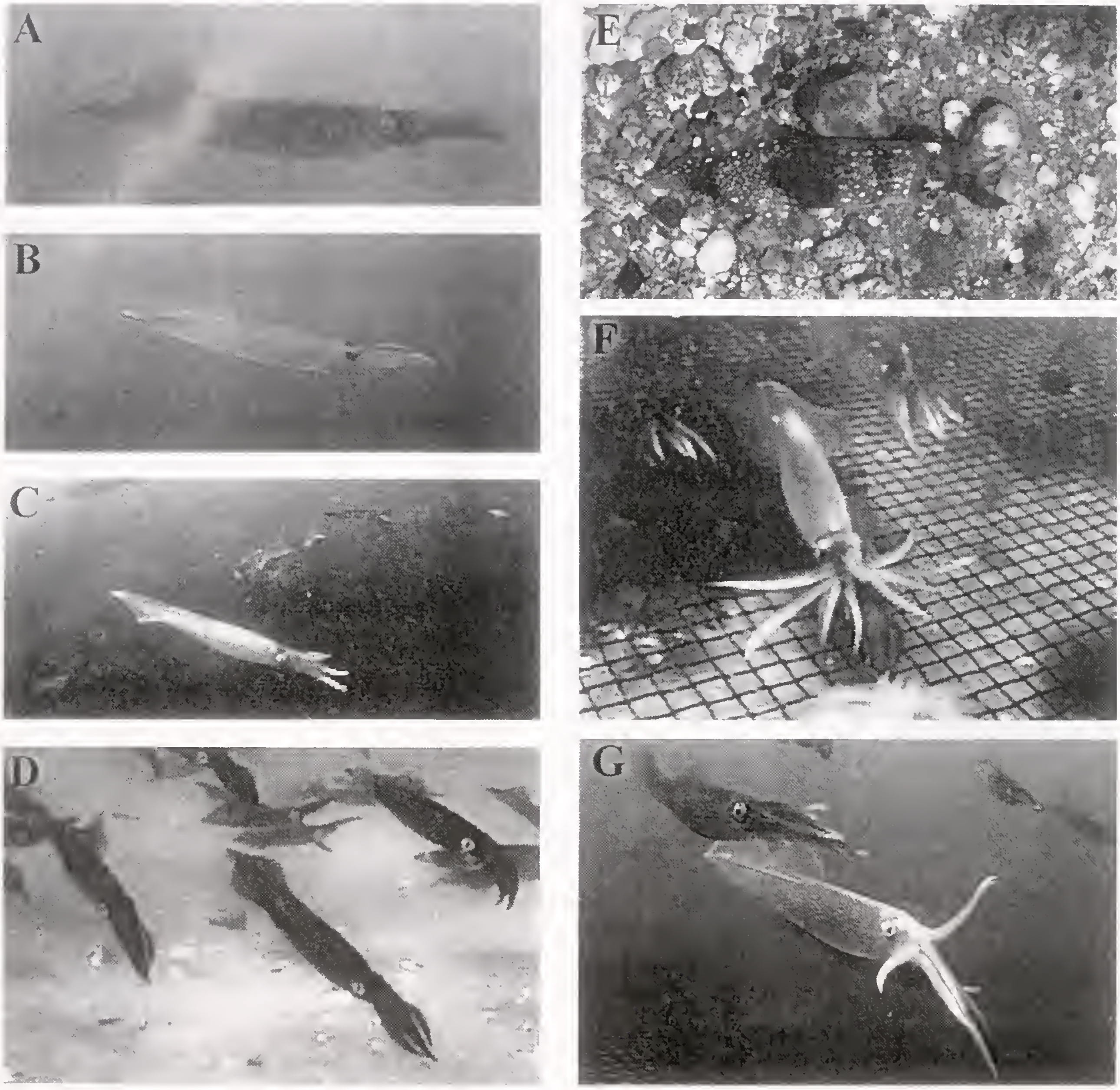

Figure 2. Underwater video images of selected components and body patterns of *Loligo pealei.* (A) The chronic Basic Amber Pattern. (B) The chronic Clear Body Pattern. (C) The chronic Bright White Pattern amidst other squids in Basic Amber. (D) The chronic All Dark pattern viewed against a sand substrate. (E) The Banded Bottom Sitting pattern showing disruptive coloration against a gravel substrate. (F) Acute Mate Guarding Pattern shown by a large consort male (female is just below him) showing the Splayed arm posture and the Accentuated testis chromatic component. (G) Raised arms postural component in a male that also shows the chromatic component of White arms/head; he is directing this signal to the lone male at upper left as he guards his female mate (barely visible behind him).

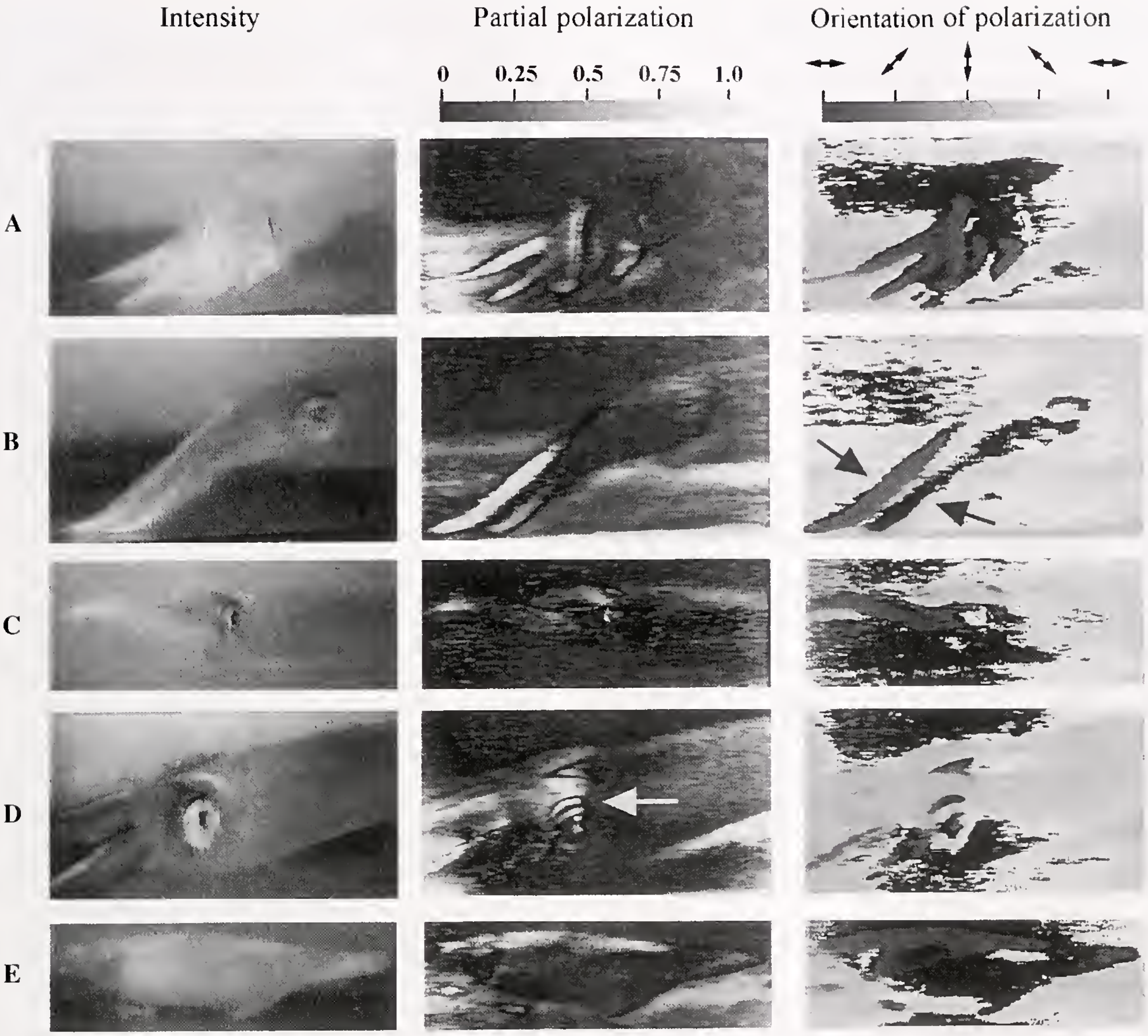

Figure 3. Selected images demonstrating the main sources of polarization components in adult squids. LEFT: Black-and-white images of the squid. CENTER: Partial polarization images in which black represents unpolarized light = 0, and white represents full linear polarization = 1. RIGHT: Orientation of polarization; horizontal polarization is coded into white or black, and vertical polarization into 50% grey. Special iridophores on the arms create the predominant components (A, B), where the partial polarization can exceed 0.75. The orientation of polarization can be equal on all arms (A) or it can vary between them (B, indicated by arrows). Structural reflection from the skin-water interface can produce a polarization pattern that changes with the animal's motion (C). The reflection from the sclera of the eye may be highly polarized (D, arrow). The top of the mantle of the squid occasionally reflects light that is partially polarized (E). This polarization may arise from structural reflection, as in C, or from reflection by the iridophores on the squid's mantle or splotches (Shashar and Hanlon, 1997).

consort males when an intruder male approaches. **Accentuated testis** is a male-only component shown when the chromatophores directly above the testis are retracted while the squid mantle is otherwise dark, thus accentuating the whiteness of the organ (Fig. 2F). This component was seen frequently in single or mate-paired males when reproductive behavior was actively occurring in the school. **Accentuated oviducal gland** is a female-only component analogous in form and function to Accentuated testis in the male. This was often seen in females paired with consort males. All of these light components except White dorsal stripe have been seen commonly in other *Loligo* spp.

Light iridescent chromatic components

Each of the light iridescent chromatic components is common to *Loligo* spp., and comparable color images may be viewed in Hanlon (1982). **Dorsal mantle collar iridophores** are on the anteriormost portion of the mantle, and they appear as bright yellow or pink iridescence; this component tends to produce disruptive coloration by breaking up the longitudinal aspect of the squid's body. It and the next component are usually seen on calm squids near the bottom in the Clear pattern. **Dorsal iridophore splotches** occur on the dorsal mantle and head. They are a distinctive yellow or golden color, and they help to produce general camouflage (Fig. 2E). **Iridescent arm stripes** extend most of the length of the first three pairs of arms. These are usually expressed lightly during camouflage in the Clear pattern, but during agonistic encounters they can be expressed very brightly (see color illustration in Hanlon, 1982). **Iridescent sclera** is the bright silver iridescence on the back (or sclera) of the eye; squids have the ability to obscure this with chromatophores with the Shaded eye component. **Dorsal iridophore sheen** is somewhat rare and is only noticeable from the side. Its function is unclear but may aid camouflage in open water by disrupting the body shape. None of these are unique to *L. pealei* but are shared by other *Loligo* spp.

Light polarization chromatic components

These linear polarization components are newly described for *Loligo* spp. **Polarized arms** are highly polarized reflections that create the most conspicuous component of polarization (Fig. 3A, B). This component often exceeds partial polarization of 0.75, which is noteworthy because Flamarique and Hawryshyn (1997) showed that the natural underwater light field rarely exhibits partial polarization as high as 0.67. The orientation of polarization can be equal in all arms (Fig. 3A), or it may differ between arms (Fig. 3B). **Skin surface polarization** results from the difference in refractive indexes between the squid's body and the water, so that light reflected from any area of the skin may be partially polarized (Fig. 3C). However, the partial polarization in this case is mostly low, rarely reaching 0.5. **Polarized eyes** result from reflection by iridophore cells that surround the eye (Fig. 3D, arrow). The dorsal mantle occasionally reflects light that is partially polarized, resulting in **Polarized dorsal sheen.** The orientation of polarization can vary, reaching 20 degrees from horizontal. This polarization reflection corresponds to the area of the Dorsal iridophore sheen, although the two components do not always coincide in time. The source of this polarization component can be either reflection from iridophores on the mantle or Skin surface polarization. Owing to the limitations of the equipment used to record polarization patterns, these are probably not the only polarization components that squids can show.

Dark chromatic components

All dark is the opposite of Clear: all or most chromatophores are expanded to some degree. The maximal expression of All dark (Fig. 2D) produces an overall deep brown coloration; it is characteristic of alarmed squids. However, the chromatophores need not be maximally expanded, and thus there are ranges of darkness. Often squids are in a "normal" or "basic" coloration that is roughly between Clear and All dark, producing an overall amber body pattern (Fig. 2A). There is also a striking *unilateral* expression of All Dark (Fig. 1). **Dark arms/head** is variable in expression (see Fig. 1) and is opposite to White arms/head. It is seen typically in mating pairs and may represent a mild state of alarm. **Dark head** is expansion of all the chromatophores around the head of the animal (but not the arms), causing the head to appear almost black. This component is frequently seen in mate pairs near the egg mop and probably represents a low-grade alarm signal.

Four striped components occur in *L. pealei*, one used for crypsis and three used during intraspecific agonistic contests. **Dark dorsal stripe** extends halfway or fully down the mid-dorsal mantle. Seen mainly on calm squids, it apparently aids camouflage because it covers some of the bright organs such as the testis, oviducal glands, and ink sac. **Ventral mantle stripe** is a thin, distinct line of fully expanded chromatophores. *L. pealei*, in contrast to *L. plei* but in common with *L. vulgaris reynaudii*, *L. vulgaris*, and *L. forbesi*, shows no protrusile flap of skin when exhibiting this component (Hanlon, 1988; Hanlon *et al.*, 1994). The function of this component is uncertain, but it is seen commonly on mating pairs and on males during mate guarding. Males often swim just above females, and pairs are frequently approached by other squids from below, so the ventral positioning of this visual signal may be useful. It is also possible that the stripe helps disrupt the body form when viewed from below by predators. **Mantle margin stripe** is a dark line running along the fin insertion. It was seen most often as a mild reaction to disturbance or alarm during agonistic bouts, and was usually expressed in conjunction with Ventral mantle stripe, Fin spots, and weak Lateral flame (see below). **Dark arm stripes** are variable, being expressed either along the third pair of arms or along pairs 1, 2, and 3. This uncommon component was seen on a female that also expressed Dark fins (also uncommon, see below) just before a male mated her, and as another mating pair bumped into them. Thus it seems to be an expression of alarm when all three arm pairs are darkened. The simultaneous expression of stripes on three arm pairs has not been reported for squids.

Three spotted components are expressed during alarm or threat situations, mainly intraspecifically, and can be shown unilaterally on the side towards the other squid. **Fin spots** are a collection of small circular and oval dark spots scattered across the fins. This component is seen mostly during agonistic bouts or rarely when an aggressive male comes close by. **Arm spots** are small and occur at the base of the third arms, the second arms, or both. This component is seen on males during mate guarding and at the early stages of agonistic encounters; it probably constitutes a low grade of alarm (see also Arnold, 1962, 1990). **Infraocular spot** appears directly in front of the eye and has variations, including a circular shape that looks like an eye ring. The avenue of achieving signals of "increasing alarm" appears to be Arm spots > Infraocular spot > expanded to eye ring > Dark head.

Various other dark components include two for crypsis and four for intraspecific alarm situations. **Bands** are variable (see Figs. 1 and 2E) and may occur on the fins, head, or arms. First reported by Stevenson (1934), this component is seen typically in calm, bottom-sitting squids and functions as disruptive coloration to break up the longitudinal outline of the squid. **Shaded eye** is a transverse head bar of expanded chromatophores that may aid crypsis by covering the bright Iridescent sclera of the eyes. **Dark fins** occur when all fin chromatophores are expanded maximally; it is not common but has been seen on females that are alarmed. **Dark posterior mantle** is similar to Dark fins, but the mantle chromatophores are expanded; it may be the next stage of alarm after Dark fins.

Several dark components associated with reproductive behavior complement the light components Accentuated testis and Accentuated oviducal gland. **Shaded testis** and **Shaded oviducal gland** are selective expansion of chromatophores over the testis or oviducal gland. Both are often indistinct and serve to mask these bright white organs, thus aiding crypsis. However, the complementary "shading/accentuating" allows rapid signaling. The **Red accessory nidamental gland** can be seen through the translucent mantle and occurs only in fully mature females, so it may be a part of communication even though it is internal. Since it turns red only upon attainment of full sexual maturity, it may be a sign of female sexual maturity or even receptivity. **Lateral mantle spot** is a female-only component expressed as a small intense dark spot of chromatophores near the anterior fin insertion. It coincides roughly with the position of the Red accessory nidamental gland, and the two may function together in some way. The Lateral mantle spot is seen only when the female is paired with a large consort male, and could indicate either receptivity or rejection. **Lateral blush** is a female-only component expressed unilaterally as a diffuse dark area on the lateral mantle. It may be comparable to a variety of similar components shown by female squids, and it may function as a repellent to courting males (Hanlon and Messenger, 1996: their fig. 6.21).

Weak lateral flame is a male-only component produced by longitudinally oriented rows of partly expanded chromatophores. It is seen during low-grade agonistic contests. There are several variations of this component in other *Loligo* spp., the most well developed and dramatic of which is in *Loligo plei* (Hanlon, 1982; DiMarco and Hanlon, 1997). In *Loligo vulgaris, Loligo vulgaris reynaudii,* and *Loligo forbesi* there are Lateral mantle streaks that are arranged a bit differently in the skin, but they all function to provide a lateral signal to an opposing male. *Loligo pealei* has perhaps the weakest expression of this component, while *L. plei* has the strongest.

Postural components

Five postural components are expressed through the arm positioning of *Loligo pealei.* They are generally comparable to postures seen in other *Loligo* spp. **Raised arms** (Fig. 2G) is the unilateral or bilateral raising of the first pair of arms, which may be light or dark, and is seen in both males and females on the mating grounds. This component appears to be a signal of alarm during agonistic contests. It was previously reported by Arnold (1962, 1990). **Splayed arms** (Fig. 2F) is a posture in which all eight arms are spread and flattened on the horizontal plane. This posture is expressed by both sexes but is most common in males that use it to guard female mates they are escorting to egg mops. **Raised and splayed arms** are a combination of the previous postures in which the arms are all splayed except for the first pair, which is raised; it is a strong signal of alarm used when a rival male approaches closely. **Drooping arms** in a swimming squid is a posture in which all the arms appear relaxed and hang downward, but its function is unknown. **Flared arms** is a rare posture in which all of the arms are held stiffly outward in a radial manner; it is seen during highly aggressive agonistic encounters between two males, and during mate guarding.

Locomotor components

Inking is the expulsion of ink mixed with mucus, either in small puffs or as a large dense cloud (Hanlon *et al.*, 1994). Inking is often followed by **Jetting/fleeing,** which is a rapid jet-propulsed escape used in avoidance of both predators and conspecifics. Females often jet from males that try to swim with them or copulate with them. **Chasing** occurs when one squid actively pursues another, usually in forward swimming. In most cases a male is pursuing another male at the conclusion of an agonistic bout. **Bottom sitting** occurs when a squid rests on the substrate (Fig. 2E). **Egg touching** consists of contacts with an egg mop by both males and females. Contact ranges from brief, exploratory touches to embraces of an egg capsule with all of the arms. Females usually lay eggs on existing egg mops, and touching may be a way of assessing the egg-laying substrate. Males commonly touch eggs, and touching is often followed by highly aggressive agonistic bouts (Hanlon, 1996), suggesting that the eggs provide a visual, tactile, or perhaps chemosensory stimulus. **Parallel positioning** occurs when two animals are hovering or swimming parallel to one another in the same direction, within one body length or each other. Courting pairs maintain this position, and agonistic encounters begin with this movement. **Jockeying and parrying** (m, males only) occur when two males maneuver to get next to a female. A successful paired male will often ward off (or parry) the jockeying movements of the unpaired male in a long sequence of swimming maneuvers. **Fin beating** (m) occurs in the parallel position when two males maneuver themselves so that they are beating their fins against each other. This is a physical and escalated stage of an agonistic context, but it results in no obvious physical damage. **Forward lunge/grab** (m) is a short, fast movement to bluff or grab another male during agonistic contests. The grab sometimes results in grappling in which the squids attempt to bite each other. It is rare and is the highest escalation of a fight. **Male-parallel mating** occurs when the male positions himself under the female and grasps her anterior mantle to pass spermatophores into her mantle cavity. **Head-to-head mating** occurs when a male and female face each other, and the male grasps the female's arms. Spermatophores are placed in a seminal receptacle below the mouth (Drew, 1911). **Oviposition** (f, females only) occurs when the female extrudes a single egg capsule and affixes it to the substrate or to existing communal egg masses; she does not hold the egg capsule for long. Among these, egg touching is newly described for *Loligo* spp., although other species do this to varying degrees.

Body patterns

Chronic patterns last for minutes or hours. There are four general chronic body patterns that are common on calm squids and function as crypsis. The **Basic Amber Pattern** (Fig. 2A) is the most common and long-lasting body pattern observed in *Loligo pealei,* and it occurs while the squids are hovering, gently rocking back and forth, or swimming slowly. It is characterized by a partial expansion of all chromatophores (*i.e.*, the All dark component). Apparently the squid detects the albedo in the immediate vicinity and neurally adjusts chromatophore expansion to match it, thus achieving crypsis by matching its surroundings. This pattern can grade into a lighter **Clear Body Pattern** (Fig. 2B) with expression of the Dorsal iridophore splotches; this is seen both when squids are swimming just above the substrate and when they are in the water column. Another subtle variation of these two patterns is **Countershading,** in which the chromatophores on the dorsal surfaces of the squid are in a rather uniform light expansion (as in Clear or Basic Amber) while the ventral portions of the animal are light (probably with help from the many iridophores in the dermis; see Cooper *et al.*, 1990; Hanlon *et al.*, 1990) to eliminate the shadow. In the natural environment, squids only a few meters away blend in almost perfectly with the water column. A more unusual situation occurs when a whole school of squids go into the **Chronic All Dark Pattern** (Fig. 2D), which is not cryptic at all. The function of this pattern is unknown, but we have observed it several times in the natural habitat on many hundreds of calm squids hovering in large schools in the water column. The **Banded Bottom Sitting** pattern (Fig. 2E) is very common and consists of Bands with Dorsal iridophore splotches and Bottom sitting. The pattern provides excellent crypsis through disruptive coloration because the bands break up the longitudinal shape of the squid, and the pattern has variations in the banding. To our knowledge, *L. pealei* is the only loliginid squid that commonly sits on the substrate, although *Loligo forbesi* was observed to bottom sit in the laboratory on rare occasions (Porteiro *et al.*, 1990).

Around egg beds, many squids that are actively engaging in sexual selection behavior remain in the **Chronic Bright White Pattern** (Fig. 2C), which is visually conspicuous. This pattern has many variations, but the most common one is seen on mating pairs near the egg beds. Males that are mate guarding are in Clear, Raised arms, White arms/head, Arm spots, and sometimes Dark head. Females that are being guarded are in Clear with Dark head, and sometimes Raised arms. In both cases the testis and the oviducal glands are clearly visible through the mantle. It is noteworthy that unpaired males (whether large or small) moving amidst a school of reproductively active squids are not in this bright white pattern, yet if a large male wins an agonistic contest and pairs with the female he will immediately go into the Chronic bright white pattern.

Acute patterns last for seconds or rarely for minutes and are seen during intra- and interspecific interactions. **Very Dark** has two variations. The first is a brief flash to a conspecific or an interspecific threat (*e.g.*, to a person in the laboratory or a fish in the field). The second variation shows several flashes over a 5-s period, producing a strong Deimatic effect that startles or bluffs (see Hanlon and Messenger, 1996). The **Blanch-Ink-Jet Maneuver** may be universal among squids: the animal blanches Clear and jets away (usually backwards, but sometimes forward) while ejecting ink in a pseudomorph that remains in the approximate position from which the squid started the maneuver. This is a typical secondary defense against predation or threat (when, for instance, the primary defense of crypsis fails). Such behavior is called Protean behavior because the variable and erratic escape response upsets target prediction by the attacker (Driver and Humphries, 1988).

Lateral Display is a complex set of behaviors performed only by males during agonistic contests. There is some stereotypy, although it is by no means a fixed sequence (see Hanlon and Messenger, 1996; DiMarco and Hanlon, 1997). It begins with Parallel positioning by two males and then includes various visual signals including Arm spots, Infraocular spot, Fin spots, Mid ventral stripe, Weak lateral flame, and Raised and splayed arms. The overall base coloration of the body is bright white: this, because it is "turned on" so quickly as the chromatophores retract when a contest begins, gives the optical illusion of flashing. The ensuing dynamic interactions between the males include flashing and escalation to Fin beating followed by Jockeying on the part of the intruder male to get near the female, and Parrying by the paired male to fend off the intruder. **Mate Guarding Pattern** (Fig. 2F) is shown by paired consort males that are approached either by paired males or by single large or small males that may be seeking an extrapair copulation. The male hovers directly between his mate and the approaching male, maintaining a bright white coloration with Arm spots and maximally Splayed arms; the Accentuated testis is often conspicuous, especially if the male goes dark or amber briefly (Fig. 2F). **Accentuated Testis** is a single component that can and does act as a body pattern, and it is particularly common on small sneaker males that swim around spawning areas attempting extrapair copulations. This pattern is often shown with the All dark component, but it may also be paired with Basic Amber. Although we list it as an acute pattern, it can sometimes be shown often enough to be considered chronic.

Comparisons With Other Loliginids

Sympatric Loligo pealei *and* Loligo plei

The components of body patterns were compared between these species by Hanlon (1988) before detailed information on *Loligo pealei* was available. The importance of these comparisons is that the species are nearly indistinguishable morphologically at hatching (McConathy *et al.*, 1980), as juveniles (*e.g.*, Cohen, 1976), or even at adult size (Vecchione *et al.*, 1998), and fisheries statistics usually lump the two species together in landing records. Hanlon (1988) should be consulted for many comparisons of these two species; only corrections or additions to that paper are discussed here. First, Accentuated testis and Accentuated oviducal gland (and their respective shaded counterparts) occur in both species, so these components cannot be used to distinguish them. Second, Lateral blush has now been seen in both species, but the Lateral mantle spot of female *L. pealei* seems to be unique. Third, Dark arm stripes in *L. pealei* seem distinctive. Fourth, Fin spots in *L. pealei* are strikingly distinguishable from Stitchwork fins in *L. plei*. Fifth, the bands are more variable and perhaps distinctive in *L. pealei*. The Lateral Displays of the two species are clearly different, especially the Mid ventral ridge and the dramatic Lateral flame of *L. plei* compared to the Mid ventral stripe (*i.e.*, no ridge of extended skin) and the weak Lateral flame of *L. pealei*. Conversely, the bright white Mate Guarding Pattern of *L. pealei* seems distinctive, although field observations of natural spawning in *L. plei* would be needed to confirm this difference.

Loligo forbesi *and* Loligo vulgaris reynaudii

In general, *Loligo pealei* is comparable in the content and diversity of its patterning with other *Loligo* spp. Porteiro *et al.* (1990) provided an ethogram of *L. forbesi* based on limited laboratory observations in the Azores Islands, and Hanlon *et al.* (1994) provided an ethogram of *L. vulgaris reynaudii* based on a moderate number of diving observations (but no laboratory trials) in South Africa. The latter two species occur in the eastern Atlantic and do not overlap in distribution with *L. pealei*. However, the adults are extremely similar in morphology, and hence the body patterns are one reasonable way to distinguish living animals. The western Atlantic *L. plei* and *L. pealei* have Lateral flame markings on the mantle, whereas the eastern Atlantic *L.*

vulgaris, *L. vulgaris reynaudii*, and *L. forbesi* all have Lateral mantle streaks; the arrangement of chromatophores in the skin is very different and can be seen in preserved specimens. All five species seem to have highly comparable body patterns for crypsis and countershading, but differences appear in the intraspecific signals used during agonistic contests, courtship, and mate guarding. Sexual signals must be specific, and these are, therefore, the components of body patterns that will continue to provide unique markers, which is critical in distinguishing sympatric species.

Conclusions

Loligo pealei has an unexpectedly rich repertoire of body patterning. Any of the 34 chromatic components can be expressed instantly and in various combinations with the 5 postural and 12 locomotor components to produce each squid's wide variety of behavior. This is a unique capacity of cephalopods because of the direct neural control of hundreds of thousands of chromatophore organs in the skin. It also reflects this group's sensory capabilities and well-developed central nervous system (Hanlon and Messenger, 1996). In *L. pealei*, the largest portion of these visual signals seem to be used for intraspecific communication. This is not unexpected in a species that schools for much of its brief life, but it calls into question just how social squids are. Our findings in this report can be explained partly in the context of the life history and ecology of this species off Cape Cod. *Loligo pealei* individuals live less than a year (Brodziak and Macy, 1996), and their inshore migration each spring is generally thought to be linked to spawning. Off of south Cape Cod (which is a prime squid fishing area and much warmer than Cape Cod Bay and other locations northward), the squids arrive around the first week of May. The inshore trawl and weir trap fishery targets these schooling squids, which often have egg mops when captured, indicating high levels of spawning. This reproductive activity can be studied by divers throughout May, but it becomes increasingly difficult to find spawning congregations of squids around the southern Cape and islands (Nantucket and Vineyard Sounds) during the summer and fall, although eggs are trawled episodically throughout this time.

Our diving operations were designed to study sexual selection processes, thus our ethogram is based mostly on squids that were mature and actively engaged in agonistic contests between males, courting, mating, mate guarding, and egg laying. In May, many females already have sperm stored in the seminal receptacle, and it is likely that some reproductive behavior occurs offshore, before the squids migrate inshore. Moreover, the squids apparently spend considerable time in reproduction while inshore during the spring and summer, and thus it is not surprising that most of the components listed in Table 1 are associated with reproductive behavior. Our many hours (more than 440) of observation over three field seasons make us confident that the ethogram is quite complete for these activities and times. Whether other forms of social behavior occur remains to be discovered. For example, behaviors of young squids and of adults not engaged in reproductive activities during other times of the year and in different habitats have yet to be studied. However, we predict that such observations will reveal only a few new body patterns.

We have included polarization components in the ethogram largely because recent discoveries have shown that *L. pealei* (and probably all cephalopods) uses its visual polarization sensitivity to detect prey (Shashar *et al.*, 1998) and produces polarization components in its skin that could be used for intraspecific signaling (Shashar and Hanlon, 1997; this paper, Fig. 3). Experiments on the cuttlefish *Sepia officinalis* suggested that it could possibly use this distinctive visual capability as a "hidden channel" of intraspecific communication (Shashar *et al.*, 1996).

One of our recurrent and peculiar observations while diving was that aggregations of squids actively engaged in reproductive behaviors were usually conspicuous (*i.e.*, bright white) rather than cryptic, thus potentially making them more easily detected by visual predators, which abound in the nearshore waters (*e.g.*, mackerel, striped bass, flatfish). By helping squids avoid predators, schooling, combined with diurnal activity, may offset the disadvantage of increased visibility.

We believe that use of our ethogram will contribute to future behavioral studies demonstrating that *L. pealei*, like other loliginids, is a species with complex sexual behavior (Hanlon *et al.*, 1997; Hanlon and Messenger, 1996; Sauer *et al.*, 1997) that must be understood by those charged with protecting the resource. This species apparently has a window of opportunity for laying eggs that is restricted in both time (mainly spring) and space (shallow nearshore waters). Many squid fisheries worldwide target spawning congregations, so the predation pressure on spawners is increased (Hanlon, 1998). State and federal fishery managers estimate that stocks of *L. pealei* are being maximally exploited by commercial fishing (NEFSC, 1995). Understanding the mating system of such short-lived species will help managers assess the true effects of fishery practices that not only capture a large number of animals but, by removing spawning individuals, may disrupt the reproductive behavior of individuals and affect the recruitment and demographic structure of populations.

Acknowledgments

We thank Mark Simonitsch, Ernie Eldridge, and Paul Lucas, who allowed us to dive in and around their weir traps to film squid spawning activity. We also thank numerous personnel of the Marine Resources Center of the MBL and many summer students who helped collect and feed squids. This work is the result of research sponsored in part by NOAA National Sea Grant College Program Office, Department of Commerce, under Grant No. NA86RG0075, Woods Hole Oceanographic Institution Sea Grant no. 22850012. Saltonstall-Kennedy Grant NA76FD0111 and NSF Grant IBN 9722805 also partially supported this work. KLB was partially funded by the Marine Models in Biological Research Program (NSF Grant DBI-9605155). ERL was supported by ONR grant NR 4221022-01 and NSF grant 9419566. Special thanks to Rosie Davis who produced the first draft of Fig. 1.

Literature Cited

Arnold, J. M. 1962. Mating behavior and social structure in *Loligo pealii. Biol. Bull.* **123:** 53–57.

Arnold, J. M. 1990. Squid mating behavior. Pp. 65–75 in *Squid as Experimental Animals,* D. L. Gilbert, W. J. Adelman, and J. M. Arnold, eds. Plenum Press, New York.

Brodziak, J. K. T., and W. K. Macy, III. 1996. Growth of long-finned squid, *Loligo pealei,* in the northwest Atlantic. *Fish. Bull.* **94:** 212–236.

Cohen, A. C. 1976. The systematics and distribution of *Loligo* (Cephalopoda, Myopsida) in the western North Atlantic, with descriptions of two new species. *Malacologia* **15:** 299–367.

Cooper, K. M., R. T. Hanlon, and B. U. Budelmann. 1990. Physiological color change in squid iridophores. II. Ultrastructural mechanisms in *Lolliguncula brevis. Cell Tissue Res.* **259:** 15–24.

Cronin, T. W., N. Shashar, and L. Wolff. 1994. Portable imaging polarimeters. *IEEE Proc. 12th IAPR Int. Conf. Pattern Recognition* 606–609.

DiMarco, R. P., and R. T. Hanlon. 1997. Agonistic behavior in the squid *Loligo plei* (Loliginidae, Teuthoidea): fighting tactics and the effects of size and resource value. *Ethology* **103:** 89–108.

Drew, G. A. 1911. Sexual activities of the squid, *Loligo pealii* (Les.). *J. Morphol., Wistar Inst. of Anat. and Biol.* **22:** 327–359.

Driver, P. M., and D. A. Humphries. 1988. *Protean Behaviour: The Biology of Unpredictability.* Oxford University Press, New York.

Dubas, F., R. T. Hanlon, G. P. Ferguson, and H. M. Pinsker. 1986. Localization and stimulation of chromatophore motoneurons in the brain of the squid, *Lolliguncula brevis. J. Exp. Biol.* **121:** 1–25.

Flamarique, I. N., and C. A. Hawryshyn. 1997. Is the use of underwater polarized light by fish restricted to crepuscular time periods? *Vision Res.* **37:** 975–989.

Gilbert, D. L., W. J. Adelman, and J. M. Arnold, eds. 1990. *Squid as Experimental Animals.* Plenum Press, New York.

Griswold, C. A., and J. Prezioso. 1981. *In situ* observations on reproductive behavior of the long-finned squid, *Loligo pealei. Fish. Bull.* **78:** 945–947.

Hanlon, R. T. 1982. The functional organization of chromatophores and iridescent cells in the body patterning of *Loligo plei* (Cephalopoda: Myopsida). *Malacologia* **23:** 89–119.

Hanlon, R. T. 1988. Behavioral and body patterning characters useful in taxonomy of field identification of cephalopods. *Malacologia* **29:** 247–264.

Hanlon, R. T. 1996. Evolutionary games that squids play: fighting, courting, sneaking, and mating behaviors used for sexual selection in *Loligo pealei. Biol. Bull.* **191:** 309–310.

Hanlon, R. T. 1998. Mating systems and sexual selection in the squid *Loligo:* How might commercial fishing on spawning squids affect them? *Calif. Coop. Oceanic Fish Invest. Rep.* **39:** 92–101.

Hanlon, R. T., and J. B. Messenger. 1996. *Cephalopod Behaviour.* Cambridge University Press, Cambridge.

Hanlon, R. T., R. F. Hixon, and W. H. Hulet. 1983. Survival, growth, and behavior of the loliginid squid, *Loligo plei, Loligo pealei* and *Lolliguncula brevis* (Mollusca: Cephalopoda) in closed sea water systems. *Biol. Bull.* **165:** 637–685.

Hanlon, R. T., K. M. Cooper, B. U. Budelmann, and T. C. Pappas. 1990. Physiological color change in squid iridophores. I. Behavior, morphology and pharmacology in *Lolliguncula brevis. Cell Tissue Res.* **259:** 3–14.

Hanlon, R. T., M. J. Smale, and W. H. H. Sauer. 1994. An ethogram of body patterning behavior in the squid *Loligo vulgaris reynaudii* on spawning grounds in South Africa. *Biol. Bull.* **187:** 1–10.

Hanlon, R. T., M. R. Maxwell, and N. Shashar. 1997. Behavioral dynamics that would lead to multiple paternity within egg capsules of the squid *Loligo pealei. Biol. Bull.* **193:** 212–214.

Horvath, G., and D. Varju. 1997. Polarization pattern of freshwater habitats recorded by video polarimetry in red, green and blue spectral ranges and its relevance for water detection by aquatic insects. *J. Exp. Biol.* **200:** 1155–1163.

Kattawar, G. W. 1994. Polarization of light in the ocean. Pp. 203–225 in *Ocean Optics,* R. W. Spinrad, K. L. Carder, and M. J. Perry, eds. Oxford University Press, New York.

McConathy, D. A., R. T. Hanlon, and R. F. Hixon. 1980. Chromatophore arrangements of hatchling loliginid squids (Cephalopoda, Myopsida). *Malacologia* **199:** 279–288.

McKiernan, D. J., and D. E. Pierce. 1995. *Loligo* squid fishery in Nantucket and Vineyard Sounds. *Mass. Div. Mar. Fish.* **Publ. No. 17648-75-200:** 1–200.

NEFSC, Northeast Fisheries Science Center. 1995. Status of fishery resources off the northeastern United States for 1993. *NOAA Tech. Mem. NMFS-F/NEC.* Woods Hole, Massachusetts. 1–138.

Packard, A., and F. G. Hochberg. 1977. Skin patterning in *Octopus* and other genera. *Symp. Zool. Soc. Lond.* **38:** 191–231.

Porteiro, F. M., H. R. Martins, and R. T. Hanlon. 1990. Some observations on the behaviour of adult squids, *Loligo forbesi,* in captivity. *J. Mar. Biol. Assoc. UK* **70:** 459–472.

Saidel, W. M., J. Y. Lettvin, and E. F. MacNichol. 1983. Processing of polarized light by squid photoreceptors. *Nature* **304:** 534–536.

Sauer, W. H. H., M. J. Roberts, M. R. Lipinski, M. J. Smale, R. T. Hanlon, D. M. Webber, and R. K. O'Dor. 1997. Choreography of the squid's "nuptial dance." *Biol. Bull.* **192:** 203–207.

Shashar, N., and R. T. Hanlon. 1997. Squids (*Loligo pealei* and *Euprymna scolopes*) can exhibit polarized light patterns produced by their skin. *Biol. Bull.* **193:** 207–208.

Shashar, N., P. S. Rutledge, and T. W. Cronin. 1996. Polarization vision in cuttlefish—a concealed communication channel? *J. Exp. Biol.* **199:** 2077–2084.

Shashar, N., R. T. Hanlon, and A. M. Petz. 1998. Polarization vision helps detect transparent prey. *Nature* **393:** 222–223.

Stevenson, J. A. 1934. On the behavior of the long-finned squid (*Loligo pealii,* (Lesueur)). *Can. Field-Nat.* **48:** 4–7.

Summers, W. C. 1983. *Loligo pealei.* Pp. 115–142 in *Cephalopod Life Cycles,* Vol. I, P. R. Boyle, ed. Academic Press, London.

Vecchione, M., T. F. Brakoniecki, Y. Natsukari, and R. T. Hanlon. 1998. A provisional generic classification of the family Loliginidae. Pp. 215–222 in *Systematics and Biogeography of Cephalopods,* Vol. I, N. Voss, M. Vecchione, R. B. Toll, and M. J. Sweeney, eds. Smithsonian Institution Press, Washington, DC.

Verrill, A. E. 1880–1881. The cephalopods of the northeastern coast of America. Part II. The smaller cephalopods, including the 'squids' and the octopi, with other allied forms. *Trans. Conn. Acad. Sci.* **5:** 259–446.

Wolff, L. B., and A. G. Andreou. 1995. Polarization camera sensors. *Image Vis. Comput.* **16:** 497–510.

Reference: *Biol. Bull.* **197:** 63–71. (August 1999)

Concurrent Signals and Behavioral Plasticity in Blue Crab (*Callinectes sapidus* Rathbun) Courtship

PAUL J. BUSHMANN*

Smithsonian Environmental Research Center, 647 Contee's Wharf Road, Edgewater, Maryland 21037

Abstract. Behavioral flexibility and behavioral regulation through courtship signals may both contribute to mating success. Blue crabs (*Callinectes sapidus*) form precopulatory pairs after courtship periods that are influenced by female and perhaps male urine-based chemical signals. In this study, male and female crabs were observed in 1.5-m circular outdoor pools for 45 min while the occurrence and sequence of courtship behaviors and pairing outcomes were recorded. These results were then compared with trials in which males or females were blindfolded; lateral antennule (outer flagellum) ablated; blindfolded and lateral antennule ablated; or had received nephropore blocks. The relative importance of visual and chemical sensory systems during blue crab courtship were then determined and urine and non-urine based chemical signals for both males and females were examined. Courtship behaviors varied considerably in occurrence and sequence; no measured behavior was necessary for pairing success. Male or female blindfolding had no effect on any measured behavior. Males and females required chemical information for normal courtship behaviors, yet blocking male or female urine release did not affect courtship behaviors. Males required chemical information to initiate pairing or to maintain stable pairs. Male urine release was necessary for stable pairing, suggesting that male urine signals may be involved in pair maintenance rather than pair formation. Females that could not receive chemical information paired faster and elicited fewer male agonistic behaviors. The results demonstrate a great variability and flexibility in blue crab courtship, with no evidence for stereotyped behavioral sequences. However, these behaviors appear regulated by urine- and nonurine-based redundant chemical signals emanating from both males and females. Although urine-based signals play roles in blue crab courtship, chemical signals from other sites appear to carry sufficient information to elicit a full range of behavioral responses in males and females.

Introduction

Courtship and mating success depend upon correct behavioral responses by both males and females. One might expect a degree of plasticity in these behaviors (Hazlett, 1995). Because behavior can quickly track changes in environmental conditions (West-Eberhard, 1989), flexibility in the occurrence and timing of reproductive behaviors might help insure successful mating. Many invertebrates do exhibit plasticity in their behaviors (Carlson and Copeland, 1978; Dejean, 1987; Elner and Beninger, 1995) and this variability may be the rule for most animal species (Lott, 1991).

Conversely, one might also expect courtship and reproductive behaviors to be controlled and regulated by conspecific communication signals. By eliciting appropriate behavioral responses, these signals could enhance mating success and help to prevent interspecies mating. Courtship and mating in a fluctuating environment could be aided by multiple or redundant signals, which would make the transmission of adequate and correct information more likely. Multiple or redundant signals have been found in both invertebrate and vertebrate species (van den Hurk and Lambert, 1983; Linn *et al.*, 1984; Rand *et al.*, 1992).

Chemical communication signals appear to be nearly universal in the animal world. For aquatic crustaceans, chemical communication signals have been well documented in courtship and reproduction (Ryan, 1966; Atema and Engstrom, 1971; Eales, 1974; rev. in Dunham, 1978, 1988; Gleeson, 1980; Borowsky, 1984, 1985), while visual (Christy and Salmon, 1991) and acoustic (Salmon and Horch, 1972) signals have received less study. Recent studies with a variety of animal taxa have begun to examine

---

Received 30 March 1998; accepted 1 June 1999.

* Current address: Anne Arundel Community College, 101 College Parkway, Arnold, MD 21012. E-mail: pjbushman@mail.aacc.cc.md.us

multiple signals and signal interactions (Hazlett, 1982; Waas and Colgan, 1992; Stauffer and Semlitsch, 1993; Hughes, 1996).

Like many crustaceans (Hartnoll, 1969), the blue crab *Callinectes sapidus* Rathbun practices a polygynous mating system involving a complex coordination of female ecdysis, maturation, and copulation. The mating process has been well described (Hay, 1905; Churchill, 1921; Van Engel, 1958; Gleeson, 1980). Immature females nearing their final maturational molt, termed prepubertal females, are approached and courted by mature males. Pairing success results in females being held beneath males in a "cradle carry" posture for a period of precopulatory guarding. They are released for their molt, mated while still soft, and carried again for a period of postcopulatory guarding. This latter guarding protects the female while she is soft and prevents subsequent inseminations by other males (Jivoff, 1997a). Females are thought to receive only one copulation in their lifetime while males mate repeatedly (Van Engel, 1958), although multiple inseminations are possible and occur occasionally (Jivoff, 1997a).

Blue crab courtship can be divided into three phases: mate attraction, pair formation, and pair maintenance. In each phase a precise signaling system would seem important to help insure mating success. The coupling of molt and reproductive condition requires individuals to ascertain the physiological state of prospective partners. Signals can function in the reduction of agonistic behaviors (Tinbergen, 1953; Bastock, 1967), and during mating female blue crabs must in some way guard against injury or death by aggressive, cannibalistic males. Reproductive behaviors and sequences might, therefore, be tightly regulated by communication signals, making appropriate responses more likely and increasing the eventual mating success of the participants (Ryan, 1990; Reynolds, 1993).

Chemoreception and vision are the two best studied sensory modalities in blue crab courtship. Teytaud (1971) reported a role for visual signals in male recognition by pre-pubertal females. However, Gleeson (1980) showed that males did not respond to female visual stimuli alone, and pairing could proceed in darkness. Chemical signals are important for both male (Gleeson, 1980) and female (Teytaud, 1971; Gibbs, 1996) mate recognition. Some mature males respond with a courtship display to chemical compounds in pre-pubertal female urine (Gleeson, 1980; Gleeson *et al.*, 1984) and reception of these chemical signals occurs via the aesthetasc sensilla on the lateral filament (outer flagellum) of the male antennules (Gleeson, 1982). This signaling theme appears common in crustaceans: urine carries chemical courtship signals (Ryan, 1966; Bushmann and Atema, 1997; Bamber and Naylor, 1997) and the antennules appear to be the site of distance chemoreception (Ache, 1975; Ameyaw-Akumfi and Hazlett, 1975; Devine and Atema, 1982; Cowan, 1991). The presence of a male chemical signal has not been firmly established, although Gleeson (1991) showed female attraction to water that contained males and Gibbs (1996) demonstrated disruption of pairing with male antennule ablation.

In this study, the occurrence and variability of courtship behaviors observed during blue crab pair formation were examined. These behaviors were then compared with those generated by male and female pairs with vision, distance chemoreception, both senses, or urine release impaired. This allowed a determination of the relative importance of visual and chemical sensory systems during blue crab courtship and an examination of urine- and nonurine-based chemical signals for both males and females.

Materials and Methods

Adult male crabs (125 mm–170 mm carapace width) were collected from the Rhode River, an upper Chesapeake Bay subestuary, with baited commercial crab traps. Premolt prepubertal females (96 mm–127 mm carapace width) were purchased from two local businesses which hold molting females for the soft crab industry. Females ranged in molt stage from late D_0 to D_3 (Drach, 1939). Animals were held in floating cages in the Rhode River or flow-through seawater tanks for no more than 48 h before participation in the study.

Behavioral interactions were observed in outdoor circular pools (150 cm d. × 20 cm h.) with three centimeters of washed river sand as substrate. Prior to a trial, pools were filled with 15 cm of new river water filtered through a felt bag with 10 μm mesh. A trial began by randomly selecting a male crab and placing him into a pool. Ten minutes later, a randomly selected prepubertal female was placed into the middle of the pool, inside an opaque plastic cylinder designed to prevent interactions prior to the start of the trial. After 10 min acclimation, the cylinder was removed, allowing the animals to freely interact. Three pools were started and watched simultaneously, and the ensuing behaviors were recorded by hand for 45 min. Carapace width and molt stage were recorded for each animal.

Prior to trials either a male or a female from each pair was subjected to an experimental treatment. They were as follows:

1. Nephropore Occlusion: Blue crabs possess bilateral nephropores, located anteriorly and just ventral to the eye stalks. Each opening is found in a pit in the carapace. A chitinous flap opens to allow urine to exit. A modification of a successful cannulation technique was used to prevent urine release. Each pit was first dried by blotting and a drop of acetone, then filled with a viscous cyanoacrylate glue. The glue was immediately hardened with a catalytic accelerator. This sealed the nephropore flap shut. Animals were occluded 30 min prior to a trial. The blocks were

checked for a tight bond with the carapace immediately before and after a trial. n = 12 males (M: URINE), 14 females (F:URINE).

3. Antennule Ablation: the distal lateral filament (outer flagellum), containing the aesthetasc sensilla, of both antennules was removed. n = 12 males (M: ANTENN), 12 females (F:ANTENN).
4. Blindfolding: two strips of black plastic (50 × 10 mm) were fastened with cyanoacrylate glue to the dorsal and ventral carapace so that each wrapped over and covered an eye stalk. n = 13 males (M:BLIND), 12 females (F:BLIND).
5. Antennule ablation and blindfolding: animals received both antennule ablation and blindfolding treatments. n = 12 males (M:ANT-BLIND), 12 females (F:ANT-BLIND).
6. Sham treatment: both animals in a pair were subjected to sham operations. Antennules were held with forceps without ablation, nephropores were treated with acetone and accelerator but not glued, and blindfolds were attached similarly, but lateral to the eye stalks so that vision was not impaired. n = 10.
7. Intact: No treatments or sham operations were performed on either animal. n = 12.

Blue crab reproductive and agonistic behaviors have been well described over the years (Churchill, 1921; Van Engel, 1958; Teytaud, 1971; Jachowski, 1974; Gleeson, 1980). This study analyzed one agonistic and five reproductive behaviors. These behaviors were common, unmistakable, and reliable indicators of the nature of the interaction occurring. They were:

1. *Male Strike:* an agonistic behavior in which the male strikes or seizes any female body part with either chelae without subsequent attempts at cradle carry.
2. *Male Display:* A courtship behavior in which the male raises high on his walking legs, spreads his chelae laterally, and raises and rotates his 5th walking legs (periopods) laterally.
3. *Female Present:* a courtship behavior in which the female faces away from the male and holds her body in a cradle carry posture, with or without spread chelae.
4. *Female Rock:* a courtship behavior in which the female rocks her body from side to side.
5. *Initiation of Pair Formation:* the male seizes the female and attempts to pull her into a cradle carry position. Females often resist, males may make many attempts, and pairing may or may not become established.
6. *Stable Pair Formation:* this was scored at the end of a trial. Pairs were in stable cradle carry if both female and male struggling had ceased, and the animals had been paired for at least 10 min.

Comparisons of the intact and sham-treated groups showed no differences in the frequency of occurrence of any measured behavior or pairing outcome. These two groups thus appeared to represent samples of the same population and their data were pooled to yield 22 intact control trials. Behaviors of these pairs were examined to determine a normal range of behavioral variability and sequence. Behaviors were scored once if they occurred in a given trial. The number of trials in which behaviors occurred for the intact control group was then compared with those generated by the treatment groups. Overall differences between treatment and control groups were evaluated with a Chi-square test for multiple independent samples (Siegel and Castellan, 1988). Where significance was found, differences between specific treatment groups and the control were evaluated with a Fisher exact test (FAT) (Siegel and Castellan, 1988). The mean times between trial start and both the first behavioral interaction and *Initiation of Pair Formation* were also compared between the control and treatment groups. Overall differences were evaluated with analysis of variance (Jaccard, 1983), while mean differences between specific treatments and the control were evaluated with a non-directional *t*-test (Jaccard, 1983).

Results

Male and female blue crabs in intact control pairs showed great variability in the occurrence of their behaviors. During courtship, no behavior occurred with a high frequency (Table I). *Male Strike, Male Display, Female Present* and *Female Rock* occurred in only 41, 41, 56, and 36 percent of intact control trials, respectively. Pairing was initiated at a high rate, however (82% of trials), with 50% of trials resulting in *Stable Pair Formation.* No single behavior more likely led to the initiation of pairing or stable pairing, nor did the exhibition of any behavior preclude these outcomes (Table I). There was no single sequence of behaviors

Table I

Frequency of courtship and agonistic behaviors in intact blue crab pairs. The number of trials in which each behavior occurred is shown for all trials, those trials in which Initiation of Pair Formation *occurred, and those trials in which a stable pair was formed*

Behaviors	Occurrence in 22 trials (%)	Trials (%) with *Initiation of Pair Formation* (n = 18)	Trials (%) with *Stable Pair Formation* (n = 11)
Male Strike	9 (41)	6 (33)	2 (18)
Male Display	9 (41)	10 (56)	3 (30)
Female Present	12 (56)	10 (56)	4 (36)
Female Rock	8 (36)	8 (44)	3 (27)
Initiation of Pair Formation	18 (82)	—	—
Stable Pair Formation	11 (50)	—	—

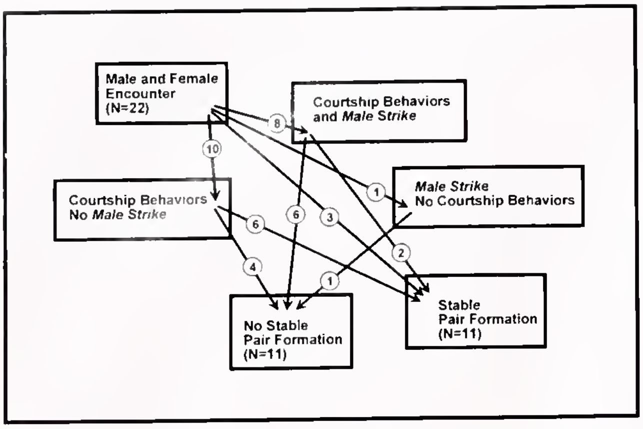
Male and Female Encounter (N=22)
Courtship Behaviors and *Male Strike*
Courtship Behaviors No *Male Strike*
Male Strike No Courtship Behaviors
No Stable Pair Formation (N=11)
Stable Pair Formation (N=11)
8
10
1
6
6
3
2
4
1

Figure 1. Flow chart showing behavioral pathways from first encounter, through courtship and/or male agonistic behavior, to stable pairing success or failure. The circled numbers represent the number of trials following that particular pathway.

that predominated, nor any single sequence that invariably led to greater or lesser pairing success. Neither male or female courtship behaviors were correlated with female molt stage (early premolt D_0 vs. late premolt D_3) or the relative sizes of males and females.

However, some general trends emerge from courtship sequences examined together with male agonistic behavior (Fig. 1). Most pairs (18 of 22) exhibited some sequence of courtship behaviors prior to pair formation ($\chi^2 = 8.91$, $P = 0.003$). The presence of male agonistic behavior significantly reduced the likelihood of stable pairing (FAT, $P = 0.040$). Of the nine pairs in which males exhibited *Male Strike*, only two (22%) formed stable pairs. Of the remaining 13 pairs in which males did not exhibit *Male Strike*, nine (69%) formed stable pairs (Fig. 1).

Examination of male agonistic and display behaviors revealed overall differences between treatment and control groups ($\chi^2 = 20.45$, $P < 0.05$; $\chi^2 = 17.62$, $P < 0.05$). The incidence of *Male Strike* was significantly diminished (FAT, $P = 0.009$) if females were antennule ablated (F: ANTENN) (Fig. 2A). Scores for females antennule ablated and blindfolded (F:ANT-BLIND) closely approached significance (FAT, $P = 0.050$). *Male Display* was significantly reduced when males were antennule ablated (M:ANTENN) (FAT, $P = 0.009$) or antennule ablated and blindfolded (M:ANT-BLIND) (FAT, $P = 0.049$), but were unaffected by female or male nephropore occlusion (F:URINE or M: URINE) (Fig. 2B). Blindfolding alone (M:BLIND and F:BLIND) had no effect on any measured behavior.

When the behaviors *Female Present* and *Female Rock* were examined, there were significant overall differences between treatment and control groups ($\chi^2 = 45.78$, $P < 0.05$; $\chi^2 = 20.2$, $P < 0.05$). The incidence of *Female Present* was reduced when females were antennule ablated (FAT, $P = 0.035$) or antennule ablated and blindfolded (FAT, $P = 0.009$) (Fig. 2C). This behavior was also reduced by male antennule ablation (FAT, $P = 0.001$). *Female Rock* (Fig. 2D) was reduced in incidence when females were antennule ablated and blindfolded (FAT, $P = 0.009$); female antennule ablation alone did not significantly reduce the occurrence of this behavior ($P = 0.083$). *Female Rock* also occurred less frequently when males were antennule ablated and blindfolded (FAT, $P = 0.009$). Male or female nephropore occlusions or blindfolding had no significant effect on either female courtship behavior.

Initiation of Pair Formation occurred frequently (80% of trials) in the intact control group (Fig. 2E). There were significant overall differences between groups in the occurrence of this behavior ($\chi^2 = 34.8$, $P < 0.05$). It occurred significantly less often than the control group when males were antennule ablated (FAT, $P = 0.007$), while the reduction for antennule ablated and blindfolded males approached statistical significance ($P = 0.062$). Examination of stable pairing at the trials' conclusions showed significant overall differences between treatment groups ($\chi^2 = 31.36$,

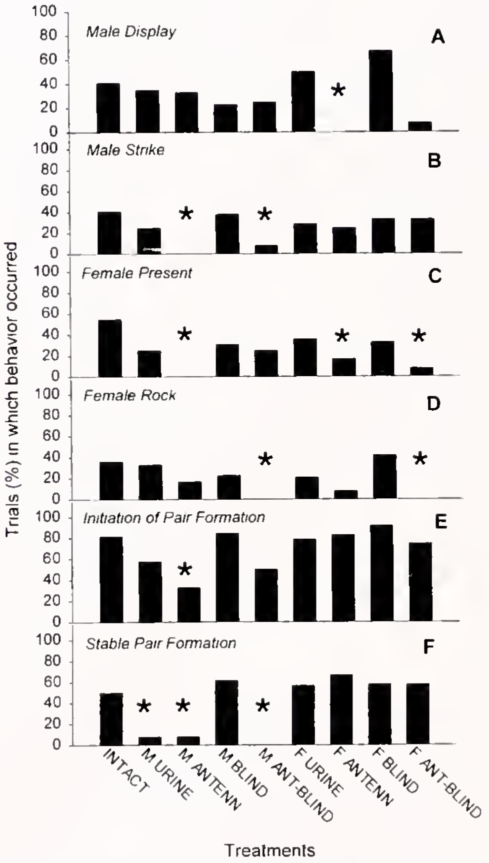

Figure 2. The percentage of trials in which *Male Strike*, (2A), *Male Display* (2B), *Female Present* (2C), *Female Rock* (2D), *Initiation of Pair Formation* (2E), and *Stable Pair Formation* (2F) occurred for the intact control and treatment groups. Differences between intact control and treatment groups were evaluated with a Fisher exact test. Stars indicate statistical significance at $\alpha = 0.05$.

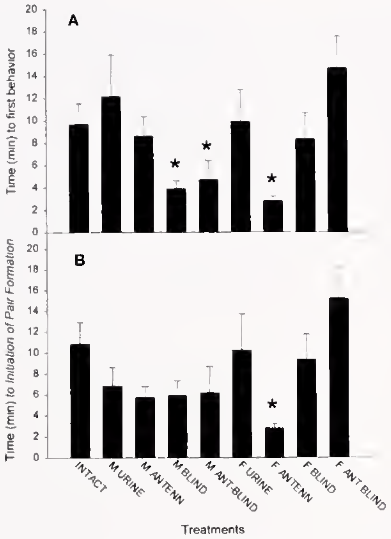

Figure 3. Mean time to first observed behavior (3A) and *Initiation of Pair Formation* (3B) for the intact control and treatment groups. Bars represent mean standard error. Differences between intact control and treatment groups were evaluated with a non-directional t-test. Stars indicate statistical significance at $\alpha = 0.05$.

$P < 0.05$). Fewer pairs were stable (Fig. 2F) if the males were antennule ablated (FAT, $P = 0.016$) or antennule ablated and blindfolded (FAT, $P = 0.002$). The incidence of stable pairing was also reduced when male nephropores were occluded (FAT, $P = 0.016$). This was the only significant effect observed with any nephropore occlusion.

An examination of the mean time between a trial's start and the first observed behavior (Fig. 3A) showed significant differences between treatment groups (ANOVA F = 2.73, $P = 0.009$). The mean time to first behavior was significantly less than the control group when males were blindfolded (t = 2.97, $P = 0.026$), when males were blindfolded and antennule ablated (t = 2.28, $P = 0.032$), and when females were antennule ablated (t = 3.69, $P = 0.001$). Overall differences were found (ANOVA F = 2.29, $P = 0.030$) when the time between trial start and *Initiation of Pair Formation* was evaluated (Fig. 3B). In this comparison only the female antennule-ablated trials showed a significant reduction in time (t = 3.90, $P = 0.001$). Time differences between the male blindfolded group and the intact controls closely approached significance (t = 2.01, $P = 0.06$), while those for the male blindfolded and antennule ablated group were not significant (t = 1.46, $P = 0.170$).

Discussion

Arthropod behavior has generally been considered stereotyped. Studies of some insects, such as many moth species, have demonstrated stereotypic courtship behavior: specific chemical signals elicit specific and predictable responses (Kaissling, 1979; Charlton and Cardé, 1990). Other insect species have shown greater flexibility, with individuals basing their behavioral responses upon current conditions and context (Carlson and Copeland, 1978; Dejean, 1987).

Similarly, the behavior of many crustacean species is not based upon stereotyped responses but instead shows great plasticity and can be modified as context changes (Ra'anan and Cohen, 1984; Elner and Beninger, 1995; Hazlett, 1995). The current study demonstrates such flexibility in *Callinectes sapidus* courtship behavior. Courtship is variable in that no single behavior must occur, nor does any behavior invariably lead to successful pairing. No single behavior occurred more than approximately half the time, yet the odds of successful pairing remained high. This suggests that courtship follows multiple behavioral pathways, all potentially leading to successful pair formation. Such flexible courtship would be useful for both males and females in a species that mates in a fluctuating estuarine environment. With intense male competition for females (Jivoff, 1997b) and only one chance for females to receive sperm, it maximizes the chances of an encounter producing pair formation, with eventual mating and reproductive success.

However, blue crab mating behavior is not without constraints and regulation. In the intact control group most pairs displayed some courtship behaviors prior to pair formation, and male agonistic behavior reduced the likelihood of stable pairing. This demonstrates the importance of controlling male aggression during courtship and, together with the treatment trials, illustrates the role that communication signals often serve in this regard (Tinbergen, 1953). For blue crabs, the most likely path to successful pairing, and therefore successful reproduction, involves courtship and reduced male aggression.

The treatment trials suggest behavioral regulation through chemical communication signals and that both female and male chemical signals play important roles in courtship and pairing. Males with ablated antennules showed reduced instances of *Male Display, Initiation of Pair Formation* and *Stable Pair Formation*. For the male, loss of distance chemoreception affected behavioral expression and directly reduced courtship success. The relevant chemical information did not seem to reside solely in female urine, however, because females with occluded nephropores induced male behaviors at frequencies similar to intact controls. Although the results were less clear, females also appeared to exhibit fewer instances of courtship behaviors when their antennules were ablated, while pairing initiation or stability was unaffected. The physical act of pairing is initiated by the male, and evidently an antennule-ablated female is still attractive to males. However, an unreceptive female can likely flee and decline pairing in the wild. Blocking male urine release had no effect on female courtship behaviors, again suggesting that the relevant chemical compounds are not restricted to urine.

It is now generally recognized that many chemical signals are mixtures or blends and thus can serve as multiple or redundant signals (van den Hurk and Lambert, 1983; Vetter and Baker, 1983; Linn *et al.*, 1984). In blue crabs and other brachyurans, a chemical signal in female urine that induces male courtship behavior has been well described (Ryan, 1966; Gleeson, 1980; Seifert, 1982; Bamber and Naylor, 1997). The present study does not refute the existence of this signal, but rather suggests urine is only one source of courtship signals and is not obligatory for the initiation of male or female courtship behaviors. There appears to be chemical information from non-urine sources capable of eliciting the same behaviors when nephropores are occluded. It is only when all chemical signals are lost through antennule ablation that behavior is negatively affected. These statements appear at odds with Ryan's (1966) work showing no male responses to seawater that had contained nephropore-blocked premolt *Portunus sanguinolentus* females. It may be that the relevant female *P. sanguinolentus* signal is sent only in urine. In addition, the females in Ryan's study were isolated in 8-l buckets during signal release, while females in the current study were placed in larger tanks in the presence of a male. This more naturalistic behavioral context may have elicited female nonurine signal release and male responses not seen in the earlier study. Lastly, Ryan used molten paraffin rather than glue as blocks; this may have affected the animals differently from the blocks used here. These apparent interspecific differences in behaviors and signals should be more closely examined.

Blue crab courtship thus appears regulated by female and male concurrent chemical signals emanating from multiple sources. It is unknown if the concurrent signals demonstrated here are different compounds or if they are the same compound released at different sites. This knowledge awaits the purification and structural description of these chemical courtship signals. The release sites of the non-urine chemical compounds are likewise unknown. In lobsters (*Homarus americanus*), the gill current has been implicated as a method for transporting chemical signals to a receiver (Atema, 1985). Because blue crabs possess a similar current, it is possible that the gills themselves or structures within the gill cavity are sources of chemical signals. Tegumental glands, found in blue crabs and other arthropods (Johnson, 1980; Talbot and Demers, 1993) have been suggested as chemical signal sources in several crustacean species (Berry, 1970; Kamiguchi, 1972; Bushmann and Atema, 1996) and also may play a role here.

Loss of chemical signals in some instances had indirect effects on behavior. Males were less aggressive toward antennule-ablated females. Ablation evidently alters either female behavior or her signaling patterns in a way that affects male agonistic behavior. Similarly, female courtship behaviors were reduced when male chemical reception was impaired. Male antennule ablations must alter male behaviors or communication signals in a way that makes them less attractive to females and less capable of inducing female courtship behavior. This is consistent with field work (Gibbs, 1996) demonstrating that antennule-ablated males in crab traps are less able to attract prepubertal females.

There is evidence for an obligatory male urine-based signal involved in pair maintenance during precopulatory guarding. When male nephropores were occluded, initiation of pair formation was not affected yet there was reduced incidence of stable pairing. This was the only evidence for a urine-based signal in this study. However, female antennule ablation did not reduce the incidence of stable pair formation. It is possible that the direct contact involved in a cradle carry produces other avenues for signal reception, such as contact chemoreceptors on the dactyls or elsewhere on the exoskeleton (Fuzessery and Childress, 1975). Although the observed reduction in stable pairing could have resulted from some male trauma associated with the occlusion procedure, occluding females produces no such pattern and blue crabs and lobsters appear capable of suspending urine release for periods of several hours without ill effect (Bushmann, unpub. data, Breithaupt and Atema, 1993).

Visual signals seem to play no role in influencing courtship behaviors or outcomes. Blindfolded males and females courted, received courtship, and paired with success rates equal to the intact controls. This is consistent with previous observations for blue crabs and lobsters that visual signals are of secondary importance during social interactions (Gleeson, 1980; Snyder *et al.*, 1993; Kaplan *et al.*, 1993). Thus, the primary function of the male courtship display is likely not transmission of a visual signal. However, it may be an excellent method for transmitting both chemical and hydrodynamic signals to a potential partner. Rotation of the periopods causes a strong and highly turbulent flow of water directed forward of the animal (Gleeson, 1991; Bushmann, unpub. data). This flow would likely entrain any chemical signal emanating from the gills or nephropores. In addition, some crustaceans use hydrodynamic information during agonistic interactions and prey capture (Barron and Hazlett, 1989; Breithaupt *et al.*, 1995). The highly turbulent, directed flow generated by male paddle waving could provide directional or other information to females.

Many aspects of the male courtship display remain unclear. It must have some energetic cost and may draw attention by predators, yet it need not occur for successful pairing and occurred in less than half the observed encounters. In this study its occurrence was not correlated with female premolt stage, the relative sizes of males and females, or pairing success during the encounter. The function of this rather spectacular behavior and the stimuli leading to its initiation require further investigation.

Loss of female chemoreception appeared to accelerate rather than retard pairing. When females were antennule-ablated, males showed little agonistic behavior, females exhibited fewer courtship behaviors, and pairs formed more quickly than in the intact control group (Fig. 3B) and they remained stable. This is at odds with Gibbs (1996), who found males to be more aggressive toward antennule-ablated females and the time required for pairing to be unaffected. The present study suggests that females use chemical information and courtship behaviors to lengthen courtship periods, perhaps as a way of better evaluating potential partners. Loss of chemical information through female antennule ablation would then result in less female evaluation and faster pairing.

The significant reduction in time until first behavior seen in the male blindfolded group was probably a general behavioral rather than specific communication effect. Blindfolded males, without visual stimuli, may have been less wary and more likely to begin moving about the pool after trial start. This male movement would result in more rapid encounters with females. The time until *Initiation of Pair Formation* was not significantly shortened, however (Fig. 3B), and blindfolding had no effect on any measured behavior.

Several studies have shown that lateral antennule ablation affects behavior by interfering with chemical reception (Ache, 1975; Ameyaw-Akumfi and Hazlett, 1975; Gleeson, 1980; Cowan, 1991). However, in any ablation experiment there is always a question of false-negative responses due to a general dampening of behavior caused by the procedure itself (Dunham, 1978). In the present study, while ablated males showed reduced reproductive behaviors, agonistic responses were unaltered. Antennule-ablated females, while not exhibiting many courtship behaviors, were nonetheless courted and carried by males. These ablations appeared to affect certain reproductive behaviors, presumably those dependent upon chemical signals, rather than causing a general reduction in behavioral responses.

A second potential problem concerns the blocks applied to the nephropores to prevent urine release. Correct interpretation of results depends upon an effective block. Several lines of evidence suggest that these blocks prevented urine release. First, they are the initial step in the attachment of a urine cannula. This cannula can collect urine from blue crabs for several days without leaking (Bushmann, unpub. data). Second, three urine blocked animals were held after their trials. These individuals were swollen from fluid retention within 6 h and died within 12 h. Lastly, the water from four blocked animals held individually in 2-l tanks showed reduced ammonia levels compared to water from four unblocked crabs (Bushmann, unpub. data). Ammonia levels from blocked crab water were not zero, because ammonia is also excreted across the gills (Mantel and Farmer, 1983). Taken together, these observations suggest that the blocks used in this experiment were effective in preventing urine release.

In summary, *Callinectes sapidus* courtship illustrates both behavioral plasticity and the importance of behavioral regulation through a signaling system. The concurrent and seemingly redundant chemical signals discussed here may be different compounds or the same compound released from different sites. Chemical rather than visual signals from both male and female seem to play crucial roles in courtship and pairing. Although these signals influence the initiation of behaviors and pairing success, there appear to be many different pathways leading to pairing success, and no single behavior and perhaps no single signal is necessary for pairing success. Courtship behaviors and chemical signaling may operate in a more complex and flexible manner than previously demonstrated.

Acknowledgments

The author thanks Dr. Anson H. Hines for his assistance, support, and review of this manuscript. This work was funded through a Smithsonian Postdoctoral Fellowship to PB, and an NSF grant OCE-9711843 to AHH.

Literature Cited

Ache, B. W. 1975. Antennular mediated host location by symbiotic crustaceans. *Mar. Behav. Physiol.* **3:** 125–130.

Ameyaw-Akumfi, C., and B. A. Hazlett. 1975. Sex recognition in the crayfish *Procambarus clarkii*. *Science* **190:** 1225–1226.

Atema, J. 1985. Chemoreception in the sea: adaptations of chemoreceptors and behavior to aquatic stimulus conditions. *Soc. Exp. Biol. Semin. Ser.* **39:** 387–423.

Atema, J., and D. G. Engstrom. 1971. Sex pheromone in the lobster, *Homarus americanus*. *Nature* **232:** 261–263.

Bamber, S. D., and E. Naylor. 1997. Sites of release of putative sex pheromone and sexual behaviour in female *Carcinus maenas* (Crustacea: Decapoda). *Estuarine, Coastal Shelf Sci.* **44:** 195–202.

Barron, L. C., and B. A. Hazlett. 1989. Directed currents: a hydrodynamic display in hermit crabs. *Mar. Behav. Physiol.* **15:** 83–87.

Bastock, M. 1967. *Courtship: an Ethological Study*. Aldiline Publishing Company, Chicago.

Berry, P. F. 1970. Mating behavior, oviposition and fertilization in the spiny lobster *Panulirus homarus* (Linnaeus). South African Association for Marine Biological Research Investigational Report no. 24. 16 pp.

Borowsky, B. 1984. Effects of receptive females' secretions on some male reproductive behaviors in the amphipod crustacean *Microdeutopus gryllotalpa*. *Mar. Biol.* **33:** 266–271.

Borowsky, B. 1985. Responses of the amphipod crustacean *Gammarus palustis* to waterborne secretions of conspecifics and congenerics. *J. Chem. Ecol.* **11:** 1545–1552.

Breithaupt, T., and J. Atema. 1993. Evidence for the use of urine signals in agonistic interactions of the American lobster. *Biol. Bull.* **185:** 318.

Breithaupt, T., B. Schmitz, and J. Tautz. 1995. Hydrodynamic orientation of crayfish (*Procambarus clarkii*) to swimming fish prey. *J. Comp. Physiol. A* **177:** 481–491.

Bushmann, P., and J. Atema. 1996. Nephropore rosette glands of the lobster *Homarus americanus:* possible sources of urine pheromones. *J. Crustac. Biol.* **16**(2): 221–231.

Bushmann, P., and J. Atema. 1997. Shelter sharing and chemical courtship signals in the lobster, *Homarus americanus. Can. J. Fish. Aquat. Sci.* **54**(3): 647–654

Carlson, A. D., and J. Copeland. 1978. Behavioral plasticity in the flash communication systems of fireflies. *Am. Sci.* **66**(3): 340–346.

Charlton, R. E., and R. T. Card(943c. 1990. Behavioral interactions in the courtship of *Lymantria dispar* (Lepidoptera: Lymantriidae). *Ann. Entomol. Soc. Am.* **83**(1): 89–96.

Christy, J. H., and M. Salmon. 1991. Comparative studies of reproductive behavior in mantis shrimps and fiddler crabs. *Am. Zool.* **31:** 329–337.

Churchill, E. P., Jr. 1921. Life history of the blue crab. *Bull. U.S. Bur. Fish.* **36:** 95–128.

Cowan, D. F. 1991. The role of olfaction in courtship behavior of the American lobster *Homarus americanus. Biol. Bull.* **181:** 402–407.

Dejean, A. 1987. Behavioral plasticity of hunting workers of *Serrastruma serrula* (Hymenoptera: Formicidae, Myrmicinae) presented with different arthropods. *Sociobiology* **13**(3): 191–208.

Devine, D. V., and J. Atema. 1982. Function of chemoreceptor organs in spatial orientation of the lobster, *Homarus americanus:* differences and overlap. *Biol. Bull.* **163:** 144–153.

Drach, P. 1939. Mue et cycle d'intermue chez les crustaces decapodes. *Ann. Inst. Oceanogr.* **19:** 103–391.

Dunham, P. J. 1978. Sex pheromones in Crustacea. *Biol. Rev. Camb. Philos. Soc.* **53:** 555–583.

Dunham, P. J. 1988. Pheromones and behaviour in Crustacea. Pp. 375–392 in *Endocrinology of Selected Invertebrate Types,* H. Laufer and G. H. Downer, eds. Liss, New York.

Eales, A. J. 1974. Sex pheromone in the shore crab *Carcinus maenas,* and the site of its release from females. *Mar. Behav. Physiol.* **2:** 345–355.

Elner, R. W., and P. G. Beninger. 1995. Multiple reproductive strategies in snow crab, *Chionoecetes opilio:* Physiological pathways and behavioral plasticity. *J. Exp. Mar. Biol. Ecol.* **193:** 93–112.

Fuzessery, Z. M., and J. J. Childress. 1975. Comparative chemosensitivity to amino acids and their role in the feeding activity of bathypelagic and littoral crustaceans. *Biol. Bull.* **149:** 522–538.

Gibbs III, D. S. 1996. Field and laboratory evidence of pheromone mediated mating behavior in the blue crab, *Callinectes sapidus.* M.S. thesis, The College of William and Mary.

Gleeson, R. A. 1980. Pheromone communication in the reproductive behavior of the blue crab, *Callinectes sapidus. Mar. Behav. Physiol.* **7:** 119–134.

Gleeson, R. A. 1982. Morphological and behavioral identification of the sensory structures mediating pheromone reception in the blue crab, *Callinectes sapidus. Biol. Bull.* **163:** 162–171.

Gleeson, R. A. 1991. Intrinsic factors mediating pheromone communication in the crab *Callinectes sapidus.* Pp. 17–32 in *Crustacean Sexual Biology,* R. T. Baur and J. N. Martin, eds. Columbia University Press, New York.

Gleeson, R. A., M. A. Adams, and A. B. Smith III. 1984. Characterization of a sex pheromone in the blue crab, *Callinectes sapidus:* Crustecdysone studies. *J. Chem. Ecol.* **10:** 913–921.

Hartnoll, R. G. 1969. Mating in the Brachyura. *Crustaceana* **16:** 161–181.

Hay, W. P. 1905. The life history of the blue crab (*Callinectes sapidus*). *Rep. U.S. Bur. Fish.* **1904:** 395–413.

Hazlett, B. A. 1982. Chemical induction of visual orientation in the hermit crab *Clibanarius vittatus. Anim. Behav.* **30**(4): 1259–1260.

Hazlett, B. A. 1995. Behavioral plasticity in crustacea: why not more? *J. Exp. Mar. Biol. Ecol.* **193:** 57–66.

Hughes, M. 1996. The function of concurrent signals: visual and chemical communication in snapping shrimp. *Anim. Behav.* **52:** 247–257.

Jaccard, J. 1983. *Statistics for the Behavioral Sciences.* Wadsworth, Belmont, CA.

Jachowski, R. L. 1974. Agonistic behavior of the blue crab, *Callinectes sapidus* Rathbun. *Behaviour* **50:** 232–253.

Jivoff, P. 1997a. The relative roles of predation and sperm competition on the duration of the post-copulatory association between the sexes in the blue crab, *Callinectes sapidus. Behav. Ecol. Sociobiol.* **40:** 175–185.

Jivoff, P. 1997b. Sexual competition among male blue crab, *Callinectes sapidus. Biol. Bull.* **193:** 368–380.

Johnson, P. T. 1980. *Histology of the Blue Crab,* Callinectes sapidus. *A Model for the Decapoda.* Praeger Publishers, New York.

Kaissling, K. E. 1979. Recognition of pheromones by moths, especially in saturnids and *Bombyx mori.* Pp. 43–56 in *Chemical Ecology: Odour Communication in Animals,* F. J. Ritter, ed. Elsevier, Amsterdam.

Kamiguchi, Y. 1972. A histological study of the "sternal gland" in the female freshwater prawn, *Palaemon paucidens,* a possible site of origin of the sex pheromone. *J. Fac. Sci. Hokkaido Univ. Ser. VI, Zool.* **18**(3): 356–365.

Kaplan, L. J., C. Lowrance, J. Basil, and J. Atema. 1993. The role of chemical and visual cues in agonistic interactions of the American lobster. *Biol. Bull.* **185:** 320–321.

Linn, C. E., L. B. Bjostad, J. W. Du, and W. L. Roelofs. 1984. Redundancy in a chemical signal: behavioral responses of male *Trichoplusia ni* to a 6-component sex pheromone blend. *J. Chem. Ecol.* **10**(11): 1635–1658.

Lott, D. F. 1991. *Intraspecific Variation in the Social Systems of Wild Vertebrates.* Cambridge University Press, Cambridge.

Mantel, L. H., and L. L. Farmer. 1983. Osmotic and ionic regulation. Pp. 53–161 in *The Biology of Crustacea* Vol. 5, L. H. Mantel, ed. Academic Press, New York.

Ra'anan, Z., and D. Cohen. 1984. The effect of group interactions on the development of size distribution in *Macrobrachium rosenbergii* (de Man) juvenile populations. *Biol. Bull.* **166:** 22–31.

Rand, A. S., M. J. Ryan, and W. Wilczynski. 1992. Signal redundancy and receiver permissiveness in acoustic mate recognition by the Túngara frog, *Physalaemus pustulosus. Am. Zool.* **32:** 81–90.

Reynolds, J. D. 1993. Should attractive individuals court more? Theory and test. *Am. Nat.* **14:** 914–927.

Ryan, E. P. 1966. Pheromone: evidence in a decapod crustacean. *Science* **151:** 340–341.

Ryan, M. J. 1990. Sexual selection, sensory systems and sensory exploitation. *Oxf. Surv. Evol. Biol.* **7:** 157–195.

Salmon, M., and K. W. Horch. 1972. Acoustic signalling and detection by semi-terrestrial crabs of the family Ocypodidae. Pp 60–96 in *Behavior of Marine Animals. Current Perspectives in Research, Vol. 1, Invertebrates.* H. E. Winn and B. L. Olla, eds. Plenum Press, New York.

Seifert, P. 1982. Studies on the sex pheromone of the shore crab. *Carcinus maenas,* with special regard to ecdysone excretion. *Ophelia* **12**(2): 147–158.

Siegel, S., and N. J. Castellan Jr. 1988. *Nonparametric Statistics for the Behavioral Sciences.* 2nd ed. McGraw-Hill, New York.

Snyder, M. J., C. Ameyaw-Akumfi, and E. S. Chang. 1993. Sex recognition and the role of urinary cues in the lobster, *Homarus americanus. Mar. Behav. Physiol.* **24:** 101–116.

Stauffer, H. P., and R. D. Semlitch. 1993. Effects of visual, chemical and tactile cues of fish on the behavioural responses of tadpoles. *Anim. Behav.* **46:** 355–364.

Talbot, P., and D. Demers. 1993. Tegumental glands of crustacea. Pp.

151–191 in *The Crustacean Integument.* M. N. Horst and J. A. Freeman, eds. CRC Press, Boca Raton.

Teytaud, A. R. 1971. The laboratory studies of sex recognition in the blue crab, *Callinectes sapidus* Rathbun. Sea Grant Technical Bulletin No. 156. University of Miami Sea Grant Program. 62 pp.

Tinbergen, N. 1953. *Social Behaviour in Animals with Special Reference to Vertebrates.* Chapman and Hall, London.

Van den Hurk, R., and J. G. D. Lambert. 1983. Ovarian steroid gluconurides function as sex pheromones for female zebrafish, *Brachydanio rerio. Can. J. Zool.* **61:** 2381–2387.

Van Engel, W. A. 1958. The blue crab and its fishery in Chesapeake Bay. Part I—Reproduction, early development, growth and migration. *Commer. Fish. Rev.* **20:** 6–17.

Vetter, R. S., and T. C. Baker. 1983. Behavioral responses of male *Heliothis virescens* in a sustained-flight tunnel to combinations of seven compounds identified from female sex pheromone glands. *J. Chem. Ecol.* **9:** 747–759.

Waas, J. R., and P. W. Colgan. 1992. Chemical cues associated with visually elaborate aggressive displays of three-spine sticklebacks. *J. Chem. Ecol.* **18**(2): 2277–2284.

West-Eberhard, M. J. 1989. Phenotypic plasticity and the origins of diversity. *Annu. Rev. Ecol. Syst.* **20:** 249–278.

Reference: *Biol. Bull.* **197:** 72–81. (August 1999)

Translocation of Photosynthetic Carbon From Two Algal Symbionts to the Sea Anemone *Anthopleura elegantissima*

HILARY P. ENGEBRETSON AND GISÈLE MULLER-PARKER*

Department of Biology and Shannon Point Marine Center, Western Washington University, Bellingham, Washington 98225-9160

Abstract. The intertidal sea anemone *Anthopleura elegantissima* contains two symbiotic algae, zoochlorellae and zooxanthellae, in the Northern Puget Sound region. Possible nutritional advantages to hosting one algal symbiont over the other were explored by comparing the photosynthetic and carbon translocation rates of both symbionts under different environmental conditions. Each alga translocated 30% of photosynthetically fixed carbon in freshly collected anemones, although zoochlorellae fixed and translocated less carbon than zooxanthellae. The total amount of carbon translocated to the host was equivalent because densities of zoochlorellae were two to three times greater than were densities of zooxanthellae. In *A. elegantissima* maintained under high and low irradiance (100 and 10 μmol photons/m^2/s) at 20°C and 13°C for 21 days, both algae fixed and translocated carbon at greater rates at 20°C (translocation rates: 0.38 pg C /zoochlorella/h; 1.12 pg C /zooxanthella/h) than at 13°C (translocation rates: 0.06 pg C /zoochlorella/h; 0.37 pg C /zooxanthella/h). However, zoochlorellate anemones received 3.5 times less carbon at 20°C than at 13°C because the higher temperature caused a significant reduction in the density of zoochlorellae. Environmental variables, like temperature, that influence the densities of the two symbionts will affect their relative nutritional contribution to the host. Whether these differences in carbon translocation rates of the two algal symbionts affect the ecology of their anemone host awaits further investigation.

Introduction

The temperate sea anemones *Anthopleura elegantissima* and *Anthopleura xanthogrammica* host both dinoflagellate zooxanthellae and green algae known only generally as zoochlorellae (Muscatine, 1971). Both algal symbionts photosynthetically fix inorganic carbon and translocate some of the products to the animal host. Zooxanthellae in corals, as well as in *A. elegantissima*, translocate carbon to the host mainly as glycerol (Muscatine, 1967; Trench, 1971; Battey and Patton, 1987). Glycerol is used by the host to support its basal metabolism, while lipids that are also translocated by the algae are used to create lipid stores (Battey and Patton, 1987). We do not know what products are translocated by marine zoochlorellae to their host, although unpublished work by Minnick and McCloskey (cited in Verde and McCloskey, 1996) indicates that zoochlorellae translocate several amino acids in addition to glycerol. For zoochlorellae in the freshwater green hydra, maltose is the principal form of translocated photosynthate (Mews and Smith, 1982).

Further understanding of the nutritional relationship between *Anthopleura* and the two algae may come from comparisons of the amount of carbon translocated from the algae to the host. Previous studies have suggested that zoochlorellae do not translocate as much carbon as zooxanthellae. Using ^{14}C, O'Brien (1980) found that zoochlorellae in excised tentacles translocate from zero to 3.6% of the total carbon fixed by the algae to the epidermal tissues of *Anthopleura xanthogrammica.* Zooxanthellae in intact anemones translocate as much as 50% of the total ^{14}C-labelled carbon fixed to the host fraction of *A. elegantissima* (Trench, 1971). Based on carbon budgets, Verde and McCloskey (1996) calculate that zooxanthellae will have photosynthetic products available to supply *A. elegantissima*

Received 12 January 1998; accepted 3 June 1999.

* To whom correspondence should be addressed. E-mail: gisele@biol.wwu.edu

with 48% of its respiratory carbon requirement, while zoochlorellae will only be able to satisfy 9% of the anemone's respiratory needs. Verde and McCloskey conclude that the higher net photosynthesis and lower algal growth demand of zooxanthellae combine to provide more photosynthetic carbon to a zooxanthellate host anemone than is the case for an anemone that contains zoochlorellae as its endosymbiont. These studies show that zooxanthellae appear to be the "better" symbiont with respect to carbon supplied to the host.

It is important to directly compare carbon translocation rates of zoochlorellae and zooxanthellae under different temperatures and irradiance levels, because intertidal *A. elegantissima* are exposed to extreme seasonal fluctuations in these parameters (Dingman, 1998). Furthermore, both irradiance and temperature are thought to influence the distribution of these two algae within anemones. Field observations of the distribution of *Anthopleura xanthogrammica* in British Columbia, Canada, by O'Brien and Wyttenbach (1980) led the authors to suggest that zooxanthellae and zoochlorellae populations in anemones may be regulated by temperature. In the lower latitude, warmer regions of *Anthopleura's* range zooxanthellae are the dominant symbiont, while zoochlorellae are more abundant in anemones in the higher latitude, colder regions of *Anthopleura's* range (Secord, 1995). Are these distribution patterns related to differences in carbon translocation of the two algae? Saunders and Muller-Parker (1997) determined that increased temperature caused a reduction in the density of zoochlorellae in *Anthopleura elegantissima* tentacles over time. How do such changes in algal density affect the rate of carbon translocation to the host?

This study compares carbon fixation and translocation rates of both zoochlorellate and zooxanthellate anemones collected from a single site and kept under different environmental conditions likely to be encountered in the field. The effects of irradiance and temperature on translocation of fixed carbon from zooxanthellae and zoochlorellae to *A. elegantissima* are examined by measuring the distribution of radioactively labelled carbon in the algae and in the animal host, and relating the carbon translocation rates to population densities of the respective algae.

Materials and Methods

Collection of anemones and determination of symbiont complement

Anthopleura elegantissima was collected from a rocky intertidal area located on Anaco Beach, Fidalgo Island, Washington (48° 29′; 122° 42′) in June and July of 1994. Ambient seawater temperature was 11°C. Both zooxanthellate and zoochlorellate anemones were collected from the same large boulder, at one tidal height (+0.6 m). Nonsymbiotic (algae-free) anemones were collected from dark crevices in a nearby rock jetty. The anemones were placed in flow-through ambient seawater tables at Shannon Point Marine Center for one day before experiments began.

The anemones were separated by color and excised tentacles from several anemones were examined microscopically to verify that anemones that appeared brown in the field actually contained zooxanthellae, that green anemones contained zoochlorellae, and that white anemones were algae-free.

The symbiont complement of all anemones was confirmed by counting the number of zoochlorellae and zooxanthellae in homogenized anemone samples after ^{14}C incubation. Zoochlorellate anemones from the field contained an average of 99.0% (±2.0 SD, n = 18) zoochlorellae, while zooxanthellate anemones contained an average of 97.3% (±3.2 SD, n = 18) zooxanthellae. Three field anemones that contained mixed populations of both symbionts contained from 40% to 60% of each alga (average = 53% zoochlorellae) within their tissues.

Experimental treatments: symbiont, light, and temperature

To examine the effects of irradiance and temperature on zooxanthellate and zoochlorellate anemones, a 2 × 2 × 2 factorial experiment was designed with factors of anemone symbiont type, irradiance level, and temperature. Two experiments were run sequentially in one incubator. For each, 28 anemones, consisting of 14 zoochlorellate anemones and 14 zooxanthellate anemones, were placed in individual 50-ml beakers containing 35 ml of 5 μm-filtered seawater. For the first experiment the anemones were incubated at 20°C; for the second experiment the anemones were incubated at 13°C. The beakers containing the anemones were arranged randomly within the incubator under a bank of fluorescent lights providing a mean irradiance of 100 μmol photons/m^2/s. For each experiment, half of each group of anemones was covered with mesh for the low irradiance treatment (10% of full irradiance; see Saunders and Muller-Parker, 1997, for details). The lights were set to a natural daylength cycle of 14 h:10 h (light:dark). The anemones were fed every three days with freshly hatched *Artemia* nauplii and were last fed two days prior to ^{14}C incubation. The anemones were maintained under the experimental conditions for 21 days prior to measuring carbon fixation and translocation rates.

Carbon fixation and translocation

The amount of carbon photosynthetically fixed by the algal symbionts and translocated to the anemone host was measured using the ^{14}C method (O'Brien, 1980; Battey and Patton, 1987), with some modifications. One hour prior to the ^{14}C incubation period each anemone was transferred to an individual clear plastic vial (Nunc® tube). Exactly 10 ml of 5 μm-filtered seawater was added to each vial and the anemones were returned to their treatment conditions.

The ^{14}C incubations were always begun at the same time of day (0900 h) to minimize variation due to any factors associated with the natural photoperiod of the anemone. The addition of ^{14}C-bicarbonate to each vial was noted as time zero. After thorough mixing, 100 μl of the seawater was subsampled to determine the total activity of the seawater in the vial, which ranged from 13.6 to 21.3 μCi/anemone. Anemones in vials that were covered completely with foil to exclude light served as controls for each experiment. These controls were used to account for dark fixation of ^{14}C by the algae and/or the animal under each set of conditions. Separate controls were run for zoochlorellate and for zooxanthellate anemones. All anemones were incubated with ^{14}C for 1.5 h under the appropriate temperature and irradiance conditions they had experienced for 21 days. After incubation, the anemones were rinsed thoroughly with non-labelled seawater, making sure that seawater retained in the coelenteron was also expelled. The seawater in the vials was replaced, and all of the vials were covered completely with foil. The vials were then returned to the appropriate incubation conditions for the dark chase period, which was 1.75 h for most experiments. Following the dark chase period, the anemones were rinsed again and individually homogenized in seawater with a motor-driven teflon tissue grinder (60 ml volume). Homogenate volume (= anemone) was measured and 1 ml of the homogenate was frozen for later protein analysis. A 0.5 ml sample of the homogenate was transferred to a 7-ml plastic scintillation vial and acidified with 0.3 ml 6 *N* HCl under a heat lamp in a fume hood to remove unincorporated inorganic ^{14}C label. Assay of homogenate was used to determine the amount of ^{14}C fixed by the whole anemone.

The algae were separated from the host fraction to measure the distribution of ^{14}C in both fractions. Ten ml of the homogenate was centrifuged in a table top swinging bucket centrifuge for 10 min. The algal pellet was rinsed two times and the final algal pellet was resuspended in 5 ml of filtered seawater. The combined supernatant was the animal fraction of the homogenate and the resuspended pellet was the algal fraction. The final animal fraction volume was measured and 1-ml samples of the animal and algal fraction were frozen for later analysis. Half-milliliter (0.5-ml) samples of each fraction were acidified with 0.3 ml 6 *N* HCl, as described above. The acidified homogenate, animal, and algal samples in the scintillation vials were then neutralized with 0.3 ml 6 *N* NaOH, 5 ml of Ecolume scintillation fluid was added, and disintegrations per minute (DPM) of each sample counted in a Packard TriCarb 1900TR liquid scintillation counter.

To compare translocation of ^{14}C by freshly collected field anemones to the anemones in the experimental treatments, anemones gathered from the field were subjected to ^{14}C analysis the day after collection. These anemones were kept under a light bank of fluorescent lamps at a photosynthetically saturating irradiance of 309 μmol photons/m^2/s in a flow-through ambient seawater table (11°C) until ^{14}C analysis.

Biomass parameters

The protein content of the homogenate and animal fractions of each anemone was determined by the method of Lowry (Lowry *et al.*, 1951), using bovine serum albumin (BSA) as a standard. Two replicates of both homogenate and animal fractions from each anemone were analyzed on a Hitachi 100-40 spectrophotometer. To ascertain the algal biomass and proportion of zoochlorellae and zooxanthellae in each anemone, cell counts were done on the frozen algal fractions. The number of each alga (zoochlorellae and zooxanthellae) in each sample was counted using a hemacytometer viewed under a compound microscope. Six replicate counts of algal numbers were done for each sample. The mean of the replicate counts was normalized to weight of anemone homogenate protein to provide an estimate of algal density in each anemone.

Percent carbon translocation

The percent of fixed ^{14}C translocated to the host during the 1.75-h dark chase time was determined by dividing the DPM calculated for the whole animal fraction by DPM in the whole homogenate fraction. Any dark carbon fixation by the algae and host was accounted for by subtracting the mean DPM per mg protein of the dark control fractions for the appropriate symbiont type from the DPM per mg protein of each experimental anemone fraction (homogenate or animal) before calculating the percent translocation. For all symbiotic anemones, dark fixation accounted for less than 10% of the total carbon fixed by anemones in the light. For the nonsymbiotic anemones, dark fixation accounted for 86% of the total carbon fixed. Because the data were in the form of percentages, they were arcsine transformed for statistical analysis.

Rates of carbon fixation and translocation

Although the percent of fixed carbon translocated to the host is important, it does not indicate the actual rate of carbon received by the anemone under different environmental conditions. For that information, the rates of carbon fixation and translocation must be examined. The specific activity of ^{14}C in the seawater was used to calculate the actual amount of carbon fixed and translocated. The weight of carbon dioxide (all forms) present in the seawater was determined by the alkalinity method described in Parsons *et al.* (1984). The weight of the total inorganic carbon present in the seawater was then multiplied by the rate of uptake (or

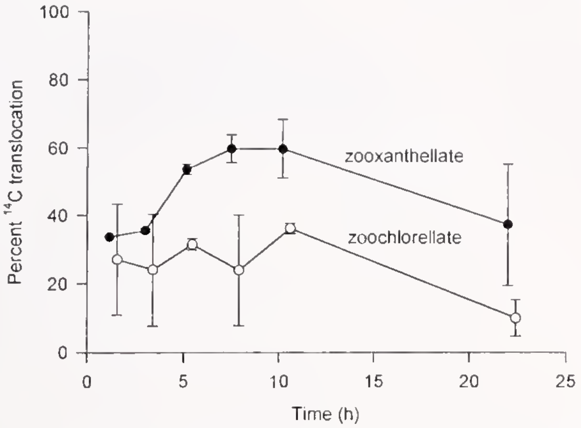

Figure 1. The effects of symbiont type and dark chase period on the percent of carbon translocated to the host anemone. $n = 2$ for each group; ± 1 SD of the mean.

translocation) of the labelled carbon in the sample, as determined by dividing DPM in the homogenate (or animal) fraction sample (corrected for DPM in the dark control) by the total activity (DPM) of the ^{14}C added and the hours of incubation with ^{14}C. The result is the rate of carbon fixation (or translocation), as amount of C fixed (or translocated) per hour.

Carbon fixation and translocation rates can be expressed on the basis of both anemone biomass (protein) and on the basis of an individual algal cell. Comparison of rates normalized to these two parameters shows how algal density affects photosynthesis and translocation. The rate of carbon fixed by anemones was calculated by using the homogenate fractions in the above calculation and normalizing to either anemone protein biomass or to number of algae. The rate of carbon translocated to the animal was calculated by using the animal fractions in the above calculation.

All analyses of variance and multiple range test statistics were examined with a significance level of 5%. Statistics were calculated using Statistix 4.1 by Analytical Software.

Results

Percent C translocation over time

A ^{14}C pulse-chase time course experiment was conducted with field anemones to determine if and how the length of the dark chase time affected the percent of carbon translocated to the host by the two symbionts. A 2 × 6 factorial analysis of variance showed that symbiont type had a significant effect on percent translocation ($P < 0.000$). Over the entire chase time period, the percent of fixed carbon translocated to the host by zooxanthellae is significantly higher than the percent of fixed carbon translocated by zoochlorellae (Fig. 1). The length of the chase time period also significantly affected the percent of carbon translocated to the host anemone ($P = 0.031$), but there was no interaction between symbiont type and chase period. Tukey's (HSD) multiple range test indicated that only chase time periods of 10.2 h and 22 h are significantly different from each other. To permit direct comparison of the effects of external factors (temperature and irradiance) on percent translocation, we used a short dark chase period (1.75 h) to compare C translocation of zoochlorellae and zooxanthellae in all subsequent experiments.

Percent translocation

There was no significant difference in the percent of carbon translocated from the algae to the animal in zoochlorellate, zooxanthellate, and mixed anemones collected from the field and incubated under saturating irradiance and at ambient seawater temperature (comparison by ANOVA). Percent carbon translocated averaged 30% for all field anemones under these conditions (Fig. 2).

The percent C translocated was higher for anemones maintained under the experimental treatments than for field anemones, and zoochlorellae translocated a greater percent of carbon (up to 65%; Fig. 2). Both temperature and symbiont type are significant main effects on percent translocation. Both symbionts translocated greater percentages of fixed carbon at 20°C than at 13°C (2 × 2 × 2 factorial analysis, $P = 0.013$). Additionally, zoochlorellae translocated a higher percent of fixed carbon than zooxanthellae ($P = 0.036$) at both temperatures. Irradiance was not a significant main effect on the percent of carbon translocated to the host ($P = 0.437$). No interaction effects were significant. Although these results show that hosting zoochlorel-

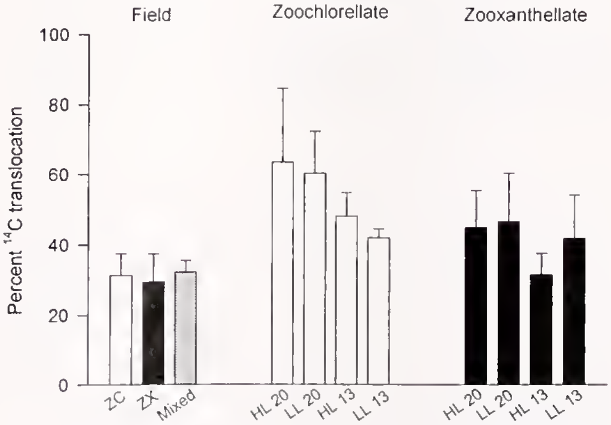

Figure 2. Percent of carbon translocated to the anemone host after a 1.75 h dark chase period. Field anemones were incubated at 11°C and a light intensity of 309 μmol photons/m^2/s (for zoochlorellate anemones, $n = 4$; for zooxanthellate and mixed anemones, $n = 2$). Experimental zoochlorellate and zooxanthellate anemones were incubated under their treatment conditions: high light (HL, 100 μmol/m^2/s) or low light (LL, 10 μmol/m^2/s) at either 13 or 20°C (20 or 13). $n = 5$ for each group; ± 1 SD of the mean.

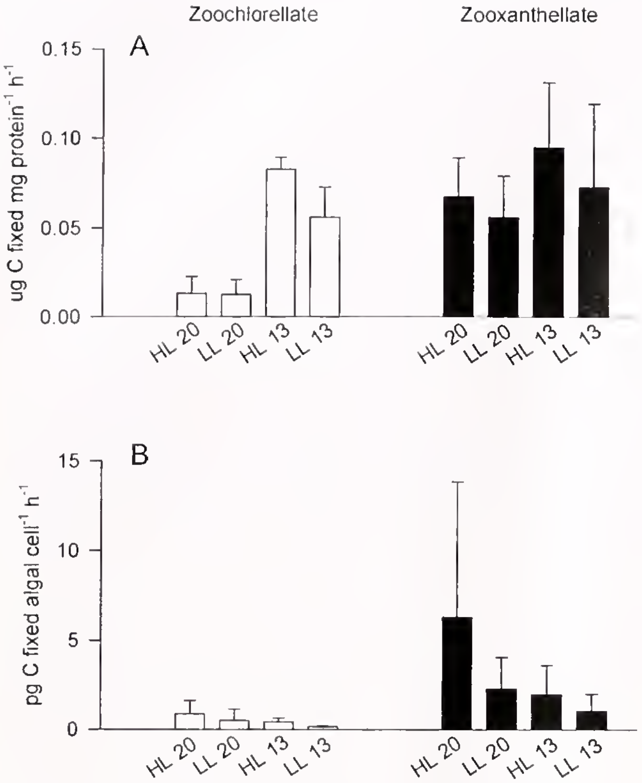

Figure 3. The rate of carbon fixation by zoochlorellate (☐) and zooxanthellate (■) anemones incubated under their treatment conditions: high light (HL, 100 μmol/m^2/s) or low light (LL, 10 μmol/m^2/s) at either 13 or 20°C (20 or 13). $n = 5$ for each group; ± 1 SD of the mean. A. The rate of carbon fixation per mg anemone protein. B. The rate of carbon fixation per algal cell.

lae at higher temperatures results in a greater *percent* of fixed carbon to the anemone, carbon translocation rates are needed to compare the actual *amounts* of carbon received by zoochlorellate and zooxanthellate anemones under field and experimental conditions.

Rates of carbon fixation and translocation

The rate of carbon fixation by zoochlorellate and zooxanthellate anemones maintained under high and low irradiance at 13°C and 20°C for 21 days was significantly affected by an interaction between temperature and symbiont type ($P = 0.009$). While zooxanthellate anemones fixed carbon at the same rate at both temperatures, zoochlorellate anemones fixed about three times more carbon at 13°C than at 20°C for rates expressed on the basis of anemone biomass (Fig. 3a). Carbon fixation and translocation rates expressed on an algal cell basis are needed to compare these processes at the level of the individual algal cell with that of the symbiotic association. When the rate of carbon fixation is normalized to algal numbers instead of to anemone protein biomass, none of the interaction effects were significant and both algae fixed carbon at a *lower* rate at 13°C than at 20°C (2.3 times less and 3 times less, respectively; $P = 0.004$; Fig. 3b). The rate of carbon fixation per algal cell is significantly greater under high irradiance than under low irradiance ($P = 0.045$), and at both temperatures the zooxanthellae fixed carbon at a significantly greater rate than did the zoochlorellae ($P = 0.000$).

As shown in Figure 4a for carbon fixation rates normalized to anemone biomass, the rate of carbon translocated to the host anemone is significantly affected by an interaction between temperature and symbiont type ($P = 0.009$). While zooxanthellate anemones experienced similar rates of carbon translocation at both temperatures, rates of translocation in zoochlorellate anemones were almost 3.5 times less at 20°C than at 13°C (Fig. 4a). At 13°C, rates of translocation are comparable for both zoochlorellate and zooxanthellate anemones, and these rates were higher at the high irradiance level at both temperatures (Fig. 4a). When carbon translocation rates are normalized to algal cell number, a significant interaction between temperature and symbiont type is again observed ($P = 0.039$; Fig. 4b). In this case, the rate of carbon translocation was also greater per

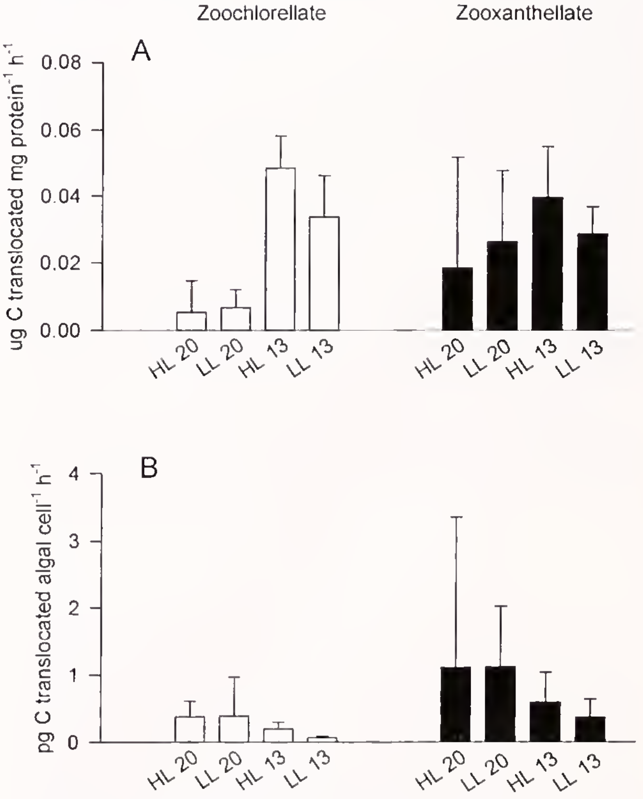

Figure 4. The rate of carbon translocation by zoochlorellate (☐) and zooxanthellate (■) anemones incubated under their treatment conditions: high light (HL, 100 μmol/m^2/s) or low light (LL, 10 μmol/m^2/s) at either 13 or 20°C (20 or 13). $n = 5$ for each group; ± 1 SD of the mean. A. The rate of carbon translocation per mg anemone protein. B. The rate of carbon translocation per algal cell.

Table I

Rates of carbon fixation and translocation by algae in zoochlorellate, zooxanthellate and mixed field anemones collected during summer, normalized to anemone protein biomass or to alga

	CARBON FIXED		CARBON TRANSLOCATED	
ANEMONE TYPE	μg C fixed/mg protein/h	pg C fixed/ alga/h	μg C translocated/mg protein/h	pg C translocated/ alga/h
Zoochlorellate	0.110 ± 0.03	0.275 ± 0.14	0.034 ± 0.007[a]	0.091 ± .06
Zooxanthellate	0.145 ± 0.06	1.236 ± 1.13	0.038 ± 0.004[a]	0.390 ± 0.042
Mixed	0.199 ± 0.02	0.684 ± 0.08	0.065 ± 0.012[b]	0.221 ± 0.01
Results of 1-way ANOVA	NS	NS	P = 0.014	NS

For zoochlorellate anemones, $n = 4$; for zooxanthellate and mixed anemones, $n = 2$. NS denotes the parameters (column headings) that are not significantly different among the three anemone types. Tukey's HSD Multiple Range Test indicated that both zoochlorellate and zooxanthellate anemones experienced similar rates of translocation per mg protein, while mixed anemones experienced a significantly greater rate of translocation per mg protein (a and b are used to indicate these differences among anemone types).

zooxanthella than per zoochlorella at both 13°C and 20°C; however, while zooxanthellae translocated approximately 2.5 times less carbon at 13°C as at 20°C, zoochlorellae translocated almost 4 times less carbon at 13°C as at 20°C (comparisons between temperatures use pooled rates from both irradiance levels, because irradiance did not affect the rate of carbon translocation per algal cell).

Although our sample size for field anemones is small, data obtained from these anemones provide a valuable comparison to treatment anemones. When mixed anemones are included in the comparison of carbon fixation and translocation rates of field anemones, the carbon fixation rates of zoochlorellate, zooxanthellate, and mixed field anemones are not significantly different from each other, whether expressed on the basis of anemone protein biomass or algal cell (Table I). Although algal cell-based translocation is not significantly different, the rate of carbon translocation per mg protein in *A. elegantissima* is significantly affected by symbiont type (Table I). However, Tukey's HSD Multiple Range Test indicated that both zoochlorellate and zooxanthellate anemones experienced similar rates of translocation per mg protein, while mixed anemones experienced a significantly greater rate of translocation per mg protein.

Algal density in anemones

Zoochlorellate field anemones contained significantly higher algal densities than did zooxanthellate field anemones (Fig. 5; $P = 0.000$). Mixed anemones had algal densities between those of zooxanthellate and zoochlorellate anemones; the density of algae in mixed anemones was not significantly different from the density of algae in either zooxanthellate or zoochlorellate anemones.

A two-way ANOVA performed on the algal density within the anemones after 21 days under the experimental treatments showed that the interaction between temperature and symbiont type was significant ($P = 0.001$). All anemones held at 20°C contained similar densities of algae; however, at 13°C zooxanthellate anemones had significantly fewer algae per mg anemone protein than did zoochlorellate anemones (Fig. 5). Anemones held in the laboratory under all experimental treatments contained significantly fewer algae than did anemones freshly collected from the field ($P = 0.000$).

Discussion

Percent translocation and translocation rates

In the field, zoochlorellate and zooxanthellate anemones receive the same amount of photosynthetic carbon from their symbionts during the summer in northern Puget Sound (Fig. 2, Table I). These results suggest that during summer

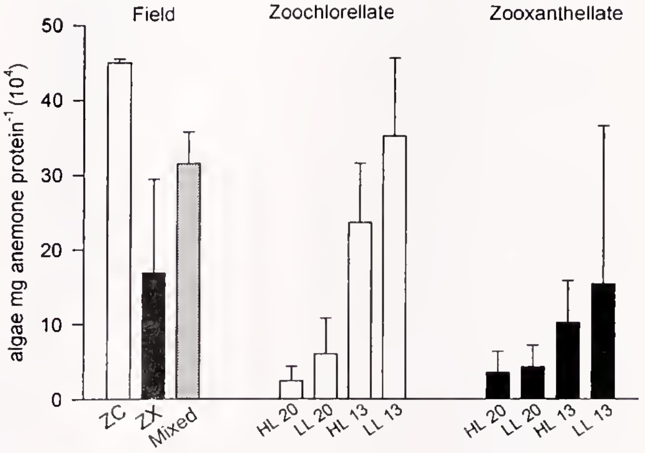

Figure 5. Density of algae in field anemones (n = 20, 17, and 3 for zoochlorellate, zooxanthellate, and mixed anemones respectively) and in zoochlorellate (□) and zooxanthellate (■) anemones after 21 days under high light (HL, 100 μmol/m^2/s) or low light (LL, 10 μmol/m^2/s) at either 13 or 20°C (20 or 13). n = 7 for each group; ± 1 SD of the mean.

there is no selective advantage, with respect to carbon, of hosting one symbiont over the other under saturating irradiance levels and ambient temperature. However, under different environmental conditions imposed in a laboratory experiment, zoochlorellae translocated a greater percent of fixed carbon to the host than did zooxanthellae, and both algal symbionts translocated a significantly greater percent of the carbon they fixed at 20°C than at 13°C (Fig. 2). The implications of these results are discussed below.

In our study, zoochlorellae translocated a much greater percent of the fixed carbon than shown by the previous studies of Muscatine (1971), O'Brien (1980), and Verde and McCloskey (1996). However, the percent carbon translocated by both algae in *A. elegantissima* is comparable to values obtained for other temperate cnidarian symbioses (Sutton and Hoegh-Guldberg, 1990; Davy *et al.*, 1997). Muscatine (1971), using ^{14}C analysis, determined that zoochlorellae translocate only 1.0% to 3.6% of the carbon they fix. However, Muscatine used only the tentacles and not whole anemones in his experiments; in addition, for some experiments the animal and algal fractions from tentacles were homogenized and separated before incubation with ^{14}C. O'Brien (1980) found that zoochlorellae translocated 1.3% to 3.9% of the carbon they fixed. O'Brien also used only tentacles of *A. xanthogrammica.* He dissected the epidermis of the anemone from the algae-containing gastrodermis after ^{14}C incubation and used the epidermis as the animal fraction and the gastrodermis as the algal fraction for translocation calculations. Any labelled carbon that the algae had translocated to the gastrodermal tissues of the host was counted as fixed carbon retained by the algal fraction. In addition, any host mechanisms acting upon translocation would be lost due to the excision of the tentacle from the remainder of the anemone body.

The ^{14}C method employed in this study accounts only for short-term carbon products fixed and released by the algae from inorganic carbon supplied in the external environment. There is substantial evidence for zooxanthellae that recently fixed carbon is released to the host (Sutton and Hoegh-Guldberg, 1990; Wang and Douglas, 1997). In contrast, translocation of carbon based on the growth-rate method takes into account the daily carbon budget of the symbiotic algae (Muscatine *et al.*, 1984). Because carbon required for algal growth may be supplied from the host animal (Trench, 1979), any contribution of host-derived carbon is wholly missed by the ^{14}C method as applied here. This may explain the discrepancy between our results and those of Verde and McCloskey (1996), who found that zoochlorellae may have only minimal excess carbon available to translocate to the host. The algae may selectively translocate photosynthetically fixed carbon while concurrently obtaining carbon for growth from the anemone host. This comparison also illustrates the importance of defining the time scales used to assess carbon translocation. Zoochlorellate and zooxanthellate anemones receive the same amount of translocated carbon during short-term (hours) ^{14}C incubations (our results), while growth rate comparisons based on longer time intervals (days to weeks) show that zoochlorellae translocate less carbon (Verde and McCloskey, 1996). The appropriate time scale for comparisons of these two algae will depend on the metabolic fate of the translocated carbon and on the external supply of carbon derived from host feeding.

Higher carbon fixation rates by both algae at the high irradiance level at both temperatures also resulted in greater carbon translocation rates (Figs. 3, 4). It appears that the symbiotic algae simply translocate fixed carbon at a higher rate under high irradiance because they have more photosynthetic product available. These results indicate that, with similar algal densities, anemones located in areas exposed to high solar irradiance should receive larger amounts of fixed carbon from their symbionts than should anemones located in areas of low light. The same is true for temperature. Both zoochlorellae and zooxanthellae fixed and translocated carbon at greater rates at 20°C. However, the advantage of greater carbon translocation at the higher temperature and irradiance level on an algal cell basis is offset by lower algal densities under these conditions, reducing the amount of carbon received by the anemone (see below).

Algal density and carbon translocation in anemones

Zoochlorellate anemones from the field contained approximately two to three times the density of algae as did zooxanthellate anemones (Fig. 5), as has been found by others (Verde and McCloskey, 1996; Dingman, 1998). Thus, although an individual zoochlorella translocates carbon to the host anemone at a lesser rate than does a zooxanthella (Table I; Fig. 4b), both anemone types receive fixed carbon at similar rates because of increased densities of zoochlorellae in field anemones (Fig. 5). Interestingly, although the zoochlorellae are numerically more abundant, volume comparisons indicate that they occupy the same "space" as the larger zooxanthellae within the anemones (unpub. data). Therefore, both anemone types in the field maintain similar ratios of algal to animal biomass and receive similar amounts of photosynthate.

Anemones in all experimental treatments contained significantly fewer algae than did field anemones, and both types of anemone had lower algal densities at the higher temperature (Fig. 5). This may be related to differences in summer field conditions and laboratory incubator conditions. Although anemones were maintained at relatively low constant irradiances in the lab (an order of magnitude lower than noon irradiance levels in the field), they probably received more light on a daily basis than field anemones because of tide-related changes in water depth and rapid light extinction due to high plankton levels in summer. Field anemones also experienced pronounced daily changes in water temperature during periods of exposure to low tide. Changes in density of symbionts may result from differences in both algal growth rate and algal expulsion rate under the experimental treatments. Although we did not measure these parameters in our study, zooxanthellate and zoochlorellate *A. elegantissima* have higher algal expulsion rates at 20°C than at 13°C (Saunders, 1995). McCloskey *et al.* (1996) also found that algal expulsion rates increase with increasing irradiance, and concluded that algal densities in *A. elegantissima* are regulated by expulsion of excess algae. In mixed anemones, the presence of the dominant symbiont is more likely due to that alga's ability to grow at a rate that meets or exceeds the rate of expulsion by the anemone and the growth rate of the other algal species. It is likely that greater numbers of algae were lost from zoochlorellate anemones than were lost from zooxanthellate anemones at 20°C since, as noted earlier, zoochlorellate anemones from the field contain higher densities of algae than do zooxanthellate anemones.

With respect to translocation of photosynthetic carbon, the relative abundance of zooxanthellae and zoochlorellae in *A. elegantissima* determines the amount of carbon translocated within anemones. How does the advantage of greater carbon translocation at the higher temperature and irradiance level on an algal cell basis affect the amount of carbon received by anemones when these also contain lower algal densities (Fig. 5)? A zoochlorellate anemone held at 13°C under high light receives 0.048 μg C/mg protein/h from its algae (Fig. 4a). To maintain this rate of carbon translocation at 20°C, the anemone would require an algal density of only 9.6×10^4 algae/mg protein because individual zoochlorellae translocate 2.5 times more at the higher temperature. However, the density of zoochlorellae at 20°C was one-fourth (26%) of this density (Fig. 5), showing that the higher translocation rate per cell was not sufficient to compensate for the reduced density of zoochlorellae at the higher temperature. A similar calculation for a zooxanthellate anemone shows that it needs 2.97×10^4 algae/mg protein at 20°C to maintain a translocation rate equivalent to that obtained at 13°C. However, zooxanthellate anemones held at 20°C contained 3.5×10^4 algae/mg protein (Fig. 5), about 18% *more* than required to maintain the translocation rate obtained at 13°C. This slightly elevated density of zooxanthellae was not sufficient to yield any significant difference in translocation rate (Fig. 4a). Using carbon translocation at 13°C as the basis of comparison, zoochlorellate anemones lost more algae than they should have at 20°C, and zooxanthellate anemones kept more algae than they needed to at this temperature. This comparison suggests that the nutritional contribution of the algae is not important to the host anemone and there is no regulation of algal densities to maintain certain carbon translocation rates. However, the cost to the host anemone of harboring symbionts at different densities is unknown. Should reduced algal densities lower the cost of maintaining the symbionts, then simply comparing carbon translocation rates is insufficient for assessing benefit to the host.

Application to the field

The *Anthopleura elegantissima*-zooxanthella nutritional relationship has been examined by determining the percent contribution of translocated carbon to animal respiration (CZAR). Shick and Dykens (1984) indicated that CZAR was greater for low intertidal (34%) than for high intertidal anemones (18%) due to self-shading of the anemone during exposure to air, while Fitt *et al.* (1982) demonstrated that CZAR for fed anemones (13%) was less than that for starved anemones (45%). In the only study to compare CZAR of anemones harboring both symbionts, Verde and McCloskey (1996) showed that CZAR for zooxanthellate anemones was much greater than CZAR for zoochlorellate anemones. The use of CZAR as a tool of comparison hinges on the assumptions that the algae will translocate all unneeded fixed carbon, that the anemone will use all of the translocated carbon, and that the form in which the fixed carbon is translocated does not matter to the anemone. Some of these assumptions may not apply to temperate anemone symbioses.

While there may be energetic advantages to the anemone to maintaining an algal population within its tissues, these advantages may be quite limited for temperate anemones (Davy *et al.*, 1997). *Anthopleura elegantissima* may not rely on carbon supplied by zooxanthellae for growth. Tsuchida and Potts (1994) demonstrated that *A. elegantissima* clones gained or lost weight in response to whether they were fed or not, regardless of whether they were kept in the light or dark, or whether they contained zooxanthellae or were algae-free. Similar results for zooxanthellate and zoochlorellate anemones were obtained by Blevins (1991). The heterotrophic supply of carbon appears to be the primary source of nutrition for these anemones. Indirect evidence for high rates of feeding under field conditions is provided by high ammonium concentrations in anemone-dominated tidepools (Jensen and Muller-Parker, 1994). Moreover, Davy *et al.* (1996) showed that reduced photosynthetic production of zooxanthellae in temperate anemones due to cloud cover, depth, and other environmental conditions could decrease the alga's translocatable carbon to just 0.7% of that fixed. Reliance on external carbon sources will be pronounced during seasonally low irradiance during the winter months. During such times the algae may represent a liability to the host, especially because algal densities in *A. elegantissima* during the winter season are the same as densities in midsummer (Dingman, 1998). In contrast with tropical symbiotic associations (Muscatine *et al.*, 1981; 1984; Davies, 1984), temperate symbiotic cnidarians like *Anthopleura* must often depend on sources outside of their algal complement for their respiratory carbon requirements as well as their growth needs (Davy *et al.*, 1997).

On the other hand, during warm and sunny periods, translocated photosynthate may be an important source of carbon. Clark and Jensen (1982) proposed that a period of high yield during such conditions may be sufficient for the anemone hosts to keep the symbionts year-round. Because their study of the anemone *Aiptasia pallida* showed that temperature also affects the nature of the translocated products, it will be important to compare the metabolites translocated by zoochlorellae and zooxanthellae under the range of environmental conditions experienced by anemones in the field. The nature of these metabolites, and the ability of the anemone host to use translocated compounds, may be more important than the amount of carbon translocated. Temperate symbioses exposed to pronounced seasonal variations in environmental factors are ideal systems in which to explore variation in the nutritional contribution of algal symbionts to the host and the consequences for the association.

The quantity of carbon translocated, as examined in this study, is only one factor in the symbiosis between zoochlorellae, zooxanthellae, and the anemone host in temperate regions. While this factor has justifiably received the greatest attention in tropical algal-cnidarian symbioses, it is not at all clear if provision of carbon is the most important benefit of the symbiosis to temperate *A. elegantissima*. If it was, our results suggest that zooxanthellae should predominate given their translocation potential under high temperature. Other selective advantages not directly related to carbon translocation must also be considered for this dual symbiosis. For example, there may be different energetic costs to hosting zooxanthellae and zoochlorellae associated with photooxidative stress resulting from photosynthesis, since host anemones must protect against toxic effects of reactive oxygen species (Shick, 1991). It would be interesting to compare antioxidant defenses in zooxanthellate and zoochlorellate anemones. There may be behavioral costs associated with harboring these two algae. If photosynthesis of zooxanthellae and zoochlorellae results in different expansion and contraction behaviors of anemones in the field, these may affect primary productivity and feeding on zooplankton (Shick and Dykens, 1984), as well as gas and dissolved organic matter exchanges with the environment. Ecological consequences of harboring different symbionts must also be considered. For example, Augustine and Muller-Parker (1998) have shown that selective predation on zooxanthellate anemones by a sculpin favors the survival and propagation of zoochlorellate anemones. Future studies should also focus on long-term comparisons of the growth and asexual reproduction of zooxanthellate and zoochlorellate anemones under a variety of environmental conditions. Continuing studies of this dual symbiosis in a temperate environment should prove useful to researchers studying tropical symbioses as well.

Acknowledgments

We thank two anonymous reviewers for their helpful comments. This study was supported by a Project Development Award from Western Washington University to Gisèle Muller-Parker.

Literature Cited

Augustine, L., and G. Muller-Parker. 1998. Selective predation by the mosshead sculpin *Clinocottus globiceps* on the sea anemone *Anthopleura elegantissima* and its two algal symbionts. *Limnol. Oceanogr.* **43:** 711–715.

Battey, J. F., and J. S. Patton. 1987. Glycerol translocation in *Condylactis gigantea. Mar. Biol.* **95:** 37–46.

Blevins, J. K. 1991. Comparative growth and metabolism of zooxanthellate and zoochlorellate *Anthopleura elegantissima.* Master's thesis, Western Washington University. 41 pp.

Clark, K. B., and K. R. Jensen. 1982. Effects of temperature on carbon fixation and carbon budget partitioning in the zooxanthellal symbiosis of *Aiptasia pallida* (Verrill). *J. Exp. Mar. Biol. Ecol.* **64:** 215–230.

Davies, P. S. 1984. The role of zooxanthellae in the nutritional energy requirements of *Pocillopora eydouxi. Coral Reefs* **2:** 181–186.

Davy, S. K., I. A. N. Lucas, and J. R. Turner. 1996. Carbon budgets in temperate anthozoan-dinoflagellate symbioses. *Mar. Biol.* **126:** 773–783.

Davy, S. K., J. R. Turner, and I. A. N. Lucas. 1997. The nature of temperate anthozoan-dinoflagellate symbioses. Proc. 8th Int. Coral Reef Symp. **2:** 1307–1312.

Dingman, H. C. 1998. Environmental influence on algal symbiont populations in the sea anemone *Anthopleura elegantissima.* Master's thesis, Western Washington University. 92 pp.

Fitt, W. K., R. L. Pardy, and M. M. Littler. 1982. Photosynthesis, respiration, and contribution to community productivity of the symbiotic sea anemone *Anthopleura elegantissima* (Brandt, 1835). *J. Exp. Mar. Biol. Ecol.* **61:** 213–232.

Jensen, S., and G. Muller-Parker. 1994. Inorganic nutrient fluxes in anemone-dominated tidepools. *Pac. Sci.* **48:** 32–43.

Lowry, O. H., N. J. Rosebrough, H. L. Farr, and R. J. Randall. 1951. Protein measurement with the Folin phenol reagent. *J. Biol. Chem.* **193:** 265–275.

McCloskey, L. R., T. G. Cove, and E. A. Verde. 1996. Symbiont expulsion from the anemone *Anthopleura elegantissima* (Brandt) (Cnidaria; Anthozoa). *J. Exp. Mar. Biol. Ecol.* **195:** 173–186.

Mews, L. K., and D. C. Smith. 1982. The green hydra symbiosis. VI. What is the role of maltose transfer from alga to animal? *Proc. R. Soc. Lond. B* **216:** 397–413.

Muscatine, L. 1967. Glycerol excretion by symbiotic algae from corals and *Tridacna* and its control by the host. *Science* **156:** 516–519.

Muscatine, L. 1971. Experiments on green algae coexistent with zooxanthellae in sea anemones. *Pac. Sci.* **25:** 13–21.

Muscatine, L., L. R. McCloskey, and R. E. Marian. 1981. Estimating the daily contribution of carbon from zooxanthellae to coral animal respiration. *Limnol. Oceanogr.* **26:** 601–611.

Muscatine, L., P. G. Falkowski, J. W. Porter, and Z. Dubinsky. 1984. Fate of photosynthetic fixed carbon in light- and shade-adapted colonies of the symbiotic coral *Stylophora pistillata. Proc. R. Soc. Lond. B* **222:** 181–202.

O'Brien, T. L. 1980. The symbiotic association between intracellular zoochlorellae (Chlorophyceae) and the coelenterate *Anthopleura xanthogrammica. J. Exp. Zool.* **211:** 343–355.

O'Brien, T. L., and C. R. Wyttenbach. 1980. Some effects of temperature on the symbiotic association between zoochlorellae (Chlorophyceae) and the sea anemone *Anthopleura xanthogrammica. Trans. Am. Microsc. Soc.* **99(2):** 221–225.

Parsons, T. R., Y. Maita, and C. M. Lalli. 1984. *A Manual of Chemical and Biological Methods for Seawater Analysis.* Pergamon Press. Oxford, England. Pp. 115–119, 140–148.

Saunders, B. K. 1995. The effects of temperature and light on populations of symbiotic algae in the sea anemone *Anthopleura elegantissima.* Master's thesis, Western Washington University. 52 pp.

Saunders, B. K., and G. Muller-Parker. 1997. The effects of temperature and light on populations of two algae in the temperate sea anemone *Anthopleura elegantissima* (Brandt, 1835). *J. Exp. Mar. Biol. Ecol.* **211:** 213–224.

Secord, D. L. 1995. Host specificity and symbiotic interactions in sea anemones. Ph.D. dissertation, University of Washington, Seattle, WA. 88 pp.

Shick, J. M. 1991. *A Functional Biology of Sea Anemones.* Chapman and Hall, London.

Shick, J. M., and J. A. Dykens. 1984. Photobiology of the symbiotic sea anemone *Anthopleura elegantissima:* photosynthesis, respiration, and behavior under intertidal conditions. *Biol. Bull.* **166:** 608–619.

Sutton, D. C., and O. Hoegh-Guldberg. 1990. Host-zooxanthella interactions in four temperate marine invertebrate symbioses: assessment of effect of host extracts on symbionts. *Biol. Bull.* **178:** 175–186.

Trench, R. K. 1971. The physiology and biochemistry of zooxanthellae symbiotic with marine coelenterates. I. Liberation of fixed 14C by zooxanthellae *in vitro. Proc. Roy. Soc. Lond. B.* **177:** 237–250.

Trench, R. K. 1979. The cell biology of plant-animal symbiosis. *Annu. Rev. Plant Physiol.* **30:** 485–531.

Tsuchida, C. B., and D. C. Potts. 1994. The effects of illumination, food and symbionts on growth of the sea anemone *Anthopleura elegantissima* (Brandt, 1835). I. Ramet growth. *J. Exp. Mar. Biol. Ecol.* **183:** 227–242.

Verde, E. A., and L. R. McCloskey. 1996. Photosynthesis and respiration of two species of algal symbionts in the anemone *Anthopleura elegantissima* (Brandt) (Cnidaria; Anthozoa). *J. Exp. Mar. Biol. Ecol.* **195:** 161–171.

Wang, J.-T., and A. E. Douglas. 1997. Nutrients, signals, and photosynthate release by symbiotic algae. *Plant Physiol.* **114:** 631–636.

Reference: *Biol. Bull.* **197:** 82–93. (August 1999)

Morphology and Epithelial Ion Transport of the Alkaline Gland in the Atlantic Stingray (*Dasyatis sabina*)

GREGORY M. GRABOWSKI,[1] JOHN G. BLACKBURN,[2] AND ERIC R. LACY[3,4]

[1] *Department of Biology, University of Detroit Mercy, 4001 W. McNichols, P.O. Box 19900, Detroit, Michigan 48219;* [2] *Department of Physiology,* [3] *Department of Cell Biology and Anatomy, Medical University of South Carolina, 171 Ashley Avenue, Charleston, South Carolina 29425; and* [4] *Marine Biomedicine and Environmental Sciences, Medical University of South Carolina, 221 Fort Johnson Road, Charleston, South Carolina 29412*

Abstract. The alkaline glands are two fluid-filled sacs that lie on the ventral, posterior surface of each kidney in skates and rays. In this study, the morphology, transepithelial ion transport, fluid constituents, and histochemistry of the alkaline glands of the Atlantic stingray, *Dasyatis sabina*, were investigated. The duct from each gland joined the corresponding vas deferens and the resulting two common ducts emptied into the cloaca. Dark burgundy, aqueous fluid (pH 8.0–8.2) was secreted into the sacs by a simple columnar epithelium with extensive rough endoplasmic reticulum and large secondary lysosomes containing lipofuscin and membrane fragments. Zonulae occludentes were deep (~22 fibrils), reflecting an electrically tight epithelium (732 ohms/cm^2). Carbonic anhydrase activity was localized histochemically within the intercellular spaces and less intensely in the mid-basal cytoplasm.

In vitro electrophysiology showed that baseline short-circuit current (Isc, 29.1 μA/cm^2) was reduced 67.0% after Cl$^-$ removal from the medium. Cl$^-$ removal also completely abolished luminal alkalinization (baseline 4.5 ± 0.7 μEq of acid/cm^2/h). Luminal exposure to the chloride-bicarbonate exchange inhibitor, DIDS, reduced Isc by 38%. Simultaneous administration of DIDS and bumetanide (Na$^+$/K$^+$/Cl$^-$ cotransport inhibitor) to the serosal side of the tissue caused the Isc to decrease >100%. Serosal exposure to ouabain (Na-K, ATPase inhibitor) decreased Isc 48%, whereas amiloride (sodium ion channel blocker) and acetazolamide (carbonic anhydrase inhibitor) had no statistically significant effect on Isc or alkalinization rates. Taken together the results suggest the presence of apical epithelial bicarbonate exchangers that are chloride or sodium dependent, basal sodium and HCO_3^- transport, and an Isc that is not totally dependent on Na$^+$-K$^+$ ATPase.

Introduction

Early anatomical studies of the male skate and stingray urogenital system reported a pair of blind-ended sacs, each of which opened into the cloaca. These structures were described initially as urinary bladders or sperm storage sacs (Borcea, 1906; Daniel, 1934), but the only evidence to support this functional nomenclature is the proximity of the sacs' openings to those of the ureters and vas deferens within the cloaca.

The sacs secrete and store a watery fluid of high pH (8.0–9.2), thus their name, alkaline gland (Maren *et al.*, 1963). On the basis of the high pH of the fluid, Smith (1929) speculated that it neutralized the potentially deleterious effects of acidic urine in the cloaca on the extruded sperm. As yet, however, no studies on the physiological function of the alkaline gland have been published.

A few reports, from various skate species (little skate, *Raja erinacea;* barndoor skate, *R. stabuliforis;* big skate, *R. ocellata*), have described the gland's morphology and epithelial transport physiology (H.W. Smith, 1929; Maren *et*

Received 12 April 1999; accepted 14 June 1999.

Send correspondence to Eric R. Lacy, Marine Biomedicine and Environmental Sciences, Medical University of South Carolina, 221 Fort Johnson Road, Charleston, SC 29412.

A portion of this work was presented in abstract form (The FASEB Journal, Part I, #3024, 1992).

al., 1963; Masur, 1984; P. L. Smith, 1981, 1985). These morphological accounts show that the gland lumen has mucosal "villar projections" lined by a simple columnar epithelium (Maren *et al.*, 1963; Masur, 1984). The mucosa generates and maintains a hundred-fold concentration gradient of OH ions and a 50-fold gradient of CO_2 from plasma to gland lumen; these are some of the steepest alkaline gradients across any epithelium in nature (Maren *et al.*, 1963). Given the unique epithelial transport properties of the alkaline gland, physiologic studies have focused on the mechanisms of fluid and bicarbonate secretion (Maren *et al.*, 1963; Smith, 1981, 1985).

Chloride and bicarbonate are the two main anions constituting alkaline gland fluid in the skate. *In vitro* experiments indicate that chloride secretion accounts for most, if not all, of the short-circuit current (Isc) (Maren *et al.*, 1963; Smith, 1981, 1985). These results led to speculation that chloride-dependent bicarbonate transport might be involved in fluid alkalinization. Although definitive evidence was lacking, secreted chloride was believed to recirculate into the epithelial cell by way of a Cl^-/HCO_3^- exchanger located at the apical plasma membrane (Maren *et al.*, 1963; Smith, 1981, 1985). Carbonic anhydrase, an enzyme associated with many bicarbonate-secreting tissues, was identified biochemically in the alkaline gland of some but not all skate species studied (Maren *et al.*, 1963). The concentration of carbonic anhydrase in the tissue was correlated with the pH of the alkaline gland fluid produced (Maren *et al.*, 1963), suggesting that this enzyme has a role in bicarbonate secretion for some skate species.

The present study uses transmission and scanning electron microscopy and freeze fracture to elucidate the ultrastructural organization of the alkaline gland in a stingray species, *Dasyatis sabina*, the Atlantic stingray. The presence and distribution of carbonic anhydrase activity, nerve fibers, and lipofusion were identified histochemically. These results are correlated with *in vitro* electrophysiological data and rates of fluid alkalinization. Some of the regulatory mechanism of ion transport were probed with various metabolic inhibitors. The composition of the fluid removed from the alkaline glands was analyzed.

Materials and Methods

Sexually mature male Atlantic stingrays (*Dasyatis sabina*, wing span ~45 cm) purchased from Gulf Specimens Inc. (Panacea, FL) or captured along the coast of South Carolina were allowed to acclimate in a 16,000-l holding tank for at least 5 days prior to experimentation. Water in the holding tank was drawn from Charleston (South Carolina) Harbor (650–850 mosm/l) and maintained at room temperature. Stingrays were fed shrimp twice a week and kept on a 12-h light/dark cycle. After acclimation, animals were anesthetized with MS222 (3-aminobenzoic acid ethyl ester, 0.5 g/l, Sigma Chemical Co.) and double pithed. The body cavity was opened by a ventral midline incision; the alkaline gland fluid was aspirated with a 25-gauge needle and saved at 4°C for further analysis; the alkaline gland was removed for use in morphology or electrophysiology experiments.

Light and electron microscopy

Fixative (2.5% paraformaldehyde, 5.0% glutaraldehyde, and 0.25% picric acid; Ito and Karnovsky, 1968) was injected into both sacs of the gland immediately after the fluid was removed. After 1 h the puboischiac bar was severed, and the alkaline gland was freed from surrounding tissue with fine forceps. Each gland was excised at its junction with the cloacal wall and placed in the same fixative for 24 h. The tissue was then rinsed, trimmed into 1-mm^2 pieces with a razor blade, and stored in 0.1 *M* sodium cacodylate buffer.

Alkaline gland fluid was centrifuged at 200 × *g* for 10 min. The pellet was fixed for 4 h in the same fixative injected into the gland sacs (Ito and Karnovsky, 1968). Both pellet and pieces of fixed gland were then postfixed (1.0% osmium tetraoxide in 0.1 *M* sodium cacodylate buffer), dehydrated in graded ethanols, and embedded in Epon-Araldite. Sections were cut, stained (semithin sections stained with alkalinized toluidine blue and ultrathin sections with uranyl acetate and lead citrate), and examined using a light microscope or a JEOL 1200 EX electron microscope.

Additional gland tissue, fixed as described above but in aldehydes only, was cryoprotected in graded concentrations of glycerols to a final concentration of 30% glycerol for freeze fracture. The tissue was then frozen rapidly in liquid propane, followed by fracturing and replication in a Balzer 360 M device (Balzers, Fürstentum Liechtenstein). Replicas were supported on 200-mesh copper grids and examined with the transmission electron microscope.

Aldehyde-fixed tissue was also used for scanning electron microscopy. It was first postfixed in 1.0% osmium tetraoxide in 0.1 *M* sodium cacodylate buffer, followed by dehydration in graded ethanols, and then critical point dried using a Sorvall critical point dryer (Newtown, CT). Tissue was coated with gold/palladium for 3 min at 2.5 kV and 20 mA using an E5100 sputter coating unit (Polaron Instruments, Doylestown, PA) and examined with a JEOL 35C scanning electron microscope.

Lipofuscin staining

Alkaline gland tissue and particulate matter from gland fluid of four stingrays were stained for lipofuscins using the Long Ziehl-Neelsen technique (Bancroft and Cook, 1984). The pellet, as described above, and gland tissue were fixed in Bouin's solution for 2 h, followed by dehydration in graded ethanols, clearing in xylene, and embedding in paraffin. Five-micrometer-thick sections were deparaffinized in xylene taken stepwise to water and stained in filtered carbol fuchsin for 1–3 h at 56°C. After staining, sections were washed in water, differentiated in 1% acid-alcohol, and counter stained in aqueous methylene blue. Slides were then rinsed in water, dehydrated, cleared in xylene, and mounted on glass slides. Lipofuscin appeared bright magenta, and nuclei stained blue against a pale magenta background.

Silver staining of neural tissue

Nerve fibers in alkaline glands were localized using the silver precipitate method of Sevier and Munger (1965). Five-micrometer-thick paraffin sections of Bouin's fixed tissue were incubated in 20% silver nitrate for 15 min, washed with distilled water, and developed in ammoniacal silver (10% silver nitrate precipitated with 28%–30% ammonium hydroxide, plus 2% formalin). After a 2-min rinse in 5% sodium thiosulfate, slides were washed in distilled water, dehydrated, cleared in xylene, and mounted.

Localization of carbonic anhydrase activity (CAH)

Alkaline glands were fixed in a solution of 2.0% paraformaldehyde, 2.5% glutaraldehyde, and 0.4% $CaCl_2$ in 0.1 *M* sodium cacodylate buffer for localization of carbonic anhydrase activity (CAH) using the Hansson's technique (Hansson, 1967; Maren, 1980b; Sugai and Ito, 1980; Lacy, 1983b). Fixed tissue was frozen in 8% sucrose and sectioned at 10 μm on an IEC CTF cryostat (International Equipment Company). Sections were floated on Hansson's medium (1.86 m*M* $CoSO_4$, 55.9 m*M* H_2SO_4, 3.73 m*M* KH_2PO_4, and 158 m*M* $NaHCO_3$) for 1–5 min. Sections were rinsed by floating on Sorensen's phosphate buffer (pH 8.0) for 1 min and then transferred onto 2% ammonium sulfide for 1–2 min. This was followed by rinsing sections on Sorensen's phosphate buffer at pH 5.0 and then mounting them in heated glycerin jelly on glass slides for observation with a light microscope (Sugai and Ito, 1980; Lacy, 1983b). After the sections were incubated on 2% ammonium sulfide, low-pH buffers were used to prevent the black precipitate indicative of CAH activity from degrading. For electron microscopy, sections were postfixed in 1.0% osmium tetraoxide in Sorensen's phosphate buffer (pH 5.0) for 30–45 min, stained *en bloc* with 1.0% uranyl acetate in maleate buffer (pH 5.2), dehydrated in graded ethanols, and embedded flat in epoxy resin. Ultrathin sections were stained and examined as described above.

Acetazolamide (10^{-5} and 10^{-6} *M*) in Hansson's medium was used to inhibit CAH, thereby serving as a negative control. For evaluation of nonspecific activity, sections were incubated either in ammonium sulfide without prior incubation on Hansson's medium, or on bicarbonate-free Hansson's medium.

Morphometric analysis

Ratios of basal cells to columnar cells were determined from counts made of cross-sectioned glands at the light microscopic level (epoxy resin sections, 50×). The size and distribution of intramembranous particles observed in freeze fracture replicas were measured on electron micrographs using a scale magnification loupe (Baxter, Atlanta, GA). The luminal surface area of columnar epithelial cells was estimated by measuring the cell diameters of luminal plasma membranes from scanning electron micrographs.

Constituents of alkaline gland fluid

Fluid from the alkaline glands of five stingrays was pooled, cooled to 5°C, and centrifuged as described above. The supernatant was then frozen by placing the tube in dry ice and shipped overnight to Mayo Medical Laboratories (Rochester, MN) for analysis of its composition.

Electrophysiology

Each sac of the alkaline gland was freed *in situ* from surrounding connective tissue, excised, and placed in a petri dish of oxygenated elasmobranch Ringer (NaCl, 280.0 m*M*; KCl, 5.0 m*M*; $MgCl_2$, 3.3 m*M*; $CaCl_2$, 3.8 m*M*; $NaHCO_3$, 10.0 m*M*; urea, 350.0 m*M*; dextrose, 5.0 m*M*; 800 mOsm/l; pH 6.9). The Ringer was gassed with 95% O_2/5% CO_2, unless otherwise noted, and used at room temperature.

Each sac was mounted between two halves of an Ussing chamber (4-mm diameter). Each half of the chamber was connected to a 20-ml circulation reservoir (Medical Research Apparatus, Clearwater, FL). The short-circuit current (Isc) and transepithelial potential difference (PD) were measured using a voltage-current clamp (Physiological Instruments, San Diego, CA). Before tissue was mounted in the Ussing chamber, electrode polarization and fluid resistance was compensated with the VCC600 voltage-current clamp. Calomel electrodes (Fisher, Atlanta, GA) placed in a saturated KCl solution were connected to the Ussing chamber *via* salt bridges (4% agar in elasmobranch Ringer) to measure the PD. Platinum electrodes (Fisher, Atlanta, GA) were placed directly into the Ussing chamber to measure Isc. The PD and Isc were displayed on a Soltec 1242 strip chart recorder (Soltec Corp., Sun Valley, CA). Transepithelial resistance was calculated using the open-circuit PD, and the closed-circuit Isc of the mounted tissue. All readings were in reference to the luminal medium.

Transport inhibitors

Once baseline electrophysiological parameters were established, the percent change of Isc was calculated after the tissue was exposed to the following transport inhibitors: ouabain, Na^+/K^+ ATPase inhibitor (10^{-4} *M*, serosal); bumetanide, $Na^+/K^+/Cl^-$ cotransport inhibitor (10^{-3} *M*, serosal); DIDS (4,4′-diisothiocyanatostilbene-2,2′-disulfonic acid, Cl^-/HCO_3^- exchange inhibitor (10^{-3} *M*, luminal); amiloride, sodium channel inhibitor, (10^{-3} *M*, luminal and serosal); acetazolamide, carbonic anhydrase inhibitor (10^{-5} *M*, luminal). Chloride was substituted in the medium with isomolar concentrations of gluconate. All reagents were purchased from Sigma Chemical Co., St. Louis, MO.

Alkalinization rates

The alkalinization rate of the luminal medium was measured using the pH stat technique on glands mounted in the Ussing chamber. Unbuffered (bicarbonate-free) Ringer bathing the luminal side of the gland was gassed with 100% oxygen during experiments and 30 min prior to tissue mounting. The serosal-bathing medium consisted of buffered elasmobranch Ringer, gassed with 95% oxygen/5% carbon dioxide. The rate of fluid alkalinization (μEq of acid/cm^2/h) was then determined *via* titration using 0.01 *M* sulfuric acid. The pH of the luminal medium was maintained at pH 5.5 for at least six consecutive intervals of 5 min each. The pH was monitored using a pH microelectrode (Microelectrode, Londonderry, NH) connected to a Beckman pH meter (Omega 40, Fullerton, CA).

Two experiments were performed to determine the presence of either chloride-dependent or sodium-dependent bicarbonate transport. Alkalinization rates were measured after each manipulation. Baseline values were made from tissues bathed on both sides with elasmobranch Ringer. The medium was changed on the luminal and serosal sides to iso-osmotic elasmobranch Ringer free of chloride or sodium. In the first experiment, chloride-containing Ringer was added back to the luminal side; in the second experiment, sodium-containing Ringer was added back to the serosal side. After a new alkalinization rate was established, a bicarbonate transport inhibitor, SITS (4-acetamido-4′-isothiocyanatostilbene-2,2′-disulfonic acid, 10^{-3} *M*), was added to the luminal medium in both experiments.

The buffering capacity of the various Ringers was determined after each experiment, using the pH stat method. The buffering capacity of each medium was then subtracted from the alkalinization rate derived under the experimental conditions.

Statistical analyses

Statistical significance was evaluated using a two-tailed-paired *t* test, with the level of significance set at $P < 0.05$.

Results

Gross anatomy

The alkaline gland of the Atlantic stingray, *Dasyatis sabina*, consists of a pair of blind-ended, bladder-like sacs located within the pelvic girdle ventral to the posterior pole of the kidney and lateral to the vas deferens. In the animals we examined, the glands were retroperitoneal and symmetrically aligned along the vertebral column. They were easily distinguished from surrounding tissue by their deep burgundy color. Each sac of the gland held a maximum of 4–5 ml of fluid. The mediocaudal portion of each gland narrowed to a single duct, which joined the respective sperm duct (vas deferens) on the same side of the animal. The resultant common duct for sperm and alkaline gland fluid was about 3-mm long and pierced the body wall to open on the crest of the urinary papilla in the cloaca.

Microscopy

The mucosa of the alkaline gland was highly folded and lined by a simple columnar epithelium (Figs. 1, 2). A rich capillary network lay immediately beneath the basement membrane. Within each fold were an arteriole and venule and dense tracts of nerve fibers (Figs. 1–3).

Two populations of epithelial cells were distinguished on the basis of their apical membrane exposure to the lumen (Fig. 1). The length of the long axis of the apical cell surface differed significantly in the two populations ($P < 0.05$, $n = 141$); in one (84.4% of the total cells) the long axis of the apical cell surface was 7.2 ± 0.14 μm; in the other (15.6%), the long axis was about twice that length (14.92 ± 0.49 μm). All cells that contacted the lumen had the same ultrastructural organization, despite the difference in lumenal membrane area.

Columnar epithelial cells had a prominent, basally located pleomorphic nucleus and exceptionally large and abundant secondary lysosomes (Figs. 1, 2). The secondary lysosomes stained positively for lipofuscin (data not shown) and were dark green-brown in unstained sections. (Fig. 3). The smooth-surfaced endoplasmic reticulum was evenly distributed throughout the cytoplasm. Mitochondria bearing lamellar cristae were located in the upper two-thirds of the cell, and Golgi complexes were abundant in the perinuclear region (Fig. 2). Many membrane-bound vesicles were present in the Golgi region and adjacent to the apical plasma membrane. Some of these vesicles were seen fusing with larger vesicles as well as with the apical plasma membrane (Fig. 2).

Basal cells were also present in the lower third of the epithelium (Fig. 4) in a ratio of about 1 basal cell to 20 columnar cells. These cells, which ranged from 1.4 to 2.6 μm in diameter, were not highly interdigitated with adjacent columnar cells and were not observed in contact with another basal cell. The cytoplasm of basal cells surrounded a proportionately large nucleus and contained only a few organelles, which were limited to the endoplasmic reticulum, and small vesicles containing material of various degrees of electron density.

The apical surface of the columnar cells was elaborated

Figure 1.

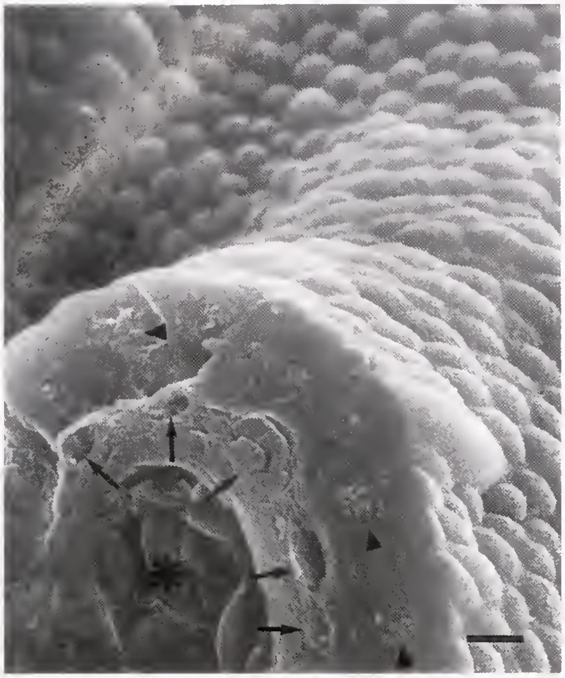

Figure 2.

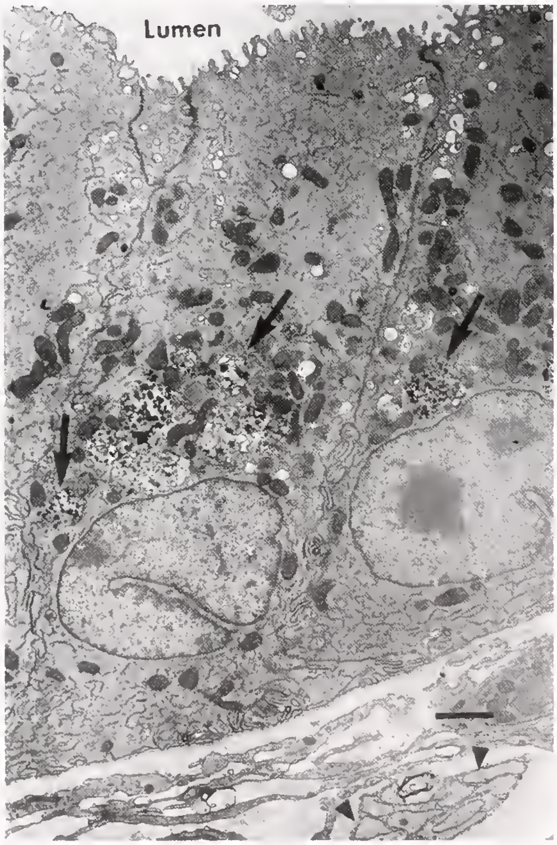

Figure 3.

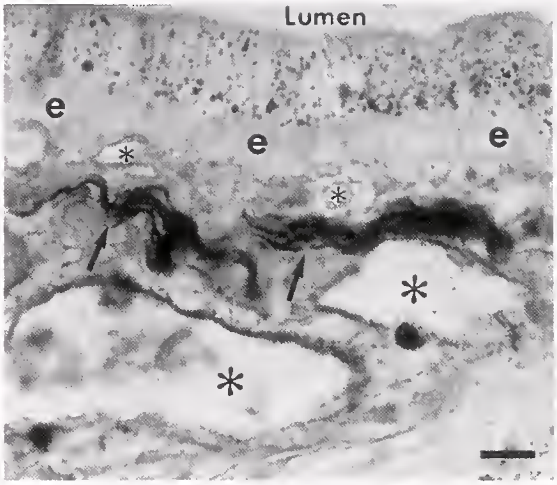

Figure 4.

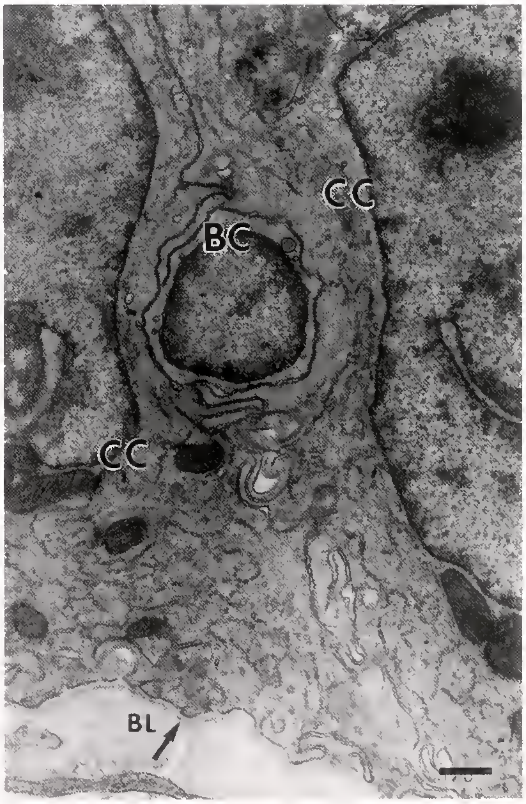

into microplicae (Figs. 1, 2). The basolateral plasma membrane was relatively straight nearest the lumen, but closer to the basal lamina it was interdigitated with itself and adjacent cells (Fig. 2). Freeze fracture of the lateral plasma membrane revealed some areas consisting only of large intramembranous particles (99 Å ± 0.1, $n = 52$) (Fig. 5) loosely arranged as single particles or in groups of up to 20 particles. Outside these areas was a mixture of large and small intramembranous particles. No rod-shaped particles were observed in either the apical or basolateral plasma membrane. The zonulae occludentes were deep (1.4 ± 0.7 μm, $n = 19$ replicas) and composed of 21.8(±4.5) fibrils (Fig. 6). Most of the fibrils were parallel to the apical plasma membrane, with those constituting the basal one-fourth of the zonulae occludentes forming a loose anastomosing network (Fig. 6).

Ultrastructural observations of the solids from alkaline gland fluid showed cellular debris including multivesicular bodies, spherical particles with electron-dense cores that stained positively for lipofuscin, membrane whorls, and a few necrotic spermatozoa (Fig. 7).

Localization of carbonic anhydrase activity

Carbonic anhydrase activity (CAH) was indicated by a black precipitate at both the light and electron microscopic level (Figs. 8, 9). A minimum of 2 min in the incubation medium was required for the precipitate to develop, at which time CAH appeared first within the intercellular space of columnar cells. In electron micrographs, CAH was localized in the intercellular space between columnar cells but excluded from the zonulae occludentes (Fig. 9). Adjacent to the basement membrane, CAH was observed only within the intercellular space formed by invaginations of the plasma membrane or interdigitation of cytoplasmic folds (Fig. 9). Regions of the basolateral plasma membrane that contacted the basement membrane did not exhibit CAH. After 3–10 min of incubation, the precipitate appeared in the basal two-thirds of columnar cell cytoplasm (Fig. 8).

Control sections incubated on bicarbonate-free Hansson's medium or on ammonium sulfide alone were similar to unstained sections that were rinsed only on Sorensen's phosphate buffer, and showed no positive staining (data not shown). Complete inhibition of CAH occurred at acetazolamide concentrations of 10^{-5} *M* in Hansson's medium (data not shown). Lower concentrations of acetazolamide (10^{-6} *M*) failed to inhibit CAH activity for incubation periods longer than 2 min.

Analysis of alkaline gland fluid (AGF)

Table I shows the analyzed constituents of AGF. Sodium and chloride were the dominant ions, with K^+, Mg^{++}, Ca^{++}, and Fe^{++} in detectable amounts. The osmolality was near that of plasma (750–875 mOsm), and significant concentrations of protein and urea were measured. The pH varied between 8.0 and 8.2.

Electrophysiology

Baseline parameters. The baseline PD was 14.5 ± 1.9 mV, Isc was 29.1 ± 4.2 μA/cm^2, and transepithelial resistance was calculated to be 732.4 ± 184.6 ohm · cm^2 ($n = 18$).

Transport inhibitors. The effect of specific ion transport inhibitors on the baseline Isc is shown in Table II. The serosal addition of ouabain, a Na^+/K^+ ATPase inhibitor, resulted in an almost 48% decrease of Isc within 45 to 50 min. Bumetanide, a $Na^+/K^+/Cl^-$ cotransport inhibitor, decreased the Isc approximately 70% within 30 min, and DIDS, a Cl^-/HCO_3-exchange inhibitor, placed on the luminal side of the epithelium decreased the Isc almost 38% within 30 to 40 min. The Isc was completely inhibited, and in fact was slightly reversed, after consecutive addition of bumetanide within 30 min of DIDS addition to the lumenal surface. The effect of luminal exposure to acetazolamide, a carbonic anhydrase inhibitor, on Isc was sporadic, and produced only a 16% overall reduction of Isc. Amiloride, a sodium ion channel inhibitor, placed in either the luminal or serosal media had no significant effect on the Isc (data not shown). The removal of chloride from the bathing media on both sides of the tissue with the substitution of gluconate resulted in a 67% reduction in Isc by 45 min.

Alkalinization rates. Two experiments investigating de-

Figure 1. Scanning electron micrograph of a transected mucosal fold. The asterisk is located in the center of an arteriole. A network of capillaries (arrows) lies directly beneath the epithelium, which has prominent secondary lysosomes (arrowheads). Bar = 50 μm.

Figure 2. Transmission electron micrograph (TEM) of the simple columnar epithelium of the alkaline gland. Arrows indicate secondary lysosomes located in the supranuclear region. Arrowheads indicate a nerve fiber closely adjacent to the epithelium. Note the numerous vesicles in the apical cytoplasm. Bar = 2 μm.

Figure 3. Light micrograph (LM) of nerve fibers (arrows) in the subepithelial lamina propria stained black using the Sevier Munger silver technique. Nerve fibers were closely associated with blood vessels (asterisks) and the epithelium (e). Note the multiple darkly staining secondary lysosomes in the apical cytoplasm of the epithelium. Bar = 4 μm.

Figure 4. TEM of a basal cell (BC) located between adjacent columnar cells (CC). Note the large proportion of the nucleus relative to the BC cytoplasm. Basal lamina (BL). Bar = 2 μm.

Figure 5.

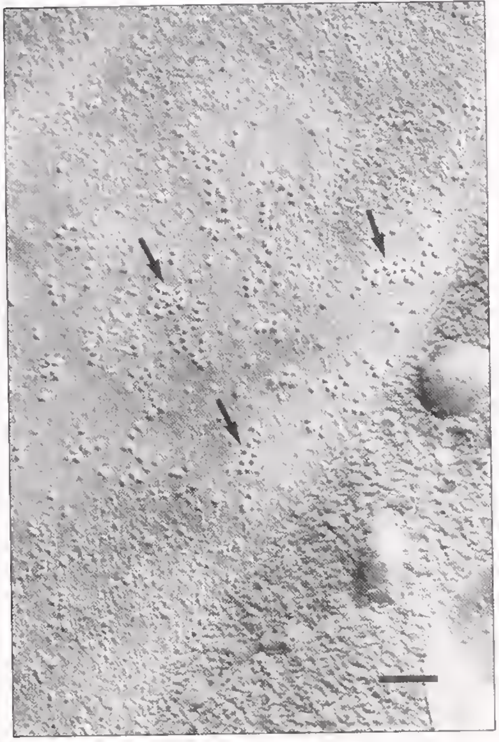

Figure 6.

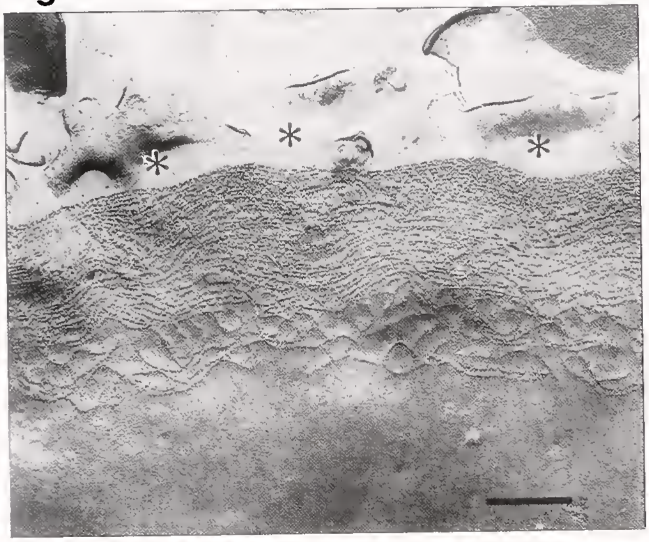

Figure 7.

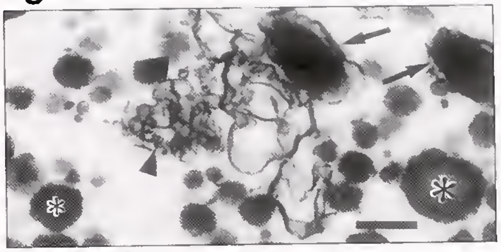

Figure 8.

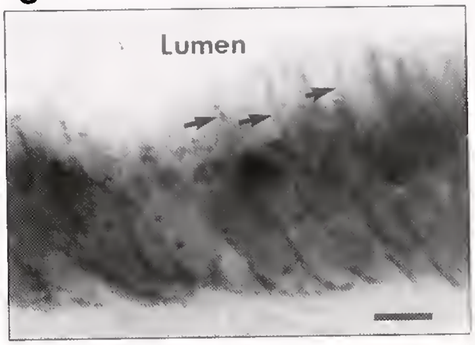

Figure 9.

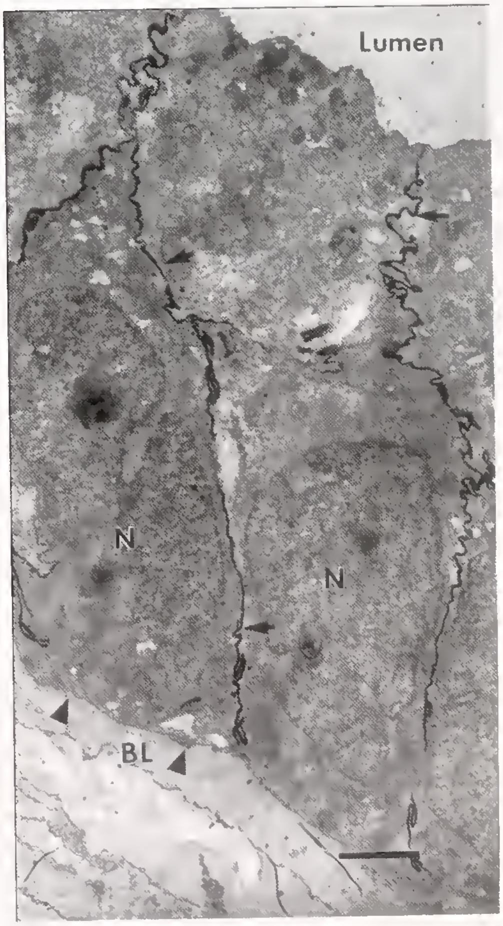

Table I

Analyzed constituents of alkaline gland fluid

Component	*Concentration*
Na^+	286 mM
K^+	3.7 mM
Cl^-	113.0 mM
Mg^{++}	1.68 mM
Ca^{++}	0.84 mM
Cu^{++}	0.58 mM
Zn^{++}	0.87 mM
Fe^{++}	0.61 mM
Urea	271 mM
Progesterone	0.012 μM
Estradiol	0.16 pM
Norepinephrine	ND
Epinephrine	ND
Dopamine	ND
Testosterone	4.3 μM
Protein	5.9 mg/ml
Osmolality	875 mosm

mosm = milliosmoles, ml = milliliter, mg = milligram, pM = picomoles, μM = micromoles, mM = millimoles, ND = none detected.

Table II

Effects of ion transport inhibitors on the short-circuit current (Isc)

Treatment	% Decrease of Isc	*n*
Ouabain (10^{-4} M), S	47.8 ± 2.9	4
Bumetanide (10^{-3} M), S	69.7 ± 5.5	8
DIDS (10^{-3} M), L	37.9 ± 5.9	6
DIDS (10^{-3} M), L + Bumetanide (10^{-3} M), S	105.9 ± 12.2	5
Acetazolamide (10^{-5} M), L	16.0 ± 9.0	3

Values are means ± SE, L = Luminal, S = Serosal, *n* = number of mounted glands. DIDS = 4,4′-diisothiocyanatostilbene-2,2′-disulfonic acid.

pendent and independent bicarbonate transport mechanisms are shown in Table III. The baseline alkalinization rate of control tissues varied from about 4 to 7.5 μEq of acid/cm^2/h depending upon the animal used.

Chloride-dependent bicarbonate secretion was demonstrated by a significant decrease in alkalinization rate when both sides of the gland were exposed to chloride-free Ringer (Table III, Experiment 1). Alkalinization returned to control levels when chloride was added back to the luminal side of the tissue. SITS (10^{-3} M), a bicarbonate transport inhibitor, when applied to the luminal medium, had no statistically significant effect on the alkalinization rate after luminal exposure to chloride (Table III). However, the results varied widely from tissue to tissue.

In the second experiment, the fluid alkalinization rate decreased significantly, 55%, after luminal and serosal exposure to sodium-free media (Table III). The alkalinization rate increased immediately with the readdition of serosal sodium-containing Ringer. Addition of the bicarbonate transport inhibitor, SITS (10^{-3} M), to the luminal medium caused a significant decrease (24%) in the alkalinization rate compared to the values after sodium readdition (Table III).

Discussion

Results of this study extend the presence of alkaline glands in the Elasmobranchii to include stingrays. Our gross anatomical explorations of several species of shark—spiny dogfish, *Squalus acanthias;* black tip, *Carcharhinus limbatus;* smooth dogfish, *Mustelus canis;* scalloped hammerhead, *Sphyrna lewini,* and Atlantic sharpnose, *Rhizoprionodon terraenovae*—did not reveal the presence of alkaline glands in these elasmobranchs. This finding is consistent with the notion that alkaline glands are present only in skates and rays and not in sharks. Furthermore, this study is the first to elucidate the morphology, ion transport mechanisms, enzyme histochemistry, and fluid composition of the alkaline gland in a species of stingray.

The gross anatomy of the Atlantic stingray alkaline gland is similar to that described for several species of skates

Figure 5. Transmission electron micrograph (TEM) of freeze fracture replica of a loose cluster of large intramembranous particles (arrows) found on the P fracture face of the lateral plasma membrane. Bar = 270 nm.

Figure 6. TEM of freeze fracture replica of the zonula occludens between two columnar cells. Note that numerous strands are arranged in a parallel array near the gland lumen (asterisk), but the more basal strands form an anastomosing network (P fracture face). Bar = 200 nm.

Figure 7. TEM of solid constituents from centrifuged alkaline gland fluid. Arrows indicate degenerate sperm with outer plasma membrane separated from the sperm head. Arrowheads indicate masses of membranes. Asterisks show roughly globular particles that composed the greatest part of the alkaline gland particulate matter. Bar = 2 μm.

Figure 8. Light micrograph of carbonic anhydrase activity in epithelial cells lining the alkaline gland. Typical staining pattern in sections incubated for 3–10 min on Hansson's medium. Enzyme activity was strongly present in the intercellular spaces (arrows), as well as in the mid to basal cytoplasm of columnar cells. Bar = 7 μm.

Figure 9. TEM of carbonic anhydrase activity in sections incubated for 2 min on Hansson's medium. Enzyme activity appears as electron-dense precipitate (arrows) confined to the intercellular space. N = nuclei of columnar cells. Note the absence of CAH activity along the basal lamina (BL). Bar = 2 μm.

Table III

In vitro *alkalinization rates of alkaline glands*

Experimental conditions	Alkalinization rate (μEq of acid/cm^2/h)
Experiment 1	
Elasmobranch Ringer (Control)	3.88 ± 0.63
Chloride-free Ringer, L&S	−1.93 ± 1.89*
Chloride readdition, L	3.65 ± 1.17**
Addition of SITS (1 m*M*), L	1.45 ± 2.22
Experiment 2	
Elasmobranch Ringer (Control)	7.65 ± 0.67
Sodium-free Ringer, L&S	3.49 ± 0.41*
Sodium readdition, S	5.64 ± 0.62**
Addition of SITS (1 m*M*), L	4.30 ± 0.45***

Values are means ± SE; $n = 5$ for each experiment. L = luminal, S = serosal. SITS = 4-acetamido-4′-isothiocyanatostilbene-2,2′-disulfonic acid.

* Significant difference compared to control, ** significant difference compared to respective chloride or sodium free conditions, *** significant difference compared to respective chloride or sodium readdition, $P < 0.05$.

(Maren *et al.*, 1963). However, one significant difference is the relationship between the alkaline gland duct and the sperm duct. In skates, Maren *et al.* (1963) reported that the alkaline gland ducts and sperm ducts have separate openings onto the urinary papilla. In the stingray, the alkaline gland duct joins the sperm duct, and the resultant common duct then opens onto the urogenital papilla. This anatomical arrangement in the Atlantic stingray allows mixing of sperm and alkaline gland fluid (AGF), suggesting that AGF may facilitate successful fertilization by its actions on spermatozoa. Furthermore, the confluence of the two ducts in the Atlantic stingray may explain the presence of some necrotic sperm and cell membranes in AGF, because residual sperm in the common duct would have retrograde access to the alkaline gland lumen. The absence of spermatozoa in the AGF supports the contention that the gland is not a *bona fide* sperm storage organ, thus contradicting reports by early anatomists (Borcea, 1906; Daniel, 1934).

Morphological features of columnar cells composing the epithelium of the alkaline gland of the Atlantic stingray are generally consistent with preliminary reports of the alkaline gland of the little skate (Maren *et al.*, 1963; Masur, 1984). Those cells exhibited a well-developed Golgi apparatus and endoplasmic reticulum, suggesting a high degree of active protein synthesis. The many vesicles we observed in the cytoplasm, especially those budding from the Golgi apparatus and fusing with larger vesicles or with the apical plasma membrane, support that idea. Although basal cells were morphologically distinct from columnar cells, we are uncertain whether they are a separate population of mature cells or are immature columnar cells.

A striking microscopic feature of stingray alkaline gland epithelial cells was large secondary lysosomes that imparted a dark green-black color to the gland and were distinctive in unstained tissue sections. An accumulation of myelin figures and lipofuscin granules in these secondary lysosomes was strongly suggestive of increased lysosomal processing of lipid membrane (Reed *et al.*, 1965; Harman, 1990). Interestingly, such features were also observed in epithelial cells of mammalian male reproductive organs such as the epididymis and seminal vesicle (Pappenheimer and Victor, 1954; Nicander, 1958; Mitchinson *et al.*, 1975). Mitchinson *et al.* (1975) suggested that the spermatozoa in the lumen of those organs may be the source of the intracellular lipofuscin granules, whereby epithelial cells perform a "salvaging" function and store insoluble fatty acids as lipofuscin. A similar process may occur in alkaline gland epithelial cells: the necrotic sperm and cell debris observed in the lumen of the gland would be the extracellular source of the intracellular lipofuscin granules.

The composition of stingray AGF differs from that previously reported for three species of skates (Maren *et al.*, 1963) in several ways. Stingray AGF is a deep burgundy color and nearly opaque; in contrast, skate AGF is clear to slightly yellow. Stingray AGF has significant amounts of protein and urea; skate AGF is reported to lack protein and have only about one-third the concentration of urea found in the Atlantic stingray (Maren *et al.*, 1963). Furthermore, the ionic concentration was different: stingray AGF had one-half the concentration of K^+ and Cl^- reported for skate AGF but 4 times more Mg^{++} and Ca^{++}. The present study is the first to show AGF with immunodetectable steroid hormones. However, the immunological methods used antibodies to human hormones, which raises the possibility that the results may be due to nonspecific binding.

A recent study (Büllesbach *et al.*, 1997) probed the possibility that AGF contained relaxin, a peptide hormone found in mammalian reproductive tissues and secreted fluids. The fact that relaxin in mammalian seminal fluid stimulates sperm motility (Essig *et al.*, 1982; Weiss, 1989) was the basis for the investigation in the stingray. Büllesbach and colleagues (1997) showed that stingray AGF contains a unique relaxin-like molecule with an apparent molecular mass of 13 kDa formed by two polypeptide chains of 4 and 9 kDa. This molecule is the only member of the relaxin family known to be glycosylated. The relaxin-like molecule of stingray AGF did not alter stingray sperm motility *in vitro* (Büllesbach *et al.*, 1997), but this finding does not rule out the possibility that the AGF relaxin-like molecule acts on a different aspect of sperm function such as capacitation or that it functions in the female reproductive tract.

The lumen of the stingray alkaline gland was not lined by the villar projections described in the skate (Maren *et al.*, 1963), but it did have mucosal folds, each of which contained a major arteriole and venule. The apical plasma membrane of the columnar epithelial cells was elaborated into microvilli characteristic of a secreting epithelium.

Freeze fracture replicas showed that the only distinguishing intramembranous particles were in the basolateral plasma membrane. The size and distribution of the particles forming these clusters was comparable to those forming gap junctions in mammalian cells. Apical and basolateral plasma membranes did not reveal any rod-shaped particles that would suggest proton transport (Brown and Montesano, 1980).

The zonulae occludentes of columnar cells consisted of about 22 strands, suggesting that the epithelium is electrically tight and imparts a high transepithelial resistance (Claude and Goodenough, 1973; Claude, 1978). Our *in vitro* electrophysiological data showed that the transepithelial resistance was 732 ohm · cm^2, confirming the tight junction morphology. The presence of "very tight" zonulae occludentes and a high transepithelial resistance suggests that there is little paracellular solute transport across the epithelium of the alkaline gland (Bowman *et al.*, 1992; Byers and Marc-Pelletier, 1992). Therefore, regulation of ion transport appears to occur primarily across the plasma membrane.

Maren *et al.* (1963) and Smith (1981, 1985) have demonstrated that both bicarbonate and chloride are secreted in the little skate alkaline gland and that chloride is the main anion responsible for most of the Isc. This finding was extended to the stingray alkaline gland in the present study in which Isc decreased almost 70% when chloride was removed from the bathing medium. Using intracellular microelectrodes, Smith (1981, 1985) showed that the apical plasma membrane was dominated by a large chloride conductance, whereas the basolateral plasma membrane contained a barium-sensitive potassium channel. However, the mechanisms involved in the alkalinization process have never been clearly established in this gland, despite speculation that a Cl^-/HCO_3^- exchanger may exist in the apical or basolateral plasma membrane or in both membranes (Maren *et al.*, 1963; Smith, 1981, 1985).

In the present study, the marked reduction in Isc after serosal addition of bumetanide, an inhibitor of $Na^+/K^+/Cl^-$ cotransport, suggests that this transporter is located in the basolateral plasma membrane. If so, it may be the main conductive pathway for chloride entry into the cell. The remaining Isc could be due to the secretion of intracellular chloride or another anion, such as bicarbonate. To test this latter possibility we added the stilbene, DIDS, which effectively inhibits bicarbonate cotransporters (Wiederholt *et al.*, 1985; Melvin and Turner, 1992) as well as chloride channels (Bretag, 1987) to the luminal side of the epithelium. The resultant 38% decrease of Isc, and its further reduction to nominal levels after the consecutive addition of serosal bumetanide, substantiates this assumption. Furthermore, complete reduction of the Isc by consecutive addition of DIDS and bumetanide suggests a pathway for chloride secretion across the epithelial cells *via* a $Na^+/K^+/Cl^-$ cotransporter at the basolateral plasma membrane, and a chloride channel at the apical plasma membrane.

Chloride movement across the epithelial basolateral plasma membrane, *via* a putative $Na^+/K^+/Cl^-$ cotransporter in epithelial cells in stingray alkaline gland, appears to be driven in part by Na^+/K^+ ATPase, as shown by the serosal addition of ouabain, which decreased the Isc by 48%. In contrast, ouabain completely abolished chloride secretion and Isc in the little skate alkaline gland (Smith, 1985).

The lack of significant alkalinization rates after the tissue was exposed to medium free of chloride and sodium suggests that there is little independent transport of bicarbonate. If a significant portion of the alkalinization process involves an apical Cl^-/HCO_3 exchanger—as our results suggest—the absence of luminal chloride could impede that process, resulting in the accumulation of intracellular bicarbonate. Such a scenario has been observed in the rat parotid acini: SITS, an inhibitor of bicarbonate transport, increased intracellular pH and was thought to stimulate bicarbonate secretion *via* anion channels (Pirani *et al.*, 1987; Melvin and Turner, 1992). Chloride channels in a number of different epithelia, including pancreatic duct, sweat gland duct, and respiratory epithelia, have been shown to transport bicarbonate (Gray *et al.*, 1989; Tabcharani *et al.*, 1989; Kunzelmann *et al.*, 1991) at a conductance as high as 50% of the conductance of chloride.

The remaining Isc may be accounted for by a Na^+/HCO_3^- symport, as demonstrated in this study by using pH stat methodology. Such mechanisms for bicarbonate transport have been demonstrated in renal proximal tubule (Yoshitomi *et al.*, 1985), corneal endothelial cells (Wiederholt *et al.*, 1985), and gastric oxyntic cells (Curci *et al.*, 1987).

Alkalinization of the luminal medium in the present study was dependent on the presence of both apical chloride and serosal sodium. The changes attributed to the absence and readdition of sodium suggests the presence of a Na^+/HCO_3^- symport. The alkalinization rate attributed to the readdition of serosal sodium, and its reduction by luminal SITS, is indirect evidence that a Na^+/HCO_3^- symport may be located at the apical plasma membrane. The stilbene, SITS, blocks not only bicarbonate transport *via* Na^+/HCO_3^- symporters (Curci *et al.*, 1987; Fitz *et al.*, 1989; Wiederholt *et al.*, 1985), but also Cl^-/HCO_3^- exchangers (Stewart *et al.*, 1989).

Maren and co-workers (1963) demonstrated a possible relationship between CAH and higher pH levels in AGF of various skate species. They showed that inhibition of CAH *in vivo* reduced the pH of newly formed fluid to levels found in species that did not have glandular CAH. This was accomplished using intravenous injections of acetazolamide at least 10 times higher than the dose we used. In a study of rat distal colon, the need for high (millimolar) concentrations of acetazolamide to inhibit bicarbonate transport was attributed to the drug's poor cellular penetration, the distribution of CAH within the cell, and the requirement of 99% inhibition of CAH for a significant decrease of Isc to occur (Feldman *et al.,* 1988). The effectiveness of acetazolamide in reducing the Isc of the stingray alkaline gland is questionable because of the erratic results from tissue to tissue. However, concentrations of acetazolamide greater than 10^{-4} *M* were not used in the present study, because reports have indicated that the drug interferes with other ion transport mechanisms (Nellens *et al.,* 1975; Weiner and Mudge, 1985). Because the response to acetazolamide in our experiments was not consistent, we conclude that, in the stingray alkaline gland, either higher concentrations of acetazolamide are required to reduce the Isc, or bicarbonate secretion is not completely dependent on the presence of CAH.

We chose Hansson's technique (Hansson, 1968) to localize CAH after indirect immunoperoxidase staining methods failed. Antibodies to mammalian carbonic anhydrase I and II failed to recognize stingray carbonic anhydrase, which has significant structural and kinetic differences from forms found in higher vertebrates (Maynard and Coleman, 1971; Maren, 1980b).

The presence of CAH in the intercellular space of epithelial cells has been demonstrated not only in the alkaline gland in the present study, but also in other tissues such as the gall bladder, duodenum, and sweat gland (Hansson, 1968), as well as in the teleost opercular epithelium (Lacy, 1983b) and the elasmobranch rectal gland (Lacy, 1983a). This subcellular site may indicate the presence of either a membrane-bound or soluble form of CAH (Maren, 1980a). The exclusion of CAH activity from portions of the plasma membrane that contact the basement membrane suggests that its function is important in areas of cell-cell contact. Another possibility is that a soluble form of CAH exists in the intercellular space. The mechanisms that would prevent its diffusion along the basal aspect of the cell are unknown. In any case, CAH in intercellular spaces suggests that a bicarbonate reservoir may exist between epithelial cells (Lacy, 1983a) or that membrane-bound CAH may transport carbon dioxide, protons, or bicarbonate into or out of the cell (Enns, 1967; Wistrand, 1984).

The exclusion of CAH from the apical region of the alkaline gland epithelial cells shown in the present study has been demonstrated in mitochondria-rich cells of the turtle bladder and interfoveolar epithelial cells of the rat stomach, both of which are thought to subserve bicarbonate secretion (Sugai and Ito, 1980; Fritsche *et al.,* 1991a). A pattern similar to that seen in the alkaline gland was displayed in microvillated cells and microplicated cells under conditions inhibiting acid secretion (Fritsche *et al.,* 1991b).

The difference in distribution pattern and stain development of CAH in the alkaline gland may reflect the presence of at least two carbonic anhydrase isozymes (Carter and Parsons, 1971). The appearance of CAH in the intercellular space after relatively short incubation periods may indicate a high-affinity membrane-bound carbonic anhydrase isozyme. A low-affinity cytoplasmic form of carbonic anhydrase in the stingray alkaline gland is suggested by the longer incubation periods necessary for intracellular stain development.

Acknowledgments

This work was supported, in part, by the Slocum-Lunz Foundation (GMG), National Science Foundation (ERL # DCB 8903369), and the University Research Council, Medical University of South Carolina.

Literature Cited

Bancroft, J. D., and H. C. Cook. 1984. Pigments. Pages 144–158 in *Manual of Histological Techniques.* Churchill Livingstone, New York.

Borcea, I. 1906. Recherches sur la systeme urogenital des Elasmobranches. *Arch. Zool. Exper. Gen.* **4(4):** 199–484.

Bowman, P. D., M. du Bois, R. R. Shivers, and K. Dorovini-Zis. 1992. Endothelial tight junctions. Pages 305–320 in *Tight Junctions,* M. Cereijido, ed. CRC Press, Ann Arbor, MI.

Bretag, A. H. 1987. Muscle chloride channels. *Physiol. Rev.* **67(2):** 618–724.

Brown, D., and R. Montesano. 1980. Membrane specialization in the rat epididymis. I. Rod-shaped intramembrane particles in the apical (mitochondria-rich) cell. *J. Cell Sci.* **45:** 187–198.

Büllesbach, E. E., C. Schwabe, and E. R. Lacy. 1997. Identification of a glycosylated relaxin-like molecule from the male Atlantic stingray, *Dasyatis sabina. Biochemistry* **36:** 10735–10741.

Byers, S., and R. Marc-Pelletier. 1992. Sertoli-sertoli cell tight junctions and blood-testis barrier. Pages 279–307 in *Tight Junctions,* M. Cereijido, ed. CRC Press, Ann Arbor, MI.

Carter, M. J., and D. S. Parsons. 1971. The isoenzymes of carbonic anhydrase: Tissue subcellular distribution and function significance, with particular reference to the intestinal tract. *J. Physiol.* **215:** 71–94.

Claude, P. 1978. Morphological factors influencing transepithelial permeability: A model for the resistance of the zonula occludens. *J. Membr. Biol.* **39:** 219–232.

Claude, P., and D. A. Goodenough. 1973. Fracture faces of zonulae occludente from "tight" and "leaky" epithelia. *J. Cell Biol.* **58:** 390–400.

Curci, S., L. Debellis, and E. Fromter. 1987. Evidence for rheogenic sodium bicarbonate cotransport in the basolateral membrane of oxyntic cells of frog gastric fundus. *Pflugers Arch.* **408:** 497–504.

Daniel, F. J. 1934. Urogenital system. Pages 300–303 in *The Elasmobranch Fishes,* F. J. Daniel, ed. University of California, Berkeley, CA.

Enns, T. 1967. Facilitation by carbonic anhydrase of carbon dioxide transport. *Science* **155:** 44–47.

Essig, M., C. Schoenfeld, R. D-Eletto, R. Amelar, L. Dubin, B. G. Steinetz, M. O'Bryne, and G. Weiss. 1982. Relaxin in human seminal plasma. *Ann. NY Acad. Sci.* **380:** 224–230.

Feldman, G. M., S. F. Berman, and R. L. Stephenson. 1988. Bicarbonate secretion in the distal colon *in vitro:* A measurement technique. *Am. J. Physiol.* **254:** C383–390.

Fitz, J. G., M. Persico, and B. F. Scharschmidt. 1989. Electrophysiological evidence for sodium-coupled bicarbonate transport in cultured rat hepatocytes. *Am. J. Physiol.* **256:** G491–500.

Fritsche, C., J. G. Kleinman, J. L. W. Bain, R. R. Heinen, and D. A. Riley. 1991a. Carbonic anhydrase in turtle bladder mitochondrial-rich luminal and subluminal cells. *Am. J. Physiol.* **260:** F431–442.

Fritsche, C., J. G. Kleinman, J. L. W. Bain, R. R. Heinen, and D. A. Riley. 1991b. Carbonic anhdrase and proton secretion in turtle bladder mitochondrial-rich cells. *Am. J. Physiol.* **260:** F443–458.

Gray, M. A., A. Harris, L. Coleman, J. R. Greenwell, and B. E. Argent. 1989. Two types of chloride channel on duct cells cultured from human fetal pancreas. *Am. J. Physiol.* **257:** C240–251.

Hansson, H. P. J. 1967. Histochemical demonstration of carbonic anhydrase activity. *Histochemie* **11:** 112–128.

Hansson, H. P. J. 1968. Histochemical demonstration of carbonic anhydrase activity in some epithelia noted for active transport. *Acta Physiol. Scand.* **73:** 427–434.

Harman, D. 1990. Lipofuscin and ceriod formation: The cellular recycling system. *Adv. Exper. Med. Biol.* **266:** 3–18.

Ito, S., and M. J. Karnovsky. 1968. Formaldehyde-glutaraldehyde fixatives containing trinitro compounds. *J. Cell Biol.* **39:** 168a.

Kunzelmann, K., L. Gerlach, U. Frobe, and R. Greger. 1991. Bicarbonate permeability of epithelial chloride channels. *Pfluger Arch.* **417:** 616–621.

Lacy, E. R. 1983a. Carbonic anhydrase localization in elasmobranch rectal gland. *J. Exp. Zool.* **226:** 163–169.

Lacy, E. R. 1983b. Histochemical and biochemical studies of carbonic anhydrase activity in the opercular epithelium of the euryhaline teleost, *Fundulus heteroclitus. Am. J. Anat.* **166:** 19–39.

Maren, T. H., J. A. Rawls, J. W. Burger, and A. C. Myers. 1963. The alkaline (Marshall's) gland of the skate. *Comp. Biochem. Physiol.* **10:** 1–16.

Maren, T. H. 1980a. Current status of membrane-bound carbonic anhydrase. *Ann. NY Acad. Sci.* **341:** 246–258.

Maren, T. H. 1980b. Kinetics, equilibrium and inhibition in the Hansson histochemical procedure for carbonic anhydrase: A validation of the method. *Histochem. J.* **12:** 183–190.

Masur, S. K. 1984. Electron microscopy of the alkaline gland epithelium of the little skate, *Raja erinacea. Bull. Mt. Desert Is. Biol. Lab.* **24:** 96–97.

Maynard, J. R., and J. E. Culeman. 1971. Elasmobranch carbonic anhydrase. Purification and properties of the enzyme from two species of shark. *J. Biol. Chem.* **246:** 4455–4464.

Melvin, J. E., and R. J. Turner. 1992. Cl^- fluxes related to fluid secretion by the rat parotid: Involvement of Cl^-/HCO_3^- exchanger. *Am. J. Physiol.* **262:** G393–398.

Mitchinson, M. J., K. P. Sherman, and A. M. Stainer-Smith. 1975. Brown patches in the epididymis. *J. Pathol.* **115:** 57–62.

Nellens, H. N., R. A. Frizzell, and S. G. Schultz. 1975. Effect of acetazolamide on sodium and chloride transport by *in vitro* rabbit ileum. *Am. J. Physiol.* **228:** 1808–1814.

Nicander, L. 1958. Studies on the regional histology and cytochemistry of the ductus epididymis in stallions, rams, and bulls. *ACTA Morph. Neerl. Scand.* **1:** 337.

Pappenheimer, A. M., and J. Victor. 1954. "Ceroid" pigment in human tissues. *Am. J. Pathol.* **22:** 395–413.

Pirani, D., L. A. Evans, D. I. Cook, and J. A. Young. 1987. Intracellular pH in the rat mandibular salivary gland: The role of Na-H and Cl-HCO_3 antiports in secretion. *Pflugers Arch.* **408:** 178–184.

Reed, R., G. McMillan, S. Hartroft, and E. Porta. 1965. Progress of medical science: Pathology and bacteriology. *Am. J. Med. Sci.* **250:** 116–137.

Sevier, A. C., and B. L. Munger. 1965. A silver method for paraffin sections of neural tissue. *J. Neuropathol. Exp. Neurol.* **24:** 130–135.

Smith, H. W. 1929. The composition of the body fluids of elasmobranchs. *J. Biol. Chem.* **81:** 407–419.

Smith, P. L. 1981. Electrolyte transport by the alkaline gland of the little skate, *Raja erinacea.* Mechanism of luminal alkalinization. *Bull. Mt. Desert Is. Biol. Lab.* **21:** 80–83.

Smith, P. L. 1985. Electrolyte transport by alkaline gland of little skate *Raja erinacea. Am. J. Physiol.* **248:** 346–352.

Stewart, C. P., J. M. Winterhages, K. Heintze, and K. U. Petersen. 1989. Electrogenic bicarbonate secretion by guinea pig gallbladder epithelium: Apical membrane exit. *Am. J. Physiol.* **256:** C736–749.

Sugai, N., and S. Ito. 1980. Carbonic anhydrase, ultrastructural localization in the mouse gastric mucosa and improvements in the technique. *J. Histochem. Cytochem.* **28(6):** 511–525.

Tabcharani, J. A., T. J. Jensen, J. R. Riordan, and J. W. Hanrahan. 1989. Bicarbonate permeability of the outward rectifying anion channel. *J. Membr. Biol.* **112:** 109–122.

Weiner, I. M., and G. H. Mudge. 1985. Pp. 887–907 in *The Pharmacological Basis of Therapeutics.* 7th Edition. MacMillan, New York.

Weiderholt, M., T. J. Jentsch, and S. K. Kellar. 1985. Electrogenic sodium-bicarbonate symport in cultured corneal endothelial cells. *Pfluger Arch.* **405 (Suppl. 1):** S167–171.

Weiss, G. 1989. Relaxin in the male. *Biol. Reprod.* **40:** 197–200.

Wistrand, P. J. 1984. Properties of membrane-bound carbonic anhydrase. *Ann. NY Acad. Sci.* **429:** 195–206.

Yoshitomi, K., B-Ch. Burckhardt, and E. Fromter. 1985. Rheogenic sodium-bicarbonate cotransport in the peritubular cell membrane of rat proximal tubule. *Pflugers Arch.* **405:** 360–366.

Reference: *Biol. Bull.* **197:** 94–103. (August 1999)

Waterborne and Surface-Associated Carbohydrates as Settlement Cues for Larvae of the Specialist Marine Herbivore *Alderia modesta*

PATRICK J. KRUG[1,*] AND ADRIANA E. MANZI[2]

[1] *Department of Biology, University of California, Box 951606, Los Angeles, California 90095-1606; and* [2] *Cytel Corp., 9393 Towne Center Drive, San Diego, California 92121-3016*

Abstract. Larvae of the specialist marine herbivore *Alderia modesta* (Opisthobranchia: Ascoglossa) metamorphose in response to a chemical settlement cue from the alga *Vaucheria longicaulis,* the obligate adult prey. Bioactivity coeluted with both high and low molecular weight carbohydrates in solution, and with insoluble high molecular weight carbohydrates associated with the algal cell wall. Larvae metamorphosed in response to water conditioned by *V. longicaulis,* as well as to frozen and homogenized algal tissue. The inducer was efficiently extracted from the algae with boiling water, but after all soluble activity was extracted, residual tissue still induced larval settlement. Ethanol precipitation of a boiled-water extract followed by gel filtration chromatography showed that the precipitate contained carbohydrates of >100,000 Da molecular weight, while the supernatant contained only low molecular weight carbohydrates (<2,000 Da); in both cases all activity was associated with the carbohydrate peak. An aqueous-insoluble 4% NaOH extract was chromatographed in 7 M urea to yield a bioactive high molecular weight carbohydrate peak. Activity was not affected by proteinase K or mild acid hydrolysis, but was significantly decreased by periodate treatment. The results indicate that larvae of *A. modesta* metamorphose in response to both water-soluble and surface-associated carbohydrates of *V. longicaulis,* and that the soluble cue exists as both high and low molecular weight isoforms.

Introduction

Most marine invertebrate species produce free-swimming larvae that disperse in the plankton until becoming competent to settle to the bottom and metamorphose into the adult form (Grahame and Branch, 1985; Levin and Bridges, 1995). Larval recruitment plays a critical role in benthic marine ecosystems, structuring communities and regulating population dynamics (Grosberg, 1982; Roughgarden *et al.*, 1988; Underwood and Fairweather, 1989). Microscopic larvae are generally viewed as passive particles transported by flow to the benthos (Eckman, 1983, 1990; Butman, 1987). Following hydrodynamic delivery of larvae to the bottom, recruitment can be divided into settlement and metamorphosis (Chia and Koss, 1988; Pawlik, 1992). Settlement is characterized by active behaviors with which larvae explore the physical and chemical characteristics of potential substrata (LeTourneux and Bourget, 1988; Rodriguez *et al.*, 1993). Larvae may reject a substrate and resume swimming, becoming resuspended in the water column (Butman *et al.*, 1988; Butman and Grassle, 1992). Alternatively, larvae may respond to surface-associated cues and commit to metamorphosis, an irreversible developmental transformation into the adult stage of the organism (Burke, 1983; Pawlik *et al.*, 1991; Roberts *et al.*, 1991; Pawlik, 1992). Larvae are capable of fine-scale discrimination among substrata both in the laboratory and in the field (Keough and Downes, 1982; Raimondi, 1988).

Recent studies have demonstrated that both surface-associated and water-soluble chemical cues can trigger larval behavioral responses that greatly increase rates of settlement and metamorphosis. Still-water laboratory assays have demonstrated the importance of surface-associated chemical cues for inducing larval metamorphosis of barnacles (Maki

---

Received 3 March 1999; accepted 1 June 1999.

[*] To whom correspondence should be addressed. E-mail: pkrug@biology.ucla.edu

Abbreviations: BVE = boiled *Vaucheria* extract.

et al., 1990), bryozoans (Hurlbut, 1991), corals (Morse *et al.*, 1988), gastropods (Morse *et al.*, 1984), and polychaetes (Kirchman *et al.*, 1982). Hydrodynamic conditions and the presence of a surface cue associated with adult conspecifics had an interactive effect on settlement of larvae of the reef-building polychaete *Phragmatopoma californica* in flow (Pawlik *et al.*, 1991). Waterborne chemical cues also affect larval settlement processes. Soluble cues secreted by the adult prey organisms induced settlement and metamorphosis in the opisthobranchs *Phestilla sibogae* and *Adalaria proxima* (Hadfield and Scheuer, 1985; Lambert and Todd, 1994). Larvae of the oyster *Crassostrea virginica* showed dramatic behavioral responses to a chemical cue secreted by adult conspecifics, increasing settlement in both still and moving water (Tamburri *et al.*, 1992; Turner *et al.*, 1994; Tamburri *et al.*, 1996). However, despite decades of research into the nature of larval chemical settlement cues, relatively little is known about the molecules that regulate this crucial aspect of the life history of most benthic marine invertebrates.

A recent study of a population of the opisthobranch mollusc *Alderia modesta* revealed several unusual features that make *A. modesta* an ideal experimental system for investigating larval life history and settlement processes (Krug, 1998a, b). *A. modesta* is an ascoglossan found in temperate estuaries in association with its obligate food source, the yellow-green alga *Vaucheria longicaulis* (Xanthophyta: Xanthophyceae) (Hartog and Swennen, 1952; Hartog, 1959; Trowbridge, 1993). In southern California, *A. modesta* exhibits a reproductive polymorphism that is extremely rare among marine invertebrates; study populations contain specimens that produce planktotrophic larvae and other individuals that produce lecithotrophic larvae (Krug, 1998b). Most lecithotrophic spawn masses contain a mixture of sibling larvae, some of which metamorphose spontaneously within 2 days of hatching; the remaining veligers delay metamorphosis until encountering a chemical cue derived exclusively from the adult host alga *V. longicaulis* (Krug, 1998a). The present work used a bioassay for larval metamorphosis to determine whether the inductive activity was soluble or surface-associated in nature, and for bioassay-guided isolation of active fractions as a preliminary step in purifying the settlement cue.

Materials and Methods

Collection of organisms and larval bioassay

Alderia modesta (Lovén, 1844) and *Vaucheria longicaulis* were collected from mudflats in the Kendall-Frost Marine Reserve and Northern Wildlife Preserve, and in the San Diego River Flood Control Channel, San Diego, California, U.S.A. All algae used in this study conformed to published descriptions of *V. longicaulis* from California (Abbott and Hollenberg, 1976). Patches of *V. longicaulis* were grown under continuous lighting in the laboratory, and blades of algae were pulled free of the sediment base and rinsed in seawater before use in assays. Adult specimens of *A. modesta* were maintained in petri dishes under 1 cm of seawater, and lecithotrophic egg masses were harvested daily for 3 days. Egg masses from each day were pooled and maintained in 0.45 μm-filtered seawater (FSW); water was changed every other day until hatching. Upon hatching, larvae were maintained in FSW for 2 days, to allow spontaneous metamorphosis to occur in cue-independent larvae (Krug, 1998a). The remaining larvae were then subsampled for use in the bioassay. For each experimental treatment, 15 larvae were added to each of 3 replicate dishes containing 4 ml FSW. After 2 days, larvae were scored for metamorphosis. Each experiment included a FSW-only treatment as a negative control and live *V. longicaulis* as a positive control. The percentage of metamorphosis for each replicate was arcsine transformed, and treatments were compared using a 1-way ANOVA. Unplanned comparisons of means were done using the Scheffé procedure (Day and Quinn, 1989).

Secretion of settlement cue

An experiment was designed to determine whether the *Vaucheria*-derived settlement cue was surface-associated or secreted by the algae. Small patches (1 cm^2) of *V. longicaulis* were cut from a growing mat and left attached to the sediment base. Conditioned seawater (CSW) was made by placing a patch in 4 ml FSW for either 3 h or 24 h, after which the CSW was filtered through cotton and placed in a sterile petri dish; larvae were added directly to the CSW for the bioassay. Conditioned fresh water (CFW) was made by placing patches of *V. longicaulis* in 4 ml deionized water for 24 h. The CFW was filtered through cotton, dried on a rotary evaporator, and resuspended in an equivalent volume of FSW for use in the bioassay. The negative control was FSW aged 24 h and filtered through cotton in parallel with treatements; the positive control was live *V. longicaulis* tissue.

To determine whether *Vaucheria longicaulis* must be alive to trigger metamorphosis, pieces of the algae were frozen at −20°C for 3 days. Frozen patches were thawed by immersion in FSW at room temperature for 1 h prior to use in the bioassay. To determine whether algal tissue must be physically intact, blades of live *V. longicaulis* were pulled free of a 2 cm^2 sediment base and washed in FSW. The algae was manually homogenized in 10 ml deionized water for 20 min, and the suspension sonicated for another 10 min. The homogenate was centrifuged (10 min, 2000 RPM) and the supernatant removed. The soluble homogenate was assayed by adding 200 μl (high concentration) or 30 μl (low concentration) aliquots to 4 ml FSW for use in the bioassay. The negative control was FSW, and the positive control was live intact *V. longicaulis* tissue.

Sequential extraction with boiling water

Four 20 × 20 cm mats of *Vaucheria longicaulis* attached to the natural sediment base were field collected (March 1997) and grown in the laboratory under continuous lighting, moistened daily with 50% seawater. After 2 weeks algal blades had grown 1–2 cm in height, and were harvested by cutting with dissecting scissors just above the sediment base. The *V. longicaulis* tissue (1.34 g wet weight) was placed in a beaker containing 50 ml deionized water and boiled for 10 min. The solution of boiled *Vaucheria* extract (BVE) was filtered through 100 μm Nitex mesh to remove *Vaucheria* residue, and then through a 0.45 μm filter membrane. The *Vaucheria* residue was collected off of the mesh filter, put in 50 ml of fresh deionized water, and again boiled for 10 min to generate a second extract. This process was repeated four more times, yielding a total of six sequential boiling water extracts. The *Vaucheria* residue remaining after the sixth extraction was collected from the filter; this residue was yellow-brown in coloration but the blades were still physically intact. Each of the six extracts was assayed by adding a 50 μl aliquot to 4 ml FSW per replicate assay dish. Pieces of live *V. longicaulis* were assayed as a positive control, and equivalently sized pieces of the *V. longicaulis* residue remaining after the six sequential extractions were also assayed.

Biochemical characterization of boiled Vaucheria longicaulis *extract (BVE)*

The initial extract made by boiling *Vaucheria longicaulis* for 10 min (described above) was subjected to preliminary biochemical characterization. Six volumes of ethanol were added to 1 ml of BVE and the solution was precipitated overnight at 4°C. The precipitate was pelleted by centrifugation, the supernatant removed, and the precipitate washed with ethanol and repelleted. The supernatant and wash ethanol were combined and dried on a rotary evaporator. The precipitate and supernatant residue were individually resuspended in 1 ml of MilliQ-purified water, such that the material in each fraction was present in solution at the same concentration as in the original extract.

Aliquots (100 μl) of the initial BVE and of the resuspended solutions of supernatant and precipitate were used in subsequent assays to determine the dry weight, carbohydrate content, protein content, and bioactivity of each sample. Lyophilized aliquots were weighed to determine dry mass. Carbohydrate content was determined for duplicate aliquots from each sample using the phenol-sulphuric colorimetric assay (DuBois *et al.*, 1956). Measurements were calibrated to a standard curve generated with known concentrations of glucose. Protein content was determined using the BCA colorimetric assay (Pierce Co.) calibrated to a standard curve generated with commercially supplied albumin standards. Bioactivity was determined using the larval settlement bioassay.

Another 3 ml of BVE was precipitated with 6 volumes of ethanol overnight, and the supernatant and precipitated material were separated as before. The carbohydrate elution profiles of both the supernatant and precipitate fractions were determined using a gel filtration column (90 cm × 1 cm) of Sephacryl S-200 resin (Pharmacia Co.). The column was calibrated for molecular weight using Blue Dextran to determine the void volume (V_o) and glucose to determine the included volume (V_i) for small molecules; size standards were detected in fractions after collection visually (Blue Dextran) or by the phenol-sulphuric colorimetric assay (glucose). The supernatant residue was dissolved in a minimal volume and loaded onto the column, eluting with MilliQ-purified water at a flow rate of 6 ml/h and collecting 0.5 ml fractions. Aliquots were taken from each fraction and analyzed for carbohydrate content by the phenol-sulphuric colorimetric assay and for protein content by the BCA assay; the detection limit for both colorimetric assays was 0.5 μg/ml. Based on the resulting carbohydrate elution profile, fractions representing every 8 ml were pooled and lyophilized to give 5 total fractions spanning the void volume and included volume. Each pooled fraction was dissolved in water and 150 μl aliquots were bioassayed. The precipitated fraction was chromatographed in an identical manner and fractions were collected, assayed for carbohydrate content, and pooled to give five total fractions. Each pooled fraction was dissolved in water and 75 μl aliquots were bioassayed. A positive control using live *Vaucheria longicaulis* induced 84 ± 10% metamorphosis, while a negative control using FSW gave 4 ± 4% background metamorphosis.

Sequential extraction of Vaucheria longicaulis *with solvents of increasing polarity*

To determine whether macromolecules associated with the algal cell wall were bioactive, *Vaucheria longicaulis* was sequentially extracted with solvents of increasing polarity and harshness to extract molecules of increasing molecular weight. Lyophilized *Vaucheria longicaulis* (500 mg) was homogenized into a fine powder and extracted with 80% aqueous ethanol (50 ml, 7 h, 75°C), cold water (50 ml, 4 d, 20°C), hot water (50 ml, 24 h, 65°C), and 4% sodium hydroxide (50 ml, 24 h, 20°C) (Cleare and Percival, 1972). The ethanol extract was partitioned into a water-soluble fraction and a water-insoluble organic fraction. The cold and hot water extracts were precipitated with ethanol as before to generate supernatant and precipitate fractions for each extract. Aliquots corresponding to 250 μg dry weight were taken from the water-soluble ethanol extract and from the cold and hot water supernatant and precipitate fractions and were assayed directly for bioactivity. An aliquot of the organic-soluble material from the ethanol extract was dissolved in methanol, added to a dry culture dish, the solvent evaporated, and 4 ml of FSW added prior to the bioassay.

The 4% NaOH extract was exhaustively dialyzed against MilliQ-purified water and lyophilized, giving a dry material (44 mg) that was completely insoluble in water but dissolved readily in 7 M urea. The S-200 Sephacryl column was equilibrated in 7 M urea and calibrated for V_0 and V_t as before. A portion of the 4% NaOH extract was dissolved in a minimal volume of 7 M urea and loaded onto the S-200 column. The sample was chromatographed and fractions were collected and assayed exactly as before, except the column was eluted with 7 M urea. Fractions comprising the high molecular weight carbohydrate peak were pooled and dialyzed exhaustively against water using 10,000 molecular weight cutoff dialysis tubing. The dialysate was reduced to a volume of 1 ml on a rotary evaporator and 100 μl aliquots were bioassayed.

Treatment of BVE with proteinase K, sodium periodate, and mild acid hydrolysis

Chemical and enzymatic treatments were performed to determine the biochemical nature of the settlement cue. A solution of sodium periodate (0.37 M, 100 μl) was added to 1.0 ml of BVE, and the solution was incubated at 4°C in the dark (Hassid and Abraham, 1957). The reaction was quenched after 24 h by the addition of excess glycerol (20 μl). As a control, 1.0 ml of BVE was incubated at 4°C in the dark for 24 h, after which excess glycerol (20 μl) was added followed immediately by periodate as in the treated sample. Both samples were incubated for 1 h to allow the consumption of excess periodate, and were then dialyzed exhaustively against deionized water for one week. Both treatment and control samples were lyophilized, dissolved in 300 μl FSW, and 100 μl aliquots used as replicate treatments in the larval settlement bioassay.

Proteinase K (600 μg) was added to a sample of BVE (300 μl) which had been adjusted to pH 7.8 and incubated at 50°C for 24 h. The proteinase was then inactivated by heating at 100°C for 15 min. A control was done by adding proteinase to BVE immediately prior to heating at 100°C for 15 min. Samples were split into three replicate 100 μl aliquots and tested in the larval bioassay. A mild acid hydrolysis was performed by adding concentrated TFA (1.5 μl) to BVE (400 μl) to achieve a final concentration of 0.1 M TFA. The solution was heated at 100°C for 75 min (Lahaye and Ray, 1996) and dried under vacuum to remove TFA. As control for the presence of residual TFA salts, BVE (400 μl) was heated in parallel at 100°C for 15 min, and concentrated TFA was added to BVE immediately prior to drying under vacuum. Samples were dissolved in 300 μl FSW, and 100 μl aliquots used as replicate treatments in the bioassay. Differences between treatment and control samples were compared using an unpaired two-tailed t-test on arcsine-transformed percentages for each of the three treatments, as different quantities of BVE were treated and bioassayed in each case.

Results

Secreted and surface-associated forms of the larval settlement cue

Previous work had demonstrated that *Alderia modesta* larvae metamorphosed specifically in response to living tissue of *Vaucheria longicaulis* (Krug, 1998a). The initial aim of the present study was to determine whether the settlement cue was secreted into seawater by living algae, and whether dead or homogenized algal tissue could induce settlement. Water previously conditioned by the presence of *V. longicaulis* was as active in promoting metamorphosis as was the living algae (Fig. 1A, and results of a 1-way ANOVA: df = 4, 22; F = 32.73; $P < 0.0001$). The

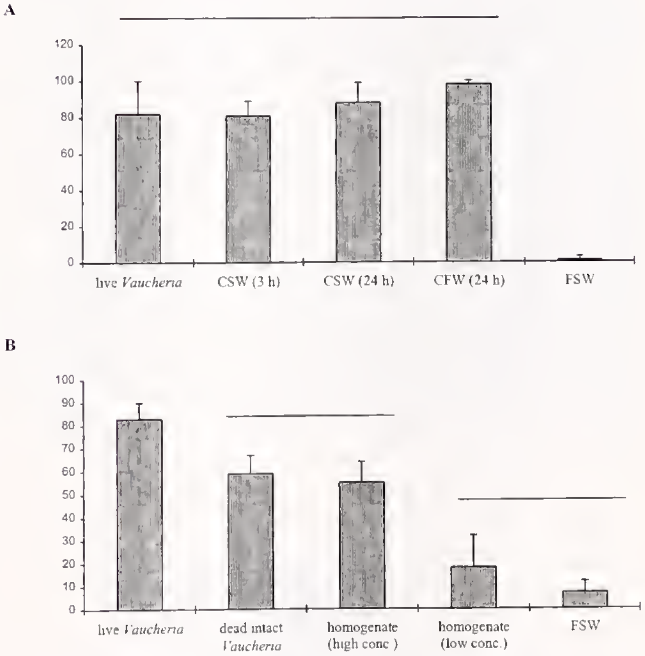

Figure 1. Induction of larval metamorphosis by live *Vaucheria longicaulis*, dead tissue, and conditioned water. Percentages of larval metamorphosis are given as means + SD (n = 3); arcsine-transformed percentages were compared with a 1-way ANOVA, with a post-hoc Scheffé test for unplanned comparisons. Live *V. longicaulis* tissue was used as a positive control and filtered sea water (FSW) as a negative control A. Secretion of larval settlement cue by living *V. longicaulis*. Means are percentages of metamorphosis induced by exposure to *Vaucheria*-conditioned seawater (CSW) or conditioned fresh water (CFW). Duration of conditioning process is given in parentheses. Means not joined by a horizontal line differed significantly ($P < 0.001$). B. Inductive effect of dead or homogenized *V. longicaulis*. Previously frozen and thawed *Vaucheria* tissue, or aliquots of homogenized algal tissue, were assayed for inductive effect. Means not joined by a horizontal line differed significantly ($P < 0.05$).

conditioning process occurred rapidly in the laboratory, such that water conditioned for 3 h induced the same level of metamorphosis as water conditioned for 24 h. Fresh water was also conditioned by the presence of *V. longicaulis* (Fig. 1A). There was no statistical difference between the level of metamorphosis induced by the living algae and any of the conditioned water treatments, all of which differed significantly from the seawater-only control (Scheffé test, $P < 0.001$).

Vaucheria longicaulis tissue that was frozen and thawed induced significant larval metamorphosis, indicating that the algae does not have to be alive to trigger settlement (Fig. 1B, and results of a 1-way ANOVA: df = 4, 16; $F = 61.55$; $P < 0.0001$). Homogenates of algal tissue were also active, confirming that *V. longicaulis* tissue does not have to be alive or intact to induce metamorphosis (Fig. 1B). Significantly higher levels of metamorphosis were induced by frozen *V. longicaulis* and the higher concentration of tissue homogenate than by the negative control (Scheffé test, $P < 0.05$). The lower concentration of homogenate did not induce significantly more metamorphosis than the negative control, indicating that the larvae may be dose-responsive to preparations of the cue; dilution experiments with conditioned seawater support this conclusion (data not shown).

When *Vaucheria longicaulis* was extracted with boiling water, the resulting aqueous extract was as active as positive controls when assayed at an 80-fold dilution (Fig. 2, and results of a 1-way ANOVA: df = 8, 18; $F = 20.45$; $P < 0.0001$). Conditioned seawater had no effect at such a dilution, indicating that boiling water extracted the settlement cue more efficiently than did the conditioning process. When the *V. longicaulis* tissue was re-extracted with boiling water for a second time, the resulting extract induced a low level of metamorphosis, but not significantly more than the negative control when assayed at an 80-fold dilution (Fig. 2). Four further extractions with boiling water yielded extracts that contained no appreciable bioactivity, even when assayed at higher concentrations. These data indicate that all of the measurable bioactivity was extracted from *V. longicaulis* in the first two boiling water treatments. The insoluble residue remaining after six sequential extractions had thus been exhaustively extracted. However, larvae exposed to this residue metamorphosed at a level comparable to those exposed to living *V. longicaulis* (Fig. 2). Significant bioactivity thus remained associated with the *Vaucheria* cell wall residue after all the soluble settlement cue had been extracted.

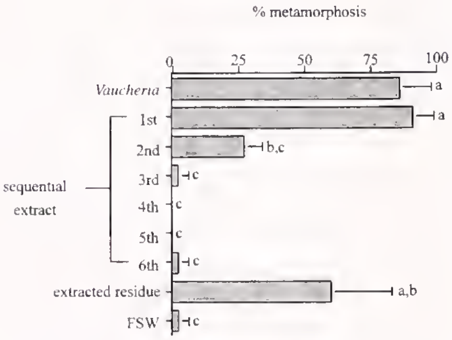

Figure 2. Serial extraction of *Vaucheria longicaulis* with boiling water. Means + SD (n = 3) are percentages of larval metamorphosis induced by aliquots of 6 sequential boiling water extracts, tested at an 80-fold dilution, along with the fully extracted algal residue. Live *V. longicaulis* was used as a positive control, and FSW as a negative control. Means not identified with the same letter differed significantly ($P < 0.05$, 1-way ANOVA with a post-hoc Scheffé comparison).

High and low molecular weight forms of the soluble settlement cue

Boiled *Vaucheria* extract (BVE) was fractionated by ethanol precipitation into a supernatant and precipitate, each of which was diluted back up to the starting volume of BVE for comparison. Biochemical analysis revealed that the carbohydrate content of BVE partitioned equally between the precipitate and supernatant, while the majority of the protein in the crude BVE went into the ethanol precipitate (Table I). There was no significant difference between the bioactivity in 100 μl of precipitate, supernatant, and BVE (1-way ANOVA, $P > 0.3$), although the supernatant consistently displayed slightly lower activity at several concentrations tested.

Both the ethanol precipitate and supernatant were further fractionated by gel filtration chromatography on a Sephacryl S-200 column. When column fractions were assayed for carbohydrate content, contrasting elution profiles were obtained for the two samples (Fig. 3). All detectable carbohydrate from the supernatant fraction eluted in the included volume of the column, indicating a molecular weight of <2,000 Da. In contrast, when the precipitate was chromatographed, all detectable carbohydrate eluted as one peak in the void volume, indicating molecules of >100,000 Da molecular weight. When fractions were pooled and bioassayed, there was significant variation in the bioactivity of different fractions (Fig. 3, and results of a 1-way ANOVA: df = 11, 24; $F = 17.33$; $P < 0.0001$). For the precipitate, a high level of metamorphosis (54 ± 23% SD) was induced by the pooled fractions containing the high molecular weight carbohydrate peak, and a lower level was induced by the adjacent fraction containing the trailing edge of the peak. The level of metamorphosis induced by the high molecular weight peak was not statistically different from that induced by the positive control (Scheffé test, $P = 0.20$) but was significantly higher than the negative control (Scheffé test, $P < 0.05$). No bioactivity significantly higher than the negative control (4 ± 4%) was detected in the low molecular weight fractions from the ethanol precipitate. The bioactivity profile of the ethanol supernatant gave the op-

Table I

Comparative dry weight, protein content, carbohydrate content, and bioactivity (±SD) of 100 μl aliquots of a standard solution of boiled Vaucheria *extract (BVE) and the precipitate and supernatant resulting from ethanol treatment of BVE. The precipitate and supernatant were dissolved in the starting volume of extract and aliquots were removed for chemical assays ($n = 2$) and bioassays ($n = 3$)*

Sample	Dry Weight (μg)	Carbohydrate (μg)	Protein (μg)	Bioactivity (%)
BVE	270 ± 10	6 ± 1	25 ± 1	82 ± 25
supernatant	110 ± 10	4 ± 1	6 ± 1	49 ± 4
precipitate	140 ± 10	3 ± 1	17 ± 1	77 ± 27

posite result. The low molecular weight fraction of the supernatant, which contained all the carbohydrate, induced a level of metamorphosis that was not significantly different from the high molecular weight carbohydrate peak from the precipitate (Scheffé test, $P = 0.79$). No other fraction from the supernatant induced significant metamorphosis. Bioactivity thus co-eluted with the major carbohydrate peak of both the supernatant and precipitate, although the active peak from the supernatant contained only low molecular weight molecules while that from the precipitate contained molecules of high molecular weight. Identical carbohydrate peak profiles were obtained when samples were chromatographed using 7 M urea as a chaotropic agent to disrupt any potential aggregation of macromolecules, and no major protein peaks were evident for either sample (data not shown).

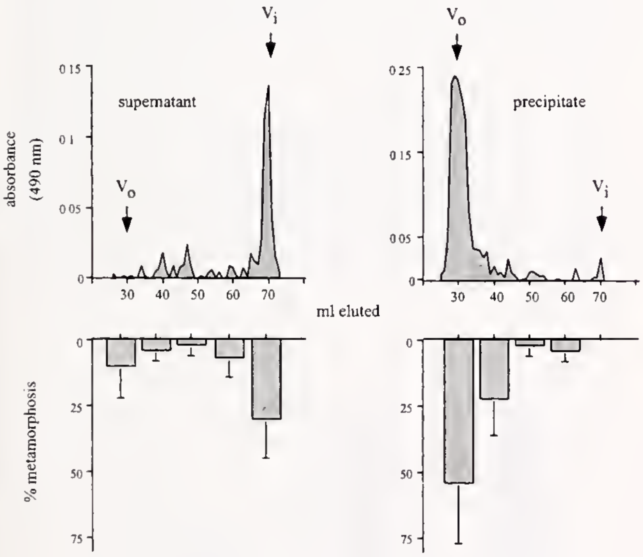

Figure 3. Gel filtration chromatography of the supernatant and precipitate from ethanol precipitation of boiled *Vaucheria* extract (BVE). Fractions were independently chromatographed on a size-calibrated column of Sephacryl S-200 gel eluting with water. Molecules of molecular weight > 100,000 Da elute in the void volume (V_o), while those of <2,000 Da elute in the included volume (V_i). Column fractions (0.5 ml) were assayed for carbohydrate content by the phenol-sulphuric colorimetric assay. Fractions were pooled as indicated, lyophilized, and bioassayed for induction of larval metamorphosis. Percentages of metamorphosis are means + SD ($n = 3$).

Sequential extraction of Vaucheria longicaulis

Lyophilized *Vaucheria longicaulis* was sequentially extracted with solvents of increasing harshness to determine if bioactivity was persistently associated with molecules of increasing molecular weight and stronger association with the algal cell wall. Aqueous extracts were ethanol precipitated to yield supernatant and precipitate fractions, and all soluble extracts were bioassayed at the same concentration per unit dry weight. The material extracted with 4% NaOH was insoluble in water but dissolved readily in 7 M urea, a chaotropic agent routinely used to solubilize and chromatograph high molecular weight polysaccharides. One major carbohydrate peak was detected in the void volume of the S-200 column when the 4% NaOH extract was chromatographed with 7 M urea as eluant (Fig. 4). This carbohydrate peak was exhaustively dialyzed, and the material which remained in aqueous solution was bioassayed. There was significant variation in the bioactivity of different extracts (Fig. 5, and results of a 1-way ANOVA: df = 8, 39; $F = 4.64$; $P < 0.0005$). The water-soluble partition of an ethanol extract of *V. longicaulis* induced significantly higher levels of metamorphosis than the water-insoluble organic layer and the negative control (Scheffé test, $P < 0.05$), indicating all bioactive molecules are highly polar. Bioactivity above the level of the negative control (8 ± 8%) was found in all water-soluble extracts as well as in the resolubilized 4% NaOH extract, indicating that molecules of increasing mo-

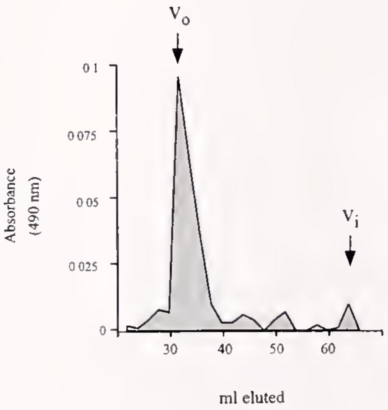

Figure 4. Carbohydrate elution profile of 4% NaOH extract of *Vaucheria longicaulis* powder. Aqueous-insoluble material from the basic extraction was eluted from Sephacryl S-200 gel with the chaotropic agent 7 M urea. Fractions containing the carbohydrate peak eluting in the void volume were pooled, dialyzed, and reduced in volume before being bioassayed.

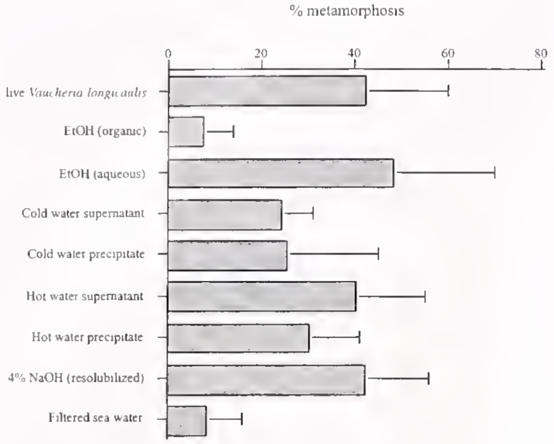

Figure 5. Bioactivity of sequential extracts of *Vaucheria longicaulis.* Lyophilized *Vaucheria* powder was sequentially extracted with aqueous ethanol, cold water, hot water, and 4% NaOH. The ethanol extract was partitioned into aqueous and organic fractions. Cold and hot water extracts were precipitated with ethanol to yield supernatant and precipitate fractions for each. Aliquots of equal dry weight were bioassayed for all water-soluble extracts; the carbohydrate peak from the 4% NaOH extract (see Fig. 4) was dissolved in water prior to the bioassay. Percentages of metamorphosis are means + SD (n = 3).

lecular weight are all active in promoting larval settlement, including those associated with structural elements of the cell wall (Fig. 5).

Chemical and enzymatic treatment of boiled Vaucheria *extract (BVE)*

To determine whether proteinacious components were required for bioactivity, BVE was treated with a high concentration (2 mg/ml) of proteinase K. Proteinase treatment did not decrease the bioactivity of BVE (Fig. 6). Bioactivity was also stable to mild acid hydrolysis using 0.1 M TFA at 100°C. In contrast, treatment with sodium periodate, a chemical agent which cleaves sugar residues, significantly decreased the bioactivity of BVE (Fig. 6).

Discussion

The present study demonstrates that larvae of the ascoglossan *Alderia modesta* metamorphose in response to both secreted and surface-associated forms of the settlement cue derived from the adult host alga, *Vaucheria longicaulis.* Seawater conditioned by the presence of *V. longicaulis* was as active as the algae itself at inducing larval metamorphosis, suggesting the algae secretes one form of the cue into the surrounding seawater. Water-soluble cues derived from the adult prey organism induce larval settlement for other specialist predators. Larvae of the aeolid nudibranch *Phestilla sibogae* metamorphosed in response to water conditioned with the hard coral *Porites compressa* (Hadfield, 1977; Hadfield and Scheuer, 1985). Larvae of the dorid nudibranch *Adalaria proxima* metamorphosed in seawater conditioned by the preferred adult prey, the bryozoan *Electra pilosa* (Lambert and Todd, 1994). However, metamorphosis of *A. proxima* larvae could only be induced by live colonies of *E. pilosa* and not by dead colonies or homogenized extracts (Todd *et al.*, 1991; Lambert and Todd, 1994). In contrast, dead and homogenized *V. longicaulis* tissue induced metamorphosis in *A. modesta.*

Secreted settlement cues are also involved in gregarious settlement of some species. Larvae of the sand dollars *Dendraster excentricus* and *Echinarachinus parma* metamorphosed in response to sand beds and seawater conditioned by the presence of adult conspecifics (Burke, 1984; Pearce and Scheibling, 1990). The most detailed studies on the effects of a secreted chemical settlement cue have focused on the oyster *Crassostrea virginica.* Larvae altered their swimming speed and turning rate in response to small basic peptides secreted by adult conspecifics, significantly increasing settlement in both still and moving water in response to the dissolved cue (Tamburri *et al.*, 1992; Turner *et al.*, 1994; Tamburri *et al.*, 1996). These results demonstrate that soluble chemicals can increase settlement rates by influencing the behavior of larvae still suspended in the water column (Turner *et al.*, 1994). The relative importance of the secretion of the *Vaucheria*-derived cue to the settlement of *Alderia modesta* larvae in the field will require further study. However, the rapidity of the conditioning process suggests that absorbent mats of *V. longicaulis* may become saturated with naturally conditioned water during high tides, which might induce settlement in larvae that enter trapped water parcels.

Extracting *Vaucheria longicaulis* with boiling water not only demonstrated that the chemical cue is stable to prolonged periods of boiling, but that a highly concentrated solution can be prepared in this manner. The diminishing bioactivity of sequential extracts indicates that

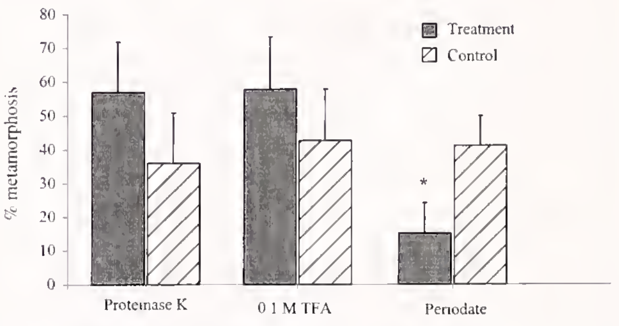

Figure 6. Effects of proteinase K, mild acid hydrolysis, and sodium periodate on bioactivity of boiled *Vaucheria* extract (BVE). Percentages of larval metamorphosis are given as means + SD (n = 3) for each treatment and the corresponding control. Percentages for each treatment and control were arcsine transformed and compared with a two-tailed unpaired t-test (* = significant at $P < 0.05$ level); the t values obtained were 2.08 (proteinase K), 1.20 (mild acid hydrolysis), and −4.46 (sodium periodate).

there is a limited amount of the waterborne cue that can be extracted with boiling water. However, after repeated extractions the residual *Vaucheria* tissue retained significant activity, indicating that a non-extractable form of the settlement cue remains associated with the algal cell wall. This is the first direct demonstration that the same substrate produces both secreted and surface-associated forms of a larval settlement cue, each of which is sufficient to induce metamorphosis.

Polysaccharide chemists routinely employ basic solvents such as NaOH to extract material that remains associated with plant cell walls following hot water extraction (Cleare and Percival, 1972). The water-insoluble material extracted with 4% NaOH contained high molecular weight carbohydrates that, when partially resolubilized in 7 M urea and then dialyzed against water, were active in the larval settlement assay. The bioactivity of this fraction is consistent with the finding that *Vaucheria* tissue exhaustively extracted with boiling water can still induce metamorphosis; together, these experiments define a surface-associated class of molecules which differ in their physical properties (size, solubility) from the water-soluble cue molecules, but share the same bioactivity. An insoluble inducer associated with cell wall polysaccharides of the crustose red alga *Hydrolithon boergesenii* triggered metamorphosis in the coral *Agaricia humilis* (Morse *et al.*, 1988; Morse and Morse, 1991). Larvae of the echinoid *Stronglyocentrotus droebachiensis* metamorphosed in response to live tissue or a homogenate of several species of coralline red algae, but the algae did not release soluble inducers into seawater (Pearce and Scheibling, 1990).

The active material in the water-soluble extracts was further divided into discrete molecular weight classes by ethanol precipitation. Chromatography revealed that the carbohydrates in the BVE precipitate were exclusively of high molecular weight, while those in the supernatant were all of low molecular weight; in both cases, the bioactivity co-eluted with the major carbohydrate peak. Studies of larval settlement inducers for other opisthobranchs have used ultrafiltration to show that the bioactive molecules are less than 1,000 Da in size (Hadfield and Pennington, 1990; Gibson and Chia, 1994; Lambert *et al.*, 1997). Distinct size-classes of water soluble settlement cue molecules have not been previously reported from other study systems.

The bioactive settlement cue molecules co-eluted with the carbohydrate peak in each extract, were stable to boiling and mild acid or base treatment, and some were firmly associated with the algal cell wall. These results suggested that the molecules were either composed of, or tightly associated with, algal carbohydrates. Proteinase K treatment did not diminish the activity of algal extracts, but bioactivity was significantly reduced by treatment with sodium periodate. Periodate reacts with monosaccharide units of polysaccharides, oxidizing consecutive hydroxyl groups to aldehydes and cleaving sugar residues having three consecutive hydroxyl groups to produce formic acid (Hassid and Abraham, 1957). Taken together, the data strongly suggest that the larvae of *Alderia modesta* metamorphose in response to a structural feature of the polysaccharides produced by *Vaucheria longicaulis*. This would account for the bioactivity of molecules of differing molecular weight, since small oligosaccharides can contain the same distinctive glycosidic linkages as are found in the full-length polymer. Consistent with this hypothesis, the activity of *Vaucheria* extract was not diminished by a mild acid hydrolysis using 0.1 M TFA; the same conditions have been used to fragment matrix polysaccharides of green algae into smaller oligosaccharides representative of the repeating unit (Lahaye and Ray, 1996).

Recognition of carbohydrates by larval lectins has been implicated in settlement induction for several taxonomically diverse marine invertebrates (Kirchman *et al.*, 1982; Maki and Mitchell, 1985; Bahamondes-Rojas and Dherbomez, 1990; Bonar *et al.*, 1990; Morse and Morse, 1991). Metamorphosis of barnacle larvae in response to glycoproteins is abolished when the oligosaccharide chains of the proteins are bound by lectins and thus rendered inaccessible to larval receptors (Matsumura *et al.*, 1998). The present study strongly indicates a carbohydrate is the settlement cue for *Alderia modesta*, but definitive proof will require the isolation of a pure oligosaccharide that induces metamorphosis. Preliminary results indicate that inductive fragments are anionic and contain uncommon sugar residues including glucuronic and galacturonic acid, rhamnose, and xylose, which are not recognized by most available enzymes and lectins (Krug, 1998a). A direct chemical analysis of the structural features of the polysaccharides of *Vaucheria longicaulis* and their bioactivity is currently underway. However, bioactivity is clearly associated with algal polysaccharides, both soluble and insoluble, making *A. modesta* an ideal experimental organism for dissecting the roles of waterborne versus surface-associated cues in the larval settlement process.

Acknowledgments

We thank Dr. K. Norgard-Sumnicht for experimental assistance, and Drs. N. Holland, L. Levin, W. Fenical, C. Derby, and two anonymous reviewers for thoughtful criticisms that greatly improved this manuscript. Access to the Kendall-Frost Reserve was made possible by Isabelle Kay and the University of California Natural Reserve System. P. J. K. was supported by an NSF Predoctoral Fellowship.

Literature Cited

Abbott, I. A., and G. J. Hollenberg. 1976. *Marine Algae of California.* Stanford University Press, Stanford.

Bahamondes-Rojas, I., and M. Dherbomez. 1990. Purification partielle de substances glycoconjuguées capables d'induire la métamorphose des larves competentes d'*Eubranchus doriae* (Trinchese, 1879), mollusque nudibranche. *J. Exp. Mar. Biol. Ecol.* **144:** 17–27.

Bonar, D. B., S. L. Coon, M. Walch, R. M. Weiner, and W. Fitt. 1990. Control of oyster settlement and metamorphosis by endogenous and exogenous chemical cues. *Bull. Mar. Sci.* **46:** 484–498.

Burke, R. D. 1983. The induction of metamorphosis of marine invertebrate larvae: stimulus and response. *Can. J. Zool.* **61:** 1701–1719.

Burke, R. D. 1984. Pheromonal control of metamorphosis in the Pacific sand dollar, *Dendraster excentricus. Science* **225:** 442–443.

Butman, C. A. 1987. Larval settlement of soft-sediment invertebrates: the spatial scales of pattern explained by habitat selection and the emerging role of hydrodynamic processes. *Oceanogr. Mar. Biol. Annu. Rev.* **25:** 113–165.

Butman, C. A., and J. P. Grassle. 1992. Active habitat selection by *Capitella* sp. I larvae: two-choice experiments in still water and flume flows. *J. Mar. Res.* **50:** 699–715.

Butman, C. A., J. P. Grassle, and C. M. Webb. 1988. Substrate choice made by marine larvae settling in still water and in a flume flow. *Nature* **333:** 771–773.

Chia, F.-S., and R. Koss. 1988. Induction of settlement and metamorphosis of the veliger larvae of the nudibranch *Onchidoris bilamellata. Int. J. Invertebr. Reprod. Devel.* **14:** 53–70.

Cleare, M., and E. Percival. 1972. Carbohydrates of the fresh water alga *Tribonema aequale.* I. Low molecular weight and polysaccharides. *Br. Phycol. J.* **7:** 185–193.

Day, R. W., and G. P. Quinn. 1989. Comparisons of treatments after an analysis of variance in ecology. *Ecol. Monogr.* **59:** 433–463.

DuBois, M., K. A. Gilles, J. K. Hamilton, P. A. Rebers, and F. Smith. 1956. Colorimetric method for the determination of sugars and related substances. *Anal. Chem.* **28:** 350–356.

Eckman, J. E. 1983. Hydrodynamic processes affecting benthic recruitment. *Limnol. Oceanogr.* **28:** 241–257.

Eckman, J. E. 1990. A model of passive settlement by planktonic larvae onto bottoms of differing roughness. *Limnol. Oceanogr.* **35:** 887–901.

Gibson, G. D., and F.-S. Chia. 1994. A metamorphic inducer in the opisthobranch *Haminaea callidegenita:* partial purification and biological activity. *Biol. Bull.* **187:** 133–142.

Grahame, J., and G. M. Branche. 1985. Reproductive patterns of marine invertebrates. *Oceanogr. Mar. Biol. Annu. Rev.* **23:** 373–398.

Grosberg, R. 1982. Intertidal zonation of barnacles: the influence of planktonic zonation of larvae on the vertical distribution of adults. *Ecology* **63:** 894–899.

Hadfield, M. G. 1977. Chemical interactions in larval settling of a marine gastropod. Pp. 403–413 in *Marine Natural Products Chemistry.* D. J. Faulkner and W. H. Fenical, eds. Plenum, New York.

Hadfield, M. G., and J. T. Pennington. 1990. Nature of the metamorphic signal and its internal transduction in larvae of the nudibranch *Phestilla sibogae. Bull. Mar. Sci.* **46:** 455–464.

Hadfield, M. G., and D. Scheuer. 1985. Evidence for a soluble metamorphic inducer in *Phestilla:* ecological, chemical and biological data. *Bull. Mar. Sci.* **37:** 556–566.

Hartog, C. Den. 1959. Distribution and ecology of the slugs *Alderia modesta* and *Limapontia depressa* in the Netherlands. *Beaufortia* **7:** 15–36.

Hartog, C. Den., and C. Swennen. 1952. On the occurrence of *Alderia modesta* (Lovén) and *Limapontia depressa* A. & H. on the salt marshes of the Dutch Wadden Sea. *Beaufortia* **2:** 1–3.

Hassid, W. Z., and S. Abraham. 1957. Chemical procedures for analysis of polysaccharides. *Methods in Enzymol.* **3:** 34–50.

Hurlbut, C. J. 1991. Community recruitment: settlement and juvenile survival of seven co-occurring species of sessile marine invertebrates. *Mar. Biol.* **109:** 507–515.

Keough, M. J., and B. J. Downes. 1982. Recruitment of marine invertebrates: the role of active larval choices and early mortality. *Oecologia* **54:** 348–352.

Kirchman, D., S. Graham, D. Reish, and R. Mitchell. 1982. Lectins may mediate in the settlement and metamorphosis of *Janua (Dexiospira) brasiliensis* (Grube). *Mar. Biol. Lett.* **3:** 131–142.

Krug, P. J. 1998a. Chemical and larval ecology of opisthobranch molluscs: variable development modes and settlement requirements for larvae of *Alderia modesta.* Ph.D. dissertation, University of California, San Diego, 227 pp.

Krug, P. J. 1998b. Poecilogony in an estuarine opisthobranch: planktotrophy, lecithotrophy, and mixed clutches in a population of the ascoglossan *Alderia modesta. Mar. Biol.* **132:** 483–494.

Lahaye, M., and B. Ray. 1996. Cell-wall polysaccharides from the marine alga *Ulva "rigida"* (Ulvales, Chlorophyta)—NMR analysis of ulvan oligosaccharides. *Carbohydr. Res.* **283:** 161–173.

Lambert, W. J., and C. D. Todd. 1994. Evidence for a water-borne cue inducing metamorphosis in the dorid nudibranch mollusc *Adalaria proxima* (Gastropoda: Nudibranchia). *Mar. Biol.* **120:** 265–271.

Lambert, W. J., C. D. Todd, and J. D. Hardege. 1997. Partial characterization and biological activity of a metamorphic inducer of the dorid nudibranch *Adalaria proxima* (Gastropoda: Nudibranchia). *Invertebr. Biol.* **116:** 71–81.

LeTourneux, F., and E. Bourget. 1988. Importance of physical and biological settlement cues used at different spatial scales by the larvae of *Semibalanus balanoides. Mar. Biol.* **97:** 57–66.

Levin, L. A., and T. S. Bridges. 1995. Pattern and diversity in reproduction and development. Pp. 1–47 in *Marine Invertebrate Larvae.* L. McEdward, ed. CRC Press, Oxford.

Maki, J. S., and R. Mitchell. 1985. Involvement of lectins in the settlement and metamorphosis of marine invertebrate larvae. *Bull. Mar. Sci.* 37: 675–683.

Maki, J. S., D. Rittschof, M.-O. Samuelsson, U. Szewzyk, A. B. Yule, S. Kjelleberg, J. D. Costlow, and R. Mitchell. 1990. Effect of marine bacteria and their exopolymers on the attachment of barnacle cypris larvae. *Bull. Mar. Sci.* **46:** 499–511.

Matsumura, K., S. Mori, M. Nagano, and N. Fusetani. 1998. Lentil lectin inhibits adult extract-induced settlement of the barnacle, *Balanus amphitrite. J. Exp. Zool.* **280:** 213–219.

Morse, A. N. C., C. A. Froyd, and D. E. Morse. 1984. Molecules from cyanobacteria and red algae that induce settlement and metamorphosis in the mollusc *Haliotis rufescens. Mar. Biol.* **81:** 293–298.

Morse, D. E., and A. N. C. Morse. 1991. Enzymatic characterization of the morphogen recognized by *Agaricia humilis* (Scleractinian coral) larvae. *Biol. Bull.* **181:** 104–122.

Morse, D. E., N. Hooker, A. N. C. Morse, and R. Jensen. 1988. Control of larval metamorphosis and recruitment in sympatric agariciid corals. *J. Exp. Mar. Biol. Ecol.* **116:** 193–217.

Pawlik, J. R. 1992. Chemical ecology of the settlement of benthic marine invertebrates. *Oceanogr. Mar. Biol. Annu. Rev.* **30:** 273–335.

Pawlik, J. R., C. A. Butman, and V. R. Starczak. 1991. Hydrodynamic facilitation of gregarious settlement of a reef-building tube worm. *Science* **251:** 421–424.

Pearce, C. M., and R. E. Scheibling. 1990. Induction of settlement and metamorphosis in the sand dollar *Echinarachnius parma:* evidence for an adult-associated factor. *Mar. Biol.* **107:** 363–369.

Raimondi, P. T. 1988. Settlement cues and determination of the vertical limit of an intertidal barnacle. *Ecology* **69:** 400–407.

Roberts, D., D. Rittschof, E. Holm, and A. R. Schmidt. 1991. Factors influencing initial larval settlement: temporal, spatial, and surface molecular components. *J. Exp. Mar. Biol. Ecol.* **150:** 203–221.

Rodriguez, S., F. Patricio Ojeda, and N. Inestrosa. 1993. Settlement of benthic marine invertebrates. *Mar. Ecol. Prog. Ser.* **97:** 193–207.

Roughgarden, J., S. Gaines, and H. Possingham. 1988. Recruitment dynamics in complex life cycles. *Science* **241:** 1460–1466.

Tamburri, M. N., R. K. Zimmer-Faust, and M. L. Tamplin. 1992. Natural sources and properties of chemical inducers mediating settlement of oyster larvae: a re-examination. *Biol. Bull.* **183:** 327–338.

Tamburri, M. N., C. M. Finelli, D. S. Wethey, and R. K. Zimmer-Faust. 1996. Chemical induction of larval settlement behavior in flow. *Biol. Bull.* **191:** 367–373.

Todd, C. D., M. G. Bentley, and J. N. Havenhand. 1991. Larval metamorphosis of the opisthobranch mollusc *Adalaria proxima* (Gastropoda: Nudibranchia): the effects of choline and elevated potassium ion concentration. *J. Mar. Biol. Assoc. U. K.* **71:** 53–72.

Trowbridge, C. 1993. Local and regional abundance patterns of the ascoglossan opisthobranch *Alderia modesta* (Lovén, 1844) in the Northeastern Pacific. *Veliger* **36:** 303–310.

Turner, E. J., R. K. Zimmer-Faust, M. A. Palmer, and M. Luckenback. 1994. Settlement of oyster (*Crassostrea virginica*) larvae: effects of water flow and a water-soluble chemical cue. *Limnol. Oceanogr.* **39:** 1579–1593.

Underwood, A. J., and P. G. Fairweather. 1989. Supply-side ecology and benthic marine assemblages. *TREE* **4:** 16–20.

Reference: *Biol. Bull.* **197:** 104–111. (August 1999)

The Velar Ciliature in the Brooded Larva of the Chilean Oyster *Ostrea chilensis* (Philippi, 1845)

O. R. CHAPARRO[1], R. J. THOMPSON[2,*], AND C. J. EMERSON[3]

[1] *Instituto de Biología Marina, Universidad Austral de Chile, Casilla 567, Valdivia, Chile;*
[2] *Ocean Sciences Centre, Memorial University of Newfoundland, St. John's, Newfoundland,*
Canada A1C 5S7; and [3] *Biology Department, Memorial University of Newfoundland,*
St. John's, Newfoundland, Canada A1B 3X9

Abstract. The Chilean oyster (*Ostrea chilensis*) broods its offspring almost to the settlement stage (about 8 weeks). Larvae are maintained inside the infrabranchial chamber of the female. Samples from all embryo and larval developmental stages were obtained from mantle cavities of brooding females and analyzed by scanning electron microscopy, with particular attention to the velar structures.

All embryos and the earliest veliger stages of *O. chilensis* are devoid of cilia. Cilia first appear when shell length reaches 290–300 μm, and the first cilia to grow on the velum form the outer preoral cilia. In larvae 340 μm long, all the ciliary rings on the velum can be distinguished. These are the apical cilia (AC), inner preoral cilia (IPC), outer preoral cilia (OPC), and adoral cilia (AOC). The absence of the apical tuft in both *O. chilensis* and the closely related species *O. edulis* represents an adaptation to brooding by the embryos and larvae, but the lack of the postoral cilia (POC) in *O. chilensis* and the lack of cilia in the embryonic and early veliger stages are associated with an extreme brooding condition in this species.

Introduction

Most bivalve molluscs exhibit external fertilization of the gametes followed by the development of pelagic larvae. In some species, however, there is a totally benthic or brooded larval development, and in other cases a period of brooding is followed by a pelagic phase (Pechenik, 1979, 1986). In brooding species the eggs, embryos, and larvae are retained in the interlamellar spaces of both demibranchs or of the inner or outer demibranchs only; alternatively, they may be confined to brood sacs, marsupia, mucous masses, capsules, or other specialized structures (Ockelmann, 1964; Solís, 1967; Franz, 1973; Mackie *et al.*, 1974; Heard, 1977; Mackie, 1984; Tankersley and Dimock, 1992, 1993; Gallardo, 1993).

Brooding is a characteristic common to all members of the subfamily Ostreinae (Harry, 1985). All species of the genus *Ostrea* brood their embryos in the infrabranchial chamber (Millar and Hollis, 1963; Galtsoff, 1964; Chanley and Dinamani, 1980; Harry, 1985; Cranfield and Michael, 1989). Brooding in oysters can be very short, as in *O. puelchana* (3 days, Morriconi and Calvo, 1980; 3 to 9 days, Fernandez Castro and Le Pennec, 1988), or very long, as in *O. chilensis* (6 to 12 weeks; Toro and Chaparro, 1990). In addition to having the longest period of brooding, the Chilean oyster produces the fewest eggs (3500 to 152,000) of any *Ostrea* species, with the largest egg diameter (approximately 250 μm), the largest pediveliger at the time of release (approximately 450 μm), and the shortest pelagic phase (minutes to 24 hours) (review by Toro and Chaparro, 1990).

Pelagic larvae possess structures specialized for swimming and feeding, but it is unlikely that brooded larvae have the same requirements, especially if the brooding period is long, as in the Chilean oyster (8 weeks). In many species, brooded larvae do not ingest particles, often because the brooding female provides nutrition through the biochemical reserves in large eggs, as in *O. chilensis*, or through body fluids or nurse eggs. Strathmann (1978) has described the adaptations of some nonfeeding brooded larvae. In other cases, the female concentrates phytoplankton and other suspended material from the external environment for the use

---

Received 22 May 1998; accepted 24 May 1999.

* To whom correspondence should be addressed. E-mail: thompson@morgan.ucs.mun.ca

of the larvae, as suggested by Buroker (1985) for *Ostrea* spp. and by Mackie (1979) for freshwater bivalves (Pisidiidae), and as demonstrated in *O. chilensis* by Chaparro *et al.* (1993). The present paper examines the velar ciliature of the larva of *O. chilensis,* an extreme case in which the larva is brooded for almost the entire developmental period, and compares the ciliature morphologically with that of the planktotrophic larvae of related species, particularly other ostreids.

Materials and Methods

Samples of oysters (*Ostrea chilensis*) were obtained at intervals throughout the brooding period (October to January) during 1992, 1993, and 1994 from a natural bank in the Quempillén estuary in the northern part of Chiloé Island (41°52'S; 73°46'W), in the south of Chile. On each sampling date, several female oysters were opened and their embryos or larvae removed. In this way, all larval development stages were sampled. Larvae were prepared for scanning electron microscopy (SEM) following Hadfield and Iaea (1989).

Larvae were anesthetized for about 10 min in a $MgCl_2$ solution isotonic with seawater, then fixed for 1 h in ice-cold 3% glutaraldehyde in 0.2 *M* sodium cacodylate buffer, pH 7.4. Fixed samples were rinsed in the buffer solution twice and post-fixed for 1 h in ice-cold 1% OsO_4 in 0.2 *M* sodium cacodylate, pH 7.4. The specimens were then rinsed two or three times with buffer solution and then once with distilled water before being dehydrated in a graded series of ethanol (Cragg, 1985).

For SEM, dehydrated specimens were critical-point dried from liquid carbon dioxide in a Polaron E3000 drying apparatus. Dried larvae were attached to aluminum viewing stubs with double-sided tape and then coated with gold in an Edwards S150A sputter-coater. When necessary, larval shells were broken with a fine needle to expose the internal structures (Cragg, 1985, 1989). Coated samples were viewed in a Hitachi S570 scanning electron microscope operated at an accelerating voltage of 20 kV. Micrographs were recorded on Polaroid Type 665 positive/negative film, and stereopairs taken with a 10° tilt angle difference.

Each brood of larvae was processed separately. Although all larvae from a given brood were at the same developmental stage, as an additional precaution at least 30–50 larvae from each brood were observed by SEM before micrographs were taken, to ensure that the structures observed were common to all of them. Measurements based on SEM are approximate, owing to foreshortening effects related to the depth of field, the tilt angle, and the curvature of the sample.

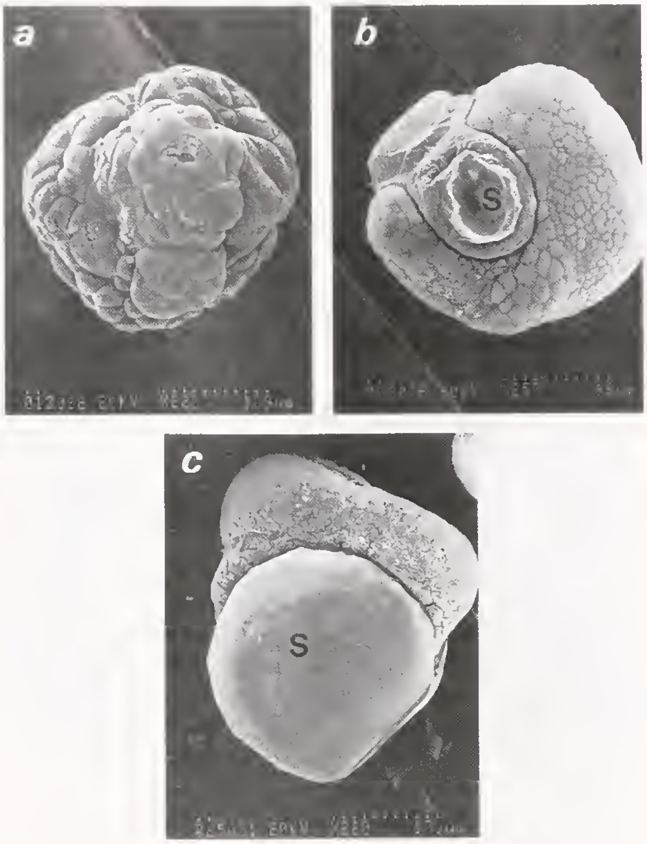

Figure 1. Early development stages in *Ostrea chilensis.* (a) Gastrula; scale bar 109 μm. (b) Dorsolateral view of late trochophore; scale bar 96 μm. (c) Lateral view of early veliger; scale bar 109 μm. In all cases, embryos or larvae are devoid of cilia.

Results

Early development stages

The earliest development stages are naked, with no cilia (Fig. 1). Only when the embryo reaches the earliest veliger stage, with a shell length of about 290 μm, is the first ciliary growth observed. Cilia appear on the upper part of the velum, and owing to their location and arrangement on the velum, they are presumed to form the future ring of outer preoral cilia (OPC) (Fig. 2a, b). These cilia are about 11–14 μm long. At this stage they are separate, with a tendency to join each other in the middle basal part of the cilia. At the same time, a group of short cilia develops in the mouth region and begins to cover the food groove. These cilia are shorter than those in the putative OPC ring, and are randomly distributed (Fig. 2c).

After 25–30 days of brooding (shell length 315–320 μm), a clear pattern of single or compound cilia has emerged which persists for the remainder of the larval phase. The ciliary belts composing the velum are shown schematically in Figure 3. Larvae exhibit a very well synchronized ciliary

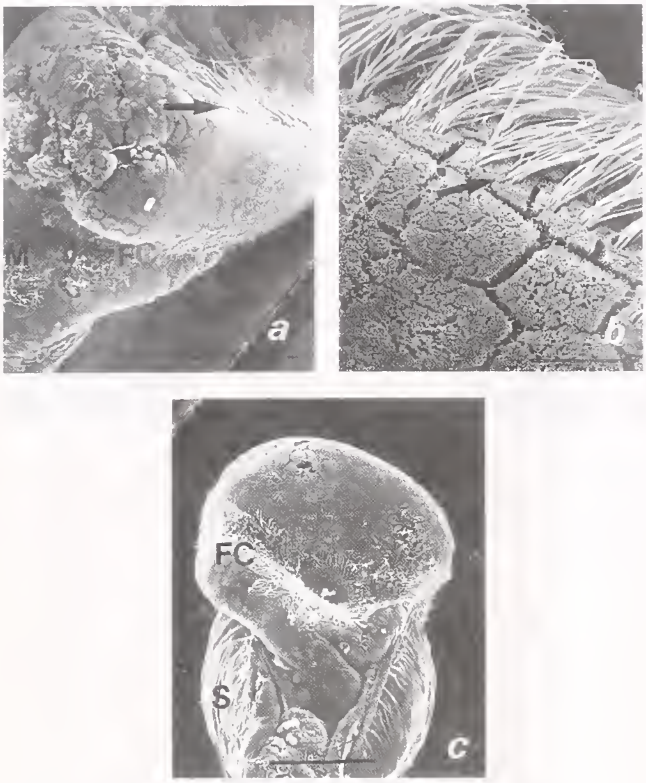

Figure 2. In a larva of *Ostrea chilensis* with a shell length of about 300 μm, the cilia first appear on top of the velum, as well as in the food groove and mouth region. (a, b) Superior-lateral view of the cilia that will form the OPC band; scale bars 60 μm and 8 μm respectively; arrows indicate future OPC. (c) Short cilia covering the adoral food groove (FC) and the mouth region (ventral aspect); scale bar 80 μm.

growth pattern, with all larvae from the same brood being at the same developmental stage.

Distribution of cilia on the velum

The ciliature of a larva of shell length 400 μm is shown in Figure 4A. A concavity about 70–80 μm in diameter is visible in the most central and apical sector of the velum (Fig. 4B). Located in its base is a group of small cilia, the apical cilia (AC), which are randomly distributed and are not organized into the apical tuft characteristic of planktonic veligers, but lie in the same position. Surrounding this depression is a bare region about 60 μm wide, delimited by a single belt of cilia constituting the inner preoral ciliary (IPC) ring.

Inner preoral cilia

The IPC form a ring of single cilia (Fig. 4C), each one about 15–20 μm long. Outside the IPC ring is a naked area, 9–10 μm wide, which is surrounded by a large ring of OPC.

Outer preoral cilia

The OPC form a band, about 10–15 μm wide, of two rows of cirri, or composite cilia (Waller, 1981), which are oriented radially from the center of the velum (Fig. 4D, E). This is the dominant ring in the velum because of its width and the size and complexity of its cirri. Each cirrus is roughly 80 μm long and is composed of 50–100 cilia,

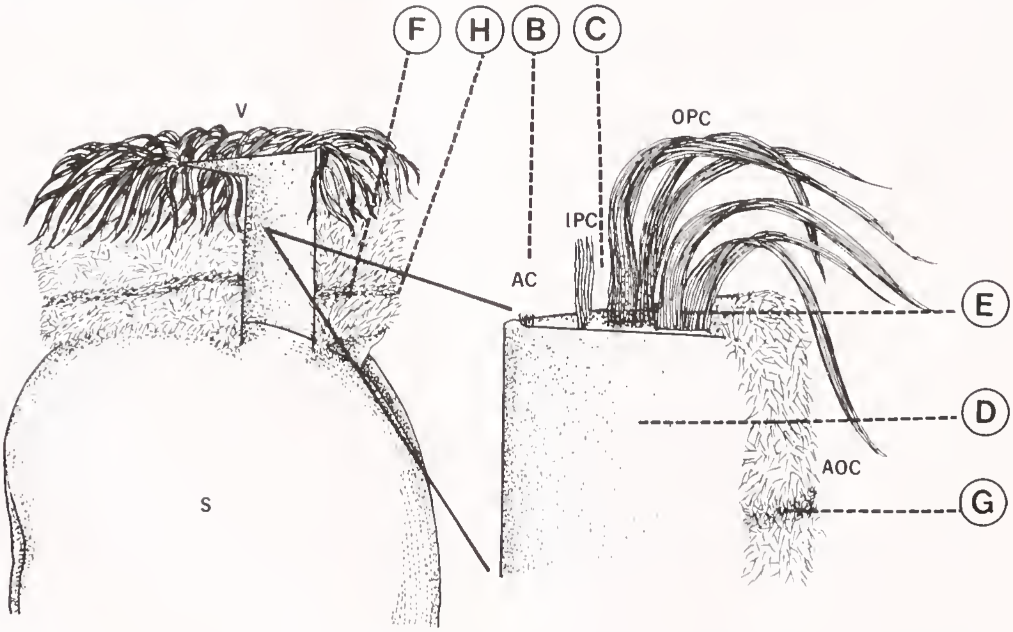

Figure 3. Schematic representation of the velum in a late pediveliger of *Ostrea chilensis* (>400 μm shell length) in lateral view. Ciliary bands are identified in an enlarged section of the velum. AC: apical cilia; AOC: adoral cilia; IPC: inner preoral cilia; OPC: outer preoral cilia; S: shell; V: velum. Circled letters refer to the scanning electron micrographs in Figure 4.

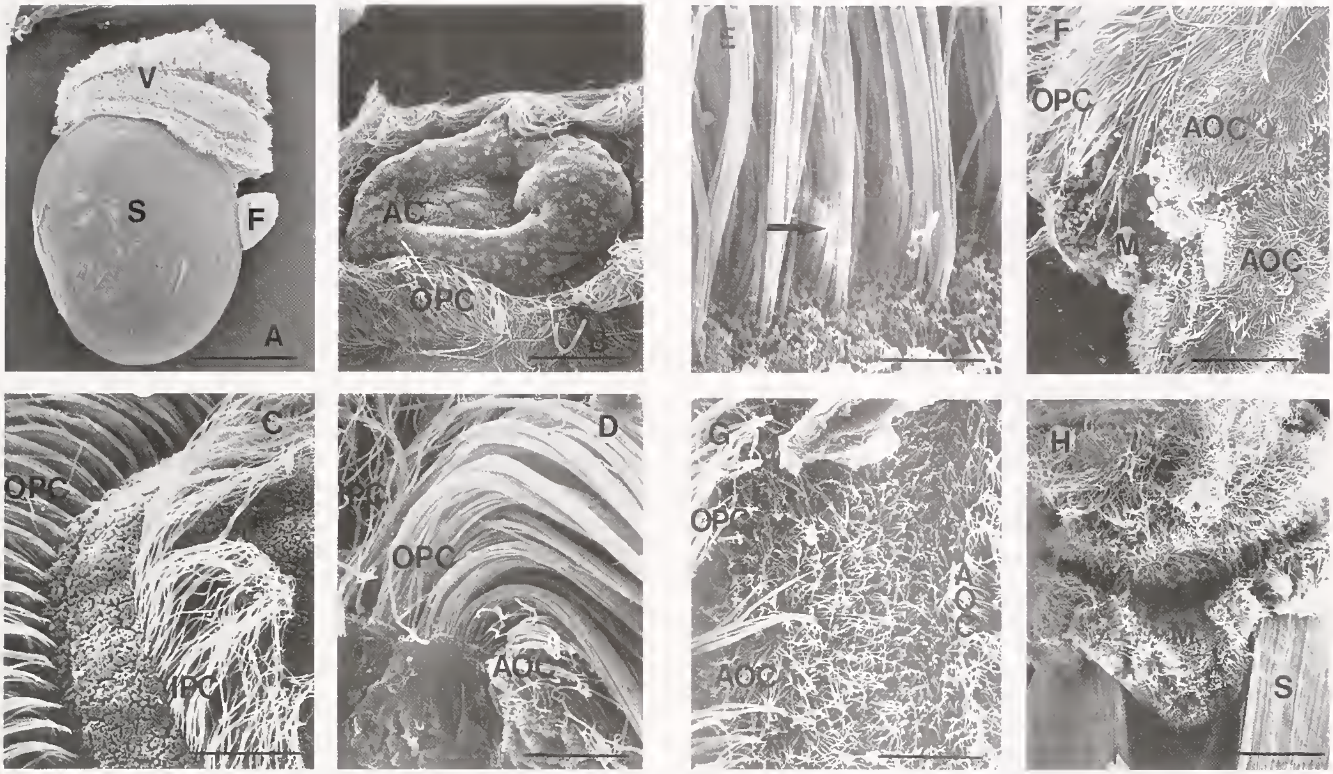

Figure 4. Ciliature of the late pediveliger of *Ostrea chilensis.* (A) Lateral view; scale bar 160 μm. (B) Superior view of the velum showing the AC band in the center; scale bar 60 μm. (C) Detail of the IPC band (superior aspect); scale bar 10.9 μm. (D) Transverse section of the velum showing the principal ciliary bands; scale bar 9.6 μm. (E) Detail of the OPC band; scale bar 3.0 μm. Arrow indicates a row of cirri. (F) Lateral view of the mouth area, showing OPC and AOC bands; scale bar 40 μm. (G) Food groove; scale bar 22 μm. (H) Ventral (= frontal) view of the mouth region; scale bar 48 μm. F = foot; for other abbreviations see legend to Figure 3.

which are in contact with each other for almost all their length. The width of the cirrus is about 1 μm, and each one is separated from its neighbor by a nonciliated space of about 1.5–2 μm.

Adoral cilia

The remainder of the velum (adoral area), from the OPC to the dorsal margin of the shell, is covered by a carpet of individual, short cilia (8–12 μm) known as the adoral cilia (AOC), which also cover the crest and floor of the food groove (the sides are not visible) and the external part of the mouth. No differentiation in the form of the AOC is apparent, although in some areas there are a few cilia of different length, and in the floor of the food groove the cilia are shorter than the rest of the AOC (Fig. 4F, G). Short cilia can also be seen on the base of the external part of the mouth (Fig. 4H). There is no clearly identifiable postoral ciliary band of the type identified in larvae of *Ostrea edulis* by Waller (1981). Below the food groove and close to the mouth lie several lobes, which resemble the tumescent cells identified by Waller (1981) in *O. edulis.*

Discussion

The inclusion of a pelagic larva in the life cycle of most marine bivalve molluscs is accompanied by anatomical adaptations, especially those associated with the velum, and is characterized by rapid development to the prodissoconch stage. These features allow the larva to survive for long periods in the water column, and the velum is an adaptation for planktonic life (Cragg, 1989). Many papers on the early development of bivalves have shown the presence of cilia on some parts of the embryo or larva, or covering the entire surface (Allen, 1961; Carriker, 1961; Bayne, 1976; Amor, 1981; Fitt *et al.*, 1984; Gustafson and Lutz, 1991). In most cases the cilia appear at the earliest stages of embryonic development (Gallardo, 1989). The few studies that have been undertaken on brooded embryos or larvae have shown that cilia first appear at later stages of development: *Ostrea lurida*, trochophore stage (Hopkins, 1936); *O. edulis*, trochophore stage (Horst 1883–1884, in Waller, 1981). However, the present study shows that in the Chilean oyster all embryonic stages, together with the trochophore and early veliger, are totally devoid of cilia. This is one of the few cases known in which cilia are totally absent at such a late stage of development in a bivalve. From the illustrations in Beauchamp (1986), it can be inferred that advanced, shelled veligers of the brooding clam *Lasaea subviridis* are also naked. This species exhibits direct development, and no pelagic phase has been detected (Beauchamp, 1986), an observation that would explain the absence of cilia during the larval stages. Oldfield (1964) demonstrated that the area normally occupied by the ciliated velum is replaced in *L. rubra* by an unciliated structure she termed the "cephalic mass," implying a specialization for brooding more extreme than is seen in the Chilean oyster. Thus loss or modification of the velar ciliature represents one of the most important and visible adaptations for brooding in a bivalve mollusc.

Cilia begin to develop when the shell length of the Chilean oyster larva is about 290 μm. By the time the larva reaches about 300 μm, the cilia have developed completely and remain throughout the rest of the larval phase. The present study supports the contention of Winter *et al.* (1984) and Toro and Chaparro (1990) that the brooding period in *O. chilensis* is the longest of any *Ostrea* species for which information is available. There is little necessity for swimming because the larva spends only a few hours in the water column and is competent to settle immediately after being released (Solís, 1973; Cranfield, 1979). According to Millar and Hollis (1963), the shortened pelagic phase in the larva of *O. chilensis* is an adaptation for survival in a habitat characterized by strong currents.

The absence of cilia during much of larval life may be considered an adaptation to brooding. The encapsulated embryos of many marine invertebrate species lacking pelagic larvae bear structures that appear to be functionally significant only in free-swimming larval stages. In some encapsulated embryos, those cilia normally associated with swimming in pelagic larvae serve to rotate the embryo within its capsule, presumably aiding the larva in the ingestion of fluid albumen and in gas exchange (Fretter and Graham, 1962). Hadfield and Iaea (1989) reported an extreme case in which encapsulated larvae of the gastropod *Petaloconchus montereyensis* showed an absence or reduction of some velar structures that are very important in closely related species with a pelagic larva. On the other hand, in another encapsulated gastropod (*Turritella communis*), cilia develop in the very earliest embryonic stages, even though these cilia are not required for swimming (Kennedy and Keegan, 1992). The velar lobes of many encapsulated gastropod veligers are known to participate in the breakdown and ingestion of nurse eggs (Fioroni, 1966), and in others the velum is greatly modified for aiding in the ingestion and perhaps in the breakdown of external nurse yolk (Hadfield and Iaea, 1989).

In Chilean oyster veligers, ciliary development is well-synchronized within a brood. Immediately after the cilia have completely developed, the larvae start to ingest particles. Thus the cilia are required for feeding more than for swimming, although data from endoscopy show that the larvae are not completely immobile, but exhibit a specific circulation pattern inside the mantle cavity of the female (Chaparro *et al.*, 1993). The larval circulation is driven by water currents produced by the female rather than by the larval velum. Furthermore, although the velar cilia are very active when the female has stopped pumping, the larvae move very little, and it is not clear whether they are capable of swimming at this stage.

The composition of the ciliary bands on the velum is similar, but not identical, to that of the closely related species *Ostrea edulis*, described by Waller (1981). Both these species have a short apical ciliary (AC) ring and no apical tuft, unlike the pelagic larvae of many other bivalves (Allen, 1961; Carriker, 1961; Ansell, 1962; Gruffydd and Beaumont, 1972; Bayne, 1976; Boyle and Turner, 1976; Chanley and Chanley, 1980; Amor, 1981). The reduced development of the AC ring in the Chilean oyster larva may be explained by a reduced sensory function during the brooding phase, and also by the short larval pelagic phase. A sensory function has been proposed for the AC because they are very short, appear to be unsuitable for locomotion and food-gathering, and are underlain by the cerebral ganglion (Hickman and Gruffydd, 1971). According to Hodgson and Burke (1988), the apical tuft remains in the larva of *Chlamys hastata* until the earliest veliger stage, but in the Chilean oyster larva the AC never develop into a tuft.

A ring composed of single cilia (inner preoral cilia, IPC) has been identified between the AC and the OPC in the Chilean oyster veliger. A similar structure has also been described by Waller (1981) for *O. edulis*, by Hodgson and Burke (1988) for *Chlamys hastata*, and by Elston (1980) for *Crassostrea virginica*. No clear function has been identified for this band (Waller, 1981). Although the IPC ring is situated in such a position that it could entrain food particles, it lies far from the mouth and the AOC and is separated from the nearest ciliated pathway to the mouth by a non-ciliated zone. Waller (1981) therefore concluded that the IPC probably do not play a role in food capture and are more likely to function as an upcurrent tactile receptor.

The outer preoral cilia (OPC) form the most prominent ciliated ring in the velum of *O. chilensis*, as they do in several other bivalve larvae including *O. edulis* (Waller, 1981), *Chlamys hastata* (Hodgson and Burke, 1988), and *Crassostrea virginica* (Elston, 1980). In some species the ring is composed of a single row of cilia in the early larval stages (*e.g.*, the D-stage veliger of *C. hastata*), but more developed larvae of *C. hastata* have two rows (Hodgson and Burke, 1988), as do all stages of the veliger in *O. edulis* (Waller, 1981). The OPC ring is believed to function in locomotion and feeding (Strathmann *et al.*, 1972; Strathmann and Leise, 1979; Waller, 1981), and it is normally the most prominent ciliated structure on the velum (Waller, 1981). Furthermore, Bayne (1971) showed that long cilia, presumably the OPC, on the velum of the pediveliger of the mussel *Mytilus edulis* provide the main force for swimming and also create the feeding currents.

In *O. chilensis,* a wide band of short adoral cilia (AOC) covers an area of the velum limited in the uppermost part by the OPC ring and in the lowest part by the shell. In the middle of this band lies the food groove. The ciliature is uniform throughout the band, although the cilia in the floor of the food groove are a little shorter. The cilia of the upper and lower regions of the AOC band are in close contact with the groove. These cilia are probably responsible for transferring particles caught by the other ciliary bands to the food groove. In many specimens of *O. chilensis* veligers, pieces of mucous strings or globules could be distinguished in the food groove, presumably moving towards the mouth. It may be significant that some descriptions of feeding in lamellibranch veligers (*e.g.,* Yonge, 1926) refer to a mucous string carrying food particles to the mouth, since the efficiency of a system that lacks postoral cilia may be improved by the presence of mucus (Bayne, 1976). Waller (1981) indicated that the AOC are in close contact with the compound cilia of the OPC when the latter are at the bottom of their effective beat; this is probably the mechanism by which the OPC transfer the entrained particles to the AOC band to be moved to the mouth.

The velar bands are almost identical in *O. chilensis* and *O. edulis,* the principal difference being that in the latter the postoral cilia (POC) represent a single cirral ring located at the base of the velum, in contact with the shell edge (Erdmann, 1935; Waller, 1981), whereas the POC were not visible in this study on the Chilean oyster and are probably not present. On a cautionary note, however, Strathmann *et al.* (1972) pointed out that some authors have not mentioned the POC when describing mollusc larvae that feed and have a well-developed preoral band. These authors suggested that in many cases this may have been an oversight, or a result of confusing the shorter cilia of the postoral band with the cilia of the food groove. However, owing to the central position of the food groove on the velum of the Chilean oyster larva, it would be easy to distinguish between food groove cilia and POC, were the latter present.

Waller (1981) associated the POC band in *O. edulis* with both swimming and particle capture. The latter has been described by Strathmann *et al.* (1972), who showed that many marine invertebrate larvae can continue swimming without feeding, presumably by stopping the beat of the POC. This band appears to be very important in filter-feeding, especially in the larvae of taxa which employ the opposing band mechanism proposed by Strathmann *et al.* (1972) and Strathmann (1978)—bivalves, annelids, echiurids, sipunculids, and entoprocts. In this system both preoral and postoral rings are essential for filter-feeding by the larva (Strathmann *et al.,* 1972), and provide an efficient mechanism to capture particles. In this context, the POC ring identified by Waller (1981) in *O. edulis* may serve to catch particles passing the tips of the cirri of the preoral band, and may also play a more direct role in particle retention and rejection (Strathmann *et al.,* 1972).

The food collected by the cirri is moved to the adoral ring and then to the mouth, where oral compound cilia are present. These may function in selecting or rejecting food particles before they enter the mouth (Hodgson and Burke, 1988).

Whatever the characteristics of the POC band, Hodgson and Burke (1988) have suggested that it may play a role in particle capture, although Strathmann (1987) has shown that the larvae of other invertebrate taxa catch particles by using only one cirral ring. In the Chilean oyster, the particle-catching mechanism was not identified in the present study, but the apparent absence of the second (POC) ring may imply that only one ciliary band is involved, probably because the brooded larva does not need to concentrate particles since the brooding female is performing this function. Furthermore, endoscopic observations have shown the larval velum to be in close contact with mucous strings from the food grooves on the gills of the female (Chaparro *et al.,* 1993). The resolution of the endoscope was insufficient to determine whether larvae were ingesting the mucous string, but the presence of larvae in the food groove, their orientation, and their behavior suggested that this was probable; furthermore, marker particles introduced into the ambient seawater were later observed in the gut of the larva. Thus the absence of the POC may represent another adaptation of the Chilean oyster larva for brooding. Hodgson and Burke (1988) identified secretory cells among the velar cilia of the pectinid *Chlamys hastata,* but such cells have not been described in other bivalve larvae, although several authors have suggested or assumed that mucus is involved in the collection of particles (Yonge, 1926; Erdmann, 1935; Strathmann *et al.,* 1972; Waller, 1981). Hodgson and Burke (1988) suggested that mucus produced by the velum serves principally to bind entrained particles into a string, which travels along the food groove, thereby ensuring the retention of the particles. Pieces of mucus were detected in the food groove of the larva of the Chilean oyster during the present study. The origin of this material could not be clearly ascertained, but two possibilities may be suggested: first, that pieces of the mucous string are taken from the food grooves of the female's gill; and second, that mucus is produced by the larva, as described by Hodgson and Burke (1988) in *C. hastata.*

The absence of the POC band is consistent with the short pelagic phase of the pediveliger in *O. chilensis* because there is no requirement to filter food particles from the water column and no necessity to swim for a long time as a dispersive strategy, since the population is confined to its own estuary. The pediveliger is competent to settle on the first hard substrate that it encounters after release. Typical settlement distances are variously given as 10 cm (Padilla *et al.*, 1969) and 40 cm (Solís, 1973) from the female parent.

Morphological adaptations of marine invertebrate larvae have been described by Strathmann (1978). The larvae of some oligomeric taxa (*e.g.*, Bryozoa, Phoronida, Brachiopoda, Hemichordata) have a single band system and have eliminated the planktotrophic stage. These taxa have lost or modified some larval structures, such as the band of cilia that captures particles. The gut is often incomplete, and the mouth, anus, or both may be absent. In some mollusc species with nonfeeding larvae, the metatroch and food groove have been lost; in contrast, other gastropod larvae, which are also not filter-feeders, retain the opposing band system, even when the larvae are not planktotrophic (Strathmann, 1978). It is clear that many species have modified some larval structures, allowing the larva to adapt more completely to the environment in which it is developing. The Chilean oyster is one such example: the morphological modifications of the velum are essential for the adaptation by the species to brooding the larva inside the mantle cavity of the female—a very different environment from that experienced by a planktonic larva. Furthermore, in *O. chilensis* and *O. lutaria,* which have the longest incubation periods of all the ostreids, the larval shells differ structurally from those of other oysters (Chanley and Dinamani, 1980). In particular, the shells of the two larvae are equivalve and edentulous, but it is not clear whether these features represent the ancestral condition or are adaptations to brooding (Chanley and Dinamani, 1980).

Acknowledgments

A large part of the field research was carried out in the Estación Experimental de Quempillén, Ancud, Chile, and in the Instituto de Biología Marina de la Universidad Austral de Chile, to whose staff we extend our appreciation. Financial help came from operating grants to ORC by the Fondo Nacional de Investigación Científica y Tecnológica-Chile (Fondecyt 1930364 and 1980984), by the International Foundation for Sciences-Sweden (IFS A/0846), and by the Dirección de Investigación of the Universidad Austral de Chile, and from a research grant to RJT from the Natural Sciences and Engineering Research Council-Canada (NSERC). ORC's stay in Canada was made possible by fellowships from the International Development Research Centre-Canada (IDRC) and NSERC (through a Networks of Centres of Excellence programme, the Ocean Production Enhancement Network). We also thank the Canadian International Development Agency (CIDA) for support during the preparation of the manuscript.

Literature Cited

Allen, J. A. 1961. The development of *Pandora inaequivalvis* (Linné). *J. Embryol. Exp. Morphol.* **92:** 252–268.

Amor, A. 1981. Observaciones sobre el desarrollo embrionario y larval de *Mytilus platensis* D'Orbigny, del sector Bonaerense (Mollusca, Bivalvia). *Physis (Buenos Aires)*, Secc. A., **39(97):** 33–39.

Ansell, A. 1962. The functional morphology of the larva, and the post-larval development of *Venus striatula* (Da Costa). *J. Mar. Biol. Assoc. U.K.* **42:** 419–443.

Bayne, B. L. 1971. Some morphological changes that occur at the metamorphosis of the larvae of *Mytilus edulis.* Pp. 259–280 in *European Marine Biology Symposium.* D. J. Crisp, ed. Cambridge University Press, London.

Bayne, B. L. 1976. The biology of mussel larvae. Pp. 81–120 in *Marine Mussels: Their Ecology and Physiology.* B. L. Bayne, ed. Cambridge University Press.

Beauchamp, K. A. 1986. Reproductive ecology of the brooding, hermaphroditic clam *Lasaea subviridis. Mar. Biol.* **93:** 225–235.

Boyle, P. J., and R. D. Turner. 1976. The larval development of the wood boring piddock *Martensia striata* (l.) (Mollusca: Bivalvia: Pholadidae). *J. Exp. Mar. Biol. Ecol.* **22:** 55–68.

Buroker, N. E. 1985. Evolutionary patterns in the family Ostreidae: larviparity *vs.* oviparity. *J. Exp. Mar. Biol. Ecol.* **90:** 233–247.

Carriker, M. R. 1961. Interrelation of functional morphology, behavior, and autecology in early stages of the bivalve *Mercenaria mercenaria. J. Elisha Mitchell Sci. Soc.* **77:** 168–242.

Chanley, P., and M. Chanley. 1980. Reproductive biology of *Arthritica crassiformis* and *A. bifurca,* two commensal bivalve molluscs (Leptonacea). *N. Z. J. Mar. Freshwater Res.* **14:** 31–43.

Chanley, P., and P. Dinamani. 1980. Comparative descriptions of some oyster larvae from New Zealand and Chile, and a description of a new genus of oyster, *Tiostrea. N. Z. J. Mar. Freshwater Res.* **14: 103–120.**

Chaparro, O. R., R. J. Thompson, and J. E. Ward. 1993. *In vivo* observations of larval brooding in the Chilean oyster, *Ostrea chilensis* Philippi, 1845. *Biol. Bull.* **185:** 365–372.

Cragg, S. M. 1985. The adductor and retractor muscles of the veliger of *Pecten maximus* (L.) (Bivalvia). *J. Molluscan Stud.* **51:** 276–283.

Cragg, S. M. 1989. The ciliated rim of the velum of larvae of *Pecten maximus* (Bivalvia: Pectinidae). *J. Molluscan Stud.* **55:** 497–508.

Cranfield, H. J. 1979. The biology of the oyster, *Ostrea lutaria* and the oyster fishery of Foveaux Strait. *Rapp. P. V. Réun. Cons. Int. Explor. Mer.* **175:** 44–49.

Cranfield, H. J., and K. P. Michael. 1989. Larvae of the incubatory oyster *Tiostrea chilensis* (Bivalvia: Ostreidae) in the plankton of central and southern New Zealand. *N. Z. J. Mar. Freshwater Res.* **23:** 51–60.

Elston, R. 1980. Functional anatomy, histology and ultrastructure of the soft tissues of the larval American oyster, *Crassostrea virginica. Proc. Natl. Shellfish Assoc.* **70:** 65–93.

Erdmann, W. 1935. Über die Entwicklung und die Anatomie der 'Ansatzreifen' Larvae von *Ostrea edulis* mit Bemerkungen uber die Lebengeschichte der Auster. *Helgol. Wiss. Meeresunters.* **19(6):** 1–25.

Fernandez Castro, N., and M. Le Pennec. 1988. Modalities of brooding and morphogenesis of larvae in *Ostrea puelchana* (D'Orbigny) under experimental rearing. *J. Mar. Biol. Assoc. U. K.* **68:** 399–407.

Fioroni, P. 1966. Zur Morphologie und Embryogenese des Darmtraktes und der Transitorischen Organe bei Prosobranchiern (Mollusca, Gastropoda). *Rev. Suisse Zool.* **73:** 621–876.

Fitt, W. K., C. R. Fisher, and R. K. Trench. 1984. Larval biology of tridacnid clams. *Aquaculture* **39:** 181–195.

Franz, D. R. 1973. Ecology and reproduction of a marine bivalve *Mysella planulata. Biol. Bull.* **144:** 93–106.

Fretter, V., and A. Graham. 1962. *British Prosobranch Molluscs.* Ray Society London. 755 pp.

Gallardo, C. S. 1989. Patrones de reproducción y ciclo vital en moluscos marinos bénticos: Una aproximación ecológica evolutiva. *Medio Ambiente* **10(2):** 25–35.

Gallardo, C. S. 1993. Reproductive habits and life cycle of the small clam *Kingiella chilenica* (Bivalvia: Cyamiidae) in an estuarine sand flat from the South of Chile. *Mar. Biol.* **115:** 595–603.

Galtsoff, P. S. 1964. *The American Oyster* Crassostrea virginica *Gmelin. U. S. Fish Wildl. Serv. Fish. Bull.* **64:** 480 pp.

Gruffydd, Ll. D., and A. R. Beaumont. 1972. A method for rearing *Pecten maximus* larvae in the laboratory. *Mar. Biol.* **15:** 350–355.

Gustafson, R. G., and R. A. Lutz. 1991. Larval and early post-larval development of the protobranch bivalve *Solemya velum* (Mollusca: Bivalvia). *J. Mar. Biol. Assoc. U. K.* **72:** 383–402.

Hadfield, M. G., and D. K. Iaea. 1989. Velum of encapsulated veligers of *Petaloconchus* (Gastropoda), and the problem of re-evolution of planktotrophic larvae. *Bull. Mar. Sci.* **45:** 377–386.

Harry, H. W. 1985. Synopsis of the supraspecific classification of living oysters (Bivalvia: Gryphaeidae and Ostreidae). *Veliger* **28:** 121–158.

Heard, W. H. 1977. Reproduction of fingernail clams (Sphaeridae: *Sphaerium* and *Musculum*). *Malacologia* **16:** 421–455.

Hickman, R. W., and Ll. D. Gruffydd. 1971. The histology of the larva of *Ostrea edulis* during metamorphosis. Pp. 281–294 in *European Marine Biology Symposium.* D. J. Crisp, ed. Cambridge University Press, London.

Hodgson, C. A., and R. D. Burke. 1988. Development and larval morphology of the spiny scallop, *Chlamys hastata. Biol. Bull.* **174:** 303–318.

Hopkins, A. E. 1936. Ecological observations on spawning and early larval development in the Olympia oyster (*Ostrea lurida*). *Ecology* **17(4):** 551–566.

Kennedy, J. J., and B. F. Keegan. 1992. The encapsular developmental sequence of the mesogastropod *Turritella communis* (Gastropoda: Turritellidae). *J. Mar. Biol. Assoc. U. K.* **72:** 783–805.

Mackie, G. L. 1979. Dispersal mechanisms in Sphaeriidae (Mollusca: Bivalvia). *Bull. Am. Malacol. Union* **1979:** 17–21.

Mackie, G. L. 1984. Bivalves. Pp. 351–418 in *The Mollusca. Vol 7. Reproduction.* A. S. Tompa, N. H. Verdonk, and J. Van Den Biggerlaar, eds. Academic Press, Orlando, Florida.

Mackie, G. L., S. U. Qadri, and H. Clarke. 1974. Development of brood sacs in *Musculium securis* (Bivalvia: Sphaeriidae). *Nautilus* **88:** 109–111.

Millar, R. H., and P. J. Hollis. 1963. Abbreviated pelagic life of Chilean and New Zealand oysters. *Nature* **197:** 512–513.

Morriconi, E., and J. Calvo. 1980. Fertilidad y periodicidad del desove en *Ostrea puelchana. Rev. Invest. Desarrollo Pesq.* **2:** 57–62.

Ockelmann, K. W. 1964. *Turtonia minuta* (Fabricus), a neotenous veneracean bivalve. *Ophelia* **1:** 121–146.

Padilla, M., M. Mendez, and F. Casanova. 1969. Observaciones sobre el comportamiento de la *Ostrea chilensis* en Apiao. *Bol. Inst. Fomento Pesquero, Santiago de Chile.* **10:** 1–28.

Pechenik, J. A. 1979. Role of encapsulation in invertebrate life histories. *Am. Nat.* **114:** 859–870.

Pechenik, J. A. 1986. The encapsulation of eggs and embryos by molluscs: an overview. *Am. Malacol. Bull.* **4:** 165–172.

Solís, I. 1967. Observaciones biológicas en ostras (*Ostrea chilensis* Philippi) de Pullinque. *Biol. Pesq.* **2:** 51–82.

Solís, I. 1973. Valoración de colectores de larvas de ostras *Ostrea chilensis* Philippi en Pullinque. *Biol. Pesq.* **6:** 1–23.

Strathmann, R. R. 1978. The evolution and loss of feeding larval stages in marine invertebrates. *Evolution* **32:** 894–906.

Strathmann, R. R., and E. Leise. 1979. On feeding mechanisms and clearance rates of molluscan veligers. *Biol. Bull.* **157:** 524–535.

Strathmann, R. R., T. L. Jahn, and J. R. C. Fonseca. 1972. Suspension feeding by marine invertebrate larvae: clearance of particles by ciliated bands of a rotifer, pluteus, and trochophore. *Biol. Bull.* **142:** 505–519.

Tankersley, R. A., and R. V. Dimock. 1992. Quantitative analysis of the structure and function of the marsupial gills of the freshwater mussel *Anodonta cataracta. Biol. Bull.* **182:** 145–154.

Tankersley, R. A., and R. V. Dimock. 1993. Endoscopic visualization of the functional morphology of the ctenidia of the unionid mussel *Pyganodon cataracta. Can. J. Zool.* **71:** 811–819.

Toro, J. E., and O. R. Chaparro. 1990. Conocimiento biológico de *Ostrea chilensis* Philippi 1845. Impacto y perspectivas en el desarrollo de la ostricultura en Chile. Pp. 231–264 in *Cultivo de Moluscos en América Latina. Memorias Segunda Reunión Grupo Trabajo Técnico, Ancud, Chile. Noviembre 1989.* A. Hernández, ed. Special publication, Canadian International Development Agency, Bogotá, Colombia.

Waller, T. R. 1981. Functional morphology and development of veliger larvae of the European oyster, *Ostrea edulis* Linné. *Smithson. Contrib. Zool.* **328:** 1–70.

Winter, J. E., J. E. Toro, J. M. Navarro, G. S. Valenzuela, and O. R. Chaparro. 1984. Recent developments, status, and prospects of molluscan aquaculture on the Pacific coast of South America. *Aquaculture* **39:** 95–134.

Yonge, C. M. 1926. Structure and physiology of the organs of feeding and digestion in *Ostrea edulis. J. Mar. Biol. Assoc. U. K.* **14:** 295–386.

Marine
Biological
Laboratory
Woods Hole
Massachusetts

One Hundred and First Report
for the Year 1998
One-Hundred and Tenth Year

Officers of the Corporation

Sheldon J. Segal, *Chairman of the Board of Trustees*
Frederick Bay, *Co-Vice Chair*
Mary J. Greer, *Co-Vice Chair*
John E. Dowling, *President of the Corporation*
John E. Burris, *Director and Chief Executive Officer*
Mary B. Conrad, *Treasurer*
Neil Jacobs, *Clerk of the Corporation*

Contents

Report of the Director and CEO R1
Report of the Treasurer R7
Financial Statements R8
Report of the Library Director R19
Educational Programs
  Summer Courses R21
  Special Topics Courses R25
  Other Programs R31
Summer Research Programs
  Principal Investigators R33
  Other Research Personnel R34
  Library Readers R35
  Institutions Represented R36
Year-Round Research Programs R41
Honors R53
Board of Trustees and Committees R60
Administrative Support Staff R64
Members of the Corporation
  Life Members R67
  Members R68
  Associate Members R78
Certificate of Organization R82
Articles of Amendment R82
Bylaws R82

Photo credits:
Beth Armstrong, R4 (bottom), R5 (bottom), R7, R21, R33, R67
Jelle Atema, R45
Ken Foreman, R32
Linda Golder, R24, R64
Roger Hanlon, R60
Diedtra Henderson, R47
Jan Hinsch, R53
Richard Howard, R2(top), R4(top), R5(top)
Alan Kuzirian, R2(bottom), R34, R49, R50
Lisa Kerr Lobel, R1
Chris Pauk, R22
P.A. Shave, R82
James Shreeve, R35
Sam Sweezy, R51

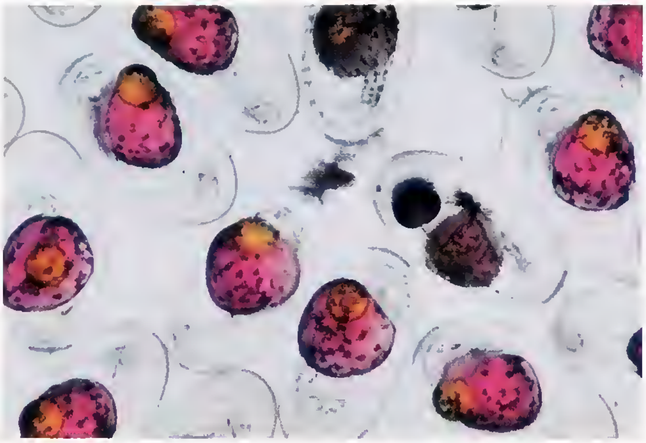

Report of the Director and Chief Executive Officer

The Marine Biological Laboratory remains a remarkable place as we approach the end of the 20th Century. At every turn there are feelings of pride and satisfaction, of excitement, curiosity, determination and anticipation of things to be discovered. These feelings are shared by both resident and visiting scientists and by students for whom time spent at MBL is an experience never to be matched. That spirit of scientific adventure and achievement is alive and thriving here, as it has been for more than a century.

The MBL continues to build on its solid history, to add programs in research and education, to recruit new scientists and to raise funds for vital improvements to this place that is like no other. After establishing research and education priorities, we were able to define funding requirements and a timeframe enabling us in August of 1997 to launch *Discovery: The Campaign for Science at the Marine Biological Laboratory*. The goal is to reach $25 million by December 31, 2000. We are gratified by the response to this fundraising effort and are grateful to many of you who have already made generous contributions to this Campaign. I'm pleased to say that, by the end of 1998, we had raised $20.6 million, which is good news indeed.

Education at the MBL

The MBL's education program is growing both in numbers of students and faculty and in courses offered. During the summer of 1998 we hosted 594 faculty for 416 students from around the world. We were able to award more than $600,000 in scholarship support for those students, making it possible for the best and the brightest to continue to come to the MBL. Even as we grow, we have retained the high quality, intensive courses that have long set the MBL apart from other educational institutions. As Purnell Choppin, president of the Howard Hughes Medical Institute, stated in announcing a $2.2 million award to support education at the MBL in April of 1999, "The Marine Biological Laboratory serves as an international schoolhouse for the biomedical research community. Young scientists and established researchers alike gather there to learn the latest developments at the cutting edges of their fields." In 1998 we continued to attract international students with over 30% of our applications from students from 68 different foreign countries.

We take great pride in maintaining the quality and dynamics of the courses and continue to be responsive to the changing face of biological research as demonstrated by our ability and interest in adding new courses to our roster of exceptional offerings. Two new courses were introduced in 1998: *Frontiers in Reproduction: Molecular and Cellular Concepts* and *Neural Development and Genetics of Zebrafish*. These were in addition to the *Molecular Mycology: Current Approaches to Fungal Pathogenesis* course and the *Semester in Environmental Sciences*, both of which were offered for the first time in 1997.

Not only have we added new courses, but we have continued to change our long-standing courses through the planned turnover in course directors. For example, in 1999 David Garbers and Randy Reed will be the co-directors of the over 100-year-old Physiology course. They will succeed Kerry Bloom and Mark Moosekar who did a superb job in leading the course for the past four years.

Our *Semester in Environmental Sciences* program was a great success again this year. Undergraduate students selected from a consortium of 34 liberal arts colleges were in residence for 14 weeks during the fall to learn about environmental sciences. The curriculum covered aquatic and terrestrial ecosystems and included electives in computational modeling and microbial ecology. Students gained a basic understanding of ecosystem structure and dynamics through intensive hands-on fieldwork at two local sites on Cape Cod. Major biogeochemical processes were studied and general problems concerning the global carbon cycle, fossil fuel emissions, increased concentrations of greenhouse gases

in the atmosphere, estuarine eutrophication, deforestation, and over-exploitation of fisheries were considered. Special emphasis was given to how changes in biodiversity affect ecosystem function.

The MBL's *Science Writing Fellowships Program*, now about to enter its fourteenth summer, added a new hands-on laboratory course in environmental science during the summer of 1998. Co-directed by John Hobbie and Jerry Melillo of the Ecosystems Center, this new component of the program was a great success, attracting environment writers from around the country.

Research at the MBL

The Marine Resources Center

While John Glenn was the most famous traveler in space late last fall, two other passengers aboard the shuttle were of considerable importance to scientific experiments conducted during that mission. Two oyster toadfish participated in an experiment overseen by Steve Highstein that was designed to provide a better understanding of the effects of microgravity on our balance system. The fish, collected from the waters off Woods Hole, traveled more than three million miles in what was a follow-up to studies conducted during the Neurolab space mission in April of 1998. Balance, location and movement are so crucial to animals that the vestibular system was one of the first sensory systems to evolve. The toadfish has become a well-known experimental model for learning more about balance disorders, such as Meniere's disease and vertigo. It also is a good model for studying motion sickness, including that experienced by astronauts during space flight.

Thanks to a $1 million challenge grant, the MBL has an exciting opportunity to build on its existing strengths as a developer of aquatic models for biomedical research. The technologically sophisticated Marine Resources Center is an ideal venue for this program. And MRC Director Roger Hanlon's expertise in the culturing of marine organisms such as Hawaiian squid and cuttlefish provides a great foundation for the expansion of aquaculture activities at MBL. Dr. Hanlon contributed his expertise in this area as a member of a National Research Council/National Academy of Sciences committee that published in 1998 a report titled "Biomedical Models and Resources: Current Needs and Future Opportunities." This paper is expected to help the National Institutes of Health structure research funding for model organisms, including many aquatic ones.

The MRC challenge grant, which stipulates that two dollars must be raised for every one dollar awarded, will enable the MBL to establish a scientific aquaculture program in the Marine Resources Center. This exceptional gift will allow scientists to develop novel research techniques and to address problems being faced by scientific and commercial aquaculture interests alike. Studies will address problems such as disease diagnosis and management, water quality requirements for specific life stages, nutrition research for optimal diets and numerous aspects of reproductive biology. For many

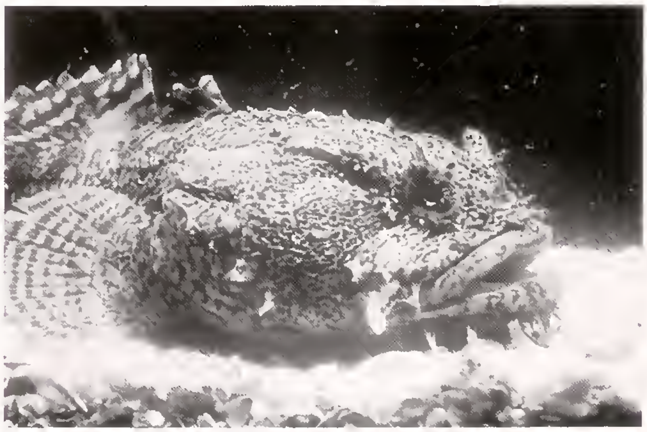

years, commercial aquaculture companies have sought the MBL's expertise in addressing all of these issues. In recent years, we successfully maintained 95,000 juvenile flounder bound for the Japanese sushi industry and raised seedling scallops for the local shellfish trade. Now we will be in an even better position to provide advice and develop appropriate aquaculture techniques in the future.

The Ecosystems Center

The Ecosystems Center recently launched a new tropical ecology program that focuses on the consequences of land-cover and land-use changes in the tropics. The possibility of a new joint research project with Brazilian scientists is being explored. The program is based on a challenge put to ecologists: "Now that you think you know how ecosystems work, why don't you try to fix some broken ones?" Perhaps we can test our understanding of ecosystem structure by working to rebuild a damaged one. The joint project would focus on large tracts of coastal forests northeast of São Paulo.

The Ecosystems Center also received the only Long-Term Ecological Research Site award made in 1998. The MBL is now the only place in the country responsible for the oversight of two LTER sites—the new one at Plum Island Sound, located north of Boston, and the long-time Arctic Toolik Lake site, located on the North Slope of the Brooks Range in Alaska—and which has major involvement in a third (Harvard Forest in Petersham, Massachusetts).

All of this research activity has resulted in remarkable growth over the past few years. Since 1979, Center staff has increased sixfold. The resulting demand for additional laboratories, offices, and staging areas for equipment and supplies used in field research has led to a severe shortage of space. And the MBL's new *Semester in Environmental Sciences* program for undergraduate liberal arts students is putting an additional squeeze on the Center's already over-taxed facilities.

In November, the MBL Board of Trustees approved the architectural plans for a new facility to house research and education activities of the Ecosystems Center. The proposed three-story building will provide a cutting-edge GIS (geographic information systems) facility, state-of-the-art laboratories for plant and soil sample analysis, a stable isotope laboratory, modern offices, teaching facilities and a classroom/conference room for the *Semester in Environmental Science* program, ample storage areas for diving gear, field samples, and equipment, and field staging areas. The 32,000-square-foot building is designed to meet the needs of Ecosystems Center scientists for many years to come, as well as serve the needs of the entire MBL research and education programs.

Fundraising is now underway, with a much appreciated $1 million challenge grant from the Clowes Fund leading the way. With groundbreaking scheduled for the spring of 2000, this new state-of-the-art Environmental Sciences Building will be a fitting tribute to a quarter century of excellence in ecological research and provide the foundation for continued scientific achievements as the MBL enters the 21st Century.

The Josephine Bay Paul Center

Under the direction of MBL Senior Scientist Dr. Mitchell Sogin, the Josephine Bay Paul Center for Comparative Molecular Biology and Evolution, dedicated in August of 1998, is flourishing. The research pace at the Center escalated during the past year, thanks to the arrival of a number of scientists and the receipt of several important grant awards.

Early in 1998, the Center received a major grant from the National Institutes of Health, to be used in an important research initiative to sequence the genome of the parasitic protist, *Giardia lamblia. Giardia* is a waterborne human pathogen that attacks the intestinal tract and exacts a terrible toll on public health worldwide. The NIH grant will provide salary support for nine scientists and technicians and has allowed us to establish a new automated DNA sequencing facility.

There was still more exciting news at the Bay Paul Center in 1998, when NASA selected MBL as a member of the new Virtual Astrobiology Institute. This program will bring together astrophysicists, biologists, chemists, physicists, planetologists, and geologists for interdisciplinary studies on life in the universe and its cosmic implications. The MBL was one of 11 institutions selected to participate from a field of nearly 70 applicants.

Dr. Michael Cummings joined the Bay Paul Center in

early 1998 as an Assistant Scientist. His work is in the field of molecular evolutionary genetics. The major focus of that research is using novel statistical methods to study relationships between genotype and phenotype. Current investigations examine how gene sequence data can be used to understand and predict drug resistance in tuberculosis, variation in color vision, and basic immune system functions at the molecular level. Dr. Cummings is also studying the evolution of pathogenic bacteria by examining species within the genus *Mycobacterium*. The analysis of *Mycobacterium* DNA sequence data will reveal evolutionary patterns that demonstrate the emergence of both new pathogens and drug resistant strains. This information will assist clinicians with diagnosis and treatment of diseases such as tuberculosis and leprosy.

Other Research Initiatives

The MBL is home not only to the above centers, but to a number of individual laboratories where, for example, the basis of bioluminescence is being investigated, the fluxes of ions from individual cells are being measured, the evolution of heme biosynthesis is being traced, new antibiotics are being sought, and microscopy is being developed and used to understand more about the cell.

A remodeled and expanded laboratory is serving Dr. Carol Reinisch, a recently appointed Senior Scientist at the MBL and a new year-round resident. She investigates how environmental factors influence the prevalence of leukemia using soft shell clams as a research model. She also studies surf clams to better understand how toxins such as PCBs disrupt nerve development in embryos that later influences normal learning and behavior.

Drs. Barbara and Bruce Furie have modernized their MBL laboratory to accommodate ongoing work on the study of hemophilia and other blood disorders using the venomous cone snail. The conotoxins produced by these invertebrate snails share an amino acid that is found in mammals. A protein containing this unusual amino acid, when linked to vitamin K, triggers blood-clotting mechanisms that are distributed widely throughout mammalian species.

Summer Research

The MBL—as it has for more than a century—will host hundreds of scientists from around the world who come each summer to the Laboratory to participate in a unique and intense research experience. Often using marine and aquatic model organisms, these investigators study basic processes in the life sciences. Their work spans research on the protein assemblies that achieve accurate chromosome segregation in cell division, on the neural processing of visual information in the brain, and on how hormones and pharmaceuticals stimulate the secretion of insulin from the pancreas.

The MBL's Fellowship Program is an important element of summer research activities. Nineteen scientists were awarded summer research fellowships at the MBL in 1998. Examples of research projects by neurobiologists

include studies by Dr. Elizabeth Jonas of Yale University School of Medicine on the intracellular channels that regulate synaptic function; studies by Dr. Matthew Halstead of the University of New Zealand on the processing of electrosensory information in the midbrain of the skate; and studies by Dr. James Zheng from the Robert Wood Johnson Medical School on the cellular mechanisms underlying the formation of nerve connections. Cell biologists included Dr. Mark Alliegro of Louisiana State University, who studied cells from sea urchins and other organisms to learn how cells differentiate, and Dr. John Eriksson of the Turku Center for Biotechnology in Finland, who studied the mitotic protein phosphatases in surf clam eggs. Fourteen other scientists whose research focused on topics ranging from global climate change to sensory physiology rounded out the group of 1998 fellows.

Improvements Around Campus

As always there is work to be done on the MBL's physical plant, all of it important, all of it requiring time, effort, and financial support. In 1998, renovations were made at the Loeb building and to the Neurobiology course laboratories. And the Lillie Auditorium got a new roof. I'm pleased to report that commitments are now in hand to install an air-conditioning system at the Library, and very soon the MBL will have a new emergency generator. One of the most the exciting changes to the MBL campus last summer was the creation of the new Robert W. Pierce Visitors Center, which shares 100 Water Street with the MBL and Satellite Clubs. This beautiful new facility, which is also home to the MBL Associates Gift Shop, was dedicated and opened in the summer of 1998. It has already introduced thousands of Woods Hole visitors to the Marine Biological Laboratory.

MBL Trustees

In 1998, the MBL Board of Trustees welcomed Dr. John E. Dowling as President of the Corporation. Dr. Dowling succeeded Dr. James D. Ebert, who retired after serving as President for seven years. Dr. Dowling is the Maria Moors Cabot Professor of Natural Science at Harvard University, as well as an MBL summer investigator and former MBL Trustee. His research focuses on the physiology of vision, especially the correlation between structure and function in the vertebrate retina. He also is interested in retinal development and uses the zebrafish as a model organism for these studies.

Last year the MBL Board of Trustees elected Ronald P. O'Hanley, President of Dreyfus Institutional Investors in Boston, and Vincent J. Ryan, President, Chairman, and CEO of Schooner Capital Corporation, also of Boston, to membership in the Class of 2003. The Laboratory is most fortunate to welcome these dynamic and thoughtful individuals to help guide our progress over the next few years. Burton J. Lee, III, Laurie J. Landeau, Darcy Brisbane Kelley, and Jean Pierce were reappointed to the

Board in November 1998 as members of the class of 2003.

Directors Emeriti

The Board of Trustees voted to name three former directors of the Marine Biological Laboratory "Directors Emeriti." James D. Ebert, Paul R. Gross, and Harlyn O. Halvorson were recognized for the contributions that each of these men made to the growth and strength of the Laboratory during their tenures as director. Each of these individuals has left a legacy of achievement that has earned the respect and gratitude of the MBL community.

In closing, 1998 was an exciting time, and 1999 should be no less so. The Marine Biological Laboratory remains a wonderful gathering place for scientists and students from around the world. Anchored by a top-notch team of year-round investigators, enlivened by some of the best students anywhere, and stimulated by the summer influx of great researchers, the MBL continues to serve science in a unique and exciting way.

—John E. Burris

Report of the Treasurer

During 1998 the Marine Biological Laboratory continued a favorable trend in operations. This progress was due to healthy increases in five of the six areas of Operating Support. Government grants increased 9.6% and now represent 42.5% of the total support and revenues. Double digit increases in Private Contracts (38.3%), Fees for Conferences and Services (10.7%) and Miscellaneous Revenues (22.3%) powered the year's success story. While there was an easing in the present value of Contributions this was predictable at the midpoint of our very successful *Discovery Campaign*. As already noted in the Report of the Director and CEO, the campaign is ahead of schedule.

Focusing on the change in Unrestricted Net Assets, we enjoyed a three-year favorable trend. The change before nonoperating activity has improved from a deficit of $1 million in 1996, to a deficit of $753 thousand in 1997, to a deficit of only $256 thousand this year. This is particularly auspicious when one realizes these figures are after approximately $1.5 million in depreciation each year.

While the Change in Net Assets before nonoperating activity was only half of 1997 results, it was still a robust $1.1 million. Total Investment Income and Earnings of only 820 thousand dollars were unsatisfactory when compared to the multi-million dollar returns in previous years. This was a result of the volatile markets and a revamping of our endowment management philosophy. As a result, Net Assets increased for the fourth year in a row, but the Return on Average Net Assets was only 1.1%.

A review of the 1998 Balance Sheet demonstrates our continued strong liquidity and low and improving leverage. Property Plant and Equipment showed a slight decline (2.4%), but this is the smallest decline in the past four years as we are in the process of upgrading the physical plant. Plans are underway to expand our capital maintenance efforts and to build a new Environmental Sciences Building. Ultimately, this will make the Laboratory an even more attractive facility to conduct science.

In summary, the Laboratory continues to demonstrate the ability to attract funds from the federal government, foundations and individuals. Our housing and conferences continue to generate surplus cash. Successful completion of the *Discovery Campaign* and a return to our history of very successful endowment performance will guarantee the financial strength of the Marine Biological Laboratory for the 21st century.

—Mary B. Conrad

Financial Statements

PRICEWATERHOUSECOOPERS

PricewaterhouseCoopers LLP
One Post Office Square
Boston MA 02109
Telephone (617) 478 5000
Facsimile (617) 478 5900

REPORT OF INDEPENDENT ACCOUNTANTS

To the Board of Trustees of
Marine Biological Laboratory
Woods Hole, Massachusetts

In our opinion, the accompanying balance sheet of Marine Biological Laboratory (the "Laboratory") as of December 31, 1998 and the related statements of activities and cash flows for the year then ended present fairly, in all material respects, the financial position of the Laboratory as of December 31, 1998, and the changes in its net assets and its cash flows for the year then ended in conformity with generally accepted accounting principles. These financial statements are the responsibility of the Laboratory's management; our responsibility is to express an opinion on these financial statements based on our audit. We conducted our audit in accordance with generally accepted auditing standards. Those standards require that we plan and perform the audit to obtain reasonable assurance about whether the financial statements are free of material misstatement. An audit includes examining, on a test basis, evidence supporting the amounts and disclosures in the financial statements. An audit also includes assessing the accounting principles used and significant estimates made by management, as well as evaluating the overall financial statement presentation. We believe that our audit provides a reasonable basis for the opinion expressed above.

Our audit was conducted for the purpose of forming an opinion on the basic financial statements taken as a whole. The supplemental schedule of functional expenses for the year ended December 31, 1998 is presented for the purpose of additional analysis and is not a required part of the basic financial statements. Such information has been subjected to the auditing procedures applied in the audit of the basic financial statements and, in our opinion, is fairly stated, in all material respects, in relation to the basic financial statements taken as a whole.

April 9, 1999

MARINE BIOLOGICAL LABORATORY

Balance Sheets

December 31, 1998

(with comparative totals as of December 31, 1997)

ASSETS	1998	1997
Cash and cash equivalents	$ 1,187,954	$ 560,801
Short-term investments, at market (Note C)	3,561,544	4,408,046
Accounts receivable, net of allowance for doubtful accounts of $34,195 in 1998 and $36,782 in 1997	1,242,530	1,221,781
Current portion of pledges receivable (Note H)	1,607,664	2,219,056
Receivables due for costs incurred on grants and contracts	1,531,083	1,157,165
Other assets	557,908	560,269
Total current assets	9,688,683	10,127,118
Long-term investments, at market (Notes C and D)	37,054,120	35,614,151
Pledges receivable, net of current portion (Note H)	2,855,352	2,238,826
Plant assets, net (Notes B, E and F)	19,536,171	20,026,580
Total long-term assets	59,445,643	57,879,557
Total assets	$69,134,326	$68,006,675
LIABILITIES AND NET ASSETS		
Current portion of long-term debt (Note E)	243,274	229,657
Accounts payable and accrued expenses	2,057,741	1,494,948
Deferred income and advances on contracts	462,873	384,258
Total current liabilities	2,763,888	2,108,863
Annuities and unitrusts payable	1,412,200	1,213,583
Long-term debt, net of current portion (Note E)	2,324,096	2,567,370
Advances on contracts	1,272,390	1,433,208
Total long-term liabilities	5,008,686	5,214,161
Total liabilities	7,772,574	7,323,024
Commitments and contingencies (Notes F and H)		
Net assets:		
Unrestricted	18,451,865	18,729,311
Temporarily restricted	25,635,237	25,596,656
Permanently restricted	17,274,650	16,357,684
Total net assets (Note B)	61,361,752	60,683,651
Total liabilities and net assets	$69,134,326	$68,006,675

The accompanying notes are an integral part of the financial statements.

MARINE BIOLOGICAL LABORATORY

STATEMENTS OF ACTIVITIES

for the year ended December 31, 1998
(with comparative totals for the year ended December 31, 1997)

	Unrestricted	Temporarily Restricted	Permanently Restricted	1998 Total	1997 Total
Operating support and revenues:					
Government grants	$10,943,239	$ —	$ —	$10,943,239	$ 9,986,800
Private contracts	1,629,283	—	—	1,629,283	1,178,192
Laboratory rental income	1,470,372	—	—	1,470,372	1,478,757
Tuition	489,726	—	—	489,726	399,703
Fees for conferences and services	3,415,519	—	—	3,415,519	3,085,616
Contributions	1,264,235	3,420,615	653,152	5,338,002	6,441,429
Investment income	490,474	1,465,261	—	1,955,735	1,709,983
Miscellaneous revenue	405,633	—	—	405,633	322,667
Present value adjustment to annuities	—	(68,849)	(7,853)	(76,702)	(164,447)
Net assets released from restrictions	4,100,624	(4,138,622)	37,998	—	—
Total operating support and revenues	24,209,105	678,405	683,297	25,570,807	24,438,700
Expenses:					
Research	12,666,746	—	—	12,666,746	11,031,914
Instruction	4,433,789	—	—	4,433,789	4,144,508
Conferences and services	1,999,433	—	—	1,999,433	1,487,705
Other programs (Note B)	5,365,530	—	—	5,365,530	5,440,808
Total expenses	24,465,498	—	—	24,465,498	22,104,935
Change in net assets before nonoperating activity	(256,393)	678,405	683,297	1,105,309	2,333,765
Nonoperating revenue:					
Total investment income and earnings	27,353	558,683	233,669	819,705	4,869,035
Less: investment earnings used for operations	(48,406)	(1,198,507)	—	(1,246,913)	(1,056,211)
Reinvested (utilized) investment earnings	(21,053)	(639,824)	233,669	(427,208)	3,812,824
Total change in net assets	(277,446)	38,581	916,966	678,101	6,146,589
Net assets, beginning of year	18,729,311	25,596,656	16,357,684	60,683,651	54,537,062
Net assets, end of year	$18,451,865	$25,635,237	$17,274,650	$61,361,752	$60,683,651

The accompanying notes are an integral part of the financial statements.

MARINE BIOLOGICAL LABORATORY

Statements of Cash Flows

for the year ended December 31, 1998

(with comparative totals for the year ended December 31, 1997)

	1998	1997
Cash flows from operating activities:		
Change in net assets	$ 678,101	$ 6,146,589
Adjustments to reconcile change in net assets to net cash provided by (used in) operating activities:		
Depreciation	1,505,696	1,483,203
Unrealized (gain) loss on investments	2,755,079	(1,740,501)
Realized (gain) loss on investments	(2,805,560)	(1,728,792)
Present value adjustment to annuities and unitrusts payable	76,702	164,447
Contributions restricted for long-term investment and annuities	(682,817)	(1,390,609)
Provision for bad debt	15,771	21,781
Provision for uncollectible pledges	250,000	89,620
Change in certain balance sheet accounts:		
Accounts receivable	(36,520)	(480,702)
Pledges receivable	(255,134)	(314,658)
Grants and contracts receivable	(373,918)	(43,083)
Other assets	2,361	(77,277)
Accounts payable and accrued expenses	562,793	(71,564)
Deferred income and advances on contracts	78,615	62,260
Annuities and unitrusts payable	163,700	120,052
Advances on contracts	(160,818)	222,258
Net cash provided by operating activities	1,774,051	2,463,024
Cash flows from investing activities:		
Purchase of property and equipment	(1,015,287)	(814,159)
Proceeds from sale of investments	18,935,050	23,450,218
Purchase of investments	(19,478,036)	(26,321,432)
Net cash used in investing activities	(1,558,273)	(3,685,373)
Cash flows from financing activities:		
Payments on annuities and unitrusts payable	(41,785)	(30,430)
Receipt of permanently restricted gifts	653,152	1,321,302
Annuity and unitrusts donations received	29,665	69,307
Loan proceeds	—	250,000
Payments on long-term debt	(229,657)	(218,557)
Net cash provided by financing activities	411,375	1,391,622
Net increase in cash and cash equivalents	627,153	169,273
Cash and cash equivalents at beginning of year	560,801	391,528
Cash and cash equivalents at end of year	$ 1,187,954	$ 560,801

The accompanying notes are an integral part of the financial statements.

Marine Biological Laboratory

Notes to Financial Statements

A. *Background:*

The Marine Biological Laboratory (the "Laboratory") is a private, independent not-for-profit research and educational institution dedicated to establishing and maintaining a laboratory or station for scientific study and investigation, and a school for instruction in biology and natural history. The Laboratory was founded in 1888 and is located in Woods Hole, Massachusetts.

B. *Significant Accounting Policies:*

Basis of Presentation

The accompanying financial statements have been prepared on the accrual basis of accounting and in accordance with the principles outlined in the American Institute of Certified Public Accountants' Audit Guide, "Not-For-Profit Organizations." The financial statements include certain prior-year summarized comparative information in total but not by net asset class. Such information does not include sufficient detail to constitute a presentation in conformity with generally accepted accounting principles. Accordingly, such information should be read in conjunction with the Laboratory's financial statements for the year ended December 31, 1997, from which the summarized information was derived.

The Laboratory classifies net assets, revenues, and realized and unrealized gains and losses based on the existence or absence of donor-imposed restrictions and legal restrictions imposed under Massachusetts State law. Accordingly, net assets and changes therein are classified as follows:

Unrestricted

Unrestricted net assets are not subject to donor-imposed restrictions of a more specific nature than the furtherance of the Laboratory's mission. Revenues from sources other than contributions are generally reported as increases in unrestricted net assets. Expenses are reported as decreases in unrestricted net assets. Gains and losses on investments and other assets or liabilities are reported as increases or decreases in unrestricted net assets unless their use is restricted by explicit donor stipulations or law. Expirations of temporary restrictions on net assets, that is, the donor-imposed stipulated purpose has been accomplished and or the stipulated time period has elapsed, are reported as reclassifications between the applicable classes of net assets.

Temporarily Restricted

Temporarily restricted net assets are subject to legal or donor-imposed stipulations that will be satisfied either by the actions of the Laboratory, the passage of time, or both. These assets include gifts plus monies for which the specific, donor-imposed restrictions have not been met, and pledges, annuities, and unitrusts for which the ultimate purpose of the proceeds is not permanently restricted. As the restrictions are met, the assets are released to unrestricted net assets. Also, realized/unrealized gains/losses associated with permanently restricted gifts which are not required to be added to principal by the donor are classified as temporarily restricted but maintain the donor requirements for expenditure.

Permanently Restricted

Permanently restricted net assets are subject to donor-imposed stipulations that they be invested to provide a permanent source of income to the Laboratory. These assets include gifts, pledges and trusts which require that the corpus be invested in perpetuity and only the income be made available for program operations in accordance with donor restrictions.

Nonoperating revenues include realized and unrealized gains on investments during the year as well as investment income on the master pooled investments. Investment income from short-term investments and investments held in trust by others are included in operating support and revenues. To the extent that nonoperating investment income and gains are used for operations as determined by the Laboratory's total return utilization policy (see below), they are reclassified from nonoperating to operating on the statement of activities as "Investment earnings used for operations." All other activity is classified as operating revenue. The Laboratory recorded net realized gains of $2,805,560, net unrealized losses of $2,755,079 and dividend and interest income of $1,478,046 in 1998.

Cash and Cash Equivalents

Cash equivalents consist of resources invested in overnight repurchase agreements and other highly liquid investments with original maturities of three months or less.

Financial instruments which potentially subject the Laboratory to concentrations of risk consist primarily of cash and investments. The Laboratory maintains cash accounts with one banking institution.

Investments

Investments purchased by the Laboratory are carried at market value. Donated investments are recorded at fair market value at the date of the gift. For determination of gain or loss upon disposal of investments, cost is determined based on the first-in, first-out method. Investments with an original maturity of three months to one year are classified as short-term. All other investments are considered long-term. Investments are maintained primarily with five institutions.

In 1924, the Laboratory became the beneficiary of certain investments, included in permanently restricted net assets, which are held in trust by others. The Laboratory has the continuing rights to the income produced by these funds in perpetuity, subject to the contractual restrictions on the use of such funds. Accordingly, the trust has established a process to conduct a review every ten years by an independent committee to ensure the Laboratory continues to perform valuable services in biological research in accordance with the restrictions placed on the funds by the agreement. The committee met in 1994 and determined that the Laboratory has continued to meet the contractual requirements. The market values of such investments are $7,673,828 and $7,440,158 at December 31, 1998 and 1997, respectively. The dividend and interest income on these investments totaled $260,805 and $254,898 in 1998 and 1997, respectively.

Investment Income and Distribution

For the master pooled investments, the Laboratory employs a total return utilization policy that establishes the amount of the investment return made available for spending each year. The Finance Committee has approved a standing policy that the withdrawal will be based on a percentage of the latest three-year average ending market values of the funds. The market value includes the principal plus reinvested income, realized and unrealized gains and losses. Spending rates in excess of 5%, but not exceeding 7%, can be utilized if approved in advance by the Finance Committee of the Board of Trustees. For fiscal 1998 and 1997, the Laboratory obtained approval to expend 6% of the latest three-year average ending market values of the investments.

The net appreciation on permanently and temporarily restricted net assets is reported together with temporarily restricted net assets until such time as all or a portion of the appreciation is distributed for spending in accordance with the total return utilization policy and applicable state law.

Investment income on the pooled investment account is allocated to the participating funds using the market value unit method (Note D).

Plant Assets

Buildings and equipment are recorded at cost. Donated facility assets are recorded at fair market value at the date of the gift. Depreciation is computed using the straight-line method over the asset's estimated useful life. Estimated useful lives are generally three to ten years for equipment and 20 to 40 years for buildings and improvements. Depreciation expense for the years ended December 31, 1998 and 1997 amounted to $1,505,696 and $1,483,203, respectively, and has been recorded in the statement of activities in the appropriate functionalized categories. When assets are sold or retired, the cost and accumulated depreciation are removed from the accounts and any resulting gain or loss is included in unrestricted income for the period.

Annuities and Unitrusts Payable

Amounts due to donors in connection with gift annuities and unitrusts are determined based on remainder value calculations, with varied assumptions of rates of return and payout terms.

Deferred Income and Advances on Contracts

Deferred income includes prepayments received on Laboratory publications and advances on contracts to be utilized within the next year. Advances on contracts includes funding received for grants and contracts before it is earned. In certain circumstances, long-term advances are invested in the master pooled account until they are expended.

Revenue Recognition

Revenue is recognized at the time it is earned. The sources of revenue include grant payments from governmental agencies, contracts from private organizations, and income from the rental of laboratories and classrooms for research and educational programs. The tuition income is net of student financial aid of $523,190 and $536,097 in 1998 and 1997, respectively. Fees for conferences and other services include the following activities: housing, dining, library, scientific journals, aquatic resources and research services.

Contributions

Contribution revenue includes gifts and pledges. Gifts are recognized as revenue upon receipt. Pledges are recognized as temporarily or permanently restricted revenue in the year pledged and are recorded at the present value of expected future cash flows, net of allowance for unfulfilled pledges. Gifts and pledges, other than cash, are recorded at fair market value at the date of contribution.

Expenses

Expenses are recognized when incurred and charged to the functions to which they are directly related. Expenses that relate to more than one function are allocated among functions using various methodologies.

Other programs expense consists primarily of fundraising, year-round labs and library room rentals, costs associated with aquatic resource sales and scientific journals. Total fundraising expense for 1998 and 1997 is $1,037,495 and $1,226,360, respectively.

Use of Estimates

The preparation of financial statements in conformity with generally accepted accounting principles requires management to make estimates and assumptions that affect the reported amounts of assets and liabilities and disclosure of contingent assets and liabilities at the date of financial statements and the reported amounts of revenues and expenses during the reporting period. Actual results could differ from those estimates.

Tax-Exempt Status

The Laboratory is exempt from federal income tax under Section 501(c)(3) of the Internal Revenue Code.

C. *Investments:*

The following is a summary of the cost and market value of investments at December 31, 1998 and 1997:

	Market		*Cost*	
	1998	*1997*	*1998*	*1997*
Certificates of deposit	$ 40,000	$ 40,000	$ 40,000	$ 40,000
Money market securities	1,052,276	2,168,958	1,052,276	2,168,958
U.S. Government securities	1,397,686	1,292,600	1,136,219	1,098,526
Corporate fixed income	2,504,507	2,587,861	2,472,653	2,472,653
Common stocks	5,033,704	5,279,266	4,290,581	4,271,853
Mutual funds	29,548,891	23,223,812	26,225,214	19,317,499
Limited partnerships	1,038,600	5,429,700	958,982	3,309,994
Total investments	$40,615,664	$40,022,197	$36,175,925	$32,679,483

Investment portfolios for the years ended December 31, 1998 and 1997 are as follows:

	Market		*Cost*	
	1998	*1997*	*1998*	*1997*
Short-Term Investments				
Certificates of deposit	$ 40,000	$ 40,000	$ 40,000	$ 40,000
Money market 1784 Fund	559,314	1,759,589	559,314	1,759,589
Common stocks	6,241	551,780	6,241	530,936
Mutual funds	2,955,989	2,056,677	2,940,929	2,056,679
Total	3,561,544	4,408,046	3,546,484	4,387,204

	Market		*Cost*	
	1998	*1997*	*1998*	*1997*
Long-Term Investments				
Pooled investments:				
Master pooled investments	$27,057,909	$26,163,702	$23,723,343	$20,201,962
Separately invested:				
General Chase trust	6,038,153	5,846,916	5,433,574	4,986,443
Library Chase trust	1,635,675	1,593,242	1,477,462	1,358,149
Annuity and unitrust investments	2,322,383	2,010,291	1,995,062	1,745,725
Total	37,054,120	35,614,151	32,629,441	28,292,279
Total investments	$40,615,664	$40,022,197	$36,175,925	$32,679,483

D. *Accounting for Pooled Investments:*

Certain net assets are pooled for investment purposes. Investment income from the pooled investment account is allocated on the market value unit basis, and each fund subscribes to or disposes of units on the basis of the market value per unit at the beginning of the calendar quarter within which the transaction takes place. The unit participation of the funds at December 31, 1998 and 1997 is as follows:

	1998	*1997*
Unrestricted	4,001	4,192
Temporarily restricted	44,455	42,693
Permanently restricted	65,016	65,411
Advances on contracts	6,437	6,506
	119,909	118,802

Pooled investment activity on a per-unit basis was as follows:

	1998	*1997*
Unit value at beginning of year	$ 220.30	$ 186.35
Unit value at end of year	225.51	220.30
Total return on pooled investments	$ 5.21	$ 33.95

E. *Long-Term Debt:*

Long-term debt consisted of the following at December 31:

	1998	*1997*
Variable rate (5.15% at December 31, 1998) Massachusetts Industrial Finance Authority Series 1992A Bonds payable in annual installments through 2012	$ 925,000	$ 960,000
6.63% Massachusetts Industrial Finance Authority Series 1992B Bonds, payable in annual installments through 2012	1,230,000	1,280,000
5.8% The University Financing Foundation, Inc., payable in monthly installments through 2000	226,024	325,210
5.8% The University Financing Foundation, Inc., payable in monthly installments through 2002	186,346	231,817
	$2,567,370	$2,797,027

The aggregate amount of principal due on long-term debt for each of the next five fiscal years and thereafter is as follows:

1999	$ 243,274
2000	267,404
2001	173,664
2002	148,028
2003	125,000
Thereafter	1,610,000
	2,567,370
Less current portion of long-term debt	(243,274)
Long-term debt net of current return	$2,324,096

In 1992, the Laboratory issued $1,100,000 Massachusetts Industrial Finance Authority (MIFA) Series 1992A Bonds with a variable interest rate and $1,500,000 MIFA Series 1992B with an interest rate of 6.63%. Interest expense debt totaled $136,340 for the year ended December 31, 1998. The Series 1992 A and B Bonds mature on December 1, 2012 and are collateralized by a first mortgage on certain Laboratory property.

On March 17, 1998, the Laboratory entered into a ten-year interest rate swap contract in connection with the Series 1992A Bonds. This contract effectively fixes the interest rate at 6.30% through December 17, 2008.

The agreements related to these bonds subject the Laboratory to certain covenants and restrictions. Under the most restrictive covenant of this debt, the Laboratory's operating surplus, exclusive of interest expense and depreciation expense, must be greater than or equal to 1.2 times all debt service payments, as defined by the agreement. The Laboratory was in compliance with these covenants and restrictions at December 31, 1998.

In 1996, the Laboratory borrowed $500,000 with an interest rate of 5.8% per annum from the University Financing Foundation, Inc. The interest expense for the year ended December 31, 1998 was $16,253. The loan matures in 2000 and is collateralized by 50,000 shares of a fixed income fund with a fair value of $595,000 at December 31, 1998.

In 1997, the MBL borrowed $250,000 with an interest rate of 5.8% per annum from the University Financing Foundation, Inc. The interest expense for the year ended December 31, 1998 was $12,249. This loan matures in 2002 and is collateralized by 19,440 shares of a fixed income mutual fund with a fair value of $231,336 at December 31, 1998.

The Laboratory has a line of credit agreement with BankBoston from which it may draw up to $1,000,000. No amounts were outstanding under this agreement as of December 31, 1998 and 1997.

F. *Plant Assets:*

Plant assets consist of the following at December 31:

	1998	*1997*
Land	$ 702,908	$ 702,908
Buildings	33,334,107	32,419,072
Equipment	4,401,184	4,300,932
Total	38,438,199	37,422,912
Less: Accumulated depreciation	(18,902,028)	(17,396,332)
Plant assets, net	$19,536,171	$20,026,580

G. *Retirement Plan:*

The Laboratory participates in the defined contribution pension plan of TIAA-CREF (the "Plan"). The Plan is available to permanent employees who have completed two years of service. Under the Plan, the Laboratory contributes 10% of total compensation for each participant. Contributions amounted to $737,156 and $715,858 for the years ended December 31, 1998 and 1997, respectively.

H. *Pledges:*

Unconditional promises to give are included in the financial statements as pledges receivable and the related revenue is recorded in the appropriate net asset category. Unconditional promises to give are expected to be realized in the following periods:

	1998	*1997*
In one year or less	$1,607,664	$2,219,056
Between one year and five years	3,110,354	2,485,851
After five years	146,586	80,000
Total	4,864,604	4,784,907
Less: discount of $301,588 in 1998 and $227,025 in 1997 and allowance of $100,000 in 1998 and $100,000 in 1997	(401,588)	(327,025)
	$4,463,016	$4,457,882

Pledges receivable at December 31 have the following restrictions:

	1998	*1997*
Research and education	$3,933,988	$3,787,882
Permanently restricted net assets	529,028	670,000
	$4,463,016	$4,457,882

I. *Postretirement Benefits:*

The Laboratory accounts for its postretirement benefits under Statement No. 106, ''Employers' Accounting for Postretirement Benefits Other than Pensions,'' which requires employers to accrue, during the years that the employee renders the necessary service, the expected cost of benefits to be provided during retirement. As permitted, the Laboratory has elected to amortize the transition obligation over 20 years commencing on January 1, 1994.

The Laboratory's policy is that all current retirees and certain eligible employees who retired prior to June 1, 1994 will continue to receive postretirement health benefits. The remaining current employees will receive benefits; however, those benefits will be limited as defined by the Plan.

Employees hired on or after January 1, 1995 will not be eligible to participate in the postretirement medical benefit plan.

The following tables set forth the Plan's funded status as of December 31:

	1998	*1997*
Benefit obligation at December 31	$ 2,171,119	$ 1,919,865
Fair value of plan assets at December 31	820,645	701,140
Funded status	$(1,350,474)	$(1,218,725)
Accrued benefit cost	$ (26,654)	$ (8,397)
Weighted-average assumptions as of December 31:		
Discount rate	6.75%	7.50%
Expected return on plan assets	7.25%	8.00%
Compensation increase rate	N/A	N/A
Benefit cost	210,339	192,082
Employer contribution	192,082	192,082
Benefits paid	109,404	111,255

For measurement purposes a 7.5% annual rate of increase in the per capita cost of covered health care benefits was assumed for 1999. The rate was assumed to decrease by half of 1.00% per year to 4.25% in 2006 and remain at that level thereafter. Pension plan assets consist of investments in a money market fund.

MARINE BIOLOGICAL LABORATORY

Supplemental Schedule of Functional Expenses

for the year ended December 31, 1998
(with comparative totals for the year ended December 31, 1997)

	Research	*Instruction*	*Conferences*	*Other*	*Facilities Maintenance*	*Administration*	*Library Services*	*Research Services*	*Aquatic Research Services*	*Total*
Salaries	$ 3,188,396	$ 368,776	$ 346,380	$ 636,238	$1,045,652	$1,722,940	$346,574	$344,199	$239,100	$ 8,238,255
Fringe benefits	852,100	99,599	93,522	171,739	282,421	468,136	93,575	92,934	64,557	2,218,583
Professional services	63,077	252,301	—	29,915	73,695	196,044	3,903	25	—	618,960
Subcontracts	981,132	—	957,949	3,127	—	—	—	—	—	1,942,208
Equipment	522,592	334,164	2,470	1,466	135,947	26,875	—	4,050	2,598	1,030,162
Supplies	537,402	391,223	40,850	110,557	217,796	138,744	15,073	353,334	42,422	1,847,401
Travel	501,316	193,823	(2,834)	31,135	8,334	39,363	10,707	915	95	782,854
Serials	627	1,466	—	15,846	628	1,305	476,119	346	—	496,337
Utilities	292	439	1285,488	1,901	730,360	99,609	367	304	1,599	1,020,359
Depreciation	—	—	—	—	1,483,203	—	—	—	—	1,483,203
Other	223,503	300,789	216,477	331,173	493,236	472,017	111,450	195,312	82,656	2,426,613
Internal direct changes	359,010	801,051	(665,077)	98,639	(147,503)	28,593	49,906	(498,532)	(26,087)	—
Total	7,229,447	2,743,631	1,175,225	1,431,736	4,323,769	3,193,626	1,107,674	492,887	406,940	22,104,935
Indirect expense allocations	3,802,467	1,400,877	312,480	4,009,072	(4,323,769)	(3,193,626)	(1,107,674)	(492,887)	(406,940)	—
Total expenses	$11,031,914	$4,144,508	$1,487,705	$5,440,808	—	—	—	—	—	$22,104,935

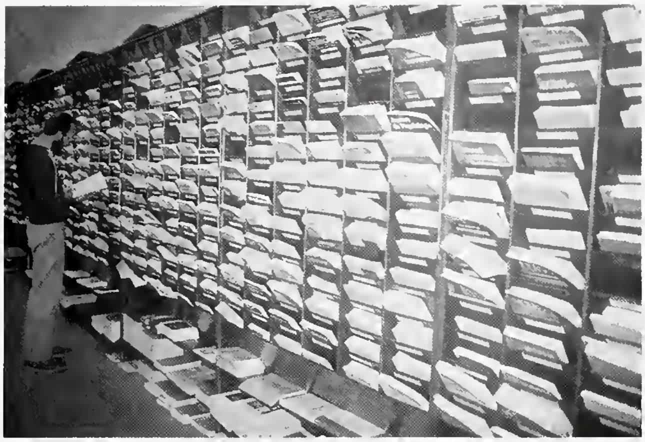

Report of the Library Director

A recent spate of articles foretelling the demise of libraries and the instant availability of information on the Internet has engendered some lively conversation about the future of the MBL/WHOI Library and the role of librarians. Among the questions being raised is "what do libraries do?" However, the more important question is, "what are libraries for?" If we fail to understand what libraries are for, we will mismanage their inevitable evolution to new environments and institutions.

Libraries as they currently exist are repositories of physical materials. As such they will be replaced as the dominant technology for communicative information moves from tangible objects to electronic bits on a network. Libraries organize information and make it readily, publicly, and economically available. Libraries are the pathways that organizations and institutions use to subsidize the distribution of information to their respective communities. Without such support, information is underused, and its potential benefit is lost. Librarians need to understand this model so that, as information distribution changes (and it will), they can help shape the information economy in order to maintain the community subsidy as new technologies enhance and extend information availability. If we think our focus is book warehousing we will fail. Librarians will still need to evaluate material and, with the advice of scientists, decide what to add to collections; then they must order, pay for, and process the material, to say nothing of helping people use it effectively.

Libraries will continue to live in the two worlds of electronic delivery and physical archive for a while because the half-life of electronic data is currently about five years. There is no improvement in sight because the high-tech industry can only reach as far as next year's upgrade. We have experienced the loss of data in our disk archives of the ALVIN dive data, which is only 20 years old but already unreadable because the programs, operating systems, and machines that wrote the files have all disappeared! Similarly, all of the early pioneer computer work at labs such as MIT's Artificial Intelligence has been lost. Digitized information created today may be similarly doomed, because the rate of digital obsolescence keeps accelerating; and there is nothing in the digital world like acid-free paper.

It was reported in a recent volume of *Nature* that Denmark's National Technical Knowledge Center and Library has decided to phase out print altogether and deliver journals direct to staff desktops via the World Wide Web. Perhaps this is a solution to our space problems, but the MBL/WHOI Library is not yet prepared to abandon print. Concern over how and by whom electronic resources will be archived remains unsolved, along with the out-of-control rise in the cost of serials in both paper and electronic formats. Academic libraries, through the SPARC Initiative, are currently supporting a move to return control of journal publishing to learned societies, and are encouraging researchers to refuse to sit on editorial boards or review papers for the publishers of expensive titles. Another move promotes the retention of copyright by researchers. Caltech may require their authors to retain copyright over their papers and only license them to publishers.

Our vision of opening an electronic window to the vast array of available information will require us to form partnerships and alliances to overcome problems of storage, cost, accessibility, and marketing. This window will be fashioned and focused to provide information that is reliable, authentic, and trustworthy as we delineate our role in the library future.

Space and Time

Since 1888, Woods Hole scientists and librarians have collected valuable works in biology and oceanography. Over the past century an invaluable learning resource has evolved, albeit one that is bulging. In the *Annual Report of 1990*, the Librarian reported on the lack of adequate storage space. In that year the staff moved the most recent twenty years of the collection and consolidated the older material to acquire just three years of growth.

In the years since, we have implemented a program of weeding, storing, discarding, and moving archival material to the Special Collection or Rare Book Room. Despite the promised electronic future, we will come to the end of our space before the millennium. We are once again moving the largest portion of the older serial volumes in the back wing of the Library with hope of obtaining one more year of growth. Even this meager amount of space will be absorbed by the addition of ductwork for the long-needed air conditioning of the stacks.

The Library committee is in preliminary discussion about solutions—increased weeding, deaccession, depository storage, electronic delivery, off-site storage, digitization, and the addition of a new wing.

Special Collections

The Special Collection area of the Library became the main focus of cataloging in 1998. A large number of nineteenth-century monographs were identified and placed in the collection. In all, more than 900 items were added during the year. Among them are many newly discovered works of Oscar Hertwig, a leading physiologist of the 19th century, and two expeditions—the *Report of the US Geological Survey of the Territories: F. V. Hayden Expedition* in 1873 by Hayden and Joseph Leidy (whose portrait hangs on the 5th stack), and the *Den Norske Nordhavs-Expedition,* 1876–1878—seven volumes which had never been cataloged elsewhere.

Preservation

The *Florence Gould Foundation* award to the library has allowed us to preserve and conserve more than 75 monographs, prepare a bibliography of eighteenth- and nineteenth-century French science books and journals in the MBL/WHOI Library collection, and develop a web page detailing this collection. This contribution allowed the restoration, rebinding, and deacidification of French books and monographs dating back to the eighteenth century. Marine zoology and comparative zoology first emerged as a recognized science in France. The studies of Audouin, Milne-Edwards, Cuvier, and Lavoisier became prototypes for future research. All of these and many more are represented in our collection.

Journals

The Library continues to hold the line in journal acquisitions, and in spite of the numeric decline in titles acquired by the Library, the number of volumes we acquire has increased. The journals we still collect in paper are publishing more volumes and more articles, hence the continued increase in shelf space demand.

Our collection of electronic journals has increased to more than 500, which in many cases accompany a paper subscription. Plans are developing for the archiving of this digitized format.

Branch libraries

Melissa Lamont became WHOI's Data Librarian in February. During the year, both the ALVIN Database and the ALVIN Bibliography were completed and brought online (http://dunkle.whoi.edu/dlaweb/alvin.html). The WHOI Contributions database is up on the Web, and a finding aid for Henry Stommel material is cataloged on Mariner. The Archives received the collections of Holger Jannasch, Frank Mather, and John Hunt. A film vault and compact shelving were added at the Data Library. A finding aid for WHOI Director's files was created in the Archives. The Northeast Document Conservation Center, funded through a grant, recommended new methods for the care and preservation of the material in WHOI's Data Center and Archive.

The Future

The National Library of Medicine has increased the award to the Library in support of two courses in Medical Informatics at the MBL. The first course was held in June 1999, and the second course in October. During the fall of 1999, the Library will host the 25th meeting of the International Association of Aquatic and Marine Science Libraries and Information Centers (IAMSLIC). Past MBL/WHOI Librarians Jane Fessenden and Carol Winn began this organization in Woods Hole in 1975. It has since grown from a small group of East Coast members to include participants from around the globe. The mission of this group is to foster innovative uses of technology and to improve scholarly communication in the fields of ocean and marine science.

As we look to the millennium, it is my hope that people will not consider it the end of something but rather the beginning. We actually have the technical understanding to solve problems such as digital degradation. What we don't have yet in our digital culture is the habit of long-term thinking that supports preservation of this resource. While technologists plan the next digital medium, librarians must think about how it lasts and how it can be made available.

Predictions of the future usually overestimate the extent of change in the short run and underestimate it in the long run. While much, if not most, of the information that is useful for scholarly research will probably be online some day, we are not even close to having the critical mass of information available online that is necessary to support faculty or even student research. By this time next year, we will be in the new millennium. The Library will still make available the published results of scientific research no matter what technology shifts or economic forces are at work.

—Cartherine Norton

PHYSIOLOGY!
CELLULAR

Educational Programs

Summer Courses

Biology of Parasitism: Modern Approaches

(June 11–August 14)

Directors

Edward Pearce, Cornell University
Christian Tschudi, Yale University School of Medicine

Faculty

Serap Aksoy, Yale University School of Medicine
Meg Phillips, University of Texas Southwest, Dallas
David Russell, Washington University Medical School
Phillip Scott, University of Pennsylvania
Murray Selkirk, Imperial College of Science, Technology and Medicine, United Kingdom
David Sibley, Washington University Medical School
Elisabetta Ullu, Yale University School of Medicine
Andrew P. Waters, University of Leiden, The Netherlands

Teaching Assistants

Deirdre Brekken, University of Texas Southwestern, Dallas
Daniel Brown, University of Chicago
Jaime Dant, Washington University Medical School
Maristela De Camargo, Federal University of Minas Gerais, Brazil
Merle Elloso, University of Pennsylvania
J. Chris Fromme, Cornell University
Brian Hondowicz, University of Pennsylvania
Ayman Hussein, Imperial College of Science, Technology and Medicine, United Kingdom
Anne Camille La Flamme, Cornell University
Andreas Lingnau, Washington University Medical School
Maren Lingnau, Washington University Medical School
Carol Lopez-Estrano, Yale University School of Medicine
Dana Mordue, Washington University Medical School
Kai Wengelnik, Imperial College of Science, Technology and Medicine, United Kingdom
Liangbiao Zheng, Yale University

Lecturers

Norma Andrews, Yale University School of Medicine
James Bangs, University of Wisconsin, Madison
Stephen Beverley, Washington University Medical School
John Boothroyd, Stanford University School of Medicine
Nino Campobasso, Cornell University
George Cross, Rockefeller University
Karen Day, Oxford University, United Kingdom
Kirk Deitsch, National Institutes of Health
Anne Dell, Imperial College of Science, Technology and Medicine, United Kingdom
Eric Denkers, Cornell University
John Donelson, University of Iowa College of Medicine
Steve Ealick, Cornell University
Durland Fish, Yale University School of Medicine
Ute Frevert, New York University Medical Center
Daniel Goldberg, Washington University Medical School
Richard K. Grencis, University of Manchester, United Kingdom
Steve Hajduk, University of Alabama, Birmingham
John Hawdon, Yale University School of Medicine
John Heuser, Washington University Medical School
Stephen Hoffman, Naval Medical Research Institute
Patricia Johnson, University of California, Los Angeles
Jean Langhorne, Imperial College of Science, Technology and Medicine, United Kingdom
Margaret Linnell, University of Georgia
Susan Little, University of Georgia
Leo Liu, Beth Israel Hospital
Philip LoVerde, State University of New York, Buffalo
James McKerrow, University of California, San Francisco
Sara Melville, University of Cambridge, United Kingdom
Timothy Nilsen, Case Western Reserve University
Scott O'Neill, Yale University
Eric Pearlman, Case Western Reserve University
David Peterson, University of Georgia
Pradip Rathod, Catholic University of America
Steve Reiner, University of Chicago
David Roos, University of Pennsylvania
David Sacks, National Institutes of Health
Alan Sher, National Institutes of Health
Mitchell Sogin, Marine Biological Laboratory
Rick Tarleton, University of Georgia
Buddy Ullman, Oregon Health Sciences University
Akhil Vaidya, Hahnemann University
Ching C. Wang, University of California, San Francisco

Course Coordinator

Stepanka Vanacova, Charles University, Czech Republic

Course Assistant

Ellenita Bridget Salko, Cornell University

Students

Fábio Alves, Fundação Oswaldo Cruz, Brazil
Myriam Arévalo, Universidad del Valle Cali, Columbia
David Artis, University of Manchester, United Kingdom
Katrin Henze, The Rockefeller University
Bolyn Hubby, University of Georgia
Laurence Lambert, Ludwig-Maximilians-Universität, München, Germany
Jennie Lovett, Washington University, St. Louis
Emily Lyons, Indiana University
Kai Matuschewski, New York University
Pius Nde, Humboldt University Berlin, Germany
Monida Oli, Auburn University
Kimberly Paul, Princeton University
Tina Saxowsky, Johns Hopkins School of Medicine
Kendra Speirs, University of Pennsylvania
Ross Waller, University of Melbourne, Australia
Colby Zaph, University of Victoria, Canada

Embryology: Concepts and Techniques in Modern Developmental Biology

(June 14–July 25)

Directors

Marianne Bronner-Fraser, California Institute of Technology
Scott Fraser, California Institute of Technology

Faculty

Andre Adoutte, University of Paris-Sud, France
Seth S. Blair, University of Wisconsin
Sean Carroll, University of Wisconsin
Andres Collazo, House Ear Institute
Richard Harland, University of California, Berkeley
Robb Krumlauf, National Institute for Medical Research, United Kingdom
Lee Niswander, Memorial Sloan-Kettering Cancer Center
Joel Rothman, University of California, Santa Barbara
John Saunders, Jr., Marine Biological Laboratory
Judith Venuti, Columbia University
Robert Zeller, University of California, San Diego

Teaching Assistants

Maria Ina Arnone, Stazione Zoologica A. Dohrn, Italy
Guillaume Balavoine, Wellcome/CRC Institute, United Kingdom
Rebecca Beach, Hollins College
Rebecca Crowe, Memorial Sloan-Kettering Cancer Center
Gabrielle Kardon, Harvard Medical School
Sung-hee Kil, House Ear Institute
Catherine Krull, University of Missouri, Columbia
Julie Kuhlman, Memorial Sloan-Kettering Cancer Center
Nicholas Lartillot, Universite Paris-Sud, France
Morris Maduro, University of California, Santa Barbara
Francesca Mariani, University of California, Berkeley
Craig Micchelli, University of Wisconsin, Madison
Carmen Pepicelli, Harvard University
Paul Trainor, Medical Research Council, United Kingdom
Emily Walsh, University of California, San Francisco
Valerie Wilson, Western General Hospital, United Kingdom

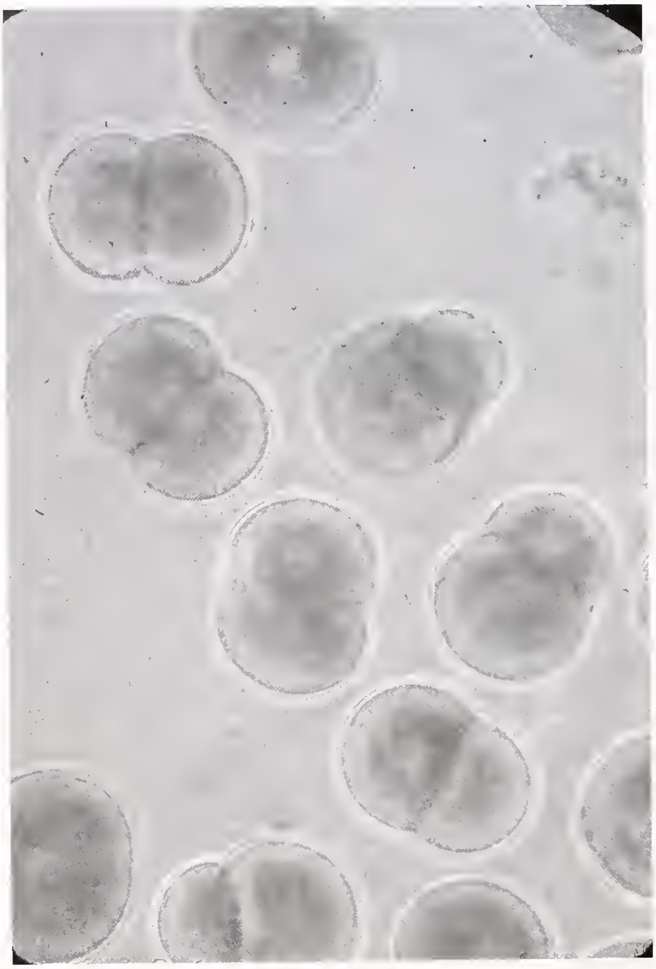

Lecturers

Eric Davidson, California Institute of Technology
Marietta Dunaway, University of California, Berkeley
Katia Georgopoulos, Massachusetts General Hospital–East
John Gerhart, University of California, Berkeley
Nancy Hopkins, Massachusetts Institute of Technology
Marc Kirschner, Harvard University Medical School
Rusty Lansford, California Institute of Technology
Michael Levine, University of California, Berkeley
Nadia Rosenthal, Massachusetts General Hospital–East
Ellen Rothenberg, California Institute of Technology
Joshua Sanes, Washington University Medical School
Marty Shankland, University of Texas
Claudio Stern, Columbia University
Clifford Tabin, Harvard Medical School

Course Assistants

Sarah Balligan, Michigan State University
Allison Freeman, Wheaton College

Lab Technician

Kim Ulandt, Marine Biological Laboratory

Lab Assistant

Sara Wylie, Marine Biological Laboratory

Students

Tonya Anderson, University of California, Los Angeles
Kirsten Berggren, University of Vermont
James Chen, Harvard University
Fabiana Geraci, Fondazione Alberto Monroy, Italy
Arjuman Ghazi, National Centre for Biological Sciences, India
Anjali Kalyani, University of Utah
Yuk Kong, University of Southern California
Paul Kulesa, California Institute of Technology
Giuseppe Lupo, University of Pisa, Italy
Helen McBride, University of Utah
Kathryn McCabe, University of Washington
David McCauley, Pennsylvania State University
David McLay, McGill University, Canada
Julie Nowicki, University of North Carolina, Chapel Hill
Elke Ober, Max-Planck-Institut Tübingen, Germany
Anne Pollack, University of Arizona
Fernando Roch, Wellcome/CRC Institute, United Kingdom
Marion Rozowski, Wellcome/CRC Institute, United Kingdom
Miguel Santos, Harvard University
Ryuichi Shirasaki, Osaka University, Japan
Laura Stimson, University of Arizona
Emilios Tahinci, Boston University
Jay Vivian, University of Texas
Alin Vonica, Cornell University Medical Center

Microbial Diversity (June 14–July 30)

Directors

Edward Leadbetter, University of Connecticut
Abigail Salyers, University of Illinois, Urbana

Faculty

Kurt Hanselmann, University of Zurich, Switzerland
Bruce Paster, Forsyth Dental Center
Thomas Pitta, Rowland Institute for Science
Bernhard Schink, University of Wisconsin

Teaching Assistants

Scott Dawson, University of California, Berkeley
Rebecca Ericson, Forsyth Dental Center
Elke Jaspers, University of Oldenburg, Germany
Carol Lau, Forsyth Dental Center
Irena Levin, Forsyth Dental Center
Dianne Newman, Harvard Medical School
Bodo Philipp, Universität Konstanz, Germany

Lecturers

John Breznak, Michigan State University
Nyles Charon, West Virginia University
Jerald Ensign, University of Wisconsin
Stephen Farrand, University of Illinois, Urbana
Dan Fraenkel, Harvard Medical School
Tillman Gerngross, Metabolix, Inc.
Olivia Harriott, Fairfield University
Stanley Holt, University of Texas Health Science Center
Mary Lidstrom, University of Washington
Margaret McFall-Ngai, University of Hawaii
John Murrell, University of Warwick, United Kingdom
Scott O'Neill, Yale University
Ronald Oremland, United States Geological Survey
Jeanne Poindexter, Barnard College
Hans Schlegel, Georg-August Universität, Germany
Thomas Schmidt, Michigan State University
Rene Schwarzenbach, EAWAG/ETH, Switzerland
Andreas Teske, Woods Hole Oceanographic Institute
Pieter Visscher, University of Connecticut, Avery Point

Course Coordinator

Angelica Seitz, Marine Biological Laboratory

Lab Assistants

Nell Ament, Marine Biological Laboratory
Joanna Levitt, H. M. Gunn High School
Kalina White, Earlham College

Students

Ana Anton Garcia, Universidad Miguel Hernandez, Spain
Cynthia Carr, Rice University
Hector Castro, University of Florida
Pat Fidopiastis, University of Hawaii
Andrea Foster, Stanford University
Christopher Francis, Scipps Institution of Oceanography
Yoshiko Fujita, Stanford University
Patricia Howard, Aquatic Resources Center
Andreas Kappler, University of Konstanz, Germany
Joel Klappenbach, Michigan State University
Min-Ken Liao, Hope College
Kathryn Patterson, University of Georgia
Milva Pepi, University of Siena, Italy
Jorge Rodrigues, Michigan State University
Karin Sauer, Max-Planck-Institut, Germany
Dmitri Sobolev, University of Alabama
John Spear, Colorado School of Mines
Silvana Tarlera, Universidad de la Republica of Uruguay, Uruguay
Julie Zilles, University of Wisconsin, Madison
Erik Zinser, Harvard University

Neural Systems & Behavior (June 14–August 7)

Directors

Janis Weeks, University of Oregon
Harold Zakon, University of Texas, Austin

Faculty

Carol Barnes, University of Arizona
Ronald L. Calabrese, Emory University
Catherine Carr, University of Maryland
Kathleen French, University of California, San Diego
David Glanzman, University of California, Los Angeles
Scott Hooper, Ohio University
Richard Hyson, Florida State University
William Kristan, University of California, San Diego
Richard Levine, University of Arizona
Bruce McNaughton, University of Arizona
Gillian Muir, University of Saskatchewan, Canada
Michael Nusbaum, University of Pennsylvania School of Medicine
Glen Prusky, University of Lethbridge, Canada
William Roberts, University of Oregon
Angela Wenning-Erxleben, Universität Konstanz, Germany

Teaching Assistants

Tatiana Arjannikova, University of Lethbridge, Canada
Cecilia Armstrong, University of Oregon
Dawn Marie Blitz, University of Pennsylvania School of Medicine
Mark Bower, University of Arizona
Shanping Chen, House Ear Institute
Raymond Chitwood, University of Texas, San Antonio
Christos Consoulas, University of Arizona
Brian Edmonds, University of Oregon
Michael Ferrari, University of California, San Diego
Georgi Gamkrelidze, George Washington University Medical Center
Jorge Golowasch, Brandeis University
Andrew Hill, Emory University
Joshua Krane, Florida State University
John Lewis, University of Ottawa, Canada
Lynne McAnelly, University of Texas
Geoffrey Murphy, University of California, Los Angeles
Kathryn S. Richards, Brandeis University
David Sandstrom, University of Arizona
Emma Wood, Boston University
Shih-Rung Yeh, University of California, Los Angeles

Lecturers

Jelle Atema, Marine Biological Laboratory
George Augustine, Duke University Medical Center
David Bodznick, Wesleyan University
Michael Dickinson, University of California, Berkeley
Lily Jan, University of California, San Francisco
Shawn Lockery, University of Oregon
Jan-Marino Ramirez, University of Chicago
Catherine Woolley, Northwestern University

Scholars-in-Residence

Sarah Bottjer, University of Southern California
George Pollak, University of Texas, Austin

Course Assistants

Sarah Doernberg, Harvard University
Krista Stogryn, Marine Biological Laboratory

Students

Jon Boyle, University of Wisconsin, Madison
Elke Buschbeck, Cornell University
Andrea d'Avella, Massachusetts Institute of Technology
Michael Farries, University of Pennsylvania
Antoinette Freeman, Boston University School of Medicine
Andrea Green, McGill University, Canada
Allan Gulledge, University of Texas, San Antonio
Cynthia Gulledge, Tufts University
Heather Henning, University of California, Berkeley
James Hitt, State University of New York Health Science Center
Adam Kepecs, Brandeis University
Achim Klug, University of Texas
Daniel Major, University of California, San Diego
Johnathan Melville, Oregon State University
Kush Paul, University of Texas, Dallas
Daphne Soares, University of Maryland
Haiyang Tao, Ohio University
Vivek Unni, Columbia University
Angela Wonsettler Ridgel, Marshall University School of Medicine
Michele Zee, University of Oregon

Neurobiology (June 14–August 15)

Directors

Gary Banker, Oregon Health Sciences University
Daniel Madison, Stanford University Medical Center

Section Directors

Michael Greenberg, Childrens' Hospital
Stephen Smith, Stanford University Medical Center

Faculty

Susan Birren, Brandeis University
Azad Bonni, Children's Hospital
Gabriel Corfas, Children's Hospital
Kerry Delaney, Simon Fraser University, Canada
Donald Faber, Allegheny University of the Health Sciences
Philip Haydon, Iowa State University
Kamran Khodakhah, University of Colorado School of Medicine
Diane Lipscombe, Brown University
David Ogden, National Institute for Medical Research, United Kingdom
Thomas Reese, National Institutes of Health
Felix Schweizer, University of California, Los Angeles
Morgan Sheng, Howard Hughes Medical Institute
Ruth E. Siegel, Case Western Reserve University
Carolyn Smith, National Institutes of Health
Mark Terasaki, University of Connecticut Health Center
Stuart Thompson, Stanford University
David Van Vactor, Harvard Medical School
Susan Wray, National Institutes of Health
Joshua Zimmerberg, National Institutes of Health

Teaching Assistants

Brie Linkenhoker, Stanford University
Alberto Pereda, Allegheny University of the Health Sciences
Martine Usdin, Stanford University Medical Center
David Jack Waters, Stanford University

Lecturers

George Augustine, Duke University Medical Center
Ann Marie Craig, University of Illinois
Tom Curran, St. Jude Children's Research Hospital
Peter Di Stefano, Millennium Pharmaceuticals
John Heuser, Washington University Medical School
Julie Ann Kauer, Duke University Medical Center
Jeff Lichtman, Washington University Medical School
Fred Sigworth, Yale University
Karel Svoboda, Cold Spring Harbor Laboratory

Course Assistants
Tara Bennett, Dartmouth College
Sarah Boies, Brandeis University

Students
Leonardo Belluscio, Columbia University
Sunghoe Chang, University of Illinois
Esther Chapin, Wayne State University
Eyal Jacobson, Technion, Israel
J. Troy Littleton, University of Wisconsin
Jennifer O'Brien, University of Washington
Francesco Rossi, Scuola Normale Superiore, Pisa, Italy
Mari Takasu, Harvard University
Kristen Thomas, Emory University
Jing Wang, Bell Laboratories
Linda Wilbrecht, Rockefeller University
Ming Zhou, State University of New York, Buffalo

Physiology: Cellular and Molecular Biology
(June 14–July 25)

Directors
Kerry Bloom, University of North Carolina, Chapel Hill
Mark Mooseker, Yale University

Faculty
Jonathan Chernoff, Fox Chase Cancer Center
Sydney P. Craig, University of North Carolina, Chapel Hill
Ann E. Eakin, University of North Carolina, Chapel Hill
Richard Fehon, Duke University Medical Center
Antony Galione, University of Oxford, United Kingdom
Daniel Kiehart, Duke University Medical Center
Daniel Lew, Duke University Medical Center
Mary Ann Sells, Fox Chase Cancer Center
Steve Stricker, University of New Mexico
Edwin Taylor, University of Chicago
Joseph S. Wolenski, Yale University

Teaching Assistants
Elaine Bardes, Duke University Medical Center
Bhutorn Canyuk, University of North Carolina, Chapel Hill
Marc Champagne, Duke University Medical Center
Elaine Chin, University of North Carolina, Chapel Hill
Janice Crawford, Duke University Medical Center
Benjamin Dale, University of New Mexico Medical School
Lisa Evans, Yale University
Tama Hasson, Yale University
Amanda Hayward-Lester, Yale University
Christian Lee, University of North Carolina, Chapel Hill
Robert Loudon, Fox Chase Cancer Center
Valerie Mermall, Yale University
Ruth Montague, Duke University Medical College
Penny Post, Yale University
Samara Reck-Peterson, Yale University
Melissa Reeder, Fox Chase Cancer Center
Chandra Theesfeld, Duke University Medical Center
Hao Zhu, Duke University Medical Center

Lecturers
Lorena Beese, Duke University Medical Center
John Condeelis, ASB/AECOM
Jennifer Doudna, Yale University
Rafael Fissore, University of Massachusetts
Robert Fletterick, University of California, San Francisco
William Kaelin, Dana-Farber Cancer Institute
Douglas Koshland, Carnegie Institution of Washington
Peter Matthias, Swiss Institute for Experimental Cancer Research, Switzerland
Ilaria Rebay, Whitehead Institute

Lab Assistant
Ben Mooseker, Hamden High School

Course Coordinator
Dawn Grant, Louisiana State University Medical Center

Course Assistant
Abigail Day, Trinity College

Students
Carolina Arancibia, Imperial College, United Kingdom
Antonia Avila, Centro de Investigacion y de Estudios Avanzados, Mexico
Christopher Bjornsson, University of Manitoba, Canada
Mia Champion, University of California, Davis
Janet Chenevert, National Center of Scientific Research, France
Brinda Dass, Texas Tech University Health Sciences
Bettina Deavours, Virginia Tech
Amy Gladfelter, Duke University
Kerimi Gokay, University of Arizona
Cruz Hinojos, University of Texas, Houston
Javier Irazoqui, Duke University
Shann Kim, University of Illinois, Chicago
Joyce King, Emory University
Svetlana Komarova, NASA Ames Research Center
Phoebe Lam, Princeton University
Samuel Lamitina, Emory University
Agnes Lee, Yale University
Emily Locke, Johns Hopkins University
Malini Mansharamani, Texas Tech University Health Science
Jonathan Marchant, University of California, Irvine
Felix Omara, Université de Québec, Canada
Koen Paemeleire, University of Ghent, Belgium
Leocadia Paliulis, Duke University
Kartik Pappu, Wesleyan University
Linda Runft, University of Connecticut
Amy Shaub, University of North Carolina, Chapel Hill
Drina Sta. Iglesia, George Washington University Medical School
Marcia Stickler, San Jose State University
Jesse Stricker, Duke University
Tsahai Tafari, University of California, San Diego
Sinji Tauhata, University of São Paulo, Brasil
Brian Uher, University of Pennsylvania
Johannes Vos, University of Massachusetts
Eric Wanger, Duke University
Stacy Weber, Ohio University
Rania Zaarour, Yale University

Special Topics Courses

Analytical & Quantitative Light Microscopy
(May 7–May 15)

Directors
Greenfield Sluder, University of Massachusetts Medical Center
David Wolf, University of Massachusetts Medical Center

Faculty
William B. Amos, Medical Research Council, United Kingdom
Richard Cardullo, University of California, Riverside
Jeff Gelles, Brandeis University
Shinya Inoué, Marine Biological Laboratory
Rudolf Oldenbourg, Marine Biological Laboratory
Peter Quinby, University of Massachusetts Medical Center
Edward Salmon, University of North Carolina, Chapel Hill
Randi Silver, Cornell University Medical College
Kenneth Spring, National Institutes of Health
Jason Swedlow, Harvard Medical School
Yu-li Wang, University of Massachusetts Medical Center

Teaching Assistants
Christine Thompson, University of Massachusetts Medical Center
Elizabeth Thompson, University of Massachusetts Medical Center

Course Coordinator
Frederick Miller, University of Massachusetts Medical Center

Students
Iain Asplin, Duke University
Marcia Babcock, Ribozyme Pharmaceuticals, Inc.
James Boyer, Yale University
Charles Capaday, Université Laval, Canada
Paul Clute, Wellcome/CRC Institute, United Kingdom
Carol Dieckmann, University of Arizona
Diane Finegood, Simon Fraser University, Canada
Alfredo Franco-Obregon, Children's Hospital
Dian Gifford, University of Rhode Island
Daniel Gist, University of Cincinnati
Makoto Goda, Kyoto University, Japan
Dean Gute, Louisiana State University
Jim Henthorn, University of Oklahoma
Ann Hubbard, Johns Hopkins Medical School
Kristine Jernigan, National Cancer Institute
David Kang, Boston University
Ed Kuczmarski, Northwestern University
Karen Lee, Hong Kong University, Hong Kong
Jerry Lin, Harvard Medical School
Didier Marguet, Johns Hopkins University
Robin Mayfield, Massachusetts General Hospital
Francis McGowan, Children's Hospital
Lennart Ohlsson, Pharmacia and Upjohn, Sweden
Aimo Oikari, University of California, Davis
Sushil Sarna, Medical College of Wisconsin
Matthew Savoian, State University of New York, Albany
Robert Tarran, University of North Carolina, Chapel Hill
Eric Weeks, University of Pennsylvania

Frontiers in Reproduction: Molecular and Cellular Concepts and Applications
(May 26–July 5)

Directors
Joan Hunt, University of Kansas Medical Center
Kelly Mayo, Northwestern University
Gerald Schatten, Oregon Health Sciences University

Faculty
Mario Ascoli, University of Iowa
Jeffery A. Bowen, University of Kansas Medical Center
Sally Camper, University of Michigan Medical School
Barbara Anne Croy, University of Guelph, Canada
Susan Fisher, University of California, San Francisco
Alan Handyside, St. Thomas' Hospital, United Kingdom
John C. Herr, University of Virginia School of Medicine
Laurinda Jaffe, University of Connecticut Health Center
Paul Linnemeyer, Veterans Administration Medical Center
Roger Pederson, University of California, San Francisco
Jeffrey W. Pollard, Albert Einstein College of Medicine
Margaret Shupnik, University of Virginia Medical Center
Calvin Simerly, Oregon Regional Primate Research Center
Paul D. Soloway, Roswell Park Cancer Institute
Tim Stearns, Stanford University
Mark Terasaki, University of Connecticut Health Center
Jonathan L. Tilly, Massachusetts General Hospital
Nancy Weigel, Baylor College of Medicine
Debra Wolgemuth, Columbia University

Teaching Assistants
Mark Berard, University of Michigan
Leigh Ann Bush, University of Virginia Health Sciences Center
Alan Diekman, University of Virginia Health Sciences Center
Tanja Dominko, Oregon Regional Primate Research Center
Laura Hewitson, Oregon Regional Primate Research Center
Kenneth Klotz, University of Virginia Health Sciences Center
Abir Mukherjee, Northwestern University
Alan Packer, Columbia University
Teresa Phillips, University of Kansas Medical Center
P. Prabhakara Reddi, University of Virginia Health Sciences Center
Brian Rowan, Baylor College of Medicine
Linda Runft, University of Connecticut Health Center
Anne Westbrook, University of Virginia Health Sciences Center

Lecturers
Richard Behringer, University of Texas
Richard Bronson, State University of New York, Stony Brook
David Carroll, University of California, Santa Barbara
Alta Charo, University of Wisconsin
William Crowley, Harvard Center for Reproduction
Harvey Florman, Tufts University School of Medicine
Lothar Hennighausen, National Institutes of Health
Joseph Hill, Brigham and Women's Hospital
David Keefe, Marine Biological Laboratory
Luigi Mastroianni, University of Pennsylvania Medical Center
D. Michael Nelson, Washington University
John Nilson, Case Western Reserve Medical School
Pasquale Patrizio, University of Pennsylvania Medical Center
Jon Pryor, University of Minnesota Medical School
JoAnne Richards, Baylor College of Medicine
Peter N. Schlegel, New York Hospital

Richard Schultz, University of Pennsylvania
Andrew Shenker, Children's Memorial Hospital
Victor Vacquier, University of California, San Diego
Gary Wessel, Brown University
Judith White, University of Virginia Health Science Center

Course Administrator

Michele Emme, Oregon Health Sciences University

Course Coordinators

Lisa D'Oger de Speville, University of the Witwatersrand, South Africa
Crista Martinovich, Oregon Regional Primate Research Center
Christopher Payne, Oregon Health Sciences University

Students

Fabian Arechavaleta-Velasco, National Institute of Nutrition, Mexico
Mohd Beg, National Institute of Immunology, India
Mary Jo Carabatsos, Tufts University
Chie-Pein Chen, MacKay Memorial Hospital, Taiwan
Débora Cohen, Instituto de Biologia y Medicina Experimental, Argentina
Susan Euling, US Environmental Protection Agency
Anna Grazul-Bilska, North Dakota State University
Lisa Halvorson, Brigham and Women's Hospital
Ricardo Moreno, Oregon Regional Primate Research Center
Todd Rosen, New York University Medical Center
Susana Rulli, Hospital General de Ninos Ricardo Gutierrez, Argentina
Ramasamy Sampath Kumar, University of Western Ontario, Canada
Luis Sánchez-Partida, University of Adelaide, Australia
João Santos, Oregon Regional Primate Research Center
Lisa Schwartz, New York University Medical Center
Yukihiro Terada, Oregon Regional Primate Research Center

Fundamental Issues in Vision Research
(August 16–August 29)

Director

David Papermaster, University of Connecticut Health Center

Faculty

Robert Barlow, State University of New York Health Science Center
Ben Barres, Stanford University
David C. Beebe, Washington University School of Medicine
Eliot Berson, Massachusetts Eye and Ear Infirmary
David Birk, Tufts University School of Medicine
Dean Bok, University of California Medical School
Constance Cepko, Harvard University Medical School
John Clark, University of Washington
Patricia D'Amore, Children's Hospital
Kay Dickersin, University of Maryland
John E. Dowling, Harvard University
Thomas Ferguson, Washington University School of Medicine
Jonathan Horton, University of California, San Francisco
Joseph Horwitz, University of California, Los Angeles
Simon John, Jackson Laboratory
Carl Kupfer, National Institutes of Health
M. Cristina Leske, State University of New York Health Science Center
Ellen Liberman, National Institutes of Health
Richard Maas, Brigham and Women's Hospital
Robert Malchow, University of Illinois, Chicago
Richard Masland, Massachusetts General Hospital
Susan McConnell, Stanford University
Orson Moritz, University of Connecticut Health Center
Jeremy Nathans, Johns Hopkins University School of Medicine
Jerry Niederkorn, University of Texas
Paul A. Overbeek, Baylor College of Medicine
Krzysztof Palczewski, University of Washington
Joram Piatigorsky, National Institutes of Health
Haohua Qian, Harvard University
Elio Raviola, Harvard University Medical School
Val Sheffield, University of Iowa Hospital & Clinics
Dwight Stambolian, University of Pennsylvania
Stephen P. Sugrue, University of Florida College of Medicine
Tung-Tien Sun, New York University Medical Center
Beatrice Tam, University of Connecticut Health Center
Paul Wasson, Eye Health Services
Scott Whitcup, National Institutes of Health
Robert Wurtz, National Institutes of Health

Students

Ananth Badrinath, University of Wisconsin, Madison
Kenneth Beckman, University of California, Berkeley
Indranil Das, Cornell University Medical College
Claudia Garcia, Harvard University
Fang-Cheng Hung, Baylor College of Medicine
Jeanette Hyer, Cornell University Medical College
Anh-Chi Le, Oregon Health Sciences University
Vivian Lee, Oregon Health Sciences University
Donna Lehman, University of Texas Health Science Center
Angelique Louie, California Institute of Technology
Donna Mackay, Institute of Ophthalmology London, United Kingdom
Morgan McNamara, Lawrence Berkeley National Laboratory
Alicia Paulson, University of Texas M.D. Anderson
James Peterson, University of California, Davis
Francesca Pignoni, University of California, Los Angeles
Luanna Putney, University of California, Davis
Susan Robinson, University of Texas Southwestern
Mark Rosenblatt, University of Miami
Noah Shroyer, Baylor College of Medicine
Kelly Wentz-Hunter, University of Illinois, Chicago

Medical Informatics (May 31–June 7)

Director

Daniel Masys, University of California, San Diego

Faculty

Paul Clayton, Columbia University
George Hripcsak, Columbia-Presbyterian Medical Center
Lawrence Kingsland, National Library of Medicine
David Landsman, National Library of Medicine
Donald D.A.B. Lindberg, National Library of Medicine
Carol Newton, University of California, Los Angeles
Richard Rodgers, National Library of Medicine
Charles Safran, Center for Clinical Computing
Soumitra Sengupta, Columbia University

Students

Martha Adamson, University of Texas Southwestern Medical Center Library
Joanna Barnett, Baystate Health System
Nancy Bryant, Morehouse School of Medicine
James Chambliss, University of Chicago
Steven Cohn, State University of New York, Brooklyn
Susan Conley, St. Christopher's Hospital for Children
Elizabeth Connor, Medical University of South Carolina
Douglas Einstadter, MetroHealth Medical Center
Kimberly Guenther, University of Virginia
Fred Hashimoto, University of New Mexico Health Sciences
Gerelyn Henry-Sam, Xavier University, Louisiana College of Pharmacy
Kellie Kaneshiro, Indiana University
Steven Karch, City of Las Vegas
Martin Klein, New York Medical College
David Munson, United States Navy
Scott Norton, Bliss Army Health Clinic
Edward Ratner, Allina Health System
Joan Redmond Leonard, Centers for Disease Control and Prevention
James Reilly, State University of New York, Brooklyn
Mary Ryan, University of Arkansas
Robert Saqueton, Cook County Hospital
Alan Silver, Long Island Jewish Medical Center
Susan Silverton, University of Pennsylvania
Steven Sivak, Saint Vincent's Hospital
Julia Sollenberger, University of Rochester Medical Center
John Stey, University of Connecticut Health Center
Lisa Traditi, University of Colorado Health Sciences
Kathleen Wagner, Gundersen Lutheran Medical Center
Susan Whitmore, National Institutes of Health
John Woodward, United States Army Graduate Program

Methods in Computational Neuroscience

(August 2–August 29)

Directors

William Bialek, NEC Research Institute
Rob de Ruyter van Steveninck, NEC Research Institute

Faculty

Lawrence Abbott, Brandeis University
Carol Colby, University of Pittsburgh
Thomas Collett, University of Sussex, United Kingdom
Kerry Delaney, Simon Fraser University, Canada
Allison Doupe, University of California, San Francisco
Bard Ermentrout, University of Pittsburgh
John Hopfield, Princeton University
Daniel Johnston, Baylor College of Medicine
Darcy Kelley, Columbia University
David Kleinfeld, University of California, San Diego
Nancy Kopell, Boston University
Eve Marder, Brandeis University
Markus Meister, Harvard University
Partha Mitra, Lucent Technologies
Fred Rieke, University of Washington
H. Sebastian Seung, Lucent Technologies
Karen Sigvardt, University of California, Davis
Haim Sompolinsky, Hebrew University of Jerusalem, Israel
Lubert Stryer, Stanford University Medical School
David Tank, AT&T Bell Laboratories
Naftali Tishby, Hebrew University of Jerusalem, Israel
Steven Zucker, Yale University

Teaching Assistants

B. Aguera y Arcas, Princeton University
Roderick Jensen, Wesleyan University
Roland Koberle, Universidade di São Paulo, Brasil
Lowell McLinskey, Wesleyan University
Maoz Shamir, Hebrew University of Jerusalem, Israel
John White, Boston University

Lecturers

Denis Baylor, Stanford University Medical Center
Simon Barry Laughlin, University of Cambridge, United Kingdom
Nikos Logothetis, Max-Planck-Institute for Biological Cybernetics, Germany

Students

Rony Azouz, University of California, Davis
Riccardo Barbieri, Massachusetts General Hospital
Francesco Battaglia, SISSA, Italy
Guoqiang Bi, University of California, San Diego
Naama Brenner, NEC Research Institute
Daniel Butts, University of California, Berkeley
Thomas Euler, Massachusetts General Hospital
Adrienne Fairhall, Weizmann Institute, Israel
Jordan Feidler, University of Pittsburgh
Matthew Fellows, Brown University
Jed Hartings, University of Pittsburgh
Mathew Jones, The Vollum Institute
Adam Kepecs, Brandeis University
Ann Lee, Brown University
Christian Machens, Humboldt University, Germany
Anna Majewska, Columbia University
Thomas Oertner, Max Planck Society, Germany
Dmitry Rinberg, NEC Research Institute
Stephanie Ruggiano, Boston University
Mark Van Rossum, University of Pennsylvania
Brian Wright, University of California, San Francisco
Ying Zhang, Harvard Medical School

Microinjection Techniques in Cell Biology

(May 19–May 26)

Director

Robert B. Silver, Marine Biological Laboratory

Faculty

Susan Cousins, Cornell University
Chris Fox, Kent State University
Suzanne Klaessig, Cornell University
Douglas Kline, Kent State University
Eric Shelden, University of Michigan

Course Assistant

Leslie King, Duke University

Students

Crislyn D'Souza-Schorey, Washington University School of Medicine
Ali Eroglu, Massachusetts General Hospital

Gyorgy Hajnoczky, Thomas Jefferson University
Georgi Kalbin, Göteborg University, Sweden
Seher Khan, Penn State University
Loro Kujjo, Northeastern University
Laura Linz, Louisiana State University
Yijuan Liu, Amgen Inc.
Jorge Maldonado, University of Puerto Rico
Philip McAllister, National Fish Health Research Laboratory
Kellene Mullin, Rockefeller University
Anna Pappalardo, University of Connecticut
Peter Peters, University of Utrecht, The Netherlands
Susan Rotenberg, Queens College–CUNY
Marcia Stickler, San Jose State University
Anne Vallerga, SRI International

Molecular Mycology: Current Approaches to Fungal Pathogenesis *(August 9–August 29)*

Directors
John Edwards, Jr., Harbor-UCLA Medical Center
Paul T. Magee, University of Minnesota
Aaron P. Mitchell, Columbia University

Faculty
Arturo Casadevall, Albert Einstein College of Medicine
Gary T. Cole, Medical College of Ohio
Beth Di Domenico, Schering Plough Research Institute
Scott Filler, Harbor-UCLA Medical Center
Gerald Fink, Whitehead Institute of Biomedical Research
William Fonzi, Georgetown University Medical Center
William Goldman, Washington University School of Medicine
Joseph Heitman, Duke University Medical Center
Margaret Hostetter, Yale University
Judith Rhodes, University of Cincinnati
Stewart Scherer, Acacia Biosciences
Stephen Sprang, Howard Hughes Medical Institute
Paula Sundstrom, Ohio State University
Theodore White, Seattle Biomedical Research Institute
Jianping Xu, Duke University Medical Center

Course Assistant
Kristin DeArruda, University of Minnesota

Students
Patricia Cisalpino, Universidade Federal de Minas Gerais, Brasil
Donna Dunyak, Pharmacia and Upjohn
Heather Edens, Montana State University
Elsa Haubold, University of Texas Medical Branch
Neil Haycocks, University of Texas Medical Branch
Samuel Lee, Yale University School of Medicine
Trina Maurice, Bristol-Myers Squibb
Mookly Nagabhushan, Loyola University
Cheryl Quinn, Pharmacia and Upjohn
Rosaria Santangelo, Public Health Research Institute
Raffael Schaffrath, University of Halle, Germany
Don Sheppard, McGill University, Canada
Susan Smith, Mitotix, Inc.
Ming Wang, Vanderbilt University School of Medicine
Ping Wang, Duke University
John Wilks, Pharmacia and Upjohn

Neural Development and Genetics of Zebrafish
(August 16–August 28)

Directors
John E. Dowling, Harvard University
Nancy Hopkins, Massachusetts Institute of Technology

Faculty
Robert Baker, New York University Medical Center
Chi-Bin Chien, University of Utah Medical Center
Andres Collazo, House Ear Institute
Pierre Drapeau, McGill University, Canada
Judith S. Eisen, University of Oregon
Mark C. Fishman, Massachusetts General Hospital
Roger Hanlon, Marine Biological Laboratory
Nigel Holder, University College London, United Kingdom
Charles Kimmel, University of Oregon
Stephen Wilson, University College London, United Kingdom

Teaching Assistants
Andrew Bass, Cornell University
Thomas Becker, Massachusetts Institute of Technology
Jau-Nian Chen, Massachusetts General Hospital
Jonathan Clarke, University College London, United Kingdom
James Fadool, Auburn University
Michael Granato, University of Pennsylvania
Cecilia Moens, Fred Hutchinson Cancer Research Center
Mary Mullins, University of Pennsylvania
Torsten Trowe, Max-Planck-Institut für Entwicklungsbiologie, Germany
Charline Walker-Durchanek, University of Oregon

Lecturers
Keith Astrosfky, Massachusetts Institute of Technology
Colleen Boggs, Massachusetts General Hospital
Corinne Houart, University College London, United Kingdom
Janet Rossant, Mount Sinai Hospital, Canada

Lab Technicians
Beth Linnon, Marine Biological Laboratory
Hiroshi Suwa, New York University Medical Center

Course Coordinator
Ellen Schmitt, Harvard University

Students
Veronica Burzio, University of Chile, Chile
Christine Byrd, Western Michigan University
Miguel Concha, University of Chile, Chile
Victoria Connaughton, National Institutes of Health
Gianluca Gallo, University of Minnesota
Tatsumi Hirata, Nagoya University, Japan
James Jontes, Stanford University
James Kappler, Rockefeller University
Matthew McFarlane, Stanford University
Christine McGiflert, University of California, San Diego
Ferenc Müller, Universite Louis Pasteur, France
Michael Rebagliati, National Institutes of Health
Louis St. Amant, McGill University, Canada
Ava Udvadia, Duke University
Feng Wang, Yale University
Andrew Waskiewicz, Fred Hutchinson Cancer Research Center

Neurobiology and Development of the Leech (August 8–August 29)

Directors

Christine Sahley, Purdue University
Martin Shankland, University of Texas, Austin

Faculty

Andreas Baader, University of Berne, Switzerland
Michael Baker, Columbia University
Shirley Bissen, University of Missouri
Peter Brodfuehrer, Bryn Mawr College
Pierre Drapeau, McGill University, Canada
Francisco Fernandez de Miguel, Universidad Nacional Autonoma de Mexico
Jorgen Johansen, Iowa State University
Anna Kleinhaus, New York Medical College
Eduardo Macagno, Columbia University
Barbara Modney, Cleveland State University
Kenneth Muller, University of Miami School of Medicine
John Nicholls, University of Basel, Switzerland
Rob Savage, Williams College
Elaine Seaver, University of Texas, Austin
Jay Yang, University of Rochester Medical Center

Course Assistant

Samantha Neubert, Marine Biological Laboratory

Students

Brian Clinton, Columbia University
Elizabeth Garcia Perez, Universidad Nacional Autonoma de Mexico
Shanta Kumar, Purdue University
Chris Lemon, Binghamton University
Riccardo Mozzachiodi, University of Pisa, Germany
Hiroshi Ohnishi, Mitsubishi Kasei Institute of Life Sciences, Japan
Amy Palmer, Purdue University
Stéphanie Ratté, McGill University, Canada
Maria Luiza, University of Brasil
Vishnu Suppiramaniam, Tuskegee University
Marie Wintzer, University of Basel, Switzerland
Gary Yamaguchi, Arizona State University

Optical Microscopy and Imaging in the Biomedical Sciences (October 7–October 15)

Director

Colin Izzard, State University of New York, Albany

Faculty

Joseph DePasquale, New York State Department of Health
Robert Hard, University of Washington
Brian Herman, University of Texas Health Science Center
Frederick Maxfield, Cornell University Medical College
John Murray, University of Pennsylvania
David M. Piston, Vanderbilt University
Kenneth Snyder, State University of New York, Buffalo
Kenneth Spring, National Institutes of Health
Jason Swedlow, University of Dundee, United Kingdom

Teaching Assistants

Kenneth Dunn, Indiana University Medical Center
Lynda Pierini, Cornell University Medical College
Wade Sigurdson, State University of New York, Buffalo

Lecturers

Shinya Inoué, Marine Biological Laboratory
H. Ernst Keller, Zeiss Optical Systems
Rudolf Oldenbourg, Marine Biological Laboratory
Martin Scott, Consultant in Scientific Imaging

Students

Holly Aaron, University of California, Berkeley
James Arden, Cornell University Medical College
Stefan Bodnarenko, Smith College
Daniel Brown, Beth Israel-Deaconess Medical Center
Antoine Caron, Biotechnology Research Institute, Canada
Richard Edelmann, Miami University
Peter Gakunga, Baylor College of Dentistry
Yimin Ge, Massachusetts General Hospital
Darren Gilmour, Max-Planck-Institut, Tübingen, Germany
Oliver Hobert, Massachusetts General Hospital
Lidia Llcus, National Institutes of Health
Brian Kinkle, University of Cincinnati
Lena McPhee, Queen's University, Canada
Kellene Mullin, Rockefeller University
Gertrude Nicklee, Princess Margaret Hospital, Canada
Peter Pryfogle, Lockheed Martin Idaho Technologies
Derrick Robinson, Johns Hopkins University
Bénédicte Sanson, MRC-Lab of Molecular Biology, United Kingdom
Jodi Shann, University of Cincinnati
Cha-Min Tang, University of Maryland School of Medicine
Barbara Tolloczko, Montreal Chest Institute, Canada
Martin Völcker, Carl Zeiss Jena, Germany
Nicki Watson, Whitehead Institute
Douglas Weidner, University of Texas MD Anderson Cancer Center

Rapid Electrochemical Measurements in Biological Systems (May 14–May 18)

Director

Greg Gerhardt, University of Colorado Health Sciences Center

Faculty

Scot Brock, University of Colorado Health Sciences Center
Wayne Cass, University of Kentucky
Daniel David, University of Colorado Health Sciences Center
Karen Giardina, University of Colorado Health Sciences Center
Alexander Hoffman, University of Colorado Health Sciences Center
Peter Huettl, University of Colorado Health Sciences Center
Michael Palmer, University of Colorado Health Sciences Center
James Michael Parrish, University of Colorado Health Sciences Center
Francois Pomerleau, Douglas Hospital Research Center, Canada
Scott Robinson, University of Colorado Health Sciences Center
Steven Robinson, University of Colorado Health Sciences Center
Ron Sullivan, Douglas Hospital Research Center, Canada

Students

Anne Andrews, National Institute of Mental Health
Subramaniam Apparsundaram, Vanderbilt University

Tracy Baker, University of Wisconsin, Madison
Paul Bartell, University of Virginia
Saloua Benmansour, University of Texas Health Science Center
Pascal Bochet, Brown University
Terry Bridal, Wyeth-Ayerst Research
Vladimir Chefer, National Institutes of Health
Michael Croning, Yale University
David Fickbohm, Georgia State University
Alan Frazer, University of Texas Health Science Center
Marc-Antoine, University of Montreal, Canada
Stefano Gustincich, Harvard Medical School
Andreas Hengstenberg, Ruhr Universität Bochum, Germany
Brad Hodgeman, University of Wisconsin, Madison
Weimin Hong, George Washington University
Adele Jackson, University of Toronto, Canada
Steven Mennerick, Washington University School of Medicine
Isabelle Mintz, Boston University
Barbara Musolf, Georgia State University
Toni Shippenberg, National Institutes of Health
James Smith, University of the West Indies, Jamaica
Istran Sziraki, N.S. Kline Institute
Akaysha Tang, University of New Mexico
Alexis Thompson, National Institutes of Health
Roger Thompson, McMaster University, Canada
Jeffery Wickens, Otago University, New Zealand
Marina Wolf, Chicago Medical School

Workshop on Molecular Evolution

(August 2–August 14)

Directors

Daniel B. Davison, Bristol-Myers Squibb PRI
Mitchell Sogin, Marine Biological Laboratory

Faculty

Michael Cummings, Marine Biological Laboratory
W. Ford Doolittle, Dalhousie University, Canada
Sean Eddy, Washington University
Theresa Gaasterland, Argonne National Laboratory
David Hillis, University of Texas
Mary Kuhner, University of Washington
James Lake, University of California, Los Angeles
David Landsman, National Library of Medicine
Laura Landweber, Princeton University
David Maddison, University of Arizona, Tucson
Michael Miyamoto, University of Florida
Spencer Muse, North Carolina State University
Gary Olsen, University of Illinois
William Pearson, University of Virginia Health Sciences Center
Monica Riley, Marine Biological Laboratory
Gary Stormo, University of Colorado, Boulder
David Swofford, Smithsonian Institution

Teaching Assistants

Andrew MacArthur, Marine Biological Laboratory
Janet Siefert, Rice University
Steven Thompson, Washington State University
Linda Amaral Zettler, Marine Biological Laboratory

Course Assistant

Marian Harris, Marine Biological Laboratory

Students

Lars Aagaard, University of Aarhus, Denmark
Luis Allende, Universidad Complutense, Spain
Judite Alves, University of Lisbon, Portugal
Lilia Ana Amigó, University of Puerto Rico
Stevan Arnold, Oregon State University
Miguel Arroyo, University of Puerto Rico
Horst Backhaus, University of Braunschweig, Germany
Heather Balchowsky, Nova Southeastern University
Elena Barbieri, University of Urbino, Italy
Arturo Becerra, Universidad Nacional Autonoma de Mexico
Andrew Bennett, University of Oxford, United Kingdom
Robb Brumfield, Smithsonian Institution
Patrick Calie, Eastern Kentucky University
Michael Charette, Dalhousie University, Canada
Yangrae Cho, Indiana University
Eddie Cytryn, Hebrew University of Jerusalem, Israel
Merel Dalebout, University of Auckland, New Zealand
Barbara Dietrich, University of Zurich, Switzerland
Kecia Echols, Morehouse School of Medicine
Matthew Fain, Southern Illinois University
Jack Fell, University of Miami
Patrick Ferree, Wake Forest University
David Graham, University of Illinois, Urbana-Champaign
Karen Hansen, University of Copenhagen, Denmark
Tetsuo Hashimoto, Institute of Statistical Mathematics, Japan
Wieger Homan, National Institute of Public Health and Environment, The Netherlands
David Horner, National History Museum, United Kingdom
Ravi Jain, University of California, Los Angeles
German Jurgens, University of Helsinki, Finland
Gila Kahila Bar-Gal, Hebrew University of Jerusalem, Israel
Patricia Lee, University of Oxford, United Kingdom
José Leguina, Universidad Nacional Autonoma de Mexico
Hsin-Fu Liu, University of Louvain, Belgium
Robert Liu, University of Florida
Mariana Mateos, Rutgers University
David McClellan, Louisiana State University
Leslie McNeil, University of Illinois
Antonia Monteiro, Harvard University
Jonathan Moore, University of California, Los Angeles
Karen Ober, University of Arizona, Tucson
Akiko Okusu, Harvard University/Woods Hole Oceanographic Institution
Matthew Olson, Vanderbilt University
Matthew Osentoski, University of Miami
Mathieu Perret, University of Geneva, Switzerland
Oxana Pickeral, Johns Hopkins University
Sanit Piyapattanakorn, Southampton University, United Kingdom
Gordon Plague, University of Georgia
Jacqueline Reich, University of California, Berkeley
Leslie Rissler, University of Virginia
Deborah Robertson, Harvard University
Axayacatl Rocha-Olivares, Scripps Institute of Oceanography
Benjamin Rosenthal, Harvard School of Public Health
Mahmood Shivji, Nova Southeastern University
Andreas Teske, Woods Hole Oceanographic Institution
Stephen Tsoi, National Institutes of Health
Sonia Van Dooren, Rega Institute, Belgium
Costantino Vetriani, Rutgers University
Eileen Wagner, University of Wisconsin, Milwaukee
Katarina Winka, Umeå University, Sweden
Gerben Zylstra, Rutgers University

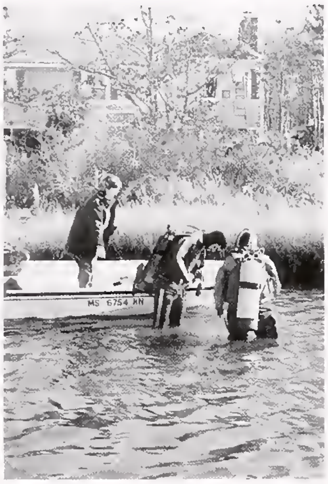

Other Programs

Semester in Environmental Science (September 6–December 17, 1998)

Directors

Jerry M. Melillo, Director
Kenneth H. Foreman, Associate Director

Faculty

Linda A. Deegan
Anne E. Giblin
John E. Hobbie
Charles S. Hopkinson, Jr.
George Lilies
Knute J. Nadelhoffer
Christopher Neill
Bruce J. Peterson
Edward B. Rastetter
Gaius R. Shaver
Paul A. Steudler
Joseph J. Vallino
Mathew Williams

Research and Teaching Assistants

Michelle Bahr
Marsha Chandler
Jeff Hughes
Sarah Jablonski
Sam Kelsey
Bonnie Kwiatkowski
Patricia Micks
Jason Wyda

Students

Ellen Carvill, Carleton College
Phoebe Chappell, Amherst College
Phoebe Congalton, Sarah Lawrence College
Cynthia Eldridge, Wellesley College
Angela Faíanunu, Middlebury College
Antonia Giardina, Colgate University
Aimee Kessler, Wellesley College
John McKay, Haverford College
Kathleen Radloff, Mt. Holyoke College
Alexis Schoppe, Dickinson College
Kyle Schwabenbauer, Allegheny College
Amanda Thimmayya, Bard College

Teachers' Workshop: Living in the Microbial World (August 16–August 22)

Course Director

Lorraine Olendzenski, University of Connecticut

Course Assistant

Arturo Beccera, Universidad Nacional Autonoma de Mexico

Presenters

Lynn Margulis, University of Massachusetts, Amherst
Steve Oliver, Boston University
Ricardo Guerrero, University of Barcelona, Spain
Beverly, University of Puget Sound
Robert Bullis, Marine Biological Laboratory
Paul Dunlap, Center of Marine Biotechnology, Maryland
Alistair Simpson, University of Sydney
Adrian Smith, Marine Biological Laboratory
Colleen Cavanaugh, Harvard University
Rebecca Gast, Woods Hole Oceanographic Institute
Art Girard, Pfizer Central Research, Groton, Connecticut
Norman Wainwright, Marine Biological Laboratory

Teacher Participants

Margaret Brumsted, Dartmouth High School, Massachusetts
Fran Shabica, Dartmouth High School, Massachusetts
Lorraine DeIlelo, Whitman Middle School, Massachusetts
Beverly Hassan, Whitman Middle School, Massachusetts
Hans Melder, Holbrook Jr./Sr High School, Massachusetts
Stacy Kaplan, Holbrook Jr./Sr High School, Massachusetts
Ann Hinson, Adams Middle School, Guilford, Connecticut
Charlotte Klinkhammer, Adams Middle School, Guilford, Connecticut
Saundra Newsom, Vigo County School Corporation, Terre Haute, Indiana
Deb Kuikendall, Vigo County School Corporation, Terre Haute, Indiana
Shirley Cox, Mitchell High School, Memphis, Tennessee
Naomi Burwell, Bernard Campbell Junior High School, Lee's Summit, Missouri
Kent Eisler, Bernard Campbell Junior High School, Lee's Summit, Missouri
Andrea Webster, Norton Knatchbull School, Kent, United Kingdom
Andrew Dyson, Norton Knatchbull School, Kent, United Kingdom
Gill Griffith, Ursiline College, Kent, United Kingdom
Franciska Maré, Ursiline College, Kent, United Kingdom

Summer Research Programs

Principal Investigators

Allen, Nina, North Carolina State University
Alliegro, Mark C., Louisiana State University Medical Center
Armstrong, Clay, University of Pennsylvania
Armstrong, Peter B., University of California, Davis
Augustine, George J., Duke University Medical Center

Barlow, Jr., Robert B., State University of New York Health Science Center
Beaugé, Luis, Instituto de Investigacion Medica "Mercedes y Martin Ferreyra," Argentina
Ben-Jonathan, Nira, University of Cincinnati
Bennett, Michael V. L., Albert Einstein College of Medicine
Bodznick, David, Wesleyan University
Bovard, Brian D., Duke University
Boyer, Barbara, Union College
Brady, Scott T., The University of Texas Southwestern Medical Center, Dallas
Brown, Joel E., Albert Einstein College of Medicine
Browne, Carole, Wake Forest University School of Medicine
Burger, Max M., Friedrich Miescher Institut, Switzerland

Cai, Wei-Jun, University of Georgia
Cardell, Robert R., University of Cincinnati
Chappell, Richard L., Hunter College, City University of New York
Cohen, Lawrence B., Yale University School of Medicine
Cohen, William D., Hunter College, City University of New York
Corwin, Jeffrey, University of Virginia
Costello, John, Providence College

De Weer, Paul, University of Pennsylvania School of Medicine
DiPolo, Reinaldo, IVIC, Venezula
Dodge, Frederick, State University of New York Health Science Center
Doetschman, Thomas, University of Cincinnati

Eckberg, William, Howard University
Ehrlich, Barbara, University of Connecticut Health Center
England, Pamela, California Institute of Technology
Eriksson, John E., Turku Center for Biotechnology, Finland

Fay, Richard, Loyola University of Chicago
Fishman, Harvey M., University of Texas Medical Branch, Galveston
Flamarique, Iñigo Novales, University of Victoria, Canada

Gadsby, David, Rockefeller University
Gerhart, John, University of California, Berkeley
Gimelbrant, Alexander A., University of Kentucky Medical Center
Giuditta, Antonio, University of Naples, Italy
Giusti, Andrew Frank, University of California, Santa Barbara
Goldman, Robert D., Northwestern University Medical School
Groden, Joanna, University of Cincinnati

Haimo, Leah, University of California, Riverside
Halstead, Matthew, University of Auckland, New Zealand
Heck, Diane, Rutgers University
Henry, Jonathan J., University of Illinois
Hershko, Avram, Technion, Israel
Highstein, Steven M., Washington University School of Medicine
Hines, Michael, Yale University School of Medicine
Holz, George, New York University Medical Center
Hoskin, Francis, US Army Natick RD&E Center

Ip, Wallace, University of Cincinnati

Jessen-Eller, Kathryn, Tufts University
Johnston, Daniel, Baylor College of Medicine
Jonas, Elizabeth, Yale University School of Medicine
Jones, Teresa, National Institutes of Health

Kaczmarek, Leonard, Yale University School of Medicine
Kaplan, Barry, National Institutes of Mental Health
Kaplan, Ilene M., Union College
Khan, Sohaib, University of Cincinnati
Kier, William, University of North Carolina, Chapel Hill
King, Jane Roche, University of Arizona
Kirschner, Marc, Harvard Medical School
Kubke, Maria Fabiana, University of Maryland
Kuhns, William, The Hospital for Sick Children, Canada

Lafer, Eileen M., University of Texas Health Science Center
Landowne, David, University of Miami School of Medicine
Langford, George, Dartmouth College
Lartillot, Nicolas, Université Paris-Sud, France
Laskin, Jeffrey, University of Medicine and Dentistry of New Jersey
Lenzi, David P., University of Oregon
Lipicky, Raymond J., Food and Drug Administration
Llinás, Rodolfo R., New York University Medical Center
Loboda, Andrey, University of Pennsylvania
Lorez, Matthias, University of Zurich, Switzerland

Major, Guy, Lucent Technologies
Martindale, Mark, University of Chicago
Martinez, Joe, University of Texas, San Antonio
McAllister, A. Kimberly, Salk Institute of Biological Studies
McNeil, Paul, Medical College of Georgia

Mead, Kristina S., University of California, Berkeley
Mensinger, Allen, Washington University School of Medicine
Metuzals, Janis, University of Ottawa Faculty of Medicine, Canada
Moore, John W., Duke University Medical Center

Nasi, Enrico, Boston University School of Medicine

Palazzo, Robert, University of Kansas
Pant, Harish, National Institutes of Health
Pierson, Beverly, University of Puget Sound
Pixley, Sarah, University of Cincinnati
Puga, Alvaro, University of Cincinnati

Quigley, James P., State University of New York, Stony Brook

Rakowski, Robert F., Finch University of Health Sciences/The Chicago Medical School
Rasmussen, Howard, Medical College of Georgia
Ratner, Nancy, University of Cincinnati
Reese, Thomas S., National Institutes of Health
Rieder, Conly, Wadsworth Center
Ripps, Harris, University of Illinois College of Medicine
Rome, Larry, University of Pennsylvania
Ruderman, Joan V., Harvard Medical School
Russell, John M., Medical College of Pennsylvania

Seaver, Elaine C., University of Texas, Austin
Siwicki, Kathleen, Swarthmore College
Sloboda, Roger D., Dartmouth College
Spiegel, Evelyn, Dartmouth College
Spiegel, Melvin, Dartmouth College
Stuart, Ann E., University of North Carolina, Chapel Hill
Sugimori, Mutsuyuki, New York University Medical Center

Telzer, Bruce, Pomona College
Tilney, Lewis, University of Pennsylvania
Trinkaus, John P., Yale University
Troll, Walter, New York University Medical Center
Tytell, Michael, Bowman Gray School of Medicine, Wake Forest University

Wachowiak, Matt, Yale University School of Medicine
Wang, Hong-Sheng, State University of New York, Stony Brook
Weidner, Earl, Louisiana State University
Wicklein, Martina, University of Arizona

Yamoah, Ebenezer, University of Cincinnati

Zecevic, Dejan P., Yale University School of Medicine
Zheng, James, University of Medicine and Dentistry of New Jersey
Zimmerberg, Joshua, National Institutes of Health
Zottoli, Steven, Williams College
Zukin, R. Suzanne, Albert Einstein College of Medicine

Other Research Personnel

Abe, Terno, Niigata University, Japan
Ahmed, Tanweer, University of Leeds, United Kingdom
Altamirano, Anibal, Universidad de Buenos Aires, Argentina
Andersen, Kristen, University of Illinois, Chicago
Antic, Srdjan, Yale University School of Medicine
Anton, Roberto, Hunter College
Armstrong, Clara, University of Pennsylvania

Baldeo, Rudolph, Hunter College
Bearer, Elaine, Brown University
Berberian, Graciela, Instituto de Investigacion Medica "Mercedes y Martin Ferreyra," Argentina
Billack, Blase, Rutgers University
Bolanos, Carlos, Northeastern University
Borst, David, Illinois State University
Boyle, Kim-Laura, Colby-Sawyer College
Burris, Jennifer, Carleton College

Campbell, Robert, Ares Advanced Technology
Carvan, Michael, University of Cincinnati
Cho, Myoung-soon, National Institutes of Health
Ciralsky, Jessica, Brown University
Crispino, Marianna, University of Southern California

DePina, Ana, Dartmouth College
Detrait, Eric, University of Texas Medical Branch
Devlin, Leah, Penn State University
Ding, J. L., National University of Singapore, Singapore

Eddleman, Christopher, University of Texas Medical Branch, Austin
Edds-Walton, Peggy, University of California, Riverside
Emons, Anne, Wagenongen Agricultural University, The Netherlands
Eyman, Maria, University of Naples, Italy

Fox, Tom, Harvard Medical School
Freidenfelds, Jason, Harvard University
Fukuda, Mitsunori, Tsukuba Life Science Center, Japan

Gainer, Harold, National Institutes of Health
Galbraith, James A., Duke University
Gallant, Paul E., National Institutes of Health
Gallo, Michael, University of Medicine and Dentistry of New Jersey
Gebhardt, Kelley, University of North Carolina, Chapel Hill
Gebre, Biniam, Williams College
Gibney, Jean, University of Medicine and Dentistry of New Jersey
Gioio, Anthony, National Institutes of Health
Gleeson, Richard, Whitney Laboratory
Goda, Makioto, Kyoto University, Japan
Goldman, Anne E., Northwestern University Medical School
Gomez, Maria del Pilar, Boston University School of Medicine
Grant, Philip, National Institutes of Health
Grassi, Daniel, Food and Drug Administration
Guevara, Michael, McGill University, Canada

Gundersen, Gregg G., Columbia University

Hagar, Robert, University of Connecticut Health Center
Hao, Weihua, University of Texas Health Science Center
Harwood, Claire, University of Leeds, United Kingdom
Heck, Kalling, Rutgers University
Hernandez, Carlos, New York University School of Medicine
Hershko, Judy, Technion, Israel
Hilfiker, Sabine, Rockfeller University
Hill, Julia, University of Massachusetts, Amherst
Hill, Susan Douglas, Michigan State University
Hinton, Shanta, Howard University
Ho, Bow, National University of Singapore, Singapore
Holmgren, Miguel, Massachusetts General Hospital

Innocenti, Barbara, Iowa State University

Klimov, Andrei, University of Pennsylvania
Kolosova, Irina, National Institutes of Health
Koroleva, Zoya, Hunter College
Koulen, Peter, Yale University School of Medicine
Krejci, Melisha, University of Puget Sound
Kuner, Thomas, Duke University Medical Center
Kuznetsov, Sergei, University of Rostock, Germany

Lam, Ying-Wan, Yale University Medical School
Lee, Kyeng, Hunter College
Lema-Foley, Christine, Hunter College
Leznick, Elena, New York University School of Medicine
Luo, Tianxiang, Chinese Academy of Sciences, China

Malchow, Robert, University of Illinois, Chicago
Marks, Andrew, Columbia University
Melishchuk, Alexey, University of Pennsylvania
Mellon, DeForest, University of Virginia
Messerli, Mark, Purdue University
Meyers, Jason, University of Virginia
Miyake, Katsuya, Fukushima Medical College, Japan
Mohan, Nishal, Hunter College
Molyneaux, Bradley, Dartmouth College
Morgan, Jennifer, Duke University Medical Center

Ndirango, Anthony, Williams College
Nigrini, Elisa, Swarthmore College
Nilsson, Helen, Goteborg University, Sweden

Onigman, Timna, Brown University
Osborn, Andrea, New England Aquarium

Parenteau, M. Niki, University of Puget Sound
Parra, Georgina, Williams College
Parshley, Michelle, State University of New York Health Science Center
Peterson, George G., Wesleyan University
Prahlad, Veena, Northwestern University
Prasad, Kondury, University of Texas Health Science Center

Quinn, Kerry, Yale University

Rebhun, Lionel, University of Virginia
Rhodes, Paul, National Institutes of Health
Robinson, Tresa, Howard University
Romero, Miryam, Yale University School of Medicine
Rose, Matthew, University of Virginia
Ruta, Vanessa, Hunter College

Schuette, Etha, Hunter College
Schweizer, Felix, University of California, Los Angeles
Sen, Boudrayan, Williams College
Shirihai, Orian, Children's Hospital
Simpson, Alastair, University of Sydney, Australia
Sistonen, Lea, Turku Center for Biotechnology, Finland
Spitzer, Nicholas, University of California, San Diego
Steffen, Walter, Biocenter, Austria
Steinacker, Antoinette, University of Puerto Rico
Stewart, Karen, State University of New York Health Science Center
Stockbridge, Norman, Food and Drug Administration
Suddith, Andrew, University of Kansas
Suwa, Hiroshi, New York University Medical Center
Swank, Douglas, San Diego State University

Tokumaru, Hiroshi, Duke University Medical Center
Tokumaru, Keiko, Duke University Medical Center
Tran, Phong, University of North Carolina, Chapel Hill

Wagg, Jonathan, Rockefeller University
Waggett, Rebecca, Providence College
Walker, Christopher, Yale University
Wen, Huajie, National Institutes of Health
Wesp, Heather, Hope College
Williams, Tracey, Howard University
Wollert, Torsten, University of Rostock, Germany

Yang, Dazhi, Howard University
Young, Ian, University of Leeds, United Kingdom

Zakevicius, Jane M., University of Illinois, Chicago
Zeno, Scotto Lavina, University of Naples, Italy
Zigman, Bunnie R., Boston University School of Science
Zochowski, Michal, Yale University Medical School

Library Readers

Abbott, Jane, Marine Research, Inc.
Ahmadmian, Vernon, Clark University
Allen, Garland E., Washington University
Anderson, Everett, Harvard Medical School
Armstrong, Samuel C., Everett, Washington

Baccetti, Baccio, University of Sienna
Barrett, Dennis, Denver, Colorado
Barry, Susan R., Mount Holyoke College
Bedard, Andre, York University
Benjamin, Thomas, Harvard Medical School
Bernhard, Jeffery D., University of Massachusetts Medical Center
Bernheimer, Alan, New York University Medical Center
Borgese, Thomas A., Lehman College-CUNY
Boyer, John, Union College
Burns, John T., Bethany College

Campbell, Robert, Ares Advanced Technology
Campos, Ana R., McMaster University
Candelas, Graciela C., University of Puerto Rico
Chang, Donald C., Hong Kong University
Child, Frank, Trinity College
Clark, Arnold M., University of Delaware
Clark, Douglas P., Johns Hopkins University
Clarkson, Kenneth L., Murray Hill, New Jersey
Cohen, Seymour S., American Cancer Society
Cohen, Leonard A., American Health Foundation
Collier, Marjorie M., The Effie Laboratory
Cooperstein, Sherwin J., University of Connecticut Health Center
Copeland, Eugene C., Woods Hole, MA
Couch, Ernest F., Texas Christian University
Cowling, Vincent F., Palm Beach Shores Florida

Duncan, Thomas, Nichols College

Epstein, Herman, Brandeis University

Gabriel, Mordecai, Brooklyn College
Galatzer-Levy, Robert, University of Chicago
Garcia-Blanco, Mariano A., Duke University Medical School
Garrick, Rita Anne, Fordham University
German, James L., New York Blood Center
Ginsberg, Harold S., National Institutes of Health
Goldstein, Moise H., Johns Hopkins University
Gross, Paul, University of Virginia
Grossman, Albert, New York University Medical Center
Gruner, John, Cephalon, Inc.
Guttenplan, Joseph, New York University Dental Center

Haimo, Leah, University of California
Haubrich, Robert, Denison University
Haugaard, Niels, University of Pennsylvania Hospital
Herskovits, Theodore T., Fordham University
Hunter, Robert, Gartnaval Royal Hospital

Ilan, Judith, Case Western University
Inoue, Sadayuki, McGill University

Jacobson, Allan S., University of Massachusetts Medical Center
Josephson, Beth, University of California
Josephson, Robert K., University of California

Kaltenbach, Jane C., Mount Holyoke College
Kamino, Kohtaro, Tokyo Medical and Dental Center
Kaminer, Benjamin, Boston University
Karlin, Arthur, Columbia University
Kelly, Robert E., Northwestern University
King, Kenneth, Falmouth, MA
Klein, Donald A., Colorado State University
Kornberg, Sir Hans, Boston University

Krane, Stephen, Harvard University Medical School

Laster, Leonard, University of Massachusetts Medical Center
Leighton, Joseph, Aeron Biotechnology, Inc. (deceased)
Lisman, John, Brandeis University
Lorand, Laszlo, Northwestern University Medical School

MacNichol, Edward F. Jr., Boston University
Martin, Donald, Toledo, Ohio
Mauzerall, David, Rockefeller University
Michaelson, James, Massachusetts General Hospital
Mitchell, Ralph, Harvard University
Mizell, Merle, Tulane University
Morgan, Lynn M., Mount Holyoke College
Morrell, Detoledo Leyla, Rush Medical College

Nagel, Ronald L., Albert Einstein College of Medicine
Narahashi, Toshio, Northwestern University Medical School
Naugle, John, National Aeronautics & Space Administration
Nickerson, Peter A., SUNY-Buffalo

Pappas, George D., University of Illinois at Chicago
Pollen, Daniel A., University of Massachusetts Medical Center
Prusch, Robert, Gonzaga University
Przybyszewski, Andrew, University of Massachusetts Medical Center

Rafferty, Keen, University of Illinois
Rafferty, Nancy, Northwestern University
Rosenbluth, Jack, New York University Medical Center

Shepro, David, Boston University
Spector, Abraham, Columbia University
Spotte, Stephen, University of Connecticut at Avery Pt.
Stein, Leonard, Stony Brook, New York
Sullivan, Gerald, Boston, MA
Sundquist, Eric, United States Geological Survey
Sweet, Frederick, Washington University School of Medicine

Tischler, Monica, Benedictine University
Trager, William, The Rockefeller University
Tweedell, Kenyon S., University of Notre Dame
Tykocinski, Mark L., Case Western University

Van Holde, Kensal, Oregon State University

Walton, Alan J., Cambridge University
Warren, Leonard, Wistar University
Whittaker, J. R., University of New Brunswick
Wirth, Dyann, Harvard School of Public Health
Wolken, Jerome J., Carnegie Mellon University (deceased)

Yevick, George, Stevens Institute of Technology

Domestic Institutions Represented

Acacia Biosciences
Alabama, University of, Birmingham
Albert Einstein College of Medicine
Allegheny University of the Health Sciences
Allina Health System
Amgen, Inc.
Aquatic Resources Center
Ares Advanced Technology

1998 Library Room Readers1

Dr. Daniel Alkon
National Institutes of Health

Dr. Lucio Cariello
Stazione-Zoologica A. Dohrn

Dr. Giuseppe D'Alessio
University of Naples

Dr. Robert D. Goldman
Northwestern Univ. Med. School

Dr. Roberto Gonzalez-Palaza
Northwest Indian College

Dr. Harlyn Halvorson
Marine Biological Laboratory

Dr. Michael Hines
Yale Univ. Sch. of Medicine

Dr. Alex Keynan
Israel Academy of Science

Dr. John W. Moore
Duke University Medical Center

Michael Rabinowitz
Marine Biological Laboratory

Dr.. George T. Reynolds
Princeton University

Dr. Gerald Weissmann
NYU Medical Center

Argonne National Laboratory
Arizona State University
Arizona, University of
Arkansas, University of
Auburn University

Barnard College
Baylor College of Dentistry
Baylor College of Medicine
Baystate Health System
Bell Laboratories
Beth Israel-Deaconess Medical Center
Binghamton University
Bliss Army Health Clinic
Boston University
Boston University School of Medicine
Brandeis University
Brigham and Women's Hospital
Bristol-Myers Squibb PRI
Brown University
Bryn Mawr College

California Institute of Technology
California, University of, Berkeley
California, University of, Davis
California, University of, Irvine
California, University of, Los Angeles
California, University of, Riverside
California, University of, San Diego
California, University of, San Francisco
California, University of, Santa Barbara
Carl Zeiss, Inc.
Carleton College
Carnegie Institution of Washington
Case Western Reserve Medical School
Case Western Reserve University
Catholic University of America
Center for Clinical Computing
Centers for Disease Control and Prevention
Chicago Medical School
Chicago, University of
Children's Hospital, Boston
Cincinnati Medical Center, University of
Cincinnati, University of
Cleveland State University
Colby-Sawyer College
Colorado Health Science Center, University of
Colorado School of Medicine, University of
Colorado School of Mines
Columbia University
Connecticut Health Center, University of
Connecticut, University of
Consultant in Scientific Imaging
Cook County Hospital
Cornell University
Cornell University Medical Center
Cornell University Medical College

Dana-Farber Cancer Institute
Dartmouth College
Duke University
Duke University Medical Center

Earlham College
Eastern Kentucky University
Emory University
Eye Health Services

Fairfield University
Finch University of Health Sciences
Florida State University
Florida, University of
Florida College of Medicine, University of
Food and Drug Administration
Forsyth Dental Center
Fox Chase Cancer Center
Fred Hutchinson Cancer Research Center

George Washington University
George Washington University Medical Center
Georgia State University
Georgia, University of
Gundersen Lutheran Medical Center

H. M. Gunn High School
Hahnemann University
Hamden High School
Harbor-UCLA Medical Center
Harvard Center for Reproduction
Harvard Medical School
Harvard University
Harvard University School of Public Health
Hawaii, University of
Hollins College
Hope College
House Ear Institute
Howard Hughes Medical Institute
Howard University
Hunter College

Illinois State University
Illinois, University of, Chicago
Illinois, University of, Urbana-Champaign
Indiana University
Indiana University School of Medicine
Iowa Hospital and Clinics, University of
Iowa State University
Iowa, University of

Jackson Laboratory
Johns Hopkins University
Johns Hopkins University School of Medicine

Kansas Medical Center, University of
Kansas, University of
Kent State University
Kentucky College of Medicine, University of
Kentucky, University of

Laboratory of Kidney and Electrolyte Metabolism
Las Vegas, City of
Lawrence Berkeley National Laboratory
Lockheed Martin Idaho Technologies
Long Island Jewish Medical Center
Louisiana State University
Louisiana State University Medical Center
Loyola University of Chicago

Lucent Technologies

Marine Biological Laboratory
Marshall University School of Medicine
Maryland, University of
Maryland School of Medicine, University of
Massachusetts Eye and Ear Infirmary
Massachusetts General Hospital
Massachusetts Institute of Technology
Massachusetts Medical School, University of
Massachusetts, University of
Medical College of Georgia
Memorial Sloan-Kettering Cancer Center
Metabolix, Inc., Cambridge
MetroHealth Medical Center
Miami School of Medicine, University of
Miami, University of
Michigan Medical School, University of
Michigan State University
Michigan, University of
Millennium Pharmaceuticals
Minnesota, University of
Missouri, University of
Mitotix, Inc.
Montana State University
Morehouse School of Medicine

N. S. Kline Institute
NASA Ames Research Center
National Cancer Institute
National Fish Health Research Laboratory
National Institute of Immunology
National Institutes of Health
National Institutes of Mental Health
National Library of Medicine
Naval Medical Research Institute
NEC Research Institute
New England Aquarium
New Jersey, University of Medicine and Dentistry
New Mexico Health Sciences, University of
New Mexico, University of
New York Health Science Center, State University of
New York Hospital
New York Medical College
New York State Department of Health
New York University Medical Center
New York University School of Medicine
New York, State University of, Albany
New York, State University of, Brooklyn
New York, State University of, Buffalo
New York, State University of, Stony Brook
North Carolina State University
North Carolina, University of, Chapel Hill
North Dakota State University
Northeastern University
Northwestern University Medical School
Nova Southeastern University

Ohio State University
Ohio University
Ohio, Medical College of
Oklahoma, University of
Oregon Health Science University
Oregon Regional Primate Research Center
Oregon State University
Oregon, University of

Pennsylvania Medical Center, University of
Pennsylvania State University
Pennsylvania, University of
Pharmacia & Upjohn
Pittsburgh, University of
Princeton University
Providence College
Public Health Research Institute
Puerto Rico, University of
Puget Sound, University of
Purdue University

Queens College

Rhode Island, University of
Ribozyme Pharmaceuticals, Inc.
Rice University
Rochester Medical Center, University of
Rockefeller University
Roswell Park Cancer Institute
Rowland Institute for Science
Rutgers University

Saint Vincents Hospital
Salk Institute
San Diego State University
San Jose State University
Schering Plough Research Institute
Scripps Institution of Oceanography
Seattle Biomedical Research Institute
Smith College
Smithsonian Institution
South Carolina, Medical University of
Southern California, University of
Southern Illinois University
SRI International
St. Christopher's Hospital for Children
St. Jude Children's Research Hospital
Stanford University
Stanford University Medical Center
Swarthmore College
Syracuse University

Texas Health Science Center, University of
Texas Medical Branch, University of
Texas Southwestern Medical Center Library, University of
Texas Southwestern Medical Center, University of
Texas Southwestern, University of
Texas Tech University Health Sciences
Texas, University of
Thomas Jefferson University
Trinity College
Tufts University
Tufts University School of Medicine
Tuskegee University

U. S. Army Graduate Program
U. S. Army Natick RD&E Center
U. S. Environmental Protection Agency
U. S. Geological Survey
U. S. Navy

Union College
Utah Medical Center, University of
Utah, University of

Vanderbilt University
Vanderbilt University School of Medicine
Vermont, University of
Veterans Administration Medical Center
Virginia Health Sciences Center, University of
Virginia School of Medicine, University of
Virginia Tech
Virginia, University of
Vollum Institute

Wadsworth Center for Labs and Research
Wake Forest University
Wake Forest University School of Medicine
Washington State University
Washington University School of Medicine
Washington University, St. Louis
Washington, University of
Wayne State University
Wesleyan University
West Virginia University
Western Michigan University
Wheaton College
Whitehead Institute for Biomedical Research
Whitney Laboratory
Williams College
Wisconsin, Medical College of
Wisconsin, University of, Madison
Wisconsin, University of, Milwaukee
Woods Hole Oceanographic Institution
Wyeth-Ayerst Research

Xavier University Louisiana College of Pharmacy

Yale University
Yale University School of Medicine

Zeiss Optical Systems

Foreign Institutions Represented

Aarhus, University of, Denmark
Adelaide, University of, Australia
Auckland, University of, Australia

Basel, University of, Switzerland
Biocenter, Austria
Biotechnology Research Institute, Canada
Braunschweig, University of, Germany
Brazil, University of, Brazil

Cambridge, University of, United Kingdom
Carl Zeiss Jena, Germany
Carl Zeiss, Inc., Germany
Centro de Investigacion y de Estudios Avanzados, Mexico
Charles University, Czech Republic
Chile, University of, Chile
Chinese Academy of Sciences, China
Copenhagen, University of, Denmark

Dalhousie University, Canada
Douglas Hospital Research Center, Canada
Dundee, University of, United Kingdom

Fondazione Alberto Monroy, Italy
Friedrich Meischer Institute, Switzerland
Fukushima Medical College, Japan
Fundação Oswaldo Cruz, Brazil

Geneva, University of, Switzerland
Georg-August Universität, Germany
Ghent, University of, Belgium
Göteborg University, Sweden
Guelph, University of, Canada

Halle, University of, Germany
Hebrew University of Jerusalem, Israel
Helsinki, University of, Finland
Hong Kong University, Hong Kong
Hospital for Sick Children, Canada
Hospital General de Ninos Ricardo Gutierrez, Argentina
Humboldt University, Germany

I.V.I.C., Venezuela
Imperial College of Science, Technology and Medicine, United Kingdom
Institute of Ophthalmology London, United Kingdom
Institute of Statistical Mathematics, Japan
Instituto de Biologia y Medicina Experimental, Argentina
Instituto de Investigacion Medica "Mercedes y Martin Ferreyra," Argentina

Konstanz, University of, Germany
Kyoto University, Japan

Laval University School of Medicine, Canada
Leeds, University of, United Kingdom
Leiden, University of, The Netherlands
Lethbridge, University of, Canada
Lisbon, University of, Portugal
Louvain, University of, Belgium
Ludwig-Maximilians-Universität München, Germany

MacKay Memorial Hospital, Taiwan
Manchester, University of, United Kingdom
Manitoba, University of, Canada
Max-Planck-Institut, Germany
Max Planck Society, Germany
McGill University, Canada
McMaster University, Canada
Medical Research Council, United Kingdom
Melbourne, University of, Australia
Minas Gerais, Universidade Federal de, Brazil
Mitsubishi Kasei Institute of Life Sciences, Japan
Montréal Chest Institute, Canada
Montréal, University of, Canada
Mount Sinai Hospital, Canada

Nagoya University, Japan
Naples, University of, Italy
National Center of Scientific Research, France
National Centre for Biological Sciences, India
National History Museum, United Kingdom
National Institute for Medical Research, United Kingdom

National Institute of Nutrition, Mexico
National Institute of Public Health and Environment, The Netherlands
Niigata University, Japan

Oldenburg, University of, Germany
Osaka University, Japan
Otago, University of, New Zealand
Ottawa, University of, Canada
Oxford, University of, United Kingdom

Pharmacia and Upjohn, Sweden
Pisa, University of, Italy
Princess Margaret Hospital, Canada

Québec, Université de, Canada
Queen's University, Canada

Rega Institute, Belgium
Republica of Uruguay, Universidad de la, Uruguay
Rostock, University of, Germany
Ruhr-Universität Bochum, Germany

São Paulo, University of, Brazil
Saskatchewan, University of, Canada
Scuola Normale Superiore Pisa, Italy
Siena, University of, Italy
Simon Fraser University, Canada
Singapore, National University of, Singapore
SISSA, Italy
Southampton University, United Kingdom
St. Thomas' Hospital London, United Kingdom
Stazione Zoologica A. Dohrn, Italy

Sussex Center for Neuroscience, United Kingdom
Swiss Institute for Experimental Cancer Research, Switzerland
Sydney, University of, Australia

Technion-Israel Institute of Technology, Israel
Toronto, University of, Canada
Tsukuba Life Science Center, Japan
Turku Center for Biotechnology, Finland

Umeä University, Sweden
Universidad Complutense Madrid, Spain
Universidad del Valle Cali, Colombia
Universidad Miguel Hernandez, Spain
Universidad Nacional Autonoma de Mexico, Mexico
Université Louis Pasteur, France
Université Paris-Sud, Frances
University College London, United Kingdom
Urbino, University of, Italy
Utrecht University, The Netherlands

Victoria, University of, Canada

Wageningen Agricultural University, The Netherlands
Warwick, University of, United Kingdom
Weizmann Institute of Science, Israel
Wellcome/CRC Institute, United Kingdom
West Indies, University of, Jamaica
Western General Hospital, United Kingdom
Western Ontario, University of, Canada
Witwatersrand, University of the, South Africa

Zurich, University of, Switzerland

Year-Round Research Programs

Architectural Dynamics in Living Cells Program

Established in 1992, this program focuses on architectural dynamics in living cells—the timely and coordinated assembly and disassembly of macromolecular structures essential for the proper functioning, division, motility, and differentiation of cells; the spatial and temporal organization of these structures; and their physiological and genetic control. The program is also devoted to the development and application of powerful new imaging and manipulation devices that permit such studies directly in living cells and functional cell-free extracts. The Architectural Dynamics in Living Cells Program promotes interdisciplinary research and consists of resident core investigators and a cadre of adjunct members.

Resident Core Investigators

Danuser, Gaudenz, Postdoctoral Fellow
Inoué, Shinya, Distinguished Scientist
Katoh, Kaoru, Postdoctoral Scientist
Oldenbourg, Rudolf, Associate Scientist

Staff

Geer, Thomas, Research Assistant
Knudson, Robert, Instrumental Development Engineer
Maccaro, Jackie, Laboratory Assistant
MacNeil, Jane, Executive Assistant

Visiting Investigators

Dogic, Zvonimir, Brandeis University
Fraden, Seth, Brandeis University
Goda, Makoto, Kyoto University, Japan
Gundersen, Gregg, Columbia University
Inoué, Theodore D., Universal Imaging Corporation, West Chester, Pennsylvania
Keefe, David, Rhode Island Women and Infant's Hospital, Providence, Rhode Island
Kinosita, Kazuhiko, Keio University, Yokohama, Japan
Liu, Lin, Rhode Island Women and Infant's Hospital, Providence, Rhode Island
Suzuki, Keisuke, Olympus Corporation, Hachioji, Japan
Takahashi, Hajime, Olympus Corporation, Hachioji, Japan
Tran, Phong, University of North Carolina, Chapel Hill

The Josephine Bay Paul Center for Comparative Molecular Biology and Evolution

Major emphasis in the Josephine Bay Paul Center in Comparative Molecular Biology and Evolution is placed upon comparative/phylogenetic studies of genes and genomes, molecular microbial ecology/biodiversity and evolution of host defense mechanisms in marine invertebrates. The Center encourages studies of genotypic diversity across all phyla and promotes the use of modern molecular genetics and phylogeny to gain insights into the evolution of molecular structure and function. The Josephine Bay Paul Center is a member of NASA's Virtual Institute for Astrobiology.

Other major research programs include Mitchell Sogin's studies of molecular evolution in eukaryotes and studies of genome sequences from parasitic microorganisms, Monica Riley's metabolic database and evolutionary studies of protein sequences, Neal Cornell's comparative molecular studies of genes critical to heme biosynthesis, Norman Wainwright's studies of the molecular basis of host defense mechanisms in marine invertebrates, and Michael Cummings' studies of evolution of pathogenetic microorganisms.

Other collaborative projects include studies of P450 evolution (M. Sogin and John Stegeman's laboratory at Woods Hole Oceanographic Institution [WHOI]), a molecular ecology component of the Long Term Ecological Research project (M. Sogin's laboratory and John Hobbie of The Ecosystems Center), and studies of molecular diversity among marine protists and bacteria (with marine microbiologists at WHOI). Future recruiting efforts will focus upon molecular evolution in developmental biology and genome sciences.

The Center has excellent resources for studies of molecular evolution: automated DNA sequencing, well-equipped research laboratories, and powerful computational facilities. In addition to participating in the Parasitology and Microbial Diversity courses, the Center sponsors the Workshop in Molecular Evolution at the MBL, which has gained an international reputation for excellence. This Workshop offers 60 students a series of lectures and minisymposia that are complemented by a state-of-the-art computational facility.

The Josephine Bay Paul Center in Comparative Molecular Biology and Evolution includes the laboratories of Neal Cornell, Michael Cummings, Monica Riley, Mitchell Sogin, and Norman Wainwright.

Resident Core Investigators

Sogin, Mitchell, Director and Senior Scientist
Cornell, Neal, Senior Scientist
Cummings, Michael, Assistant Scientist
Riley, Monica, Senior Scientist
Wainwright, Norman, Senior Scientist

Laboratory of Neal Cornell

Research in this laboratory is concerned with the comparative molecular biology of genes that encode the enzymes for heme biosynthesis, with particular emphasis on 5-aminolevulinate synthase, the first enzyme in the pathway. Because the ability to produce heme from common metabolic materials is a near universal requirement for living organisms, these genes provide useful indicators of molecular aspects of evolution. For example, 5-aminolevulinate synthase in vertebrate animals and simple eukaryotes such as yeast and *Plasmodium falciparum* have high sequence similarity to the enzyme from the alpha-purple subgroup of eubacteria. This supports the suggestion that alpha-purple bacteria are the closest contemporary relatives of the ancestor of eukaryotic mitochondria. The analysis also raises the possibility that plant and animal mitochondria had different origins. Aminolevulinate synthase genes in mitochondria-containing protists are currently being analyzed to obtain additional insight into endosymbiotic events. Also, genes of primitive chordates are being sequenced to gain information about the large-scale gene duplication that played a very important role in the evolution of higher vertebrates. Other studies in the laboratory have been concerned with the effects of environmental pollutants on heme biosynthesis in marine fish, and it has been shown that polychlorinated biphenyls (PCBs) enhance the expression of the gene for aminolevulinate synthase.

Staff

Cornell, Neal W., Senior Scientist
Dunlap, Rachel, Research Associate
Faggart, Maura A., Research Assistant
Kreiling, Jill, Research Assistant
Frisbee, Cameran, Laboratory Assistant
O'Neil, Brendan, Laboratory Assistant

Visiting Scientist

Fox, T. O., Harvard Medical School

Laboratory of Michael Cummings

The research in this laboratory is in the area of molecular evolutionary genetics and includes the study of the mechanisms of molecular genetic processes, molecular systematics and population genetics. The basis for much of the research is comparative, at several levels of biological organization, and involves both empirical and computer-based studies. Past work has involved a wide range of organisms including plants, vertebrates, invertebrates, fungi, and bacteria.

Using drug resistance in Mycobacterium tuberculosis as a model system, we are investigating how well phenotype (level of drug resistance) can be predicted with genotype information (DNA sequence data). Drug resistance is a major problem in the treatment of infectious diseases. Understanding of the evolution of drug resistance, and developing accurate methods of its prediction, are specific goals of this research. More generally, the relationship of genotype to phenotype is a fundamental problem in genetics, and through these investigations it is hoped that insight will be gained.

Mycobacterium provides an excellent model system for the study of the evolution of pathogenicity and emergent pathogens; it is a large and widely distributed group that occupies a range of habitats (*e.g.*, soil, water, skin), and exhibits a broad range of relationships with other organisms (*e.g.*, free-living, commensal, parasitic). Importantly, the group contains a number of major human pathogens (*e.g.*, those that cause tuberculosis and leprosy), including recently emerged pathogens. We are using phylogenetic analysis of DNA sequence data to study the evolutionary patterns of pathogenicity within Mycobacterium to discern patterns in the emergence of new pathogens.

These and other projects involve DNA sequencing, computer based phylogenetic and statistical analyses, and the development or application of new analytical approaches.

Staff

Cummings, Michael, Assistant Scientist

Laboratory of Monica Riley

The genome of the bacterium *Escherichia coli* contains all of the information required for a free-living chemoautotrophic organism to live, adapt, and multiply. The information content of the genome can be dissected from the point of view of understanding the role of each gene and gene product in achieving these ends. The many functions of *E. coli* have been organized in a hierarchical system representing the complex physiology and structure of the cell. In collaboration with Dr. Peter Karp of SRI International, an electronic encyclopedia of information is being constructed on the genes, enzymes, metabolism, transport processes, regulation, and cell structure of *E. coli*. The interactive EcoCyc program is now publicly available and has graphical hypertext displays, including literature citations, on nearly all of *E. coli* metabolism, all genes and their locations, a hierarchical system of cell functions and some regulation processes. This work is continuing.

In addition, the *E. coli* genome contains valuable information on molecular evolution. We are analyzing the sequences of proteins of *E. coli* in terms of their evolutionary origins. By grouping like sequences and tracing back to their common ancestors, one learns not only about the paths of evolution for all contemporary *E. coli* proteins, but one extends even further back before *E. coli*, traversing millennia to the earliest evolutionary times when a relatively few ancestral proteins served as ancestors to all contemporary proteins of all living organisms. The complete genome sequence of *E. coli* and sophisticated sequence analysis programs permit us to identify evolutionary related protein families, determining ultimately what kinds of unique ancestral sequences generated all of present-day proteins. The data developed in the work has proven to be valuable to the community of scientists sequencing microbial genomes. *E. coli* data serve as needed reference points.

Staff

Riley, Monica, Senior Scientist
Pellegrini-Toole, Alida, Research Assistant II

Kerr, Alastair, Postdoctoral Scientist
Porterfield, Pamela, Lab Clerk

Laboratory of Norman Wainwright

The mission of the laboratory is to understand the molecular defense mechanisms exhibited by marine invertebrates in response to invasion by bacteria, fungi, and viruses. The primitive immune systems demonstrate unique and powerful strategies for survival in diverse marine environments. The key model has been the horseshoe crab *Limulus polyphemus. Limulus* hemocytes exhibit a very sensitive LPS-triggered protease cascade which results in blood coagulation. Several proteins found in the hemocyte and hemolymph display microbial binding proteins that contribute to antimicrobial defense. Commensal or symbiotic microorganisms may also augment the antimicrobial mechanisms of macroscopic marine species. Secondary metabolites are being isolated from diverse marine microbial strains in an attempt to understand their role. Microbial participation in oxidation of the toxic gas hydrogen sulfide is also being studied.

Staff

Wainwright, Norman, Senior Scientist
Child, Alice, Research Assistant

Visiting Investigator

Anderson, Porter, University of Rochester

Program in Comparative Molecular Biology and Evolution: Laboratory of Mitchell L. Sogin

This laboratory in molecular evolution employs comparative phylogenetic studies of genes and genomes to define patterns of evolution that gave rise to contemporary biodiversity on the planet Earth. The laboratory is especially interested in discerning how the eukaryotic cell was invented as well as the identity of microbial groups that were ancestral to animals, plants, and fungi. The lab takes advantage of the extraordinary conservation of ribosomal RNAs to define phylogenetic relationships that span the largest of evolutionary distances. These studies have overhauled traditional eukaryotic microbial classifications systems. The laboratory has discovered new evolutionary assemblages that are as genetically diverse and complex as plants, fungi, and animals. The nearly simultaneous separation of these eukaryotic groups (described as the eukaryotic "Crown") occurred approximately one billion years ago and was preceded by a succession of earlier diverging protist lineages, some as ancient as the separation of the prokaryotic domains.

At the same time, this data base provides a powerful tool for the newly emerging discipline of molecular ecology. Using the ribosomal RNA data base and nucleic acid-based probe technology, it is possible to detect and monitor microorganisms including those that cannot be cultivated in the laboratory. This strategy has uncovered new habitats and major revelations about geographical distribution of microorganisms.

The laboratory has initiated a program to sample genomic diversity from eukaryotic microorganisms that do not have mitochondria. The lab previously demonstrated that these taxa represent some of the earliest diverging lineages in the evolutionary history of eukaryotes. The objective is to develop a set of additional molecular markers for studying molecular evolution. These will be invaluable in unraveling sudden evolutionary radiations that cannot be resolved by rRNA comparisons and will provide insights into the presence or absence of important biochemical properties in the earliest ancestors common to all eukaryotic species.

More recently, we initiated a study of the complete genome of *Giardia lamblia.*

Staff

Sogin, Mitchell L., Director and Senior Scientist
Amaral-Zettler, Linda, Postdoctoral Scientist
Eakin, Nora, Research Assistant
Edgcomb, Virginia, Postdoctoral Scientist
Harris, Marian, Executive Assistant
Hinkle, Greg, Investigator
Holder, Michael, Research Assistant
Kim, Ulandt, Research Assistant
Lim, Pauline, Executive Assistant
McArthur, Andrew, Postdoctoral Scientist
Medina, Monica, Posdoctoral Scientist
Morrison, Hilary G., Staff Scientist II
Nixon, Julie, Postdoctoral Scientist
Roger, Andrew, Postdoctoral Scientist
Shakir, Muhhamed Afaq, Postdoctoral Scientist
Silberman, Jeffrey, Postdoctoral Scientist

Visiting Investigators

Bahr, Michele, The Ecosystems Center
Campbell, Robert, Serono Laboratories, Inc.
Laderman, Aimlee, Yale University
Podar, Mircea, Woods Hole Oceanographic Institution
Weil, Jennifer, Joslin Diabetes Center

BioCurrents Research Center

The Biocurrents Research Center (BRC), one of the NIH National Centers for Research Resources, has for many years been pioneering methods in the study of transmembrane currents and has hosted a variety of research pursuits. The Center provides visiting investigators access to a variety of unique technologies as well as new approaches to experimentation in the biomedical sciences.

Since the early 1980s, when NIH's Biomedical Research Technology Program established a resource at the MBL, a number of probes have been introduced. Four systems are available at the BRC. All these probe technologies are based on the principle of a self-referencing electrode, maximizing sensitivity by noise and drift reduction. All the probes are non-invasive and generally placed in close proximity to the membrane of cells or tissues, in some cases at sub-micron distances. The two older techniques are designed to measure the movement of ions across the membranes of living tissues or cells with the minimum of disturbance. The current probe, developed in 1974, is still available for the study of external current densities resulting from the general net balance of ion transport. Most use is made of the ion-selective probes (Seris), which measure and follow the transmembrane transport of specific ions such as calcium, potassium and protons. This system also can detect nonelectrogenic transporters. Two newer techniques, now fully developed for applications to biological material, are the BioKelvin probe and the non-invasive electrochemical or polarographic oxygen probe (Serp). The BioKelvin probe measures voltages around living tissues in air. This device is now being used to characterize artificial skin. A radically different approach is being taken to the measurements of biocurrents using the electrochemical microprobes. Presently applied to molecular oxygen, such a technique offers opportunity for the study of molecular transport using redox potentials. During 1998 this probe has been applied to single neurons, β-pancreatic cells and developing embryos. We are currently developing further applications of the Serp probes to measure nitric oxide, ascorbic acid and insulin. Our first recording of nitric oxide release from single activated macrophages was made in the summer of 1998.

A state-of-the-art system offers non-invasive ion probes coupled with current and voltage clamp (both single, two electrode, and patch) along with ratio imaging via a Zeiss Attofluor system, all of which are finding uses in the hosted biomedical studies, as well as BRC research and development.

This year a wide variety of biological and biomedical subjects have been studied by BRC staff and visitors. In R&D we have continued with developing the application of ion-selective and electrochemical microsensors, all applicable to single cells with square micron spatial resolution. We are currently exploring ways to combine these sensors with a variety of techniques known collectively as near field optical microscopy. In an experimental context we have advanced our technology into several fields, including reproductive physiology, diabetes research, neuroscience, development, gravitropic responses, ion transport and homeostasis. Details of our research program and a list of publications can be found at www.mbl.edu/BioCurrents.

MBL year-round laboratories with which BRC is in active collaboration are the Laboratory of Rudolf Oldenbourg and the Laboratory for Reproductive Medicine, headed by David Keefe. Dr. Keefe and Dr. Peter Smith, BRC Director, are Co-Investigators on a grant to support the development of new technology to assess the developmental potential of preimplantation embryos and to study the pathophysiology of oocyte dysfunction.

Staff

Smith, Peter J. S., Director and Associate Scientist
Baikie, Iain D., Associate Scientist
Danuser, Gaudenz M., Postdoctoral Fellow
Hammar, Katherine, Research Assistant
Jaffe, Lionel F., Senior Scientist
McLaughlin, Jane A., Research Assistant
Porterfield, D. Marshall, Staff Scientist
Sanger, Richard H., Research Assistant
Tamse, Catherine T., Graduate Student, University of Rhode Island

Visiting Scientists and Publications

This year the Research Center hosted 42 visitors, 36 from the United States with the remaining from Canada, Denmark, France and United Kingdom. Scientific publications during the year numbered 22.

Boston University Marine Program

Faculty

Atema, Jelle, Professor of Biology, Director
Dionne, Vincent, Professor of Biology
Humes, Arthur, Professor of Biology Emeritus
Kaufman, Les, Associate Professor of Biology
Lobel, Phillip, Associate Professor of Biology
Ward, Nathalie, Lecturer

Staff

Decarie, Linette, Senior Staff Coordinator
DiNunno, Paul, Research Assistant, Dionne Lab
Hall, Sheri, Program Manager
Magee, Jennifer, Administrative Secretary
Olson, Nancy, Program Assistant
Proft, Heinz, Research Assistant, Lobel Lab
Tomasky, Gabby, Research Assistant, Valiela Lab
Wheatley, MaryJo, Information Officer
Zackrison, Rebecca, Staff Assistant

Postdoctoral Investigators

Basil, Jenny, Atema Laboratory
Cebrian, Just, Valiela Laboratory
Cohen, Anne, Lobel Laboratory
Grasso, Frank, Atema Laboratory
Lavalli, Kari, Atema Laboratory
Trott, Thomas, Atema Laboratory

Visiting Faculty and Investigators

Hanlon, Roger, Marine Biological Laboratory
Hecker, Barbara, Hecker Consulting
Hinkle, Gregory, Marine Biological Laboratory
McFall-Ngai, Margaret, Kewalo Marine Laboratory
Moore, Michael, Woods Hole Oceanographic Institution
Ruby, Edward, Kewalo Marine Laboratory
Silver, Robert, Marine Biological Laboratory
Simmons, Bill, Sandia National Laboratory
Wainwright, Norman, Marine Biological Laboratory

Other

Dolan, Mike, Visiting Teaching Assistant
Drucker, Sam, Visiting Teaching Assistant

Graduate Students

PhD Students

Existing
Batjakas, Ioannis
Cole, Marci
Dale, Jonathon
Economakis, Alistair
Hauxwell, Jennifer
Kroeger, Kevin
Lindholm, James
Ma, Diana
McClelland, James
Oliver, Steven
Sloan, Kevin
Stieve, Erica
Zhao, Jing
New
Miller, Carolyn
Zettler, Eric

Masters Students

Existing
Atkinson, Abby
Barlas, Margaret
Bowen, Jennifer
Cavanaugh, Joseph
DeCou, Domenique
Ferland, Amy
Griffin, Martin
Homkow, Laura

Keith, Lucy
Lawrence, David
Smith, Spence
Thompson, Sarah
Tober, Joanna
Valentini, Stefanie
Watson, Elise
Wright, Dana
New
Allen, Christel
Bentis, Christopher
Chichester, Heather
D'Ambrosio, Alison
Evgenidou, Angeliki
Fern, Sophie
Fredland, Inga
Konkle, Anne
Lamb, Amy
Levine, Michael
McKenna, Ian
Neviackas, Justin
Ramon, Marina

Undergraduate Students

Spring 98
Banik, Amy
Joyce, Kelly
Lolli, Amanda
Strongin, Dan
Fall 98
Alton, Jocelyn
Anselmo, Keri
Apple, Allegra
Brown, Elizabeth
Caudill, Mara
Champagne, Jaimie
Corcoran, Alina
Corcoran, Devin
Costanza, Jennifer
Dearholt, Courtney
Deshpande, Chetan
Doyle, Jamie
Edattukaran, Margaret
Folsom, Corrie
Freidlinger, Francis
Fuller, Katrina
Gaito, Steven
Gauss, Ilana
Hagberg, Erik
Healey, Danielle
Josef, Jennifer
Kelly, Brian
Koenig, Eduardo
LeVay, Adam
Mallidis, Maria
Malmstrom, Rex
Mauch, Jennifer
McCann, Jessica
Michalowski, Jennifer
Monette, Michelle
Moorman, Jesse
Morrison, Jodi
Munger, Lydia

Neuendorffer, Andrea
Patel, Alpa
Plotkin, Anna
Prendeville, Holly
Preto, Luca
Ruegg, Ian
Ryerson, Stephanie
Thompson, Rebecca
Voegtle, Holly Ann
Walker, Ryan
Watkins, Cari
Weisbaum, Dolores

Summer 1998 Interns

Appleman, Greg
Davis, Jessica
Graham, Suzanne
Harris, Jennifer
Kirkpatrick, John
Lazenby, Gweneth
Legra, Jessica
Rogers, Jennifer
Schmitt, Catherine
Sufran, Roselle

Volunteers

Shenning, Ryan
Duffy, Hugh

Laboratory of Jelle Atema

Many organisms and cellular processes use chemical signals as their main channel of information about the environment. All environments are noisy and require some form of filtering to detect important signals. Chemical signals are transported by turbulent currents, viscous flow, and molecular diffusion. Receptor cells extract chemical signals from the environment through various filtering processes. In our laboratory, fish, marine snails, and crustacea have been investigated for their ability to use chemical signals under water. Currently, we use the lobster and its exquisite senses of smell and taste as our major model to study the signal-filtering capabilities of the whole animal and its narrowly tuned chemoreceptor cells.

Research in our laboratory focuses on amino acids, which represent important food signals for the lobster, and on the function and chemistry of pheromones used in lobster courtship. We examine animal behavior in the sea and in the lab. This includes social interactions and chemotaxis. To understand the role of chemical signals in the sea we use real lobsters and untethered small robots. Our research includes measuring and computer modeling odor plumes and the water currents lobsters generate to send and receive chemical signals. Other research interests include neurophysiology of receptor cells and anatomical studies of receptor organs and pheromone glands.

Laboratory of Vincent Dionne

Odors are powerful stimuli. They can focus the attention, elicit behaviors (or misbehaviors), and even resurrect forgotten memories. These actions are directed by the central nervous system, but they depend upon the initial transduction of chemical signals by olfactory receptor neurons in the nasal passages. More than just a single process appears to underlie odor transduction, and the intracellular pathways that are used are far more diverse than once thought. Hundreds of putative odor receptor molecules have been identified that work through several different second messengers to modulate the activity of various types of membrane ion channels.

Our studies are being conducted with aquatic salamanders using amino acids and other soluble chemical stimuli that these animals perceive as odors. Using electrophysiological and molecular approaches, the research examines how these cellular components produce odor detection, and how odors are identified and discriminated.

Laboratory of Arthur G. Humes

Research interests include systematics, development, host specificity, and geographical distribution of copepods associated with marine invertebrates. Current research is on taxonomic studies of copepods from invertebrates in the tropical Indo-Pacific area, and poecilostomatoid and siphonostomatoid copepods from deep-sea hydrothermal vents and cold seeps.

Laboratory of Les Kaufman

Current research projects in the laboratory deal with speciation and extinction dynamics of haplochromine fishes in Lake Victoria. We are studying the systematics, evolution, and conservation genetics of a species flock encompassing approximately 700 very recently evolved taxa in the dynamic and heavily impacted landscape of northern East Africa. In the lab we are studying evolutionary morphology, behavior, and systematics of these small, brightly colored cichlid fishes.

Another area of study is developmental and skeletal plasticity in fishes. We are studying the diversity of bone tissue types in fishes, differential response to mineral and mechanical challenge, and matrophic *versus* environmental effects in the development of coral reef fishes.

We also study the biological basis for marine reserves in the New England fisheries. We are involved in collaborative research with NURC, NMFS and others studying the relative impact on groundfish stocks of juvenile habitat destruction *versus* fishing pressure.

Laboratory of Phillip Lobel

Fishes are the most diverse vertebrate group and provide opportunities to study many aspects of behavior, ecology and evolution. We primarily study how fish are adapted to different habitats and behavioral ecology of species interactions. Current research focuses on fish acoustic communications.

We are also conducting a long-term study of the marine biology of Johnston Atoll, Central Pacific Ocean. Johnston Atoll has been occupied continuously by the military since the 1930s and proved a unique opportunity for assessing the biological impacts of island industrialization and its effects on reefs. Johnston Atoll is the site of the US Army's chemical weapons demilitarization facility, JACADS.

Laboratory of Ivan Valiela

A focus of our work is the link between land use on watersheds and consequences in the receiving estuarine ecosystems. The work examines how landscape use and urbanization increase nutrient loading to groundwater and streams. Nutrients in groundwater are transported to the sea, and, after biogeochemical transformation, enter coastal waters. There, increased nutrients bring about a series of changes on the ecological components. To understand the coupling of land use and consequences to receiving waters, we study the processes involved, assess ecological consequences, and define opportunities for coastal management.

A second long-term research topic is the structure and function of salt marsh ecosystems, including the processes of predation, herbivory, decomposition and nutrient cycles.

Calcium Imaging Laboratory

This laboratory investigates the roles of calcium patterns in development. Our main tool—our ultralow light imaging system—uses the aequorins, a family of chemiluminescent proteins ultimately obtained from a jellyfish and long studied by Dr. Osamu Shimomura at the MBL. Aequorins can either be microinjected into cells or transgenically expressed. Aequorins introduced in both of these ways do not disturb normal function or development. The patterns of chemiluminescence that are emitted by aequorinated cells reveal changing patterns and levels of free calcium within the organisms that develop from these cells. Much of what we know about the roles of calcium in development has been obtained in this way.

The four systems under present or planned investigation are the *Drosophila* egg, the zebrafish egg, the mouse egg and the cellular slime mold, *Dictyostelium*.

Staff

Jaffe, Lionel, Senior Scientist
Créton, Robbert, Postdoctoral Scientist

Center for Advanced Studies in the Space Life Sciences at the MBL

(supported by the National Aeronautics
and Space Administration)

The Marine Biological Laboratory and the National Aeronautics and Space Administration have established a cooperative arrangement with the formation of the Center for Advanced Studies in the Space Life Sciences at the MBL. This Center serves as an interface between NASA and the basic science community, addressing issues of mutual interest. A series of symposia, workshops, and seminars are held at the MBL to advise NASA on a wide variety of topics in the life sciences, including cellular, molecular, developmental, plant, neuro-, and evolutionary biology. Special attention is directed at examining how gravity and its control impact on biological processes, and how variations in gravity can be used as a probe to better understand such processes. This center provides a forum for scientists to think and discuss, often for the first

time, the role that gravity and other aspects of space flight may play in fundamental cellular and physiological processes. These interactions also serve to inform the community of research opportunities in the life sciences that are of interest to NASA. In addition, a newsletter will be published to disseminate this information to a wider audience.

During 1998 the Center sponsored a workshop at the MBL: *Developmental Gene Regulation and Mechanisms of Evolution* held June 10–13, 1998, chaired by Eric Davidson and Michael Levine.

Staff

Dawidowicz, Eliezar A., Administrator
Amit, Udeni, Administrative Assistant

The Ecosystems Center

The Center carries out research and education in ecosystems ecology. Terrestrial and aquatic scientists work in a wide variety of ecosystems ranging from the streams, lakes and tundra of the Alaskan Arctic (limits on plant primary production) to sediments of Massachusetts Bay (controls of nitrogen cycling), to forests in New England (effects of soil warming on carbon and nitrogen cycling), and South America (effects on greenhouse gas fluxes of conversion of rain forest to pasture) and to large estuaries in the Gulf of Maine (effects on plankton and benthos of nutrients and organic matter in stream runoff). Many projects, such as those dealing with carbon and nitrogen cycling in forests, streams, and estuaries, use the stable isotopes ^{13}C and ^{15}N to investigate natural processes. A mass spectrometer facility is available. Data from field and laboratory research are used to construct mathematical models of whole-system responses to change. Some of these models are combined with geographically referenced data to produce estimates of how environmental changes affect key ecosystem indexes such as net primary productivity and carbon storage throughout the world's terrestrial biosphere.

The results of the Center's research are applied, wherever possible, to the questions of the successful management of the natural resources of the earth. In addition, the ecological expertise of the staff is made available to public affairs groups and governmental agencies who deal with problems such as acid rain, coastal eutrophication, and possible carbon dioxide-caused climate change. The Semester in Environmental Science was offered again in Fall 1998. Twelve students from 11 colleges participated in the program. There are opportunities for postdoctoral fellows.

Administrative Staff

Hobbie, John E., Co-Director
Melillo, Jerry M., Co-Director
Berthel, Dorothy J., Administrative Assistant
Chandler, Marsha, Administrative Assistant, Semester in Environmental Science
Donovan, Suzanne J., Executive Assistant
Foreman, Kenneth H., Associate Director of Semester in Environmental Sciences Program
Nuñez, Guillermo, Research Administrator
Seifert, Mary Ann, Administrative Assistant
Scanlon, Deborah G., Executive Assistant, LMER Coordination Office

Scientific Staff

Hobbie, John E., Senior Scientist
Melillo, Jerry M., Senior Scientist
Peterson, Bruce J., Senior Scientist
Shaver, Gaius R., Senior Scientist
Giblin, Anne E., Associate Scientist
Holmes, Robert M., Staff Scientist
Hopkinson, Charles S., Senior Scientist
Nadelhoffer, Knute J., Associate Scientist
Deegan, Linda A., Associate Scientist
Rastetter, Edward B., Associate Scientist
Steudler, Paul A., Senior Research Specialist
Neill, Christopher, Assistant Scientist
Tian, Hanqin, Staff Scientist
Vallino, Joseph J., Assistant Scientist
Williams, Mathew, Assistant Scientist

Educational Staff Appointments

Bovard, Brian, Postdoctoral Research Assistant
Buzby, Karen, Postdoctoral Research Assistant
Garcia, Diana, Postdoctoral Research Associate
Gough, Laura, Postdoctoral Research Associate
Hartley, Anne, Postdoctoral Research Associate
Herbert, Darrell A., Postdoctoral Research Associate
Hughes, Jeffrey E., Postdoctoral Research Associate

Technical Staff

Bahr, Michele P., Research Assistant
Bettez, Neil D., Research Assistant
Byun, Jimmy, Research Assistant
Carpino, Elizabeth, Research Assistant
Catricala, Christina E., Research Assistant
Clark, Tamara, Research Assistant
Claessens, Luc, Research Assistant
Downs, Martha R., Senior Research Assistant
Garritt, Robert H., Senior Research Assistant
Helfrich, John V.K., III, Senior Research Assistant
Holland, Keri, Research Assistant
Hooker, Bethanie, Research Assistant
Hrywna, Yarek, Research Assistant
Jablonski, Sarah, Research Assistant
Jillson, Tracy, Research Assistant

Kelsey, Samuel, Research Assistant
Kicklighter, David W., Senior Research Assistant
Kwiatkowski, Bonnie L., Research Assistant
Laundre, James A., Senior Research Assistant
Micks, Patricia, Research Assistant
Newkirk, Kathleen M., Research Assistant
Nolin, Amy L., Research Assistant
Pan, Shufen, Research Assistant
Pratt, Sara, Research Assistant
Regan, Kathleen M., Research Assistant
Ricca, Andrea, Research Assistant
Schwamb, Carol, Laboratory Assistant
Slavik, Karie A., Research Assistant
Soucy, Lori, Research Assistant
Thieler, Kama, Research Assistant
Thomas, Suzanne, Research Assistant
Tholke, Kristin A., Research Assistant
Tucker, Jane, Senior Research Assistant
Vasiliou, David, Research Assistant
Weston, Nat, Research Assistant
Wollheim, Wilfred M., Research Assistant
Wright, Amos, Research Assistant
Wyda, Jason, Research Assistant

Consultants

Bowles, Frances P., Research Systems Consultant Principal, Research Designs
Bowles, Margaret C., Administrative Consultant

Laboratory of Aquatic Animal Medicine and Pathology

The laboratory provides diagnostic, consultative research, and educational services to the institutions and scientists of the Woods Hole community concerned with marine animal health. Diseases of wild, captive, and cultured animals are investigated.

Staff

Abt, Donald A., Director and The Robert R. Marshak Term Professor of Aquatic Animal Medicine and Pathology, School of Veterinary Medicine, University of Pennsylvania
Bullis, Robert A., Research Associate in Microbiology, University of Pennsylvania
Leibovitz, Louis, Director Emeritus (deceased)
McCafferty, Michelle, Histology Technician, University of Pennsylvania
Moniz, Priscilla C., Administrative Assistant
Smolowitz, Roxanna M., Research Associate in Pathology, University of Pennsylvania
Wadman, Elizabeth A., Microbiology Technician, University of Pennsylvania

Laboratory of Aquatic Biomedicine

Work in this laboratory centers on comparative immunopathology and molecular biology using marine invertebrates as experimental models. Examples of current research include determining the prevalence of leukemia in *Mya arenaria* (the soft shell clam) in Massachusetts. Monoclonal antibodies developed by this laboratory are being used to diagnose clam leukemia, identify and characterize a tumor-specific protein, and differentiate other leukemias in bivalve molluscs. Development and chemically induced changes in gene expression and neuronal growth are also being studied in the surf clam, *Spisula solidissima*. Work in molecular biology is creating a clearer understanding of the comparative etiology and pathogenesis of tumors, particularly in environmentally impacted aquatic animals.

Staff

Reinisch, Carol L., Senior Scientist
Jessen-Eller, Kathryn, Postdoctoral Scientist
Steele, Marjorie, Research Assistant

Visiting Scientists

Stephens, Raymond, Boston University
Walker Charles, Professor of Zoology, University of New Hampshire

Student

Smith, Cynthia, Tufts University School of Veterinary Medicine

Laboratory of Cell Communication

Established in 1994, this laboratory is devoted to the study of intercellular communication. The research focuses on the cell-to-cell channel, a membrane channel built into the junctions between cells. This channel provides one of the most basic forms of intercellular communication in organs and tissues. The work is aimed at the molecular physiology of this channel, in particular, at the mechanisms that regulate the communication. The channel is the conduit of growth-regulating signals. It is instrumental in a basic feedback loop whereby cells in organs and tissues control their number; in a variety of cancer forms it is crippled.

This laboratory has shown that transformed cells lacking communication channels lost the characteristics of cancer cells, such as unregulated growth and tumorigenicity, when their communication was restored by insertion of a gene that codes for the channel protein. Work is now in progress to track the channel protein within the cells from its point of synthesis, the endoplasmic reticulum, to its functional destination in the plasma membrane, the cell-to-cell junction, by expressing a fluorescent variant of the channel protein in the cells. Knowledge about the cellular regulation of this process will aid our understanding of what goes awry when a cell loses the ability to form cell-to-cell channels and thus to communicate with its neighbors, thereby taking the path towards becoming cancerous.

Another line of work is taking the first steps at applying information theory to the biology of cell communications. Here, the intercellular information spoor is tracked to its source: the macromolecular intracellular information core. The outlines of a coherent information network inside and between the cells are beginning to emerge.

Staff

Loewenstein, Werner, Senior Scientist
Rose, Birgit, Senior Scientist
Jillson, Tracy, Research Assistant

Laboratory of Barbara and Bruce Furie

γ-Carboxyglutamic acid is a calcium-binding amino acid that is found in the conopeptides of the predatory marine cone snail, *Conus*. This

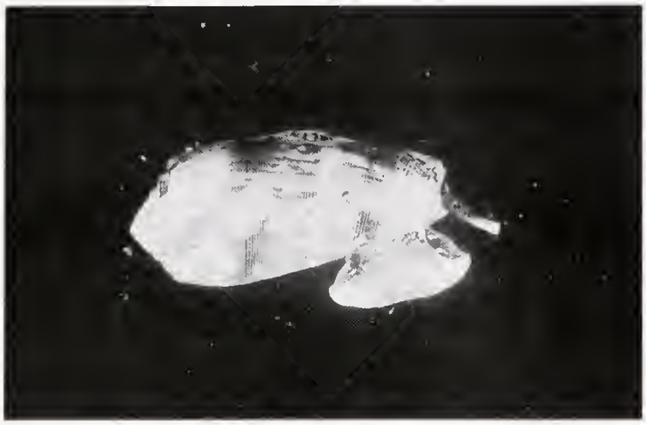

laboratory has been investigating the biosynthesis of this amino acid in *Conus* and the structural role of γ-carboxyglutamic acid in the conopeptides. This satellite laboratory relates closely to the main laboratory on the Harvard Medical School campus in Boston; the main focus of the primary laboratory is the synthesis and function of γ-carboxyglutamic acid in blood clotting proteins and the role of vitamin K.

Cone snails from Fiji have been obtained and are being maintained in the Marine Resources Center. The marine cone snail is the sole invertebrate known to synthesize γ-carboxyglutamic acid (Gla). The venomous cone snail produces neurotoxic conopeptides, some rich in Gla, which it injects into its prey. To examine the biosynthetic pathway for Gla, we have studied the *Conus* carboxylase which converts glutamic acid to γ-carboxyglutamic acid. Of the *Conus* species tested, *C. bandanus, C. marmoreus, C. textile,* and *C. leopardus* had high specific γ-carboxylase activity. This activity has an absolute requirement for vitamin K. The *Conus* carboxylase has been extensively purified. Its substrates appear to contain a carboxylation recognition site on the conotoxin precursor. The *Conus* vitamin K-dependent carboxylase should be an excellent model for determining the mechanism of action of vitamin K in the synthesis of γ-carboxyglutamic acid.

Fifteen novel γ-carboxyglutamic acid-containing conopeptides have been isolated from the venom of *Conus textile.* The amino acid sequence, amino acid composition and molecular weights of these peptides have been determined. For five peptides, the cDNA encoding the precursor conotoxin has been cloned.

The three-dimensional structure of ϵ-TxIX and conantokin G have been determined by 2D NMR spectroscopy. Complete resonance assignments were made from 2D ^{1}H NMR spectra via identification of intraresidue spin systems using ^{1}H-^{1}H through-bond connectivities. NOESY spectra provided $d_{\alpha N}$, d_{NN} and $d_{\beta N}$ NOE connectivities and vicinal spin-spin coupling constants $^3J_{HN\alpha}$ were used to calculate ϕ torsion angles. Structure generation based on interproton distance restraints and torsion angle measurements yield convergent structures generated using distance geometry and simulated annealing methods. The goal of this project is to determine the structural role of γ-carboxyglutamic acid in the Gla-containing conotoxins.

Staff

Barbara C. Furie, Scientist
Bruce Furie, Scientist
Johan Stenflo, Visiting Scientist
Eva Czerwiec, Postdoctoral Fellow
Gail Begley, Postdoctoral Fellow
Alan Rigby, Postdoctoral Fellow

Laboratory of Roger Hanlon

This laboratory investigates the behavior and neurobiology of cephalopods. Studies of various learning capabilities are currently being conducted, as are studies on reproductive strategies that include agonistic behavior, female mate choice, and sperm competition. The latter studies involve DNA fingerprinting to determine paternity and help assess alternative mating tactics. Currently we are studying sensory mechanisms and functions of polarization vision in cephalopods. Complementary field studies are conducted locally and on coral reefs. The functional morphology and neurobiology of the chromatophore system of cephalopods are also studied on a variety of cephalopod species, and image analysis techniques are being developed to study crypsis and the mechanisms that enable cryptic body patterns to be neurally regulated by visual input.

Staff

Hanlon, Roger, Senior Scientist
Sussman, Raquel, Investigator
Hatfield, Emma, Postdoctoral Fellow
Maxwell, Michael, Postdoctoral Scientist
Rummel, John, Visiting Scientist
Shashar, Nadav, Postdoctoral Scientist

Visiting Investigators

Boal, Jean, Visiting Scientist
Gabr, Howaida, Graduate Student, Suez Canal University, Egypt
Cavanaugh, Joseph, Graduate Student, Boston University Marine Program
Fern, Sophie, Graduate Student, Boston University Marine Program
Wittenberg, Kim, Boston University Marine Program

Laboratory of Shinya Inoué

Scientists in this laboratory study the molecular mechanism and control of mitosis, cell division, cell motility, and cell morphogenesis, with emphasis on biophysical studies made directly on single living cells, especially developing eggs in marine invertebrates. Development of biophysical instrumentation and methodology, such as the centrifuge polarizing microscope, high-extinction polarization optical and video microscopy, digital image processing techniques, and exploration of their underlying theory are an integral part of the laboratory's efforts.

Staff

Inoué, Shinya, Distinguished Scientist
Knudson, Robert, Instrument Development Engineer
Maccaro, Jackie, Laboratory Assistant
MacNeil, Jane, Executive Assistant

Laboratory of Alan M. Kuzirian

Research in the laboratory explores the functional morphology and ultrastructure of various organ systems in molluscs. The program includes mariculture of the nudibranch, *Hermissenda crassicornis,* with emphasis on developing reliable culture methods for rearing and maintaining the animal as a research resource. The process of metamorphic induction by natural and artificial inducers is being explored in an effort to understand the processes involved and as a

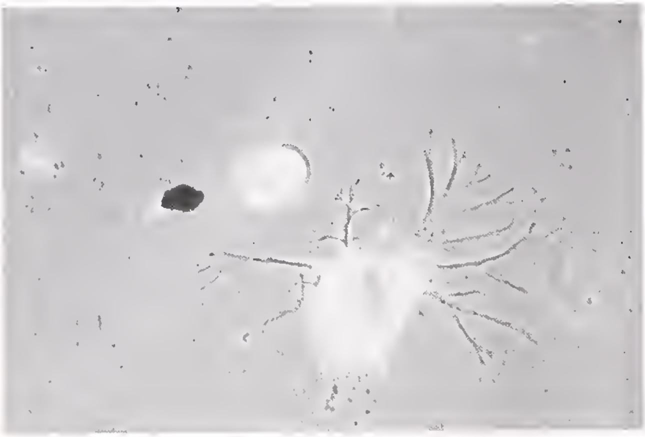

means to increase the yield of cultured animals. Morphologic studies stress the ontogeny of neural and sensory structures associated with the photic and vestibular systems which have been the focus of learning and memory studies, as well as the spatial and temporal occurrence of regulatory and transmitter neurochemicals. Concurrent studies detailing the toxic effects of lead on *Hermissenda* learning and memory, feeding, and the physiology of cultured neurons are also being conducted. New studies include cytochemical investigations of the Ca^{2+}/GTP binding protein, calexcitin, and its modulation with learning and lead exposure.

Collaborative research includes histochemical investigations on strontium's role in initiating calcification in molluscan embryos (shell and statoliths), immunocytochemical labelling of cell-surface antigens, neurosecretory products, second messenger proteins involved with learning and memory, as well as intracellular transport organelles using mono- and polyclonal antibodies on squid (*Loligo pealei*) giant axons and *Hermissenda* sensory and neurosecretory neurons. Additional collaborations involve studying neuronal development and defects, as well as nerve regeneration and repair in phylogenetically conserved nervous systems.

Additional collaborative research includes DNA fingerprinting using RAPD-PCR techniques in preparation for isogenic strain development of laboratory-reared *Hermissenda* and hatchery-produced bay scallops (*Argopectin irradians*) with distinct phenotypic markers for the rapid field identification. Systematic and taxonomic studies of nudibranch molluscs, to include molecular phylogenetics, are also of interest.

Staff

Kuzirian, Alan M., Associate Scientist

Visiting Scientists

Chikarmane, Hemant, Assistant Scientist, MBL
Clay, John R., NINDS/NIH
Gould, Robert, NYS Institute of Basic Research

Laboratory of Rudolf Oldenbourg

The laboratory investigates the molecular architecture of living cells and of biological model systems using optical methods for imaging and manipulating these structures. For imaging non-invasively and non-destructively cell architecture dynamically and at high resolution, we have developed a new polarized light microscope (Pol-Scope). The Pol-Scope combines microscope optics with new electro-optical components, video, and digital image processing for fast analysis of specimen birefringence over the entire viewing field. Examples of biological systems currently investigated with the Pol-Scope are: microtubule-based structures (asters, mitotic spindles, single microtubules); actin-based structures (acrosomal process, stress fibers, nerve growth cones); zona pellucida of vertebrate oocytes; and biopolymer liquid crystals.

Staff

Oldenbourg, Rudolf, Associate Scientist
Katoh, Kaoru, Postdoctoral Research Associate
Geer, Thomas, Research Assistant
Knudson, Robert, Instrument Development Engineer
Baraby, Diane, Laboratory Assistant

Laboratory for Reproductive Medicine, Brown University and Women and Infants Hospital, Providence

Work in this laboratory centers on the investigation of the underlying mechanisms behind female infertility. Particular emphasis is placed on the physiology of the oocyte or early embryo, with the aim of assessing developmental potential and mitochondria dysfunction arising from mtDNA deletions. The studies taking place at the MBL branch of the Brown Laboratory use some of the unique instrumentation available through the resident programs directed by Rudolf Oldenbourg and Peter J. S. Smith. Most particularly, non-invasive methods for oocyte and embryo study are being sought. Of several specific aims, one is to use the Pol-Scope to analyze the birefringence of the preimplantation mammalian zona pellucida—a structure most predictive of successful implantation. We also have used this instrument to examine meiotic spindles. An additional aim is to continue the studies on transmembrane ion transport using the non-invasive electro-physiological techniques available at the BioCurrents Research Center. Preliminary studies indicate that the calcium transport may form an accurate predictor of oocyte and embryo health. The newly developed oxygen probe also offers the possibility of looking directly at abnormalities in the mitochondria arising from accumulated mtDNA damage. Our laboratory has also focused on studying the mechanism underlying age-associated infertility in terms of oocyte quality, attempting to rescue the developmentally compromised oocytes or embryos through nuclear-cytoplasmic transfer technology. We have characterized oxidative stress-induced mitochondrial dysfunctions, developmental arrest and cell death in early embryos using animal models. Ultimately, in addition to investigating the mechanisms behind cellular aging underlying infertility, this laboratory aims to produce clinical methods for assessing preimplantation embryo viability, a development that will make a significant contribution to the health of women and children.

Staff

Keefe, David, Director
Liu, Lin, Research Scientist
Pepperell, John, Visiting Investigator
Trimarchi, James, Postdoctoral Scientist

Laboratory of Sensory Physiology

Members of this laboratory have conducted research on various facets of vision since 1973. Current investigations use UV/VIS light microspectrophotometry on vertebrate retinal photoreceptors for the determination of visual pigment absorbance characteristics. One aim is to arrive at a better understanding of the method of spectral tuning that forms the chemical basis of color vision. Polarized light microscopic techniques are used to measure linear dichroism and linear birefringence aimed at revealing structure-function relationships and biophysical mechanisms. An area of interest is polarization discrimination, the mechanisms that could account for the ability of some fish species to detect the direction of polarization of light collected by their eyes. As a recent development, investigations are carried out on sickling in fish red blood cells due to hemoglobin polymerization, once again making extensive use of polarized light microscopic techniques.

Staff

Hárosi, Ferenc I., Senior Scientist, MBL, and Boston University School of Medicine
Novales Flamarique, I., Postdoctoral Fellow

Laboratory of Osamu Shimomura

Biochemical mechanisms involved in the bioluminescence of various luminescent organisms are investigated. Based on the results obtained, various improved forms of bioluminescent and chemiluminescent probes are designed and produced for the measurements of intracellular free calcium and superoxide anion.

Staff

Shimomura, Osamu, Senior Scientist, MBL, and Boston University School of Medicine
Shimomura, Akemi, Research Assistant

Laboratory of Robert B. Silver

The members of this laboratory study how living cells make decisions. The focus of the research, typically using marine models, is on two main areas: the role of calcium in the regulation of mitotic cell division (sea urchins, sand dollars, etc.) and structure and function relationships of hair cell stereociliary movements in vestibular physiology (oyster, toadfish). Other related areas of study, *i.e.* synaptic transmission (squid), are also, at times, pursued. Tools include video light microscopy, multispectral, subwavelength, and very high speed (sub-millisecond frame rate) photon counting video light microscopy, telemanipulation of living cells and tissues, and modeling of decision processes. A cornerstone of the laboratory's analytical efforts is high performance computational processing and analysis of video light microscopy images and modeling. With luminescent, fluorescent, and absorptive probes, both empirical observation and computational modeling of cellular, biochemical, and biophysical processes permit interpretation and mapping of space-time patterns of intracellular chemical reactions and calcium signaling in living cells. A variety of *in vitro* biochemical, biophysical, and immunological methods are used. In addition to fundamental biological studies, the staff designs and fabricates optical hardware, and designs software for large video image data processing, analysis, and modeling.

Staff

Silver, Robert, Associate Scientist

Visiting Scientist

Pearson, John, Los Alamos Nations Laboratory

Interns

King, Leslie A., REU Intern, Duke University
Wise, Alyssa, REU Intern, Yale University

Laboratory of Seymour Zigman

This laboratory is investigating basic mechanisms of photooxidative stress to the ocular lens due to environmentally compatible UVA radiation. This type of oxidative stress contributes to human cataract formation. Other studies are the search for and use of chemical antioxidants to retard the damage that occurs. Cultured mammalian lens epithelial cells and whole lenses *in vitro* are exposed to environmentally compatible UVA radiation with or without previous antioxidant feeding. The following parameters of lens damage are examined: molecular excitation to singlet states via NADPH (the absorber); cell growth inhibition and cell death; catalase inactivation; cytoskeletal description (of actin, tubulin, integrins); and cell membrane damage (lipid oxidation, loss of gap junction integrity and intercellular chemical communications). Thus far, the most successful antioxidant to reduce these deficiencies is alpha-tocopherol (10 μg/ml) and tea polyphenols (especially from green tea). The preliminary phases of the research are usually carried out using marine animal eyes (*i.e.:* smooth dogfish) as models. Our goal is to provide information that will suggest means to retard human cataract formation.

Staff

Seymour Zigman, Laboratory Director, Professor of Ophthalmology, Boston University Medical School
Keen Rafferty, Research Associate, Boston University Medical School
Nancy S. Rafferty, Research Associate, Boston University Medical School
Bunnie R. Zigman, Laboratory Manager, Boston University Medical School

The Marine Resources Center

The Marine Resources Center (MRC) is one of the world's most advanced facilities for maintaining and culturing aquatic organisms essential to advanced biological, biomedical, and ecological research. Service and education also play an important and complementary role in the modern, 32,000-square-foot facility.

The MRC and its life support systems have already increased the ability of MBL scientists to conduct research and have inspired new concepts in scientific experiments. Vigorous research programs focusing on basic biological and biomedical aquatic models are currently being developed at the Center. The Program in Scientific Aquaculture was initiated in 1998.

In addition to research, the MRC provides a variety of services to the MBL community through its Aquatic Resources Division, the Water Quality and System Engineering Division, and the Administrative Division.

Research and educational opportunities are available at the facility to established investigators, postdoctoral fellows, graduate, and undergraduate students. Investigators and students will find that the MRC's unique life support and seawater engineering systems make this a favorable environment in which to conduct independent research and masters and doctoral theses using a variety of aquatic organisms and flexible tank space for customized experimentation on live animals. Prospective investigators and students should contact the Director of the MRC for further information.

Staff

Hanlon, Roger, Director and Senior Scientist
Sussman, Raquel, Investigator
Kuzirian, Alan, Associate Scientist
Maxwell, Michael, Postdoctoral Scientist
Shashar, Nadav, Postdoctoral Scientist

Visiting Investigators

Adamo, Shelly, Dalhousie University, Canada
Baker, Robert, New York University
Boal, Jean, Visiting Scientist
Cavanaugh, Joseph, Boston University Marine Program
Gabr, Howaida, Graduate Student, Suez Canal University, Egypt
Gilland, Edwin, Staff Scientist
Kier, William, University of North Carolina
Spotte, Stephen, University of Connecticut
Wittenberg, Kim, Boston University Marine Program

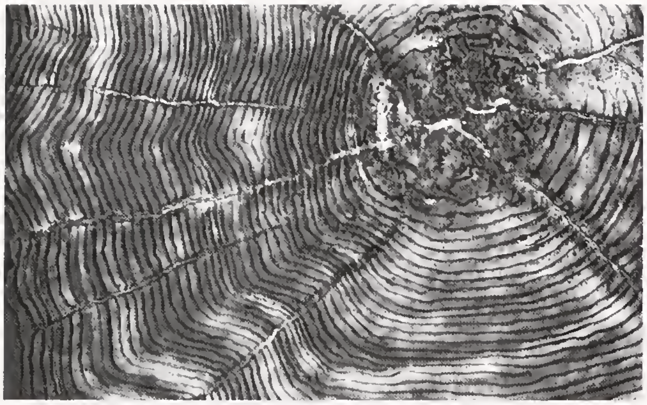

Honors

Friday Evening Lectures

June 19	Stephen L. Hajduk, School of Medicine and Dentistry, University of Alabama at Birmingham "Carriers of Death: Civil War and Tsetse Flies"
June 26	Mary Lidstrom, College of Engineering, University of Washington, Seattle "Borrowing Genes to Create New Metabolism" (Glassman Lecture)
July 3	David Garbers, Howard Hughes Medical Center, Dallas "From Sea Urchins To High Blood Pressure: Smell and Vision"
July 10	Donald Brown, Department of Embryology, Carnegie Institution of Washington "How Tadpoles Turn Into Frogs"
July 17	Irene Pepperberg, Department of Ecology and Evolutionary Biology, University of Arizona, Tucson "In Search of King Solomon's Ring: Studies on Cognitive and Communicative Abilities of Grey Parrots" (Lang Lecture)
July 23, 24	Nicolas Spitzer, Department of Biology, University of California, San Diego 1. "The Development of Electrical Excitability in Nerve and Muscle" 2. "Breaking the Code: Regulation of Differentiation by Patterns of Calcium Transients" (Forbes Lectures)
July 31	Eric Kandel, Center for Neurobiology and Behavior, Howard Hughes Medical Institute, Columbia University "Genes, Synapses and Long-Term Memory"
August 7	Peter Raven, Missouri Botanical Gardens, St. Louis "Biodiversity, the Global Environment, and the New Millennium"
August 14	Matthew Meselson, Harvard University "Evolution Without Sexual Reproduction and Genetic Recombination"

Fellowships and Scholarships

Robert Day Allen Fellowship Fund

Drs. Joseph and Jean Sanger

MBL Associates Endowed Scholarship Fund

MBL Associates
Mr. and Mrs. Douglas P. Amon
Dr. and Mrs. Leonard Laster

Frank A. Brown, Jr. Memorial Readership

Dr. and Mrs. Francis D. Carlson

C. Lalor Burdick Scholarship Fund

The Lalor Foundation

Gary Nathan Calkins Scholarship Fund

Ms. Sarah A. Calkins

Charles R. Crane Fellowship Fund

Friendship Fund
Mr. Thomas S. Crane

John O. Crane Fellowship Fund

Friendship Fund
Mr. Thomas S. Crane

Jean and Katsuma Dan Fellowship Fund

Drs. Joseph and Jean Sanger
Mrs. Eleanor Steinbach

Bernard Davis Fellowship Fund

Mrs. Elizabeth M. Davis

E. E. Just Research Fellowship Fund

Ayco Charitable Foundation
Dr. Jewel Plummer Cobb
Mr. and Mrs. Jonathan Conrad
Fiduciary Trust Company International

Daniel Grosch Scholarship Fund

Ms. Alice C. Leech
Ms. Lena T. Lord
Ms. Enid K. Sichel
Dr. Margaret W. Taft

Aline D. Gross Scholarship Fund

Dr. and Mrs. Benjamin Kaminer
Technic, Inc.

Keffer Hartline Fellowship Fund

Dr. Lloyd M. Beidler
Dr. Lawrence Eisenberg
Dr. Paul Rosen
Mr. Robert L. Schoenfeld
Dr. and Mrs. Jonathan D. Victor
Dr. Earl Weidner
Dr. Torsten Wiesel and Ms. Jean Stein

Fred Karush Endowed Library Readership

Dr. and Mrs. Laszlo Lorand
Dr. and Mrs. Arthur M. Silverstein

Stephen W. Kuffler Fellowship Fund

Dr. and Mrs. Edward A. Kravitz

Frank R. Lillie Fellowship and Scholarship Fund

Dr. and Mrs. George H. Acheson
Mr. and Mrs. John J. Valois

Josiah Macy, Jr. Research Fellowship Fund

Josiah Macy, Jr. Foundation

James A. and Faith Miller Fellowship Fund

Drs. David and Virginia Miller

Frank Morrell Scholarship Fund

Dr. and Mrs. Maynard M. Cohen
Dr. Leyla de Toledo Morrell
Mr. Paul Morrell

Mountain Memorial Fund

Dr. and Mrs. Dean C. Allard, Jr.
Ms. Brenda J. Bodian
Dr. and Mrs. Benjamin Kaminer
Ms. Anne C. Kimball, Ph.D.
Mr. and Mrs. Amos L. Roberts
Mr. and Mrs. William B. Sanford
Mr. and Mrs. Hans L. Schlesinger
Dr. and Mrs. R. Walter Schlesinger

Neural Systems & Behavior Scholarship Fund

Dr. Ronald Calabrese and Dr. Christine Cozzen
Dr. and Mrs. Alan Gelperin
Dr. Warren M. Grill
Dr. Ronald Hoy and Dr. Margaret Nelson
Drs. Darcy B. Kelley and Richard M. Bockman
Dr. William Kristan and Dr. Kathleen French
Dr. Richard and Mrs. Jane Levine
Dr. Janis C. Weeks and Dr. William M. Roberts

Nikon Fellowship Fund

Nikon, Inc.

The Ann Osterhout Edison/Theodore Miller Edison and Olga Osterhout Sears/Harold Bright Sears Endowed Scholarship Fund

Mrs. Jean S. Holden
Dr. Susan M. Plourde

William Townsend Porter Scholarship Fund

William Townsend Porter Foundation

Phillip H. Presley Scholarship Fund

Carl Zeiss, Inc.

Ruth Sager Endowed Scholarship

Dr. Arthur B. Pardee

Science Writing Fellowships Program

Association for Research in Vision and Ophthalmology
American Society for Biochemistry and Molecular Biology
American Society for Cell Biology
American Society for Photobiology
Charles A. Dana Foundation
Federation of American Society for Experimental Biology
Foundation for Microbiology
Friendship Fund
New York Times Foundation
Nicholas B. Ottaway Foundation
Society for Integrative and Comparative Biology
The Times Mirror Foundation
The Washington Post Company

Milton L. Shifman Endowed Scholarship

Milton L. Shifman Scholarship Trust

The Evelyn and Melvin Spiegel Fellowship Fund

Drs. Joseph and Jean Sanger
Drs. Melvin and Evelyn Spiegel
The Sprague Foundation

H. B. Steinbach Fellowship Fund

Mrs. Eleanor Steinbach

Marjorie R. Stetten Scholarship Fund

Ms. Pauline F. Blanchard
Mr. and Mrs. John C. Campbell
Cognos Corporation
Cognos Inc.
Ms. Ann P. B. Fitzgerald
Mr. and Mrs. Douglas W. Lucy
Mr. and Mrs. William Morton
Ms. Linda A. O'Donnel
Mrs. Jane Lazarow Stetten
Mrs. Janet L. Vanderweil
Ms. Ann M. White

Horace W. Stunkard Scholarship Fund

Dr. Albert Stunkard and Dr. Margaret Maurin

Walter L. Wilson Endowed Scholarship

Dr. Paul N. Chervin
Mr. and Mrs. Rexford A. English
Dr. Jean R. Wilson

Fellowships Awarded

MBL Summer Research Fellows

- Mark C. Alliegro, Ph.D., Louisiana State University. Dr. Alliegro uses sea urchins, and a variety of mammalian cells in culture to study the mechanisms of cell differentiation. He was supported by the *Frederik B. Bang Fellowship Fund,* the *James A. and Faith Miller Memorial Fund,* and an *MBL Associates Fellowship.*
- Brian D. Bovard, Ph.D., Duke University. Dr. Bovard worked at a field site located in Abisko, Sweden, this summer. He studies relations between plants and water as part of a climate change project being conducted by scientists at the MBL's Ecosystem Center. He was supported by the *William Townsend Porter Fellowship for Minority Investigators.*
- Wei-Jun Cai, Ph.D., University of Georgia. Dr. Cai is developing microelectrodes to aid in the study of benthic carbon recycling. He was supported by the *Lucy B. Lemann Fellowship.*
- William Cohen, Ph.D., Hunter College. Dr. Cohen uses blood clams in his studies of the formation and function of the cellular framework known as the cytoskeleton. He was supported by the *Erik B. Fries Endowed Fellowship.*
- John Costello, Ph.D., Providence College. Dr. Costello studies the feeding behavior in the comb jelly, *Mnemiopsis leidyi.* He was supported by the *Erik B. Fries Endowed Fellowship,* the *Lucy B. Lemann Fellowship,* and an *MBL Associates Fellowship.*
- John E. Eriksson, Ph.D., Turku Center for Biotechnology, Finland. Dr. Eriksson is studying mitotic protein phosphatases in the eggs of the surf clam, *Spisula.* He was a *Herbert W. Rand Fellow.*
- Andrew F. Giusti, University of California, Santa Barbara. Mr. Giusti investigates the role of the SRC tyrosine kinase during egg activation at fertilization. He was supported by the *Frederik B. Bang Fellowship Fund.*
- Matthew Halstead, Ph.D., University of Auckland, New Zealand. Dr. Halstead studies sensory processing of electrosensory information in the midbrain of the little skate, *Raja.* He was supported by the *M.G.F. Fuortes Fellowship,* the *Frank R. Lillie Fellowship,* and an *MBL Associates Fellowship.*
- Jonathan J. Henry, Ph.D., University of Illinois. Dr. Henry examines the cellular and molecular mechanisms involved in embryonic cell fate and axis determination using barnacles as his research model. He was supported by the *Evelyn and Melvin Spiegel Fellowship Fund* and the *NASA Life Science Program Fellowship.*
- Elizabeth Jonas, Ph.D., Yale University School of Medicine. Dr. Jonas studies the intracellular channels that regulate synaptic function. She was supported by the *Ann E. Kammer Memorial Fellowship Fund,* the *H. B. Steinbach Fellowship,* an *MBL Associates Fellowship,* the *Charles R. Crane Fellowship,* and the *John O. Crane Fellowship Fund.*
- Nicholas Lartillot, Université Paris Sud. Mr. Lartillot conducted a molecular study of mesoderm specification in marine spiralians. He was an *MBL Associates Fellow.*
- Guy Major, a Research Fellow from Lucent Technologies. Mr. Major took voltage-sensitive dye recordings from multiple parts of single brain cells. He was a *Herbert W. Rand Fellow.*
- Mark Martindale, Ph.D., University of Chicago. Dr. Martindale studies the evolution of development, in particular axial specification and the role of the cleavage program in body plan evolution. He was a *NASA Life Sciences Program Fellow.*
- Paul McNeil, Ph.D., Medical College of Georgia. Dr. McNeil hopes to discover how cells reseal tears in their outer covering, the plasma membrane, and to demonstrate that such membrane tears are physiological events. He uses sea urchins, starfish eggs, and squid in his studies. He was supported by a *Robert Day Allen Fellowship* and a *NASA Life Science Program Fellowship.*
- Allen Mensinger, Ph.D., Washington University School of Medicine. Dr. Mensinger is developing an acoustical transmitter tag for neural telemetry. He was a *NASA Life Science Program Fellow* and an *MBL Associates Fellow.*
- Inigo Novales Flamarique, Ph.D., University of Victoria, Canada. Dr. Novales Flamarique studies the functional organization of visual pathways from the retina to the brain in fishes. He was a *Herbert W. Rand Fellow* and an *MBL Associates Fellow.*
- Elaine C. Seaver, Ph.D., University of Texas, Austin. Dr. Seaver studies the mechanism of segmentation in polychaetes. She was supported by the *Evelyn and Melvin Spiegel Fellowship Fund.*
- Matt Wachowiak, Ph.D., University of California, Berkeley. Dr. Wachowiak studies the transmission of olfactory information from sensory cells to the central nervous system. He was supported by a *Stephen W. Kuffler Fellowship* and an *MBL Associates Fellowship.*
- James Q. Zheng, Ph.D., Robert Wood Johnson Medical School. Dr. Zheng studies the cellular mechanisms underlying the formation of nerve connections. He was a *Nikon Fellow.*

Grass Fellows

- Pamela England, Ph.D., California Institute of Technology. Project: Probing the role of the protein tyrosine kinase SRC in long-term potentiation.
- Alexander Gimelbrant, Ph.D., University of Kentucky Medical Center. Project: Characterization of cDNAs specific to individual lobster olfactory receptor neurons.
- Kathryn Jessen-Eller, Ph.D., Tufts University School of Veterinary Medicine. Project: Serotonergic growth and p53 expression in developing embryos.
- Jane Roche King, Ph.D., University of Arizona. Project: Vestibular contribution to escape turning and orientation to prey in the leopard frog, *Rana pipiens.*
- Maria Fabiana Kubke, Ph.D., University of Maryland. Project: Analysis of early position as a function of best frequency in the hindbrain auditory nuclei of the chicken.
- David P. Lenzi, Ph.D., University of Oregon. Project: The role of the synaptic ribbon at sensory cell output synapses.
- Andrey Loboda, University of Pennsylvania. Project: Elucidation of the role of the S4-S5 linker in gating of the shaker potassium channel by site-directed crosslinking and gating current measurements.
- Matthias Lorez, University of Zurich. Project: The role of HRS-2 in synaptic transmission in the giant synapse of the squid *Loligo pealei.*
- Kimberly McAllister, Ph.D., The Salk Institute for Biological Studies. Project: Properties of synapse formation between cultured cortical neurons.
- Kristina S. Mead, Ph.D., University of California, Berkeley. Project: The biomechanics and neurobiology of chemoreception in stomatopods.
- Hong-Sheng Wang, Ph.D., SUNY at Stony Brook. Project: Angiotensin modulation of transient outward current of cardiac myocytes.

MBL Science Writing Fellowships Program

Fellows

Monica Allen, *Bangor Daily News*
Kevin P. Carmody, *Chicago Daily Southtown*

Thomas Carney, *Des Moines Register*
Randall J. Edwards, *Columbus Dispatch*
Don Finley, *San Antonio Express-News*
Joel Greenberg, *The Los Angeles Times*
Ralph K. M. Haurwitz, *Austin American-Statesman*
Diedtra Henderson, *Seattle Times*
Edie Lau, *Sacramento Bee*
Larry Proulx, *The Washington Post*
Frank D. Roylance, *Baltimore Sun*
Angela Swafford, Mas Vida/CBS
Diane Toomey, WUNC Radio
Ulysses Torassa, *Cleveland Plain Dealer*
Karin Vergoth, National Public Radio/Science Friday
Joby S. Warrick, *The Washington Post*
Philip Yam, *Scientific American*

Program Directors

Robert D. Goldman, Northwestern University
Boyce Rensberger, Knight Science Journalism Program

Hands-On Laboratory Course Directors

Rex Chisholm, Northwestern University (Biomedical)
John Hobbie, Marine Biological Laboratory (Environment)
Jerry Melillo, Marine Biological Laboratory (Environment)
Robert Palazzo, University of Kansas (Biomedical)

SPINES—Summer Program in Neuroscience Ethics and Survival

SPINES is a month-long program directed by Joe L. Martinez, Jr., and James Townsel. The program is supported by grants from NIMH administered by the American Psychological Association and the Association of Neuroscience Departments and Programs. SPINES offers an introduction to the opportunities available at the MBL and in the field of neuroscience in general. Fellows are taught responsible conduct in research and other survival skills such as scientific writing, poster construction, presentations, grant mechanisms, and how to seek a postdoctoral or job position.

Fellows

Carlos Bolanos-Guzman
Morry Brown
Winfred Monica Bryan
Damani Nabet-Yero Bryant
Jameel Dennis
Cynthia Gentry
Karen Gilliams
Caterina Maria Hernandez
William Meilandt
Silke Morin
Nivia Perez Acevedo
Osceola Whitney

Scholarships Awarded

Aline D. Gross Scholarship Fund

Tao, Haiyang, Ohio University

American Society for Cell Biology Minorities Affairs Committee

Anderson, Tonya, University of California, Los Angeles
Foster, Andrea, Stanford University
Freeman, Antoinette, Boston University School of Medicine
Hinojos, Cruz, University of Texas, Houston
Tafari, Tsahai, University of California, San Diego

Arthur Klorfein Scholarship and Fellowship Fund

Garcia, Ana Anton, Universidad Miguel Hernandez, Spain
Jacobson, Eyal, Technion, Israel
Rossi, Francesco, Scuola Normale Superiore, Pisa
Tarlera, Silvana, Universidad de la Republica of Uruguay

Biology Club of the College of the City of New York

Belluscio, Leonardo, Columbia University

Burroughs Wellcome Fund Biology of Parasitism Course

Alves, Fábio, Fundação Oswaldo Cruz, Brazil
Arévalo, Myriam, Universidad del Valle Cali
Artis, David, University of Manchester
Henze, Katrin, The Rockefeller University
Hubby, Bolyn, University of Georgia
Lambert, Laurence, Universität München
Lovett, Jennie, Washington University
Lyons, Emily, Indiana University
Matuschewski, Kai, New York University
Nde, Pius, Humboldt University, Germany
Oli, Monica, Auburn University
Paul, Kimberly, Princeton University

Burroughs Wellcome Fund Frontiers In Reproduction Course

Arechavaleta-Velasco, Fabian, National Institute of Nutrition, Mexico
Beg, Mohd, National Institute of Immunology, India
Chen, Chie-Pein, MacKay Memorial Hospital
Moreno, Ricardo, Oregon Regional Primate Research Center
Kumar, Ramasamy Sampath, University of Western Ontario
Sánchez-Partida, Luis, University of Adelaide
Santos, João, Oregon Regional Primate Research Center

Burroughs Wellcome Fund Molecular Mycology Course

Cisalpino, Patricia, Universidade Federal de Minas Gerais
Edens, Heather, Montana State University
Haycocks, Neil, University of Texas Medical Branch
Lee, Samuel, Yale University School of Medicine
Nagabhushan, Moolky, Loyola University, Chicago
Santangelo, Rosaria, Public Health Research Institute, Italy
Schaffrath, Raffael, University of Halle, Germany
Sheppard, Don, McGill University

C. Lalor Burdick Scholarship

Shirasaki, Ryuichi, Osaka University

Caswell Grave Scholarship Fund

Champion, Mia, University of California, Davis
Pollack, Anne, University of Arizona
Tao, Haiyang, Ohio University
Wagner, Eric, Duke University

Charles Baker Metz and William Metz Scholarship Fund in Reproductive Biology

Arechavaleta-Velasco, Fabian, National Institute of Nurtrition, Mexico
Carabatsos, Mary Jo, Tufts University
Euling, Susan, US Environmental Protection Agency
Grazul-Bilska, Anna, North Dakota State University
Halvorson, Lisa, Brigham and Women's Hospital
Rulli, Susan, Hospital General de Ninos Ricardo Gutierrez
Sánchez-Partida, Luis, University of Adelaide

Daniel S. Grosch Scholarship Fund

Castro, Hector, University of Florida

Edwin Grant Conklin Memorial Fund

Wagner, Eric, Duke University

Frank R. Lillie Fellowship and Scholarship Fund

Lee, Agnes, Yale University
Stricker, Jesse, Duke University
Vos, Johannes, University of Massachusetts

Gary N. Calkins Memorial Scholarship Fund

Bjornsson, Christopher, University of Manitoba

Herbert W. Rand Fellowship and Scholarship Fund

Azouz, Rony, University of California, Davis
Battaglia, Francesco, SISSA, Italy
Bi, Guoqiang, University of California, San Diego
Brenner, Naama, NEC Research Institute
Buschbeck, Elke, Cornell University
Cai, Rick, University of California, Los Angeles
d'Avella, Andrea, Massachusetts Institute of Technology
Fairhall, Adrienne, Weizmann Institute, Israel
Fellows, Matthew, Brown University
Hartings, Jed, University of Pittsburgh
Kepecs, Adam, Brandeis University
Klug, Achim, University of Texas
Lee, Ann, Brown University
Machens, Christian, Humboldt University, Germany
Majewska, Anna, Columbia University
Pollack, Anne, University of Arizona
Ruggiano, Stephanie, Boston University
Shaub, Amy, University of North Carolina, Chapel Hill
Soares, Daphne, University of Maryland
Van Rossum, Mark, University of Pennsylvania
Weber, Stacy, Ohio University
Wright, Brian, University of California, San Francisco
Zhang, Ying, Harvard Medical School

Howard A. Schneiderman Endowed Scholarship

Buschbeck, Elke, Cornell University
Shirasaki, Ryuichi, Osaka University
Tahinci, Emilios, Boston University
Wonsettler, Angela, Marshall University School of Medicine

Howard Hughes Medical Institute Educational Scholarship Funding

Berggren, Kirsten, University of Vermont
Bjornsson, Christopher, University of Manitoba
Castro, Hector, University of Florida
Chang, Sunghoe, University of Illinois
Gladfelter, Amy, Duke University
Jacobson, Eyal, Technion, Israel
Locke, Emily, Johns Hopkins University
Mansharamani, Malini, Texas Tech University Health Science Center
Marchant, Jonathan, University of California, Irvine
Ober, Elke, Max-Planck-Institut Tübingen
Pappu, Kartik, Wesleyan University
Roch, Fernando, Wellcome/CRC Institute, United Kingdom
Rozowski, Marion, Wellcome/CRC Institute, United Kingdom
Runft, Linda, University of Connecticut
Shaub, Amy, George Washington University Medical Center
Stricker, Jesse, Duke University
Wagner, Eric, Duke University
Zhou, Ming, State University of New York, Buffalo

Indo-U.S. Contraceptive and Reproductive Health Initiative Program Award

Beg, Mohd, National Institute of Immunology, India

International Brain Research Organization Scholarships

Burzio, Veronica, University of Chile
Concha, Miguel, University of Chile
Gallo, Gianluca, University of Minnesota
Müller, Ferenc, IGBMC, Strasbourg
St. Amant, Louis, McGill University
Wang, Feng, Yale University

Jacques Loeb Founders' Scholarship Fund

Gladfelter, Amy, Duke University

Marjorie W. Stetten Scholarship Fund

Avila, Antonia, CINVESTAV-IPN, Mexico
Pepi, Milva, University of Siena
Speirs, Kendra, University of Pennsylvania

Massachusetts Space Grant Consortium Awards

Monteiro, Antonia, Harvard University
Rocha-Olivares, Axayacatl, Scripps Institution of Oceanography
Rosenthal, Benjamin, Harvard University

MBL Pioneers Scholarship Fund

Geraci, Fabiana, Dip di Biologia Cellulare e dello Sviluppo, Italy
Lupo, Guiseppe, University of Pisa
Ober, Elke, Max-Planck-Institut Tübingen
Vonica, Alin, Cornell University Medical Center

Merck & Company, Inc. Scholarships

Locke, Emily, Johns Hopkins University
Paul, Kimberly, Princeton University
Runft, Linda, University of Connecticut
Saxowsky, Tina, Johns Hopkins School of Medicine
Speirs, Kendra, University of Pennsylvania
Waller, Ross, University of Melbourne
Zaph, Colby, University of Victoria

Mountain Memorial Fund Scholarship

Chenevert, Janet, CNRS, France
Deavours, Bettina, Virginia Tech
Lam, Phoebe, Princeton University
Lamitina, Samuel, Emory University
Omara, Felix, Université de Québec
Zaarour, Rania, Yale University

Pfizer Inc. Endowed Scholarship Fund

Locke, Emily, Johns Hopkins University
Runft, Linda, University of Connecticut

Phillip H. Presley Scholarship Award, Funded by Carl Zeiss, Inc.

Kappler, Andreas, University of Konstanz
Paemeleire, Koen, University of Ghent
Paliulis, Leocadia, Duke University
Pepi, Milva, University of Siena
Rossi, Francesco, Scuola Normale Superiore, Pisa
Takasu, Mari, Harvard University

Planetary Biology Internship Awards

Klappenbach, Joel, Michigan State University
Spear, John, Colorado School of Mines

Ruth Sager Memorial Scholarship

Weber, Stacy, Ohio University

S. O. Mast Memorial Fund

d'Avella, Andrea, Massachusetts Institute of Technology
Komarova, Svetlana, NASA Ames Research Center

Society for Developmental Biology Scholarships

Carabatsos, Mary Jo, Tufts University
Chen, James, Harvard University
Euling, Susan, US Environmental Protection Agency
Grazul-Bilska, Anna, North Dakota State University
Halvorson, Lisa, Brigham and Women's Hospital
McBride, Helen, University of Utah
McCauley, David, Pennsylvania State University
Smith, Katherine, University of Virginia
Stimson, Laura, University of Arizona

Surdna Foundation Scholarship

Ghazi, Arjuman, National Centre for Biological Sciences, India
Lupo, Giuseppe, University of Pisa
Pappu, Kartik, Wesleyan University
Roch, Fernando, Wellcome/CRC Institute, United Kingdom
Tahinci, Emilios, Boston University

Walter L. Wilson Endowed Scholarship Fund

Mansharamani, Malini, Texas Tech University Health Science Center

William F. and Irene C. Diller Memorial Scholarship Fund

Champion, Mia, University of California, Davis

William Morton Wheeler Family Founders' Scholarship

Bjornsson, Christopher, University of Manitoba
Soares, Daphne, University of Maryland
Zhou, Ming, State University of New York, Buffalo

William Randolph Hearst Foundation Scholarships

Wang, Jing, Bell Laboratories
Lee, Agnes, Yale University

William Townsend Porter Fellowship and Scholarship Fund

Anderson, Tonya, University of California, Los Angeles
Foster, Andrea, Stanford University
Freeman, Antoinette, Boston University School of Medicine
Hinojos, Cruz, University of Texas, Houston
McFarlane, Matthew, Stanford University
McGiffert, Christine, University of California, San Diego
Tafari, Tsahai, University of California, San Diego

World Health Organization Scholarships

Arechavaleta-Velasco, Fabian, National Institute of Nutrition, Mexico
Cohen, Débora, IBYME, Argentina
Rulli, Susan, Hospital General de Ninos, Argentina

Post Course Research Awards

Brinda Dass, Texas Tech University Health Sciences Center, Physiology
Bettina Deavours, Virginia Tech, Physiology
James Hitt, SUNY Health Science Center, Syracuse, Neural Systems and Behavior
Adam Kepecs, Brandeis University, Neural Systems and Behavior
Shann Kim, University of Illinois, Chicago, Physiology
Malini Mansharamani, Texas Tech University Health Science Center, Physiology
Jonathan Marchant, University of California, Irvine, Physiology
David McCauley, Penn State University, Embryology
Linda Runft, University of Connecticut, Physiology
Tshai Tafari, University of California, San Diego, Physiology
Sinju Tauhata, Dep. de bioquimica FMRP/USP, Brazil, Physiology
Johannes Vos, University of Massachusetts, Physiology

Board of Trustees and Committees

Corporation Officers & Trustees

Chairman of the Board of Trustees, Sheldon J. Segal, The Population Council
Co-Vice Chair of the Board of Trustees, Frederick Bay, Josephine Bay Paul and C. Michael Paul Foundation
Co-Vice Chair of the Board of Trustees, Mary J. Greer, New York, NY
President of the Corporation, John E. Dowling, Harvard University
Director and Chief Executive Officer, John E. Burris, Marine Biological Laboratory*
Treasurer of the Corporation, Mary B. Conrad, Fiduciary Trust International*
Clerk of the Corporation, Neil Jacobs, Hale and Dorr
Chair of the Science Council, Kerry S. Bloom, University of North Carolina*

Class of 1999

Mary-Ellen Cunningham, Grosse Pointe Farms, MI
Darcy Brisbane Kelley, Columbia University
Laurie J. Landeau, Marinetics, Inc.
Burton J. Lee, III, Vero Beach, FL
Robert E. Mainer, The Boston Company
Jean Pierce, Boca Grande, FL

Class of 2000

Alexander W. Clowes, University of Washington School of Medicine
Story C. Landis, Case Western Reserve University
Irwin B. Levitan, Brandeis University
G. William Miller, G. William Miller and Co., Inc.
Frank Press, The Washington Advisory Group
Christopher M. Weld, Sullivan and Worcester

Class of 2001

Porter Anderson, North Miami Beach, FL
Frederick Bay, Josephine Bay Paul and C. Michael Paul Foundation, Inc.
Martha W. Cox, Hobe Sound, FL
Mary J. Greer, New York, NY
William C. Steere, Jr., Pfizer Inc.
Gerald Weissmann, New York University School of Medicine

**Ex officio*

Class of 2002

Sydney M. Cone, III, Cleary, Gottlieb, Steen & Hamilton
John R. Lakian, The Fort Hill Group, Inc.
Joan V. Ruderman, Harvard Medical School
Sheldon J. Segal, The Population Council
William T. Speck, New York Presbyterian Hospital
Alfred Zeien, The Gillette Company

Honorary Trustees

James D. Ebert, Baltimore, MD
William T. Golden, New York, NY
Ellen R. Grass, The Grass Foundation

Trustees Emeriti

Edward A. Adelberg, Yale University
John B. Buck, Sykesville, MD
Seymour S. Cohen, Woods Hole, MA
Arthur L. Colwin, Key Biscayne, FL
Laura Hunter Colwin, Key Biscayne, FL
Donald Eugene Copeland, Woods Hole, MA
Sears Crowell, Jr., Indiana University
Alexander T. Daignault, Falmouth, MA (deceased)
Teru Hayashi, Woods Hole, MA
Ruth Hubbard, Cambridge, MA
Lewis Kleinholz, Reed College
Maurice Krahl, Tucson, AZ
C. Ladd Prosser, University of Illinois
W.D. Russell-Hunter, Syracuse University
John W. Saunders, Waquoit, MA
D. Thomas Trigg, Wellesley, MA
Walter S. Vincent, Woods Hole, MA

Directors Emeriti

James D. Ebert, Baltimore, MD
Paul R. Gross, Falmouth, MA
Harlyn O. Halvorson, Woods Hole, MA

Executive Committee of the Board of Trustees

Sheldon J. Segal, Chair
Frederick Bay, Co-Vice Chair
Mary J. Greer, Co-Vice Chair
John E. Burris*
Ronald L. Calabrese (1998)
Kerry S. Bloom
Mary B. Conrad
Mary Ellen Cunningham
Robert Mainer
Joan V. Ruderman
Gerald Weissmann

Science Council

Ronald L. Calabrese, Chair (8/98)
Donald Abt (1999)
Clay M. Armstrong (8/98–8/2000)
Peter Armstrong (8/98–8/2000)
Vincent E. Dionne (1999)
John Dowling (8/98)
Barbara Ehrlich (1999)
Laurinda Jaffe (8/98–8/99)
Charles Hopkinson (8/98–8/2000)
Bruce J. Peterson (8/98)
Mitchell Sogin (8/98–8/2000)

Standing Committees of the Board of Trustees

Development

Mary Ellen Cunningham, Chair
Porter W. Anderson
Robert Barlow
Fred Bay
Mary B. Conrad
Martha Cox
James Ebert
Philip Grant
Neil Jacobs
John Lakian
Burton Lee
G. William Miller
Jean Pierce
William Speck
William Steere
Christopher Weld

Facilities & Capital Equipment

Joan Ruderman, Chair
Porter W. Anderson
Frederick Bay
Lawrence Cohen
Neal Cornell
Story Landis
Irwin Levitan
Jean Pierce
Frank Press
Christopher Weld

Investment

Robert Mainer, Chair
Sydney M. Cone
Mary B. Conrad
John R. Lakian
G. William Miller
Sheldon Segal
Alfred Zeien

Finance

Robert Mainer, Chair
Alexander Clowes
Sydney M. Cone
Mary B. Conrad
Donald DeHart
Neil Jacobs
Darcy Kelley
John R. Lakian
Laurie Landeau
Werner Loewenstein
Robert Manz
G. William Miller
Ronald O'Hanley
Alfred Zeien

Nominating

Gerald Weissmann
Ronald L. Calabrese
Alexander Clowes
Martha Cox
Mary Ellen Cunningham
Mary Greer
Story Landis
Sheldon Segal
William Steere

Standing Committees of the Corporation and Science Council

Buildings and Grounds

Lawrence B. Cohen, Chair
Barbara C. Boyer
Alfred B. Chaet
Richard Cutler*
William R. Eckberg

**Ex officio*

Barry Fleet*
Ferenc Harosi
Joe Hayes*
Bruce J. Peterson
Kenyon S. Tweedell
Ivan Valiela

Education Committee

John Dowling, Chair
Kerry S. Bloom
Elaine Bearer
Vincent Dione
Paul Dunlap
Rachel Fink
Roger Hanlon
Holger Jannasch
George M. Langford
Michael Mendelsohn
Steve Zottoli
Ron Calabrese*
E.A. Dawidowicz*
Dorianne Chrysler Mebane*

Fellowships

Thoru Pederson, Chair
Linda Deegan
Barbara Ehrlich
George M. Langford
Jose Lemos
Cindy Lee VanDover
E.A. Dawidowicz*
Sandra Kaufmann*

Housing, Food Service and Child Care

Carole Browne, Chair
Kerry S. Bloom
LouAnn King*
Robert P. Malchow
Darrell R. Stokes
Ann E. Stuart
Janis C. Weeks

MBL/WHOI Library Joint Advisory Committee

David Shepro, Chair, MBL
Judy Ashmore, MBL*
David Dow, NMFS
Daniel Fornari, WHOI
G. Richard Harbison, WHOI
John Hobbie, MBL
Sylvia Kane, NMFS
Mark Kurz, WHOI
Colleen Hurter, WHOI*
Cathy Norton, MBL*
James Robb, USGS
Birgit Rose, MBL
Peter J.S. Smith, MBL
Bruce Warren, WHOI

Research Services and Space

Hans Laufer, Chair
Peter B. Armstrong
Neal Cornell
Richard Cutler*
E.A. Dawidowicz*
Kenneth Foreman
Louis M. Kerr*
David Landowne
Andrew Mattox*
Merle Mizell
Peter J.S. Smith
Paul Steudler
Ivan Valiela

Discovery: The Campaign for Science at the Marine Biological Laboratory Steering Committee

Frederick Bay, Campaign Chair
William T. Golden, Honorary Chair
Ellen R. Grass, Honorary Chair
Alexander W. Clowes, Vice-Chair
Martha W. Cox, Vice-Chair
G. William Miller, Vice-Chair
Gerald Weissmann, Vice-Chair
Porter W. Anderson
Robert B. Barlow, Jr.
Norman Bernstein
Jewell Plummer Cobb
Mary B. Conrad
Mary Ellen Cunningham
John E. Dowling
James D. Ebert
Gerald D. Fischbach
Robert D. Goldman
Mary J. Greer
M. Howard Jacobson
Laurie J. Landeau
George M. Langford
Burton J. Lee, III
Jean Pierce
Robert A. Prendergast
David Shepro
William T. Speck
William C. Steere, Jr.
Christopher M. Weld
Alfred M. Zeien

**Ex officio*

Council of Visitors

Norman B. Asher, Esq., Hale and Dorr, Boston, MA

Mr. Donald J. Bainton, Chairman & CEO, Continental Can Co., Boca Raton, FL
Mr. David Bakalar, Chestnut Hill, MA
Mr. Charles A. Baker, The Liposome Company, Inc., Princeton, NJ
Dr. George P. Baker, Massachusetts General Hospital, Boston, MA
Dr. Sumner A. Barenberg, Bernard Technologies, Chicago, IL
Mr. Robert P. Beech, President/CEO, Component Software International, Inc., Mason, Ohio
Mr. George Berkowitz, Chairman and Founder, Legal Sea Foods, Allston, MA
Dr. Elkan R. Blout, Harvard Medical School, Boston, MA
Mr. and Mrs. Philip Bogdanovitch, Lake Clear, New York
Mr. Malcolm K. Brachman, Northwest Oil Company, Dallas, TX
Dr. Goodwin M. Breinin, New York University Medical Center, New York, NY

Mr. John Callahan, President, Carpenter, Sheperd & Warden, New London, NH
Mrs. Elizabeth Campanella, West Falmouth, MA
Thomas S. Crane, Esq., Mintz Levin Cohen Ferris Glovsky & Popeo, PC, Boston, MA
Dr. Stephen D. Crocker, Chief Technology Officer, Cyber Cash Inc., Reston, VA
Ms. Lynn W. Piasecki Cunningham, Film and Videomaker, Piasecki Productions, Brookline, MA
Dr. Anthony J. Cutaia, Sr. Director, Office of Health Issues, Anheuser-Busch, Inc., St. Louis, Missouri

Dr. Georges de Ménil, DM Foundation, New York, NY
Mrs. Sara Greer Dent, Chevy Chase, MD
Mr. D. H. Douglas-Hamilton, Vice President, Research and Development, Hamilton Thorne Research, Beverly, MA
Mr. Benjamin F. Du Pont, Du Pont Company, Deepwater, New Jersey

Dr. Sylvia A. Earle, Founder, Deep Ocean Engineering, Oakland, CA

Mr. Anthony B. Evnin, General Partner, Venrock Associates, New York, NY

Stuart Feiner, Esq., Vice President and Secretary, General Counsel, Inco Limited, Toronto, Ontario, Canada
Mrs. Hadley Mack French, Consultant, Edsel & Eleanor Ford House, Grosse Pointe Farms, MI

Mr. William J. Gilbane, Jr., Gilbane Building Company, Providence, RI
Dr. Michael J. Goldblatt, Intelligent Biocides, Tewksbury, MA
Mr. Maynard Goldman, President, Maynard Goldman & Associates, Boston, MA

Ms. Charlotte I. Hall, Edgartown, MA
Mr. Thomas J. Hynes, Jr., President, Meredith & Grew, Inc., Boston, MA

Mr. M. Howard Jacobson, Bankers Trust Westborough, MA

Mrs. Elizabeth Ford Kontulis, New Canaan, CT

Mr. and Mrs. Robert Lambrecht, Boca Grande, FL
Dr. Catherine C. Lastavica, Tufts University School of Medicine, Boston, MA
Mr. Joel A. Leavitt, Boston, MA
Mr. Stephen W. Leibholz, President, TechLabs, Inc., Huntingdon, PA
Mrs. Margaret Lilly, West Falmouth, MA
Mr. George W. Logan, Chairman, Valley Financial Corp., Roanoke, VA

Mr. Michael T. Martin, SportsMark, Inc., New York, NY
Mrs. Christy Swift Maxwell, Grosse Pointe Farms, MI
Mr. Ambrose Monell, G. Unger Vetlesen Foundation, Palm Beach, FL

Dr. Mark Novitch, Washington, DC

Ms. Julie Packard, Executive Director, Monterey Bay Aquarium, Monterey, CA
Mr. David R. Palmer, Founder & Managing Director, David Ross Palmer & Associates, Waquoit, MA
Dr. Roderic B. Park, Richmond, CA

Mr. Santo P. Pasqualucci, President/CEO Falmouth Co-Operative Bank, Falmouth, MA
Mr. Robert Pierce, Jr., Pierce Aluminum Co., Canton, MA

Mr. Richard Reston, Editor and Publisher, Vineyard Gazette, Edgartown, MA
Mr. Marius Robinson, Managing Partner, Fundamental Investors Ltd., Key Biscayne, FL
John W. Rowe, M.D., President, Mt. Sinai School of Medicine and Mt. Sinai Medical Center, New York, NY
Mr. Edward Rowland, Tucker, Anthony, Inc., Boston, MA

Mr. Gregory A. Sandomirsky, Mintz Levin Cohen Ferris Glovsky & Popeo, PC, Boston, MA
Mrs. Mary Schmidek, Marion, MA
Dr. Cecily C. Selby, New York, NY
Mr. Robert S. Shifman, St. Simon's Island, GA
Mr. and Mrs. Gregory Skau, Grosse Pointe Farms, MI
Mr. Malcolm B. Smith, Vice Chairman, General American Investors Co., New York, NY
Mr. John C. Stegeman, Owner, Campus Rentals, Ann Arbor, MI
Mr. Joseph T. Stewart, Jr., Skillman, NJ
Mr. John W. Stroh, III, Chief Executive Officer, The Stroh Brewery Company, Detroit, MI
Mr. Gerard L. Swope, Washington, DC
Mr. John F. Swope, Concord, NH

Mr. and Mrs. Stephen E. Taylor, Boston, MA

Mrs. Donna Vanden Bosch-Flynn, Spring Lake, NJ
Mrs. Carolyn W. Verbeck, Vineyard Haven, MA

Mr. Benjamin S. Warren, III, Grosse Pointe Farms, MI
Nancy B. Weinstein, R.N., The Hospice, Inc., Glen Ridge, NJ
Stephen S. Weinstein, Esq., Morristown, NJ
Mr. Frederick J. Weyerhaeuser, Beverly, MA
Mr. Tony L. White, The Perkin Elmer Corporation, Norwalk, CT
Dr. Torsten N. Wiesel, President Emeritus, The Rockefeller University, New York, NY

Administrative Support Staff[1]

Biological Bulletin

Greenberg, Michael J., Editor-in-Chief
Hinkle, Pamela Clapp, Managing Editor
  Burns, Patricia
  Gibson, Victoria R.
  Schachinger, Carol H.

Financial Services Office

Lane, Jr., Homer W., Chief Financial Officer
Roddy, Timothy, Chief Financial Officer
Bowman, Richard, Controller
  Afonso, Janis
  Barry, Maureen
  Dwyer, Patricia E.
  Eidelman, Dana
  Hopkins, Ann E.
  Lancaster, Cindy
  Poravas, Maria
  Ranzinger, Laura
  Sprague, Patricia A.
  Stark, Judy M.
  Stellrecht, Lynette

Stock Room

Schorer, Timothy M., Supervisor
Capano, Holly[2]
O'Connor-Lough, Susan

Purchasing

Hall Jr., Lionel E., Supervisor
Shamon, Lynne R.
Stone, Janice G.[2]

Director's Office

Burris, John E., Director and Chief Executive Officer
  Donovan, Marcia H.
  MacNeil, Jane L.

External Affairs

Carotenuto, Frank C., Director
  Butcher, Valerie
  Callahan Jr., John L.[2]
  Faxon, Wendy P.
  Martin, Theresa H.
  Maxwell, Thanh L.[2]
  Patch-Wing, Dolores
  Quigley, Barbara A.
  Scibek, John C.
  Shaw, Kathleen L.

Associates Program

Bohr, Kendall B.
Brown, Shannon K.[2]
Gault, Miciah Bay[2]

Communications Office

Hinkle, Pamela Clapp, Director
Burton, Anne E.
Flynn, Bridget
Hinkle, Kristen[2]
Joslin, Susan
Liles, Beth R.

Housing and Conferences

King, LouAnn D., Director
  Barry, Maureen J.
  Grasso, Deborah
  Hanlon, Arlene K.[2]
  Johnson-Horman, Frances N.
  Masse, Todd C.
  Perito, Diana

Switchboard

Baker, Ida M.[2]
Ridley, Alberta W.[2]

Human Resources

Goux, Susan P., Director
  Cox, Sarah[2]
  Drange, Stacey B.
  Houser, Carmen
  Renaud, Nina L.

Marine Resources Center

Hanlon, Roger T., Director
  Moniz, Priscilla

---

[1] Including persons who joined or left the staff during 1998.
[2] Summer or temporary.

Aquatic Resources Department

Enos, Jr., Edward G., Superintendent
Bourque, Ryan M.[2]
Chappell, P. Dreux[2]
DeGiorgis, Joseph A.[2]
Grossman, William M.
Gudas, Christopher N.[2]
Kilpatrick, Brian[2]
Klimm III, Henry W.
Luther, Herbert
Mansfield, Darren P.[2]
Sexton, Andrew W.
Smith, Gary[2]
Sullivan, Daniel A.
Tassinari, Eugene

MRC Life Support System

Mebane, William N., Systems Operator
Hanley, Janice S.
Kuzirian, Alan
Solbo, Jr., Steven[2]
Stukey, Jetley M.
Till, Geoffrey A.

MBL/WHOI Library

Norton, Catherine N., Director
Ashmore, Judith A.
Costa, Marguerite E.
Crocker, Daniel[2]
Cullen, Cynthia M.[2]
Deveer, Joseph M.
Duda, Laurel E.
Farrar, Stephen R. L.
Medeiros, Melissa
Monahan, A. Jean
Moniz, Kimberly L.
Nelson, Heidi
Riley, Jacqueline
Swasey, Anne E.[2]

Copy Center

Mountford, Rebecca J., Supervisor
Abisla, Richard L.[2]
Clark, Tamara L.
Delaney, Elizabeth S. (Suwijn)[2]
Kefeauver, Lee
LaPlante, Robert F.
Mancini, Mary E.
Sorocco, Debra[2]
Wallace, Jennifer[2]
Warner, Kathleen[2]

Information Systems Division

Smith, Adrian P., Assistant Director
Berrios, Kelly[2]
Ennis, Douglas E.[2]
Gage, Timothy J.[2]
Katz, Corey[2]
Malchow, Robert[2]
Mountford, Rebecca J.
Moynihan, James V.
Remsen, David P.
Renna, Denis J.
Space, David B.

Safety Services

Mattox, Andrew H., Environmental, Health, and Safety Manager
Bradley, Margaret[2]
O'Neill, Maureen D.[2]

Service, Projects and Facilities

Cutler, Richard D., Director
Enos, Joyce B.

Apparatus

Baptiste, Michael G.
Barnes, Franklin D.
Haskins, William A.

Building Services & Grounds

Hayes, Joseph H., Superintendent
Anderson, Lewis B.
Atwood, Paul R.
Baker, Harrison S.
Barnes, Susan M.
Berrios, Jessica L.[2]
Boucher, Richard L.
Brenerman, Brian[2]
Brereton, Richard S.[2]
Callahan, John J.
Cameron, Lawrence M.[2]
Collins, Paul J.
Cowan, Matthew B.[2]
Cutler, Matthew D.[2]
Dimond, Jay[2]
Dorris, John J.
Eldridge, Myles[2]
Fernandez, Peter R.[2]
Gibbons, Roberto G.
Gonsalves, Nelson
Gray, Joshua[2]
Hannigan, Catherine
Harrington, James D.
Illgen, Robert F.
Lawrence, Adam[2]
Ledwell, L. Patrick[2]
Luther, Herbert
Lynch, Henry L.
Maccaro, Jackie
Mayock, Michael J.[2]
McNamara, Noreen M.
McQuillan, Jeffrey[2]
Plant, Stephen W.
Rattacasa, Frank[2]
Ryan, Timothy A.[2]
Sholkovitz, David[2]
Silva, Cynthia C.
Stites, Clint[2]
Tardif, Joseph G. R.[2]
Ware, Lynn M.

Plant Operations and Maintenance

Fleet, Barry M., Superintendent
Cadose, James W., Maintenance Supervisor

Barnes, John S.
Blunt, Hugh F.
Bourgoin, Lee E.
Carini, Robert J.
Carroll, James R.
Deree, Dana J.
Fish Jr., David L.
Fuglister, Charles K.
Goehl, George
Gonsalves, Jr., Walter W.
Hathaway, Peter J.
Henderson, Jon R.
Justason, C. Scott
Langill, Richard
Lochhead, William M.
McAdams III, Herbert M.
McHugh, Michael O.
Mills, Stephen A.
Olive, Jr., Charles W.
Schoepf, Claude
Settlemire, Donald
Shepherd, Denise M.
Sylvia, Frank E.[2]
Toner, Michael
Wetzel, Ernest D.[2]

Photolab
Nelson, Linda M.

Research Administration & Educational Programs

Dawidowicz, Eliezar A., Director
Hamel, Carol C.
Kaufmann, Sandra J.
Kefauver, Lee
Iwaszko, Nicole[2]
Lynn, Rebecca
Mebane, Dorianne C.
Malmude-Davis, Anna[2]
Palmer, Pamela[2]
Patten, Brooke A.[2]
Stukey, Jetley

Central Microscopy Facility and General Use Rooms
Kerr, Louis M., Supervisor
DeProto, Jamin E.[2]
Luther, Herbert
Peterson, Martha B.

Josephine Bay Paul Center for Comparative Molecular Biology and Evolution Administrative Staff

Harris, Marian
Lim, Pauline

Journal of Membrane Biology

Loewenstein, Werner R., Editor
Fay, Catherine H.
Howard Isenberg, Linda L.
Lynch, Kathleen F.

Satellite/Periwinkle Children's Programs

Robinson, Paulina H.[2]
Browne, Jennifer L.[2]
Collins, Anne E.[2]
Curran, Kelly[2]
Douglas, Alicia D.[2]
Fitzelle, Annie[2]
Gallant, Carolyn A.[2]
Gallant, Cynthia[2]
Guiffrida, Beth[2]
Griffin, Courtney A.[2]
Jenkins, Michelle[2]
Laundy, Jennifer[2]
McCusker, Stephanie[2]
Robinson, Jayma L.[2]

NASA Center for Advanced Studies in the Space Life Sciences

Dawidowicz, Eliezar A., Administrator
Amit, Udeni P.

Ecosystems Center Administrative Staff

Berthel, Dorothy J.
Donovan, Suzanne J.
Nunez, Guillermo
Seifert, Mary Ann

Members of the Corporation

Life Members

Acheson, George H., 25 Quissett Avenue, Woods Hole, MA 02543
Adelberg, Edward A., 204 Prospect Street, New Haven, CT 06511-2107
Afzelius, Bjorn, University of Stockholm, Wenner-Gren Institute, Department of Ultrastructure Research, Stockholm, SWEDEN
Amatniek, Ernest, address unknown
Arnold, John M., 329 Sippewissett Road, Falmouth, MA 02540

Bang, Betsy G., 76 F. R. Lillie Road, Woods Hole, MA 02543
Bartlett, James H., University of Alabama, Department of Physics, Box 870324, Tuscaloosa, AL 35487-0324
Berne, Robert M., University of Virginia School of Medicine, Department of Physiology, Box 1116, MR4, Charlottesville, VA 22903
Bernheimer, Alan W., New York University Medical Center, Department of Microbiology, 550 First Avenue, New York, NY 10016
Bertholf, Lloyd M., Westminster Village, #2114, 2025 East Lincoln Street, Bloomington, IL 61701-5995
Bosch, Herman F., P.O. Box 353, Woods Hole, MA 02543
Buck, John B., Fairhaven C-020, 7200 Third Avenue, Sykesville, MD 21784
Burbanck, Madeline P., P.O. Box 15134, Atlanta, GA 30333
Burbanck, William D., P.O. Box 15134, Atlanta, GA 30333

Carlson, Francis D., Johns Hopkins University, Biophysics Department Jenkins Hall, North Charles Street, Baltimore, MD 21218 (deceased)
Clark, Arnold M., 53 Wilson Road, Woods Hole, MA 02543
Clark, James M., 258 Wells Road, Palm Beach, FL 33480-3625
Cohen, Seymour S., 10 Carrot Hill Road, Woods Hole, MA 02543-1206
Colwin, Arthur L., 320 Woodcrest Road, Key Biscayne, FL 33149-1322
Colwin, Laura Hunter, 320 Woodcrest Road, Key Biscayne, FL 33149-1322
Cooperstein, Sherwin J., University of Connecticut, School of Medicine, Department of Anatomy, Farmington, CT 06030-3405
Copeland, D. Eugene, Marine Biological Laboratory, Woods Hole, MA 02543
Corliss, John O., P.O. Box 2729, Bala Cynwyd, PA 19004-2116
Costello, Helen M., Carolina Meadows, Villa 137, Chapel Hill, NC 27514-8512
Crouse, Helen, Rte. 3, Box 213, Hayesville, NC 28904

DeHaan, Robert L., Emory University School of Medicine, Department of Anatomy & Cell Biology, 1648 Pierce Drive, Room 108, Atlanta, GA 30322
Dudley, Patricia L., 3200 Alki Avenue SW, #401, Seattle, WA 98116

Edwards, Charles, 3429 Winding Oaks Drive, Longboat Key, FL 34228
Elliott, Gerald F., The Open University Research Unit, Foxcombe Hall, Berkeley Road, Boars Hill, Oxford OX1 5HR, ENGLAND

Failla, Patricia M., 2149 Loblolly Lane, Johns Island, SC 29455
Ferguson, James K. W., 56 Clarkehaven Street, Thornhill, Ontario L4J 2B4, CANADA

Glusman, Murray, New York State Psychiatric Institute, 722 W. 168th St., Unit #70, New York, NY 10032
Goldman, David E., 140 Ter Heun Drive, Room 212, Falmouth, MA 02540 (deceased)
Graham, Herbert, 36 Wilson Road, Woods Hole, MA 02543

Hamburger, Viktor, Washington University, Department of Biology, 740 Trinity Avenue, St. Louis, MO 63130
Hamilton, Howard L., University of Virginia, Department of Biology, 238 Gilmer Hall, Charlottesville, VA 22901
Harding, Jr., Clifford V., 54 Two Ponds Road, Falmouth, MA 02540
Haschemeyer, Audrey E. V., 21 Glendon Road, Woods Hole, MA 02543-1406
Hauschka, Theodore S., 333 Fogler Road, Bremen, ME 04551
Hayashi, Teru, 15 Gardiner Road, Woods Hole, MA 02543-1113
Hisaw, Frederick L., 1765 SW Tamarack Street, Apt 11, McMinnville, OR 97128-7416
Hoskin, Francis C. G., c/o Dr. John E. Walker, U.S. Army Natick RD&E Center, SAT NC-YSM, Kansas Street, Natick, MA 01760-5020
Humes, Arthur G., Marine Biological Laboratory, Boston University Marine Program, Woods Hole, MA 02543
Hunter, W. Bruce, 305 Old Sharon Road, Peterborough, NH 03458-1736

Hurwitz, Charles, Stratton VA Medical Center, Research Service, Albany, NY 12208

Katz, George, Merck, Sharp and Dohme, Fundamental & Experimental Research Laboratory, PO Box 2000, Rahway, NJ 07065
Kingsbury, John M., Cornell University, Department of Plant Biology, Plant Science Building, Ithaca, NY 14853
Kleinholz, Lewis, Reed College, Department of Biology, 3203 SE Woodstock Boulevard, Portland, OR 97202
Kusano, Kiyoshi, National Institutes of Health, Building 36, Room 4D-20, Bethesda, MD 20892

Laderman, Ezra, Yale University, New Haven, CT 06520
LaMarche, Paul H., Eastern Maine Medical Center, 489 State Street, Bangor, ME 04401
Lauffer, Max A., Penn State University Medical Center, Department of Biophysics & Physiology, Hershey, PA 17033
LeFevre, Paul G., 15 Agassiz Road, Woods Hole, MA 02543 (deceased)
Lochhead, John H., 49 Woodlawn Road, London SW6 6PS, UK
Loewus, Frank A., Washington State University, Institute of Biological Chemistry, Pullman, WA 99164
Loftfield, Robert B., University of New Mexico, School of Medicine, Albuquerque, NM 87131

Malkiel, Saul, 174 Queen Street, #9A, Falmouth, MA 02540
Marsh, Julian B., 9 Eliot Street, Chestnut Hill, MA 02467-1407
Martin, Lowell V., 10 Buzzards Bay Avenue, Woods Hole, MA 02543
Mathews, Rita W., East Hill Road, P.O. Box 237, Southfield, MA 01259-0237
Moore, John A., University of California, Department of Biology, Riverside, CA 92521
Moscona, Aron A., University of Chicago, Department Molecular Genetics & Cell Biology, Chicago, IL 60637
Musacchia, X. J., P.O. Box 5054, Bella Vista, AR 72714-0054

Nasatir, Maimon, P.O. Box 379, Ojai, CA 93024

Passano, Leonard M., University of Wisconsin, Department of Zoology, Birge Hall, Madison, WI 53706
Prosser, C. Ladd, University of Illinois, Department of Physiology, 524 Burrill Hall, Urbana, IL 61801
Prytz, Margaret McDonald, address unknown

Ratner, Sarah, Public Health Research Institute, Department of Biochemistry, 455 First Avenue, New York, NY 10016
Renn, Charles E., address unknown
Reynolds, George T., Princeton University, Department of Physics, Jadwin Hall, Princeton, NJ 08544
Rice, Robert V., 30 Burnham Drive, Falmouth, MA 02540
Rockstein, Morris, 600 Biltmore Way, Apt. 805, Coral Gables, FL 33134
Ronkin, Raphael R., 3212 McKinley Street, NW, Washington, DC 20015-1635

Sanders, Howard L., Woods Hole Oceanographic Institution, Woods Hole, MA 02543
Sato, Hidemi, Nagoya University, 3-24-101, Oakinishi Machi, Toba Mie 517-0023, JAPAN
Saz, Arthur K., Georgetown University Medical School, Department of Immunology, Washington, DC 20007
Schlesinger, R. Walter, 7 Langley Road, Falmouth, MA 02540-1809
Scott, Allan C., Colby College, Waterville, ME 04901
Silverstein, Arthur M., Johns Hopkins University, Institute of the History of Medicine, 1900 E. Monument Street, Baltimore, MD 21205
Sjodin, Raymond A., University of Maryland, Department of Biophysics, Baltimore, MD 21201
Smith, Paul F., P.O. Box 264, Woods Hole, MA 02543-0264
Speer, John W., 293 West Main Road, Portsmouth, RI 02871
Sperelakis, Nicholas, University of Cincinnati, Department of Physiology/Biophysics, 231 Bethesda Avenue, Cincinnati, OH 45267-0576
Spiegel, Evelyn, Dartmouth College, Department of Biological Sciences, 204 Gilman, Hanover, NH 03755
Spiegel, Melvin, Dartmouth College, Department of Biological Sciences, 204 Gilman, Hanover, NH 03755
Steinhardt, Jacinto, 1508 Spruce Street, Berkeley, CA 94709 (deceased)
Stephens, Grover C., University of California, School of Biological Sciences, Department of Ecology and Evolution/Biology, Irvine, CA 92717
Strehler, Bernard L., 2310 N. Laguna Circle Drive, Agoura, CA 91301-2884
Sussman, Maurice, 72 Carey Lane, Falmouth, MA 02540
Sussman, Raquel B., Marine Biological Laboratory, Woods Hole, MA 02543
Szent-Gyorgyi, Gwen P., 45 Nobska Road, Woods Hole, MA 02543

Taylor, Robert E., 339 Gifford Street, Apt. 303, Falmouth, MA 02540 (deceased)
Thorndike, W. Nicholas, Wellington Management Company, 200 State Street, Boston, MA 02109
Trager, William, The Rockefeller University, 1230 York Avenue, New York, NY 10021-6399
Trinkaus, J. Philip, 870 Moose Hill Road, Guilford, CT 06437

Villee, Jr., Claude A., Harvard Medical School, Carrel L. Countway Library, 10 Shattuck Street, Boston, MA 02115
Vincent, Walter S., 16 F.R. Lillie Road, Woods Hole, MA 02543

Wald, Ruth, Harvard University, Biological Laboratories, Cambridge, MA 02138
Waterman, Talbot H., Yale University, Box 208103, 912 KBT Biology Department, New Haven, CT 06520-8103
Wigley, Roland L., 35 Wilson Road, Woods Hole, MA 02543
Wilber, Charles G., Colorado State University, Department of Biology, Forensic Science Laboratory, Fort Collins, CO 80523 (deceased)

Members

Abt, Donald A., Marine Biological Laboratory, Laboratory of Aquatic Animal Medicine and Pathology, Woods Hole, MA 02543
Adams, James A., 3481 Paces Ferry Road, Tallahassee, FL 32308
Adelman, William J., 160 Locust Street, Falmouth, MA 02540
Alkon, Daniel L., NIH Laboratory of Adaptive Systems, 36 Convent Drive, MSC 4124, 36/4A21, Bethesda, MD 20892-4124
Allen, Garland E., Washington University, Department of Biology, Box 1137, One Brookings Drive, Street Louis, MO 63130-4899
Allen, Nina S., North Carolina State University, Department of Botany, Box 7612, Raleigh, NC 27695
Alliegro, Mark C., Louisiana State University Medical Center, Department of Cell Biology and Anatomy, 1901 Perdido Street, New Orleans, LA 70112
Anderson, Everett, Harvard Medical School, Department of Cell Biology, 240 Longwood Avenue, Boston, MA 02115-6092
Anderson, John M., 110 Roat Street, Ithaca, NY 14850

Anderson, Porter W., 100 Bayview Drive #2224, North Miami Beach, FL 33160
Arnett-Kibel, Christine, University of Massachusetts, Dean of Science Faculty, Boston, MA 02125
Armstrong, Clay M., University of Pennsylvania School of Medicine, B701 Richards Building, Department of Physiology, 3700 Hamilton Walk, Philadelphia, PA 19104-6085
Armstrong, Ellen Prosser, 57 Millfield Street, Woods Hole, MA 02543
Arnold, William A., Oak Ridge National Laboratory, Biology Division, 102 Balsalm Road, Oak Ridge, TN 37830
Ashton, Robert W., Bay Foundation, 17 West 94th Street, New York, NY 10025
Atema, Jelle, Boston University Marine Program, Marine Biological Laboratory, Woods Hole, MA 02543

Baccetti, Baccio, University of Sienna, Institute of Zoology, 53100 Siena, ITALY
Baker, Robert G., New York University Medical Center, Department Physiology and Biophysics, 550 First Avenue, New York, NY 10016
Baldwin, Thomas O., Texas A and M University, Department of Biochemistry and Biophysics, College Station, TX 77843-2128
Baltimore, David, California Institute of Technology, 204-31, Pasadena, CA 91125
Barlow, Robert B., SUNY Health Science Center at Syracuse, 750 East Adams Street, Center for Vision Research, 3258 Weiskotten Hall, Syracuse, NY 13210
Barry, Daniel T., 2415 Fairwind Drive, Houston, TX 77062-4756
Barry, Susan R., Mount Holyoke College, Department of Biological Sciences, South Hadley, MA 01075
Bass, Andrew H., Cornell University, Department of Neurobiology and Behavior, Seely Mudd Hall, Ithaca, NY 14853
Battelle, Barbara-Anne, University of Florida, Whitney Laboratory, 9505 Ocean Shore Boulevard, Street Augustine, FL 32086
Bay, Frederick, Bay Foundation, 17 W. 94th Street, First Floor, New York, NY 10025-7116
Baylor, Martha B., P.O. Box 93, Woods Hole, MA 02543
Bearer, Elaine L., Brown University, Division of Biology and Medicine, Department of Pathology, Box G, Providence, RI 02912
Beatty, John M., University of Minnesota, Department of Ecology and Behavioral Biology, 1987 Gortner, Street Paul, MN 55108
Beaugè, Luis Alberto, Instituto de Investigacion Medica, Department of Biophysics, Casilla de Correo 389, 5000 Cordoba, ARGENTINA
Begenisich, Ted, University of Rochester, Medical Center, Box 642, 601 Elmwood Avenue, Rochester, NY 14642
Begg, David A., University of Alberta, Faculty of Medicine, Department of Cell Biology and Anatomy, Edmonton, Alberta T6G 2H7, CANADA
Bell, Eugene, Tissue Engineering, Inc., 451 D Street, Boston, MA 02210
Benjamin, Thomas L., Harvard Medical School, Pathology, D2-230, 200 Longwood Avenue, Boston, MA 02115
Bennett, Michael V. L., Albert Einstein College of Medicine, Department of Neuroscience, 1300 Morris Park Avenue, Bronx, NY 10461
Bennett, Miriam F., Colby College, Department of Biology, Waterville, ME 04901
Berg, Carl J., P.O. Box 681, Kilauea, Kauai, HI 96754-0681
Berlin, Suzanne T., 5 Highland Street, Gloucester, MA 01930
Bernstein, Norman, Columbia Realty Venture, 5301 Wisconsin Avenue, NW, #600, Washington, DC 20015-2015
Bezanilla, Francisco, Health Science Center, Department of Physiology, 405 Hilgard Avenue, Los Angeles, CA 90024
Biggers, John D., Harvard Medical School, Department of Physiology, Boston, MA 02115
Bishop, Stephen H., Iowa State University, Department of Zoology, Ames, IA 50010
Blaustein, Mordecai P., University of Maryland, School of Medicine, Department of Physiology, Baltimore, MD 21201
Blennemann, Dieter, 1117 East Putnam Avenue, Apt. #174, Riverside, CT 06878-1333
Bloom, George S., The University of Texas Southwestern Medical Center, Department of Cell Biology and Neuroscience, 5323 Harry Hines Boulevard, Dallas, TX 75235-9039
Bloom, Kerry S., University of North Carolina, Department of Biology, 623 Fordham Hall CB#3280, Chapel Hill, NC 27599-3280
Bodznick, David A., Wesleyan University, Department of Biology, Lawn Avenue, Middletown, CT 06497-0170
Boettiger, Edward G., 17 Eastwood Road, Storrs, CT 06268-2401
Boolootian, Richard A., Science Software Systems, Inc., 3576 Woodcliff Road, Sherman Oaks, CA 91403
Borgese, Thomas A., Lehman College, CUNY, Department of Biology, Bedford Park Boulevard, West, Bronx, NY 10468
Borst, David W., Illinois State University, Department of Biological Sciences, Normal, IL 61790-4120
Bowles, Francis P., Marine Biological Laboratory, Ecosystems Center, Woods Hole, MA 02543
Boyer, Barbara C., Union College, Biology Department, Schenectady, NY 12308
Brandhorst, Bruce P., Simon Fraser University, Institute of Molecular Biology/Biochemistry, Barnaby, B.C. V5A 1S6, CANADA
Brinley, F. J., NINCDS/NIH, Neurological Disorders Program, Room 812 Federal Building, Bethesda, MD 20892
Bronner-Fraser, Marianne, California Institute of Technology, Beckman Institute Division of Biology, 139-74, Pasadena, CA 91125
Brown, Stephen C., SUNY, Department of Biological Sciences, Albany, NY 12222
Brown, William L., 80 Black Oak Road, Weston, MA 02193
Browne, Carole L., Wake Forest University, Department of Biology, Box 7325 Reynolds Station, Winston-Salem, NC 27109
Browne, Robert A., Wake Forest University, Department of Biology, Box 7325, Winston-Salem, NC 27109
Bucklin, Anne C., University of New Hampshire, Ocean Process Analysis Laboratory, 142 Morse Hall, Durham, NH 03824
Bullis, Robert A., Marine Biological Laboratory, 7 MBL Street, Woods Hole, MA 02543
Burger, Max M., Friedrich Miescher Institute, P.O. Box 2543, CH 4002 Basel, SWITZERLAND
Burgess, David R., Boston College, Academic Vice President and Dean of Facilities, Bourneuf House, 84 College Road, Chestnut Hill, MA 02467-3838
Burgos, Mario H., IHEM Medical School, UNC Conicet, Casilla de Correo 56, 5500 Mendoza, ARGENTINA
Burky, Albert, University of Dayton, Department of Biology, Dayton, OH 45469
Burris, John E., Marine Biological Laboratory, 7 MBL Street, Woods Hole, MA 02543
Burstyn, Harold Lewis, United States Air Force, Air Force Materiel Command, Rome Research Site RL/JA, 26 Electronic Parkway, Rome, NY 13441-4514
Bursztajn, Sherry, LSU Medical Center, 1501 Kings Highway, Building BRIF 6-13, Shreveport, LA 71130

Calabrese, Ronald L., Emory University, Department of Biology, 1510 Clifton Road, Atlanta, GA 30322
Callaway, Joseph C., New York Medical College, Department of Physiology, Basic Sciences Building, Valhalla, NY 10595
Cameron, R. Andrew, California Institute of Technology, Division of Biology 156-29, Pasadena, CA 91125

Campbell, Richard H., Bang-Campbell Associates, Eel Pond Place, Box 402, Woods Hole, MA 02543

Candelas, Graciela C., University of Puerto Rico, Department of Biology, P.O. Box 23360, UPR Station, San Juan, PR 00931-3360

Cariello, Lucio, Stazione Zoologica "A. Dohrn", Villa Comunale, 80121 Naples, ITALY

Case, James F., University of California, Marine Science Institute, Santa Barbara, CA 93106

Cassidy, Joseph D., Providence College, Priory of Street Thomas Aquinas, Providence, RI 02918-0001

Cavanaugh, Colleen M., Harvard University, Biological Laboratories, 16 Divinity Avenue, Cambridge, MA 02138

Chaet, Alfred B., University of West Florida, Department of Cell and Molecular Biology, 11000 University Parkway, Pensacola, FL 32514

Chambers, Edward L., University of Miami School of Medicine, Department of Physiology and Biophys., P.O. Box 016430, Miami, FL 33101

Chang, Donald C., Hong Kong University, Science and Technology, Department of Biology, Clear Water Bay, Kowloon, HONG KONG

Chappell, Richard L., Hunter College, CUNY, Department of Biological Sciences, Box 210, 695 Park Avenue, New York, NY 10021

Child III, Frank M., 28 Lawrence Farm Road, Woods Hole, MA 02543-1416

Chisholm, Rex Leslie, Northwestern University, Medical School, Department of Cell Biology, Chicago, IL 60611

Citkowitz, Elena, Hospital of Street Raphael, Lipid Disorders Clinic, 1450 Chapel Street, New Haven, CT 06511

Clark, Eloise E., Bowling Green State University, Biological Sciences Department, Bowling Green, OH 43403

Clark, Hays, 150 Gomez Road, Hobe Sound, FL 33455

Clark, Wallis H., 12705 NW 112th Avenue, Alachua, FL 32615

Claude, Philippa, University of Wisconsin, Department of Zoology, Zoology Research Building 125, 1117 W Johnson Street, Madison, WI 53706

Clay, John R., NIH-NINDS, Building 36, Room 2-CO2, Bethesda, MD 20892

Clowes, Alexander W., University of Washington, School of Medicine, Department of Surgery, Box 356410, Seattle, WA 98195-6410

Cobb, Jewel Plummer, California State University, 5151 University Drive, Health Center 205, Los Angeles, CA 90032-8500

Cohen, Carolyn, Brandeis University, Rosenstiel Basic Medical, Sciences Research Center, Waltham, MA 02254

Cohen, Lawrence B., Yale University School of Medicine, Department of Physiology, 333 Cedar Street, New Haven, CT 06520

Cohen, Maynard M., Rush Medical College, Department of Neurological Sciences, 600 South Paulina, Chicago, IL 60612

Cohen, William D., Hunter College, Department Biological Sciences, New York, NY 10021

Coleman, Annette W., Brown University, Division of Biology and Medicine, Providence, RI 02912

Colinvaux, Paul, Smithsonian Tropical Research Institute, Unit 0948, Apo AA 34002-0948, USA

Collier, Jack R., 3431 Highway, #107, P.O. Box 139, Effie, LA 71331

Collier, Marjorie McCann, 3431 Highway 107, P.O. Box 139, Effie, LA 71331

Cook, Joseph A., Edna McConnell Clark Foundation, 250 Park Avenue, New York, NY 10177-0026

Cornell, Neal W., Marine Biological Laboratory, Woods Hole, MA 02543

Cornwall, Melvin C., Boston University School of Medicine, Department of Physiology L714, Boston, MA 02118

Corson, D. Wesley, Storm Eye Institute, Room 537, 171 Ashley Avenue, Charleston, SC 29425

Corwin, Jeffrey T., University of Virginia, School of Medicine, Department Otolaryngology and Neuroscience, Box 396, Charlottesville, VA 22908

Couch, Ernest F., Texas Christian University, Department of Biology, TCU Box 298930, Fort Worth, TX 76129

Cox, Rachel Llanelly, Woods Hole Oceanographic Institute, Biology Department, Woods Hole, MA 02543

Crane, Sylvia E., 438 Wendover Drive, Princeton, NJ 08540

Cremer-Bartels, Gertrud, Universitats Augenklinik, 44 Munster, GERMANY

Crow, Terry J., University of Texas Medical School, Department of Neurobiology and Anatomy, Houston, TX 77225

Crowell, Sears, Indiana University, Department of Biology, Bloomington, IN 47405

Crowther, Robert J., Shriners Hospitals for Children, 51 Blossom Street, Boston, MA 02114

Cunningham, Mary-Ellen, 62 Cloverly Road, Grosse Pointe Farms, MI 48236-3313

Cutler, Richard D., Marine Biological Laboratory, Woods Hole, MA 02543

Daignault, Alexander T., Edgewood #6308, 575 Osgood Street, North Andover, MA 01845 (deceased)

Davidson, Eric H., California Institute of Technology, Division of Biology, 156-29, 391 South Holliston, Pasadena, CA 91125

Davison, Daniel B., Bristol-Myers Squibb PRI, Bioinformatics Department, 5 Research Parkway, Wallingford, CT 06492

Daw, Nigel W., 5 Old Pawson Road, Branford, CT 06405

Dawidowicz, Eliezar A., Marine Biological Laboratory, Office of Research Administration and Education, Woods Hole, MA 02543

De Weer, Paul J., University of Pennsylvania, B400 Richards Building, Department of Physiology, 3700 Hamilton Walk, Philadelphia, PA 19104-6085

Deegan, Linda A., Marine Biological Laboratory, The Ecosystems Center, Woods Hole, MA 02543

DeGroof, Robert C., 145 Water Crest Drive, Doylestown, PA 18901-3267

Denckla, Martha Bridge, Johns Hopkins University, School of Medicine, Kennedy-Krieger Institute, 707 North Broadway, Baltimore, MD 21205

DePhillips, Henry A., Trinity College, Department of Chemistry, 300 Summit Street, Hartford, CT 06106

DeSimone, Douglas W., University of Virginia, Department of Cell Biology, Box 439, Health Sciences Center, Charlottesville, VA 22908

Dettharn, Wolf-Dietrich, Vanderbilt University, School of Medicine, Department of Pharmacology, Nashville, TN 37232

Dionne, Vincent E., Boston University Marine Program, Marine Biological Laboratory, Woods Hole, MA 02543

Dowling, John E., Harvard University, Biological Laboratories, 16 Divinity Street, Cambridge, MA 02138

Drapeau, Pierre, Montreal General Hospital, Department of Neurology, 1650 Cedar Avenue, Montreal, Que. H3G 1A4, CANADA

DuBois, Arthur Brooks, John B. Pierce Foundation Laboratory, 290 Congress Avenue, New Haven, CT 06519

Duncan, Thomas K., Nichols College, Environmental Sciences Department, Dudley, MA 01571

Dunham, Philip B., Syracuse University, Department of Biology, 130 College Place, Syracuse, NY 13244-1220

Dunlap, Paul V., University of Maryland Biotechnology Institute, Center of Marine Biotechnology, Columbus Center, Suite 236, 701 East Pratt Street, Baltimore, MD 21202

Ebert, James D., The Johns Hopkins University, Department of

Biology, Homewood, 3400 North Charles Street, Baltimore, MD 21218-2685
Eckberg, William R., Howard University, Department of Biology, P.O. Box 887, Administration Building, Washington, DC 20059
Edds, Kenneth T., R & D Systems, Inc., Hematology Division, 614 McKinley Place, NE, Minneapolis, MN 55413
Eder, Howard A., Albert Einstein College of Medicine, 1300 Morris Park Avenue, Bronx, NY 10461
Edstrom, Joan, 53 Two Ponds Road, Falmouth, MA 02540
Egyud, Laszlo G., Cell Research Corporation, P.O. Box 67209, Chestnut Hill, MA 02167-0209
Ehrlich, Barbara E., Yale University Medical School, B207 SHM, New Haven, CT 06473
Eisen, Arthur Z., Washington University, Division of Dermatology, Street Louis, MO 63110
Eisen, Herman N., Massachusetts Institute of Technology, Center for Cancer Research, E17-128, 77 Massachusetts Avenue, Cambridge, MA 02139-4307
Elder, Hugh Young, University of Glasgow, Institute of Physiology, Glasgow G12 8QQ, SCOTLAND
Englund, Paul T., Johns Hopkins Medical School, Department of Biological Chemistry, 725 North Wolfe Street, Baltimore, MD 21205
Epel, David, Stanford University, Hopkins Marine Station, Ocean View Boulevard, Pacific Grove, CA 93950
Epstein, Herman T., 18 Lawrence Farm Road, Woods Hole, MA 02543
Epstein, Ray L., 1602 W. Olympia Street, Hernando, FL 34442

Farb, David H., Boston University School of Medicine, Department of Pharmacology L603, 80 East Concord Street, Boston, MA 02118
Farmanfarmaian, A. Verdi, Rutgers University, Department of Biological Sciences, Nelson Biology Laboratory POB 1059, Piscataway, NJ 08855
Feldman, Susan C., University of Medicine and Dentistry, New Jersey Medical School, 100 Bergen Street, Newark, NJ 07103
Festoff, Barry William, VA Medical Center, Neurology Service (151), 4801 Linwood Boulevard, Kansas City, MO 64128
Fink, Rachel D., Mount Holyoke College, Department of Biological Sciences, Clapp Laboratories, South Hadley, MA 01075
Finkelstein, Alan, Albert Einstein College of Medicine, 1300 Morris Park Avenue, Bronx, NY 10461
Fischbach, Gerald D., National Institute of Health, Neurological Disorders and Strokes, 31 Center Drive, MSC 2540, Bldg 31, Rm 8A03, Bethesda, MD 20892-2540
Fishman, Harvey M., University of Texas Medical Branch, Department of Physiology and Biophysics, 301 University Boulevard, Galveston, TX 77555-0641
Flanagan, Dennis, 12 Gay Street, New York, NY 10014
Fluck, Richard Allen, Franklin and Marshall College, Department of Biology, Box 3003, Lancaster, PA 17604-3003
Foreman, Kenneth H., Marine Biological Laboratory, Woods Hole, MA 02543
Fox, Thomas Oren, Harvard Medical School, Division of Medical Sciences, MEC 435, 260 Longwood Avenue, Boston, MA 02115
Franzini-Armstrong, Clara, University of Pennsylvania, School of Medicine, 330 South 46th Street, Philadelphia, PA 19143
Fraser, Scott, California Institute of Technology, Beckman Institute 139-74, 1201 East California Boulevard, Pasadena, CA 91125
Frazier, Donald T., University of Kentucky Medical Center, Department of Physiology and Biophysics, MS501 Chandler Medical Center, Lexington, KY 40536
French, Robert J., University of Calgary, Health Sciences Centre, Alberta, T2N 4N1, CANADA
Fulton, Chandler M., Brandeis University, Department of Biology, MS 008, Waltham, MA 02454-9110
Furie, Barbara C., Beth Israel Deaconess Medical Center, BIDMC Cancer Center, Kirstein 1, 330 Brookline Avenue, Boston, MA 02215
Furie, Bruce, Beth Israel Deaconess Medical Center, BIDMC Cancer Center, Kirstein 1, 330 Brookline Avenue, Boston, MA 02215
Furshpan, Edwin J., Harvard Medical School, Department of Neurobiology, 220 Longwood Avenue, Boston, MA 02115
Futrelle, Robert P., Northeastern University, College of Computer Science, 360 Huntington Avenue, Boston, MA 02115

Gabr, Howaida, Suez Canal University, Department of Marine Science, Faculty of Science, Ismailia, EGYPT
Gabriel, Mordecai L., Brooklyn College, Department of Biology, 2900 Bedford Avenue, Brooklyn, NY 11210
Gadsby, David C., The Rockefeller University, Laboratory of Cardiac Physiology, 1230 York Avenue, New York, NY 10021-6399
Gainer, Harold, NIH, NINDS,BNP,DIR, Neurochemistry, Building 36, Room 4D20, Bethesda, MD 20892-4130
Galatzer-Levy, Robert M., 180 North Michigan Avenue, Suite 2401, Chicago, IL 60601
Gall, Joseph G., Carnegie Institution, 115 West University Parkway, Baltimore, MD 21210
Garber, Sarah S., Allegheny University of the Health Sciences, Department of Physiology, 2900 Queen Lane, Philadelphia, PA 19129
Gascoyne, Peter, University of Texas, M. D. Anderson Cancer Center, Experimental Pathology, Box 89, Houston, TX 77030
Gelperin, Alan, Bell Labs Lucent, Department Biology Comp., Rm 1C464, 600 Mountain Avenue, Murray Hill, NJ 07974
German, James L., The New York Blood Center, Laboratory of Human Genetics, 310 East 67th Street, New York, NY 10021
Gibbs, Martin, Brandeis University, Institute for Photobiology of Cells and Organelles, Waltham, MA 02254
Giblin, Anne E., Marine Biological Laboratory, The Ecosystems Center, Woods Hole, MA 02543
Gibson, A. Jane, Cornell University, Department of Biochemistry, Biotech. Building, Ithaca, NY 14850
Gifford, Prosser, 540 North Street, SW, Apt. #S-903, Washington, DC 20024-4557
Gilbert, Daniel L., National Institutes of Health, Biophysics Sec., BNP, Building 36, Room 5A-27, Bethesda, MD 20892
Giudice, Giovanni, Universita di Palermo, Dipartimento di Biologia, Cellulare e Dello Sviluppo, I-90123 Palermo, ITALY
Giuditta, Antonio, University of Naples, Department of General Physiology, Via Mezzocannone 8, Naples, 80134, ITALY
Glynn, Paul, P.O. Box 6083, Brunswick, ME 04011-6083
Golden, William T., Chairman Emeritus, American Museum of Natural History, Rm. 4201, 40 Wall Street, New York, NY 10005
Goldman, Robert D., Northwestern University Medical School, Department of Cell and Molecular Biology, 303 E. Chicago Avenue, Chicago, IL 60611-3008
Goldsmith, Paul K., National Institutes of Health, Building 10, Room 9C-101, Bethesda, MD 20892
Goldsmith, Timothy H., Yale University, Department of Biology, New Haven, CT 06510
Goldstein, Moise H., The Johns Hopkins University, ECE Department, Barton Hall, Baltimore, MD 21218
Goodman, Lesley Jean (deceased)
Gould, Robert Michael, NYS Institute of Basic Research, 1050 Forest Hill Road, Staten Island, NY 10314-6399
Govind, C. K., Scarborough College, Life Sciences Division, 1265 Military Trail, West Hill, Ontario M1C 1A4, CANADA
Grace, Dick, Doreen Grace Fund, The Brain Center, Promontory Point, New Seabury, MA 02649
Graf, Werner M., College of France, 11 Place Marcelin Berthelot, 75231 Paris Cedex 05, FRANCE

Grant, Philip, National Institutes of Health, NINDS.BN.DIR.Neurochemistry, Building 36, Room 4D20, Bethesda, MD 20892-4130
Grass, Ellen R., The Grass Foundation, 77 Reservoir Road, Quincy, MA 02170-3610
Grassle, Judith P., Rutgers University, Institute of Marine and Coastal Studies, Box 231, New Brunswick, NJ 08903
Graubard, Katherine G., University of Washington, Department of Zoology, NJ-15, Box 351800, Seattle, WA 98195-1800
Greenberg, Everett Peter, University of Iowa, College of Medicine, Department of Microbiology, Iowa City, IA 52242
Greenberg, Michael J., University of Florida, The Whitney Laboratory, 9505 Ocean Shore Boulevard, St. Augustine, FL 32086-8623
Greer, Mary J., 176 West 87th Street, #12A, New York, NY 10024-2902
Griffin, Donald R., Harvard University, Concord Field Station, Old Causeway Road, Bedford, MA 01730
Gross, Paul R., 111 Perkins Street, Apt. 45, Jamaica Plain, MA 02130-4320
Grossman, Albert, New York University Medical Center, 550 First Avenue, New York, NY 10016
Grossman, Lawrence, The Johns Hopkins University, Department of Biochemistry, 615 North Wolfe Street, Baltimore, MD 21205
Gruner, John A., Cephalon, Inc., 145 Brandywine Parkway, West Chester, PA 19380-4245
Gunning, A. Robert, P.O. Box 165, Falmouth, MA 02541
Gwilliam, G. F., Reed College, Department of Biology, Portland, OR 97202

Haimo, Leah T., University of California, Department of Biology, Riverside, CA 92521
Hajduk, Stephen L., University of Alabama, School of Medicine/Dentistry, Department of Biochemistry/Molecular Genetics, University Station, Birmingham, AL 35294
Hall, Linda M., SUNY, Department of Biochemstry Pharmacology, 329 Hochstetter Hall, Buffalo, NY 14260-1200
Hall, Zach W., University of California, Department Physiology, San Francisco, CA 94114
Halvorson, Harlyn O., University of Massachusetts, Policy Center for Marine Biosciences and Technology, 100 Morrissey Boulevard, Boston, MA 02125-3393
Haneji, Tatsuji, Kyushu Dental College, Department of Anatomy, 2-6-1, Manazuru, Kokurakita-Ku, Kitakyushu 803, JAPAN
Hanlon, Roger T., Marine Biological Laboratory, Woods Hole, MA 02543
Harosi, Ferenc, New College of the USF, Division of Natural Sciences, 5700 North Tamiami Trail, Sarasota, FL 34243-2197
Harrigan, June F., 7415 Makaa Place, Honolulu, HI 96825
Harrington, Glenn W., Weber State University, Department of Microbiology, Ogden, UT 84408
Harrison, Stephen C., Harvard University, Department of Molecular and Cell Biology, 7 Divinity Avenue, Cambridge, MA 02138
Haselkorn, Robert, University of Chicago, Department of Molecular Genetics and Cell Biology, Chicago, IL 60637
Hastings, J. Woodland, Harvard University, The Biological Laboratories, 16 Divinity Avenue, Cambridge, MA 02138-2020
Haydon-Baillie, Wensley G., Porton Institute, 2 Lowndes Place, London SW1X 8Dd, ENGLAND
Hayes, Raymond L., Howard University, College of Medicine, 520 W Street, NW, Washington, DC 20059
Heck, Diane E., EOHSI, Department of Pharmacology/Toxicology, 681 Frelinghuysen Road, Piscataway, NJ 08855
Henry, Jonathan Joseph, University of Illinois, Department of Cell and Struct. Biology, 601 South Goodwin Avenue #B107, Urbana, IL 61801-3709
Hepler, Peter K., University of Massachusetts, Department of Biology, Morrill III, Amherst, MA 01003
Herndon, Walter R., University of Tennessee, Department of Botany, Knoxville, TN 37996-1100
Herskovits, Theodore T., Fordham University, Department of Chemistry, John Mulcahy Hall, Room 638, Bronx, NY 10458
Hiatt, Howard H., Brigham and Women's Hospital, Department of Medicine, 75 Francis Street, Boston, MA 02115
Highstein, Stephen M., Washington University, Department of Otolaryngology, Box 8115, 4566 Scott Avenue, Street Louis, MO 63110
Hildebrand, John G., University of Arizona, ARL Division of Neurobiology, P.O. Box 210077, Tucson, AZ 85721-0077
Hill, Richard W., Michigan State University, Department of Zoology, East Lansing, MI 48824
Hill, Susan D., Michigan State University, Department of Zoology, East Lansing, MI 48824
Hillis, Llewellya W., Smithsonian Tropical Research Institute, Unit 0948, APO, AA 34002-0948
Hinkle, Gregory J., Bioinformatics Group, Cereon Genomics, One Kendall Square, Building 200, Cambridge, MA 02139
Hinsch, Gertrude W., University of South Florida, Department of Biology, Tampa, FL 33620
Hinsch, Jan, Leica, Inc., 110 Commerce Drive, Allendale, NJ 07401
Hobbie, John E., Marine Biological Laboratory, The Ecosystems Center, Woods Hole, MA 02543
Hodge, Alan J., 3843 Mount Blackburn Avenue, San Diego, CA 92111
Hoffman, Joseph F., Yale University School of Medicine, Cellular and Molecular Physiology, 333 Cedar Street, New Haven, CT 06520-8026
Hollyfield, Joe G. address unknown
Holz IV, George G., New York University Medical Center, Medical Sciences Building Room 442, 550 First Avenue, New York, NY 10016
Hopkinson, Charles S., Marine Biological Laboratory, Woods Hole, MA 02543
Houk, James C., Northwestern University Medical School, 303 East Chicago Avenue, Ward 5-315, Chicago, IL 60611-3008
Hoy, Ronald R., Cornell University, Section of Neurobiology and Behavior, 215 Mudd Hall, Ithaca, NY 14853
Huang, Alice S., California Institute of Technology, Mail Code 1-9, Pasadena, CA 91125
Hufnagel-Zackrolf, Linda A., University of Rhode Island, Department of Microbiology, Kingston, RI 02881
Hummon, William D., Ohio University, Department of Biological Sciences, Athens, OH 45701
Humphreys, Susie H., Food and Drug Administration, HFS-308, 200 C Street, SW, Washington, DC 20204-0001
Humphreys, Tom, University of Hawaii, Kewalo Marine Laboratory, 41 Ahui Street, Honolulu, HI 96813
Hunt, Richard T., ICRF, Clare Hall Laboratories, South Mimms Potter's Bar, Herb EN6-3LD, ENGLAND
Hunter, Robert D., Oakland University, Department of Biological Sciences, Rochester, MI 48309-4401
Huxley, Hugh E., Brandeis University, Rosenstiel Center, Biology Department, Waltham, MA 02154

Ilan, Joseph, Case Western Reserve University, School of Medicine, Department of Anatomy, Cleveland, OH 44106
Ingoglia, Nicholas A., New Jersey Medical School, Department of Pharmacology/Physiology, 185 South Orange Avenue, Newark, NJ 07103
Inoué, Saduyki, McGill University, Department of Anatomy, 3640 University Street, Montreal,PQ H3A 2B2, CANADA
Inoué, Shinya, Marine Biological Laboratory, Woods Hole, MA 02543

Isselbacher, Kurt J., Massachusetts General Hospital Cancer Center, Charlestown, MA 02129
Issidorides, Marietta Radovic, University of Athens, Department of Psychiatry, Monis Petraki 8, Athens, 140, GREECE
Izzard, Colin S., SUNY-Albany, Department of Biological Sciences, 1400 Washington Avenue, Albany, NY 12222

Jacobs, Neil, Hale and Dorr, 60 State Street, Boston, MA 02109
Jaffe, Laurinda A., University of Connecticut Health Center, Department of Physiology, Farmington Avenue, Farmington, CT 06032
Jaffe, Lionel, Marine Biological Laboratory, Woods Hole, MA 02543
Jannasch, Holger W., Woods Hole Oceanographic Institute, Department of Biology, Woods Hole, MA 02543 (deceased)
Jeffery, William R., University of Maryland, Department of Biology, College Park, MD 20742
Johnston, Daniel, Baylor College of Medicine, Division of Neuroscience, Baylor Plaza, Houston, TX 77030
Josephson, Robert K., University of California, School of Biological Science, Department of Psychobiology, Irvine, CA 92697

Kaczmarek, Leonard K., Yale University School of Medicine, Department of Pharmacology, 333 Cedar Street, New Haven, CT 06520
Kaley, Gabor, New York Medical College, Department of Physiology, Basic Sciences Building, Valhalla, NY 10595
Kaltenbach, Jane, Mount Holyoke College, Department Biological Sciences, South Hadley, MA 01075
Kaminer, Benjamin, Boston University Medical School, Physiology Department, 80 East Concord Street, Boston, MA 02118
Kaneshiro, Edna S., University of Cincinnati, Biological Sciences Department, JL 006, Cincinnati, OH 45221-0006
Kaplan, Ehud, 450 E 63rd Street, New York, NY 10021-7928
Karakashian, Stephen J., Apartment 16-F, 165 West 91st Street, New York, NY 10024
Karlin, Arthur, Columbia University, Center for Molecular Recognition, 630 West 168th Street, Room 11-401, New York, NY 10032
Keller, Hartmut Ernst, Carl Zeiss, Inc., One Zeiss Drive, Thornwood, NY 10594
Kelley, Darcy B., Columbia University, Department of Biological Sciences, 911 Fairchild, Mailcode 2432, New York, NY 10027
Kelly, Robert E., 5 Little Harbor Road, Woods Hole, MA 02543
Kemp, Norman E., University of Michigan, Department of Biology, Ann Arbor, MI 48109
Kendall, John P., Faneuil Hall Associates, 176 Federal Street, 2nd Floor, Boston, MA 02110
Kerr, Louis M., Marine Biological Laboratory, Woods Hole, MA 02543
Keynan, Alexander, Israel Academy of Science and Humanity, P.O. Box 4040, Jerusalem, ISRAEL
Khan, Shahid M.M., Albert Einstein College of Medicine, Department of Physiology and Biophysics, 1300 Morris Park Avenue, Room U273, Bronx, NY 10461
Khodakhah, Kamran, University of Colorado School of Medicine, Department of Physiology and Biophysics, 4200 East 9th Avenue, C-240, Denver, CO 80262
Kiehart, Daniel P., Duke University Medical Center, Department of Cell Biology, Box 3709, 308 Nanaline Duke Building, Durham, NC 27710
Kleinfeld, David, University of California, Department of Physics, 0319 9500 Gilman Drive, La Jolla, CA 92093
Klessen, Rainer, Address unknown.
Klotz, Irving M., Northwestern University, Department of Chemistry, Evanston, IL 60201
Knudson, Robert A., Marine Biological Laboratory, Woods Hole, MA 02543
Koide, Samuel S., The Rockefeller University, The Population Council, 1230 York Avenue, New York, NY 10021
Kornberg, Hans, Boston University, The University Professors, 745 Commonweath Avenue, Boston, MA 02215
Kosower, Edward M., Tel-Aviv University, Department of Chemistry, Ramat-Aviv, Tel Aviv, 69978, ISRAEL
Krahl, Maurice E., 2783 West Casas Circle, Tucson, AZ 85741
Krane, Stephen M., Massachusetts General Hospital, Arthritis Unit, Fruit Street, Boston, MA 02114
Krauss, Robert, P.O. Box 291, Denton, MD 21629
Kravitz, Edward A., Harvard Medical School, Department of Neurobiology, 220 Longwood Avenue, Boston, MA 02115
Kriebel, Mahlon E., SUNY Health Science Center, Department of Physiology, Syracuse, NY 13210
Kristan Jr., William B., University of California, Department of Biology 0357, 9500 Gilman Drive, La Jolla, CA 92093-0357
Kropinski, Andrew M., Queen's University, Department of Microbiology/Immunology, Kingston, Ontario K7L 3N6, CANADA
Kuffler, Damien P., Institute of Neurobiology, 201 Boulevard del Valle, San Juan 00901, PR
Kuhns, William J., Hospital for Sick Children, Biochemistry Research, 555 University Avenue, Toronto, Ontario M5G 1X8, CANADA
Kunkel, Joseph G., University of Massachusetts, Department of Biology, Amherst, MA 01003
Kuzirian, Alan M., Marine Biological Laboratory, Woods Hole, MA 02543-1015

Laderman, Aimlee D., Yale University, School of Forestry and Environmental Studies, 370 Prospect Street, New Haven, CT 06511
Landeau, Laurie J., Listowel, Inc., 2 Park Avenue, Suite 1525, New York, NY 10016
Landis, Dennis M.D., University Hospital of Cleveland, Department Neurology, 11100 Euclid Avenue, Cleveland, OH 44106
Landis, Story C., National Institutes of Health, Building 36, Room 5A05, 36 Convent Drive, Bethesda, MD 20892-4150
Landowne, David, University of Miami Medical School, Department of Physiology, P.O. Box 016430, Miami, FL 33101
Langford, George M., Dartmouth College, Department of Biological Sciences, 6044 Gilman Laboratory, Hanover, NH 03755
Laskin, Jeffrey, University of Medical and Dentistry of New Jersey, Robert Wood Johnson Medical School, 675 Hoes Lane, Piscataway, NJ 08854
Lasser-Ross, Nechama, New York Medical College, Department of Physiology, Valhalla, NY 10595
Laster, Leonard, University of Massachusetts Medical School, 55 Lake Avenue, North, Worcester, MA 01655
Laties, Alan, Scheie Eye Institute, Myrin Circle, 51 North 39th Street, Philadelphia, PA 19104
Laufer, Hans, University of Connecticut, Department of Molecular and Cell Biology, U-125, 75 North Eagleville Road Storrs, CT 06269-3125
Lazarow, Paul B., Mount Sinai School of Medicine, Department of Cell Biology and Anatomy, 1190 Fifth Avenue, Box 1007, New York, NY 10029-6574
Lazarus, Maurice, Federated Department Stores, Sears Crescent, City Hall Plaza, Boston, MA 02108
Leadbetter, Edward R., University of Connecticut, Department of Molecular and Cell Biology, U-131, Beach Hall, Room 249, 354 Mansfield Road, Storrs, CT 06269-2131
Lederberg, Joshua, The Rockefeller University, 1230 York Avenue, New York, NY 10021

Lee, John J., City College of CUNY, Department of Biology, Convent Avenue and 138th Street, New York, NY 10031
Lehy, Donald B., 35 Willow Field Drive, North Falmouth, MA 02556
Leibovitz, Louis, 3 Kettle Hole Road, Falmouth, MA 02540 (deceased)
Leighton, Joseph, Aeron Biotechnology, Inc., 1933 Davis Street #310, San Leandro, CA 94577 (deceased)
Leighton, Stephen B., National Institutes of Health, Building 13, 3W13, Bethesda, MD 20892
Lemos, Jose Ramon, University of Massachusetts Medical Center, Worcester Foundation Campus, 222 Maple Avenue, Shrewsbury, MA 01545-2737
Lerner, Aaron B., Yale University School of Medicine, Department of Dermatology, P.O. Box 3333, New Haven, CT 06510
Levin, Jack, Veterans Administration, Medical Center, 111 H2, 4150 Clement Street, San Francisco, CA 94121
Levine, Michael, University of California, Department MCB, 401 Barker Hall, Berkeley, CA 94720
Levine, Richard B., University of Arizona, Division of Neurobiology, Room 611, Gould Simpson Building, P.O. Box 210077, Tucson, AZ 85721-0077
Levinthal, Francoise, Columbia University, Department of Biological Sciences, Broadway and 116th Street, New York, NY 10026
Levitan, Herbert, National Science Foundation, 4201 Wilson Boulevard, Room 835, Arlington, VA 22230
Levitan, Irwin B., Brandeis University, Volen Center for Complex Systems, 415 South Street, Waltham, MA 02254
Linck, Richard W., University of Minnesota School of Medicine, Cell Biology and Neuroanatomy Department, 4-135 Jackson Hall, 321 Church Street, Minneapolis, MN 55455
Lipicky, Raymond J., FDA/CDER/ODEI/HFD-110, 5600 Fishers Lane, Rockville, MD 20857
Lisman, John E., 199 Coolidge Avenue, #902, Watertown, MA 02172-1572
Liuzzi, Anthony, 320 Beacon Street, Boston, MA 02116
Llinas, Rodolfo R., New York University Medical Center, Department of Phsyiology/Biophysics, 550 First Avenue, Room 442, New York, NY 10016
Lobel, Phillip S., Boston University Marine Program, Marine Biological Laboratory, Woods Hole, MA 02543
Loew, Franklin M., Becker College, 61 Sever Street, Worcester, MA 01615-0071
Loewenstein, Birgit Rose, Marine Biological Laboratory, Woods Hole, MA 02543
Loewenstein, Werner R., Marine Biological Laboratory, Woods Hole, MA 02543
London, Irving M., Harvard-MIT, Division, E-25-551, Cambridge, MA 02139
Longo, Frank J., University of Iowa, Department of Anatomy, Iowa City, IA 52442
Lorand, Laszlo, Northwestern University Medical School, CMS Biology, Searle 4-555, 303 East Chicago Avenue, Chicago, IL 60611-3008
Luckenbill, Louise M., Ohio University, Department of Biological Sciences, Irvine Hall, Athens, OH 45701

Macagno, Eduardo R., Columbia University, 109 Low Memorial Library, Mail Code 4306, New York, NY 10027
MacNichol Jr., Edward F., Boston University School of Medicine, Department of Physiology, 80 East Concord Street, Boston, MA 02118
Maglott-Duffield, Donna R., American Type Culture Collection, 12301 Parklawn Drive, Rockville, MD 20852-1776
Maienschein, Jane Ann, Arizona State University, Department of Philosophy, P.O. Box 872004, Tempe, AZ 85287-2004
Mainer, Robert E., The Boston Company, Inc., One Boston Place, OBP-15-D, Boston, MA 02108
Malbon, Craig C., SUNY, University Medical Center, Pharmacology-HSC, Stony Brook, NY 11794-8651
Malchow, Robert P., University of Illinois, Department of Ophthalmology, 1855 West Taylor Street N/C 648, Chicago, IL 60612
Manalis, Richard S., Indiana-Purdue University, Department of Biological Science, 2101 Coliseum Boulevard East, Fort Wayne, IN 46805
Mangum, Charlotte P., College of William and Mary, Department of Biology, Williamsburg, VA 23187-8795 (deceased)
Manz, Robert D., 304 Adams Street, Milton, MA 02186
Margulis, Lynn, University of Massachusetts, Department of Geosciences, Morrill Science Center, Box 35820, Amherst, MA 01003-5820
Marinucci, Andrew C., 102 Nancy Drive, Mercerville, NJ 08619
Martinez, Joe L., The University of Texas, Division of Life Sciences, 6900 North Loop 1604 West, San Antonio, TX 78249-0662
Martinez-Palomo, Adolfo, CINVESTAV-IPN, Sec. de Patologia Experimental, 07000 Mexico, D.F.A.P.140740, MEXICO
Mastroianni, Luigi, Hospital of University of Pennsylvania, 106 Dulles, 3400 Spruce Street, Philadephia, PA 19104-4283
Mauzerall, David, Rockefeller University, 1230 York Avenue, New York, NY 10021
McCann, Frances V., Dartmouth Medical School, Department of Physiology, Lebanon, NH 03756
McLaughlin, Jane A., Marine Biological Laboratory, Woods Hole, MA 022543
McMahon, Robert F., University of Texas, Arlington, Department of Biology, Box 19498, Arlington, TX 76019
Meedel, Thomas, Rhode Island College, Biology Department, 600 Mount Pleasant Avenue, Providence, RI 02908
Meinertzhagen, Ian A., Dalhousie University, Department of Psychology, Halifax, NS B3H 4J1, CANADA
Meiss, Dennis E., Immunodiagnostic Laboratories, 488 McCormick Street, San Leandro, CA 94577
Melillo, Jerry M., Marine Biological Laboratory, Ecosystems Center, Woods Hole, MA 02543
Mellon Jr., DeForest, University of Virginia, Department of Biology, Gilmer Hall, Charlottesville, VA 22903
Mellon, Richard P., P.O. Box 187, Laughlintown, PA 15655-0187
Mendelsohn, Michael E., New England Medical Center, Molecular Cardiology Laboratory, NEMC Box 80, 750 Washington Street, Boston, MA 02111
Merriman, Melanie Pratt, 7511 Beach View Drive, North Bay Village, FL 33141
Meselson, Matthew, Harvard University, Fairchild Biochemistry Building, 7 Divinity Avenue, Cambridge, MA 02138
Metuzals, Janis, University of Ottawa, Department of Pathology and Laboratory Medical, 451 Smyth Road, Ottawa, Ontario K1H 8M5, CANADA
Miledi, Ricardo, University of California, Irvine, Department of Psychobiology, 2205 Biology Sci. II, Irvine, CA 92697-4550
Milkman, Roger D., University of Iowa, Department of Biological Sciences, Biology Building, Room 318, Iowa City, IA 52242-1324
Miller, Andrew L., Hong Kong University of Science and Technology, Department of Biology, Clearwater Bay, Kowloon, HONG KONG
Mills, Robert, 10315 44th Avenue, W 12 H Street, Brandenton, FL 34210
Misevic, Gradimir, University Hospital of Basel, Department of Research, Mebelstr. 20, CH-4031 Basel, SWITZERLAND
Mitchell, Ralph, Harvard University, Division of Applied Sciences, 29 Oxford Street, Cambridge, MA 02138

Miyakawa, Hiroyoshi, Tokyo College of Pharmacy, Laboratory of Cellular Neurobiology, 1432-1 Horinouchi, Hachiouji, Tokyo 192-03, JAPAN

Miyamoto, David M., Drew University, Department of Biology, Madison, NJ 07940

Mizell, Merle, Tulane University, Department of Cell and Molecular, Biology, New Orleans, LA 70118

Moore, John W., Duke University Medical Center, Department of Neurobiology, Box 3209, Durham, NC 27710

Moreira, Jorge E., NIH/NICHD, Department of Cell and Molecular Biol., Bethesda, MD 20852

Morin, James G., address unknown

Morrell, Leyla de Toledo, Rush-Presbyterian-Street Lukes, Medical Center, 1653 West Congress Parkway, Chicago, IL 60612

Morse, M. Patricia, National Science Foundation, Room 885, Esie, Arlington, VA 22230

Morse, Stephen S., DARPA/DSO, 3701 North Fairfax Drive, Arlington, VA 22203-1714

Mote, Michael I., Temple University, Department of Biology, Philadelphia, PA 19122

Muller, Kenneth J., University of Miami School of Medicine, Department of Physiology and Biophysics, 1600 NW 10th Avenue, R-430, Miami, FL 33136

Murray, Andrew W., University of California, Department of Physiology, Box 0444, 513 Parnassus Avenue, San Francisco, CA 94143-0444

Nabrit, S. M., 686 Beckwith Street, SW, Atlanta, GA 30314

Nadelhoffer, Knute J., Marine Biological Laboratory, 7 MBL Street, Woods Hole, MA 02543

Naka, Ken-ichi, 2-9-2 Tatumi Higashi, Okazaki, 444, JAPAN

Nakajima, Yasuko, University of Illinois, College of Medicine, Anatomy and Cell Biology Department, M/C 512, Chicago, IL 60612

Narahashi, Toshio, Northwestern University Medical School, Department of Pharmacology, 303 East Chicago Avenue, Chicago, IL 60611

Nasi, Enrico, Boston University School of Medical, Department of Physiology, R-406, 80 East Concord Street, Boston, MA 02118

Neill, Christopher, Marine Biological Laboratory, 7 MBL Street, Woods Hole, MA 02543

Nelson, Leonard, Medical College of Ohio, Department of Physiology, CS 10008, Toledo, OH 43699

Nelson, Margaret C., Cornell University, Section of Neurobiology and Behavior, Ithaca, NY 14850

Nicholls, John G., University of Basel, Department of Pharmacology Biocenter, Klingelbergstrasse 70, Basel, CH-4056, SWITZERLAND

Nickerson, Peter A., SUNY, Buffalo, Department of Pathology, Buffalo, NY 14214

Nicosia, Santo V., University of South Florida, College of Medicine, Box 11, Department of Pathology, Tampa, FL 33612

Noe, Bryan D., Emory University School of Medicine, Department of Anatomy and Cell Biology, Atlanta, GA 30322

Norton, Catherine N., Marine Biological Laboratory, 7 MBL Street, Woods Hole, MA 02543

Nusbaum, Michael P., University of Pennsylvania School of Medicine, Department of Neuroscience, 215 Stemmler Hall, Philadelphia, PA 19104-6074

O'Herron, Jonathan, Lazard Freres and Company, 30 Rockefeller Plaza, 59th Floor, New York, NY 10020-1900

Obaid, Ana Lia, University of Pennsylvania School of Medicine, Neuroscience Department, 234 Stemmler Hall, Philadelphia, PA 19104-6074

Ohki, Shinpei, SUNY at Buffalo, Department of Biophysical Sciences, 224 Cary Hall, Buffalo, NY 14214

Oldenbourg, Rudolf, Marine Biological Laboratory, 7 MBL Street, Woods Hole, MA 02543

Olds, James L., George Mason University, Krasnow Institute for Advanced Studies, Mail Stop 2A1, Fairfax, VA 22030-4444

Olins, Ada L., 45 Eastern Promenade, #7-D, Portland, ME 04101

Olins, Donald E., 45 Eastern Promenade, #7-D, Portland, ME 04101

Oschman, James L., Nature's Own Research Association, P.O. Box 5101, Dover, NH 03820

Palazzo, Robert E., University of Kansas, Department of Physiology and Cell Biology, Lawrence, KS 66045

Palmer, John D., University of Massachusetts, Department of Zoology, 221 Morrill Science Center, Amherst, MA 01003

Pant, Harish C., NINCDS/NIH, Laboratory of Neurochemistry, Building 36, Room 4D20, Bethesda, MD 20892

Pappas, George D., University of Illinois, College of Medicine, Department of Anatomy, Chicago, IL 60612

Pardee, Arthur B., Dana-Farber Cancer Institute, D810, 44 Binney Street, Boston, MA 02115

Pardy, Rosevelt L., University of Nebraska, School of Life Sciences, Lincoln, NE 68588

Parmentier, James L., 175 S. Great Road, Lincoln, MA 01773-4112

Pederson, Thoru, University of Massachusetts Medical Center, Worcester Foundation Campus, 222 Maple Avenue, Shrewsbury, MA 01545

Perkins, Courtland D., 400 Hilltop Terrace, Alexandria, VA 22301

Person, Philip, 137-87 75th Road, Flushing, NY 11367

Peterson, Bruce J., Marine Biological Laboratory, 7 MBL Street, Woods Hole, MA 02543

Pethig, Ronald, University College of North Wales, School of Electronic Engineering, Bangor, Gwynedd, LL 57 IUT, UNITED KINGDOM

Pfohl, Ronald J., Miami University, Department of Zoology, Oxford, OH 45056

Pierce, Sidney K., University of Maryland, Department of Zoology, College Park, MD 20742

Pleasure, David E., Children's Hospital, Neurology Research, 5th Floor, Ambramson Building, Philadelphia, PA 19104

Poindexter, Jeanne S., Barnard College, Columbia University, 3009 Broadway, New York, NY 10027-6598

Pollard, Harvey B., NIH/NIDDKD, Building 8, Room 401, Bethesda, MD 20892

Pollard, Thomas D., Salk Institute for Biological Studies, 10010 N. Torrey Pines Road, La Jolla, CA 92037

Porter, Beverly H., 5542 Windysun Court, Columbia, MD 21045

Porter, Mary E., University of Minnesota, Department of Cell Biology and Neuroanatomy, 4-135 Jackson Hall, 321 Church Street SE, Minneapolis, MN 55455

Potter, David D., Harvard Medical School, Department of Neurobiology, 25 Shattuck Street, Boston, MA 02115

Potts, William T., University of Lancaster, Department of Biology, Lancaster, ENGLAND

Powers, Maureen K., Vanderbilt University, Department of Psychology, 301 Arts and Science Psychology Building, Nashville, TN 37240

Prendergast, Robert A., Wilmer Institute, Johns Hopkins Hospital, 600 North Wolfe Street, Baltimore, MD 21287-9142

Price, Carl A., Rutgers University, Waksman Institute of Microbiology, P.O. Box 759, Piscataway, NJ 08855-0759

Prior, David J., Northern Arizona University, Arts and Sciences Dean's Office, Box 5621, Flagstaff, AZ 86011

Prusch, Robert D., Gonzaga University, Department of Life Sciences, Spokane, WA 99258

Purves, Dale, Duke University Medical Center, Department of Neurobiology, Box 3209, 101-I Bryan Research Building, Durham, NC 27710

Quigley, James P., SUNY Health Sciences Center, Department of Pathology, BHS Tower 9, Room 140, Stony Brook, NY 11794-8691

Rabb, Irving W., 1010 Memorial Drive, Cambridge, MA 02138
Rabin, Harvey, P.O. Box 4022, Wilmington, DE 19807
Rabinowitz, Michael B., Marine Biological Laboratory, 7 MBL Street, Woods Hole, MA 02543
Rafferty, Nancy S., Marine Biological Laboratory, 7 MBL Street, Woods Hole, MA 02543
Rakowski, Robert F., UHS/The Chicago Medical School, Department of Physiology and Biophysics, 3333 Greenbay Road, N. Chicago, IL 60064
Ramon, Fidel, Universidad Nacional Autonoma de Mexico, Division EStreet Posgrado E Invest., Facultad de Medicina, 04510, D.F., MEXICO
Ranzi, Silvio, Sez. Zoologia Scienze Naturali, Dip. di Biologia, Via Celoria, 26, 20133 Milano, ITALY (deceased)
Rastetter, Edward B., Marine Biological Laboratory, The Ecosystems Center, Woods Hole, MA 02543
Rebhun, Lionel I., University of Virginia, Department of Biology, Gilmer Hall 45, Charlottesville, VA 22901
Reddan, John R., Oakland University, Department of Biological Sciences, Rochester, MI 48309-4401
Reese, Thomas S., NIH, NINDS, Building 36, Room 2A29, Bethesda, MD 20892
Reinisch, Carol L., Marine Biological Laboratory, 7 MBL Street, Woods Hole, MA 02543
Rickles, Frederick R., 2633 Danforth Lane, Decatur, GA 30033
Rieder, Conly L., Wadsworth Center, Division of Molecular Medicine, P.O. Box 509, Albany, NY 12201-0509
Riley, Monica, Marine Biological Laboratory, 7 MBL Street, Woods Hole, MA 02543
Ripps, Harris, University of Illinois at Chicago, Department of Ophthalmology/Visual Sciences, 1855 West Taylor Street, Chicago, IL 60612
Ritchie, J. Murdoch, Yale University School of Medicine, Department of Pharmacology, 333 Cedar Street, New Haven, CT 06510
Rome, Lawrence C., University of Pennsylvania, Department of Biology, Philadelphia, PA 19104
Rosenbluth, Jack, New York University School of Medical, Department of Physiology and Biophysics, RR 714, 400 East 34th Street, New York, NY 10016
Rosenbluth, Raja, Simon Fraser University, Institute of Molecular Biology and Biochemistry, Burnaby, BC, BC V5A 1S6, CANADA
Rosenfield, Allan, Columbia University School of Public Health, 600 West 168th Street, New York, NY 10032-3702
Rosenkranz, Herbert S., 130 Desoto Street, Pittsburgh, PA 15213-2535
Roslansky, John D., 57 Buzzards Bay Avenue, Woods Hole, MA 02543
Roslansky, Priscilla F., Associates of Cape Cod, Inc., P.O. Box 224, Woods Hole, MA 02543
Ross, William N., New York Medical College, Department of Physiology, Valhalla, NY 10595
Roth, Jay S., P.O. Box 692, Woods Hole, MA 02543-0692
Rottenfusser, Rudi, Marine Biological Laboratory, 7 MBL Street, Woods Hole, MA 02543
Rowland, Lewis P., Neurological Institute, 710 West 168th Street, New York, NY 10032
Ruderman, Joan V., Harvard Medical School, Department of Cell Biology, 240 Longwood Avenue, Boston, MA 02115
Rummel, John D., Marine Biological Laboratory, 7 MBL Street, Woods Hole, MA 02543
Rushforth, Norman B., Case Western Reserve University, Department of Biology, Cleveland, OH 44106
Russell-Hunter, W. D., 711 Howard Street, Easton, MD 21601-3934

Saffo, Mary Beth, Arizona State University West, Life Science Department, MC 2352, P.O. Box 37100, Phoenix, AZ 85069-7100
Salama, Guy, University of Pittsburgh, Department of Physiology, Pittsburgh, PA 15261
Salmon, Edward D., University of North Carolina, Department of Biology, CB 3280, Chapel Hill, NC 27514
Salyers, Abigail, University of Illinois, Department of Microbiology, 407 South Goodwin Avenue, Urbana, IL 61801
Salzberg, Brian M., University of Pennsylvania School of Medicine, Department of Neuroscience, 215 Stemmler Hall, Philadelphia, PA 19104-6074
Sanger, Jean M., University of Pennsylvania School of Medicine, Department of Anatomy, 36th and Hamilton Walk, Philadelphia, PA 19104
Sanger, Joseph W., University of Pennsylvania Medical Center, Department of Cell and Developemental Biology, 36th and Hamilton Walk, Philadelphia, PA 19104-6058
Saunders Jr., John W., Marquette University, P.O. Box 3381, Waquoit, MA 02536
Schachman, Howard K., University of California, Molecular and Cell Biology Department, 229 Stanley Hall, #3206, Berkeley, CA 94720-3206
Schatten, Gerald P., Oregon Health Sciences University, Oregon Regional Primate Research Center, 505 N.W. 185th Avenue, Beaverton, OR 97006
Schatten, Heide, University of Wisconsin, Department of Zoology, Madison, WI 53706
Schmeer, Arlene C., Mercenene Cancer Research Institute, 790 Prospect Street, New Haven, CT 06511
Schuel, Herbert, SUNY at Buffalo, Department of Anatomy/Cell Biology, Buffalo, NY 14214
Schwartz, James H., New York State Psychiatric Institute, Research Annex, 722 West 168th Street, 7th floor, New York, NY 10032
Schwartz, Lawrence, University of Massachusetts, Department of Biology, Morrill Science Center, Amherst, MA 01003
Schweitzer, A. Nicola, Brigham and Women's Hospital, Immunology Division, Department of Pathology, 221 Longwood Avenue, LMRC 521, Boston, MA 02115
Segal, Sheldon J., The Population Council, One Dag Hammarskjold Plaza, New York, NY 10036
Senft, Stephen Lamont, Neuroengineering/Neuroscience Center, P.O. Box 208205, New Haven, CT 06520-8205
Shanklin, Douglas R., University of Tennessee, Department of Pathology, Room 576, 800 Madison Avenue, Memphis, TN 38117
Shashoua, Victor E., Harvard Medical School, Ralph Lowell Labs, McLean Hospital, 115 Mill Street, Belmont, MA 02178
Shaver, Gaius R., Marine Biological Laboratory, The Ecosystems Center, Woods Hole, MA 02543
Shaver, John R., Michigan State University, Department of Zoology, East Lansing, MI 48824
Sheetz, Michael P., Duke University Medical Center, Department of Cell Biology, Bx 3709, 388 Nanaline Duke Building, Durham, NC 27710
Shepro, David, Boston University, CAS Biology, 5 Cummington Street, Boston, MA 02215
Shimomura, Osamu, Marine Biological Laboratory, 7 MBL Street, Woods Hole, MA 02543
Shipley, Alan M., P.O. Box 2036, Sandwich, MA 02563

Silver, Robert B., Marine Biological Laboratory, 7 MBL Street, Woods Hole, MA 02543
Siwicki, Kathleen K., Swarthmore College, Biology Department, 500 College Avenue, Swarthmore, PA 19081-1397
Skinner, Dorothy M., Oak Ridge National Laboratory, Biology Division, P.O. Box 2009, Oak Ridge, TN 37831
Sloboda, Roger D., Dartmouth College, Department of Biological Science, 6044 Gilman, Hanover, NH 03755-1893
Sluder, Greenfield, University of Massachusetts Medical School, Room 324, 377 Plantation Street, Worcester, MA 01605
Smith, Peter J.S., Marine Biological Laboratory, 7 MBL Street, Woods Hole, MA 02543
Smith, Stephen J., Stanford University School of Medicine, Department of Molecular and Cellular Physiology, Beckman Center, Stanford, CA 94305
Smolowitz, Roxanna S., Marine Biological Laboratory, 7 MBL Street, Woods Hole, MA 02543
Sogin, Mitchell L., Marine Biological Laboratory, 7 MBL Street, Woods Hole, MA 02543
Sorenson, Martha M., Cidade Universitaria-UFRJ, Department Bioquimica Medica-ICB, 21941-590 Rio de Janerio, BRAZIL
Speck, William T., Columbia-Presbyterian Medical Center, 161 Fort Washington Avenue, 14th Floor, Room 1470, New York, NY 10032-3784
Spector, Abraham, Columbia University, Department of Ophthalmology, 630 West 168th Street, New York, NY 10032
Speksnijder, Johanna E., University of Groningen, Department of Genetics, Kerklaan 30, 9751 NN Haren, THE NETHERLANDS
Spray, David C., Albert Einstein College of Medicine, Department of Neuroscience, 1300 Morris Park Avenue, Bronx, NY 10461
Spring, Kenneth R., National Institutes of Health, 10 Center Drive, MSC 1598, Building 10, Room 6N260, Bethesda, MD 20892-1603
Steele, John H., Woods Hole Oceanographic Institution, Woods Hole, MA 02543
Steinacker, Antoinette, University of Puerto Rico, Instituet of Neurobiology, 201 Boulevard Del Valle, San Jan, PR 00901
Steinberg, Malcolm, Princeton University, Department of Molecular Biology, M-18 Moffett Laboratory, Princeton, NJ 08544-1014
Stemmer, Andreas C., Institut fur Robotik, ETH-Sentrum, 8092 Zurich, SWITZERLAND
Stenflo, Johan, University of Lund, Department of Clinical Chemistry, Malmo General Hospital, S-205 02 Malmo, SWEDEN
Stetten, Jane Lazarow, 4701 Willard Avenue, #1413, Chevy Chase, MD 20815-4627
Steudler, Paul A., Marine Biological Laboratory, The Ecosystems Center, Woods Hole, MA 02543
Stokes, Darrell R., Emory University, Department of Biology, 1510 Clifton Road NE, Atlanta, GA 30322-1100
Stommel, Elijah W., Darmouth Hitchcock Medical Center, Neurology Department, Lebanon, NH 03756
Stracher, Alfred, SUNY Health Science Center, Department of Biochemistry, 450 Clarkson Avenue, Brooklyn, NY 11203
Strumwasser, Felix, P.O. Box 2278, East Falmouth, MA 02536-2278
Stuart, Ann E., University of North Carolina, Department of Physiology, Medical Research Building 206H, Chapel Hill, NC 27599-7545
Sugimori, Mutsuyuki, New York University Medical Center, Department of Physiology and Neuroscience, Room 442, 550 First Avenue, New York, NY 10016
Summers, William C., Western Washington University, Huxley College of Environmental Studies, Bellingham, WA 98225-9181
Suprenant, Kathy A., University of Kansas, Department of Physiology and Cell Biology, 4010 Haworth Hall, Lawrence, KS 66045
Swenson, Katherine I., Duke University Medical Center, Department of Molecular Cancer Biology, Box 3686, Durham, NC 27710
Sydlik, Mary Anne, Hope College, Peale Science Center, 35 East 12th St./P.O. Box 9000, Holland, MI 49422
Szent-Gyorgyi, Andrew G., 9 Westgate Road, Wellesley, MA 02181

Tabares, Lucia, University of Seville School of Medicine, Department of Physiology, Avda. Sanchez Pizjuan 4, Seville 41009, Spain
Tamm, Sidney L., Boston University, 725 Commonwealth Avenue, Boston, MA 02215
Tanzer, Marvin L., University of Conn School of Dental Medicine, Department of Biostructure and Function, Farmington, CT 06030-3705
Tasaki, Ichiji, NIMH/NIH, Laboratory of Neurobiology, Building 36, Room 2B-16, Bethesda, MD 20892
Taylor, D. Lansing, Carnegie Mellon University, Center for Flurorescence Research, 4400 Fifth Avenue, Pittsburgh, PA 15213
Taylor, Edwin W., University of Chicago, Department of Molecular Genetics, 920 E. 58th Street, Chicago, IL 60637
Teal, John M., Woods Hole Oceanographic Institute, Department of Biology, Woods Hole, MA 02543
Telfer, William H., University of Pennsylvania, Department of Biology, Philadelphia, PA 19104
Telzer, Bruce, Pomona College, Department of Biology, Thille Building, 175 West 6th Street, Claremont, CA 91711
Townsel, James G., Meharry Medical College, Department of Physiology, 1005 DB Todd Boulevard, Nashville, TN 37208
Travis, David M., 19 High Street, Woods Hole, MA 02543-1221
Treistman, Steven N., University of Massachusetts Medical Center, Department of Pharmacology, 55 Lake Avenue North, Worcester, MA 01655
Trigg, D. Thomas, One Federal Street, 9th Floor, Boston, MA 02211
Troll, Walter, NYU Medical Center, 550 First Avenue, New York, NY 10016
Troxler, Robert F., Boston University School of Medicine, Department of Biochemistry, 80 East Concord Street, Boston, MA 02118
Tucker, Edward B., Baruch College, CUNY, Department of Natural Sciences, 17 Lexington Avenue, New York, NY 10010
Turner, Ruth D., Harvard University, Museum of Comparative Zoology, Mollusk Department, Cambridge, MA 02138
Tweedell, Kenyon S., University of Notre Dame, Department of Biological Sciences, Notre Dame, IN 46556-0369
Tykocinski, Mark L., Case Western Reserve University, Institute of Pathology, 2085 Adelbert Road, Cleveland, OH 44106
Tytell, Michael, Wake Forest University, Bowman Gray School of Medicine, Department of Anatomy and Neurobiology, Winston-Salem, NC 27157

Ueno, Hiroshi, Kyoto University, AGR Chemistry, Faculty of Agriculture, Sakyo, Kyoto 606-8502, JAPAN

Valiela, Ivan, Boston University Marine Program, Marine Biological Laboratory, Woods Hole, MA 02543
Vallee, Richard, University of Massachusetts Medical Center, Worcester Foundation Campus, 222 Maple Avenue, Shrewsbury, MA 01545
Valois, John J., 420 Woods Hole Road, Woods Hole, MA 02543
Van Holde, Kensal E., Oregon State University, Biochemistry and Biophysics Department, Corvallis, OR 97331-7503
Van Dover, Cindy Lee, University of Alaska, P.O. Box 757220, Fairbanks, AK 99775
Vogl, Thomas P., Environmental Research Institute of Michigan, 1101 Wilson Boulevard, Arlington, VA 22209

Wainwright, Norman R., Marine Biological Laboratory, 7 MBL Street, Woods Hole, MA 02543

Waksman, Byron H., New York University Medical Center, Department of Pathology, 550 First Avenue, New York, NY 10016

Wall, Betty, 9 George Street, Woods Hole, MA 02543

Wang, Hsien-Yu, State University of New York, University Medical Center, Physiology and Biophysics-HSC, Stony Brook, NY 11794-8633

Wangh, Lawrence J., Brandeis University, Department of Biology, 415 South Street, Waltham, MA 02254

Warner, Robert C., University of California, Irvine, Molecular Biology and Biochemistry, Irvine, CA 92717

Warren, Leonard, Wistar Institute, 36th and Spruce Streets, Philadelphia, PA 19104

Waterbury, John B., Woods Hole Oceanographic Institution, Department of Biology, Woods Hole, MA 02543

Waxman, Stephen G., Yale Medical School, Neurology Department, 333 Cedar Street, P.O. Box 208018, New Haven, CT 06510

Webb, H. Marguerite, 184 Chestnut Street, Foxboro, MA 02035-1548

Weber, Annemarie, University of Pennsylvania School of Medicine, Department of Biochemstry and Biophysics, Philadelphia, PA 19066

Weeks, Janis C., University of Oregon, Institute of Neuroscience, Eugene, OR 97403-1254

Weidner, Earl, Louisiana State University, Department of Biological Sciences, 508 Life Sciences Building, Baton Rouge, LA 70803-1715

Weiss, Alice Sara, 105 University Boulevard West, Silver Spring, MD 20901

Weiss, Dieter, University of Rostock, Institute of Zoology, D-18051 Rostock, GERMANY

Weiss, Leon P., University of Pennsylvania School of Vet Medicine, Department of Animal Biology, Philadelphia, PA 19104

Weiss, Marisa C., Paoli Memorial Hospital, Department of Radiation Oncology, 255 W. Lancaster Avenue, Paoli, PA 19301

Weissmann, Gerald, New York University Medical Center, Department of Medicine/Division Rheumatology, 550 First Avenue, New York, NY 10016

Westerfield, Monte, University of Oregon, Institute of Neuroscience, Eugene, OR 97403

Whittaker, J. Richard, University of New Brunswick, Department of Biology, BS 4511, Frederiction, NB E3B 6E1, CANADA

Wilkens, Lon A., University of Missouri, Department of Biology, 8001 Natural Bridge Road, Street Louis, MO 63121-4499

Wilson, Darcy B., San Diego Regional Cancer Center, 3099 Science Park Road, San Diego, CA 92121

Wilson, T. Hastings, Harvard Medical School, Department of Physiology, 25 Shattuck Street, Boston, MA 02115

Witkovsky, Paul, NYU Medical Center, Department of Ophthalmology, 550 First Avenue, New York, NY 10016

Wittenberg, Beatrice, Albert Einstein College of Medicine, Department of Physiology and Biophysics, Bronx, NY 10461

Wittenberg, Jonathan B., Albert Einstein College of Medicine, Department of Physiology and Biophysics, Bronx, NY 10461

Wolken, Jerome J., Carnegie Mellon University, Department of Biological Sciences, 440 Fifth Avenue, Pittsburgh, PA 15213 (deceased)

Wonderlin, William F., West Virginia University, Pharmacology and Toxicology Department, Morgantown, WV 26506

Worden, Mary Kate, University of Virginia, Department of Neuroscience, McKim Hall Box 230, Charlottesville, VA 22908

Worgul, Basil V., Columbia University, Department of Ophthalmology, 630 West 168 Street, New York, NY 10032

Wu, Chau Hsiung, Northwestern University Medical School, Department of Pharmacology (S215), 303 East Chicago Avenue, Chicago, IL 60611-3008

Wyttenbach, Charles R., University of Kansas, Biological Sciences Department, 2045 Haworth Hall, Lawrence, KS 66045-2106

Yeh, Jay Z., Northwestern University Medical School, Department of Pharmacology, Chicago, IL 60611

Zacks, Sumner I., 65 Saconesset Road, Falmouth, MA 02540-1851

Zigman, Seymour, University of Rochester Medical School, Ophthalmology Research, Box 314, 601 Elmwood Avenue, Rochester, NY 14640

Zigmond, Michael J., University of Pittsburgh, S-526 Biomedical Science Tower, 3500 Terrace Street, Pittsburgh, PA 15213

Zimmerberg, Joshua J., National Institutes of Health, LCMB, NICHD, Building 10, Room 10D14, 10 Center Drive, Bethesda, MD 20892

Zottoli, Steven J., Williams College, Department of Biology, Williamstown, MA 01267

Zucker, Robert S., University of California, Neurobiology Division, Molecular and Cellular Biology Department, Berkeley, CA 94720

Zukin, R. Suzanne, Albert Einstein College of Medicine, Department of Neuroscience, 1410 Pelham Parkway South, Bronx, NY 10461

MBL Associates

Executive Board

Ruth Ann Laster, President
Jack Pearce, Vice President
Hanna Hastings, Treasurer
Molly Cornell, Secretary
Elizabeth Farnham, Membership Chair

Tammy Smith Amon
Duncan Aspinwall
Barbara Atwood
Kitty Brown
Julie Child
Seymour Cohen
Michael Fenlon
Alice Knowles
Rebecca Lash
Barbara Little
Cornelia McMurtrie
Jack Moakley
Joan Pearlman
Virginia R. Reynolds
Volker Ulbrich
John Valois
Kensal E. Van Holde

Patrons

Mr. and Mrs. David Bakalar
Josephine B. Crane Foundation
Dr. and Mrs. James J. Ferguson, Jr.

Sustaining Associate

Mr. Robert A. Jaye
George Frederick Jewett Foundation
Dr. and Mrs. Edward F. MacNichol, Jr.
Plymouth Savings Bank
Mr. and Mrs. William A. Putnam, III

Supporting Associate

Mrs. George H.A. Clowes
Dr. and Mrs. James D. Ebert
Mr. and Mrs. David Fausch
Dr. and Mrs. Prosser Gifford
Mr. and Mrs. Lon Hocker
Mrs. Mary D. Janney
Drs. Luigi and Elaine Mastroianni
Dr. and Mrs. William M. McDermott
Drs. Matthew & Jeanne Meselson
Dr. and Mrs. Courtland D. Perkins
Ms. Linda Sallop and Mr. Michael Fenlon
Mrs. Anne W. Sawyer
Dr. Maxine F. Singer

Dr. John Tochko and Mrs. Christina Myles-Tochko
Mr. and Mrs. John J. Valois
Drs. Walter S. Vincent and Dore J. Butler

Family Membership

Dr. Frederick W. Ackroyd
Dr. and Mrs. Edward A. Adelberg
Mr. and Mrs. Douglas F. Allison
Drs. Peggy and Fred Alsup
Drs. James and Helene Anderson
Dr. and Mrs. Samuel C. Armstrong
Mr. and Mrs. Duncan P. Aspinwall
Mr. and Mrs. Donald R. Aukamp
Mr. and Mrs. John M. Baitsell
Mr. and Mrs. William L. Banks
Dr. and Mrs. Robert B. Barlow, Jr.
Mr. and Mrs. John E. Barnes
Dr. and Mrs. Robert M. Berne
Drs. Harriet and Alan Bernheimer
Mr. and Mrs. Robert O. Bigelow
Dr. and Mrs. Edward G. Boettiger
Mr. and Mrs. Kendall B. Bohr
Dr. and Mrs. Alfred F. Borg
Dr. and Mrs. Thomas A. Borgese
Mr. and Mrs. Richard M. Bowen
Dr. and Mrs. Francis P. Bowles
Dr. and Mrs. John B. Buck
Dr. and Mrs. John E. Burris
Mr. and Mrs. William O. Burwell
Mr. and Mrs. G. Nathan Calkins, Jr.
Mr. and Mrs. D. Bret Carlson
Prof. and Mrs. James F. Case
Dr. and Mrs. Alfred B. Chaet
Dr. and Mrs. Richard L. Chappell
Dr. and Mrs. Frank M. Child, III
Dr. and Mrs. Arnold M. Clark
Mrs. LeRoy Clark
Mr. and Mrs. James Cleary
Dr. and Mrs. Laurence P. Cloud
Mr. and Mrs. Lawrence H. Coburn
Dr. and Mrs. Neal W. Cornell
Mr. and Mrs. Norman C. Cross
Mr. and Mrs. Bruce G. Daniels
Mr. and Mrs. Joel P. Davis
Mr. and Mrs. Richard C. Dierker
Dr. and Mrs. Arthur Brooks DuBois
Mr. and Mrs. John Eustis, II
Mr. and Mrs. Harold Frank
Mr. and Mrs. Howard G. Freeman
Dr. and Mrs. Robert A. Frosch
Dr. and Mrs. John J. Funkhouser
Dr. and Mrs. Mordecai L. Gabriel
Dr. and Mrs. David Garber
Dr. and Mrs. Sydney Gellis
Dr. and Mrs. James L. German, III
Mr. and Mrs. Robert S. Gillette
Dr. and Mrs. Murray Glusman
Drs. Alfred and Joan Goldberg
Mr. and Mrs. Charles Goodwin
Dr. and Mrs. Philip Grant
Dr. and Mrs. Thomas C. Gregg
Prof. and Mrs. Lawrence Grossman
Dr. and Mrs. Antoine F.O. Hadamard
Mr. and Mrs. Peter A. Hall
Dr. and Mrs. Harlyn O. Halvorson
Capt. and Mrs. Frederick J. Hancox
Drs. Alexander and Carol Hannenberg
Mrs. Janet Harvey and Dr. Richard Harvey
Dr. and Mrs. J. Woodland Hastings
Mr. and Mrs. Gary G. Hayward
Dr. and Mrs. Howard H. Hiatt
Mr. and Mrs. David Hibbitt
Dr. and Mrs. John E. Hobbie
Drs. Francis C. G. Hoskin and Elizabeth M. Farnham
Dr. and Mrs. Robert J. Huettner
Dr. and Mrs. Shinya Inoué
Dr. and Mrs. Kurt J. Isselbacher
Dr. and Mrs. Gary Jacobson
Dr. and Mrs. Benjamin Kaminer
Mr. and Mrs. Paul W. Knaplund
Mr. and Mrs. A. Sidney Knowles, Jr.
Dr. and Mrs. S. Andrew Kulin
Dr. and Mrs. George M. Langford
Dr. and Mrs. Leonard Laster
Dr. and Mrs. Hans Laufer
Mr. William Lawrence and Mrs. Barbara Buchanan
Mr. and Mrs. Stephen R. Levy
Mr. and Mrs. Robert Livingstone, Jr.
Mr. and Mrs. James E. Lloyd
Mr. and Mrs. Bernard Manuel
Dr. and Mrs. Julian B. Marsh
Mr. and Mrs. Joseph C. Martyna
Mr. and Mrs. Frank J. Mather, III
Mr. and Mrs. John E. Matthews
Dr. and Mrs. Robert T. McCluskey
Mr. Paul McGonigle
Dr. and Mrs. Jerry M. Melillo
Dr. Martin Mendelson
Mr. and Mrs. Richard Meyers
Dr. and Mrs. Daniel G. Miller
Dr. and Mrs. Merle Mizell
Dr. and Mrs. Charles H. Montgomery
Mr. and Mrs. Charles F. Murphy
Dr. and Mrs. John E. Naugle
Dr. Pamela Nelson and Mr. Christopher Olmsted
Mr. and Mrs. Frank L. Nickerson
Dr. and Mrs. Clifford T. O'Connell
Mr. and Mrs. David R. Palmer
Dr. and Mrs. George D. Pappas
Mr. and Mrs. Robert Parkinson
Mr. and Mrs. Richard M. Paulson, Jr.
Mr. and Mrs. William J. Pechilis
Mr. and Mrs. John B. Peri
Dr. and Mrs. Philip Person
Mr. and Mrs. Frederick S. Peters
Mrs. and Mr. Grace M. Peters
Mr. and Mrs. George H. Plough
Dr. and Mrs. Aubrey Pothier, Jr.
Dr. and Mrs. Carl A. Price
Mr. Allan Ray Putnam
Dr. and Mrs. Lionel I. Rebhun
Dr. and Mrs. George T. Reynolds
Mr. and Mrs. John Ripple
Dr. and Mrs. Harris Ripps
Ms. Jean Roberts
Drs. Priscilla and John Roslansky
Dr. and Mrs. John D. Rummel
Dr. and Mrs. John W. Saunders, Jr.
Dr. and Mrs. R. Walter Schlesinger
Mr. and Mrs. Harold H. Sears
Mr. John Seder and Ms. Frances Plough
Dr. and Mrs. Sheldon J. Segal
Dr. and Mrs. Douglas R. Shanklin
Dr. and Mrs. David Shepro
Mr. and Mrs. Bertram R. Silver
Mr. and Mrs. Jonathan O. Simonds
Drs. Frederick and Marguerite Smith
Dr. and Mrs. Heinz Specht (Dr. Specht deceased)
Drs. William and Phoebe Speck
Dr. and Mrs. William K. Stephenson
Mr. and Mrs. E. Kent Swift, Jr.
Mr. and Mrs. Gerard L. Swope, III
Mr. and Mrs. Emil D. Tietje, Jr.
Mr. Norman N. Tolkan
Dr. and Mrs. Walter Troll
Mr. and Mrs. Volker Ulbrich
Drs. Claude and Dorothy Villee
Mr. and Mrs. Samuel Vincent
Dr. and Mrs. Samuel Ward
Mr. J. Ware and Ms. Sharon McCarthy
Dr. and Mrs. Henry B. Warren
Dr. and Mrs. Gerald Weissmann
Dr. and Mrs. Paul S. Wheeler
Dr. Martin Keister White
Mr. and Mrs. Geoffrey G. Whitney, Jr.
Mr. and Mrs. Leonard M. Wilson
Mr. and Mrs. Leslie J. Wilson
Mr. and Mrs. Dick S Yeo
Dr. and Mrs. Sumner I. Zacks

Individual Membership

Mr. David C. Ahearn
Mr. Henry Albers
Mrs. Constance M. Allard
Dr. Nina S. Allen
Mrs. Tammy Amon
Mr. Dean N. Arden
Mrs. Ellen Prosser Armstrong
Mrs. Kimball C. Atwood, III
Dr. Serena Baccetti
Mr. Everett E. Bagley
Mr. C. John Berg
Ms. Avis Blomberg
Mrs. Elinor W. Bodian
Mr. Thomas C. Bolton
Mrs. Jennie P. Brown
Mrs. M. Kathryn S. Brown
Ms. Henriete Bull
Dr. Alan H. Burghauser
Mrs. Barbara Gates Burwell
Mr. Bruce E. Buxton
Mr. Patrick J. Calie
Dr. Graciela C. Candelas
Mrs. Winslow G. Carlton (deceased)
Mr. Frank C. Carotenuto

Dr. Robert H. Carrier
Mrs. Patricia A. Case
Dr. Sallie Chisholm
Mrs. Octavia C. Clement
Mr. Allen W. Clowes
Dr. Jewel Plummer Cobb
Mrs. Margaret H. Coburn
Dr. Seymour S. Cohen
Ms. Anne S. Concannon
Mr. Robert J. Cook
Prof. D. Eugene Copeland
Dr. Helen M. Costello
Dr. Vincent Cowling
Mrs. J. Sterling Crandall
Ms. Dorothy Crossley
Ms. Helen M. Crossley
Mrs. Villa B. Crowell
Mr. Norman Dana
Dr. Morton Davidson
Ms. Carol Reimann DeYoung
Dr. Marie A. DiBerardino
Mrs. Shirley Dierolf
Mr. David L. Donovan
Mr. Stephen Doyle
Ms. Suzanne Droban
Mr. Roy A. Duffus
Mrs. Charles Eastman
Dr. Frank Egloff
Mr. Raymond Eliott
Mr. William M. Ferry
Mr. Robert Fitzpatrick
Ms. Sylvia M. Flanagan
Mr. Robert P. Flynn, Jr.
Mr. John W. Folino, Jr.
Mr. John H. Ford
Dr. Krystyna Frenkel
Mr. Paul J. Freyheit
Mrs. Paul M. Fye
Mr. Joseph C. Gallagher
Miss Eleanor Garfield
Dr. Patricia E. Garrett
Mr. Charles Gifford
Mrs. James R. Glazebrook
Mrs. Mary L. Goldman
Mr. Michael P. Goldring
Mrs. Phyllis Goldstein
Ms. Muriel Gould
Mrs. Deborah Ann Green
Dr. B. Herold Griffith
Mrs. Edith T. Grosch (deceased)
Mrs. Barbara Grossman
Mrs. Valerie A. Hall
Dr. Peter J. Hamre
Ms. Mary Elizabeth Hamstrom
Ms. Elizabeth E. Hathaway
Dr. Robert R. Haubrich
Mrs. Jane M. Heald
Mr. Michael W. Herlihy
Mrs. Nathan Hirschfeld
Mrs. Eleanor D. Hodge
Mr. Roger W. Hubbell
Ms. Susan A. Huettner
Miss Elizabeth B. Jackson
Dr. Joseph Jacobson

Mr. Raymond L. Jewett
Mrs. Barbara W. Jones
Mrs. Margaret H. Jones
Mrs. Barbara Kanellopoulos
Mrs. Joan T. Kanwisher
Mrs. Sally Karush
Mrs. Marcella Katz
Ms. Patricia E. Keoughan
Dr. Peter N. Kivy
Lady Haber Kornberg
Dr. Bruno P. Kremer
Ms. Norma Kumin
Mr. Bernard H. Labitt
Mrs. Janet W. Larcom
Ms. Rebecca Lash
Dr. Marian E. LeFevre
Dr. Mortimer Levitz
Mr. Edwin M. Libbin
Mr. Lennart Lindberg
Mrs. Barbara C. Little
Mrs. Sarah J. Loessel
Mrs. Ermine W. Lovell
Mr. Richard C. Lovering
Mrs. Margaret M. Macleish
Ms. Anne Camille Maher
Mrs. Annemarie E. Mahler
Mr. Patrick J. Mahoney
Dr. Phillip B. Maples
Mr. Daniel R. Martin
Dr. G. C. Matthiessen
Dr. Miriam Jacob Mauzerall
Mrs. Mary Hartwell Mavor
Mrs. Jane C. McCormack
Ms. Suzanne McDermott
Mrs. Nella W. McElroy (deceased)
Dr. Susan Gerbi McIlwain
Ms. Mary W. McKoan
Ms. Geraldine G. McLean
Ms. Cornelia Hanna McMurtrie
Mrs. Ellen L. Meigs
Mr. Ted Melillo
Mrs. Grace S. Metz
Mrs. Mary G. Miles
Mrs. Florence E. Mixer
Mr. John T. Moakley
Mrs. Mary E. Montgomery
Ms. Cynthia Moor
Mr. Stephen A. Moore
Mr. Alan F. Morrison
Dr. M. Patricia Morse
Mrs. Eleanor M. Nace
Mr. William G. Neall
Mrs. Anne Nelson
Mrs. Catherine N. Norton
Mr. Thomas J. Novitsky
Mr. John J. O'Connor
Dr. Renee Bennett O'Sullivan
Miss Carolyn L. Parmenter
Mrs. Dolores Patch-Wing
Dr. John B. Pearce
Ms. Joan Pearlman
Dr. Judith Pederson
Ms. Joyce S. Pendery
Dr. Murray E. Pendleton

Mr. Raymond W. Peterson
Ms. Victoria A. Powell
Mrs. Julia S. Rankin
Mr. Fred J. Ravens, Jr.
Mrs. Adell R. Rawson
Dr. Robert M. Reece
Ms. Anecia Kathy Regis
Dr. Renato A. Ricca
Dr. Mary Esther Rice
Mr. John Riina
Dr. Monica Riley
Mrs. Alison A. Robb
Mrs. Lola E. Robertson
Mrs. Ruth J. Robinson
Mrs. Arlene Rogers
Mrs. Wendy E. Rose
Ms. Hilde Rosenthal
Mrs. Atholie K. Rosett
Dr. Virginia F. Ross
Mr. Raymond A. Sanborn
Mrs. Joyce Waksman Schambacher
Ms. Elaine Schott
Mrs. Elsie M. Scott
Sea Education Association, Inc.
Dr. Cecily C. Selby
Mrs. Deborah G. Senft
Mrs. Charlotte Shemin
Mrs. Phyllis J. Silver
Mrs. Cynthia C. Smith
Mrs. Perle Sonnenblick
Dr. Evelyn Spiegel
Dr. Guy L. Steele, Sr.
Dr. Robert E. Steele
Mrs. Eleanor Steinbach
Mrs. Judith G. Stetson
Mrs. Jane Lazarow Stetten
Dr. Dorothy A. Stracher
Mr. Robert Stump
Dr. Maurice Sussman
Mr. Albert H. Swain
Mr. James K. Taylor
Mrs. Alice Todd
Mr. Arthur D. Traub
Ms. Natalie Trousof
Ms. Ciona Ulbrich
Mrs. Barbara Van Holde
Dr. Kensal E. Van Holde
Ms. Sylvia Vatuk
Ms. Susan Veeder
Mr. Lee D. Vincent
Mr. Arthur D. Voorhis
Mrs. Eve Warren
Mr. John T. Weeks
Ms. Lillian Wendorff
Dr. William M. Wheeler
Ms. Mabel E. Whelpley
Mrs. Barbara Whitehead
Mrs. A.A. Wickersham
Mrs. Clare M. Wilber
Mrs. Ann S. Wilke
Mr. Albert Wilson
Dr. T. Hastings Wilson
Ms. Nancy Woitkoski
Mrs. Elizabeth S. Yntema

Mrs. Donald J. Zinn

MBL Gift Shop Volunteers

Marion Adelberg
Barbara Atwood
Caroline Banks
Harriet Bernheimer
Avis Blomberg
Gloria Borgese
Kitty Brown
Elisabeth Buck
Vera Clark
Peggy Clowes
Jewel Cobb
Janet Daniels
Carol DeYoung
Fran Eastman
Alma Ebert
Jane Foster
Becky Glazebrook
Muriel Gould
Barbara Grossman
Jean Halvorson
Pat Hancox
Hanna Hastings
Sally Karush
Alice Knowles
Donna Kornberg
Evelyn Laufer
Barbara Little
Sally Loessel
Winnie Mackey
Miriam Mauzerall
Mary Mavor
Jane McCormack
Louise McManus
Phyllis Meyers
Polly Miles
Florence Mixer
Lorraine Mizell
Elizabeth Moseley
Stacia Palmer
Bertha Person
Margareta Pothier
Julie Rankin
Millie Rebhun
Jean Ripps
Arlene Rogers
Lil Saunders
Louise Specht
Cynthia Smith
Peggy Smith
Jane Stetten
Elaine Troll
Natalie Trousof
Barbara Van Holde
Susan Veeder
Carol Ann Wagner
Mabel Whelpley
Clare Wilber

MBL Summer Tour Guides

Sears Crowell
Barbara Little
Steve Oliver
Julie Rankin
Priscilla Roslansky
Mary Ulbrich
John Valois

Certificate of Organization
Articles of Amendment
Bylaws

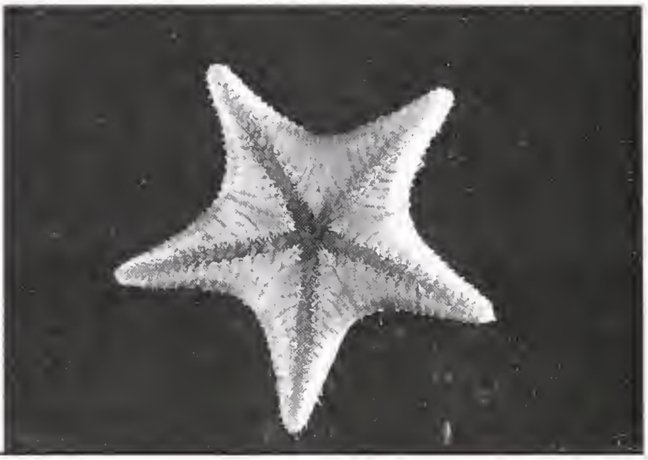

Certificate of Organization

(On File in the Office of the Secretary of the Commonwealth)

No. 3170

We, Alpheus Hyatt, President, William Stanford Stevens, Treasurer, and William T. Sedgwick, Edward G. Gardiner, Susan Mims and Charles Sedgwick Minot being a majority of the Trustees of the Marine Biological Laboratory in compliance with the requirements of the fourth section of chapter one hundred and fifteen of the Public Statutes do hereby certify that the following is a true copy of the agreement of association to constitute said Corporation, with the names of the subscribers thereto:

We, whose names are hereto subscribed, do, by this agreement, associate ourselves with the intention to constitute a Corporation according to the provisions of the one hundred and fifteenth chapter of the Public Statutes of the Commonwealth of Massachusetts, and the Acts in amendment thereof and in addition thereto.

The name by which the Corporation shall be known is
THE MARINE BIOLOGICAL LABORATORY.

The purpose for which the Corporation is constituted is to establish and maintain a laboratory or station for scientific study and investigations, and a school for instruction in biology and natural history.
The place within which the Corporation is established or located is the city of Boston within said Commonwealth.
The amount of its capital stock is none.
In Witness Whereof, we have hereunto set our hands, this twenty seventh day of February in the year eighteen hundred and eighty-eight, Alpheus Hyatt, Samuel Mills, William T. Sedgwick, Edward G. Gardiner, Charles Sedgwick Minot, William G. Farlow, William Stanford Stevens, Anna D. Phillips, Susan Mims, B. H. Van Vleck.
That the first meeting of the subscribers to said agreement was held on the thirteenth day of March in the year eighteen hundred and eighty-eight.
In Witness Whereof, we have hereunto signed our names, this thirteenth day of March in the year eighteen hundred and eighty-eight, Alpheus Hyatt, President, William Stanford Stevens, Treasurer, Edward G. Gardiner, William T. Sedgwick, Susan Mims, Charles Sedgwick Minot.
(Approved on March 20, 1888 as follows:
I hereby certify that it appears upon an examination of the within written certificate and the records of the corporation duly submitted to my inspection, that the requirements of sections one, two and three of chapter one hundred and fifteen, and sections eighteen, twenty and twenty-one of chapter one hundred and six, of the Public Statutes, have been complied with and I hereby approve said certificate this twentieth day of March A.D. eighteen hundred and eighty-eight.

Charles Endicott
Commissioner of Corporations)

Articles of Amendment

(On File in the Office of the Secretary of the Commonwealth)

We, James D. Ebert, President, and David Shepro, Clerk of the Marine Biological Laboratory, located at Woods Hole, Massachusetts 02543, do hereby certify that the following amendment to the Articles of Organization of the Corporation was duly adopted at a meeting held on August 15, 1975, as adjourned to August 29, 1975, by vote of 444 members, being at least two-thirds of its members legally qualified to vote in the meeting of the corporation:

Voted: That the Certificate of Organization of this corporation be and it hereby is amended by the addition of the following provisions:
"No Officer, Trustee or Corporate Member of the corporation shall be personally liable for the payment or satisfaction of any obligation or liabilities incurred as a result of, or otherwise in connection with, any commitments, agreements, activities or affairs of the corporation.
"Except as otherwise specifically provided by the Bylaws of the corporation, meetings of the Corporate Members of the corporation may be held anywhere in the United States.
"The Trustees of the corporation may make, amend or repeal the Bylaws of the corporation in whole or in part, except with respect to any provisions thereof which shall by law, this Certificate or the bylaws of the corporation, require action by the Corporate Members."

The foregoing amendment will become effective when these articles of amendment are filed in accordance with Chapter 180, Section 7 of the General Laws unless these articles specify, in accordance with the vote adopting the amendment, a later effective date not more than thirty days after such filing, in which event the amendment will become effective on such later date.

In Witness whereof and Under the Penalties of Perjury, we have hereto signed our names this 2nd day of September, in the year 1975, James D. Ebert, President; David Shepro, Clerk.
(Approved on October 24, 1975, as follows:
I hereby approve the within articles of amendment and, the filing fee in the amount of $10 having been paid, said articles are deemed to have been filed with me this 24th day of October, 1975.

Paul Guzzi
Secretary of the Commonwealth)

Bylaws

(Revised August 7, 1992 and December 10, 1992)

ARTICLE I—THE CORPORATION

A. *Name and Purpose.* The name of the Corporation shall be The Marine Biological Laboratory. The Corporation's purpose shall be to establish and maintain a laboratory or station for scientific study and investigation and a school for instruction in biology and natural history.

B. *Nondiscrimination.* The Corporation shall not discriminate on the basis of age, religion, color, race, national or ethnic origin, sex or sexual preference in its policies on employment and administration or in its educational and other programs.

ARTICLE II—MEMBERSHIP

A. *Members.* The Members of the Corporation ("Members") shall consist of persons elected by the Board of Trustees (the "Board"), upon such terms and conditions and in accordance with such procedures, not inconsistent with law or these Bylaws, as may be determined by the Board. At any regular or special meeting of the Board, the Board may elect new Members. Members shall have no voting or other rights with respect to the Corporation or its activities except as specified in these Bylaws, and any Member may vote at any meeting of the Members in person only and not by proxy. Members shall serve until their death or resignation unless earlier removed with or without cause by the affirmative vote of two-thirds of the Trustees then in office. Any Member who has retired from his or her home institution may, upon written request to the Corporation, be designated a Life Member. Life Members shall not have the right to vote and shall not be assessed for dues.

B. *Meetings.* The annual meeting of the Members shall be held on the Friday following the first Tuesday in August of each year, at the Laboratory of the Corporation in Woods Hole, Massachusetts, at 9:30 a.m. The Chairperson of the Board shall preside at meetings of the Corporation. If no annual meeting is held in accordance with the foregoing provision, a special meeting may be held in lieu thereof with the same effect as the annual meeting, and in such case all references in these Bylaws, except in this Article II.B., to the annual meeting of the Members shall be deemed to refer to such special meeting. Members shall transact business as may properly come before the meeting. Special meetings of the Members may be called by the Chairperson or the Trustees, and shall be called by the Clerk, or in the case of the death, absence, incapacity or refusal by the Clerk, by any other officer, upon written application of Members representing at least ten percent of the smallest quorum of Members required for a vote upon any matter at the annual meeting of the Members, to be held at such time and place as may be designated.

C. *Quorum.* One hundred (100) Members shall constitute a quorum at any meeting. Except as otherwise required by law or these Bylaws, the affirmative vote of a majority of the Members voting in person at a meeting attended by a quorum shall constitute action on behalf of the Members.

D. *Notice of Meetings.* Notice of any annual meeting or special meeting of Members, if necessary, shall be given by the Clerk by mailing notice of the time and place and purpose of such meeting at least 15 days before such meeting to each Member at his or her address as shown on the records of the Corporation.

E. *Wavier of Notice.* Whenever notice of a meeting is required to be given a Member, under any provision of the Articles or Organization or Bylaws of the Corporation, a written waiver thereof, executed before or after the Meeting by such Member, or his or her duly authorized attorney, shall be deemed equivalent to such notice.

F. *Adjournments.* Any meeting of the Members may be adjourned to any other time and place by the vote of a majority of those Members present at the meeting, whether or not such Members constitute a quorum, or by any officer entitled to preside at or to act as Clerk of such meeting, if no Member is present or represented. It shall not be necessary to notify any Members of any adjournment unless no Member is present or represented at the meeting which is adjourned, in which case, notice of the adjournment shall be given in accordance with Article II.D. Any business which could have been transacted at any meeting of the Members as originally called may be transacted at an adjournment thereof.

ARTICLE III—ASSOCIATES OF THE CORPORATION

Associates of the Corporation. The Associates of the Marine Biological Laboratory shall be an unincorporated group of persons (including associations and corporations) interested in the Laboratory and shall be organized and operated under the general supervision and authority of the Trustees. The Associates of the Marine Biological Laboratory shall have no voting rights.

ARTICLE IV—BOARD OF TRUSTEES

A. *Powers.* The Board of Trustees shall have the control and management of the affairs of the Corporation. The Trustees shall elect a Chairperson of the Board who shall serve until his or her successor is elected and qualified. They shall annually elect a President of the Corporation. They shall annually elect a Vice Chairperson of the Board who shall be Vice Chairperson of the meetings of the Corporation. They shall annually elect a Treasurer. They shall annually elect a Clerk, who shall be a resident of Massachusetts. They shall elect Trustees-at-Large as specified in this Article IV. They shall appoint a Director of the Laboratory for a term not to exceed five years, provided the term shall not exceed one year if the candidate has attained the age of 65 years prior to the date of the appointment. They shall choose such other officers and agents as they shall think best. They may fix the compensation of all officers and agents of the Corporation and may remove them at any time. They may fill vacancies occurring in any of the offices. The Board shall have the power to choose an Executive Committee from their own number as provided in Article V, and to delegate to such Committee such of their own powers as they may deem expedient in addition to those powers conferred by Article V. They shall, from time to time, elect Members to the Corporation upon such terms and conditions as they shall have determined, not inconsistent with law or these Bylaws.

B. *Composition and Election.*

(1) The Board shall include 24 Trustees elected by the Board as provided below:

(a) At least six Trustees ("Corporate Trustees") shall be Members who are scientists, and the other Trustees ("Trustees-at-Large") shall be individuals who need not be Members or otherwise affiliated with the Corporation.

(b) The 24 elected Trustees shall be divided into four classes of six Trustees each, with one class to be elected each year to serve for a term of four years, and with each such class to include at least one Corporate Trustee. Such classes of Trustees shall be designated by the year of expiration of their respective terms.

(2) The Board shall also include the Chief Executive Officer, Treasurer and the Chairperson of the Science Council, who shall be *ex officio* voting members of the Board.

(3) Although Members or Trustees may recommend individuals for nomination as Trustees, nominations for Trustee elections shall be made by the Nominating Committee in its sole discretion. The Board may also elect Trustees who have not been nominated by the Nominating Committee.

C. *Eligibility.* A Corporate Trustee or a Trustee-at-Large who has been elected to an initial four-year term or remaining portion thereof, of which he/she has served at least two years, shall be eligible for re-election to a second four-year term, but shall be ineligible for re-election to any subsequent term until one year has elapsed after he/she has last served as a Trustee.

D. *Removal.* Any Trustee may be removed from office at any time with or without cause, by vote of a majority of the Members entitled to vote in the election of Trustees; or for cause, by vote of two-thirds of the Trustees then in office. A Trustee may be removed for cause only if notice of such action shall have been given to all of the Trustees or Members entitled to vote, as the case may be, prior to the meeting at which such action is to be taken and if the Trustee to be so removed shall have been given reasonable notice and opportunity to be heard before the body proposing to remove him or her.

E. *Vacancies.* Any vacancy in the Board may be filled by vote of a majority of the remaining Trustees present at a meeting of Trustees at which a quorum is present. Any vacancy in the Board resulting from the resignation or removal of a Corporate Trustee shall be filled by a Member who is a scientist.

F. *Meetings.* Meetings of the Board shall be held from time to time, not less frequently than twice annually, as determined by the Board. Special meetings of Trustees may be called by the Chairperson, or by any seven Trustees, to be held at such time and place as may be designated. The Chairperson of the Board, when present, shall preside over all meetings of the Trustees. Written notice shall be sent to a Trustee's usual or last known place of residence at least two weeks before the meeting. Notice of a meeting need not be given to any Trustee if a written waiver of notice executed by such Trustee before or after the meeting is filed with the records of the meeting, or if such Trustee shall attend the meeting without protesting prior thereto or at its commencement the lack of notice given to him or her.

G. *Quorum and Action by Trustees.* A majority of all Trustees then in office shall constitute a quorum. Any meeting of Trustees may be adjourned by vote of a majority of Trustees present, whether or not a quorum is present, and the meeting may be held as adjourned without further notice. When a quorum is present at any meeting of the Trustees, a majority of the Trustees present and voting (excluding abstentions) shall decide any question, including the election of officers, unless otherwise required by law, the Articles of Organization or these Bylaws.

H. *Transfers of Interests in Land.* There shall be no transfer of title nor long-term lease of real property held by the Corporation without prior approval of not less than two-thirds of the Trustees. Such real property transactions shall be finally acted upon at a meeting of the Board only if presented and discussed at a prior meeting of the Board. Either meeting may be a special meeting and no less than four weeks shall elapse between the two meetings. Any property acquired by the Corporation after December 1, 1989 may be sold, any mortgage or pledge of real property (regardless of when acquired) to secure borrowings by the Corporation may be granted, and any transfer of title or interest in real property pursuant to the foreclosure or endorsement of any such mortgage or pledge of real property may be effected by any holder of a mortgage or pledge of real property of the Corporation, with the prior approval of not less than two-thirds of the Trustees (other than any Trustee or Trustees with a direct or indirect financial interest in the transaction being considered for approval) who are present at a regular or special meeting of the Board at which there is a quorum.

ARTICLE V—COMMITTEES

A. *Executive Committee.* There shall be an Executive Committee of the Board of Trustees which shall consist of not more than eleven (11) Trustees, including *ex officio* Trustees, elected by the Board.

The Chairperson of the Board shall act as Chairperson of the Executive Committee and the Vice Chairperson as Vice Chairperson. The Executive Committee shall meet at such times and places and upon such notice and appoint such subcommittees as the Committee shall determine.

The Executive Committee shall have and may exercise all the powers of the Board during the intervals between meetings of the Board except those powers specifically withheld, from time to time, by vote of the Board or by law. The Executive Committee may also appoint such committees, including persons who are not Trustees, as it may, from time to time, approve to make recommendations with respect to matters to be acted upon by the Executive Committee or the Board.

The Executive Committee shall keep appropriate minutes of its meetings, which shall be reported to the Board. Any actions taken by the Executive Committee shall also be reported to the Board.

B. *Nominating Committee.* There shall be a Nominating Committee which shall consist of not fewer than four nor more than six Trustees appointed by the Board in a manner which shall reflect the balance between Corporate Trustees and Trustees-at-Large on the Board. The Nominating Committee shall nominate persons for election as Corporate Trustees and Trustees-at-Large, Chairperson of the Board, Vice Chairperson of the Board, President, Treasurer, Clerk, Director of the Laboratory and such other officers, if any, as needed, in accordance with the requirements of these Bylaws. The Nominating Committee shall also be responsible for overseeing the training of new Trustees. The Chairperson of the Board of Trustees shall appoint the Chairperson of the Nominating Committee. The Chairperson of the Science Council shall be an *ex officio* voting member of the Nominating Committee.

C. *Science Council.* There shall be a Science Council (the "Council") which shall consist of Members of the Corporation elected to the Council by vote of the Members of the Corporation, and which shall advise the Board with respect to matters concerning the Corporation's mission, its scientific and instructional endeavors, and the appointment and promotions of persons or committees with responsibility for matters requiring scientific expertise. Unless otherwise approved by a majority of the members of the Council, the Chairperson of the Council shall be elected annually by the Council. The chief executive officer of the Corporation shall be an *ex officio* voting member of the Council.

D. *Board of Overseers.* There shall be a Board of Overseers which shall consist of not fewer than five nor more than eight scientists who have expertise concerning matters with which the Corporation is involved. Members of the Board of Overseers may or may not be Members of the Corporation and may be appointed by the Board of Trustees on the basis of recommendations submitted from scientists and scientific organizations or societies. The Board of Overseers shall be available to review and offer recommendations to the officers, Trustees and Science Council regarding scientific activities conducted or proposed by the Corporation and shall meet from time to time, not less frequently than annually, as determined by the Board of Trustees.

E. *Board Committees Generally.* The Trustees may elect or appoint one or more other committees (including, but not limited to, an Investment Committee, a Development Committee, an Audit Committee, a Facilities and Capital Equipment Committee and a Long-Range Planning Committee) and may delegate to any such committee or committees any or all of their powers, except those which by law, the Articles of Organization or these Bylaws the Trustees are prohibited from delegating; provided that any committee to which the powers of the Trustees are delegated shall consist solely of Trustees. The members of any such committee shall have such tenure and duties as the Trustees shall determine. The Investment Committee, which shall oversee the management of the Corporation's endowment funds and marketable securities shall include as *ex officio* members, the Chairperson of the Board, the Treasurer and the Chairperson of the Audit Committee, together with such Trustees as may be required for not less than two-thirds of the Investment Committee to consist of Trustees. Except as otherwise provided by these Bylaws or determined by the Trustees, any such committee may make rules for the conduct of its business, but, unless otherwise provided by the Trustees or in such rules, its business shall be conducted as nearly as possible in the same manner as is provided by these Bylaws for the Trustees.

F. *Actions Without a Meeting.* Any action required or permitted to be taken at any meeting of the Executive Committee or any other committee elected by the Trustees may be taken without a meeting if all members of such committees consent to the action in writing and such written consents are filed with the records of meetings. Members of the Executive Committee or any other committee elected by the Trustees may also participate in any meeting by means of a telephone conference call, or otherwise take action in such a manner as may, from time to time, be permitted by law.

G. *Manual of Procedures.* The Board of Trustees, on the recommendation of the Executive Committee, shall establish guidelines and modifications thereof to be recorded in a Manual of Procedures. Guidelines shall establish procedures for: (1) Nomination and election of members of the Corporation, Board of Trustees and Executive Committee; (2) Election of Officers; (3) Formation and Function of Standing Committees.

ARTICLE VI—OFFICERS

A. *Enumeration.* The officers of the Corporation shall consist of a President, a Treasurer and a Clerk, and such other officers having the powers of President, Treasurer and Clerk as the Board may determine, and a Director of the Laboratory. The Corporation may have such other officers and assistant officers as the Board may determine, including (without limitation) a Chairperson of the Board, Vice Chairperson and one or more Vice Presidents, Assistant Treasurers or Assistant Clerks. Any two or more offices may be held by the same person. The Chairperson and Vice Chairperson of the Board shall be elected by and from the Trustees, but other officers of the Corporation need not be Trustees or Members. If required by the Trustees, any officer shall give the Corporation a bond for the faithful performance of his or her duties in such amount and with such surety or sureties as shall be satisfactory to the Trustees.

B. *Tenure.* Except as otherwise provided by law, by the Articles of Organization or by these Bylaws, the President, Treasurer, and all other officers shall hold office until the first meeting of the Board following the annual meeting of Members and thereafter, until his or her successor is chosen and qualified.

C. *Resignation.* Any officer may resign by delivering his or her written resignation to the Corporation at its principal office or to the President or Clerk and such resignation shall be effective upon receipt unless it is specified to be effective at some other time or upon the happening of some other event.

D. *Removal.* The Board may remove any officer with or without cause by a vote of a majority of the entire number of Trustees then in office, at a meeting of the Board called for that purpose and for which notice of the purpose thereof has been given, provided that an officer may be removed for cause only after having an opportunity to be heard by the Board at a meeting of the Board at which a quorum is personally present and voting.

E. *Vacancy.* A vacancy in any office may be filled for the unexpired balance of the term by vote of a majority of the Trustees present at any meeting of Trustees at which a quorum is present or by written consent of all of the Trustees, if less than a quorum of Trustees shall remain in office.

F. *Chairperson.* The Chairperson shall have such powers and duties as may be determined by the Board and, unless otherwise determined by the Board, shall serve in that capacity for a term coterminous with his or her term as Trustee.

G. *Vice Chairperson.* The Vice Chairperson shall perform the duties and exercise the powers of the Chairperson in the absence or disability of the Chairperson, and shall perform such other duties and possess such other powers as may be determined by the Board. Unless otherwise determined by the Board, the Vice Chairperson shall serve for a one-year term.

H. *Director.* The Director shall be the chief operating officer and, unless otherwise voted by the Trustees, the chief executive officer of the Corporation. The Director shall, subject to the direction of the Trustees, have general supervision of the Laboratory and control of the business of the Corporation. At the annual meeting, the Director shall submit a report of the operations of the Corporation for such year and a statement of its affairs, and shall, from time to time, report to the Board all matters within his or her knowledge which the interests of the Corporation may require to be brought to its notice.

I. *Deputy Director.* The Deputy Director, if any, or if there shall be more than one, the Deputy Directors in the order determined by the Trustees, shall, in the absence or disability of the Director, perform the duties and exercise the powers of the Director and shall perform such other duties and shall have such other powers as the Trustees may, from time to time, prescribe.

J. *President.* The President shall have the powers and duties as may be vested in him or her by the Board.

K. *Treasurer and Assistant Treasurer.* The Treasurer shall, subject to the direction of the Trustees, have general charge of the financial affairs of the Corporation, including its long-range financial planning, and shall cause to be kept accurate books of account. The Treasurer shall prepare a yearly report on the financial status of the Corporation to be delivered at the annual meeting. The Treasurer shall also prepare or oversee all filings required by the Commonwealth of Massachusetts, the Internal Revenue Service, or other Federal and State Agencies. The account of the Treasurer shall be audited annually by a certified public accountant.

The Assistant Treasurer, if any, or if there shall be more than one, the Assistant Treasurers in the order determined by the Trustees, shall, in the absence or disability of the Treasurer, perform the duties and exercise the powers of the Treasurer, shall perform such other duties and shall have such other powers as the Trustees may, from time to time, prescribe.

L. *Clerk and Assistant Clerk.* The Clerk shall be a resident of the Commonwealth of Massachusetts, unless the Corporation has designated a resident agent in the manner provided by law. The minutes or records of all meetings of the Trustees and Members shall be kept by the Clerk who shall record, upon the record books of the Corporation, minutes of the proceedings at such meetings. He or she shall have custody of the record books of the Corporation and shall have such other powers and shall perform such other duties as the Trustees may, from time to time, prescribe.

The Assistant Clerk, if any, or if there shall be more than one, the Assistant Clerks in the order determined by the Trustees, shall, in the absence or disability of the Clerk, perform the duties and exercise the powers of the Clerk and shall perform such other duties and shall have such other powers as the Trustees may, from time to time, prescribe.

In the absence of the Clerk and an Assistant Clerk from any meeting, a temporary Clerk shall be appointed at the meeting.

M *Other Powers and Duties.* Each officer shall have in addition to the duties and powers specifically set forth in these Bylaws, such duties and powers as are customarily incident to his or her office, and such duties and powers as the Trustees may, from time to time, designate.

ARTICLE VII—AMENDMENTS

These Bylaws may be amended by the affirmative vote of the Members at any meeting, provided that notice of the substance of the proposed amendment is stated in the notice of such meeting. As authorized by the Articles of Organization, the Trustees, by a majority of their number then in office, may also make, amend or repeal these Bylaws, in whole or in part, except with respect to (a) the provisions of these Bylaws governing (i) the removal of Trustees and (ii) the amendment of these Bylaws and (b) any provisions of these Bylaws which by law, the Articles of Organization or these Bylaws, requires action by the Members.

No later than the time of giving notice of meeting of Members next following the making, amending or repealing by the Trustees of any Bylaw, notice thereof stating the substance of such change shall be given to all Members entitled to vote on amending the Bylaws.

Any Bylaw adopted by the Trustees may be amended or repealed by the Members entitled to vote on amending the Bylaws.

ARTICLE VIII—INDEMNITY

Except as otherwise provided below, the Corporation shall, to the extent legally permissible, indemnify each person who is, or shall have been, a Trustee, director or officer of the Corporation or who is serving, or shall have served at the request of the Corporation as a Trustee, director or officer of another organization in which the Corporation directly or indirectly has any interest as a shareholder, creditor or otherwise, against all liabilities and expenses (including judgments, fines, penalties, and reasonable attorneys' fees and all amounts paid, other than to the Corporation or such other organization, in compromise or settlement) imposed upon or incurred by any such person in connection with, or arising out of, the defense or disposition of any action, suit or other proceeding, whether civil or criminal, in which he or she may be a defendant or with which he or she may be threatened or otherwise involved, directly or indirectly, by reason of his or her being or having been such a Trustee, director or officer.

The Corporation shall provide no indemnification with respect to any matter as to which any such Trustee, director or officer shall be finally adjudicated in such action, suit or proceeding not to have acted in good faith in the reasonable belief that his or her action was in the best interests of the Corporation. The Corporation shall provide no indemnification with respect to any matter settled or comprised unless such matter shall have been approved as in the best interests of the Corporation, after notice that indemnification is involved, by (i) a disinterested majority of the Board of the Executive Committee, or (ii) a majority of the Members.

Indemnification may include payment by the Corporation of expenses in defending a civil or criminal action or proceeding in advance of the final disposition of such action or proceeding upon receipt of an undertaking by the person indemnified to repay such payment if it is ultimately determined that such person is not entitled to indemnification under the provisions of this Article VIII, or under any applicable law.

As used in the Article VIII, the terms "Trustee," "director," and "officer" include their respective heirs, executors, administrators and legal representatives, and an "interested" Trustee, director or officer is one against whom in such capacity the proceeding in question or another proceeding on the same or similar grounds is then pending.

To assure indemnification under this Article VIII of all persons who are determined by the Corporation or otherwise to be or to have been "fiduciaries" of any employee benefits plan of the Corporation which may exist, from time to time, this Article VIII shall be interpreted as follows: (i) "another organization" shall be deemed to include such an employee benefit plan, including without limitation, any plan of the Corporation which is governed by the Act of Congress entitled "Employee Retirement Income Security Act of 1974," as amended, from time to time, ("ERISA"); (ii) "Trustee" shall be deemed to include any person requested by the Corporation to serve as such for an employee benefit plan where the performance by such person of his or her duties to the Corporation also imposes duties on, or otherwise involves services by, such person to the plan or participants or beneficiaries of the plan; (iii) "fines" shall be deemed to include any excise tax plan pursuant to ERISA, and (iv) actions taken or omitted by a person with respect to an employee benefit plan in the performance of such person's duties for a purpose reasonably believed by such person to be in the interest of the participants and beneficiaries of the plan shall be deemed to be for a purpose which is in the best interests of the Corporation

The right of indemnification provided in this Article VIII shall not be exclusive of or affect any other rights to which any Trustee, director or officer may be entitled under any agreement, statute, vote of Members or otherwise. The Corporation's obligation to provide indemnification under this Article VIII shall be offset to the extent of any other source of indemnification of any otherwise applicable insurance coverage under a policy maintained by the Corporation or any other person. Nothing contained in the Article shall affect any rights to which employees and corporate personnel other than Trustees, directors or officers may be entitled by contract, by vote of the Board or of the Executive Committee or otherwise.

ARTICLE IX—DISSOLUTION

The consent of every Trustee shall be necessary to effect a dissolution of the Marine Biological Laboratory. In case of dissolution, the property shall be disposed of in such a manner and upon such terms as shall be determined by the affirmative vote of two-thirds of the Trustees then in office in accordance with the laws of the Commonwealth of Massachusetts.

ARTICLE X—MISCELLANEOUS PROVISIONS

A. *Fiscal Year.* Except as otherwise determined by the Trustees, the fiscal year of the Corporation shall end on December 31st of each year.

B. *Seal.* Unless otherwise determined by the Trustees, the Corporation may have a seal in such form as the Trustees may determine, from time to time.

C. *Execution of Instruments.* All checks, deeds, leases, transfers, contracts, bonds, notes and other obligations authorized to be executed by an officer of the Corporation in its behalf shall be signed by the Director or the Treasurer except as the Trustees may generally or in particular cases otherwise determine. A certificate by the Clerk or an Assistant Clerk, or a temporary Clerk, as to any action taken by the Members, Board of Trustees or any officer or representative of the Corporation shall as to all persons who rely thereon in good faith be conclusive evidence of such action.

D. *Corporate Records.* The original, or attested copies, of the Articles of Organization, Bylaws and records of all meetings of the Members shall be kept in Massachusetts at the principal office of the Corporation, or at an office of the Corporation's Clerk or resident agent. Said copies and records need not all be kept in the same office. They shall be available at all reasonable times for inspection by any Member for any proper purpose, but not to secure a list of Members for a purpose other than in the interest of the applicant, as a Member, relative to the affairs of the Corporation

E. *Articles of Organization.* All references in these Bylaws to the Articles of Organization shall be deemed to refer to the Articles of Organization of the Corporation, as amended and in effect, from time to time.

F. *Transactions with Interested Parties.* In the absence of fraud, no contract or other transaction between this Corporation and any other corporation or any firm, association, partnership or person shall be affected or invalidated by the fact that any Trustee or officer of this Corporation is pecuniarily or otherwise interested in or is a director, member or officer of such other corporation or of such firm, association or partnership or in a party to or is pecuniarily or otherwise interested in such contract or other transaction or is in any way connected with any person or person, firm, association, partnership, or corporation pecuniarily or otherwise interested therein; provided that the fact that he or she individually or as a director, member or officer of such corporation, firm, association or partnership in such a party or is so interested shall be disclosed to or shall have been known by the Board of Trustees or a majority of such Members thereof as shall be present at a meeting of the Board of Trustees at which action upon any such contract or transaction shall be taken; any Trustee may be counted in determining the existence of a quorum and may vote at any meeting of the Board of Trustees for the purpose of authorizing any such contract or transaction with like force and effect as if he/she were not so interested, or were not a director, member or officer of such other corporation, firm, association or partnership, provided that any vote with respect to such contract or transaction must be adopted by a majority of the Trustees then in office who have no interest in such contract or transaction.

VOLUME 197

NUMBER 2

THE BIOLOGICAL BULLETIN

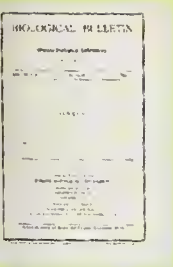

BIOLOGICAL BULLETIN

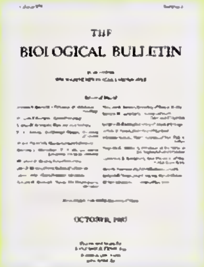

THE
BIOLOGICAL BULLETIN

CENTENNIAL ISSUE
OCTOBER
1899-1999

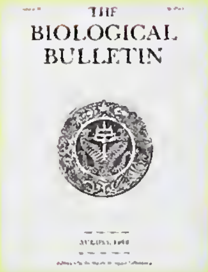

THE
BIOLOGICAL
BULLETIN

THE
BIOLOGICAL
BULLETIN

Published by the Marine Biological Laboratory

It's Wort Look.

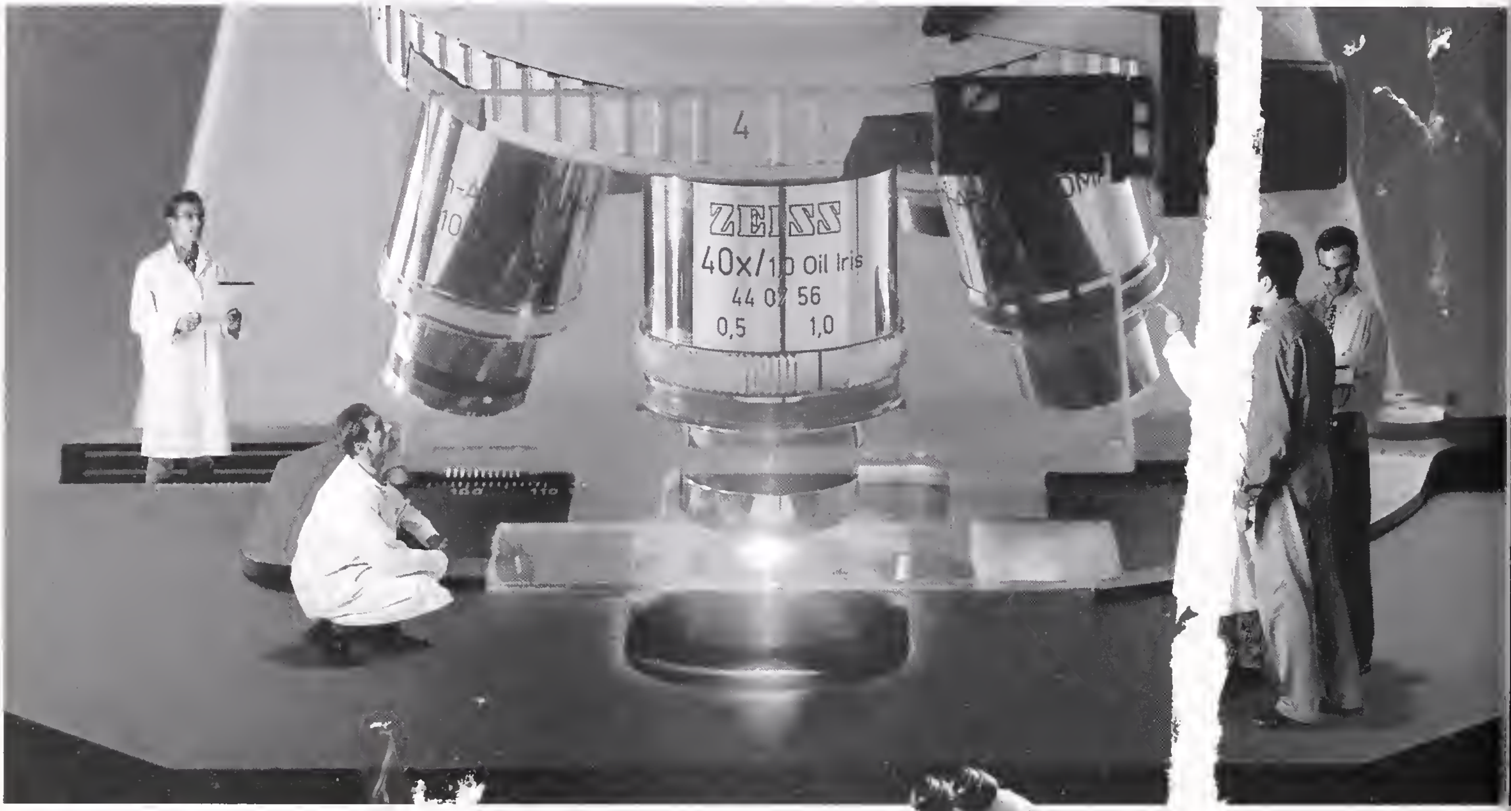

Brilliant and easy.

The **Axioskop 2** is the microscope that brings new levels of comfort and productivity to biomedical research. Renowned ICS infinity optics provide top quality images, and its operating convenience adds extra efficiency to your work.

Fluorescence 4-fold.

Carry out demanding fluorescence applications with flexibility and optimal illumination. Reflector turret for 4 fluorescence modules, 6-place excitation filter slide, plus the power of 100 watts.

Motorized automation.

In the **Axioskop 2 MOT** option, motorized functions include stage focusing and universal condenser setting (including Koehler). These and other functions can be automated for high productivity and precision when examining large numbers of specimens.

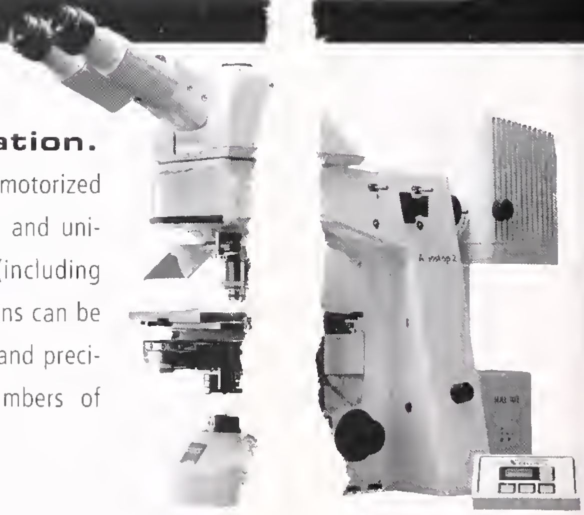

Contact Zeiss today for the full stor, ie ***Axioskop 2.***

It's smart microscopy m ea .

Carl Zeiss, Inc.
Microscopy & Imaging Systems
One Zeiss Drive
Thornwood, NY 10594

800.233.2343
Fax 914.681.7446
micro@zeiss.com
www.zeiss.com

ZEISS

THE
BIOLOGICAL BULLETIN

OCTOBER 1999

NOV 11 1999

Editor	Michael J. Greenberg	The Whitney Laboratory, University of Florida
Associate Editors	Louis E. Burnett	Grice Marine Biological Laboratory, College of Charleston
	R. Andrew Cameron	California Institute of Technology
	Charles D. Derby	Georgia State University
	Michael LaBarbera	University of Chicago
Section Editor	Shinya Inoué, *Imaging and Microscopy*	Marine Biological Laboratory
Online Editors	James A. Blake, *Keys to Marine Invertebrates of the Woods Hole Region*	ENSR Marine & Coastal Center, Woods Hole
	William D. Cohen, *Marine Models Electronic Record and Compendia*	Hunter College, City University of New York
Editorial Board	Peter B. Armstrong	University of California, Davis
	Ernest S. Chang	Bodega Marine Lab., University of California, Davis
	Thomas H. Dietz	Louisiana State University
	Richard B. Emlet	Oregon Institute of Marine Biology, Univ. of Oregon
	David Epel	Hopkins Marine Station, Stanford University
	Gregory Hinkle	Cereon Genomics, Cambridge, Massachusetts
	Makoto Kobayashi	Hiroshima University of Economics, Japan
	Donal T. Manahan	University of Southern California
	Margaret McFall-Ngai	Kewalo Marine Laboratory, University of Hawaii
	Mark W. Miller	Institute of Neurobiology, University of Puerto Rico
	Tatsuo Motokawa	Tokyo Institute of Technology, Japan
	Yoshitaka Nagahama	National Institute for Basic Biology, Japan
	Sherry D. Painter	Marine Biomed. Inst., Univ. of Texas Medical Branch
	J. Herbert Waite	University of California, Santa Barbara
	Richard K. Zimmer	University of California, Los Angeles
Editorial Office	Pamela Clapp Hinkle	Managing Editor
	Victoria R. Gibson	Staff Editor
	Carol Schachinger	Editorial Associate
	Patricia Burns	Subscription & Advertising Secretary

Published by
Marine Biological Laboratory
Woods Hole, Massachusetts

Cover

The three-dimensional stereo anaglyph on the cover is a ventral view of a brachiolaria larva of *Patiriella regularis,* a starfish; the brachiolaria depicted is about 1500 μm in length. Serotonergic neurons in the larva were stained with a rabbit antiserum and appear, in confocal fluorescent microscopy, as bright dots lining the ciliated bands and brachiolar arms. The image (which should be viewed through the stereo glasses provided with this issue) is composed of 145 optical sections and was reconstructed as described in the article by Francis Chee and Maria Byrne (p. 123).

Immunoreactive serotonergic cells are already visible in the gastrulae of echinoderms; but they increase in number and form an increasingly complex neural system as development proceeds. Because the immunoreactivity is associated with the ciliary bands of free-swimming, planktotrophic larval forms—as well as with their sensory structures and buccal cavity—the serotonergic system has been thought to coordinate the locomotory and feeding behaviors of these larvae.

In their paper, Chee and Byrne focus on the larval stages of *Patiriella regularis,* which are all planktotrophic; thus the development of the serotonergic system can be monitored throughout development, from the gastrula, through the brachiolaria (the last larval stage), and on to metamorphosis. The authors have used confocal fluorescence microscopy to reconstruct the development of the serotonergic nervous sytsem in three dimensions and have related the increase in complexity to morphogenetic changes in the larvae. They have demonstrated a complex network of cells with varicose processes that connect the preoral and postoral ciliated bands, supporting the hypothesis that this network is regulating larval feeding and swimming.

In a related article in this issue (see p. 115), Michael Dailey and his colleagues use the mammalian brain as a model to show how multidimensional confocal fluorescence microscopy can enhance studies of biological structure and function. The images in this article are fine examples of the techniques described, and readers should use the stereo glasses to examine them. This is the third in a series of papers on Concepts in Imaging and Microscopy; the series is supported by the Optical Imaging Association, which has also provided the stereo glasses.

Finally, this issue marks the end of *The Biological Bulletin's* first century of publication and the beginning of its second. The four small images on the cover, below the anaglyph, show how the face of the journal changed as the decades passed, biology expanded, the world shrank, and scientific publishing entered its greatest revolution since the invention of movable type. A metamorphosis is certainly at hand, but the nature of the imago remains unresolved.

CONTENTS

Volume 197, No. 2: October 1999

EDITORIAL

Greenberg, Michael J.
A century of science: *The Biological Bulletin* looks back—and forward 113

IMAGING AND MICROSCOPY

Dailey, Michael, Glen Marrs, Jakob Satz, and Marc Waite
Concepts in Imaging and Microscopy: Exploring biological structure and function with confocal microscopy 115

NEUROBIOLOGY AND BEHAVIOR

Chee, Francis, and Maria Byrne
Development of the larval serotonergic nervous system in the sea star *Patiriella regularis* as revealed by confocal imaging 123
Hartline, D.K., E.J. Buskey, and P.H. Lenz
Rapid jumps and bioluminescence elicited by controlled hydrodynamic stimuli in a mesopelagic copepod, *Pleuromamma xiphias* 132
Harrison, Paul J.H., and David C. Sandeman
Morphology of the nervous system of the barnacle cypris larva (*Balanus amphitrite* Darwin) revealed by light and electron microscopy 144

PHYSIOLOGY

Gainey, Louis F., Jr., Kelly J. Vining, Karen E. Doble, Jennifer M. Waldo, Aurora Candelario-Martinez, and Michael J. Greenberg
An endogenous SCP-related peptide modulates ciliary beating in the gills of a venerid clam, *Mercenaria mercenaria* 159

DEVELOPMENT AND REPRODUCTION

Saigusa, Masayuki, and Hiroshi Iwasaki
Ovigerous-hair stripping substance (OHSS) in an estuarine crab: purification, preliminary characterization, and appearance of the activity in the developing embryos 174

IMMUNOLOGY

Shirae, Maki, Euichi Hirose, and Yasunori Saito
Behavior of hemocytes in the allorejection reaction in two compound ascidians, *Botryllus scalaris* and *Symplegma reptans* 188

ECOLOGY AND EVOLUTION

Skorokhod, Alexander, Vera Gamulin, Dietmar Gundacker, Vadim Kavsan, Isabel M. Müller, and Werner E.G. Müller
Origin of insulin receptor-like tyrosine kinases in marine sponges 198
Crain, Jennifer A.
Functional morphology of prey ingestion by *Placetron wosnessenskii* Schalfeew Zoeae (Crustacea: Anomura: Lithodidae):. 207

SHORT REPORTS FROM THE 1999 GENERAL SCIENTIFIC MEETINGS OF THE MARINE BIOLOGICAL LABORATORY

Featured Article

Rome, Lawrence C.
Introduction. Bringing the script to life: the role of muscle in behavior 225
Rome, Lawrence C., Andrei A. Klimov, and Iain S. Young
A new approach for measuring real-time calcium pumping and SR function in muscle fibers 227

Physiology

Malchow, Robert Paul, and David J. Ramsey
Responses of retinal Müller cells to neurotransmitter candidates: a comparative study 229
Clay, John R., and Alan M. Kuzirian
Fluorescence localization of K^+ channels in the membrane of squid giant axons 231
Ruta, Vanessa J., Frederick A. Dodge, and Robert B. Barlow
Evaluation of circadian rhythms in the *Limulus* eye. . . 233

Novales Flamarique, Iñigo, and Ferenc I. Hárosi
Photoreceptor pigments of the blueback herring (*Alosa aestevalis*, Clupeidae) and the Atlantic silverside (*Menidia menidia*, Atherinidae) 235

Hanley, Janice S., Nadav Shashar, Roxanna Smolowitz, William Mebane, and Roger T. Hanlon
Soft-sided tanks improve long-term health of cultured cuttlefish 237

Piscine Neurobiology and Behavior

Zottoli, S.J., F.R. Akanki, N.A. Hiza, D.A. Ho-Sang, Jr., M. Motta, X. Tan, K.M. Watts, and E.-A. Seyfarth
Physiological characterization of supramedullary/dorsal neurons of the cunner, *Tautogolabrus adspersus*. . . . 239

Fay, R.R., and P.L. Edds-Walton
Sharpening of directional auditory input in the descending octaval nucleus of the toadfish, *Opsanus tau*. 240

Kaatz, Ingrid M., and Phillip S. Lobel
Acoustic behavior and reproduction in five species of *Corycoras* catfishes (Callichthyidae) 241

Lobel, Phillip S., and Lisa M. Kerr
Courtship sounds of the Pacific damselfish, *Abudefduf sordidus* (Pomacentridae) 242

Oliver, Steven J., and Elise Watson
Threat-sensitive nest defense in domino damselfish (*Dascyllus albisella*) 244

Price, Nichole N., and Allen F. Mensinger
Predator-prey interactions of juvenile toadfish, *Opsanus tau*. 246

Tang, Kathleen Q., Nichole N. Price, Maureen D. O'Neill, Allen F. Mensinger, and Roger T. Hanlon
Temperature effects on first-year growth of cultured oyster toadfish, *Opsanus tau*. 247

Chemoreception and Behavior

Mjos, Katrin, Frank Grasso, and Jelle Atema
Antennule use by the American lobster, *Homarus americanus*, during chemo-orientation in three turbulent odor plumes. 249

Hanna, John P., Frank W. Grasso, and Jelle Atema
Temporal correlation between sensor pairs in different plume positions: A study of concentration information available to the American lobster, *Homarus americanus*, during chemotaxis 250

Zettler, Erik, and Jelle Atema
Chemoreceptor cells as concentration slope detectors: preliminary evidence from the lobster nose . . . 252

Berkey, Cristin, and Jelle Atema
Individual recognition and memory in *Homarus americanus* male-female interactions 253

McLaughlin, Leslie C., Jennifer Walters, Jelle Atema, and Norman Wainwright
Urinary protein concentration in connection with agonistic interactions in *Homarus americanus*. 254

King, Alison J., Shelley A. Adamo, and Roger T. Hanlon
Contact with squid eggs increases agonistic behavior in male squid (*Loligo pealei*) 256

Cell Motility

Bearer, E.L., M.L. Schlief, X.O. Breakefield, D.E. Schuback, T.S. Reese, and J.H. LaVail
Squid axoplasm supports the retrograde axonal transport of herpes simplex virus 257

Gould, Robert, Concetta Freund, Frank Palmer, Pamela E. Knapp, Jeff Huang, Hilary Morrison, and Douglas L. Feinstein
Messenger RNAs for kinesins and a dynein are located in neural processes 259

Fukui, Yoshio, Taro Q.P. Uyeda, Chikako Kitayama, and Shinya Inoué
Migration forces in *Dictyostelium* measured by centrifuge DIC microscopy. 260

Tran, P.T., P. Maddox, F. Chang, and S. Inoué
Dynamic confocal imaging of interphase and mitotic microtubules in the fission yeast, *S. pombe*. 262

Maddox, Paul, Arshad Desai, E.D. Salmon, T.J. Mitchison, Karen Oogema, Tarun Kapoor, Brian Matsumoto, and Shinya Inoué
Dynamic confocal imaging of mitochondria in swimming *Tetrahymena* and of microtubule poleward flux in *Xenopus* extract spindles 263

Wöllert, Torsten, Ana S. DePina, and George M. Langford
Effects of vanadate on actin-dependent vesicle motility in extracts of clam oocytes 265

Cell and Developmental Biology

Billack, Blase, Jeffrey D. Laskin, Michael A. Gallo, and Diane E. Heck
Effects of α-bungarotoxin on development of the sea urchin *Arbacia punctulata*. 267

Silver, Robert B., and Nicole M. Deming
Leukotriene B_4 as calcium agonist for nuclear envelope breakdown: an enzymological survey of endomembranes of mitotic cells 268

Weidner, Earl, and Ann Findley
Extracellular survival of an intracellular parasite (*Spraguea lophii*, Microsporea) 270

Kaltenbach, Jane C., William J. Kuhns, Tracy L. Simpson, and Max M. Burger
Intense concanavalin A staining and apoptosis of peripheral flagellated cells in larvae of the marine sponge *Microciona prolifera*: significance in relation to morphogenesis 271

Comparative Biochemistry

Harrington, John M., and Peter B. Armstrong
A cuticular secretion of the horseshoe crab, *Limulus polyphemus:* a potential anti-fouling agent 274
Asokan, Rengasamy, and Peter B. Armstrong
Cellular mechanisms of hemolysis by the protein limulin, a sialic-acid-specific lectin from the plasma of the American horseshoe crab, *Limulus polyphemus* 275
Biswas, Chhanda, and Peter B. Armstrong
Identification of a hemolytic activity in the plasma of the gastropod *Busycon canaliculatum* 276
Kuhns, William J., Max M. Burger, and Eva Turley
Hyaluronic acid: a component of the aggregation factor secreted by the marine sponge, *Microciona prolifera* 277
Popescu, Octavian, Rey Interior, Gradimir Misevic, Max M. Burger, and William J. Kuhns
Biosynthesis of tyrosine O-sulfate by cell proteoglycan from the marine sponge, *Microciona prolifera* 279
Vasse, Aimee, Alice Child, and Norman Wainwright
Prophenoloxidase is not activated by microbial signals in *Limulus polyphemus* 281
Ogunseitan, O.A., S.L. Yang, and E. Scheinbach
The δ-aminolevulinate dehydratase of marine *Vibrio alginolyticus* is resistant to lead (Pb) 283
Hoskin, Francis C.G., Diane M. Steeves, and John E. Walker
Substituted cyclodextrin as a model for a squid enzyme that hydrolyzes the nerve gas soman 284
Zigman, Seymour, Nancy S. Rafferty, Keen A. Rafferty, and Nathaniel Lewis
Effects of green tea polyphenols on lens photooxidative stress 285

Ecology and Evolution

Mondrup, Thomas
Salinity effects on nutrient dynamics in estuarine sediment investigated by a plug-flux method 287
Pease, Katherine M., L. Claessens, C. Hopkinson, E. Rastetter, J. Vallino, and N. Kilham
Ipswich River nutrient dynamics: preliminary assessment of a simple nitrogen-processing model 289
Wolfe, Felisa L., Kevin D. Kroeger, and Ivan Valiela
Increased lability of estuarine dissolved organic nitrogen from urbanized watersheds 290
Evgenidou, A., A. Konkle, A. D'Ambrosio, A. Corcoran, J. Bowen, E. Brown, D. Corcoran, C. Dearholt, S. Fern, A. Lamb, J. Michalowsky, I. Ruegg, and J. Cebrián
Effects of increased nitrogen loading on the abundance of diatoms and dinoflagellates in estuarine phytoplanktonic communities 292
Cubbage, Andrea, David Lawrence, Gabrielle Tomasky, and Ivan Valiela
Relationship of reproductive output in *Acartia tonsa,* chlorophyll concentration, and land-derived nitrogen loads in estuaries in Waquoit Bay, Massachusetts. 294
Canfield, Susannah, Luc Claessens, Charles Hopkinson Jr., Edward Rastetter, and Joseph Vallino
Long-term effect of municipal water use on the water budget of the Ipswich River Basin. 295
Young, Talia, Sharon Komarow, Linda Deegan, and Robert Garritt
Population size and summer home range of the green crab, *Carcinus meanus,* in salt marsh tidal creeks. 297
Komarow, Sharon, Talia Young, Linda Deegan, and Robert Garritt
Influence of marsh flooding on the abundance and growth of *Fundulus heteroclitus* in salt marsh creeks . . . 299
Widener, Justin W., and Robert B. Barlow
Decline of a horseshoe crab population on Cape Cod 300
Kerr, Lisa M., Phillip S. Lobel, and J. Mark Ingoglia
Evaluation of a reporter gene system biomarker for detecting contamination in tropical marine sediments. 303

Oral Presentations

Published by Title Only 307

THE BIOLOGICAL BULLETIN

THE BIOLOGICAL BULLETIN is published six times a year by the Marine Biological Laboratory, 7 MBL Street, Woods Hole, Massachusetts 02543.

Subscriptions and similar matter should be addressed to Subscription Manager, THE BIOLOGICAL BULLETIN, Marine Biological Laboratory, 7 MBL Street, Woods Hole, Massachusetts 02543. Subscription per year (six issues, two volumes): $205 for libraries; $95 for individuals. Subscription per volume (three issues): $102.50 for libraries; $47.50 for individuals. Back and single issues (subject to availability): $40 for libraries; $20 for individuals.

Communications relative to manuscripts should be sent to Michael J. Greenberg, Editor-in-Chief, or Pamela Clapp Hinkle, Managing Editor, at the Marine Biological Laboratory, 7 MBL Street, Woods Hole, Massachusetts 02543. Telephone: (508) 289-7428. FAX: 508-289-7922. E-mail: pclapp@mbl.edu.

http://www.mbl.edu/BiologicalBulletin/

The home page for the electronic companion to THE BIOLOGICAL BULLETIN—*the Marine Models Electronic Record*—and other BIOLOGICAL BULLETIN publications is available on the World Wide Web at the address shown above.

THE BIOLOGICAL BULLETIN is indexed in bibliographic services including *Index Medicus* and MEDLINE, *Chemical Abstracts, Current Contents, Elsevier BIOBASE/Current Awareness in Biological Sciences,* and *Geo Abstracts.*

Printed on acid free paper,
effective with Volume 180, Issue 1, 1991.

POSTMASTER: Send address changes to THE BIOLOGICAL BULLETIN, Marine Biological Laboratory,
7 MBL Street, Woods Hole, MA 02543.

Copyright © 1999, by the Marine Biological Laboratory

Periodicals postage paid at Woods Hole, MA, and additional mailing offices.
ISSN 0006-3185

INSTRUCTIONS TO AUTHORS

The Biological Bulletin accepts outstanding original research reports of general interest to biologists throughout the world. Papers are usually of intermediate length (10–40 manuscript pages). A limited number of solicited review papers may be accepted after formal review. A paper will usually appear within four months after its acceptance.

Very short, especially topical papers (less than 9 manuscript pages including tables, figures, and bibliography) will be published in a separate section entitled "Research Notes." A Research Note in *The Biological Bulletin* follows the format of similar notes in *Nature.* It should open with a summary paragraph of 150 to 200 words comprising the introduction and the conclusions. The rest of the text should continue on without subheadings, and there should be no more than 30 references. References should be referred to in the text by number, and listed in the Literature Cited section in the order that they appear in the text. Unlike references in *Nature,* references in the Research Notes section should conform in punctuation and arrangement to the style of recent issues of *The Biological Bulletin.* Materials and Methods should be incorporated into appropriate figure legends. See the article by Lohmann *et al.* (October 1990, Vol. **179:** 214–218) for sample style. A Research Note will usually appear within two months after its acceptance.

The Editorial Board requests that regular manuscripts conform to the requirements set below; those manuscripts that do not conform will be returned to authors for correction before review.

1. ***Manuscripts.*** Manuscripts, including figures, should be submitted in quadruplicate, with the originals clearly marked. (Xerox copies of photographs are not acceptable for review purposes.) The submission letter accompanying the manuscript should include a telephone number, a FAX number, and (if possible) an E-mail address for the corresponding author. The original manuscript must be typed in no smaller than 12 pitch or 10 point, using double spacing (*including* figure legends, footnotes, bibliography, etc.) on one side of 16- or 20-lb. bond paper, 8 by 11 inches. Please, no right justification. Manuscripts should be proofread carefully and errors corrected legibly in black ink. Pages should be numbered consecutively. Margins on all sides should be at least 1 inch (2.5 cm). Manuscripts should conform to the *Council of Biology Editors Style Manual,* 5th Edition (Council of Biology Editors, 1983) and to American spelling. Unusual abbreviations should be kept to a minimum and should be spelled out on first reference as well as defined in a footnote on the title page. Manuscripts should be divided into the following components: Title page, Abstract (of no more than 200 words), Introduction, Materials and Methods, Results, Discussion, Acknowledgments, Literature Cited, Tables, and Figure Legends. In addition, authors should supply a list of words and phrases under which the article should be indexed.

2. ***Title page.*** The title page consists of a condensed title or running head of no more than 35 letters and spaces, the manuscript title, authors' names and appropriate addresses, and footnotes listing present addresses, acknowledgments or contribution numbers, and explanation of unusual abbreviations.

3. ***Figures.*** The dimensions of the printed page, 7 by 9 inches, should be kept in mind in preparing figures for publication. We recommend that figures be about 1 times the linear dimensions of the final printing desired, and that the ratio of the largest to the smallest letter or number and of the thickest to the thinnest line not exceed 1:1.5. Explanatory matter generally should be included in legends, although axes should always be identified on the illustration itself. Figures should be prepared for reproduction as either line cuts or halftones. Figures to be reproduced as line cuts should be unmounted glossy photographic reproductions or drawn in black ink on white paper, good-quality tracing cloth or plastic, or blue-lined coordinate paper. Those to be reproduced as halftones should be mounted on board, with both designating numbers or letters and scale bars affixed directly to the figures. All figures should be numbered in consecutive order, with no distinction between text and plate figures and cited, in order, in the text. The author's name and an arrow indicating orientation should appear on the reverse side of all figures.

Color: The Biological Bulletin will publish color figures and plates, but must bill authors for the actual additional cost of printing in color. The process is expensive, so authors with more than one color image should—consistent with editorial concerns, especially citation of figures in order—combine them into a single plate to reduce the expense. On request, when supplied with a copy of a color illustration, the editorial staff will provide a pre-publication estimate of the printing cost.

4. ***Tables, footnotes, figure legends, etc.*** Authors should follow the style in a recent issue of *The Biological Bulletin* in preparing table headings, figure legends, and the like. Because of the high cost of setting tabular material in type, authors are asked to limit such material as much as possible. Tables, with their headings and footnotes, should be typed on separate sheets, numbered with consecutive Roman numerals, and placed after the Literature Cited. Figure legends should contain enough information to make the figure intelligible separate from the text. Legends should be typed double spaced, with consecutive Arabic numbers, on a separate sheet at the end of the paper. Footnotes should be limited to authors' current addresses, acknowledgments or contribution numbers, and explanation of unusual abbreviations. All such footnotes should appear on the title page. Footnotes are not normally permitted in the body of the text.

5. ***Literature cited.*** In the text, literature should be cited by the Harvard system, with papers by more than two authors cited as Jones *et al.*, 1980. Personal communications and material in preparation or in press should be cited in the text only, with author's initials and institutions, unless the material has been formally accepted and a volume number can be supplied. The list of references following the text should be headed Literature Cited, and must be typed double spaced on separate pages, conforming in punctuation and arrangement to the style of recent issues of *The Biological Bulletin*. Citations should include complete titles and inclusive pagination. Journal abbreviations should normally follow those of the U. S. A. Standards Institute (USASI), as adopted by BIOLOGICAL ABSTRACTS and CHEMICAL ABSTRACTS, with the minor differences set out below. The most generally useful list of biological journal titles is that published each year by BIOLOGICAL ABSTRACTS (BIOSIS List of Serials; the most recent issue). Foreign authors, and others who are accustomed to using THE WORLD LIST OF SCIENTIFIC PERIODICALS, may find a booklet published by the Biological Council of the U.K. (obtainable from the Institute of Biology, 41 Queen's Gate, London, S.W.7, England, U.K.) useful, since it sets out the WORLD LIST abbreviations for most biological journals with notes of the USASI abbreviations where these differ. CHEMICAL ABSTRACTS publishes quarterly supplements of additional abbreviations. The following points of reference style for THE BIOLOGICAL BULLETIN differ from USASI (or modified WORLD LIST) usage:

A. Journal abbreviations, and book titles, all underlined (for *italics*)

B. All components of abbreviations with initial capitals (not as European usage in WORLD LIST *e.g., J. Cell. Comp. Physiol.* NOT *J. cell. comp. Physiol.*)

C. *All* abbreviated components must be followed by a period, whole word components *must not* (*i.e., J. Cancer Res.*)

D. Space between all components (*e.g., J. Cell. Comp. Physiol.*, not *J.Cell.Comp.Physiol.*)

E. Unusual words in journal titles should be spelled out in full, rather than employing new abbreviations invented by the author. For example, use *Rit Vísindafjélags Islendinga* without abbreviation.

F. All single word journal titles in full (*e.g., Veliger, Ecology, Brain*).

G. The order of abbreviated components should be the same as the word order of the complete title (*i.e., Proc.* and *Trans.* placed where they appear, not transposed as in some BIOLOGICAL ABSTRACTS listings).

H. A few well-known international journals in their preferred forms rather than WORLD LIST or USASI usage (*e.g., Nature, Science, Evolution* NOT *Nature, Lond., Science, N.Y.; Evolution, Lancaster, Pa.*)

6. ***Reprints, page proofs, and charges.*** Authors of articles in black and white (no color figures) receive their first 50 reprints (without covers) free of charge. Color reprints and additional black-and-white reprints may be purchased; authors will receive order forms. Reprints normally will be delivered about 2 to 3 months after the issue date. Authors (or delegates for foreign authors) will receive page proofs of articles shortly before publication. They will be charged the current cost of printers' time for corrections to these (other than corrections of printers' or editors' errors). Other than these charges for authors' alterations, *The Biological Bulletin* does not have page charges.

Reference: *Biol. Bull.* **197:** 113–114. (October 1999)

A Century of Science: *The Biological Bulletin* Looks Back—and Forward

The first number of *The Biological Bulletin* was published in October 1899; so with the current issue we celebrate the 100th anniversary of this journal. The founder was Prof. C. O. Whitman, director of the Marine Biological Laboratory at Woods Hole, Massachusetts (MBL), who aimed to publish short articles with simple illustrations as rapidly as possible. Progress was halting at first: a predecessor, the *Zoölogical Bulletin* (with C. O. Whitman and W. M. Wheeler as editors, but unassociated with the MBL), failed in 1898 after two volumes; and *The Biological Bulletin* itself ceased publication for a time, also after two volumes.[1] But guided by general policies set out in a prospectus written in June 1902,[2] the *Bulletin* began to function smoothly under the editorship of Frank R. Lillie. Those policies, paraphrased below, have informed the operation of the journal ever since:

- The *Bulletin* will be published under the auspices of the Marine Biological Laboratory.
- Its scope will include "Zoology, General Biology, and Physiology"; it is a general interest journal.
- It will contain original articles, occasional reviews, reports of work and lectures at the MBL; and preliminary statements of important results will be special feature.
- It will meet the need for rapid publication of results.
- It will be open to contributions from any source.

A general journal. *The Biological Bulletin* was meant to be, in some measure, an institutional journal; and indeed, the Annual Report of the MBL Corporation has been published by the *Bulletin* since 1908. Moreover, the scientific agenda of the MBL has always been very broad, so the close association of the *Bulletin* with the Laboratory has ensured that the scope of the journal would also be so. Probably every editor has considered this characteristic of the journal. Indeed, Alfred C. Redfield (1941) called it "one of the most perplexing problems of policy with which the . . . editor must deal," and he concluded that "in this day of specialization [*in 1941!*] one journal at least should present a rather broad cross-section of biology as a whole." This is not a necessary conclusion, but it has been accepted by the seven editors that succeeded Lillie. Today we expect—beyond technical competence—that a publishable submission will contain data resulting from the experimental testing of some hypothesis, and that it will advance its own area significantly. Moreover, we suppose that if such an investigation is not too narrowly focused, it is likely to interest a generous fraction of our diverse readership.

Of course, the actual scope of *The Biological Bulletin* has always been determined by those who contribute manuscripts; and the composition of that pool of potential authors—which is unconstrained by policy—has changed markedly through the years. In the decade 1930–1940, roughly 700 papers were published in the *Bulletin*; of these, 29% originated from the MBL, and 40% were written by members of the Corporation. These values began to decline during the late '60s, as investigators at the MBL (as elsewhere) began to send their work to specialty journals. The pace of specialization increased markedly, so that in the most recent decade (1989–1999), only about 10% of articles were authored by members of the Corporation. Moreover, the rate of acceptance by foreign authors, which began to increase in the '60s, reached 30% of papers published in the last decade. So today more than ever before, the contributors to the *Bulletin* are widely distributed throughout a shrinking world.

We are able, in a way, to ask these contributors whether *The Biological Bulletin* is actually a general journal, because authors select the headings under which their papers are published. The profile varies from issue to issue, but over 50% of recent articles have appeared under the rubric of either Physiology or Development & Reproduction; 20% are listed under Ecology & Evolution; and a quarter are distributed between Cell Biology and Neurobiology & Behavior. These data suggest that, although the pool of authors is different than it was a century ago, the scope of published material is similar to that in 1903 or 1941. On the other hand, of the animals reported on in the past two years, all but 6 were invertebrates from 13 different phyla, mostly marine, and mostly molluscs, crustaceans, cnidarians, and echinoderms. Insects are virtually absent, only one paper is about nematodes, and of 37 molluscan articles, only one is about *Aplysia;* current marine biomedical models appear largely in specialty journals. The subject matter in *Bulletin* articles is diverse and thus difficult to characterize in brief. But it is predominantly experimental and functional, and the functions tend to be complex, sometimes appearing in unusual, primitive, or extremeophilic animals, and often at the intersection of fields, *e.g.*, the development of symbiosis; or neural or pheromonal regulation of development, activity, or metamorphosis. In summary, *The Biological Bulletin,* like all general journals, has its special focus. We might predict that so long as its publication is under the auspices of the MBL, the scope of the *Bulletin* will remain general; but its focus might well shift with time or new leadership.

---

[1] The history of *The Biological Bulletin* has been described thoroughly twice before: by Alfred C. Redfield (1941), who was Managing Editor of this journal from 1930 to 1942; and (on the occasion of the 100th anniversary of the founding of the MBL) by Pamela L. Clapp (1988), who was Editorial Assistant to Charles B. Metz, the Editor from 1980–1989.

[2] The prospectus is published in the Tenth Report for the Years 1903–1906 including Financial Report from 1900–1906, Section XI Publications, pp. 42–44. (1907) Marine Biological Laboratory, Woods Holl, Massachusetts.

Enhancing the contents. Although *The Biological Bulletin* contains primarily research reports, successive editors have leavened the diet with reviews, some based on lectures. The series of lectures on *Concepts in Imaging and Microscopy,* one of which appears in this issue, is exemplary. During the past decade, the *Bulletin* has also published symposia and workshops, about one per year, on a variety of topics. These proceedings have also served to broaden the scope of the journal.

As part of its association with the MBL, *The Biological Bulletin* has, since 1936, published the abstracts of the General Scientific Meetings held at the Laboratory each summer. Investigators, postdoctoral fellows, and students present their work at these meetings, so the abstracts provide a snapshot of the research taking place at the MBL. The abstracts have been enhanced since 1991: they are longer and contain a figure or table; moreover, they are reviewed and are thus more credible and valuable than the old abstracts were. In the past nine years, about 420 of these short reports have been published, which has also served to widen the focus of the *Bulletin.*

Response to electronic publishing. Printing, design, graphic techniques, and the quality of paper have improved slowly over the past 100 years, brightening and enhancing the data published in *The Biological Bulletin,* as in other journals. This improvement in appearance is symbolized by the images on the cover of this issue. But these technical advances are trivial compared with the sea change that electronic communication has brought in the last decade. This revolution is not close to peaking, but it has already fundamentally altered the way that scientists do business.

To date, *The Biological Bulletin* has responded to the potential for electronic publishing with three online products: the *Compendia, the Marine Models Electronic* Record (MMER), and the *Keys to the Invertebrates of the Woods Hole Region (The Keys).* These products, or their contents, are composed of relatively independent units of data or methods. They are therefore well adapted to navigation and viewing on-screen and are amenable to the advantages of online editing and publication, especially continual updating. The *Compendia* consist of tabulated data: *e.g.*, composition of physiological solutions, breeding seasons and gamete characteristics, and invertebrate anesthetics and relaxants (in review). The *MMER* is a completely electronic journal devoted to the collection, culture, and preparation of marine animals for experimentation. *The Keys,* first published in 1954, were particularly useful to researchers who are not systematists; unfortunately, this guide is now out-of-date, but it is undergoing revision online. These three products are accessible on the home page of Biological Bulletin Publications at: www.mbl.edu/BiologicalBulletin/. Biological Bulletin Publications also manages the classical print journal. Tables of contents and the abstracts of articles published in each issue of the *Bulletin* are published electronically as soon as they have all been accepted and proofread. Moreover, videos and data supplemental to published articles are also maintained online.

The full text of the papers in *The Biological Bulletin* are still not available electronically; but this state of affairs cannot continue forever. Our readers do not want to store paper journals. They want to store a collection of articles, selected from a variety of journals, and tailored to their specific needs. Overwhelmingly, now, these papers are obtained, not as reprints, but by photocopying or, where available, by downloading from the internet. More important, our authors expect that, when the paper is accepted and the editorial process is complete, their paper will be distributed as rapidly and widely as possible. If this expectation is to be met, then *The Biological Bulletin* should be published electronically, and since fees limit distribution, access should be free of cost to readers.

The present Biological Bulletin Publications could produce an online journal, but two major, well-ventilated questions remain: First, who should pay for this significant service to authors? Probably authors—at least in part. At present, however, *The Biological Bulletin* has no page charges, and revenue comes almost entirely from libraries. Second, although paper documents last for hundreds of years, electronic storage technology turns over in about five; so if we only publish electronically, how do we solve the problem of archiving? Clearly paper archival copies must be produced. But who will pay for them? Probably the libraries—at least in part. In any event, scientific publication will be revolutionized in the next decade, and *The Biological Bulletin*—if it survives its inevitable transmogrification—will bear about as much physical resemblance to its earlier life as a butterfly does to a caterpillar.

—MICHAEL J. GREENBERG, Editor-in-Chief

References

Clapp, P. L. 1988. The history of *The Biological Bulletin. Biol. Bull.* **174:** 1–3.

Redfield, A. C. 1941. Annual report of the Marine Biological Laboratory for the year 1940. Report of the Managing Editor. *Biol. Bull.* **81:** 12–17.

Reference: *Biol. Bull.* **197:** 115–122. (October 1999)

Concepts in Imaging and Microscopy

Exploring Biological Structure and Function with Confocal Microscopy

MICHAEL DAILEY, GLEN MARRS[1], JAKOB SATZ[1], AND MARC WAITE

Department of Biological Sciences and [1]Program in Neuroscience, The University of Iowa, Iowa City, Iowa 52242

Abstract. Confocal microscopy is providing new and exciting opportunities for imaging cell structure and physiology in thick biological specimens, in three dimensions, and in time. The utility of confocal microscopy relies on its fundamental capacity to reject out-of-focus light, thus providing sharp, high-contrast images of cells and subcellular structures within thick samples. Computer controlled focusing and image-capturing features allow for the collection of through-focus series of optical sections that may be used to reconstruct a volume of tissue, yielding information on the 3-D structure and relationships of cells. Tissues and cells may also be imaged in two or three spatial dimensions over time. The resultant digital data, which encode the image, are highly amenable to processing, manipulation and quantitative analyses. In conjunction with a growing variety of vital fluorescent probes, confocal microscopy is yielding new information about the spatiotemporal dynamics of cell morphology and physiology in living tissues and organisms. Here we use mammalian brain tissue to illustrate some of the ways in which multidimensional confocal fluorescence imaging can enhance studies of biological structure and function.

Introduction

Marvin Minsky's quest to understand how the brain works led him to develop the first confocal microscope (Minsky, 1961, 1988). He reasoned that to make sense of the seemingly insuperable complexity of neural tissue, one needed a microscope that could resolve the fine details of neural structure. Indeed, the structural complexity of brain tissue has provided a formidable challenge to optical microscopy, and the problems are compounded if the physiological aspects of cells and tissues are also considered. A major problem is that conventional (widefield) microscopy of brain tissue—or any other thick biological sample—often yields blurred, low-contrast images in which the fine details of cell structure are obscured. This results primarily from the scatter of light due to interaction with the specimen, and from contaminating light from out-of-focus optical planes. Minsky's solution to these problems was to (a) brightly illuminate only a single spot in the tissue at a time; (b) reject light from out-of-focus regions of the specimen by using a (confocal) pinhole aperture positioned where the objective focused light from the brightly illuminated spot, and (c) scan the sample relative to the illuminating spot to generate a 2-D image of the specimen (see Lichtman, 1994). Thus, he developed a new optical technique—confocal microscopy—which yields substantially improved image contrast and clarity in thick samples. An important feature of this system was the ability to *optically section* through the thick specimen, that is, to systematically collect 2-D images from different levels of depth in the tissue with the same high contrast and clarity.

There are currently a variety of confocal systems, with differing configurations and capabilities, that all operate on

---

Received 26 March 1999; accepted 21 July 1999.

To whom correspondence should be addressed: Dr. Michael Dailey, Dept. of Biological Sciences, 335 Biology Building, University of Iowa, Iowa City, IA 52242. E-mail: michael-e-dailey@uiowa.edu

This is the third in a series of articles entitled "Concepts in Imaging and Microscopy." This series is supported by the Optical Imaging Association (OPIA) and was introduced with an editorial in the April 1998 issue of this journal (*Biol. Bull.* **194:** 99). Other articles in the series are listed on *The Biological Bulletin*'s website at <http://www.mbl.edu/html/BB/home.BB.html>.

the principle of illuminating a small portion of the tissue and restricting the collection of light from a rather narrow focal plane in the sample. The capacity afforded by these modern confocal microscopes to peer into a relatively thick biological specimen at high spatial resolution has greatly impacted neurobiology and many other areas of biological investigation. Thus, confocal microscopy is enjoying wide application in the biological sciences, enabling studies from the molecular level to that of the whole organism (Summers *et al.*, 1993; Lichtman, 1994; Gard *et al.*, 1995; Turner *et al.*, 1996; Pedley, 1997; Hepler and Gunning, 1998).

Dissecting the 3-D Structure of Tissue

As alluded to above, confocal microscopy provides a means for describing the 3-D architecture of cells in tissues, including the relationships of cells to each other and to other tissue structures. These capabilities are especially useful for examining the complex structure and organization of mammalian brain tissue, for the complexities can be daunting. In many brain regions, for example, various types of neuronal and glial cells are intermingled; moreover, most of the cells have very intricate morphologies with thin, highly branching, tortuous processes that can extend for distances up to several millimeters. Therefore, confocal microscopy has been used in numerous studies to gain high-resolution information about the structure of neural tissue elements.

The advantages of confocal imaging are several-fold. First, many probes of cell and tissue structure are amenable to light microscopy, especially fluorescence microscopy, and commercially available confocal microscopes can be equipped with multiple light sources of differing wavelengths so that a variety of fluorophores can be excited. Some confocal systems use arc lamp illumination, while many use lasers. Commonly used sources of excitation in laser-based confocal microscopes include argon (Ar; 488 nm and 514 nm), krypton (Kr; 568 nm), argon-krypton (Ar-Kr; 488 nm, 514 nm, and 568 nm), and helium-neon (He-Ne; 633 nm) lasers. Shorter wavelength lasers (Ar; 458 nm) are also available at a substantially higher cost and are thus less frequently found on confocal systems. Nevertheless, most systems can excite a set of fluorescent probes spanning nearly the full range of visible wavelengths.

The availability of a variety of excitation wavelengths on a single microscope setup offers the power and convenience of using combinations of fluorescent probes in a single specimen. For double- and triple-labeling experiments, lasers (Kr and He-Ne) and probes (*e.g.*, Cy5) in the far red are very widely separated for the standard green (FITC) and red (TRITC) dyes, precluding concern for bleed-through or crossover between channels (Sargent, 1994; Wouterlood *et al.*, 1998). Thus, the excitation power can be increased to obtain a better signal-to-noise ratio in each of the channels, providing exceptional multiprobe imaging of samples. An example of a brain tissue sample double-labeled to reveal two different glial cell populations is shown in Figure 1.

An important problem that must be considered in multiprobe imaging is the potential artifact introduced by chromatic (wavelength-dependent) aberration in the imaging system (see Pawley, 1995). In essence, when different structures are labeled with different fluorophores, their *x,y,z* positions will appear to shift relative to one another. The magnitude of this lateral (*x-y*) and axial (*z*) chromatic aberration varies with different microscope systems, particularly with different microscope objectives, but under typical, low-magnification imaging conditions, the apparent displacement can be up to several microns. The chromatic aberration of an optical system can be determined quantitatively with the aid of individual latex microspheres containing two different fluorophores with known, identical distributions (available from Molecular Probes, Eugene, OR). If an *x-y* image of a double-labeled microsphere is collected in each channel, and the images (*e.g.*, red and green images) are superimposed, then the lateral displacement of the red and green representations of the microsphere can be calculated, yielding the value of the aberration. The same procedure can be followed to determine the axial chromatic aberration using the *x-z* scanning feature found on many confocal microscopes. Once these values are known for a given set of imaging conditions, adjustments can be made (by image processing) to compensate for the aberration. In the case of axial chromatic aberration, the focus position may simply be adjusted a defined amount for one of the channels. Thus, as long as potential problems with chromatic aberration are considered and handled adequately, multiple-probe confocal imaging can provide important information on the morphology, distribution, and relationships of different cell populations and tissue structures with good spatial resolution.

A second advantage of confocal microscopy is that rather large regions of intact or semi-intact tissue may be imaged at subcellular resolution. For example, it is quite feasible to collect a single stack of confocal optical sections spanning a tissue volume as large as 0.1 mm^3 (containing perhaps as many as 100,000 cells) that can still be observed with a lateral resolution of 1 μm per pixel. Resolution greater than 1 μm may be achieved, usually with the trade-off of a smaller field of view. In fluorescence confocal microscopy, useful images are usually limited to depths into the sample of less than about 100 μm; the limitation is due in large part to light scatter by the tissue. Use of fluorophores with adsorption and emission spectra in the far red (*e.g.*, Cy5) can significantly improve depth penetration over the standard red and green fluorescent dyes.

Third, the optical sectioning capabilities of a confocal microscope, coupled with the ability to collect through-focus stacks of digital images, make it possible for cells in their native tissue setting to be reconstructed and rendered

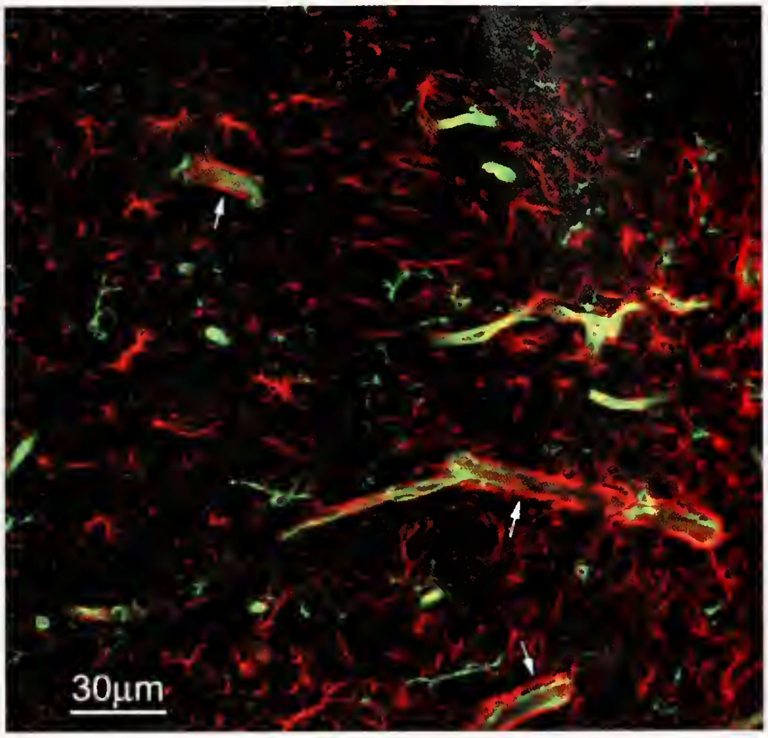

Figure 1. Dual-channel confocal imaging shows the distribution and morphological relationships of microglia (*green*) and astrocytes (*red*) in a double-labeled rat brain tissue slice. Microglia and blood vessels were stained with a fluorescein (FITC)-conjugated isolectin, IB$_4$ (Sigma, St. Louis; see Dailey and Waite, 1999). Astrocytes were immunohistochemically labeled with monoclonal antibodies against the glial fibrillary acidic protein (GFAP; Sigma, St. Louis, MO), followed by Cy5 conjugated secondary antibodies (Amersham Pharmacia). Note the astrocyte processes (end-feet) that line the surface of the blood vessels (*arrows*).

in three dimensions. One advantage of volume rendering from confocal image stacks is that the sample can be viewed from any angle. This can help clarify the spatial relationships of cells and tissue structures. As an example, we show, in Figure 2, a 3-D rendering of four microglial cells adjacent to a branching blood vessel within a volume of brain tissue reconstructed from a stack of confocal optical sections. It would be very difficult to distinguish the small cellular processes adjacent to the brightly staining blood vessels with conventional widefield fluorescence microscopy.

In most cases, the images generated by the confocal microscope are in digital form. Thus, a wide range of digital image processing capabilities can be applied to the data set. Features of cell and tissue structure can be quantified and analyzed with the aid of software packages that either stand alone or are already integrated into the confocal system software.

Imaging the Dynamics of Cell and Tissue Development and Morphology

In addition to the spatial information about cell structure, we can collect, with time-lapse confocal microscopy, information about the dynamics of cellular structure over time—from seconds to days. In many organisms, cell growth and locomotion play critical roles in tissue morphogenesis during development. Morphological changes may also reflect important responses to changing physiological conditions, as well as to tissue injury.

Among the first applications of time-lapse confocal imaging was a series of studies of the growth of axon terminals within the intact brain of *Xenopus* (O'Rourke and Fraser, 1990; O'Rourke *et al.*, 1994). Similar phenomena have also been amenable to study by time-lapse confocal microscopy in mammalian brain tissue (Smith *et al.*, 1990). For example, the mitotic cycle of neuroblasts (Chenn and McConnell, 1995; Adams, 1996), migration of neurons (O'Rourke *et al.*, 1992; Barber *et al.*, 1993; Fishell *et al.*, 1993; Komuro and Rakic, 1995, 1996, 1998), axonal growth and guidance (Dailey *et al.*, 1994), and the development of dendrites (Dailey and Smith, 1996) have all been imaged by time-lapse confocal microscopy in tissue slices of developing mammalian brain and spinal cord. Time-lapse confocal imaging has also been used to study morphological changes in synaptic structures such as dendritic spines under conditions of physiological plasticity (Hosokawa *et al.*, 1992, 1995). And finally, confocal imaging has been employed to study

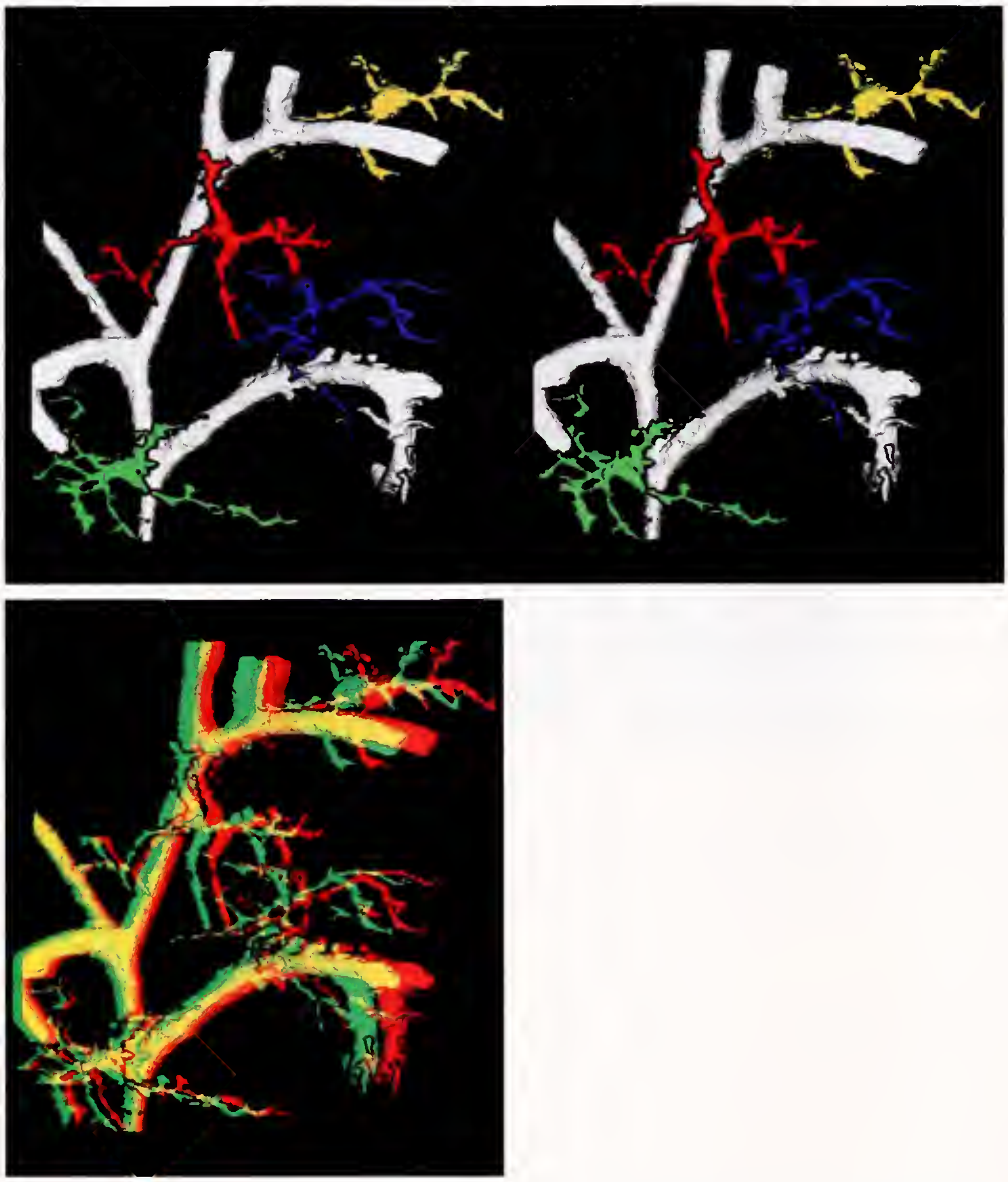

Figure 2. Three-dimensional confocal reconstruction of microglial cells in relation to a branching blood vessel in a rat hippocampal brain slice. A through-focus stack of 93 confocal images was collected at 0.4 μm z-step intervals through a tissue depth of 37 μm. The volume was reconstructed and rendered using Voxblast (Veytek, Fairfield, IA). (Top pair of images) Individual microglial cells were digitally "painted" different colors to distinguish one from another. The left and right images (a stereopair) represent views from slightly different perspectives (offset by 10°) to provide depth information. A 3-D image of the cells can be seen by crossing your eyes as you look at the pair of images. (*Bottom image*) A 3-D image of the same field may be seen using red-blue stereo glasses (red over left eye). Note that some microglial processes appear to contact the surfaces of the blood vessel. An animated movie of this tissue volume is available for viewing on *The Biological Bulletin* Website at <http://www.mbl.edu/html/BB/VIDEO/BB.video.html>.

the dynamics of glial cells responding to neural tissue injury (Brockhaus *et al.*, 1996; Dailey and Waite, 1999). In each case, the dynamic features of cell structure and movement could be viewed in a near-native tissue environment.

One of the under-utilized features of confocal microscopy is the ability to image dynamic cell and tissue structures in four dimensions (4-D); that is, in three spatial dimensions over time (*e.g.*, Kriete and Wagner, 1993; Konijn *et al.*, 1996; Errington *et al.*, 1997; Zimmermann and Siegert, 1998). This can be accomplished by collecting stacks of confocal images at set time intervals The resultant time series of confocal image stacks can be used to reconstruct 3-D views of dynamic cell and tissue development. Mark Cooper's group has elegantly applied this approach to early

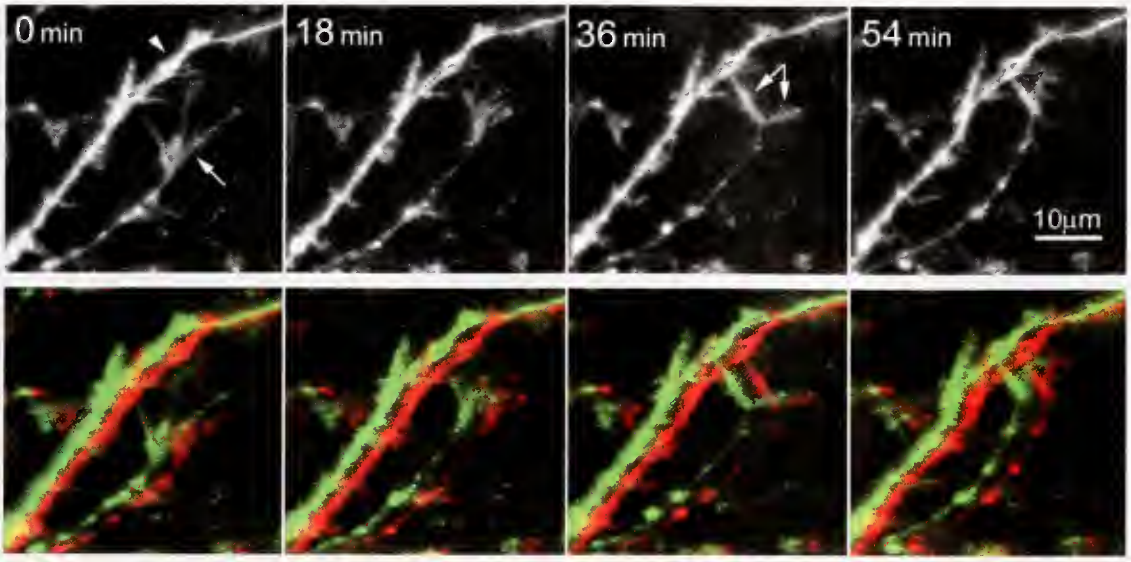

Figure 3. Time-lapse sequence shows the dynamics of axon growth and contact with a dendrite in a developing rat hippocampal slice. Neurons were labeled with a fluorescent membrane dye, DiI. To image growth of neuronal processes in three dimensions, stacks of 16 optical sections spanning 30 μm in the axial dimension (2-μm z-steps) were collected at time intervals of 6 min. Images in the top sequence represent a simple axial projection of the 16 images in the through-focus stack. The bottom series of images are red-green stereo images of the same data to provide depth information (viewing requires red-green or red-blue stereo glasses). A thin axon (*arrow*) extends parallel to a dendrite (*arrowhead*). Note the long thin filopodia at the leading edge of the growth cone (0 min), which advances (18 min) and bifurcates (*arrows*, 36 min). The left branch of the growth cone contacts the adjacent dendrite, and the axon growth is subsequently reoriented in that direction (54 min). A time-lapse movie of the axon growth is available for viewing on *The Biological Bulletin* Website at <http://www.mbl.edu/html/BB/VIDEO/BB.video.html>.

zebrafish development (Cooper, 1999), demonstrating the power of time-resolved, 4-D confocal imaging in a fully intact, experimental vertebrate preparation. In Figure 3 we illustrate the use of 4-D confocal imaging to capture the dynamic behavior of an axonal growth cone extending and contacting a dendrite within a rat hippocampal brain slice.

Imaging Cell and Tissue Physiology

With increasing frequency, it is becoming necessary—and feasible—to gather information about both the structure and physiology of the biological specimen. This is especially essential for studies on neural tissue, where spatial and temporal patterns of electrical and chemical signals play critical roles in brain function. Optical imaging of the physiology of individual cells within the context of a 3-D tissue can provide a powerful means of exploring tissue organization and function. Within a single field of view, the activity of many tens or hundreds of cells may be observed simultaneously. This can help elucidate physiological features of populations of cells, reveal distinct functional properties and relationships of different cell types, and define functional domains within a tissue.

In conjunction with the various fluorescent probes used in cell physiology, confocal imaging can provide information on absolute values of, as well as transient changes in, membrane potential, pH, intracellular calcium, and several other ions and physiological factors. For example, fluorescent calcium indicator dyes (such as fluo-3) have been used often to investigate the dynamics of intracellular calcium fluctuation in a variety of cell and tissue preparations. Such studies have helped define the spatiotemporal aspects of intra- and inter-cellular calcium signals (Cornell-Bell *et al.*, 1990; Cleemann *et al.*, 1998; Wier *et al.*, 1997). Confocal physiological imaging also has been feasible for studies in thick brain tissue slices (Dani *et al.*, 1993; van den Pol *et al.*, 1992; Dailey and Smith, 1994; Komuro and Rakic, 1996; Guerineau *et al.*, 1998) and in other complex neural preparations, such as the intact zebrafish (Cox and Fetcho, 1996) and the neuromuscular junctions of frog (Reist and Smith, 1992) and fly (Karunanithi *et al.*, 1997). Figure 4 illustrates the use of confocal imaging to examine, in cultured brain tissue, the spatiotemporal patterns of intra- and inter-cellular activity in neuroglial cells in response to a physiological perturbation.

Many calcium imaging experiments that use laser confocal microscopy have employed nonratiometric calcium indicator dyes (*e.g.*, fluo-3, calcium green), primarily because the most popular ratiometric dyes (fura-2 and indo-1) re-

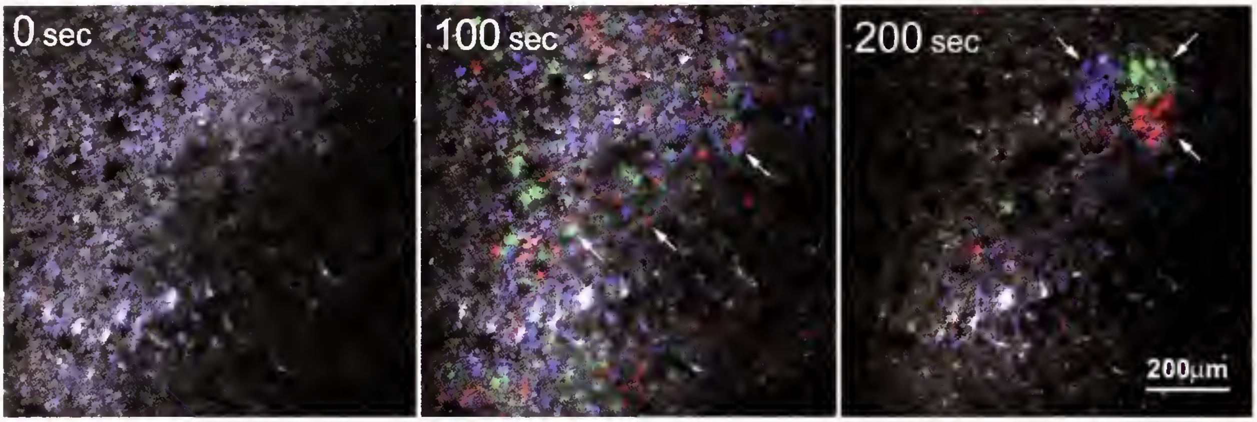

Figure 4. Physiological time-lapse imaging reveals changing spatiotemporal patterns of intracellular calcium (Ca^{2+}) activity in brain tissue in response to potassium (K^{+}) depolarization. The slice was loaded with fluo-4 AM (Molecular Probes, Eugene, OR), a membrane-permeant fluorescent indicator of intracellular calcium, and mounted in an open chamber for imaging. Single confocal scans were collected at 7-s intervals to detect changes in fluorescence intensity, which reflect changes in intracellular calcium levels. Each panel (left, center, right) is a composite of three images acquired at three slightly different time-points (7 s apart) and encoded red, green, or blue. Thus, the colors represent points in time when cells are active. Inactive cells appear black, and cells with sustained high calcium levels appear white. The left panel, corresponding to a time-point prior to K^{+} depolarization, shows a low level of spontaneous calcium activity (few colored cells). The center panel, taken just after addition of medium containing high (9 m*M*) K^{+}, shows a much higher level of calcium activity in cells. Note that the small colored patches (corresponding to individual, active cells; *arrows*) are dispersed across the field of view. In the right panel, taken about 100 s later, the isolated cell activity has diminished, and a new pattern of activity emerges corresponding to groups of 5–15 synchronously active cells within patches that are 100–200 μm in diameter. The active cells are probably astrocytes, and the emergence of synchronously active groups of neighboring cells probably represents electrical (gap junction) coupling among astrocytes (Charles, 1998; Harris-White *et al.*, 1998). A time-lapse movie is available for viewing on *The Biological Bulletin* Website at <http://www.mbl.edu/html/BB/VIDEO/BB.video.html>.

quire excitation wavelengths in the ultraviolet (UV) range. Such short-wavelength lasers are expensive and thus less widely available; moreover, chromatic aberration problems associated with UV excitation make confocal microscope design very challenging (Blinton and Lechleiter, 1995). However, several studies have shown that ratiometric physiological data can be obtained by visible wavelength confocal imaging. These studies utilize two calcium-sensitive dyes (fluo-3 and fura red) simultaneously (Lipp and Niggli, 1993, 1994; Schild *et al.*, 1994), or a calcium sensitive (fluo-3) and a calcium-insensitive (rhodamine) dye in combination (Stricker, 1996).

Since many physiological events occur on a very fast time-scale, an imaging system must sample at a sufficiently high rate to resolve such events. Many of the early confocal systems were severely limited by the rate at which they were able to collect and store images. This limitation is increasingly being overcome in two ways. First, with standard laser scanning confocal microscopes, the sampling rate can be increased by reducing the size of the field over which image data are collected. In the extreme case, the "field size" is reduced to a single line that can be repeatedly scanned at high rates (>300 Hz), a so-called line-scanning mode. This yields limited spatial information, but provides the extremely high time-resolution necessary for resolving fast physiological events such as neural synaptic activity (Schild *et al.*, 1994; Korkotian and Segal, 1998; Yuste *et al.*, 1999).

Second, several video rate or "real-time" confocal systems have been developed, some of which are capable of collecting over one hundred *x-y* (2-D) images per second. These systems have been utilized to study preparations as diverse as individual mesenchymal cells (Vesely and Boyde, 1996), perfused whole rat heart (Hama *et al.*, 1998), kidney (Andrews, 1996), and mammalian nerve and blood vessels *in vivo* (Bussau *et al.*, 1998; Papworth *et al.*, 1998).

While confocal imaging is permitting unprecedented observations of intact tissues and organisms, it is also extending our view into the dynamic subcellular and molecular world. This new capability has been closely coupled with the development and use of vital fluorescent probes such as green fluorescent protein (GFP)-tagged proteins (Chalfie *et al.*, 1994). Such probes can be engineered to target particular organelles, delivered to living cells and organisms, and imaged by time-lapse confocal microscopy, so that the growth, dynamics, and reorganization of subcellular compartments can be studied (Cole *et al.*, 1996; Terasaki *et al.*, 1996).

Outlook

The plethora of cell and molecular probes now available will, with increasing frequency, permit studies aimed at elucidating both morphological and physiological features of biological specimens. An especially exciting aspect of current biological investigation is the ability to assess the spatiotemporal dynamics of molecules in living cells, tissues, and intact organisms. Progress in such studies critically depends upon the availability of imaging tools that provide sufficient spatial and temporal resolution and that are, to the extent possible, noninvasive and nondestructive. We can anticipate that advances in confocal microscopy will continue to play a role in extending our capacity to probe the relationship between biological structure and function, from molecule to organism.

Acknowledgments

This work was supported in part by grants from the Roy J. Carver Charitable Trust, the National Institutes of Health (NS37159), the Whitehall Foundation (#S98-6), and an American Cancer Society seed grant (#IN-122R) administered through the University of Iowa Cancer Center. Voxblast was developed at the University of Iowa Image Analysis Facility.

Literature Cited

Adams, R. J. 1996. Metaphase spindles rotate in the neuroepithelium of rat cerebral cortex. *J. Neurosci.* **16(23):** 7610–7618.

Andrews, P. 1996. Tandem scanning confocal microscopic imaging of the living kidney. *Intl. Rev. Exper. Path.* **36:** 131–143.

Barber, R. P., P. E. Phelps, and J. E. Vaughn. 1993. Preganglionic autonomic motor neurons display normal translocation patterns in slice cultures of embryonic rat spinal cord. *J. Neurosci.* **13(11):** 4898–4907.

Blinton, A. C., and J. D. Lechleiter. 1995. Optical considerations at ultraviolet wavelengths in confocal microscopy. Pp. 431–444 in *Handbook of Biological Confocal Microscopy*, 2nd ed. Plenum Press, New York.

Brockhaus, J., T. Moller, and H. Kettenmann. 1996. Phagocytozing ameboid microglial cells studied in a mouse corpus callosum slice preparation. *Glia* **16:** 81–90.

Bussau, L. J., L. T. Vo, P. M. Delaney, G. D. Papworth, D. H. Barkla, and R. G. King. 1998. Fibre optic confocal imaging (FOCI) of keratinocytes, blood vessels and nerves in hairless mouse skin *in vivo*. *J. Anatomy* **192(2):** 187–194.

Chalfie, M., Y. Tu, G. Euskirchen, W. W. Ward, and D. C. Prasher. 1994. Green fluorescent protein as a marker for gene expression. *Science* **263:** 802–805.

Charles, A. 1998. Intercellular calcium waves in glia. *Glia* **24(1):** 39–49.

Chenn, A., and S. K. McConnell. 1995. Cleavage orientation and the asymmetric inheritance of Notch 1 immunoreactivity in mammalian neurogenesis. *Cell* **82:** 631–641.

Cleemann, L., W. Wang, and M. Morad. 1998. Two-dimensional confocal images of organization, density, and gating of focal Ca^{2+} release sites in rat cardiac myocytes. *Proc. Natl. Acad. Sci. USA* **95(18):** 10984–10989.

Cole, N. B., C. L. Smith, N. Sciaky, M. Terasaki, M. Edidin, and J. Lippincott-Schwartz. 1996. Diffusional mobility of Golgi proteins in membranes of living cells. *Science* **273:** 797–801.

Cooper, M. 1999. FishScope (Online). Available: http://depts.washington.edu/fishscop (accessed 9 July 1999).

Cornell-Bell, A. H., S. M. Finkbeiner, M. S. Cooper, and S. J. Smith. 1990. Glutamate induces calcium waves in cultured astrocytes: long-range glial signalling. *Science* **247:** 470–473.

Cox, K. J., and J. R. Fetcho. 1996. Labeling blastomeres with a calcium indicator: a non-invasive method of visualizing neuronal activity in zebrafish. *J. Neurosci. Methods* **68(2):** 185–191.

Dailey, M. E., and S. J. Smith. 1994. Spontaneous Ca^{2+} transients in developing hippocampal pyramidal cells. *J. Neurobiol.* **25(3):** 243–251.

Dailey, M. E., and S. J. Smith. 1996. The dynamics of dendritic structure in developing hippocampal slices. *J. Neurosci.* **16(9):** 2983–2994.

Dailey, M. E., and M. Waite. 1999. Confocal imaging of microglial cell dynamics in hippocampal slice cultures. *Methods* **18(2):** 222–230.

Dailey, M. E., J. Buchanan, D. E. Bergles, and S. J. Smith. 1994. Mossy fiber growth and synaptogenesis in rat hippocampal slices *in vitro*. *J. Neurosci.* **14(3):** 1060–1078.

Dani, J. W., A. Chernjavsky, and S. J. Smith. 1992. Neuronal activity triggers calcium waves in hippocampal astrocyte networks. *Neuron* **8:** 429–440.

Errington, R. J., M. D. Fricker, J. L. Wood, A. C. Hall, and N. S. White. 1997. Four-dimensional imaging of living chrondrocytes in cartilage using confocal microscopy: a pragmatic approach. *Am. J. Physiol.* **273:** C1040–1051.

Fishell, G., C. Mason, and M. Hatton. 1993. Dispersion of neural progenitors within the germinal zones of the forebrain. *Nature* **362:** 636–638.

Gard, D. L., B. J. Cha, and M. M. Schroeder. 1995. Confocal immunofluorescence microscopy of microtubules, microtubule-associated proteins, and microtubule-organizing centers during amphibian oogenesis and early development. *Curr. Topics Dev. Biol.* **31:** 383–431.

Guerineau, N. C., X. Bonnefont, L. Stoeckel, and P. Mollard. 1998. Synchronized spontaneous Ca^{2+} transients in acute anterior pituitary slices. *J. Biol. Chem.* **273(17):** 10389–10395.

Hama, T., A. Takahashi, A. Ichihara, and T. Takamatsu. 1998. Real time *in situ* confocal imaging of calcium wave in the perfused whole heart of the rat. *Cellular Signalling* **10(5):** 331–337.

Harris-White, M. E., S. A. Zanotti, S. A. Frautschy, and A. C. Charles. 1998. Spiral intercellular calcium waves in hippocampal slice cultures. *J. Neurophysiol.* **79(2):** 1045–1052.

Hepler, P. K., and B. E. S. Gunning. 1998. Confocal fluorescence microscopy of plant cells. *Protoplasma* **201(3–4):** 121–157.

Hosokawa, T., T. V. P. Bliss, and A. Fine. 1992. Persistence of individual dendritic spines in living brain slices. *NeuroReport* **3:** 477–480.

Hosokawa, T., D. A. Rusakov, T. V. Bliss, and A. Fine. 1995. Repeated confocal imaging of individual dendritic spines in the living hippocampal slice: evidence for changes in length and orientation associated with chemically induced LTP. *J. Neurosci.* **15(8):** 5560–5573.

Karunanithi, S., J. Georgiou, M. P. Charlton, and H. L. Atwood. 1997. Imaging of calcium in *Drosophila* larval motor nerve terminals. *J. Neurophysiol.* **78(6):** 3465–3467.

Komuro, H., and P. Rakic. 1995. Dynamics of granule cell migration: a confocal microscopic study in acute cerebellar slice preparations. *J. Neurosci.* **15(2):** 1110–1120.

Komuro, H., and P. Rakic. 1996. Intracellular Ca^{2+} fluctuations modulate the rate of neuronal migration. *Neuron* **17(2):** 275–285.

Komuro, H., and P. Rakic. 1998. Distinct modes of neuronal migration in different domains of developing cerebellar cortex. *J. Neurosci.* **18(4):** 1478–1490.

Konijn, G. A., N. J. Vardaxis, M. E. Boon, L. P. Kok, D. C. Rietveld,

and J. J. Schut. 1996. 4D confocal microscopy for visualisation of bone remodelling. *Path. Res. Prac.* **192(6):** 566–572.

Korkotian, E., and M. Segal. 1998. Fast confocal imaging of calcium released from stores in dendritic spines. *Eur. J. Neurosci.* **10(6):** 2076–2084.

Kriete, A., and H. J. Wagner. 1993. A method for spatio-temporal (4-D) data representation in confocal microscopy: application to neuroanatomical plasticity. *J. Microsc.* **169(1):** 27–31.

Lichtman, J. W. 1994. Confocal Microscopy. *Sci. Am.* **271:** 40–45.

Lipp, P., and E. Niggli. 1993. Microscopic spiral waves reveal positive feedback in subcellular calcium signaling. *Biophysical J.* **65(6):** 2272–2276.

Lipp, P., and E. Niggli. 1994. Sodium current-induced calcium signals in isolated guinea-pig ventricular myocytes. *J. Physiol.* **474(3):** 439–446.

Minsky, M. 1961. Microscopy Apparatus, U.S. Patent 3,013,467.

Minsky, M. 1988. Memoir on inventing the confocal scanning microscope. *Scanning* **10(4):** 128–138.

O'Rourke, N. A., and S. E. Fraser, 1990. Dynamic changes in optic fiber terminal arbors lead to retinotopic map formation: an *in vivo* confocal microscopic study. *Neuron* **5:** 159–171.

O'Rourke, N. A., M. E. Dailey, S. J. Smith, and S. K. McConnell. 1992. Diverse migratory pathways in the developing cerebral cortex. *Science* **258:** 299–302.

O'Rourke, N. A., H. T. Cline, and S. E. Fraser. 1994. Rapid remodeling of retinal arbors in the tectum with and without blockade of synaptic transmission. *Neuron* **12:** 921–934.

Papworth, G. D., P. M. Delaney, L. J. Bussau, L. T. Vo, and R. G. King. 1998. *In vivo* fibre optic confocal imaging of microvasculature and nerves in the rat vas deferens and colon. *J. Anatomy* **192:** 489–495.

Pawley, J. B., ed. 1995. *Handbook of Biological Confocal Microscopy, 2nd ed. Plenum Press, New York.*

Pedley, K. C. 1997. Applications of confocal and fluorescence microscopy. *Digestion* **58 Suppl 2:** 62–68.

Reist, N. E., and S. J. Smith. 1992. Neurally evoked calcium transients in terminal Schwann cells at the neuromuscular junction. *Proc. Natl. Acad. Sci. USA* **89:** 7625–7629.

Sargent, P. B. 1994. Double-label immunofluorescence with the laser scanning confocal microscope using cyanine dyes. *Neuroimage* **1(4):** 288–295.

Schild, D., A. Jung, and H. A. Schultens. 1994. Localization of calcium entry through calcium channels in olfactory receptor neurones using a laser scanning microscope and the calcium indicator dyes Fluo-3 and Fura-Red. *Cell Calcium* **15(5):** 341–348.

Smith, S. J., M. Cooper, and A. Waxman. 1990. Laser microscopy of subcellular structure in living neocortex: Can one see dendritic spines twitch? *Symp. Med. Hoechst* **23:** 49–71.

Stricker, S. A. 1996. Changes in the spatiotemporal patterns of intracellular calcium transients during starfish early development. *Invert. Reprod. Devel.* **30(1–3):** 135–152.

Summers, R. G., S. A. Stricker, and R. A. Cameron. 1993. Applications of confocal microscopy to studies of sea urchin embryogenesis. *Methods Cell Biol.* **38:** 265–287.

Terasaki, M., L. A. Jaffe, G. R. Hunnicutt, and J. A. Hammer, 3rd. 1996. Structural change of the endoplasmic reticulum during fertilization: evidence for loss of membrane continuity using the green fluorescent protein. *Dev. Biol.* **179(2):** 320–328.

Turner, J. N., J. W. Swann, D. H. Szarowski, K. L. Smith, W. Shain, D. O. Carpenter, and M. Fejtl. 1996. Three-dimensional confocal light and electron microscopy of central nervous system tissue and neurons and glia in culture. *Intl. Rev. Exper. Path.* **36:** 53–72.

van den Pol, A. N., S. M. Finkbeiner, and A. H. Cornell-Bell. 1992. Calcium excitability and oscillations in suprachiasmatic nucleus neurons and glia *in vitro. J. Neurosci.* **12(7):** 2648–2664.

Vesely, P., and A. Boyde. 1996. Video rate confocal laser scanning reflection microscopy in the investigation of normal and neoplastic living cell dynamics. *Scanning Microsc.* **Suppl. 10:** 201–211.

Wier, W. G., H. E. ter Keurs, E. Marban, W. D. Gao, and C. W. Balke. 1997. Ca^{2+} 'sparks' and waves in intact ventricular muscle resolved by confocal imaging. *Circ. Res.* **81(4):** 462–469.

Wouterlood, F. G., J. C. Van Denderen, N. Blijleven, J. Van Minnen, and W. Hartig. 1998. Two-laser dual-immunofluorescence confocal laser scanning microscopy using Cy2- and Cy5-conjugated secondary antibodies: unequivocal detection of colocalization of neuronal markers. *Brain Res. Protocols* **2(2):** 149–159.

Yuste, R., A. Majewska, S. S. Cash, and W. Denk. 1999. Mechanisms of calcium influx into hippocampal spines: heterogeneity among spines, coincidence detection by NMDA receptors, and optical quantal analysis. *J. Neurosci.* **19(6):** 1976–1987.

Zimmermann, T., and F. Siegert. 1998. 4D confocal microscopy of *Dictyostelium discoideum* morphogenesis and its presentation on the Internet. *Dev. Genes Evol.* **208(7):** 411–420.

Reference: *Biol. Bull.* **197:** 123–131. (October 1999)

Development of the Larval Serotonergic Nervous System in the Sea Star *Patiriella regularis* as Revealed by Confocal Imaging

FRANCIS CHEE* AND MARIA BYRNE

Department of Anatomy and Histology, University of Sydney F13, NSW 2006, Australia

Abstract. Development of the nervous system in the larvae of the sea star *Patiriella regularis* was reconstructed in three dimensions. The optical sectioning and image processing capabilities of the confocal microscope made it possible to identify the precise location and timing of development of serotonergic cells in relation to subsequent development of larval features. Similarities between this system and the serotonergic systems in larvae of other echinoderms were explored. Neuronal-like immunoreactive cells and processes first appeared in late gastrulae as a collection of cells scattered across the animal pole. These cells subsequently gave rise to basal axons positioned along the basal lamina. Immunopositive cells located in the stomodaeal region marked the beginnings of formation of the adoral ciliated band. Cells were also present in the mid-dorsal epithelium. Advanced bipinnaria had pyramidal immunoreactive cells within the adoral band and ovoid immunoreactive cells within the preoral and postoral ciliated bands. Processes originating from neurons in the transverse region of the preoral ciliated band extended into the buccal cavity, suggesting that these cells have a sensory role in feeding. An anterior ganglion formed in the late bipinnaria, innervating the preoral and postoral ciliated bands. This connection has not previously been described. It thus appears that the ciliated bands in the bipinnaria larvae of *P. regularis* communicate *via* serotonergic nerve tracts.

Introduction

Serotonin (5-hydroxytryptamine, 5-HT) is a ubiquitous monoamine and functions as a neurotransmitter in the adult nervous systems of a large range of animal groups (Collier, 1958). In echinoderms, serotonin was first isolated in the gonads of adult asteroids (Welsh and Moorehead, 1960), and its cellular location has been documented in studies of the larval nervous system of echinoids, asteroids, and holothuroids (Bisgrove and Burke, 1986; Burke *et al.*, 1986; Bisgrove and Burke, 1987; Nakajima, 1988; Bisgrove and Raff, 1989; Nakajima *et al.*, 1993; Moss *et al.*, 1994; Chee and Byrne, 1997). These studies indicate that serotonin functions in a neuronal capacity in these larvae. The feeding larvae of echinoderms typically have a well-developed serotonergic nervous system that innervates the ciliated bands and is suggested to play a sensory role in feeding and metamorphosis. The similarities between the serotonergic systems in the larvae of several echinoderm classes have been taken to suggest that these systems are homologous (Burke *et al.*, 1986). In general, the increasing complexity of the serotonergic nervous system in the feeding larvae of echinoderms parallels the development of the ciliated bands (Burke, 1983).

During sea star development the number of serotonergic immunoreactive cells increases from a few cells at the gastrula stage to a complex nervous system in competent larvae prior to metamorphosis (Nakajima, 1988). In this study we investigate the larval nervous system of the sea star *Patiriella regularis*. This species has planktotrophic development through bipinnaria and brachiolaria feeding stages (Byrne and Barker, 1991). Following from previous observations (Chee and Byrne, 1997), we document the expression of serotonin in *P. regularis* from the first appearance of neurons in gastrulae through the formation of a complex three-dimensional nervous system. Assisted by confocal microscopy, we were able to reconstruct development of the serotonergic-like nervous system in three dimensions with respect to morphogenetic change. Although

---

Received 2 November 1998; accepted 28 June 1999.

* E-mail: francis@anatomy.usyd.edu.au

Abbreviations: ADNP, adoral nerve plexus; FSW, filtered seawater; PBS, phosphate buffered saline; AG, anterior ganglion; 5-HT, serotonin.

previous studies have successfully used epifluorescence microscopy to follow the formation of the larval serotonergic nervous system in echinoderms (Burke, 1983; Nakajima, 1988; Moss *et al.*, 1994), insights into cell structure and the three-dimensional nature of the system were limited with this technique.

For echinoderms, development through feeding larvae is considered to be the ancestral life-history pattern (Strathmann, 1978; Hart *et al.*, 1997). In *Patiriella*, developmental evolution has resulted in the loss of a feeding larva and adaption of various forms of planktotrophic, benthic, intragonadal, and lecithotrophic larvae (Byrne and Cerra, 1996; Hart *et al.*, 1997). A major aim of this study was to obtain a more complete picture of 5-HT-like expression in the ancestral-type larvae of *P. regularis* and demonstrate that during the development of *P. regularis* small changes in gross morphology coincide with large changes in serotonergic architecture. The significance of the distribution of serotonergic neurons is assessed with respect to the functional morphology of the larvae and the roles these neurons may play in modulating larval behavior. Parallels in the immunocytochemical expression of 5-HT with other neurotransmitters in the feeding larvae of other echinoderms are discussed. The nomenclature used to describe the ciliated bands follows that established by previous authors (Strathmann, 1975; Moss *et al.*, 1994).

Materials and Methods

Patiriella regularis were collected from the Derwent Estuary, Tasmania. Mature oocytes were obtained by intracoelomic injection of the starfish with 10^{-5} M 1-methyladenine (Sigma) in 0.2-μm filtered seawater (FSW). Testes were dissected from mature males, and a dilute solution of sperm was added to the eggs. Fertilization success was visually checked after 15 min. The fertilized eggs were washed three times in FSW to remove any remaining sperm. Embryos and larvae were cultured at 22°C in FSW, and the larvae were fed *Dunaliella tertiolecta, Rhodomonas* sp., or both.

Gastrulae, early and late bipinnariae, and early brachiolariae were immunolabeled for microscopic examination. Gastrulae were obtained from four cultures derived from different fertilizations. The bipinnaria were derived from six different cultures. All of the stages were transferred to glass scintillation vials, fixed in 4% paraformaldehyde in FSW at 22°C for 1–2 h, rinsed briefly in FSW, and then placed into phosphate buffered saline (PBS) at pH 8.2–8.3. Prior to antibody incubation, specimens were treated for 30 min in PBS containing normal goat serum and 0.3% Triton × 100 to reduce nonspecific staining and to aid antibody penetration. After each incubation step the specimens were washed with gentle agitation in three 10-min changes of 0.1 M PBS pH 8.2. Specimens were then incubated first in the primary antibody, rabbit anti-serotonin (Incstar/DiaSorin) diluted 1 in 100, for 16 to 22 h at 4°C, and then in the secondary antibody, biotinylated goat anti rabbit IgG (H+L) (Vector Laboratories) 1 in 50, for 2 h. The final incubation was in a 1-in-100 dilution of fluorescein (FITC)-labeled streptavidin (Vector Laboratories) for 20 min in the dark at 23°C. Controls consisted of omitting the primary antibody, omitting the secondary antibody, using normal rabbit serum as a substitute for the primary antibody, and checking for autofluorescence using only paraformaldehyde-fixed gastrulae and larvae. Immunolabeled gastrulae ($n > 100$) and larvae were mounted on welled slides in a drop of Fluoroguard antifade reagent (Bio-Rad), and the coverslips were sealed with nail polish. Slides were viewed immediately or stored at 4°C in the dark. Slides refrigerated for several months showed no sign of fading when examined. All times quoted are postfertilization.

The specimens were examined with a confocal laser scanner coupled to an epifluorescence microscope (a Bio Rad MRC600 scanner and a Zeiss Axiophot microscope or an MRC1024 and an Olympus BX 60). The 488-nm line of the krypton/argon laser was used with a 520DF32-nm filter block. Various numbers of optical sections were collected at different depth intervals. The depth of collection was determined by the thickness of the specimen and the degree of immunolabeling. The number of immunoreactive cell bodies was determined by optically sectioning the various larvae. All images are displayed in ventral or lateral view, anterior at the top of the page. Image projections (extended focal length) were created using Confocal Assistant (Software version 4.02), and three-dimensional (3D) stereo anaglyphs were produced using Laser Sharp (Bio-Rad Laboratories) and Confocal Assistant. Computer animations were produced using a Silicon Graphics XS24 4000 with Voxel View Ultra software.

Patiriella regularis larvae were prepared for scanning electron microscopy according to Byrne and Barker (1991) and examined with a Philips XL30 at 10 Kv.

Results

Gastrula

The first cells exhibiting specific 5-HT-like immunoreactivity occurred in mid gastrulae (Fig. 1A), about 24 h postfertilization. As the gastrulae began to elongate, these cells formed a partial dome-like array across the animal region and included monopolar, bipolar, and tripolar cells (Fig. 1B). Varicosities were occasionally observed on these processes (Fig. 1C). Both the soma and the neurites of these cells were immunopositive (Fig. 1C). In cross section the cells spanned the epithelium (Fig. 1D). With 3D computer reconstructions or extended focus projections, these cells were shown to be pyramidal. Control gastrulae ($n = 15$), were nonfluorescent.

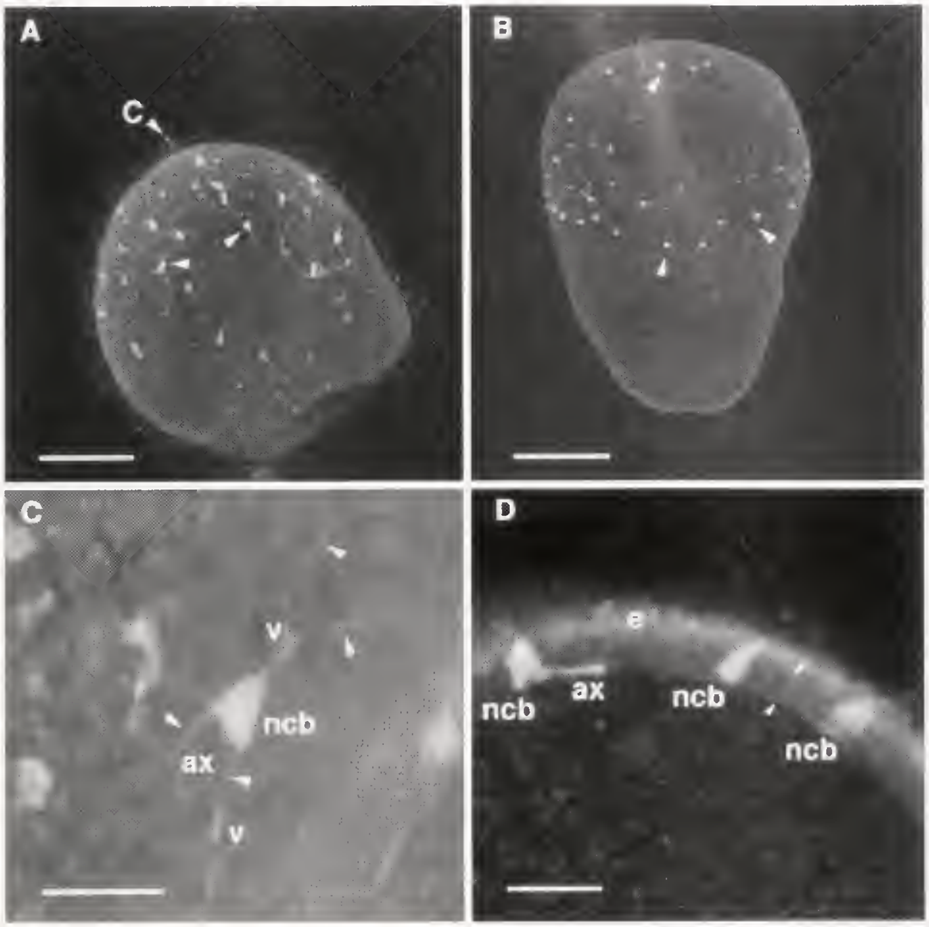

Figure 1. Confocal images showing bodies and processes of cells with 5-HT-like immunoreactivity in early and advanced gastrula. (A) A projection from 16 optical sections taken at 4.5-μm intervals of a mid gastrula shows cells with 5-HT-like immunoreactivity (arrowheads) scattered in the epithelium. C, cilia. Bar, 63 μm. (B) Advanced gastrula, projection created from 14 images at 4.5-μm depth intervals showing the concentration of immunoreactive cells (arrowheads) in the animal half. Bar, 95 μm. (C) 5-HT-like immunoreactivity in a tripolar nerve cell in a 34-h gastrula. ax, axonal-like processes; v, varicosities; ncb, nerve cell body. Bar, 16 μm. (D) Advanced gastrula/early bipinnaria epithelium (e) showing nerve cell bodies (ncb) and axonal-like processes (ax) traveling along the basal lamina in a single confocal section. Bar, 20 μm.

Bipinnaria

Prior to the opening of the mouth, early bipinnariae had a distinct stomodaeal invagination while the blastopore was still located at the vegetal pole (Fig. 2A). The larvae could now be orientated according to their dorsoventral axis (Fig. 2A). A 144-μm-thick projection reconstructed from 32 optical sections showed that cells with 5-HT-like immunoreactivity were abundant on both sides of the larva (Fig. 2A). On the ventral surface, the cells around the stomodaeum, about 10 in number, were monopolar and marked the position at which the adoral ciliated band will form (Fig. 2A). A collection of bipolar ovoid immunoreactive cells on the dorsal surface was positioned roughly opposite the stomodaeal invagination (Fig. 2A).

At about 48 h postfertilization, the mouth opened. The larvae were further elongated and the anus opened ventrally. With completion of the gut, the larvae were able to feed. As seen above, 5-HT-like immunoreactivity was conspicuous in the cells surrounding the mouth, which marked the position of the developing adoral ciliated band (Fig. 2B). A few immunoreactive cell bodies were also observed on the upper right region of the buccal cavity (Fig. 2B). Immunoreactive cells and processes on the mid-dorsal surface formed an incomplete ring that wrapped partially around the larva but did not extend to the ventral surface (Fig. 2C). Axonal-like processes from these cell bodies extended towards the posterior end of the larva (Fig. 2C). Although the fate of the immunoreactive cells in this ring could not be followed, their mid-body position indicates that they were subsequently

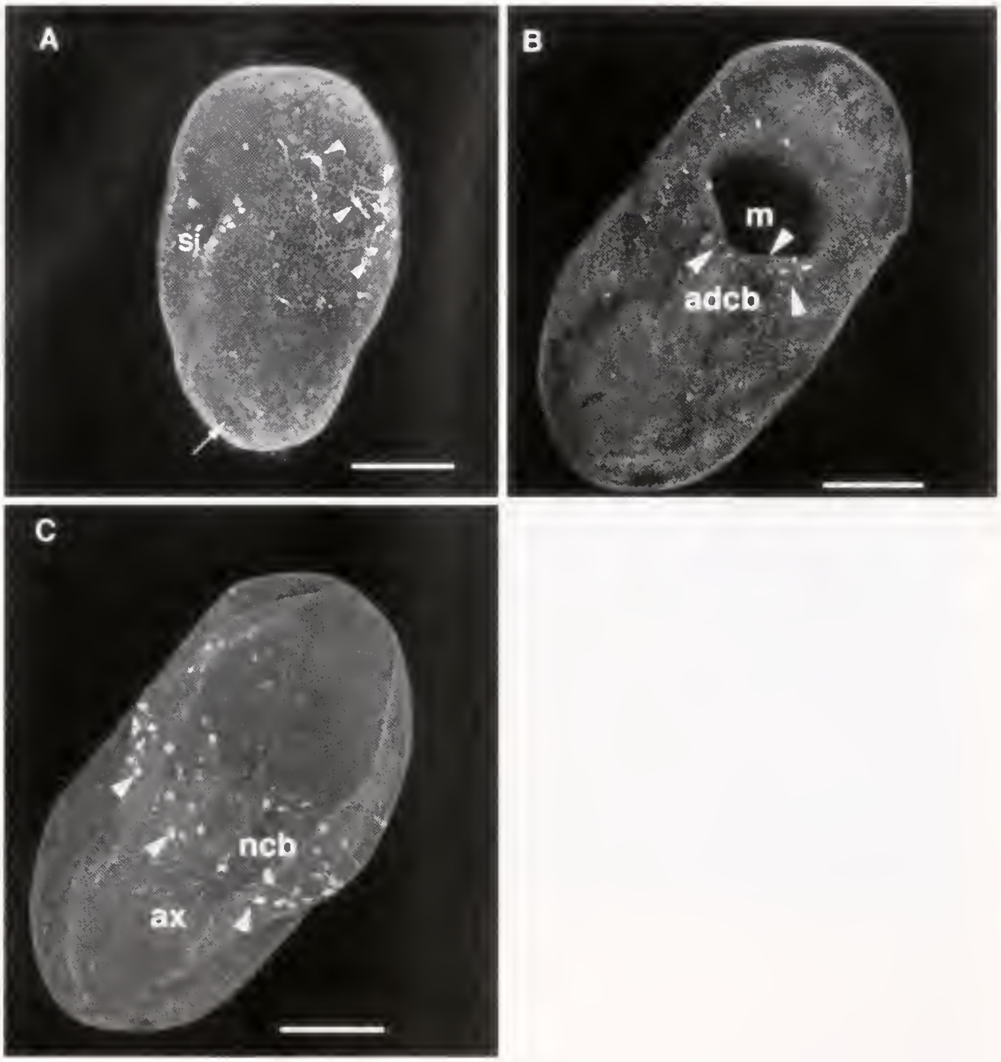

Figure 2. Confocal optical projections of early bipinnariae. (A) Early bipinnaria reconstructed from 32 optical sections. Cells with 5-HT-like immunoreactivity can be clearly seen around the stomodaeal invagination (si) and the dorsal surface (arrowheads) of the larva. (B) Projection of 5 confocal sections from the ventral side of a 48-h bipinnaria. 5-HT-like immunoreactivity is present in cell bodies (arrowheads) in the adoral ciliated band (adcb), and a few immunoreactive cells are also present on the upper left-hand side of the mouth (m). (C) Projection of 5 optical sections from the dorsal side of the larva in panel B. Immunoreactive cell bodies (ncb) and axonal-like processes (ax) form a band partially wrapping around the larva. Bars, 95 μm.

incorporated into the serotonergic tracts associated with the preoral and postoral ciliated bands.

As the preoral, postoral and adoral ciliated bands developed, the oral hood was also beginning to form (Fig. 3A, B). Serotonin-like immunoreactivity was observed along the ciliated bands in the form of monopolar cell bodies with axonal-like tracts following the path of these bands (Fig. 3A). By this stage, a ganglion was evident at the anterior end of the larva. This anterior ganglion (AG) consisted of the immunopositive cells and processes innervating the preoral and postoral ciliated bands and processes interconnecting these bands (Fig. 3A).

Advanced bipinnaria (about 18 days old) underwent a distinct shape change with the formation of an extension at the anterior end of the larva (Fig. 4A, B). The three ciliated bands were well developed in these larvae (Fig. 4A, B). Internally, the larva had a well-developed gut, and the right and left enterocoels had formed. The distribution of immunoreactive cells in these bands, discussed below, was consistent in all larvae examined ($n = 100$).

Adoral ciliated band

The adoral ciliated band was located along the posterior margin of the mouth and was characteristically paraboloidal (Fig. 5A). Along this band were densely packed cells with

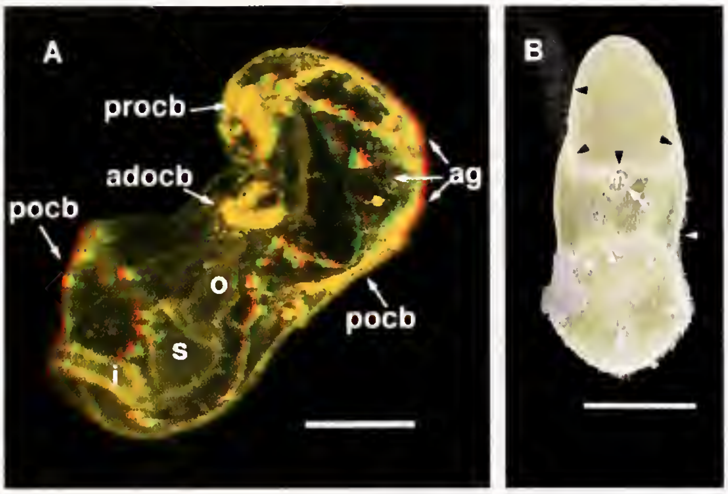

Figure 3. Three-dimensional red/green anaglyph and a scanning electron micrograph (false colored) of early bipinnariae. (A) A 3-D lateral view of an early bipinnaria showing immunoreactive cell bodies and axonal-like tracts following the ciliated bands. The anterior ganglion (ag) has formed and connects the preoral (procb) and postoral (pocb) ciliated bands. adocb, adoral ciliated band; o, esophagus; s, stomach; i, intestine. Bar, 95 μm. (B) Ventral view of an early bipinnaria at the same stage as in panel A. The ciliated bands are developing, but the anterior extension has not yet formed. Black arrowheads, preoral ciliated band; white arrowheads, postoral ciliated band; white arrow, adoral ciliated band; m, mouth; a, anus. Bar, 100 μm.

5-HT-like immunoreactivity; the apical ends of these cells extended to the edge of the ciliated epithelium. These cells were pyramidal and connected basally *via* a thick immunopositive tract (Fig. 6A). Compared with the other ciliated bands, the adoral ciliated band had the highest concentration of immunoreactive cells and processes, forming the adoral nerve plexus (ADNP). The ADNP innervated the epithelium of the adoral ciliated band. Confocal optical sectioning revealed that the apical region of these cells protruded to the exterior of the ciliated band epithelium. Computer animations (data not illustrated) and a 3D anaglyph (Fig. 5A) showed that this plexus was also connected by serotonergic processes with the nerve plexus in the preoral transverse band *via* two thin (approximately 2.5 μm) lateral immunoreactive tracts.

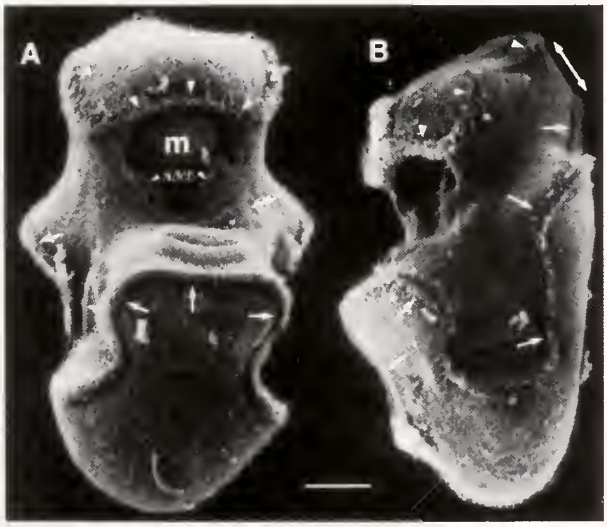

Figure 4. Scanning electron micrographs of a bipinnaria showing fully developed ciliated bands (arrowheads and arrows): (A) Ventral view of a bipinnaria with a flexed oral hood and mouth (m) open showing the position of the adoral ciliated band (adcb). (B) Lateral view of a bipinnaria showing the anterior extension of the oral hood, top right-hand side. Double-ended arrow indicates the anterior region where the anterior ganglion links the preoral and postoral ciliated bands. Arrowheads, preoral ciliated band; arrows, postoral ciliated band: Bar, 200 μm.

Preoral ciliated band

The preoral ciliated band was located on the ventral surface of the larva and outlined the oral hood (Fig. 4A). Where this band traversed the larva above the mouth (preoral transverse region), a large number of flask-shaped cell bodies with 5-HT-like immunoreactivity ($\bar{x} = 21$, SE $= 0.1$ $n = 10$ larvae) were found in the epithelium (Fig. 4B). From these cell bodies, confocal sectioning into the larva from the ventral surface revealed axonal-like processes from the basal portion of the cells extending inwards toward the buccal cavity (Fig. 4B). In its lateral region, the preoral ciliated band contained a few immunopositive cells scattered along its path. Occasionally, a collection of cell bodies forming a pair of lateral ganglia were seen in the lateral region of the postoral ciliated band. These structures were not seen in all larvae and appear to be ephemeral. In the late bipinnaria, a ganglion developed at the anterior end of the larva. This ganglion consisted of immunoreactive cells

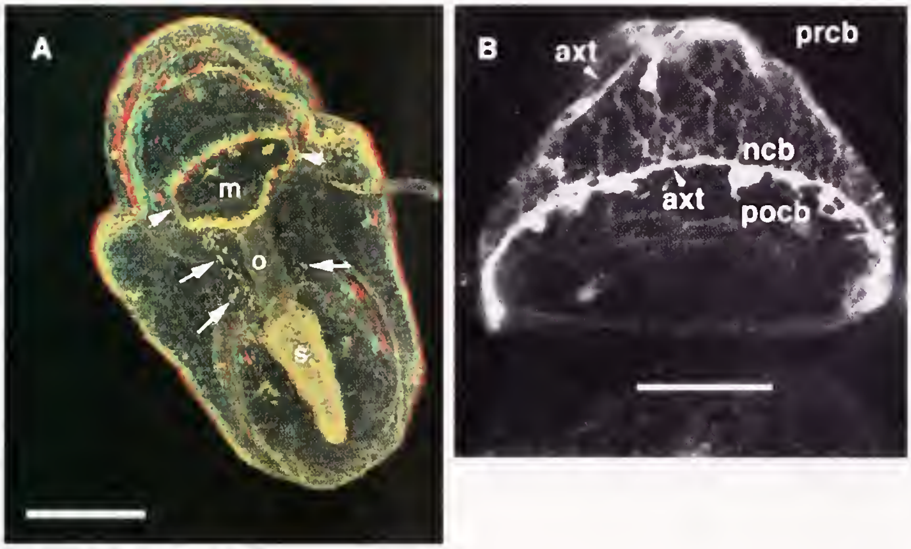

Figure 5. Bipinnaria: 3-D anaglyph and a high-magnification confocal image projection of the anterior ganglion. Images were constructed from a series of optical sections covering a distance of 132 μm. (A) 3-D anaglyph of a bipinnaria detailing the serotonergic nervous system following the pathway of the ciliated bands. White arrowheads, serotonergic connection between preoral and adoral ciliated bands; s, stomach; m, mouth; o, esophagus; arrows, immunoreactive coelomic cells. Bar, 200 μm. (B) A projection of the anterior ganglion in a late bipinnaria. Parallel axonal-like tracts on the opposing sides of the preoral ciliated band (prcb) and the postoral ciliated bands (pocb) interconnecting in a fine network of processes with 5-HT-like immunoreactivity. axt, axonal-like processes; ncb, nerve cell bodies. Bar, 50 μm.

associated with the preoral and postoral ciliated bands and a network of varicose processes spanning the two bands. This structure innervated the two bands and is a prominent neuroanatomical feature in the bipinnaria of *Patiriella regularis* (Fig. 5B).

Postoral ciliated band

The postoral ciliated band formed a continuous loop traversing the ventral surface adjacent to the mouth and continued laterally along either side of the larva (Figs. 4A, B; 5C). It then extended posteriorly, crossing to the dorsal surface and then extending anteriorly, where it formed part of the AG (Fig. 4A, B). Cells and axonal-like processes with 5-HT-like immunoreactivity occurred along the band (Fig. 5A, C). In the transverse region adjacent to the mouth, a group of immunoreactive ovoid cells were connected by a thin immunopositive tract (Fig. 6C). In general, the immunoreactive cells and processes were more sparsely distributed in the postoral ciliated band than in the other bands (Fig. 6A–C).

Numerous cells of the left and right coelomic pouches exhibited 5-HT-like immunoreactivity (Fig. 5A). These cells were not neuronal in morphology, but they appeared to be exhibiting a general expression for serotonin. Immunoreactive cells were also concentrated around the anal opening (Fig. 7) and were observed in the intestinal epithelium, extending as much as 100 μm towards the stomach. In some instances the entire stomach was immunoreactive, but this was not consistent and may have been due to incorporation of algal pigments (Fig. 7).

Discussion

Serotonergic cells were first seen at the animal pole of the gastrula of *Patiriella regularis.* Similar findings have been reported for other asteroids and echinoids with planktotrophic development (Bisgrove and Burke, 1986; Nakajima, 1988). As the gastrula elongated, these cells formed a hemispherical array at the anterior end of the larva, indicating the onset of migration and rearrangement of these cells. Cell-fate studies would be required to determine cell migration and rearrangement. The neuronal-like cells present in the gastrula included monopolar, bipolar, and tripolar cells. The cell bodies of the monopolar and bipolar neurons appeared to be flask shaped, similar to the cell bodies described for neurons in the bipinnaria larvae of an asteroid (Lacalli *et al.*, 1990). Flask-shaped nerve cells have also been observed in an echinoid pluteus (Bisgrove and Burke, 1986; Bisgrove and Raff, 1989). Burke (1983) noted that nerve cells in the bipinnaria of the asteroid *Pisaster ochraceus* had a fusiform profile. We did not observe any neuron-like cells in *P. regularis* with a similar shape. Three-dimensional reconstructions of the tripolar cells revealed that they were pyramidoid, a structure not previously reported. This observation would, however, be dependent on the imaging

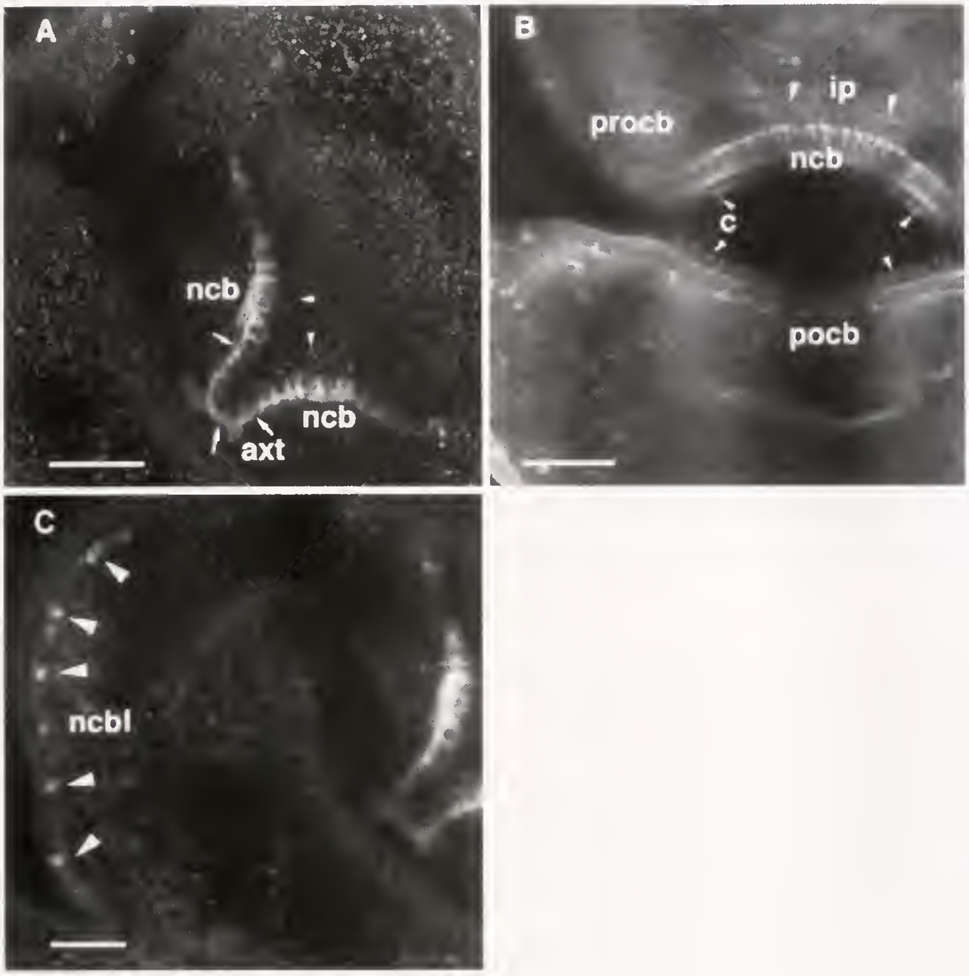

Figure 6. Confocal images detailing immunoreactive cells in ciliated bands. (A) Image from 15 optical sections (total thickness 139 μm) showing nerve cell bodies (ncb) with 5-HT-like immunoreactivity and an axonal-like tract (axt and arrows) in the adoral ciliated band. The entire band is immunoreactive. Note that the apical region of the neuron-like cells extend to the edge of the epithelium of the ciliated band. Arrowheads, cilia projecting into the buccal cavity. Bar, 20 μm. (B) The preoral and postoral ciliated bands of a fully developed bipinnaria. Note the greater number of cells with 5-HT-like immunoreactivity (ncb) present in the preoral ciliated band (procb) compared with the postoral ciliated band (pocb). The preoral ciliated band has immunoreactive processes (ip and lateral arrowheads) extending towards the buccal cavity. c and arrowheads, cilia. Bar, 63 μm. (C) Nerve cell bodies (ncbl and arrowheads) in the right lateral postoral ciliated band. Bar, 50 μm.

technique employed. Monopolar cells were the most common type of immunoreactive cell in the preoral and postoral ciliated bands, whereas multipolar pyramidal cells were the most common cell type in the adoral nerve plexus (ADNP) of the adoral ciliated band.

The presence of the apical projection arising from the cell bodies in the ADNP suggests that this plexus may have a sensory role. This interpretation is similar to that of Komatsu *et al.* (1991), who defined sensory neurons in the bipinnaria of *Luidia senegalensis* as neurons whose apical surface contacts the external environment. Strathmann (1975) demonstrated that the cilia of the adoral ciliated band in bipinnariae are involved in carrying food particles into the esophagus. It is possible that the adoral ciliated band of *P. regularis* plays a gustatorial function under the influence of serotonergic activity in the ADNP.

In the bipinnaria of *P. regularis*, serotonin-like immunoreactivity was conspicuous in the adoral ciliated band, in the preoral and postoral ciliated bands, and in the anterior ganglion. The adoral ciliated band was strongly fluorescent and connected to the preoral ciliated band by an immunoreactive tract. Detection of this connection was possible through generation of 3D anaglyphs from confocal optical sections, which allowed visualization, and tracing of the complex immunostained network with respect to larval anatomy. On-screen animations (Chee and Byrne, 1997) were also employed to view immunolabeled larvae to determine the structure and direction of the immunolabeled

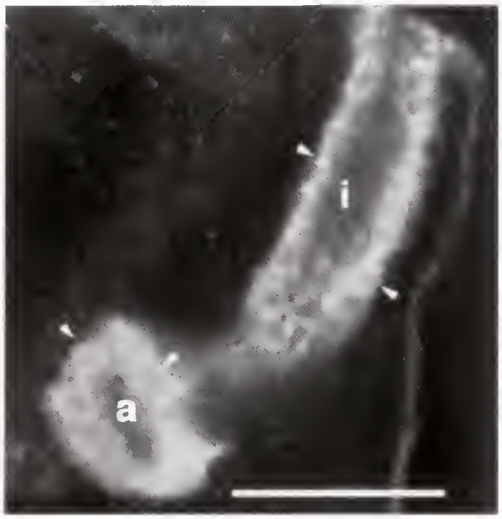

Figure 7. Confocal image showing immunoreactive cells (arrowheads) in the intestinal wall (i) and surrounding the anus (a): Bar, 50 μm.

processes. Although serotonergic immunoreactivity of the adoral ciliated band has been described in several studies (Nakajima, 1988; Moss *et al.,* 1994), the connections between the adoral and preoral ciliated bands have not been seen before. The conventional epifluorescence microscopy used in these earlier studies would not, however, have allowed resolution of this fine structure. Our observations demonstrate the presence of an extensive serotonergic communication network that connects all the ciliated bands and may govern reactions to stimuli and generate the behavioral patterns associated with feeding and swimming.

Optical sections through the oral region revealed that the immunoreactive cells in the preoral ciliated band gave rise to basal immunoreactive processes that project dorsally along the roof of the buccal cavity. The high density of immunoreactive cells in the region of the preoral ciliated band along the buccal opening suggests that these cells may play a sensory role in feeding. Selection and rejection of particles during feeding is thought to be associated with sensory cells in the buccal cavity (Strathmann, 1975). The cell processes in the roof of the buccal cavity in the larvae of *P. regularis* may connect with receptor sites that lie within the buccal cavity and are involved in particle selection in feeding. The 5-HT immunopositive tract connecting the adoral and preoral ciliated bands indicates a serotonergic link between the adoral ciliated band and the preoral ciliated band; this link could be important in feeding.

The anterior ganglion (AG) is first seen in early bipinnaria prior to formation of the anterior extension. As this extension develops, the ganglion becomes more intricate, forming a highly complex network. In advanced bipinnaria the AG consisted of prominent, strongly fluorescent tracts traversing the anterior region of the preoral and postoral ciliated bands. The anterior ganglion was the only serotonergic connection between these ciliated bands.

In contrast to that suggested for sea stars (Lacalli, 1994), the AG of *P. regularis* does not split to form a pair of lateral ganglia. On the contrary, the pair of lateral ganglia occasionally seen in *P. regularis* (Chee and Byrne, 1997) are distinct from the AG. This bilateral collection of nerve cells may be homologous to those seen in other sea star larvae (Nakajima, 1988; Moss *et al.,* 1994), and it also corresponds to the position of peptidergic GFNSALMFamide (S1) ganglia seen in *P. regularis* (Byrne *et al.,* 1999).

At the brachiolaria stage, the AG is incorporated into the attachment complex, which contains many serotonergic neuronal-like cells suggested to be involved in the settlement process (Chee and Byrne, 1999). What appears to be a serotonergic AG has been observed in other echinoderms. Immunocytochemical labeling with anti-serotonin in the auricularia larvae of a holothuroid produced a structure described as an apical ganglion (Burke *et al.,* 1986). Unlike the AG of *P. regularis,* this structure was not composed of many immunoreactive tracts. Serotonergic AG that differ structurally from that of sea stars but are still anterior in position have been extensively described for sea urchin plutei (Bisgrove and Burke, 1987; Bisgrove and Raff, 1989; Nakajima *et al.,* 1993).

The AG in the bipinnaria of *P. regularis* is similar to the anterior concentration of serotonergic neurons, variously called apical organs or apical ganglia, characteristic of many invertebrate larvae (Lacalli, 1994). These appear to be highly conserved structures in marine invertebrate larvae and are thought to have a sensory function (Lacalli, 1994; Marois and Carew, 1997). The function of the AG and the significance of the connection between the preoral and postoral ciliated bands of *P. regularis* are not known. The position of the AG, considered together with the bipinnaria's anterior direction of swimming, suggests that it may have a sensory role in directional swimming; a similar function has been suggested for the apical ganglion of other invertebrate larvae (Marois and Carew, 1997). Moreover, in an ultrastructural study of the bipinnaria of *Luidia senegalensis,* sensory cells were found in the preoral and postoral ciliated bands (Komatsu *et al.,* 1991) in the region where the AG is located in *P. regularis.* Immuno-electron microscopic examination of thin sections from the anterior region of *P. regularis* would be needed to determine whether similar cells are present in this species.

The anterior ganglion in *P. regularis* is also similar to non-serotonergic neuronal structures in other asteroids. Similar catecholaminergic anterior structures in the bipinnaria of *Archaster typicus* were described as a "fluorescent anastomosis" (Chen *et al.,* 1995). Nakajima (1987) described a similar catecholaminergic structure as a "fibrous network" in the bipinnariae of *Asterias amurensis.* We believe that confocal imaging would reveal that these structures are similar to the AG in *P. regularis*.

This study presents the most detailed immunocytochemical description of the development of the serotonergic system in a larval sea star. The organization of the serotonergic nervous system in the bipinnaria of *Patiriella regularis* reflects the bilateral symmetry of the larva. A striking bilateral symmetry is also seen in the S1-like peptidergic system in *P. regularis* (Byrne *et al.*, 1999). For a complete picture of the expression of serotonin in nerve-like cells during development, we will continue this study in the brachiolaria of *P. regularis* through metamorphosis. Interestingly, serotonin has never been localized immunocytochemically in the nervous system of adult sea stars. It appears that complex serotonergic innervation is a feature common to the swimming and feeding larval form across a range of marine invertebrate phyla. Changes in expression of serotonin in the lecithotrophic larvae of the other *Patiriella* species are being examined to document the evolution of neurogenesis in these asteroids.

Acknowledgments

We thank Paulina Selvakumaraswamy, Anna Cerra and Paula Cisternas, and Gillian Anderson for their comments and help with the manuscript. Ray Ritchie kindly supplied the algal cultures. Tony Romeo at the Electron Microscope Unit at the University of Sydney also provided assistance. This work was supported by an Australian Research Council grant.

Literature Cited

Bisgrove, B. W., and R. D. Burke. 1986. Development of serotonergic neurons in embryos of the sea urchin, *Strongylocentrotus purpuratus*. *Dev. Growth Differ.* **28:** 569–574.

Bisgrove, B. W., and R. D. Burke. 1987. Development of the nervous system of the pluteus larvae of *Strongylocentrotus droebachiensis*. *Cell Tissue Res.* **248:** 335–343.

Bisgrove, B. W., and R. A. Raff. 1989. Evolutionary conservation of the larval serotonergic nervous system in a direct developing sea urchin. *Dev. Growth Differ.* **31:** 363–370.

Burke, R. D. 1983a. Development of the larval nervous system of the sand dollar, *Dendraster excentricus*. *Cell Tissue Res.* **229:** 145–154.

Burke, R. D. 1983b. The structure of the larval nervous system of *Pisaster ochraceus* Echinodermata: Asteroidea. *J. Morphol.* **178:** 23–35.

Burke, R. D., D. G. Brand, and B. W. Bisgrove. 1986. Structure of the nervous system of the auricularia larva of *Parasticopus californicus*. *Biol. Bull.* **170:** 450–460.

Byrne, M., and M. F. Barker. 1991. Embryogenesis and larval development of the asteroid *Patiriella regularis* viewed by light and scanning electron microscopy. *Biol. Bull.* **180:** 332–345.

Byrne, M., and A. Cerra. 1996. Evolution of intragonadal development in the diminutive asterinid sea stars *Patiriella vivipara* and *P. parvivipara* with an overview of development in the Asterinidae. *Biol. Bull.* **191:** 17–26.

Byrne, M., F. Chee, P. Cisternas, and M. Thorndyke 1999. Localisation of the neuropeptide S1 in the larval and adult nervous system of the sea star *Patiriella regularis*. Pp. 187–191 in *Echinoderm Research 1998*, M.D. Candia Carneval and F. Bonasoro, eds. Balkema, Rotterdam.

Chee, F., and M. Byrne. 1997. Visualization of the developing serotonergic nervous system in the larvae of the sea star, *Patiriella regularis*, using confocal microscopy and computer generated 3D reconstructions. *Invertebr. Reprod. Dev.* **31:** 151–158.

Chee, F., and M. Byrne. 1999. Serotonin-like immunoreactivity in the brachiolaria larvae of *Patiriella regularis*. *Invertebr. Reprod. Dev.* **36:** 111–115.

Chen, C. P., C. H. Tseng, and B. Y. Chen. 1995. The development of the catecholaminergic nervous system in starfish and sea cucumber larvae. *Zool. Stud.* **34:** 248–256.

Collier, H. O. J. 1958. The occurrence of 5-hydroxytryptamine in nature. Pp. 5–19 in *The Third Symposia on Drug Action*, G. P. Lewis, ed. Pergamon Press, London.

Hart, M. W., M. Byrne, and M. J. Smith. 1997. Molecular phylogenetic analysis of life-history evolution in asterinid starfish. *Evolution* **51:** 1848–1861.

Komatsu, M., F. Chia, and R. Koss. 1991. Sensory neurons in the bipinnaria larvae of the sea star, *Luidia senegalensis*. *Invertebr. Reprod. Dev.* **19:** 203–211.

Lacalli, T. 1994. Apical organs, epithelial domains, and the origin of the chordate central nervous system. *Am. Zool.* **34:** 533–541.

Lacalli, T. C., T. H. J. Gilmour, and J. E. West. 1990. Ciliary band innervation on the bipinnaria larva of *Pisaster ochraceus*. *Philos. Trans. R. Soc. Lond. B. Biol. Sci.* **330:** 371–390.

Marois, R., and T. J. Carew. 1997. Fine structure of the apical ganglion and its serotonergic cells in the larva of *Aplysia californica*. *Biol. Bull.* **192:** 388–398.

Moss, C., R. D. Burke, and M. C. Thorndyke. 1994. Immunocytochemical localization of the neuropeptide S1 and serotonin in larvae of the starfish *Pisaster ochraceus* and *Asterias rubens*. *J. Mar. Biol. Assoc. UK.* **74:** 61–71.

Nakajima, Y. 1987. Localisation of catecholaminergic nerves in larval echinoderms. *Zool. Sci.* **4:** 293–299.

Nakajima, Y. 1988. Serotonergic nerve cells of starfish larvae. Pp. 235–239 in *Echinoderm Biology*, R. D. Burke, P. V. Mladenov, P. Lambert, and R. L. Parsley, eds. Balkema, Rotterdam.

Nakajima, Y., R. D. Burke, and Y. Noda. 1993. The structure and development of the apical ganglion in the sea urchin pluteus larvae of *Strongylocentrotus droebachiensis* and *Mesipilia globulus*. *Dev. Growth Differ.* **35:** 531–538.

Strathmann, R. R. 1975. Larval feeding in echinoderms. *Am. Zool.* **15:** 717–730.

Strathmann, R. R. 1978. The evolution and loss of feeding larval stages of marine invertebrates. *Evolution* **32:** 894–906.

Welsh, J. H., and M. Moorehead. 1960. The quantitative distribution of 5-hydroxytryptamine in the invertebrates, especially in their nervous systems. *J. Neurochem.* **6:** 146–169.

Reference: *Biol. Bull.* **197:** 132–143. (October 1999)

Rapid Jumps and Bioluminescence Elicited by Controlled Hydrodynamic Stimuli in a Mesopelagic Copepod, *Pleuromamma xiphias*

D. K. HARTLINE[1]*, E. J. BUSKEY[2], AND P. H. LENZ[1]

[1] *Békésy Laboratory of Neurobiology, Pacific Biomedical Research Center, University of Hawaii at Manoa, 1993 East-West Rd., Honolulu, Hawaii 96822; and* [2] *Marine Science Institute, University of Texas at Austin, 750 Channelview Drive, Port Aransas, Texas 78373*

Abstract. Actively vertically migrating mesopelagic copepods are preyed upon by a wide variety of fishes and invertebrates. Their responses to predatory attacks include vigorous escape jumps and discharge of bioluminescent material. Escape jumps and bioluminescent discharges in the calanoid copepod *Pleuromamma xiphias* were elicited by quantified hydrodynamic disturbances. Brief weak stimuli (peak water velocity 64 ± 21 μm s^{-1}) elicited weak (peak force 6.5 dynes) propulsive responses ("jumps") and no bioluminescence. Moderate stimuli (1580 ± 780 μm s^{-1}) produced strong propulsive responses consisting of long trains of coordinated power strokes by the four pairs of swimming legs ("kicks"). Peak forces averaged 42 dynes. Strong stimuli (5520 ± 3420 μm s^{-1}) were required to elicit both a jump and a bioluminescent discharge. In several cases, multiple stimuli were needed to evoke bioluminescence, given the limits on stimulus magnitude imposed by the apparatus. Repeated bioluminescent discharges could be evoked, but this responsiveness waned rapidly. Latencies for the jump response (14 ± 4 ms) were shorter than for the accompanying bioluminescent discharge (49 ± 26 ms). The higher threshold for eliciting bioluminescent discharge compared to escape jumps suggests that the copepods save this defense mechanism for what is perceived to be a stronger threat.

Introduction

Planktonic copepods are preyed upon by a wide variety of fishes and invertebrates (Hopkins and Baird, 1985; Hopkins *et al.*, 1996). Thus, predator evasion strategies are key to the survival of these animals in pelagic communities. Planktonic copepods respond to perceived attacks with rapid and powerful escape "jumps" (Singarajah, 1969, 1975; Strickler, 1975). The Augaptiloidea (Calanoida), which typically inhabit the mesopelagic region, possess the ability to discharge bioluminescent material (Clarke *et al.*, 1962; Herring, 1988). These discharges are thought to either startle a potential predator away or misdirect a possible attack (David and Conover, 1961; Morin, 1983; Young, 1983). Although we have a qualitative understanding that bioluminescent discharges in these calanoids are used as a defense mechanism, we know less about how these discharges are triggered in the natural environment. In the laboratory, electrical stimulation and mechanical agitation are routinely used to elicit bioluminescent discharges (*e.g.*, Latz *et al.*, 1987, 1990; Widder, 1992). However, we know little about the magnitude of stimuli required to elicit this behavior. Neither do we understand the relationship between the escape jump and the bioluminescence. We addressed some of these questions in a laboratory study, working with tethered *Pleuromamma xiphias*. This calanoid is a metridinid (Augaptiloidea) and belongs to a widespread and abundant genus in this group. Here we report on the minimum hydrodynamic stimuli necessary to elicit a jump response, and how this compares to the minimum stimulus that triggers bioluminescence. By concurrently monitoring jump behavior with a force transducer and bioluminescence with

Received 13 May 1999; accepted 6 August 1999.

* Author to whom correspondence should be addressed. E-mail: danh@pbrc.hawaii.edu

a photomultiplier tube, we are able to describe the temporal sequences for the two behaviors following a quantitative stimulus.

Materials and Methods

Collection

Animals were collected at night (2000 to 2200 h), about 1 mile offshore from Keauhou Bay, Kona, Island of Hawaii, at a depth of 70 to 100 m. A plankton net (0.5-m diam, 333-μm mesh) was towed from a small boat at idle speeds (<2 knots) for 15 to 20 min. Within 2 h of collection the animals were sorted into jars with clean seawater, cooled to 6°C, and flown, in coolers, to Oahu. Once the animals were brought into the laboratory (within 16 h of collection), they were kept in the dark at 6° to 8°C. Every 2 to 3 days the copepods were fed under dim red light with a mixture of *Artemia* nauplii and *Isochrysis galbana* cells.

Tethering

Copepods were affixed to aluminum wire tethers with cyanoacrylate glue (Borden or Loctite) under red light in an otherwise darkened room. They were corralled in a droplet of seawater, which was then drawn down until a portion of the dorsal prosome was briefly exposed to air. The wire, with some glue on its tip, was applied and held in place while the animal was reimmersed. During this procedure the animals typically bioluminesced in response to the tactile stimulation. Once a copepod was glued and transferred to the experimental setup, 3 h were allowed to elapse before it was tested for mechanical sensitivity. Good experimental animals had high mechanical sensitivity, maintained their swimming appendages in the promoted position (tucked under the body, anteriorly directed), and were bioluminescently competent. In the experiments presented, the animals maintained their mechanical sensitivity for at least 2 days, although the force produced during the jump typically declined. Toward the end of the experiments we observed either a loss in sensitivity or a failure to maintain the swimming appendages in the promoted position. All animals were still bioluminescently competent at the end of the experiments and responded to direct tactile stimulation with a discharge. While on the tether, copepods were fed *Isochrysis galbana*.

Health

To test the bioluminescent competence of *P. xiphias*, five specimens were tested for total mechanically stimulable luminescence (TMSL) using methods described in Buskey and Swift (1990). A single *P. xiphias* was placed in each of five liquid scintillation vials containing 10 ml of filtered seawater. After allowing the copepods to recover for about 2 h from the disturbance of being transferred, we placed a vial inside an integrating sphere (Labsphere, Polane coated) and stimulated bioluminescence by stirring the vial with a battery-powered test-tube stirrer until no additional bioluminescence was detected. Bioluminescence was quantified using a photomultiplier tube (PMT; Hamamatsu R464) and a photon-counting photometer (Hamamatsu C1230). Values for TMSL of *P. xiphias* ranged from 5.3×10^{10} to 5.5×10^{11} photons, with a mean of 2.4×10^{11} photons. These results are similar to previously measured values of TMSL for *P. xiphias* (Buskey and Swift, 1990; Latz *et al.*, 1990) and indicate that our experimental animals were capable of full bioluminescence and were in good physiological condition.

Experimental protocol

The experimental setup is diagrammed in Figure 1 and is described in detail in Lenz and Hartline (1999). After the tethered copepod was positioned in the apparatus, red background lights were turned off, and illumination was switched to infrared light from four Optek OP-293A LEDs emitting 875 ± 20 nm and positioned about 1 cm behind the animal, outside of the field of view of the video camera. Hydrodynamic stimuli were generated using a piezoelectric pusher to control movement of a plastic sphere of either 3- or 5-mm diameter positioned about 3 mm in front of the animal. At maximum amplitude, the experimental sphere was displaced vertically by 40 μm. A behavioral response was elicited at threshold by vertical movements of the larger sphere of less than 0.5 μm. Water displacement at the rostrum, approximately parallel to the long axes of the first antennae, was calculated based on the dipole attenuation expected of near-field laminar water flow (Kalmijn, 1988; Gassie *et al.*, 1993). Although there are some errors and approximations inherent in this indirect approach to determining stimulus magnitude (see Gassie *et al.*, 1993, and Lenz and Hartline, 1999, for detailed discussion), it is widely used in behavioral and physiological studies on hydrodynamic reception in aquatic organisms (*e.g.*, Coombs *et al.*, 1989; Bleckmann, 1994; Coombs, 1994) and provides a reasonable measure given uncertainties in such factors as the location of receptors. Computer-controlled stimuli included short and long sinusoidal movements ranging in frequency from 50 to more than 1000 Hz.

Force measurement

During a rapid swim the copepod exerted a force on the tether. The displacement this produced along a horizontal axis, roughly parallel to the copepod's body axis, was measured with a fiberoptic displacement sensor (Philtec 88N) positioned opposite to a small reflective disk mounted on the tether (Fig. 1). The force was calibrated by pushing

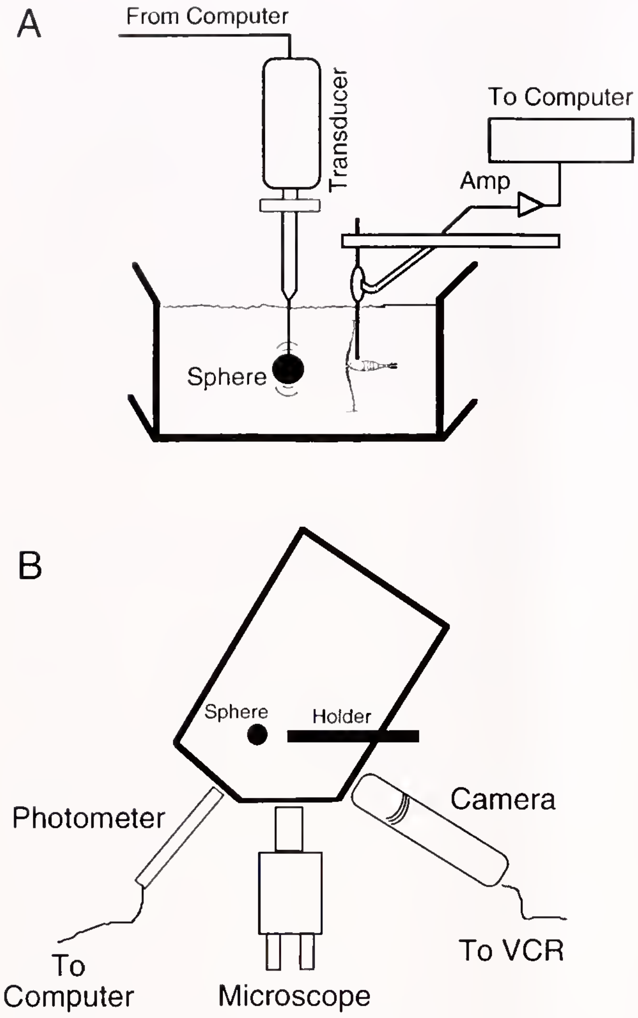

Figure 1. Diagram of the experimental setup. (A) Side view showing the positions of the dipole (sphere) and the glued copepod. The sphere used in the stimulus was either 3 or 5 mm in diameter. The distance between the center of the sphere and the rostrum of the animal ranged from 3 to 5 mm. (B) View from the top. Location of the photometer, dissecting microscope, and camera are shown. The experimental dish was made out of microscope slides and designed to allow positioning of the equipment at right angles to the glass.

against the tether with a wire, the deflection of which had been calibrated using weights. Force-transducer responses were monitored with an oscilloscope, digitized at 42 kHz per channel, and stored on computer. Resonance frequency of the transducer (1.5-2 kHz) was kept as high as possible while maintaining sufficient sensitivity for measurements. The transducer was underdamped, with an overshoot of around 20% to abruptly applied (0.5 ms rise) forces; it had a damping time-constant of 4 ms. Force signals were filtered at 2 kHz with an 8-pole Bessel filter. Further details of the recording system are given in Gassie *et al.* (1993) and Lenz and Hartline (1999).

Optical train

Mounted perpendicular to the view presented in Figure 1A were a photometer, a dissecting microscope, and a video camera (Fig. 1B). Each of these instruments faced one of the five sides of the experimental chamber. Light from the I-R LEDs was blocked from the photometer with an interference filter (center wavelength 480 nm), and background recordings were very low. The spatial and temporal patterns of bioluminescent emission of *P. xiphias* were recorded on videotape using a Cohu monochrome CCD (charge-coupled-device) camera (30 fps) fitted with a 55-mm Micro-NIKKOR macro lens, coupled to a Videoscope International KS-1381 microchannel plate image intensifier. The video output signal was recorded on a Mitsubishi HU-770 videocassette recorder. The stimulus-trigger from the computer also triggered a 30-ms-long flash in an I-R LED, producing a single video frame with an elevated light level. This was used to correlate video with force and PMT records, which thus had an uncertainty of 30 ms. Characteristics of the bioluminescence monitored by the PMT could frequently be used to estimate the relative timing with higher temporal resolution.

Light measurement

The bioluminescent emissions of *P. xiphias* were measured in two ways: with a photomultiplier photometer and with an image intensifier. In early experiments, photometer measurements were made using a Hamamatsu C1230 photon counter and a Hamamatsu R464 PMT. This system was convenient for measuring the total integrated bioluminescence emitted by *P. xiphias*, but it did not provide the temporal resolution necessary to accurately measure flash kinetics since it integrates counts over 0.1-s intervals. It was replaced with a Pacific Instruments model 126 wide-range photometer using an EMI QL-30 PMT. Amplified voltage from the PMT was sent directly to the computer and digitized along with other components of the data stream. Before and after being shipped to Hawaii, both photometer systems were calibrated using cultures of bioluminescent bacteria (*Photobacterium* sp.) and a calibrated Quantalum 2000 luminescence photometer with a highly stable silicon photodiode sensor. A secondary standard (^{14}C emission standard made from Sylvania Type 132 blue phosphor, peak wavelength 455 nm) was also calibrated. The secondary standard was measured frequently to allow for calibration of readings of bioluminescence.

Results

Sudden hydrodynamic disturbances were capable of eliciting behavioral responses in *Pleuromamma xiphias;* we interpret these responses as "rapid swims," or "jumps." In tethered animals, a complex temporal pattern of force development followed closely on the presentation of such a stimulus. Figure 2A shows a typical response to a brief (2-ms) water movement of peak-to-peak amplitude computed at 3.83 μm at the copepod's rostrum. Following a short latency ("L"), there was an abrupt rise ("R") in forward propulsive force. Then a relatively rapid return past zero force to a smaller reverse force ("Rv") led to the development of a second forward component. As in a previous study on the epipelagic copepod *Undinula vulgaris* (Lenz and Hartline, 1999), we interpret these propulsive units to be kicks generated by the combined power strokes of the four pairs of swimming legs (pereiopods). The features of strong locomotor responses in *P. xiphias* were similar in most respects to those of *U. vulgaris* (Lenz and Hartline, 1999). They were characterized by short latencies, measured from the onset of the stimulus to the onset of the forward propulsion, typically around 10 ms (minimum: 6 ms). A weak brief backward propulsion, or "preparatory movement," was observed in some animals immediately preceding the forward propulsion (*e.g.*, Fig. 3A, "Pr"). Following the peak of forward propulsion, there was often an irregular pattern of peaks and valleys for the remainder of the short stroke duration (mean: 8.7 ms, Table I). As in *U. vulgaris* (Lenz and Hartline, 1999) and *Calanus helgolandicus* (Svetlichnyy, 1987), the major peaks can be assigned to the individual strokes of pereiopod pairs. Minor peaks caused by resonance in the underdamped force-transducer system were also often apparent (Fig. 2A "res"). The distinct reverse propulsion following the termination of the forward phase was a feature found consistently in *P. xiphias* but not in previous studies on *U. vulgaris.* A pattern of multiple kicks in quick succession characterized a strong response to a stimulus. This is illustrated in Figure 2B, which shows the same response as Figure 2A on a compressed time scale. In *P. xiphias*, a train of kicks was typical, producing a cohesive propulsive response we term a "jump." Within the train, kicks occurred at repetition rates of 80 Hz (Table I; range 59 to 98 Hz).

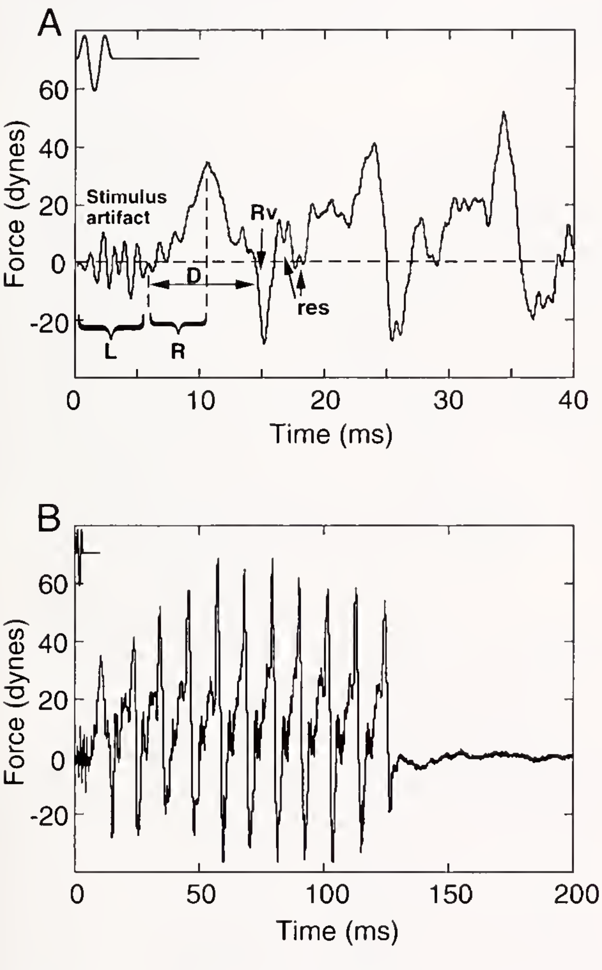

Figure 2. Force record of a fast swim response of a *Pleuromamma xiphias* adult female to a suprathreshold hydrodynamic stimulus. (A) Expanded temporal scale showing the first four kicks of the response. (B) Record showing the complete response to the stimulus. Stimulus: 700 Hz, 1.5 cycles, maximum water velocity of 8400 μm s^{-1} at the rostrum. Piezoelectric transducer: PZL-060; vertical movement of sphere: 40 μm; sphere diameter: 5.1 mm; distance from center of ball to rostrum: 4.4 mm (BPL97-8.D04, second trace).

Response depended on stimulus magnitude

With the experimental setup described, we were able to monitor jumps and bioluminescence simultaneously. As with other copepods we have tested, *P. xiphias* is very sensitive to water movement. Figure 3 shows records from the PMT and the force transducer at three stimulus intensities. We observed several degrees of response, graded with the intensity of the stimulus (Table II). Figure 3A shows a "weak" response given to the lowest intensity of a 1.5-cycle stimulus that elicited a measurable response in this animal. Peak water velocity produced by this stimulus at the rostrum was calculated to be 50 μm s^{-1} (BPL97-10: Table II). Neither the PMT nor the image intensifier recorded any sign of bioluminescence. The force trace shows first one small 12-dyne kick followed by a 100-ms delay and then three additional kicks. The cumulative force impulse generated by these kicks (the integral of force over time; related to total distance moved in a linear viscous medium) reaches only 0.2 dyne-second. In general, a weak response consisted of a brief force transient, which often barely registered on the force transducer (*e.g.*, mean of 6.5 dynes, Table I). These weak responses consisted of a small number of propulsive events (*e.g.*, 1–3) with moderate latencies (15–20 ms). We term them "weak kicks," but determining what is involved in their production awaits high-resolution cinematography. As in Figure 3A, a weak kick was sometimes

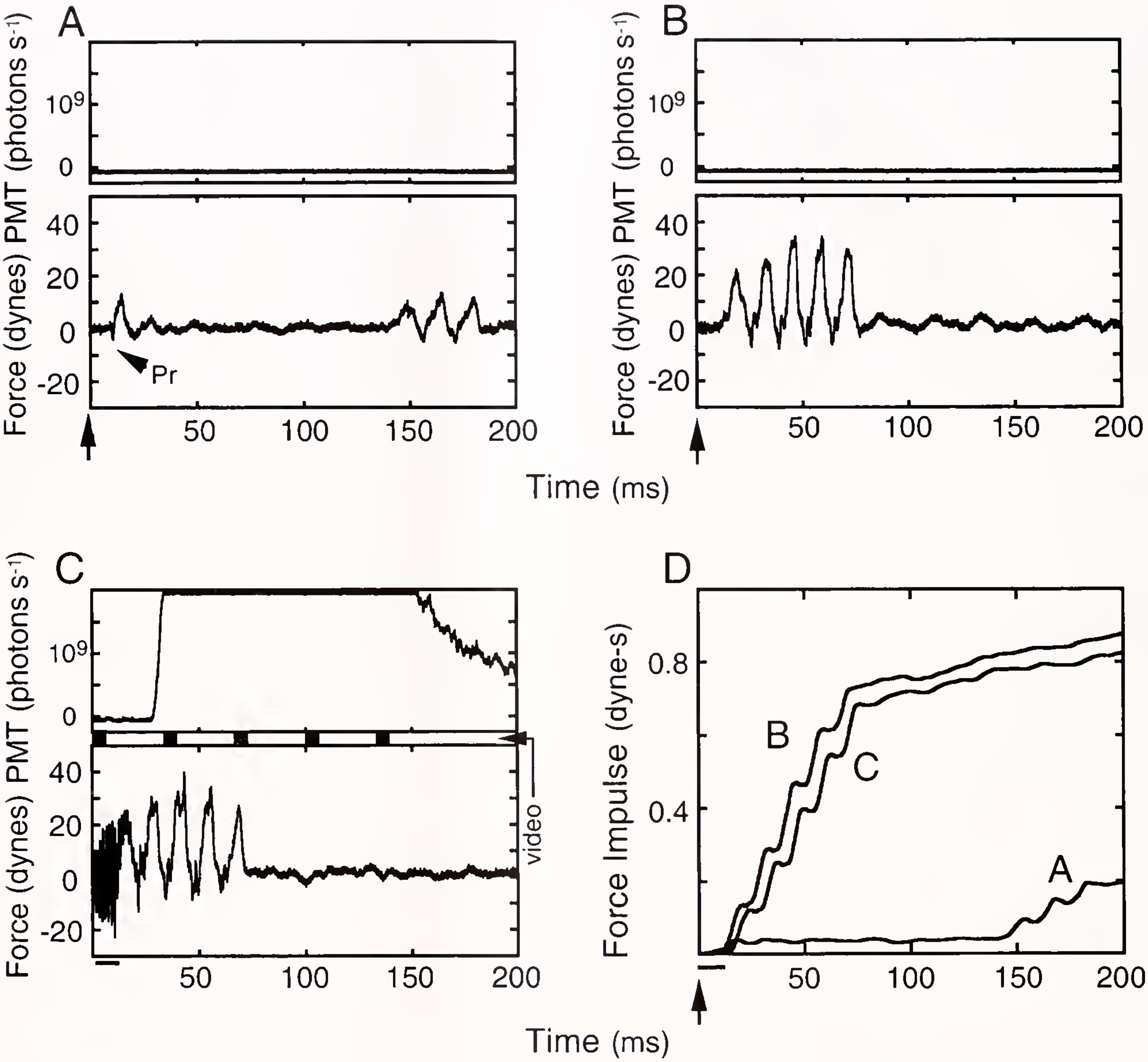

Figure 3. Behavioral responses of a *Pleuromamma xiphias* adult female to three stimulus intensities. Hydrodynamic stimulus was produced by a piezoelectric transducer (PZL-060) with a 5.1-mm sphere, the center of which was located 4.3 mm from the animal's rostrum. (A) Photomultiplier tube (PMT) and force records showing response to a small stimulus: 700 Hz, 1.5 cycles, maximum water velocity of 50 μm s^{-1} at the rostrum (vertical peak-to-peak movement of sphere: 0.22 μm). (B) PMT and force records showing response to a moderate stimulus: 700 Hz, 1.5 cycles, maximum water velocity of 1600 μm s^{-1} at the rostrum (vertical peak-to-peak movement of sphere: 7.1 μm). (C) PMT and force records showing response to a large stimulus: 700 Hz, 8 cycles, maximum water velocity of 8900 μm s^{-1} at rostrum (vertical peak-to-peak movement of sphere: 40 μm). Response is to fourth stimulus in a series of five presented at 1-s intervals (the animal also luminesced to the fifth presentation). Estimated times of video frames shown in Figure 5 indicated with marks along the time axis. (D) Integral of force over time for the force records shown in A, B, and C. Arrows indicate stimulus presentation. Bar in C indicates the length of time the stimulus was on (11.5 ms). Stimulus length in A and B: 2 ms (BPL97-10.D02, D04, D06).

followed by a 50–200 ms period of quiescence and then a cluster of delayed, sometimes stronger, kicks.

As stimulus intensity was progressively increased above the threshold level, a point was passed at which the intensity of the response increased abruptly (Tables I, II). Figure 3B shows force and PMT records for a stimulus intensity that is

Table I

Characteristics of escape response elicited by a hydrodynamic stimulus

Experiment	Sex	Weak kick force (dynes)	Max kick force (dynes)	Latency (ms)	Kick duration (ms)	Kick frequency (Hz)
BPL97-3	M	7.5 ± 1.7 (5)	60.0 ± 6.4 (5)	12.9 ± 9.1 (6)	8.1 ± 1.2 (4)	89 ± 3 (5)
BPL97-6	M	4.7 (1)	24.8 ± 6.8 (5)	11.5 ± 1.0 (6)	6.9 ± 0.6 (5)	98 ± 5 (6)
BPL97-8	F	4.3 (1)	55.9 ± 3.5 (6)	7.4 ± 0.6 (6)	8.5 ± 0.7 (6)	89 ± 5 (6)
BPL97-10	F	10.4 ± 3.2 (8)	36.8 ± 6.8 (19)	11.1 ± 3.3 (16)	11.3 ± 0.8 (8)	75 ± 4 (8)
BPL97-11	F	5.5 ± 1.5 (3)	34.2 ± 6.8 (4)	15.6 ± 1.7 (4)	8.8 ± 2.4 (6)	56 ± 5 (7)

Weak kick forces were measured from escape responses to near-threshold stimuli. Maximum kick force, latency, kick duration, and kick frequency were all measured from responses to suprathreshold stimuli. Maximum kick force refers to the largest force produced in a train of kicks. Latency and kick duration were measured as shown in Figure 2 (L, D). Kick frequency was calculated by averaging the number of kicks over time either for the complete jump or over the data record (200 ms) in the cases where the jumps extended beyond the sampling window. Means and standard deviations are given; sample size (in parentheses) indicates the number of measurements used for the mean and SD.

30 times higher than that shown in Figure 3A. The PMT record shows no sign of bioluminescence. However, many characteristics of the force record are substantially augmented (Fig. 3B). The response typically involved multiple strong kicks with maximum forces produced by individual kicks registering nearly 40 dynes (Fig. 3B). The force impulse produced in the example shown in Figure 3B over a 75-ms interval approached 1 dyne-second (Fig. 3D). In general, such "strong" responses were elicited at stimulus strengths 15 to 30 times above threshold for the weak kicks (Table II). Peak amplitudes (mean = 42 dynes) were greater by a factor of 5 or more than for the weak kicks (Table I). Duration of individual kicks averaged 8.7 ms (Table I). The overall envelope of peak forces during a jump was "spindle" shaped (Fig. 2B). The first few kicks increased progressively in amplitude, then continued with several (sometimes 35 or more) kicks, and finally tapered off somewhat before ending. Figure 4 shows an example of the initial phase of one of these very long spindle-shaped jumps. In a multiple-stimulus protocol, the first or second stimulus of a train of five at 1.5-s intervals usually evoked the longest spindle-shaped jump.

Further increase in stimulus intensity would in some cases result in a bioluminescent discharge. Figure 3C shows

Table II

Calculated water velocities that elicited behavioral responses: weak kicks, strong kicks, and strong kicks and bioluminescent discharges

		Weak kick response		Strong kick response		Jump + biolum response	
Expt	Sex	Stim	Velocity (μm s^{-1})	Stim	Velocity (μm s^{-1})	Stim	Velocity (μm s^{-1})
BPL97-3	M	S700	70	S700	2220	S700	2220
BPL97-6	M	S700	66	S700	1170	S700	6590
BPL97-7	F	ND	ND	ND	ND	S700	8420
BPL97-8	F	S700	84	S700	840	ND	ND
BPL97-9	F	S700	28	S700	890	ND	ND
BPL97-10	F	S700	50	S700	1570	F700	8860
BPL97-11	F	S700	89	S700	2770	F700	8860
BPL97-1	F	F700	58	ND	ND	F700	1830
BPL96-1	M	ND	ND	ND	ND	F700	1830
Mean			64		1580		5520
SD			21		780		3420

Water velocities at the copepod were calculated using dipole equations. Sinusoidal vertical movements of sphere at 700 Hz were either short (S700, 1.5 cycles) or long (F700, 8 cycles). ND = not determined; threshold could not be established.

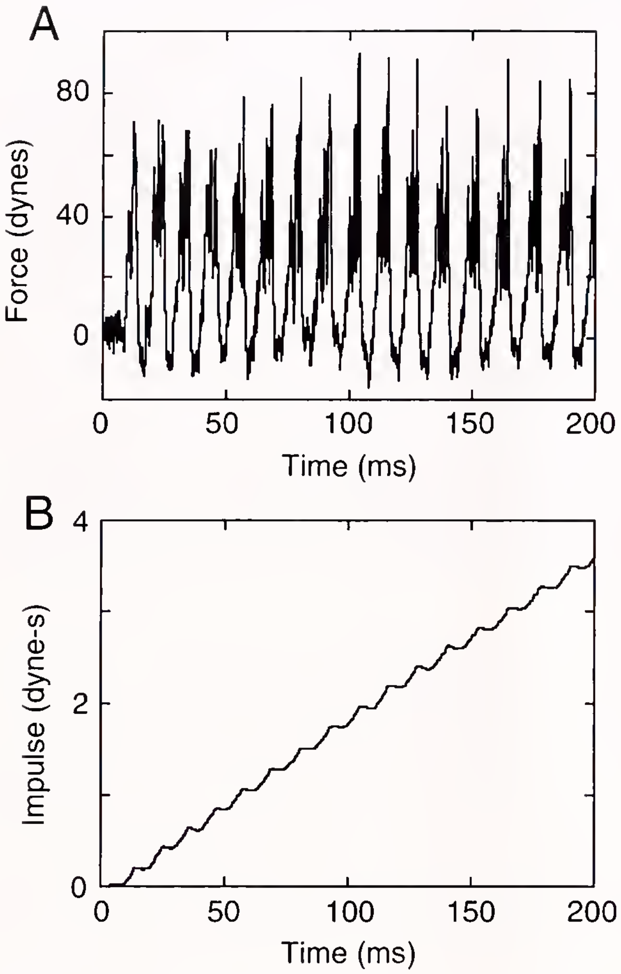

Figure 4. (A) Force record of a long series of multiple kicks in response to a large stimulus in *Pleuromamma xiphias*, adult female. (B) Integral of force over time for the force record shown in A. Stimulus: 700 Hz, 1.5 cycles, maximum water velocity of 8900 μm s^{-1} at rostrum. Piezoelectric transducer: PZL-060; sphere diameter: 5.1 mm; distance from center of ball to rostrum: 4.4 mm; vertical peak-to-peak movement of sphere: 40 μm.

the response of the same animal as in Figures 3A and 3B to a stimulus with an amplitude 180 times greater (and of longer duration) than threshold for eliciting the weak jump. Both a jump and a bioluminescent discharge were produced. The jump response was initiated well before (18 ms) the bioluminescence (Fig. 3C, top panel). The bioluminescent discharge started at the end of the second kick in a train of five and lasted for about 200 ms. The integrated force for the train of kicks was about 0.8 dyne-second (Fig. 3D). Bioluminescence was usually accompanied by strong spindle-shaped jumps. Near threshold for bioluminescence, discharges were likely to be given in response to one of the later stimuli in a sequence of five, and were thus not clearly associated with the strongest (=longest) jump.

We were not able to elicit bioluminescent discharges to hydrodynamic stimuli in all cases. This was not due to a lack of bioluminescent competence, as electrical stimuli or more vigorous mechanical disturbance would invariably elicit bioluminescence even if our strongest hydrodynamic stimulus would not. In five experiments, we obtained thresholds for both jump and bioluminescence, and the mean and standard deviations for the stimulus intensities are shown in Table II. The mean threshold of computed peak water velocity for a jump response was 64 μm s^{-1}, whereas that for eliciting bioluminescence was 5520 μm s^{-1}. The variability of the threshold for bioluminescence was greater than that for the jump. On average the stimulus magnitude had to be 90 times greater to elicit bioluminescent discharge than to produce a weak jump, but this ratio ranged from 30 to 180 in the five experiments. Once we established a threshold for bioluminescence for an experimental animal, we usually were able to elicit bioluminescence multiple times at that stimulus level, sometimes within half an hour from the previous discharge.

Water velocity was not the only stimulus characteristic that affected the likelihood of a bioluminescent discharge, as shown in Table II. Stimulus length was important: the multi-cycle sinusoidal stimulus (F700) was more effective than the 1.5-cycle one (S700; Table II). Furthermore, repeated presentation of stimuli in quick succession was even more effective. In these cases, the animals would respond with only a jump to the first and second stimulus presentations, but would bioluminesce as well as jump to the subsequent one or two stimuli.

Characteristics of evoked bioluminescence

In our tethered animals, bioluminescence typically (though not always) outlasted the jump. The PMT record in Figure 3C shows that bioluminescence was initiated at about 30 ms post-stimulus, corresponding to the second kick. It lasted throughout the recording period, although by 200 ms post-stimulus it was well along an exponential decay. Excerpts from the corresponding video record are shown in Figure 5. Taken at 30 frames per second (fps), with the frame following stimulus delivery tagged by a light flash, the first frame shows no bioluminescence and the onset of the major kick transients occur in this interval. Bioluminescence begins to appear from the region of the abdomen in the next frame, and reaches a peak in the third. Its near-absence from the last two frames is partly a result of decay and partly that much of the material has left the field of view. Thirty-five minutes later a second trial for the same animal as in Figures 3 and 5 elicited an escape as well as a bioluminescent discharge from both head and abdomen (Fig. 6). The animal bioluminesced in response to the sec-

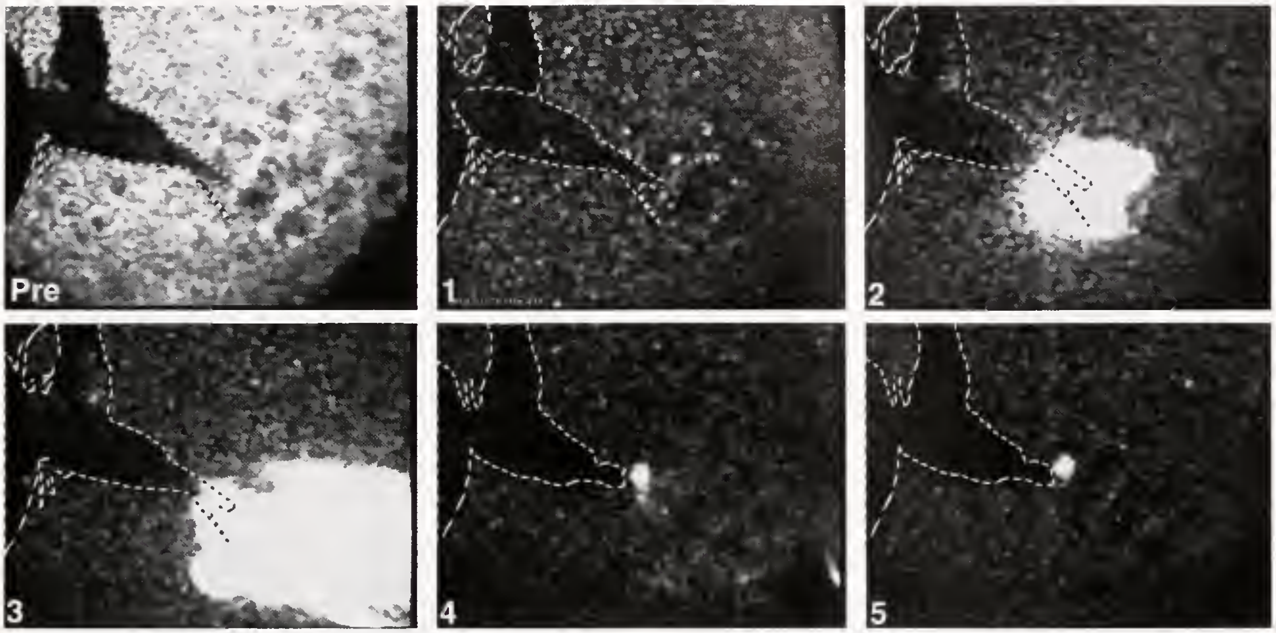

Figure 5. Video frames showing the bioluminescent discharge associated with the records in Figure 3C. The pre-stimulus frame is a composite of the 10 frames preceding stimulus presentation. The next five video stills are from frames 3–7, counting the first post-stimulus frame as 1 (30 fps). Ventral-posterior aspect of animal faces camera. Discharge is primarily from abdominal glands. Broken outlines up to frame 3 indicate position of body prior to stimulation.

ond stimulus of a train of five. It was somewhat more delayed (50-ms latency) and shorter (100-ms duration) than the earlier response (peak amplitude could not be measured owing to saturation of the PMT), but the jump was twice the length (10 kicks *versus* 5).

Records of jumps and bioluminescent discharges from a male *Pleuromamma xiphias* are shown in Figure 7. In this case the animal completed its jump before the bioluminescence. This example was chosen to illustrate a double reaction. The animal responded with two sets of kicks and matching bioluminescent discharges. The discharges were small and short in duration. The animals routinely push the bolus of bioluminescence away from them by flicking their urosomes. This can be seen in Figure 7 as the streaks of bioluminescence move across the screen. The force generated by this behavior is very small compared to the pereiopod power strokes and does not register on the force record.

Comparing this record with the data from the female of Figures 3, 5, and 6 shows the differences that occur when the pereiopods beat during emission of bioluminescent material. The combined kicking and bioluminescence produce the explosion of bioluminescence seen in the video frames. This is in contrast to the male (Fig. 7), in which the luminescent material clung to the urosome, presenting a streaky appearance.

Temporal relations between jump and bioluminescence

The rapid swim was always initiated before the bioluminescence, as illustrated in Figure 8, a scatter plot of jump latencies *versus* bioluminescence latencies. All points are above the line with a slope of one. Rapid swims were initiated within 7 to 20 ms (mean ± SD = 14 ± 4 ms), whereas bioluminescence latencies ranged from 20 to 50 ms (with one very delayed response that started at 110 ms; mean ± SD = 49 ± 26 ms). In general, the longer the rapid swim latency the greater the delay for the bioluminescence, although the correlation coefficient was not significant ($r = 0.508$, $n = 8$). Bioluminescent discharges in response to the hydrodynamic stimulus were typically short, lasting from 50 to 350 ms. Luminescence often (*e.g.*, Figs. 3C; 7), but not always (Fig. 6), extended well after the termination of the jump.

Discussion

Escape jumps

Like all pelagic calanoids, mesopelagic *Pleuromamma xiphias* has an impressive escape jump at its disposal. When sensitivity to water perturbations and jump kinematics measured in tethered animals are compared to similar data for neritic *Undinula vulgaris* (Lenz and Hartline, 1999), a pat-

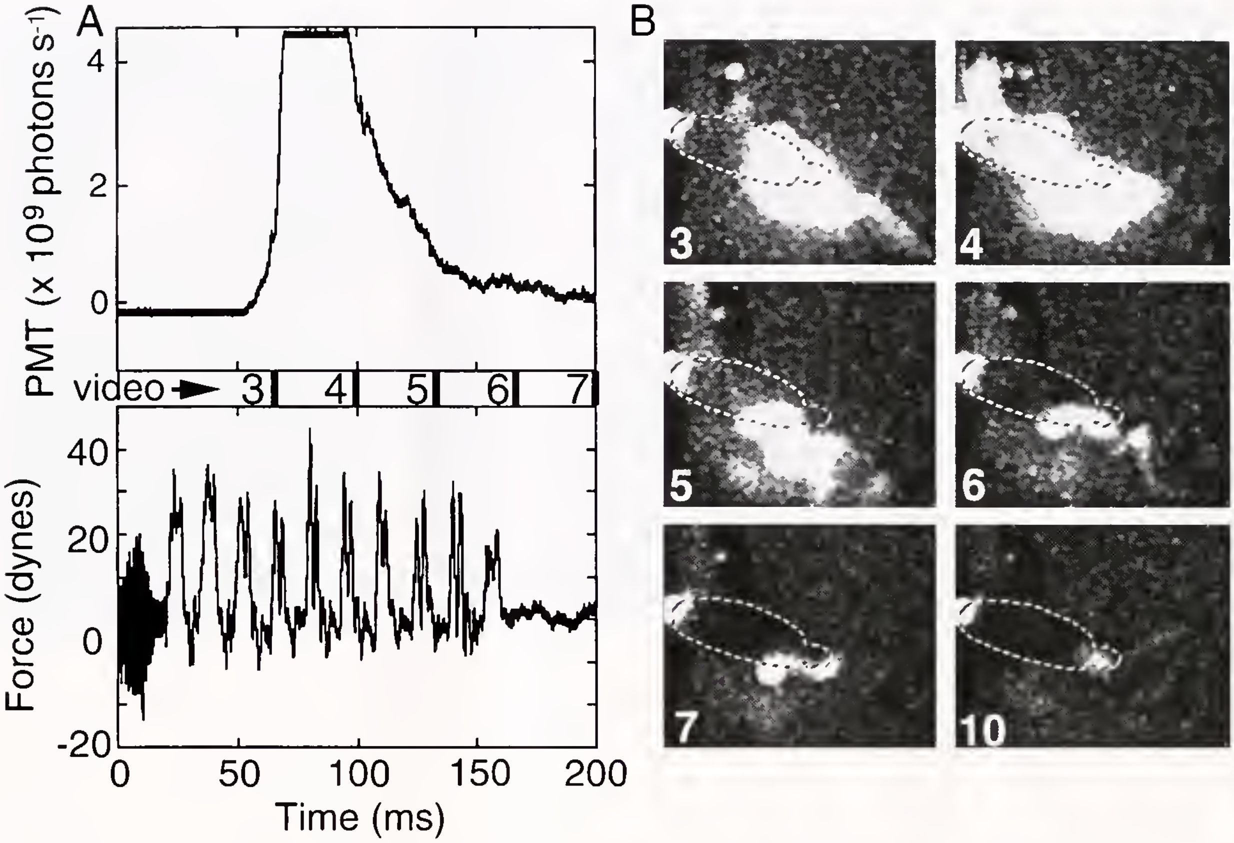

Figure 6. (A) Force record of a second response from the animal in Figures 3 and 5. Comparison shows variability in propulsion and bioluminescence. Note the greater duration of the jump and the shorter duration of the bioluminescent discharge. Stimulus: second in a train of five identical to that for Figures 3 and 5, delivered 35 min following. (B) Video frames 3–7 and 10 following stimulus, showing bioluminescent discharge associated with records of A (30 fps). Broken outline indicates position of body prior to stimulation. Note luminescent discharge from cephalic gland.

tern of characteristics emerges that is similar in broad scope but distinctive in detail. *P. xiphias* sensitivities (~60 μm s^{-1}) are similar to, though perhaps somewhat lower than, those in *U. vulgaris* (~40 μm s^{-1}). Minimum latencies for *P. xiphias* (~6 ms) were distinctly longer than for *U. vulgaris* (~2 ms). This difference in reaction times is in part explained by the lack of myelination of nerve fibers in the Augaptiloidea (Davis *et al.*, 1999). Peak forces of kicks from *U. vulgaris* showed a small gradation in magnitude as a function of the strength of the triggering stimulus and over the course of an escape jump. In contrast, those of *P. xiphias* exhibited a much wider range, with a 5- to 10-fold difference between the weak kicks produced to near-threshold stimuli and the strongest kicks in the middle of a spindle-shaped jump. The strongest kicks registered in our apparatus by *U. vulgaris* (100 dynes) were almost twice the peak forces measured from *P. xiphias* (Table 1). In *U. vulgaris*, the initial one or two kicks were the strongest, whereas in *P. xiphias*, the strength of kick built up over several cycles, and then waned, giving rise to the spindle-shaped envelope. Although both species produced multiple kicks in response to threshold and well supra-threshold stimuli, *U. vulgaris* consistently produced fewer (2–3 typical; up to 9) than did *P. xiphias* (5–10 typical; up to 35). For comparably sized animals, this should result in longer jump distances in the latter species. This expectation is in agreement with casual observations made while attempting to catch *P. xiphias* in an open vessel: jumps of tens of centimeters are not atypical, while those of *U. vulgaris* are shorter (3 to 5 cm).

Bioluminescent discharges can be evoked by hydrodynamic stimuli

Pleuromamma xiphias will produce a bioluminescent discharge to a brief water disturbance; tactile stimulation is not

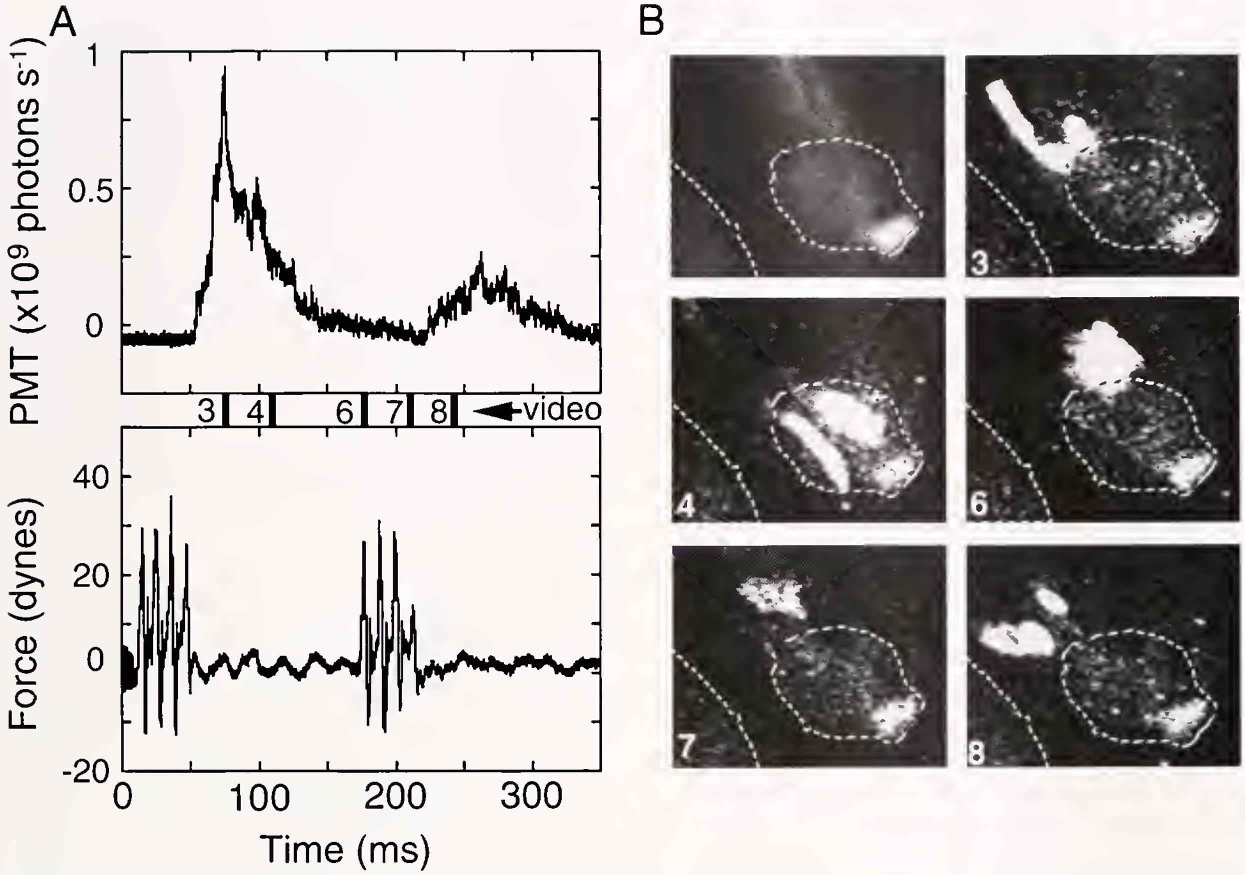

Figure 7. Response of *Pleuromamma xiphias* adult male to a large hydrodynamic stimulus. (A) PMT and force records. (B) Video frames of bioluminescent discharge. The pre-stimulus frame is a composite of 10 frames preceding stimulus presentation. The next five video stills are post-stimulus frames 3–8. Approximate times of frames are indicated with marks along time axis of A. Note the occurrence of two jumps and two separate bioluminescent discharges, spaced 150 ms apart. Stimulus: 700 Hz, 1.5 cycles, maximum water velocity of 6600 μm s^{-1} at rostrum. Piezoelectric transducer: PZL-060; sphere diameter: 5.1 mm; distance from center of ball to rostrum: 4.8 mm, vertical peak-to-peak movement of sphere: 40 μm. Broken outlines indicate position of body prior to stimulation and a portion of the stimulating sphere in lower left corner; posterior view of animal with dorsal toward lower right corner of frames. Glowing material appears associated with abdominal glands (BPL97-6.D03).

required. The magnitude of the stimulus required varied among experimental animals, but in general was significantly greater than that sufficient to trigger strong escape jumps (velocities of 2000 to 9000 μm s^{-1}). When presented with a threat, *P. xiphias* preferentially responds with an escape jump. However, if the threat is prolonged or persists as in the case of repetitive strong stimulation, then the jump is more likely to be accompanied by a bioluminescent discharge. Widder (1992) found a similar pattern for *Gaussia princeps*. During a train of electrical stimulation (3 s^{-1}) *G. princeps* would respond with an escape alone until the fifth stimulus, when it finally produced a bioluminescent discharge as well.

Bioluminescence is delayed compared to the jump

Bioluminescence was always initiated after the onset of a jump sequence. Although the numbers of animals tested were insufficient for complete reliability, in two animals of our study (both males), jumps were completed before the bioluminescence began. In four others (all females), the bioluminescent discharge commenced during the train of kicks. This resulted in a qualitative difference in the visual effect of the bioluminescence, the luminescent bolus being swept along by water propelled posteriorly by the power strokes. An animal that bioluminesces after it has stopped swimming would seem more likely to become a victim of a predatory attack if the luminescent bolus attracts a predator.

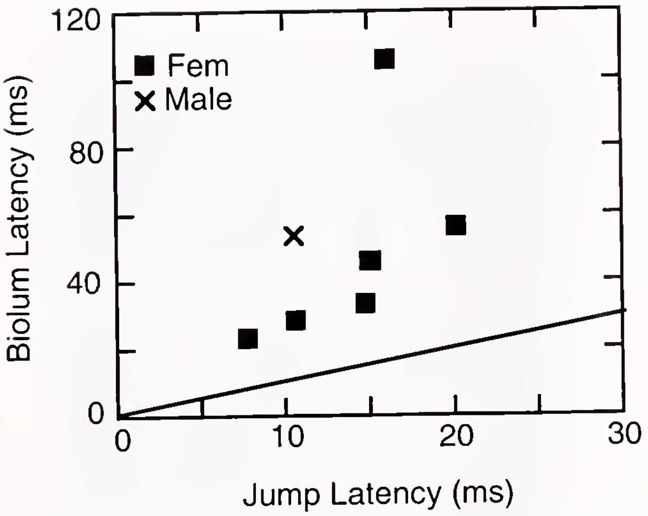

Figure 8. Scatter plot of fast swim latencies (x axis) *versus* bioluminescence latencies (y axis). Squares: adult females ($n = 7$); crosses: adult male ($n = 1$). All points lie above the line, which has a slope of one.

The possibility that there might be a sexual difference in the response patterns is intriguing.

Characteristics of bioluminescence and its relation to other cases reported in the literature

The kinetics and spatial patterns of bioluminescence released by copepods have been studied for copepods stimulated with electrical pulses (Latz *et al.*, 1987; Bowlby and Case, 1991) and for copepods stimulated by mechanical disturbance of undefined frequency and intensity (Latz *et al.*, 1990). For the large mesopelagic copepod *Gaussia princeps*, Bowlby and Case (1991) identified three types of flash in response to single electrical stimuli: a fast flash of about 2-s duration, a long flash of 7-s duration, and a slow flash of 17-s duration. Latz *et al.* (1987) found two components to flashes in *P. xiphias* stimulated with a single electrical pulse: a fast component that reached maximum intensity in < 100 ms and a slow component that reached peak intensity in > 600 ms. Double flashes with fast and slow characteristics were also observed. Using an intensified video system, he observed that the fast component originated from thoracic and abdominal glands, without obvious discharge of bioluminescent material away from the body; the slow component of flashes was caused by the discharge of luminescent fluid from the abdominal organ. Flashes with similar kinetics were observed for *P. xiphias* exposed to mechanical stimulation from a stirring paddle with three tines rotated at 2000 rpm for < 1 s. Since the spatial relationship between the copepod and the rotating tines is unknown during the stimulation period, neither the frequency nor the intensity of mechanical stimulation is known. In addition to strong hydrodynamic stimulation caused by the velocity of the water and the shear created by the spinning tines, mechanical stimulation is possible through direct contact of the copepods with the tines or by contact with the walls of the scintillation vial following an escape jump. In our observations of bioluminescence evoked by hydrodynamic stimuli of known intensity, only fast flashes were observed. In contrast to the observations of Latz *et al.* (1990), we observed bioluminescence having fast flash kinetics originating from abdominal glands, and with obvious discharge of bioluminescent material away from the body. We have noted that a copepod's ability to produce a second bioluminescent discharge shortly after a previous one is not necessarily precluded. Thus recovery times measured in TMSL protocols (8–24 h) are probably overly long for most natural situations.

Ecological significance

Vertically migrating copepods such as *Pleuromamma xiphias* are important components of mesopelagic food webs, and *Pleuromamma* spp. are often preferred prey of mesopelagic fish (Hopkins and Baird, 1985; Hopkins *et al.*, 1996). To help them avoid predation, these copepods have evolved several defensive behaviors, including vertical migration (Bennett and Hopkins, 1989), strong escape jumps (Buskey *et al.*, 1987; present study), and bioluminescence (Clarke *et al.*, 1962). In contrast to the diversity of strategies possessed by *P. xiphias*, neritic *Undinula vulgaris* appears to have relied on enhancing the speed and strength of the escape response itself as a survival mechanism (Davis *et al.*, 1999; Lenz and Hartline, 1999). The production of light in an otherwise dark environment may at first seem counterintuitive as a defense mechanism against visual predators; discharge of bioluminescence while the predator is still remote might help the predator locate its prey. However, the higher stimulus threshold for eliciting bioluminescence compared to escape jumps suggests that copepods save this defense for what are perceived to be the strongest threats by predators in close proximity. Mesopelagic predators have sensitive eyes adapted to low light levels, and the discharge of bioluminescence when the predator is nearby may serve to temporarily blind and confuse the predator (Buck, 1978; Morin, 1983). Since copepods initiate escape jumps prior to release of bioluminescence, and leave behind distinct droplets or clouds of bioluminescent material (Widder, 1992), the bioluminescent discharge may also serve as a decoy to confuse visual predators (Morin, 1983).

Acknowledgments

We thank P. Couvillon, B. Kodama, and S. Lum for major alterations to the experiment room; C. Kosaki for administrative assistance; H. Akaka and A. Davis for technical assistance; C. Unabia for providing the algal cultures; and P. Cunningham for making the copepod collections possible. The Natural Energy Laboratory of Hawaii provided access to the laboratory facilities at Keahole Point, Hawaii. This is University of Texas Marine Science Institute Contribution number 1118. The research was supported by NSF grant OCE 95-21375.

Literature Cited

Bennett, J. L., and T. L. Hopkins. 1989. Aspects of the ecology of the calanoid copepod genus *Pleuromamma* in the eastern Gulf of Mexico. *Contrib. Mar. Sci.* **31:** 119–136.

Bleckmann, H. 1994. *Reception of Hydrodynamic Stimuli in Aquatic and Semiaquatic Animals.* G. Fischer, New York, 115 pp. (*Progress in Zoology* vol. **41**).

Bowlby, M. R., and J. F. Case. 1991. Flash kinetics and spatial patterns of bioluminescence in the copepod *Gaussia princeps. Mar. Biol.* **110:** 329–336.

Buck, J. B. 1978. Functions and evolutions of bioluminescence. Pp. 419–460 in *Bioluminescence in Action,* P. J. Herring, ed. Academic Press, New York.

Buskey, E. J., and E. Swift. 1990. An encounter model to predict natural bioluminescence. *Limnol. Oceanogr.* **35:** 1469–1485.

Buskey, E. J., C. G. Mann, and E. Swift. 1987. Photophobic responses of calanoid copepods: possible adaptive value. *J. Plankton Res.* **9:** 857–870.

Clarke, G. L., R. J. Conover, C. N. David, and J. A. C. Nicol. 1962. Comparative studies of luminescence in copepods and other pelagic marine animals. *J. Mar. Biol. Assoc. UK* **42:** 541–564.

Coombs, S. 1994. Nearfield detection of dipole sources by the goldfish (*Carassius auratus*) and the mottled sculpin (*Cottus bairdi*). *J. Exp. Biol.* **190:** 109–129.

Coombs, S., R. R. Fay, and J. Janssen. 1989. Hot-film anemometry for measuring lateral line stimuli. *J. Acoust. Soc. Am.* **85:** 2185–2193.

David, C. N., and R. J. Conover. 1961. Preliminary investigation on the physiology and ecology of luminescence in the copepod *Metridia lucens. Biol. Bull.* **121:** 92–107.

Davis, A. D., T. M. Weatherby, D. K. Hartline, and P. H. Lenz. 1999. Myelin-like sheaths in copepod axons. *Nature* **398:** 571.

Gassie, D. V., P. H. Lenz, J. Yen, and D. K. Hartline. 1993. Mechanoreception in zooplankton first antennae: electrophysiological techniques. *Bull. Mar. Sci.* **53:** 96–105.

Herring, P. J. 1988. Copepod luminescence. *Hydrobiologia* **167/168:** 183–195.

Hopkins, T. L., and R. C. Baird. 1985. Aspects of the trophic ecology of the mesopelagic fish *Lampanyctus alatus* (Family Myctophidae) in the eastern Gulf of Mexico. *Biol. Oceanogr.* **3:** 285–313.

Hopkins, T. L., T. T. Sutton, and T. M. Lancroft. 1996. The trophic structure and predation impact of a low latitude midwater fish assemblage. *Prog. Oceanogr.* **38:** 205–239.

Kalmijn, A. J. 1988. Hydrodynamic and acoustic field detection. Pp. 83–130 in *Sensory Biology of Aquatic Animals,* J. Atema, R. R. Fay, A. N. Popper, and W. N. Tavolga, eds. Springer Verlag, New York.

Latz, M. R., T. M. Frank, M. R. Bowlby, E. A. Widder, and J. F. Case. 1987. Variability in flash characteristics of a bioluminescent copepod. *Biol. Bull.* **173:** 489–503.

Latz, M. R., M. R. Bowlby, and J. F. Case. 1990. Recovery and stimulation of copepod bioluminescence. *J. Exp. Mar. Biol. Ecol.* **136:** 1–22.

Lenz, P. H., and D. K. Hartline. 1999. Reaction times and force production during escape behavior of a calanoid copepod, *Undinula vulgaris. Mar. Biol.* **133:** 249–258.

Morin, J. G. 1983. Coastal bioluminescence: patterns and functions. *Bull. Mar. Sci.* **33:** 787–817.

Singarajah, K. V. 1969. Escape reactions of zooplankton: avoidance of a pursuing siphon tube. *J. Exp. Mar. Biol. Ecol.* **3:** 171–178.

Singarajah, K. V. 1975. Escape reactions of zooplankton: effects of light and turbulence. *J. Mar. Biol. Assoc. UK* **55:** 627–639.

Strickler, J. R. 1975. Swimming of planktonic *Cyclops* species (Copepoda, Crustacea): pattern, movements and their control. Pp. 599–613 in *Swimming and Flying in Nature, Vol. 2,* T. Y.-T. Wu, C. J. Brokaw, and C. Brennan, eds. Plenum Press, New York.

Svetlichnyy, L. S. 1987. Speed, force and energy expenditure in the movement of copepods. *Oceanology* **27:** 497–502.

Widder, E. A. 1992. Mixed light imaging system for recording bioluminescence behaviours. *J. Mar. Biol. Assoc. UK* **72:** 131–138.

Young, R. E. 1983. Oceanic bioluminescence: an overview of general functions. *Bull. Mar. Sci.* **33:** 829–845.

Reference: *Biol. Bull.* **197:** 144–158. (October 1999)

Morphology of the Nervous System of the Barnacle Cypris Larva (*Balanus amphitrite* Darwin) Revealed by Light and Electron Microscopy

PAUL J. H. HARRISON* AND DAVID C. SANDEMAN

School of Biological Science, University of New South Wales, Sydney, Australia 2052

Abstract. The central nervous system of the cypris larva of *Balanus amphitrite* consists of a brain and posterior ganglion. The neuropil of the brain includes protocerebral and deutocerebral divisions, with nerve roots from the protocerebrum extending to the eyes and frontal filaments, and nerve roots from the deutocerebrum extending to the first antennae (antennules) and cement glands. The neuropil of the posterior ganglion includes subesophageal and thoracic divisions, with nerve roots from subesophageal divisions extending to the gut, and nerve roots from each of the six thoracic divisions extending to their corresponding thoracic appendage. The antennular nerve is the major peripheral extension of the nervous system and is composed in part by afferent fibers that innervate setae on the antennules. The cyprid nervous system is small, containing fewer than 2000 neurons, but is well organized for coordinating a response to settlement cues.

Introduction

The cyprid (cypris larva) is the final larval stage of the barnacle. Cyprids are specialized for settlement (Anderson, 1994), a behavioral process in which a site is selected for permanent attachment and metamorphosis (Anderson, 1994; Walker, 1995). Cyprid settlement is known to be mediated by specific environmental cues (Clare, 1995; Walker, 1995), but little is known about the mechanisms of cue detection and, in particular, how the detection of cues results in the centrally coordinated motor patterns of settlement behavior.

Cyprids are highly mobile and bear numerous sense organs (Walley, 1969). The nauplius eye (= median eye) is present during the cyprid stage and is remodeled into the adult ocelli during metamorphosis (Takenaka *et al.*, 1993). A pair of compound eyes are also present, which are unique to the cyprid. These develop during the final naupliar stage and are lost during metamorphosis (Walley, 1969; Hallberg and Elofsson, 1983). The compound eyes are closely associated with a pair of frontal filaments (Walker, 1974), and many setae are located on the antennules (Nott and Foster, 1969; Nott, 1969; Clare and Nott, 1994; Glenner and Høeg, 1995), thoracic appendages (Glenner and Høeg, 1995), caudal rami (Walker and Lee, 1976; Glenner and Høeg, 1995), and carapace valves (Walker and Lee, 1976; Jensen *et al.*, 1994; Glenner and Høeg, 1995). Many of these setae are thought to function as mechano- and chemoreceptors. Putative sensory structures located on the carapace include dermal pits, wheel organs (Elfimov, 1995), and lattice organs (Jensen *et al.*, 1994; Høeg *et al.*, 1998). Recently, cilia-type dendritic segments were shown to innervate the lattice organs, suggesting a chemosensory function (Høeg *et al.*, 1998).

To date, morphological studies of the cyprid have focused primarily on external structures (Elfimov, 1995), and particularly on the antennules because of the role played by these appendages during settlement (Nott and Foster, 1969; Nott, 1969; Moyse *et al.*, 1995). Fewer details are available on the internal organization of the cyprid. Walley (1969) described the larval development of *Semibalanus balanoides* (previously *Balanus balanoides*) and outlined the nervous system and major sense organs of both the cyprid and nauplius. Other studies have shown that the antennules (Nott and Foster, 1969), frontal filaments (Kauri, 1961; Walker, 1974), dermal pits (Walker and Lee, 1976), lattice organs (Høeg *et al.*, 1998), and cement glands (Walker, 1971; Okano *et al.*, 1996) are innervated, but the nerves

Received 22 March 1999; accepted 27 July 1999.

* Current address: Department of Biology, Georgia State University, PO Box 4010, Atlanta, Georgia 30302.

associated with each of these structures have not been traced back to the central nervous system.

The cyprid is well equipped to detect settlement cues, but little is known about the underlying role of the nervous system. Recent studies have suggested that cyprid settlement behavior is affected by exposing cyprids to certain neuroactive substances (Clare *et al.*, 1995; Kon *et al.*, 1995; Yamamoto *et al.*, 1995, 1996; Okano *et al.*, 1996, 1998). Studies aimed at investigating the underlying mechanisms of settlement would benefit from a detailed account of the cyprid nervous system. We report here the results of an anatomical study of the central nervous system and the major sense organs of the cypris larva of *B. amphitrite*, gained from microdissection, semithin serial sections, and electron microscopy. We find that the central nervous system is made up of about 2000 neurons and that it contains regionalized neuropils, many of which are linked to peripheral sense organs. Although the cyprid nervous system is small, it is well organized, which is consistent with the cyprids' need to detect and respond to multiple cues for settlement.

Materials and Methods

Cyprids used in this study were obtained from a laboratory culture of *Balanus amphitrite* (see DeNys *et al.*, 1995). The selected individuals were between 1 and 3 days old (nauplius-cyprid molt = day 0), were active, and had clear (*i.e.*, non-milky) carapaces, obvious cement glands, and compound eyes. Dissection of the animals provided a useful overview of their structure, including the placement of the antennules and limbs within the bivalved carapace and the gross organization of internal organs. Specimens were placed on a stereomicroscope and dissected using tungsten microscalpels and pins (Conrad *et al.*, 1993). Individuals were placed in a calcium-free saline (in mmol · l^{-1}, 485 NaCl, 13 KCl, 10 MgCl$_2$, 10 HEPES, pH 7.4) to reduce movement and secured (ventral surface upward) to a silicon-coated microscope slide using either tungsten pins or a nontoxic, rapid-setting silicon adhesive (Kwik-Sil, World Precision Instruments). A cut along the ventral midline allowed separation of the carapace valves to expose the central nervous system and internal organs of the cephalon (see Figs. 1, 2). The carapace valves, antennules, and thoracic appendages were then secured with fine (<10 µm diameter) tungsten pins. The secured preparation was transferred to a fixed-stage Olympus BH-2 microscope and viewed and photographed using water immersion objectives.

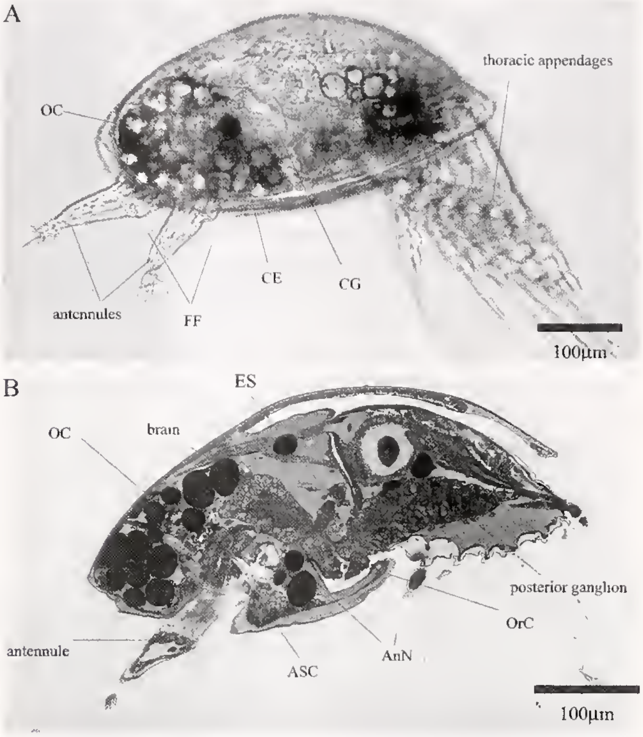

Figure 1. The cypris larva of *Balanus amphitrite*. (A) Light micrograph of a live cyprid with antennules and thoracic appendages extending from the bivalved carapace. Internal structures visible include a compound eye (CE), translucent oil cells (OC), and a cement gland (CG). Frontal filaments (FF) extend posterior to each antennule. (B) Longitudinal section of the cyprid showing the central nervous system, which consists of a brain and posterior ganglion. The brain connects *via* paired circumesophageal connectives (not visible in this section) to the posterior ganglion. A single antennular nerve (AnN) and its associated antennular soma cluster (ASC) are visible. The ASC contains the somata of bipolar sensory neurons. Also apparent in this section are densely stained oil cells, the oral cone, esophagus, and gut. The compound eyes and cement glands are located lateral to this plane and are not seen (0.5 µm section; stained with toluidine blue and osmium tetroxide).

Fixation and embedding. Larvae were placed in equal volumes of 0.4 *M* MgCl$_2$ and 0.22 µm-filtered seawater (FSW) and gently agitated for up to 3 h, which had the effect of relaxing the carapace adductor muscles and exposing the antennules. Specimens were cooled to 4°C for 30 min, transferred to chilled (4°C) fixative consisting of 2.5% glutaraldehyde and 2.0% formalin in FSW (pH 8.2; 950 mosmol). The formalin used was prepared fresh from paraformaldehyde (37% w/v paraformaldehyde in H$_2$O). Microwave treatment was used to facilitate the penetration of fixative. For microwave fixation, specimens were placed in 20-ml glass vials filled with chilled fixative; the vials were secured in a beaker filled with chilled water, which in turn was placed in a beaker of crushed ice. Microwave treatment continued until the water in the beaker reached a temperature of 37°C (typically 50 s). Specimens were then removed from the oven and allowed to cool to ambient temperature; fixation continued overnight. The following day, specimens were rinsed in FSW for 1 h (three changes of 20 min each), post-fixed in 2% osmium tetroxide (in H$_2$O) for 30 min, 2% uranyl acetate (in H$_2$O) for 20 min, dehydrated through an ethanol series, cleared in propylene oxide, exposed to

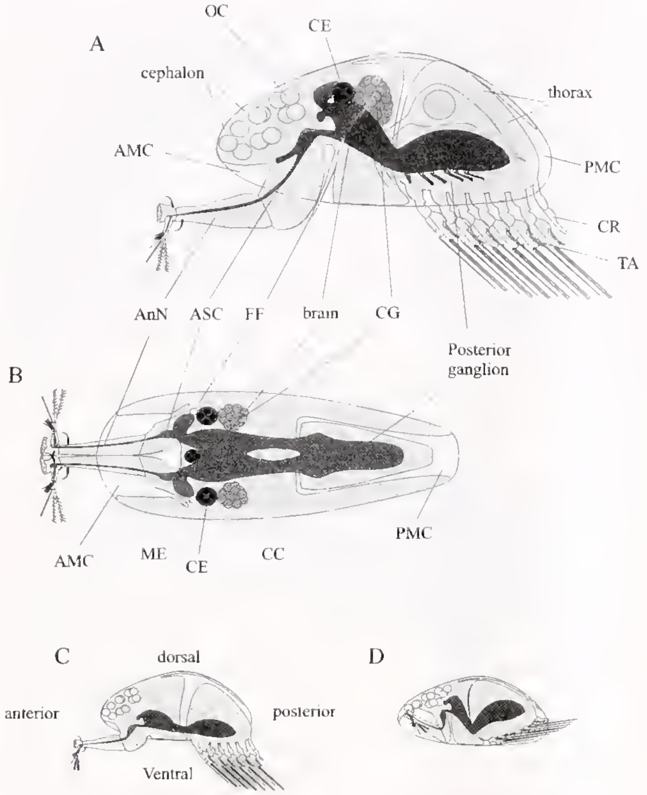

Figure 2. Schematic drawings of the cyprid nervous system and major organs in longitudinal and horizontal planes. (A–B) The body of the cyprid is organized in two main compartments, the cephalon and the thorax. The bivalve carapace encloses anterior (AMC) and posterior (PMC) mantle cavities about the cephalon and thorax respectively. The brain, compound eyes (CE), median eye (ME), and cement glands (CG) are contained within the cephalon. The antennules extend from the cephalon and bear the adhesive discs and putative chemoreceptive and mechanoreceptive sensilla. The brain connects with the posterior ganglion *via* circumesophageal connectives (CC). The posterior ganglion and gut are contained within the thorax. Six pairs of thoracic appendages (TA) and a pair of caudal rami (CR) extend from the thorax. (C–D) The orientation of neural structures in the cyprid depends on the relative position of the antennules and thoracic appendages, both of which extend beyond the carapace when the cyprid either swims or contacts the substratum (C), or can be withdrawn for protection (D). Planes are identified on the basis of the orientation of the nervous system in (C). Other abbreviations: ASC, antennular soma cluster; OC, oil cell; FF, frontal filament.

increasing concentrations of Araldite epoxy resin, and flat-embedded on microscope slides. Flat embedding allowed the orientation of the specimen to be determined using a light microscope. The Araldite was then removed from the slides by cold shock (using liquid nitrogen) and specimens cut from the blocks and remounted on Araldite stubs for sectioning.

Light microscopy. Twelve animals were serially sectioned at either 0.5 or 1.0 μm (six in sagittal plane, three frontal, and three horizontal—see Fig. 2 for orientation) with a Reichert-Jung ultramicrotome and diamond histology knife. Sections were transferred to microscope slides and stained with toluidine blue (1% in 6% borax, 0.6% boric acid, pH 8.3) or methylene blue (1% in 0.1% borax, pH 8.0); reconstructions were made from camera lucida drawings and photographs and with the aid of PC-based, Adobe Illustrator software.

Electron microscopy. Specimens for transmission electron microscopy were prepared as described above, sectioned at 60–70 nm on a Reichert-Jung ultramicrotome using a diamond knife, and viewed and photographed using a Hitachi H-7000 transmission electron microscope. For scanning electron microscopy, anesthetized and fixed animals were washed for 10 min in H_2O (three changes of 3 min each) with sonication during the first two steps, dehydrated, and transferred to acetone for critical-point drying. Dried specimens were mounted on microscope stubs with double-sided carbon tape, then gold coated and photographed on a Leica/Cambridge S-360 scanning electron microscope.

Results

General anatomy

Live cyprids of *B. amphitrite* typically measure 500–550 μm in length from the rostral to the caudal end of the carapace (Fig. 1A) (Glenner and Høeg, 1995), but minor size variations occurred in our cultured animals. When fixed, the average dimensions for 12 individuals were 480 μm in length, 220 μm in height, and 170 μm across the broadest part of the carapace.

The body of the *B. amphitrite* cyprid, like that of *S. balanoides* (Walley, 1969), is arranged as two separate compartments, the cephalon and thorax (Fig. 2). A bivalved carapace encloses anterior and posterior mantle cavities around the cephalon and thorax respectively (Fig. 2). The cephalon houses the brain, eyes, and cement glands, together with many large, densely staining oil cells (Figs. 1, 2), which are thought to supply energy for the lecithotrophic larva and its subsequent metamorphosis (Walley, 1969). First antennae (antennules) project anteriorly from the cephalon and can be extended well beyond the carapace during temporary attachment (Fig. 2C), or completely retracted within the anterior mantle cavity (Fig. 2D). Frontal filaments extend from the ventral surface of the cephalon, posterior to the antennules (Figs. 1A, 2A, 6C). The thorax houses the posterior ganglion and the undifferentiated gut (Figs. 1, 2). Six pairs of thoracic appendages and the caudal rami project from the ventral surface of the thorax, which may extend beyond the ventral edge of the carapace or be completely withdrawn within the posterior mantle cavity (Fig. 2C–D).

The central nervous system (CNS) can be seen in near-sagittal section (Fig. 1B) and is drawn schematically in Figure 2. The CNS consists of a cerebral ganglion, or "brain," linked by paired circumesophageal connectives to a posterior ganglion. Nerve roots extend from central ganglia toward peripheral organs (Figs. 1, 2). The major peripheral nerves include the antennular nerve and thoracic nerve roots (Fig. 2A). The relative position of neural structures depends on the degree of contraction of the appendages. When the appendages are fully extended (*e.g.*, Fig. 2C), the central nervous system lies essentially flat along the ventral surface, and this orientation is used to identify planes throughout this study. When the appendages are withdrawn (*e.g.*, Fig. 2D), the central nervous system can bend to an angle of 60° relative to the longitudinal axis, and the antennular nerve bends accordingly to accommodate flexion of the antennule.

The brain and associated structures

The brain (Figs. 3, 4) is composed of centrally positioned neuropil surrounded by the somata of central cells (Figs. 3, 4). The neuropil is composed of fine fibers and nerve endings and on close inspection contains membrane-bound vesicles and densely staining clefts typical of invertebrate synapses (Fig. 4C). Central somata are relatively uniform in size, measuring 4–8 μm in diameter, and form an outer layer of between one and five cells thick (Figs. 3, 4). The somata of these cells typically contain lightly stained granular nuclei and have a relatively thin layer of cytoplasm between the nucleus and cell membrane (Fig. 3B–C). Distinct clusters project neurites together in bundles to the central neuropil (Fig. 3B–C); based on a calculation of soma volume, we estimate the total number of neuronal cells in the cyprid brain to be approximately 750.

The brain is enclosed in a thin sheath, but the broad perineural glial layer present beneath the sheath in decapod crustacean ganglia (Sandeman, 1982) is absent. Small, densely stained, spindle-shaped glial cells lie between the somata and central neuropil and delineate neuropil regions (Fig. 3C). Two broad areas of neuropil can be discerned in the cyprid brain, and the lateral lobes of each division link *via* transverse fiber tracts (Fig. 4). The anterior division is connected to the eyes and frontal filaments *via* the optic tracts, and the posterior division is connected to the antennules *via* the antennular nerves (Fig. 4A). These divisions appear similar to the protocerebral and deutocerebral divisions of the decapod brain. We find no evidence of a tritocerebrum in the cyprid, which is consistent with the absence of antenna II during this stage (Sandeman *et al.*, 1992).

The protocerebrum. The protocerebrum can be subdivided into three regions, based on connections with peripheral sense organs and delineation by spindle-shaped glia (Fig. 5). We refer to these regions as the dorsofrontal neuropil, optic lobe neuropil, and median protocerebral neuropil. The dorsofrontal neuropil is dorsal to the protocerebral commissure (Fig. 5) and receives input from the median eye. The optic lobe neuropils are located within the anterolateral extensions of the brain and are linked to more posterior regions of the protocerebrum *via* the optic tract (Figs. 4, 5). Each optic lobe neuropil receives input from the adjacent frontal filament and compound eye (Figs. 4, 5). The median protocerebral neuropils elongate along the anteroposterior axis of the brain (Fig. 5) and are not directly linked with peripheral sense organs. Neurites from surrounding somata project into the median protocerebral neuropils (Figs. 3B, C) and longitudinal fibers that extend from the posterior regions of these neuropils contribute to the circumesophageal connectives (Fig. 5). Lateral lobes of the median protocerebral neuropil connect *via* the protocerebral commissure (Figs. 4, 5).

The nauplius eye (= median eye) is located on the anterodorsal margin of the brain. The nauplius eye has been studied in *B. amphitrite hawaiiensis* (Takenaka *et al.*, 1993) and in *S. balanoides* and *B. crenatus* (Kauri, 1961). In the *B. amphitrite* cyprid, the nauplius eye is composed of three pigment "cups" (two lateral and one ventral), with each cup containing four retinular cells. Axons from each of the three pigment cups were traced to the dorsofrontal neuropil. In one of three preparations in which these axons were traced, however, some axons appeared to bypass the dorsofrontal neuropil and contribute directly to the protocerebral commissure.

A frontal filament is attached to the anteromedial margin of each compound eye. The fine structure of the frontal filament in the nauplius of *S. balanoides* has been described previously (Walker, 1974). In the relaxed cyprid, the filaments extend beyond the carapace margin (Figs. 1A, 6C) and each contains large internal vesicles in its basal region (Fig. 6B). A frontal filament tract connects each frontal filament to its adjacent optic lobe neuropil (Figs. 5, 6B).

The structure of *the compound eye* in *B. amphitrite* is consistent with that described for *S. balanoides* (Walley, 1969; Hallberg and Elofsson, 1983). Each eye is located within a lateral "pocket" of the cephalon and composed of radially arranged ommatidia, each with a spherical lens and underlying retinular cells (Figs. 2, 5, 6A, B). Retinular cell axons converge to form a short optic nerve (Figs. 6A, B), which emerges from the medial surface of each compound eye and projects anteriorly to the optic lobe neuropil (Figs. 5, 6A, B).

The deutocerebrum. The deutocerebrum can be subdivided into two distinct regions, which we call the circular deutocerebral neuropils and median deutocerebral neuropils (Figs. 3B, 4A, 5). All peripheral nerves associated with the deutocerebrum travel within the antennular nerves. The circular deutocerebral neuropils are located lateral and slightly posterior to the brain-antennular nerve junction (see Fig. 3B). These neuropils are clearly delineated by glial cells and, based on their position and shape, are possible candidates for olfactory lobes. However, glomeruli that characterize the olfactory lobes in many animals (Hallberg

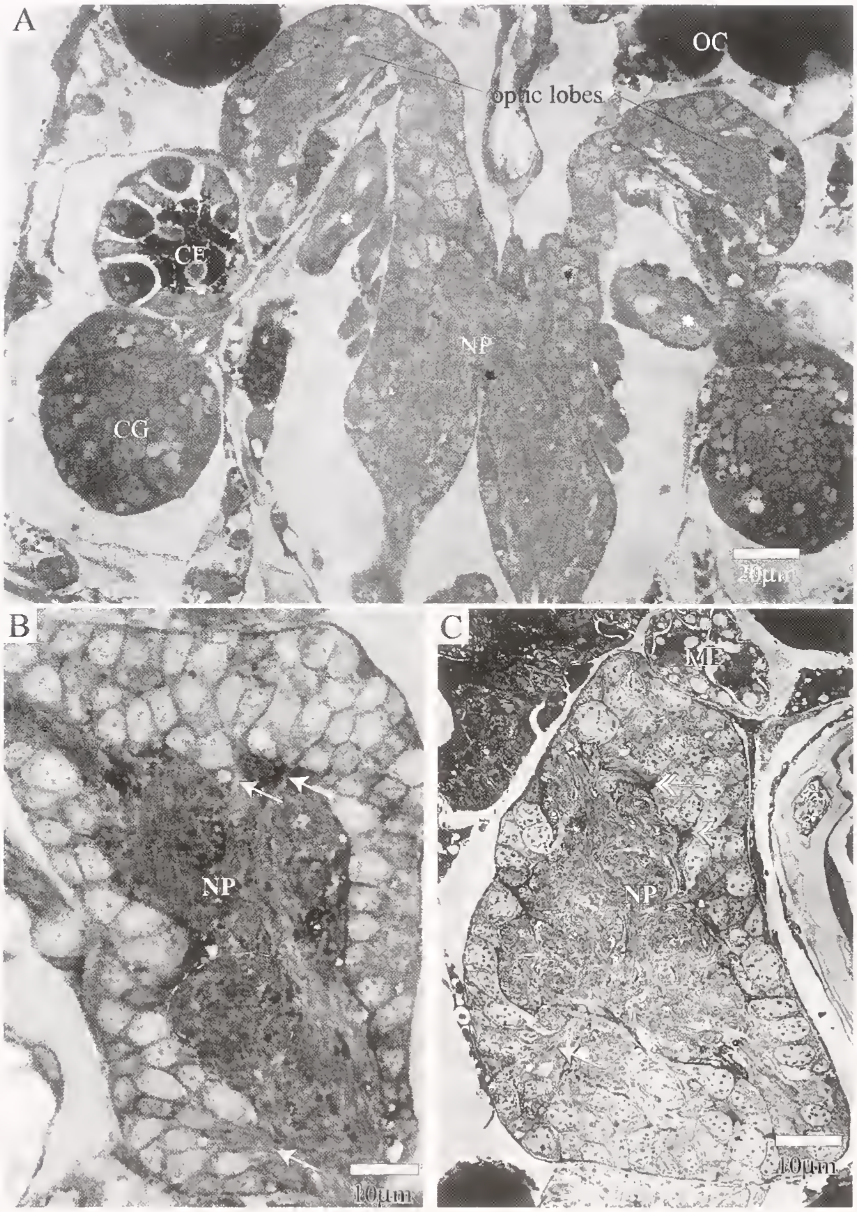

Figure 3. (A) Horizontal section through the cyprid brain. The brain is composed mainly of centrally positioned neuropil (NP) and surrounding cell somata. The anterior portion of the brain extends laterally to form the optic lobes. Also apparent are the compound eyes (CE), cement glands (CG), and cross-sections of the cement ducts (*), which extend to the adhesive discs of the antennules (see also Figure 7). OC, oil cell. (B) Longitudinal section of the cyprid brain showing clusters of somata with primary neurites (arrows) that project to the neuropil (NP). The circular deutocerebral neuropil (see also Fig. 5) is outlined. (C) Electron micrograph of the brain in near sagittal section highlighting projections of neurons (single arrow) into the central neuropil (NP) and the delineation of the neuropil by spindle-shaped glia (double arrows). ME, median eye.

et al., 1992; Hildebrand and Shepherd, 1997) were not seen in this region. Lateral lobes of the median deutocerebral neuropil are linked by the deutocerebral commissure and receive primary neurites from surrounding cell somata, particularly those located ventrolaterally to this neuropil. Posterior projections from the median protocerebral neuropils contribute to the circumesophageal connectives and travel in bundles distinct from those associated with the median protocerebral neuropil (Fig. 5).

The antennules and associated cement glands are innervated by the antennular nerves, which link to the deutocerebral neuropil (Fig. 4A, B). Detailed morphological descriptions of the cyprid antennule are available for both *B. amphitrite* (Clare and Nott, 1994; Glenner and Hoeg, 1995)

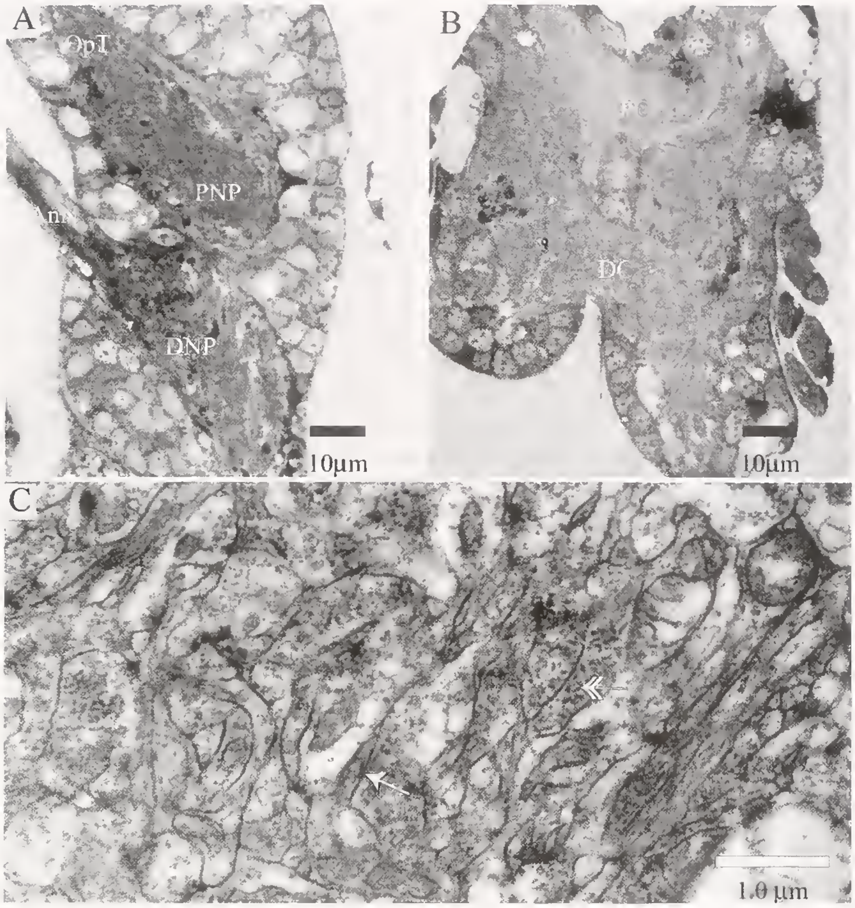

Figure 4. Two distinct neuropil divisions in the cyprid brain as seen in (A) longitudinal and (B) horizontal planes. (A) The anterior, or protocerebral, neuropil (PNP) is associated with the optic tract (OpT); the posterior, or deutocerebral, neuropil (DNP) is associated with the antennular nerve (AnN). (B) Protocerebral and deutocerebral commissures (PC, DC respectively) are the transverse fiber tracts that link lateral lobes of these two major neuropil divisions. (C) Electron micrograph of the neuropil showing many dark clefts (*e.g.*, single arrow) and membrane-bound vesicles (*e.g.*, double arrow) indicative of synapses.

and *S. balanoides* (Nott and Foster, 1969). We provide a brief description here to account for the neural innervation of this appendage. The antennule, represented schematically in Figure 7, consists of four articulating segments. Segment I projects ventrally from the cephalon and attaches to the slightly longer and slender segment II. Segment III functions as an adhesive disc and is used for attachment to the substratum (Nott and Foster, 1969; Nott, 1969; Walker, 1971). Segment IV is the terminal segment and extends laterally from the disc. Cuticular setae project from the antennular segments, particularly from the disc (Nott and Foster, 1969; Moyse *et al.*, 1995) and from segment IV (Nott and Foster, 1969; Gibson and Nott, 1971; Clare and Nott, 1994; Glenner and Høeg, 1995). Two large cement glands are associated with the antennules (Fig. 7). These are located within the cephalon, posterior to the compound eyes (Figs. 1, 2, 7; Walker, 1971), and ducts from these glands extend the length of the antennule to open through the adhesive disc. A muscular sac surrounds each duct (Walley, 1969) near the base of the antennule. In addition to the cement glands, antennulary glands are present in segment II of the antennule, which are thought to mediate the controlled release of adhesive used for temporary attachment (Nott and Foster, 1969; Walker, 1971).

The antennular nerve extends from the ventrolateral margin of the brain to the distal region of the antennule (Fig. 7). Distally, the antennular nerve is composed almost exclusively of neural processes associated with the distal setae (Figs. 8, 9). The external morphology of setae on segment IV has been described previously (Clare and Nott, 1994; Glenner and Hoeg, 1995). There are nine setae on the fourth segment, which are arranged in terminal and subterminal rows (Fig. 8); their associated neural processes can be seen in cross-section of segment IV (Fig. 9A). Most neural processes in this segment are between 0.5 and 1.0 μm in diameter and contain between one and three mitochondria

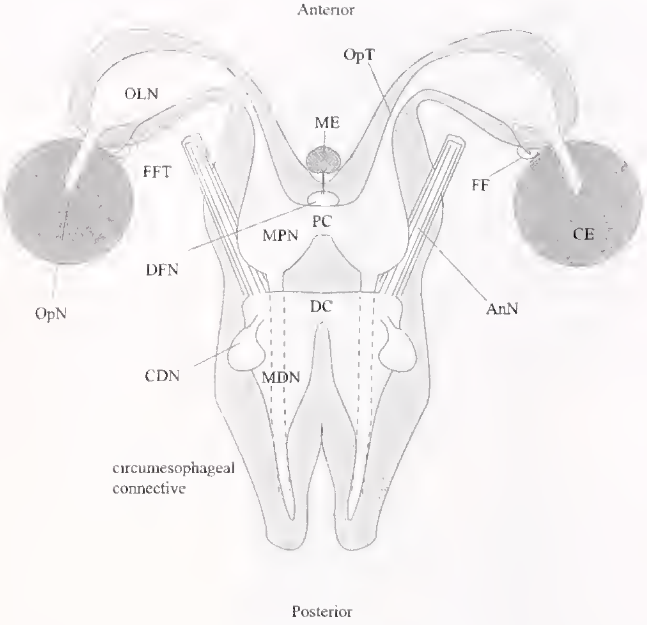

Figure 5. Schematic drawing of the neuropils and fiber tracts in the cyprid brain, showing further possible subdivision. The protocerebrum includes the paired optic lobe neuropils (OLN), median protocerebral neuropils (MPN), and an unpaired dorsofrontal neuropil (DFN). Optic lobe neuropils receive input from compound eyes (CE) *via* the optic nerve (OpN), and from frontal filaments (FF) *via* the frontal filament tract (FFT). The small dorsofrontal neuropil (DFN) lies anterior to the PC and receives input *via* the median eye (ME). Median protocerebral neuropils are not directly linked to peripheral sense organs, but the lateral lobes are connected by the protocerebral commissure (PC). The deutocerebrum includes paired circular and median deutocerebral neuropils (CDN, MDN, respectively). Peripheral nerves from the deutocerebrum form the antennular nerve (AnN), and lateral lobes of the median deutocerebral neuropil are connected by the deutocerebral commissure (DC). Longitudinal fiber tracts extend from the posterior of both the MPN and MDN and contribute to the circumesophageal connectives.

(Fig. 9B). Narrow "cilia-type" dendritic profiles (0.1–0.2 μm in diameter), which can be identified by a $9 \times 2 + 2$ microtubule arrangement, are also present (Fig. 9C). The larger processes can be traced as far as the distal portion of this segment, whereas the outer dendritic segments of smaller cilia-type processes extend into each of the four short subterminal setae (Fig. 9C).

Approximately 50 μm from the brain, the antennular nerve is associated with a cluster of neurons, which we refer to as the *antennular soma cluster* (Fig. 10). This group of cells was referred to as the antennular "ganglion" by Walley (1969), who proposed that the somata were those of motorneurons that had migrated out from the brain. From light micrographs, the cells in this cluster appear to be bipolar, with processes extending both proximally to the brain and distally along the antennular nerve. The somata, which measure 6–8 μm in length, have large nuclei and a relatively thin layer of cytoplasm (Figs. 10B, 3C). From electron micrographs, we found no evidence of branching or of synapses within the antennular soma cluster, which leads us to conclude that these cells do not form a ganglion in the usual sense. The morphology of these cells and their association with the antennular nerve suggest that they are receptor cells and are, therefore, possible candidates for chemoreceptors or mechanoreceptors whose dendrites extend to the distal setae.

The antennular nerve splits midway between the antennular soma cluster and the brain (Fig. 7), sending a fine branch toward the *cement duct.* This fine branch splits again before reaching the duct, and minor branches project toward both the *cement gland* and the muscular sac. These branches of the antennular nerve travel adjacent to the cement duct and are difficult to trace in serial section. They are more obvious, however, during dissection of this region and will typically separate from the collecting duct following slight enzymatic treatment (0.01 mg · ml^{-1} trypsin for 5 min). We were unable to trace projections of these fine branches beyond the muscular sac.

The posterior ganglion and associated structures

The posterior ganglion is composed largely of centrally positioned neuropil and fiber tracts surrounded by neuronal somata (Fig. 11A). The somata in this region, like those in the brain, measure 4–8 μm in diameter, contain lightly stained granular nuclei, and are gathered into clusters with neurites that project together to the central neuropil. Densely stained glial cells are present and delineate the neuropil (Fig. 11A, B).

The posterior ganglion is composed of several fused divisions. Longitudinal fiber tracts extend through the length of this ganglion, and individual divisions can be discerned by the presence of transverse commissures (Fig. 11A). We identified six divisions in the posterior portion of this ganglion as thoracic divisions on the basis that paired nerve roots extend ventrally from each division toward the corresponding thoracic appendage (Figs. 2, 11A–C). We were unable to determine whether a seventh thoracic division, which might be expected in cirripedes (see Grygier, 1987), was present in the cyprid. Individual divisions are more difficult to distinguish in the anterior portion of the ganglion, which elongates laterally and is compressed longitudinally (Fig. 11A). However, we identified three divisions in this region (from two of the three preparations sectioned in the horizontal plane), which might reflect the presence of the three pairs of gnathopods that can be seen with either scanning electron microscopy or light microscopy (Fig. 12B).

Thoracic appendages and the caudal rami. Six pairs of thoracic appendages (thoracopods) and the paired caudal rami extend from the ventral surface of the thorax. The extrinsic muscles of thoracic appendages and the caudal rami attach dorsally in the thorax and can be seen in both

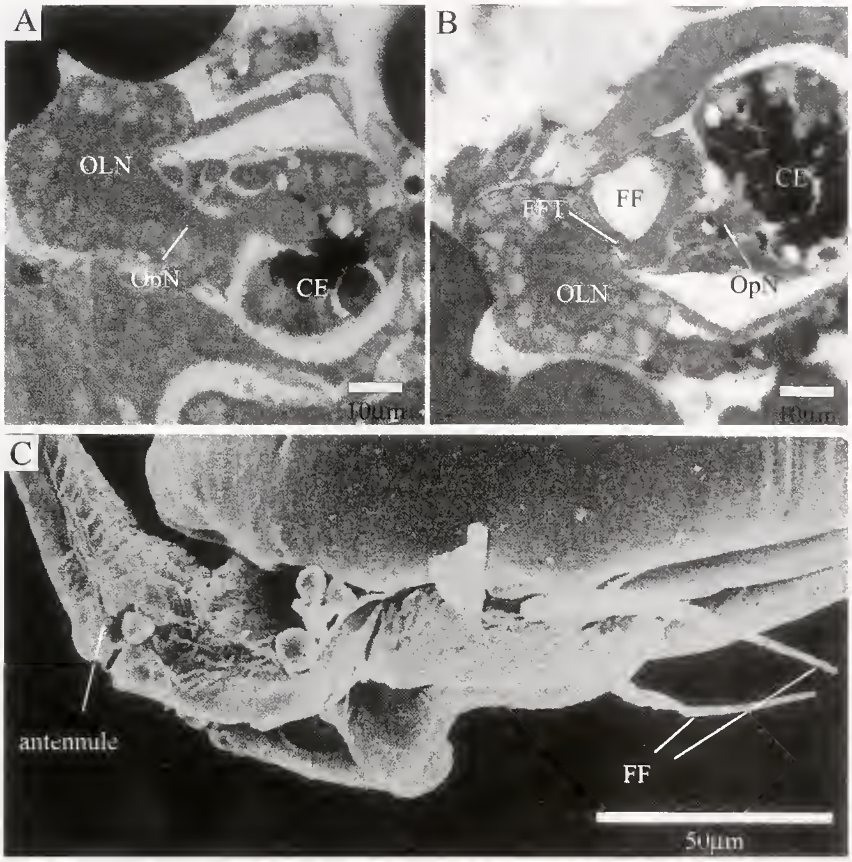

Figure 6. Compound eyes and frontal filaments. (A) The optic nerve (OpN) connects the compound eye (CE) to the optic lobe neuropil (OLN). (B) Frontal filaments are closely associated with compound eyes, and a transverse section through the base of a frontal filament (FF) is shown. The frontal filament tract (FFT) connects the frontal filament with the optic lobe neuropil proximal to the point of entry of the optic nerve (OpN) (see Fig. 5). (C) Scanning electron micrograph of the anterior ventral surface of a cyprid in which the cephalon is extended from the bivalve carapace. Frontal filaments (FF) extend from the ventral surface of the cephalon, posterior to the antennules.

horizontal and longitudinal sections (Fig. 11A, B). Paired nerve roots to the thoracic appendages extend from each thoracic division (Fig. 11B, C). Paired nerve roots extend to the caudal rami, but unlike those to thoracic appendages, are not associated with an obvious ganglionic division. Instead, these nerve roots appear to extend from a terminal loop of the longitudinal fibers (Fig. 11A, D).

Oral cone. The gnathopods of the cyprid form an oral cone, which opens to the ventral surface of the cephalon (Figs. 1, 2, 12A). The cyprid does not eat, and gnathopods are rudimentary during this stage (Walley, 1969). There are no obvious nerves connecting the gnathopods to the central nervous system in *B. amphitrite.* However, the posterior ganglion extends laterally in the region adjacent to the oral cone. It is likely that the three ganglionic divisions located adjacent to the oral cone reflect the presence of three pairs of gnathopods and are, therefore, referred to as subesophageal divisions.

Esophagus and digestive system. The digestive system of the cyprid is not fully developed (Walley, 1969). The esophagus has an oral opening (Fig. 12A), but we found no evidence of a rostral opening of the digestive system. In some sections the esophagus appears to be closed in the region where it passes between the cephalon and thorax (Fig. 12A, B), but it remains possible that this represents a sectioning artifact. Fine nerves can be traced from the dorsal surface of the subesophageal ganglionic divisions to the esophagus and midgut (Fig. 12B). These nerves are most obvious when they converge to pass between the cephalon and thorax, but they disperse among the cells surrounding the midgut (Fig. 12C).

Discussion

Our results show that the cypris larva of *B. amphitrite* has a well-developed nervous system that, in spite of being relatively small, contains the full complement of neural elements necessary for mediating complex interactions with

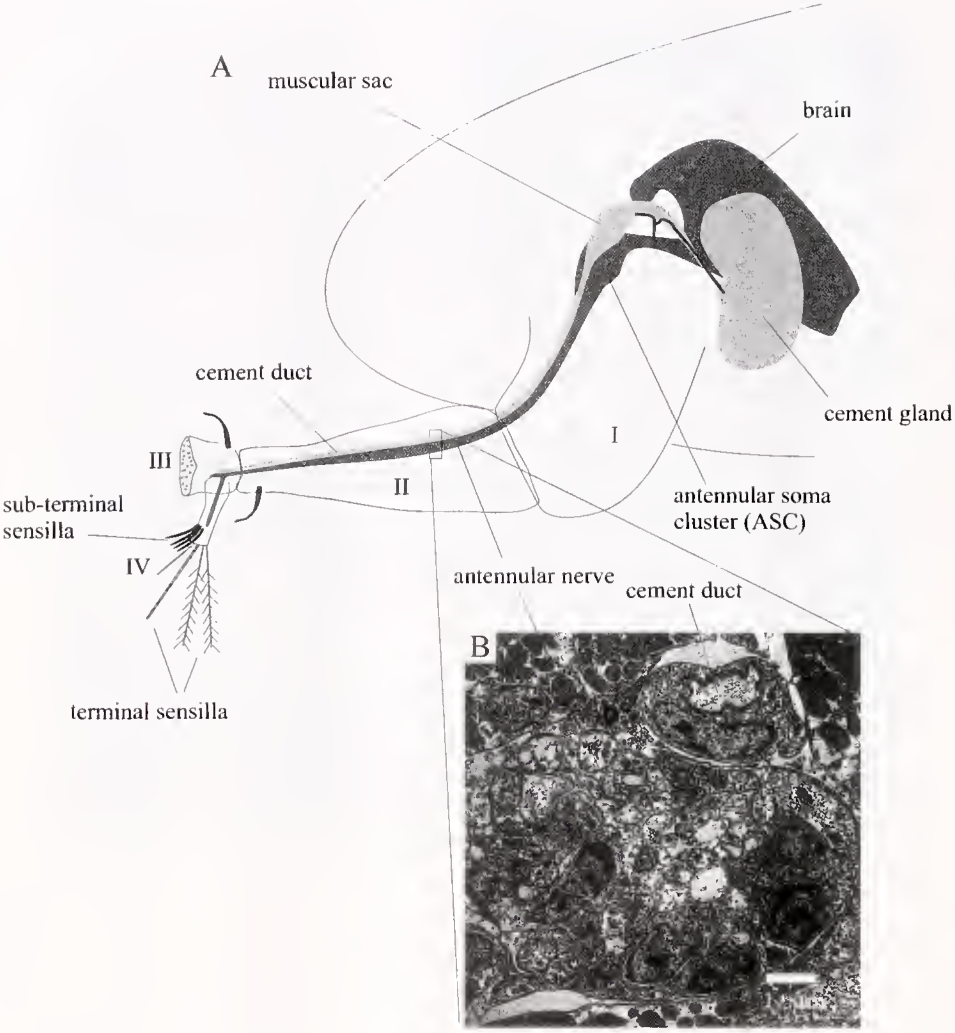

Figure 7. (A) Schematic drawing of the antennule to show the extension of the antennular nerve and its association with the collecting duct of the cement gland. The antennule has four segments (I–IV). The antennular nerve consists of neural processes associated with the distal setae (innervation of setae not drawn here, but see Figs. 8, 9). The antennular nerve is also expected to contain the motor neurons to the antennular musculature. The antennular soma cluster (ASC), located near the base of the antennule, contains bipolar cells, which are candidates for receptor cell somata whose dendrites innervate the distal setae (discussed in text). Midway between the ASC and the brain, a small branch of the antennular nerve extends to the muscular sac, a node of muscle surrounding the collecting duct of the cement gland, and a separate branch extends toward a cement gland.

the environment. The presence of regionalized neuropils, some of which clearly receive input from peripheral sensory structures, suggests a level of neural integration that goes beyond simple reflexive responses.

Observations of complex behavior displayed by cyprids during settlement support the claim that the nervous system has the capacity for more than simple reflex responses. For example, cyprids of *S. balanoides* settle gregariously in response to a proteinaceous cue associated with the cuticle of conspecifics (Crisp and Meadows, 1962; Gabbott and Larman, 1987). Upon encountering this cue, however, the cyprids' response is not indiscriminate. For example, in "favored" areas (those containing conspecifics), individual cyprids will still conduct a meticulous inspection phase and reject the substratum if the immediate barnacle density is too high or if the surface topography is inadequate (Crisp, 1961).

The cyprids' need to settle is reflected by the fact that the barnacle nervous system is most "complete" during the cyprid stage. The cyprid has a well-developed brain and a large investment in cephalic sense organs, whereas the brain is greatly reduced in the naupliar stages and almost completely absent in the adult barnacle (Walley, 1969). The "upgrade" from the nauplius to the cyprid nervous system is

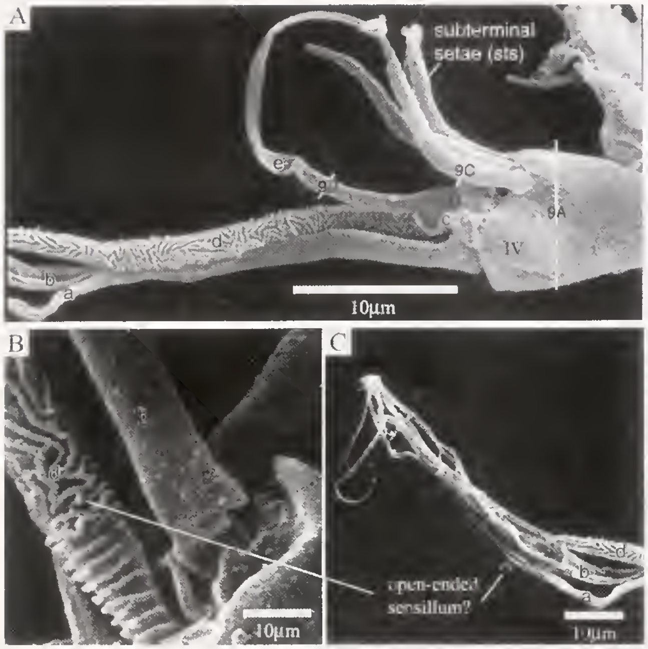

Figure 8. (A) The setae on the fourth antennular segment (IV) are arranged in terminal and subterminal rows. (A) The four subterminal setae (sts) do not articulate at the base. These are short and taper toward the tip with a general morphology similar to that of the aesthetasc (olfactory) sensilla described in other crustaceans. The terminal row consists of two plumose setae (a, b), a short, sickle-shaped seta (c), a longer "sculptured" seta with many cuticular ridges along its length (d), and a shorter unsculptured seta (e). Terminology following Clare and Nott (1994) and Glenner and Høeg (1995). (B) Higher power micrograph highlighting the articulating bases of two of the terminal setae (b, d). (C) High power of the distal tips of setae a, b, and d. The setules of a and b are folded back on themselves, and seta d appears open-ended. 9A, 9C, 9D in (A) refer to cross-sectional planes shown in Figure 9.

consistent with the cyprids' need to detect and actively respond to settlement cues. The restructuring to the adult nervous system (Walley, 1969), in which most of the anterior neuropil regions and cephalic sensory structures that we describe here degenerate, is presumably an adaptation to sedentary life.

The nervous system and associated structures

Neural input from cephalic sense organs is structurally organized in discrete neuropils within the cyprid brain (see Fig. 5). The cephalic sensory input in the cyprid can be summarized as follows: primary nerves from the median eye project to the dorsofrontal neuropil; primary nerves from each compound eye form an optic tract and project to the optic lobe; primary nerves from each frontal filament form a frontal filament tract and project also to the optic lobe; and primary nerves that innervate setae on the antennule project to the deutocerebrum.

Eyes and frontal filaments. Optic nerves connect the compound eyes with their adjacent optic lobe neuropils (Figs. 5, 6A, B). Under the light microscope, this neuropil appears to be unstructured, lacking the geometrically ordered segments seen in the optic lobes of decapods (Dahl, 1965). Nevertheless, compound eyes are morphologically well developed in the cyprid (Hallberg and Elofsson, 1983), and the fact that these eyes are present only during the cyprid stage is suggestive of a significant role in settlement. The exact function of these eyes is not yet known. Crisp (1955) argued, on the basis of the simple structure of these eyes, that image formation was unlikely, but suggested a role in mediating responses to fine-scale topographic features such as cracks and grooves. It is likely that compound eyes enable the detection of reflected light levels (Yule and Walker, 1984), thereby mediating light-guidance behavior (Barnes *et al.*, 1951). However, this function might equally be attributed to the median eye.

The frontal filament tract connects each of the frontal filaments with the adjacent optic lobe (Fig. 6B), proximal to the point of entry of the optic nerve (Figs. 5, 6A–B). The optic lobe of decapods includes neuropil divisions of the lamina ganglionaris, external and internal medullae, terminal medulla, and hemiellipsoid body (Dahl, 1965). We were unable to identify these divisions in the cyprid and have therefore chosen to use the general term of optic lobe. The exact nature of the frontal filaments and their function remains a contentious issue. Frontal organs are found in many Crustacea but, to date, frontal filaments of barnacle larvae have been considered only as pressure sensors on the basis of their suspected homology with the SPX organs (or organ of Bellonci) of Pericarida (Kauri, 1964; Walker, 1974).

Antennules. The antennules play a role as attachment organs during exploration and settlement (Nott and Foster, 1969) and have been implicated in the detection of chemical and physical cues (Nott and Foster, 1969; Walker, 1971; Clare *et al.*, 1994; Clare and Nott, 1994; Walker, 1995). The antennular nerve extends through the length of the antennule (Fig. 1B) and *during dissection* can be dissected into smaller individual bundles. Recently, electrical activity has been recorded from this nerve in response to chemical and mechanical stimulation of the distal segments of the antennule (Harrison, 1998).

The setae on the fourth antennular segment, and the nerves that innervate them, vary considerably in their morphology (Figs. 7–9). The functional properties of individual setae on this segment are not known. However, the innervation of segment IV suggests that these are sensilla, and some appear to be morphologically similar to chemoreceptors and mechanoreceptors of other Crustacea (Nott and Foster, 1969; Bush and Laverack, 1982; Heimann, 1984; Schmidt, 1989; Clare and Nott, 1994). The external morphology of the four subterminal setae, for example, is similar to that of the olfactory

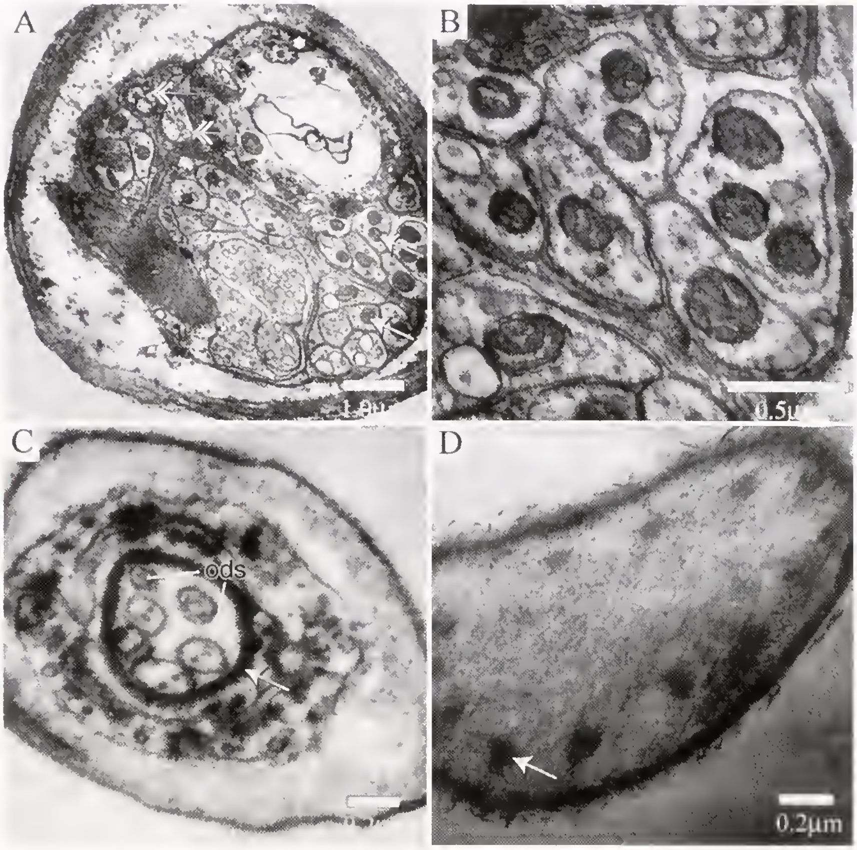

Figure 9. Innervation of antennular segment IV (see Fig. 8A for orientation). (A) The dendritic profiles in segment IV vary in diameter. Most profiles are between 0.5 and 1.0 μm in diameter and contain between one and three mitochondria (single arrow). Smaller-diameter processes (typically 0.1–0.3 μm in diameter) are also present (double arrows), and in some cases a 9 × 2 + 2 pattern of microtubules is apparent (*). (B) Enlargement of part of (A) to highlight the variation in the number of mitochondria in neural profiles. (C) Transverse section through a single subterminal seta showing the outer dendritic segments (ods) that extend into each of the subterminal setae. At this level, the dendrites are contained within an electron-dense tube (arrow), which is encircled by two glial cells. (D) A transverse section through seta e (see Fig. 8a) reveals densely stained peripheral structures (arrow) that possibly support this seta. Neural processes were not observed to extend into this seta, nor into any of the other terminal setae.

aesthetascs of Decapoda (Hallberg *et al.*, 1992; Clare and Nott, 1994). Furthermore, our results show that up to six outer dendritic segments (each 0.1–0.2 μm in diameter) project into the lumen of each subterminal seta (Fig. 9C). The outer dendritic segments are contained within a central cavity bordered by electron-dense material and a pair of ensheathing cells. This arrangement is similar to that reported for olfactory aesthetascs of crayfish (Tierney *et al.*, 1986).

It is generally accepted that the setae on the antennule include both chemoreceptors and mechanoreceptors (Clare and Nott, 1994; Clare, 1995), but the location of the somata of receptor cells has not been shown. In an effort to locate receptor cell somata, we traced serial sections of the antennule and were led to the bundle of cells that form the antennular soma cluster (Fig. 10). The cells in this bundle are 6–8 μm in length, 4–6 μm in width, and are located about 150 μm from the fourth segment of the antennule. Interestingly, the size and shape of these soma is again consistent with olfactory receptor neurons of many decapods (Laverack and Ardill, 1965; Snow, 1973; Tierney *et al.*, 1986; Hallberg *et al.*, 1992). These cells, however, are located at the base of the antennule in the cyprid and not, as in decapods, at the base of the sensilla.

The antennules are used for temporary attachment during surface exploration, which enables the cyprid to "walk" across the substratum (Nott and Foster, 1969; Walker, 1971). This involves the controlled release of cement from the adhesive disc *via* the antennulary glands (Nott and Foster, 1969; Walker, 1971; Okano *et al.*, 1996) and the coordination of motor activity. Motor neurons to the antennular musculature are expected to travel in the main branch of the antennular nerve. The

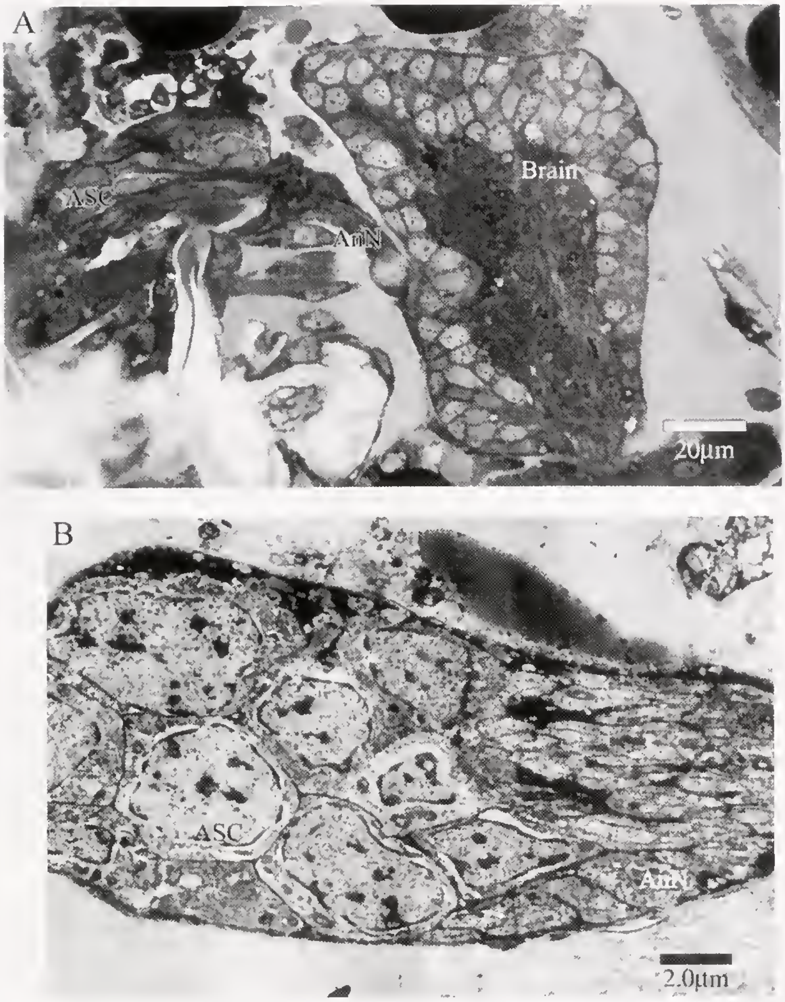

Figure 10. Longitudinal sections of the antennular soma cluster (ASC). (A) Light micrograph of the ASC shows its position relative to the brain, and association with the antennular nerve (AnN). The bipolar cells in this cluster are likely candidates for receptor cells that project to distal setae. (B) Electron micrographs of the ASC do not reveal synapses in this region, as would be expected for motor neurons, suggesting that these cells do not form a ganglion of antennular motorneurons as previously suggested (discussed in text).

location of efferent cell soma within the central nervous system is not known, but cells located ventrolateral to the median protocerebral neuropil that project anteriorly in the deutocerebrum are possible candidates (see Fig. 3B). The location of cells that control the release from the antennular glands for temporary attachment and the explosive release from cement glands for permanent attachment remains to be shown.

Thoracic appendages and caudal rami. The nerves that project to the thoracic appendages are, together with the antennular nerve, the most obvious peripheral extensions from the central nervous system. Thoracic appendages are used for swimming and bear many setae (Glenner and Høeg, 1995). These appendages, however, serve a natatory function, and it is not known whether the setae play a sensory role. Setae are also present on the caudal rami (Walker and Lee, 1976; Glenner and Høeg, 1995), and behavioral observations suggest that caudal rami might play a sensory role (Crisp and Barnes, 1954).

The nervous system and settlement

Cyprids settle in response to a range of environmental cues. It follows that the cyprid nervous system must sort and process input from various sense organs, and coordinate an appropriate behavioral response. We have traced neural connections between the central nervous system and many of the peripheral sense organs, but connections to the lattice organs (Jensen *et al.*, 1994b; Høeg *et al.*, 1998) and other sensory structures on the carapace remain to be shown. The small size of the cyprid raises questions about the behavioral capacity of this

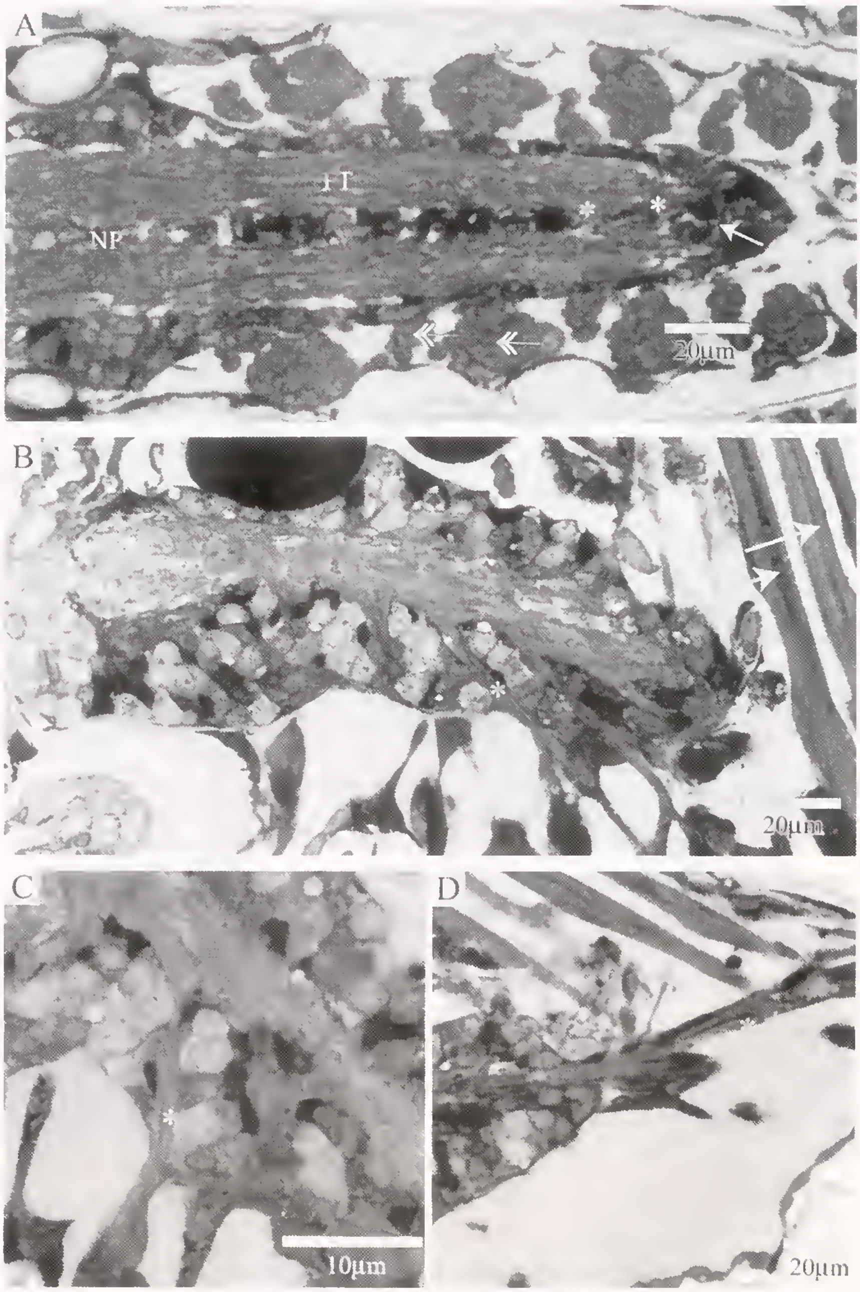

Figure 11. Light micrographs of the posterior ganglion. (A) Horizontal section showing regions of neuropil (NP), parallel fiber tracts (FT) and transverse fiber tracts (*). The transverse fibers distinguish individual divisions of this ganglion. The parallel fiber tracts end in a terminal loop (arrow). Extrinsic muscles of the thoracic appendages are seen in cross-section (double arrows). (B) A longitudinal section through the posterior ganglion. Paired nerve roots (*) extend from the ventral portion of each ganglionic division to the corresponding thoracic appendage. Extrinsic muscles of the thoracic appendages are seen (arrows). (C) Higher power of a thoracic nerve root (*) extending ventrally from the posterior ganglion. (D) Paired nerve roots (*) extend from the terminal loop of the transverse fiber tract to the caudal rami.

organism (Rittschof *et al.*, 1998). However, the large investment in sensory structures, each of which links to a discrete neuropil within the brain, suggests that the cyprid nervous system has the capacity for a relatively sophisticated level of neural processing.

Acknowledgments

We thank Renate Sandeman for discussion and advice during the course of this work and particularly for advising on many of the techniques used. We also thank Holly Cate

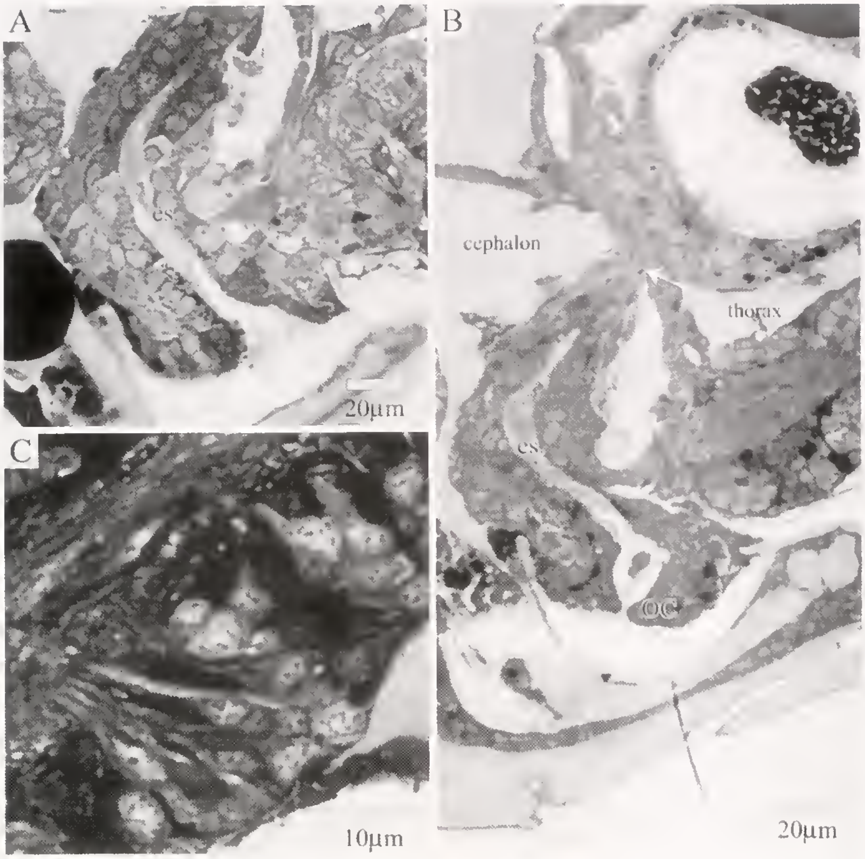

Figure 12. Light micrographs showing possible innervation of the esophagus and gut. (A–B) The esophagus of the cyprid opens on the ventral surface through the oral cone (consisting of vestigial mouthpart appendages). In these sections the esophagus appears to be closed in the region where it passes between the cephalon and thorax. Nerve roots arising from the anterior ganglionic divisions can be traced along the length of the esophagus and extend toward the gut (arrows). Innervation of mouthpart appendages was not observed. (C) The neurites of ventrally located cells project to the neuropil of anterior ganglionic divisions, but few nerves could be traced out of this region.

and two anonymous reviewers, whose comprehensive feedback was used to significantly improve the manuscript.

Literature Cited

Anderson, D. T. 1994. *Barnacles. Structure, Function, Development and Evolution.* Chapman & Hall, London. 357 pages.

Barnes, H., D. J. Crisp, and H. T. Powell. 1951. Observations on the orientation of some species of barnacles. *J. Anim. Ecol.* **20:** 227–241.

Bush, B. M. H., and M. S. Laverack. 1982. Mechanoreception. Pp. 399–468 in *The Biology of Crustacea, Vol. 3. Neurobiology, Structure and Function,* H. L. Atwood and D. C. Sandeman, eds. Academic Press, New York.

Clare, A. S. 1995. Chemical signals in barnacles: old problems, new approaches. Pp. 49–67 in *Crustacean Issues 10: New Frontiers in Barnacle Evolution,* F. R. Schram and J. T. Høeg, eds. A. A. Balkema, Rotterdam.

Clare, A. S., and J. A. Nott. 1994. Scanning electron microscopy of the fourth antennular segment of *Balanus amphitrite amphitrite. J. Mar. Biol. Assoc. UK* **74:** 967–970.

Clare, A. S., R. K. Freet, and M. McClary, Jr. 1994. On the antennular secretion of the cyprid of *Balanus amphitrite amphitrite,* and its role as a settlement pheromone. *J. Mar. Biol. Assoc. UK* **74:** 243–250.

Clare, A. S., R. F. Thomas, and D. Rittschof. 1995. Evidence for the involvement of cyclic AMP in the pheromonal modulation of barnacle settlement. *J. Exp. Biol.* **198:** 655–664.

Conrad, G. W., J. A. Bee, S. M. Roche, and M. A. Teillet. 1993. Fabrication of microscalpels by electrolysis of tungsten wire in a meniscus. *J. Neurosci. Methods* **50:** 123–127.

Crisp, D. J. 1955. The behavior of barnacles in relation to water movement over a surface. *J. Exp. Biol.* **32:** 569–590.

Crisp, D. J. 1961. Territorial behavior in barnacle settlement. *J. Exp. Biol.* **38:** 429–446.

Crisp, D. J., and H. Barnes. 1954. The orientation and distribution of barnacles at settlement with particular reference to surface contour. *J. Anim. Ecol.* **23:** 142–162.

Crisp, D. J., and P. S. Meadows. 1962. The chemical basis of gregariousness in cirripedes. *Philos. Trans. R. Soc. Lond. B* **156:** 500–520.

Dahl, E. 1965. Frontal organs and protocerebral neurosecretory systems in Crustacea and Insecta. *Gen. Comp. Endocrinol.* **5:** 614–617.

DeNys, R., P. D. Steinberg, P. Willemsen, S. A. Dworjanyn, C. L. Gabelish, and R. J. King. 1995. Broad spectrum effects of secondary metabolites from the red alga *Delisea pulchra* in antifouling assays. *Biofouling* **8:** 259–271.

Elfimov, A. S. 1995. Comparative morphology of the thoracican cyprid larvae: studies on the carapace. Pp. 137–152 in *Crustacean Issues 10. New Frontiers in Barnacle Evolution.* F. R. Schram and J. T. Høeg, eds. A. A. Balkema, Rotterdam.

Gabbott, P. A., and V. N. Larman. 1987. The chemical basis of gregariousness in cirripedes: A review (1953–1984). Pp. 377–388 in *Crustacean Issues 5. Barnacle Biology,* A. J. Southward, ed. A. A. Balkema, Rotterdam.

Gibson, P. H., and J. A. Nott. 1971. Concerning the fourth antennular segment of the cypris larva of *Balanus balanoides.* Pp. 227–236 in *Fourth European Marine Biology Symposium,* D. J. Crisp ed. Cambridge University Press, Cambridge.

Glenner, H., and J. T. Høeg. 1995. Scanning electron microscopy of cypris larvae of *Balanus amphitrite* (Cirripedia: Thoracica: Balanomorpha). *J. Crustac. Biol.* **15:** 523–536.

Grygier, M. J. 1987. New records, external and internal anatomy, and systematic position of Hansen's Y-larvae (Crustacea: Maxillopoda: Facetoteca). *Sarsia* **72:** 261–278.

Hallberg, E., and R. Elofsson. 1983. The larval compound eye of barnacles. *J. Crustac. Biol.* **3:** 17–24.

Hallberg, E., K. U. Johansson, and R. Elofsson. 1992. The aesthetasc concept: structural variations of putative olfactory receptor cell complexes in Crustacea. *J. Microsc. Res. Tech.* **22:** 325–335.

Harrison, P. J. H. 1998. The nervous system and settlement of barnacle cypris larvae. PhD Thesis, University of New South Wales. 150 pages.

Heimann, P. 1984. Fine structure and molting of aesthetasc sense organs on the antennules of the isopod, *Asellus aquaticus* (Crustacea). *Cell Tissue Res.* **235:** 117–128.

Hildebrand, J. G., and G. M. Shepherd. 1997. Mechanisms of olfactory discrimination: converging evidence for common principles across phyla. *Annu. Rev. Neurosci.* **20:** 595–631.

Hoeg, J. T., B. Hosfeld, and P. G. Jensen. 1998. TEM studies on the lattice organs of cirripede cypris larvae (Crustacea, Thecostraca, Cirripedia). *Zoomorphology* **118:** 195–205.

Jensen, P. G., J. Moyse, J. Høeg, and H. Al-Yahya. 1994. Comparative SEM studies of lattice organs: putative sensory structures on the carapace of larva from Ascothoracica and Cirripedia (Crustacea Maxillopoda Thecostraca). *Acta Zool.* **75:** 125–142.

Kauri, T. 1961. On the frontal filaments and nauplius eye in *Balanus. Crustaceana* **4:** 131–142.

Kauri, T. 1964. On the sensory papilla X organ in cirriped larvae. *Crustaceana* **11:** 115–122.

Kon, Y., W. Miki, and M. Endo. 1995. L-tryptophan and related compounds induce larval settlement of the barnacle *Balanus amphitrite* Darwin. *Fish. Sci.* **61:** 800–803.

Laverack, M. S., and D. J. Ardill. 1965. The innervation of the aesthetasc hairs of *Panulirus argus. Q. J. Microsc. Sci.* **106:** 45–60.

Moyse, J., J. T. Høeg, P. G. Jensen, and H. A. D. Al-Yahya. 1995. Attachment organs in cypris larvae: using scanning electron microscopy. Pp. 153–177 in *Crustacean Issues 10. New Frontiers in Barnacle Evolution,* F. R. Schram and J. T. Høeg, eds. A. A. Balkema, Rotterdam.

Nott, J. A. 1969. Settlement of barnacle larvae: surface structure of the antennular attachment disc by scanning electron microscopy. *Mar. Biol.* **2:** 248–251.

Nott, J. A., and B. A. Foster. 1969. On the structure of the antennular attachment organ of the cypris larva of *Balanus balanoides* (L.). *Philos. Trans. R. Soc. Lond. B* **256:** 115–134.

Okano, K., K. Shimizu, C. G. Satuito, and N. Fusetani. 1996. Visualization of cement exocytosis in the cypris cement gland of the barnacle *Megabalanus rosa. J. Exp. Biol.* **199:** 2131–2137.

Okano, K., K. Shimizu, C. G. Satuito, and N. Fusetani. 1998. Enzymatic isolation and culture of cement secreting cells from cypris larvae of the barnacle. *Biofouling* **12:** 149–159.

Rittschof, D., J. Forward, G. Cannon, J. M. Welsh, J. McClary, E. R. Holm, A. S. Clare, S. Conova, L. M. McKelvey, P. Bryan, and C. L. van Dover. 1998. Cues and context: larval responses to physical and chemical cues. *Biofouling* **12:** 31–44.

Sandeman, D., R. Sandeman, C. Derby, and M. Schmidt. 1992. Morphology of the brain of crayfish, crabs, and spiny lobsters: a common nomenclature for homologous structures. *Biol. Bull.* **183:** 304–326.

Sandeman, D. C. 1982. Organization of the central nervous system. Pp. 1–61 in *The Biology of Crustacea, Vol. 3. Neurobiology, Structure and Function,* H. L. Atwood and D. C. Sandeman, eds. Academic Press, New York.

Schmidt, M. 1989. The hair-peg organs of the shore crab, *Carcinus maenas* (Crustacea, Decapoda): ultrastructure and functional properties of sensilla sensitive to changes in seawater concentration. *Cell Tissue Res.* **257:** 609–621.

Snow, P. J. 1973. Ultrastructure of the aesthetasc hairs of the littoral decapod, *Paragrapsus gaimardii. Z. Zellforsch.* **138:** 489–502.

Takenaka, M., A. Suzuki, T. Yamamoto, M. Yamamoto, and M. Yoshida. 1993. Remodeling of the nauplius eye into the adult ocelli during metamorphosis of the barnacle *Balanus amphitrite hawaiiensis. Dev. Growth Differ.* **35:** 245–255.

Tierney, A. J., C. S. Thompson, and D. W. Dunham. 1986. Fine structure of aesthetasc chemoreceptors in the crayfish *Orconectes propinquus. Can. J. Zool.* **64:** 392–399.

Walker, G. 1971. A study of the cement apparatus of the cypris larva of the barnacle *Balanus balanoides. Mar. Biol.* **9:** 205–212.

Walker, G. 1974. The fine structure of the frontal filament complex of barnacle larvae (Crustacea: Cirripedia). *Cell Tissue Res.* **152:** 449–465.

Walker, G. 1995. Larval settlement: historical and future perspectives. Pp. 69–85 in *Crustacean Issues 10. New Frontiers in Barnacle Evolution,* F. R. Schram and J. T. Høeg, eds. A. A. Balkema, Rotterdam.

Walker, G., and V. E. Lee. 1976. Surface structures and sense organs of the cypris larva of *Balanus balanoides* as seen by scanning and transmission electron microscopy. *J. Zool. (Lond.).* **178:** 161–172.

Walley, L. J. 1969. Studies on the larval structure and metamorphosis of *Balanus balanoides* (L.). *Philos. Trans. R. Soc. Lond. B* **256:** 237–279.

Yamamoto, H., A. Tachibana, K. Matsumura, and N. Fusetani. 1995. Protein kinase C (PKC) signal transduction system involved in larval metamorphosis of the barnacle, *Balanus amphitrite. Zool. Sci.* **12:** 391–396.

Yamamoto, H., A. Tachibana, S. Kawaii, K. Matsumura, and N. Fusetani. 1996. Serotonin involvement in larval settlement of the barnacle, *Balanus amphitrite. J. Exp. Zool.* **275:** 339–345.

Yule, A. B., and G. Walker. 1984. The temporary adhesion of barnacle cyprids: effects of some differing surface characteristics. *J. Mar. Biol. Assoc. UK* **64:** 429–439.

Reference: *Biol. Bull.* **197:** 159–173. (October 1999)

An Endogenous SCP-Related Peptide Modulates Ciliary Beating in the Gills of a Venerid Clam, *Mercenaria mercenaria*

LOUIS F. GAINEY, JR.[1,*], KELLY J. VINING[1], KAREN E. DOBLE[2], JENNIFER M. WALDO[2], AURORA CANDELARIO-MARTINEZ[2], AND MICHAEL J. GREENBERG[2]

[1] *Department of Biological Sciences, University of Southern Maine, Portland, Maine 04104; and*
[2] *the Whitney Laboratory of the University of Florida, 9505 Ocean Shore Blvd.,*
St. Augustine, Florida 32086-8623

Abstract. The activities of both the lateral and frontal cilia of *Mercenaria mercenaria* were unaffected, either by the two endogenous SCP-related peptides AMSFYFPRMamide and YFAFPRQamide, or by FMRFamide (all at 10^{-6} *M*). Dopamine (DA) inhibited the lateral cilia; the mean EC_{50} was 2×10^{-6} *M*. The peptide YFAFPRQamide—but neither AMSFYFPRMamide nor FMRFamide—antagonized the inhibition induced by DA; this effect was dependent on both time and dose. At a DA concentration of 5×10^{-7} *M*, the effect of YFAFPRQamide appeared within 20 min and became maximal within 40–60 min; the mean EC_{50} at these times was 4.7×10^{-11} *M*. If the concentration of DA was increased to 10^{-6} *M*, the maximal effect of the peptide was delayed to 50 min, and the mean EC_{50} increased to 1.1×10^{-7} *M*. Particle transport by the frontal cilia was inhibited by 5-hydroxytryptamine (5HT); the mean EC_{50} was 5.7×10^{-7} *M*. Again, only YFAFPRQamide had an antagonistic effect on the 5HT-induced inhibition. At a 5HT concentration of 10^{-6} *M*, the effects of YFAFPRQamide did not appear until 45 min; the mean EC_{50} was 10^{-6} *M*. When radioimmunoassayed with an SCP antiserum, the elution profile of a gill extract overlapped those of the SCP-related peptides that had previously been identified in extracts of whole animals. These data suggest that all three SCP analogs occur in the gill. Immunohistochemistry of the gill, carried out with a monoclonal antibody raised to SCP_B, stained many varicose neuronal fibers. Most of these were associated with the gill musculature, but a sparse innervation of the filaments underlying the cilia was also observed. Some fluorescent nerve cell bodies were also seen in the gill tissue. Our results are consistent with the hypothesis that YFAFPRQamide modulates branchial activities—muscular as well as ciliary—that are associated with feeding.

Introduction

Molluscs are ciliary organisms; they are among the largest animals, yet cilia perform mechanical functions that, in many other taxa, are carried out primarily by muscles. For example, cilia are responsible for locomotion in gastropods as large as the lightning whelk *Busycon contrarium* and the helmet conch *Cassis tuberosa* (see Gainey, 1976; and Miller, 1974, respectively). Cilia are particularly well known for generating the currents that provide for respiration and feeding in all bivalves, except the Septibranchia. These currents are substantial; clearance rates generated by cilia in the American oyster *Crassostrea virginica* are as high as 24 to 27 l/h (Loosanoff and Nomeijko, 1946; Collier, 1959 [both cited in Foster-Smith, 1975]).

The ctenidial water currents are created by the lateral cilia (Purchon, 1968; Morton, 1983), although the abfrontal cilia may contribute between 30% and 40% of the flow in *Mytilus edulis* (Jones and Richards, 1993). The control of lateral ciliary activity, especially in *Mytilus*, has been studied for nearly a century (early work reviewed in Aiello, 1960; Paparo, 1972, 1985). In brief, the ciliated cells of bivalve gills are electrically coupled (Motokawa and Satir, 1975; Murakami and Machemer, 1982; Saimi *et al.*, 1983b; Stom-

---

Received 7 April 1999; accepted 22 July 1999.

* To whom correspondence should be addressed. Department of Biological Sciences, University of Southern Maine, P.O. Box 9300, Portland, ME 04104-9300. E-mail: gainey@usm.maine.edu

mel, 1984a), and branches of the branchial nerve run beneath the lateral and frontal ciliated cells (Aiello and Guideri, 1965; Paparo, 1972; Owen, 1974; Aiello, 1979). Apparently not all of the ciliated cells are innervated, but those that do receive neural input are reported to act as pacemakers (Paparo, 1972).

Both 5-hydroxytryptamine (5HT) and dopamine (DA) have been localized in the branchial nerves of *Mytilus* (Paparo and Finch, 1972; Stefano and Aiello, 1975). Moreover, electrical stimulation of either the cerebrovisceral connective or the branchial nerve at a stimulus frequency of 10 Hz increased the rate of beat of the lateral cilia, whereas stimulation at a frequency of 20 Hz decreased the rate. These excitatory and inhibitory effects of electrical stimulation were blocked, respectively, by serotonergic and dopaminergic antagonists (Catapane *et al.*, 1978, 1979; Catapane, 1983). Applied exogenously to isolated gills, 5HT stimulates the lateral cilia of all bivalves studied to date, including those of *Mercenaria mercenaria* (see Aiello, 1962, 1970, 1990; Paparo, 1972; Motokawa and Satir, 1975; Catapane, 1983). In contrast to the effect of 5HT, the response of lateral cilia to DA is variable. For example, the lateral cilia of *Mytilus edulis, Crassostrea virginica* (Paparo and Aiello, 1970; Catapane, 1983; Paparo, 1985), *Ostrea edulis, Mercenaria mercenaria,* and *Modiolus modiolus* (Gainey and Shumway, 1991) are inhibited by DA; but the lateral cilia of *Geukensia (=Modiolus) demissa* (Catapane, 1983), *Argopecten irradians,* and *Mya arenaria* (Gainey and Shumway, 1991) are unaffected. In summary, both 5HT and DA are present in the gills of at least some bivalves, and they appear to serve as endogenous transmitters regulating, in part, the activity of the lateral cilia.

Dose-response curves for 5HT and DA (see Catapane, 1983) show that the lateral cilia of *Mytilus* have a maximal beat frequency of about 25 beats/s, and that synchronous beating is lost below about 10 beats/s. Between these narrow limits (*i.e.*, 25 and 10 beats/s), the cilia respond in a graded manner, both to stimulation by 5HT and to inhibition by DA. At the lower limit (10 beats/s), these compounds seem to be activating a simple on-off switch. That such a switch controls pumping in intact animals has yet to be demonstrated unequivocally (Stefano *et al.*, 1977; Jorgensen, 1989; Jones and Richards, 1993).

In contrast to the lateral cilia, which transport water, the frontal cilia receive material that has been retained by the branchial filter and transport it to the food grooves; there it is packaged in mucus and carried to the labial palps (Purchon, 1968; Morton, 1983; Murakami, 1989). The frontal cilia are therefore intimately involved in feeding, and their activity is correlated with the rate of mucus secretion (Aiello, 1979). Beyond that generality, the pharmacology and control of the frontal cilia is poorly understood (reviewed by Aiello, 1990).

The inconsistency between the range of clearance rates in intact bivalves and the pharmacology of isolated gill cilia, as well as the distinct functions of cilia in different tracts, suggests that ciliary activity is probably not controlled by motoneurons that release only dopamine or serotonin. Studies of a pair of neurons in the pedal ganglia of the nudibranch *Tritonia diomedea* clearly show that, in this mollusc, peptides are also involved. These neurons innervate the locomotory cilia on the foot of *Tritonia*, augment the frequency of ciliary beat when stimulated, and synthesize and store a family of three pedal peptides (Peps). Moreover, the action of these peptides mimics neuronal stimulation by increasing the frequency of ciliary beating (reviewed by Willows *et al.*, 1997). The beat frequency of vertebrate cilia, particularly those of airway epithelia, are also regulated by neuropeptides, including Substance P (Lindberg and Mercke, 1986; Lindberg *et al.*, 1986; Lindberg and Dolata, 1993; Aiello *et al.*, 1991); vasoactive intestinal polypeptide (VIP) (Lindberg *et al.*, 1988); neuropeptide Y (NPY) (Cervin *et al.*, 1991; Wong *et al.*, 1998); endothelin (Tamaoki *et al.*, 1991); and vasopressin (Tamaoki *et al.*, 1998).

Among bivalved molluscs, three members of the SCP-related family of peptides have been isolated from the quahog *Mercenaria mercenaria:* 1AMSFYFPRMamide, AMSFYFPRMamide, and YFAFPRQamide; the second peptide is likely a degradation product of the first. Furthermore, high levels of these peptides occur in the gills, and SCP-related immunoreactivity has been localized to neural fibers in the gill. But though these peptides affect gut motility in the clam (Candelario-Martinez *et al.*, 1993), their effects upon ciliary activity in the gill have not yet been tested. We have, therefore, examined two of these SCPs—YFAFPRQamide and AMSFYFPRMamide—as well as DA, 5HT, and another neuropeptide, FMRFamide, for their actions upon both the lateral and frontal gill cilia of *Mercenaria.* The results indicate that one of the peptides, YFAFPRQamide, modulates the effects of the amines. Preliminary results of this study were presented to the Society for Integrative and Comparative Biology (Gainey *et al.*, 1997).

Materials and Methods

Animals

Quahogs (*Mercenaria mercenaria* L.) were obtained from Poquoson and Wachapreague, Virginia. The animals were held at 10°C in natural seawater (30‰) on a 12 h light/dark cycle. Individuals were held a minimum of 3 days prior to use.

The preparation

Gills were dissected away from the body wall distal to the visceral ganglia and were then separated into demibranchs. The dissection caused the beating of the lateral cilia to cease for an hour or more. But once the beating had resumed, the frequency remained unchanged for up to 24 h. Therefore, the gills were excised between 4 and 15 h before an experiment. Dorsoventral strips about 1 cm wide were cut from the isolated demibranchs and pinned to strips of rubber band that had been glued with rubber cement to the bottom of petri dishes (4.7 cm diameter). The dishes were filled with 5 ml of artificial seawater (recipe in Welsh *et al.*, 1968).

Drugs

Peptides were synthesized at the Protein Chemistry Core Facility of the Interdisciplinary Center for Biotechnology Research at the University of Florida, Gainesville. Dopamine (DA) and 5-hydroxytryptamine (5HT) were purchased from Sigma Chemical, St. Louis, Missouri.

Responses of the lateral cilia

The activity of the lateral cilia was measured as follows: Isolated, pinned-out strips of gill were placed on the stage of a compound microscope and observed at a magnification of 100×. The substage illuminator on the microscope was replaced with a mirror, and the rate of beating of the lateral cilia was determined by their synchrony with a Pasco Sf-9211 strobe light. Details of the measurement procedure are described in Gainey and Shumway (1991).

At the outset of each experiment, we would locate an area of the gill with well-defined metachronal waves and with frequencies between 12 and 25 beats/s. Once the initial rate was measured, the gill was not moved, and the same patch of cilia was used for all subsequent measurements. In all but the initial set of experiments on the effects of the peptides alone, two pieces of gill were used on separate microscopes, with one of these pieces serving as a control.

Larger quahogs (7 to 9 cm long) had lateral cilia that were consistently less sensitive to DA than those of smaller quahogs (5 to 7 cm). Moreover, the sensitivity of the lateral cilia of the smaller quahogs followed a seasonal pattern; they were less sensitive to DA from April to June. Therefore, all of the experiments reported here were done with gills from smaller animals and were carried out from June to April.

Effects of peptides: (1) Stimulation. Freshly dissected gill strips showing no lateral ciliary activity were exposed to one of the peptides at 10^{-6} *M;* controls were untreated. 5HT at 10^{-6} *M* was used as a positive control because it excites quiescent lateral cilia of *Mercenaria mercenaria* (Aiello, 1970). The rate of beat of the lateral cilia on the treated and control strips was measured hourly for 3 h. In a separate observation, we examined 10 areas on each strip of gill for the presence or absence of metachronal waves; the percentage of areas with metachronal waves (percent activity) was taken as an estimate of the ciliary activity of the strip. The data on rate and on percent activity were analyzed with ANCOVA with time as a covariate; the analysis was performed with the general linear models (GLM) procedure in SAS, version 6.

Effects of peptides: (2) Inhibition. Isolated strips of gill with active lateral cilia were exposed to one of the peptides at 10^{-6} *M;* controls were untreated. Measurements were made every 2 min for the first 10 min and then at 20, 40, and 60 min. The effects of the peptides on the rate of ciliary beating were evaluated with a two-way ANOVA with treatment, time, and treatment*time as factors; the analysis was performed with the GLM procedure in SAS.

Effects of peptides and DA. Previous studies have shown that 10^{-4} *M* DA will, within several minutes, completely arrest the lateral cilia of *Mercenaria* (Gainey and Shumway, 1991). This effect is temporary because DA slowly oxidizes, and the cilia eventually return to their initial rate of beating. To assess the effects of the peptides on this DA arrest, we exposed isolated demibranch strips to concentrations of 10^{-6} *M* of each peptide; 10 min later, the same demibranch was exposed to 10^{-4} *M* DA. Controls were exposed only to 10^{-4} *M* DA. The activity of the lateral cilia was recorded every 2 min until it returned to the initial rate. In some instances, the ciliary beating on one of the gill strips did not return to its initial rate before the end of the experiment; data of this type were designated *censored.* The results were analyzed with the Wilcoxon test with the lifetest procedure in SAS; this program adjusts for censored data.

Dose-dependent effects. In these experiments, two strips taken from the same demibranch were pinned out and observed with separate microscopes. The initial rate of ciliary beating of both strips was then determined. Thereafter, the measurement of ciliary activity at any time was expressed as a fraction of the initial rate; *i.e.*, the *fractional rate* of beat. After a drug of interest was applied, the fractional rate of the treated strip was corrected by subtraction of the fractional rate of the control strip. This *fractional difference* was taken as the measure of peptide effect and was used as the ordinate on dose-response curves.

(1) *Dopamine.* In these experiments, oxidation of DA was retarded with an ascorbic acid buffer as described by Malanga (1975a). DA was added to the treated strip; the control strip was untreated; and the rate of beat of both strips was determined every 10 min for 1 h. Each pair of gill strips was used to measure only one dose of DA. Because DA is inhibitory, the value of the fractional difference becomes larger and more negative with dose. Therefore, to make the DA dose-response plots more comprehensible, the effect was expressed as the *adjusted fractional difference:* $[1 + (\text{fractional rate}_{\text{treated}} - \text{fractional rate}_{\text{control}})]$.

(2) *YFAFPRQamide.* After the measurement of initial rate, a dose of peptide was added to the treatment strip. Ten minutes later, DA (either 5×10^{-7} *M* or 10^{-6} *M*) was added to both the treatment and control gills. Thereafter, rates

were measured every 10 min for 1 h. The fractional difference was used as the measure of effect in the dose-response curves; notice that when the response of peptide is maximal, no inhibition by DA is observable, so the fractional rate of the control strip approximates zero.

Responses of the frontal cilia

The activity of the frontal cilia was measured as follows: Isolated, pinned-out strips of gill were observed at a magnification of 100× with a compound microscope, and the activity of the frontal cilia was determined by the rate of transport of polystyrene microspheres (diameter, 0.85–1.0 μm; Polysciences, Inc., Warrington, Pennsylvania). The time (in seconds) required for these particles to travel 0.5 mm was measured with a stopwatch and an ocular micrometer. Particle transport rates (mm/s) were expressed as a fraction of the initial rate. During the experiments on peptides, five readings were taken on each gill strip at each time. But during the experiments on the effects of the peptides and 5HT, three readings were made at each time. Once the initial rate was measured, the gill strips were not moved, and the same gill filaments were used for all subsequent measurements.

Effects of peptides. Isolated strips of gill were exposed to one of the peptides at 10^{-6} *M;* controls were untreated. Particle transport rates were measured every 5 min for 25 min. Initial analysis of these data indicated a positive correlation between the standard deviation and the mean of the fractional initial rate. Therefore, the data were transformed with natural logarithms, which removed this correlation. The effects of the peptides on the frontal cilia, as well as the effects of the peptides plus 5HT, were evaluated using repeated measures ANOVA; the analyses were performed using the GLM procedure in SAS.

Effects of peptides with 5-hydroxytryptamine. We found that 5HT inhibits the rate of particle transport by the frontal cilia. To assess the effects of the SCPs on this inhibition, we first exposed isolated strips of gill to the SCPs at 10^{-6} *M;* 10 min later, the same gill strip was exposed to 10^{-6} *M* 5HT. Control strips were exposed only to 10^{-6} *M* 5HT. Particle transport rates were measured every 15 min for 1 h.

Dose-dependent effects. We followed almost the same protocols and analyses that were used to examine the effects of DA and of YFAFPRQamide plus DA on the lateral cilia. The exceptions were that (1) readings were taken every 15 min for 1 h; and (2) three replicate readings on each gill strip at each time were averaged, and the average rates were expressed as a fraction of the average initial rate of each strip. In the experiments on the effects of YFAFPRQamide plus 5HT, the concentration of 5HT was 10^{-6} *M.*

Regression analyses, significance levels

All dose-response curves, and the concentrations of agonists giving half-maximal responses (EC_{50}), were estimated, at each time, from a logistic model [response $= 1/(1 + e^{(\beta 0 + \beta 1 * \log \ \mathrm{dose})})$], with a nonlinear regression procedure (Nlin) in SAS. *F* tests were used to compare the regression lines using a general linear test approach (Bates and Watts, 1988; Neter *et al.*, 1990). In most instances, means are reported with their standard errors and sample sizes. All test statistics, including ANCOVA and ANOVAs, were considered significant at probabilities less than 0.05.

Detection of SCPs in clam gill

Radioimmunoassay of a fractionated extract. In 1993, Candelario-Martinez *et al.* tabulated the distribution of SCP-related immunoreactivity among the tissues of *M. mercenaria* (see their table 1). In this paper, we present the unpublished immunoreactive profile of the SCPs in gill, which were obtained as follows.

Gills from 20 animals were extracted in acetone. The extract was evaporated, and the aqueous portion was loaded onto a Prep-10 Octyl column (10 × 100 mm, 4 ml/min) and eluted with a gradient of acetonitrile (16%–40% over 30 min) in water with 0.1% trifluoroacetic acid. Fractions were collected every half minute and analyzed by radioimmunoassay; elution patterns were plotted from these data. Details of the fractionation and the assay are set out in Candelario-Martinez *et al.* (1993).

Immunohistochemistry. Small, rectangular pieces of tissue were cut from the outer demibranchs of several clams; the samples usually included the ventral edge of the gill and were 2–3 mm wide and 3–5 mm high. A few minutes after dissection, the tissues were fixed in a solution of paraformaldehyde, prepared freshly as follows. A solution of paraformaldehyde (4 g in 45 ml distilled water) was heated at 60°C for 10 min, clarified by the addition of 1 *N* NaOH, brought to a final volume of 50 ml, and cooled on ice for about 20 min. Thereafter, 50 ml of 0.2 *M* sodium potassium phosphate buffer (SPB) was added, together with 15 g of sucrose to approximate the osmolality of seawater. The tissues were left in this fixative overnight at 4°C.

After fixation, the tissues were rinsed twice (5 min each) with Tris buffered saline (TBS; pH 7.4), and then placed in 30% sucrose/PBS and left overnight at 4°C. The tissues were then embedded in Tissue Tek O.C.T., frozen, and sectioned (10 μm). The sections were collected onto gelatin-coated slides, and stored at −80°C for at least 24 h prior to staining.

The sections were preincubated for 30 min at 37°C in TBS containing 0.1% Triton X-100 and 2% normal goat serum. The preincubation medium was then poured off and replaced with the primary antibody—a monoclonal raised to SCP_B (Masinovsky *et al.*, 1988)—which was diluted 1:100

in the preincubation medium. After 4 h in the primary antibody at room temperature, the sections were rinsed three times (5 min each) in TBS, and secondary antibody—fluoresceine isothiocyanate-conjugated goat anti-mouse IgG (FITC-GAM IgG)—was then applied to the sections; incubation continued for 2 h, at room temperature, in the dark. The sections were then washed once for 5 min in TBS containing 10 μg/ml of 4′,6-diamidino-2-phenylindole (DAPI), an ultraviolet-excitable, nucleic acid-binding dye. The sections were washed twice more (5 min each) in TBS, and coverslips were applied; the mounting medium was 60% glycerol/TBS containing *p*-phenylenediamine (PPD). Controls were treated as described above, except that the primary antibody, before being applied to the sections, was incubated overnight, at 4°C, on a rotating shaker, with either YFAFPRQamide or AMSFYFPRMamide (10^{-3} *M*).

Micrographs were generated with a Leica/Leitz DMRB microscope equipped with filters that allow the mutually exclusive visualization of fluorochrome and DAPI staining. Digital images were gathered with a Hamamatsu color chilled 3CCD camera (C5810) and were prepared for printing with Adobe Photoshop.

Results

Lateral cilia

Peptides. Analysis of preliminary experiments on gill strips exposed to either AMSFYFPRMamide, YFAFPRQamide, or FMRFamide (all at 10^{-6} *M*) revealed that none of the peptides had any significant stimulatory or inhibitory effect upon the activity of the lateral cilia: stimulation (ciliary rate), $F_{(3,119)} = 0.85$, $P = 0.47$; stimulation (percent activity), $F_{(3,79)} = 0.37$, $P = 0.78$ (Table I); inhibition (ciliary rate), $F_{(3,28)} = 0.26$, $P = 0.85$. In the experiment on the inhibition of spontaneous ciliary activity, the mean rate of beat of the control cilia, as well as those treated with any of the three peptides, was 25 beats/s ($n = 9$ gills for each treatment).

Table I

Responses of quiescent lateral cilia exposed to peptides and 5HT at 10^{-6} M

Treatment	Frequency (beats/s)	SE	% activity	SE	*n*
Control	11	1.1	36	5.5	6
AMSFYFPRMa	12	1.1	31	5.5	6
YFAFPRQa	10	1.1	30	5.5	6
FMRFamide	12	1.1	30	5.5	6
5HT*	12	1.1	57**	5.8	6

Controls were untreated; *n* = number of gill-strip preparations. Responses are frequency (beats/s); or as the percent occurrence of metachronal waves in 10 separate areas of each gill (% activity). The data are all expressed as least square means.

* Excluded from the ANCOVA in text.

** Significantly greater ($P < 0.05$) than the control and the peptides.

Table II

Comparison of mean times to recovery (±SE) for lateral cilia exposed simultaneously to peptides (10^{-6} M*) and DA (*10^{-4} M*), and for lateral cilia exposed only to DA (*10^{-4} M*)*

Treatment	Recovery time Treated (min)	 Control (min)	*n*	*P***
AMSFYFPRMa	62 ± 9.26	60 ± 9.44	5	0.60
YFAFPRQa	43 ± 9.04	64 ± 8.19	6	0.02
FMRFamide	69 ± 9.16	62 ± 5.36	6	0.93

n = number of gill strip preparations.

** *P* values were generated with a Wilcoxan test.

Peptides and dopamine. To determine whether the peptides might alter the activity of lateral cilia inhibited by DA, we exposed isolated gill strips to individual peptides at 10^{-6} *M*, and 10 min later to 10^{-4} *M* DA. Control strips were exposed only to DA. An ascorbic acid buffer was omitted in these experiments, so DA oxidized and the ciliary beat recovered. The recovery times of lateral cilia exposed, at first, to either AMSFYFPRMamide or FMRFamide, and then to DA, were not significantly different from those of the controls (DA only, Table II). In contrast, the lateral cilia of gill strips exposed to YFAFPRQamide and then to DA returned to their initial rates within 42 ± 9.0 min, whereas the DA controls required 64 ± 8.2 min to return to their initial rates; these times are significantly different (Table II).

Dose-dependent effects. The adjusted fractional differences, measured at several times, were plotted against the log of the DA concentration, and the family of calculated regression lines is set out in Figure 1A. This graph shows that the effects of DA appear within 10 min of the treatment and remain constant for 1 h; there is no statistical difference among the regression lines plotted in Figure 1A ($F_{(10,120)} = 0.22$, $P = 0.99$). The mean EC_{50}, as estimated from the regression parameters, is 2.0×10^{-6} *M* ($\pm 6.9 \times 10^{-8}$ *M*). But the dose-response curves are very steep; the change from 90% to 10% maximal activity is effected by an increase of only half a log unit in the concentration of DA (3–4 μM). Moreover, Figure 1B shows that the response is essentially biphasic; *i.e.*, the cilia are either beating or not at a DA concentration of about 3 μM.

The dose-dependent effects of YFAFPRQamide on DA-treated cilia were studied on gills exposed to 5×10^{-7} *M* DA. This concentration of the amine was chosen because it was predicted (from the dose-response regression equation) to inhibit the cilia by 17% of their initial rate; thus the peptide could, in theory, either potentiate or inhibit the effects of DA. The actual response of the control gills to DA was quite variable, ranging from 10% to 100% inhibition of the original rate, but YFAFPRQamide always had an antagonistic effect on the action of DA. That is, gill strips treated with varying concentrations of the peptide and 5×10^{-7} *M* DA were inhibited less than gill strips exposed to DA alone. The threshold for the effect of YFAFPRQamide was about 5×10^{-12} *M*. The maximal response (*i.e.*, complete block of inhibition) was produced by about 10^{-8} *M*. Moreover, the antagonistic effects of the peptide were time dependent. A set of dose-response regression lines produced at 10-min intervals shows that the effects of the peptide began to appear within 20 min after the addition of DA. The regression lines from 40 to 60 min are not statistically different ($F_{(4,44)} = 0.71$, $P > 0.05$; Fig. 2A).

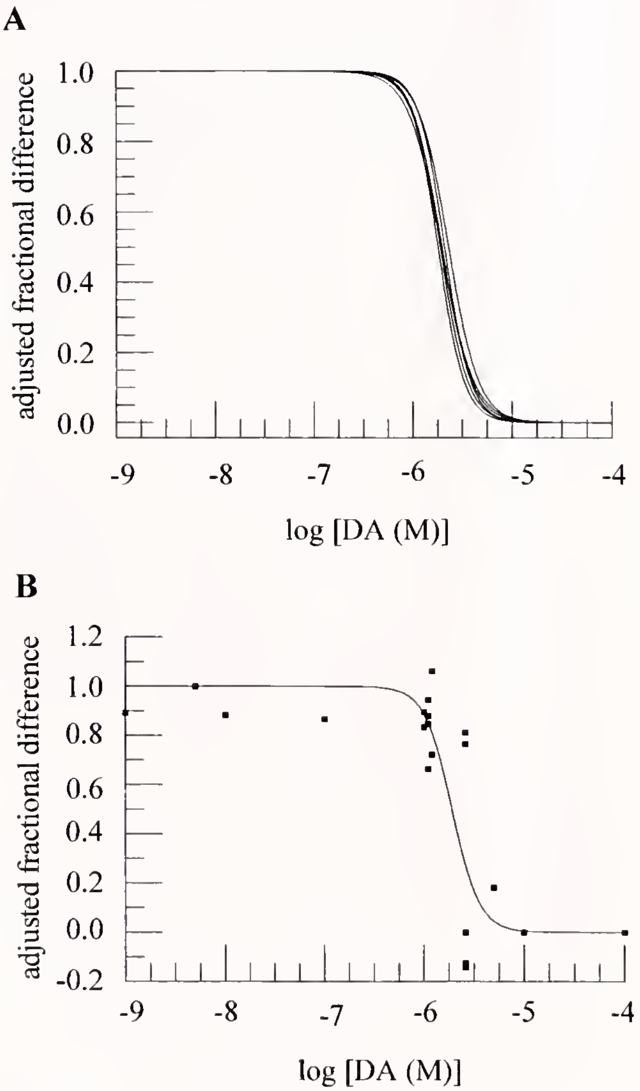

Figure 1. (A) Dose-response curves for the inhibitory effect of dopamine (DA) on lateral cilia. Ordinate: the *adjusted fractional difference*: [1+ (fractional treatment rate − fractional control rate)]; this measure is described in the Methods section. The regression lines were derived from measurements made every 10 min after the addition of DA, continuing to 60 min. Data points are omitted for clarity. (B) The regression line at 60 min with data points shown.

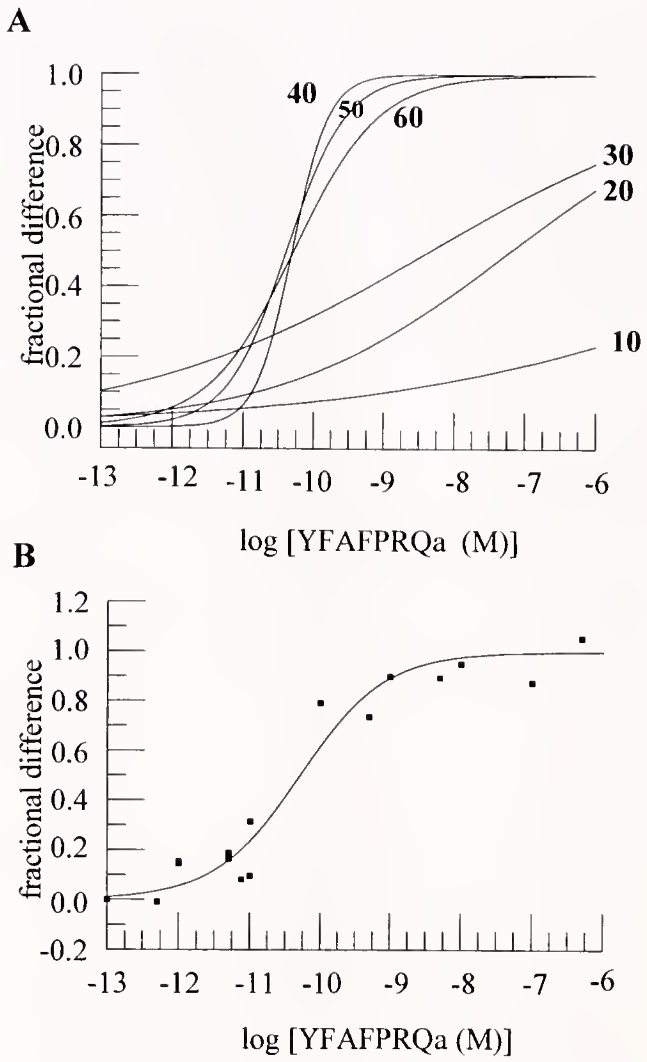

Figure 2. (A) Dose-response curves illustrating the antagonistic effect of YFAFPRQamide on the dopamine- (DA-) induced inhibition of lateral cilia. Ordinate: the *fractional difference* between lateral cilia exposed to 5×10^{-7} *M* DA plus various concentrations of YFAFPRQamide, and lateral cilia exposed only to 5×10^{-7} *M* DA. Peptides were added 10 min before the cilia were exposed to DA. The regression lines were generated at the times indicated *after the addition of DA*. The slope parameter ($\beta 1$) of the line at 10 min is not significantly different from 0. Data points are omitted for clarity. (B) The regression line at 60 min with data points included.

The mean EC_{50} for these times is 4.7×10^{-11} *M* ($\pm 3.5 \times 10^{-12}$ *M*).

To determine whether the latency in the effect of YFAFPRQamide might reflect the permeability of the gills to the peptide, the concentration of DA was increased, from 5×10^{-7} *M*, to 10^{-6} *M*. If the latency were due primarily to the low permeability of the peptide, then increasing the dose of DA should only increase the EC_{50} of YFAFPRQamide and not alter the time course of the response. In fact, the threshold for the effect of the peptide increased from

5×10^{-12} *M* to about 10^{-8} *M;* the dose producing the maximal effect increased from 10^{-8} *M* to about 5×10^{-7} *M*. Again, the antagonistic effects of the peptide on the DA-induced inhibition were time dependent, and the effect began to appear 20 min after the addition of DA. But, the response did not stabilize until 50 min after the addition of dopamine (Fig. 3A), as opposed to 40 min previously (compare with Fig. 2A). Moreover, the 40-min regression lines for the two doses of DA are significantly different (compare Figs. 2A and 3A; $F_{(2,28)} = 10.3$; $P = 0.0004$). And, the regression lines at 50 and 60 min in Figure 3A are not statistically different ($F_{(2,26)} = 0.45$, $P = 0.64$); the mean EC_{50} for these times is 1.1×10^{-7} *M* ($\pm 2.6 \times 10^{-8}$ *M*). Finally, a Mann-Whitney *U* test revealed that the mean EC_{50} of gills exposed to YFAFPRQamide and 10^{-6} *M* DA was significantly greater than that of gills exposed to YFAFPRQamide and 5×10^{-7} *M* DA ($P = 0.04$). Thus, the latency of the peptide response cannot be due entirely to permeability.

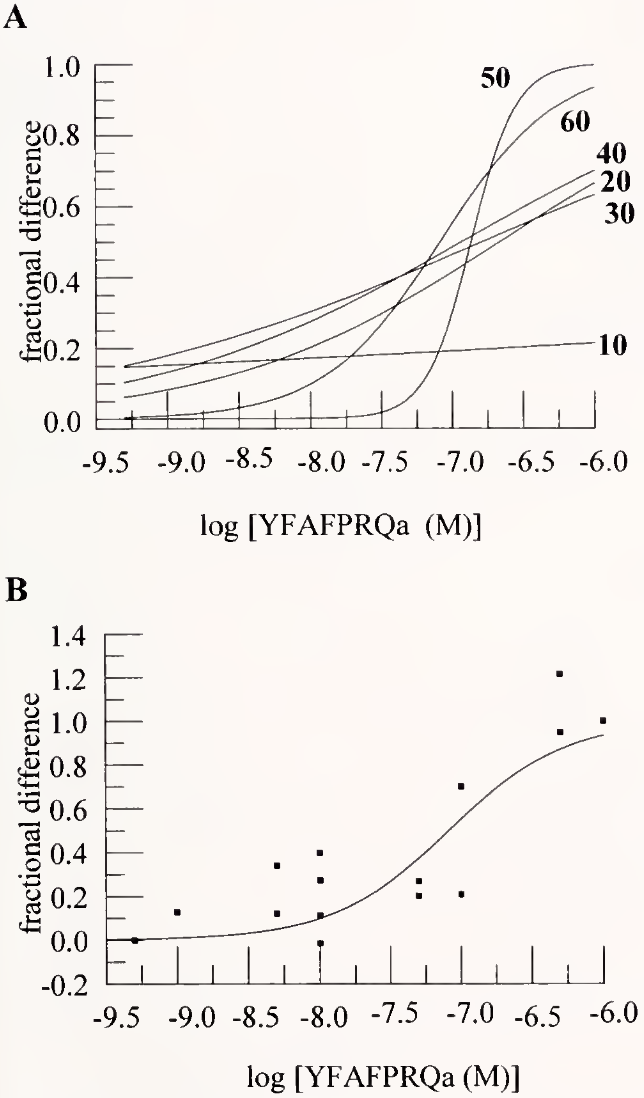

Figure 3. (A) Effect of a higher dose of dopamine (DA) on the dose-response curves for the antagonistic effect of YFAFPRQamide (compare with Fig. 2). Ordinate: the *fractional difference* between lateral cilia exposed to 10^{-6} *M* DA plus various concentrations of YFAFPRQamide, and lateral cilia exposed only to 10^{-6} *M* DA. Peptides were added 10 min before the cilia were exposed to DA. The regression lines were generated at the times indicated after the addition of DA. The slope parameter ($\beta 1$) of the line at 10 min is not significantly different from 0. Data points are omitted for clarity. (B) The regression line at 60 min with data points included.

Beat frequencies. The lateral cilia used in dose-response studies, including controls, beat in metachronal waves at frequencies from 7 to 27 beats/s, or they did not beat at all. That is, no metachronal waves appeared at frequencies lower than 7 beats/s ($n = 888$ on 148 pieces of gill).

Frontal cilia

Peptides. Preliminary experiments on gill strips exposed to the three peptides, all at 10^{-6} *M*, revealed that none of the peptides had a significant effect on the activity of the frontal cilia: AMSFYFPRMamide, $F_{(1,78)} = 0.05$, $P = 0.81$; YFAFPRQamide, $F_{(1,78)} = 1.66$, $P = 0.20$; FMRFamide, $F_{(1,48)} = 3.18$, $P = 0.08$; the mean rate of particle transport in all cases was 0.29 mm/s.

SCPs and 5-hydroxytryptamine. To determine whether the two SCPs might alter the activity of frontal cilia inhibited by 10^{-6} *M* 5HT, we first exposed isolated gill strips to either AMSFYFPRMamide or YFAFPRQamide (10^{-6} *M*) and then, 10 min later, to 10^{-6} *M* 5HT. Controls were exposed only to 5HT. Neither peptide had a significant effect upon the 5HT-induced inhibition: AMSFYFPRMamide, $F_{(1,16)} = 1.22$, $P = 0.28$; YFAFPRQamide, $F_{(1,8)} = 3.93$, $P = 0.08$.

Dose-dependent effects. In Figure 4A, the regression lines of the adjusted fractional difference are plotted against the log of the 5HT concentration and time. The graph shows that the inhibitory effects of 5HT on the frontal cilia appear within 15 min and remain constant for 1 h; there is no statistical difference between these regression lines ($F_{(6,34)} = 0.32$, $P = 0.92$). The mean EC_{50} is 5.7×10^{-7} *M* ($\pm 3.5 \times 10^{-7}$ *M*). Particle transport was, however, never completely inhibited; the maximal inhibition was about 80% of the initial rate at 10^{-3} *M* 5HT.

The effect of YFAFPRQamide on frontal cilia inhibited by 5HT was not statistically significant. But because the probability of the "*F*" value from the ANOVA was 0.08, which is close to the significance level of 0.05, and because the peptide had modulated the action of DA on lateral cilia, we decided to measure the dose-dependency of the effects of the peptide on 5HT-induced inhibition. The frontal cilia were exposed to 10^{-6} *M* 5HT, a concentration predicted to inhibit the cilia by 39% of their initial rates, and to varying concentrations of the peptide. The threshold for the effect of

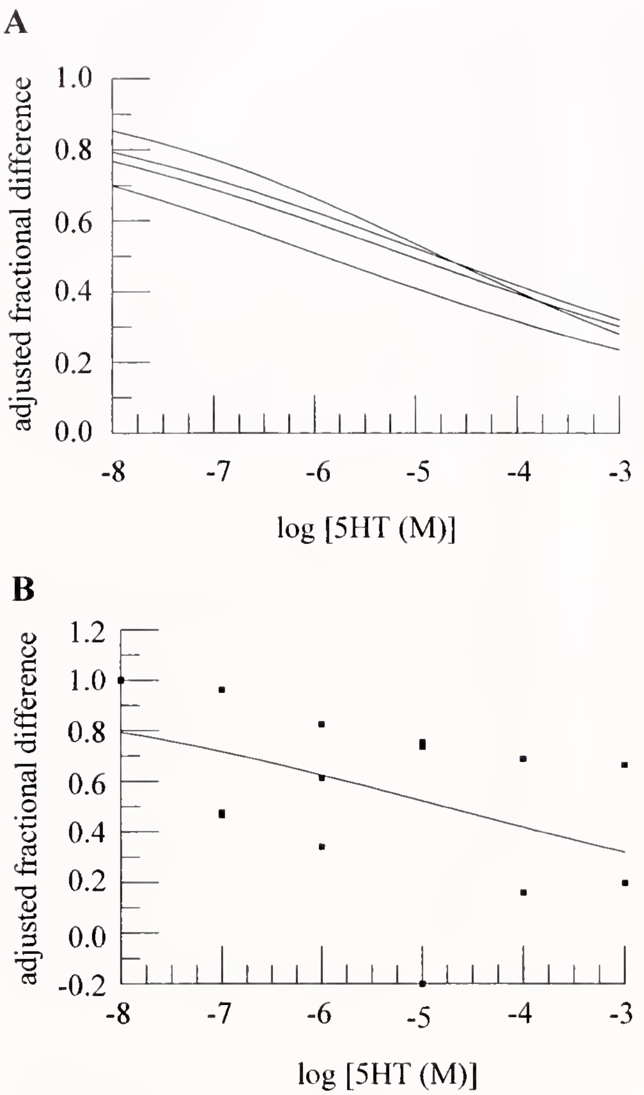

Figure 4. (A) Dose-response curves for the inhibitory effect of 5-hydroxytryptamine (5HT) on frontal cilia. Ordinate: the *adjusted fractional difference:* [1+ (fractional treatment rate − fractional control rate)]; explained in the Methods section. The regression lines were derived from measurements made every 10 min after the addition of 5HT, continuing to 60 min. Data points are omitted for clarity. (B) The regression line at 60 min with data points included.

YFAFPRQamide was about 5 × 10^{-7} *M*. At the maximum dose of YFAFPRQamide used (3 × 10^{-6} *M*), there was about a 30% difference between the controls and the treatment cilia. This means that the cilia returned to their original rates because the 5HT did not completely inhibit them. The effects of the peptide did not appear until 45 min after the addition of 5HT, and there was no statistical difference between the regression lines at 45 and 60 min ($F_{(3,32)} = 0.1$, $P = 0.91$; Fig 5A). The mean EC$_{50}$ is 10^{-6} *M* (±1.5 × 10^{-7}).

Particle transport rates. Particle transport rates of both treated and control cilia varied from 0.05 to 0.56 mm/s (n = 1560 on 52 pieces of gill), but the rates were never zero in any of the experiments.

Identification of SCPs in clam gill

Radioimmunoassay. The purification of SCPs from clam extracts is strongly influenced by two features of the longest SCP, IAMSFYFPRMamide: First, even as the purification proceeds, this peptide is degrading by stepwise cleavage at

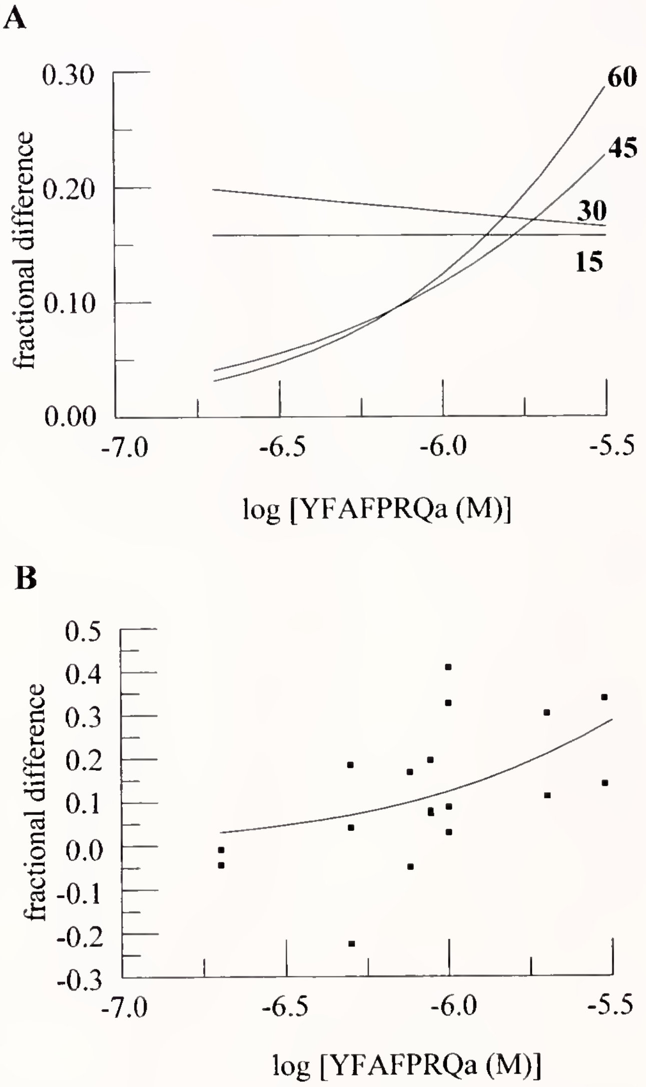

Figure 5. A) Dose-response curves illustrating the antagonistic effect of YFAFPRQamide on the 5-hydroxytryptamine- (5HT-) induced inhibition of frontal cilia. Ordinate: the *fractional difference* between frontal cilia exposed to 10^{-6} *M* 5HT plus various concentrations of YFAFPRQamide, and frontal cilia exposed only to 10^{-6} *M* 5HT. Peptides were added 10 min prior to exposure of the cilia to 5HT. The regression lines were generated at the times indicated *after the addition of 5HT*. The slope parameter ($\beta 1$) of the lines at 15 and 30 min are not significantly different from 0. Data points are omitted for clarity. (B) The regression line at 60 min with data points included.

the N-terminal. Second, the peptide and its degradation products oxidize at one or both methionine residues. Thus, peaks of immunoreactivity tend to be wide, and their position tends to shift from step to step of the purification. Nevertheless, SCP-related peptides were isolated and identified, either by mass spectroscopy or chemical sequencing, from extracts of whole clam (Candelario-Martinez *et al.*, 1993). This work is summarized in Figure 6A, which shows that, although YFAFPRQamide occurred only in fraction 10, IAMSFYFPRMamide and its oxidized forms were identified from fractions 18 to 27. The truncated peptide AMSFYFPRMamide and its oxidized forms were distributed from fraction 14 to 27. The smaller degradation products of IAMSFYFPRMamide all eluted early.

When extracts of gill were fractionated on the same HPLC system, most of the immunoreactivity eluted between 5 and 15 min (fractions 10–30). The elution profiles generated from three extracts were all very similar; *i.e.*, three peaks centered, respectively, at fractions 11, 18, and 24 (*e.g.*, Fig. 6B). No SCPs have been successfully purified from extracts of clam gills, but the near congruence of the elution profiles of extracts of gill and whole clams suggests that all of the substances found in whole clams are also present in gills. Moreover, a search for the major products (YFAFPRQamide, AMSFYFPRMamide, and IAMSFYFPRMamide) would probably begin with an examination of the three obvious peaks seen in the gill extract.

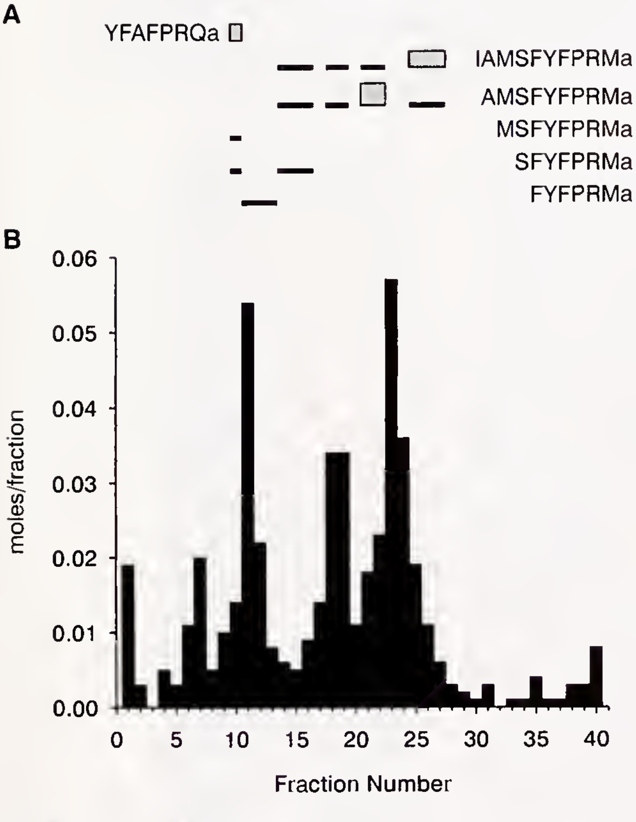

Figure 6. An assessment of the distribution of SCP-related peptides in acetone extracts of tissues of *Mercenaria mercenaria*. (A) SCP-related peptides identified in extracts of whole clams (replotted data from Candelario-Martinez *et al.*, 1993). The extract was fractionated on HPLC, as described in the Methods section. Five peaks were selected for purification, and the labeled peptides were identified, either by sequencing (grey boxes) or by FAB-ms (thickened lines). Note that IAMSFYFPRMamide, AMSFYFPRMamide, and their presumed degradation products are widely distributed in the whole clam extract, whereas YFAFPRQamide is restricted to fraction 10. (B) Elution profile of an extract of gills for comparison with the peptide distribution in A.

Immunocytochemistry. SCP-like immunoreactive staining in the gill tissue was apparent only in the fibers and cell bodies of neurons. Most of the fibers seen were varicose and occurred in the interior of the gill, in the interlamellar septa, and associated with muscle (Fig. 7A). But a very few, fine immunoreactive fibers were also observed in the proximal walls of the filament projecting toward the ciliary tracts (Fig. 7B, C). Infrequently, these fibers could be followed to the distal end of the filament, and to the base of the epithelial cells bearing the frontal cilia (Fig. 7D). Neuronal cell bodies were also stained; they appeared interior to the bands of horizontal muscle underlying the filaments (Fig. 8A). Under UV illumination, the nuclei of these cells, which were stained with DAPI, were clearly visible (Fig. 8B).

When we preabsorbed the primary SCP antibody with either YFAFPRQamide or AMSFYFPRMamide, staining was abolished (not shown). In addition, preabsorption of this monoclonal antibody with FMRFamide affected neither its immunostaining of *Tritonia diomedia* ganglia (Masinovski *et al.*, 1988) nor that of crustacean neurons (Arbiser and Beltz, 1991). However, the immunostaining is reduced or abolished upon preabsorption with TNRNFLRFamide (Arbiser and Beltz, 1991), a native peptide discovered in the lobster *Homarus americanus* (Trimmer *et al.*, 1987). On the other hand, no N-terminally extended FLRFamide analogs could be detected by a specific immunochemical analysis of HPLC fractions of ganglion extracts from *M. mercenaria* (K. E. Doble, D. A. Price, and M. J. Greenberg, unpublished results).

Discussion

We have shown that the activity of the lateral and frontal cilia of the *Mercenaria* gill are modulated specifically by low concentrations of an endogenous SCP-related neuropeptide, YFAFPRQamide. We suppose that YFAFPRQamide is a modulator because its effect—a diminution of inhibition—is apparent only on lateral and frontal cilia that have been treated with their inhibitory transmitters (DA and 5HT, respectively); *i.e.*, none of the peptides had any direct effect upon the activity of untreated, spontaneously beating cilia. Finally, the specificity of the modulation is suggested by the lack of activity, not only of FMRFamide, but also of AMSFYFPRMamide, the other SCP-related peptide tested.

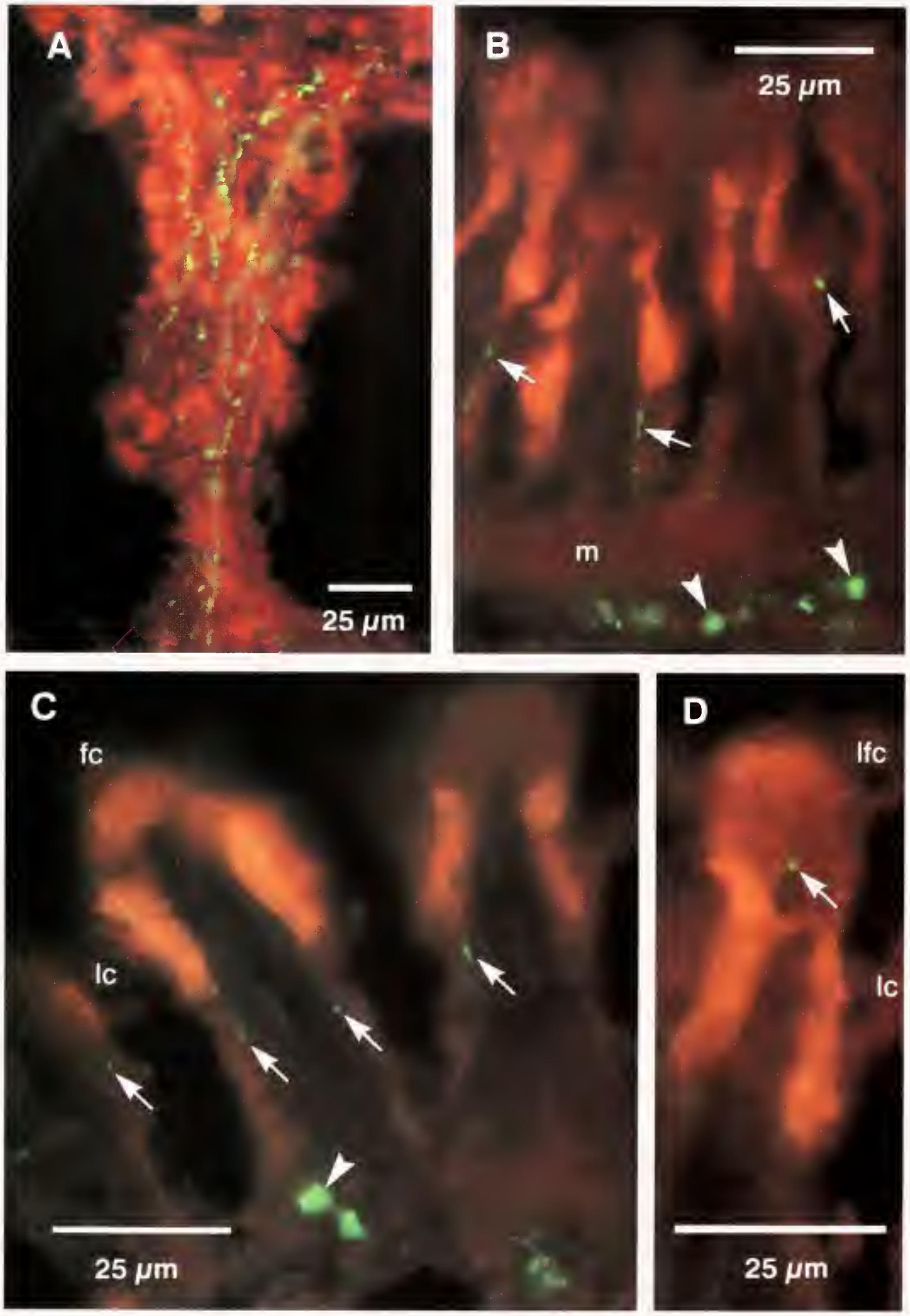

Figure 7. Frontal-sections through the gill of *Mercenaria mercenaria.* (A) SCP-related immunoreactivity occurs within varicose neural fibers in the interlamellar septa. (B–D) Innervation of the gill filaments that bear the ciliary tracts. Thin, sparse fibers (small arrows) can be followed from the base of the filament (B), to the level of the lateral cilia (C), and occasionally to the distal end of the filament below the frontal and laterofrontal cilia (D). Cell bodies (large arrowheads) are usually (*e.g.,* B), but not always (C), found proximal to the filaments. Abbreviations: fc, frontal cilia; lc, lateral cilia; lfc, laterofrontal cilia.

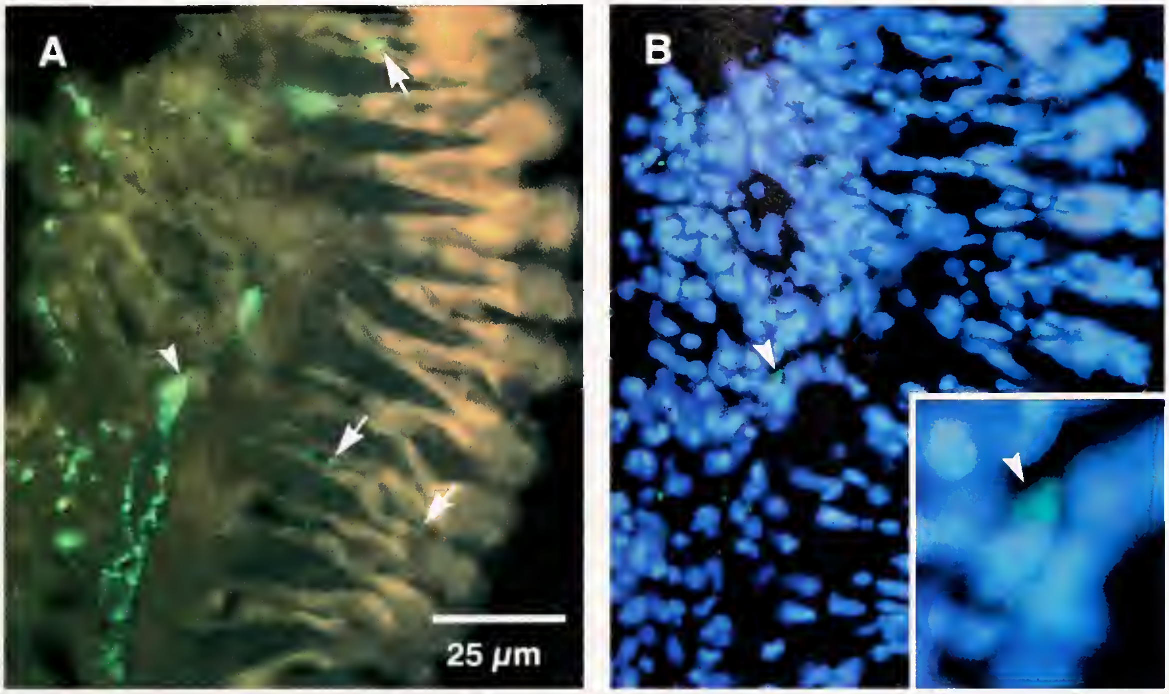

Figure 8. Neuronal cell bodies stained with the primary SCP-antibody are apparent in the gill tissue (A, arrowhead). Under UV illumination, the nucleus of such putative cell bodies can be seen to be stained with DAPI (B). The small arrows indicate fine fibers that innervate the gill filaments (see also Fig. 7).

That YFAFPRQamide and AMSFYFPRMamide (as well as the untruncated analog IAMSFYFPRMamide) are endogenous peptides of *Mercenaria mercenaria* was clearly demonstrated by Candalario-Martinez *et al.* (1993). More to the point, however, the immunoreactive elution profile seen when gill extracts are fractionated on HPLC, taken together with our immunocytochemical observations, is consistent with the hypothesis that these peptides occur in the gill, and specifically within neurons. Furthermore, our demonstration of immunoreactive neuronal cell bodies in the gill suggests that some of the SCP-related peptides are actually synthesized within this tissue. We note, however, that the individual branchial neuropeptides have yet to be unambiguously identified in gill, and that the organization of the precursor RNA and its pattern of expression remains completely unresolved.

Although most of the immunostained SCPergic nerves are associated with muscle, particularly in the interlamellar septa, some of these fibers project out along the filament toward the lateral cilia. At the distal end of the filament, fibers appear to run along the dorsoventral axis of the filament, under the frontal and laterofrontal cilia. That these fibers actually innervate ciliated cells (and not, for example, mucus glands), and whether their origin is in the visceral ganglion or the gill, remains to be established. Nerves in the same locations have been reported in the gill filaments of *Mytilus edulis* (references in Introduction), and also in *Chlamys varia* and *Ostrea edulis* (see Owen and McCrae, 1976). Moreover, Setna (1930) and Elsey (1935) observed nerve cell bodies in, respectively, the gills of *Pecten maximus* and *Ostrea (=Crassostrea) gigas.* But all of these animals are in the subclass Pteriomorphia, and mussels and scallops possess filibranch gills. Nerve fibers have been observed, from time to time, in the eulamellibranch gills of heterodonts like *Mercenaria mercenaria,* (*e.g., Ensis siliqua* in Atkins, 1937), but the *innervation* of such gills has not been described. So broad generalizations about branchial innervation in the Bivalvia must be made cautiously, at present.

The effects, reported here, of endogenous YFAFPRQamide on the branchial cilia of *Mercenaria* are, in their general characteristics, reminiscent of those of VIP on the cilia of the intact rabbit maxillary sinus (Lindberg *et al.,* 1988). Immunoreactive VIP occurs in neural fibers under the epithelium, as well as in the sphenopalatine ganglion. Moreover, although arterial infusion of the peptide alone is without effect on mucociliary activity, VIP does potentiate the stimulatory action of infused methacholine. In contrast, the other peptides affecting mammalian airway cilia have observable effects on intact tissues (references in Introduction)—as do the endogenous pedal peptides (T-Peps) on the pedal cilia of *Tritonia* (see Willows *et al.,* 1997).

The T-Peps and the SCP-related peptides of *Mercenaria* also differ in the specificity of their actions. That is, only one of the bivalve homologs (YFAFPRQamide) is a ciliary modulator, whereas all three *Tritonia* homologs are roughly equipotent in their direct stimulation of cilia. Nevertheless, an ortholog of the T-Peps—an A-Pep isolated from *Aplysia californica* (Lloyd *et al.*, 1996)—is also ineffective on the pedal cilia of *Tritonia* (Willows *et al.*, 1997).

All but one of the amino acid residues in YFAFPRQamide are either highly conserved or identical to those in the 13 known molluscan SCPs (see table II in Candelario-Martinez *et al.*, 1993). The exception is the C-terminal glutaminyl amide, and so the specific modulatory action of YFAFPRQamide on the clam gill cilia can probably be attributed to this residue. Since YFAFPRQamide is consistently more potent than AMSFYFPRMamide on the contractility and rhythmicity of the various parts of the clam gut (Candelario-Martinez *et al.*, 1993), we might suggest that the C-terminal Gln-NH_2 improves binding to a particular SCP receptor in the branchial epithelium of *Mercenaria*, as for example, the action of substance P on the ciliated epithelium of the rabbit maxillary sinus seems to be specifically at the NK1 receptor (Lindberg and Dolata, 1993). However, the rapid degradation of IAMSFYFPRMamide and AMSFYFPRMamide, relative to YFAFPRQamide, in extracts and presumably in the intact tissue, might also explain the differences in potency. If this were the case, the prolonged onset of the YFAFPRQamide modulation might be telling us that AMSFYFPRMamide is ineffective because a threshold concentration is never reached. We note that the stimulatory effects of substance P on the ciliary beat of cultured, brushed human nasal epithelial cells were also dependent upon endopeptidease activity (Smith *et al.*, 1996).

In any event, the slow development of the YFAFPRQamide effect is striking. The modulation did not appear until 20 min after treatment of the lateral cilia with DA. Moreover, when the concentration of DA was increased from 5×10^{-7} *M* to 10^{-6} *M*, the maximal effect of the SCP was delayed further, from 40 min to 50 min, and this increase was statistically significant. In comparison, the latencies of various neuropeptide effects on other molluscan tissues, though varied, are shorter. For some examples, the effects of FMRFamide on neurons of the snail *Helix aspersa* (Green *et al.*, 1994), of pedal peptides on the cilia of *Tritonia* (A. O. D. Willows, Univ. of Washington, pers. comm.), and of YFAFPRQamide on the rectum of *Mercenaria* (Candelario-Martinez *et al.*, 1993) are all evident in less than a minute. A myomodulin-related peptide (MMc) required 3 to 4 min to fully activate an L-type calcium current in the ARC muscle of *Aplysia californica* (Brezina *et al.*, 1995). The peptide achatin I maximally reduced the inward current in neurons of the snail *Achatina fulica* in about 15 min (Liu and Takeuchi, 1995). Finally, SCP_B took up to 30 min to maximize adenylate cyclase activity in ganglionic homogenates of the snail *Planorbis corneus* (Ferretti *et al.*, 1996). Thus, the time required for YFAFPRQamide to exert its full effect on the lateral and frontal cilia of *Mercenaria* is the longest reported in molluscs.

Because the inhibitory effect of DA develops much more rapidly than that of YFAFPRQamide, and the molecular weight of DA (189.6 Da) is less than that of YFAFPRQamide (927.44 Da), the slow onset of the peptide action might reflect the inverse proportionality between the diffusion coefficient of a molecule and the square root or cube root of its molecular weight (Alberty, 1983; Denny, 1993). Thus, the ratio of the diffusion coefficients of YFAFPRQamide and DA should be between 0.47 and 0.59. But pyroantimonate (223.74 Da) penetrates the intercellular spaces in excised gills of the fresh-water mussel *Elliptio complanatus*, presumably through septate junctions in the ctenidial epithelium (Satir and Gilula, 1970; see also Machin, 1977; Stommel, 1984a). And Uglem *et al.* (1985) demonstrated that molecules up to the size of inulin (5250 Da) would cross the pedal epithelium of the slug *Lehmannia valentiana* by a paracellular route with a molecular weight cutoff of 10^4 Da. Similarly, inulin seems to cross the ctenidia of the oyster *Crassostrea gigas* by a paracellular route (Hevert, 1984). Finally, DA, 5HT, AMSFYFPRMamide, and YFAFPRQamide all act upon the musculature of the labial palps of *Mercenaria* within several minutes (L. F. Gainey, unpublished observations). In conclusion, if we assume that the ctenidial epithelium of *Mercenaria* is similar to that of other molluscs, then DA, 5HT, and the SCPs could have entered the gills readily *via* a paracellular route, and the time for YFAFPRQamide to exert its effect on the lateral cilia would have been limited only modestly by the peptide's lower rate of diffusion.

The robust cardioexcitation, as well as other effects of the SCPs on various pulmonate and opisthobranch tissues, is accompanied by an increase in levels of cAMP (references in Reich *et al.*, 1997a, b). Furthermore, experiments on the accessory radula closer muscle of *Aplysia californica* (Probst *et al.*, 1994) and on isolated myocardial cells of *Helix aspersa* (Reich *et al.*, 1997a, b) showed that the peptide is exerting its effect by activating a cAMP-dependent protein kinase in the tissue. However, the isolated heart of *Mercenaria* responds only weakly and unreliably to the SCPs (Candelario-Martinez *et al.*, 1993); moreover, the strong mechanical responses of bivalve hearts to 5HT and FMRFamide may not, after all, be mediated by cAMP (reviewed by Bayakly and Deaton, 1992). Thus, the YFAFPRQamide antagonism of DA ciliary inhibition could be due to another mechanism, or the peptide could even be stimulating serotonergic neurons, releasing 5HT. Most evidence suggests that substance P also has such an indirect effect on mucociliary activity (*e.g.*, Lindberg and Mercke, 1986; Khan *et al.*, 1986; Wong *et al.*, 1991; Schlosser *et al.*, 1995).

Our experiments do not allow us to distinguish among the possibile mechanisms. But work with the gills of *Mytilus* *edulis* showed that lateral cilia arrested by calcium ion—the likely mechanism of DA inhibition (Stommel 1984b; Stommel and Stephens, 1985a)—are stimulated to beat within seconds by 5HT and cAMP (Murakami and Takahashi, 1975; Stommel and Stephens, 1985b; for reviews of ciliary control mechanisms see Murakami, 1989, and Aiello, 1990). These data suggest that the much delayed onset of YFAFPRQamide action after the DA concentration has been raised from 5×10^{-7} *M* to 10^{-6} *M*, is due neither to 5HT release nor to augmented levels of cAMP.

The pharmacology of the frontal cilia is much more poorly known than that of the lateral cilia, and some of the data are contradictory. For example, reports agree that particle transport by the frontal cilia in *Mytilus* is stimulated by 5HT (Gosselin and O'Hara, 1961; Jorgensen, 1975; Malanga, 1975b). Yet 5HT also inhibits the "crawling" of isolated pieces of *Mytilus* gill that is effected by the frontal cilia (Malanga, 1975a). And species also matters, because, in contrast to the situation in *Mytilus*, particle transport by the frontal cilia of *Lampsilis* sp. is inhibited by 5HT (Malanga, 1975b). In this study, we found that 5HT inhibited the rate of particle transport in frontal cilia of *Mercenaria* in a dose-dependent manner. But we were unable to stop the transport completely, even with 10^{-3} *M* 5HT.

The physiological mechanisms underlying the control of the frontal cilia are also largely unexplained. Walter and Satir (1978) found that the frontal cilia of *Elliptio complanatus* are several orders of magnitude less sensitive to an influx of Ca^{++} than are the lateral cilia. Aiello (1979) reported that frontal ciliary activity in *Mytilus* increases in response to mechanical stimulation; similar results have been reported for the abfrontal cilia (Stommel and Stephens, 1988), where mechanical stimulation is accompanied by an influx of calcium. Thus, the mechanism of inhibition of frontal cilia by 5HT and the modulation of this response by the SCPs are probably different from those in lateral cilia. Frontal cilia remain difficult to work with, but the data reported here demonstrate that, since each ciliary tract has its distinct function (reviewed by Aiello, 1990), its physiology and regulatory mechanisms should also be distinct, a well-established principle with respect to muscles and other organs and tissues.

The lateral cilia often "vibrate" in an apparently uncoordinated manner, and then suddenly switch into well-defined metachronal waves [this report, and Catapane *et al.*, 1978 (*Mytilus edulis*)]; the waves are formed by the viscous coupling of cilia (reviewed in Satir and Sleigh, 1990). Now an examination of the data reveals that the lateral cilia in *Mercenaria* do not beat in a continuous range of frequencies; they especially do not beat in metachronal waves below 7 beats/s. The dose-response graph of DA (Fig. 1B) also reveals this behavior; *i.e.*, the cilia slow down, but only modestly, and then abruptly stop. A similar discontinuity is readily apparent in the DA (inhibitory) and 5HT (excitatory) dose-response curves for lateral cilia of *Mytilus* (Catapane, 1983). Assuming that 5HT and DA activate the initiation and cessation of ciliary beating, we suppose that YFAFPRQamide has the effect of smoothing out the transition between cessation and metachronal beating. This idea is supported by the following data from *Mytilus:* Stimulation of the branchial nerve with a single depolarizing pulse led to a single action potential on the lateral cells and complete cessation of ciliary beating, which lasted for as long as a second (Saimi *et al.*, 1983a). But stimulation of the branchial nerve at 25 to 50 Hz led to a decrease in, not an arrest of, the ciliary beat frequency; moreover, the cilia took 30 min to recover (Paparo and Aiello, 1970). Finally, there is strong evidence that the SCPs and acetylcholine are co-transmitters in *Aplysia* (Cropper *et al.*, 1987, 1990). Taken together, these data suggest that, in *Mercenaria* gills, DA and YFAFPRQamide are co-transmitters.

Candelario-Martinez *et al.* (1993) found that YFAFPRQamide and AMSFYFPRMamide are most concentrated in the labial palps and visceral ganglia, with substantial concentrations in the gills and gut. Moreover, immunoreactive, varicose fibers were found in all ganglia and peripheral tissues involved in feeding. Finally, YFAFPRQamide, and to a lesser extent AMSFYFPRMamide, caused relaxation of the gut. Based upon these findings, these authors proposed that one role of these SCP-related peptides in *M. mercenaria* is to regulate feeding and gut motility, as in a variety of gastropods (reviewed in Lloyd, 1989; Prior and Welsford, 1989; Weiss *et al.*, 1992). Our results are consistent with this hypothesis.

Acknowledgments

We thank Karen Emery and Christy Leigh (University of Southern Maine) for their help in measuring ciliary rates. Dr. James Kenyon (Pharmaceutical Research Institute, Bristol-Myers Squibb, New Brunswick, NJ) gave valuable statistical advice; Prof. A. O. D. Willows (Friday Harbor Laboratories, University of Washington) made us a gift of the monoclonal antibody against SCP_B; Dr. Paul J. Linser (Whitney Laboratory, University of Florida) provided instruction and help with the immunohistochemistry; and M. Lynn Milstead prepared the immunocytochemical images for publication. Support was provided by a grant to LFG from Maine EPSCoR (NSF) administered by the Maine Science and Technology Foundation, by an NIH grant (HL28440) to MJG, and by the Grass Foundation (A. C-M). This is Publication No. 322 of the Tallahassee, Sopchoppy & Gulf Coast Marine Biological Association.

Literature Cited

Aiello, E. L. 1960. Factors affecting ciliary activity on the gill of the mussel *Mytilus edulis. Physiol. Zool.* **23:** 120–135.

Aiello, E. L. 1962. Identification of the cilioexcitatory substance present in the gill of the mussel *Mytilus edulis*. *J. Cell. Comp. Physiol.* **60:** 17–21.

Aiello, E. L. 1970. Nervous and chemical stimulation of gill cilia in bivalve molluscs. *Physiol. Zool.* **43:** 60–70.

Aiello, E. L. 1979. Nervous and local mediator control of mucociliary transport in a bivalve gill. *Malacologia* **18:** 469–472.

Aiello, E. L. 1990. Nervous control of gill ciliary activity in *Mytilus edulis*. Pp. 189–208 in *Neurobiology of* Mytilus edulis. G. B. Stefano, ed. Manchester University Press, Manchester, UK.

Aiello, E. L., and G. Guideri. 1965. Distribution and function of the branchial nerve in the mussel. *Biol. Bull.* **129:** 431–438.

Aiello, E. L., J. Kennedy, and C. Hernandez. 1991. Stimulation of frog ciliary cells in culture by acetylcholine and Substance P. *Comp. Biochem. Physiol.* **99:** 497–506.

Alberty, R. A. 1983. *Physical Chemistry*. 6th ed. Wiley, New York.

Arbiser, Z. K., and B. S. Beltz. 1991. SCPB- and FMRFamide-like immunoreactivities in lobster neurons: colocalization of distinct peptides or colabeling of the same peptide(s)? *J. Comp. Neurol.* **306:** 417–424.

Atkins, D. 1937. On the ciliary mechanisms and interrelationships of lamellibranchs. Part I: New observations on sorting mechanisms. *Q. J. Microsc. Sci.* **79 (New Series):** 181–308.

Bates, D. M., and D. G. Watts. 1988. *Nonlinear Regression Analysis and Its Applications*. Wiley, New York.

Bayakly, N. A., and L. E. Deaton. 1992. The effects of FMRFamide, 5-hydroxytryptamine and phorbol esters on the heart of the mussel *Geukensia demissa*. *J. Comp. Physiol. B* **162:** 463–468.

Brezina, V., B. Bank, E. C. Cropper, S. Rosen, F. S. Vilim, I. Kupfermann, and K. R. Weiss. 1995. Nine members of the myomodulin family of peptide cotransmitters at the B16-ARC neuromuscular junction of *Aplysia*. *J. Neurophysiol.* **74:** 54–72.

Candelario-Martinez, A., D. M. Reed, S. J. Prichard, K. E. Doble, T. D. Lee, W. Lesser, D. A. Price, and M. J. Greenberg. 1993. SCP-related peptides from bivalve mollusks: identification, tissue distribution, and actions. *Biol. Bull.* **185:** 428–439.

Catapane, E. J. 1983. Comparative study of the control of lateral ciliary in marine bivalves. *Comp. Biochem. Physiol.* **75C:** 403–405.

Catapane, E. J., G. B. Stefano, and E. Aiello. 1978. Pharmacological study of the reciprocal dual innervation of the lateral ciliated gill epithelium by the CNS of *Mytilus edulis* (Bivalvia). *J. Exp. Biol.* **74:** 101–113.

Catapane, E. J., G. B. Stefano, and E. Aiello. 1979. Neurophysiological correlates of the dopaminergic cilio-inhibitory mechanism of *Mytilus edulis*. *J. Exp. Biol.* **83:** 315–323.

Cervin, A., S. Lindberg, and U. Mercke. 1991. The effect of neuropeptide Y on mucociliary activity in the rabbit maxillary sinus. *Acta Oto-laryngol.* **111:** 960–966.

Cropper, E. C., P. E. Lloyd, W. Reed, R. Tenenbaum, I. Kupfermann, and K. R. Weiss. 1987. Multiple neuropeptides in cholinergic motor neurons of *Aplysia:* evidence for modulation intrinsic to the motor circuit. *Proc. Natl. Acad. Sci. USA.* **84:** 3486–3490.

Cropper, E. C., D. Price, R. Tenenbaum, I. Kupfermann, and K. R. Weiss. 1990. Release of peptide cotransmitters from a cholinergic motor neuron under physiological conditions. *Proc. Natl. Acad. Sci. USA.* **87:** 933–937.

Denny, M. W. 1993. *Air and Water*. Princeton University Press, Princeton, NJ.

Elsey, C. R. 1935. On the structure and function of the mantle and gill of *Ostrea gigas* (Thunberg) and *Ostrea lurida* (Carpenter). *Trans. R. Soc. Can.* **29 (Section 5):** 131–160.

Ferretti, M. E., D. Sonetti, M. C. Pareschi, M. Buzzi, M. L. Colamussi, and C. Biondi. 1996. Effect of serotonin and neuropeptides on adenylate cyclase of the central nervous system and peripheral organs of the freshwater snail *Planorbis corneus*. *Neurochem. Int.* **28:** 417–424.

Foster-Smith, R. L. 1975. The effect of concentration of suspension on the filtration rates and pseuodfaecal production for *Mytilus edulis* L., *Cerastoderma edule* (L.) and *Venerupis pullastra* (Montagu). *J. Exp. Mar. Biol. Ecol.* **17:** 1–22.

Gainey, L. F., Jr. 1976. Locomotion in the Gastropoda: functional morphology of the foot in *Neritina reclivata* and *Thais rustica*. *Malacologia* **15:** 411–431.

Gainey, L. F., Jr., and S. E. Shumway. 1991. The physiological effect of *Aureococcus anophagefferens* ("brown tide") on the lateral cilia of bivalve mollusks. *Biol. Bull.* **181:** 298–306.

Gainey, L. F., Jr., K. J. Vining, and M. J. Greenberg. 1997. Modulation of gill ciliary activity of *Mercenaria mercenaria* by a neuropeptide. *Am. Zool.* **37:** 148A.

Gosselin, R. E., and G. O'Hara. 1961. An unsuspected source of error in studies of particle transport by lamellibranch gill cilia. *J. Cell. Comp. Physiol.* **58:** 1–9.

Green, K. A., S. W. P. Falconer, and G. A. Cottrell. 1994. The neuropeptide Phe-Met-Arg-Phe-NH_2 (FMRFamide) directly gates two ion channels in an identified *Helix* neurone. *Pfluegers Arch.* **428:** 232–240.

Hevert, F. 1984. Urine formation in the lamellibranchs: evidence for ultrafiltration and quantitative description. *J. Exp. Biol.* **111:** 1–12.

Jones, H. D., and O. G. Richards. 1993. The effects of acetylcholine, dopamine and 5-hydroxytryptamine on water pumping rate and pressure in the mussel *Mytilus edulis* L. *J. Exp. Mar. Biol. Ecol.* **170:** 227–240.

Jorgensen, C. B. 1975. On gill function in the mussel *Mytilus edulis* L. *Ophelia* **13:** 187–232.

Jorgensen, C. B. 1989. Water processing in ciliary feeders, with special reference to the bivalve filter pump. *Comp. Biochem. Physiol.* **94A:** 383–394.

Khan, A. R., B. Bengtsson, and S. Lindberg. 1986. Influence of substance P on ciliary beat frequency in airway isolated preparations. *Eur. J. Pharmacol.* **130:** 91–96.

Lindberg, S., and J. Dolata. 1993. NK1 receptors mediate the increase in mucociliary activity produced by tachykinins. *Eur. J. Pharmacol.* **231:** 375–380.

Lindberg, S., and U. Mercke. 1986. Capsaicin stimulates mucociliary activity by releasing substance P and acetylcholine. *Eur. J. Respir. Dis.* **68:** 96–106.

Lindberg, S., U. Mercke, and R. Uddman. 1986. The morphological basis for the effect of substance P on mucociliary activity in rabbit maxillary sinus. *Acta Oto-laryngol.* **101:** 314–319.

Lindberg, S., A. Cervin, U. Mercke, and R. Uddman. 1988. VIP potentiates cholinergic effects on the mucociliary system in the maxillary sinus. *Otolaryngol. Head Neck Surg.* **99:** 401–407.

Liu, G. J., and H. Takeuchi. 1995. Suppressing effects of neuroactive peptides on the inward current caused by Achatin-I, an *Achatina* endogenous peptide. *Gen. Pharmacol.* **26:** 765–772.

Lloyd, P. E. 1989. Peripheral actions of the SCPs in *Aplysia* and other gastropod molluscs. *Am. Zool.* **29:** 1265–1274.

Lloyd, P. E., G. A. Phares, N. E. Phillips, and A. O. D. Willows. 1996. Purification and sequencing of neuropeptides from identified neurons in the marine mollusc, *Tritonia*. *Peptides* **17:** 17–23.

Machin, J. 1977. Role of integument in molluscs. Pp. 735–762 in *Transport of Ions and Water in Animals*. B. L. Gupta, R. B. Moreton, J. L. Oschman, and B. J. Wall, eds. Academic Press, New York.

Malanga, C. J. 1975a. Dopaminergic stimulation of frontal ciliary activity in the gill of *Mytilus edulis*. Comp. Biochem. Physiol. **51C:** 25–34.

Malanga, C. J. 1975b. Effects of serotonin (5HT) and dopamine (DA) on particle transport by frontal cilia of three species of bivalve mollusc. *Fed. Proc.* **34:** 800.

Masinovsky, B., S. C. Kempf, J. S. Callaway, and A. O. D. Willows.

1988. Monoclonal antibodies to the molluscan small cardioactive peptide SCP_B: immunolabeling of neurons in diverse invertebrates. *J. Comp. Neurol.* **273:** 500–515.

Miller, S. L. 1974. The classification, taxonomic distribution, and evolution of locomotor types among prosobranch gastropods. *Proc. Malacol. Soc. Lond.* **41:** 233–272.

Morton, B. 1983. Feeding and digestion in Bivalvia. Pp. 65–147 in *The Mollusca, Vol. 5, Physiology Part 2.* A. S. M. Saleuddin and K. M. Wilbur, eds. Academic Press, New York.

Motokawa, T., and P. Satir. 1975. Laser-induced spreading arrest of *Mytilus* gill cilia. *J. Cell Biol.* **66:** 377–391.

Murakami, A. 1989. The control of cilia in metazoa: ciliary functions and Ca-dependent responses. *Comp. Biochem. Physiol.* **94A:** 375–382.

Murakami, A., and H. Machemer. 1982. Mechanoreception and signal transmission in the lateral ciliated cells on the gills of *Mytilus. J. Comp. Physiol.* **145A:** 351–362.

Murakami, A., and K. Takahashi. 1975. The role of calcium in the control of ciliary movement in *Mytilus.* II. The effects of calcium ionophores X537A and A23187 on the lateral cilia. *J. Fac. Sci. Univ. Tokyo, Sect. 4.* **13:** 251–256.

Neter, J., W. Wasserman, and M. H. Kutner. 1990. *Applied Linear Statistical Models.* 3rd ed. Irwin, Homewood, IL.

Owen, G. 1974. Studies on the gill of *Mytilus edulis:* the eu-laterofrontal cirri. *Proc. R. Soc. Lond.* **187:** 83–91.

Owen, G., and J. M. McCrae. 1976. Further studies on the latero-frontal tracts of bivalves. *Proc. R. Soc. Lond. B* **194:** 527–544.

Paparo, A. 1972. Innervation of the lateral cilia in the mussel, *Mytilus edulis* L. *Biol. Bull.* **143:** 592–604.

Paparo, A. 1985. The role of the cerebral and visceral ganglia in ciliary activity. *Comp. Biochem. Physiol.* **81A:** 647–651.

Paparo, A., and E. Aiello. 1970. Cilio-inhibitory effects of branchial nerve stimulation in the mussel, *Mytilus edulis. Comp. Gen. Pharmacol.* **1:** 241–250.

Paparo, A., and C. E. Finch. 1972. Catecholamine localization, content, and metabolism in the gill of two lamellibranch molluscs. *Comp. Gen. Pharmacol.* **3:** 303–309.

Prior, D. J., and I. G. Welsford. 1989. The role of small cardioactive peptide, SCP_B, in the regulatory responses of terrestrial slugs. *Am. Zool.* **29:** 1255–1263.

Probst, W. C., E. C. Cropper, J. Hierhorst, S. L. Hooper, H. Jaffe, F. Vilim, S. Beushausen, I. Kupferman, and K. R. Weiss. 1994. cAMP-dependent phosphorylation of *Aplysia* twitchin may mediate modulation of muscle contractions by neuropeptide cotransmitters. *Proc. Natl. Acad. Sci. USA* **91:** 8487–8491.

Purchon, R. D. 1968. *The Biology of Mollusca.* Pergamon, New York.

Reich, G., K. E. Doble, D. A. Price, and M. J. Greenberg. 1997a. Effects of cardioactive peptides on myocardial cAMP levels in the snail *Helix aspersa. Peptides* **18:** 355–360.

Reich, G., K. E. Doble, and M. J. Greenberg. 1997b. Protein phosphorylation in snail cardiocytes stimulated with molluscan peptide SCPb. *Peptides* **18:** 1311–1314.

Saimi, Y., A. Murakami, and K. Takahashi. 1983a. Electrophysiological correlates of nervous control of ciliary arrest response in the gill epithelial cells of *Mytilus. Comp. Biochem. Physiol.* **74A:** 499–506.

Saimi, Y., A. Murakami, and K. Takahashi. 1983b. Ciliary and electrical responses to intracellular current injection in the ciliated gill epithelium of *Mytilus. Comp. Biochem. Physiol.* **74A:** 507–511.

Satir, P., and N. B. Gilula. 1970. The cell junction in a lamellibranch gill ciliated epithelium. *J. Cell Biol.* **47:** 468–487.

Satir, P., and M. A. Sleigh. 1990. The physiology of cilia and mucociliary interactions. *Annu. Rev. Physiol.* **52:** 137–155.

Schlosser, R. J., J. M. Czaja, B. Yang, and T. V. McCaffrey. 1995. Signal transduction mechanisms in substance P-mediated ciliostimulation. *Otolaryngol. Head Neck Surg.* **11:** 582–588.

Setna, S. B. 1930. The neuromuscular mechanism of the gill of *Pecten. Q. J. Microsc. Sci.* **73:** 365–392.

Smith, R. P., R. Shellard, G. Di Benedetto, C. J. Magnus, and A. Mehta. 1996. Interaction between calcium, neutral endopeptidase and the substance P mediated ciliary response in human respiratory epithelium. *Eur. Respir. J.* **9:** 86–92.

Stefano, G. B., and E. Aiello. 1975. Histofluorescent localization of serotonin and dopamine in the nervous system and gill of *Mytilus edulis* (Bivalvia). *Biol. Bull.* **148:** 141–156.

Stefano, G. B., E. J. Catapane, and J. M. Stefano. 1977. Temperature dependent ciliary rhythmicity in *Mytilus edulis* and the effects of monoaminergic agents on its manifestation. *Biol. Bull.* **153:** 618–629.

Stommel, E. W. 1984a. Calcium regenerative potentials in *Mytilus edulis* gill abfrontal ciliated epithelial cells. *J. Comp. Physiol. A* **155:** 445–456.

Stommel, E. W. 1984b. Calcium activation of mussel gill abfrontal cilia. *J. Comp. Physiol. A* **155:** 457–469.

Stommel, E. W., and R. E. Stephens. 1985a. Calcium-dependent phosphatidylinositol phosphorylation in lamellibranch gill lateral cilia. *J. Comp. Physiol. A* **157:** 441–449.

Stommel, E. W., and R. E. Stephens. 1985b. Cyclic AMP and calcium in the differential control of *Mytilus* gill cilia. *J. Comp. Physiol. A* **157:** 451–459.

Stommel, E. W., and R. E. Stephens. 1988. EGTA induces prolonged summed depolarizations in *Mytilus* gill coupled ciliated epithelial cells: implications for the control of ciliary motility. *Cell Motil. Cytoskeleton* **10:** 464–470.

Tamaoki, J., T. Kanemura, N. Sakai, K. Isono, K. Kobayashi, and T. Takizawa. 1991. Endothelin stimulates ciliary beat frequency and chloride secretion in canine cultured tracheal epithelium. *Am. J. Respir. Cell Mol. Biol.* **4:** 426–431.

Tamaoki, J., M. Kondo, S. Takeuchi, H. Takemura, and A. Nagai. 1998. Vasopressin stimulates ciliary motility of rabbit tracheal epithelium: role of V1b receptor-mediated Ca2+ mobilization. *Am. J. Respir. Cell Mol. Biol.* **19:** 293–299.

Trimmer, B. A., L. Kobiarski, and E. A. Kravitz. 1987. Purification and characterization of FMRFamidelike immunoreactive substances from the lobster nervous system: isolation and sequence analysis of two closely related peptides. *J. Comp. Neurol.* **266:** 16–26.

Uglem, G. L., D. J. Prior, and S. D. Hess. 1985. Paracellular water uptake and molecular sieving by the foot epithelium of terrestrial slugs. *J. Comp. Physiol. B* **156:** 285–289.

Walter, M. F., and P. Satir. 1978. Calcium control of ciliary arrest in mussel gill cells. *J. Cell Biol.* **79:** 110–120.

Weiss, K. R., V. Brezina, E. C. Cropper, S. L. Hooper, M. W. Millewr, W. C. Probst, F. S. Villim, and I. Kupfermann. 1992. Peptidergic co-transmission in *Aplysia:* functional implications for rhythmic behaviors. *Experientia* **48:** 456–463.

Welsh, J. H., R. I. Smith, and A. E. Kammer. 1968. *Laboratory Exercises in Invertebrate Physiology.* 3rd ed. Burgess, Minneapolis, MN.

Willows, A. O. D., G. A. Pavlova, and N. E. Phillips. 1997. Modulation of ciliary beat frequency by neuropeptides from identified molluscan neurons. *J. Exp. Biol.* **200:** 1433–1439.

Wong, L. B., I. F. Miller, and D. B. Yeates. 1991. Pathways of substance P stimulation of canine tracheal ciliary beat frequency. *J. Appl. Physiol.* **70:** 267–273.

Wong, L. B., C. L. Park, and D. B. Yeates. 1998. Neuropeptide Y inhibits ciliary beat frequency in human ciliated cells *via* nPKC, independently of PKA. *Am. J. Physiol.* **275:** 440–448.

Reference: *Biol. Bull.* **197:** 174–187. (October 1999)

Ovigerous-Hair Stripping Substance (OHSS) in an Estuarine Crab: Purification, Preliminary Characterization, and Appearance of the Activity in the Developing Embryos

MASAYUKI SAIGUSA AND HIROSHI IWASAKI

Department of Biology, Faculty of Science, Okayama University, Tsushima 2-1-1
(General Education Buildings), Okayama 700-8530, Japan

Abstract. Ovigerous-hair stripping substance (OHSS) is an active factor in crab hatch water (*i.e.*, filtered medium into which zoea larvae have been released). This factor participates in stripping off the egg attachment structures (*i.e.*, egg case, funiculus, and the coat investing ovigerous hairs) that remain attached to the female's ovigerous hairs after larval release. Thus this activity prepares the hairs for the next clutch of embryos. OHSS activity of an estuarine crab, *Sesarma haematocheir*, eluted as a single peak on molecular-sieve chromatography, but this peak still showed two protein bands at 32 kDa and 30 kDa on SDS-PAGE. The two protein bands stained with a polyclonal antiserum raised to the active fractions from molecular-sieve chromatography. Moreover, antibodies purified from this polyclonal OHSS antiserum also recognized both the 32-kDa and 30-kDa bands. OHSS immunoreactivity and biological activity were associated with the attachment structures that remained connected to the ovigerous hairs after hatching. In developing embryos, both protein bands could be stained immunochemically at least 10 days before hatching. But OHSS biological activity appeared only 3 days before hatching. The immunoreactive protein bands were not observed in the zoea, but OHSS bioreactivity was present, though greatly reduced. The 32-kDa protein, at least, is probably an active OHSS, and the 30-kDa protein band may also be OHSS-related. The OHSS appears to be produced and stored by the developing embryo. Upon hatching, most of the material may be trapped by the remnant structures, and the remainder is released into the ambient water.

Received 16 January 1997; accepted 16 June 1999.

Introduction

After egg-laying, the embryos of intertidal and estuarine crabs—and indeed most decapod crustaceans—are encased in a thick, protective capsule composed of two or three layers; these capsules are then attached to the female's ovigerous hairs through the funiculus and investment coat (Yonge, 1937, 1946; Cheung, 1966; Goudeau and Lachaise, 1983). The capsule breaks open during or after embryonic development, and hatching occurs (Davis, 1968, 1981; Saigusa, 1997).

The funiculus and investment coat, as well as the broken egg capsule, remain attached to the hairs after hatching (for further details, see Saigusa, 1994). But at the time of hatching, an active factor we call ovigerous-hair stripping substance (OHSS) is released from the embryo and causes these remnant structures to slip off the hairs (Saigusa, 1994). The stripping of these remnant structures is very important because it leaves the hairs clean, unbroken, and thus prepared to incubate the next clutch of embryos (Saigusa, 1995).

The funiculus, the coat that wraps the ovigerous hairs, and the outermost layer of the egg capsule are all composed of the same material (Saigusa *et al.*, unpub. data), and OHSS may be an enzyme that acts on this material. In many other animals, a hatching enzyme is released from the embryos upon hatching and digests the layers of the egg case (*e.g.*, Yamagami, 1988; Lepage and Gache, 1989; Roe and Lennarz, 1990; Helvik *et al.*, 1991). However, there is no evidence, even after electron microscopy studies, that the layers of the egg capsule encasing crab embryos are digested by OHSS (Saigusa *et al.*, unpubl. data). So the notion that OHSS is a crustacean hatching enzyme remains unsubstantiated.

Although the cells that produce OHSS have not yet been identified, we do know that this substance is secreted by the embryo, and not by the female. The molecular mass of OHSS was estimated by primary gel filtration to be 15–20 kDa (Saigusa, 1995), but no other chemical characteristics are known. If we are ever to characterize the physiological mechanism of OHSS, or its expression during development under the control of a circatidal clock (Saigusa, 1992, 1993, 1997), a purified preparation must first be obtained.

Here we describe a relatively simple procedure for purifying OHSS from the hatch water of an estuarine terrestrial crab, *Sesarma haematocheir*, and we also provide a preliminary characterization of this material. A polyclonal antiserum was raised against OHSS and purified so that, by immunochemical staining, we could examine the appearance of OHSS in the developing embryos and its disappearance after hatching. Furthermore, we assessed whether OHSS is still associated with the remnants of the embryonic attachment structures that remain after hatching and larval release.

Materials and Methods

Larval release and collection of hatch water

Specimens of *Sesarma haematocheir*, the estuarine terrestrial crab used in this study, were collected at Kasaoka, Okayama Prefecture, Japan. Here, the thicket inhabited by the crabs is separated from the shore of a tidal creek by a small road (for their habitat, see Saigusa, 1982). Just after sunset, between 1900 and 2000 h, for several days around the time of the full or new moon, large numbers of ovigerous female appear onto this road on their way to the shore. Thus exposed, they can easily be captured.

In 1994, more than 3000 females were captured on the road and placed individually into large plastic containers (10 cm in diameter, 15 cm in height) containing 30 ml of very clean ground water obtained near the collecting site. The females released their larvae into this water. Immediately thereafter, the females were removed from the containers, and the water was filtered through a nylon mesh that retained the larvae. The filtered hatch water was accumulated in 1-liter bottles, transported 50 km to the laboratory, and finally frozen at −20°C.

The method of collection was changed in 1996. In the three years 1996, 1997, and 1998, ovigerous females were still collected at the same site at Kasaoka, but they were first disinfected in ice-cold 70%–80% ethanol for a few minutes, then washed with distilled water, and finally placed individually in the large plastic containers, but without water. These containers were transferred to the laboratory, where each crab was immediately placed in a small, covered plastic cup (5 cm in diameter, 6 or 8 cm in height) containing 9 ml of distilled water. As soon as larvae were released, the zoeas were removed by filtration through nylon mesh, and the remaining water was then passed again through a filter paper. The resulting hatch water was pooled in a 50-ml plastic bottle and immediately stored at −40°C until used. Most females incubate their next clutch of embryos a few days after larval release. The females were therefore kept in the laboratory for a month, and hatch water was obtained from their second larval release.

Since the OHSS activity of hatch water declines constantly at ambient temperatures, the second method, in which the material is frozen immediately after production, yielded hatch water solutions with higher concentrations of OHSS. Moreover, since all of the female crabs survived and were able to incubate another clutch of embryos, we are confident that the disinfection in ethanol and the dry transport were not deleterious to the animals.

Most of the hatch water used in this study was collected in 1994, but some experiments were carried out with material collected in 1996–1998. The concentrations of OHSS obtained by the two methods would certainly have been different, but the biochemical properties observed were virtually identical.

Bioassay of OHSS activity

Our biological assay of OHSS is based on the ability of chemically fixed ovigerous setae to respond to OHSS. In brief, an ovigerous seta with its attached embryos, all in early stages of development, were excised from a female crab, fixed in 70% ethanol, and then stored in the refrigerator at 4°C until used. Ethanol-fixed setae with their attached clumps of embryos respond well to exogenous OHSS, even after several years of cold storage at 4°C (unpub. data).

Shortly before a bioassay was to be performed, the fixed setae were suspended in distilled water (DW) to wash out the ethanol, and then placed in a glass dish with DW. The tip of each ovigerous seta was cut away, and the remainder was subdivided into four segments under the stereomicroscope (see Saigusa, 1995). Each segment was placed on a paper towel to remove attached water, and one or two (or three in some experiments) of these segments were placed in each of the wells (each 0.8 cm in diameter, 1.7 cm in height) of a plastic culture dish; the wells also contained 300–500 μl of a fraction eluted through chromatography. The culture dish was shaken slowly on a mechanical shaker for 1.0–2.2 h at about 23°C.

Recall that each seta is equipped with 10–15 whorls of ovigerous hairs to which the embryos are actually attached, and that the number of ovigerous hairs is about 10–20 per whorl (see Saigusa, 1994, 1995). For example, each of the three segments of a seta would contain 2–5 whorls (30–100 ovigerous hairs). After the incubation described above, each setal segment with its cluster of embryos was again placed in a glass dish with DW. This dish was put under a stereomicroscope, and fine forceps were used to pull the embryos gently away from the ovigerous hairs. The percentage of hairs in each whorl that were stripped clean but were still undamaged was calculated. The activity of OHSS was usually taken as the mean of 3–10 whorls (one or two segments); the standard deviation was also calculated.

Purification procedure

Stored, frozen, crude hatch water was thawed and centrifuged at 18,000 rpm for 30 min at 4°C to remove the solid materials. The hatch water was saturated with $(NH_4)_2SO_4$ powder, left overnight, and centrifuged at 18,000 rpm for 30 min. The supernatant contained no OHSS activity. The precipitate was dissolved in 100 m*M* Tris-HCl buffer (pH 9.0) and, at this stage, could also be stored at −20°C. This material was called "concentrated hatch water." OHSS was purified further in three steps, as described below. The procedures were all carried out with a fast protein liquid chromatography system (FPLC; Pharmacia) in an experimental chamber with the temperature controlled at 4°C; protein elution was monitored at 280 nm. OHSS rapidly loses its activity during purification, so the following procedures were completed within 12 h.

Step 1: Hydrophobic chromatography. Concentrated hatch water (described above) was mixed with an equal quantity of 20 m*M* Tris-HCl buffer (pH 9.0) containing 300 m*M* Na_2SO_4. This medium was applied to a column containing 10 ml of HiTrap-Octyl-Sepharose 4FF (prepack column, Pharmacia) equilibrated with 20 m*M* Tris-HCl buffer containing 300 m*M* Na_2SO_4 (pH 9.0). The column was eluted with a linear gradient of Na_2SO_4: −8 m*M*/min (−2 m*M*/ml and a flow rate maintained at 4.0 ml/min). Fractions of 10 ml were collected.

Step 2: Ion-exchange chromatography. The active fractions from step 1 were pooled (60 ml), and this sample was applied to an anion-exchange column (MONO-Q HR5/5, prepack, Pharmacia; 0.5 × 5 cm). The column had been pre-equilibrated with 20 m*M* Tris-HCl buffer (pH 9.0), and the sample was eluted with the same solution. The flow rate was 1.0 ml/min, and 2-ml fractions were collected. The fractions from the void volume were pooled, and were concentrated to 500 μl with an ultrafiltration membrane (YM 10, Amicon).

Step 3: Molecular-sieve chromatography. A sample of these concentrated active fractions (500 μl) was fractionated by molecular-sieve chromatography (gel filtration) (Superdex 75 HR10/30, prepack, Pharmacia). The column had been equilibrated previously with 20 m*M* Tris-HCl buffer containing 150 m*M* NaCl (pH 9.0). The sample was eluted with the same buffer at a flow rate of 0.25 ml/min, and 1-ml fractions were collected. The molecular mass of OHSS was determined by comparison with the elution volume of the following marker proteins: glutamate dehydrogenase (55.6 kDa), aldolase (39.2 kDa), trypsin inhibitor (20.1 kDa) (Sigma Chemical Co.).

Effects of temperature and pH

The active fractions from molecular-sieve chromatography (fractions 6–8; Fig. 2A) were pooled and incubated for 15 min at temperatures from 4°C to 100°C, and were immediately returned to 23°C. Segments of the ovigerous seta with their attached embryos were incubated with these solutions for 1 h at 23°C, and OHSS activity was bioassayed. In another experiment, the pooled active fractions were maintained at 4°C and 23°C for 0–120 h. These solutions were then bioassayed for 1 h.

The effects of pH were examined similarly. Buffers used for this study were as follows: 100 m*M* Na-acetate (pH 3.0 and 5.0; 100 m*M* Tris-HCl (pH 7.0 and 8.5); and 100 m*M* glycine-NaOH (pH 10.5). Active fractions were mixed with an equal quantity of each buffer, and the OHSS activity was bioassayed for 1 h.

In each experiment (A–C), assays were repeated three times with the same OHSS solution. The mean percentage of stripped hairs in 2–5 whorls of the hair was first estimated, and the mean of three assays was estimated.

Electrophoretic analysis (SDS-PAGE)

SDS (sodium dodecyl sulfate)-polyacrylamide gel electrophoresis (SDS-PAGE) was carried out according to the method of Laemmli (1970). Each fraction from gel filtration was concentrated by passage through an ultrafiltration membrane (Centricon 10, Amicon). The filtered material was dissolved in an equal quantity of lysis buffer [composition: 5% SDS, 5% 2-mercaptoethanol, 8 *M* urea, 5 m*M* EDTA (ethylenediaminetetraacetic acid), 5% sucrose, in 125 m*M* Tris-HCl (pH 6.8)], and then kept at room temperature for 30 min. The molecular mass markers employed were glutamate dehydrogenase (55.6 kDa), aldolase (39.2 kDa), triosephosphase isomerase (26.6 kDa), trypsin inhibitor (20.1 kDa), and lysozyme (14.3 kDa) (Sigma Chemical Co.). The gels (15%) were transblotted onto PVDF (polyvinyliden difluoride) membranes (Clear Blot Membrane P; Atto, Japan), and were stained with Coomassie brilliant blue R-250 (CBB).

Electrophoresis of the active fractions without denaturation (native SDS-PAGE) and bioassay with the crushed gel

The active fractions from gel filtration were pooled (2 ml) and concentrated to less than 200 μl by passage through the ultrafiltration membrane. This material (80 μl) was dissolved in a solution containing 45 mg of saccharose added in 100 μl of 0.5 *M* Tris-HCl (pH 6.8), and was electrophoresed on an SDS-polyacrylamide gel (15%). After electrophoresis, a narrow strip of this gel was cut parallel to the direction of migration, and then stained with CBB. This strip was used to indicate the position of the protein bands. The remainder of the gel was cut into four equal segments perpendicular to the direction of migration. Each of these gel segments was crushed with a pestle, 500 μl of DW was added, and the OHSS activity was bioassayed.

Preparation of polyclonal antiserum, electrophoresis, and western blotting of OHSS

In preliminary experiments, a 32-kDa protein band seen on SDS-PAGE was cut from the gel with a sharp knife, mixed with Freund's complete adjuvant, and injected into a commercial white rabbit. These treatments—four injections, 2 weeks apart—yielded no antiserum when assayed by western blotting. Therefore, the pooled active fractions from gel filtration (2 ml; 6 and 7 in Fig. 2A) were mixed with the adjuvant, and two additional injections, 2 weeks apart, were given to the same rabbit.

In western blotting, the electrophoresed sample was transblotted onto PVDF membrane, and immunoreactivity was detected by chemobioluminescence with ECL western blotting reagents (Amersham). For the primary antibody, the polyclonal antiserum was diluted 1:1000 with 0.5% nonfat milk in T-TBS (10 m*M* Tris-HCl, 150 m*M* NaCl, and 0.05% Tween 20). The PVDF membrane was incubated with the primary antibody for 1 h at room temperature, then washed five times with T-TBS. The secondary antibody was peroxidase-conjugated goat anti-rabbit immunoglobulin (Cappel) diluted 1:5000 with 0.5% nonfat milk in T-TBS. After a 1 h incubation with the secondary antibody at room temperature, the membrane was washed five times with T-TBS, and was further incubated (for 1 min at room temperature) with ECL western blotting reagents. This membrane was exposed to Hyperfilm ECL (Amersham).

Affinity purification of the OHSS antiserum

The pooled active fractions from molecular sieve chromatography (6 and 7 in Fig. 2A) were concentrated, electrophoresed on 15% SDS gel, and then transferred to a PVDF membrane. A narrow strip of this membrane was then cut on both edges (5 mm in width), parallel to the direction of migration. These filter strips were stained with CBB and were used to indicate the position of each protein band; the membrane was not stained with CBB, except these strips.

Two protein bands located with the CBB-stained filter strips, an upper (32 kDa) and lower (30 kDa), were cut separately from the membrane. Each band was further cut into pieces and was incubated for 24 h in 1 ml antiserum at 4°C. The pieces of membrane were then rinsed in PBS (pH 7.4) for 10 min, and this operation was repeated 5–6 times. The membrane pieces were overlain with 200 μl of 0.2 *M* glycine-HCl (pH 2.0) for 10 min, on ice, to elute bound antibody. The eluate was adjusted to pH 7.4–7.5 by the addition of 30–32 μl of 1 *M* Tris.

For staining, a 1:1000 dilution of the antibody that was eluted from either the 32-kDa or 30-kDa band was used as the primary; dilution was with 0.5% nonfat milk in T-TBS. The secondary antibody was peroxidase-conjugated goat-rabbit immunoglobulin (Cappel) diluted 1:5000 with 0.5% nonfat milk in T-TBS.

Because the two bands were at most 2 mm apart on the gel and were not stained with CBB, we could not be sure that the two proteins had been completely separated. Therefore, concentrated active fractions from molecular-sieve chromatography (6 and 7 in Fig. 2A) were electrophoresed on 15% SDS gel for a longer period (9 h), and were then transferred to a PVDF membrane. This procedure produced a gap of 5–6 mm between the upper and lower bands. The whole membrane was stained with 0.01% Ponceau S (Sigma) in 5% acetic acid for 10 min. The protein bands, 2 mm wide, were cut out and the middle strip (about 2 mm wide) was excluded. The bound antibodies were then eluted, as described above.

Immunochemical detection of OHSS during embryonic development

At various times before hatching, an embryo cluster with its attached hairs and seta (*i.e.*, one-third of an ovigerous seta altogether) was detached from a single female, crushed with a pestle in distilled water (300 μl) for 5 min, and denatured by the addition of 300 μl of the lysis buffer (pH 6.8). The solution was centrifuged at 15,000 rpm for 20 min. Fifty microliters of the supernatant was pipetted, and 100 μl of DW and 100 μl of the lysis buffer were added to this supernatant. Thirty microliters of this solution was subjected to electrophoresis, and OHSS was examined by the immunochemical staining of western blots. The purified antibody was used in the experiments.

OHSS was also examined as follows. Embryo clusters were crushed with a pestle in 500 μl of DW, and immediately centrifuged for 20 min. Then the supernatant was denatured in the lysis buffer described above for 1 h, electrophoresed, and the OHSS was examined by the immunochemical staining of western blots. The sediment was denatured separately by the addition of the lysis buffer for 1 h. The solution was further centrifuged for 20 min, and the supernatant was subjected to electrophoresis followed by immunochemical detection.

Appearance of OHSS activity in developing embryos: bioassay with crushed embryos

One-third of the embryo clusters attached to an ovigerous seta were detached from a single female every day until hatching, crushed in 500 μl of DW, and then centrifuged at

15,000 rpm. The OHSS activity contained in these samples (*i.e.*, the supernatant and sediment of crushed embryos) was bioassayed.

Bioassay of OHSS activity in broken egg cases

As described elsewhere (Saigusa, 1994), remnants of the embryonic attachment system (*i.e.*, broken egg cases, funiculi, and the coat investing ovigerous hairs) remain on the ovigerous hairs after hatching and larval release. These remnants were removed with fine forceps after hatching, and stored at −20°C until used. Ovigerous hairs and setae were not contained in these remnants. So the possibility that the OHSS activity is present in the ovigerous hairs and setae of the female was excluded.

Five hundred milligrams of the remnant matter (wet weight) was thawed and washed repeatedly with DW, and centrifuged for 20 min (15,000 rpm). The sediment was crushed in 600 μl of DW; the suspension was divided into two wells of a plastic dish (each 300 μl), and OHSS activity was bioassayed for 1.5 h and 2.0 h.

We also determined whether the OHSS activity could be extracted with the detergent (Triton-X). Remnant matter (500 mg wet weight) was thawed and washed repeatedly with DW. The remnants were then crushed in 600 μl of Triton-X solution dissolved in DW (5%, 10%, and 20%), and were held for 30 min at room temperature (23°C). Each suspension was centrifuged for 20 min (15,000 rpm), the supernatant was divided into two wells of a plastic culture dish (each 300 μl), and OHSS activity was bioassayed for 1.5 and 2.2 h.

Results

Chromatography and estimation of the molecular mass

Crude hatch water from about 90 females was saturated with $(NH_4)_2SO_4$ overnight; no OHSS activity was found in the supernatant. The precipitate was dissolved in 100 m*M* Tris-HCl buffer. This solution (concentrated hatch water) was subjected to hydrophobic chromatography, and each fraction (10 ml) was bioassayed for 1.5 h.

As shown in Figure 1, most proteins were removed by this fractionation. The peak of OHSS activity was very

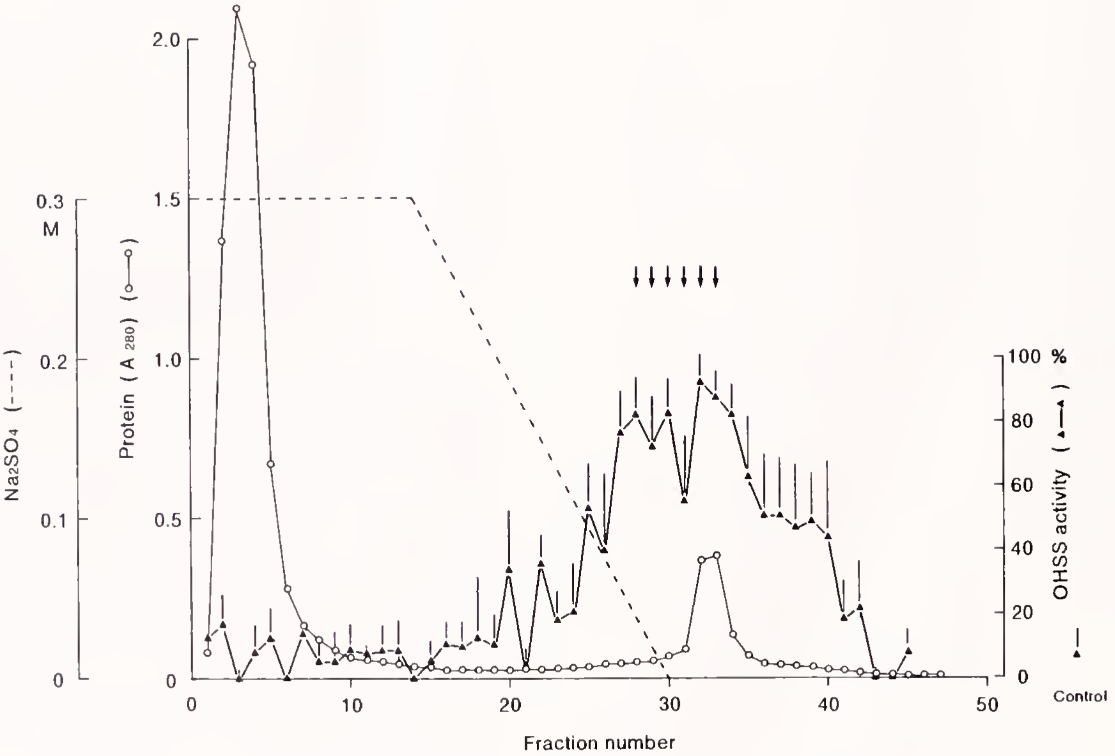

Figure 1. Elution of OHSS activity from a hydrophobic column (HiTrap-Octyl-Sepharose 4FF; Pharmacia). Concentrated hatch water from 90 females was applied to a column previously equilibrated with 20 m*M* Tris-HCl buffer containing 300 m*M* Na_2SO_4, and the proteins were eluted with a linear gradient: −8 m*M* Na_2SO_4/min (broken line). Open circles (○): 280 nm absorption indicating protein concentration in each fraction (10 ml). Bioassay: incubation time, 1.5 h; OHSS activity, percentage of stripped, unbroken ovigerous hairs per whorl; data points are the mean percentages of 3–10 whorls (▲ solid triangles); vertical bars indicate standard deviation; control assay (▲ bottom right), incubation with buffer (details of assay in Methods). Vertical arrows indicate the 6 active fractions (60 ml) applied to anion exchange chromatography.

broad, and only half of it coincided with a protein peak that eluted after 0 mM Na_2SO_4 was reached. A bioassay with an incubation of 1.0 h was also attempted; the results were similar to those shown in Figure 1, although the peak of activity was narrower than that with the longer incubation (not shown).

The pooled active fractions from hydrophobic chromatography (60 ml; six vertical arrows in Fig. 1) were subjected to anion exchange chromatography. The OHSS activity appeared in the pass-through fractions (not shown).

These active fractions (60 ml) were concentrated to 500 μl by ultrafiltration and were then subjected to molecular-sieve chromatography. Each fraction was bioassayed for 1.5 h. As shown in Figure 2A, the activity appeared as a single peak in fractions 6–8. The molecular mass of the eluted protein peak was estimated at 35 kDa by comparison with standard proteins. Similar results were also obtained with the solutions bioassayed for 1.0 h (not shown).

SDS-PAGE

Each fraction eluted in molecular-sieve chromatography (Fig. 2A) was concentrated, and the proteins were analyzed by SDS-PAGE. As shown in Figure 2B, two common protein bands appeared in fractions 6 and 7, both of which had high OHSS activity (Fig. 2A). Fraction 8, which also had high OHSS activity, had little or no staining. The molecular masses of these bands were estimated to be 32 kDa and 30 kDa by comparison with the marker proteins. An additional band (22 kDa) appeared in fractions 5 and 6; it is very weak in Figure 2B, but is clear in Figure 5A. It was clear that the OHSS activity bioassayed with ovigerous setal segments does not correspond to the 22-kDa band in fractions 5 and 6 (compare Fig. 2A with Fig. 2B).

The concentrated active fractions (6 and 7) from molecular-sieve chromatography were also electrophoresed without denaturation; the proteins were clearly separated (Fig. 3A). The gel was cut into quarters, and each segment of the gel was bioassayed for 1.5 h and 2.0 h. The OHSS activity appeared in the second segment (b) of the gel strip (molecular mass between 40 kDa and 23 kDa), which contained the 32-kDa and 30-kDa protein bands (Fig. 3B).

Characterization

Active fractions 6–8 from molecular-sieve chromatography (Fig. 2A) were pooled, and the thermostability of the OHSS solution was examined. Active solutions that were exposed for 15 min to temperatures between 4°C and 80°C showed virtually no decrease in OHSS activity. In contrast, solutions exposed to 100°C lost activity (Fig. 4A).

Least-square regression lines fitted to the data (Fig. 4B) indicated that active solutions incubated at either 4°C or room temperature (about 23°C) for up to 70 h showed no significant decrease in activity, and that there was no sig-

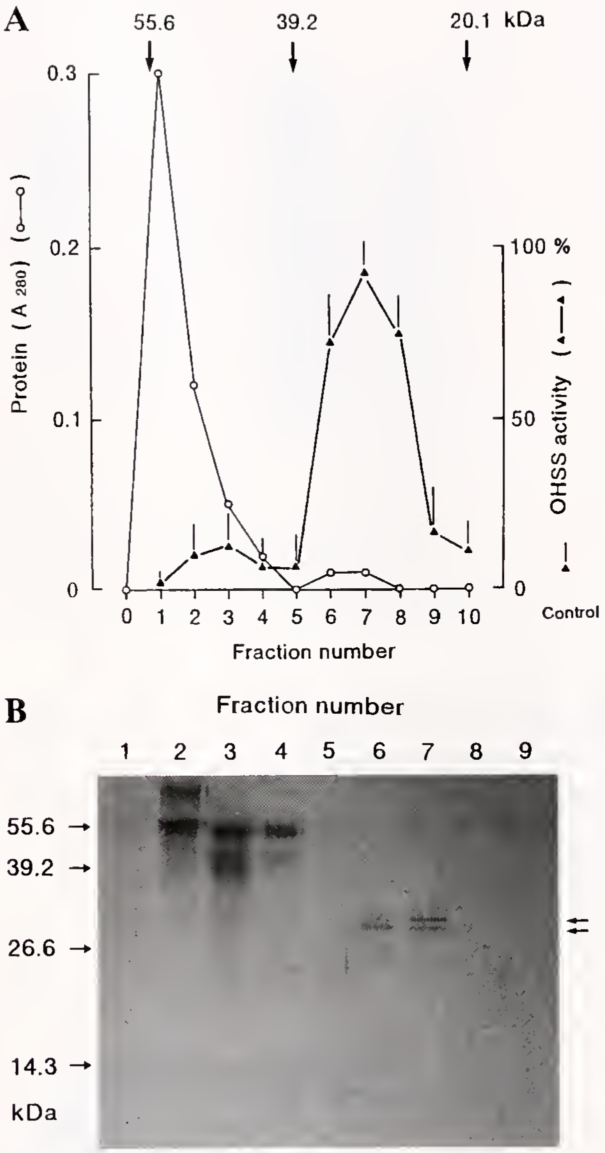

Figure 2. Purification of OHSS activity by molecular-sieve chromatography with protein analysis on SDS-PAGE. (A) The pass-through fractions (60 ml) from anion-exchange chromatography were concentrated by ultrafiltration, and an aliquot (500 μl) was applied to molecular-sieve chromatography; fractions are 1 ml. Open circles (○): protein concentration in each fraction (280 nm absorption). Solid triangles (▲): the OHSS activity of each fraction; bioassays carried out for 1.5 h with one (or two) ovigerous setal segments per fraction; error bars: standard deviation. Control assay (▲ bottom right). Downward-pointing arrows indicate the molecular masses of marker proteins: glutamate dehydrogenase (55.6 kDa), aldolase (39.2 kDa), and trypsin inhibitor (20.1 kDa). (B) Analysis, by SDS-PAGE, of the proteins in each fraction (1–9) eluted from molecular-sieve chromatography. The polyacrylamide gel was transblotted to a PVDF membrane which was stained with Coomassie brilliant blue. The marker proteins were glutamate dehydrogenase (55.6 kDa), aldolase (39.2 kDa), triosephosphate isomerase (26.6 kDa), and lysozyme (14.3 kDa). The two bands that appear in fractions 6 and 7 (arrows to the right) have molecular masses of 32 kDa and 30 kDa.

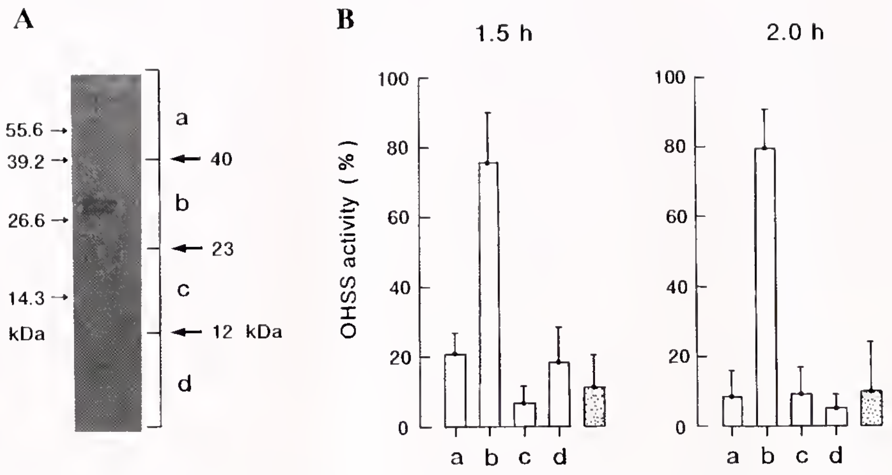

Figure 3. Distribution of OHSS activity in a polyacrylamide gel divided into four equal segments after SDS-PAGE. (A) The gel. Numbers at the left of the small arrows indicate the molecular masses of the standards (see Fig. 2B). The molecular mass limits of each gel segment are indicated by the large arrows. (B) Bioassay with two or three ovigerous setal segments. Open bars indicate OHSS activity of each gel segment. Incubation periods for the bioassay: 1.5 h and 2.0 h. Stippled bars: controls; the ovigerous setal segments were incubated in DW for 1.5 h and 2.0 h. Error bars: standard deviation.

nificant difference between the two experiments. Solutions maintained for longer times (100 and 120 h) decreased in activity in both experiments.

Figure 4C shows the pH dependency of OHSS activity. After an assay incubation of 1 h, the pH optimum was quite broad, about 7.0–11.0.

Specificity of antibodies and affinity purification

An antiserum raised from molecular-sieve chromatography (fractions 6 and 7) detected only two strong protein bands on SDS-PAGE, and they appeared in fractions 6–8 (Fig. 5). These immunostained protein bands clearly corresponded to the peak of OHSS activity in Figure 2A.

The antibodies that had stained the 32-kDa and 30-kDa protein bands were purified by immunochemical affinity to determine the specificity of binding. As shown in Figure 6A, the antibodies eluted from the 32-kDa protein band on SDS-PAGE stained the 30-kDa protein as well; and the antibodies eluted from the 30-kDa band similarly stained both the 30-kDa and 32-kDa proteins.

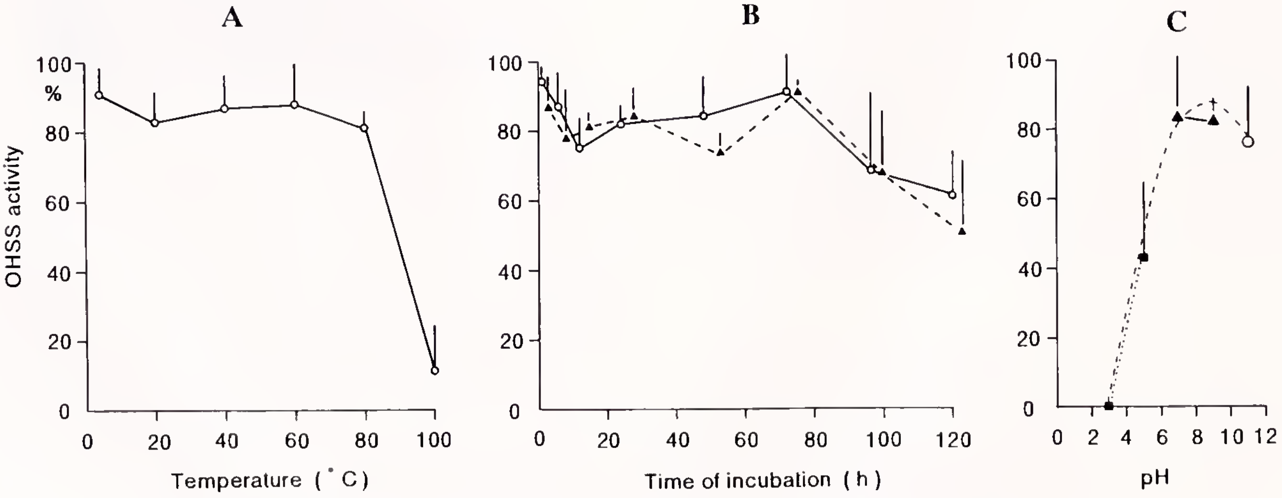

Figure 4. Characteristics of OHSS activity. (A) Heat stability. Active solutions were incubated for 15 min at each temperature, and OHSS activity was bioassayed for 1 h. (B) Effects of prolonged incubation (up to 5 days). For each time, active solutions were maintained at either 4°C (○) or 23°C (▲), and the activity was bioassayed for 1 h. (C) Dependence of activity on pH. Buffers: 100 m*M* Na-acetate (■); 100 m*M* Tris-HCl (▲); 100 m*M* Gly-NaOH (○). The activity was bioassayed for 1 h. Broken line in (C) indicates the least-square regression curve fitted to the data. Error bars: standard deviation of three experiments.

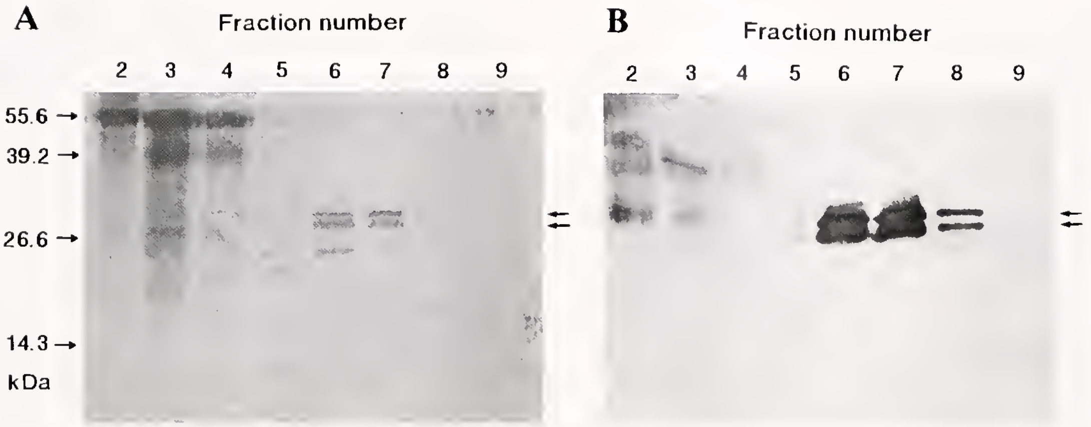

Figure 5. Specificity of the polyclonal antiserum raised against OHSS. (A) SDS-PAGE of fractions eluted from molecular-sieve chromatography. The polyacrylamide gel was transblotted onto a PVDF membrane and stained with Coomassie brilliant blue. (B) Immunostaining of the PVDF membrane with a polyclonal antiserum raised to OHSS. Numbers to the left show the molecular masses of the standards shown in Figure 2B. The intensely immunostained bands in fractions 6–8 have masses of about 32 kDa and 30 kDa (arrows to the right).

In this experiment (Fig. 6A), however, the 32-kDa band was at most 2 mm apart from the 30 kDa band on the gel. In addition, the PVDF membrane was not stained with CBB, except the narrow strip that had been cut on both sides (5 mm in width), because the antibodies were not bound to CBB-stained proteins. So these protein bands could have been incompletely separated.

In Figure 6B, concentrated active fractions from molecular sieve chromatography (6 and 7 in Fig. 2A) were electrophoresed for a longer period (9 h), which produced a gap of 5–6 mm between the upper and lower bands. The whole membrane was stained by Ponceau S, and each protein band (2 mm in width) was subjected to affinity purification. Again, the antibody raised from the 32-kDa band bound to the 30-kDa band as well; and the antibody produced from the 30-kDa band also recognized the 32-kDa band (Fig. 6B).

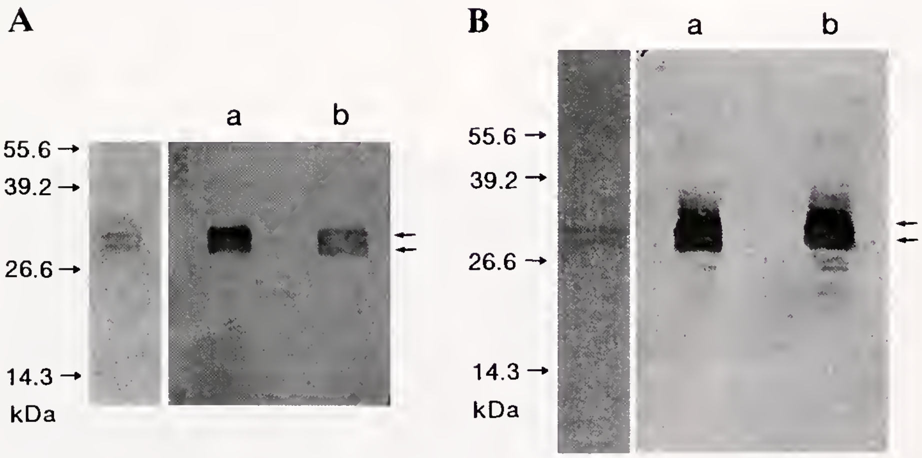

Figure 6. Immunostaining with antibodies affinity purified from SDS-PAGE bands that had OHSS activity. SDS-PAGE of the proteins from molecular-sieve fractions 6 and 7 (see Fig. 2A) was carried out for either 3.5 h (A) or 9h (B), the longer electrophoresis producing the greater separation between the active bands at 32 kDa and 30 kDa. The bands were cut out of the PVDF membranes, incubated with a polyclonal antiserum raised to OHSS, and the bound antibodies were eluted (see Methods). These antibodies, obtained from the short and long electrophoresis, were applied to two new SDS-PAGE runs, both of 3.5 h; these final runs are shown in this figure. Immunostaining was effected by antibodies bound (a) to protein in the upper band (32 kDa), and (b) to the protein in the lower band (30 kDa). The strips to the left of the two panels were stained with Coomassie brilliant blue (A) and Ponceau S (B); the numbers (with arrow) are the molecular masses of the standard molecules (identified in Fig. 2B).

OHSS activity in the post-hatching remnants of the embryo attachment system

After hatching, the broken egg cases, funiculus, and investment coat remain attached to the ovigerous hairs. The female picks these remnant attachment structures off the ovigerous hairs, but this must occur after the OHSS released with the hatch water has been greatly diluted in the estuary. We therefore examined the possibility that at least some OHSS is present in the remnant attachment structures themselves.

The remnants were collected and stained with FITC-conjugated, OHSS antiserum (Fig. 7). OHSS was clearly detected all over the remnants, including the prezoeal cuticles. In contrast, the egg capsule, funiculus, and investment coat did not react to the FITC-conjugated OHSS antiserum when the embryos were squeezed in the egg cases (not shown).

When samples for electrophoresis and immunoblotting were prepared from remnants that had been crushed and denatured, only the 32-kDa band was detected (Fig. 7, right).

Remnants stored at −20°C were thawed and crushed, and suspensions of this material (not centrifuged) were bioassayed for 1.5 h and 2.0 h. As shown in Table I, strong OHSS was detected in this solution. In another experiment, the remnants were thawed and crushed, and then treated with 5%, 10%, and 20% Triton-X. After centrifugation for 20 min (15,000 rpm), the supernatant was bioassayed for 1.5 h and 2.2 h and showed strong OHSS activity, particularly at the longer incubation (Table II).

Appearance of OHSS in the developing embryos

Because OHSS immunoreactivity and biological activity occur in the remnants after hatching, we determined when, during development, these activities would appear. Immunochemical and biological observations were made.

Immunochemistry. Embryo clusters (one-third of an ovigerous seta) were taken at successive times from a single female and crushed; the suspensions were denatured with the lysis buffer *before* centrifugation. As shown in Figure 8, the 32- and 30-kDa proteins became noticeable at least 2 weeks before hatching. The 30-kDa band was the stronger of the two bands at 10 and 6 days before hatching; but its intensity declined and became very faint in embryos 4 h before hatching; and it disappeared completely in post-hatched zoeas. In contrast, the 32-kDa band appeared later than the 30-kDa band, but it was still quite clear in embryos 4 h before hatching, and again was not detected in the post-hatched zoeas. In addition to the two bands of OHSS-related protein, an immunoreactive band appeared at about 55 kDa, from 14 to about 2 days before hatching (Fig. 8).

In another female, the supernatant and the sediment were denatured separately by the lysis buffer *after* the embryo clusters had been crushed and centrifuged. In the supernatant (Fig. 9A), OHSS first appeared as a weak 32-kDa band 14 days before hatching. The 30-kDa band was noticeable 10 days before hatching, and the amount increased abruptly in the embryos collected 6 days before. This protein decreased markedly just before hatching, but was still visible 4 h before hatching.

On the other hand, the sediment contained broken egg cases, funiculi, the investment coat, ovigerous hairs, prezoeal cuticles, and probably only a portion of the embryos. When this material was centrifuged and the supernatant was examined on the same female (Fig. 9B), the 30-kDa band appeared weakly in the lanes derived from embryos collected 10, 6, and 4 days before hatching; but it was absent at other times. In contrast, the 32-kDa band

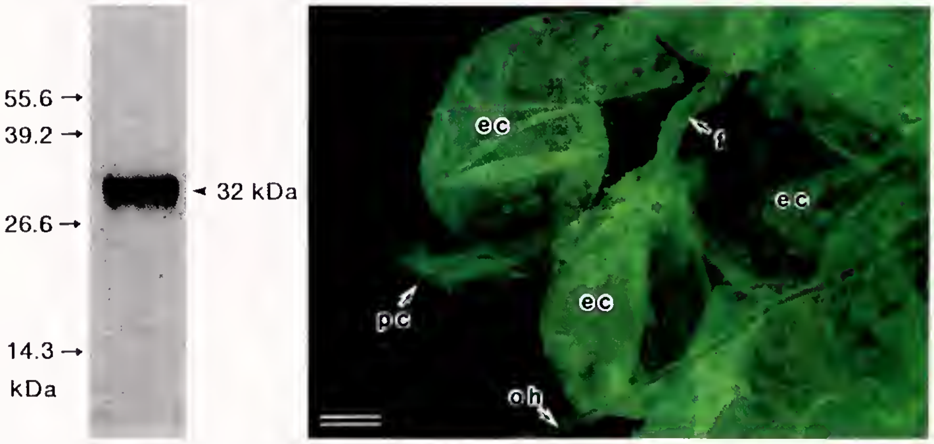

Figure 7. Immunochemical staining of the structures remaining attached to a female's ovigerous hairs after hatching. Left: the immunoblot of an extract of the remnants subjected to SDS-PAGE. Arrowhead: 32-kDa protein band. Numbers to the left show the molecular masses of the standard molecules (as in Fig. 2B). Right: the remnants stained with polyclonal FITC-conjugated OHSS antiserum. *ec*: broken egg case; *f*: funiculus; *pc*: prezoeal cuticle; *oh*: female ovigerous hair (see fig. 2 in Saigusa, 1994). Scale: 100 μl.

Table I

Bioassay of suspensions of crushed attachment structures remaining after hatching

	Incubation*	
	1.5 h	2.0 h
Control†	1.2 ± 2.4%(5)	3.8 ± 6.3%(6)
Experiment	81.1 ± 7.4%(6)	93.5 ± 4.3%(4)

* Values are the mean percentage of unbroken, stripped ovigerous hairs on each whorl; number of whorls on the subdivided segments of the ovigerous seta is given in parentheses.

† Incubation of embryo clusters in distilled water.

became very distinct 6 days before hatching, and was virtually the only band that appeared from 2 days before, until hatching. A 55-kDa band was also detected in the sediment, but was less clear than in the supernatant (Fig. 9A).

Bioassay. Embryo clusters (one-third of an ovigerous seta) were detached from a single female, and were frozen at −20°C. The embryo clusters were thawed and crushed in distilled water, centrifuged, and the OHSS activity in the supernatant was bioassayed for 1.5 h and 2.2 h (Fig. 10A). The OHSS activity began to appear 3 days before hatching, became very strong 6 h before hatching, and was markedly decreased in the zoeas.

The sediment of the embryo clusters was also examined (Fig. 10B). The OHSS activity was again detectable 3 days before hatching; the activity increased near hatching and, like the supernatant, was very strong 6 h before hatching. The zoeas, again, had weak OHSS activity.

Discussion

Ovigerous-hair stripping substance (OHSS) from an estuarine terrestrial crab was purified through three steps of chromatography (Fig. 2A). The activity eluted as a single peak on molecular-sieve chromatography, but still showed two protein bands at 32 kDa and 30 kDa on SDS-PAGE (Fig. 2B). Affinity purified antibodies raised to the active fractions (6 and 7 in Fig. 2A) also bound to two bands at 32 kDa and 30 kDa, corresponding to the bands shown in Figure 2B. Furthermore, immunochemical staining indicated that OHSS-related 32-kDa and 30-kDa bands appear in developing embryos at least 10 days before hatching. This time course, however, did not correspond to the appearance of OHSS activity as bioassayed with ovigerous setal segments. These features invite the following four issues for discussion.

Stability of OHSS

As shown in Figure 4B, purified OHSS retains its activity for at least 80 h, even at room temperature. When crude or concentrated hatch water was frozen to temperatures lower than −20°C, OHSS was stable. But instability appeared after thawing. For example, active fractions that were eluted from the hydrophobic column lost most of their activity within 12 h (unpub. data).

Crude hatch water contains multiple proteases, and these proteases digest casein (Katsube *et al.,* 1999; see also Saigusa, 1996), and they are not excluded by the hydrophobic chromatography shown in Figure 1. So the disappearance of OHSS activity could be due to its digestion by the caseinolytic proteases that still remain in active solutions.

These caseinolytic proteases do, however, bind to an anion exchange column (MONO-Q) and are therefore excluded with this chromatography. Thus, caseinolytic proteases are not present in the materials applied to the column for molecular-sieve chromatography (Fig. 2A). Consequently, purified OHSS retains its activity for a long period even at room temperature (Fig. 4B).

Evidence that the 32-kDa band is active OHSS

As shown in Figure 2A, OHSS activity always appeared in fractions 6–8 on molecular-sieve chromatography. On SDS-PAGE, 32-kDa and 30-kDa protein bands appeared very clearly in these fractions (Fig. 2B). The second segment (b) of the gel strip containing these two bands certainly showed OHSS activity (Fig. 3). An additional band (22 kDa) appeared in fractions 5 and 6 (Figs. 2B and 5A), but did not correspond to the OHSS activity bioassayed with ovigerous setal segments (compare Fig. 2A with Fig. 2B). Thus, we might speculate that OHSS consists of either or both of the two protein bands at 32 kDa and 30 kDa.

Antibodies raised from fractions 6 and 7 stained the 32-kDa and 30-kDa protein bands (Fig. 5B). These bands also appeared in fraction 8, indicating a good correspondence with the bioassayed OHSS activity (Fig. 2A). OHSS is clearly detected all over the remnants that remain on the ovigerous hairs after hatching (Fig. 7). However, only the

Table II

Bioassay with the extract from the remnants with the detergent (Triton-X)

	Incubation*	
	1.5 h	2.2 h
Control†	3.6 ± 8.7%(7)	5.8 ± 7.9%(5)
5% Triton-X	27.5 ± 9.3%(4)	92.0 ± 5.7%(3)
10% Triton-X	72.5 ± 15.1%(3)	91.0 ± 2.8%(3)
20% Triton-X	88.3 ± 7.3%(3)	98.5 ± 2.6%(4)

* Values are the mean percentage of unbroken, stripped ovigerous hairs on each whorl; number of whorls on the subdivided segments of ovigerous seta is given in parentheses.

† Incubation of embryo clusters in distilled water.

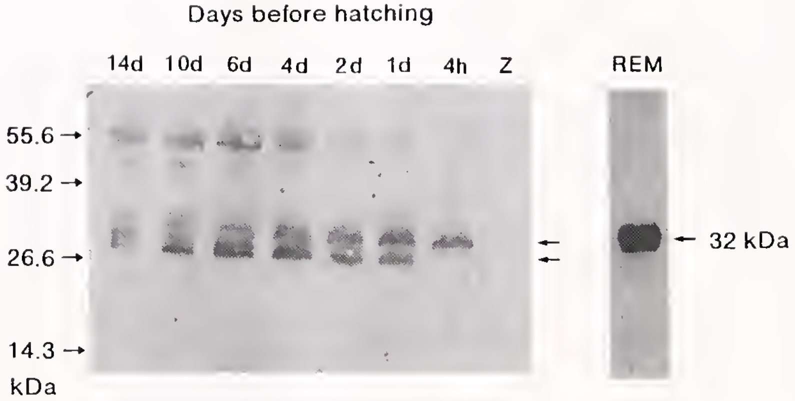

Figure 8. The appearance of immunoreactive OHSS in developing crab embryos. Embryo clusters (one-third of an ovigerous seta) were detached from a single female, crushed, and then denatured with the lysis buffer. The extracts (supernatant) were subjected to SDS-PAGE, and blots were stained immunochemically with the polyclonal OHSS antiserum. *d* (or *h*): days (or hours) before hatching. *Z*: post-hatched embryos (zoeas) released from the same female. REM: remnant structures remaining attached to the female's ovigerous hairs after hatching. Numbers to the left are the molecular masses of the same markers shown in Figure 2B. Note that only the 32-kDa band is detected in the remnant structures (see Fig. 7).

32-kDa protein band was detected in these remnants (Fig. 8). Furthermore, a strong OHSS activity was also detected in these remnants (Table I), as well as in the supernatant after treatment with detergent (Table II). Hence, we speculate that the 32-kDa band is an active OHSS.

On the other hand, we cannot yet hypothesize that the 30-kDa protein band also has OHSS activity. Since purified antibodies recognized both the 32-kDa and 30-kDa bands (Figs. 6A and 6B), we suppose that these two proteins have very similar sequences; *i.e.*, the bands detected by immunochemical staining are probably both OHSS-related proteins.

The OHSS antiserum detected not only 32-kDa and 30-kDa proteins, but also a band at 55 kDa (Figs. 8 and 9). When the active fractions 6 and 7 of molecular-sieve chromatography were studied (Fig. 3A), this band was not detected at all. In contrast, when the crushed embryos (Figs. 8 and 9) were examined, the 55-kDa band often appeared clearly; but it did not appear in the remnant (Fig. 7). The 55-kDa band also appeared on molecular-sieve chromatography (Fig. 2B), but it did not have OHSS activity (Fig. 2A). This band also did not appear in any fraction (1–8) of immunostained PVDF membranes (Fig. 5B). So the 55-kDa band in Figure 2B might be different from that appearing in Figures 8 and 9.

As shown in Figure 8, the 55-kDa protein appeared clearly between 14 days and 4 days before hatching; and it became very faint after 2 days before hatching. Figure 9A

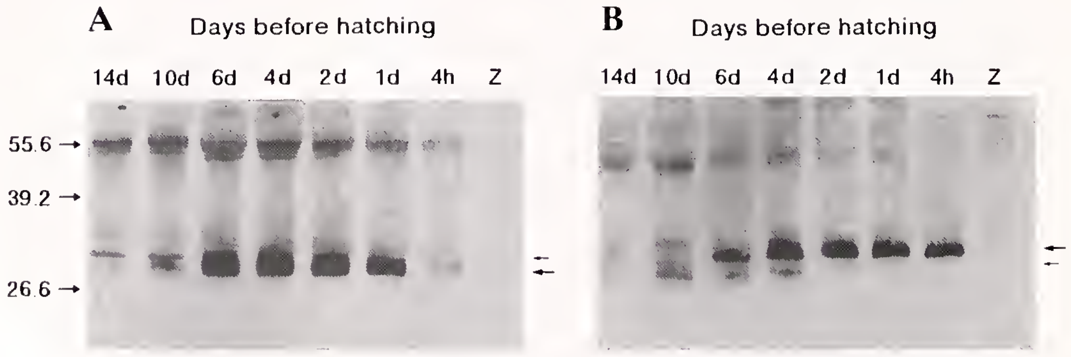

Figure 9. Appearance of immunoreactive OHSS in developing crab embryos. Embryo clusters (one-third of an ovigerous seta) were detached from a single female, crushed, and then centrifuged. The supernatant and sediment were separately denatured with lysis buffer after centrifugation. (A) The supernatant subjected to SDS-PAGE, and the blots immunostained. (B) Extracts of precipitate of the crushed embryos run on SDS-PAGE and immunostained. *d* (or *h*): days (or hours) before hatching. *Z*: post-hatched embryos (zoeas) released from the same female. Arrows indicate immunostained 32-kDa and 30-kDa bands. Numbers to the left are the molecular masses of the same markers as in Figure 2B.

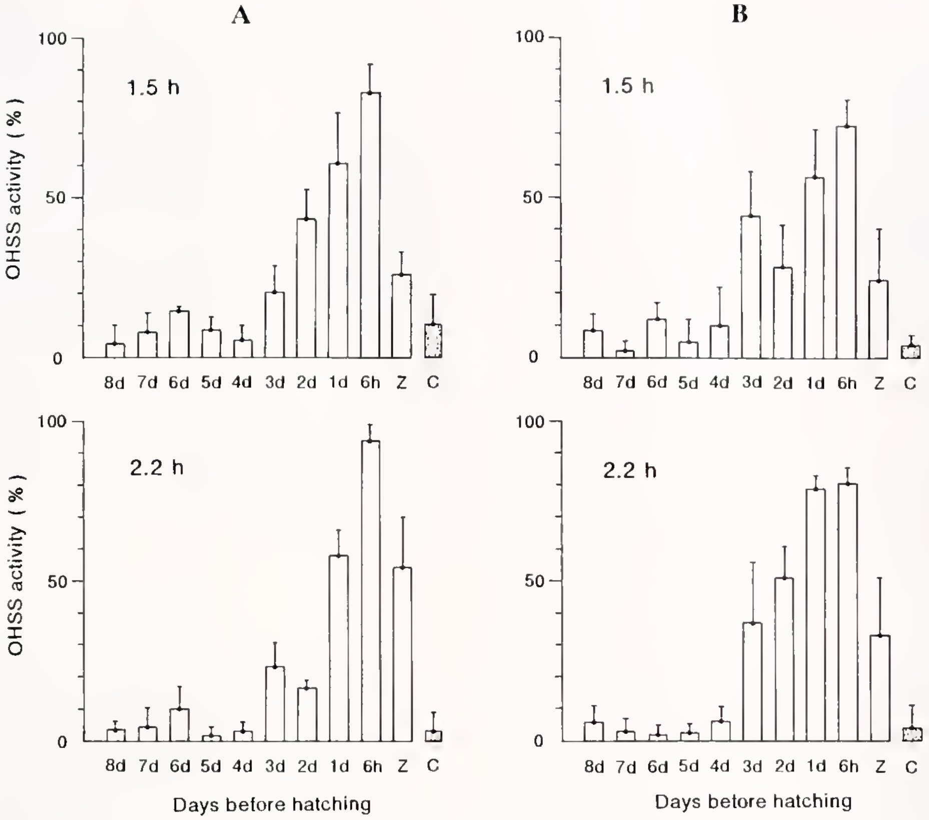

Figure 10. Appearance of OHSS activity in developing crab embryos. Every day, an embryo cluster attached to one-third of an ovigerous seta was detached from a single female. These embryos were crushed, centrifuged, and then the OHSS activity was bioassayed with one or two ovigerous setal segments (open bars). A: Bioassay of the supernatant for 1.5 h (upper panel) and for 2.2 h (lower panel). B: Bioassay of the sediment for 1.5 h (upper panel) and 2.2 h (lower panel). C: Control (incubation with DW; stippled bar). Error bars: standard deviation.

also shows that this protein appears 2 weeks before hatching, and that it stains intensely until 1 day before hatching. These results favor the notion that the 55-kDa protein is, perhaps, a precursor to the 32 and 30 kDa forms.

Behavior of OHSS before and at hatching

When the ovigerous hairs with their attached embryo clusters are gently pulled by a forceps, they are easily broken until the time of hatching. Just after hatching, however, the hairs easily slip out of the coat without damage (see fig. 6 in Saigusa, 1995). Nevertheless, if embryos are crushed before hatching, and the extract is bioassayed, OHSS activity is shown to be present (Fig. 10A and 10B).

The egg capsule, funiculus, and the coat investing ovigerous hairs are not stained by FITC-conjugated OHSS antiserum at least 4 h before hatching (unpub. data). On the other hand, as shown in Tables I and II, remnant structures that are still attached to the ovigerous hairs after hatching show a strong OHSS activity, and immunoreactive OHSS is associated with the remnants (Fig. 7). We speculate that OHSS is stored somewhere in the embryos as they approach hatching, and that it is released outside the egg capsule when hatching occurs or the embryos are crushed. This OHSS would be strongly attached to broken egg capsules, funiculus, and investment coat, which would be stained by FITC-conjugated OHSS antiserum. As shown in Figure 7, a large amount of immunoreactivity was detected in the broken egg cases. We speculate that most of the OHSS is trapped by the egg capsules upon hatching, and the remainder is released into the ambient water.

With immunochemical staining, the 32-kDa band already appears as a faint band between 14 days (Fig. 9A) and 10 days (Fig. 9B) before hatching. However, bioassay of OHSS (Fig. 10A and 10B) shows the OHSS activity appearing no earlier than 3 days before hatching. Moreover, neither the 32-kDa nor 30-kDa band was detected in post-hatched larvae upon immunochemical staining (Fig. 9A and 9B), but at least some OHSS activity was detected by bioassay (Fig. 10A and 10B). We cannot fully explain this discrepancy. As described above, OHSS could be stored somewhere in the embryo after it has been produced; at first it may be in an inactive form, being activated a few days before hatching.

Active substances in other species

Morphologically, the coat that wraps the ovigerous hairs, the funiculus, and the outermost layer (E1) of the egg case are all composed of the same material (Saigusa *et al.*, unpub. data). OHSS is likely to be an enzyme that acts on this material, but electron microscopical observations suggest that OHSS does not digest any portion of the egg case (unpub. data). OHSS is neither a collagenase nor a chitinase. If the main component of the embryo attachment structures were glycoproteins, OHSS might act by partially digesting the sugar, and thus softening the coat wrapping the ovigerous hairs.

Since the layers forming the egg case are not digested by OHSS, the notion that this substance is a crustacean hatching enzyme remains unsubstantiated. However, OHSS can be compared with active substances that are released to the outside by the embryos of other species, upon hatching.

Medaka hatching enzyme, which digests a thick inner layer of the egg case, consists of two kinds of proteases: a high choriolytic enzyme (HCE) and a low choriolytic enzyme (LCE) (Yasumasu *et al.*, 1989a, b). The molecular masses of these enzymes are similar—24.0 kDa for HCE and 25.5 kDa for LCE, as determined by SDS-PAGE—but their actions on the egg case are different. That is, HCE digests the inner layer, causing it to swell markedly, and LCE efficiently digests this swollen inner layer; but acting alone, LCE has no effect on this structure. These are distinct enzymes, and they are not interconvertable (Yasumasu *et al.*, 1989a, b; Yasumasu *et al.*, 1992).

Hatching enzymes in sea urchin embryos are known to be released first as a large molecular mass, and then converted into a smaller mass. For example, the hatching enzyme of *Paracentrotus lividis*, purified by Lepage and Gache (1989), is a 57-kDa glycoprotein, highly active on the fertilization envelope. But this enzyme is soon converted into a 30-kDa form with a reduced proteolytic activity on dimethylcasin (about 80%) and with no activity on the fertilization envelope. The reduced molecular size and the loss of activity were hypothesized to be due to autolysis.

Similar results have been reported for *Strongylocentrotus purpuratus* embryos (Roe and Lennarz, 1990); *i.e.*, the hatching enzyme is secreted from the embryos as a 57-kDa form on SDS-PAGE, but it is converted to a 33-kDa form during purification. This conversion was speculated to be due either to autolysis or to proteolysis by a different protease contained in the sample solution.

Acknowledgments

We thank Dr. Masatsugu Hatakeyama, Kobe University, for help in raising the polyclonal antiserum. Thanks are also due to Dr. Yasushi Yamamoto, Biochemistry Laboratory, and the students of the Molecular Biology Laboratory, for their kind help and many suggestions about SDS-PAGE and immunochemical techniques. Dr. Tadashi Akiyama helped M. S. in the collection of hatch water in 1994. Supported by Grant-in-Aid for Scientific Research (C) (2) from the Ministry of Education, Science, Sports, and Culture, Japan, to M. S. (Nos. 06839017 and 08833009, Marine Biology; No. 10836014, Natural History). Also supported by Narishige Zoological Science Award to M. S. in 1997.

Literature Cited

Cheung, T. S. 1966. The development of egg-membranes and egg attachment in the shore crab, *Carcinus maenas*, and some related decapods. *J. Mar. Biol. Assoc. UK* **46:** 373–400.

Davis, C. C. 1968. Mechanisms of hatching in aquatic invertebrate eggs. *Oceanogr. Mar. Biol. Annu. Rev.* **6:** 325–376.

Davis, C. C. 1981. Mechanisms of hatching in aquatic invertebrate eggs. II. *Oceanogr. Mar. Biol. Annu. Rev.* **19:** 95–123.

Goudeau, M., and F. Lachaise. 1983. Structure of the egg funiculus and deposition of embryonic envelopes in a crab. *Tissue Cell* **15:** 47–62.

Helvik, J. V., D. O. Oppen-Bernsten, and B. T. Walther. 1991. The hatching mechanism in Atlantic halibut (*Hippoglossus hippoglossus*). *Int. J. Dev. Biol.* **35:** 9–16.

Katsube, Y., M. Terajima, and M. Saigusa. 1999. Caseinolytic protease in crab hatch water: preliminary studies of purification, characterization, and its putative role. *Proc. Arthropod. Embryol. Soc. Jpn.* **34:** 1–9.

Laemmli, U. K. 1970. Cleavage of structural proteins during the assembly of the head of bacteriophage T4. *Nature* **227:** 680–685.

Lepage, T., and C. Gache. 1989. Purification and characterization of the sea urchin embryos hatching enzyme. *J. Biol. Chem.* **264:** 4787–4793.

Roe, J. L., and W. J. Lennarz. 1990. Biosynthesis and secretion of the hatching enzyme during sea urchin embryogenesis. *J. Biol. Chem.* **265:** 8704–8711.

Saigusa, M. 1982. Larval release rhythm coinciding with solar day and tidal cycles in the terrestrial crab *Sesarma*. *Biol. Bull.* **162:** 371–386.

Saigusa, M. 1992. Control of hatching in an estuarine terrestrial crab. I. Hatching of embryos detached from the female and emergence of mature larvae. *Biol. Bull.* **183:** 401–408.

Saigusa, M. 1993. Control of hatching in an estuarine terrestrial crab. II. Exchange of a cluster of embryos between two females. *Biol. Bull.* **184:** 186–202.

Saigusa, M. 1994. A substance inducing the loss of premature embryos from ovigerous crabs. *Biol. Bull.* **186:** 81–89.

Saigusa, M. 1995. Bioassay and preliminary characterization of ovigerous-hair stripping substance (OHSS) in hatch water of crab larvae. *Biol. Bull.* **189:** 175–184.

Saigusa, M. 1996. Two kinds of active factor in crab hatch water: ovigerous-hair stripping substance (OHSS) and protease. *Biol. Bull.* **191:** 234–240.

Saigusa, M. 1997. Hatching and its control by the circatidal clock in marine crustaceans. *Proc. Arthropod. Embryol. Soc. Jpn.* **32:** 1–23.

Yamagami, K. 1988. Mechanisms of hatching in fish. Pp. 447–499 in *Fish Physiology,* Vol. 11A, W. S. Hoar and D. J. Randall, eds. Academic Press, San Diego, California.

Yasumasu, S., I. Iuchi, and K. Yamagami. 1989a. Purification and partial characterization of high choriolytic enzyme (HCE), a component of the hatching enzyme of the teleost, *Oryzias latipes. J. Biochem.* **105:** 204–211.

Yasumasu, S., I. Iuchi, and K. Yamagami. 1989b. Isolation and some properties of low choriolytic enzyme (LCE), a component of the hatching enzyme of the teleost, *Oryzias latipes. J. Biochem.* **105:** 212–218.

Yasumasu, S., S. Katow, T. S. Hamazaki, I. Iuchi, and K. Yamagami. 1992. Two constituent proteases of a teleostean hatching enzyme: concurrent syntheses and packaging in the same secretory granules in discrete arrangement. *Dev. Biol.* **149:** 349–356.

Yonge, C. M. 1937. The nature and significance of the membranes surrounding the developing eggs of *Homarus vulgaris* and other Decapoda. *Proc. Zool. Soc. Lond.* (*Ser. A*). **107:** 499–517.

Yonge, C. M. 1946. Permeability and properties of the membranes surrounding the developing egg of *Homarus vulgaris. J. Mar. Biol. Assoc. UK* **26:** 432–438.

Reference: *Biol. Bull.* **197:** 188–197. (October 1999)

Behavior of Hemocytes in the Allorejection Reaction in Two Compound Ascidians, *Botryllus scalaris* and *Symplegma reptans*

MAKI SHIRAE[1]*, EUICHI HIROSE[2], AND YASUNORI SAITO[1]

[1] *Shimoda Marine Research Center, University of Tsukuba, Shimoda 5-10-1, Shizuoka 415-0025, Japan; and* [2] *Department of Chemistry, Biology and Marine Science, Faculty of Science, University of the Ryukyus, Nishihara, Okinawa 903-0213, Japan*

Abstract. In botryllid ascidians, the type of allorejection reaction differs among species. Comparative studies of these different reactions contribute to our understanding of the allorecognition and nonself-rejection system. We studied the morphology of hemocyte behavior during allorejection reactions in two species, *Botryllus scalaris* and *Symplegma reptans,* which stand at important points in botryllid phylogeny. In *B. scalaris,* phagocytes mediated hemocyte aggregation, resulting in interruption of blood flow just after vascular fusion of incompatible colonies. Although previous studies indicate that morula cells (MCs) play a central role in the rejection reaction, the MCs of *B. scalaris* did not participate in the rejection reaction. Colonies of *S. reptans* showed two types of allorejection reaction that started at different points in the process of vascular fusion between two colonies. In both types of rejection reaction, the MCs played a central role and behaved similarly to those of all botryllids except *B. scalaris* and a botryllid from Israel. These observations suggest that the differences in hemocyte behavior and allorecognition site observed in this study reflect the variation in allorejection reactions among botryllids.

Introduction

Colony specificity is a type of self-nonself recognition and rejection reaction against conspecifics that occurs in many colonial forms of animals; allogeneic colonies fuse to form a single mass or reject each other when the colonies come into contact at their growing edges, whereas syngeneic colonies always fuse with each other. The phenomenon has been studied in various species in different phyla (*e.g.,* Porifera, Cnidaria, Bryozoa, and Urochordata), and the significance of the fusion and the rejection to survival has been discussed. However, it is difficult to reach a reasonable conclusion by comparing the features of colony specificity among a broad range of species because they differ in body plan and physiological condition.

In botryllid ascidians, the morphological process of fusion and rejection reactions in colony specificity has been described in detail for five species: *Botryllus primigenus* (Oka and Watanabe, 1957, 1960; Tanaka, 1973; Tanaka and Watanabe, 1973; Taneda and Watanabe, 1982a, 1982b); *Botryllus schlosseri* (Sabbadin, 1962; Boyd *et al.,* 1990); *Botrylloides simodensis* (Mukai and Watanabe, 1974; Hirose *et al.,* 1988, 1997); *Botrylloides fuscus* (Hirose *et al.,* 1994, 1997); and *Botrylloides violaceus* (Hirose *et al.,* 1988). In these botryllid ascidians, the processes of fusion are essentially the same. When rejection reactions occur, they interrupt the progress of fusion, and the beginning stages of rejection differ among species. That is, the variation in allorejection types is thought to be caused by differences in the allogeneic recognition stage in the colony fusion process (Taneda *et al.,* 1985; Saito *et al.,* 1994).

Hemocytes play important roles in the allorejection reactions of botryllid ascidians (Taneda *et al.,* 1985; Saito *et al.,* 1994). An earlier comparative study on the ultrastructure of hemocytes in some botryllids, including *Botryllus scalaris* and *Symplegma reptans,* showed that hemocytes could be commonly classified into five morphological types: hemoblasts, morula cells (MCs), granular leukocytes, vacuolated cells, and phagocytes (Shirae, unpub. data). Transient cells in differentiation were also observed. We hypothesize that

Received 30 September 1998; accepted 26 June 1999.

Abbreviations: MCs, morula cells.

* To whom correspondence should be addressed. Email: shirae@kurofune.shimoda.tsukuba.ac.jp

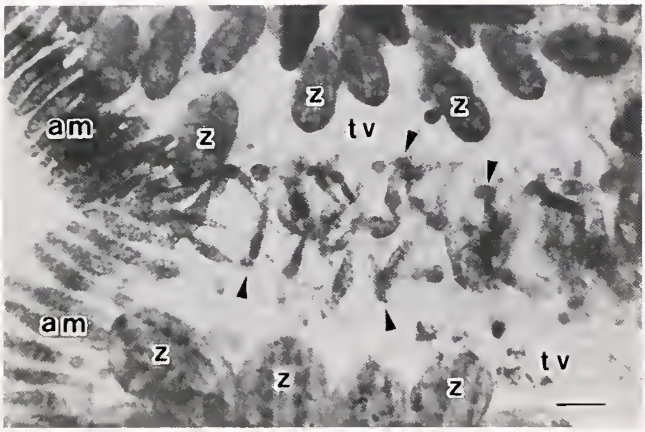

Figure 1. Allorejection reaction in *Botryllus scalaris* under a stereomicroscope. Two incompatible colonies are in contact at their growing edges. Their tunics and ampullae are fused, and hemocyte aggregation in the fused ampullae induces interruption of blood flow (arrowheads). am, ampullae; tv, tunic vessels; z, zooids. Bar = 0.5 mm.

differences in these hemocyte characteristics reflect the variety in allorejection reactions among botryllids.

Botryllus scalaris is thought to be the most primitive botryllid species known to date, based on its manner of sexual reproduction (Mukai, 1977; Mukai *et al.*, 1987; Saito *et al.*, 1981a, 1981b; Saito and Watanabe, 1985). Recently, the molecular phylogeny of botryllids, based on 18S rRNA sequencing, indicated that *B. scalaris* branched off from the lineage earlier than the other botryllids studied thus far (Cohen *et al.*, 1998). In *B. scalaris*, the allorejection reaction begins at the latest stage of the fusion process, that is, soon after fusion of blood vessels and the beginning of blood exchange between two incompatible colonies (Saito and Watanabe, 1982). Therefore, the rejection reaction in *B. scalaris* may be the most primitive type of rejection among botryllid ascidians (Saito *et al.*, 1994). However, there are few descriptions of hemocyte behavior in the rejection reaction to compare with hemocyte behavior of other botryllids.

Symplegma reptans, of the family Styelidae, might be the nearest phylogenetic relative of botryllids for the following reasons. Styelidae is a sister family of Botryllidae (Berrill, 1936), and some researchers (*cf.* Kott, 1969) argue that botryllid ascidians should be classified in a subfamily Botryllinae, belonging to an enlarged family Styelidae. Among compound styelids, *S. reptans* is the species most similar to botryllids morphologically. In botryllids and *S. reptans*, all zooids in a colony are interconnected *via* a common vascular system, and vascular ampullae occur at the growing edge of a colony. Furthermore, the occurrence of colony specificity in *S. reptans* was reported, on the basis of stereomicroscopic observation, by Mukai and Watanabe (1974). They showed that the manner of colony specificity of *S. reptans* resembles that of botryllids.

In this study, we used light and electron microscopy to investigate the processes of allorejection reactions in *B. scalaris* and *S. reptans*, paying special attention to the behavior of hemocytes. In *B. scalaris*, we found that the hemocytes with a central role in the rejection reaction are not morula cells (MCs) but phagocytes. In *S. reptans*, we describe two types of allorejection reaction—the particular combination of allogeneic colonies determines which type occurs. Finally, we discuss the variation in the allorejection reaction in botryllids based on the behavior of hemocytes.

Materials and Methods

Colonies of *Botryllus scalaris* and *Symplegma reptans* were collected in the vicinity of Shimoda (Shizuoka Prefecture), Japan. They were attached to glass slides and reared in culture boxes immersed in Nabeta Bay near the Shimoda

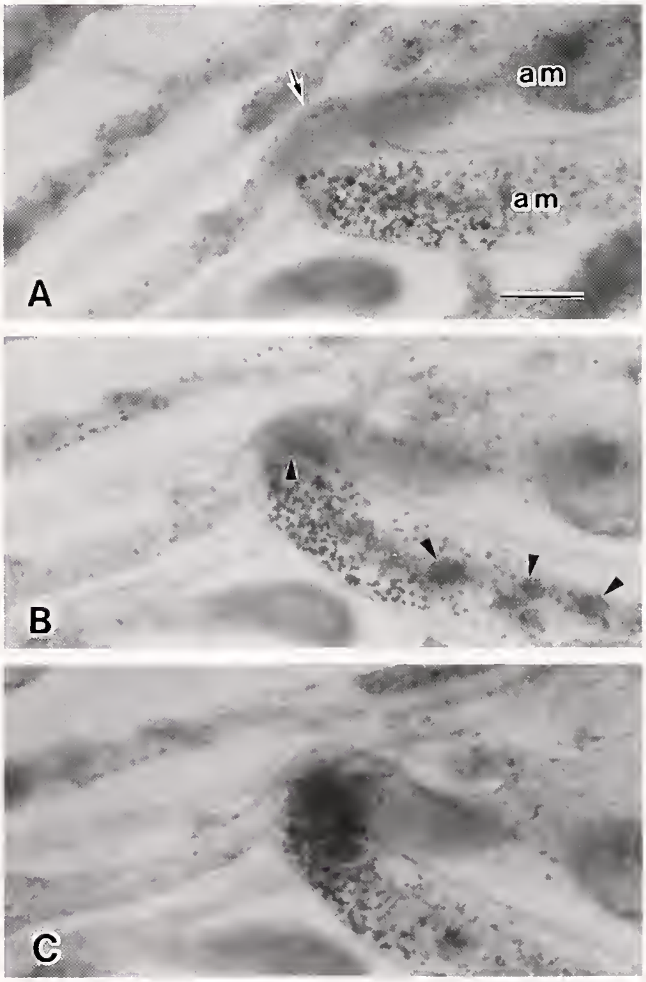

Figure 2. Rejection reaction in *Botryllus scalaris.* (A) Vascular fusion has just occurred and blood of the two incompatible colonies is exchanged. Arrow indicates the fusion point of two ampullae (am) between the incompatible colonies. (B) Hemocytes gradually aggregate in the fused vessels. Arrowheads indicate clusters of aggregating hemocytes. (C) Blood flow is interrupted by the mass of aggregating hemocytes in a few minutes. A, B, and C are the same magnification. Bar = 100 μm.

Marine Research Center, University of Tsukuba. Colonies that grew well were used for the experiments.

Fusion experiments to test fusibility (compatibility) between two colonies were routinely carried out as follows. A small piece was cut from the periphery of each colony with a razor blade. Two allogeneic or syngeneic colony pieces of the same size were brought into contact at their growing edges on a glass slide and were allowed to adhere to the slide in a moisture chamber for 30 min. These colony pieces were subsequently reared in a running seawater aquarium and were observed periodically under a binocular stereomicroscope.

Specimens undergoing fusion or rejection were fixed for 2 h on ice in a 2.5% glutaraldehyde solution containing 0.45 *M* sucrose buffered with 0.1 *M* sodium cacodylate at pH 7.4. The fixed specimens were rinsed in the same buffer and were then postfixed with 1% osmium tetroxide in the same buffer without sucrose for 1.5 h. After dehydration through an ethanol series, the specimens were cleared with *n*-butyl glycidyl ether and embedded in low-viscosity epoxy resins. Thick sections were stained with 1.0% toluidine blue and examined under a light microscope. Thin sections were double-stained with uranyl acetate and lead citrate and then examined with a Hitachi HS-9 transmission electron microscope at 75 kV.

Results

Allorejection reaction in Botryllus scalaris

In *B. scalaris,* as in other botryllids, autogeneic or syngeneic colony pairs fuse and form a single mass. The fusion process was the same as that of other botryllids (Katow and Watanabe, 1980; Saito and Watanabe, 1982). First, the tunics of two colonies fused. Second, the ampullae (termini of blood vessels) penetrated into the opposite colony and the ampullar tips came into contact with the sides of opposite ampullae (tip-to-side contact); at these contact points the colonies fused with each other. Blood started to flow between the two colonies, and finally those colonies formed a single mass. The rejection reaction between allogeneic colonies began after the fusion of opposing ampullae (Fig. 1). Soon after blood exchange through the fused vessels of the two colonies (Fig. 2A), hemocytes aggregated in the vascular lumen of the fused ampullae (Fig. 2B, arrowheads). These aggregates formed a cluster that plugged the opening of the fused ampullae (Fig. 2C) and interrupted the blood flow within a few minutes. Histological observations of the rejection area in the same stage are shown in Figure 3A. As the aggregation gradually proceeded, the volume of hemocyte clusters in the blood vessels increased (Fig. 3, B and C). Subsequently, the vessels collapsed in the rejection area, the surrounding tunic disintegrated, and the two colonies became separate.

The behavior of the hemocytes, as observed by electron microscopy, is shown in Figures 4 and 5. Immediately after the stoppage of blood flow, the cell density of the phagocytes (including hyaline amebocytes, macrophage-like cells, and signet ring cells, as described by Ballarin *et al.*, 1994) increased significantly in the rejection reaction area. The phagocytes had variable shapes, contained many round granules of 0.5 μm in diameter, and often engulfed other hemocytes. Moreover, the phagocytes adhered to other hemocytes and began to aggregate with one another inside the fused ampullae (Fig. 4A). After about half an hour, hemocytes in the aggregates were packed more tightly in the fused ampullae (Fig. 4B), and some of them disintegrated. The aggregates in the ampullae gradually enlarged by

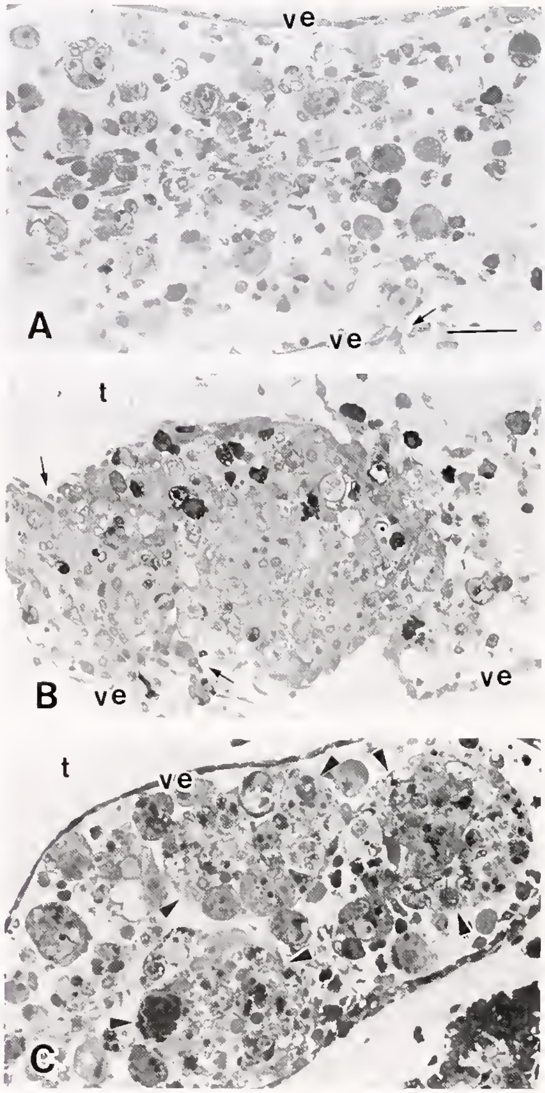

Figure 3. Histological sections in rejection reaction area in *B. scalaris.* (A) Immediately after interruption of blood exchange. Arrow indicates fusion point of vascular epithelia. (B) About 10 h after interruption of blood exchange. Arrow indicates fusion point of vascular epithelia. (C) Two days after interruption of blood exchange. Three clusters encapsulated by phagocytes are shown. t, tunic; ve, vascular epithelia; arrow indicates fusion point of vascular epithelia; arrowheads indicate periphery of hemocyte clusters. A, B, and C are the same magnification. Bar = 50 μm.

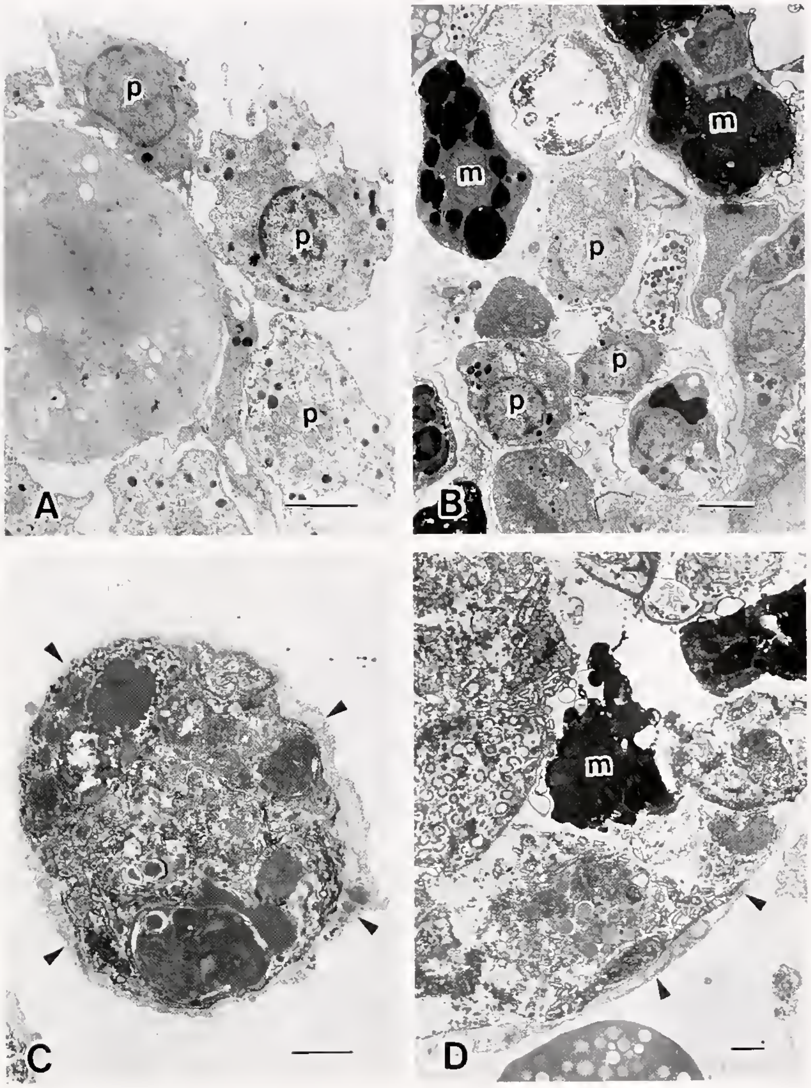

Figure 4. Hemocytes in allorejection reaction in *Botryllus scalaris.* (A) Several phagocytes adhere to a hemocyte. (B) Aggregation. (C) Phagocytosis. Arrowheads indicate outer edges of a phagocyte that surrounded and engulfed a hemocyte cluster. (D) Encapsulation. Arrowheads indicate the periphery of a phagocyte that encapsulated a hemocyte cluster. m, encapsulated and disintegrated morula cell; p, phagocyte. Bars = 2 μm.

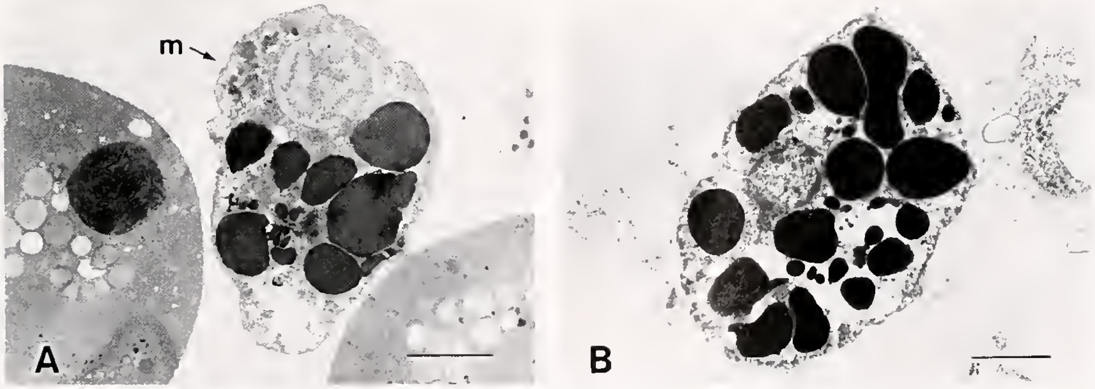

Figure 5. Morula cells in *Botryllus scalaris:* (A) inside the vascular lumen in an allorejection reaction; (B) in an intact colony. m, morula cell. Bars = 2 μm.

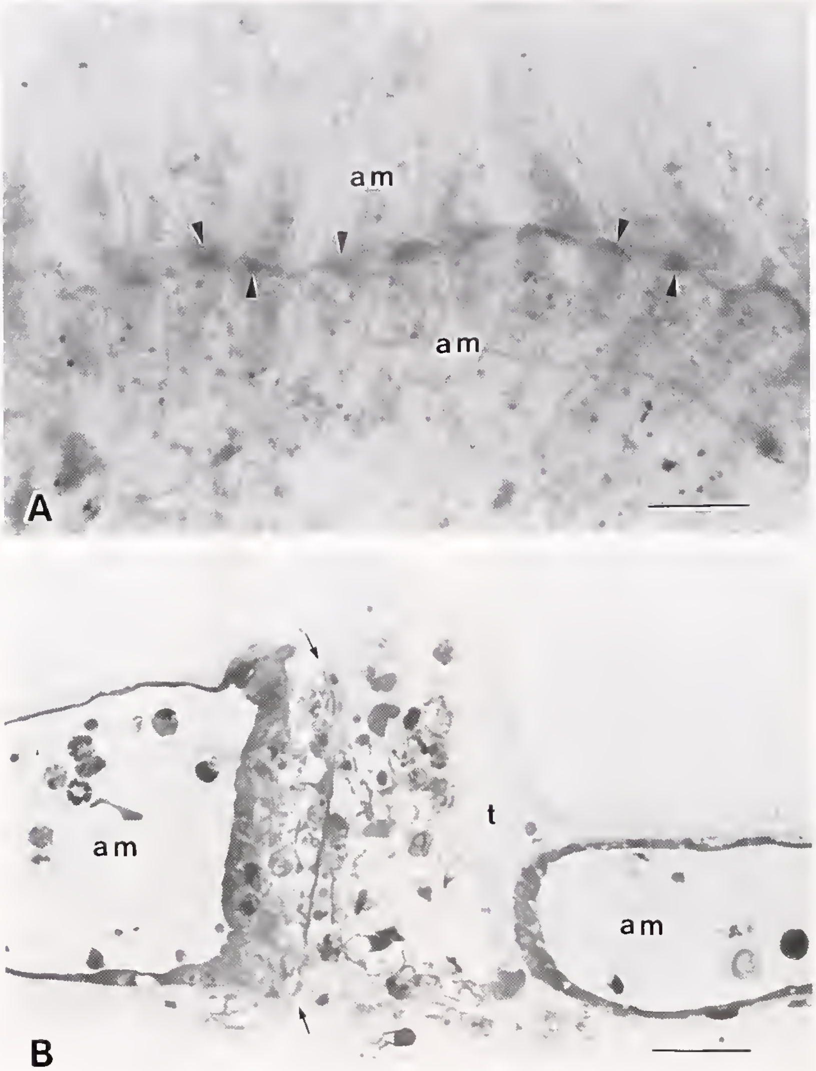

Figure 6. The rejection type of *Symplegma reptans* that is initiated before fusion of ampullae. (A) View of allorejection under stereomicroscope. Ampullae of two incompatible colonies make contact at their growing edges, and infiltrated hemocytes (arrowheads) are observed at the tips of ampullae. (B) Contact area of two incompatible colonies. Arrows indicate the contact point of these two colonies. Many hemocytes infiltrate the tunic and disintegrate, and the surrounding tunic is broken. am, ampulla; t, tunic. Bars: A = 200 μm; B = 50 μm.

recruiting cells from the circulating blood. Furthermore, 3 to 4 h after the stoppage of blood flow, phagocytes engulfed other hemocytes or hemocyte clusters in the rejection areas of blood vessels (Fig. 4C). The hemocyte clusters were encapsulated by phagocytes (Fig. 4D), and the encapsulated clusters sometimes attained a diameter of about 50 μm. All types of hemocytes, including MCs, were engulfed or encapsulated by phagocytes. In the allorejection reaction of other botryllids, MCs always infiltrate the tunic from the blood vessels and disintegrate, but in the allorejection reaction of *B. scalaris,* MCs showed neither infiltration nor disintegration; they also did not show any morphological change inside the blood vessels (Fig. 5).

Allorejection reactions in Symplegma reptans

In botryllid ascidians the ampullae exhibit tip-to-side fusion after extension into the facing colony (Katow and Watanabe, 1980). In *S. reptans,* the fusion process in autogeneic and syngeneic colony pairs has been reported (Mukai and Watanabe, 1974) as tip-to-tip fusion: ampullae of the two colonies did not extend into the facing colony and the ampullae of both colonies came into contact with each other at their tips. But as far as we observed, tip-to-side fusion of ampullae always occurred in the fusion reaction of *S. reptans,* as in botryllid ascidians.

Unlike botryllids, *S. reptans* showed two types of allorejection reaction. The first type was the same as that

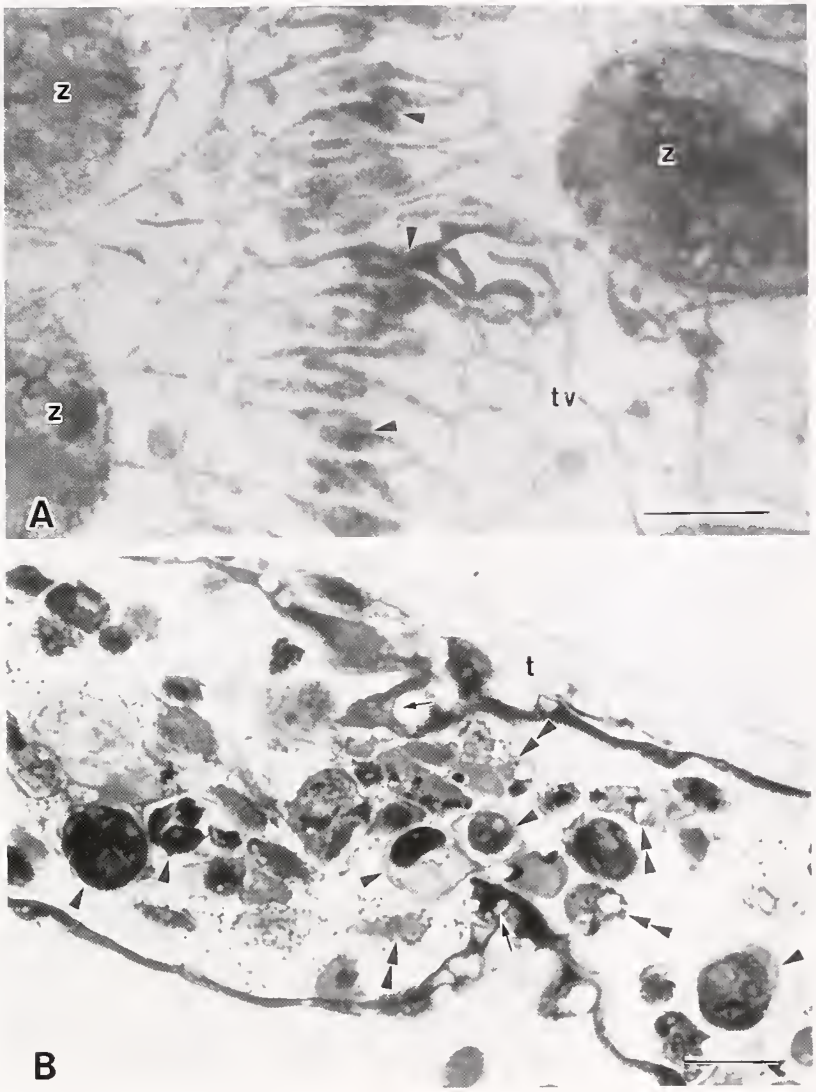

Figure 7. The rejection type of *Symplegma reptans* that is initiated after fusion of ampullae. (A) View of rejection area under stereomicroscope. Arrowheads indicate fused ampullae of two incompatible colonies and aggregation of hemocytes in their ampullae. (B) Inside of fused blood vessels during rejection reaction. Single arrows indicate fused points of vascular epithelia in the two incompatible colonies. Arrowheads indicate phagocytes engulfing other hemocytes. Double arrowheads indicate disintegrating cells. tv, tunic vessels; z, zooid. Bars: A = 500 μm; B = 10 μm.

described by Mukai and Watanabe (1974). In this type of rejection reaction, when two allogeneic colonies came into contact with each other, their tunics fused, but their ampullae neither extended into the opposite colony nor fused with each other. Then, within about 12 h of the contact hemocytes infiltrated the tunic from the ampullar tips at the contact area (Fig. 6A). Then, at the contact area, the tunic around the infiltrating hemocytes disintegrated (Fig. 6B).

In the second type of rejection reaction, which was discovered in this work, fusion of blood vessels and exchange of blood occurred between two incompatible colonies as it does in fusion between compatible colonies. Twelve to fourteen hours after the fusion, hemocytes began to aggregate in blood vessels, and cell aggregation progressed inside the fused ampullae. Thereafter, the vessels were filled with aggregated hemocytes until finally the blood exchange was interrupted completely, within about 24 to 48 h after vascular fusion (Fig. 7A). Histological observations showed phagocytosis and disintegration of cells in this area (Fig. 7B). In addition, hemocytes infiltrated the tunic mainly from the fused ampullae, and these hemocytes and the surrounding tunic disintegrated.

With respect to hemocyte behavior, the two types of rejection reaction were similar. In both types, most of the hemocytes infiltrating the tunic were MCs. During the rejection reaction, MCs disintegrated inside and outside the blood vessels (Figs. 8 and 9), as in some botryllids (such as *Botryllus primigenus* and *Botryllus schlosseri*). Disintegra-

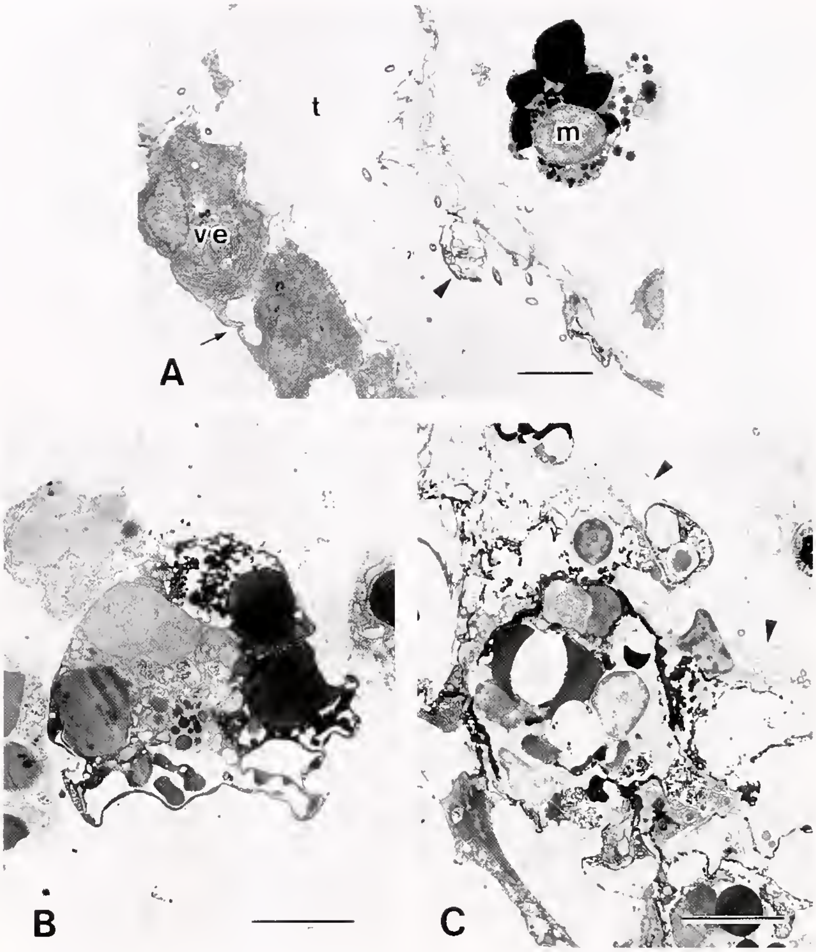

Figure 8. Hemocytes and vascular epithelium in the rejection type initiated before fusion of ampullae in *Symplegma reptans.* (A) Blood vessel and outside of blood vessel. (B) Disintegration of morula cell inside blood vessel. (C) Disintegration of infiltrating morula cell in tunic. Arrowheads indicate electron-dense fiber in the tunic. m, infiltrating morula cell; t, tunic; ve, vascular epidermal cell. Bars = 2 μm.

tion of MCs in the tunic promoted disintegration of the tunic matrix. Phagocytosis occurred in both types of rejection reaction, but encapsulated hemocyte clusters were not found. In the first type of rejection reaction (rejection before vascular fusion), tunic disintegration was limited to the regions surrounding the tips of ampullae in the contact area, and it was more intensive than in the second type (rejection after vascular fusion). However, MC disintegration and phagocytosis inside blood vessels was more common in the second type of rejection reaction than in the first. In the second type of rejection, electron-dense material that might have been discharged from MCs was often found in the vascular lumen (Fig. 9, arrowheads). This material was most abundant in the fused ampullae. The second type of rejection reaction in *S. reptans* progressed more slowly than the rejection reaction of *B. scalaris.* In both types of rejection reaction in *S. reptans,* cellular junctions between the epithelial cells of ampullar tips became loose, and some gaps appeared (arrow in Fig. 8A).

Some *S. reptans* colonies could exhibit both types of rejection reaction, but others showed only the first type (Fig. 10). The fusion experiments with the same pair of colonies were repeated several times and always showed the same results.

Discussion

In five botryllids, *Botryllus primigenus, Botryllus schlosseri, Botrylloides simodensis, Botrylloides fuscus,* and *Botrylloides violaceus,* the rejection reaction between incompatible colonies starts before the fusion of ampullae, although the beginning stages differ among species. These reactions involve activation of a few types of hemocytes, especially MCs, which are ubiquitous hemocytes in ascidians (Wright, 1981). In contrast to these allorejections accompanied by MC activation, the first stage of the rejection reaction in *B. scalaris* was hemocyte aggregation in fused ampullae mediated by phagocytes, especially hyaline amebocytes. The hemocyte clusters clearly caused the interruption of blood exchange between incompatible colonies, as

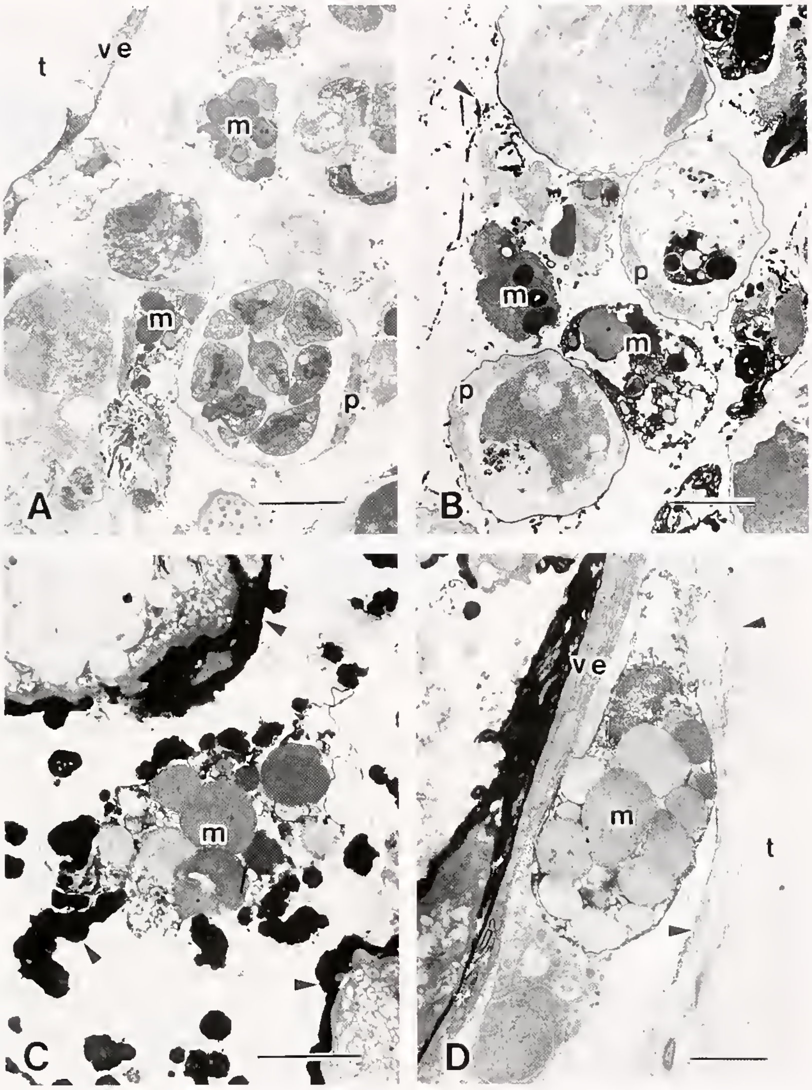

Figure 9. Hemocytes and vascular epithelium in the rejection type initiated after fusion of ampullae in *Symplegma reptans.* (A) Hemocytes in blood vessel where the hemocytes have not aggregated yet. Phagocytosis often occurred. (B) Aggregation of hemocytes mediated by highly electron-dense material. (C) Disintegration of morula cell inside blood vessel. (D) Disintegration of infiltrating morula cell in tunic. Arrowheads in B, C, and D indicate highly electron-dense material inside blood vessel. Arrows in D indicate disintegrated tunic around morula cells. m, infiltrating morula cell; p, phagocyte; t, tunic; ve, vascular epidermal cell. Bars: A and B = 5 μm; C and D = 2 μm.

shown in Figure 2. We labeled this phagocyte-mediated rejection reaction as P-type rejection, to distinguish it from the M-type rejection reaction primarily mediated by MCs in the other botryllids studied thus far. In *S. reptans,* the two types of allorejection reaction shown here could be regarded as M-type rejection, although the second type did not involve remarkable MC infiltration. Morula cell infiltration, which occurs in allorejection in most botryllid species, might be facilitated by the change of permeability in the ampullar epithelium (Taneda and Watanabe, 1982a). This rejection reaction is always accompanied by disintegration of MCs, and their disintegration occurs not only outside but also inside of the ampullae in some botryllids (Rinkevich *et al.,* 1994, 1998; Shirae, unpub. data). Therefore, we regard the standard character of M-type rejection as disintegration of MCs and discharging of their vacuolar contents.

Both MCs and phagocytes are known to have important functions in the defense system of ascidians (Wright, 1981; Raftos, 1990; Cammarata *et al.,* 1997). In the M-type rejection in botryllids and in *S. reptans,* the accumulation of the electron-dense material at the allorejection area is distinctive. Moreover, in the second type of rejection in *S. reptans,* that material seems to mediate hemocyte aggregation, resulting in interruption of blood exchange. Since phenoloxidase activity was demonstrated in MCs (Ballarin *et al.,* 1995), the electron-dense material might be a mela-

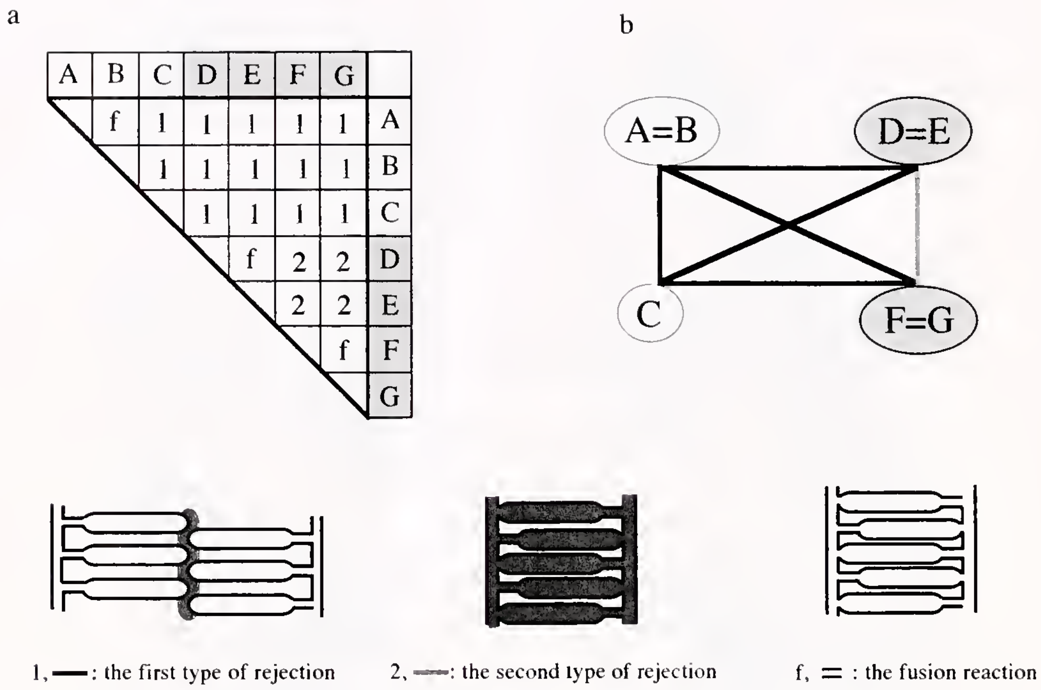

A	B	C	D	E	F	G	
	f	1	1	1	1	1	A
		1	1	1	1	1	B
			1	1	1	1	C
				f	2	2	D
					2	2	E
						f	F
							G

1, ▬ : the first type of rejection   2, ▬ : the second type of rejection   f, = : the fusion reaction

Figure 10. A pairwise allorejection assay among seven strains of *Symplegma reptans* (a) and relationships among *S. reptans* colonies concerning allorejection/fusion type (b).

nin-like substance. A recent cytochemical study by Ballarin *et al.* (1998) suggested that phenoloxidase activity of MCs caused cytotoxicity in the allorejection reaction of *Botryllus schlosseri.* However, in the P-type rejection reaction of *B. scalaris,* such a defense system might not act. In *B. scalaris,* phagocytes might involve some functions in mediation of hemocyte aggregation. Consequently, the diversity of hemocyte characteristics among botryllid ascidians may lead to the observed variation in allorejection. Comparative studies of hemocyte histochemistry might further highlight the variation in allorejection systems of botryllids.

A "fusion-rejection" reaction resembling the allorejection reaction in *B. scalaris* was described in an Israeli *Botrylloides* (Rinkevich *et al.,* 1994). In that botryllid, the allorejection reaction started after vascular fusion and involved much phagocytosis, but cell disintegration occurred inside fused ampullae. Because the hemocyte behavior in the Israeli botryllid is unclear, it is unknown whether the rejection reaction is M-type or P-type.

In *S. reptans,* colonies of four strains exhibited the second type of rejection when they contacted and rejected each other (as shown in Fig. 10); colonies of the other three strains always showed the first type of rejection or fusion. Contact between the colonies of the two groups always resulted in the first type of rejection. Thus, the expression of allorejection reaction type might be controlled genetically. In addition, we found that in the second type of rejection, hemocyte aggregation accompanied by accumulation of electron-dense materials was always initiated only at the fused ampullae of the incompatible colonies, although blood was exchanged well through the fused ampullae just after the fusion. The ampullar epithelial cells might lead to the rejection reaction, at least in *S. reptans.* More studies of the two rejection reactions are needed to fully understand the M-type rejection system.

In the present work, we studied the behavior of hemocytes during allorejection reactions, and showed that differences in hemocyte behavior, as well as differences in allorecognition site, reflect the variation in allorejection reactions among botryllids. Differences in hemocyte behavior are probably caused by changes in hemocyte function, in which case the cytochemical and histochemical characteristics of hemocytes may change. Therefore, to understand the allorejection reaction in botryllids, cytochemical and histochemical studies, as well as morphological studies, should be performed using as many botryllid species as possible.

Acknowledgments

This study was supported in part by a grant-in-aid to Y. S. (#08459005) from the Ministry of Education, Science and Culture of Japan. We are grateful to the staff of the Shimoda Marine Research Center (SMRC), University of Tsukuba, for their assistance and hospitality during this work. We also thank Professor K. Tanaka, Dr. T. Otake (Nihon University), and Dr. T. Ishii (Akita University) for their advice. Finally, special thanks to Dr. A. Bellgrove for her kindness in reading the manuscript for grammatical correctness. This report is contribution No. 633 from SMRC.

Literature Cited

Ballarin, L., F. Cima, and A. Sabbadin. 1994. Phagocytosis in the colonial ascidian *Botryllus schlosseri*. *Dev. Comp. Immunol.* **18:** 467–481.

Ballarin, L., F. Cima, and A. Sabbadin. 1995. Morula cells and histocompatibility in the colonial ascidian *Botryllus schlosseri*. *Zool. Sci.* **12:** 757–764.

Ballarin, L., F. Cima, and A. Sabbadin. 1998. Phenoloxidase and cytotoxicity in the compound ascidian *Botryllus schlosseri*. *Dev. Comp. Immunol.* **22:** 479–492.

Berrill, N. J. 1936. Studies in tunicate development. V. The evolution and classification of ascidians. *Philos. Trans. R. Soc. Lond. B.* **22:** 43–70.

Boyd, H. C., I. L. Weissman, and Y. Saito. 1990. Morphologic and genetic verification that Monterey *Botryllus* and Woods Hole *Botryllus* are the same species. *Biol. Bull.* **178:** 239–250.

Cammarata, M., V. Arizza, N. Parrinello, G. Candore, and C. Caruso. 1997. Phenoloxidase-dependent cytotoxic mechanism in ascidian (*Styela plicata*) hemocytes active against erythrocytes and K562 tumor cells. *Eur. J. Cell. Biol.* **74(3):** 302–307.

Cohen, S. C., Y. Saito, and I. L. Weissman. 1998. Evolution of allorecognition in botryllid ascidians inferred from molecular phylogeny. *Evolution* **52(3):** 746–756.

Hirose, E., Y. Saito, and H. Watanabe. 1988. A new type of the manifestation of colony specificity in the compound ascidian, *Botrylloides violaceus* Oka. *Biol. Bull.* **175:** 240–245.

Hirose, E., Y. Saito, and H. Watanabe. 1994. Surgical fusion between incompatible colonies of the compound ascidian, *Botrylloides fuscus*. *Dev. Comp. Immunol.* **18:** 287–294.

Hirose, E., Y. Saito, and H. Watanabe. 1997. Subcuticular rejection: an advanced mode of the allogeneic rejection in the compound ascidians *Botrylloides simodensis* and *B. fuscus*. *Biol. Bull.* **192:** 53–61.

Katow, H., and H. Watanabe. 1980. Fine structure of fusion reaction in compound ascidian *Botryllus primigenus* Oka. *Dev. Biol.* **76:** 1–14.

Kott, P. 1969. Antarctic Ascidiacea. *Antarct. Res. Ser.* **13:** 1–239.

Mukai, H. 1977. Comparative studies on the structure of reproductive organs of botryllid ascidians. *J. Morphol.* **152:** 363–380.

Mukai, H., and H. Watanabe. 1974. On the occurrence of colony specificity in some compound ascidians. *Biol. Bull.* **147:** 411–421.

Mukai, H., Y. Saito, and H. Watanabe. 1987. Viviparous development in *Botrylloides* (compound ascidians). *J. Morphol.* **193:** 263–276.

Oka, H., and H. Watanabe. 1957. Colony specificity in compound ascidians as tested by fusion experiments (a preliminary report). *Proc. Jpn. Acad.* **33:** 657–659.

Oka, H., and H. Watanabe. 1960. Problems of colony specificity in compound ascidians. *Bull. Mar. Biol. Stn. Asamushi* **10:** 153–155.

Raftos, D. A. 1990. The morphology of allograft rejection in *Styela plicata* (Urochordata: Ascidiacea). *Cell Tissue Res.* **261:** 389–396.

Rinkevich, B., T. Linker-Levav, and M. Goren. 1994. Allorecognition/xenorecognition responses in *Botrylloides* (Ascidiacea) subpopulations from the Mediterranean coast of Israel. *J. Exp. Zool.* **270:** 302–313.

Rinkevich, B., S. Tartakover, and M. Goren. 1998. Contribution of morula cells to allogeneic responses in the colonial urochordate *Botryllus schlosseri*. *Mar. Biol.* **131:** 227–236.

Sabbadin, A. 1962. Le basi genetiche della capacita di fusione fra colonies in *Botryllus schlosseri* (Ascidiacea). *Rend. Accad. Naz. Lincei Ser.* **8, 32:** 1031–1035.

Saito, Y., and H. Watanabe. 1982. Colony specificity in colonial ascidian, *Botryllus scalaris*. *Proc. Jpn. Acad.* **58B:** 105–108.

Saito, Y., and H. Watanabe. 1985. Studies on Japanese compound styelid ascidians. IV. Three new species of the genus *Botrylloides* from the vicinity of Shimoda. *Publ. Seto Mar. Biol. Lab.* **30:** 227–240.

Saito, Y., H. Mukai, and H. Watanabe. 1981a. Studies on Japanese compound styelid ascidians. I. Two new species of *Botryllus* from the vicinity of Shimoda. *Publ. Seto Mar. Biol. Lab.* **26:** 347–355.

Saito, Y., H. Mukai, and H. Watanabe. 1981b. Studies on Japanese compound styelid ascidians. II. A new species of the genus *Botrylloides* and redescription of *B. violaceus* Oka. *Publ. Seto Mar. Biol. Lab.* **26:** 357–368.

Saito, Y., E. Hirose, and H. Watanabe. 1994. Allorecognition in compound ascidians. *Int. J. Dev. Biol.* **38:** 237–247.

Tanaka, K. 1973. Allogeneic inhibition in a compound ascidian, *Botryllus primigenus* Oka. II. Cellular and humoral responses in "nonfusion" reaction. *Cell. Immunol.* **7:** 427–443.

Tanaka, K., and H. Watanabe. 1973. Allogeneic inhibition in a compound ascidian. *Botryllus primigenus* Oka. I. Processes and features of "nonfusion" reaction. *Cell. Immunol.* **7:** 410–426.

Taneda, Y., and H. Watanabe. 1982a. Studies on colony specificity in the compound ascidian, *Botryllus primigenus* Oka. I. Initiation of "nonfusion" reaction with special reference to blood cell infiltration. *Dev. Comp. Immunol.* **6:** 43–52.

Taneda, Y., and H. Watanabe. 1982b. Studies on colony specificity in the compound ascidian, *Botryllus primigenus* Oka. II. *In vivo* bioassay for analyzing the mechanism of "nonfusion" reaction. *Dev. Comp. Immunol.* **6:** 243–252.

Taneda, Y., Y. Saito, and H. Watanabe. 1985. Self or non-self discrimination in ascidians. *Zool. Sci.* **2:** 433–442.

Wright, R. K. 1981. Urochordates. Pp. 565–626 in *Invertebrate Blood Cells*. Vol. 2. N. A. Ratcliffe and A. F. Rowley, eds. Academic Press, London.

Reference: *Biol. Bull.* **197:** 198–206. (October 1999)

Origin of Insulin Receptor-Like Tyrosine Kinases in Marine Sponges

ALEXANDER SKOROKHOD[1,2], VERA GAMULIN[3], DIETMAR GUNDACKER[1],
VADIM KAVSAN[2], ISABEL M. MÜLLER[1], AND WERNER E. G. MÜLLER[1,*]

[1] *Institut für Physiologische Chemie, Abteilung Angewandte Molekularbiologie, Universität, Duesbergweg 6, D-55099 Mainz, Germany;* [2] *Ukrainian Academy of Sciences, Department of Biosynthesis of Nucleic Acids, Institute of Molecular Biology and Genetics, 252627 Kiev, Ukraine; and* [3] *Institute Rudjer Boskovic, Department of Molecular Genetics, 10000 Zagreb, Croatia*

Abstract. One autapomorphic character restricted to all Metazoa including Porifera [sponges] is the existence of transmembrane receptor tyrosine kinases (RTKs). In this study we screened for molecules from one subfamily within the superfamily of the insulin receptors. The subfamily includes the insulin receptors (InsR), the insulin-like growth factor I receptors, and the InsR-related receptors—all found in vertebrates—as well as the InsR-homolog from *Drosophila melanogaster*. cDNAs encoding putative InsRs were isolated from the hexactinellid sponge *Aphrocallistes vastus*, the demosponge *Suberites domuncula*, and the calcareous sponge *Sycon raphanus*. Phylogenetic analyses of the catalytic domains of the putative RTKs showed that the sponge polypeptides must be grouped with the InsRs. The relationships revealed that all sponge sequences fall into one branch of this group, whereas related sequences from mammals (human, mouse, and rat), insects and molluscs, and polypeptides from one cephalochordate, fall together into a second branch. We have concluded that (*i*) the InsR-like molecules evolved in sponges prior to the "Cambrian Explosion" and contributed to the rapid appearance of the higher metazoan phyla; (*ii*) the sponges constitute a monophyletic taxon, and (*iii*) epidermal growth factor (EGF)-like domains are present in sponges, which allows the insertion of this domain into potential receptor and matrix molecules.

Introduction

The Porifera [sponges] are the oldest metazoan phylum; they existed 40 to 50 million years prior to the onset of the "Cambrian Explosion" (Valentine *et al.*, 1996), the time of main divergence of metazoan phyla (Valentine, 1994). Highly conserved amino acid (aa) sequences in sponges indicate that the Porifera share one common ancestor with other metazoan phyla (Müller *et al.*, 1994; also see Müller, 1995, 1997, and 1998). These sequences include those (*i*) for transmembrane receptors, *e.g.*, transmembrane tyrosine kinase [TK] receptors [RTKs] (Müller and Schäcke, 1996); (*ii*) for transmembrane adhesion molecules, *e.g.*, the integrins (Pancer *et al.*, 1997a); and (*iii*) for G-protein linked transmembrane receptors for signaling molecules, *e.g.*, the metabotropic glutamate receptor (Perovic *et al.*, 1999). Additional sequences from homeodomain transcription factors show that the transcriptional control of gene expression in the oldest Metazoa is similar to that of the most recent phyla (Seimiya *et al.*, 1994; Richelle-Maurer *et al.*, 1998; Coutinho *et al.*, 1998). One metazoan autapomorphic character restricted to Porifera is the presence of high telomerase activity in all (or almost all) cells, including somatic cells (Koziol *et al.*, 1998).

The discovery that sponges contain transmembrane (Schäcke *et al.*, 1994a), cytoplasmic (Ottilie *et al.*, 1992), and nuclear TKs (Cetkovic *et al.*, 1998) suggests that the

Received 13 January 1999; accepted 26 July 1999.

To whom correspondence should be addressed. E-mail: WMUELLER@mail.UNI-Mainz.DE

The sequences reported here are deposited in the EMBL/GenBank data base: *Suberites domuncula*, cDNA for InsR-like molecule, SDINR: accession number Y17880; *Aphrocallistes vastus*, cDNA for InsR-like molecule AVINR: accession number Y17881; *Sycon raphanus*, cDNA for type 1 InsR-like molecule, SRINR1: accession number Y17877; *Sycon raphanus*, cDNA for type 2 InsR-like molecule, SRINR2: accession number Y17878; *Sycon raphanus*, cDNA for type 3 InsR-like molecule, SRINR3: accession number Y17879.

Abbreviations: aa, amino acid; kb, kilobase; nt, nucleotide; InsR, insulin receptor; ORF, open reading frame; EGF, epidermal growth factor; IGF-1-R, insulin growth factor I receptor; PTK, protein tyrosine kinase; RTK, receptor tyrosine kinase; TK, tyrosine kinase

signaling system in these animals is sophisticated enough to respond to peptide growth factors and to cell adhesion (Müller and Müller, 1999). The catalytic domain of the RTKs is related to that of the cytoplasmic protein tyrosine kinases [PTKs] and the Ser/Thr kinases (Hanks and Hunter, 1995; Kruse *et al.*, 1997). The catalytic domain of the TKs is subdivided into 12 smaller subdomains, the first eight of which are most highly conserved (Hardie and Hanks, 1995). In addition to the characteristic tyrosine protein kinase-specific active-site signature, the previously described catalytic domain of the RTK from the demosponge *Geodia cydonium* contains no further site that marks this molecule as belonging to a specific class of RTKs (Schäcke *et al.*, 1994a). In this study, we have demonstrated for the first time that one distinct subfamily of the RTKs is already present in all three classes of Porifera, and that it contains the TK class II signature with the consensus pattern D-[LIV]-Y-x$_3$-Y-Y-R (PC/GENE, 1995 [Prosite]). By choosing appropriate primers for the polymerase chain reaction, sequences were obtained from sponges that must be grouped with the insulin receptors [InsRs] of vertebrates (Ullrich *et al.*, 1985), the insulin-like growth factor I receptors [IGF-I-Rs] of vertebrates (Ullrich *et al.*, 1986), the InsR-related receptors of vertebrates (Shier and Watt, 1989), and the InsR homolog from *Drosophila melanogaster* (Fernandez *et al.*, 1995). These molecules are all members of the class II RTKs which display, within subdomain VII, the following consensus for InsRs, GF-I-Rs, and InsR-homologs R-D-[IV]-Y-E-[TS]-D-Y (Hardie and Hanks, 1995).

Here we present the TK domains of InsR-(like) molecules that have been isolated from the hexactinellid sponge *Aphrocallistes vastus*, the demosponge *Suberites domuncula*, and the calcareous sponge *Sycon raphanus*. From *S. raphanus*, three full-length clones from the InsR-like molecules are given. All of the sequences were used for phylogenetic analyses. These revealed that the sponge InsR-like molecules are statistically significantly distinct from the related molecules of higher Metazoa, and allowed an assessment of the evolutionary order in which the three classes of Porifera appeared.

Materials and Methods

Materials

Restriction endonucleases and other enzymes for recombinant DNA techniques and vectors were obtained from Stratagene (La Jolla, CA; USA), QIAGEN (Hilden; Germany), Boehringer Mannheim (Mannheim; Germany), GibcoBRL (Grand Island, NY; USA), Amersham (Buckinghamshire; UK), USB (Cleveland, OH; USA), DUPONT (Bad Homburg; Germany), Epicentre Technologies (Madison, WI; USA), and Promega (Madison, WI; USA). *Taq* DNA polymerase, DIG [digoxigenin] DNA labeling kit, DIG-11-dUTP, anti-DIG AP Fab fragments, and CDP [disodium 2-chloro-5-(4-methoxyspiro{1,2-dioxetane-3,2′-(5′-chloro)-tricyclo[3.3.1.1^{3,7}]decan}-4-yl)phenyl phosphate] were from Boehringer Mannheim (Mannheim; Germany).

Sponges

Live specimens of *Sycon raphanus* [Schmidt] (Porifera, Calcarea, Calcaronea, Leucosoleniida, Sycettidae) and *Suberites domuncula* [Olivi] (Porifera, Demospongiae, Tetractinomorpha, Hadromerida, Suberitidae) were collected from the Adriatic Sea near Rovinj (Croatia). The specimens of *Aphrocallistes vastus* [Schulze] (Porifera, Hexactinellida, Hexasterophora, Hexactinosida, Aphrocallistidae) were collected from Saanich Inlet and Barkley Sound, British Columbia (Canada) by scuba diving. They were a gift of Dr. Sally P. Leys (Department of Biology, University of Victoria, P.O. Box 1700, Victoria, BC, Canada). The material was immediately frozen in liquid nitrogen until use.

Construction of cDNA library from A. vastus

Total RNA was extracted from sponge tissue, and polyadenylated mRNA was isolated from total RNA as already described (Pfeifer *et al.*, 1993a and b). cDNA was prepared with a ZAP Express cDNA synthesis kit. The cDNA library of *A. vastus* was prepared in Hybri ZAPII (Stratagene) and packaged *in vitro* with the MaxPlax Packaging Extract (Epicentre Technologies). The library contained approximately 2.4 × 10^6 independent plaque forming units (pfu); the amplified library was stored at 4°C.

Screening and isolation of the cDNAs encoding InsR-like molecules

The complete cDNAs as well as those encoding the catalytic domains were cloned by the polymerase chain reaction (PCR) from the *A. vastus* cDNA library (see above), the *S. domuncula* (Kruse *et al.*, 1997), or the *S. raphanus* cDNA libraries (Kruse *et al.*, 1997). The degenerate sense primer 5′-TTYGGIATGGTITAYGARGG-3′ (Y = pyrimidine, R = purine, I = inosine) and the downstream primer (anti sense) 5′-TARTARTCIGTYTCRTADATRTC-3′ were designed against the conserved regions of TK subdomain I (FGMVYEG) and TK subdomain VII (DIYETDY) of InsRs as well as IGF-I-Rs from mammalian species; these regions are different from the corresponding protein kinases of other classes (Scavo *et al.*, 1991). The two primers define a 470–490 bp long sequence encoding part of the TK catalytic domain (Fig. 1). The PCR was carried out using a GeneAmp 9600 thermal cycler (Perkin Elmer), with an initial denaturation at 95°C for 3 min, then 35 amplification cycles each at 95°C for 30 s, 50°C for 45 s, 72°C for 1.5 min, and a final extension step at 74°C for 10 min. The reaction mixture of 50 μl included 20 pmol of the respective degenerate primer and 10 pmol of the primer T7 (Stratagene), 200 μM of each nucleotide, 1 μl of the respective cDNA libraries, buffer, and 2.5 units of *Taq* DNA polymerase. The expected amplified products were purified and concentrated using Geneclean Spin Kit and directly ligated into pGEM-T vector. After isolation and purification, the plasmid DNAs were sequenced with an automatic DNA sequenator [Li-Cor 4200].

The TK catalytic domains of the three *S. raphanus* InsR-like molecules were used and completed by both 5′- and 3′-RACE, using the kits "5′-" and "3′-RACE System" to full-length cDNAs.

Sequence analyses

Sequences were analyzed using PC/GENE, release 14.0, from IntelliGenetics, Mountain View, CA (USA). Similarity searches and sequence retrieval were performed *via* the e-mail servers at the European Bioinformatics Institute, Hinxton Hall, UK (BLITZ and FASTA), and the National Institutes of Health, Bethesda, MD, USA (BLAST). The phylogenetic tree was constructed from an aa alignment by the neighbor-joining method (Saitou and Nei, 1987) applying the PHYLIP package version 3.5c program (Felsenstein, 1993). The degree of support for internal branches was further assessed by bootstrapping. The distance matrix was calculated as described (Dayhoff *et al.*, 1978). Multiple alignments were performed with CLUSTAL W version 1.6 (Thompson *et al.*, 1994) and their graphic presentations by the program GeneDoc (Nicholas and Nicholas, 1997).

Northern blot

RNA was extracted from liquid-nitrogen-pulverized sponge tissue with TRIzol Reagent (GibcoBRL) as recommended by the manufacturer. Total RNA (1 μg) was electrophoresed through formaldehyde/agarose gel and blotted onto Hybond N^+ membrane following the manufacturer's instructions (Amersham). Hybridization experiments were performed with the probes *SRINR1*, *SRINR2*, or *SRINR3* [≈600 bp segments] from *S. raphanus*. These probes were labeled with DIG-11-dUTP by the DIG DNA labeling kit. Hybridization was performed with the anti sense DIG-labeled probes at 42°C overnight using 50% formamide containing 5×SSC, 2% blocking reagent [Boehringer], 7% [w/v] SDS, and 0.1% [w/v] N-lauroylsarcosine, following the instructions of the manufacturer [Boehringer]. After washing, DIG-labeled nucleic acid was detected with anti-DIG Fab fragments [conjugated to alkaline phosphatase] and visualized by a chemiluminescence technique using CDP, the chemiluminescence substrate for alkaline phosphatase, according to the instructions of the manufacturer [Boehringer].

Results

Cloning and sequencing the cDNAs encoding the InsR-like molecules

The *S. domuncula* nt sequence, *SDINR*, is 491 nt long and has a potential open reading frame [ORF] of 489 bases encoding a deduced protein sequence of 163 aa residues. The sequence from *A. vastus*, *AVINR*, is 490 nt long with an ORF of 489 nt (163 aa).

Three putative sequences of InsR-like molecules were isolated from the cDNA library of *S. raphanus*. The cDNA for type 1 InsR, *SRINR1*, is 2026 nt long with an ORF of 1848 nt encoding a putative sequence of 616 aa (Figs. 1 and 2); type 2 InsR, *SRINR2*, is 2150 nt long with an ORF of 1842 nt (614 aa); and type 3 InsR (Fig. 2), *SRINR3*, is 1433 nt long with an ORF of 1368 nt (456 aa) (Fig. 2). Northern blot analyses were performed with these *S. raphanus* cDNA probes. One band each of approximately 2.2 kb (type 1), 2.3 kb (type 2), and 1.6 kb (type 3) were obtained, confirming that the full-length cDNAs were isolated (Fig. 3).

Deduced aa sequences of the catalytic domains of the putative sponge InsRs

The deduced aa sequences of the catalytic domains of the InsR-like sequences between subdomains I to VII have been aligned (Fig. 1). The borders of subdomains I to VII (according to Hardie and Hanks, 1995), could be defined for all sponge sequences unequivocally (Fig. 1). Specific sites and sequence characteristics were also present as outlined earlier (Müller and Schäcke, 1996): in subdomain I, the ATP-binding site [consensus: GxGxxGxV; but in the hexactinellid INR_AV sequence G is replaced by R]; within subdomain II, the residue Lys in the consensus VAxK, which is required for kinase activity; within subdomain VIb: the aa D [Asp] and N [Asn] as well as in subdomain VII: the DFG tripeptide is present. The DFG segment has been implicated in ATP binding (Hanks *et al.*, 1988) and represents the most conserved portion within the catalytic domain. The tyrosine residue (Y) in subdomain VII (aa no. 180 of the catalytic domain, with respect to the *G. cydonium* RTK) undergoes phosphorylation and is the tyrosine kinase phosphorylation site. Signatures within subdomains VIII, IX, X, and XI are generally less well conserved. Therefore, the PCR-based sequencing was restricted to the part within subdomains I to VII. The TK-specific active-site signature, D-L-A-T/A-R-N, characteristic for both vertebrate and invertebrate TKs (Ottilie *et al.*, 1992; Hanks *et al.*, 1988) is found in subdomain VIb. Within the subdomain VII the signature for the TK class II receptors with the consensus pattern is found, D-[LIV]-Y-x_3-Y-Y-R (PC/GENE, 1995 [Prosite]).

The PCR primers were chosen to identify, in sponges, those catalytic domains of class II RTKs that share the highest similarity to InsRs, IGF-1-Rs, to InsR-related receptors, and to the insulin receptor homolog from *D. melanogaster* (Fernandez *et al.*, 1995). These receptors have the consensus within the class II signature of R-D-[IV]-Y-E-[TS]-D-Y (Hardie and Hanks, 1995). As seen in Figure 1, this consensus is, as expected, present in all sponge sequences; therefore the sequences from the demosponge *S. domuncula*, the calcareous sponge *S. raphanus*, and the hexactinellid sponge *A. vastus* were termed InsR-like molecules.

Complete aa sequences of the InsR-like sequences from S. raphanus

Three cDNAs encoding complete putative InsR-like sequences from *S. raphanus* have been isolated from the library. The sequences are termed type 1, *SRINR1*, type 2, *SRINR2*, and type 3, *SRINR3*, InsR-like molecules. The putative 616 aa sequence INR_SR1 (deduced from SRINR1) has a calculated M_r of 69,477; INR_SR2 of 614 aa has an M_r of 69,213, and INR_SR3 of 456 aa has an M_r of 51,259.

The sequence INR_SR2 was selected for the analysis given here. The transmembrane segment, determined according to the program "RAOARGOS" (PC/GENE, 1995) ranges from aa_{181} to aa_{196}. The intracellular domain is, as in other RTKs (Hardie and Hanks, 1995), divided into a juxtamembrane domain (aa_{197} to aa_{242}) and the catalytic domain [TK domain] (aa_{243} to aa_{521}) (Fig. 2). The catalytic domain is subdivided into 12 subdomains and contains the characteristic TK-specific active-site signature and the RTK class II signature (see above); in addition, the putative ATP-binding site (Hanks *et al.*, 1988) is present (Fig. 2).

The extracellular domain contains one calcium-binding, epidermal growth factor receptor [EGF]-like domain that reads D-x-N-E-C^1-D-x_5-C^2-D-E-C^3-Q-N-C^4-x-N-x_6-C^5-x-N-x_3-C^6-D; it is located from aa_{129} to aa_{162} [the Cys residues are numbered consecutively]. This EGF-like domain consists of six Cys residues, flanked by aa with carbonyl oxygen atoms, which are arranged slightly differently from those found in molecules from higher Metazoa. In particular, the Cys^4 and Cys^5 are separated by more than one aa (Bork *et al.*, 1996). Furthermore, an incomplete EGF-like domain is present from aa_{49} to aa_{128}. The two other types of InsR-like molecules from *S. raphanus* also have two EGF-like domains, and they are similarly arranged. This finding is the first demonstration that EGF-like domains are present in the lowest metazoan phylum. Until now, this domain, which is widely found in vertebrate receptors—*e.g.*, mammalian epidermal growth factor receptors (Geer *et al.*, 1994) and matrix proteins like fibulin (Pan *et al.*, 1993)—has only been identified among invertebrates in *Caenorhabditis elegans* (Campbell and Bork, 1993).

Phylogenetic analyses

When the deduced aa sequences of the TK catalytic domains from the three sponge species were analyzed using the programs BLITZ, FASTA, and BLAST, they displayed highest similarity to the polypeptides from both invertebrates and vertebrates. Among invertebrates, these domains were most similar to the insulin-like receptors from the insects *Aedes aegypti* and *D. melanogaster*, as well as to the insulin receptor of the mollusc *Aplysia californica*. In addition an InsR-homolog sequence isolated, so far, from one cephalochordate, *Branchiostoma lanceolatum*, as well as InsRs, IGF-1-Rs, or InsR-homologs from selected vertebrates (human, mouse and rat) were highly similar to the sponge sequences. They share about 40%–45% of identical aa and about 60%–65% of similar aa (including identical aa) with the selected corresponding molecules. Taking only the sponge sequences, the sequence from *S. raphanus*, type 1, is identical in 67% of the aa (similarity of 78%) within the catalytic domain with *A. vastus* and in 69% (79%) with *S. domuncula*. The finding that the three sequences obtained from *S. raphanus* differ considerably from each other is interesting; type 1 shares only 75% identical aa (similarity 86%) with type 2 and only 79% identical aa (similarity 88%) with type 3.

The phylogenetic tree was constructed and rooted with the sequence of the catalytic domain of the Fes/FER non-receptor TK domain from *S. raphanus* (Cetkovic *et al.*, 1998; Fig. 4A). All sequences used were cut for the alignment to obtain the 12 subdomains, comprising approximately 300 aa. All of the sponge sequences fall into one branch of the tree, whereas the selected sequences of InsRs, IGF-1-Rs, or InsR-related sequences from invertebrates and vertebrates are grouped together into a second one. This relationship is statistically very robust as analyzed by bootstrapping. Hence, support for monophyly of Porifera can be deduced. In consequence, the presented findings, based on the data obtained with the catalytic domains of the InsR-like molecules from sponges, shed new light on the assumed uncertain position of sponges as reviewed by Rodrigo *et al.* (1994). In addition, the data given do not support earlier notions which suggested that the phylum Porifera might be paraphyletic (Cavalier-Smith *et al.*, 1996).

Rate of evolution of the catalytic domains of sponge InsR-like molecules

Use of our data collected on the percentage of aa identity among the polypeptide sequences from the different sponge species on one side and the sponge sequences in comparison to those from higher metazoan allows a relative approach to determining the time of divergence of the sponge classes from a common ancestor. This estimation, which is based on the number of point mutations per 100 aa within given polypeptides, might reflect the time of divergence of two

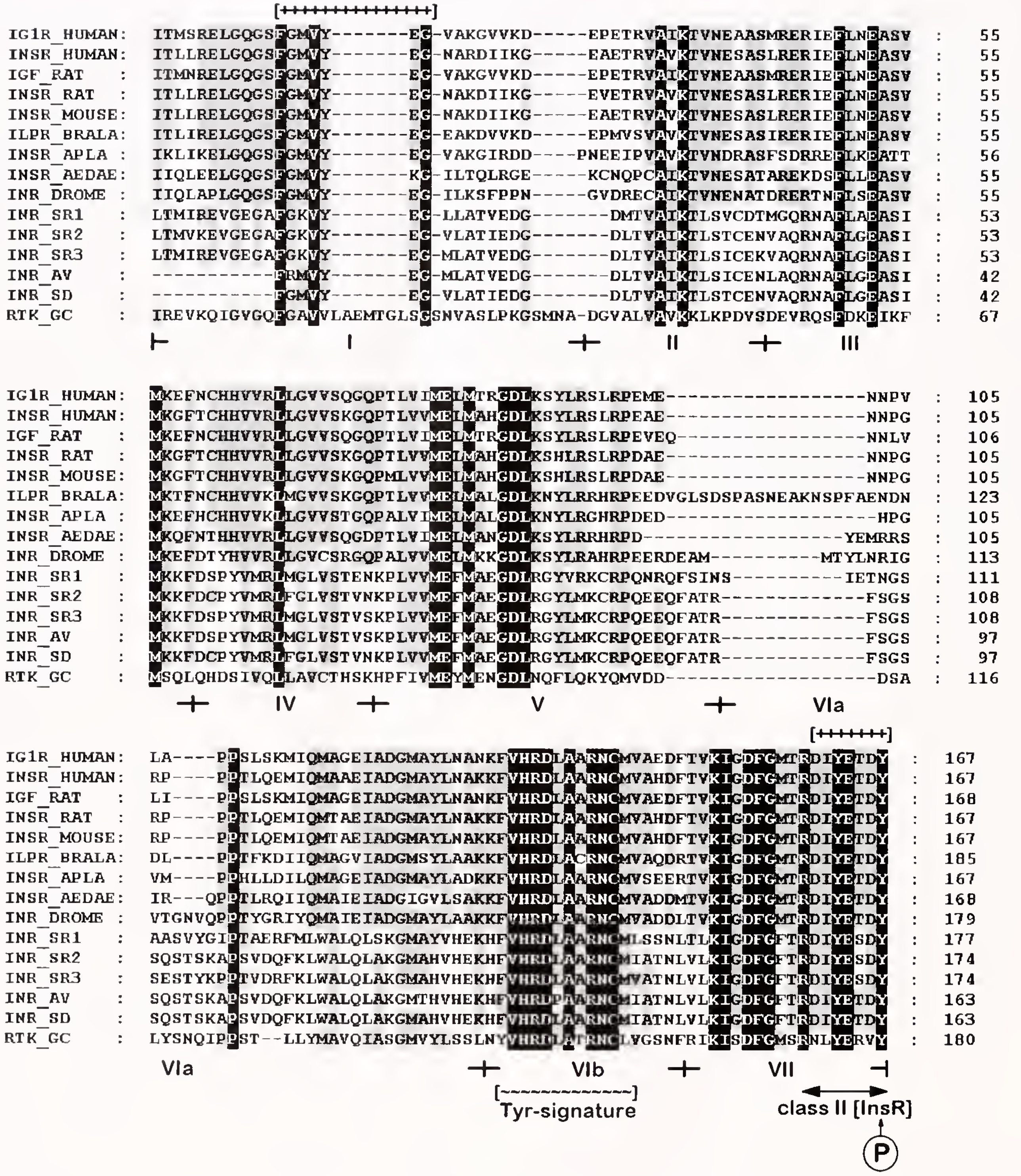

```
IG1R_HUMAN:  ITMSRELGQGSFGMVY--------EG-VAKGVVKD-----EPETRVAIKTVNEAASMRERIEFLNEASV  :  55
INSR_HUMAN:  ITLLRELGQGSFGMVY--------EG-NARDIIKG-----EAETRVAVKTVNESASLRERIEFLNEASV  :  55
IGF_RAT   :  ITMNRELGQGSFGMVY--------EG-VAKGVVKD-----EPETRVAIKTVNEAASMRERIEFLNEASV  :  55
INSR_RAT  :  ITLLRELGQGSFGMVY--------EG-NAKDIIKG-----EVETRVAVKTVNESASLRERIEFLNEASV  :  55
INSR_MOUSE:  ITLLRELGQGSFGMVY--------EG-NAKDIIKG-----EAETRVAVKTVNESASLRERIEFLNEASV  :  55
ILPR_BRALA:  ITLIRELGQGSFGMVY--------EG-EAKDVVKD-----EPMVSVAVKTVNESASIRERIEFLNEASV  :  55
INSR_APLA :  IKLIKELGQGSFGMVY--------EG-VAKGIRDD----PNEEIPVAVKTVNDRASFSDRREFLKEATT  :  56
INSR_AEDAE:  IIQLEELGQGSFGMVY--------KG-ILTQLRGE-----KCNQPCAIKTVNESATAREKDSFLLEASV  :  55
INR_DROME :  IIQLAPLGQGSFGMVY--------EG-ILKSFPPN-----GVDRECAIKTVNENATDRERTNFLSEASV  :  55
INR_SR1   :  LTMIREVGEGAFGKVY--------EG-LLATVEDG-------DMTVAIKTLSVCDTMGQRNAFLAEASI  :  53
INR_SR2   :  LTMVKEVGEGAFGKVY--------EG-VLATIEDG-------DLTVAIKTLSTCENVAQRNAFLGEASI  :  53
INR_SR3   :  LTMIREVGEGAFGKVY--------EG-MLATVEDG-------DLTVAIKTLSICEKVAQRNAFLGEASI  :  53
INR_AV    :  -----------FRMVY--------EG-MLATVEDG-------DLTVAIKTLSICENLAQRNAFLGEASI  :  42
INR_SD    :  -----------FGMVY--------EG-VLATIEDG-------DLTVAIKTLSTCENVAQRNAFLGEASI  :  42
RTK_GC    :  IREVKQIGVGQFGAVVLAEMTGLSGSNVASLPKGSMNA-DGVALVAVKKLKPDVSDEVRQSFDKEIKF  :  67

IG1R_HUMAN:  MKEFNCHHVVRLLGVVSQGQPTLVIMELMTRGDLKSYLRSLRPEME------------------NNPV  :  105
INSR_HUMAN:  MKGFTCHHVVRLLGVVSKGQPTLVVMELMAHGDLKSYLRSLRPEAE------------------NNPG  :  105
IGF_RAT   :  MKEFNCHHVVRLLGVVSQGQPTLVIMELMTRGDLKSYLRSLRPEVEQ-----------------NNLV  :  106
INSR_RAT  :  MKGFTCHHVVRLLGVVSKGQPTLVVMELMAHGDLKSHLRSLRPDAE------------------NNPG  :  105
INSR_MOUSE:  MKGFTCHHVVRLLGVVSKGQPMLVVMELMAHGDLKSHLRSLRPDAE------------------NNPG  :  105
ILPR_BRALA:  MKTFNCHHVVKLMGVVSKGQPTLVVMELMALGDLKNYLRRHRPEEDVGLSDSPASNEAKNSPFAENDN  :  123
INSR_APLA :  MKEFHCHHVVKLLGVVSTGQPALVIMELMALGDLKNYLRGHRPDED-------------------HPG  :  105
INSR_AEDAE:  MKQFNTHHVVRLLGVVSQGDPTLVIMELMANGDLKSYLRRHRPD------------------YEMRRS  :  105
INR_DROME :  MKEFDTYHVVRLLGVCSRGQPALVVMELMKKGDLKSYLRAHRPEERDEAM----------MTYLNRIG  :  113
INR_SR1   :  MKKFDSPYVMRLMGLVSTENKPLVVMEFMAEGDLRGYVRKCRPQNRQFSINS----------IETNGS  :  111
INR_SR2   :  MKKFDCPYVMRLFGLVSTVNKPLVVMEFMAEGDLRGYLMKCRPQEEQFATR-------------FSGS  :  108
INR_SR3   :  MKKFDSPYVMRLMGLVSTVSKPLVVMEFMAEGDLRGYLMKCRPQEEQFATR-------------FSGS  :  108
INR_AV    :  MKKFDSPYVMRLMGLVSTVSKPLVVMEFMAEGDLRGYLMKCRPQEEQFATR-------------FSGS  :  97
INR_SD    :  MKKFDCPYVMRLFGLVSTVNKPLVVMEFMAEGDLRGYLMKCRPQEEQFATR-------------FSGS  :  97
RTK_GC    :  MSQLQHDSIVQLLAVCTHSKHPFIVMEYMENGDLNQFLQKYQMVDD-------------------DSA  :  116

IG1R_HUMAN:  LA----PPSLSKMIQMAGEIADGMAYLNANKFVHRDLAARNCMVAEDFTVKIGDFGMTRDIYETDY  :  167
INSR_HUMAN:  RP----PPTLQEMIQMAAEIADGMAYLNAKKFVHRDLAARNCMVAHDFTVKIGDFGMTRDIYETDY  :  167
IGF_RAT   :  LI----PPSLSKMIQMAGEIADGMAYLNANKFVHRDLAARNCMVAEDFTVKIGDFGMTRDIYETDY  :  168
INSR_RAT  :  RP----PPTLQEMIQMTAEIADGMAYLNAKKFVHRDLAARNCMVAHDFTVKIGDFGMTRDIYETDY  :  167
INSR_MOUSE:  RP----PPTLQEMIQMTAEIADGMAYLNAKKFVHRDLAARNCMVAHDFTVKIGDFGMTRDIYETDY  :  167
ILPR_BRALA:  DL----PPTFKDIIQMAGVIADGMSYLAAKKFVHRDLACRNCMVAQDRTVKIGDFGMTRDIYETDY  :  185
INSR_APLA :  VM----PPHLLDILQMAGEIADGMAYLADKKFVHRDLAARNCMVSEERTVKIGDFGMTRDIYETDY  :  167
INSR_AEDAE:  IR---QPPTLRQIIQMAIEIADGIGVLSAKKFVHRDLAARNCMVADDMTVKIGDFGMTRDIYETDY  :  168
INR_DROME :  VTGNVQPPTYGRIYQMAIEIADGMAYLAAKKFVHRDLAARNCMVADDLTVKIGDFGMTRDIYETDY  :  179
INR_SR1   :  AASVYGIPTAERFMLWALQLSKGMAYVHEKHFVHRDLAARNCMLSSNLTLKIGDFGFTRDIYESDY  :  177
INR_SR2   :  SQSTSKAPSVDQFKLWALQLAKGMAHVHEKHFVHRDLAARNCMIATNLVLKIGDFGFTRDIYESDY  :  174
INR_SR3   :  SESTYKPPTVDRFKLWALQLAKGMAHVHEKHFVHRDLAARNCMVATNLVLKIGDFGFTRDIYESDY  :  174
INR_AV    :  SQSTSKAPSVDQFKLWALQLAKGMTHVHEKHFVHRDPAARNCMIATNLVLKIGDFGFTRDIYETDY  :  163
INR_SD    :  SQSTSKAPSVDQFKLWALQLAKGMAHVHEKHFVHRDLAARNCMIATNLVLKIGDFGFTRDIYETDY  :  163
RTK_GC    :  LYSNQIPPST--LLYMAVQIASGMVYLSSLNYVHRDLATRNCLVGSNFRIKISDFGMSRNLYERVY  :  180
```

Figure 1. Alignment of the catalytic domains of the insulin-like receptors as well as of the related sequences within the class II tyrosine kinase receptors (RTKs). The deduced amino acid sequences of InsR homologs from the polypeptides of the three classes of the phylum Porifera (sponges) were aligned with the related sequences for three invertebrates (mosquito, fruit fly, and mollusc); one cephalochordate (amphioxus); and the three vertebrates (human, mouse, rat). In addition, the RTK domain from the sponge *Geodia cydonium* was used for the comparison. Specific sequence codes are identified below. The borders of the subdomains [I to VII] are shown in the figure below the sequences; the nomenclature follows that of Hardie and Hanks (1995). Also marked are the tyrosine protein kinase specific active-site signature (Tyr-signature [~~~~]), the TK class II

taxa. The evolutionary rates—expressed as k_{aa}-values—vary between different proteins (Zuckerkandl and Pauling, 1965; Kimura, 1983; Li *et al.*, 1987). In a previous study, the galectin protein from the sponge *G. cydonium* (Pfeifer *et al.*, 1993b) was calculated to have an estimated evolutionary rate of 0.97×10^{-9} aa substitutions/site/year (Hirabayashi and Kasai, 1993); a value of 1.24×10^{-9} was calculated for the RTK from *G. cydonium* (Schäcke *et al.*, 1994b) from the same animal.

Dating based on the molecular clock is inaccurate because its rate often varies. If we accept this insecurity, reject the estimated evolutionary rate from sponge genes, and accept the one calculated from the time of protostome-deuterostome divergence—700 MYA (Dayhoff 1978)—we can postulate the time of separation of the sponges from the common metazoan ancestor, as follows. If we take the calculated k_{aa}-value for the human to *D. melanogaste* (0.46) as a reference for the protostome-deuterostome split, then the hexactinellid sponge *A. vastus* branched off 1400 MYA (k_{aa}-value of 0.92), followed by the demosponge *S. domuncula* 1300 (k_{aa}-value of 0.84) and the calcareous sponge *S. raphanus* 1200 MYA for type 1 and 2 (k_{aa}-value of 0.80) and for type 3 1100 MYA (k_{aa}-value of 0.77). Recent fossil data show (Li *et al.*, 1998) that sponges existed in much their present form 580 MYA (Fig. 4B).

Discussion

We have shown that all three classes of the phylum Porifera express molecules related to InsR; and these molecules display, in their extracellular domains, EGF-like sequences (as shown here for *S. raphanus*). This finding implies that animals of the lowest metazoan phylum already contain growth factor receptors that allow them to react to nutrient cues and also to neighboring, individual cells, with a complex intracellular signaling reaction. The InsR-homologs, which are putative transmembrane receptors, presumably allow the transduction of signals through the cellular membrane. Usually signaling by RTKs involves ligand-mediated receptor dimerization (Geer *et al.*, 1994), a process that has not yet been studied in Porifera. InsRs, IGF-1-Rs, and InsR-related receptors or InsR-homologs of higher metazoan taxa do not contain, in their extracellular loops, EGF-like domains, but rather cysteine-rich regions (Geer *et al.*, 1994). This finding underlines again previous findings, that most polypeptides deduced from the cDNA sequences of sponges are assembled by an unusually large variety of modules. For one example, the putative sponge aggregation receptor is composed of scavenger receptor cysteine-rich domains as well as of short consensus repeats (Pancer *et al.*, 1997b; Blumbach *et al.*, 1998) in a structural complexity not known in higher Metazoa.

From the evolutionary point of view, the present contribution makes three points. First, it establishes that molecules similar to the InsR-homologs have evolved prior to the "Cambrian Explosion." Suga *et al.* (1997) suggested that most of the PTK subfamilies, including InsRs, diverged by domain shufflings, together with gene duplications before the diploblast-triploblast split. As a result of recent findings that the Porifera already existed before this event (Li *et al.*, 1998), we can assume that this class of key molecules, involved in the complex network of intracellular signaling, could have been one major driving force that allowed the

signature [specific for InsRs and related sequences] (←class II→ [InsR]) as well as the TK phosphorylation site (P). The positions of the primers are indicated ([+ + + +]) above the sequences. Identical aa residues in all 15 sequences are shown in white-on-black, and residues conserved in at least eight sequences are shaded.

Vertebrates
IG1R_HUMAN = Human insulin-like growth factor 1 receptor precursor (XO4434)
INSR_HUMAN = Human InsR precursor (PO6213)
INSR_MOUSE = InsR precursor house mouse (*Mus musculus;* P15208),
IGF_RAT = IGF-1-RI receptor precursor rat (*Rattus norvegicus;* A33837)
INSR_RAT = InsR precursor from rat (*R. norvegicus;* P15127)
Cephalochordate
ILPR_BRALA = Insulin-like peptide receptor precursor amphioxus (*Branchiostoma lanceolatum;* O02466)
Invertebrates
INSR_AEDAE = Insulin-like receptor precursor mosquito (*Aedes aegypti;* Q93105)
INR_DROME = InsR homolog fruit fly (*Drosophila melanogaster;* U28136)
INSR_APLA = InsR the mollusc (*Aplysia californica;* 1587845)
Sponges
INR_SD = Insulin-like receptor demosponge *Suberites domuncula*
INR_SR1 = Insulin-like receptor calcareous sponge *Sycon raphanus* type 1
INR_SR2 = Insulin-like receptor calcareous sponge *S. raphanus* type 2
INR_SR3 = Insulin-like receptor calcareous sponge *S. raphanus* type 3
INR_AV = Insulin-like receptor hexactinellid sponge *Aphrocallistes vastus*
RTK_GC = Receptor tyrosine kinase demosponge *Geodia cydonium* (X77528)

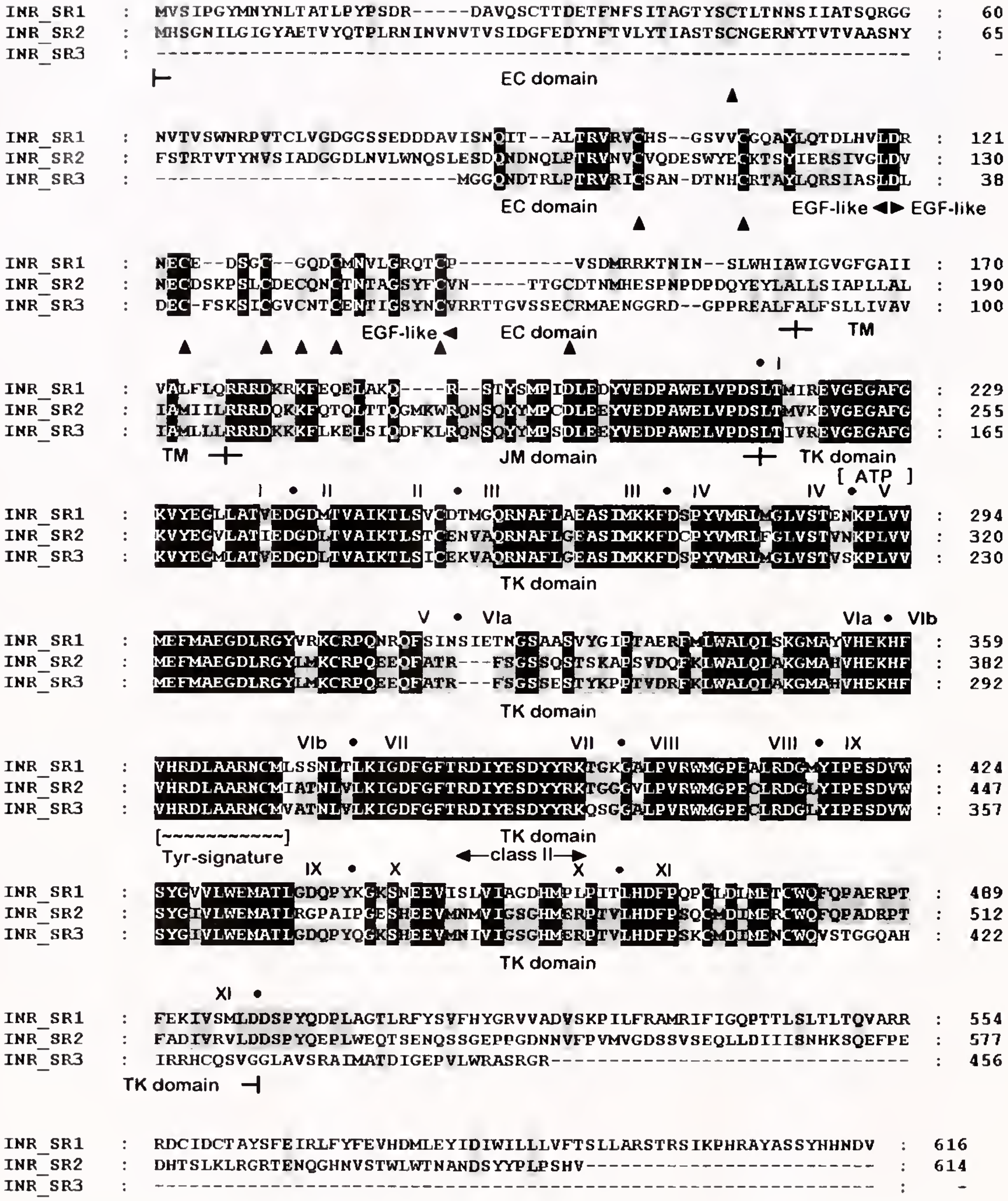
INR_SR1 : MVSIPGYMNYNLTATLPYPSDR-----DAVQSCTTDETFNFSITAGTYSCTLTNNSIIATSQRGG : 60
INR_SR2 : MHSGNILGIGYAETVYQTPLRNINVNVTVSIDGFEDYNFTVLYTIASTSCNGERNYTVTVAASNY : 65
INR_SR3 : : -
EC domain
INR_SR1 : NVTVSWNRPVTCLVGDGGSSEDDDAVISNQIT--ALTRVRVCHS--GSVVCGQAYLQTDLHVLDR : 121
INR_SR2 : FSTRTVTYNVSIADGGDLNVLWNQSLESDQNDNQLPTRVNVCVQDESWYECKTSYIERSIVGLDV : 130
INR_SR3 : MGGQNDTRLPTRVRICSAN-DTNHCRTAYLQRSIASLDL : 38
EC domain
EGF-like ◄► EGF-like
INR_SR1 : NECE--DSGC--GQDCMNVLGRQTCP----------VSDMRRKTNIN--SLWHIAWIGVGFGAII : 170
INR_SR2 : NECDSKPSLCDECQNCTNTAGSYFCVN-----TTGCDTNMHESPNPDPDQYEYLALLSIAPLLAL : 190
INR_SR3 : DEC-FSKSICGVCNTCENTIGSYNCVRRTTGVSSECRMAENGGRD--GPPREALFALFSLLIVAV : 100
EGF-like◄
EC domain
TM
• I
INR_SR1 : VALFLQRRRDKRKKFEQELAKQ----R--STYSMPIDLEDYVEDPAWELVPDSLTMIREVGEGAFG : 229
INR_SR2 : IAMIILRRRDQKKFQTQLTTQGMKWRQNSQYYMPCDLEEYVEDPAWELVPDSLTMVKEVGEGAFG : 255
INR_SR3 : IAMLLLRRRDKKKFLKELSIDDFKLRQNSQYYMPSDLEEYVEDPAWELVPDSLTIVREVGEGAFG : 165
TM
JM domain
TK domain
[ATP]
I • II II • III III • IV IV • V
INR_SR1 : KVYEGLLATVEDGDMTVAIKTLSVCDTMGQRNAFLAEASIMKKFDSPYVMRLMGLVSTENKPLVV : 294
INR_SR2 : KVYEGVLATIEDGDLTVAIKTLSTCENVAQRNAFLGEASIMKKFDCPYVMRLFGLVSTVNKPLVV : 320
INR_SR3 : KVYEGMLATVEDGDLTVAIKTLSICEKVAQRNAFLGEASIMKKFDSPYVMRLMGLVSTVSKPLVV : 230
TK domain
V • VIa VIa • VIb
INR_SR1 : MEFMAEGDLRGYVRKCRPQNRQFSINSIETNGSAASVYGIPTAERFMLWALQISKGMAYVHEKHF : 359
INR_SR2 : MEFMAEGDLRGYLMKCRPQEEQFATR---FSGSSQSTSKAPSVDQFKLWALQLAKGMAHVHEKHF : 382
INR_SR3 : MEFMAEGDLRGYLMKCRPQEEQFATR---FSGSSESTYKPPTVDRFKLWALQLAKGMAHVHEKHF : 292
TK domain
VIb • VII VII • VIII VIII • IX
INR_SR1 : VHRDLAARNCMLSSNLTLKIGDFGFTRDIYESDYYRKTGKGALPVRWMGPEALRDGMYIPESDVW : 424
INR_SR2 : VHRDLAARNCMIATNLVLKIGDFGFTRDIYESDYYRKTGGGVLPVRWMGPECLRDGLYIPESDVW : 447
INR_SR3 : VHRDLAARNCMVATNLVLKIGDFGFTRDIYESDYYRKQSGGALPVRWMGPECLRDGLYIPESDVW : 357
[~~~~~~~~~~~]
Tyr-signature
TK domain
←class II→
IX • X X • XI
INR_SR1 : SYGVVLWEMATLGDQPYKGKSNEEVISLVIAGDHMPLPITLHDFPQPCLDIMEMCWQFQPAERPT : 489
INR_SR2 : SYGIVLWEMATLRGPAIPGESHEEVMNMVIGSGHMERPTVLHDFPSQCMDIMERCWQFQPADRPT : 512
INR_SR3 : SYGIVLWEMATLGDQPYQGKSHEEVMNIVIGSGHMERPTVLHDFPSKCMDIMENCWQVSTGGQAH : 422
TK domain
XI •
INR_SR1 : FEKIVSMLDDSPYQDPLAGTLRFYSVFHYGRVVADVSKPILFRAMRIFIGQPTTLSLTLTQVARR : 554
INR_SR2 : FADIVRVLDDSPYQEPLWEQTSENQSSGEPPGDNNVFPVMVGDSSVSEQLLDIIISNHKSQEFPE : 577
INR_SR3 : IRRHCQSVGGLAVSRAIMATDIGEPVLWRASRGR : 456
TK domain ⊣
INR_SR1 : RDCIDCTAYSFEIRLFYFEVHDMLEYIDIWILLLVFTSLLARSTRSIKPHRAYASSYHHNDV : 616
INR_SR2 : DHTSLKLRGRTENQGHNVSTWLWTNANDSYYPLPSHV : 614
INR_SR3 : : -

Figure 2. Alignment of the deduced aa sequences of the InsR-like sequences from *Sycon raphanus* type 1 (INR_SR1), type 2 (INR_SR2), and type 3 (INR_SR3). The four segments of the sequences are the extracellular domains (EC domain); the transmembrane segments (TM); and the two intracellular domains, the juxtamembrane domain (JM domain) and the catalytic domain (TK domain). The TK domain is subdivided into the 12 subdomains (above the sequence) with the characteristic TK-specific active-site signature (Tyr-signature [~~~~]) and RTK class II signature (←class II→) (below the sequence); in addition, the putative ATP-binding-site (ATP) is marked. In the extracellular domain, the conserved Cys residues (arrowhead) of the two EGF-like domains (EGF-like) are indicated. Identical amino acid residues are shown in white-on-black type, and residues conserved in at least two sequences are shaded.

other metazoan phyla to arise. Second, the phylogenetic analyses confirm that, based on the autapomorphic character for Metazoa, the RTKs, sponges as a taxon are monophyletic; the Hexactinellida have been calculated to be the oldest class, followed by the Demospongia and finally by the Calcarea. Third, EGF-like domains are already present in sponges, where they were inserted into potential cell surface receptors and also into matrix molecules.

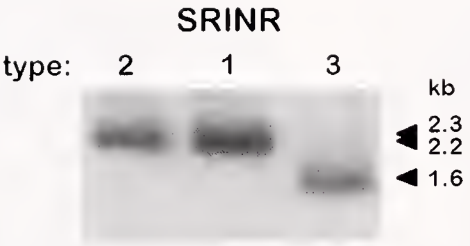

Figure 3. Northern blot analyses to determine the sizes of the transcripts of the mRNA encoding the *Sycon raphanus* InsR-like molecules (*SRINR*) type 1 (*SRINR1*), type 2 (*SRINR2*), and type 3 (*SRINR3*). RNA was prepared from sponge tissue and 1 μg each was subjected to analysis. Molecular masses of marker RNAs, which were run in parallel, are given on the right (in kilobytes).

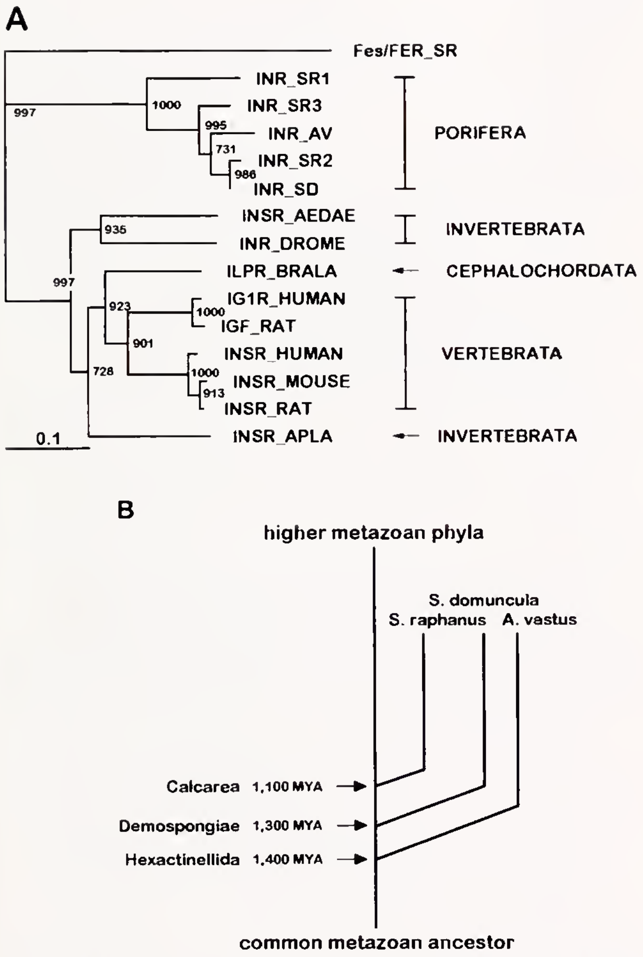

Figure 4. (A) Rooted phylogenetic tree of the catalytic domains of the sequences listed in Figure 1. The numbers at the nodes refer to the levels of confidence as determined by bootstrap analysis. The scale bar indicates an evolutionary distance of 0.1 amino acid substitution per position in the sequence. The catalytic domain of the Fes/FER nonreceptor TK domain from *Sycon raphanus* (Fes/FER_SR, Y17051) was used as the outgroup sequence. (B) Proposed branching order of the three classes of the phylum Porifera (Hexactinellida, Demospongiae, and Calcarea) from a common metazoan ancestor. The dates of the approximate times of divergence are indicated.

Acknowledgments

This work was supported by grants from the Deutsche Forschungsgemeinschaft [Mü 348/12-1] and from the International Human Frontier Science Program [W. E. G. Müller; RG-333/96-M].

Literature Cited

Blumbach, B., Z. Pancer, B. Diehl-Seifert, R. Steffen, J. Münkner, I. Müller, and W. E. G. Müller. 1998. The putative sponge aggregation receptor: isolation and characterization of a molecule composed of scavenger receptor cysteine-rich domains and short consensus repeats. *J. Cell. Sci.* **111:** 2635–2644.

Bork, P., A. K. Downing, B. Kieffer, and I. D. Campbell. 1996. Structure and distribution of modules in extracellular proteins. *Q. Rev. Biophys.* **29:** 119–167.

Campbell, I. D., and P. Bork. 1993. Epidermal growth factor-like molecules. *Curr. Opin. Struct. Biol.* **3:** 385–392.

Cavalier-Smith, T., M. T. E. P. Allsopp, E. E. Chao, N. Boury-Esnault, and J. Vacelet. 1996. Sponge phylogeny, animal monophyly, and the origin of the nervous system: 18S rRNA evidence. *Can. J. Zool.* **74:** 2031–2045.

Cetkovic, H., I. M. Müller, W. E. G. Müller, and V. Gamulin. 1998. Characterization and phylogenetic analysis of a cDNA encoding the Fes/FER related, non-receptor protein-tyrosine kinase in the marine sponge *Sycon raphanus*. *Gene* **216:** 77–84.

Coutinho, C. C., J. Seack, G. Van de Vyver, R. Borojevic, and W. E. G. Müller. 1998. Origin of metazoan bodyplan: characterization and functional testing of the promotor of the homeobox gene *EmH-3* from the freshwater sponge *Ephydatia muelleri* in mouse 3T3 cells. *Biol. Chem. Hoppe-Seyler* **379:** 1243–1251.

Dayhoff, M. O. 1978. Survey of new data and computer methods of analysis. Pp. 1–8 in *Atlas of Protein Sequence and Structure*. Vol. 5, suppl. 3, M. Dayhoff, ed. National Biomedical Research Foundation, Washington, DC.

Dayhoff, M. O., R. M. Schwartz, and B. C. Orcutt. 1978. A model of evolutionary change in protein. Pp. 345–352 in *Atlas of Protein Sequence and Structure*. Vol. 5, suppl. 3, M. Dayhoff, ed. National Biomedical Research Foundation, Washington, DC.

Felsenstein, J. 1993. PHYLIP (Phylogeny Inference Package), ver. 3.5. University of Washington, Seattle.

Fernandez, R., D. Tabarini, N. Azpiazu, M. Frasch, and J. Schlessinger. 1995. The *Drosophila* insulin receptor homologue: a gene essential for embryonic development encodes two receptor isoforms with different signaling potential. *EMBO J.* **14:** 101–112.

Geer, P. v. d., T. Hunter, and R. A. Lindberg. 1994. Receptor protein-tryosine kinases and their signal transduction pathways. *Annu. Rev. Cell Biol.* **10:** 251–337.

Hanks, S. K., and T. Hunter. 1995. The eukaryotic protein kinase superfamily: kinase (catalytic) domain structure and classification. *FASEB J.* **9:** 579–596.

Hanks, S. K., M. A. Quin, and T. Hunter. 1988. The protein kinase family: conserved features and deduced phylogeny of the catalytic domains. *Science* **241:** 42–52.

Hardie, G., and S. Hanks. 1995. *The Protein Kinase FactsBook: Protein-tyrosine Kinases*. Academic Press, London.

Hirabayashi, J., and K. Kasai. 1993. The family of metazoan metal-independent β-galactoside-binding lectins: structure, function and molecular evolution. *Glycobiology* **3:** 297–304.

Kimura, M. 1983. *The Neutral Theory of Molecular Evolution.* Cambridge University Press, Cambridge.

Koziol, C., R. Bornjevic, R. Steffen, and W. E. G. Müller. 1998. Sponges (Porifera) model systems to study the shift from immortal- to senescent-somatic cells: the telomerase activity in somatic cells. *Mech. Ageing Dev.* **100:** 107–120.

Kruse, M., I. M. Müller, and W. E. G. Müller. 1997. Early evolution of metazoan serine/threonine and tyrosine kinases: identification of selected kinases in marine sponges. *Mol. Biol. Evol.* **14:** 1326–1334.

Li, W. H., M. Tanimura, and P. M. Sharp. 1987. An evaluation of the molecular clock hypothesis using mammalian DNA sequences. *J. Mol. Evol.* **25:** 330–342.

Li, C. W., J. Y. Chen, and T. E. Hua. 1998. Precambrian sponges with cellular structures. *Science* **279:** 879–882.

Müller, W. E. G. 1995. Molecular phylogeny of Metazoa (animals): monophyletic origin. *Naturwissenschaften* **82:** 321–329.

Müller, W. E. G. 1997. Origin of metazoan adhesion molecules and adhesion receptors as deduced from their cDNA analyses from the marine sponge *Geodia cydonium. Cell Tissue Res.* **289:** 383–395.

Müller, W. E. G. 1998. Origin of Metazoa: sponges as living fossils. *Naturwissenschaften* **85:** 11–25.

Müller, W. E. G., and I. M. Müller. 1999. Primordial endocrinology in the lowest invertebrates: The Porifera. in *Reproductive Biology of Invertebrates,* A. Dorn, ed. J. Wiley & Sons, Chichester. In press.

Müller, W. E. G., and H. Schäcke. 1996. Characterization of the receptor protein-tyrosine kinase gene from the marine sponge *Geodia cydonium. Prog. Mol. Subcell. Biol.* **17:** 183–208.

Müller, W. E. G., I. M. Müller, and V. Gamulin. 1994. On the monophyletic evolution of the Metazoa. *Braz. J. Med. Biol. Res.* **27:** 2083–2096.

Nicholas, K. B., and H. B. Nicholas, Jr. 1997. *GeneDoc: a Tool for Editing and Annotating Multiple Sequence Alignments.* Distributed by the author. Version 1.1.004. www.cris.co./~ketchupTgenedoc.shtml.

Ottilie, S., F. Raulf, A. Barnekow, G. Hannig, and M. Schartl. 1992. Multiple *src*-related genes, *srk1-4,* in the fresh water sponge *Spongilla lacustris. Oncogene* **7:** 1625–1630.

Pan, T. C., T. Sasaki, R. Z. Zhang, R. Fassler, R. Timpl, and M. L. Chu. 1993. Structure and expression of fibulin-2, a novel extracellular matrix protein with multiple EGF-like repeats and consensus motifs for calcium binding. *J. Cell Biol.* **123:** 1269–1277.

Pancer, Z., M. Kruse, I. Müller, and W. E. G. Müller. 1997a. On the origin of adhesion receptors of metazoa: cloning of the integrin α subunit cDNA from the sponge *Geodia cydonium. Mol. Biol. Evol.* **14:** 391–398.

Pancer, Z., J. Münkner, I. Müller, and W. E. G. Müller. 1997b. A novel member of an ancient superfamily: sponge (*Geodia cydonium,* Porifera) putative protein that features scavenger receptor cysteine-rich repeats. *Gene* **193:** 211–218.

PC/GENE. Data Banks CD-ROM. 1995. [EMBL, Swiss Prot]; Release 14.0. IntelliGenetics, Inc. Mountain View, CA.

Perovic, S., I. Prokic, A. Krasko, I. M. Müller, and W. E. G. Müller. 1999. Origin of neuronal receptors in Metazoa: cloning of a metabotropic glutamate-like receptor from the marine sponge *Geodia cydonium. Cell Tissue Res.* **296:** 395–404.

Pfeifer, K., M. Haasemann, V. Gamulin, H. Bretting, F. Fahrenholz, and W. E. G. Müller. 1993a. S-type lectins occur also in invertebrates: high conservation of the carbohydrate recognition domain in the lectin genes from the marine sponge *Geodia cydonium. Glycobiology* **3:** 179–184.

Pfeifer, K., W. Frank, H. C. Schröder, V. Gamulin, B. Rinkevich, R. Batel, I. M. Müller, and W. E. G. Müller. 1993b. Cloning of the polyubiquitin cDNA from the marine sponge *Geodia cydonium* and its preferential expression during reaggregation of cells. *J. Cell Sci.* **106:** 545–554.

Richelle-Maurer, E., G. Van de Vyver, S. Visser, and C. C. Coutinho. 1998. Homeobox-containing genes in freshwater sponges: characterization, expression, and phylogeny. *Prog. Mol. Subcell. Biol.* **19:** 157–175.

Rodrigo, A. G., P. R. Bergquist, P. L. Bergquist, and R. A. Reeves. 1994. Are sponges animals? An investigation into the vagaries of phylogenetic interference. Pp. 47–54 in *Sponges in Time and Space,* R. W. M. v Soest, T. M. G. v. Kempen, and J. C. Braekman, eds. Balkema Press, Rotterdam.

Saitou, N., and M. Nei. 1987. The neighbour-joining method: a new method for reconstructing phylogenetic trees. *Mol. Biol. Evol.* **4:** 406–425.

Scavo, L. M., A. R. Shuldiner, J. Serrano, R. Dashner, J. Roth, and F. de Pablo. 1991. Genes encoding receptors for insulin and insulin growth factor I are expressed in *Xenopus* oocytes and embryos. *Proc. Natl. Acad. Sci. USA* **88:** 6214–6218.

Schäcke, H., H. C. Schröder, V. Gamulin, B. Rinkevich, I. M. Müller, and W. E. G. Müller. 1994a. Molecular cloning of a receptor tyrosine kinase from the marine sponge *Geodia cydonium:* a new member of the receptor tyrosine kinase class II family in invertebrates. *Mol. Membr. Biol.* **11:** 101–107.

Schäcke, H., I. M. Müller, and W. E. G. Müller. 1994b. Tyrosine kinase from the marine sponge *Geodia cydonium:* the oldest member belonging to the receptor tyrosine kinase class II family. Pp. 201–211 in *Use of Aquatic Invertebrates as Tools for Monitoring of Environmental Hazards,* W. E. G. Müller, ed. Gustav Fischer Verlag, Stuttgart.

Seimiya, M., H. Ishiguro, K. Miura, Y. Watanabe, and Y. Kurosawa. 1994. Homeobox-containing genes in the most primitive Metazoa, the sponge. *Eur. J. Biochem.* **221:** 219–225.

Shier, P., and V. M. Watt. 1989. Primary structure of a putative receptor for a ligand of the insulin family. *J. Biol. Chem.* **264:** 14605–14608.

Suga, H., K. Kuma, N. Iwabe, N. Nikoh, K. Ono, M. Koyanagi, D. Hoshiyama, and T. Miyata. 1997. Intermittent divergence of the protein kinase family during animal evolution. *FEBS Lett.* **412:** 540–546.

Thompson, J. D., D. G. Higgins, and T. J. Gibson. 1994. CLUSTAL W: improving the sensitivity of progressive multiple sequence alignment through sequence weighting, position-specific gap penalties and weight matrix choice. *Nucleic Acids Res.* **22:** 4673–4680.

Ullrich, A., J. R. Bell, E. Y. Chen, R. Herrera, L. M. Petruzzelli, T. J. Dull, A. Gray, L. Coussens, Y. C. Liao, M. Tsubokawa, A. Mason, P. H. Seeburg, C. Grunfeld, O. M. Rosen, and J. Ramachandran. 1985. Human insulin receptor and its relationship to the tyrosine kinase family of oncogenes. *Nature* **313:** 756–761.

Ullrich, A., A. Gray, A. W. Tam, T. Yang-Feng, M. Tsubokawa, C. Collins, W. Henzel, T. Le Bon, S. Kathuria, E. Chen, S. Jacobs, U. Francke, J. Ramachandran, and Y. Fujita-Yamaguchi. 1986. Insulin-like growth factor I receptor primary structure: comparison with insulin receptor suggests structural determinants that define functional specificity. *EMBO J.* **5:** 2503–2512.

Valentine, J. W. 1994. The Cambrian explosion. Pp. 401–412 in *Early Life on Earth,* S. Bengtson, ed. Columbia University Press, New York.

Valentine, J. W., D. H. Erwin, and D. Jablonski. 1996. Developmental evolution of metazoan bodyplan: the fossil evidence. *Dev. Biol.* **173:** 373–381.

Zuckerkandl E., and L. Pauling. 1965. Evolutionary divergence and convergence in proteins. Pp. 97–166 in *Evolving Genes and Proteins.* V. Bryson and H. J. Vogel, eds. Academic Press, New York.

Reference: *Biol. Bull.* **197:** 207–218. (October 1999)

Functional Morphology of Prey Ingestion by *Placetron wosnessenskii* Schalfeew Zoeae (Crustacea: Anomura: Lithodidae)

JENNIFER A. CRAIN

Shannon Point Marine Center, 1900 Shannon Point Road, Anacortes, Washington 98221

Abstract. The relationship between the morphology and functions of the feeding appendages of first-stage zoeae of the lithodid crab *Placetron wosnessenskii* Schalfeew during ingestion is explored in this study. The preoral chambers of these zoeae are bordered on all sides, with the labrum and mandibles forming the anterior borders, the paragnaths and sternal projection together creating the posterior boundaries, and the maxillules forming the sides. The maxillules are the sole pair of appendages responsible for prey manipulation immediately preceding ingestion. Maxillules are capable of remarkable plasticity of movement, enabling them to grasp, control, and redirect violently struggling prey (*Artemia* sp. metanauplii). The asymmetrical mandibles tear and grind the prey, working against each other with rotating motions.

Two separate ratchet-like coordinations of the appendages were seen, each of which enabled the zoea to maintain a firm grasp on the prey while renewing points of leverage for ingestion. The mandibles hold prey in position while the maxillules regrab it to push it farther into the mouth. Similarly, the labrum holds the prey while the mandibles prepare for a new grinding rotation.

Capture and ingestion of an algal cell by a rapid outward flinging and inward clasping of the mouthparts was seen in one videotaped sequence. Gut fluorescence after introduction of various algal species reveals an ability to ingest a range of particle sizes. This plasticity of feeding behaviors allows the zoeae to ingest a range of food items, and thus meet their nutritional needs.

Introduction

Behavioral observations, especially in conjunction with detailed morphological descriptions, are valuable in relating form and function of the mouthparts of adult crustaceans. Among decapod crustaceans, feeding behavior has been studied by many authors (*e.g.*, Orton, 1927; Roberts, 1968; Greenwood, 1972; Kunze and Anderson, 1979; Manjulatha and Babu, 1991). In adult crabs, the tasks of manipulating, tearing, shredding, and retaining food are divided among their six pairs of feeding appendages. These small, rapidly moving appendages (the mandibles, maxillules, maxillae, and first, second, and third maxillipeds) are obliquely layered, forming the confines and manipulatory structures of the preoral chamber. Gross accounts of feeding behavior in crustaceans commonly include descriptions of the functions of the outer mouthparts, emphasizing the maxillipeds, in manipulation of food items. Detailed accounts of the movements of the inner mouthparts during ingestion are less common, because these appendages are usually blocked from view either by the food being ingested or by adjacent appendages. Schembri (1982) accounted for the motions of the inner mouthparts in his description of feeding in the brachyuran crab *Ebalia tuberosa* (Pennant), and Alexander and Hindley (1985) described the functional morphology of these appendages during food ingestion by the banana prawn *Penaeus merguiensis* De Man.

To date, studies of the functional morphology of decapod zoeal mouthparts have focused on descriptions of morphological features, with few or no behavioral observations available. The development of the feeding apparatus in decapods, with special emphasis on the mandibles and gastric mill, has been extensively reviewed by Factor (1989). Lavalli and Factor (1992) used scanning electron microscopy to detail the functional morphology of mouthparts of

Received 16 July 1998; accepted 29 July 1999.

Current address: College of Oceanic and Atmospheric Sciences, Oregon State University, Corvallis, OR 97331-5503. E-mail: jcrain@oce.orst.edu

juvenile and larval lobsters. Decapod zoeae have fewer pairs of functional mouthparts than the adults. The zoeal maxillipeds are used for locomotion, and are not used for feeding until the megalopal stage. In these earlier stages, all the actions involved with manipulation and ingestion of food are therefore divided among the maxillules, mandibles, labrum, and, possibly, maxillae. Although detailed analyses of the motions and functions of the inner mouthparts of decapod zoeae during ingestion have not been made, it is reasonable to expect a situation similar to that found in copepods (Paffenhofer and Lewis, 1989), with the functions of zoeal mouthparts being quite different from those observed in adult crabs.

The species used in this study is *Placetron wosnessenskii* Schalfeew, a somewhat dorsoventrally flattened, long-legged lithodid crab found at depths from 0 to 110 m in rocky areas from the Aleutian Islands in Alaska to Puget Sound, Washington (Hart, 1982). This species exhibits a reproductive pattern typical of lithodids, with mating in the spring, brooding for nearly a year, and hatching between March and early May (Nyblade, 1987). There is a short prezoeal stage (several minutes in duration; pers. obs.), followed by four planktonic zoeal stages and one megalopal stage (pers. obs.), during which settlement as a megalopa occurs. A morphological description of the first zoeal stage was published by Haynes (1984), and a description of larval and megalopal development and morphology is currently in preparation (Crain and McLaughlin, unpubl. data). *P. wosnessenskii* was chosen for this study because of the large size of the first-stage zoeae (carapace length is about 3 mm) and their willingness to feed under the conditions necessary for videotape recording.

The present paper relates form to function for the appendages involved in the ingestion of large prey items (*Artemia* metanauplii) and unicellular algae by first-stage *P. wosnessenskii* zoeae. Feeding appendages and accompanying setal types of newly hatched zoeae are described and related to their functions during prey ingestion. Descriptions of appendage functions are based on direct observations and on analysis of videotaped feeding activity of untethered first-feeding zoeae.

Materials and Methods

Morphological descriptions of the mouthparts and behavioral observations were based on zoeae from two separate broods. The first brood was from an ovigerous female *Placetron wosnessenskii* collected on 5 March 1992 and the second from an ovigerous female collected in late October of 1993. Both ovigerous females were collected from depths of about 13 to 15 m at rocky sites near Anacortes, Washington. Each ovigerous female was transported in a bucket of seawater to Shannon Point Marine Center, where it was transferred to a sea table with continuously flowing natural seawater and held throughout the hatching period. Upon hatching, normal larvae underwent a brief prezoeal stage, after which they shed the prezoeal cuticles and swam actively in the sea table as first-stage zoeae. Only actively swimming, healthy zoeae were used in the study. A careful comparison showed no morphological differences among the zoeae or between broods.

Specimens were preserved in 70% ethanol. Dissection and mounting of preserved specimens in polyvinyl alcohol lactophenol followed staining with 1% chlorozol black (3% in equal parts lactic acid and phenol). Details of appendages and setae were described with the aid of Nomarski differential interference microscopy. Illustrations of morphological features were drawn with camera lucida attachments mounted on dissecting and compound microscopes. Setal descriptions follow the system of Lavalli and Factor (1992) in general terminology and categorization. Terminology used for morphological descriptions follows that of McLaughlin *et al.* (1988).

Appendage movements during ingestion of *Artemia* metanauplii were observed with a dissecting microscope. Because preliminary attempts to tether the zoeae to thin glass rods with cyanoacrylate glue or modeling clay were unsuccessful, newly hatched zoeae (less than 24 h old) were videotaped while they swam freely in a small glass dish containing about 7.5 ml of filtered seawater. During observations of feeding behavior, each zoea was isolated individually in the observation chamber and allowed to adjust to the dish for one to several minutes prior to addition of *Artemia* metanauplii or, in several cases, algal cells. Feeding sequences were videotaped using a black-and-white CCD (charge-coupled device) video camera mounted on a dissecting microscope and connected to a VHS video recorder equipped with an onscreen stopwatch. Frame duration of 1/1000 s enhanced the clarity of the images.

Analysis of videotaped feeding sequences was based on review of the tapes both on normal speed (30 frames per second) and in slow motion using a jog shuttle advance mechanism or stepping through individual frames. Durations of sequences were determined either by use of the onscreen stopwatch or by an actual count of the number of frames used for a given sequence.

Selected frames from ingestion sequences were digitized with Bioscan Optimas image analysis software and illustrated from projected negatives. Illustrations of the ratcheting mechanisms observed from the videotapes were pieced together by copying morphological illustrations into the positions in which the appendages were observed for the relevant sequences.

A preliminary experiment to test the ability of first-stage *P. wosnessenskii* zoeae to capture algal cells was performed using five species of algae. Eight zoeae were isolated in each of six small glass bowls with 75 ml of filtered (2 μm) seawater. Each bowl except the control received one of the

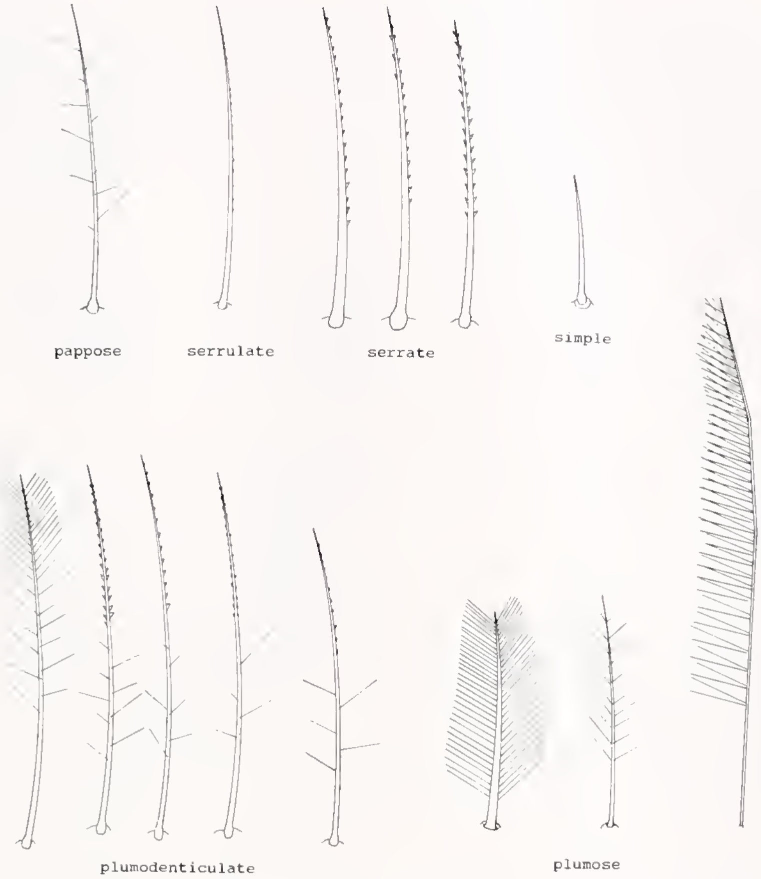

Figure 1. Setal types found on the mouthparts of first-stage *Placetron wosnessenskii* zoeae. Illustrations not to scale.

following algal species: *Cryptomonas* sp., *Prorocentrum micans*, *Gyrodinium dorsum*, *Chaetoceros calcitrans*, or *Isochrysis galbana*. In bowls containing algae, the concentration of cells was such that the algal cells were visible under a dissecting microscope. The bowls were placed in a dark incubator at 12° C. Zoeae were removed after 12 h, rinsed with deionized water, placed in groups of four on GF/C glass filters, and frozen at 4° C. After 16 h, the filters and zoeae were removed from the freezer, cut into small pieces, and ground in 90% acetone in a tissue grinder. The resultant slurry was poured into volumetric test tubes and refrigerated for 24 h. The tubes were then centrifigued and the supernatant was tested for fluorescence using a Turner fluorometer calibrated with a 90% acetone blank.

Results

Types of setae

The types of setae found on the maxillules and maxillae of first-stage *P. wosnessenskii* zoeae (Fig. 1) can be grouped into six of Lavalli and Factor's (1992) categories, differentiated by the armature of the setal shaft. All of these setae have ampullae and basal septae that are readily visible by differential interference microscopy. Size and shape of the ampulla, prominence of the basal socket, thickness of the walls of the shaft, and shaft length are all variable characters both among and within these six major setal groupings. They are defined as follows:

Simple setae (Lavalli and Factor's Type I). No setules or other secondary processes present on setal shaft.

Plumose setae (Lavalli and Factor's Type A). Secondary processes long; thin setules arranged in two distinct rows along length of setal shaft; setule density and distances between rows variable.

Pappose setae (Lavalli and Factor's Type B). Secondary processes long; thin setules arranged in no apparent order on setal shaft; setule density highly variable.

Serrate setae (Lavalli and Factor's Type D). Secondary processes relatively short; thick, pointed denticles; denticle density variable, size often decreasing along length of setal shaft.

Serrulate setae (Lavalli and Factor's Type F). Secondary processes minute scales, often visible only as slight indentations of outer walls, arranged along setal shaft in one or more rows, concentrated on the distal half.

Plumodenticulate setae (Lavalli and Factor's Type C). Secondary processes not homogeneous; proximal half of setal shaft usually bearing long setules arranged in no apparent order; setules increasing in thickness to form one or two rows of denticles on distal half of shaft, often decreasing in size toward the tip. Secondary process densities variable on all subtypes.

Morphology and movements of oral region and appendages

Comparisons of the mouthparts of the zoeae used in behavioral analysis with those used for morphological descriptions showed no differences between the two broods. The morphology and movements of preoral chamber structures and of the appendages expected to be involved in ingestion are as follows:

Preoral chamber. The anterior portion of the preoral chamber (Figs. 2, 3) is bordered by the labrum (Fig. 4f), a large, subquadrate lobe with two rows of five or six slender spines medially on the posterior face and a small, dense patch of posteroventrally directed simple setae located between the rows of spines. The observed range of motion of this lobe was limited to a short ventral-to-dorsal movement in which the spines were tilted toward the mouth.

The two ventrally directed lobes of the paragnaths (Figs. 2, 3, 4e) form the posterior lateral borders of the preoral chamber. Each paragnathal lobe is fringed with many fine, anteriorly directed, simple setae along the inner and distal margins. The paragnaths were not seen to move during ingestion, but were difficult to observe because of their position deep in the preoral chamber.

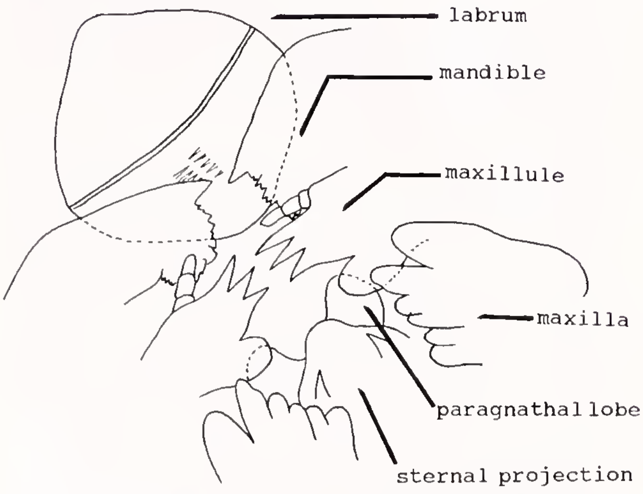

Figure 2. Ventral view of the oral region of a first-stage *Placetron wosnesseuskii* zoea, showing locations and orientations of the mouthparts. Setae have been omitted from illustration in order to clearly illustrate appendage positions. Orientation: anterior is top left, posterior is bottom right.

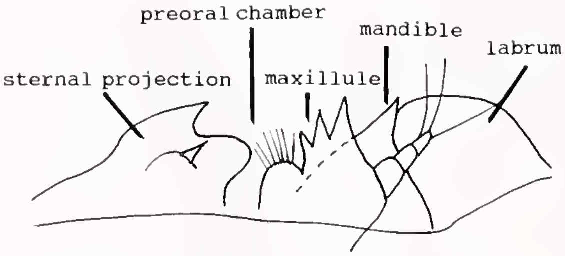

Figure 3. Lateral view of the oral region of first-stage *Placetron wosnesseuskii* zoea, showing locations and orientations of the mouthparts. Orientation: anterior is to the right, posterior to the left; ventral is at the top of the figure, and dorsal at the bottom.

Posterior to the paragnathal lobes is a large, immobile projection of the sternite (Figs. 2, 3), which completes the posterior boundary of the preoral chamber. The sides of the chamber are bordered, anteriorly to posteriorly, by the highly mobile mandibles, maxillules, and maxillae.

Mandibles. The cutting edges of the mandibles are divided into distinct incisor and molar processes and are asymmetrical with respect to the armament of these processes. The incisor process of the left mandible (Fig. 4b) is slightly larger than that of the right (Fig. 4a), consisting of one very large tooth and three or four smaller denticulate teeth. The left molar process is a large, rounded section of the mandible bearing two to four serrate or denticulate ridges culminating in a group of jagged denticles at the extreme (dorsal) edge. The right mandible (Fig. 4a) also bears a large, denticulate incisor process that includes one very large tooth, but in contrast to the left bears approximately 6 to 10 smaller denticulate teeth. The molar region of the right mandible has a complex jagged margin and several serrate ridges. The cutting edges of the mandibles are aligned in a ventrodorsal plane, perpendicular to the sagittal plane of the animal. The incisor processes are positioned farthest ventrally, adjacent to the oral opening.

The mandibles have rolling ventral-dorsal (down-up), mesial-lateral (inside-outside), and anterior-posterior (front-back) components to their movement. Each mandibular motion begins with a lateral-to-mesial movement that brings the cutting edges together and ends with a mesial-to-lateral movement that draws them apart. The ventral-dorsal rolling motions serve to tear and subsequently grind the prey by bringing the two mandibles together in an arcing slice, with contact made first at the extreme (dorsal) ends of the molar regions. Simultaneously, the mandibles make short anterior-posterior motions that grind the ridges of the molar regions against each other. The point of contact between the mandibles is then smoothly shifted from the molars to the incisors over the duration of the arcing movement. Although the actions of the mandibles bring the grinding

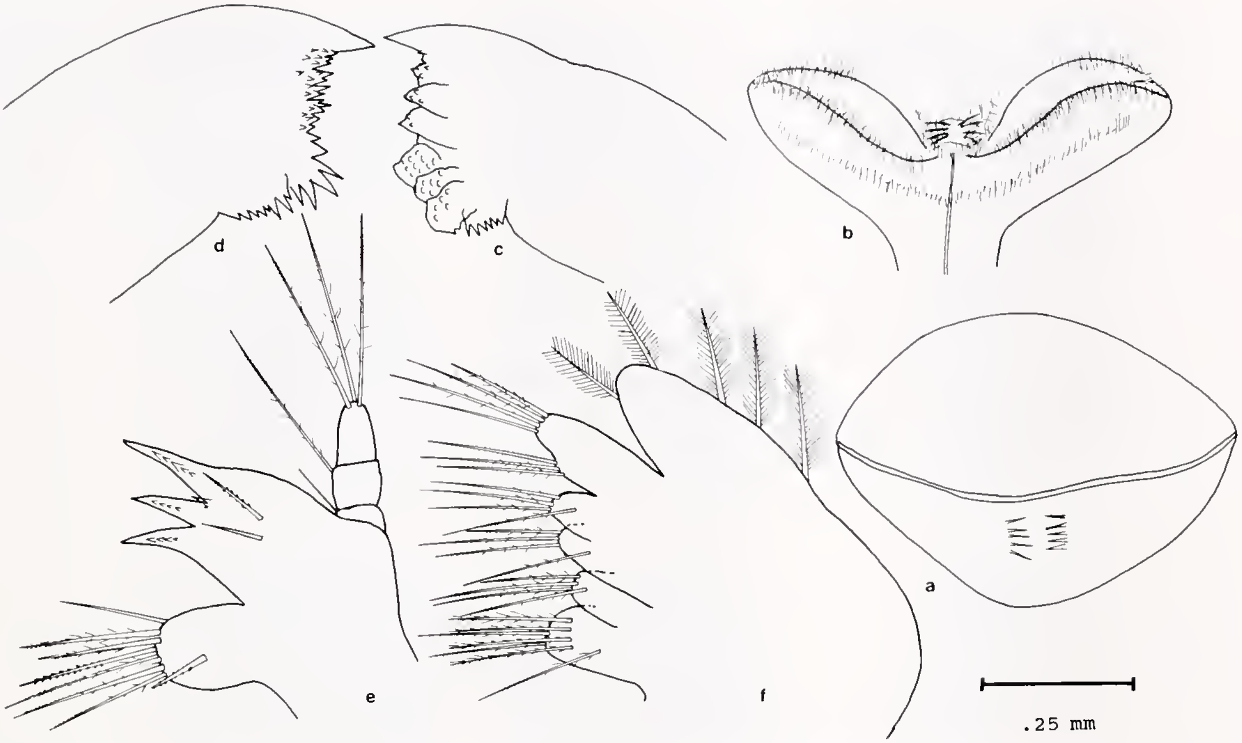

Figure 4. Illustrations of the preoral chamber features and mouthparts of first-stage *Placetron wosnessenskii* zoeae: (a) labrum; (b) paragnaths; (c) right mandible; (d) left mandible; (e) maxillule; (f) maxilla.

molar regions together first, prey entering the oral region initially contact the tearing incisor processes. As the incisors are drawn across each other, the rolling motion of the mandibles results in a mouthward push of torn material from the incisors to the molar regions, to be crushed by the next mandibular roll. In this way, food is broken into sequentially smaller fragments by the mandibles before entering the oral cavity.

Maxillules. Each maxillule (Fig. 4c) has a three-segmented endopodite located distolaterally; a large, toothed, mesially directed basal endite; and a smaller setose coxal endite that is also mesially directed. The setae of the three endopodal segments are (progressing distally): one simple, one pappose, and three plumodenticulate or pappose setae. The basal endite is armed with three large cuspidate teeth, each tooth with two to five denticles, and often with one very small, naked tooth developing between the others. The basal endite also bears two submarginal serrate or serrulate setae. The coxal endite bears six to eight marginal setae that are plumodenticulate, serrate, simple, or a combination of these types and one submarginal serrate seta.

The maxillules position the food prior to ingestion. An overall mesial-lateral motion is most common, with the entire maxillule moving as a lever that uses the basal attachment as the fulcrum, and the tips of the endites describing a large arc. Anterior-posterior motions of the maxillule are also observed, with the base of the appendage again serving as the fulcrum. The endopodite of each maxillule is muscularized and seems to be capable of some independent motion both in the anterior-posterior and mesial-lateral directions.

The radically different morphologies of the endopodite and coxal and basal endites facilitate the plasticity of functions that this appendage is capable of performing. The denticulate teeth of the basal endite are used primarily for grasping and holding a captured metanauplius. The row of denticles on each tooth presumably aids in maintaining a grip on a struggling metanauplius, and although many of the metanauplii captured struggled energetically, very few of them were able to escape from the maxillules. The two submarginal setae on the basal endite may also aid in this grasping and holding. The three-segmented endopodite was seen to act as an outer guide for captured metanauplii, with the distal setae considerably extending the effective reach of the appendage in the anterior direction. The mobility of this endopodite adds a certain amount of fine control to the positioning of large prey. The location of the coxal endite was often difficult to distinguish in the videotapes, but was clearly at the posterior end of the preoral chamber during the final phase of ingestion. This endite was sometimes used to sweep small fragments of loose food back into the preoral chamber during phases 2 and 3 of ingestion. The setae of the coxal endites of the two maxillules were also seen to overlap each other along the midline of the zoea when the maxillules were not in motion, thus forming a stationary border to the preoral chamber when at rest.

Maxillae. Each maxilla (Fig. 4d) of the first zoeal stage consists of a large scaphognathite (exopodite fused with epipodite) on the lateral portion of the appendage, a weakly bilobed endopodite and two bilobed endites on the mesial portion. The scaphognathite bears four to six plumose setae on the outer margin; the proximal lobe is completely fused with the protopod. There are two or occasionally three small groupings (one to five setae per grouping) of setae on the distal portion of the endopodite, in combinations of serrate, plumodenticulate, simple, and pappose setae. The coxal endite is divided into two distinct lobes, with three plumodenticulate or serrate marginal setae and one plumodenticulate or pappose submarginal seta on the distal lobe. The proximal lobe of the coxal endite bears two plumodenticulate marginal setae, a ridge with four or five plumodenticulate setae, and one plumodenticulate submarginal seta. A similar division into two distinct lobes is characteristic of the basal endite, with the distal lobe bearing three plumodenticulate or pappose marginal setae and one plumodenticulate submarginal seta. There are three or four plumodenticulate or pappose marginal setae and one plumodenticulate or pappose submarginal seta on the proximal lobe of the basal endite.

The maxillae beat continuously during ingestion, with the entire appendages moving water over the thoracic area. The scaphognathites, with their fringe of plumose setae, create a large functional "paddle" that increases the amount of current flow over the developing gill buds at the bases of the maxillipeds and adjacent area. This beating pattern is apparently respiratory, as it is in adults, and is undisturbed by the motions of adjacent appendages. Involvement of maxillae in prey ingestion was not observed.

Behavioral observations: ingestion of Artemia *metanauplii*

Not all of the videotaped zoeae were observed to feed. Many individuals failed to capture or attempt to capture metanauplii. Those that successfully captured and ingested *Artemia* metanauplii nearly always exhibited an initial period of several minutes during which no metanauplii were captured. This interval prior to capture and ingestion of the first metanauplius tended to be longer than the pauses between subsequent captures. Initial capture preceded a rapid series of capture and ingestion events, after which the zoea was apparently satiated and ceased feeding. At this point, the appendages even failed to respond to direct contact with the mouthparts by an *Artemia* metanauplius. In two separate sequences, the zoea spent several minutes merely holding, twisting, rotating, and finally rejecting a metanauplius captured during the preceding feeding event.

Zoeae captured and ingested metanauplii both while actively swimming and while stationary. Prey manipulation and ingestion were apparently unaffected by movements of the exopodites and endopodites of the maxillipeds, which were used only for locomotion. Similarly, positioning of the abdomen and telson had no apparent effect on ingestion mechanisms.

Because of complications in the use of untethered larvae, compounded by limitations of both field of view and of field of focus, only one sequence was recorded in which the ingestion of an *Artemia* metanauplius was traceable in its entirety (Fig. 5). Partial sequences in which only portions of the ingestion process were recorded were more numerous. Consequently, ingestion events have been separated into three consecutive phases to analyze appendage motions throughout the ingestion process. Each phase is easily distinguished and possesses a distinct beginning and end.

Phase 1. During the initial phase of *Artemia* ingestion, only the maxillules are in direct contact with the prey item. As noted above, the principal movements of the maxillules involve the rotating of the entire appendage from the base. In this way, they push the prey around or catch it between opposing endites, and the whole maxillule acts as a large paddle. The maxillules coordinate simultaneous and alternating motions as necessary to manipulate prey into position for ingestion. The first motion of ingestion is a rapid outward fling of the paired appendages, followed by an inward squeezing action, bringing the endites of the maxillules into contact with the metanauplius as it enters the preoral chamber. Metanauplii are held between the basal endites of the opposing maxillules, with the endopodites acting as outer guides and presumably aiding in stabilization of the struggling prey. Symmetrical motions of the opposing maxillules control the anterior-posterior positioning of the metanauplius, while asymmetrical motions are involved with lateral repositioning of the metanauplius or with rotating it about its long axis. In two sequences, the metanauplius was turned end over end by the maxillules employing both symmetrical and asymmetrical motions. Metanauplii can be grasped by the maxillules in any position, but are usually manipulated into either a head-first or tail-first position (with the long axis of the metanauplius perpendicular to the long axis of the zoea) prior to ingestion. In some cases, ingestion sequences are initiated with the metanauplius in a sideways position (with the long axis parallel to the long axis of the zoea), but are completed with the metanauplius in a head-first or tail-first position.

Variations of this basic sequence were seen with two or more metanauplii involved. In four of the five multiple ingestion sequences analyzed, a newly captured metanauplius was used to push a partially ingested metanauplius into the mandibles. In two separate sequences, two metanauplii were ingested simultaneously, although sequential ingestions were far more common. In two of the analyzed

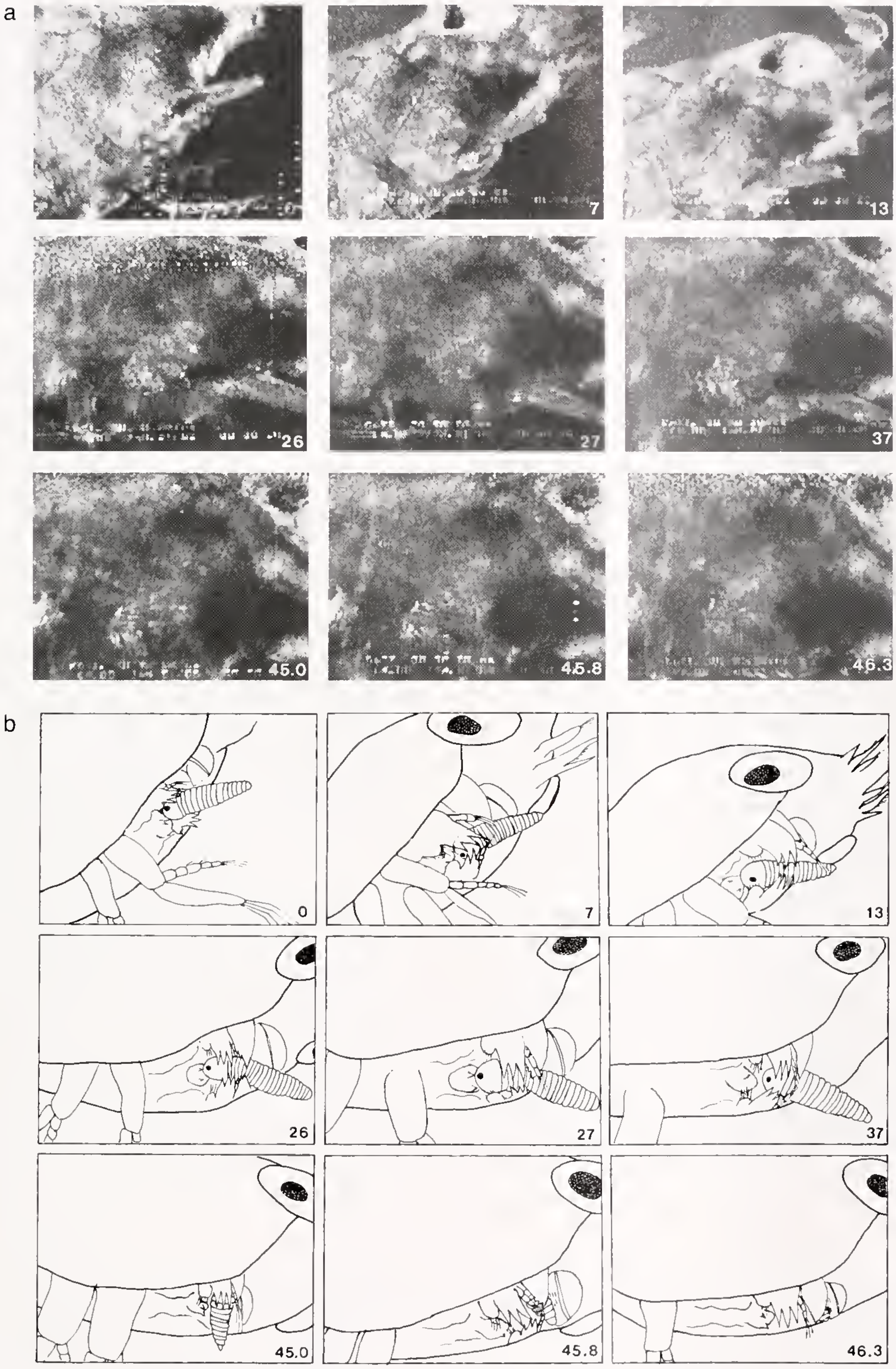
a
0
7
13
26
27
37
45.0
45.8
46.3
b
0
7
13
26
27
37
45.0
45.8
46.3

Figure 5. Selected frames from a sequence of ingestion of an *Artemia* metanauplius by a first-stage *Placetron wosnessenskii* zoea at 0, 7, 13, 26, 27, 37 (phase 1), 45.0 (phase 2), 45.8 and 46.3 (phase 3) seconds elapsed time: (a) photographs from images captured from a videotaped sequence; (b) illustration drawn from photographs in (a) to enhance clarity.

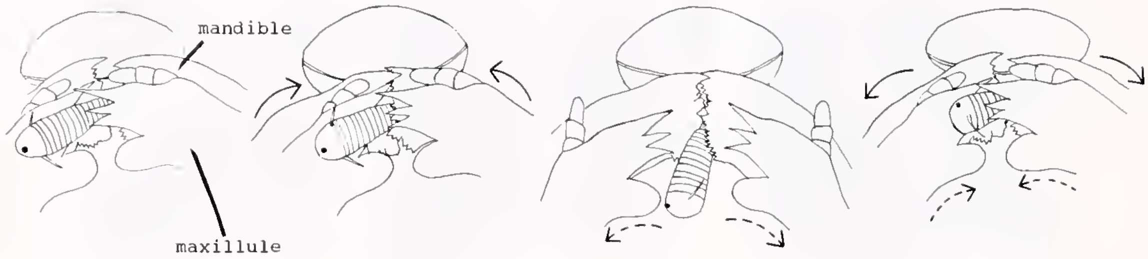

Figure 6. Coordination of maxillule and mandible movements during phase 2 of ingestion of an *Artemia* metanauplius by a first-stage *Placetron wosnessenskii* zoea. Approximate duration: 0.1 to 0.6 s.

sequences, phase 1 of ingestion was shortened to merely the fling and capture steps, which were followed immediately by the maceration associated with phase 2.

Recorded phase 1 duration ranged from 0.2 to 5.9 s in sequences involving only a single metanauplius, and from 6.1 to 233.0 s in sequences involving two or more metanauplii. Mean durations were 3.9 (n = 14; SD = 5.8) and 56.8 (n = 5; SD = 93.2) s respectively.

Phase 2. This phase of ingestion involves the maxillules, mandibles, and labrum. Phase 2 begins with the first contact of the metanauplius with the mandibles and ends with the loss of direct contact with the prey item by the basal endites of the maxillules. The maxillules, after manipulating the metanauplius into position in phase 1, begin pushing the prey toward the mouth, bringing it into contact with the mandibles. In one sequence, phase 2 was initiated by repeated nudging of the metanauplius into and out of range of the mandibles by the maxillules.

The maxillules and labrum press the metanauplius against the mandibles as the latter tear and grind the prey on its way into the mouth. Two separate ratcheting mechanisms were observed, each of which maintains a steady net movement of the metanauplius into the mouth, while enabling the appendages to renew points of contact for leverage. First, the maxillules and mandibles alternate motions, maintaining a firm grip on the metanauplius as it is masticated (Fig. 6). The maxillules press the prey against the mandibles as they shred bits of tissue with their rolling motions. The mandibles then hold the metanauplius as the maxillules regrasp it once every two or three mandibular rotations, or as seen in two sequences, with each mandibular roll. Second, the mandibles and the labrum work in conjunction to prevent food from escaping from the mouth when the mandibles are on the recovery stroke of their motion (Fig. 7). The labrum moves downward, pinning the metanauplius in the preoral chamber with its spiny processes as the mandibles return to their initial (lateral) position in preparation for the next grinding roll, with a 1:1 ratio of alternating movements.

The recorded total durations of phase 2 range from 6.5 to 150 s, with a mean duration of 49 s (n = 11; SD = 45.7).

Phase 3. This phase of ingestion begins when the basal endites of the maxillules are no longer in contact with the prey, and continues until the entire metanauplius has passed through the mandibular region into the oral cavity. The mandibles and labrum continue to work together as in phase 2 until the entire metanauplius has been ingested. Although the maxillules are apparently no longer in direct contact with the prey, they often continue to make the sweeping mesial-lateral motions associated with phase 2, and direct small, easily lost fragments of masticated food back into the preoral chamber. A variation of phase 3 was seen in four sequences, when the maxillules pushed one metanauplius through the final stage of ingestion with a second metanauplius.

The range of durations recorded for this phase was from 4 to 84 s, with a mean duration of 23.2 s (n = 9; SD = 31.6).

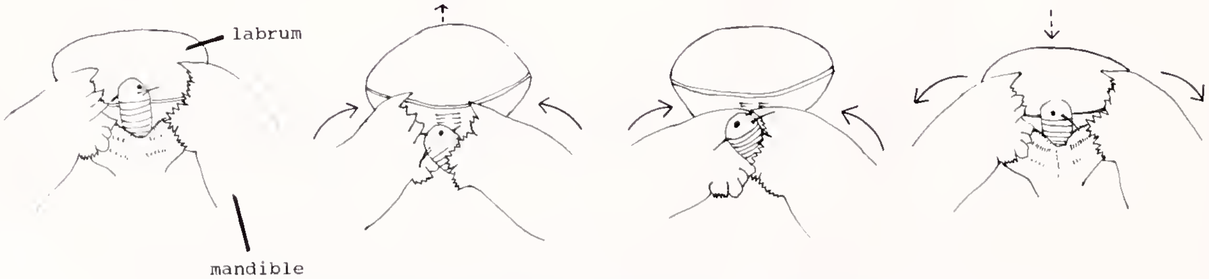

Figure 7. Coordination of mandible and labrum movements during phases 2 and 3 of ingestion of an *Artemia* metanauplius by a first-stage *Placetron wosnessenskii* zoea. Approximate duration: 0.1 to 0.3 s.

Behavioral observations: capture of algal cells

Although several instances of algal capture by zoeae were observed, only one, in which a *Prorocentrum micans* cell was caught and ingested, was recorded on videotape. This capture took place very quickly, with the maxillules and mandibles drawing laterally, then held open momentarily before closing over the algal cell, which had apparently been drawn into the mouth by the suction created in the oral region. In preliminary gut fluorescence experiments, *P. wosnessenskii* ingested four species of unicellular algae: *Cryptomonas* sp. (approximately 12 × 7 μm), *Prorocentrum micans* Ehrenberg (approximately 39 × 30 μm), *Gyrodinium* sp. (approximately 40 × 35 μm), and *Isochrysis galbana* Parke (approximately 4 × 3 μm). These experiments did not contain sufficient numbers of replicates to determine clearance rates, but did indicate that the zoeae were able to ingest a range of particle sizes.

Discussion

Comparison of morphological descriptions

A comparison of the present description of the mouthparts of first-stage *P. wosnessenskii* zoeae with that of Haynes (1984) reveals few differences. Haynes commented on asymmetry between the left and right mandibles and on the jagged ridge of denticles located at the extreme end of the molar process of each, as noted here. The descriptions of the maxillules and maxillae differed only slightly in terminology and degree of detail.

Mechanical functions of setae

Function can sometimes be inferred by the types and placement of setae on an appendage. Detailed descriptions of setal types and locations, using both light and scanning electron microscopy, have been instrumental in revealing the function of the corresponding appendages or body areas (*e.g.*, Roberts, 1968; Farmer, 1974; Factor, 1978; Ajmal-Khan and Natarajan, 1981; Ohtsuka and Onbe, 1991; Lavalli and Factor, 1992). In some cases specific setal types have been linked to specific functions, especially in feeding and grooming (*e.g.*, Barker and Gibson, 1977; Kunze and Anderson, 1979; Schembri, 1982; Fryer, 1983; Pohle, 1989).

Crustacean setal types have been described in detail by many authors, as reviewed in Jacques (1989). Lavalli and Factor (1992), in their work on the lobster *Homarus americanus*, used light microscopy to produce detailed descriptions of the range and locations of setal types found on the mouthparts of larval and juvenile lobsters. They grouped the setae into 13 categories based on external features, especially the form and position of setules. Each category included variations in form, and several of the setal types found on the mouthparts of first-stage *P. wosnessenskii* zoeae fit into Lavalli and Factor's (1992) groupings.

The setae found on the tips and edges of the feeding appendages of *P. wosnessenskii* were often more setulose than those on the inner surfaces, a condition that is also reported for crayfish by Thomas (1970), lobsters by Factor (1978) and Lavalli and Factor (1992), and leucosids by Schembri (1982). Farmer (1974) reported smoother setae on the inner surfaces of the mouthparts of *Nephrops norvegicus* (Linnaeus) than on the fringes, attributing this pattern of distribution to the different functions of the two locations. Farmer ascribed primarily a gripping function to the setae located on the insides of the mouthparts, a role for which setulose setae would be less suited because of the recurring need for removal of bits of trapped food. Following this line of reasoning, the submarginal serrulate setae on the inner surface of the maxillules of *P. wosnessenskii* zoeae are well suited for gripping: their minute scales enhance the ability to clutch food without retaining or becoming clogged by small particles. Similarly, the serrate setae on the endites of the maxillules and maxillae may perform gripping functions along with grooming of other setose appendages, as suggested by several authors, *e.g.*, Roberts (1968), Farmer (1974), and Schembri (1982).

A variety of functions have been reported for setae armed with long setules, such as the plumose, pappose, and plumodenticulate setae found on the maxillules and maxillae of *P. wosnessenskii* zoeae. Plumose setae like those found in this study on the scaphognathites of the maxillae aid in generating water currents for respiration (Thomas, 1970; Farmer, 1974; Factor, 1978; Ajmal-Khan and Natarajan, 1981; Schembri, 1982), filter feeding (Rubenstein and Koehl, 1977; Cheer and Koehl, 1987), and locomotion (Fryer, 1983). If the setules are closely spaced, the boundary layer surrounding each will overlap that of adjacent setules, increasing the effective area of the appendage. As the thickness of these boundary layers changes with velocity, a given group of setae can effectively function either as large solid areas or as sieves (Cheer and Koehl, 1987). In this respect, although the planar configuration of the setules on plumose setae may cause them to function as flat paddles, the seemingly haphazard arrangement of the setules on the shafts of pappose setae such as those found on the maxillary endites of *P. wosnessenskii* may in turn cause the setae to function more like cylinders.

Plumodenticulate setae on the maxillules and maxillary endites of *P. wosnessenskii* may act as a combination of pappose and denticulate setae. Schembri (1982) observed that the tendency toward smaller denticles on the distal portions of plumodenticulate setae served to direct stray particles toward the tips of the setal shafts. The large number of these setae on the endites of the maxillae and maxillules of first-stage *P. wosnessenskii* zoeae, coupled with the diversity of secondary processes, suggests that they may be quite versatile, performing grasping, brushing, cleaning, and current-controlling functions.

The chemosensory and tactile roles of setae have been studied in detail by a number of authors, including Shelton and Laverack (1970), Derby (1982), Atema (1985), and Lavalli and Factor (1992). Regrettably, the electron microscopy and neurological experimentation necessary to attribute chemosensory or tactile function to specific setal types was beyond the scope of this study.

Behavioral and morphological analysis

The wide ranges of time for each phase of ingestion were due in large part to the variability of levels and types of activity in which the zoeae were engaged. Lapses in ingestion activity were frequent, often corresponding with increased swimming or capture of a second metanauplius, but in some cases not attributable to any obvious external cause. The shortest phase durations were recorded for zoeae that were actively engaged in sequential capture and ingestion events, and were often followed by long periods of reduced interest in feeding.

Although not usually included in most morphological descriptions, the functional significance of the paragnathal lobes warrants mention. It has been observed that in at least some crustaceans the paragnaths are mobile and are mechanically coupled with the mandibles (Wales, 1982). The paragnaths of *P. wosnessenskii* zoeae were not observed to move in this study, which is consistent with the findings of Alexander (1988), who noted that although the paragnaths of anomurans do not move by themselves, they can passively shift position as the mandibles open. Alexander also noted that the many large setae on the inner margins of anomuran paragnaths seem to aid in food retention. This appears to be true in *P. wosnessenskii.*

The labrum is another feature of crustacean anatomy often omitted from morphological descriptions. The functional significance of this structure and its complement of spines and setae in prey ingestion by zoeal *P. wosnessenskii* cannot be overlooked. In all of the observed sequences, the labrum was instrumental in maintaining a steady movement of food into the mouth. Its location at the opening to the oral chamber places it in position to give food items the final push into the foregut as well as to grip large prey items while the mandibles reposition themselves between motions. Similar accounts of labrum and mandible coordination in other crustaceans can be found in Manton (1977) and Schembri (1982).

The mandibles are the masticating appendages, responsible for all tearing, shredding, and grinding of the prey prior to entry into the mouth. Although the rotational motion of the mandibles brings the molar processes into contact with each other before the rest of the cutting edges, the prey item actually contacts the ventrally located incisor processes first. The incisor portion of the cutting edge tears off large pieces of the prey; the rotational motion of the mandible then aids in pushing those pieces farther toward the mouth to be further shredded and ground by the molar processes. The asymmetry of the molar processes of the left and right mandibles and the complexity of these regions provides a variety of masticating surfaces. As these surfaces are moving past each other, the prey is torn, shredded, and ground into tiny pieces in the final preparation for ingestion.

The maxillules manipulate prey during the initial phase of ingestion. The radically different morphologies of the endopodite and coxal and basal endites facilitate a wide range of functions. The denticulate teeth of the basal endite were used primarily for grasping and holding a captured metanauplius. The row of denticles on each tooth presumably aids in maintaining a firm grip on a struggling metanauplius, and although many of the metanauplii captured struggled energetically, very few of them escaped from the grip of the maxillules. The two submarginal setae on the basal endite may also aid in this grasping and holding process. The three-segmented endopodite acts as an outer guide for the manipulation of captured metanauplii, with the distal setae extending its effective reach in the anterior direction. Endopodite mobility enhances fine control over the positioning of a large prey item. The position of the coxal endite was often difficult to distinguish in the videotapes, but it clearly was at the posterior end of the preoral chamber during the final phase of ingestion. The range of motion demonstrated by manipulation of preserved specimens shows that the coxal endite is capable of at least some movement independent of the rest of the maxillule. Small fragments of floating food were often swept back into the preoral chamber by the coxal endite during phases 2 and 3 of ingestion. The setae of the coxal endites of the two maxillules overlapped each other along the midline of the zoea when the maxillules were not in motion, thus forming a stationary border to the preoral chamber when at rest. Fryer (1983) observed that the naupliar maxillules of the anostracan *Branchinecta ferox* (Milne-Edwards) retained food particles in a similar manner.

The lack of observed feeding function of the endites of the maxillae of *P. wosnessenskii* zoeae is probably related to their more posterior position in the zoeal stages compared to the adults, in which they are presumed to be involved in ingestion. In adult crabs, all of the feeding appendages, including the three pairs of maxillipeds, overlap one another obliquely and are limited in their posterior extension by the sternites of the pereopods. In this arrangement, the maxillary endites are more directly in the path of the food particles than they are in the larvae. Greenwood (1972) observed that the movements of the endites in adult hermit crabs were coupled with those of the scaphognathites, resulting in a continuous beating, "threshing the sides of the food" in the preoral chamber. It is also quite possible that the setae of the maxillary endites of both zoeae and adult crabs aid in the ingestion of smaller food items either through physical contact with the food or by the creation of a strong feeding current.

Other possible food sources for zoeae: ecological implications

For some decades, the focus of studies on zoeal diet has been its effect on growth and survival under laboratory and natural conditions (*e.g.*, Kurata, 1959; Sulkin, 1975, 1978; Paul *et al.*, 1979; McConaugha, 1985; Harms and Seeger, 1989; Paul *et al.*, 1989; Epifanio *et al.*, 1991). There is increasing agreement that under natural conditions, zoeae are unlikely to encounter zooplankton prey in the concentrations routinely used in laboratory rearing experiments, and therefore they can probably utilize a variety of food sources (Incze and Paul, 1983; Harms and Seeger, 1989; Paul *et al.*, 1989; Epifanio *et al.*, 1991). Sulkin found that the zoeae of *Callinectes sapidus* Rathbun, a brachyuran crab that cannot successfully complete development to metamorphosis on purely algal diets, nonetheless ingested unicellular organisms (Sulkin, 1975). The lithodid crab *Paralithodes camtschatica* (Tilesius) can be reared in the laboratory on polychaete larvae or *Artemia* nauplii, but not on a diet made up solely of diatoms (Kurata, 1959). However, Paul *et al.* (1989) found that when first-stage *P. camtschatica* zoeae ingested phytoplankton soon after hatching, they molted to the second zoeal stage at higher rates than those that did not. The algal diet did not sustain the zoeae through metamorphosis, and an increasing dependence on carnivory through the zoeal stages was hypothesized for this species (Paul *et al.*, 1989). First-feeding *P. wosnessenskii* zoeae are able to take advantage of a wide range of prey items and probably rely on a variety of planktonic food sources throughout their development.

Factor and Dexter (1993) found that the larvae of the brachyuran crab *Carcinus maenas* (Linnaeus) could capture suspended algal cells, and hypothesized that the setose mouthparts were involved in suspension feeding. In preliminary gut fluorescence experiments, *P. wosnessenskii* ingested unicellular algae covering a range of sizes. How these zoeae capture small algal cells is not known, but we assume that the mechanism is similar to that seen for ingestion of a *Prorocentrum micans* cell. In the one sequence of particle capture recorded on videotape, a *P. micans* cell was captured and ingested using a "fling and clap" method similar to that described for copepods by Koehl and Strickler (1981). The mouthparts were flung outward, enlarging the space between them, thus drawing the cell into the mouth. The mouthparts were then closed over the cell, squeezing water out through the spaces between the setae and endites, as seen in algal capture by copepods (Koehl and Strickler, 1981).

This study demonstrates that *P. wosnessenskii* zoeae can utilize prey items ranging from unicellular algae (*Cryptomonas* sp., *Prorocentrum micans*, *Gyrodinium* sp., and *Isochrysis galbana*) to relatively large, active zooplankton (*Artemia* sp. metanauplii). McConaugha (1985) identified three criteria for suitability of prey items as food sources for larval crustaceans: (1) appropriate size for capture and consumption, (2) adequate concentration, and (3) essential dietary nutrients to meet the larvae's needs for survival, growth, and metamorphosis. Natural plankton assemblages are varied in composition both spatially and temporally. The ability to capture and ingest a variety of sizes and shapes, expanding the diversity of prey species that meet McConaugha's first criterion, increases the probability that the zoea will be able to fulfill its nutritional requirements for successful development.

Acknowledgments

This project was funded by a grant from the PADI Foundation. Special thanks go to Drs. P. A. McLaughlin, R. R. Strathmann, S. D. Sulkin, D. Schneider, and C. B. Miller for invaluable advice and assistance. Use of space and equipment at Shannon Point Marine Center and Friday Harbor Laboratories is gratefully acknowledged.

Literature Cited

Ajmal-Khan, S., and R. Natarajan. 1981. Functional morphology of mouth parts and feeding behavior in the estuarine hermit crab *Clibanarius longitarsus* (De Haan). *Indian J. Mar. Sci.* **10:** 357–362.

Alexander, C. G. 1988. The paragnaths of some intertidal crustaceans. *J. Mar. Biol. Assoc. U.K.* **68:** 581–590.

Alexander, C. G., and J. P. R. Hindley. 1985. The mechanism of food ingestion by the banana prawn, *Penaeus merguiensis*. *Mar. Behav. Physiol.* **12:** 33–46.

Atema, J. 1985. Chemoreception in the sea: adaptations of chemoreceptors and behavior to aquatic stimulus conditions. Pp. 387–423 in *Physiological Adaptations of Marine Animals, Society of Experimental Biology Symposium 39*, M. S. Laverack, ed. Company of Biologists, Cambridge, U.K.

Barker, P. L., and R. Gibson. 1977. Observations on the feeding mechanism, structure of the gut, and digestive physiology of the European lobster *Homarus gammarus* (L.) (Decapoda: Nephropidae). *J. Exp. Mar. Biol. Ecol.* **26:** 297–324.

Cheer, A. Y. L., and M. A. R. Koehl. 1987. Paddles and rakes: fluid flow through bristled appendages of small organisms. *J. Theor. Biol.* **129:** 17–39.

Derby, C. D. 1982. Structure and function of cuticular sensilla of the lobster *Homarus americanus*. *J. Crustac. Biol.* **2:** 1–21.

Epifanio, C. E., J. S. Cope, P. M. Rowe, and F. M. Jenkins. 1991. Comparison of rates of development of Atlantic mud crab larvae in the laboratory and in field-deployed enclosures. *J. Crustac. Biol.* **11:** 540–545.

Factor, J. R. 1978. Morphology of the mouthparts of larval lobsters, *Homarus americanus* (Decapoda: Nephropidae), with special emphasis on their setae. *Biol. Bull.* **154:** 383–408.

Factor, J. R. 1989. Development of the feeding apparatus in decapod crustaceans. Pp. 185–203 in *Functional Morphology of Feeding and*

Grooming in Crustacea, B. E. Felgenhauer, L. Watling, and A. B. Thistle, eds. A. A. Balkema, Rotterdam.

Factor, J. R., and B. L. Dexter. 1993. Suspension feeding in larval crabs (*Carcinus maenas*). *J. Mar. Biol. Assoc. U.K.* **73:** 207–211.

Farmer, A. S. 1974. The functional morphology of the mouthparts and pereiopods of *Nephrops norvegicus* (L.) (Decapoda: Nephropidae). *J. Nat. Hist.* **8:** 121–142.

Fryer, G. 1983. Functional ontogenetic changes in *Branchinecta ferox* (Milne-Edwards) (Crustacea: Anostraca). *Philos. Trans. R. Soc. Lond., B* **303:** 229–343.

Greenwood, J. G. 1972. The mouthparts and feeding behavior of two species of hermit crabs. *J. Nat. Hist.* **6:** 325–337.

Harms, J., and B. Seeger. 1989. Larval development and survival in seven decapod species (Crustacea) in relation to laboratory diet. *J. Exp. Mar. Biol. Ecol.* **133:** 129–139.

Hart, J. F. L. 1982. *Crabs and Their Relatives of British Columbia.* British Columbia Provincial Museum Handbook No. 40. British Columbia Provincial Museum, Victoria, B.C.

Haynes, E. B. 1984. Early zoeal stages of *Placetron wosnessenskii* and *Rhinolithodes wosnessenskii* (Decapoda, Anomura, Lithodidae) and review of lithodid larvae of the northern North Pacific Ocean. *Fish. Bull.* **82:** 315–324.

Incze, L. S., and A. J. Paul. 1983. Grazing and predation as related to energy needs of stage I zoeae of the Tanner crab *Chionoecetes bairdi* (Brachyura, Majidae). *Biol. Bull.* **165:** 197–208.

Jacques, F. 1989. The setal system of crustaceans: types of setae, groupings, and functional morphology. Pp. 6–13 in *Crustacean Issues 6: Functional Morphology of Feeding and Grooming in Crustacea,* B. E. Felgenhauer, L. Watling, and A. B. Thistle, eds. A. A. Balkema, Rotterdam.

Koehl, M. A. R., and J. R. Strickler. 1981. Copepod feeding currents: food capture at low Reynolds number. *Limnol. Oceanogr.* **26:** 1062–1073.

Kunze, J., and D. T. Anderson. 1979. Functional morphology of the mouthparts and gastric mill in the hermit crabs *Clibanarius taeniatus* (Milne Edwards), *Clibanarius virescens* (Krauss), *Paguristes squamosus* (McCulloch) and *Dardanus setifer* (Milne-Edwards) (Anomura: Paguridae). *Aust. J. Freshwater Res.* **30:** 683–722.

Kurata, H. 1959. Studies on the larva and postlarva of *Paralithodes camtschatica.* I. Rearing of the larvae, with special reference to the food of the zoea. *Bull. Hokkaido Reg. Fish. Res. Lab.* **20:** 76–83.

Lavalli, K. L., and J. R. Factor. 1992. Functional morphology of the mouthparts of juvenile lobsters, *Homarus americanus* (Decapoda: Nephropidae), and comparison with the larval stages. *J. Crustac. Biol.* **12:** 467–510.

Manjulatha, C., and D. E. Babu. 1991. Functional organisation of mouthparts, and filter feeding, in *Clibanarius longitarsus* (Crustacea: Anomura). *Mar. Biol.* **109:** 121–127.

Manton, S. M. 1977. *The Arthropoda, Habits, Functional Morphology, and Evolution.* Clarendon Press, Oxford.

McConnaugha, J. R. 1985. Nutrition and larval growth. Pp. 127–154 in *Crustacean Issues 3: Larval growth,* A. M. Wenner, ed. A. A. Balkema, Rotterdam.

McLaughlin, P. A., R. H. Gore, and J. A. Crain. 1988. Studies on the *Provenzanoi* and other pagurid groups: II. A reexamination of the larval stages of *Pagurus hirsutiusculus hirsutiusculus* (Dana) (Decapoda: Anomura: Paguridae) reared in the laboratory. *J. Crustac. Biol.* **8:** 430–450.

Nyblade, C. P. 1987. Phylum or Subphylum Crustacea, Class Malacostraca, Order Decapoda, Anomura. Ch. 20 in *Reproduction and Development of Marine Invertebrates of the Northern Pacific Coast,* M. F. Strathmann, ed. University of Washington Press, Seattle.

Ohtsuka, S., and T. Onbe. 1991. Relationship between mouthpart structures and *in situ* feeding habits of species of the family Pontellidae (Copepoda: Calanoida). *Mar. Biol.* **111:** 213–225.

Orton, J. H. 1927. On the mode of feeding of the hermit-crab, *Eupagurus bernhardus,* and some other Decapoda. *J. Mar. Biol. Assoc. U.K.* **14:** 909–921.

Paffenhofer, G. A., and K. D. Lewis. 1989. Feeding behavior of metanauplii of the genus *Eucalanus* (Copepoda, Calanoida). *Mar. Ecol. Prog. Ser.* **57:** 129–136.

Paul, A. J., J. M. Paul, P. A. Shoemaker, and H. M. Feder. 1979. Prey concentrations and feeding response in laboratory reared stage one zoeae of king crab, snow crab, and pink shrimp. *Trans. Am. Fish. Soc.* **108:** 440–443.

Paul, A. J., J. M. Paul, and K. O. Coyle. 1989. Energy sources for first feeding zoeae of king crab *Paralithodes camtschatica* (Tilesius) (Decapoda: Lithodidae). *J. Exp. Mar. Biol. Ecol.* **130:** 55–69.

Pohle, G. 1989. Gill and embryo grooming in lithodid crabs: comparative functional morphology based on *Lithodes maja.* Pp. 75–94 in *Crustacean Issues 6: Functional Morphology of Feeding and Grooming in Crustacea,* B. E. Felgenhauer, L. Watling, and A. B. Thistle, eds. A. A. Balkema, Rotterdam.

Roberts, M. H., Jr. 1968. Functional morphology of the mouthparts of the hermit crabs *Pagurus longicarpus* and *Pagurus pollicaris. Chesapeake Sci.* **9:** 9–20.

Rubenstein, D. I., and M. A. R. Koehl. 1977. The mechanisms of filter feeding: some theoretical considerations. *Am. Nat.* **3:** 981–994.

Schembri, P. J. 1982. The functional morphology of the feeding and grooming appendages of *Ebalia tuberosa* (Pennant) (Crustacea: Decapoda: Leucosidae). *J. Nat. Hist.* **16:** 467–480.

Shelton, R. G. S., and M. S. Laverack. 1970. Receptor hair structure and function in the lobster *Homarus gammarus* (L.). *J. Exp. Mar. Biol. Ecol.* **4:** 201–210.

Sulkin, S. D. 1975. The significance of diet in the growth and development of larvae of the blue crab *Callinectes sapidus* Rathbun, under laboratory conditions. *J. Exp. Mar. Biol. Ecol.* **20:** 119–135.

Sulkin, S. D. 1978. Nutritional requirements during larval development of the portunid crab, *Callinectes sapidus* Rathbun. *J. Exp. Mar. Biol. Ecol.* **34:** 29–41.

Thomas, W. J. 1970. The setae of *Austropotomobius pallipes* (Crustacea: Astacidae). *J. Zool. Lond.* **160:** 91–142.

Wales, W. 1982. Control of mouthparts and gut. Pp. 165–191 in *The Biology of Crustacea,* Volume 4. Academic Press, New York.

Reports of Papers Presented at THE GENERAL SCIENTIFIC MEETINGS OF THE MARINE BIOLOGICAL LABORATORY, Woods Hole, Massachusetts 16 to 18 August 1999

Program Chairs:
BARBARA BOYER, Union College
WILLIAM ECKBERG, Howard University
CHARLES HOPKINSON, Ecosystems Center, MBL
ROBERT PAUL MALCHOW, University of Illinois at Chicago

Each of these reports was reviewed by two members of a special editorial board drawn from the research community of Woods Hole, Massachusetts. Reviewers included scientists from THE MARINE BIOLOGICAL LABORATORY, THE WOODS HOLE OCEANOGRAPHIC INSTITUTION, AND THE NATIONAL MARINE FISHERIES SERVICE.

SHORT REPORTS FROM THE 1999 GENERAL SCIENTIFIC MEETINGS OF THE MARINE BIOLOGICAL LABORATORY

Featured Article

Rome, Lawrence C.
Introduction. Bringing the script to life: the role of muscle in behavior 225

Rome, Lawrence C., Andrei A. Klimov, and Iain S. Young
A new approach for measuring real-time calcium pumping and SR function in muscle fibers 227

Physiology

Malchow, Robert Paul, and David J. Ramsey
Responses of retinal Müller cells to neurotransmitter candidates: a comparative study 229

Clay, John R., and Alan M. Kuzirian
Fluorescence localization of K^+ channels in the membrane of squid giant axons 231

Ruta, Vanessa J., Frederick A. Dodge, and Robert B. Barlow
Evaluation of circadian rhythms in the *Limulus* eye. . . 233

Novales Flamarique, Iñigo, and Ferenc I. Hárosi
Photoreceptor pigments of the blueback herring (*Alosa aestevalis*, Clupeidae) and the Atlantic silverside (*Menidia menidia*, Atherinidae) 235

Hanley, Janice S., Nadav Shashar, Roxanna Smolowitz, William Mebane, and Roger T. Hanlon
Soft-sided tanks improve long-term health of cultured cuttlefish 237

Piscine Neurobiology and Behavior

Zottoli, S.J., F.R. Akanki, N.A. Hiza, D.A. Ho-Sang, Jr., M. Motta, X. Tan, K.M. Watts, and E.-A. Seyfarth
Physiological characterization of supramedullary/dorsal neurons of the cunner, *Tautogolabrus adspersus*. . . . 239

Fay, R.R., and P.L. Edds-Walton
Sharpening of directional auditory input in the descending octaval nucleus of the toadfish, *Opasnus tau*. 240

Kaatz, Ingrid M., and Phillip S. Lobel
Acoustic behavior and reproduction in five species of *Corycoras* catfishes (Callichthyidae) 241

Lobel, Phillip S., and Lisa M. Kerr
Courtship sounds of the Pacific damselfish, *Abudefduf sordidus* (Pomacentridae) 242

Oliver, Steven J., and Elise Watson
Threat-sensitive nest defense in domino damselfish (*Dascyllus albisella*) 244

Price, Nichole N., and Allen F. Mensinger
Predator-prey interactions of juvenile toadfish, *Opsanus tau*. 246

Tang, Kathleen Q., Nichole N. Price, Maureen D. O'Neill, Allen F. Mensinger, and Roger T. Hanlon
Temperature effects on first-year growth of cultured oyster toadfish, *Opsanus tau*. 247

Chemoreception and Behavior

Mjos, Katrin, Frank Grasso, and Jelle Atema
Antennule use by the American lobster, *Homarus americanus*, during chemo-orientation in three turbulent odor plumes. 249

Hanna, John P., Frank W. Grasso, and Jelle Atema
Temporal correlation between sensor pairs in different plume positions: A study of concentration information available to the American lobster, *Homarus americanus*, during chemotaxis 250

Zettler, Erik, and Jelle Atema
Chemoreceptor cells as concentration slope detectors: preliminary evidence from the lobster nose . . . 252

Berkey, Cristin, and Jelle Atema
Individual recognition and memory in *Homarus americanus* male-female interactions 253

McLaughlin, Leslie C., Jennifer Walters, Jelle Atema, and Norman Wainwright
Urinary protein concentration in connection with agonistic interactions in *Homarus americanus*. 254

King, Alison J., Shelley A. Adamo, and Roger T. Hanlon
Contact with squid eggs increases agonistic behavior in male squid (*Loligo pealei*) 256

Cell Motility

Bearer, E.L., M.L. Schlief, X.O. Breakefield, D.E. Schuback, T.S. Reese, and J.H. LaVail
Squid axoplasm supports the retrograde axonal transport of herpes simplex virus 257

Gould, Robert, Concetta Freund, Frank Palmer, Pamela E. Knapp, Jeff Huang, Hilary Morrison, and Douglas L. Feinstein
Messenger RNAs for kinesins and a dynein are located in neural processes 259
Fukui, Yoshio, Taro Q.P. Uyeda, Chikako Kitayama, and Shinya Inoué
Migration forces in *Dictyostelium* measured by centrifuge DIC microscopy 260
Tran, P.T., P. Maddox, F. Chang, and S. Inoué
Dynamic confocal imaging of interphase and mitotic microtubules in the fission yeast, *S. pombe* 262
Maddox, Paul, Arshad Desai, E.D. Salmon, T.J. Mitchison, Karen Oogema, Tarun Kapoor, Brian Matsumoto, and Shinya Inoué
Dynamic confocal imaging of mitochondria in swimming *Tetrahymena* and of microtubule poleward flux in *Xenopus* extract spindles 263
Wöllert, Torsten, Ana S. DePina, and George M. Langford
Effects of vanadate on actin-dependent vesicle motility in extracts of clam oocytes 265

Cell and Developmental Biology

Billack, Blase, Jeffrey D. Laskin, Michael A. Gallo, and Diane E. Heck
Effects of α-bungarotoxin on development of the sea urchin *Arbacia punctulata* 267
Silver, Robert B., and Nicole M. Deming
Leukotriene B_4 as calcium agonist for nuclear envelope breakdown: an enzymological survey of endomembranes of mitotic cells 268
Weidner, Earl, and Ann Findley
Extracellular survival of an intracellular parasite (*Spraguea lophii*, Microsporea) 270
Kaltenbach, Jane C., William J. Kuhns, Tracy L. Simpson, and Max M. Burger
Intense concanavalin A staining and apoptosis of peripheral flagellated cells in larvae of the marine sponge *Microciona prolifera:* significance in relation to morphogenesis 271

Comparative Biochemistry

Harrington, John M., and Peter B. Armstrong
A cuticular secretion of the horseshoe crab, *Limulus polyphemus:* a potential anti-fouling agent 274
Asokan, Rengasamy, and Peter B. Armstrong
Cellular mechanisms of hemolysis by the protein limulin, a sialic-acid-specific lectin from the plasma of the American horseshoe crab, *Limulus polyphemus* 275
Biswas, Chhanda, and Peter B. Armstrong
Identification of a hemolytic activity in the plasma of the gastropod *Busycon canaliculatum* 276
Kuhns, William J., Max M. Burger, and Eva Turley
Hyaluronic acid: a component of the aggregation factor secreted by the marine sponge, *Microciona prolifera* 277
Popescu, Octavian, Rey Interior, Gradimir Misevic, Max M. Burger, and William J. Kuhns
Biosynthesis of tyrosine O-sulfate by cell proteoglycan from the marine sponge, *Microciona prolifera* 279
Vasse, Aimee, Alice Child, and Norman Wainwright
Prophenoloxidase is not activated by microbial signals in *Limulus polyphemus* 281
Ogunseitan, O.A., S.L. Yang, and E. Scheinbach
The δ-aminolevulinate dehydratase of marine *Vibrio alginolyticus* is resistant to lead (Pb) 283
Hoskin, Francis C.G., Diane M. Steeves, and John E. Walker
Substituted cyclodextrin as a model for a squid enzyme that hydrolyzes the nerve gas soman 284
Zigman, Seymour, Nancy S. Rafferty, Keen A. Rafferty, and Nathaniel Lewis
Effects of green tea polyphenols on lens photooxidative stress 285

Ecology and Evolution

Mondrup, Thomas
Salinity effects on nutrient dynamics in estuarine sediment investigated by a plug-flux method 287
Pease, Katherine M., L. Claessens, C. Hopkinson, E. Rastetter, J. Vallino, and N. Kilham
Ipswich River nutrient dynamics: preliminary assessment of a simple nitrogen-processing model 289
Wolfe, Felisa L., Kevin D. Kroeger, and Ivan Valiela
Increased lability of estuarine dissolved organic nitrogen from urbanized watersheds 290
Evgenidou, A., A. Konkle, A. D'Ambrosio, A. Corcoran, J. Bowen, E. Brown, D. Corcoran, C. Dearholt, S. Fern, A. Lamb, J. Michalowsky, I. Ruegg, and J. Cebrián
Effects of increased nitrogen loading on the abundance of diatoms and dinoflagellates in estuarine phytoplanktonic communities 292
Cubbage, Andrea, David Lawrence, Gabrielle Tomasky, and Ivan Valiela
Relationship of reproductive output in *Acartia tonsa*, chlorophyll concentration, and land-derived nitrogen loads in estuaries in Waquoit Bay, Massachusetts 294
Canfield, Susannah, Luc Claessens, Charles Hopkinson Jr., Edward Rastetter, and Joseph Vallino
Long-term effect of municipal water use on the water budget of the Ipswich River Basin 295

Young, Talia, Sharon Komarow, Linda Deegan, and Robert Garritt
Population size and summer home range of the green crab, *Carcinus meanus,* in salt marsh tidal creeks. 297
Komarow, Sharon, Talia Young, Linda Deegan, and Robert Garritt
Influence of marsh flooding on the abundance and growth of *Fundulus heteroclitus* in salt marsh creeks . . . 299
Widener, Justin W., and Robert B. Barlow
Decline of a horseshoe crab population on Cape Cod 300
Kerr, Lisa M., Phillip S. Lobel, and J. Mark Ingoglia
Evaluation of a reporter gene system biomarker for detecting contamination in tropical marine sediments. 303

ORAL PRESENTATIONS

PUBLISHED BY TITLE ONLY 307

Reference: *Biol. Bull.* **197:** 225–226. (October 1999)

Introduction to the Featured Article
Bringing the Script to Life: the Role of Muscle in Behavior

A goal of *Neuroscience's* soon-to-be-completed "Decade of the Brain" is to integrate nervous function from molecule to behavior. But behavior does not begin and end in the nervous system. Muscles actuate the movements that constitute most behaviors—and if the properties of the muscle are not "tuned" to the overall biomechanics of the body, then the behavior will not occur as planned in the brain. Thus, the properties of the muscles and the overall biomechanics of the body are also determinants of behavior, sometimes equal in importance to that of the nervous system. Two central concepts dictate that experimental approaches to the properties of muscles must also be integrative. First, one cannot understand how a muscle is designed without knowing exactly what it does during normal behavior (1), and second, the adaptation of muscle for different motor activities takes place at the molecular level.

Our goal over the past few years has therefore been to understand, from the level of molecular biophysics to whole-animal biomechanics, how muscles are designed to power different activities. This ambitious goal has only become feasible because of a revolution that has taken place in the field of integrative muscle physiology and biomechanics over the past decade. This revolution has been largely fueled by technological improvements in three areas: biophysics, whole-animal measurements, and computer modeling.

The development of new biophysics technologies (*e.g.*, Ca^{2+}-sensitive dyes and caged compounds) enables us, for the first time, to measure the kinetics of the pertinent molecular processes of muscle contraction. Indeed, we will soon begin to develop a model of muscle contraction that is based on principles of chemical kinetics. At the organismal end of the scale, development and miniaturization of transducers (*e.g.*, sonomicrometry, strain gauges) and telemetry now facililate measuring the performance of muscles in the animal during normal behavior. Further, recent development of musculoskeletal modeling systems and 3-D laser scanners permits us to construct virtual animals with anatomical features that are exactly like those of living animals. Because the movements of these virtual animals are dictated by biomechanics rather than an animator's imagination, simulation of a set of muscle contractions will allow us to test how whole-animal motor performance would be altered if the kinetics of a molecular process were changed in a specific manner. This approach will show how changes in single molecular components might affect whole-animal performance in real life, and thus how simple genetic changes might have affected the evolution of behavior.

Finally, this current revolution in muscle physiology and biomechanics would not have been possible without the development of exceptional experimental models. Fish have led the way in this regard. In contrast to the mixing of different fiber types that occurs in the muscles of mammals and most other vertebrates, the different muscle fiber types in fish are organized into large, homogenous, and anatomically separated regions that are visible to the naked eye. In fish, as opposed to mammals, we can monitor which motor activities are powered by each fiber type because we can implant electromyography electrodes in these anatomically separate regions. In addition, one can dissect bundles of fibers that are all of the same type, so that the mechanical, biochemical, and ultrastructural properties of each muscle fiber type can be determined.

The fish that best exemplifies the diversity of muscular function and design is the toadfish (*Opsanus tau*) (Fig. 1, left). These animals rest on the bottom and wait for a fish or crustacean to pass; then they grab the prey with their immense jaws. The swimming muscles of the toadfish reflect this sluggish behavior. Their slow-twitch muscles, which in most fish are used for steady swimming, are almost nonexistent; the few that do occur are among the slowest ever measured—they work at about 1 Hz. Toadfish "fast"-twitch white muscle, used in a short burst of activity to capture prey, is also unimpressive—it has about the same speed as *slow*-twitch muscle in other fish.

But when it comes to calling for a mate, the male toadfish is an athlete of Olympic stature. The muscles that surround his heart-shaped swimbladder (Fig. 1, center) alternately contract down on the organ and relax at up to 200 Hz to produce the "boat-whistle" mating call. In fact, the swimbladder muscle is the fastest vertebrate muscle known.

The diversity of muscles in toadfish strikingly illustrates how muscle can be so exquisitely tuned for one

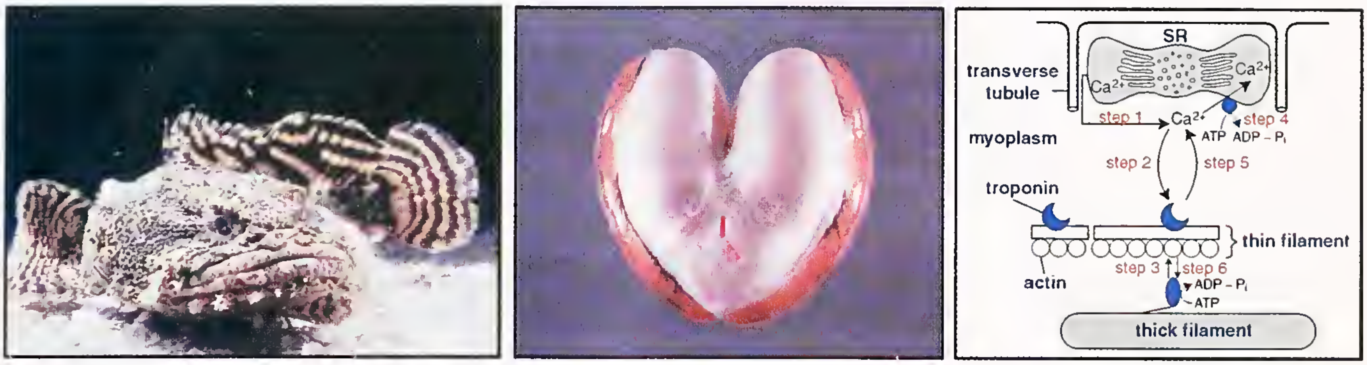

Figure 1. *Left: The toadfish* Opsanus tau *(Photo by A. Kuzirian). Center: Toadfish swimbladder; the red swimbladder muscle runs circumferentially around the white swimbladder (Photo by L. Nelson). Right: Molecular processes of muscle activation and relaxation (Drawing: T. Clark).*

behavior that it can't be used for another. Neither the red nor the white swimming muscle can physically produce high-frequency sounds because it can't relax fast enough. By contrast, at the low frequencies of steady swimming, the swimbladder muscle's extremely low mechanical power output and extremely high energetic cost make it unable to power locomotion (2).

The challenge of studying the adaptations of the fastest vertebrate muscle is irresistible. My colleagues and I (3, 4) had already determined that the immense speed of the swimbladder is principally due to its extremely fast relaxation rate, which in turn is due to three specific adaptations: the swimbladder removes Ca^{2+} from the cytoplasm 50-fold faster than the red muscle does (Fig. 1, right: Step 4), swimbladder troponin C has a far faster Ca^{2+} off-rate than red muscle (Step 5), and swimbladder crossbridges have a 50-fold faster detachment rate constant than red muscle (Step 6).

In our attempt to further dissect the molecular mechanisms responsible for the swimbladder's rapid clearing of Ca^{2+}, we ran into a snag in distinguishing the three competing mechanisms. One of these mechanisms is fast Ca^{2+} pumping by the sarcoplasmic reticulum (SR); but two other mechanisms—binding of Ca^{2+} to the soluble protein parvalbumin and binding to the SR-Ca^{2+} pumps themselves—may also make a very large contribution. Consider that when toadfish call with the swimbladder muscle, it is not a single twitch but a series of many contractions that is produced. When the muscle relaxes after a stimulus, the interval before the next stimulus (1/200 s) is not long enough for all the Ca^{2+} to be pumped back into the SR. So Ca^{2+} is left attached to the parvalbumin and the Ca^{2+} pumps, and thus less Ca^{2+} is pumped back into the SR than was originally released. During calling, therefore, the SR may ultimately run out of Ca^{2+} to release. Perhaps reflecting this limitation, toadfish call in short bursts rather than continuously. Therefore, if we could determine the relative importance of these three mechanisms we could understand, not only how the system is designed to be so quick, but why these animals behave as they do.

Unfortunately, these processes can't be differentiated in an intact cell. We turned, therefore, to permeabilized ("skinned") muscle cells because the parvalbumin can be washed out through the leaky cell membrane while the SR membrane remains intact. The following paper describes the development of a new technique for measuring Ca^{2+} uptake by the SR in skinned muscle fibers. This technique is a small but necessary step towards solving the puzzle of how these biological machines have evolved to perform so many functions. It will also help us better understand the biological basis of behavior.

—Lawrence C. Rome
August 1999

Literature Cited

1. **Rome, L. C., R. P. Funke, R. M. Alexander, G. Lutz, H. D. J. N. Aldridge, F. Scott, and M. Freadman. 1988.** *Nature* **355:** 824–827.
2. **Rome, L. C., and S. L. Lindstedt. 1998.** *News Physiol. Sci.* **13:** 261–268.
3. **Rome, L. C., D. A. Syme, S. Hollingworth, S. L. Lindstedt, and S. M. Baylor. 1996.** *Proc. Natl. Acad. Sci. USA* **93:** 8095–8100.
4. **Rome, L. C., C. Cook, D. A. Syme, M. A. Connaughton, M. Ashley-Ross, A. A. Klimov, B. A. Tikunov, and Y. E. Goldman. 1999.** *Proc. Natl. Acad. Sci. USA* **96:** 5831.

Reference: *Biol. Bull.* **197:** 227–228. (October 1999)

A New Approach for Measuring Real-time Calcium Pumping and SR Function in Muscle Fibers

Lawrence C. Rome[1], *Andrei A. Klimov, and Iain S. Young*
(Biology Department, University of Pennsylvania, Philadelphia, Pennsylvania 19104)

Different muscles are designed to perform a wide variety of motor activities that extend over a large range of frequencies. To increase our understanding of the molecular basis for these different designs, we are attempting to model the activation-relaxation cycle of different muscles by obtaining kinetic information about each of the constituent processes (1, 2). An important component in muscle relaxation is Ca^{2+} sequestration by sarcoplasmic reticulum (SR)-Ca^{2+} pumps, but the pump turnover rate in different fiber types is not known precisely.

Previous measurements of SR function have generally involved one of two approaches. One approach involves homogenizing muscle, making SR preparations and measuring the rate of Ca^{2+} accumulation in the presence of oxalate (*e.g.*, 3). It is unclear, however, whether homogenization alters the pumping rate compared to that of intact SR in muscle fibers. Further, the presence of oxalate probably increases the rate of accumulation above that in normal fibers by reducing the free Ca^{2+} concentration inside the SR. An alternate approach involves physiological measurements of intracellular free $[Ca^{2+}]$ using calcium sensitive dyes (*e.g.*, 1, 4). However, this approach provides direct information only about the small amount of Ca^{2+} that is actually free in the myoplasm. The total movements of Ca^{2+} can only be estimated by modelling the large quantities of other Ca^{2+} buffers in the cell (*e.g.*, parvalbumin and troponin; 4), but the amounts and the kinetics of these calcium buffers are not always known in detail.

We have developed a technique and an instrument that permit direct measurements of Ca^{2+} sequestration by intact SR of muscle fibers as a function of $[Ca^{2+}{}_{free}]$. Single muscle fibers are exposed to 50 μg/ml saponin (20 min), which permeablizes the cell membrane, but leaves the SR membrane intact (5). The "skinned" muscle fibers are then bathed in solutions that contain various concentrations of $Ca^{2+}{}_{free}$; and calcium sequestration (*i.e.*, Ca^{2+} leaving the bath) is monitored by using a Ca^{2+} sensitive dye, FURA-2. This approach solves two important problems. First, during the "skinning" procedure, most of the intracellular Ca^{2+}-buffer (the soluble parvalbumin) leaks out of the cell membrane and is washed away. Second, the amounts of remaining intracellular buffers (*e.g.*, troponin), become very small compared to the total buffer in the bath, which is well defined in terms of amounts and kinetics, and can be accurately calibrated. Hence Ca^{2+} sequestration by the SR can be accurately measured as a removal of Ca^{2+} from the bathing solution.

This approach, unfortunately, involves a high bath volume to fiber volume ratio. The fiber diameter (and hence fiber volume) must be kept small because of potential diffusion limitations. Further, the necessity of stirring the bathing solution rapidly in the long and thin chamber fitted to the morphology of muscle fibers prevents reduction of the bath volume below a critical value. In this study we used a bath volume of 5 μl and typical fiber volumes of ~5 nl, giving a bath to fiber volume ratio of about 1000:1.

We overcame the large bath volume to fiber volume ratio by using three approaches to optimize the detection of the fluorescence change associated with the uptake of Ca^{2+}. First, by using FURA-2 as the main Ca^{2+} buffer (in addition to its use as Ca^{2+} indicator), we maximized the absolute fluorescence change for a given uptake of Ca^{2+}. By avoiding using additional buffers (*e.g.*, EGTA), at low $[Ca^{2+}{}_{free}]$, we achieved a nearly stoichiometric fluorescent change in one FURA molecule for every Ca^{2+} molecule taken up by the SR. Second, we also improved detection by employing only a low concentration (50 μM) of the FURA Ca^{2+} buffer. Note that at high $[Ca^{2+}{}_{free}]$, the ATP in the solution also bound Ca^{2+}, thus leading to a decline in sensitivity. Third, as illustrated in the optics diagram (Fig. 1B), the FURA was excited at 400–420 nm. With this excitation, only unbound FURA absorbs light (6). Hence the emission measured at 480–610 nm with a solid state photodetector is proportional to the concentration of unbound FURA. Thus, those solutions containing high $[Ca^{2+}{}_{free}]$ have low fluorescence. This is important because, under conditions where Ca^{2+} sequestration was measured (*i.e.*, high $[Ca^{2+}{}_{free}]$), Ca^{2+} sequestration was observed as an increase in fluorescence over a low initial fluorescence (Fig. 1C), thereby further improving detection.

In addition to the optics for measuring the fluorescence change, the calcium sequestration device contained a cuvette in which the muscle fiber is positioned and in which solutions containing the appropriate FURA and Ca^{2+} concentrations can be very rapidly exchanged (~200 ms, Fig. 1A). Because the cuvette is well stirred (with air jets—Fig. 1A), the FURA fluorescence can be sampled anywhere within it, except in the small volume occupied by the fiber itself.

For development of this technique, our preparation consisted of one or two toadfish swimbladder muscle fibers with a maximum diffusion distance of about 20 μm. This fiber type is thought to have the highest density of Ca^{2+} pumps (7) and the fastest calcium transient of any vertebrate muscle (1). Our base solution (pH 7.1, 15°C, pCa = 7.4) contained 50 mM HDTA, 8

---

[1] To whom correspondence should be addressed.

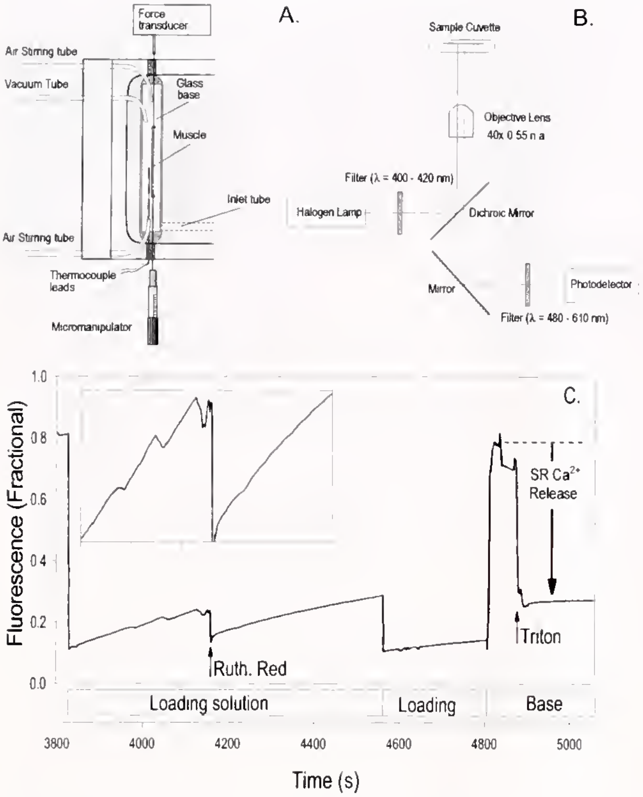

Figure 1. *An apparatus for measuring the Ca^{2+} sequestration rate of single muscle fibers. (A) The chamber consists of an anodized aluminum block with a 5 μl solution well. Slots cut at the ends of the well allow a pin attached to a force transducer and a fixed pin to enter the well; the muscle fiber is "T-clipped" onto the tips of these pins. A glass coverslip covers the bottom of the well. Solutions enter the well at one end via a stainless steel inlet tube, pass through the well and are removed at the opposite end* via *a vacuum tube placed at the surface of the well. The solutions are held in thermostated reservoirs, and driven under pressure into the cuvette through Lee valves controlled by a computer. The solution is stirred by jets of humidified air directed over the surface of the chamber. (B) The chamber is mounted on a Leica DM-IRB inverted microscope fitted with epi-fluorescent illumination. During Ca^{2+} sequestration, violet light from a halogen light source is focused into the sample cuvette by the objective lens, causing the unbound FURA to fluoresce. The emission light (dashed line) passes back down through the lens, dichroic mirror, and filter before detection by a solid state photodetector. (C) A sample trace in which fluorescence is normalized for maximized fluorescence in the presence of relaxing solution (all FURA unbound). At low $[Ca^{2+}_{free}]$ (Base solution), fluorescence is high and changes little with time. Upon influx of high $[Ca^{2+}_{free}]$ loading solution, the fluorescence drops to a low level and subsequently increases. The initial drop signifies a low unbound FURA concentration appropriate for a high $[Ca^{2+}_{free}]$. The increase in fluorescence signifies that Ca^{2+} is leaving FURA (increasing unbound [FURA]) as it is sequestered by the SR. After taking up some Ca^{2+}, the fluorescence levels showed oscillations (see inset for expanded scale) which is stopped by the injection of 50 μM ruthenium red (Ruth. Red). The loading solution is exchanged several times, so that the SR can take up a large quantity of Ca^{2+}. Then the excess bath Ca^{2+} was washed out by base solution. Finally, 1 μl of base solution was removed, and 1 μl 15% Triton in base solution was injected into the bath, raising the bath Triton concentration to 3%. There was an immediate drop in fluorescence corresponding to release of all Ca^{2+} from the SR.*

m*M* ATP, 10 m*M* creatine phosphate, 8.4 m*M* $MgCl_2$ ($[Mg^{2+}_{free}] = \sim 1$ m*M*), 30 units/ml of creatine phosphokinase, 70 m*M* TES, ~140 m*M* K^+, and 50 μ*M* FURA-2. To this base solution various reagents were added to make additional solutions. To make the relaxing solution, 1 m*M* EGTA was added; to make caffeine solution, 40 m*M* caffeine and 1 m*M* EGTA were added; to make loading solutions, various amounts of $CaCl_2$ were added to produce a $[Ca^{2+}_{free}]$ of 0.5–2 μ*M*,; and to make Triton solutions, Triton-X-100 was added to make 3% (V/V).

Figure 1C shows a sample trace. The fibers were exposed to caffeine solution to empty the SR of Ca^{2+} (not shown). The caffeine was then washed out in relaxing solution (not shown). The EGTA was subsequently washed out in rapid exchanges with base solution. The solution was then exchanged for a loading solution with a $[Ca^{2+}_{free}]$ of ~ 2 μ*M* (note the much lower initial fluorescence in the loading solution). The subsequent increase in fluorescence signifies an increase in unbound FURA in the bath. That is, the Ca^{2+} being pumped into the SR is being removed from the bath. The slope represents the rate of Ca^{2+} uptake by the SR in the muscle fiber—the maximum being about 0.8 pmoles per s.

In addition to measuring Ca^{2+} uptake rate, this instrument can also be used for exploring other functions of the SR. For example, as more Ca^{2+} is taken up by the SR, oscillations of the bath $[Ca^{2+}_{free}]$ level were often observed. The presence of these oscillations, and the fact that they could be ended by injection of ruthenium red (Fig. 1C and inset), are suggestive of calcium-induced-calcium-release. Our instrument enables us to quantify how much Ca^{2+} is released and how quickly it is taken back up. Finally, this instrument also permits the measurement of total Ca^{2+} stored in the SR, which is crucial in understanding the cycling of Ca^{2+} during calling in toadfish. By exposing the fiber to Triton solution, the SR membrane is rapidly permeablized and all the Ca^{2+} is released (8). The released Ca^{2+} binds to FURA, causing a drop in fluorescence equivalent to ~180 pmoles of Ca^{2+}.

Supported by NSF IBN-9514383, NIH AR38404, and NIH AR46125 to L. Rome. We thank S. M. Baylor for suggesting the use of FURA as a Ca^{2+} buffer.

Literature Cited

1. **Rome, L. C., D. A. Syme, S. Hollingworth, S. L. Lindstedt, and S. M. Baylor. 1996.** *Proc. Natl. Acad. Sci. USA* **93:** 8095–8100.
2. **Rome, L. C., C. Cook, D. A. Syme, M. A. Connaughton, M. Ashley-Ross, A. A. Klimov, B. A. Tikunov, and Y. E. Goldman. 1999.** *Proc. Natl. Acad. Sci. USA* **96:** 5831.
3. **Feher, J. J., T. D. Waybright, and M. L. Fine. 1998.** *J. Muscle Res. Cell Motil.* **19:** 661–674.
4. **Baylor, S. M., and S. Hollingworth. 1988.** *J. Physiol. (Lond.)* **403:** 151–192.
5. **Launikonis, B. S., and D. G. Stephenson. 1997.** *J. Physiol. (Lond.)* **504:** 425–437.
6. **Konishi, M., A. Olson, S. Hollingworth, and S. M. Baylor. 1988.** *Biophys. J.* **54:** 1089–1104.
7. **Appelt, D., V. Shen, and C. Franzini-Armstrong. 1991.** *J. Muscle Res. Cell Motil.* **12:** 543–552.
8. **Fryer, M. W., and D. G. Stephenson. 1996.** *J. Physiol. (Lond.)* **493:** 357–370.

Reference: *Biol. Bull.* **197:** 229–230. (October 1999)

Responses of Retinal Müller Cells to Neurotransmitter Candidates: A Comparative Survey

Robert Paul Malchow (Departments of Biological Sciences and Ophthalmology and Visual Sciences, University of Illinois at Chicago, Chicago, Illinois 60607), and David J. Ramsey[1]

Radial glial cells of the retina (commonly referred to as Müller cells) are believed to play a crucial role in maintaining the normal functional capabilities of this most peripheral extension of the central nervous system. Like glia elsewhere in the nervous system, these cells have been implicated in such diverse functions as metabolic support for neighboring neurons (1), maintenance of the ionic composition of the external milieu (2), regulation of extracellular pH (3), clearance of extracellular neurotransmitters (including glutamate and GABA) from the perisynaptic space (4), and regulation of synaptogenesis during the course of development (5). Recent experiments have also demonstrated that Müller cells possess a variety of receptors for extracellular signals; these receptors enable the cells to sense changes in the external environment that result from neuronal activity. For example, glutamate, the neurotransmitter likely released by photoreceptors, has been reported to modulate potassium conductances of Müller cells (6), and increases in internal calcium have been reported to be induced in retinal Müller cells by mechanical and neurochemical stimulation, eliciting calcium waves that course though glia adjacent to the stimulated site (7). Moreover, changes in the properties of the Müller cells are likely to affect the activity of neighboring neurons. The most recent and exciting demonstration of such an effect has been in experiments that link the increases in internal calcium elicited in glial cells to changes in the pattern of electrical discharges of neighboring ganglion cells (8). Given the potential importance of such modulation, we have begun to ask which neurotransmitters and neuromodulators can promote increases in calcium in Müller cells, and whether there is a consistent pattern of responses across species.

To address these questions, we have chosen to compare alterations in calcium levels in Müller cells isolated from an amphibian (the neotenous tiger salamander, *Ambystoma tigrinum*), and an elasmobranch (the skate, *Raja ocelatta* and *R. erinacea*). The Müller cells of these two types of animals have been used in the past as models to study the electrophysiological properties associated with Müller cell function. Individual Müller cells were isolated using a variation of the procedure outlined by Malchow *et al.* (9). In brief, animals were pithed, the eyes enucleated, and the retinas isolated. The retinas were immersed for 45–60 min in Ringer's or other appropriate culture medium that also contained 2 mg/ml papain and 1 mg/ml L-cysteine. After extensive washing to remove the papain, the retinas were mechanically agitated through a glass-graduated pipette, and aliquots of the solution containing isolated cells were placed on glass cover slips that had previously been coated with protamine sulfate and concanavalin A. Cells isolated from the tiger salamander matched closely those described by previous investigators (10) and possessed clear cell endfeet, cell somas, and apical regions normally associated with the photoreceptors. Identification of skate Müller cells was based on their morphological resemblance to cells previously shown to display positive staining using a polyclonal antiserum raised to chick glutamine synthetase, which selectively stains glial cells in the intact retina of skate and other vertebrates (11).

Isolated cells were loaded with the calcium dye Fura-2 by incubating the cells for 30 min at 14°C in 5 μM of the acetoxymethyl ester form of the dye. Cells were then rinsed three times with Ringer and allowed to incubate for at least an additional hour in the dark at 14°C. The dye incorporated into the cells was excited

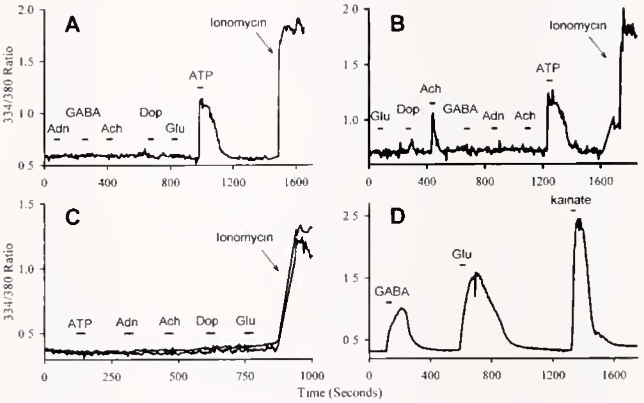

Figure 1. *Changes in intracellular calcium levels in isolated retinal cells upon superfusion of a variety of neurotransmitter agents. Increases in internal calcium were indicated by increases in the ratio of Fura-2 fluorescence induced by stimulation with 334 and 380 nm light. (A) Responses from an isolated tiger salamander Müller cell, showing that of the agents tested, only ATP was able to produce an increase in the ratio of 334/380 fluorescence. This result was typical of the majority of the cells tested. (B) Responses from another tiger salamander Müller cell. In this cell, as in 47% of the others tested, both acetylcholine and ATP induced an increase in the ratio of 334/380 fluorescence. The increase induced by acetylcholine was always smaller and more transient than that produced by ATP. (C) Responses from two skate Müller cells. None of the neurotransmitter candidates induced changes in intracellular calcium levels in these cells. However, ionomycin, a calcium ionophore, induced a significant increase in the 334/380 ratio, indicating that the system could indeed detect increases in intracellular calcium. (D) Responses from an isolated external horizontal cell from the skate. As expected, the neurotransmitters GABA and glutamate, and the glutamate analog kainate, all produced significant increases in intracellular calcium levels. All drugs were bath superfused at a concentration of 1 mM, except ionomycin. In the latter case, 2 μl of a 5 mM solution was added to the central well of the dish, resulting in a final concentration of 50 μM. Superfusion was turned off during the application of ionomycin. Abbreviations: Adn, adenosine; GABA, gamma-amino butyric acid; Ach, acetylcholine; Dop, dopamine; glu, glutamate; ATP, adenosine triphosphate.*

---

[1] Biological Laboratories, Harvard University, Cambridge, Massachusetts.

Table I

Cells responding with an increase in intracellular calcium after addition of neurotransmitter agents

	ATP	Acetylcholine	Glutamate	GABA	Dopamine	Adenosine
Tiger Salamander Müller	64 (65)	16 (34)	5 (42)	2 (40)	1 (15)	5 (34)
Skate Müller	1 (24)	— (21)	1 (22)	— (12)	— (17)	— (17)

The number of cells tested in each condition is shown in parentheses. The number of cells responding with an increase in calcium (defined as producing a 334/380 ratio greater than 25% of the initial baseline) is shown to the left of the parentheses. A dash (—) indicates that none of the cells tested responded with an increase. All chemicals were applied at 1 m*M* concentrations *via* bath superfusion.

alternately with 334 and 380 nm light every 2 seconds, and the resultant fluorescence, emitted through a 520 nm filter, was quantified with a Zeiss Attofluor calcium imaging system. Drugs were applied onto the cells, in random order at about 1–2.5 ml/min *via* a gravity superfusion system. Cells were rinsed for at least two minutes with Ringer in between applications of drugs. A response was considered to have been induced when the ratio of 334/380 fluorescence exceeded, by 25%, the baseline level recorded prior to the application of a drug. A transient increase in calcium was frequently observed when the flow of Ringer was started; typically, drugs were applied 2 min after this initial transient had declined to a steady baseline level.

We examined the responses of these cells to applications of 1 m*M* gamma-aminobutyric acid (GABA), glutamate, acetylcholine, adenosine, adenosine triphosphate (ATP) and dopamine. As first reported by Keirstead and Miller (12), extracellularly-applied ATP elicited a marked increase in calcium in the tiger salamander Müller cells (Fig. 1A). Of 65 cells examined, ATP induced an increase in calcium in 64 cells. Acetylcholine was less consistent in raising internal calcium, producing smaller and more transient calcium increases in 47% of the cells tested (Fig. 1B; see also Table I). These data are of interest in light of work by Wakakura *et al.* (13), demonstrating that one-half of all rabbit Müller cells examined responded to acetylcholine with increases in calcium. We were, however, unable to evoke an increase in calcium with 1 m*M* glutamate, despite previous evidence supporting the presence of metabotropic glutamate receptors on the Müller cells of the tiger salamander (12). This result was unexpected, but we note that glutamate has also been reported to be ineffective in inducing calcium waves in Müller cells in the intact retina of the tiger salamander (7). None of the other neurotransmitters caused an increase in calcium in the majority of cells tested.

The same array of neuroactive agents were ineffective in increasing calcium in 24 skate Müller cells. Positive controls to ensure that the imaging system was working properly included demonstrations: (a) that increases in calcium were observed in skate Müller and horizontal cells upon application of the calcium ionophore ionomycin (Fig. 1C); and (b) that glutamate and GABA both increased calcium levels in isolated skate retinal horizontal cells (Fig. 1D), as had been described previously (14).

Electrophysiological data also support significant differences in the responses of the Müller cells of the two species to neurotransmitter agents. For example, skate Müller cells respond to GABA with a brisk electrical current mediated by GABA$_a$ receptors (9), while no such similar current has yet been reported in tiger salamander Müller cells. While we cannot rule out the possibility that the enzyme used to produce isolated cells might have altered the properties of some of the membrane proteins present in the cells, our results suggest that Müller cells of disparate species can differ widely in their responses to neurotransmitter agents. Consequently, the conditions under which Müller cells might alter the function of neighboring neurons is likely to differ from species to species.

The authors would like to thank Kasia Hammar and Rudi Rottenfusser for guidance and assistance in using the Zeiss Attofluor system, Naomi Rosenkranz for help with cell culture, Richard Sanger for computer and equipment assistance, and Peter J. S. Smith and Barbara Innocenti for comments on the manuscript. This research was supported by grant EY09411 from the National Eye Institute, grant DBI-9605155 from the National Science Foundation, and grants NCCR P41 RR01395 and R21 RR12718 from the National Center for Research Resources.

Literature Cited

1. **Carter-Dawson, L., F. Shen, R. S. Harwerth, E. L. Smith 3rd, M. L. Crawford, and A. Chuang. 1998.** *Exp. Eye Res.* **66:** 537–45.
2. **Newman, E. A. 1985.** *Trends Neurosci.* **8:** 156–159.
3. **Newman, E. A. 1996.** *J. Neurosci.* **16:** 159–168.
4. **Sarthy, P. V. 1982.** *J. Neurosci. Methods* **5:** 77–82.
5. **Wilbold, E., and P. G. Layer. 1998.** *Histol. Histopathol.* **13:** 531–552.
6. **Schwartz, E. A. 1993.** *Neuron* **10:** 1141–1149.
7. **Newman, E. A., and K. A. Zahs. 1997.** *Science* **275:** 844–847.
8. **Newman, E. A., and K. A. Zahs. 1998.** *J. Neurosci.* **18:** 4022–4028.
9. **Malchow, R. P., H. H. Qian, and H. Ripps. 1989.** *Proc. Natl. Acad. Sci. U.S.A.* **86:** 4226–4230.
10. **Newman, E. A. 1985.** *J. Neurosci.* **5:** 2225–2239.
11. **Linser, P. J., K. Smith, and K. Angelides. 1985.** *J. Comp. Neurol.* **237:** 264–272.
12. **Keirstead, S. A., and R. F. Miller. 1997.** *Glia* 194–203.
13. **Wakakura, M., I. Utsunomiya-Kawasaki, and S. Ishikawa. 1998.** *Graefe's Arch. Clin. Exp. Ophthalmol.* **236:** 934–939.
14. **Haugh-Scheidt, L., R. P. Malchow, and H. Ripps. 1995.** J. Physiol. **488:** 565–576.

Reference: *Biol. Bull.* **197:** 231–232. (October 1999)

Fluorescence Localization of K^+ Channels in the Membrane of Squid Giant Axons

John R. Clay[1] and *Alan M. Kuzirian (Marine Biological Laboratory, Woods Hole, Massachusetts 02543)*

Modern neuroscience can be said to have begun with the seminal work of Hodgkin and Huxley (1) who demonstrated the existence of Na^+ and K^+ specific conductances in the membrane of squid giant axons. These conductances underlie the action potential that propagates along the nerve and then triggers contraction of the mantle, *i.e.*, the jet-propelled escape response (2). In the last few years, Na^+ and K^+ channel proteins from this preparation have been cloned and sequenced (3, 4). Moreover, a polyclonal antiserum has been raised against a portion of the NH_2-terminal amino acid sequence of the SqKv1A K^+ channel (4)—an intracellular epitope. We have used this antiserum to localize with fluorescence immunocytochemistry K^+ channels in the axonal membrane.

Because the target for the antibody we have used is intracellular, we necessarily had to deliver it to the interior of the axon. We were unable to accomplish this by external application of the antibody, even with Triton-X-100, because of barriers outside the axolemma—particularly the basement membrane and the glial cell layer (5). We circumvented this problem by using intracellular perfusion. This is a novel approach for histologists, but not for electrophysiologists, who have for decades used intracellular perfusion together with the axial wire voltage-clamp technique to investigate the effects of intracellular factors on ionic currents in squid giant axons (6, 7). The method used is illustrated in Figure 1. The axoplasm was extruded with a roller (Fig. 1A). A small piece or "plug" of axoplasm was left near one end of the axon. The preparation was then placed in a Lucite chamber and tied onto a small hook (Fig. 1B). A small hole was cut in the axon, and a glass cannula was guided into the axon through the remaining plug of axoplasm. The axon was ligated onto the cannula, and perfusion with a 1-ml syringe was initiated. The syringe was attached to the apparatus which held the cannula in place (not shown). Throughout the experiment, the exterior surface of the central portion of the axon (1 cm length) was superperfused with filtered seawater (fsw). The standard intracellular perfusion buffer consisted of 100 m*M* K glutamate and 500 m*M* sucrose (pH = 7.2; referred to below as "standard buffer").

Even though we were able to introduce antibodies inside the axon with this preparation, no immunostaining was observed unless we used procedures to circumvent the inner cortical layer of axoplasm that remains after extrusion (5). This layer prevents antibodies from reaching the inner membrane surface. Specifically, we used either potassium iodide (KI)—a chaotropic agent—to completely wash away the cortical layer, or Triton-X-100 to permeabilize the layer. In the former experiments, we perfused for 10 min with 300 m*M* KI and 500 m*M* sucrose, and then for 1 h with standard buffer containing primary K^+ channel antibody (1:500 dilution). After a wash with standard buffer for 30 min, we perfused with secondary antibody (goat anti-rabbit/Oregon Green, Molecular Probes Inc., Eugene, Oregon) at the recommended dilution of 1:200, followed by a wash with standard buffer for 30 min. In the experiments with Triton-X-100, we perfused with standard buffer containing 4% paraformaldehyde for 1 h, followed by perfusion with 0.2% Triton-X-100 in standard buffer for 1 h. Antibodies were applied as above. The axon was subsequently tied closed at both ends, removed from the chamber, and mounted on a slide with Aqua Poly/Mount (Polysciences, Warrington, Pennsylvania). The preparation was viewed either with a confocal laser microscope or conventional epifluorescence. Control preparations were treated in the same way as the test axons, but with the K^+ channel antibody replaced by an antibody that does not cross-react with squid.

Observed by conventional epifluorescence microscopy, the test axons were intensely immunofluorescent in discrete areas or patches throughout the membrane, with a spacing of ~25 μm between patches (Fig. 2A). A pattern in the immunostaining was not clearly apparent, although the punctate patches of fluorescence appeared to lie along linear elements longitudinally oriented along the axon. The result in Figure 2A was obtained with the KI pretreatment described above. A control preparation (different axon) for these conditions is shown in Figure 2B in which the SqKv1A antibody was replaced with a K^+ channel antibody that does not crossreact with squid. All other procedures were the same as for the test result. A clear fluorescence signal was not observed, which demonstrates lack of nonspecific binding by the secondary antibody (Fig. 2B). Results similar to those in Figure 2A were obtained when fixation and permeabilization of the cortical axoplasm layer was carried out with Triton-X-100, as described above. Using confocal laser microscopy, we observed in test preparations a

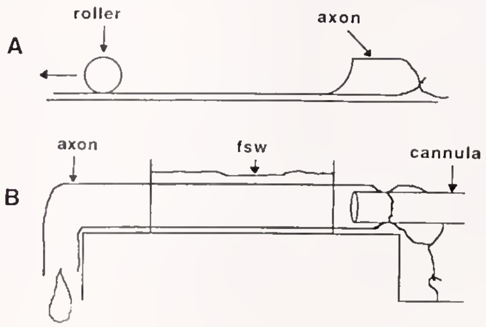

Figure 1. *Schematic diagram illustrating the method for intracellular perfusion of antibodies in the squid giant axon. See text for details.*

---

[1] Laboratory of Neurophysiology, National Institute of Neurological Disorders and Stroke, National Institutes of Health, Bethesda, Maryland 20892.

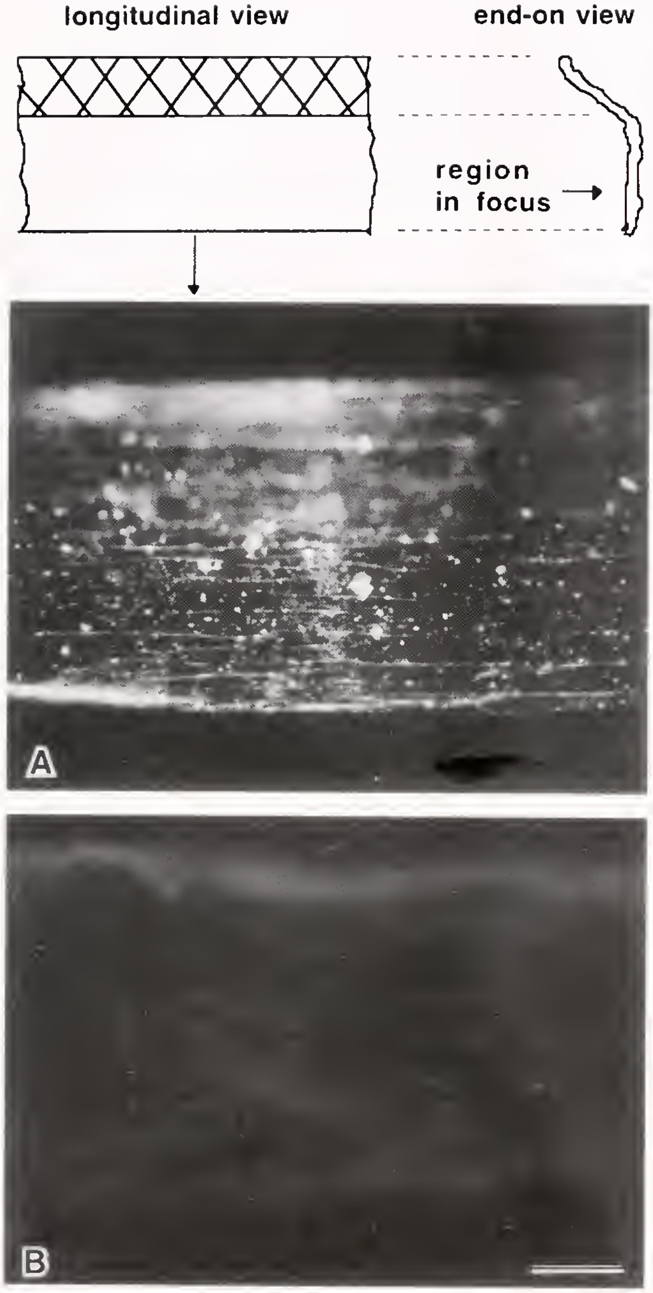

Figure 2A. *Epifluorescent image of immunolabeled K⁺ channels in an intracellularly perfused squid giant axon. Without the central axoplasmic core, the unsupported axonal membrane folded and collapsed as it was mounted on the slide (top panel). The bottom part of the image (in focus) illustrates patches of immunofluorescence from two membrane surfaces. The top part of the image (out of focus) showed staining similar to that in the bottom part of the image when it was brought into focus. B. Epifluorescent image of an axon (different than the one described in A) perfused with a K⁺ channel antibody that does not crossreact with squid. All other experimental procedures were the same as the test axon, as described in the text. The bar below this image represents 100 μm (same for A and B).*

diffuse signal throughout the membrane—not present in the control axons—in addition to the patches of intense immunofluorescence shown in Figure 2A. Preliminary results with immunogold suggest that the immunofluorescence is attributable to K^+ channels in the axonal membrane rather than to K^+ channel containing vesicles which have not been removed during extrusion of the axoplasm. Our results provide further support to the argument that SqKv1A mediates the classic delayed rectifier potassium ion current in the squid giant axon (4).

Punctate ion-channel immunofluorescence has been observed in a number of preparations. The results most relevant to this study are those of Johnson *et al.* (8). They demonstrated, in cultured *Aplysia* axons, clusters of Na^+ channels that were separated by regions where channels were not present, *i.e.*, similar to nodes of Ranvier in myelinated axons (9). Our results are consistent with the punctate nature of immunofluorescence observed in *Aplysia* axons, but the patches of fluorescence in squid axons appear to be uniform throughout. We speculate that the membrane patches of ion channels suggested by the results in Figure 2A are targets for K^+ channel-containing vesicles, which we have isolated from the axoplasm and which may be involved in turnover of ion channels in the membrane (J. R. Clay and A. M. Kuzirian, unpublished). The punctate distribution of immunostaining is very similar to clustering of Kv1 channels by PDZ proteins in heterologous expression systems (10). We note that the squid SqKv1A K^+ channel does have a consensus sequence for PDZ protein binding at its C terminus (4, 10). However, it is premature to speculate on the role of PDZ proteins in the clustering of K^+ channels in squid axons.

We gratefully acknowledge William Gilly and Zora Lebaric for generous gifts of their K^+ channel antibodies.

Literature Cited

1. **Hodgkin, A. L., and A. F. Huxley. 1952.** *J. Physiol. (Lond.).* **116:** 449–472.
2. **Otis, T. S., and W. F. Gilly. 1990.** *Proc. Natl. Acad. Sci. U.S.A.* **87:** 2911–2915.
3. **Rosenthal, J. J. C., and W. F. Gilly. 1993.** *Proc. Natl. Acad. Sci. U.S.A.* **90:** 10026–10030.
4. **Rosenthal, J. J. C., R. G. Vickery, and W. F. Gilly. 1996.** *J. Gen. Physiol.* **108:** 207–219.
5. **Brown, A., and R. J. Lasek. 1990.** Pp. 235–302 in *Squid as Experimental Animals*, D. L. Gilbert, W. J. Adelman, Jr., and J. M. Arnold, eds. Plenum Press, New York.
6. **Baker, P. F., A. L. Hodgkin, and T. I. Shaw. 1961.** *Nature* **190:** 885–887.
7. **Adelman, W. J., Jr., and D. L. Gilbert. 1964.** *J. Cell. Comp. Physiol.* **64:** 423–428.
8. **Johnson, W. L., J. R. Dyer, V. F. Castellucci, and R. J. Dunn. 1996.** *J. Neurosci.* **16:** 1730–1739.
9. **Dugandzija-Novakovic, S., A. G. Koszowski, S. R. Levinson, and P. Shrager. 1995.** *J. Neurosci.* **15:** 492–503.
10. **Sheng, M., and M. Wyszynski. 1997.** *Bioessays* **19:** 847–853.

Reference: *Biol. Bull.* **197:** 233–234. (October 1999)

Evaluation of Circadian Rhythms in the *Limulus* Eye

Vanessa J. Ruta, Frederick A. Dodge, and Robert B. Barlow
(Marine Biological Laboratory, Woods Hole, Massachusetts 02543)

The visual system of the horseshoe crab, *Limulus polyphemus*, shows a remarkable circadian rhythm in sensitivity. About the time of sunset, a circadian oscillator in the brain of the animal generates efferent optic nerve signals to the lateral eye modulating both its structure and function. The overall increase in sensitivity nearly compensates for the reduction in ambient light at night (1, 2). High nighttime visual sensitivity appears to be important for mating, a visually guided behavior that the animals can accomplish as well at night as in the day (3). The mechanisms underlying the elegant adaptation of the *Limulus* eye to dim nighttime illumination include anatomical changes in the retina that increase photon catch at the expense of spatial resolution, and physiological changes that enhance the summation of photon events at the expense of temporal resolution.

Here we evaluate further the effect of the circadian clock on two properties that shape the dynamics and strength of the eye's response. We first asked whether the elevated nighttime response resulted from a clock-induced reduction in the strength of lateral inhibitory interactions between ommatidia. We then asked whether the loss of temporal resolution at night resulted from an increase in the dispersion of latencies of optic nerve responses. We report here that the circadian clock does not change the latencies of the optic nerve responses but decreases the strength of lateral inhibition at night.

To evaluate the possible clock influence on the strength of lateral inhibitory interactions, we compared the steady state optic nerve discharge of a single dark-adapted ommatidium over a wide range of light intensities during the day and at night. To maximize the inhibitory influences exerted on the recorded ommatidium, we uniformly illuminated the entire eye by placing a Teflon diffusing screen in contact with the cornea and illuminating it with a large (5 mm) light pipe (4). We recorded the intensity response function of the single optic nerve fiber during the day. At dusk efferent optic nerve fiber activity begins to transform the retina to its highly sensitive nighttime state, and we tracked the transformation by measuring the shift in threshold of the dark-adapted ommatidium. We define threshold as the intensity of brief (35 ms) test flashes to which the optic nerve responds 50% of the time; test flashes are triggered at 20 s intervals allowing complete decay of lateral inhibition. We remeasure the intensity-response function about 2100 h when the eye has attained its nighttime state.

Figure 1A shows the intensity response functions for a single dark-adapted ommatidium during the day and at night. Plotted are the steady-state optic nerve responses as a function of the log of the light intensity. To compare the level of lateral inhibitory interactions in the two states of the retina, we subtracted the mean rate of spontaneous activity from all steady-state responses. We then shifted the nighttime intensity-response function to the right to account for the increase in sensitivity as measured by the threshold shift (5). Barlow and Fraioli (4) reported that inhibitory effects are not detectable at low firing rates (~1–2 impulses/s). Note that in Figure 1A the "Night" and "Day" functions separate above ~5 impulses/s. The elevated nighttime responses indicate a weakening of lateral inhibition. At firing rates greater than 10 impulses/s another circadian mechanism comes into play—one that increases response gain. The increased gain at night is thought to result from a reduction in the efficacy of a voltage-dependent light adapting mechanism which acts to reduce the eye's response to light during the day (5). The contribution of increases in response gain to the separation of the two functions limits our ability to evaluate the clock's role in lateral inhibition strength at higher light intensities.

For a more quantitative measure of the changes in lateral inhibition at night, independent of the changes in gain, we designed a second experiment in which lateral inhibition was induced by antidromic stimulation of the optic nerve trunk. We recorded the response of a single, optically-isolated ommatidium to a steady 30-s light stimulus and every two seconds applied a brief (100 ms) train of four current pulses to the optic nerve trunk. To avoid transients at the onset of illumination, we discarded the response to the first antidromic stimulus, averaged the following 14 responses, and plotted the two-second cycle averages in Figure 1B. Brief periods of inhibition occur immediately following the antidromic stimuli (0.9–1.0 s). In addition to exerting inhibition, antidromic stimulation also activates the efferent fibers, simulating the circadian clock and driving the retina into the higher sensitivity nighttime state (1). We reduced the light intensity by over 300 times to compensate for the increased sensitivity of the eye and maintain roughly the same firing rate as in the daytime state. Note that the depth and duration of inhibition in the nighttime state (thick black line) are less than in the daytime state (thin black line). As measured by the change in response rate, inhibition is approximately 60% less in the nighttime state. Other experiments exhibited equivalent or smaller decreases in inhibition. After cessation of efferent input, inhibition (broken line) recovered to that recorded during the daytime state.

To monitor response latencies of the dark-adapted retina, we measured the delay of the optic nerve response to a brief (35 ms) test flash. As in the experiment shown in Figure 1A, we adjusted the intensity of the test flash to produce a threshold response of 50%. Figure 1C shows a histogram of the latencies of response for both the day and nighttime state of the retina. During the day, the average latency of response at threshold was 140 ± 21 ms. After converting the eye into the nighttime state by delivering current pulses to the optic nerve, the threshold intensity decreased tenfold, but the average response latency remained unchanged (145 ± 22 ms). There is no significant change in either the length of the latency of response or in the distribution of latencies as a consequence of circadian input.

We conclude that the clock increases retinal sensitivity with a concomitant reduction in lateral inhibition but without a significant change in the latency between the absorption of a photon and the discharge of an optic nerve impulse.

Literature Cited

1. **Barlow, R. B., S. J. Bolanowski, and M. L. Brachman. 1977.** *Science* **197:** 86–89.
2. **Barlow, R. B., S. C. Chamberlain, and J. Z. Levinson. 1980.** *Science* **210:** 1037–1039.
3. **Barlow, R. B., R. B. Ireland, and L. Kass. 1982.** *Nature* **296:** 65–66.
4. **Barlow, R. B., and A. J. Fraioli. 1978.** *J. Gen. Physiol.* **71:** 699–718.
5. **Barlow, R. B., E. Kaplan, G. H. Renninger, and T. Saito. 1987.** *J. Gen. Physiol.* **89:** 353–378.

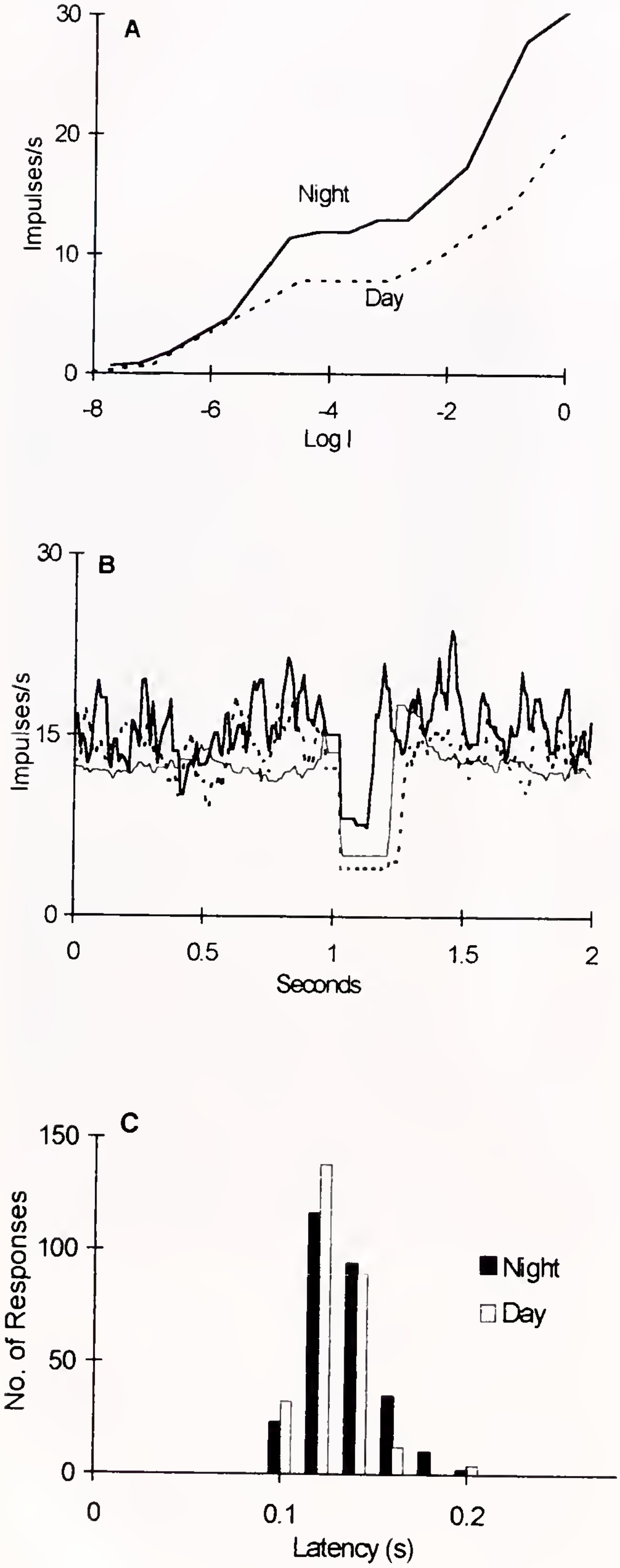

Figure 1. *Input from the circadian clock in the nighttime eye increases sensitivity by weakening lateral inhibition but does not affect the dispersion of response latencies. (A) Intensity functions of the steady-state response of a single dark-adapted ommatidium in a* Limulus *eye during the day and at night. The steady-state response is defined as the last 2 s of a 5-s light flash, although at low intensities the flash duration and the count interval were increased to compensate for variability in the spike discharge. The whole eye was uniformly illuminated by placing a Teflon diffusion screen over the eye. At log I = 0 the light incident on a single ommatidium was ~10^{12} photons/s. (B) Inhibition of the response of a single ommatidium by antidromic stimulation of the optic nerve in the daytime state (thin black line), in the simulated nighttime state (thick black line), and after recovery back to the daytime state (broken line). (C) The dispersion of optic nerve response latencies is not affected by efferent input. The histogram for the daytime state includes the latencies of 275 responses and that for the nighttime state includes the latencies of 280 responses.*

Reference: *Biol. Bull.* **197:** 235–236. (October 1999)

Photoreceptor Pigments of the Blueback Herring (*Alosa aestevalis,* Clupeidae) and the Atlantic Silverside (*Menidia menidia,* Atherinidae)

Iñigo Novales Flamarique and Ferenc I. Hárosi
(Marine Biological Laboratory, Woods Hole, Massachusetts 02543)

Since the discovery of an ultraviolet (UV) visual pigment in the retina of the Japanese dace (1), other freshwater fishes have been found to possess UV pigments (2). Among marine species, UV pigments have been reported for the adults of only one tropical species (3). Here we examine the pigments in the retinal cones from two marine coastal species, the blueback herring and the Atlantic silverside. The blueback herring is strictly a saltwater species (stenohaline), whereas the Atlantic silverside is euryhaline; *i.e.,* it can live in a wide range of salinities. Both the Atlantic silverside and the juvenile blueback herring inhabit coastal surface waters (<10 m depth) where light from 320–800 nm is available to stimulate all potential photoreceptor types (UV, blue, green, and red) present in fish retinas. Adult blueback herring also dwell in deeper waters (50–100 m) where UV light is absent and the spectrum narrower and centered around 560 nm (4).

We used the technique of microspectrophotometry (MSP) to measure photoreceptor pigments *in situ.* After enucleation of the eye from a recently euthanized dark-adapted animal, pieces of retina were extracted and teased apart in Ringer solution. These pieces were placed between coverslips, and individual photoreceptors lying on their sides were examined with the dichroic microspectrophotometer (5). Sample measurements were carried out by placing a beam of light (0.6 × 2 μm cross section) on the structure of interest and taking an average of eight consecutive transmission scans from 270–648 nm. Similarly, reference measurements were recorded from adjacent areas devoid of tissue, and sample absorbance was computed in 2 nm increments (5).

The blueback herring showed single cones, double cones, and rods. The single cones were sensitive to blue or short (S) wavelengths with maximum absorbance (λ_{max}) at 447 nm. The double cones were composed of a green or middle (M) wavelength-sensitive cone (λ_{max} = 517 nm) and a red or long (L) wavelength-sensitive cone (λ_{max} = 566 nm). The λ_{max} of the rod was 510 nm (Figs. 1A, B). The average spectral bandwidth at half maxima for the cones and the rod was about 4000 cm^{-1}. This measurement suggests that the primary visual pigment chromophore in this retina is vitamin A_1 (6).

The retina of the Atlantic silverside also showed rods, as well as single and double cones; but the distal parts of the cones' inner segments and the pigment spectra were different from those in the blueback herring. Double cones in the Atlantic silverside were of two kinds, M/L and L/L pairs. The average λ_{max} of the M pigment was 472 nm, while that of the L pigment was 580 nm (Fig. 1D). M/L pairs exhibited pinkish globular structures at the distal end of their inner segments, termed ellipsosomes (7). These organelles were first documented in the double cones of killifishes and guppies and are known to be of mitochondrial origin (7). The M ellipsosome had the highest absorbance, with a spectral profile indicative of cytochrome-c (Fig. 1E). Ellipsoid absorbance by the L member was always lower than that of the M member (Fig. 1F). L/L double cones showed an ellipsosome in one member with absorbance similar or higher than that of the L member in M/L pairs, and minute traces of cytochrome-c in the other member. There were two types of single cones: large ones (S cones) with inner segment structures that looked exactly like ellipsosomes, but did not contain any cytochrome-c (pseudoellipsosomes, Fig. 1F), and smaller ones with normal ellipsoids. The average λ_{max} of the S cones was 410 nm (Fig. 1C). Although we were unable to secure good average spectra from the smaller cones, our records nonetheless show that they contain a UV pigment (λ_{max} around 365 nm). The average spectrum of the rod peaked at 511 nm (Fig. 1C), and its half bandwidth was ~4010 cm^{-1}. The latter is indicative of a visual system predominantly based on vitamin A_1.

The pigment complement found in the retina of the blueback herring resembles that of other stenohaline fishes and may be the basis for maximal quantal catch over an extensive depth range, > 0–100 m (8). Fishes that live closer to the water surface, where UV and blue wavelengths are more prevalent, may instead benefit from a pigment complement shifted toward shorter wavelengths, as with the Atlantic silverside. If the presence of UV cones in the Atlantic silverside were confirmed, the visual pigment complement of this fish would then be similar to those of the killifishes, with λ_{max} at 360, 410, 470 and 570 nm for the cones, and at 510 nm for the rods (2). Beyond the visual pigments, these euryhaline species also share the presence of ellipsosomes in double cones, which were previously hypothesized to act as optical filters for the reduction of β-band absorption by M cones (7). A similar mechanism could operate here to improve discrimination and contrast detection at short wavelengths. Since the Atlantic silverside is often found in the same habitat as the killifishes, the similarities in their visual systems may be due to convergent evolution.

Literature Cited

1. **Hárosi, F. I., and Y. Hashimoto. 1983.** *Science* **222:** 1021–1023.
2. **Hárosi, F. I. 1991.** *Vision Res.* **34:** 1359–1367.
3. **McFarland, W. N., and E. W. Loew. 1994.** *Vision Res.* **34:** 1393–1396.
4. **Novales Flamarique, I., and C. W. Hawryshyn. 1993.** *Can. J. Fish. Aquat. Sci.* **50:** 1706–1716.
5. **Hárosi, F. I. 1987.** *J. Gen. Physiol.* **89:** 717–743.
6. **Bridges, C. D. B. 1967.** *Vision Res.* **7:** 349–369.
7. **MacNicholl, E. F. Jr., Y. W. Kunz, J. S. Levine, F. I. Hárosi, and B. A. Collins. 1978.** *Science* **200:** 549–552.
8. **Hárosi, F. I. 1996.** *Biol. Bull.* **190:** 203–212.

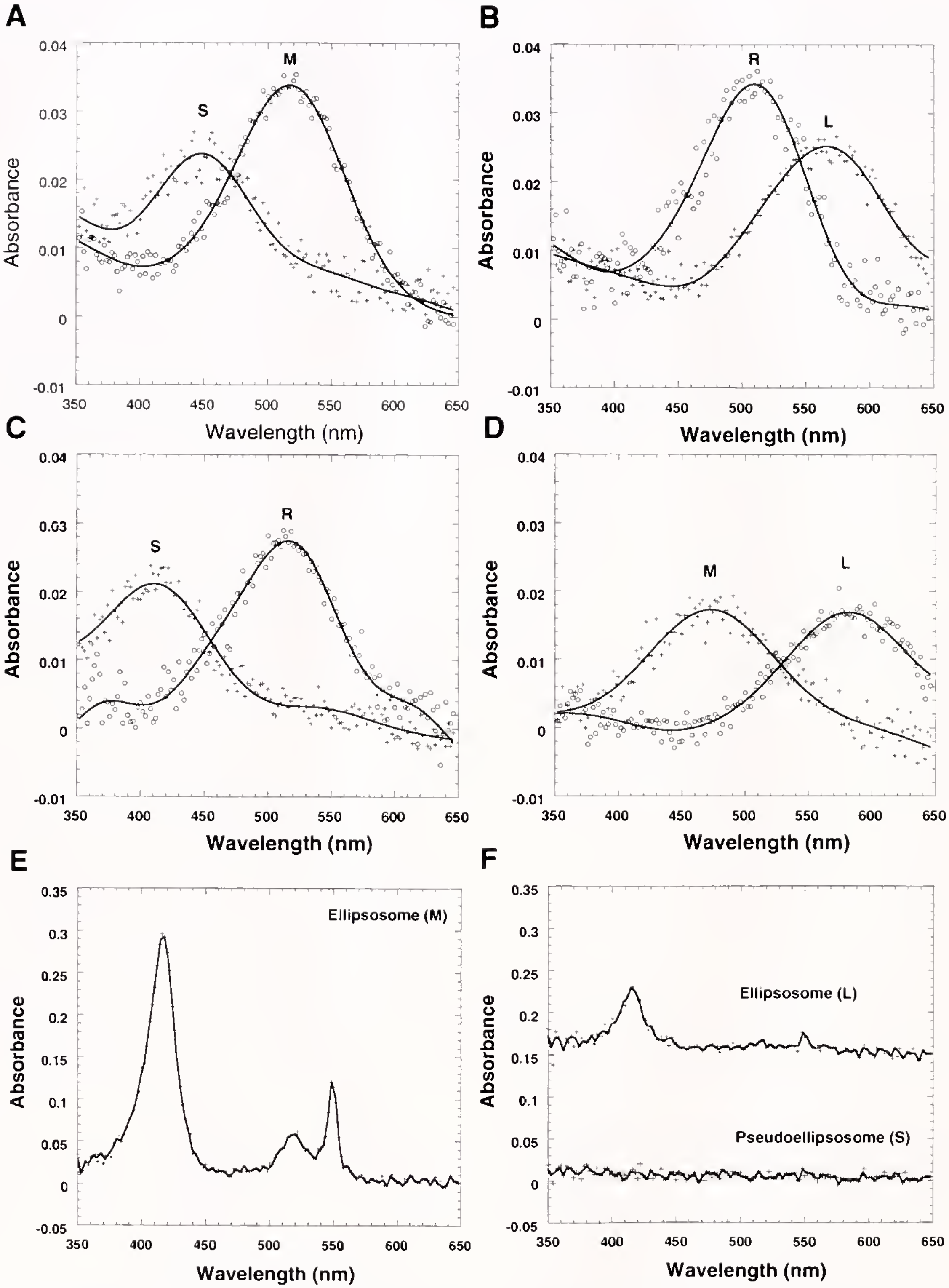

Figure 1. *Photoreceptor pigments of the blueback herring and the Atlantic silverside. (A, B) Blueback herring: average spectral absorbances of the S* (n = 3)*, M* (n = 13) *and L* (n = 11) *cones, and the rod (R,* n = 6*). (C, D) Atlantic silverside: average spectral absorbances of the S* (n = 9)*, M* (n = 11) *and L* (n = 15) *cones, and the rod (R,* n = 8*). (E, F) Atlantic silverside: typical ellipsosomes of the M and L members of double cones, and pseudoellipsosome of the S cone. A value of 0.15 has been added to the L ellipsosome trace to separate it from that of the S pseudoellipsosome. Ellipsosomes exhibited the typical cytochrome-c spectrum with a prominent Soret (γ) peak at 414 nm, and secondary β and α peaks at 518 nm and 548 nm, respectively.*

Reference: *Biol. Bull.* **197:** 237–238. (October 1999)

Soft-sided Tanks Improve Long-term Health of Cultured Cuttlefish

Janice S. Hanley, Nadav Shashar[1]*, Roxanna Smolowitz, William Mebane, and Roger T. Hanlon (Marine Resources Center, Marine Biological Laboratory, Woods Hole, Massachusetts 02543).*

The common European cuttlefish, *Sepia officinalis* Linnaeus, 1758, is being cultured in captivity to provide experimental animals for biological and biomedical research, and for testing methods applicable to larger-scale mariculture. This species adapts quite well to captivity, and several generations of cuttlefish have been grown in facilities in Europe and the United States (*e.g.*, 1–5). However, while jetting away from other animals during social interactions, or from human observers who have inadvertently startled them, cuttlefish occasionally collide into the walls of holding tanks (3). Moreover, recent work by Boal *et al.* (7) shows that social interactions (many of them deleterious) increase substantially when sub-adult and adult cuttlefish are maintained or cultured in higher densities, which they usually are. The accumulated damage to the skin caused by the collisions (see also 6) often contributes substantially to mortalities in the course of the one-year life cycle. Repetitive collision causes trauma, particularly to the posterior mantle tip, because the cuttlefish are most often jetting backwards when they hit the wall. The mantle tip is particularly vulnerable because the layer of muscle and skin overlying the posterior tip of the cuttlebone is quite thin. As a result, focally extensive, deep ulcerative dermatitis and cellulitis develop. We term this posterior mantle tip dermatitis (PMTD). Severe cases result in hemolymph loss, bacteremia, and death. Subacute, chronic cases result in fibrosing cellulitis and abnormal cuttlebone formation at the posterior apex; occasionally, the apex of the cuttlebone fractures. Because culturing a cuttlefish through its life cycle is expensive, methods that will increase survival to adulthood need to be developed.

We counted collisions for a total of 7 h over 3 days; the cuttlefish were males of about 1 kg, and females of about 0.5 kg. Collisions with tank walls can occur quite frequently: we counted rates of 0.75–1.25 events per animal per hour in a variety of tanks (n = 4 tanks), even when the animals were relatively calm (*e.g.*, when they were not sexually active, when the tanks contained only females or immature animals, and when human distraction was minimized). These rates increased to over 4.0 wall collisions per animal per hour when the animals were sexually active (*e.g.*, when two males were placed in a tank with mature females, or when human observers startled the cuttlefish).

Hulet *et al.* (8) suggested that a "bumper system" be installed along the walls of squid holding tanks to reduce skin damage from collisions with the hard surfaces. Modifying their concept, we have developed a simple system in which black plastic cushioning curtains were hung parallel to, and 10 cm away from, the inner surfaces of the tank walls (Fig. 1). The resulting holding arena was smaller—1.65 × 1.3 m (surface area = 2.145 m^2)—than the control tank. Water depth was held at 0.28 m, providing an overall volume of 0.6 m^3.

An identical control tank (1.85 × 1.5 × 0.28 m, surface area = 2.775 m^2, volume = 0.777 m^3) was set adjacent to the experimental tank. Animals in both tanks experienced the same water input, outside disturbances, light conditions, cleaning schedule, etc. Since no space was taken by cushioning curtains, the cuttlefish could roam through the entire volume of the control tank.

Hulet *et al.* (8) used cushioning walls that created a slope between the bottom of the tank and its hard walls. Although this design greatly reduced the impact when the side surfaces were hit, it restricted water movement behind this angled curtain, so the medium became increasingly anoxic, and hydrogen sulfide built up. The new tank design circumvents the water quality problem. First, we are using a flow-through seawater system and no substrate. We improved water circulation by placing the cushioning curtains parallel to the tank walls and by pumping fresh seawater into the area between the curtains and the walls. Two airlift pumps were used, each working at 9.45 l/min (2.5 gal/minute); the pumps were placed near the curtains at opposite sides of the tank and moved water from behind the curtains to the central area. The volume of water behind the curtains was 176.4 liters, and with both pumps operating that entire volume could be exchanged approximately every 9.3 minutes. No significant difference in pH or in oxygen concentration was found between the water in the control tank and that in the center arena of the experimental tank, or in the area between the cushioning curtains and the walls of the experimental tank.

Two sequential trials were conducted. In each trial, 4 sexually mature cuttlefish (2 males and 2 females, all free of any body

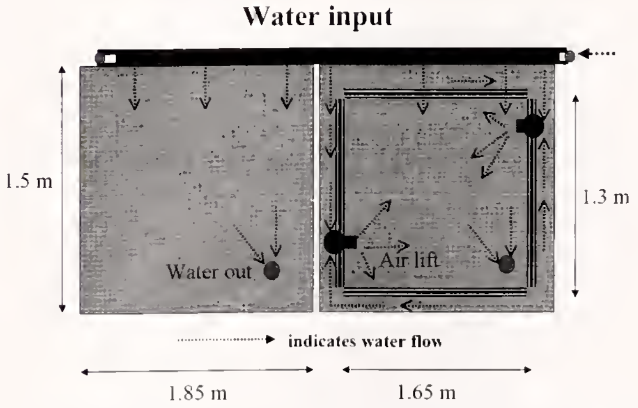

Figure 1. *Setup for testing the use of cushioning curtains in cuttlefish holding tanks. Left, a control tank. Right, the experimental tank with the cushioning curtain (bold lines) set along its sides. Two airlifts moved water from behind the curtain to the center of the tank, thus maintaining high-quality water on both sides of the curtain.*

---

[1] Hebrew University, H. Steinitz Interuniversity Institute, P.O. Box 469, Eilat 8800, Israel.

injury) were placed in each tank. Hence, the density in the experimental tank was slightly higher than in the control tank (0.54 *vs.* 0.69 m^2 per cuttlefish, respectively). The health of these adult animals was monitored throughout the trials.

Trial 1 lasted for 40 days. On day 11, one of the cuttlefish in the control tank developed PMTD. On day 17, a second cuttlefish in the control tank developed PMTD. None of the animals in the experimental tank showed any signs of PMTD, although two animals developed unrelated illnesses.

Trial 2 was conducted with four new healthy cuttlefish in each tank (2 males, 2 females). In the control tank, PMTD first occurred at day 7, and this animal died on day 11; thus animal density in this tank was lower during the remainder of the trial. By day 26, the three remaining animals in this tank showed PMTD; one died on day 42, one on day 49, and one is still alive at this writing (day 105). Once again, in contrast, none of the animals in the experimental tank developed PMTD. More importantly, the second trial is still in progress, and all four cuttlefish in the experimental tank are completely free of PMTD at day 105. Overall, for both trials, none of the 8 cuttlefish in the tank equipped with the cushioning sides exhibited PMTD, as compared with 6 out of 8 (75%) of the animals in the control tank (χ^2, $P < 0.014$).

The new tank design increases the maintenance effort in rearing the cuttlefish. Eight additional surfaces must be scrubbed as compared with traditional hard-sided holding tanks. Furthermore, the soft sides of the tank are more difficult to scrub than hard surfaces. Nevertheless, the efforts are worthwhile because cuttlefish nurtured through the life cycle in captivity have a relatively high value. Although our tank design did not reduce the number of social interactions among cuttlefish, which occur even at low densities (7), it reduced the resulting skin damage experienced by the animals, and thus increased their longevity.

Acknowledgments

We thank Geoff Till for help in culturing the animals, and Aaron Hoffman for animal observations. This study was partly supported by NSF Grant IBN 9729598.

Literature Cited

1. **Schroeder, W. 1966.** *Sber. Ges. naturf. Freunde* (N.F.) **6:** 101–107.
2. **Pascual, E. 1978.** *Invest. Pesq.* **42(2):** 421–442.
3. **Forsythe, J. W., R. T. Hanlon, and R. DeRusha. 1991.** Pp. 313–323 in *The Cuttlefish*, E. Boucaud-Camou, ed. Centre de publication de l'Université de Caen, France.
4. **Forsythe, J. W., R. H. DeRusha, and R. T. Hanlon. 1994.** *J. Zool. Lond.* **233:** 175–192.
5. **Hanley, J. S., N. Shashar, R. Smolowitz, R. A. Bullis, W. N. Mebane, H. R. Gabr, and R. T. Hanlon. 1998.** *Biol. Bull.* **195:** 223–225.
6. **Hanlon, R. T., and J. W. Forsythe. 1990.** Pp. 23–46 in *Diseases of Marine Animals. Vol. III: Cephalopoda to Urochordata*, O. Kinne, ed. Biologische Anstalt Helgoland, Hamburg, Germany.
7. **Boal, J. G., R. A. Hylton, S. A. Gonzalez, and R. T. Hanlon. 1999.** *Contemp. Top. Lab. Anim. Sci.* **38:** 49–55.
8. **Hulet, W. H., M. R. Villoch, R. F. Hixon, and R. T. Hanlon. 1979.** *Lab. Anim. Sci.* **29:** 528–533.

Reference: *Biol. Bull.* **197:** 239–240. (October 1999)

Physiological Characterization of Supramedullary/Dorsal Neurons of the Cunner, *Tautogolabrus adspersus*

S. J. Zottoli, F. R. Akanki, N. A. Hiza, D. A. Ho-Sang Jr., M. Motta, X. Tan, K. M. Watts
(Department of Biology, Williams College, Williamstown, Massachusetts 01267) and E.-A. Seyfarth[1]

The somata of large neurons can be found on the dorsal surface of the medulla oblongata (supramedullary neurons) and spinal cord (dorsal cells) in many teleost fish (1, 2). Thirty-five to forty of these neurons are arranged in a single, median, longitudinal row, from the posterior end of the fissura rhomboidalis through the anterior portion of the spinal cord of the cunner, *Tautogolabrus adspersus* (3). Comparative physiological studies have indicated that these cells in the cunner and other teleost fish make electrotonic connections with one another, and that they respond to tactile inputs from the skin (4). We report on some physiological properties of these cells with the ultimate goal of determining their function.

Cunner, 9.8–11.5 cm in body length, were secured in a holding chamber and a respiratory current of chilled water was passed through the mouth and over the gills. D-tubocurarine was injected intramuscularly. After the application of local anesthetic (20% benzocaine, Ultradent, Inc.), the medulla oblongata and rostral spinal cord were exposed and single microelectrode recordings (KCl-filled; 8–11 MΩ) were made from dorsal cell somata. The skin was stimulated either electrically with bipolar stainless-steel electrodes, or mechanically with a probe mounted on the face of an audio speaker. A sphere, 2-mm in diameter, located at the end of the probe contacted the skin.

In 17 neurons from 6 fish, resting potentials ranged from −56 to −71 mV (mean = −64.5), and evoked action potentials ranged in amplitude from 92–115 mV (mean = 103.7). Intracellular depolarization caused repetitive firing with no apparent change in spike height (Fig. 1A). Electrical stimulation of the skin resulted in depolarizations that, in some cases, could activate the dorsal cells (Fig. 1B1). Repetitive stimulation of the skin at rates of about 1 per 15 s reduced the depolarizations (Fig. 1B2, arrow) revealing long-duration post-synaptic potentials (PSPs). PSPs were graded and were depressed at stimulation rates of 1 per s (Fig. 1B3). PSPs could be evoked from many but not all skin locations in an individual neuron, suggesting that each cell may have a different pattern of skin innervation. Mechanical stimulation of the skin just caudal to the posterior limit of the dorsal fin produced PSPs in many cells. An action potential was elicited when these PSPs were combined with subthreshold intracellular depolarization of the somata (Fig. 1C). The apparent firing level in Figure 1C is much lower than that in Figure 1B. Thus, the impulse is most likely arising at a distance from the soma. This interpretation is consistent with results from the puffer that indicate that synapses and the site of physiological impulse initiation are far from the soma (5).

Supramedullary neurons in puffer and other teleost fish are electrotonically coupled and discharge synchronously to tactile stimulation (6). These neurons also respond to visual stimulation and saccular movement in the toadfish and boxfish (7). The activity of these cells in puffer is correlated with an efferent discharge in the dorsal roots (5). Immunohistological studies of the puffer supramedullary cells indicate that they project to cutaneous mucous glands and the epidermal layer of the skin (8). We speculate that these neurons in cunner and puffer discharge in response to skin stimulation that is associated with a threat. We also suggest that the output of supramedullary/dorsal neurons affects mucous secretion that may aid in protection from predation or may help prevent infection from a wound that would follow a predatory strike.

This work was supported in part by Howard Hughes Medical Institute and Essel Foundation grants to Williams College. We thank Liz Jonas and Len Kaczmarek for their support during this study.

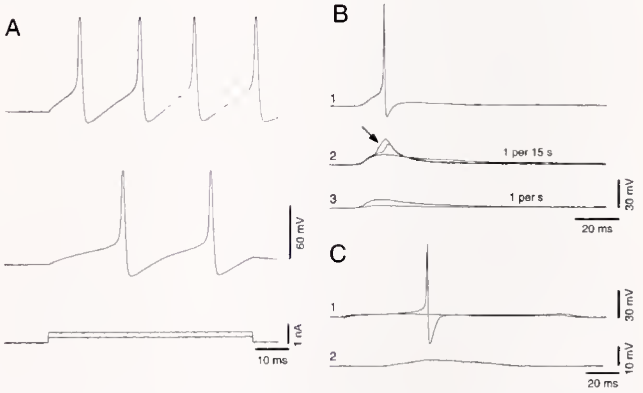

Figure 1. *Physiological responses of supramedullary/dorsal neurons to electrical and mechanical stimulation. A. Response of a neuron to two levels of intracellular current injection (bottom traces). Current was injected for 60 ms and membrane voltage was recorded with a single electrode using bridge-balanced mode of an Axoclamp 2A amplifier. With increased current the cell shows increased rates of discharge from the middle to the upper trace. B (1) Electrical stimulation of the skin excites the cell. (2) Discrete depolarizations (arrow) are lost with repetitive stimulation (1 per 15 s) revealing a long-lasting PSP (every other stimulus is shown). (3) The PSP amplitude is depressed at stimulation rates of 1 per s (intervening stimuli between the last stimulus in 2 and the first in this panel are not shown). C. Mechanical stimulation causes a PSP that, when combined with a subthreshold intracellular stimulation, elicits an action potential. C1. Superimposed traces of a subthreshold intracellular stimulation (no action potential) and a mechanical stimulus (10 ms delay) combined with the subthreshold intracellular stimulation (action potential). C2. PSP, shown at higher gain, was evoked by mechanical stimulation alone.*

---

[1] Zoologisches Institut, J. W. Goethe-Universität, D-60054, Frankfurt a.M., Germany.

Literature Cited

1. **Marini, M., and I. Benedetti. 1992.** Pp. 217–236 in *Neurology Today*. I. Benedetti, B. Bertolini, and E. Capanna, eds. Selected Symposia and Monographs U.Z.I., 7, Mucchi, Modena.
2. **Zottoli, S. J., E.-A. Seyfarth, C. J. Tyler, and D. S. Palmer. 1999.** *Neurosci. Abstr.* **25:** 104.
3. **Sargent, P. E. 1899.** *Anat. Anz.* **15:** 212–225.
4. **Bennett, M. V. L. 1960.** *Biol. Bull.* **119:** 303.
5. **Bennett, M. V. L., S. M. Crain, and H. Grundfest. 1959.** *J. Gen. Physiol.* **43:** 221–250.
6. **Bennett, M. V. L., Y. Nakajima, and G. D. Pappas. 1967.** *J. Neurophysiol.* **30:** 161–179.
7. **Barry, M. A., M. Weiser, R. Baker, and M. V. L. Bennett. 1986.** *Biol. Bull.* **171:** 490–491.
8. **Funakoshi, K., T. Kadota, Y. Atobe, M. Nakano, R. C. Goris, and R. Kishida. 1998.** *Neurosci. Letters* **258:** 171–174.

Reference: *Biol. Bull.* **197:** 240–241. (October 1999)

Sharpening of Directional Auditory Input in the Descending Octaval Nucleus of the Toadfish, *Opsanus tau*

R. R. Fay and P. L. Edds-Walton
(Parmly Hearing Institute, Loyola University Chicago, Chicago, Illinois 60626)

This investigation concerns the fate of acoustic directional encoding in the medulla of *Opsanus tau*. The descending octaval nucleus (DON) is the nucleus receiving the majority of auditory input from the saccule. Previous work has shown that saccular afferents encode directional auditory information that could be used to determine the location of a sound source (1, 2). Each saccular afferent projects to multiple sites along the rostral-caudal axis of the DON (3). Most saccular afferents show a cosinusoidal response pattern to motional stimuli in the horizontal and mid-sagittal planes (2). Recently, we reported that directional auditory responses were present in the DON (4). In this study, we examine directional response properties of cells in the DON that were sharpened compared to primary saccular afferents.

Prior to surgery, the toadfish was anesthetized lightly (3 aminobenzoic acid), and the tail muscles were paralyzed (pancuronium bromide). The dorsal surface of the cranium was removed to expose the left lateral surface of the medulla between the posterior ramus of the eighth cranial nerve ($\mathrm{VIII_p}$) and cranial nerve IX, near the rostral and mid-region of the DON, respectively. The fish's head was secured in a circular dish (containing seawater) that is mounted on a three-dimensional shaker table described in detail elsewhere (2). Minishakers produced sinusoidal, translatory motion of the dish in the horizontal and mid-sagittal planes at 30° intervals. This stimulus simulates the particle motion component of underwater sound.

Extracellular recordings were made using woodsmetal-filled electrodes (4, 5), with 10–12 μm tip diameters and NaCl-filled capillary tubes with 5–7 μm tips and resistances of 3–8 mΩ. These electrodes produced comparable data. A three-axis micromanipulator was used to position the electrode, and recording sites were documented by noting micromanipulator position during recording. Neurobiotin was injected (4% in 2*M* NaCl, 1900–2000 nA for 10–20 min) once per animal at an auditory site. This procedure helped document recording location for use in future neuroanatomical analyses.

The 88 recordings made in the DON contain two categories of directional responses: primary-like and sharpened. Primary-like DON cells have cosinusoidal directional response patterns similar to those seen in saccular afferents (1, 2). Many cells recorded in the DON had directional response patterns that differed from simple cosine functions: they are sharpened (see Fig. 1A) with torpedo-shaped patterns (63% of 88). Sharpened cells were further categorized as slightly (23%), moderately (28%), or highly (12%) sharpened based on the magnitude of their deviation from a cosine function. Some cells were sharpened in only one plane (n = 15, with only mid-sagittal plane sharpening in 11 cells, and only horizontal plane sharpening in 4 cells). The rest (n = 40) were sharpened in both planes to some extent. Although we cannot

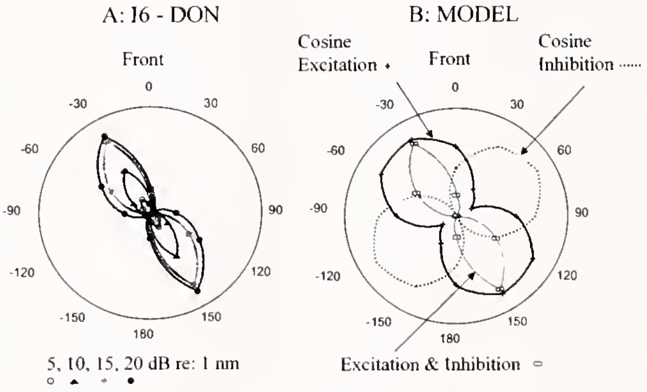

Figure 1. *A: Directional responses for cell 6 (animal I) at four iso-displacement levels in the horizontal plane in polar coordinates. The angular axis is the orientation of linear translatory motion. The radial axis is response magnitude (the Z-statistic: $Z = R^2N$, where R is vector strength—a phase-locking metric (2), where $0 \leq R \leq 1$, and N is the number of spikes recorded for eight repetitions of a 500 ms sinusoid at 100 Hz). The circular axis indicates a Z value of 350. In this polar plot, each directional stimulus axis is represented on the circle in degrees with respect to straight ahead (0°). For each stimulus axis, response magnitude (Z) was plotted twice (at the nominal axis angle, and at this angle plus 180°). Thus, the distance between the polar plot origin and the plotted points represent the value of Z at each stimulus axis. B: Hypothetical excitatory (solid lines, + symbol) and inhibitory (dotted lines) cosine-shaped directional inputs to a DON cell. The amplitudes and orientations of the inputs were adjusted to form a difference function (gray lines and ☐ symbols, negative values set to zero) closely modeling the directional response in Figure 1A for the 15 dB level. The difference function is also plotted in Figure 1A, which overlaps the cell's response completely.*

determine with certainty whether these recordings were made from primary afferent axons or from cells of the DON, response patterns classified as very sharpened or moderately sharpened (40%) were never observed in over 400 recordings from saccular afferents (2). Further work using intracellular recording and neurobiotin injection will help resolve this ambiguity.

Figure 1A illustrates directional response patterns of a representative sharpened DON cell in the horizontal plane. Sharpening is level-independent for this cell and results in a responsiveness maximum oriented about 30° to the left front. Idealized cosine responsiveness functions are illustrated in Figure 1B. Clearly, the directional response of the DON cell is not well modeled by a single cosine function. The directional responses of most sharpened cells in the DON are well modeled by a combination of excitation and inhibition from at least two inputs with cosinusoidal directional response patterns. Fitting excitatory and inhibitory cosinusoidal influences to a cell's directional response function gives the relative magnitudes and orientations of the hypothetical inputs. For this cell, hypothetical excitatory and inhibitory magnitudes are approximately equal at all levels, with the excitatory cosine oriented at about 36° to the left front, and the inhibitory cosine oriented at about 34° to the right front. The origin of the putative inhibition remains to be determined, but could arise from the contralateral ear via commissural DON connections (6).

Research funded by a National Institutes of Health R01 grant to the Parmly Hearing Institute.

Literature Cited

1. **Edds-Walton, P. L., and R. R. Fay. 1995.** *Biol. Bull.* **189:** 211–212.
2. **Fay, R. R., and P. L. Edds-Walton. 1997.** *Hear. Res.* **111:** 1–21.
3. **Edds-Walton, P. L., R. R. Fay, and S. M. Highstein. 1999.** *J. Comp. Neurol.* **411**(2): 212–238.
4. **Edds-Walton, P. L., and R. R. Fay. 1998.** *Biol. Bull.* **195:** 191–192.
5. **Dowben, R. M., and J. E. Rose. 1953.** *Science* **118:** 22–24.
6. **Edds-Walton, P. L. 1998.** *Hear. Res.* **123:** 41–54.

Reference: *Biol. Bull.* **197:** 241–242. (October 1999)

Acoustic Behavior and Reproduction in Five Species of *Corydoras* Catfishes (Callichthyidae)

Ingrid M. Kaatz and Phillip S. Lobel (Boston University Marine Program,
Marine Biological Laboratory, Woods Hole, Massachusetts 02543)

Many catfishes produce stridulation and swimbladder sounds when disturbed (1, 2, 3, 4, 5, 6), although the role of catfish sound production in intraspecific contexts has not been widely studied (7, 8). Males of the neotropical catfish *Corydoras paleatus* are known to produce agonistic and courtship stridulation sounds when reproductively active (9). Catfish stridulation sounds are produced by microscopic bony ridges located on the distal end of the pectoral fin spine that are rubbed against the wall of the spinal fossa (3). In *Corydoras,* these ridges are narrower and more acute than in other catfishes (4). Identifying a species' acoustic repertoire (*i.e.,* the full range of contexts in which sound is produced) and if or how sounds differ is a necessary first step in understanding how a species communicates (10). To further describe the acoustic repertoire of *Corydoras* catfishes, we conducted a study of five species in aquaria. Our objectives were to determine (1) the behavioral context for sound production, and (2) whether acoustic activity levels (numbers and types of sounds) differed when the same fishes were reproductively and non-reproductively active.

Individual fishes ($n = 122$) were obtained through the pet trade as juveniles and raised to sexual maturity. The mean number of individuals per group was 10 (range 3–15). *C. paleatus* juveniles were born in captivity while others were wild caught. All fishes were similar in length and weight. Five species (10 groups) were kept in 20-gallon aquaria in a soundproof room (Acoustic Systems Inc.). The acoustic behavior of adults was monitored using a hydrophone (BioAcoustics Inc., frequency response 10–3000 Hz, sensitivity at 10 psi of -162 dBv/μPa $\pm$ 2.0 dB) and amplifier-speaker (frequency response 100 Hz–10,000 Hz). The average monitoring time for each species was 10 months (range 6–15 months). Sounds were recorded on videotape with a Panasonic VHS recorder (professional/industrial model AG-180, frequency response 100–8000 Hz).

The behavioral context for each sound produced was determined by observing behavior, beginning with feeding, at night using a red light. The mean number of hours sampled per species was 50 (19–77). Five species (*C. aeneus, C. arcuatus, C. leopardus, C. paleatus, C. reticulatus*) were stimulated into reproductive activity by simulating a tropical freshwater rainy season (6). For reproductive fishes, the total number of 1-h samples was 81 and the mean number of hours sampled per species was 10 (6–25). Groups were maintained in non-reproductive condition by using a dry-season simulation (6). For non-reproductive fishes, the total number of 1-h samples was 171 and the mean number of hours sampled per species was 34 (5–63). Chi-square was used to test for differences in sound production between reproductive and non-reproductive fishes for all groups and samples. Student's t test was used to compare acoustic activity immediately preceding and following spawning for five groups that each had more than 10 individuals per group.

The software package SIGNAL (Engineering Systems Inc., Belmont, MA) was used to determine total pulse number and frequency range. These acoustic parameters are believed to be of significance to fishes in intraspecific contexts (7, 8). A minimum of 40 courtship sounds per species were analyzed for determining pulse number for *C. aeneus, C. leopardus,* and *C. paleatus* (177 sounds total). A minimum of 30 sounds per species for agonistic chase sounds were analyzed for the same three species (90 total). A minimum of 6 agonistic pre-chase sounds were analyzed for *C. arcuatus* and *C. reticulatus* (total 18). For startle sounds, a minimum of three sounds were analyzed for *C. leopardus* and *C. aeneus* (8 total).

Table 1

Differences in the number of sounds for reproductive and non-reproductive Corydoras *catfishes*

	Total sounds[1] (mean sounds/h ± SD)			
Species	Reproductive	Non-reproductive	n = 1-h samples[2]	t test[3] (P value)
C. aeneus	314 (24 ± 33)	2 (0.1 ± 0.1)	13	<0.01
C. arcuatus	439 (41 ± 25)	2 (0.2 ± 0.6)	13	<0.0002
C. leopardus	206 (21 ± 17)	1 (1.0 ± 0.3)	10	<0.002
C. paleatus	373 (62 ± 61)	2 (0.3 ± 0.5)	6	<0.03
C. reticulatus	72 (12 ± 8)	1 (0.2 ± 0.4)	6	<0.01

[1] Total number of sounds for 1-h samples immediately preceding and following spawning for one group per species (10–15 individuals per group).

[2] Number of 1-h samples analyzed for reproductive and non-reproductive each.

[3] Significance level for differences between total number of sounds per hour for reproductive *vs.* non-reproductive fishes.

Sounds were grouped as one of four types based on the behavioral context in which they were observed: (1) courtship, (2) agonistic chase, (3) agonistic pre-chase, and (3) startle. Fish activities without sound production included schooling, resting on the substrate, or testing the substrate with barbels. Courtship-associated sounds were high-pitched "creaks" (600–8000 Hz) produced when, prior to spawning, males hovered near females beating pectoral and dorsal fins. All five species produced these sounds when reproductive. The pulse number per sound ranged from 10 to 112. Agonistic chase sounds were high-pitched creaks (600–8000 Hz) produced when males chased both other males or females. These sounds were only observed several days before, during, and after spawning and consisted of 2 to 16 pulses. All five species produced these sounds when reproductive. Agonistic pre-chase sounds were low-pitched "wooden claps" (430–750 Hz) consisting of 2 to 6 pulses. They were produced when two individuals hovered near each other and a chase ensued. This sound was observed in *C. arcuatus* and *C. reticulatus*. Startle sounds were high-pitched "creaks" (600–8000 Hz). They consisted of 26 to 100 pulses and were produced when fishes, reproductive and non-reproductive, were resting on the substrate and suddenly scattered across the bottom or into the water column.

The number of 1-h samples that included sound production was higher for reproductive (63% of 81 1-h samples) than non-reproductive (22% of 171 1-h samples) fishes. The range of percentages of 1-h samples in which fishes were acoustically active was 43% to 71% for reproductive animals and 10% to 40% for non-reproductive animals. These differences were significant (Chi-square, $P < 0.001$). The two 1-h sample periods with the highest number of sounds were from reproductive fishes (120 and 185 sounds). All other reproductive-period samples ranged between 1 and 75 sounds per hour. Non-reproductive samples ranged from a total of 1 to 4 sounds per hour. Significantly more sounds were produced when fishes were reproductive than non-reproductive (Table 1).

The results of this study suggest that (1) *Corydoras* catfishes produce sounds in four behavioral contexts; and (2) acoustic activity is low for non-reproductive fishes and significantly higher for the same individuals when they are reproductive.

Literature Cited

1. **Pfeiffer, W., and J. F. Eisenberg. 1965.** *Z. Morph. Oekol. Tiere* **54:** 669–679.
2. **Kaatz, I. M., and D. S. Stewart. 1995.** *Am. Zool.* **35**(5): 16a. (abstract).
3. **Fine, M. L., J. P. Friel, D. McElroy, C. B. King, K. E. Loesser, and S. Newton. 1997.** *Copeia:* 777–790.
4. **Kaatz, I. M., and D. J. Stewart. 1997.** *J. Morphol.* ICVM-5 232(3): 272. (abstract).
5. **Ladich, F. 1997.** *Bioacoustics* **8:** 185–191.
6. **Kaatz, I. M. 1999.** Ph.D. Dissertation, State University of New York, College of Environmental Science and Forestry, Syracuse, NY. Pp. 80–112.
7. **Myrberg, A. A. 1981.** Pp. 395–424 in *Hearing and Sound Communication in Fishes,* W. N. Tavolga, A. N. Popper, and R. R. Fay, eds. Springer-Verlag, New York.
8. **Hawkins, A. D. 1986.** Pp. 129–169 in *Behavior of Teleost Fishes,* T. J. Pitcher, ed. Chapman and Hall, London.
9. **Pruzsinsky, I., and F. Ladich. 1998.** *Environ. Biol. Fishes* **53:** 183–191.
10. **Kroodsma, D. E., and E. H. Miller. 1996.** *Ecology and Evolution of Acoustic Communication in Birds.* Cornell University Press, Ithaca, NY. Pp. 136–177.

Reference: *Biol. Bull.* **197:** 242–244. (October 1999)

Courtship Sounds of the Pacific Damselfish, *Abudefduf sordidus* (Pomacentridae)

Phillip S. Lobel (Boston University Marine Program, Marine Biological Laboratory, Woods Hole, Massachusetts 02543) and Lisa M. Kerr[1]

The courtship-associated sounds (CAS) produced by *Abudefduf sordidus* (Forsskål, 1775) are different than those of other well-known sonic pomacentrids (*e.g., Dascyllus* spp., *Stegastes* spp.). Pomacentrids, unlike many other fishes, generally produce loud, clear, pulsed calls that are easily heard by scuba divers. The bioacoustic patterns associated with courtship have been particularly well described for the Caribbean species *Stegastes partitus* and the Pacific species *Dascyllus albisella* (1, 2, 3). During courtship, the males of the sympatric *D. albisella* produce loud and organized pulsed calls that are very consistent in such temporal qualities as pulse rate, individual pulse duration, interpulse interval duration, call duration, and number of pulses in a call (4, 5). Most importantly, these calls are associated with a stereotypical courtship behavior (the "courtship dip") in which a male rises in the water column and rapidly swims downward while producing the loud call. It makes sense that, if these acoustic signals evolved to attract conspecific females from a distance, the sound patterns would be easily identifiable and consistent.

---

[1] University of Massachusetts, Biology Department, 100 Morrissey Blvd., Boston, Massachusetts 02125.

Abudefduf sordidus is found on coral reefs throughout the Indo-west Pacific to Hawaii. This study was conducted at Johnston Atoll, using a specialized underwater video and hydrophone assembly (see methods in ref. 4). The hydrophone had a frequency range of 10 to 3000 Hz and sensitivity at 10 psi of −162 dBv/μPa ± 2 dB (model FishFone, BioAcoustics Inc, Woods Hole, Massachusetts). In general, about 40% of the total recording time on videotape was lost due to scuba bubble noise obscuring the signal sufficiently to affect the accuracy of measurements. Signals were digitized at 44 kHz (Canary Software, Cornell University, Ithaca, New York). Sonograms were produced using the following parameters: filter bandwidth 389.7 Hz, frame length 512 pts, FFT size 2048 pts, time grid resolution 5.805 ms, 50% overlap, frequency grid resolution 21.53 Hz, window function Hamming, amplitude logarithmic.

The courtship and spawning behavior of four males was recorded between March 1995 and June 1998 (total 3.5 h of recording), resulting in a data set of clear recordings of 53 CAS and four aggressive "pops" by three males. Of these, 40 recordings were from one male. The adult males and female fish in this study ranged in size from about 13 cm standard length, SL (160 g weight and age 7 years) to 15 cm SL (225 g weight and age 9 years) and produced more than 400,000 embryos in a nest (6, 7).

The acoustic recordings from one male demonstrate a high degree of individual variability in the pulse pattern and timing of the CAS (Fig. 1). The mean CAS duration was 620 ms ± 276 SD (range 188 to 1387). The mean number of pulses per call was 5 ± 2 SD (range 2 to 10). The coefficient of variation was high for duration (0.45) and number of pulses (0.4); these values are about four times greater than those observed in *D. albisella* (4). The CAS produced by *A. sordidus* did not exhibit a consistent repeated

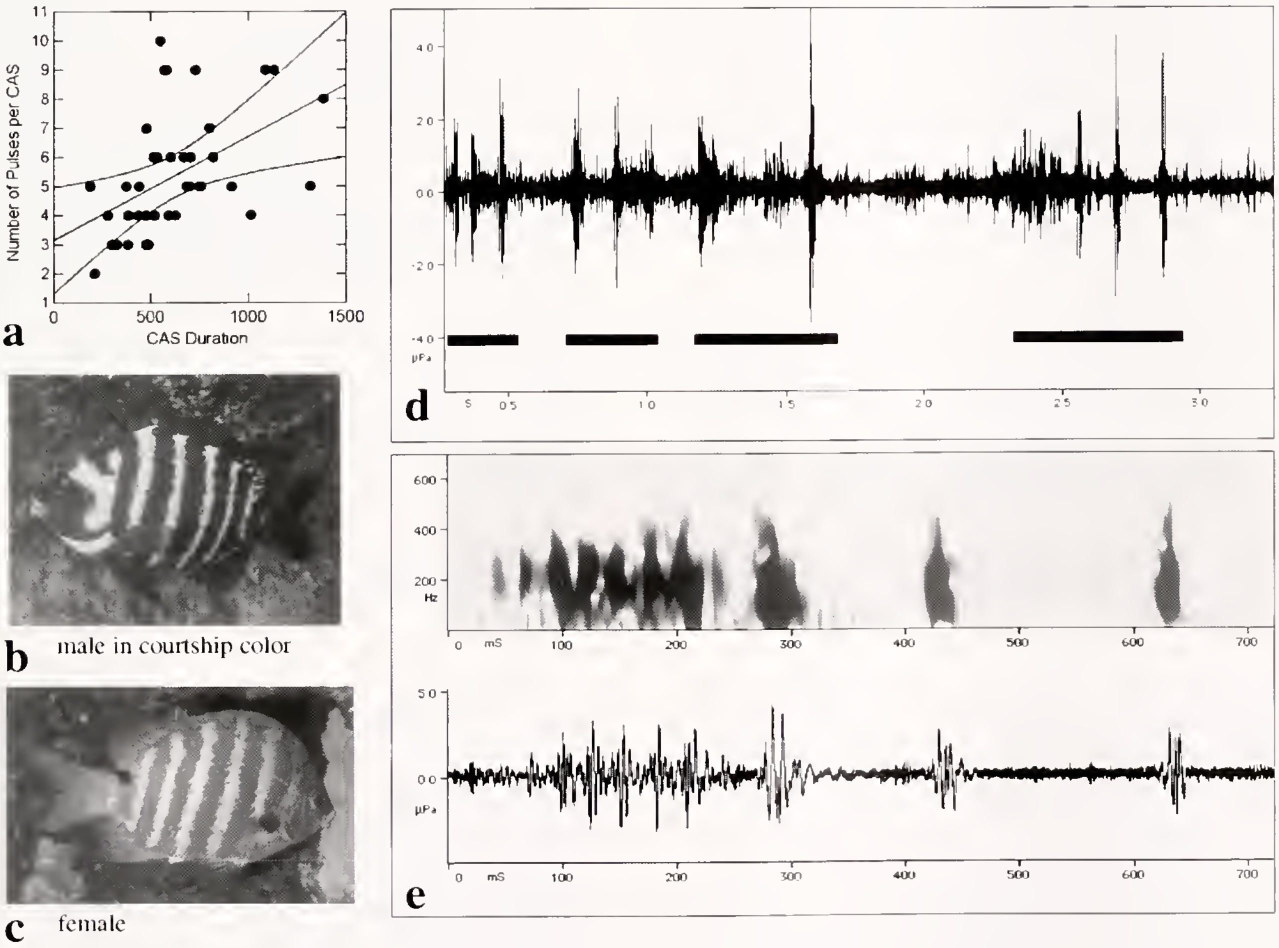

male in courtship color

female

Figure 1. *Individual variability of the courtship-associated sound (CAS) by* Abudefduf sordidus. *Data in a, d and e are from one male. (a) Plot of CAS duration against number of pulses in that CAS* (n = *40) for one male. Linear regression* (r^2 = *0.23) is shown by the straight line with the curved lines on either side delineating the 95% CI. (b) male in courtship coloration. (c) female, both about 15 cm total length. (d) A series of CAS showing intra-individual variability in pulse pattern and overall timing. Black horizontal bars span individual CAS units. (e) An example of one CAS shown in detail as a sonograph (top) showing frequency (Hz) plotted against time (ms), and an oscillograph (bottom) showing relative amplitude by time (ms).*

pattern found in other pomacentrids. The CAS were highly variable in pulse number and length, and the linear relationship between the two factors was very weak ($r^2 = 0.23$; Fig. 1a). Furthermore, the CAS of *A. sordidus* were relatively low amplitude and could not be detected unless the hydrophone was within about 2 m. In contrast, *D. albisella* sounds were detected at distances up to about 9 m (8).

Male *A. sordidus* establish and maintain territories for nesting, often returning to the same nest site every year (9). Males compete aggressively for their own exclusive nest site. These nests are arranged in a colonial arena layout. Courting males change coloration from the drab barred pattern shown by non-courting males and by females to a bright contrasting pattern of white bars on a black background (Fig. 1b, c). A male responds to a female in the vicinity of the nest by rapidly swimming out toward her in a zigzag pattern, swimming first on one side, then flipping to the other. Often more than one male is seen swimming out to meet a female. The successful male leads the female back to his nest; when near the nest, he swims rapidly around her in a figure-eight pattern. During this courtship behavior, sounds are produced (Fig. 1d, e). Clearly, the female will be aware of the male's activity in front of her, with or without sounds. The male continues this behavior, apparently trying to entice the female to enter the nest. Once she does, both male and female take turns swimming with pelvic fins pressed against the nest substrate. This behavior may last up to 20 min before actual spawning begins. If the female tries to leave, or pauses in her passing over the nest, the male resumes swimming in the rapid figure-eight pattern and producing sounds. (For an audio-video clip see web site http://www.mbl.edu/html/BB/VIDEO/BB.video.html). Once spawning begins, the male no longer produces sound. A male will often nest with several females over a few days.

A. sordidus possibly uses CAS acoustics only to attract attention. In contrast, males in the genera *Dascyllus* and *Stegastes* repeatedly swim in vertical loops over their nest sites while making a stereotypical, loud, clear, pulsed sound without detectable hydrodynamic noise. In these species, the female approaches the male in his nest before the male responds specifically to her. The notion is that females are attracted by the information content of the sounds or the pattern of production (1, 2, 4).

The CAS patterns produced by the four male *A. sordidus* examined were irregular and highly variable. The sound appears to result from a combination of hydrodynamic noise produced by vigorous swimming movements with fins extended, and biological sounds produced by the movement of muscles and bones, possibly amplified by the swimbladder. The exact mechanism of sound production is unknown. It seems unlikely that the pulsed sounds produced by *A. sordidus* represent advanced coded signals; they are possibly, at least in part, adventitious. When compared to the highly stylized and repetitious acoustic and swimming display exhibited by *Dascyllus* and *Stegastes* spp., the courtship-associated sounds and behavior of *A. sordidus* seem rudimentary. This difference in acoustic displays probably reflects a species-specific reproductive tactic by which males attract females to the nest.

Supported by the Army Research Office grant DAAG 55-98-1-0304 for the Johnston Atoll Reef Study.

Literature Cited

1. **Myrberg, A. A. 1972.** *Anim. Behav. Monogr.* **5:** 197–283.
2. **Myrberg, A. A., S. J. Ha, and M. J. Shamblott. 1993.** *J. Acoust. Soc. Am.* **94:** 3067–3070.
3. **Mann, D. A., and P. S. Lobel. 1998.** *Environ. Biol. Fishes* **51:** 421–428.
4. **Lobel, P. S., and D. A. Mann. 1995.** *Bioacoustics* **6:** 187–198.
5. **Mann, D. A., and P. S. Lobel. 1995.** *Bioacoustics* **6:** 199–213.
6. **Kerr, L. M. 1996.** *Biol. Bull.* **191:** 306–307.
7. **Kerr, L. M., K. L. Lang, and P. S. Lobel. 1997.** *Biol. Bull.* **193:** 279–281.
8. **Mann, D. A., and P. S. Lobel. 1997.** *J. Acoust. Soc. Am.* **101:** 3783–3791.
9. **Stanton, F. G. 1985.** *Proc. Fifth Int. Coral Reef Congr. Tahiti.* **5:** 361–366.

Reference: *Biol. Bull.* **197:** 244–246. (October 1999)

Threat-Sensitive Nest Defense in Domino Damselfish, *Dascyllus albisella*

Steven J. Oliver and Elise Watson (Boston University Marine Program, Woods Hole, Massachusetts)

Among fishes with paternal care of eggs, damselfish (Pisces: Pomacentridae) are particularly well-studied (1). Species-specific aggression has been reported for algal-gardening damselfish (2, 3, 4, 5, 6). We initiated this study to determine whether the planktivorous Domino damselfish (*Dascyllus albisella*) exhibits species-specific nest-defense patterns. *D. albisella* is a common and conspicuous reef fish endemic to the Hawaiian archipelago. Males guard nest-territories against conspecifics year round, and chase potential egg predators when defending embryos. Courtship includes an acoustic and visual display and is followed by the deposition of demersal eggs, which the male fertilizes and guards until they hatch (4 days) as planktonic larvae (7).

Williams (8) suggested that paternal care in fishes adds little additional cost to defending mating territories. In algal-gardening species, such as *Stegastes* spp., there is evidence of non-depreciable care: eggs do not appreciably increase defense costs because heterospecifics are already excluded from the territories of these species. In *D. albisella*, however, the cost of nest defense in terms of energy expenditure (attacking of intruders) and energy uptake (time spent feeding) is largely additive because the fish undergo a behavioral shift in territoriality upon reception of eggs. One strategy for ameliorating the cost of paternal care is selective defense proportional to the threat of egg predation posed by different species.

The authors observed male *D. albisella* ($n = 23$; standard length (SL) ± SD = 89.9 ± 11.2 mm) at Johnston Atoll, Central Pacific Ocean, in March–July 1998. Water depth of the lagoon study site ranged from 4 to 5 m. Using scuba, 15-min focal samples were conducted at times ranging from sunrise (0545 h) to sundown

(2030 h), with more than 80% of the observations made between 0800 and 1100 h. Males were tagged to allow individuals to be recognized. We measured attack distances by placing three 5-m nylon lines (marked in 0.5-m intervals) on the substrate, radiating outward from the nest. The observer estimated attack distances to the nearest 0.25 m. Heterospecific intrusions within 1 m of the nest were recorded (noting species, response, and distance from nest), as were all attacks by the focal male. Encounters were defined as any incursion within 1 m of the nest, or as an attack on an intruder regardless of the distance from the nest. We defined attacks as those encounters in which males oriented towards, swam at, or physically struck the intruder and the intruder fled. Males often pursued intruders several meters from the nest.

Encounters between *D. albisella* and other fishes occurred for 43 species. Twenty-three species (representing 10 families) were excluded from analysis because they were encountered only in the presence of eggs. A total of 346 encounters, resulting in 119 attacks (34.4% attack rate) were observed for 19 species (Table I). Wrasses (Labridae) were the only family in which individual species differed in the response elicited from *D. albisella*, and are listed both by family and by species. The remaining 13 species are listed by family. One species, the piscivorous *Oxycheilinus unifasciatus* (Labridae), was consistently attacked by *D. albisella* in the absence of embryos. Because *O. unifasciatus* appears to be unique in this regard, we excluded it from further analysis.

To test the hypothesis that *D. albisella* selectively attacks active egg predators, we divided the species into two groups. At Johnston atoll, the wrasses *Thalassoma duperrey* and *T. lutescens* hybridize (9), making identification of species difficult. This hybrid complex was the only group of fish that were observed to actively search for nests, and to persistently return to a nest once it was discovered. We grouped the *Thalassoma* spp. together as the *T. duperrey* × *T. lutescens* species complex (hereafter referred to as "*Thalassoma* hybrids"). We grouped the other fishes (Acanthuridae, Monacanthidae, Chaetodontidae, Mullidae, Scaridae, and the labrids *Epibelus insidiator, Gomphosis varius*, and *Coris gaimard*) together because they were not observed to actively search for, and raid, nests, although they would consume embryos if they discovered a nest. With the exception of *Aluterus scriptus* (Monacanthidae), which can achieve a standard length of 760 mm, the fishes being attacked were roughly 2 to 3 times the size of the territorial male.

We compared differences in attack distance between *Thalassoma* hybrids and the other fishes using a one-tailed paired t test of means ($\alpha = 0.05$; H_1: μ Others $< \mu$ *Thalassoma* hybrids; calculated using Data Desk 6.0.1 for Windows). *Thalassoma* hybrids were attacked at significantly (t-stat = $^{-}10.51$ with 83 d.f. $P < 0.0001$) greater distances (2.41 ± 1.02 m) than the other fishes (0.88 ± 0.54 m). *Thalassoma* hybrids were responsible for 103 of 109 (95%) egg predation events. They were attacked a combined 59 times, accounting for 50% of all attacks by *D. albisella*.

Attacks on *Thalassoma* hybrids appeared to be qualitatively more aggressive, rapid, and persistent, often continuing until the wrasse was driven off the coral head entirely. Attacks on *Thalassoma* hybrids occasionally resulted in the male leaving the nest unguarded for as long as 30 seconds. However, secondary predation, in which other fish exploited the elevated aggression towards *Thalassoma* hybrids, was rare ($n = 4$). In these cases, a second *Thalassoma* hybrid would exploit the opportunity to search for or raid a nest, but the *D. albisella* males were usually able to fend off all intruders. These same species (often the same individuals,

Table I

Encounters, attacks, and mean attack distance based on the presence of embryos in Dascyllus albisella *nests*

	No embryos in nest		Embryos present in nest				
Family	Encounters	Attacks	Encounter	Attacks	Distance[1]	SD	Percent[2]
Acanthuridae	11	0	32	10	0.70	0.31	100
Chaetodontidae	13	0	70	14	0.54	0.32	100
Labridae	65	3	103	64	2.21	1.09	95.52
Coris gaimard	4	0	3	3	1.00	0.50	100
Epibelus insidiator	14	0	32	4	0.50	0.35	100
Gomphosis varius	2	0	1	1	1.50	n/a	100
Thalassoma duperrey	27	1	26	22	2.48	0.94	95.65
Thalassoma duperrey × *lutescens*	13	1	19	18	2.61	1.10	94.74
Thalassoma lutescens	5	1	22	16	2.08	1.02	94.12
Monacanthidae	3	0	2	2	0.88	0.18	100
Mullidae	2	0	4	4	0.81	0.43	100
Scaridae	8	0	33	22	0.81	0.61	100
TOTALS[3,4]:							
All families	102	3	244	116	1.54	1.11	97.48
Thalassoma hybrids	45	3	67	56	2.41	1.02	94.92
Other Fishes	57	0	177	60	0.77	0.50	100.00

[1] Mean attack distance in meters.

[2] The percentage of total attacks (sum of attacks with and without embryos present) that occurred when embryos were present.

[3] Totals do not include the individual species listed under Labridae. The Labridae family total includes the species data.

[4] Totals of mean attack distance and standard deviation are calculated by combining all observations, rather than by summing the columns.

which we identified by their unique markings) that were attacked when embryos were present were tolerated in the nest when there were no embryos. Since none of these species are cryptic, and many of them are highly conspicuous (see 9), it is unlikely that the ability of *D. albisella* to perceive the fishes explains this pattern.

These patterns suggest that *D. albisella* exhibits a threat-dependent level of aggression in which the size of the defended area around the nest varies as a function of relative threat of egg predation.

Funding provided by Army Research Office Grant DAAG 559810304.

Literature Cited

1. **Petersen, C. W. 1995.** *Bull. Mar. Sci.* **57:** 690–704.
2. **Draud, M. J., and M. Itzkowitz. 1995.** *Copeia* **2:** 431–435.
3. **Ebersole, J. P. 1980.** *Am. Nat.* **115(4):** 492–509.
4. **Myrberg, A. A., and R. E. Thresher. 1974.** *Am. Zool.* **14:** 81–96.
5. **Thresher, R. E. 1976.** *Anim. Behav.* **24:** 562–569.
6. **Thresher, R. E. 1979.** *Mar. Behav. Physiol.* **6:** 83–94.
7. **Mann, D. A., and P. S. Lobel. 1995.** *Bioacoustics* **6:** 199–213.
8. **Williams, G. C. 1975.** *Sex and Evolution.* Princeton, New Jersey.
9. **Randall, J. E. 1996.** *Shore Fishes of Hawaii.* Natural World Press, Vida, Oregon.

Reference: *Biol. Bull.* **197:** 246–247. (October 1999)

Predator-prey Interactions of Juvenile Toadfish, *Opsanus tau*

Nichole N. Price[1,2] *and Allen F. Mensinger*[2]
(Washington University School of Medicine, St. Louis, Missouri 63110)

The oyster toadfish, *Opsanus tau,* is a benthic teleost that inhabits estuaries and coastal waters along the eastern seaboard of the United States (1). The toadfish is an ambush predator that commonly feeds on crabs, shrimps, and fishes (2).

The toadfish has also been historically an important marine model for research on auditory physiology, muscle physiology, vestibular system, and nerve regeneration (3, 4, 5). Although much is known about this animal in its adult stages, the behavior of juvenile toadfish is poorly understood. A concurrent project at the Marine Biological Laboratory is attempting to culture toadfish (6). If this effort is to be successful, the feeding behaviors of these young fish must be understood. The aim of this study was to investigate the relationship between strike distance and strike success of first year toadfish.

One-year old juvenile *Opsanus tau* (n = 6; 5.9 ± 0.3 cm, standard length) were maintained separately in 80-l Plexiglas tanks provided with flow-through ambient seawater (20° ± 2°C). The toadfish were transferred to feeding arenas (opaque 6.5-l aquariums) containing seawater at 20° ± 1°C and allowed to acclimate for 30 min, which was sufficient time for the fish to resume their normal respiration rates and initiate their feeding behaviors. For each feeding trial, five feeder guppies (about 2 cm sl) were placed in the arena, and the experiment was conducted for 30 min. The interval between trials was no less than 48 h to prevent satiation. Trials were recorded on 8-mm tape with a Sony video High 8 Handycam positioned 0.5 m above the tank. Grids (0.25 cm^2) were placed on the bottom of the tank so that measurements on the VHS recordings could be calibrated. All strikes were re-recorded onto VHS to be viewed frame by frame on a ZenithInteq VCR (30 frames per second).

The typical toadfish strike sequence consists of an orientation towards the prey followed by a sudden contraction of the pectoral fins, which propels the toadfish at the prey. Just prior to striking, the toadfish begins to raise its head and lower its mandible rapidly, generating an inward rush of water that may assist in the capture of the prey (7). Upon contacting the prey, the toadfish quickly snaps its jaws around it. Strike initiation was defined as the frame in which the pectoral fins begin to contract. Strike distance was defined as the distance between the head of the fish and the head of the guppy measured at the time of strike initiation (8).

The toadfish exhibited a 34.6% success rate at capturing the guppies (n = 78 attempts). Successful attempts were initiated at an average distance of 1.26 ± 0.16 cm, while unsuccessful strike attempts were initiated at a significantly greater distance (2.43 ± 0.24 cm, unpaired t test with Welch correction, $P < 0.0004$). Strike distances were binned in 0.5 cm increments so that the effect of distance on strike success could be illustrated (Fig. 1). The majority (54%) of successful attempts were made when the fish were within 0.5 and 1.5 cm of the prey, while most failures (35%)

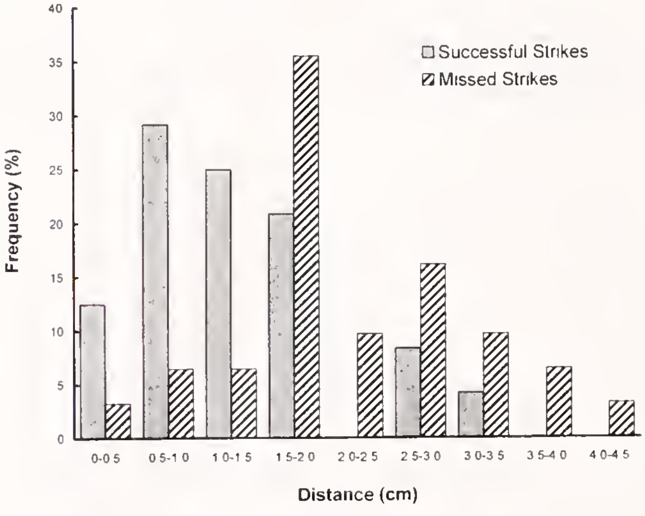

Figure 1. *Bar graph showing percentage of strike frequency. The frequency of missed (65.4%) and successful (34.6%) strikes* (n = *78) is plotted against distance (cm) from prey at strike initiation.*

---

[1] Connecticut College, New London, Connecticut 06320-4196.

[2] Marine Biological Laboratory, Woods Hole, Massachusetts 02543.

occurred at 1.5 to 2.0 cm (Fig. 1). Strike success was similar when compared to prey number remaining, indicating that earlier predation events did not influence predation success.

Juvenile toadfish are effective short-range ambush predators. At strike distances between 0 and 1.5 cm they strike successfully 76.2% of the time. But between 1.5 and 2.0 cm, strike success is mixed, and it continues to decline with distance. Future experiments will examine the efficacy of prestrike orientation on predation success.

We thank L. C. Rome, S. M. Highstein, W. Mebane, and J. Hanley for their contributions to this study. We also show our appreciation to M. Tytell and C. Browne, directors of the undergraduate Marine Models in Biological Research program. The experiment was funded by the Lawrence Scholarship of Connecticut College and the NSF grant NSFDBI-9605155.

Literature Cited

1. **Schwartz, F. J., and B. W. Dutcher. 1963.** *Trans. Am. Fish. Soc.* **92:** 170–173.
2. **Bisker, R., M. Gibbons, and M. Castagna. 1989.** *J. Shellfish Res.* **8:** 25–31.
3. **Edds-Walton, P. L., and R. R. Fay. 1997.** *Hear. Res.* **111:** 1–21.
4. **Rome, L. C., and S. L. Lindstedt. 1998.** *News Physiol. Sci.* **13:** 261–268.
5. **Mensinger, A. F., and S. M. Highstein. 1999.** *J. Comp. Neurol.* **410:** 653–676.
6. **Tang, K. Q., N. N. Price, M. D. O'Neill, A. F. Mensinger, and R. T. Hanlon. 1999.** *Biol. Bull.* **197:** 247–248.
7. **Gosline, W. A. 1996.** *Environ. Biol. Fishes.* **47:** 399–405.
8. **Walton, W. E., S. S. Easter, C. Malinoski, and N. G. Hairston. 1994.** *Can. J. Fish. Aquat. Sci.* **51:** 2017–2026.

Reference: *Biol. Bull.* **197:** 247–248. (October 1999)

Temperature Effects on First-Year Growth of Cultured Oyster Toadfish, *Opsanus tau*

Kathleen Q. Tang (Marine Biological Laboratory, Woods Hole, Massachusetts)[1], *Nichole N. Price*[2], *Maureen D. O'Neill, Allen F. Mensinger*[3], *and Roger T. Hanlon*

The toadfish, *Opsanus tau*, has been the focus of scientific research for more than a century. Since its development was first outlined by Ryder (1), it has continued to be an important marine model for muscle (2), auditory (3), and vestibular physiology (4), as well as for nerve regeneration (5). Recent studies (6) have established baseline blood chemistries to help understand biological requirements of the toadfish in captivity. Despite the many studies of toadfish physiology, little is known about the basic life history of the animal, such as its growth rate and nutritional requirements.

Recently, the availability of wild-caught toadfish has declined, making it difficult for the Marine Biological Laboratory (MBL) to provide the necessary numbers and size classes for research. In addition, captive populations of adults have been affected by diseases such as bacterial pericarditis, *Flexibacter* sp. dermatitis, and parasitic infestations (7). To provide researchers with healthy toadfish and reduce pressure on wild populations, a mariculture program has been initiated to examine husbandry techniques needed to propagate captive populations. To our knowledge, *Opsanus tau* has never been cultured. This paper summarizes aspects of growth and survival during the first year posthatching.

Two toadfish nests (with guardian males) were transported to the Marine Resources Center of the MBL from Waquoit Bay in early July 1998. Physical detachment of the larval fish from the nest was completed by late July. One hundred (100) juvenile toadfish from an original pool of about 200 fish were randomly selected in mid-October for this study and separated into 90-l fiberglass tanks (130 × 70 × 10 cm). Each tank was provided with rock and sandy substrate and artificial habitats (PVC pipe). Half of the toadfish were maintained at a constant temperature (Temperature A) of 19.5° ± 1°C. The other toadfish were maintained at predominantly cooler temperatures (Temperature B) using ambient (October–November 1998, 10°–15°C) or recirculating seawater (December 1998–May 1999 13° ± 2°C). These fish were subsequently switched to ambient in June 1999 and experienced temperatures ranging from 15°C to 23°C by the end of July 1999. Each experimental group was further subdivided into two groups consisting of 10 (11.3 fish/m^2) or 40 fish (45.0 fish/m^2) to study the effects of density on toadfish growth.

Many food types were presented to the fish, which were fed every other day. The initial diet consisted of live, newly hatched squid (*Loligo pealei*), *Artemia* sp., and mysid shrimps. As the fish increased in size, the diet was switched to approximately 10% live food (guppies), and 90% prepared food such as chopped butterfish (*Peprilus triacanthus*), oyster (*Crassostrea virginica*), bloodworms (*Glycera capitata*), krill, and thawed squid. Due to the faster growth exhibited by the fish in Temperature A, they were placed on the prepared food diet several months earlier than the other group.

Toadfish were removed bimonthly and weighed (wet weight in grams) and measured (standard length in centimeters). All 10 fish in the low-density tanks were examined, while at least 10 of the 40 were randomly chosen from the high-density tanks for measurement.

After detachment from nests, juveniles had an average length of 1.36 ± 0.1 cm. After one year of culturing, fish kept at the constant 19°C temperature were significantly (*t* test with Welch correction, $P < 0.0001$) larger (mean 6.10 ± 0.3 cm compared to 4.1 ± 0.4 cm) and heavier (7.70 ± 0.5 g compared to 1.7 ± 0.1 g) than conspecifics maintained on the lower temperature regime (Fig. 1). No differences in average length or weight were found between the two densities in each temperature regime (*t* test, $P > 0.21$).

The survival rate from day 80 through day 365 was 78%. Many

---

[1] Washington University, St. Louis, Missouri 63110.

[2] Connecticut College, New London, Connecticut.

[3] Washington University School of Medicine, St. Louis, Missouri 63110.

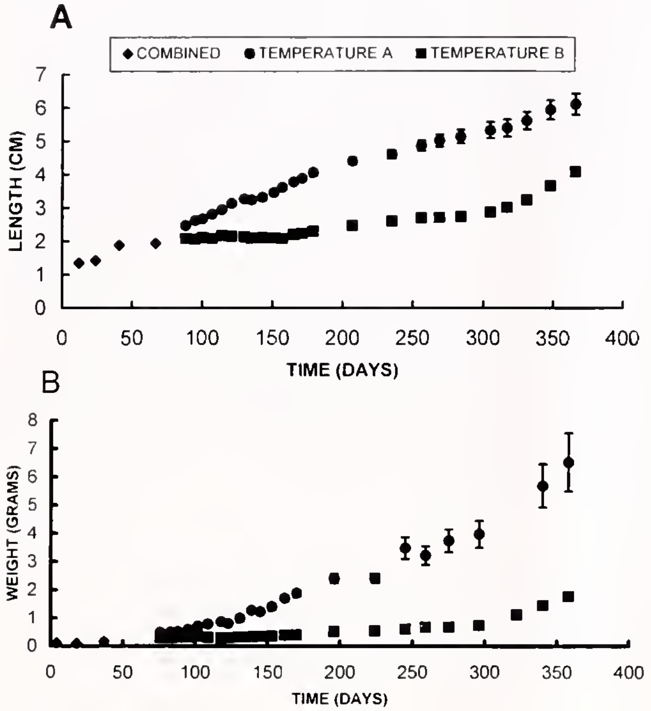

Figure 1. *Standard length in centimeters (A) and wet weight in grams (B) are plotted against time (days) from physical detachment of larval toadfish from the nest. Fish from the two nests were combined (diamonds) and maintained at ambient water temperatures until late October 1998. Fish* (n = *50) were then subdivided into two temperature regimes: Temperature A fish (circles) were maintained at 19.5° ± 1°C; Temperature B fish (squares) were kept at temperatures ranging 10°C to 23°C (see text for details). The Temperature A and B data represent the means ± 1 SE for the fish* (n = *10) kept in the low-density tanks.*

of the mortalities were smaller fish that showed signs of conspecific attack, which is consistent with the cannibalistic nature of batrachadoids (8). Future studies will test whether fish sorted by size class fare better and reduce the effects of cannibalism.

A similar mariculture study conducted at approximately the same temperature range (15° to 20°C) on the congener *Porichthys notatus* showed slightly faster growth rates (6.2 cm at 8 months and 8.8 cm at 13 months) (8). These fish were maintained mostly on live prey, which may have contributed to faster growth.

Our study has shown that full-life-cycle mariculture of *Opsanus tau* may be possible. Surprisingly, growth rate did not appear to be density-dependent. It was, however, temperature-dependent as predicted. It remains to be determined how culture temperatures, which are warmer than the normal winter/spring ambient temperatures, may affect development. Concurrent behavioral studies indicate that the cultured toadfish can accurately detect and capture various forms of prey (9). We also plan to increase genetic variation in future years by obtaining multiple nests from different geographical locations. At current growth rates, cultured toadfish will reach the size desired by researchers in about 3 years.

We would like to thank J. Hanley and W. Mebane for assisting with this project. The project has been funded an MBL Associates Fellowship (AFM), Lawrence Scholarship (NNP), NSF grant DBI-9605515, and NIH grant DC01837.

Literature Cited

1. **Ryder, J. A. 1886.** *Am. Nat.* **20:** 77–80.
2. **Rome, L. C., D. A. Syme, S. Hollingworth, S. L. Lindstedt, and S. M. Baylor. 1996.** *Proc. Natl. Acad. Sci. USA.* **93:** 8095–8100.
3. **Fay, R. R., and P. L. Edds-Walton. 1997.** *Hearing Res.* **111:** 1–21.
4. **Mensinger, A. F., J. P. Carey, R. Boyle, and S. M. Highstein. 1997.** *J. Comp. Neurol.* **384:** 71–85.
5. **Mensinger, A. F., and S. M. Highstein. 1999.** *J. Comp. Neurol.* **410:** 653–676.
6. **O'Neill, D. O., H. M. Wesp, A. F. Mensinger, and R. T. Hanlon. 1998.** *Biol. Bull.* **195:** 228–229.
7. **Smolowitz, R., E. Wadman, and H. M. Chikarmane. 1998.** *Biol. Bull.* **195:** 229–230.
8. **Mensinger, A. F., and J. F. Case. 1991.** *Biol. Bull.* **181:** 181–188.
9. **Price, N. N., and A. F. Mensinger. 1999.** *Biol. Bull.* **197:** 246–247.

Reference: *Biol. Bull.* **197:** 249–250. (October 1999)

Antennule Use by the American Lobster, *Homarus americanus*, During Chemo-orientation in Three Turbulent Odor Plumes

Katrin Mjos[1], *Frank Grasso, and Jelle Atema*
(Boston University Marine Program, Marine Biological Laboratory, Woods Hole, Massachusetts)

The American lobster, *Homarus americanus*, may use the dynamics and spatial distribution of chemical signals for guidance to the source of a turbulent odor plume (1, 2, 3). Other studies have shown that lobsters orient most efficiently when they are able to use both of their lateral antennules (4, 5). These results lead us to wonder whether the use of antennules by the plume-tracking lobster varies with the type of turbulence the lobster encounters. Such variations would suggest that the lobster is actively sensing rather than merely adjusting to the mechanical stresses presented by turbulence.

One way to answer this question is to measure the positions and orientations of the antennules of a lobster as it tracks different turbulent odor plumes. In this report we describe new methods for making these types of measurements and present preliminary results.

We observed the plume tracking behavior of 24 locally caught lobsters (~84 mm carapace length) in a flow-through seawater flume (3 m × 0.9 m and 0.22 m water depth). During trials, a plume was injected into the background flow (1.5 cm/s) at one of three rates: 1, 12, or 120 ml/min. The source was a glass tube (0.25 cm I.D.) positioned parallel to the flume floor, at antennule height (~9 cm), and in the middle of the flume. The downstream distance was selected to lie within the zone where the boundary layer had reached asymptote.

A shelter was positioned 1.5 m directly downstream from the source. The lobsters (tested one at a time) were given 30 min to habituate to the flume and settle in to this shelter before the plume was turned on. If a lobster had not settled within the allotted time, it was given another 30 min to habituate. If, after this, the lobster had not habituated, it was removed from the flume, and the habituation process was begun with a different lobster. After habituation, the stimulus was turned on, and the lobster was given 20 min to track the plume. Lobsters that did not track the plume were removed at the end of 20 min and given an additional trial 8 or more hours later. Each lobster was presented with three different injection rates (*i.e.*, plume types) in random order.

We recorded the tracking behavior of the lobsters with overhead video cameras. The dorsal surface of the lateral antennules and the anterior and posterior tips of the carapace were marked with fluorescent paint. Black lights were suspended over the testing section of the flume. This arrangement allowed us to score the positions of the antennules and the body in the X and Y coordinates of the flume floor. We then used the Metamorph Image Processing System™ to digitize the animals' paths from video images. The video was sampled at 6 Hz, and in each sampled frame the positions of the left and right lateral antennules were collected in source-centered coordinates. Once calibrated to distances in centimeters, these positions were used to compute the angle between the two antennules. Because the antennules are fixed in length, the angle is a measure of the bilateral sampling distance from which the lobster derives odor information. We only scored those trials in which the lobster: 1) started in the shelter or the downstream end of the behavioral section; 2) moved its rostrum within 5 cm of the source; 3) did not contact the side walls of the flume during its tracking; and 4) did this within the 20-min time limit.

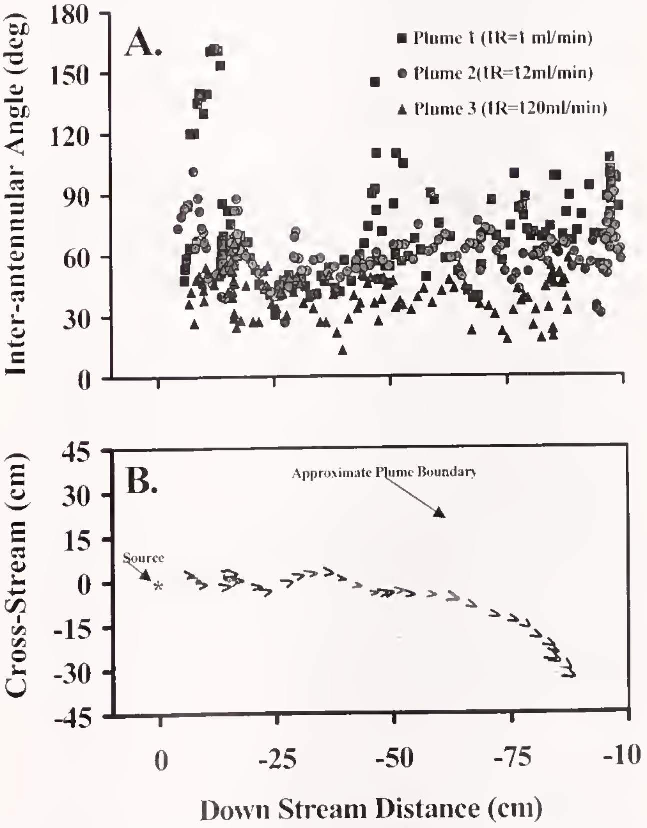

Figure 1. *(A) The angle between the two antennules for three paths made by lobster 28 while tracking. The data taken from paths associated with three different injection rates are shown at 6 Hz sampling rate. Note the higher inter-antennular angle at the lowest injection rate, particularly at farther downstream distances. (B) The actual positions of the antennules from the 120 ml/min injection rate in A. Display is at 2 Hz. The asterisk marks the location of the source. Each "V" drawn has its vertex at the location of the lobster's rostrum. The tips of each "V" mark the location of the antennule tips. Variations in antennule length reflect the elevation of the antennule.*

---

[1] Department of Biology, University of Massachusetts at Dartmouth, North Dartmouth, Massachusetts.

The animals met the criteria in 26 of 125 trials. However, only three animals did so for for all three injection rates. For these nine trials, we measured the animals' body orientation, walking speed, projected antennule length (an indirect measure of antennule tip elevation), the angle between the antennules, and the absolute antennular orientation from the digitized video. We report here the results for the analysis of inter-antennular angle. An analysis of variance for repeated measures (on the individual animals) indicated a significant primary effect of injection rate $F(2,2,708) = 29.06$ ($P < 0.001$) and a significant animal-by-injection-rate interaction (Fig. 1). Inter-antennular angle increased with distance from the source during tracking at the lowest of the three injection rates. The two higher injection rates are significantly different from the lowest injection rate in this analysis, but are not distinct from one another.

The three animals that were analyzed held their antennules more widely at the lower injection rates, meaning that less turbulent flow leads to wider spatial sampling. Obviously, the results taken from three animals must be interpreted conservatively. However, we take these results to indicate the power of this methodology for revealing the different sampling behavior lobsters employ with their lateral antennules. If the relationship between antennular separation and plume structure demonstrated here represents lobster tracking behavior in general, we will continue to use these methods to further examine the relationships between sampling strategies and stimulus environment.

This work was supported by NSF-REU (OCE-960599) Site Grant to Boston University and DARPA-ONR Award (N00014-98-1-0822) to FG and JA. The authors wish to thank Mimi Sheik for valuable technical assistance and Dr. Jennifer Basil, Marjorie Steele, Kirsten Pohlman, Michael van der Waal, and Thomas Breithaupt for advice and David Sandeman for thoughtful discussions that suggested this approach.

Literature Cited

1. **Moore, P. A., N. Scholz, and J. Atema. 1991.** *J. Chem. Ecol.* **17:** 1293–1307.
2. **Basil, J., and J. Atema. 1994.** *Biol. Bull.* **187:** 272–273.
3. **Dittmer, K., F. Grasso, and J. Atema. 1995.** *Biol. Bull.* **189:** 232–233.
4. **Devine, D., and J. Atema. 1982.** *Biol. Bull.* **163:** 144–153.
5. **Beglane, P., F. Grasso, J. Basil, and J. Atema. 1997.** *Biol. Bull.* **193:** 214–215.

Reference: *Biol. Bull.* **197:** 250–251. (October 1999)

Temporal Correlation Between Sensor Pairs in Different Plume Positions: A Study of Concentration Information Available to the American Lobster, *Homarus americanus*, During Chemotaxis

John P. Hanna[1], *Frank W. Grasso, and Jelle Atema (Boston University Marine Program, Marine Biological Laboratory, Woods Hole, Massachusetts)*

The American lobster requires both lateral antennules for efficient tracking of a turbulent jet odor plume (1, 2). We set out to determine what bilateral cues are available to a lobster while it tracks a "leaky" plume to its source. To do this we characterized the dynamics of a turbulent odor plume. We made video recordings of a 5-mm thick horizontal plane through a plume at the same height above the substrate that the lobster holds its lateral antennules and then analyzed the spatial patterns of concentration dynamics in that plane.

The experiments were conducted in a transparent-sided recirculating flume (10 m long; 2 m wide; water depth, 0.44 m). We analyzed a momentum-free ("leaky") plume that issued from a length of 0.5 cm diameter Tygon tubing (terminating in a stoppered porous section, 2 cm long) situated centrally on the floor of the flume. The tubing oozed 1×10^{-4} *M* rhodamine b dye (in seawater) at a rate of 15 ml/min, producing a "puddle" of dye about 10 cm in diameter on the floor of the flume. This dye was then lifted from the viscous sub-layer into the free-stream by the small amount of intrinsic vertical turbulence of our flume, which, in turn, created a plume that was transported downstream by the 9 cm/s free-stream current. This plume is a good model of a decomposing carcass or other benthic odor source typical of lobster food items. In addition, lobsters in our laboratory track an identical, odor-laden plume to the source under these exact conditions.

We used a pulsed YAG CO_2 laser (532 nm) and appropriate optics to produce a horizontal laser sheet that covered a 1 m^2 area of the flume 10 cm off the flume floor. The laser light within this sheet excited the fluorescent dye that constituted the plume. The intensity of the light emitted from the excited rhodamine B (excitation 540 nm emission 625 nm) molecules (and detected by the overhead CCD camera) was proportional to their concentration. Synchronizing signals were sent from an overhead CCD camera (Hitachi KP-M2U) to a 400 MHz Pentium computer running MetaMorph™ imaging software; the computer then synchronized the firing of the laser with the acquisition of images. We made seven recordings, each 2.35 min in duration, with the source positioned sequentially at 50, 100, 150, 200, 250, 300, and 350 cm upstream from the center of the recording area. The recordings were streamed directly to the computer disk at a rate of 10 frames per sec. At each recording location, we made separate recordings with the plume off to correct for background illumination, background dye accumulation from flume water re-circulation, and intensity variations in the laser sheet. Reference concentration series were also recorded so that pixel intensities could be calibrated to molar units. The individual images in each recording were corrected for background illumination and dye accumulation in the flume by subtracting the average background image. The effects from uneven light distribution in the laser sheet were corrected by using this same average background image as a normalizing mask. Each image was then filtered with a 7 × 7 pixel median filter to remove speckle noise. The dye reference images were corrected in the same manner and used to create a linear calibration curve ($R^2 = 0.98$) to convert the pixel values into molar units of dye concentration.

---

[1] Department of Biology, University of Delaware, Newark, Delaware.

In general, this plume resembled a series of discontinuous filaments and patches of dye, with their long axes aligned with the direction of flow. As the plume progressed downstream, these filaments became more diffuse and blended into an unhomogenous cloud at the furthest downstream recording location. At the 350-cm recording location this diffusion led to signal levels too low to analyze.

Once all the recordings were appropriately calibrated (above), we extracted concentration profiles (time series) at various spatial positions within the plume. We collected from pairs of sites separated by 1, 3, and 9 cm cross-stream distances. Three centimeters approximates the inter-antennular separation of a plume-tracking lobster. We centered these pairs at coordinates directly downstream and at 15 cm to the left and right of the source in a given image stack. One such set of six points was collected from the image stack corresponding to each distance from the source. This spatial distribution of concentration profiles provided a sampling, in regular x-y coordinates, of the plume concentration dynamics within the laser sheet.

We studied the cross correlation functions (CCF) of these paired concentration series (Fig. 1) to look for spatial cues that would indicate source direction and that might be available to a pair of sensors (*e.g.*, the lobster's paired lateral antennules). For each spatial location, we measured the best correlation magnitude, best-matched delay, peak half width, and peak asymmetry. The delay and asymmetry indicated the existence of left-right differences in odor patch arrival time, half width reflected variation in odor patch size. The correlation magnitude gave an indication of reliability of any of these cues. All 54 CCFs had significant correlations centered at 0 delay ($P < 0.0001$ for all CCF maximum peaks, many $P < 0.0001$, R^2 ranged between 0.99 at 1 cm and 0.25 at 9 cm inter-sensor separation). The magnitude of the correlations fell off with increased separation between sampling pairs, but did not vary systematically with the spatial location of the pairs in the plume. We also found no significant variations in CCF asymmetry or half width with spatial location.

Although American lobsters are more accurate plume trackers when they use both antennules, we found no indications in this rigorous quantitative study that bilaterally relevant information exists in the plume generated by this "leaky" source. The earlier lobster studies were conducted with plumes from non-zero momentum (jet) sources, where such directional cues are known to exist (3, 4, 5, 6). Since lobsters can track this exact momentumless (leaky) plume, however, we are left with two alternatives: 1) that lobsters use other bilateral cues than instantaneous cross correlation of concentration when tracking such plumes; or 2) that no bilateral information is required by these animals to track leaky plumes. These negative results are important because leaky plumes are common in the natural world and contrast the 'jet' sources which have received greater attention in previous physical plume characterizations (5, 6) and behavioral studies with lobsters (1, 2). These results support the idea that lobsters are more likely to use different tracking strategies in different plumes than one universally effective strategy for all plumes.

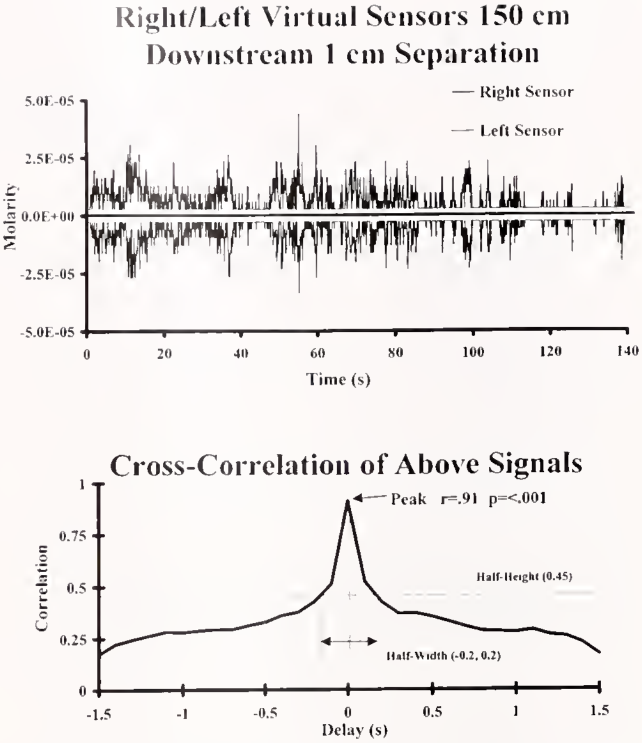
Right/Left Virtual Sensors 150 cm Downstream 1 cm Separation

Cross-Correlation of Above Signals

Figure 1. *A representative cross-correlation (n = 1411) from our data set. Only the first second and half of the 2.35-min range of the cross-correlation is shown. All of the cross-correlations showed a zero delay and a high degree of symmetry around that delay. The method of determining the half-width of the cross-correlation is illustrated in the diagram. We measured half width by finding the two points of intersection between the horizontal line at the 50% maximum correlation level and the correlogram. The half-width was the distance between these two points projected onto the time axis. Peak asymmetry was measured by comparing the integrated areas beneath the correlogram between these two half-widths and the delay of the peak correlation.*

We thank Dr. Deborah Compton of the Boston University Aeronautical Engineering department for fluid dynamics advice, and the loan of the laser and optical equipment. We thank Doug Bowman and Neil Glickman from Universal Imaging, and Meg Steele and Carla Guenther for valuable technical assistance. This work was supported by NSF-REU (OCE-960599) Site Grant to Boston University and DARPA-ONR Award (N00014-98-1-0822) to FG and JA.

Literature Cited

1. **Devine, D., and J. Atema. 1982.** *Biol. Bull.* **163:** 144–153.
2. **Beglane, P., F. W. Grasso, J. Basil, and J. Atema. 1997.** *Biol. Bull.* **193:** 214–215.
3. **Grasso, F. W., J. H. Dale, T. R. Consi, D. C. Mountain, and J. Atema. 1996.** *Biol. Bull.* **191:** 312–313.
4. **Grasso, F. W., J. H. Dale, T. R. Consi, D. C. Mountain, and J. Atema. 1997.** *Biol. Bull.* **193:** 215–216.
5. **Dittmer, K., F. W. Grasso, and J. Atema. 1996.** *Biol. Bull.* **191:** 313–314.
6. **Dittmer, K., F. W. Grasso, and J. Atema. 1995.** *Biol. Bull.* **189:** 232–233.

Reference: *Biol. Bull.* **197:** 252–253. (October 1999)

Chemoreceptor Cells as Concentration Slope Detectors: Preliminary Evidence from the Lobster Nose

Erik Zettler[1] *and Jelle Atema (Boston University Marine Program, Marine Biological Laboratory, Woods Hole, Massachusetts 02543)*

Chemoreceptor cells of the American lobster *Homarus americanus* distinguish between different chemical compounds, as well as their concentrations (1, 2, 3). After an initial phasic response to an increase in stimulus concentration, chemoreceptor cells quickly adapt to the higher background and, within one to a few seconds, spike frequency reverts to zero or to a low tonic level (2, 3). The chemical signature of an odor source is dispersed through its fluid medium by generally turbulent flow resulting in patches of different sizes and shapes. As these spatial patches pass by a sensor they appear as concentration peaks over time. The onset slopes of these peaks depend on the shape and concentration of the individual patches. Despite the chaotic nature of turbulence there is a spatial gradient of patches within such an odor plume. Patches disperse in statistically describable patterns, creating "odor landscapes" such that, closer to the source, the average odor peak heights and onset slopes are greater (1, 4). If an animal could distinguish between shallow and steep odor onset slopes, it could orient itself in a turbulent plume and move towards or away from the odor source.

We have investigated the response of chemoreceptor cells of the lateral antennule of the American lobster *Homarus americanus* to odor onset slopes generated by computer-controlled piston pumps (Millipore model 510). The odor stimulus (a 0.01% aqueous extract of TetraMarin fish food) was mixed with a dopamine tracer that allowed us to measure the actual stimulus concentration profile of each slope with high spatial and temporal resolution; the measurement was made with an IVEC-5 system (In Vivo Electro-Chemistry, Harvard Apparatus). Lateral antennules were excised and inserted, with aesthetasc sensilla facing up, into an acrylic olfactometer chamber that permitted perfusion with cold oxygenated Ringers and use of a suction electrode to record from the proximally exposed nerve bundle. The distal section bearing the aesthetascs was bathed with a constant flow of 10 ml min^{-1} of filtered seawater into which the food odor and tracer dissolved in seawater could be injected by the piston pumps. Using a micromanipulator, the measuring tip of the IVEC electrode was placed within the aesthetasc tuft. Details of this tracer system, the olfactometer, and the extracellular recording techniques for this preparation are found elsewhere (3).

Four cells were tested with each of two stimulus slopes (Low and Medium). One of these cells was tested with an additional slope (High) generated by suddenly opening a valve to gravity feed the stimulus to the preparation. This delivery system is similar to one used earlier (3) to achieve steep onset ramps but does not allow for easily controlled slope variation. Because all cells tested showed a similar response, we chose to show results from the cell with the greatest number of treatments (Fig. 1). Average spike frequency, calculated during the first second of stimulus concentration rise, was higher for steeper onset slopes, ranging from 3 spikes per second for the Low slope to 60 spikes per second for the High slope. Despite this 20-fold increase in spike frequency in response to steeper slopes, the ratio of spike frequency to stimulus concentration change varied only by a factor of two. Since the length of the slopes and the peak concentrations varied between treatments and the purpose of this study was to investigate the effects of onset slopes, we also compared the spike frequency during the initial rise from background to when the dopamine tracer reached 8 μM (the highest concentration reached by the Low slope). Examined in this way, the change in concentration is identical across treatments, so differences in spike frequency

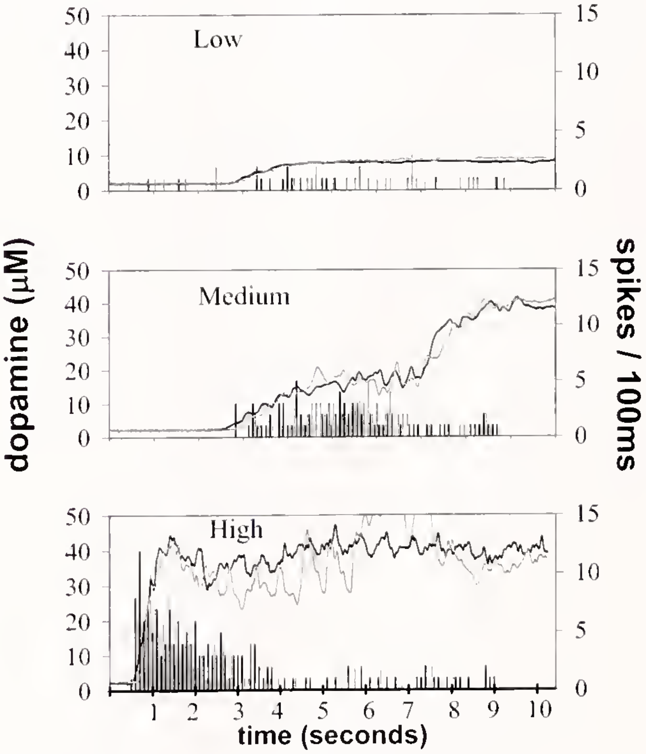

Figure 1. *Duplicate odor pulses for the three slopes (top traces in each panel), and the resulting spikes from a single chemoreceptor cell. The concentration of the dopamine tracer (measured at 200 Hz using IVEC-5) is plotted on the left y-axis; the dopamine was mixed in seawater with the odor stimulus and is assumed to disperse in a manner similar to the odor (4). The lower section of each panel represents the occurrence of individual spikes grouped into 100 ms bins (right y-axis). For both the stimulus trace and the spikes, the first run is shown in black, and the second run in gray. Despite some variation in the pump outputs (especially after the peak concentration was reached) agreement during the initial rise in concentration was good between replicates. Spikes were digitized and sorted to ensure that they would represent a single receptor cell. Spike frequency increased with increasing odor onset slope.*

---

[1] Also at Sea Education Association, Woods Hole, Massachusetts.

should be due mainly to the different slopes. The spike frequency (and rise time) during this portion of each slope was 3.1 Hz (1800 ms) for the Low slope, 5.5 Hz (980 ms) for the Medium slope, and 70 Hz (160 ms) for the High slope. Once the concentration stopped rising, cells adapted to the constant background within a couple of seconds. We note that the lack of a response to the second slope rise in the Medium slope (middle panel between 7 and 8 seconds) of Figure 1 may be due to the large fluctuations in the output of the piston pumps preceding this rise. These periodic fluctuations (some of which exceed 5 μM) would cause cumulative adaptation in the chemoreceptor cell such that the overall response is depressed (5). Because spike adaptation can occur rapidly, beginning within 500 ms of the stimulus presentation, a steeper onset slope may minimize adaptation and provide the highest frequency for a given concentration. We will not discuss here the intracellular signal transduction pathways that may be involved in the excitation and adaptation phenomena observed.

These preliminary results demonstrate the feasibility of delivering measured concentration slopes and provide initial evidence that chemoreceptor cells can act as "slope detectors." Odor slope discrimination could be very useful for orienting and tracking in a fluid environment, because so much physical information about the plume and odor source is present in the distribution of slopes in the eddy field (4). In this study, single cells could discriminate between a range of odor onset slopes with rise times similar to those measured in laboratory studies of jet plumes (1, 4). In general, animals may have different chemoreceptor cells "tuned" to particular ranges of pulse characteristics, such as frequency, height, length, and slope (1, 2, 3).

Thanks to D. Mellon and G. Gomez for helpful discussions. Supported by NSF grant IBN-9723542 to JA and a B.U.M.P. Humes alumni Award to EZ.

Literature Cited

1. **Atema, J. 1996.** *Biol. Bull.* **191:** 129–138.
2. **Borroni, P., and J. Atema. 1988.** *J. Comp. Physiol. A.* **164:** 67–74.
3. **Gomez, G., and J. Atema. 1996.** *J. Exp. Biol.* **199:** 1771–1779.
4. **Moore, P., and J. Atema. 1991.** *Biol. Bull.* **181:** 408–418.
5. **Voigt, R., and J. Atema. 1990.** *J. Comp. Physiol. A.* **166:** 865–874.

Reference: *Biol. Bull.* **197:** 253–254. (October 1999)

Individual Recognition and Memory in *Homarus americanus* Male-Female Interactions

Cristin Berkey[1] *and Jelle Atema (Boston University Marine Program, Woods Hole, Massachusetts 02543)*

Individual recognition and memory have been studied in *Homarus americanus,* the American lobster. It has previously been demonstrated, through lobster boxing matches, that males can recognize individuals. When a male encounters the same male it lost to previously, it avoids a new fight. The same animal will fight on subsequent occasions if presented with an unfamiliar opponent (1). The ability to recognize a previous opponent lasts for up to a week, and it is based on olfactory recollection of the opponents' urine (2). The same results have been obtained in female-female encounters (3). We therefore hypothesize that male-female pairs of *Homarus americanus* can also recognize individuals, as demonstrated by shorter periods of fighting on the second encounter with familiar individuals.

Males and females were paired by carapace length, with no pair differing by more than 3 mm. It was also ensured that in all matched pairs, the animals had not previously met. Animals were kept in isolation for 24 h before their first boxing match and for the 24 h between the first and second matches. All boxing matches took place in a 240-l glass aquarium and were videotaped. One male and one female were placed in the tank and separated by a removable, opaque divider. The lobsters were allowed to acclimate for 10 min before the divider was removed, and then allowed to interact for 20 min. There were two sets of fights, group A and group B. In group A, the same pair of animals fought twice. In group B, the animals were rotated so that each animal met a new opponent in the second fight. In both sets, the first and second fights were separated by 24 h. Any pair of animals that did not show a definite loser and winner after the first 20-min period was disqualified and the fight was not included in the data analysis.

The fights were scored using a pre-established scale of agonistic levels (1) with some additions made for differences that arose as a result of the fights being between males and females. An agonistic level was assigned to each animal every 5 s. The levels ranged from -2 to 5, with -2 demonstrating fleeing behavior and 5 demonstrating claw snapping or claw ripping at the opponent. An overall agonistic scale was calculated for each animal in each fight by summing all of the agonistic values. A fight was determined to be over when one animal ceased to show an agonistic level above one. In this way, the duration of each fight was scored. To prevent bias during analysis of the behavioral tapes, the scorer was blind to whether the tapes were from a first or second fight.

In group A, 10 pairs of fights were carried out. Significantly, in 9 out of 10 instances, no fighting occurred on the second encounter; fighting did occur in the tenth case. In group B, 13 pairs of fights were carried out. Two sets were disqualified because there was no clear winner after the first fight. In 3 out of 11 instances, no fighting occurred on the second encounter. In 8 instances, fighting occurred. The fraction of times in which fighting occurred on the second encounter is significantly different between the two groups ($P < 0.005$ $x^2 = 8.416$ df = 1).

When a fight was between familiar opponents, the aggression level of the loser was significantly lower in the second boxing match than in the first boxing match ($P < 0.05$ paired t test). However, for unfamiliar opponents, the aggression level of the loser was not significantly lower in the second boxing match than in the first (paired t test). The aggression level of the winner was not significantly different between the two fights in either group A or group B (paired *t* test).

---

[1] Tufts University, Medford, Massachusetts.

We observed two behaviors that had not previously been seen in either male-male (1) or female-female (3) matches. One of these was mounting behavior, which typically occurs just prior to mating (4): the male climbs on the back of the female and attempts to turn her onto her back using his first two pairs of walking legs and his third maxillipeds. In our encounters, however, this mounting behavior never progressed to actual mating. We observed male-female mounting behavior in five separate encounters, two of which involved the same pair of animals. A second form of behavior not seen in same-sex boxing matches was nonreactive contact. This included any situation in which the two animals were in physical contact but did not seem to be reacting to each other. The average time spent in contact across the 42 fights analyzed was 179 s per 20-min fight. This value had no obvious correlation with previous exposure to the opponent. In addition to the differences already mentioned, fight duration in first encounters was significantly shorter in male-female fights than in male-male fights ($P < 0.05$, *t* test). The average fight duration was 250 s (SE ± 50 s) in male-female pairs, but 457 (SE ± 73 s) in male-male pairs (1). However, there was no significant difference in fight duration between male-female and female-female first fights: the average fight duration in female-female pairs was 206 s (SE ± 73 s) (3). The similarity in fight duration between female-female and male-female pairs is consistent with the observation that the loser determines the end of the fight: in male-female pairs, females typically lost.

The fact that second encounters were much shorter, to the point that no fighting occurred, supports the hypothesis that male and female lobsters can recognize each other as individuals. The results also demonstrated differences, such as nonreactive contact and mounting behavior, in the way male and female lobsters interact within the boxing match situation, compared to male-male and female-female interactions. It is possible that these differences parallel the natural interactions between male and female lobsters. Females are allowed to enter male shelters, whereas other males are not (5). Therefore, males and females must be capable of being near to each other without demonstrating aggressive behavior.

Financial support from NSF-REU (OCE-9605099 site award to Boston University). We thank Leslie McLaughlin, Jennifer Walters, and Dr. Frank Grasso for their assistance with this project.

Literature Cited

1. **Karavanich, C., and J. Atema. 1998.** *Anim. Behav.* **56:** 1553–1560.
2. **Karavanich, C., and J. Atema. 1998.** *Behaviour* **135:** 719–730.
3. **Atema, J., T. Breithaupt, A. LeVay, J. Morrison, M. Mallidis, and M. Edattukaran. 1999.** *Chem. Senses* (in press).
4. **Atema, J., and D. G. Engstrom. 1971.** *Nature* **232:** 261–263.
5. **Bushmann, P., and J. Atema. 1997.** *Can. J. Fish. Aquat. Sci.* **54:** 647–656.

Reference: *Biol. Bull.* **197:** 254–255. (October 1999)

Urinary Protein Concentration in Connection with Agonistic Interactions in *Homarus americanus*

Leslie C. McLaughlin[1], *Jennifer Walters*[2], *Jelle Atema, and Norman Wainwright*
(Boston University Marine Program, Marine Biological Laboratory, Woods Hole, Massachusetts 02543)

Homarus americanus, the American lobster, relies heavily on chemical signals as a source of information (1). Urine in particular has notable behavioral effects on these animals, suggesting that it is an important source of chemical information, specifically in social communication. Lobsters store urine and, in different behavioral contexts, release it from two paired, frontally facing nephropores into their gill current (2, 3). Previous studies (4, 5, 6) have shown that lobsters recognize conspecifics as individuals for at least 24 h and up to a week after one 20-min staged agonistic interaction. Both urine release and antennular chemoreception are necessary for this recognition (7). Evidently lobster urine carries a chemical signal that allows for individual recognition among animals; the challenge is to identify the chemical composition of the signal. One candidate is the proteinaceous content of the nephropore gland (8). We set out to study protein concentration in the urine of lobsters subjected to two agonistic encounters separated by 24 h.

Twenty-three wild-caught female lobsters (79–83 mm carapace length) were used. They were kept in groups of 5 to 15 in 400-l communal tanks with flow-through seawater and artificial shelters made from PVC pipe. All lobsters were healthy and fed squid twice a week. Lobsters were isolated in individual aquaria 48 h before their first agonistic encounters with unfamiliar lobsters, following Karavanich and Atema (4). Isolated lobsters were fed a small piece of squid at least 1 h before each interaction. All agonistic interactions took place in a 240-l glass aquarium that was rinsed and filled with unfiltered seawater immediately before each lobster interaction. Two female lobsters unfamiliar to one another were placed in the aquarium on either side of a removable, opaque divider and were allowed 10 min to acclimate to their new surroundings. To initiate the encounter, the plastic divider was raised and the lobsters were allowed to interact for 20 min, after which they were returned to their respective isolation tanks. Twenty-four hours later this procedure was repeated: about half ($n = 13$) of the animals were exposed to the same lobster they had encountered the day before; the other half ($n = 10$) were paired with an unfamiliar lobster. All encounters were videotaped for later analysis.

---

[1] Brown University, Providence, Rhode Island.

[2] Oregon State University, Corvallis, Oregon.

Table I

Mean urinary protein concentrations[1] *(μg/ml)*

	Pre-fight I	Fight I	Post-fight I	Pre-fight II	Fight II	Post-fight II
WINNERS						
Mean	224	138	167	214	215	144
Standard Error	22	31	32	73	96	42
Range	119–305	8–233	8–284	5–635	14–848	14–298
LOSERS						
Mean	218	146	180	206	189	221
Standard Error	40	46	39	32	32	34
Range	32–364	26–346	38–349	15–310	60–340	25–352

[1] Day I Winners $n = 11$, Day II Winners, $n = 12$; Day I Losers, $n = 10$, Day II Losers, $n = 11$.

Lobsters were catheterized following Breithaupt, Lindstrom, and Atema (3), except that only the right nephropore was catheterized. While we collected urine from one nephropore, the other was thus free to function normally—most importantly, as a source of chemical signals. To minimize contamination, all equipment to be in contact with urine was cleaned with 100% ethanol and rinsed with deionized water prior to use. Six urine samples were collected from each lobster. The first sample was labeled *pre-fight I* and was collected from the time of catheterization until the start of the first agonistic encounter (about 20 h of collection). The second sample, *fight I,* was collected during the 10 min of acclimation and the subsequent 20 min of agonistic interactions. The third sample, *post-fight I,* was collected for the first 6 h after the first fight, after which collection of *pre-fight II* was begun; *pre-fight II* was replaced by *fight II* at fight time on the second day. *Fight II* and *post-fight II* were collected on the same schedule as their counterparts on the first day. All urine samples were stored at −80°C, then thawed in a cool water bath immediately before analysis. The Pierce BCA protein assay kit was used to detect and quantify protein in the samples. It has a working range of 20 μg/ml to 2000 μg/ml (9). Samples were prepared, incubated, and read in a spectrophotometer at 562 nm along with a set of protein standards of known concentration.

Most of the urine samples showed protein concentrations of 100–300 μg/ml. Differences in protein concentration were evaluated for correlation with the status of the animal (winner or loser), the fight (I or II), and the opponent (familiar or unfamiliar), and with all combinations of these factors. No significant differences in protein concentrations were found among the different conditions (Table I). Any differences that might exist would be difficult to determine due to great variation within and between individuals. The most extreme protein concentration difference in samples collected from one animal was between 244 and 848 μg/ml. The most extreme values among all animals ranged from 3 to 848 μg/ml. Since all animals were fed the same diet systematically, this variation is unlikely to be due to diet.

The high levels of protein found in female lobster urine suggest that these proteins may not be simply waste products but may function as a chemical signal. The finding that protein concentration did not vary systematically with any of the fight conditions tested indicates that such a signal is more likely to be involved in individual recognition than in social status or in recent fight experience. For recognition, the signal of each individual needs to be only qualitatively reliable. Identification of the proteins in lobster urine is needed to substantiate these suggestions.

Financial support from NSF-REU (OCE-9605099 site award to Boston University). We thank Alice Child, Felisa Wolfe, and Andrea Cubbage for technical support, Kirsten Pohlmann and Dr. Thomas Breithaupt for design ideas and a crash course in catheterization, and Dr. Frank Grasso, Dr. Jenny Basil, and Meg Steele for scientific insight.

Literature Cited

1. **Atema, J., and R. Voigt. 1995.** Pp. 313–348 in *Biology of the Lobster* Homarus americanus, J. R. Factor, ed. Academic Press, New York.
2. **Atema, J., and D. F. Cowan. 1985.** *J. Chem. Ecol.* **12:** 2065–2080.
3. **Breithaupt, T., D. P. Lindstrom, and J. Atema. 1999.** *J. Exp. Biol.* **202:** 837–844.
4. **Karavanich, C., and J. Atema. 1998.** *Anim. Behav.* **56:** 1553–1560.
5. **Atema, J., T. Breithaupt, A. LeVay, J. Morrison, M. Mallidis, and M. Edattukaran. 1999.** *Chem. Senses.* (in press).
6. **Berkey, C., and J. Atema. 1999.** *Biol. Bull.* **197:** 253–254.
7. **Karavanich, C., and J. Atema. 1998.** *Behaviour* **135:** 719–730.
8. **Bushmann, P. J., and J. Atema. 1996.** *J. Crustac. Biol.* **16(2):** 221–231.
9. **Pierce. 1997.** BCA Protein Assay Kit (23225). 3747 N. Meridian Road P.O. Box 117, Rockford IL 61105. Tel. 800-8-PIERCE.

Reference: *Biol. Bull.* **197:** 256. (October 1999)

Contact with Squid Egg Capsules Increases Agonistic Behavior in Male Squid (*Loligo pealei*)

Alison J. King, Shelley A. Adamo (Departments of Biology and Psychology, Dalhousie University, Halifax, Nova Scotia, Canada B3H 4J1), and Roger T. Hanlon[1]

Agonistic (aggressive) behavior is costly (1). For this reason, males should fight only when it will increase their reproductive fitness. In some species, the last male to mate with a female before she oviposits sires most of the offspring (2). If *Loligo pealei* has a similar system of sperm precedence, a male should drive away nearby males when females are about to lay their eggs. In *L. pealei*, conspecific egg capsules induce other females to lay their eggs (3). Therefore, the presence of egg capsules could provide male squid with the information that females are about to begin ovipositing. To determine whether male squid might use this information, we tested the effect of squid egg capsules on male agonistic behavior. An earlier report suggested that squid egg capsules may increase male agonistic behavior (4). We also explored which stimuli connected with the egg capsules might influence male behavior.

Agonistic behavior in *L. pealei* is similar to that observed in *Loligo plei* (5). First there is a variety of signaling through skin patterns; then the behavior escalates to Fin Beating, Chasing, (or Fleeing) and finally to Open Arm Charges. In the highly aggressive Open Arm Charge, one squid rushes toward the other squid with his arms in a tight cone. Once he is close to his opponent, he throws open his arms. Sometimes the charging squid contacts and wrestles with the conspecific, but more often he stops short of the other squid.

The effect of egg capsules on male agonistic behavior was tested as follows. Male squid were isolated for 14 to 21 h prior to a trial. Squid were randomly assigned as either the "resident" or "intruder." Resident squid were isolated in circular tanks (3 m in diameter, 0.5 m deep). Intruder squid were isolated in rectangular tanks (132 × 76 × 43 cm). The mantle lengths of the resident and intruder (16–21 cm) were size-matched to within 1 cm. Water temperature in the tanks was maintained between 14.5°–22.5°C, and the tanks were exposed to an ambient light cycle (June–Aug.). Squid were fed *Fundulus* spp. on the evening before the trials, which were run early the next day. Each squid was used only once. During a trial, an intruder male was introduced into the circular tank containing the resident. Incidences of Fin Beating, Chases, Open Arm Charges, and other behaviors were recorded. After 20 min ($n = 23$) or 30 min ($n = 10$), squid egg mops (16–20 egg capsules attached to an airstone), were placed in the center of the tank for 20 min ($n = 16$) or 30 min ($n = 5$) and then removed. One min (median: 1 min, 1st and 3rd quartiles: 1 min, $n = 21$) after the addition of an egg mop, squid swam towards it, blew water on it, and finally touched it with their arms. In one set of control trials, airstones were added without egg capsules (Table I).

As Table I shows, the presence of egg mops induced a large increase in Open Arm Charges, while the airstone alone had no effect. The increase in Open Arm Charges never occurred prior to physical contact with the egg capsules (49/49 trials).

Table I

The effect of different treatments on the number of Open Arm Charges

Treatment	Number of Open Arm Charges/10 min Median (1st quartile, 3rd quartile)	*n*
Nothing added to tank	0 (0, 0)	33
Airstones only	0 (0, 0)	5
Egg mop	9.7 (6.5, 17.3)*	21
Covered egg mop	0 (0, 0)	7
Egg mop in glass box	0 (0, 1.5)	8

* Significantly different from "Airstones only" treatment ($Z = 3.41$, $P < 0.001$).

In a further set of experiments, we placed an egg mop under a perforated cover. The cover blocked squid from seeing the eggs, but allowed chemical substances to flow from under the cover into the tank. Experiments in which a bolus of dye was introduced under the cover indicated that substances could pass into the tank from this location. While the egg mop was under the cover, the number of Open Arm Charges did not increase (Table I: Covered egg mop). Once the cover was removed, and the squid had seen and touched the egg capsules, the number of Open Arm Charges increased (7/7 trials).

We also placed an egg mop in an uncovered glass box, which was lowered into the tank containing the squid. The glass box allowed visual, and possibly chemical, stimuli to enter into the squids' tank, but prevented the squid from contacting the egg mop. Squid visually inspected the egg mop through the glass box, but there was no increase in the number of Open Arm Charges (Table I: Egg mop in glass box). When the egg capsules were placed outside of the glass box, agonistic behavior increased after the squid contacted the egg mop (7/7 trials). Contact with the egg capsules appears to be critical for inducing the effect.

These results suggest that contact with squid egg capsules increases agonistic behavior in male squid. Although visual cues may be important for locating the egg mop, the stimulus that 'turns on' agonistic behavior may be a chemical embedded in the egg capsule that the male must touch to sense. By using a cue from the egg capsule to regulate their agonistic behavior, male squid may be able to target the expression of this costly behavior to times when it will produce the maximum reproductive benefit.

This study was supported by NSERC (SA and AJK), the Grass Foundation (SA) and a WHOI Sea Grant NA46RG0470 (RTH).

Literature Cited

1. **Archer, J. 1988.** *Behavioural Biology of Aggression.* Cambridge University Press, Cambridge.
2. **Birkhead, T. R., and A. P. Møller. 1992.** *Sperm Competition in Birds: Evolutionary Causes and Consequences.* Academic Press, San Diego.
3. **Arnold, J. M. 1962.** *Biol. Bull.* **123:** 53–57.
4. **Hanlon, R. T. 1996.** *Biol. Bull.* **191:** 309–310.
5. **DiMarco, F. P., and R. T. Hanlon. 1997.** *Ethology.* **103:** 89–108.

---

[1] Marine Biological Laboratory, Woods Hole, Massachusetts 02543.

Reference: *Biol. Bull.* **197:** 257–258. (October 1999)

Squid Axoplasm Supports the Retrograde Axonal Transport of Herpes Simplex Virus

E. L. Bearer (Brown University), M. L. Schlief[1]*, X. O. Breakefield*[2]*, D. E. Schuback*[2]*, T. S. Reese*[1]*,*
and J. H. LaVail[3]

Neurotropic viruses, such as Herpes simplex virus type 1 (HSV1), first enter the axon terminal and are transported to the cell body where they replicate in the nucleus. Based on previous studies using whole animal assays (1), as well as assays of whole cells *in vitro* (2, 3), we know that HSV enters axons and travels as an unenveloped particle—capsid plus associated tegument proteins—in a retrograde direction toward the cell body. The rate of transport has been estimated to be 3–5 mm/hr (2).

Although these earlier studies provided important insight into the delivery of virus to the nucleus, they were limited. What has been needed is an experimental system in which HSV can be applied to a particular region of a neuron at a known concentration and time, and the transport of the virus assayed quantitatively within the axon. With such an assay one could address questions about the real time motility of the viral particle and about the viral and cellular proteins that are essential for this behavior.

The giant axon of the squid, *Loligo pealei*, serves as a powerful model for the molecular mechanisms of axoplasmic transport. The microtubule-based motor, kinesin, was discovered in squid (4); and microtubule-based transport in both anterograde and retrograde directions has been extensively characterized. Recently, actin-based transport of squid axoplasmic organelles has also been described (5, 6). Organelles move in either direction in the giant axon at 2–4 μm/s. Organelles isolated from squid axons move towards the barbed ends of actin filaments (6, 7) at 1.6 μm/s (8) and in either direction on microtubules at 2 μm/s (9). The axon contains long tracks of microtubule-actin filament bundles that appear to serve collectively as tracks for axonal transport (10). Thus, the squid axon contains all the requisite molecular machinery for transport. In this report, we describe the use of the squid giant axon as an alternative to previous approaches and present for the first time direct observation of the movement of HSV in living axons.

To image the virus in the axon, we used a viral HSV strain in which a major tegument protein, viral protein (VP) 16, was generated as a fusion protein with GFP at the C terminal. This virus was grown in Vero cells, purified, and concentrated to a titer of about 1.0×10^9 pfu/ml. Different aliquots of the viral stock were treated in various ways to remove the viral envelope. This mimics the first step in viral infection in which the viral envelope fuses with the cell membrane, releasing the capsid together with its tegument into the cytosol. *In vitro* removal of the envelope was necessary for these experiments because injection of virus into the axon by-passes the normal membrane fusion step. Several treatments were found that produced motile, fluorescent particles in the axon after injection.

The viral preparation was co-injected with non-fluorescent oil. The oil droplet was used to determine an appropriate focal plane and as a fixed reference marker, since it remains stationary after injection (11). The movement of viral particles was recorded on a laser scanning confocal microscope. Movement was sampled ~1 frame/3 s, and transport rates were determined by analyzing sequential frames.

When we examined fields upstream from the oil droplet, *i.e.*, closer to the cell body, we identified rapidly moving particles. One of these moved ~36 μm in 18 s for an overall rate of 1.9 μm/s in the retrograde direction (Fig. 1). At the end of this sequence, this particle went out of the plane of focus. Of 113 moving particles examined, all were found in the region of the axon between the oil droplet and the cell body, moving in the retrograde direction.

The effect on the virus of the pre-injection treatment was determined by electron microscopy of negatively stained preparations. Of the virus in those samples that produced motile particles when injected in the axon, ~90% had lost their surface envelope. Since the GFP-labeled protein, VP16, is a tegument protein, the moving particles we observed must include at least tegument, either as whole virus, tegument plus capsid, or simply as tegument aggregates. Since neither capsid nor membrane are GFP-labeled, we cannot know from these studies whether they also are capable of moving.

We have demonstrated the rapid and preferential retrograde axonal transport of HSV particles in the living axon. The rate of movement of these viral particles in the squid giant axon is similar to the estimated rates of retrograde transport of this human virus in rat dorsal root ganglia in culture (2). Furthermore, this rate is consistent with the rates of retrograde transport of endogenous organelles in the squid axon and of isolated organelles on either microtubules or actin filaments. Both the direction and rate of movement suggest that a host cell motor molecule, such as the retrograde microtubule motor, dynein, may be co-opted by invading virus. Thus, by combining the power of the squid axon with a biochemical and genetic dissection of the virus, we expect to be able to identify the viral proteins required for transport, as well as the cellular transport machinery that they recruit.

Supported by NIH EY08773 (JHL), GM47638 (ELB), NINDS (TSR), NINDS24279 (XDB), and by the Frederik B. Bang Fellowship Fund and the Evelyn and Melvin Spiegel Fellowship Fund, Marine Biological Laboratory, Woods Hole, MA, and by a predoctoral NINDS fellowship (MLS).

Literature Cited

1. **Topp, K. S., L. B. Meade, and J. H. LaVail. 1994.** *J. Neurosci.* **14:** 318–325.
2. **Lycke, E., K. Kristensson, B. Svennerholm, A. Vahlne, and R. Zeigler. 1984.** *J. Gen. Virol.* **65:** 55–64.

---

[1] NINDS, National Institutes of Health, Bethesda, Maryland.

[2] Massachusetts General Hospital, Boston, Massachusetts.

[3] University of California, San Francisco.

3. **Sodeik, B., M. W. Ebersold, and A. Helenius. 1997.** *J. Cell Biol.* **136:** 1007–1021.
4. **Vale, R. D., T. S. Reese, and M. P. Sheetz. 1985.** *Cell* **42:** 39–50.
5. **Kuznetsov, S. A., G. M. Langford, and D. G. Weiss. 1992.** *Nature* **356:** 722–725.
6. **Bearer E. L., J. A. DeGiorgis, R. A. Bodner, A. W. Kao, and T. S. Reese. 1993.** *Proc. Natl. Acad. Sci. USA* **90:** 11252–11256.
7. **Langford, G. M., S. A. Kuznetsov, D. Johnson, D. L. Cohen, and D. G. Weiss. 1994.** *J. Cell Sci.* **107:** 2291–8.
8. **Bearer, E. L., J. A. DeGiorgis, N. A. Medeiros, and T. S. Reese. 1995.** *Cell Motil. Cytoskeleton* **33:** 106–114.
9. **Schnapp, B. J., R. D. Vale, M. P. Sheetz, and T. S. Reese. 1985.** *Cell* **40:** 455–462.
10. **Bearer, E. L., and T. S. Reese. 1999.** *J. Neurocytol.* **28:** 85–98.
11. **Galbraith, J. A., T. S. Reese, M. L. Schlief, and P. E. Gallant. 1999.** *Proc. Natl. Acad. Sci. USA* (in press).

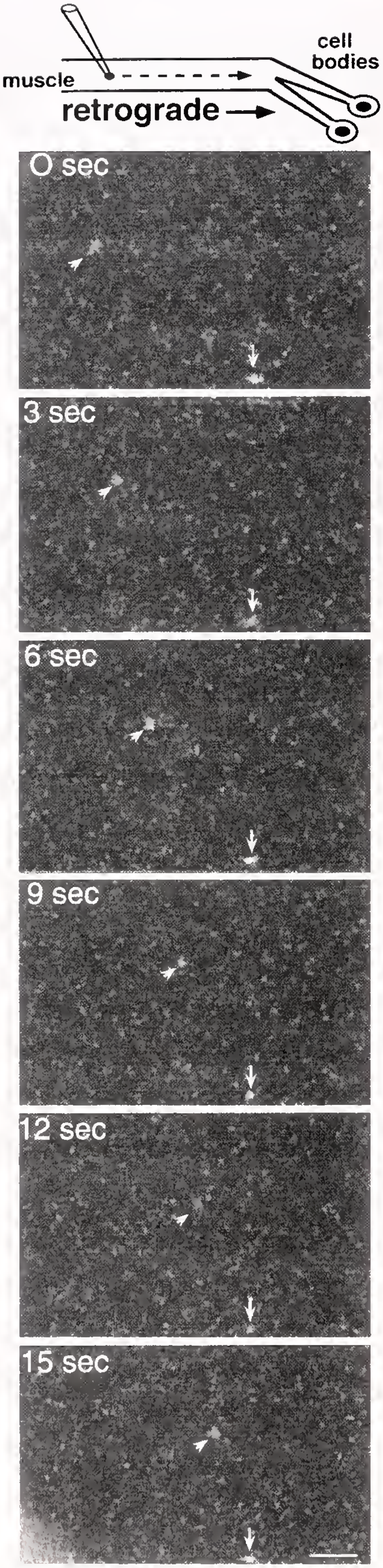

Figure 1. *Retrograde transport of a GFP-labeled viral particle in a living squid axon. The giant axon was dissected in Ca^{++}-containing seawater and injected with >100 pfu of GFP-VP16 labeled and extracted Herpes simplex virus. Still frames were taken from a BioRad confocal microscope sequence captured at 2–3 sec intervals and processed with NIH Image software. The diagram shows the orientation of the giant axon and site of injection relative to observed movements (dashed arrow). In this preparation, the cell body is to the right. GFP-labeled particle (oblique arrowhead) moves at 1.9 μm/s towards the cell body, contrasting with a stationary fluorescent spot (vertical arrow). Axons were dissected away from cell bodies and synapses, and their two ends labeled with color coding string. Bar = 10 μm.*

Reference: *Biol. Bull.* **197:** 259–260. (October 1999)

Messenger RNAs for Kinesins and Dynein are Located in Neural Processes

Robert Gould (NYS Institute for Basic Research, Staten Island, New York), Concetta Freund, Frank Palmer, Pamela E. Knapp[1], *Jeff Huang*[2], *Hilary Morrison*[3], *and Douglas L. Feinstein*[4]

The nervous systems of all jawed animals are fully myelinated. During development, the largest caliber axons are separated from smaller neighbors by oligodendrocyte (OL) processes that envelop them with compacted multilayered myelin sheaths. Usually a single OL myelinates many axon segments. Proteins used in the sheaths are synthesized at two sites, OL soma and OL processes. Myelin basic protein (MBP) and isoforms of a second small, highly basic protein, myelin-associated oligodendrocytic basic protein (MOBP) are the only proteins known to be synthesized in OL processes. The synthesis of these two proteins is ideally situated to coordinate the compaction of the cytoplasmic leaflets into the major dense line. As a prelude to their synthesis in OL processes, the mRNAs encoding MBP and MOBP must be transported to each of the sites where myelin sheaths are formed. Morphologically, these sites are thin cytoplasmic fingers, called outer tongue processes, that overlie the compacted myelin. When one homogenizes nervous tissue, these cytoplasmic fingers become entrapped in vesicles that form from compacted myelin lamellae. The resulting myelin vesicles are readily purified by subcellular fractionation. Because they trap cytoplasm derived from OL processes, they have high levels of MBP mRNA (1). In contrast, they contain relatively little of the mRNAs that originate in other neural cell compartments, including OL soma, astrocytes, neuronal soma, and their dendritic processes (2, 3).

We used mRNAs purified from a low-speed supernatant (S) of homogenized rat brain and mRNAs purified from the myelin fraction (M)—material that accumulates at a 0.25 *M* sucrose/0.85 *M* sucrose interface—as starting materials for suppression-subtractive hybridization (4). Briefly, the "S" mRNA is used to make double-stranded cDNA "driver," and "M" mRNA is used to make "M" cDNA tester. Both cDNAs are digested with RsaI to make small pieces. Different adaptors are ligated to each of two separate batches of digested "M" cDNAs. One round of hybridization is performed in which each batch of "M" cDNA is melted and annealed with excess "S" cDNA. A second hybridization is performed with the individual hybridization reactions combined. Then, the double-stranded cDNAs, which are derived from the separate testers (*i.e.*, they have different adaptors at each end), are selectively amplified by nested PCR. All of the above protocols follow the Clontech kit manual. The PCR product, which represents mRNAs enriched in myelin, is incorporated into vector, transformed into bacteria, and colonies that represent individual cDNAs are screened by southern blot hybridization with full-length cDNA probes of the mRNAs for MBP and MOBP. The fact that 60%–80% of the cDNAs obtained from the transformed cells are derived from MBP and MOBP mRNAs is proof that subtractive hybridization selectively purifies the mRNAs from OL processes.

Among the cDNAs that were sequenced were ones with significant identities to KIF1A (5), a molecular motor involved in anterograde transport of synaptic vesicles (6), and to dynein light intermediate chain protein (DLIC-2), a constituent of the dynein motor protein complex (7). Northern blot analysis studies were used to confirm that the mRNAs are concentrated in rat brain myelin (Fig. 1). Probes to MBP and 2′, 3′-cyclic nucleotide 3′-phosphodiesterase (CNP) mRNAs served as controls. MBP mRNA, located in OL processes, is enriched in rat brain myelin, whereas CNP mRNA, located in OL soma, is not (8). Here we show that mRNAs to two high molecular weight bands of KIF1A and one of two DLIC-2 mRNAs are enriched in myelin (M > S).

DNA sequences known from five other neuronal kinesin family mRNAs were used as probes in a Northern blot analysis to determine whether any other kinesins were enriched in myelin. Messenger RNA isoforms of two other kinesins, KHC and KIF2, were found to be enriched in myelin (data not shown). The mRNA for the major KHC was quite large, 7–9 kb, whereas that for KIF2 was small, less than 2.5 kb. Northern blots were used to determine the tissue distributions and developmental appearances of these mRNAs. The low molecular weight mRNA for KIF2 had tissue distribution and developmental expression patterns similar to those of the MBP and CNP mRNAs. Unlike these "myelination-specific" mRNAs, non-neural tissues also expressed KHC and DLIC-2 (data

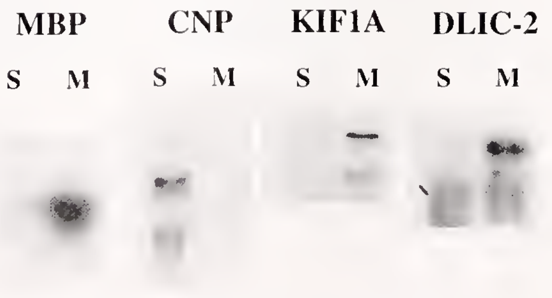

Figure 1. *Equal amounts (10 μg RNA/lane) of RNA from the starting material supernatant (S) and myelin fraction (M) were run on 1% agarose/formaldehyde gels and transferred to nylon membranes. The membranes were probed with ^{32}P-labeled cDNAs for MBP, CNP, and two novel cDNAs obtained by subtractive hybridization (see text) according to methods used in our lab (8). We have not checked these membranes for equal loading, but have found the same results for each probe on several occasions. The sizes of the mRNAs are roughly 2 kb (MBP), 5 kb (CNP), 7 and 9 kb for the larger KIF1A bands and more than 6 kb for the DLIC-2 band enriched in myelin. The sizes for MBP, CNP and DLIC mRNAs are the same as expected from the sizes of the cDNAs (accessed through GenBank).*

---

[1] Department of Anatomy and Neurobiology, University of Kentucky, Lexington, Kentucky.

[2] Brookdale Center for Developmental and Molecular Biology, Mount Sinai Medical Center, New York, New York.

[3] Josephine Bay Paul Center for Comparative Molecular Biology and Evolution, Marine Biology Laboratory, Woods Hole, Massachusetts.

[4] Department of Anesthesiology, University of Illinois, Chicago, Illinois.

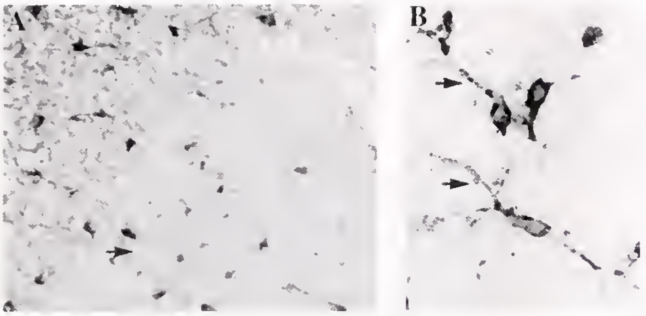

Figure 2. In situ *hybridization of KIF1A mRNA in (A) the dorsal column of P10 rat spinal cord and in (B) cultured mouse OL. In both pictures the arrows point to labeled cell processes. The resolution in cultured cells is sufficient to see that the mRNA is present in discrete granules, which would be an indicator that the mRNA was transported in granules.*

not shown). Their developmental expression patterns also differed from MBP and CNP mRNAs; they were expressed throughout postnatal development. *In situ* hybridization studies confirm the presence of these mRNAs in OL processes *in vivo* and in culture. We have demonstrated that the KIF1A probe recognizes mRNAs in a cluster of OLs in the dorsal column of a young rat spinal cord and in cultured mouse brain OLs (Fig. 2). In cells *in vivo* and in culture, mRNA is clearly seen in long cell processes, indicative of mRNA transport. Synthesis of motor proteins in OL processes indicates that complex "microtubule-based" communication systems are in place to transport vesicles from sites of myelin sheath assembly back to the OL soma. This system could function to transport those proteins that must be removed from the OL plasma membrane so that the myelin sheaths will be left with their select and rather simple protein composition. We hypothesize that the appearance of KIF1A, KHC, and DLIC-2 mRNAs early in development indicates that these proteins are formed in OL processes at early developmental stages, *i.e.*, when OLs first contact the axons they myelinate. If this is the case, the motors may play a role in transporting axon-derived material back to the OL soma.

Supported by a grant (RG2944AG/1) from the National Multiple Sclerosis Society.

Literature Cited

1. **Colman, D. R., G. Kreibich, A. B. Frey, and D. D. Sabatini. 1982.** *J. Cell Biol.* **95:** 598–608.
2. **Gillespie, C. S., L. Bernier, P. J. Brophy, and D. R. Colman. 1990.** *J. Neurochem.* **54:** 656–661.
3. **Gould, R. M. 1998.** *J. Neurochem.* **70 Suppl. 1** S53.
4. **Diatchenko, L., Y.-F. C. Lau, A. P. Campbell, A. Chenchik, F. Monadam, B. Huang, S. Lukyanov, K. Lukyanov, N. Gurskaya, E. D. Sverdlov, *et al.* 1996.** *Proc. Natl. Acad. Sci. USA* **93:** 6025–6030.
5. **Altschul, S. F., T. L. Madden, A. A. Schaffer, J. Zhang, Z. Zhang, W. Miller, and D. J. Lipman. 1997.** *Nucleic Acids Res.* **25:** 3389–3402.
6. **Okada, Y., Y. Yamazaki, Y. Sekine-Aizawa, and N. Hirokawa. 1995.** *Cell* **81:** 769–780.
7. **Hughes, S. M., K. T. Vaughan, J. S. Herskovits, and R. B. Vallee. 1995.** *J. Cell Sci.* **108:** 24.
8. **Gould, R. M., C. M. Freund, and E. Barbarese.** *J. Neurochem.* **73:** (in press).

Reference: *Biol. Bull.* **197:** 260–262. (October 1999)

Migration Forces in *Dictyostelium* Measured by Centrifuge DIC Microscopy

Yoshio Fukui[1], *Taro Q. P. Uyeda*[2], *Chikako Kitayama*[2], *and Shinya Inoué*
(Marine Biological Laboratory, Woods Hole, Massachusetts 02543-1015)

Amoeboid locomotion represents an important biological activity involved in cell growth and development (1). Forces that underlie movement of the giant amoeba, *Chaos chaos*, have been estimated to be 1.5×10^2 pN/μm^2 as measured by Kamiya's double chamber method (2). For a slime mold, *Dictyostelium discoideum*, the forces of cell locomotion have been unknown, but the cortex resists poking with a microneedle (cortical tension) at 1.4×10^3 pN/μm^2 (3). By micropipette aspiration, the cortical tension of *D. discoideum* has been measured as 1.55×10^3 pN/μm^2 (4). In the present study, we determined the migration stalling forces of *D. discoideum* by using a centrifuge polarizing microscope (CPM) equipped with DIC optics (5). The results demonstrated that individual wild type (NC4) amoebae (6) can crawl centripetally on a glass surface, resisting gravitational forces larger than 11,465 × *g*. NC4 amoebae can also undergo normal cytokinesis at forces of at least 8376 × *g*.

Dictyostelium cells were washed with Bonner's saline solution (BSS: 10 m*M* NaCl, 10 m*M* KCl, 3 m*M* $CaCl_3$) and allowed to attach to an ethanol-cleaned glass slide in a custom centrifuge chamber filled with BSS. Frozen images of the spinning microscopic field containing 20–50 cells were recorded onto Sony ED-Beta tape through an Olympus SLC Plan Fl 40× (N.A. 0.55) or LC Plan Fl 20× (N.A. 0.40) objective lens and a condenser lens (LC Plan Fl 20×/N.A. 0.40). The images illuminated by a 532-nm pulsed laser were captured in real time with a Hamamatsu C5946 CCD camera equipped with an interference-fringe-free filter. The centrifuge disk rotates horizontally, and its speed was controlled in

---

[1] Cell and Molecular Biology, Northwestern University Medical School, Chicago, Illinois 60611-3008.

[2] Biomolecular Research Group, National Institute for Advanced Interdisciplinary Research, Tsukuba, Ibaraki 305-8562, Japan.

Table 1

Migration stall forces in Dictyostelium

Measurement	Strain* NC4	Ax3	HS1	A5
	A. Reduced mass of different strains and myosin mutants			
Radius ($\times 10^{-4}$ cm)	4.81 ± 0.95	5.47 ± 1.05	5.14 ± 0.83	5.48 ± 0.98
Volume ($\times 10^{-10}$ cm^3)	3.78 ± 1.44	4.87 ± 1.80	4.26 ± 1.34	4.87 ± 1.69
ΔMass† ($\times 10^{-11}$ g)	2.57 ± 0.98	3.32 ± 1.23	2.90 ± 0.91	3.31 ± 1.15
	B. Migration stall forces of different strains and myosin mutants			
Maximum Rotation (rpm)‡	>11,700	6,400	3,500	3,400
Gravity (× g)	>11,465	3,431	1,025	968
Force § ($\times 10^3$ pN)	>8.77 ± 1.10	1.08 ± 0.42	0.28 ± 0.09	0.30 ± 0.11

C. Migration stall forces and medium density in HS1

Percoll (%)	0%	10%	25%	50%	75%	100%
Density (g/ml)	1.000	1.024	1.032	1.064	1.104	1.186
Maximum Rotation (rpm)‡	3,500	4,100	4,900	6,800	7,800	8,600
Gravity (× *g*)	1,025	1,408	2,011	3,873	5,096	6,195

* NC4: wild type, Ax3: axenic mutant, HS1: myosin II knock-out mutant, A5: triple (myoIA, myoIB, myosin II) knock-out mutant.

† ΔMass = (Cell density − Medium density) × Volume = (1.068 − 1.000) × Volume = 0.068 (g/cm^3) × Volume (cm^3)

‡ Maximum rotor rpm beyond which the amoebae were unable to crawl centripetally.

§ Standard deviation each based on measurements of diameters of more than 100 cells.

100-rpm increments up to a maximum speed of 11,700 rpm. The radius from the center of the disk to the center of the observation chamber was 7.5 cm. We determined the maximum rotation speed at which the cell's geometric center ("centroid") exhibited centripetal movement, *i.e.*, movement towards the center of the rotor. The measurement was done for wild type (NC4) (6), axenic strain (Ax3) (6), and two myosin knock-out mutants. Of the two, HS1 is a myosin II null mutant that does not express conventional myosin, which is responsible for production of major mechanochemical forces (7). A5 is a triple knock-out mutant that does not express myoIA, myoIB, or myosin II (8).

Migration forces were calculated from Newton's Force Law, *i.e.*, $F = m \times a$, where F is force (in pico Newton: pN), m is mass (in grams), and a is acceleration (in centimeters per second squared). We measured cell volumes from the diameter of round cells and calculated the reduced mass by multiplying the volume by the density difference (1.068 − 1.000 g/cm^3) (9). The average radius, calibrated volume, and reduced mass of NC4, Ax3, HS1, and A5 are shown in Table 1A. As shown, the maximum rotational speeds at which the amoebae were able to crawl centripetally were 11,700, 6400, 3500, and 3400 rpm, respectively. No centripetal migration occurred when the rotor speed was increased by 100 rpm. These values correspond to 11,465 × *g*, 3431 × *g*, 1025 × *g*, and 968 × *g*, respectively. These results showed that the gravitational forces equivalent to the migration stall forces are, respectively, >2.77 × 10^3 pN, 1.08 × 10^3 pN, 0.28 × 10^3 pN, and 0.30 × 10^3 pN (Table 1B).

We also examined the "maximum rotation speed" as a function of density of the medium (Table 1C). The results of these experiments were unexpected; the ability of the amoebae to migrate centripetally continued to increase with the density of the medium, even when it substantially exceeded the density of the amoebae themselves, so that detached amoebae would float. Since all strains exhibited the same level of adhesion up to maximum rotation (*i.e.*, 11,700 rpm), we propose that the capacity for centripetal movement in fact represents the migration forces of those amoebae. The behavior of an amoeba in a medium with a density greater than its own must signify a stalling mechanism based not on the overall buoyant density of the amoeba, but perhaps on some stratified components on or within the amoeba.

This study demonstrates that the axenic strain (Ax3) is in fact a type of mutant (10) that can generate less than 39% of the migration force generated by the original wild type (NC4). This study further demonstrates that a myosin II knock-out mutant (HS1) can generate only 26% of the migration force that its axenic parent (Ax3) can produce. In contrast, knocking-out myoIA and IB (A5) produces no additional decrease in the generation of migration forces. The migration stall forces exhibited by those mutants are obviously not dependent on myoIA, myoIB or myosin II, suggesting a significant contribution by other actin-based, force-generating mechanisms.

Literature Cited

1. **Fukui, Y. 1993.** *Int. Rev. Cytol.* **144:** 85–127.
2. **Kamiya, N. 1964.** Pp. 257–277 in *Primitive Motile Systems in Cell Biology*, R. D. Allen and N. Kamiya, eds. Academic Press, New York.
3. **Pasternak, C., J. A. Spudich, and E. L. Elson. 1989.** *Nature* **341:** 549–551.
4. **Gerald, N., J. Dai, H. P. Ting-Beall, and A. De Lozanne. 1998.** *J. Cell Biol.* **141:** 483–492.
5. **Goda, M., S. Inoué, and R. Knudson. 1998.** *Biol. Bull.* **195:** 212–214.

6. **Raper, K. B. 1984.** Pp. 19, 74–75 in *The Dictyosteliads*, Princeton University Press, Princeton, New Jersey.
7. **Ruppel, K. M., T. Q. P. Uyeda, and J. A. Spudich. 1994.** *J. Biol. Chem.* **269:** 18773–18780.
8. **Kitayama, C., J. Dai, H. P. Ting-Beall, M. A. Titus, and T. Q. P. Uyeda. 1998.** *Mol. Biol. Cell* **9:** 387a.
9. **Fukui, Y. 1976.** *Dev. Growth Differ.* **18:** 145–155.
10. **Kayman, S. C., and M. Clarke. 1983.** *J. Cell Biol.* **97:** 1001–1010.

Reference: *Biol. Bull.* **197:** 262–263. (October 1999)

Dynamic Confocal Imaging of Interphase and Mitotic Microtubules in the Fission Yeast, *S. pombe*

P. T. Tran[1], *P. Maddox*[2], *F. Chang*[1], *and S. Inoué*
(Marine Biological Laboratory, Woods Hole, Massachusetts 02543)

In the fission yeast, *S. pombe*, microtubules are required for multiple cellular processes, including maintenance of cell polarity, positioning of cellular organelles, and mitosis. Thus, microtubules are dynamic polymers (1), remodeling themselves within the living cell throughout the cell cycle.

Unfortunately, our current view of the cytoskeletal architecture of the fission yeast microtubule comes from immunofluorescence microscopy and electron microscopy of static, fixed cells (2). However, recent technical advances in wide-field epifluorescence imaging of microtubules, made possible by fusions of green fluorescent protein to tubulin (GFP-tubulin), have allowed direct observation of microtubule behavior in living fission yeast cells (3). We have now applied real-time confocal microscopy to GFP-tubulin in haploid fission yeast, and can report dynamic changes in the microtubule cytoskeleton with unprecedented spatial and temporal resolution.

A wild type haploid strain of fission yeast was transformed with a plasmid carrying the GFP-α2/tubulin gene. GFP-tubulin was therefore expressed along with endogenous tubulin. The behavior of the GFP-tubulin yeast strain is identical to that of the wild type in terms of cellular morphology and cell cycle duplication time (3). For imaging, cells were mounted on a thin layer of 20% gelatin mixed with yeast medium, between coverslip and slide. Images were digitally acquired at room temperature (23° to 26°C) with Metamorph Software (Universal Imaging Corp.) controlling a

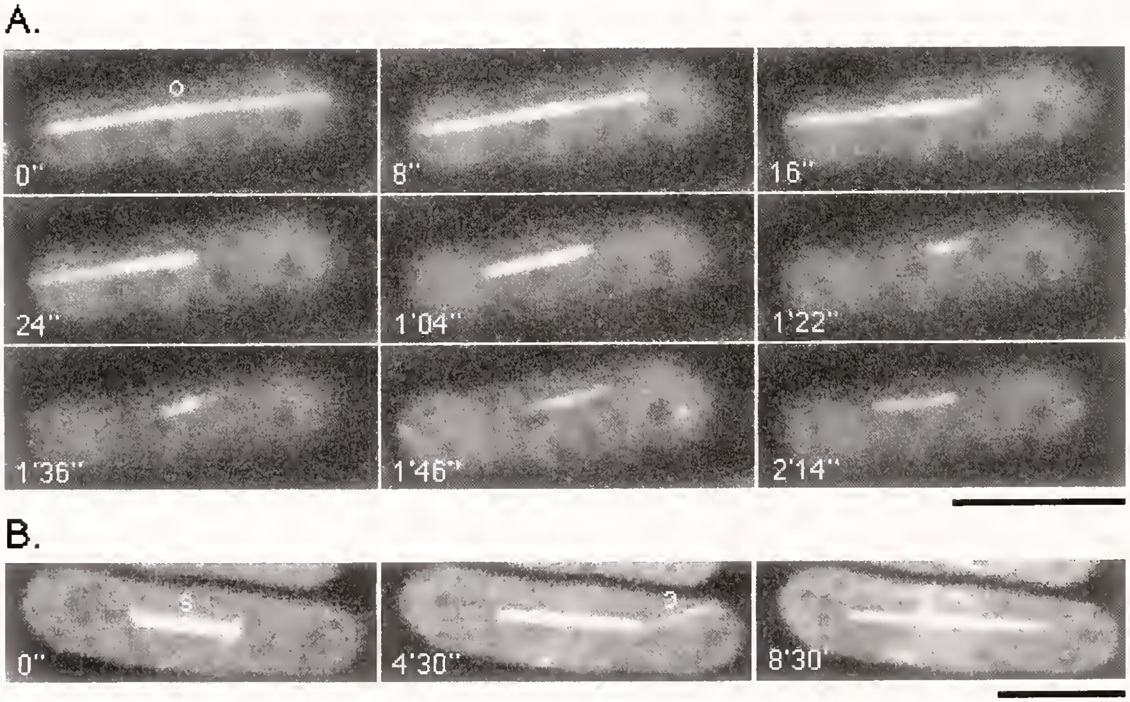

Figure 1. *Real-time confocal imaging of GFP-tubulin in the haploid fission yeast,* S. pombe. *Images are extracted at the noted time intervals to show cell cycle progression of microtubule reorganization and dynamics. Panel A shows an interphase microtubule bundle. Note the dynamic changes in microtubule lengths and the persistence of the overlap region; o = overlap region. Panel B shows a mitotic microtubule spindle. Note the rapid increase in spindle length at both ends, as well as astral microtubules and newly nucleated microtubules from the central region of the cell at the late stage of mitosis; s = spindle, a = astral microtubules. Scale bar = 5 μm.*

---

[1] Columbia University, New York, New York 10032.

[2] University of North Carolina, Chapel Hill, North Carolina 27514.

CCD digital camera (Orca-1, Hamamatsu Corp.), mounted on a real-time confocal unit at 488 nm excitation (CSU-10, Yokogawa Corp.) attached to the Leica DMRX microscope stand equipped with a 100×/1.3N.A. oil-immersion objective (Leica Corp.).

During interphase, about 4–6 bundles of microtubules extend along the long axis of the cell. Each bundle consists of 2–4 individual microtubules arranged in a characteristic manner suggestive of anti-parallel microtubules overlapping each other within a small region near the center of the cell (Fig. 1A). The microtubules are very dynamic, exhibiting a growth rate of 2.5 μm/min and a shrinkage rate of 15 μm/min. Switching between growth and shrinkage is frequent. Microtubule shrinkage starts at one tip of the cell, progresses to the overlap region near the center of the cell, and abruptly stops, never advancing beyond the overlap region (Fig. 1A). The behavior of the opposing microtubule in the overlap appears to be independent of the shrinking microtubule. In instances where both ends of the same microtubule bundle shrink completely, the overlapping region remains in the center of the cell as a small bright dot which eventually nucleates new microtubules (Fig. 1A). This suggests that the overlapping region in each microtubule bundle contains secondary microtubule-organizing-centers (MTOCs), whereas the SPB is the primary MTOC.

At the onset of mitosis, all interphase microtubules abruptly and completely shrink, not to be renucleated. The secondary MTOCs also disappear. The SPBs appear as one bright dot, which subsequently elongates to form the mitotic spindle. Spindle elongation appears biphasic. There is an initial slow rate of elongation of 0.2 μm/min until the spindle reaches a length of about 2–3 micrometers. Then the spindle elongates rapidly, at 0.8 μm/min. Coincident with the fast elongation phase, astral microtubules, which appear to be more or less perpendicular to the long axis of the spindle, begin to nucleate from the SPBs (Fig. 1B). The ends of the astral microtubule bundle seem to interact with the cell cortex, as the spindle elongates to the length of the cell. Before the spindle has completely elongated to the tips of the cell, numerous microtubule nucleations can be observed at the center of the cell, where the division ring and septum eventually constrict to separate the two new cells (Fig. 1B). The new microtubules undergo dynamics similar to those of the interphase microtubules. At the end of mitosis, the spindle microtubules disassemble, septation occurs, and the two new cells are once again in interphase. The complete cell cycle lasts about 2.5 h.

These preliminary observations on microtubule cytoskeleton dynamics and reorganization throughout the fission yeast cell cycle were made directly on living cells at high spatial and temporal resolution. Because a myriad of mutants in fission yeast are available for study with this imaging technique, important new opportunities for probing and analyzing the molecular mechanisms of microtubule-dependent cellular processes and activities are now open.

P.T.T. thanks Dr. Rudolf Oldenbourg for generously providing lab space and equipment during this study. This work was funded in part by NIH grants to P.T.T. and F.C.

Literature Cited

1. **Desai, A., and T. J. Mitchison. 1997.** *Annu. Rev. Cell Dev. Biol.* **13:** 83–117.
2. **Hagan, I. M. 1988.** *J. Cell Sci.* **111:** 1603–1612.
3. **Ding, D. Q., Y. Chikashige, T. Haraguchi, and Y. Hiraoka. 1998.** *J. Cell Sci.* **111:** 701–712.

Reference: *Biol. Bull.* **197:** 263–265. (October 1999)

Dynamic Confocal Imaging of Mitochondria in Swimming *Tetrahymena* and of Microtubule Poleward Flux in *Xenopus* Extract Spindles

Paul Maddox[1], *Arshad Desai*[2], *E. D. Salmon*[1], *T. J. Mitchison*[3], *Karen Oogema*[2], *Tarun Kapoor*[3], *Brian Matsumoto*[4], *and Shinya Inoué (Marine Biological Laboratory, Woods Hole, Massachusetts 02543)*

We report here the use of a real-time, spinning-disk confocal scanning unit (Yokogawa Electric CSU-10; 1) mounted on a Leica microscope to investigate the internal dynamics of fluorescently labeled microtubules in mitotic spindles. We aimed, in particular, to test the spatial and temporal resolution and the optical sectioning capability of the microscope setup.

Live *Tetrahymena* were stained with the fluorescent probe, Mito Tracker Green FM (Molecular Probes, Cat#M7514). Excitation was provided by the 488-nm line from a Krypton-Argon gas laser, which was passed through the spinning disk in the CSU-10. Green fluorescence from the mitochondria was collected back through the confocal unit by a SIT (Silicon Intensified Target) camera (Dage-MTI 66) mounted at the primary image plane. Video output from the camera was recorded directly onto ED-Beta tape at 30 frames per second, *i.e.*, in real time. The objective lens used for this experiment was the 100×/1.3 NA Fluotar on the Leica DMRX microscope.

Conventional wide field microscopy showed bright signals from all the mitochondria, so the image was blurred. With confocal observation, optical sections of the swimming *Tetrahymena* showed fluorescence only where mitochondria came to intersect the plane of focus.

We next explored the ability of the microscope system to produce confocal images of assembly dynamics and motility of microtubules within mitotic spindles. The mitotic spindles were produced in the cell-free *Xenopus* extract system described elsewhere (2). Briefly, cytoplasm was isolated from eggs of *Xenopus laevis*. This extract, arrested by a metaphase cytostatic-factor (CSF), was driven into interphase by Ca^{++} addition, then induced

---

[1] University of North Carolina, Chapel Hill, North Carolina.

[2] EMBL, Heidelburg, Germany.

[3] Harvard Medical School, Boston, Massachusetts.

[4] University of California, Santa Barbara, California.

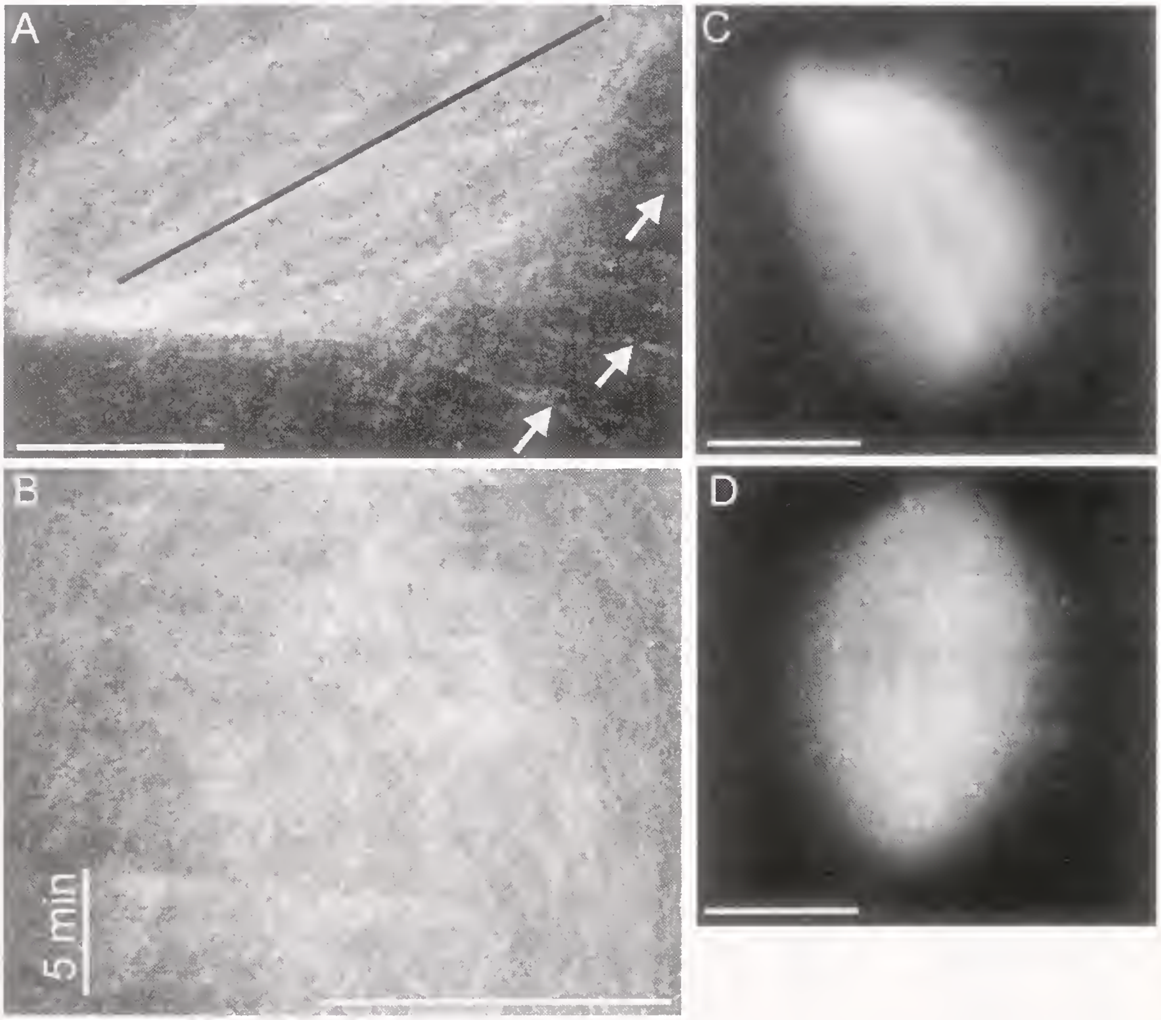

Figure 1. *(A) Mitotic spindle in* Xenopus *egg extract. Fluorescent speckles in the microtubules were visualized by adding x-rhodamine-labeled tubulin (~ 1% of total tubulin in extract) and using the CSU-10 confocal unit as described in the text. Arrows point to free microtubules extending from the spindle. (B) Kymograph showing the dynamics of fluorescent speckle flux. The kymograph is made up by displaying, on the horizontal axis, the fluorescence distribution along the black line in (A) as a function of time (vertical axis). The diagonal streaks are bright spots of fluorescent speckles which move over time within the spindle, indicating microtubule poleward flux. (C) Wide field fluorescence image of a different* Xenopus *extract spindle (~ 5% labeled-tubulin). Notice the homogeneity of the spindle. (D) Another* Xenopus *extract spindle (~ 0.05% labeled-tubulin) imaged by wide field fluorescence microscopy. Fluorescent speckles are visible, but finer details of the spindle are not visible due to fluorescence from out-of-focus planes. Bars: (A) and (B) = 10 μm; (C) and (D) = 15 μm.*

back into mitosis by addition of a small amount of CSF-arrested extract. The resulting cytoplasmic extract contained metaphase spindles (sperm nuclei were added for a source of chromatin) that were easily observed by addition of fluorescent labels (DAPI for DNA and x-rhodamine-labeled purified tubulin for microtubules).

In previous studies, photo-uncaging of fluorescently labeled tubulin in spindles was used to show that there is a bulk flow of polymer originating near the spindle mid-zone and progressing toward each pole region. This flow, termed microtubule poleward flux, was found to move at about 2 μm/min in *Xenopus* extract spindles; this is the same rate as the chromosome-to-pole movement during anaphase in this system. Therefore, it was proposed that poleward microtubule flux could be the force generator for anaphase A chromosome separation (3).

The object of this study was to image the dynamics of individual microtubules within spindles. Because the spindles are about 40-μm long and contain thousands of microtubules, conventional wide-field fluorescence micrographs lack fine structural detail (Fig. 1C). Lowering the ratio of labeled to unlabeled tubulin subunits in the cytoplasmic extract leads to a low density of label along the polymerized microtubule lattice (4, 5). This distribution in turn creates bright speckles of fluorescence that serve nicely as internal fiduciary marks along the lattice. One is then able to visualize either polymerization or depolymerization, as well as the flux of subunits within polymers and the movement of whole polymers (5). A problem with this technique, however, is that the small amounts of labeled tubulin (less than 0.1%) make visualization of gross spindle morphology difficult (Fig. 1D).

Mitotic *Xenopus* extract spindles with more than 0.1% of the total tubulin pool labeled were observed with the CSU-10 real-time confocal unit, which was coupled to an Orca cooled CCD camera (Hamamatsu Photonics, Bridgewater, New Jersey). With this system, the dynamics of microtubules in the middle of spindles could be seen, as could the fibrous structure of the polymer mass (Fig. 1A). MetaMorph software (Universal Imaging Corp., West Chester, Pennsylvania) was used to control the CSU-10 shutter as well as the camera. This allowed time-lapse imaging for up to 10 min, exposing the sample for 0.75 s to the 568-nm line of the laser every 10 s, with little photobleaching. A Leica 100×/1.3 NA objective lens was used to increase light-gathering efficiency, as well as to match magnification to the resolution limit imposed by the pixel size of the CCD chip.

Analysis of the time-lapse images revealed that microtubules add subunits to their plus ends while losing subunits from their minus ends near the spindle poles. Plus ends were located throughout the half spindle, and the movement of fluorescent speckles was often seen traversing the entire spindle (Fig. 1B). Preliminary measurements of the poleward movement of fluorescent speckles indicated a rate of about 2 μm/min, corresponding nicely to previous values (4, 5). The confocal images revealed that microtubules were clustered into bundles within the spindle (Fig. 1A). Also clearly visible were fluorescent-speckled microtubules extending out and away from the main spindle (Fig. 1A, arrows), often for great lengths (up to 50 μm). Poleward speckle movement was detected in this population of microtubules, indicating that plus ends do not have to be within the spindle to facilitate poleward microtubule flux and disassembly near the poles.

We thank Yokogawa Electric, Universal Imaging, Leica, Hamamatsu Photonics, and Nikon for generous support. EDS was supported in part by the 1999 Nikon Fellowship. TJM and EDS were supported by NIH grants.

Literature Cited

1. **Fukui, Y., E. L. de Hostos, and S. Inoué. 1997.** *Biol. Bull.* **193:** 224–225.
2. **Murray, A. W. 1991.** *Methods Cell Biol.* **36:** 581–605.
3. **Desai A., P. S. Maddox, T. J. Mitchison, and E. D. Salmon. 1998.** *J. Cell Biol.* **141:** 703–713.
4. **Waterman-Storer, C. M., and E. D. Salmon. 1998.** *Biophys. J.* **75:** 2059–2069.
5. **Waterman-Storer, C. M., A. Desai, J. C. Bulinski, and E. D. Salmon. 1998.** *Curr. Biol.* **8:** 1227–1230.

Reference: *Biol. Bull.* **197:** 265–266. (October 1999)

Effects of Vanadate on Actin-dependent Vesicle Motility in Extracts of Clam Oocytes

Torsten Wöllert[1], *Ana S. DePina, and George M. Langford*
(Dartmouth College, Hanover, New Hampshire 03755)

The effect of sodium orthovanadate on actin-based vesicle transport (1) was examined in extracts obtained from oocytes of the surf clam *Spisula solidissima.* Vanadate, an analog of inorganic phosphate (Pi), inhibits microtubule-based motors at low concentrations (5–50 μ*M*) without affecting actin-based motors, and inhibits tyrosine phosphatases selectively at higher concentrations (0.5–1.0 m*M*) (2). The higher concentrations of vanadate were used to determine whether myosin-dependent vesicle transport in clam oocyte extracts is regulated by tyrosine phosphatase activity.

Clam oocyte extracts were incubated at 18°C for 45 min and then treated with 0.5 μ*M* rhodamine-phalloidin to fluorescently label actin filaments, and 0.5 or 1.0 m*M* vanadate to inhibit tyrosine phosphatases. Vesicle transport on actin filaments was monitored for 60 min by video microscopy, and images of the actin filaments on the coverslip surface were recorded at regular intervals by epi-fluorescence microscopy. Vesicle transport on actin filaments was unaffected by vanadate during these experiments. Both motile activity and the velocity of vesicle transport in the control and the treated extracts were the same. However, the actin filament network in the extracts was altered significantly by vanadate treatment. Vanadate reduced actin filament nucleation and stimulated the formation of actin bundles. In the control samples at 15 and 60 min (C in Fig. 1), single actin filaments formed on the coverslip surface and bundles were rarely seen. In the vanadate-treated samples (V in Fig. 1), a 3-D network of bundles formed, and the density of the network increased over time (60 min). The bundles of actin filaments in the vanadate-treated extracts supported bi-directional movement of vesicles. The actin filament bundles in these extracts were disrupted by treatment with Triton X-100 (0.05 and 0.1%), indicating that actin assembly may be dependent on the presence of membranes in the extracts, as observed in *Xenopus* oocyte extracts (3, 4). These results suggest that some of the membranes in these extracts have the ability to nucleate actin filament assembly, although vesicle transport was driven by myosin motors.

The inhibitory effect of vanadate on tyrosine phosphatases is well established (2, 5), and the actin filament bundle formation observed in these extracts was most likely due to an increase in actin cross-linking activity upon inhibition of tyrosine phosphatases by vanadate. However, vanadate can influence many different activities in cells when used at high concentration. At millimolar concentrations, it can inhibit the myosin motor by forming a stable complex with ADP (6), but under our assay condition, in the presence of ATP, formation of myosin-ADP-Vi is slow, with an inhibition $t_{1/2}$ of 1.5 h (7). Therefore, the slow formation of the inhibitory complex explains the failure to inhibit myosin-dependent vesicle transport in clam oocyte extracts. Vanadate has the potential to inhibit other activities requiring ATP, including Na^+/K^+ ATPase (8), acid and alkaline phosphatases (9, 10), phosphofructokinase (11), and adenylate kinase (12), as well as actin polymerization (13). The complexity of the vanadate effect

[1] University of Rostock, Rostock, Germany.

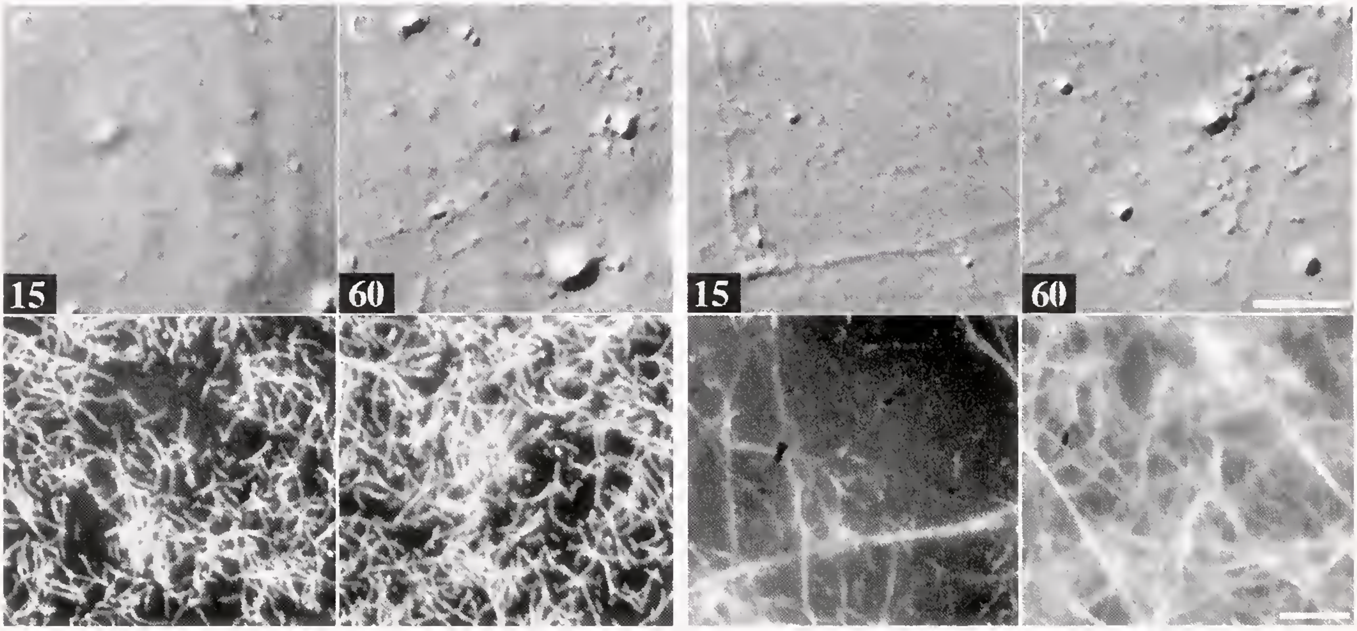

Figure 1. *Vanadate-induced actin filament bundles in clam oocyte extracts: the DIC (top row) and corresponding fluorescent images (bottom row) of extracts that were stained with rhodamine-phalloidin. Actin filaments were present in control samples (C) at the initial time point (15 min) as well as the final time point (60 min). In vanadate (1 mM)-treated samples (V), bundles rather than filaments were detected at the 15 and 60 min time points. Concentrated extracts of clam oocytes were clarified, incubated at 18°C for 45 min, and stained with 0.5 μM rhodamine-phalloidin which stabilizes actin filaments and enables their detection through fluorescence microscopy. Scale bar, 5 μm.*

does not allow us to state categorically that the effect we observed is due solely to inhibition of protein tyrosine dephosphorylation. To resolve this potential complication, future experiments are planned to determine the level of tyrosine phosphorylation in the extract when vanadate is present, and to monitor the level of phosphotyrosine in specific actin cross-linking proteins.

Literature Cited

1. **DePina, A. S., and G. M. Langford. 1999.** *Microsc. Res. Tech.* (In press).
2. **Gilbert-McClain, L. I., A. D. Verin, S. Shi, R. P. Irwin, and J. G. Garcia. 1998.** *J. Cell. Biochem.* **70:** 141–155.
3. **Moreau, V., and M. Way. 1998.** *FEBS Lett.* **427:** 353–356.
4. **Ma, L., L. C. Cantley, P. A. Janmey, and M. W. Kirschner. 1998.** *J. Cell Biol.* **140:** 1125–1136.
5. **Swarup, G., S. Cohen, and D. L. Garbers. 1982.** *Biochem. Biophys. Res. Commun.* **107:** 1104–1109.
6. **Goodno, C. C. 1982.** *Methods Enzymol.* **85:** 116–123.
7. **Goodno, C. C. 1979.** *Proc. Natl. Acad. Sci. U. S. A.* **76:** 2620–2624.
8. **Huang, W. H., and A. Askari. 1984.** *J. Biol. Chem.* **259:** 13287–13291.
9. **Vescina, C. M., V. C. Salice, A. M. Cortizo, and S. B. Etcheverry. 1996.** *Biol. Trace Elem. Res.* **53:** 185–191.
10. **Seargeant, L. E., and R. A. Stinson. 1979.** *Biochem. J.* **181:** 247–250.
11. **Khoja, S. M., A. O. Abuelgassim, and O. A. al-Bar. 1996.** *Comp. Biochem. Physiol. C. Pharmacol. Toxicol. Endocrinol.* **115:** 217–221.
12. **Cremo, C. R., J. A. Loo, C. G. Edmonds, and K. M. Hatlelid. 1992.** *Biochemistry* **31:** 491–497.
13. **Combeau, C., and M. Carlier. 1988.** *J. Biol. Chem.* **263:** 17429–17436.

Reference: *Biol. Bull.* **197:** 267–268. (October 1999)

Effects of α-bungarotoxin on Development of the Sea Urchin *Arbacia punctulata*

Blase Billack (Rutgers University, Piscataway, New Jersey 08854), Jeffrey D. Laskin[1],
Michael A. Gallo[1], and Diane E. Heck[2]

Recent evidence suggests that the expression of acetylcholine receptors is important in regulating growth and development (1). Normally, as sea urchins develop and progress through the pluteus stage, the postoral arms of the embryo elongate, the stomach develops into a large sack, the esophagus becomes muscular, the mouth opens and the digestive track begins to function (2, 3). During this time, the animal begins to feed, a requirement for further development (4).

The purpose of the present work was to evaluate the role of α-bungarotoxin-sensitive acetylcholine receptors in the development of the sea urchin *Arbacia punctulata.* For these studies, we used the fluorescent labeled drug (BODIPY-paclitaxel)—which binds polymerized microtubules with high affinity (4)—to visualize subtle alterations in the architecture of developing structures within the sea urchin embryo. In untreated embryos, we observed polymerized microtubules appearing in the cilia, the cells lining the mouth, esophagus, and gut, and in distinct punctuate regions within the epithelium during development through the pluteus stages (Fig. 1, panel A). Treatment with α-bungarotoxin (1 *μM*), a neurotoxin known to bind α subunits of the acetylcholine receptor (5), dramatically altered this pattern of accumulation. Prior to the pluteus stage no teratogenic effects of α-bungarotoxin were evident. We observed that the gross morphology, the developing internal structures that could be visualized using BODIPY-paclitaxel, and swimming behavior were indistinguishable from untreated animals. However, using both light and fluorescence microscopy, we observed marked alterations in development from early to late pluteus induced by α-bungarotoxin. These alterations included diminished extension of the postoral arms, lack of differentiation of the gut and mouth, failure to feed and impaired swimming (Fig. 1). In α-bungarotoxin-treated zygotes, the pattern of microtubule accumulation within the cells surrounding the gut, which normally develops during the pluteus stage, was not observed.

We also used rhodamine-labeled α-bungarotoxin in conjunction with confocal microscopy to study the uptake of this acetylcholine receptor antagonist into zygotes. We found that, prior to the extension of postoral arms and gut enlargement, distinct accumu-

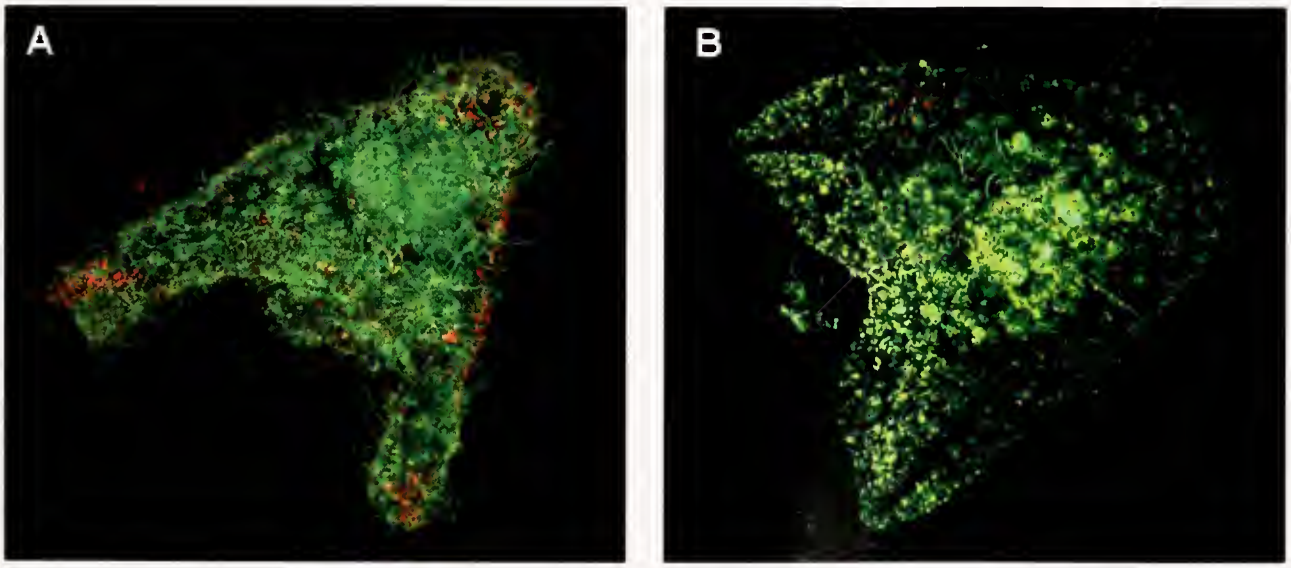

Figure 1. *Fluorescence localization of polymerized microtubules bound to paclitaxel and acetylcholine receptors in the sea urchin embryo. Fertilized eggs from the sea urchin* Arbacia punctula *(Marine Biological Laboratories, Woods Hole, Massachusetts) were grown for three days in seawater, at room temperature, in the dark and in the presence or absence of 1* μM *biotin-α-bungarotoxin (Molecular Probes, Eugene OR). The embryos were then treated with 1.25* μM *BODIPY-paclitaxel (panels A and B) and 1* μM *rhodamine-labeled α-bungarotoxin (panel A, Molecular Probes, Eugene OR) or 1 μg/ml rhodamine strepavidin (Sigma, panel B) for 30 min. The specimens were then fixed in 1% buffered formalin. After 1 h, embryos were washed and examined with a BIO-RAD confocal imaging system fitted with argon and helium-neon lasers on a Nikon ES800 microscope. Panel A, normal pluteus labeled with BODIPY-paclitaxel and rhodamine-conjugated α-bungarotoxin; panel B, pluteus grown in biotin-α-bungarotoxin and labeled with BODIPY-paclitaxel and rhodamine strepavidin.*

---

[1] Environmental and Occupational Health Sciences Institute (EOHSI), UMDNJ-Robert Wood Johnson Medical School, 170 Frelinghuysen Road, Piscataway, New Jersey 08854.

[2] EOHSI, Rutgers University, 170 Frelinghuysen Road, Piscataway, New Jersey 08854.

lations of α-bungarotoxin-sensitive acetylcholine receptors could be observed in these areas. Figure 1 (panel A) demonstrates this pattern in an untreated embryo. Rhodamine labeled α-bungarotoxin binding at the distal ends of the expanding arms and within the developing gut are clearly evident. Panel B in Figure 1 demonstrates the altered morphology of an animal grown in biotin-α-bungarotoxin. In this animal the postoral arms are undeveloped and the skeletal structure remains immature. Finally, animals that were incubated with rhodamine strepavidin, which binds biotin-α-bungarotoxin, and observed by fluorescent confocal microscopy revealed small clusters of α-bungarotoxin in distinct areas adjacent to the developing skeletal structures.

Taken together these data indicate that α-bungarotoxin disrupts zygote development during the pluteus stages in the sea urchin *Arbacia punctulata.* We speculate that α-bungarotoxin-sensitive acetylcholine receptors are necessary for the development of postoral arms and the gut in this sea urchin.

Supported in part by NIH grants ES 03647, ES 05022 and ES 06897

Literature Cited

1. **Lauder, J. M., and U. B. Schambra. 1999.** *Environ. Health Perspect.* **107:** S65–S69.
2. **Okazaki, K. 1975.** Pp. 177–232 in *The Sea Urchin Embryo. Biochemistry and Morphogenesis,* G. Czihak, ed. Springer-Verlag, New York.
3. **Gustafson, T. 1975.** Pp. 233–266 in *The Sea Urchin Embryo. Biochemistry and Morphogenesis,* G. Czihak, ed. Springer-Verlag, New York.
4. **Bicamumpaka, C., and M. Page. 1998.** *Int. J. Mol. Med.* **2:** 161–165.
5. **Carr, C., G. D. Fischbach, and J. B. Cohen. 1989.** *J. Cell. Biol.* **109:** 1753–64.

Reference: *Biol. Bull.* **197:** 268–270. (October 1999)

Leukotriene B_4 as Calcium Agonist for Nuclear Envelope Breakdown: An Enzymological Survey of Endomembranes of Mitotic Cells

Robert B. Silver and Nicole M. Deming (Marine Biological Laboratory, Woods Hole, Massachusetts 02543)

The requisite calcium signal that precedes nuclear envelope breakdown (NEB) is generated, acts, and is degraded very near to the site of action (1, 2). Neither calcium nor an agonist that would trigger release of calcium diffuse over distances greater than 1 micrometer from the site of agonist production and calcium release (2). In addition, this laboratory has shown that: a) leukotriene B_4 (LtB_4), but no other products of the arachidonic acid (AA) pathway, can evoke calcium release from endomembrane stores *in vitro* and *in vivo* in a pattern quite similar to that of the pre-NEB calcium signal (3) in sand dollar (*Echinaracnius parma*) eggs and mitotic cells (2–9); b) both the pre-NEB calcium signal and NEB are blocked by inhibitors of LtB_4 synthesis (8, 9); c) phospholipase A_2 (PLA_2) is present on calcium regulatory endomembranes of prophase mitotic apparatus (MA) and is selectively concentrated in the MA relative to the whole cell (9, 10); and d) phospholipase C activity, and thus production of 1,4,5-inositol trisphosphate, is absent from prophase MA (8–10). These four findings led Silver to hypothesize that LtB_4, and not IP_3, is the calcium agonist that produces the space-time patterned calcium QEDs essential for NEB (3, 8, and 9).

Leukotriene B_4 is produced by a well-established mechanism (11). Phospholipase A_2 acts on phospholipids to yield AA and monoacylglycerols. In turn, AA is converted to LtB_4 through the 5′-lipoxygenase (5-LO) branch of the AA pathway. Leukotriene A_4 (LtA_4), the precursor of LtB_4, can be converted by glutathione S-transferase (GST) to leukotriene C_4 (LtC_4) by the conjugation of reduced glutathione (GSH) to LtA_4. Oxidized glutathione is reduced to GSH by glutathione reductase through a reaction in which NADPH serves as the proton donor. The primary source for NADPH in animal and plant cells is the oxidative branch of the pentose phosphate pathway, specifically through the actions of glucose-6-phosphate dehydrogenase (G6PD) and 6-phosphogluconate dehydrogenase (6PGD).

We now report that: a) LtB_4 is a stereospecific agonist of endomembrane calcium release *in vivo;* b) observed PLA_2 activity is "calcium-independent"; c) kinetic analyses show that the prophase MA endomembrane GST activity represents two distinct microsomal GST enzymes; and d) enzymes of the oxidative branch of the pentose phosphate pathway are present on prophase MA membranes.

Our studies were conducted with cells from the first and second cell cycles, eggs, and isolated native prophase MA, all from the sand dollar (*Echinaracnius parma*) (*e.g.,* 1, 2, 4, 12, 13). Eggs were obtained from mature females as previously described (1, 2). Endomembranes were subfractionated as previously described (4, 12). Native prophase MA were isolated according to our standard methods (4, 12). Spectrophotometric assays for enzyme activities developed for these studies are adaptations of published methods for PLA_2 (14), PLC (15) GST (16, 17), GSR (18), creatine kinase (19), G6PD (17), lactonase (9), 6PGD (17), and pentose phosphate isomerase (9). Standard curves for identification of enzyme product were generated for each experiment at log/2 and linear/2 concentration steps (R^2 typically > 0.995). Kinetic analyses were performed with GraFit™, version 4 (Erathicus Software). Protein concentration was measured with the biuret assay, where standard curves had an R^2 of > 0.9985 across at least three orders of magnitude of protein concentration (*e.g.,* 12, 13). Triplicate assays were performed for each membrane subfraction. Specific and total

Table I

Glutathione S-transferase activity of calcium regulatory endomembranes

Enzyme Activity	Source	Km (mM GSH)	S.E. (±)	Vmax (mM sec^{-1} mg protein^{-1})	S.E. (±)
Total microsomal GST activity	Calcium regulatory endomembranes	0.1518	0.0307	0.2246	0.0149
Microsomal GST-α activity	Parsed from above data	0.0097	0.0015	0.0814	0.0052
Microsomal GST-β activity	Parsed from above data	0.2707	0.0528	0.2824	0.0188
Microsomal GST-α activity	Reduced glutathione affinity column	0.0092	0.0020	0.0981	0.0052
Microsomal GST-β activity	Reduced glutathione affinity column	0.2171	0.0947	0.2335	0.0307

activities for the enzyme activities of each subfraction were determined, and the values compared. Quantitative direct-pressure microinjection studies were performed as previously described (1, 2, 13, 20).

This laboratory has demonstrated that LtB_4 evokes release of calcium from MA-associated endomembranes *in vivo* and *in vitro* (3, 7–9). Intracellular microinjection of 2—10 picoliters of LtB_4 (10^{-4} to 10^{-8} M) evokes release of calcium from endomembranes in intact eggs and prophase cells (3, 8, 9). In contrast, microinjection of similar doses of structural homologues of LtB_4 such as LtA_4 (3, 8, 9) LtC_4 (3, 8, 9), 6-*trans*-LtB_4, or 5[S],15[S]-DiHETE do not evoke calcium release from intracellular stores. This is the first report of a stereospecific-dependence of LtB_4-evoked calcium release from endomembranes in echinoderms or from mitotic cells. Thus, among the lipoxins, LtB_4 is a stereospecific agonist of MA endomembrane calcium release *in vivo*.

The PLA_2 superfamily is composed of four PLA_2 families, two secretory (Types I and II), and two cytosolic (Types III (calcium-dependent) and IV (calcium-independent)) (21). The activities of these enzymes have distinguishing requirements for calcium concentration. Types I, II and III PLA_2 require 5, 3 and 0.08 mM $CaCl_2$, respectively (22). Type IV PLA_2 requires no calcium ions for its activity and is thus considered to be calcium independent. The PLA_2 activity measured as a component of the calcium regulatory endomembranes of isolated prophase MA, using methods previously described (9, 10, 25), does not require addition of calcium to the reaction milieu. This is consistent with the observed MA associated PLA_2 being a Type IV calcium-independent PLA_2.

Kinetic analyses of the GST activity in calcium regulatory endomembranes from prophase MA, measured across a substrate concentration range of 0.001 to 1.0 mM GSH, revealed values for Km and Vmax of 0.1518 mM GSH and 0.2246 mM sec^{-1} mg protein^{-1}, respectively (Table I). Lineweaver-Burke plots of the results indicated that the overall observed activity comprises two components. Parsing the data revealed two distinct microsomal GST enzyme activities designated GST-α and GST-β whose values for Km and Vmax differ by 27.9-fold and 3.5-fold, respectively (Table I). Both GST-α and GST-β bind to immobilized GSH and, consistent with their kinetic properties, elute at 0.3 and 0.01 mM GSH, respectively. The kinetic parameters of the affinity purified GST-α and GST-β are consistent with values parsed from the crude microsomal GST activity (Table I). Based upon kinetic properties comparable to published values for mammalian hepatic microsomal GST (*e.g.*, 23) and LtC_4 synthase (*e.g.*, 24), relative associations with S-hexyl-glutathione, and their microsomal origin, GST-α appears to be a LtC_4 synthase, while GSH-β appears to be a microsomal GST. This is the first demonstration of such activities in echinoderms, mitotic apparatuses, or mitotic cells.

In animal and plant cells, two dehydrogenases of the pentose phosphate pathway, specifically G6PD and 6PGD, serve as the catalytic source for NADPH. NADPH is necessary for GSR to produce GSH from oxidized glutathione. Reduced glutathione is a substrate for GST in the production of LtC_4 and "deactivation" of reactive oxygen intermediates. Present experiments show that GSR and active enzymes of the oxidative branch of the pentose phosphate pathway are present on prophase MA membranes. Specifically, we have identified GSR, G6PD, lactonase, 6PGD, and pentose phosphate isomerase as constitutive enzymes of the calcium regulatory endomembranes proximal to the nucleus during prophase. Thus, we propose that in the presence of glucose-6-phosphate and $NADP^+$, the calcium regulatory endomembranes of prophase MA can produce NADPH essential for GSR-mediated reduction of oxidized glutathione. Reduced glutathione is, in turn, necessary and available for the observed microsomal GST to produce either LtC_4 or glutathione-derivatized reactive oxygen intermediates. The presence of the pentose phosphate pathway enzymes also suggests a site for biosynthesis of purines, pyrimidines and amino acids essential for the subsequent cell cycle (*e.g.*, 8, 9).

These results, together with earlier findings from this laboratory (*e.g.*, space-time patterns of pre-NEB calcium signals (*e.g.*, 1, 2), LtB_4 as an agonist of pre-NEB calcium signals (3, 8, 9, 25), distribution of PLA_2 and PLC activities (7–10)), reveal a network of enzymes within prophase MA that is available for regulated production of LtB_4 as an agonist of the space-time patterned pre-NEB calcium signal (2, 8, 9).

This is the first report of stereospecificity for LtB_4 evocation of calcium release from MA endomembrane stores, of two distinguishable forms of microsomal GST (tentatively identified as microsomal GST and leukotriene C_4 synthase), and of a calcium-independent PLA_2 in echinoderms, mitotic apparatus, or mitotic cells. These findings support Silver's hypothesis of an intracellular control network in which LtB_4 is the agonist for the space-time patterned pre-NEB calcium signal and cell activation (2, 8, and 9).

Research grant support by NSF (MCB-99082680) is gratefully acknowledged. The authors are grateful to the reviewers and editor for their many helpful and well considered suggestions made in the final preparation of this manuscript.

Literature Cited

1. **Silver, R. B. 1989.** *Dev. Biol.* **131:** 11–26.
2. **Silver, R. B. 1996.** *Cell Calcium* **20:** 161–179.
3. **Silver, R. B. 1995.** *Biol. Bull.* **189:** 203–204.
4. **Silver, R. B., R. D. Cole, and W. Z. Cande. 1980.** *Cell* **19:** 505–516.
5. **Bansal, V. S., and P. W. Majerus. 1990.** *Annu. Rev. Cell Biol.* **6:** 41–67.
6. **Chow, S. C., and M. Jondel. 1990.** *J. Biol. Chem.* **265:** 902–907.
7. **Silver, R. B., D. E. Strongin, L. R. Hurwitz, and A. P. Reeves. 1997.** *Biol. Bull.* **193:** 236–237.
8. **Silver, R. B. 1999.** *FASEB J.* (in press).
9. **Silver, R. B. 1999.** *Science* (accepted).
10. **Silver, R. B., L. A. King, and A. F. Wise. 1998.** *Biol. Bull.* **195:** 209–210.
11. **Samuelsson, B. 1983.** *Science* **220:** 568–575.
12. **Silver, R. B. 1986.** *Methods Enzymol.* **134:** 200–217.
13. **Silver, R. B. 1986.** *Proc. Natl. Acad. Sci. U.S.A.* **83:** 4302–4306.
14. **Reynolds, L. J., L. L. Hughes, L. Yu, and E. A. Dennis. 1994.** *Anal. Biochem.* **217:** 25–32.
15. **Kurioka, S., and M. Matsuda. 1976.** *Anal. Biochem.* **75:** 281–289.
16. **Keen, J. H., W. H. Habig, and W. B. Jakoby. 1976.** *J. Biol. Chem.* **251:** 6183–6188.
17. **Pabst, M. J., W. H. Habig, and W. B. Jakoby. 1976.** *J. Biol. Chem.* **249:** 7140–7147.
18. **Racker, E. 1955.** *J. Biol. Chem.* **190:** 855–865.
19. **Silver, R. B., M. S. Saft, A. R. Taylor, and R. D. Cole. 1983.** *J. Biol. Chem.* **258:** 13287–13291.
20. **Silver, R. B. 1997.** Pp 83.1–20 in *Cells: A Laboratory Manual*. D. L. Spector, R. D. Goldman, and L. Leinwand, eds. CSHL Press.
21. **Dennis, E. A. 1995.** *J. Biol. Chem.* **269:** 13057–13060.
22. **Leslie, C. C. 1977.** *J. Biol. Chem.* **272:** 16709–16712.
23. **Gupta, N., M. J. Gresser, and A. W. Ford-Hutchinson. 1998.** *Biochim. Biophys. Acta* **139:** 157–168.
24. **Oesch, F., and C. R. Wolf. 1989.** *Biochem. Pharmacol.* **38:** 353–359.
25. **Silver, R. B., J. B. Oblak, G. S. Jeun, J. Sung, and T. Dutta. 1994.** *Biol. Bull.* **187:** 242–244.

Reference: *Biol. Bull.* **197:** 270–271. (October 1999)

Extracellular Survival of an Intracellular Parasite (*Spraguea lophii,* Microsporea)

Earl Weidner and Ann Findley[1] *(Biology, Louisiana State University, Baton Rouge, Louisiana)*

Microsporeans are intracellular parasites; they are located directly in host cell cytoplasm with only a plasma membrane as an interface (1). Microsporeans have an infective spore stage that discharges the sporoplasm from a long, fine tube. The spore has but one plasma membrane which is left behind within the spore ghost during discharge. The extruded sporoplasm is surrounded by a membrane, but this structure is derived from the extrusion apparatus within the spore. Since microsporeans have not been cultured or maintained extracellularly for more than short periods, it became an objective of this study to: (a) develop a simple protocol for isolating pure populations of discharged sporoplasms; and (b) develop a procedure for maintaining pure populations of extruded microsporean sporoplasms in culture for 24 h for further biochemical investigations.

To initiate spore discharge, spores of *Spraguea lophii* were incubated in 0.1 *M* HEPES buffer at pH 7.0 (with 50 n*M* Ca^{++}) for 1 h. Subsequently, 10–100 μl of spore suspension were transferred into a thin pool on a glass coverslip. These spores were triggered to discharge by the addition of 1–2 μl of filtered (0.45 μm pore size) mammalian or fish mucus onto the spore film, followed a few seconds later by the addition of 1–5 μl of 0.1 *M* HEPES buffer (pH 10). After several minutes, most of the spores had discharged sporoplasms that were attached to the cover glass surface. The unfired and discharged spore ghosts were removed from the surface by rapid washes with 0.1% concanavalin A (Con A) made up in HEPES (pH 7.0). The sporoplasms were transferred to a Medium 199 enriched with 5 m*M* ATP pH 7.2 (1).

The support medium that was tested at first included vitamins A and C (1 n*M*), L-phosphatidycholine (0.1 mg/ml), glucose (0.01%), 5% bovine serum albumen, 5% fetal calf serum, cofactors NAD and Co-A (1 n*M*) and 5 μ*M* concentrations of ATP and GTP. The cells were maintained at 15°C and 20°C. Although the sporoplasms showed some stability in this medium, the cells lost much

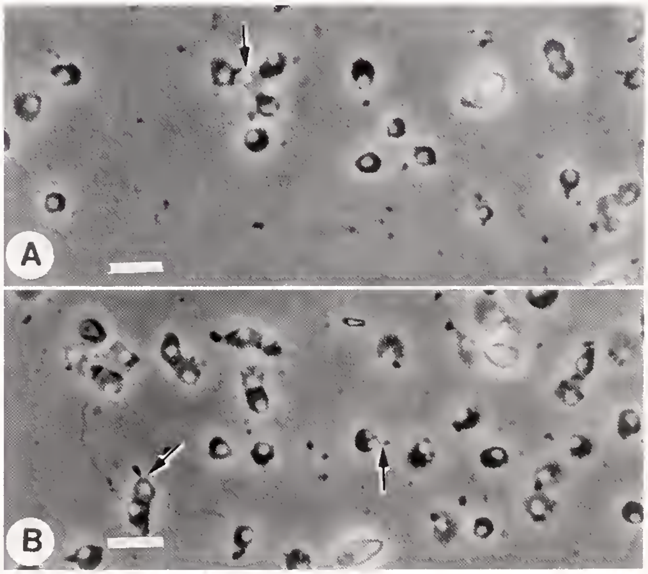

Figure 1. Spraguea lophii *sporoplasms after 24 h in Medium 199 with ATP supplement and 10%* Xenopus *oocyte cytosol. (A) Sporoplasms (arrow) frequently fuse or attach to one another. (B) Sporoplasms (arrows) also attach or fuse with other elements in medium. Bar scale represents 4 μm.*

---

[1] Biology, Northeastern Louisiana University, Monroe, Louisiana.

of their cytosol and frequently fused during the first 6 h of incubation. When the support medium was suspended onto a 2%–5% gelatin matrix, the cells incubated within it developed a vacuolated cytoplasm. However, the sporoplasms appeared to have a more robust stability when they were added to Medium 199 made up in 0.15 *M* potassium phosphate buffer with 5 m*M* ATP, and were supplemented with 10%–30% *Xenopus* oocyte cytosol (Fig. 1). After 12–24 h, these sporoplasms retained cytoplasm and did not vacuolate, although the sporoplasms appeared to still attach to each other or fuse. There was no evidence of nuclear division during 24 h of incubations.

Microsporean sporoplasms were clearly stabilized in Medium 199 (pH 7.1–7.2) with ATP (5 m*M*) on a 2% gelatin substrate onto which was added 0.01–0.02 m*M* cholesterol with no *Xenopus* cytosol. There was no evidence of vacuolation or nuclear division. However, after 12 h, the sporoplasms remained segregated and retained their cytoplasmic matrix. This significant positive effect of cholesterol addition to the medium indicates that the sporoplasm outer envelope may be devoid of cholesterol. Insertion of cholesterol into plasma membrane is an essential component of eukaryote plasma membranes; it affects membrane fluidity and reduces the permeability of membranes (2). Because newly extruded sporoplasms acquire an outer membrane that is believed to be derived from the extrusion apparatus (and is not the original plasma membrane of the spore), we expect that this second-hand membrane may lack a cholesterol component. This may account for the leaky condition of discharged sporoplasms when they are first entering into extracellular environs. Other primitive cells, such as mycoplasmas, also have an outer membrane that requires an external source of cholesterol from the outside environs for any level of stability. Once the cholesterol is acquired, these cells begin to regulate their internal milieu.

Literature Cited

1. **Weidner, E., A. Findley, V. Dolgikh, and J. Sokolova. 1999.** Pp. 172–195 in *The Microsporidia and Microsporidiosis.* American Society of Microbiology, Washington, D.C.
2. **Dahl, J. 1993.** Pp. 167–188 in *Subcellular Biochemistry.* Vol. 20. Plenum, New York.

Reference: *Biol. Bull.* **197:** 271–273. (October 1999)

Intense Concanavalin A Staining and Apoptosis of Peripheral Flagellated Cells in Larvae of the Marine Sponge *Microciona prolifera:* Significance in Relation to Morphogenesis

Jane C. Kaltenbach[1], *William J. Kuhns*[2], *Tracy L. Simpson*[3], *and Max M. Burger*[4]
(Marine Biological Laboratory, Woods Hole, Massachusetts 02543)

Free-swimming larvae are released from adult *Microciona* sponges during a brief period in late June and early July. The larvae are covered by a layer of flagellated epithelial cells, which disappear within 24 h, at about the time of larval settlement, to a substrate such as rocks, shells, etc. (1, 2). The fate of the flagellated cells has long been discussed. As early as 1892, the inversion of these cells to form choanocytes was proposed for some species of sponge (3). However, more recent evidence (*e.g.*, electron microscopy and autoradiography) indicates that, in certain species including *Microciona prolifera*, flagellated cells do not differentiate into other cell types but, near the time of settlement, are engulfed by large phagocytic cells presumed to be archaeocytes (4, 5).

The present study addresses the fate of peripheral flagellated cells in *Microciona* larvae with methods other than those used in previous reports. We used lectin-based histochemical staining of surface sugars, as well as terminal UDP, nick-end labeling, commonly known as the TUNEL assay, and DNA gel electrophoresis, to define apoptosis.

Lectins, which have binding sites for specific sugars, can be conjugated to markers, such as horseradish peroxidase (HRP), and used as probes to localize sites of terminal sugar residues of the glycans of membrane glycoproteins (6). To this end, larvae were fixed in 10% formalin, embedded in paraffin, and sectioned (5 μm). The sections were treated with H_2O_2 to block endogenous peroxidase, and with bovine serum albumin to block non-specific staining. Sections were then incubated with HRP lectins (Table I). A brown color was developed with 3,3′diaminobenzidine (DAB)-H_2O_2 to indicate sites of specific sugars in the larvae. Control

Table I

Lectins and their specific affinities

Lectin	Sugar
Concanavalin A (Con A)	α-Mannose
Wheat Germ Agglutinin (WGA)	N-Acetyl-Glucosamine (GlcNAc)
Soybean Agglutinin (SBA) and *Dolichos biflorus* Agglutinin (DBA)	N-Acetyl-Galactosamine (GalNAc)
Peanut Agglutinin (PNA)	β-Galactose
Ulex europaeus Agglutinin (UEA-1)	α-L-Fucose

---

[1] Mount Holyoke College, South Hadley, Massachusetts.
[2] Hospital for Sick Children, Toronto, Canada.
[3] University of Hartford, Hartford, Connecticut.
[4] Friedrich Miescher Institute, Basel, Switzerland.

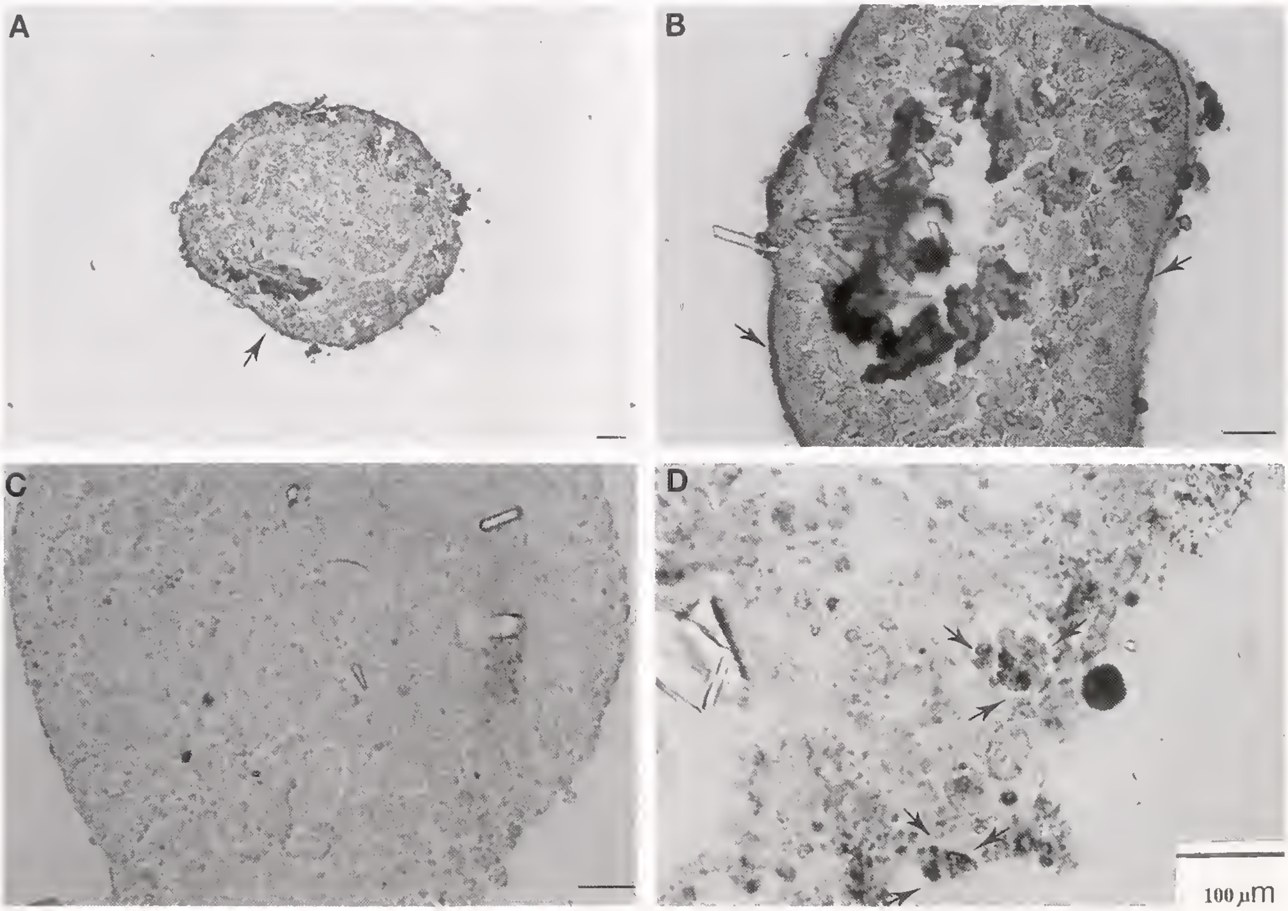

Figure 1. *Sections of* Microciona prolifera *larvae: A, B: Peripheral flagellated epithelium stained intensely with con A for mannose (arrows). Some large inner cells also gave a positive con A stain. Scale bars, (A): 20 µm, (B) 60 µm. C: Peripheral epithelium stained lightly with WGA for GlcNAc. Scale bar, 60 µm. D: Peripheral flagellated epithelium containing darkly stained apoptotic cells or cell fragments (TUNEL assay). Lighter background staining is due to hematoxylin counterstain. Two large phagocytic cells (arrows) have light cell membranes and contain darkly stained apoptotic cells or cell fragments within the cytoplasm (dark brown with TUNEL).*

sections were treated with lectin solutions containing high concentrations of specific sugars.

The TUNEL assay for apoptosis involves labeling the strand breaks of disrupted DNA (7). Sections of larvae were treated successively with proteinase K and endogenous peroxidase blocking solution, and were then permeabilized with 0.1% Triton-X-100. Non-specific reactive sites were also blocked. Sections were treated with TUNEL mixture followed by sheep antifluorescein-HRP conjugate. A brown color, developed by DAB-H_2O_2, showed sites of apoptosis. The sections were counterstained with hematoxylin. For controls, the TUNEL mixture was omitted from the procedure.

The occurrence of apoptosis was confirmed by DNA gel electrophoresis. Samples of DNA (3 µg) extracted from sponge cells (8) were loaded into wells prepared on 2% agarose gel and were separated electrophoretically. Standards consisted of Hind III (high molecular weight) DNA ladder and 100-bp low molecular weight (LMW) DNA ladder. The gel was stained with ethidium bromide and washed in several changes of water to remove excess stain.

Peripheral flagellated cells showed an intense brown stain with the con A probe for mannose (Fig. 1A,B), but only a weak stain with GlcNAc (Fig. 1C), and no stain at all with the other lectins tested (SBA, DBA, PNA, UEA-1) (not shown). This suggests that mannose was the only terminal lectin-binding sugar residue on the surface of the flagellated cells. The diagram of a high mannose N-glycan shows the two terminal mannose residues (arrows) that are able to bind to the lectin con A or to similar structures (receptors) on the surface of phagocytes. The diagram also illustrates our notion that the weak WGA staining reflects GlcNAc residues that are covered by mannose. The negative results by other lectins indicate that the corresponding sugars were non-terminal or not present.

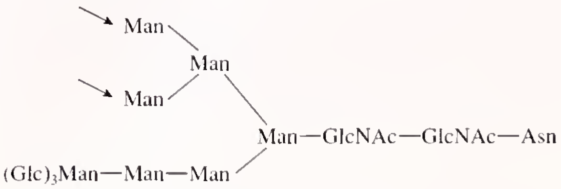

The brown staining of fragmented DNA produced by the TUNEL assay indicated that apoptosis was only located in the peripheral region of flagellated cells. However, brown staining was sometimes seen within large cells adjacent to the peripheral region (Fig. 1D), suggesting that apoptotic cells or fragments had been engulfed by large phagocytic cells (probably archaeocytes).

Comparison of sponge DNA extracts with the standards showed a ladder of LMW DNA fragments (not shown), which is characteristic of apoptotic cells (indicated in larvae by the TUNEL assay).

In summary, the results demonstrate that, in *Microciona* larvae, mannose is the only terminal, lectin-binding sugar on the surface of the flagellated cells as shown by con A staining. The cells undergo apoptosis and engulfment, indicated by dark staining of fragmented DNA (TUNEL assay).

We suggest that mannose receptors are present on the surface of phagocytes in the larvae (as shown in a variety of other organisms) (9) and that such receptors recognize and bind with mannose on apoptotic flagellated cells. A mannose-mannose receptor reaction may be required for ingestion of the apoptotic cells (9, 10). Membrane surface changes are characteristic in cell development and cell death. The changes may include turnover and externalization of high mannose N-glycans as a terminal expression in apoptotic cells and thus provide a unique method for their disposal by phagocytes (10).

Other sugars that are associated with terminal differentiation and apoptosis include those that specify histo-blood group H (L-fucose) (11). Our study supports the theory that peripheral flagellated cells in *Microciona* larvae are terminally differentiated; their fate is apoptosis and eventually phagocytosis.

Literature Cited

1. **Bergquist, P. R. 1978.** *Sponges.* University of California, Berkeley.
2. **Simpson, T. L. 1984.** *The Cell Biology of Sponges.* Springer-Verlag, New York.
3. **Delage, Y. 1892.** *Arch. Zool. Exp. Gén.* **2° série:** 345–498.
4. **Bergquist, P. R., and K. Glasgow. 1986.** *Exp. Biol.* **45:** 111–122.
5. **Misevic, G. N., V. Schulep, and M. M. Burger. 1990.** Pp. 182–187 in *New Perspectives in Cell Biology*, K. Rützler, ed. Smithsonian Press, Washington, DC.
6. **Faszewski, E. E., and J. C. Kaltenbach. 1995.** *Cell Tissue Res.* **281:** 169–177.
7. **Kuhns, W. J., M. Ho, M. M. Burger, and R. Smolowitz. 1997.** *Biol. Bull.* **193:** 239–241.
8. **Gavriela, Y., Y. Sherman, and S. A. Ben-Sasson. 1992.** *J. Cell Biol.* **119:** 493–501.
9. **Drickamer, K., and M. E. Taylor. 1993.** *Annu. Rev. Cell Biol.* **9:** 237–264.
10. **Platt, N., R. P. da Silva, and S. Gordon. 1998.** *Trends Cell Biol.* **8:** 365–372.
11. **Kuhns, W. J., and C. Pann. 1972.** *Nat. New Biol.* **240:** 22–24.

Reference: *Biol. Bull.* **197:** 274–275. (October 1999)

A Cuticular Secretion of the Horseshoe Crab, *Limulus polyphemus:* A Potential Anti-fouling Agent

John M. Harrington (Biological Sciences Department, University of South Alabama, Mobile, AL 36688) and Peter B. Armstrong[1]

Solid surfaces placed in the ocean are targets for colonization by all manner of sessile fouling organisms. Although the carapace of the horseshoe crab presents just such an opportunity for colonization, it is usually surprisingly clean of macroscopic colonizers. The dorsal surfaces of the cephalothorax of 8 of 16 randomly chosen animals from the Marine Resources Center at the Marine Biological Laboratory were completely free of macroscopic fouling organisms and in a second sample of 10 randomly chosen animals, 6.09% of the dorsal surface of the cephalothorax was occupied by macroscopic colonizers. In these samples, the commonest fouling organisms were members of the genera *Crepidula* (a sessile gastropod) and *Balanus* (barnacles). Some common sessile organisms, such as bryozoans, tunicates, and green algae, were not present on these animals.

We have identified a viscous secretion (dermal exudate) released onto the entire dorsal and ventral surfaces of the carapace of the American horseshoe crab that may have anti-fouling activity. Only a small fraction of the animals freshly collected from Chatham, Massachusetts, and brought into the Marine Resources Center show detectable traces of dermal exudate, but we found that the secretion is produced when the animal is exposed to waters containing concentrated decaying animal material. We had modest success in eliciting exudate secretion by challenging animals with dense mixed cultures of marine bacteria grown up on marine broth. A more robust and a prolonged response was achieved when the horseshoe crabs were housed in a live car in Eel Pond in the company of decaying fish parts (the head, viscera, and skeleton that remains after filleting striped bass). The dorsal surface of the cephalothorax of the pollution-challenged animal was harvested with a rubber scraper and Pasteur pipette, yielding 0.5–1 ml of dermal exudate. This material was stored at −20°C, or with NaN_3, to prevent microbial growth. The animals reconstituted the layer of secreted exudate within 2 h after its removal.

The exudate is probably the product of the hypodermal glands, whose ducts pass through the dermis and terminate at the surface of the cuticle (1). This secretion is different from the material released from animals injected with lipopolysaccharide (2), which we now believe is a secretion of the gastrointestinal tract. The protein content of dermal exudate is low, approximately 20 μg/ml, as determined by the bicinchoninic acid assay (Pierce Cat. #23225).

The activities of the dermal exudate included hemolytic, hemagglutinating, and bacteriolytic activities. Hemolysis was assayed according to standard procedures (3) with sheep red cells in a buffer containing 0.25 *M* NaCl, 10 m*M* $CaCl_2$, 0.14 *M* dextrose, 10 m*M* Tris, pH 7.3. The positive control was limulin, a sialic acid-binding lectin that is responsible for the hemolytic activity of the plasma of the horseshoe crab (4). A robust hemolytic activity was caused by a 1:16 dilution of dermal exudate (Table I). Hemagglutination of sheep red cells was found at a 1:8 dilution when tested in a buffer containing 0.15 *M* NaCl, 10 m*M* $CaCl_2$, 50 m*M* Tris, pH 7.3. Bacteriocidal activity was assayed on confluent lawns of the marine Gram-negative bacterium, *Vibrio alginolyticus,* grown on nutrient agar. Aliquoits (5 μl) of dermal extract (azide-free) were placed at equally spaced intervals on the surface of the culture shortly after bacterial plating, and the culture was checked periodically for zones of clearance in the bacterial lawn, at sites of deposited exudate. Controls were 5 μl deposits of sterile 3% NaCl. Bacteriolysis was observed only in one of four separate collections of dermal exudate, so this may be a variable property of the exudate.

Table I

Hemolysis of sheep red cells by dermal exudate

Hemolytic agent	Hemolysis (%)
10 n*M* Limulin	27.5 ± 11.3
1:16 Dermal exudate, preparation #1	38.5 ± 7.4
1:16 Dermal exudate, preparation #2	13.3 ± 2.2
1:16 Dermal exudate, preparation #3	36.4 ± 1.3

We propose that the dermal exudate is a barrier to colonization of the cuticle by fouling organisms. Two distinct mechanisms probably collaborate in this function. The exudate, which is continuously secreted onto the surface of the exoskeleton, would present a mechanical barrier to contact with the solid surface of the cuticle. In addition, the exudate has antibiological properties that may kill or disable potential colonizers. Production of the exudate is stimulated by polluted water. The dermal exudate is not a perfect barrier. Green algae and cyanobacteria that succeed in establishing colonies on the cuticle slowly destroy the exoskeleton, which can prove fatal for adult horseshoe crabs (5). Thus, the prevention of this condition clearly has important health benefits.

Supported by Grant No. MCB-97-26771 from the National Science Foundation. We thank Dr. Chhanda Biswas for help with the bacteriolytic assay and Mr. Edward Enos and Dr. Norman Wainwright for suggestions on methods to elicit secretion of the dermal exudate.

Literature Cited

1. **Stagner, J. I., and J. R. Redmond. 1975.** *Mar. Fish. Rev.* **37:** 11–19.
2. **Quigley, J. P., G. Corcoran, and P. B. Armstrong. 1997.** *Biol. Bull.* **193:** 273.

---

[1] Molecular and Cellular Biology, University of California, Davis, California 95616, <pbarmstrong@ucdavis.edu>.

3. **Armstrong, P. B., R. Melchior, S. Swarnakar, and J. P. Quigley. 1998.** *Mol. Immunol.* **35:** 47–53.

4. **Armstrong, P. B., S. Swarnakar, S. Srimal, S. Misquith, E. A. Hahn, R. T. Aimes, and J. P. Quigley. 1996.** *J. Biol. Chem.* **271:** 14717–14721.

5. **Liebovitz, L., and G. A. Lewbart. 1987.** *Biol. Bull.* **173:** 430.

Reference: *Biol. Bull.* **197:** 275–276. (October 1999)

Cellular Mechanisms of Hemolysis by the Protein Limulin, a Sialic-Acid-Specific Lectin From the Plasma of the American Horseshoe Crab, *Limulus polyphemus*

Rengasamy Asokan[1] *and Peter B. Armstrong (Department of Molecular and Cellular Biology, University of California, Davis, California 95616)*

The cytolytic destruction of foreign cells by proteins of the plasma is an important immune defense strategy of higher animals. In the American horseshoe crab, *Limulus polyphemus,* the plasma-based cytolytic system is mediated by a single protein, the sialic acid-binding lectin, limulin (1). Limulin is a member of the pentraxin protein family and is present in the plasma of the horseshoe crab at 30–50 n*M* (2). In assays using sheep red cells as the model foreign cell, the entire hemolytic activity of plasma is the province of limulin (1). Hemolysis depends on the sialic acid-binding activity of limulin, because sialylated glycoconjugates, such as fetuin and the sialic acids N-acetyl neuraminic acid and colominic acid, inhibit hemolysis, and desialylation of the target cells renders them immune to cytolysis (1).

Limulin was purified from *Limulus* plasma by sequential affinity chromatography on phosphorylethanolamine-agarose to isolate the pentraxins followed by chromatography on fetuin-Sepharose to isolate limulin, the sole pentraxin with sialic acid-binding capability. The cytolytic activity of *Limulus* plasma proteins was assayed with sheep red blood cells as described previously (3).

The hemolytic action of purified limulin is sensitive to the ionic environment and shows a broad activity maximum at NaCl concentrations between 0.2 and 0.35 *M*. These salt concentrations would be non-physiological for an immune effector from a vertebrate, but the blood of the horseshoe crab has the ionic composition of seawater, 0.5 *M* NaCl. The curve showing the Ca^{+2} dependence for hemolysis is sigmoidal, with a surprisingly sharp rise from zero activity at 0.65 m*M* to maximal activity at 0.85 m*M*. This may reflect the Ca^{+2} dependency of binding of limulin to the red cell, because hemagglutination shows a similar dose-dependence on the concentration of Ca^{+2}. Under optimized conditions, hemolysis is dependent upon the concentration of limulin between 2–8 n*M*.

The macromolecular osmolites dextran-8 (Mr 8–12 kDa) and, to a lesser extent, dextran-4 (Mr 4–6 kDa) block hemolysis (Table I). This result suggests that limulin inserts into the plasma membrane to generate hydrophilic channels that allow water to flow into the cell in response to the high concentration of internal macromolecular osmolites, principally the protein hemoglobin. Protection is imagined to result from the establishment of a concentration of osmolites larger than the channel pore size in the external milieu that is equal to the concentration of hemoglobin in the cell so that the dextrans external to the cell exert an osmotic pressure equal to that of the hemoglobin within the cell and the cell is thus protected from osmotic rupture (4). Protection is partially reversible because red cells treated with limulin plus dextran show partial lysis when washed into limulin- and dextran-free buffer (data not shown). Dextran-8 fails to block hemagglutination at low Ca^{+2} concentrations (data not shown) and exerts the same protective effect against hemolysis at standard (0.85 m*M*) and high (10 m*M*) Ca^{+2} concentrations (Table I), so dextran's activity does not involve Ca^{+2} sequestration. The molecular size of dextran-4 is approximately 1.7 nm (5), indicating an effective pore size for membrane-associated limulin that is smaller than this.

One of the indicators of microbial intrusion into higher animals is the plasma protein α_2-macroglobulin, which is activated by proteases of the intruding microbes. Furthermore, α_2-macroglobulin can be activated by small primary amines, such as methylamine, as well as by the reaction with proteases. In the context of this study, activated forms of *Limulus* α_2-macroglobulin inhibit the hemolytic activity of purified limulin (3). Only the activated form

Table I

Inhibition of limulin-mediated hemolysis by high molecular mass osmolites

Osmolite[1]	Hemolysis (%)[2]
None	47.4 ± 2.3
30 m*M* Sucrose	36.7 ± 1.6
30 m*M* Melezitose	30.2 ± 2.3
30 m*M* Inulin	17.9 ± 1.6
30 m*M* Dextran-4	13.7 ± 2.1
30 m*M* Dextran-8	2.7 ± 0.9
30 m*M* Dextran-8 + 10 m*M* $CaCl_2$	1.5 ± 1.0

[1] All samples contained 7 n*M* limulin in standard hemolysis buffer, 0.25 *M* NaCl, 0.85 m*M* $CaCl_2$, 10 m*M* Tris, pH 7.3.

[2] Mean of 3 determinations, ± standard error of the mean.

---

[1] Molecular and Cellular Biology, University of California, One Shields Avenue, Davis, California 95616, <rasokan@ucdavis.edu>.

of α_2-macroglobulin inhibits limulin-mediated cytolysis; native, unreacted α_2-macroglobulin has no effect (3).

Treatment of methylamine-reacted *Limulus* α_2-macroglobulin with the thiol alkylating agent iodoacetamide abolished the ability of activated α_2-macroglobulin to inhibit hemolysis, indicating an important role for free thiols in inhibition. Activation of α_2-macroglobulin involves cleavage of an internal thiol ester bond which, in *Limulus* α_2-macroglobulin, links Cys 999 with Glx 1002. Thiol ester cleavage generates a new free thiol at Cys 999 (6). This is the only free thiol of the protein (7, 8), and, based on the effects of thiol alkylation, appears to be important for the ability of thiol ester-reacted α_2-macroglobulin to inhibit limulin-mediated hemolysis.

Cytolysis of foreign cells is an important immune defense strategy for a broad array of animals. In *Limulus*, foreign cell cytolysis is produced by the plasma protein, limulin. Limulin appears to exert this action by inserting into the plasma membrane of the targeted foreign cell to establish a hydrophilic channel that compromises the integrity of the cell membrane. This cytolytic activity is modulated by a second plasma protein, α_2-macroglobulin, and that activity appears to depend on the generation of a new free thiol group when α_2-macroglobulin is activated by its reaction with proteases.

This research was supported by NSF Grant No. MCB 26771.

Literature Cited

1. **Armstrong, P. B., S. Swarnakar, S. Srimal, S. Misquith, E. A. Hahn, R. T. Aimes, and J. P. Quigley. 1996.** *J. Biol. Chem.* **271:** 14717–14721.
2. **Swarnakar, S., R. Melchior, J. P. Quigley, and P. B. Armstrong. 1995.** *Biol. Bull.* **189:** 226–227.
3. **Armstrong, P. B., R. Melchior, S. Swarnakar, and J. P. Quigley. 1998.** *Mol. Immunol.* **35:** 47–53.
4. **Hatakeyama, T., H. Nagatomo and N. Yamasaki. 1995.** *J. Biol. Chem.* **270:** 3560–3564.
5. **Scherrer, R. and P. Gerhardt. 1971.** *J. Bacteriol.* **107:** 718–735.
6. **Ikawi, D., S.-I. Kawahata, Y. Miura, A. Kato, P. B. Armstrong, J. P. Quigley, K. L. Nielsen, K. Dolmer, and S. Iwanaga. 1996.** *Eur. J. Biochem.* **242:** 822–831.
7. **Armstrong, P. B. and J. P. Quigley. 1987.** *Biochem. J.* **248:** 703–707.
8. **Dolmer, K., L. B. Husted, P. B. Armstrong, and L. Sottrup-Jensen. 1996.** *FEBS Lett.* **393:** 37–40.

Reference: *Biol. Bull.* **197:** 276–277. (October 1999)

Identification of a Hemolytic Activity in the Plasma of the Gastropod *Busycon canaliculatum*

Chhanda Biswas (Immunobiology Division, Indian Institute of Chemical Biology, Calcutta 700 032, India), and Peter B. Armstrong[1]

The immune protection of higher animals from parasitic invasion depends on the activities of immune effector proteins in the blood. These agents must discriminate between host tissues and the surfaces of foreign cells and direct their actions only against the latter. The most effective strategy to deal with pathogenic invasion is the immediate cytolytic destruction of the pathogen. In several well-characterized examples, the agents of cytolytic destruction of invading pathogens are present in the blood, either as soluble molecules of the plasma or as molecules secreted from blood cells. In mammals, the principal agent of foreign cell cytolysis is the complement system, which consists of several dozen proteins that act either in the direct complement activation cascade or as ancillary regulatory molecules and receptors (1). In *Limulus polyphemus*, the American horseshoe crab, the plasma-based cytolysis of foreign cells is mediated by a single protein, the sialic acid-binding lectin limulin (2). Here we report the presence of a cytolytic activity in the plasma of the channeled whelk, *Busycon canaliculatum*, and present preliminary evidence that the cytolytic activity is mediated by hemocyanin, the major protein of the plasma.

To obtain blood, adult animals were removed from the tank and prompted to express the sea water held inside the shell. The animal was then placed in a large beaker, the shell and underlying tissue were punctured adjacent to the operculum, and blood flowed from the wound into the beaker. A large animal yielded 20–25 ml of blood, which was centrifuged to remove the blood cells, and was then fractionated by differential precipitation with polyethylene glycol-8000 (PEG) (Sigma cat #P-2139). A majority of the hemocyanin was precipitated at 4% PEG and gave a voluminous blue pellet upon centrifugation. PEG precipitation fractionates protein solutions largely by size, with proteins in excess of 1,000 kDa precipitating at low concentrations of PEG. *Busycon* hemocyanin exists in solution as aggregates that range in size from dimers to heptamers of the basic decameric aggregate of the polypeptide chain, yielding molecular assemblies ranging from 9,000 kDa to 35,000 kDa (3, 4). The *Busycon* hemocyanin molecule truly is a huge protein. Plasma contains approximately 80 mg/ml of protein, the great majority of which is hemocyanin. Precipitation by 4% PEG yielded a preparation that showed a major protein band with a subunit molecular mass in the vicinity of 300 kDa when examined by SDS-PAGE in the presence of 2-mercaptoethanol. This is close to the reported subunit molecular mass of *Busycon* hemocyanin, 290 kDa (5).

Whole plasma and the protein precipitated by PEG were hemolytic when tested with horse red cells in a standard hemolysis assay (2) (Fig. 1). In this context, the mammalian red cell is a model foreign cell, albeit not a relevant parasite, and it is used because hemolysis is a convenient assay of cytolysis of foreign cells. Removal of Ca^{+2} diminished, but did not eliminate completely, the hemolytic activity of the PEG-precipitable protein (Fig. 1).

---

[1] Molecular and Cellular Biology, University of California, Davis, California 95616.

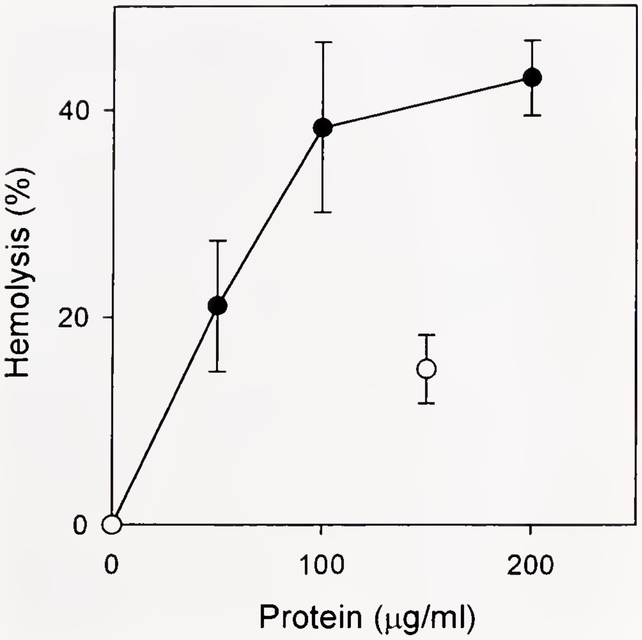

Figure 1. *Hemolysis of horse red cells by the proteins precipitated by 4% PEG-8000. Hemolysis was conducted in 0.15* M *NaCl, 0.14* M *dextrose, 10 mM* $CaCl_2$*, 10 mM Tris, pH 7.3. The hemolytic activity of the plasma was determined with triplicate samples using horse red blood cells obtained from Becton Dickinson and Company, Cockeysville, MD. The reaction mixtures contained* 3×10^7 *washed red cells in a final volume of 800 μl. The samples were incubated at 22–23°C for 4 h, and the reaction was terminated by adding 2 ml of ice-cold phosphate-buffered saline containing 5 mM ethylenediaminetetraacetic acid, followed by centrifugation to remove the red cells. The extent of hemolysis was determined by monitoring released hemoglobin in the supernatant by the optical absorbance at 412 nm and was compared to full hemolysis produced by hypotonic lysis of the red cells. The filled circles report hemolysis in the presence of 10 mM* Ca^{+2}*; the open circle reports hemolysis in a* Ca^{+2}*-free buffer system.*

Hemolysis appears to result from the insertion of the hemolytic protein into the plasma membrane of the target red cell to establish hydrophilic pores that mediate osmotic lysis of the cell. We draw this conclusion because the macromolecular osmolites dextran-4 (Mr 4–6 kDa) and dextran-8 (Mr 8–12 kDa) blocked hemolysis completely. In this situation, the dextrans appear to act as osmolites that are too large to enter the red cell through the presumed hydrophilic channels and thus act to balance the osmotic pressure gradient across the red cell membrane and thus to protect the cell against osmotic damage (6). The molecular size of dextran-4 is approximately 1.7 nm (7), indicating that the effective pore size is smaller than this value.

We suggest that *Busycon* has a cytolytic system in the plasma that functions to destroy invading pathogens. Hemocyanin has tentatively been identified as the cytolytic agent. This is the first example of which we are aware of an immune function for molluscan hemocyanin.

This research was supported by Grant MCB 97-26771 from the National Science Foundation.

Literature Cited

1. **Law, S. D., and K. B. M. Reid. 1988.** Complement. IRL Press, Oxford.
2. **Armstrong, P. B., S. Swarnakar, S. Srimal, S. Misquith, E. A. Hahn, R. T. Aimes, and J. P. Quigley. 1996.** *J. Biol. Chem.* **271:** 14717–14721.
3. **Herskovits, T. T., S. E. Carberry, and G. B. Villanueva. 1985.** *Biochim. Biophys. Acta* **828:** 278–289.
4. **Herskovits, T. T., A. E. Guzman, and M. G. Hamilton. 1989.** *Comp. Biochem. Physiol.* **92B:** 181–187.
5. **Waxman, L. 1975.** *J. Biol. Chem.* **250:** 3796–3806.
6. **Hatakeyama, T., H. Nagatomo, and N. Yamasaki. 1995.** *J. Biol. Chem.* **270:** 3560–3564.
7. **Scherrer, R., and P. Gerhardt. 1971.** *J. Bacteriol.* **107:** 718–735.

Reference: *Biol. Bull.* **197:** 277–279. (October 1999)

Hyaluronic Acid: A Component of the Aggregation Factor Secreted by the Marine Sponge, *Microciona prolifera*

William J. Kuhns[1], *Max M. Burger*[2], *and Eva Turley*[1] *(Marine Biological Laboratory, Woods Hole, Massachusetts, 02543)*

The aggregation factor (MAF) of *Microciona* sponge is a secreted proteoglycan with a molecular weight of about 20×10^6 daltons. As observed by electron microscopy (EM), MAF has a sunburst type structure comprising a number of linear, primarily carbohydrate appendages extending from a rounded protein core (1). The integrity of the whole molecule is maintained by calcium, which unites the low molecular weight subunits of MAF to each other *via* salt linkages, and to cells by a linkage that is not yet defined. In the absence of calcium, MAF disintegrates; concomitantly, EM reveals partially denuded cores ("bracelets"), and cell-cell binding is lost (2). A form of MAF-cell binding that is calcium-independent is presumed to exist (3) but has not been characterized. We hypothesized that polymers of the disaccharide hyaluronic acid (HA) might play a role in cell attachment, because

---

[1] Hospital for Sick Children, 555 University Avenue, Toronto, Ontario, Canada, M5G 1X8.

[2] Friedrich Miescher Institute, Box 2543, CH 4002, Basel, Switzerland. Correspondence should be addressed to Dr. Kuhns.

its constituent monosaccharides (glucuronic acid and N-acetylglucosamine) are known to be present in MAF glycans (4). Among our aims was to test our hypothesis that MAF contains an HA polymer and to show that this polymer constitutes a central link in the binding of MAF to an HA-binding protein (HABP).

Various HABPs have been identified in vertebrates; moreover, the consensus amino acid sequence at the HA binding site can be expressed by the formula $(B(X_{6-7})B)$, where B is arginine (R) or lysine (K), and X is any non-acidic amino acid, except that one or more must be a basic residue (5). An HA-binding peptide sequence has recently been identified within the amino acid sequence of the MAF core protein, which was translated from the cDNA (6). The sequence of the novel sponge binding site, designated MAF-HABP, is RRYRNRVR; it clearly fits the requirements of the consensus (5). MAF-HABP has been synthesized at the University of Toronto Biotechnology Center and has been probed, in a Western blot, with a biotin-labeled hyaluronic acid (BHA), as described by us in an earlier report (7).

A second non-MAF HABP has also been demonstrated by immunohistochemistry on *Microciona* cell surfaces. The antibody probe was prepared from RHAMM protein, *i.e.*, the receptor for hyaluronic acid (HA) mediated motility. This protein occurs on vertebrate cell membranes and possesses amino acid sequences that, again, conform to the consensus formula given above (5). Double labeling studies indicated that immunoreactivity to FITC-labeled anti-RHAMM could be blocked by the prior exposure of cells to BHA; conversely, a reaction with BHA was blocked by previous exposure to anti-RHAMM (5). We concluded that MAF binding to a cell could occur, if a RHAMM on the cell surface were linked to the MAF-HABP *via* an HA polymer, and if this polymer were a component of the MAF macromolecule.

In the experiments to be described, we provide further evidence in support of this hypothesis. First we show that treatment of MAF with hyaluronidase (HAase), an HA depolymerizing enzyme, abrogates MAF binding to an HABP (**experiment 1**). Second, we establish that when MAF is premixed with synthetic MAF-HABP, binding occurs, and the MAF is subsequently incapable of binding to a labeled HABP probe (**experiment 2**).

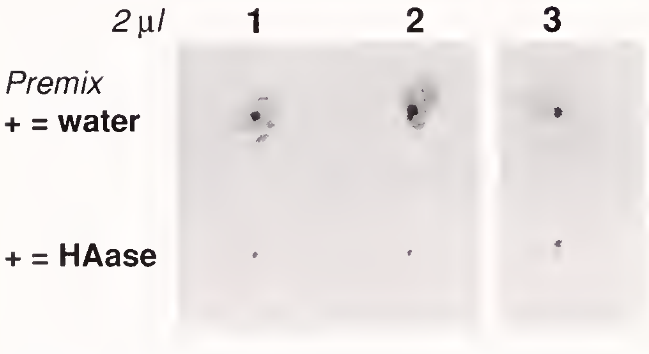

Figure 1. *Dot blots illustrating the effects of hyaluronidase (HAase) and synthetic MAF-HABP on the binding of purified* Microciona *aggregation factor (MAF) to biotin-labeled, hyaluronic acid binding protein (B-HABP). Experiment 1 (Lanes 1 and 2): Upper blots, MAF premixed with water, incubated, and spotted, the spots treated with B-HABP, and the color developed (methods in text); Lower blots, MAF premixed with HAase (method as above). Experiment 2 (Lane 3, Upper blot): MAF premixed with synthetic MAF-HABP (method as above). Lane 3, Lower blot: color control.*

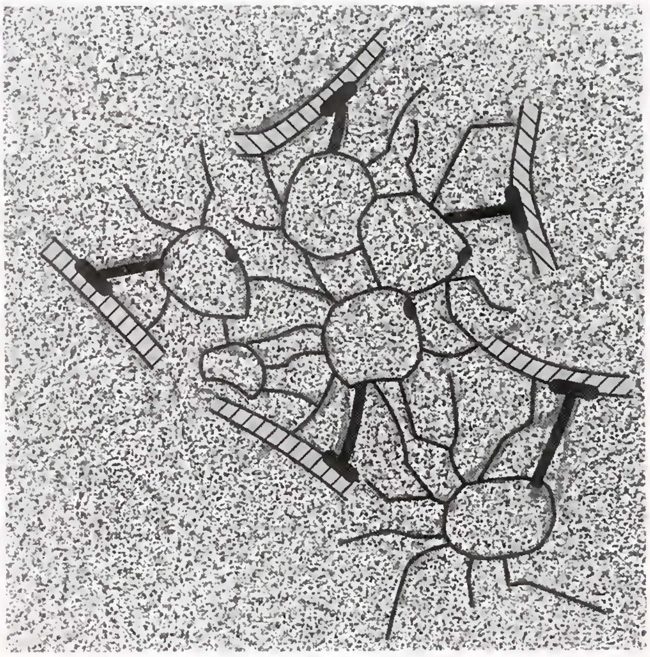

Figure 2. *A semi-schematic diagram drawn upon a portion of an electron micrograph adapted from (1). MAF is visualized by us as a three-dimensional pattern (grey circles and lines) etched within a stack of very thin grey carpets. A portion of the pattern on one layer of the stack is outlined in dark black; it represents a nest of MAF macromolecules attached to five* Microciona *cells (only fragments of cell membranes are shown as curved hatched structures). The core protein of the MAF are circular structures, and the thin lines extending away from the cores are the primarily carbohydrate arms. The arms appear to bind to other MAF cores as well as to cell membranes. Cores also seem able to bind to one another, but there may be overlapping that cannot be visualized in one dimension. Arms that appear to be short, or to have a free end, may be attached to an underlying portion of MAF. Similarly, portions of cores that appear to lack arms may have arms that extend vertically to MAF in a different horizontal plane. A single MAF-HABP (see text) is thought to occur on each protein core; it is attached to HA (thick dark line) which binds at its distal end to a cell surface HABP (short dark lines at right angles to the HA). RHAMM is an example of a cell surface HABP, but other molecules with similar HA binding motifs may exist in sponges.*

Adult *Microciona* sponge was processed, in accordance with previous reports, to yield the crude adhesive proteoglycan (MAF) (8, 9). Purified MAF was isolated by cesium gradient centrifugation, and the concentrated product was desalted. Viscosity was reduced by extensive dialysis in de-ionized water containing 1 m*M* EDTA. The final compound was lyophilized and reconstituted at 1 mg/ml as needed. Synthetic MAF-HABP was used in these studies at a concentration of 1 mg/ml.

For **experiment 1**, aliquots of MAF were premixed with an equal volume of a solution of hyaluronidase (HAase). The latter solution was prepared by adding 50 units of HAase, together with protease inhibitors (25 μg/ml) in acetate buffer at pH 5.0, to make 50 μl. Mixtures in a total volume of 10 μl, as well as dilution controls lacking HAase, were incubated at 4°C overnight. For **experiment 2**, MAF was premixed with synthetic MAF-HABP, both products being combined in equal amounts and incubated as above.

Dot blots were prepared for both experiments by spotting 2 μl of one of the two premixtures on nitrocellulose. Non-specific reactive sites were blocked with 1% bovine serum albumin in phosphate buffered saline. The spots were then treated with 2 μg of biotin-labeled hyaluronic acid binding protein (B-HABP) (Seikagaku No. 400763-1) for one hour, and then washed. This was followed by streptavidin-conjugated peroxidase and color development with 3′3 diaminobenzidine and hydrogen peroxide. If binding occurred, a brown coloration would appear at sites where substrates were applied to the nitrocellulose.

In **experiment 1**, two preparations of MAF gave a strong brown color at the sites of application of B-HABP; but MAF that was incubated with HAase showed no coloration. This result shows that the depolymerization of HA prevents the binding of MAF to B-HABP. In experiment 2, the site that contained MAF pre-treated with synthetic MAF-HABP remained almost colorless after the application of biotin-labeled HABP. This finding indicated that HA in MAF had combined with the synthetic binding site and was unable to bind to the HABP probe. Taken together, the results of the two experiments demonstrate that the MAF macromolecule contains HA, presumably in polymeric form (Fig. 1).

These results extend our earlier findings that had demonstrated the binding of biotin-labeled HA to the synthetic MAF-HABP (7). The existence of an HA binding amino acid sequence within the MAF core peptide suggests that its coupling to HA is a likely event. Our belief that HA-HABP coupling derives from a single site on the MAF core is supported by recent studies of Fernandez-Busquets (manuscript in preparation). The occurrence of RHAMM, or other HA receptors on *Microciona* cell populations may thus provide a means of MAF-cell binding that is calcium independent and distinct from the low molecular weight anionic carbohydrate epitopes previously described (10, 11). A signalling role for HA and its receptors has also been proposed (7); such linkages may enable Microciona cells to cross-communicate (Fig. 2).

Literature Cited

1. **Henkart, P., S. Humphreys, and T. Humphreys. 1973.** *Biochemistry* **12:** 3045–3050.
2. **McLaurin, J., T. Franklin, W. Kuhns, and P. Fraser. 1999.** *Amyloid* (In press).
3. **Jumblatt, J., V. Schlup, and M. Burger. 1980.** *Biochemistry* **19:** 1038–1042.
4. **Misevic, G., and M. Burger. 1986.** *J. Biol. Chem.* **261:** 2853–2859.
5. **Yang, B., L. Zhang, and E. Turley. 1993.** *J. Biol. Chem.* **268:** 8617–8623.
6. **Fernandez-Busquets, X., R. Kammerer, and M. Burger. 1996.** *J. Biol. Chem.* **271:** 23558–23565.
7. **Kuhns, W., X. Fernandez-Busquets, M. Burger, M. Ho, and E. Turley. 1998.** *Biol. Bull.* **195:** 216–218.
8. **Misevic, G., J. Finne, and M. Burger. 1987.** *J. Biol. Chem.* **262:** 5870–5877.
9. **Misevic, G., and M. Burger. 1993.** *J. Biol. Chem.* **268:** 4922–4929.
10. **Spillmann, D., K. Hard, J. Thomas-Oates, J. Vliegenthart, G. Misevic, M. Burger, and J. Finne. 1993.** *J. Biol. Chem.* **268:** 13378–13387.
11. **Spillmann, D., J. Thomas-Oates, A. van Kuik, J. Vliegenthart, G. Misevic, M. Burger, and J. Finne. 1995.** *J. Biol. Chem.* **270:** 5089–5097.

Reference: *Biol. Bull.* **197:** 279–281. (October 1999)

Biosynthesis of Tyrosine O-Sulfate by Cell Proteoglycan from the Marine Sponge, *Microciona prolifera*

Octavian Popescu[1], *Rey Interior*[4], *Gradimir Misevic*[2], *Max M. Burger*[3], *and William J. Kuhns*[4]
(Marine Biological Laboratory, Woods Hole, Massachusetts, 02543)

Tyrosine sulfation is a post-translational modification of protein that takes place in the trans-Golgi system (1). The inclusion of such a modified tyrosine in their native sequence confers strong bioactivity to a variety of ligands and peptides involved in motility, secretion, cell binding, and the promotion of complement action and blood coagulation (2–7). Tyrosine sulfation is catalyzed by a specific tyrosylprotein sulfotransferase (TPST); the enzyme has a particularly strong affinity for peptide substrates with a consensus sequence that features acidic amino acid residues adjacent, or at least close to, tyrosine (8). Sequences with these criteria can be identified in translated portions of the cDNA encoding the protein core of the *Microciona* adhesive proteoglycan (MAF) (9). A related earlier finding of ours established that restriction of environmental sulfate in *Microciona* cell suspensions is accompanied by a diminution of secreted MAF and a loss of cell motility (10). These findings motivated a search for a functional correlate. We now describe, for the first time, the biosynthesis of tyrosine sulfate by cell preparations from the marine sponge, *Microciona prolifera*.

Cell suspensions (10^7/ml) were prepared in sulfate-free artificial seawater (ASW) from whole sponge fragments and rotated for 24 h at 16°C. The cells were then pulsed with 50 μCi of sulfur-35 (DuPontNEN NEX-041) and 50 μCi tyrosine-ring 3,5 ^{3}H (NEN) for 8 h. The pellets were washed 3 times: lysates were prepared in 20 m*M* Tris (pH 7.4) containing 1% Triton-X-100 and protease inhibitors (25 μg/ml). Several aliquots (20

---

[1] Institute for Biological Research, Cluj/Napoca, Romania (O.P.).

[2] Biocenter, University of Basel, Switzerland.

[3] Friedrich Miescher Institute, Box 2543, CH4002, Basel, Switzerland.

[4] Hospital for Sick Children, 555 University Avenue, Toronto, Ontario, Canada, M5G 1X8.

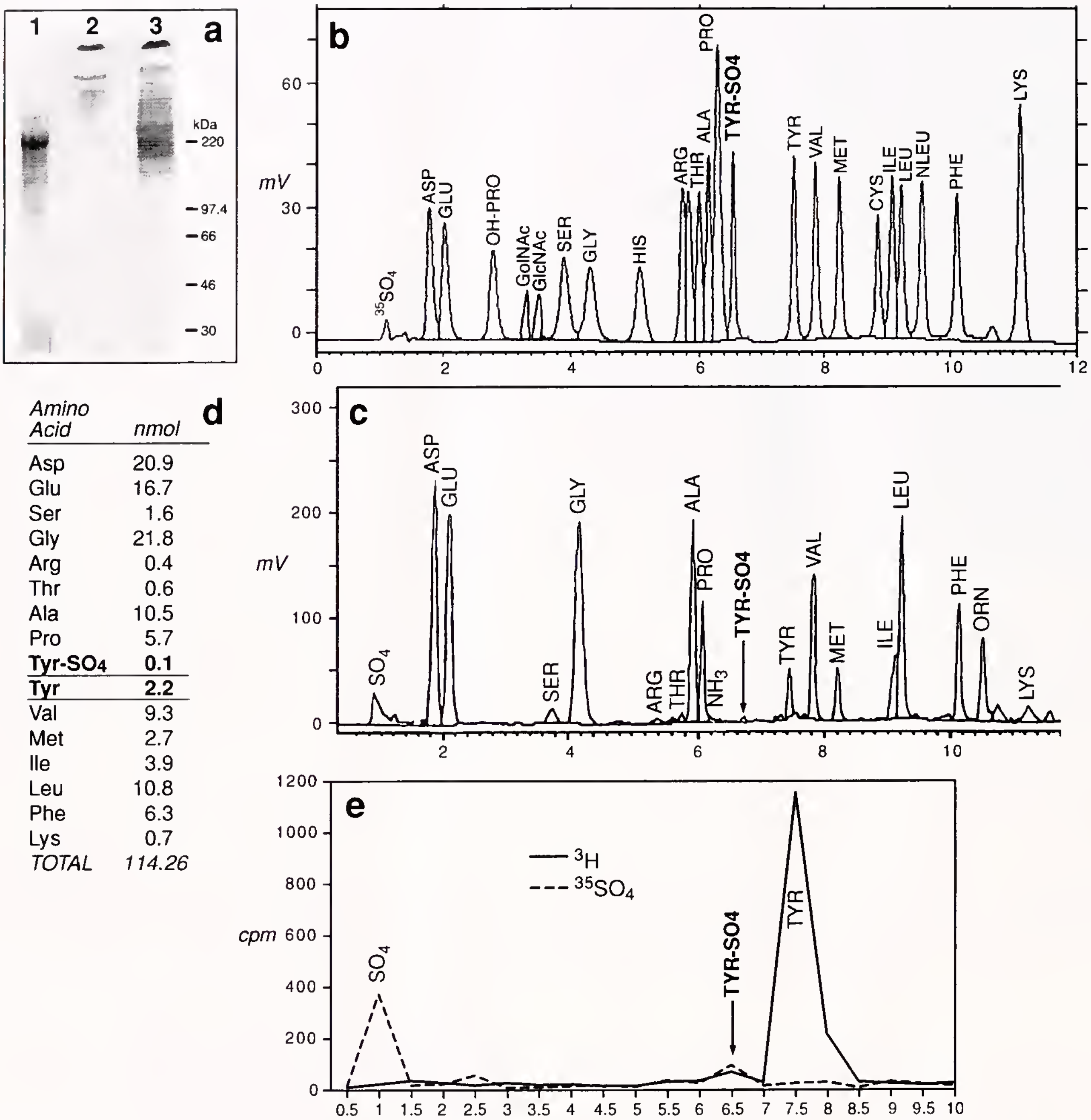

Amino Acid	nmol
Asp	20.9
Glu	16.7
Ser	1.6
Gly	21.8
Arg	0.4
Thr	0.6
Ala	10.5
Pro	5.7
Tyr-SO4	**0.1**
Tyr	**2.2**
Val	9.3
Met	2.7
Ile	3.9
Leu	10.8
Phe	6.3
Lys	0.7
TOTAL	*114.26*

Figure 1. *(a) SDS-PAGE separation, on 7.5% gel slab, of MAF (bands at about 210 kDa) from Triton-X-100 sponge cell lysates. Lane 1, MAF sample stained by Alcian blue; lane 2, autoradiograph of lysate from cells rotated in ASW with normal sulfate content; lane 3, autoradiograph of lysate from sulfate restricted cells. (b) Profile of reference amino acids after HPLC separation. The position of radiolabeled sulfate is based upon a separate run and is shown in relation to the amino acid peaks. (c) The position of amino acids derived from hydrolyzed sponge cell lysates. (d) Figures for amino acids recovered from lysates and expressed as nanomoles. (e) Counts for radioactive sulfate and tyrosine in cell lysates.*

μg) of the lysate, as well as a sample of purified MAF, were loaded onto a 7.5% SDS-polyacrylamide gel slab. After electrophoretic separation of protein bands, a portion of the slab was removed and stained for acidic proteoglycans with Alcian blue. A second portion of the slab was electrically blotted onto nitrocellulose and probed with block 2 antibody, which identified a self-binding epitope of MAF. A third portion was autoradiographed to identify isotopically labeled protein bands. From these procedures, a major band of about 210 kDa was identified and excised from the gel. The protein contained in the gel was solubilized in water, and then desalted.

Samples of this protein were hydrolyzed under alkaline conditions (0.2 *M* KOH) for 24 h. Acid hydrolysis, normally employed to dissociate amino acids from proteins, was avoided in this instance because of the acid lability of tyrosine sulfate. The recovered amino acids were derivatized and assayed with a Model ALC 204 liquid chromatograph equipped with a Pico-Tag analysis column (11). A mixture of known and calibrated amino acids was similarly derivatized for reference standards. After sample injection, the column was eluted with an acetonitrile/water (AN/W) gradient consisting of 10% AN increasing to 51% AN in 12 min. A bolus of 10 μl containing 12 μg of test sample was injected for each run. Recovery data for the standards was established by converting areas for individual peaks to nanomoles. Test samples of the radio-labeled protein were injected separately into the same machine for radioactive counts (1 ml/assay), and 0.05 ml aliquots were removed at 0.5 min intervals for 10 min, and counted. The figures represent the average of duplicate counts.

The results are presented in Figure 1a–e. In the first panel (a) (Fig 1a, lane 3), a radioactive band at about 210 kDa is visualized upon autoradiography, and it corresponds in size to an Alcian blue band shown by MAF (lane 1). On a Western blot this protein gave a positive signal when reacted with block 2 antibody (not shown). Lysates from 26 m*M* sulfate ASW (*i.e.*, not desulfated), showed very little incorporation of isotope (lane 2). The recoveries and analysis of amino acids are shown for the standards and test samples in Figure 1b and c, respectively. Tyrosine sulfate is characterized by a peak at 6.6–6.7 min; this peak is very small in the test sample. The areas of these peaks were scanned and converted to nanomoles (Fig. 1d). Recoveries of those amino acids present in large amounts (larger peaks) gave values within 10–15% on duplicate runs, but the reproducibility of yields from very small peaks was poor. As an example, the nanomolar recovery ratio of tyrosine sulfate to tyrosine was 0.1/2.2 in one run as shown, and 0.03/2.5 in a second run. ^{35}S and ^{3}H radioactivity peaked at 1 min and 7.5 min, respectively (Fig. 1e). The sample collected at 6.5 min had counts for both isotopes, close to the position at which cold tyrosine sulfate was demonstrated. The results indicate that a small portion of the tyrosine had become sulfated.

The data presented here demonstrate that cell-derived MAF (defined by molecular size and by co-precipitation with specific anti-MAF block 2 antibody)—and perhaps other sponge proteins—possess tyrosine sulfate residues, but in small amounts relative to non-sulfated tyrosine. This finding is consistent with others in established literature (12). The presence of tyrosine sulfate in MAF conforms to the sequence data derived from the translated MAF core protein cDNA, from which strongly acidic consensus sequences could be identified. Some of them also contained other favorable residues such as a low count of basic amino acids, a minimum of hydrophobic residues, and one or more turn-inducing amino acids such as glycine. The translated sequence that appears to be most favorable as a sulfation substrate is given by the 15 amino acid sequence VGFDPTDYEVNEADG (9), and it compares well with peptide segments in other systems in which sulfate activation converts a non-binding ligand to one with cell-binding properties (4). The information from these experiments may be of value in future studies on the sulfation of tyrosine residues as it applies to such issues as environmental stress or cell-cell communication.

The authors express their gratitude to Dr. Glen Horton who kindly supplied the tyrosine-0-sulfate used as a reference standard in these assays.

Literature Cited

1. **Huttner, W. 1988.** *Annu. Rev. Physiol.* **50:** 363–376.
2. **Pouyani, T., and B. Seed. 1995.** *Cell* **83:** 333–343.
3. **Dong, J., C. Li, and J. Lopez. 1994.** *Biochemistry* **33:** 13946–13953.
4. **Sako, D., K. Comess, K. Barone, R. Camphausen, D. Cumming, and G. Shaw. 1995.** *Cell* **83:** 323–331.
5. **Mutt, V. 1980.** Pp. 169–221 in *Gastrointestinal Hormones*, G. B. J. Glass, ed. Raven Press, New York.
6. **Baeuerle, P. 1987.** *J. Cell Biol.* **105:** 2655–2664.
7. **Lin, W., K. Larsen, G. Hortin, and J. Roth. 1992.** *J. Biol. Chem.* **267:** 2876–2878.
8. **Hille, A., A. Braulke, K. von Figura, and W. Huttner. 1990.** *Eur. J. Biochem.* **188:** 577–586.
9. **Fernandez-Busquets, X., D. Gerosa, D. Hess, and M. Burger. 1998.** *J. Biol. Chem.* **273:** 29545–29553.
10. **Kuhns, W., O. Popescu, M. Burger, and G. Misevic. 1995.** *J. Cell. Biochem.* **57:** 71–89.
11. **Bidlingmeyer, B., S. Cohen, and T. Tarvin. 1984.** *J. Chromatogr.* **336:** 93–104.
12. **Huttner, W., and P. Baeuerle. 1988.** *Mod. Cell Biol.* **6:** 97–140.

Reference: *Biol. Bull.* **197:** 281–282. (October 1999)

Prophenoloxidase Is Not Activated by Microbial Signals in *Limulus polyphemus*

Aimee Vasse, Alice Child, and Norman Wainwright (Marine Biological Laboratory, Woods Hole, Massachusetts 02543)

Prophenoloxidase (proPO) has been found in many invertebrates as a zymogen component of the non-inducible defense cascade involved in local melanization. The microbial cell wall constituents, lipopolysaccharide (LPS), β-1,3-glucan, and peptidoglycan are known to activate proPO, and thus, the melanin cascade, by activating prophenoloxidase-activating-enzyme (ppA). PpA proteolytically cleaves proPO into two active peptides, which can then function as opsonins (1, 2), catalyze the hydroxylation of tyrosine to dopa, or both. Dopa is further oxidized to dopaquinone, which autocatalytically produces melanin as a modified clot at a wound site, or as an encapsulation of microbial invaders in the circulatory system.

Soderhall and coworkers (2, 3, 4, 5) deemed proPO absent from the horseshoe crab *Limulus polyphemus*, claiming that the primary

Table I

The reaction of Limulus *hemolymph preparations to various detergents and microbial agents*

HEMOLYMPH PREPARATION	SDS[1]	LPS[2]	*E. coli*[3]	β-Glucan[4]	Peptidoglycan[5] in DMSO	DMSO[6]	*B. subtilis*[7]
Plasma	++	—	—	—	++	++	—
Amoebocytes in H_2O	—	—	—	—	—	—	—
Amoebocytes in saline	—	—	—	—	—	—	—
Whole hemolymph	+	—	—	—	+	+	—

Hemolymph was collected from an adult *Limulus* and immediately spun at 14,000 rpm for 8 min to separate plasma (supernatant) from amoebocytes (pellet). The pellet was rinsed three times with deionized water, but rapidly, to avoid osmotic lysis. The final pellet, containing amoebocytes separated from a 1.5-ml aliquot of hemolymph, was suspended in 1.5 ml of deionized water by stirring vigorously. This was followed by vortexing for 20 s, or until the suspension was slightly turbid. The same procedure was repeated with saline substituted for the deionized water. The whole hemolymph preparation was made with equal amounts of plasma and amoebocytes in saline. Each hemolymph preparation was then tested for reaction with the horizontally listed factors in the presence of catechol. Symbols: —, no color change (the factor did not elicit any proPO activation); +, color changed to red (thus the ability of the factor to activate proPO, because PO must be present to elicit the oxidation of catechol to produce a red product); ++; a more vivid color change. Visual analysis was used because a precipitation of plasma in catechol precluded spectrophotometric analysis.

[1] SDS, or sodium dodecyl sulfate is a detergent which activates proPO by changing its conformation to expose the active site (6).

[2] LPS (lipopolysaccharide), otherwise known as endotoxin, comprises the most exterior parts of the gram-negative cell wall. LPS activates the *Limulus* coagulin cascade.

[3] This gram-negative bacterium was obtained from a culture in Luria broth.

[4] β-Glucan is a component of the fungal and yeast cell walls.

[5] Peptidoglycan is a primary constituent of the gram-positive bacterium cell wall.

[6] The peptidoglycan did produce a color change in *Limulus* plasma and whole hemolymph, but it was dissolved in DMSO, so DMSO was tested to verify the actual cause of the color change (DMSO).

[7] This gram-positive bacterium was cultured in TSB.

Limulus defense mechanism exists in a similar proteolytic clotting cascade that yields coagulin. Nellaiappan and Sugumaran, however, recently detected proPO in *Limulus* hemolymph homogenate (6). They demonstrated that this proPO activity can be stimulated both by anionic and cationic detergents. It is presently believed that detergents bind proPO, resulting in a conformational change in the enzyme and exposure of the active site (7). The source of the proPO activity within the *Limulus* hemolymph remains unclear and may represent contributions from amoebocytes, plasma, or whole hemolymph.

In the present study, we examined the distribution of proPO activity in the different components of *Limulus* hemolymph. In an effort to understand the role of proPO in *Limulus* defense, we also examined the effects of several microbial cell wall constituents on the activity of the proPO enzyme. Dopamine and catechol were used as chromogenic substrates to assess proPO activity. In the presence of activated proPO, these compounds were oxidized to colored products. Each component of the hemolymph was first tested for proPO activation by SDS. Only the plasma and the whole hemolymph showed a visually obvious activation in response to the detergent. SDS elicited a greater response in the plasma than in the whole blood, leading to the hypothesis that the proPO cascade in *Limulus* is located in the plasma, unlike most invertebrates in which the hemocytes contain the cascade. Next, activation of the *Limulus* proPO cascade was attempted with LPS, β-1,3-glucan, peptidoglycan, and liquid cultures of assorted gram-positive and gram-negative bacteria. No activation of the proPO system could be detected visually. We conclude that the *Limulus* proPO cascade does not respond to microbial signals *in vitro*. However, we continue to explore the possibility that other factors necessary for proPO activation by microbial factors exist outside the hemolymph, thus allowing the system to work as a defense mechanism *in vivo*. We speculate that the proPO cascade may be a mechanism for pigmentation rather than defense.

Literature Cited

1. **Soderhall, K. 1982.** *Dev. Comp. Immunol.* **6:** 601–611.
2. **Soderhall, K., L. Cerenius, and M. W. Johansson. 1994.** *Ann. NY Acad. Sci.* **712:** 155–161.
3. **Soderhall, K., J. Levin, and P. B. Armstrong. 1985.** *Biol. Bull.* **169:** 661–674.
4. **Johansson, M. W., and K. Soderhall. 1989.** *Parasitol. Today* **5:** 171–176.
5. **Smith, V., and K. Soderhall. 1991.** *Dev. Comp. Immunol.* **15:** 251–261.
6. **Sugumaran, M., and K. Nellaiappan. 1991.** *Biochem. Biophys. Res. Commun.* **176:** 1371–1376.
7. **Nellaiappan, K., and M. Sugumaran. 1996.** *Comp. Biochem. Physiol. B.* **113:** 163–168.

Reference: *Biol. Bull.* **197:** 283–284. (October 1999)

The δ-Aminolevulinate Dehydratase of Marine *Vibrio alginolyticus* is Resistant to Lead (Pb)

O. A. Ogunseitan, S. L. Yang, and E. Scheinbach (Department of Environmental Analysis and Design, University of California at Irvine, California 92697-7070)

Vibrio alginolyticus is a ubiquitous marine bacterium that causes vibriosis in shellfish (1). The association of *V. alginolyticus* with biofilms in marine ecosystems that are contaminated with toxic metals has led to the discovery of an inducible copper-binding protein produced by this bacterium as a mechanism for copper detoxification through the formation of organic complexes (2, 3). However, the role of organic ligands produced by marine bacteria in trace metal cycling remains poorly understood at the molecular level. The aim of our research is to determine whether the production of certain other proteins by *V. alginolyticus* can be used as a biosensor for the bioavailability of lead (Pb), a potent neurotoxin in contaminated marine habitats. δ-aminolevulinate dehydratase (ALAD) is a phylogenetically conserved metalloprotein that catalyses the second step in the synthesis of porphobilinogen, the universal precursor of tetrapyrroles found in hemes and chlorophylls (4, 5). It is well known that the ALAD in humans and other eukaryotic organisms is very sensitive to Pb toxicity, because the required zinc atoms in the protein are stoichiometrically replaced by Pb. In fact, the accumulation of aminolevulinic acid (ALA) due to the inhibition of ALAD activity by Pb is responsible for the adverse neurological effects of lead poisoning. Consequently, the excretion of ALA and the level of ALAD activity have both been used as biomarkers for lead exposure in human populations and in wildlife (6, 7). To our knowledge, this is the first report on the response of marine bacterial ALAD to Pb.

Two strains of *V. alginolyticus* were isolated from Buzzards Bay in July 1999. The strains were purified by colony streaking and were identified through fingerprint analysis of fatty acids and methyl esters (FAME). There was a 94.7% match between the FAME profile of a non-swarming isolate and prototype *V. alginolyticus* subgroup A, whereas a swarming isolate exhibited a 91% FAME profile match with *V. alginolyticus* subgroup B. To determine the sensitivity of ALAD activity to Pb exposure in the two strains, total protein was extracted through sonication of cell pellets from cultures grown overnight without Pb. The protein extracts were suspended in a buffer containing 20 m*M* Tris-Cl, 1 m*M* dithiothreitol, and 1 m*M* phenylmethylsulfonyl fluoride (pH 7.4). Protein concentration was determined by means of the Bradford assay (USB Biochemicals, Cleveland, Ohio), and ALAD activity (μmol porphobilinogen/mg protein/h) was determined according to the method of Battistuzi *et al.* (4) after incubation of 1 mg aliquots of protein with 0, 10, or 500 μM of Pb^{++} as lead nitrate (Oguseitan *et al.*, unpublished). As a control, parallel experiments were conducted with a freshwater strain of *Pseudomonas putida* ATCC 700097 known to be sensitive to lead toxicity (Oguiseitan *et al.*, unpublished).

The results (Table I) show that ALAD activity in both strains of *V. alginolyticus* is not inhibited by Pb. The effect of Pb on ALAD activity in protein extracts from *V. alginolyticus* was not significant ($P > 0.05$), whereas 0.5 m*M* of Pb caused greater than 90% inhibition of ALAD activity in the control strain, *P. putida* ATCC 700097. The average concentration of Pb in Buzzards Bay sediment was about 20 mg/kg (8), but the extent to which this amount of Pb is biologically available at a level that would constitute a selective pressure on the molecular evolution of ALAD is not known. The metallic component of ALAD varies according to species. Zinc is required for ALAD activity in mammals, yeast, and *Escherichia coli*, whereas magnesium is required for ALAD activity in most plants and in bacteria that are associated with plants, *e.g.*, *Bradyrhizobium japonicum* (9). The identity of the metallic component of ALAD, as well as the amino acid sequence of the metal-binding site of the protein, have likely evolved in response to environmental factors, including the presence of toxic chemicals. Further work to identify the metallic component of ALAD in *V. alginolyticus* is ongoing in our laboratory as an approach to the molecular basis of Pb-resistance.

Table I

Effect of Pb on bacterial δ-aminolevulinate dehydratase activity

Bacterial Strain*	[Pb] μM	ALAD Activity (μmol Porphobilinogen/mg protein/h)**	% Change in Enzyme Activity due to Pb
Control, *P. putida*	0	5.70 ± 0.01	
ATCC 700097	10	4.51 ± 0.09	−20.9
	500	0.41 ± 0.01	−92.3
Vibrio alginolyticus	0	7.38 ± 0.01	
Group A (Swarmer)	10	7.64 ± 0.04	+3.5
	500	8.09 ± 0.01	+9.6
Vibrio alginolyticus	0	2.37 ± 0.01	
Group B	10	2.58 ± 0.04	+8.9
(Non-swarmer)	500	2.54 ± 0.07	+7.2

* Data in the Table are from experiments conducted with proteins extracted from cells before Pb exposure. Pb at the specified concentrations was then incubated with proteins for 1 h before enzyme assay. Similar results were obtained when viable cells were exposed to the specified concentrations of Pb before protein extraction and enzyme assay.

** Experiments were replicated five times. Values reported are the means ± standard deviation.

This research was supported by a Josiah Macy Jr. fellowship awarded to Ogunseitan.

Literature Cited

1. **Elston, R., E. L. Elliot, and R. R. Colwell. 1982.** *J. Fish Diseases* **5:** 265–284.

2. **Schreiber, D. R., F. J. Millero, and A. S. Gordon. 1990.** *Mar. Chem.* **28:** 275–284.
3. **Harwood, V. J. and A. S. Gordon. 1994.** *Appl. Environ. Microbiol.* **60:** 1794–1753.
4. **Battistuzi, G., R. Petrucci, L. Silvagni, F. R. Urbani, and S. Caiola. 1981.** *Ann. Hum. Genet.* **45:** 223–229.
5. **Duncan, R., M. A. Faggart, A. J. Roger, and N. W. Cornell.** *Mol. Biol. Evol.* **16:** 383–396.
6. **Fleming, D. E. B., D. R. Chettle, J. G. Wetmur, R. J. Desnick, J-P. Robin, D. Boulay, N. S. Richard, C. L. Gordon, and C. E. Webber. 1998.** *Environ. Res.* **77:** 49–61.
7. **Burden, V. M., M. B. Sandheinrich, and C. A. Caldwell. 1998.** *Environ. Pollut.* **101:** 285–289.
8. **Shine, J. P., R. V. Ika, and T. E. Ford. 1995.** *Environ. Sci. Technol.* **29:** 1781–1788.
9. **Chauhan, S., and M. R. O'Brian. 1995.** *J. Biol. Chem.* **270:** 19823–19827.

Reference: *Biol. Bull.* **197:** 284–285. (October 1999)

Substituted Cyclodextrin as a Model for a Squid Enzyme that Hydrolyzes the Nerve Gas Soman

Francis C. G. Hoskin (Marine Biological Laboratory, Woods Hole, Massachusetts 02543),
Diane M. Steeves[1], and John E. Walker[1]

Certain phosphorus-fluorine (P-F) compounds are powerful inhibitors of the nerve enzyme acetylcholinesterase (AChE), and are thus termed "nerve gases." One such compound is soman, 1,2,2-trimethylpropyl methylphosphonofluoridate. An enzyme that hydrolyzes, and thus detoxifies soman has been purified from squid nerve and immobilized on agarose resin. However, this enzyme, termed organophosphorus acid anhydrolase (OPAA), hydrolyzes the relatively non-toxic pair of diastereoisomers, C(±)P(+), more rapidly than the toxic pair C(±)P(−) (1). Cyclodextrins are donut-shaped heptahexose molecules that can also act as P-F hydrolyzing "synzymes" (2, 3); but their rates are much lower than those of the OPAAs. We now report the rapid hydrolysis and detoxication of soman by a substituted cyclodextrin: 2-O-(4-carboxy-3-iodosobenzoyl)-β-cyclodextrin (IBA-βCD) (4). Dimebu (3,3-dimethylbutyl methylphosphonofluoridate) (5), an isomer of soman with only one chiral center, P(±), is also hydrolyzed by IBA-βCD. Information about the catalysis of these reactions by IBA-βCD contributes to our understanding of the active site of the naturally occurring OPAA.

The hydrolysis of soman or dimebu was monitored with a fluoride-sensitive electrode (1); the loss of AChE inhibitory potency, by a modified Ellman reaction (1). A 5-ml solution was made 25 m*M* in Pipes buffer, 3 m*M* in soman or dimebu, and 0.03 m*M* in IBA-βCD; pH 7, 22°–23°C. After approximately half hydrolysis, as measured by the fluoride electrode, 0.1 ml of the reaction solution was removed, diluted at ice-water temperature, and tested for AChE inhibitory potency. The results of the AChE determinations, and the fluoride measurements at that point are presented in Table I. Semi-log plots of fluoride release up to that point and well beyond are shown in Figure 1.

Figure 1 shows that the hydrolysis of both soman and dimebu by IBA-βCD is catalytic. Had it been stoichiometric, about 95% of either P-F compound would have remained unhydrolyzed at 200 min. Figure 1 further suggests that the catalyzed hydrolysis of soman involves two simultaneous reactions, one with a $t_{1/2}$ of about 20 min, and the other with a $t_{1/2}$ of 300 min or more. In contrast, dimebu is hydrolyzed by a single reaction with a $t_{1/2}$ of about 15 min. Table I, on the other hand, shows that soman or dimebu are hydrolyzed at about the same rate at which they lose potency as AChE inhibitors. That is, when soman is about 35% hydrolyzed as determined by the fluoride-sensitive electrode, 44% has been destroyed judging by the loss of AChE inhibitory potency. The same values for dimebu are 46% and 59%, respectively.

Table I

Soman or dimebu degradation by IBA-βCD determined by two methods

Compound	Method	% Degraded
Soman	Fluoride-sensitive electrode	34, 36
Soman	AChE inhibitory loss	41, 47
Dimebu	Fluoride-sensitive electrode	44, 47
Dimebu	AChE inhibitory loss	57, 60

These observations can be explained in the following way. From the manner of its synthesis, IBA is covalently bonded to the rim of the βCD torus. The enhanced activity of IBA-βCD over IBA alone suggests that soman fits inside the torus and that the CH_3 of the

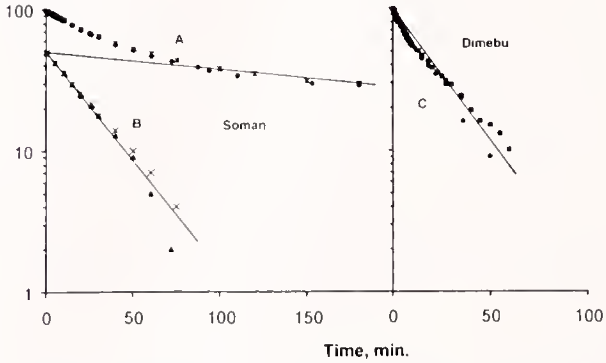

Figure 1. *Hydrolysis of soman and dimebu by IBA-βCD, determined in duplicate with the fluoride-sensitive electrode. Soman hydrolysis is resolvable into two reactions: (A) observed values; (B) derived values. Dimebu hydrolysis appears to be a single reaction: (C) observed values.*

---

[1] U.S. Army Natick RD&E Center, Natick, Massachusetts 01760.

methylphosphono part of soman is oriented away from the IBA. No matter whether the P=O or the P-F is to one side or the other of the IBA, about equal hydrolysis of the AChE inhibitory P(−)F isomers and the relatively non-inhibitory P(+)F pair will result. However, the chiral C-CH_3 at the 1-propyl position of soman will, in one configuration, allow a close approach of the P-F to the IBA, but in the other configuration will increase the distance of the P-F from the IBA by 1–2Å. The increased distance would cause a much slower hydrolysis rate for half of the racemic soman. The same reasoning applies to dimebu, but since there is no chiral C-CH_3 on the 3,3-dimethylbutyl portion, dimebu is hydrolyzed at a single fast rate.

Both AChE, which is inhibited by soman, and OPAA, the enzyme that hydrolyzes soman, seem to be indifferent to the configuration around the C chiral center (1). In contrast, IBA-βCD, in its catalytic hydrolysis of soman, shows the reverse stereospecificity with respect to the two chiral centers. This conclusion is supported by the use of dimebu, in which there is no C-chiral center. These findings and speculations have important implications for protection against, and disposal of, the acid anhydride type nerve gases, of which soman is an important example.

Literature Cited

1. **Hoskin, F. C. G. 1990.** Pp. 469–480 in *Squid as Experimental Animals.* D. L. Gilbert, W. J. Adelman, Jr., and J. M. Arnold, eds. Plenum Press, New York.
2. **Klotz, I. M., G. P. Royer, and I. S. Scarpa. 1971.** *Proc. Natl. Acad. Sci. USA* **68:** 263–264.
3. **Breslow, R., and S. D. Dong. 1998.** *Chem. Rev.* **98:** 1997–2012.
4. **Seltzman, H. H. 1992.** Pp. 24–29 in *Final Report of Contract No. DAMD 17-89-C-9012. Synthesis of Soman Scavengers.* Requests for this document should be addressed to: Commander, U.S. Army Medical Research and Development Command, Attention SGRD-RMI-S, Fort Detrick, MD 21702 USA.
5. **Chettur, G., J. J. DeFrank, B. J. Gallo, F. C. G. Hoskin, S. Mainer, F. M. Robbins, K. E. Steinmann, and J. E. Walker. 1988.** *Fundam. Appl. Toxicol.* **11:** 373–380.

Reference: *Biol. Bull.* **197:** 285–286. (October 1999)

Effects of Green Tea Polyphenols on Lens Photooxidative Stress

Seymour Zigman, Nancy S. Rafferty, Keen A. Rafferty, and Nathaniel Lewis (Eye Research Laboratory, Department of Ophthalmology, Boston University School of Medicine, and Marine Biological Laboratory, Woods Hole, Massachusetts 02543)

Our purpose was to determine whether tea polyphenols such as epigallocatechin gallate (EGCG) would protect certain functions of rabbit and dogfish lenses *in vitro* against the photooxidative stress of UVA irradiation. We have asked specifically whether catalase activity was protected.

New Zealand white rabbit eyes were obtained from PelFreeze Biologicals within 20 hours of death. Dogfish (*Mustelus canis*) lenses were obtained fresh (under conditions approved by the MBL Institutional Animal Use Committee), and kept on ice for 5 h before use. The media used to maintain the lenses were Tyrode's solution (Sigma) for rabbit tissues and elasmobranch Ringer's medium (Marine Biological Laboratory) for dogfish tissues.

The HPLC-purified EGCG (one elution peak) was supplied in solid form by the Lipton Company (Englewood Cliffs, NJ), and the solid material was dissolved in Tyrode's or Ringer's solutions to make 50 μg/ml. Whole eyes were placed with their anterior surfaces up in small glass beakers on gauze soaked with medium. Only the corneas were protruding into the air, and the beakers were filled with Tyrode's or Ringer's.

Whole eyes were exposed to the EGCG solutions as follows. Filled plastic bottle reservoirs were placed on a shelf above the beakers of eyes so that the solutions were delivered through plastic tubing connected to shortened micro-pipette tips at about 12 drops per min for 4 h. For comparison, solutions not containing EGCG were dropped onto control eyes at the same rate.

Cornea epithelia and lens capsule epithelia were dissected, washed in their respective media, and homogenized in glass homogenizers in 1.5 ml of medium. Homogenates were cleared of the insoluble residues by precipitation with an Eppendorf centrifuge at 12,000 rpm for 10 min. The presence of EGCG (50 μg/ml) was detected in the cornea and lens, which were found to exhibit the same fluorescent and absorptive spectral qualities as the pure EGCG (excited at 490 nm, emission at 540 nm). We therefore attribute the fluorescences of these ocular tissues to the presence of EGCG.

Extracted lenses were pre-incubated in Tyrode's (rabbit) or elasmobranch Ringer's (dogfish) solutions containing 5 μg/ml of EGCG. After the presoaking period, three lenses per group were placed in beakers containing 15 ml of fresh Tyrode's or Ringer's solutions without EGCG. The beakers containing lenses with anterior surface pointing upward were placed on a rack in our UVA exposure chamber.

The UVA radiation was provided by 15 Osram Sylvania 15 W BL (maximum emission at 355 nm) lamps. Total exposure was 20 J/cm^2. Lenses were kept on ice until examined.

When the experimental procedures were complete, the lenses were blotted, weighed analytically, and assayed for catalase activity (*i.e.*, O_2 production from H_2O_2) with an O_2 meter and probe (Microelectrodes) connected to an (XY) LKB recorder. The slope of O_2 generation per minute was used as a measure of catalase activity. Controls for the EGCG-treated lenses and for UV-exposed lenses were included in every experiment.

The enzyme catalase is quite sensitive to inactivation due to UVA exposure (1, 2). This was shown to occur in lenses of

Table I

Protection of lens catalase activity from UVA inactivation by EGCG

	Dark control	UV exposed	% of control	UV exposed after EGCG soak	% of control
Rabbit catalase* (% O_2 increase)	4.0 ± 0.9	1.5 ± 0.3	38%	2.9 ± 0.5	73%
Dogfish catalase (% O_2 increase)	2.78 ± 0.5	0.63 ± 0.2	23%	1.38 ± 0.3	50%

* Average of 3 determinations ± the Standard Deviations.

numerous species. In this report, we confirm that the inactivation of catalase due to UVA exposure is significantly reduced by the antioxidant action of EGCG. The protection of lens catalase by 5 μg/ml of EGCG ranged from 10% to 50% (Table I).

This study indicates that EGCG in physiological solutions can penetrate the anterior surface of the eye *in vitro* so as to reach the lens. It also shows that when EGCG reaches the lens, it is incorporated into the capsule epithelium. EGCG is known to be an antioxidant that reduces oxidative stress in non-ocular tissues (3). This report shows that it enters the eye so as to reach the lens as well and provides beneficial antioxidant effects, as shown by others in non-ocular tissues (3).

Further research is needed to determine whether EGCG can reduce oxidative stress to the human lens, thus delaying some cataractous changes that are due to environmental photo-oxidants.

Literature Cited

1. **Zigman, S. 1997.** *Biol. Bull.* **193:** 253–254.
2. **Zigman, S., J. Reddan, J. B. Schultz, and T. McDaniel. 1996.** *Photochem. Photobiol.* **63:** 818–824.
3. **Mitscher, L. A., M. Jung, D. Shankel, J-H. Don, L. Steele, and S. P. Pillar. 1997.** *Med. Res. Rev.* **17:** 327–365.

Reference: *Biol. Bull.* **197:** 287–288. (October 1999)

Salinity Effects on Nitrogen Dynamics in Estuarine Sediment Investigated by a Plug-flux Method

Thomas Mondrup (Department of Life Sciences and Chemistry, Roskilde University, Denmark)

The efficiency of nitrification and coupled denitrification of regenerated N is greater in fresh water than in the marine and estuarine environments (1). Salinity or factors related to salinity thus play a major role in determining the fate of regenerated N. Increasing salinity decreases the amount of exchangeable ammonium, which is thought to diminish the substrate availability for nitrifiers (1). Sulfide, which is associated with sulfate reduction in saline environments, inhibits nitrification and denitrification (2). Lastly, nitrifiers and denitrifiers presumably suffer direct physiological salinity stress (3).

The relative significance and interaction of these relations are unclear. The purpose of this study was to investigate the effect of salinity on estuarine sediment in the absence of potential sulfide effects. We employed a plug-flux method (4) in which thin layers of sediment are incubated with a small volume of overlying water after porewater concentrations have achieved steady state in a large volume of overlying water. The advantage of the method is that steady state can be attained relatively fast, and that linear fluxes during incubation can be interpreted as production rates (4).

Surface sediment (0–2 cm) was collected in April 1999 from a station with seasonally varying salinity in the Parker River Estuary, Massachusetts. Salinity was ~0‰ at collection. Sediment was sieved (1 mm), kept dark at 2°C, and stirred daily for 2 weeks prior to incubations. Sediment was incubated at different concentrations of artificial seawater lacking sulfate (0, 3, 10, and 30‰ under oxic conditions, and 0 and 30‰ under anoxic conditions). At each treatment, 14 plugs (0.8 cm deep, 4.8 cm diameter) filled with 14.5 cm^3 of sediment were each placed in open 125-ml cups, and afterwards placed in a tank containing 25 l of treatment water. The experiment was kept at 20°C. After 50 h, steady state was assumed and the cups were sealed. Exchangeable and porewater ammonium concentrations were hereafter measured to be constant in each treatment between 0 and 72 h, thus indicating that steady state had been achieved. Microelectrode measurements of oxygen concentrations indicated that only the top 2 mm of sediment in the plugs was oxygenated. Rates of ammonification, nitrification, denitrification, and oxygen consumption were calculated from differences in final and initial concentrations in the overlying water in the sealed cups after 0, 18, 40, 48, 72, and 161 h. At every timepoint, two cups from each treatment were removed for analysis. For sediments removed after 161 h, potential nitrification was measured as nitrate production in oxic conditions. The samples were shaken with treatment water enriched with 500 μM NH_4^+ and 200 μM PO_4^{3-} (5).

Ammonium concentrations were measured fluorometrically (6). Nitrate (+nitrite) concentrations were measured on a Lachat autoanalyzer. Oxygen consumption and denitrification were measured by membrane inlet mass spectrometry (MIMS) (7). Differences ($P < 0.05$) in flux rates among treatments were tested using a one-way ANOVA after determining whether data were homogeneous and normally distributed. If the differences were significant, treatment means were compared using a Tukey test. Nitrate efflux data were not homogeneous and were therefore analyzed with a Kruskal-Wallace nonparametric ANOVA.

The ammonification rates (Fig. 1A), expressed on an areal basis were ~0.6–0.9 mmol $m^{-2}d^{-1}$, which is typical for estuarine sediment. The ammonification rate was significantly higher at 3‰ than at all other salinities. There was no significant difference between the anoxic and oxic treatments at either 0 or 30‰. Measured nitrification rates (Fig. 1B) were very low (0–2% of ammonification rates), suggesting either low nitrification or efficient coupling to denitrification. Nitrate decreased at all treatments, suggesting net denitrification. Potential nitrification (Fig. 1C) was significantly higher at 3‰ than at 30‰. Oxygen consumption (Fig. 1D) was similar for all four oxic salinity treatments, suggesting that the difference in ammonification at 3‰ might reflect a difference in anaerobic metabolism. If Redfield ratio (C:N = 7:1) is assumed for the decomposed organic matter, then an oxygen consumption of 500 nmol would produce ~70 nmol of ammonification. Thus oxygen consumption alone is not sufficient to explain the ammonification rate at 3‰. The measured rates of denitrification (Fig. 1E) were highly variable and not significantly different from 0 in any treatment. The measurements ranged from 0 to 100 nmol N g^{-1} ww d^{-1}. However, because ammonification did not differ between anoxic and oxic treatments, because there was no nitrate in overlying water at the beginning of the experiment, and because there was very low measured nitrification, we believe that denitrification was very low.

In conclusion, there was a relative stimulation of ammonification and potential nitrification at 3‰. Neither sulfide inhibition nor the relative amount of exchangeable ammonium could explain this result, pointing to a direct physiological response of the bacterial community to salinity. This response could be due either to a larger number of active bacteria or to an increase in bacterial activity. Potential and actual nitrification was lowest at 30‰, which was expected due to severe salinity stress. Decrease in substrate availability could also acount for the low actual nitrification, but not for the low potential nitrification. However, the experimental setup was not optimal for investigating actual nitrification and denitrification. First, changes in oxygen conditions influenced the conditions for nitrification and denitrification, so that fluxes were nonlinear at several treatments. To investigate the effects on actual rates of nitrification and denitrification more thoroughly, it would be advisable to look at the two processes separately. This could have been done by investigating nitrification at thinner sediment plugs without an anoxic interface, and by investigating denitrification in plugs with an oxic anoxic interface as described above, but with a substantial addition of nitrate to the treatment water.

This research was supported by an NSF-LTER Grant (OCE 9726921), NOAA Sea Grant, the Mellon Foundation, and Roskilde University. I thank Gary T. Banta, Anne E. Giblin, Charles S. Hopkinson, Jane Tucker, Nathaniel Weston, and Yongchen Wang for help and assistance in carrying out this research.

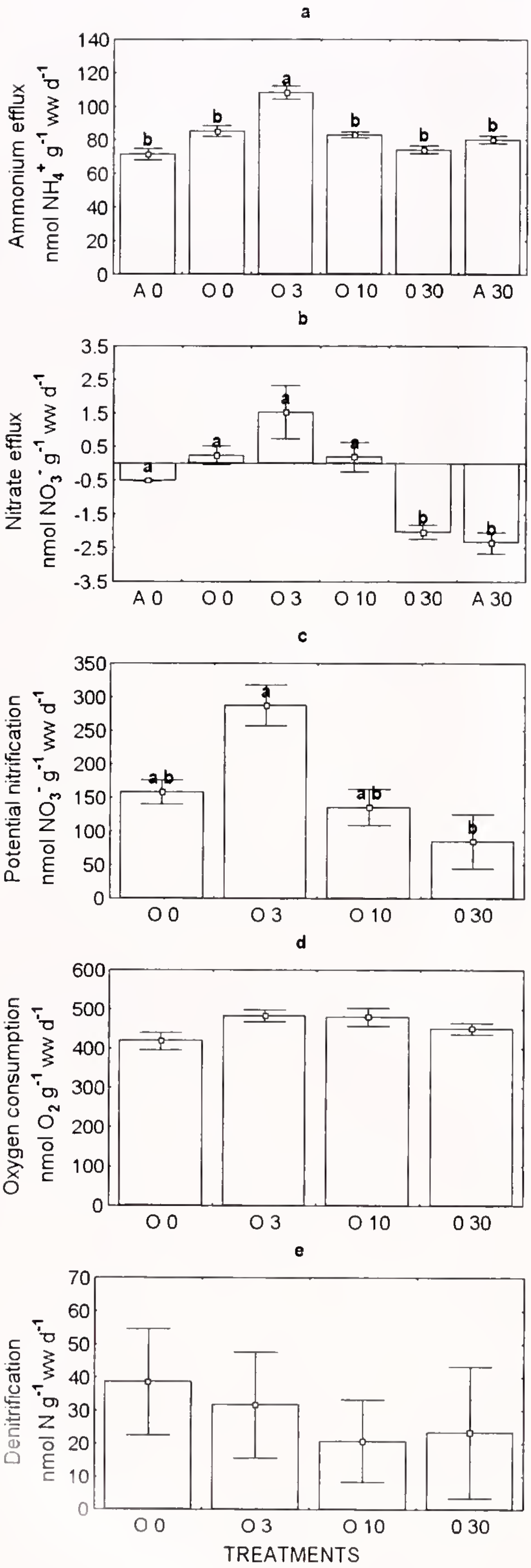

Figure 1. *Average flux rates ± SE for each treatment (A 0 and A 30 = anoxic 0 and 30‰, O 0, O 3, O 10, and O 30 = oxic 0, 3, 10, and 30‰): (A) ammonium efflux, (B) nitrate efflux, (C) potential nitrification, (D) oxygen consumption, and (E) denitrification. Treatments shown to be significantly different* ($P < 0.05$) *by ANOVA following multiple comparison are indicated with different letters (A and B).*

Literature Cited

1. **Seitzinger, S. P. 1988.** *Limnol. Oceanogr.* **33:** 702–724.
2. **Joy, S. B., and J. T. Hollibaugh. 1995.** *Science* **270:** 623–625.
3. **Rysgaard, S., P. Thastum, T. Dalsgaard, P. B. Christensen, and N. P. Sloth. 1999.** *Estuaries* **22:** 21–30.
4. **Aller, R. C., and J. E. Mackin. 1989.** *J. Mar. Res.* **47:** 441–456.
5. **Henriksen, K., J. I. Hansen, and T. H. Blackburn. 1981.** *Mar. Biol.* **61:** 299–304.
6. **Holmes, R. M., A. Aminot, R. Kérouel, B. A. Hooker, and B. J. Peterson. 1999.** *Can. J. Fish. Aquat. Sci.* (in press).
7. **Kana, T. M., C. Darkangelo, M. D. Hunt, J. B. Oldham, G. E. Bennett, and J. C. Cornwell. 1994.** *Anal. Chem.* **66:** 4166–4170.

Reference: *Biol. Bull.* **197:** 289–290. (October 1999)

Ipswich River Nutrient Dynamics: Preliminary Assessment of a Simple Nitrogen-Processing Model

Katherine M. Pease[1], *L. Claessens, C. Hopkinson, E. Rastetter, J. Vallino, and N. Killham*
(Marine Biological Laboratory, Woods Hole, Massachusetts)

The Ipswich River is a low-gradient, coastal river in northeastern Massachusetts. It is about 55 km long and drains an area of 401 km^2. Previous observations and studies indicate high levels of dissolved inorganic nitrogen (DIN) in the headwaters of the river due to urban and residential land use (1). However, concentrations drop quickly with distance downstream, presumably due to biological processing of the nitrogen. A mass balance budget of nitrogen indicates a large unknown nitrogen sink in the Ipswich River (1). To further investigate the dynamics of N cycling in the Ipswich River, nutrient concentrations were measured along transects running the length of the river, and a simple nitrogen-processing model was constructed and analyzed.

Water samples were collected on 1 and 2 July 1998 and analyzed for NH_4^+, NO_3^- (collectively dissolved inorganic N-DIN), PO_4^{3-}, total dissolved N (TDN), and total dissolved P (TDP). The samples were collected in the main channel between river kilometers 6 and 50 at intervals of 1 to 5 km (river mouth = km 0). Samples were also collected from three headwater sites (between river km 60 to 63) and analyzed for nutrients. A simple nitrogen-cycling model was developed that included compartments for

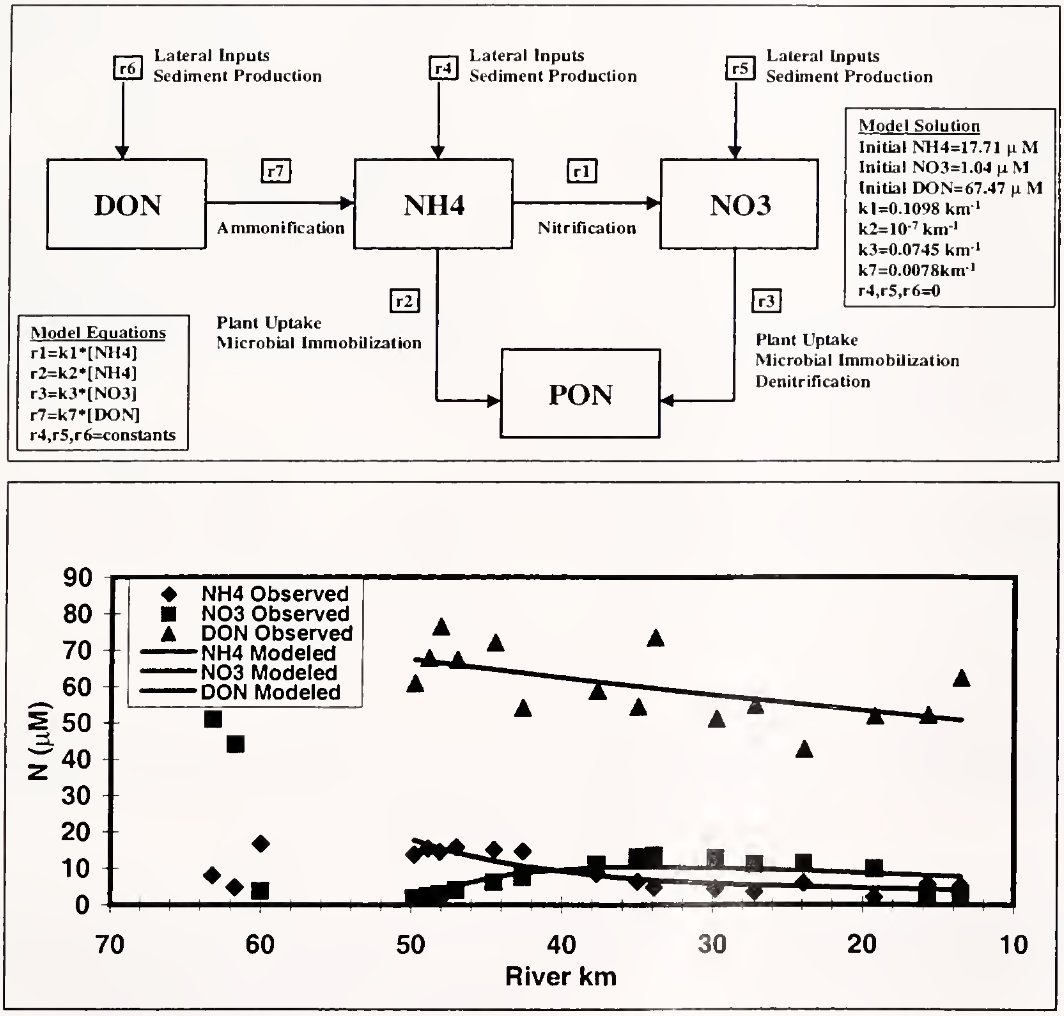

Figure 1. *(Top): A simple N-processing model showing compartments, equations, and calculated rate coefficients. (Bottom): Observed (symbols) and predicted (lines) concentrations of* NH_4^+, NO_3^-, *and dissolved organic nitrogen (DON) for the Ipswich River in July 1998.*

---

[1] Barnard College, New York.

NH_4^+, NO_3 , dissolved organic N (DON), and particulate organic N (PON) and considered the processes of ammonification, nitrification, and immobilization (Fig. 1, top). First-order kinetics were assumed for all processes except for lateral inputs. Concentrations were modeled as functions of distance. The least squares approach was used to fit the model to the main channel concentration data. The concentration data from the headwater sites were not used in the model. Constraints were placed on the model so that the initial concentrations, rate coefficients (k), and uptake rates (r) were greater than zero. Uptake lengths (1/k) were calculated from the rate coefficients; an uptake length is an estimate of the average distance traveled by an element before it is removed from the water column.

Phosphate concentrations were very low at the headwater sites, averaging only 0.3 μM P (data not shown). Further downstream in the main stem of the river, PO_4^{3-} was roughly the same as upstream (0.6 μM). TDP concentrations showed no apparent downstream pattern and were only slightly higher than PO_4^{3-}, indicating very low DOP concentrations (0–1.5 μM). DIN concentrations at the headwater sites were high, approaching 60 μM N (Fig. 1, bottom). Further downstream in the main stem of the river, DIN concentrations were markedly lower (averaging 17 μM). TDN concentrations were much higher than DIN but, as with TDP, showed no apparent spatial pattern. Of the DIN fractions, NO_3^- exhibited a large drop in concentration with distance down the headwater stream. Although NO_3^- dropped, NH_4^+ increased slightly, suggesting denitrification of the NO_3^- and ammonification without subsequent nitrification. In contrast, in the main channel, NH_4^+ and NO_3^- concentrations were mirror images of each other but with NH_4 dropping and NO_3 increasing. This pattern suggests nitrification.

Our simple N model tracked observed data well (Fig. 1, bottom). Plots of predicted *versus* observed concentrations of NH_4^+, NO_3^-, and DON illustrated close agreement for all fractions. Slopes of regression lines were between 0.96 and 1.2 for the three components. Not only was there close agreement in a general sense, but the spatial patterns were also close to observed patterns for all components.

Rate coefficients determined with the model differed greatly between the various N fractions, ranging from 0.0078 km^{-1} for ammonification to 10^7 km^{-1} for plant uptake and microbial immobilization (Fig. 1, top). For all fractions, uptake, or transformation, lengths calculated from the rate coefficients were much longer than those usually reported for more pristine stream systems (2). The uptake lengths for NH_4^+ and NO_3^- were 9 km and 13 km, respectively. The uptake length for NO_3^- was dominated by nitrification, as the rate of nitrification was 10^6 times that of plant uptake. The uptake length for DON exceeded the length of the river. NH_4^+ uptake lengths reported in the literature for low-nitrogen, pristine stream systems are often between 30 and 400 m (2). Reported NO_3^- uptake lengths for similar systems typically range from 40 to 690 m (2). The long Ipswich River uptake lengths are probably due to the relatively high concentrations of inorganic and organic N in the Ipswich River. For a given rate of processing, calculated uptake rate coefficients vary inversely with concentration. The observed uptake lengths may also represent slow overall rates of N cycling in this system, which as evidenced by extremely high inorganic N:P ratios, is probably P limited.

Patterns of nutrient concentration and the results of the N model suggest that an important location for N retention or loss is in the headwater streams of the Ipswich River. Inorganic N concentrations decrease markedly in this region. The N-cycling model indicates very long uptake lengths in the mid and lower stretches of the river. It is possible that nutrient processing is greater in the headwaters because of greater relative contact with the riverbed. There may also be more active exchange between surface and hyporheic waters in the headwater streams. We would expect high rates of denitrification in anoxic hyporheic waters. Additional studies, such as tracer-nutrient releases and ^{15}N additions could be profitably conducted in the upper reaches. Study of nutrient processing in the Ipswich River is increasingly important because N loading is rising in this rapidly urbanizing watershed. It is unclear how long the Ipswich River will be able to continue to process the high loads of inorganic N before the uptake capacity is reached.

This research was funded by NSF grants (LTER: OCE-9726921, DEB-9726862, and EAR-9807632) and a gift from the Jessie B. Cox Charitable Trust.

Literature Cited

1. **Ingram, K. K., C. S. Hopkinson, K. Bowman, R. Garritt, and J. Vallino. 1994.** *Biol. Bull.* **187:** 277–278.
2. **Marti, E., and F. Sabater. 1996.** *Ecology* **77:** 854–869.

Reference: *Biol. Bull.* **197:** 290–292. (October 1999)

Increased Lability of Estuarine Dissolved Organic Nitrogen From Urbanized Watersheds

Felisa L. Wolfe[1], *Kevin D. Kroeger, and Ivan Valiela (Boston University Marine Program, Marine Biological Laboratory, Woods Hole, Massachusetts 02543)*

Inputs of nitrogen from land can lead to eutrophication of estuaries (1–5, 6). Terrestrial N is transported as NO_3^-, NH_4^+, PON (particulate organic nitrogen), and DON (dissolved organic nitrogen), but most estimates of N loading are based on DIN (NO_3^- + NH_4^+). DON had been thought to be mostly refractory to organisms, but recent studies show that some portion of the DON may be labile (6, 7). Land-derived DON may thus be mineralized within estuaries, and the NH_4^+ released may be available to organisms (4). Most calculations of N inputs to estuaries are based on DIN; to the extent that DON is labile, nitrogen loads calculated on the basis of land-derived DIN inputs alone underestimate effective N loads (6, 7).

---

[1] Oberlin College, Oberlin, Ohio.

There is evidence that urbanization of watersheds alters the lability as well as the amount of DON loaded to receiving waters (6). We evaluated these issues by use of estuaries of Waquoit Bay, Massachusetts (Sage Lot Pond, Quashnet River, and Childs River), that receive different N inputs from their watersheds because of different degrees of urbanization (1, 4, 5). Sage Lot Pond (SLP) has a primarily forested watershed that provides a N load of 14 kg N ha^{-1} y^{-1}; Quashnet River (QR) has a watershed with an intermediate degree of urbanization and a N load of 350 kg N ha^{-1} y^{-1}; Childs River (CR) has a watershed with the greatest degree of urbanization, and a N load of 601 kg N ha^{-1} y^{-1} (4, 5).

To gain a better understanding of how urbanization alters DON, we measured the lability of DON from the three different estuaries. In each estuary we collected surface water from a station with a salinity of 25‰. Samples were placed in acid-washed bottles and kept on ice. The water was filtered through precombusted 0.7-μm glass fiber filters to remove larger consumers and particulates. Triplicate samples (1000-ml/flask) were incubated at 25°C in the dark with continuous shaking. Each flask was re-sampled at 12, 24, 36, 48, 96, and 192 h. The water samples were filtered (0.2-μm Durapore membrane Millipore filter, prerinsed with deionized water); placed in acid-washed, high-density polyethylene bottles; and frozen for later analysis. Nutrient concentrations were determined by standard methods (Lachat QuikChem 8000 Automatic Ion Analyzer, 8).

DON concentrations decreased in all incubations (Fig. 1, top right) and as a percentage of the total N (Fig. 1, middle row). The loss of DON generated NH_4^+, which increased in concentration during all incubations (Fig. 1, middle panel in top row, and all panels in middle row). NO_3^- concentrations remained relatively constant during the incubations (Fig. 1, top left). The total dissolved nitrogen (TDN) did not change significantly (data not shown) within the measurement error (*F* values for regressions were 0.56 for SLP, 0.95 for QR, and 0.9 for CR), which implies that the transformation of TDN to particulate forms was not significant during the incubation; the concentrations of NH_4^+, NO_3^-, and DON accounted for measured TDN throughout.

The degree of urbanization on the different watersheds did alter the lability of DON generated from the watersheds. Concentrations of DON were largest in SLP (Fig. 1, top right), the estuary with the smallest N load (Fig. 1, bottom left) and the largest ratio of forest to residential land on its watershed (Fig. 1, bottom right). Our results thus suggest that increased N loads during urbanization (Fig. 1, bottom right) are accompanied by proportionally more labile DON (Fig. 1, bottom right).

We conclude that since DON is quantitatively a large part of inputs from land (6), a labile fraction of 20%–40% (Fig. 1, bottom left) could indeed make a significant contribution of available N to estuarine organisms. Nutrient-loading protocols should therefore include assessments of the amounts and lability of DON entering estuaries. This is particularly important in cases of eutrophication of estuaries with watersheds exposed to greater degrees of urban land use.

The DON in the incubation was derived from a mix of terrestrial and marine sources. Internal sources (exudation from producers, regeneration from sediments) of DON are qualitatively important (our unpublished data). In addition, we collected samples from stations at which salinity was high and marine sources could have been important. Both of these features would diminish the possibility of our finding differences in lability due to land-derived DON. Nevertheless, we did find such differences, suggesting that despite the potentially confounding effects of internal estuarine and marine sources of DON, we can still detect measurable influences tied to land-use mosaics on watersheds. Clearly, further mass balance studies will be useful to clarify issues, but our present results point to a substantive coupling between land use on watersheds and the nature of the DON in estuarine waters. This coupling has considerable importance to the management of N loads to estuaries.

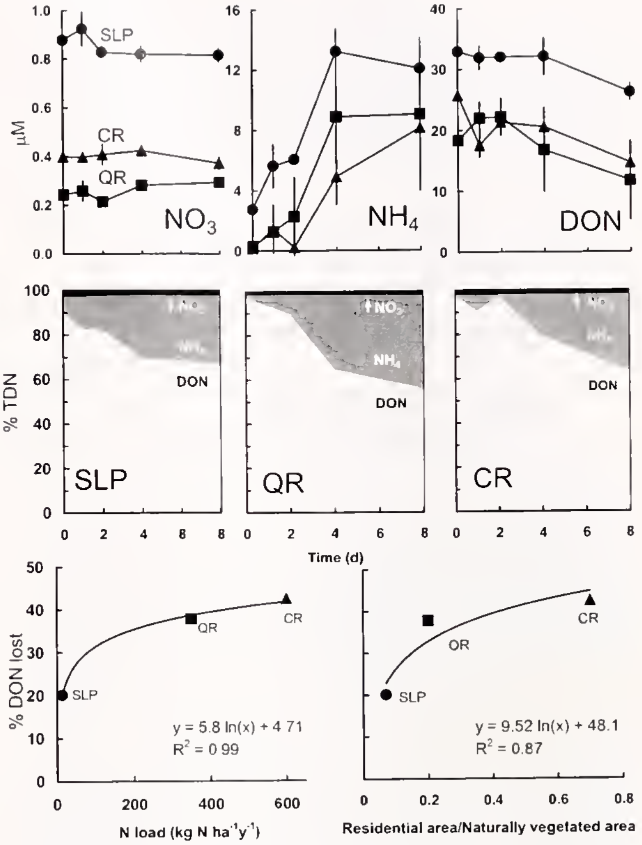

Figure 1. *Top row: concentration (mean ± SE) of nitrate, ammonium, and dissolved organic nitrogen (DON) during the incubation. Middle row: percentage composition of N measured in each of the three estuaries (Sage Lot Pond, Quashnet River, and Childs River) during the incubations. Bottom row: relationship of total percent DON lost during the incubations vs. land-derived nitrogen load (left panel) and vs. ratio of residential to vegetated land acreage on the watersheds (right panel).*

We thank Caroline Plugge, Kurt Hanselmann, Gabrielle Tomasky, and Jennifer Walters for analytical assistance. Also special thanks to Kenneth Foreman and The Ecosystems Center for use of the Lachat autoanalyzer and to Eric Davidson of the Woods Hole Research Center for suggestions. This research was supported by funds from the NSF Research Experience for Undergraduates program (OCE-9605099).

Literature Cited

1. **Valiela, I., J. Costa, K. Foreman, J. M. Teal, B. Howes, and D. Aubrey. 1990.** *Biogeochemistry* **10:** 177–197.
2. **Valiela, I., *et al.* 1992.** *Estuaries* **15:** 443–457.
3. **D'Avanzo, C., and J. Kremer. 1994.** *Estuaries* **17:** 131–139.
4. **McClelland, J. W., and I. Valiela. 1998.** *Limnol. Oceanogr.* **43:** 577–585.
5. **Valiela, I., G. Collins, J. Kremer, K. Lajtha, M. Geist, B. Seely, J. Brawley, and C. H. Sham. 1997.** *Ecol. Appl.* **7:** 358–380.
6. **Seitzinger, S. P., and R. W. Sanders. 1997.** *Mar. Ecol. Prog. Ser.* **159:** 1–12.
7. **Bronk, D. A., P. M. Gilbert, and B. B. Ward. 1994.** *Science* **265:** 1843–1846.
8. **D'Elia, C. *et al.* 1977.** *Limnol. Oceanogr.* **22:** 760–764.

Reference: *Biol. Bull.* **197:** 292–294. (October 1999)

Effects of Increased Nitrogen Loading on the Abundance of Diatoms and Dinoflagellates in Estuarine Phytoplanktonic Communities

A. Evgenidou, A. Konkle, A. D'Ambrosio, A. Corcoran, J. Bowen, E. Brown, D. Corcoran, C. Dearholt, S. Fern, A. Lamb, J. Michalowski, I. Ruegg, and J. Cebrián (Boston University Marine Program, Marine Biological Laboratory, Woods Hole, Massachusetts, 02543)

Coastal and estuarine ecosystems are among the most anthropogenically affected ecosystems on earth (1). Increased urbanization, deforestation, and agricultural land uses are some of the main factors that cause increased nitrogen loading in the estuaries (2). The effects of this increased delivery of nitrogen on the receiving estuarine waters include increased abundance of benthic macroalgae and phytoplankton, reduced oxygen content of the water, and deterioration of shellfish and finfish populations (2, 3). However, knowledge of how and why estuaries subject to different rates of nitrogen loading differ in the composition of their phytoplanktonic communities is not as extensive, even though many laboratory experiments have addressed this question (4, 5, 6, 7). Changes in phytoplanktonic composition may have important effects on the receiving estuaries, such as changes in the food web structure (8) or in the sedimentation rates of organic matter (9).

In our study, we describe the abundance of diatoms and dinoflagellates in three estuaries of Waquoit Bay, Massachusetts, which have similar physical properties but differ greatly in their degree of urbanization and subsequent nitrogen loading rates (2). Childs River, Quashnet River, and Sage Lot Pond exhibit high (601 kg ha^{-1} y^{-1}), medium (350 kg ha^{-1} y^{-1}), and low (14 kg ha^{-1} y^{-1}) nitrogen loading rates respectively (10). To describe the natural assemblages of diatoms and dinoflagellates in the three estuaries, we took water samples from one site at the mouth of each estuary, at ~2 m depth on 12 November 1998. Temperature and salinity were very similar in the three sites examined. We took six samples from Childs River and Sage Lot Pond, and three samples from Quashnet River. Natural abundance was low during the sampling period; therefore, samples were concentrated 50 times by filtering 50 l of water through a 10-μm-mesh filter to collect the phytoplankton. The phytoplankton was then placed in 1 l of water and fixed with Lugol's solution. The two phytoplanktonic groups were identified and cells were counted under compound microscopes.

In addition, we conducted a laboratory experiment to test whether the observed differences in composition of the phytoplanktonic groups examined were driven by increased nitrogen loading. Phytoplankton from Sage Lot Pond was collected using a 10-μm mesh, and then placed in two 35-l tanks filled with Childs River water that had been previously filtered through 1-μm filters. The control tank contained phytoplankton from Sage Lot Pond placed in water from the same estuary using the procedure described above. Similar quantities of phytoplankton were placed in the three tanks. All tanks were oxygenated and kept with seasonal light and temperature conditions in an incubation chamber. In each tank, three replicates were taken at 0, 3, 6, and 9 days to measure phytoplankton abundance. We used the nitrogen content in the water column as a proxy for nitrogen loading. Nitrogen concentrations in Sage Lot Pond and Childs River water in November were 1 and 5 μM respectively. Therefore, every 3 days we measured the nitrogen concentration in all tanks and added nitrogen as needed to maintain these natural levels.

Analysis of the natural abundance of diatoms and dinoflagellates showed that diatoms were the dominant group in all three estuaries (Fig. 1A), while dinoflagellates represented less than 10% of the phytoplanktonic community examined. Both diatom and dinoflagellate abundances increased from low- to high-nitrogen estuaries (Fig. 1A; ANOVA, $P < 0.01$ for both groups). In addition, diatoms increased to a much greater extent than dinoflagellates did and, as a consequence, the ratio of diatoms to dinoflagellates increased more than one order of magnitude from low- to high-nitrogen estuaries (Fig. 1B; ANOVA, $P < 0.01$). Dinoflagellates represented about 10% of the total community examined in Sage Lot Pond, but were less than 1% in Childs River (Fig. 1B). A further examination of the diatom community showed that both centric and pennate diatoms increased from low- to high-nitrogen estuaries (Fig. 1C; ANOVA, $P < 0.01$ for both types). The two groups increased in similar proportions and, consequently, the ratio of centric to pennate did not change significantly with higher loading rates (ANOVA, $P > 0.05$).

The results from the experiment showed that the Sage Lot diatom community in Childs River water responded differently than the control, the same community kept in its own water (Fig. 2). Diatom abundance in Childs River water increased over the course of the experiment (t test, $P < 0.01$). Conversely, diatom abundance in Sage Lot water at the end of the experiment was not higher than the initial abundance (t test, $P > 0.05$), in spite of the observed peak on the third day. At the end of the experiment, diatoms were more abundant in Childs River water than in Sage Lot water (t test, $P < 0.01$). Dinoflagellate abundance increased over the experiment in both Childs and Sage Lot water (t test, $P < 0.01$), reaching similar values in both types of water (t test, $P > 0.05$).

Results from the natural abundance survey indicate that diatoms were more abundant than dinoflagellates in the estuaries examined (Fig. 1A). Moreover, these results suggest that the dominance of diatoms is promoted by increased nitrogen loading. The results of the experiment also show that by the end of the study period diatoms were more abundant in Childs River water than in Sage Lot Pond water. However, diatom abundance in Sage Lot Pond water was inconsistent over the course of the experiment, increasing for the first 3 days before declining to levels not different from their initial abundance. Therefore, the results of this preliminary experiment can only suggest that nitrogen loading rates may be promoting diatom dominance in these estuaries (Fig. 2). Moreover, there may be some other factors that could account for the increasing abundance of diatoms, such as differences in silica and other trace metals among estuaries.

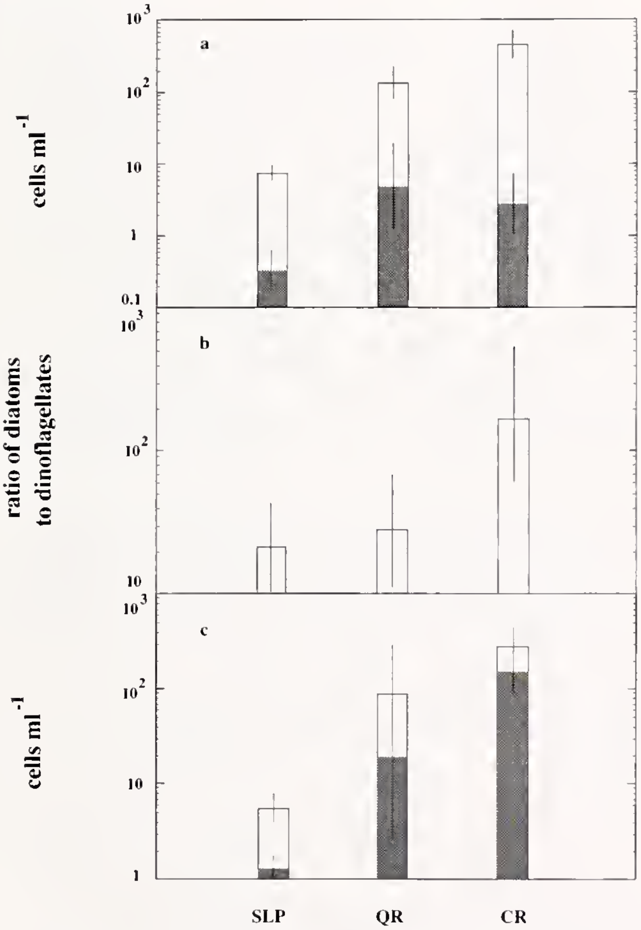

Figure 1. *Analysis of the natural phytoplanktonic communities in the three estuaries of Waquoit Bay. (A) The abundance of diatoms (open bins) and dinoflagellates (grey bins) in Sage Lot Pond (SLP), Quashnet River (QR), and Childs River (CR). (B) The ratio of diatoms to dinoflagellates in the three estuaries examined. (C) The abundance of centric diatoms (open bins) and pennate diatoms (grey bins) in the three estuaries. Bins represent mean values and bars show confidence intervals calculated from six replicates for CR and SLP and from three replicates for QR. Variables were log-transformed to comply with the assumptions of the ANOVA test employed.*

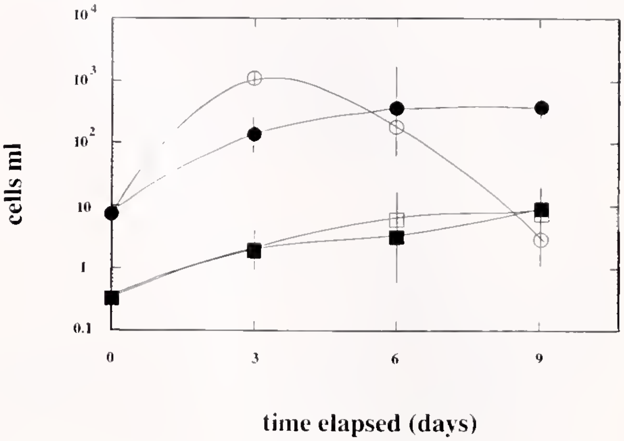

Figure 2. *Abundance of diatoms (circles) and dinoflagellates (squares) during the laboratory experiment. Sage Lot Pond phytoplankton in Childs River water (experimental) is represented by solid symbols; Sage Lot Pond phytoplankton in Sage Lot Pond water (control) is represented by open symbols. Symbols represent mean values and bars show confidence intervals calculated from six replicates for experimental tanks and from three replicates for control tanks. Lines depict the spline-smoothed trends. Variables were log-transformed to comply with the assumptions of the ANOVA test employed.*

Our findings are consistent with the results of previous laboratory manipulations. Many authors have shown that experimental nitrate enrichment results in phytoplanktonic communities dominated by centric diatoms (4, 5, 7). This is attributed to the higher growth rates of diatoms compared to dinoflagellates (5, 6, 7). Therefore, it is possible that diatoms could build up large stocks of biomass faster than dinoflagellates.

Changes in the relative abundance of diatoms and dinoflagellates under increasing nitrogen loading may have important ecological implications for the receiving estuaries. Large centric diatoms are the main diet of some copepods species, which in turn are preyed upon by commercial fish species (8). Therefore, increases in abundance of centric diatoms could cause changes in the food web structure of the receiving estuaries. In addition, diatoms have higher sinking rates than other groups of phytoplankton, which could lead to enhanced sedimentation rates of carbon in the estuary (9). Examination of these hypotheses is needed to assess the effects of nitrogen induced shifts in phytoplankton composition, particularly among diatoms and dinoflagellates, on the ecology of the receiving estuaries.

Literature Cited

1. **Vitousek, P. M., H. A. Mooney, J. Lubchenco, and J. M. Melillo. 1997.** *Science* **277:** 494–499.
2. **Valiela, I., K. Foreman, M. LaMontagne, D. Hersh, J. Costa, P. Peckol, B. DeMeo-Andreson, C. D'Avanzo, M. Babione, C. Sham, J. Brawley, and K. Lajtha. 1992.** *Estuaries* **15:** 443–457.
3. **Nixon, S. W. 1986.** *J. Limnol. Soc. S. Afr.* **12:** 43–71.

4. **Davis, C. O. 1982.** Pp. 323–332 in *Marine Mesocosms*, G. D. Grice and M. R. Reeve, eds. Springer-Verlag, New York.
5. **Takahashi, M., I. Koike, K. Iseki, P. K. Bienfang, and A. Hattori. 1982.** Pp. 333–340 in *Marine Mesocosms*, G. D. Grice and M. R. Reeve, eds. Springer-Verlag, New York.
6. **Ishizaka, J., M. Takahashi, and S. Ichimura. 1983.** *Mar. Biol.* **76:** 271–278.
7. **Parsons, T. R., P. J. Harrison, and R. Waters. 1978.** *J. Exp. Mar. Biol. Ecol.* **32:** 285–294.
8. **Greve, W., and T. R. Parsons. 1977.** *Helgol. Wiss. Meeresunters* **30:** 666–672.
9. **KiØrboe, T. 1993.** *Adv. Mar. Biol.* **29:** 1–72.
10. **Valiela, I., G. Collins, J. Kremer, K. Lajtha, M. Geist, B. Seely, J. Brawley, and C. H. Sham. 1997.** *Ecol. Appl.* **7:** 358–380.

Reference: *Biol. Bull.* **197:** 294–295. (October 1999)

Relationship of Reproductive Output in *Acartia tonsa*, Chlorophyll Concentration, and Land-Derived Nitrogen Loads in Estuaries of Waquoit Bay, Massachusetts

Andrea Cubbage[1], David Lawrence, Gabrielle Tomasky, and Ivan Valiela (Boston University Marine Program, Marine Biological Laboratory, Woods Hole, Massachusetts 02543)

Anthropogenic nutrient enrichment of estuaries and coastal waters has a profound impact on ecosystem structure and function. Such impacts include increases in abundance of planktonic and benthic macroalgae (1). Because estuaries of Waquoit Bay, Massachusetts (Childs River, Quashnet River, and Sage Lot Pond), receive different land-derived nitrogen loads (601, 350, 14 kg N ha^{-1} y^{-1}, respectively) (2), the ecological effects of different nitrogen loads can be compared. The differences are directly related to the degree of urbanization on each watershed, with primary production highest in the estuary with the most urbanized watershed (2).

The objective of this study was to determine the effect of nutrient enrichment, *via* increased phytoplankton biomass, on the reproductive output of the copepod *Acartia tonsa*, the dominant summer zooplankter of Waquoit Bay (>90% of the individuals, D. Lawrence, unpublished data). *A. tonsa* has a high rate of population turnover and a low capacity for energy storage (3), so it is a suitable organism to use in assessing short-term responses to food supply. We expected that changes in available food supply created by the different nitrogen enrichment regimes would be reflected in the egg output of *A. tonsa*, a variable known to respond rapidly to food supply (3).

Egg production experiments were conducted in the field from 10 to 20 July 1999 to measure reproductive output of *A. tonsa* in relation to chlorophyll concentration and to nitrogen load. Adult *A. tonsa* females were collected from each site by towing a 153-μm Nitex nylon net obliquely at a depth of 0.5 m. To minimize the influence of temperature and salinity, animals were collected from sites that ranged in temperature from 24°C to 27°C and in salinity from 25‰ to 30‰. The incubation water was collected, using a Lamotte water sampler, from the same site and depth as the tows, and filtered through a 45-μm sieve to remove all mesozooplankton and copepod eggs but retain phytoplankton. This filtered water, now devoid of eggs, was used to fill the 2-l incubation bottles.

In the laboratory, adult females were isolated and 6 to 10 were placed in each incubation bottle. For each site, six bottles were incubated in Waquoit Bay for 24 h. This is sufficient time to measure changes in egg production in these animals (4). Incubations were run *in situ* to maintain field conditions of light and temperature. After the incubations the water was sieved twice, first through a 200-μm mesh to isolate the adult females and then through a 53-μm mesh to concentrate the eggs and nauplii. After the copepods were fixed in 70% ethanol, we measured the prosome length of adult females to determine average size, and the eggs and nauplii were counted in each sample. We determined daily egg production (EP) as $(E + N)/F$, where E = number of eggs, N = number of nauplii, and F = number of adult females in each sample. The adult females may have cannibalized nauplii, but probably at an ingestion rate of only 1% day^{-1} (5).

Water for determination of chlorophyll *a* concentration was collected on 20 July 1999 from five sites in each estuary, from near surface and bottom depths, using a Lamotte water sampler. Spectrophotometric measurements (6) were averaged to estimate mean chlorophyll *a* concentration in each incubation.

Reproductive output of *A. tonsa* increased as chlorophyll concentrations increased (Fig. 1, top left). Chlorophyll concentrations in the water increased at higher nitrogen loads (Fig. 1, top middle). We interpret these results to mean that increases in nitrogen supply led to increases in chlorophyll concentration, which in turn supplied greater amounts of food to copepods, which responded by increasing egg production. There is, therefore, an indirect correlation between reproductive output and nitrogen loads (Fig. 1, top right).

Of course, the greater reproductive production could be caused by the somewhat larger female size in the higher loaded estuaries (Fig. 1, bottom left). Nitrogen load increased both reproductive output and adult size, but egg production rates were not related to size of females (Fig. 1, bottom right). The increased reproductive output measured was therefore mediated by conditions in the estuary, not by the size of females alone.

The results suggest that with increasing nitrogen loads, phytoplankton populations increase, providing more food for *A. tonsa*, thus probably increasing its reproductive output. The reproductive output by this calanoid zooplankter seems therefore indirectly linked, through the response of phytoplankton to increased nutrient concentration, to the nitrogen loading rate derived from the watershed land-use mosaic.

This research was supported by NSF Research Experience for

---

[1] Lafayette College, Easton, Pennsylvania.

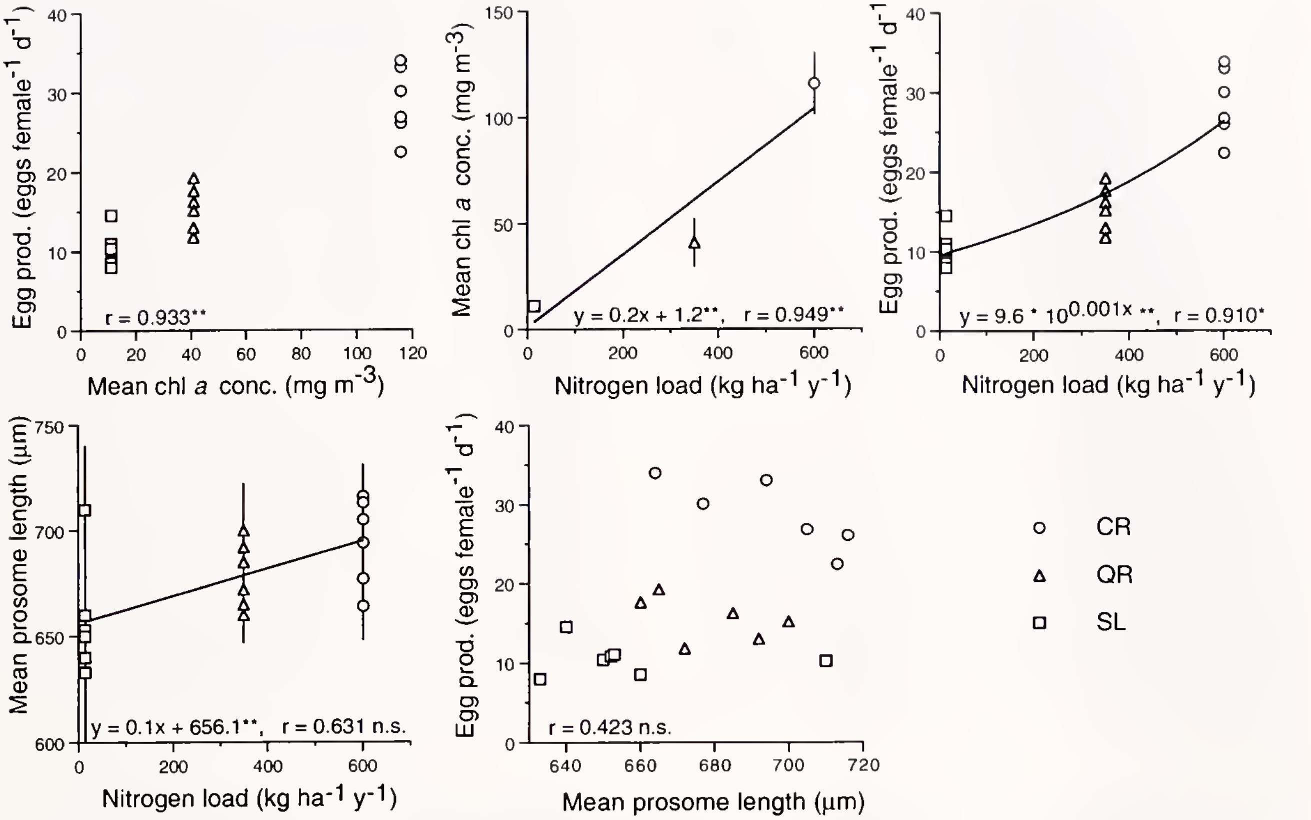

Figure 1. *Top left: Egg production rate (eggs female^{-1} day^{-1})* versus *mean chlorophyll concentration (mg m^{-3}). Top middle: Mean chlorophyll concentration* versus *land-derived nitrogen load (kg ha^{-1} y^{-1}). The lines represent standard error. Nitrogen loads obtained from Valiela* et al. *(2). Top right: Egg production rate* versus *land-derived nitrogen load. Bottom left: Mean prosome length* versus *nitrogen load. The lines represent standard error. Bottom right: Egg production rate* versus *mean prosome length of females (µm). One asterisk indicates significance of <0.05 and two asterisks indicate significance of <0.01.*

Undergraduates grant. Special thanks to Felisa Wolfe, Amy Watson, Erica Stieve, and the Waquoit Bay National Estuarine Research Reserve.

Literature Cited

1. **Valiela, I., K. Foreman, M. LaMontagne, D. Hersh, J. Costa, P. Peckol, B. DeMeo-Anderson, C. D'Avanzo, M. Babione, C-H. Sham, J. Brawley, and K. Lajtha. 1992.** *Estuaries* **15:** 443–457.
2. **Valiela, I., J. McClelland, J. Hauxwell, P. Behr, D. Hersh, K. Foreman.** *Ecol. Appl.* (in press).
3. **Kleppel, G. S., C. A. Burkart, and C. Tomas. 1998.** *Estuaries* **21:** 328–339.
4. **Bellantoni, D. C., and W. T. Peterson. 1987.** *J. Exp. Mar. Biol. Ecol.* **107:** 199–208.
5. **Lonsdale, D. J., D. R. Heinle, and C. Siegfried. 1979.** *J. Exp. Mar. Biol. Ecol.* **36:** 235–248.
6. **Lorenzen, C. J. 1967.** *Limnol. Oceanogr.* **12:** 343–346.

Reference: *Biol. Bull.* **197:** 295–297. (October 1999)

Long-Term Effect of Municipal Water Use on the Water Budget of the Ipswich River Basin

Susannah Canfield[1], *Luc Claessens, Charles Hopkinson Jr., Edward Rastetter, and Joseph Vallino*
(The Ecosystems Center, Marine Biological Laboratory, Woods Hole, Massachusetts 02543)

The Ipswich River watershed has served as a public water supply to suburban communities north of Boston since the late 1800s. Population growth and land-use changes have affected the hydrology of the watershed by increasing the amount of water pumped from the basin and altering the land cover—a problem that is prevalent nationwide (1). In recent years, the river has suffered from low flows in the summer (2). Low streamflow can be detrimental to the ecosystem of the river, the surrounding wetlands, and the estuary into which the river drains (1). The purpose of this study was to examine the effect of municipal water use on the overall water budget of the Ipswich River basin.

---

[1] Bates College, Lewiston, Maine 04240.

Monthly water budgets were constructed for the period 1931–1989 as: $\Delta S = P - ET - R - D$, where P is precipitation; ET is evapotranspiration; R is streamflow; D is net diversions, including drinking water and wastewater; and ΔS is change in storage. Precipitation data were obtained from observations of the National Weather Service (NWS) and cooperative network. Observations from NWS first-order weather stations were used to calculate evapotranspiration using a mathematical model (3). Streamflow data were obtained from the U.S. Geological Survey. Data on monthly water pumpage and wastewater systems were collected from individual town water departments, the Department of Environmental Protection, the Massachusetts Area Planning Council, and the Massachusetts Water Resources Authority. Public drinking water was divided into public water supply from within and from outside the watershed based on the locations of pumping stations relative to the boundary of the Ipswich River basin. Using population data and the relative distribution of urban land use for each town, we separated the total public water supply into water delivered inside and outside the basin. To account for lawn and plant watering, an irrigation coefficient was calculated for the summer months by considering the difference between summer and winter pumpage. Finally, the remaining water, for commercial and household use, was divided into wastewater exported out of the basin *via* sewer systems and wastewater retained in the watershed by on-site septic disposal. Sewered water was assumed to have a 65% infiltration component from groundwater (4). Linear regression analyses were performed to examine time-dependent trends in annual, monthly, and seasonal data.

On a long-term annual scale (Fig. 1a), precipitation, streamflow, and evapotranspiration are highly variable but do not display any significant time-dependent trends. Only diversions have increased significantly over time ($r = 0.96$, $P < 0.001$) and currently represent 15%–20% of streamflow. One would expect that with a significant increase in diversions, streamflow would decrease significantly. It is plausible, however, that changes in land use have masked the effect of diversions on streamflow and the overall water budget; for example, the conversion of forested area to impervious land cover could lead to an increase in streamflow and a decrease in evapotranspiration (5). Our analysis of the main diversion components shows an increase in water drawn from within and outside the basin, tripling over the 59-year period (Fig. 1b). Water supply from outside the basin constitutes 30% of the total supply; of this total water supply, 71% is delivered outside the watershed. The septic wastewater component levels off after 1966, when sewer systems became more prevalent.

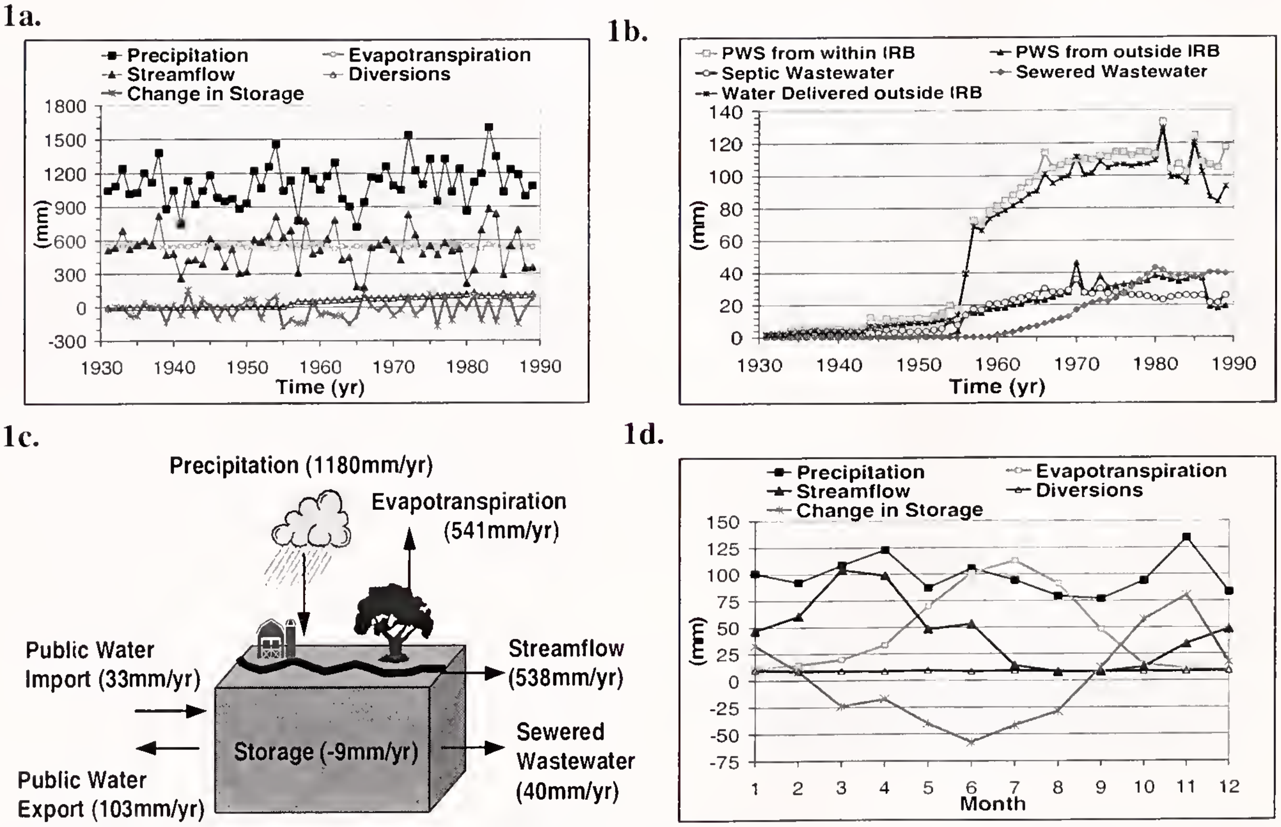

Figure 1. *(a) 1931–1989 annual time series of the main components of the water budget, with only diversions increasing significantly. (b) 1931–1989 annual time series of the components of diversions, including public water supply (PWS) from within and from outside the Ipswich River basin (IRB), water delivered outside the basin, septic and sewered wastewater, including infiltration. (c) Main components of the Ipswich River basin water budget, including 1979–1988 annual averages. (d) 1979–1988 average monthly time series of the main components of the water budget.*

In the 1979–1988 water budget (Fig. 1c), which is representative of current conditions, evapotranspiration (541 mm/y) and streamflow (538 mm/y) each account for about 45% of precipitation (1180 mm/y). Diversions leaving the basin (143 mm/y) are greater than diversions entering the basin (33 mm/y). The change in storage (−9 mm/y) is small. However, in this study, we ignored the absolute value of the storage component because it is highly dependent on the evapotranspiration estimate, which is the least accurate component of any large-scale water budget; only the temporal variation is considered. During the summer months (Fig. 1d), the change in storage is most negative, due to increasing evapotranspiration, and it is coincident with decreasing rainfall and streamflow. Diversions remain relatively constant throughout the year, with high groundwater pumping during the summer balanced by surface water withdrawals into reservoirs during the rest of the year. The effect of diversions should be most apparent during the summer months because streamflow is lowest at this time.

With increasing water demands, diversions have become a major component of the water budget—they currently represent 15%–20% of the streamflow. Our analyses of the water budget did not reveal any significant long-term trend in change in storage or in streamflow. This suggests that to understand the impact of diversions on the system we ought to reduce the time step (to daily or hourly) to examine changes in streamflow; focus the study area on the upper Ipswich basin where low flows occur and the river dries up most frequently; and look at different indices of hydrological change, such as the number of days of low flow and groundwater levels. Low streamflow is detrimental not only to the river ecosystems, but also to the downstream estuary, where alterations in salinity during the summer months could increase the stress on estuarine communities, a topic that requires further research.

This research has been supported by the NSF-BUMP REU program, the Cox Charitable Trust, and the NSF grants: OCE-9726921, DEB-9726862, and EAR-9807632. We thank the water departments of those towns that provided data and assistance, the Ipswich River Watershed Association, the Department of Environmental Protection, and Gil Pontius and colleagues at Clark University.

Literature Cited

1. **U.S. Geological Survey. 1997.** Pp. 41–45 in *Watershed Research in the U.S. Geological Survey*. National Academy Press, Washington, DC.
2. **USGS website** *(http://ma.water.usgs.gov/ipswich/)*.
3. **Morton, F. I., F. Ricard, and S. Fogarasi. 1985.** *National Hydrology Research Institute*, Paper No. 24. Ottawa, Canada.
4. **Allen, Scott. 1999.** *Boston Globe*. July 16:A16.
5. **Van Patten, Peg. 1997.** *Nor'Easter*. Spring/Summer: 15. Northeast Sea Grant Programs, University of Rhode Island, Narragansett, RI.

Reference: *Biol. Bull.* **197:** 297–299. (October 1999)

Population Size and Summer Home Range of the Green Crab, *Carcinus maenas*, in Salt Marsh Tidal Creeks

Talia Young (Swarthmore College, Swarthmore, Pennsylvania 19081), Sharon Komarow[1], *Linda Deegan*[2] *and Robert Garritt*[2]

The green crab, *Carcinus maenas*, is native to the Atlantic coast of Europe. First reported in the western Atlantic in 1817, it is abundant today in salt marshes and on rocky shores from Nova Scotia to Virginia. As a predator, it has been linked to the sharp decline of the New England soft-shell clam (*Mya arenaria*) industry in the 1940s (1). Since the crab was first found in San Francisco Bay in 1989, scientists and fishers have been anxiously monitoring its movement northward and its effects on the ecosystem (2). Despite interest in the extension of the species' geographic distribution, little work has been conducted on the home range of individual crabs. We examined the population size and summer home range of green crabs in a New England salt marsh tidal creek.

We conducted a mark-recapture experiment in a branched primary tidal creek off of the Rowley River in the Plum Island Sound Estuary in northeastern Massachusetts. The upper 200 m of the creek has about 7274 m^3 of volume and about 7128 m^2 of creek bed area. Water temperature (16°–25°C) and salinity (28‰–31‰) in the creek were typical of New England salt marshes in late spring and summer. From 29 June to 6 August 1999, crawfish traps (20 × 30 × 45 cm with 1.3-cm mesh and 8-cm opening) baited with tuna fish or dog food soaked in fish oil were laid along both branches and downstream of the confluence at seven sites 100 m apart. From 29 June to 30 July, each trapped crab measuring 40 mm or more was marked either with colored oil-based marker paint on the carapace or with a plastic loop behind the claws. The carapace width (in millimeters), sex (male or female), and carapace color (red or green) of each crab were also noted. Crabs trapped at each of the seven sites were marked with a distinct color scheme and then released at the same site. Marked crabs that were recaptured were marked a second time with the color scheme corresponding to their recapture location. Crabs trapped from 3 to 6 August were counted and removed from the creek. We used the Lincoln index and the Schnabel method to estimate population size (3). We also conducted two catch-per-unit-effort collections in five other similar-sized primary tidal creeks off of the Rowley River (Sand Creek, Shad Creek, West Creek, Club Head Creek, and Nelson Island Creek) by deploying traps from high tide to low tide (~6 h).

We estimated the population of green crabs in the study creek to be 30,000–40,000 individuals (~5 crabs per m^2) (Table 1). Recapture rate of marked crabs was between 5% and 11%. The average number of crabs caught over a 6-h period did not differ significantly between the study creek and the other five creeks

---

[1] Earth Systems Program, Stanford University, Stanford, California 94035.

[2] Ecosystems Center, Marine Biological Laboratory, Woods Hole, Massachusetts 02543.

Table I

Estimates of the population size of green crabs, Carcinus maenas, *in a tidal creek in Rowley, Massachusetts*

Marking technique	Marking period	Number of crabs marked	recaptured	captured	Recapture rate	Estimated population	95% confidence interval
Paint[1]	29 June–1 July	87	9	4095	10.35%	39585	23852–118948
Plastic tags[1]	12 July–16 July	240	25	3735	10.42%	35856	25636–59627
Paint[2]	26 July–30 July	1887	109	1848	5.78%	31992	26979–39295
All marking techniques[2]	29 June–30 July	2378	120	1848	5.05%	36621	31126–44473
All marking techniques[3]	29 June–30 July	2629	145	4251	5.52%	32746	28082–39268

[1] Estimates calculated using the Lincoln index, counting all crabs trapped in subsequent weeks as the single capture sample (6). The number of marked crabs used in these calculations was 66% of the actual number marked because approximately 33% of marked crabs in the laboratory lost their marks in two weeks.

[2] Estimates calculated using the Lincoln index with the collection from 3 to 6 August as the single recapture sample (6).

[3] Estimate calculated using the Schnabel method, treating each marking technique as one of the repeated recapture samples (6).

sampled. We caught slightly more male crabs (n = 1257) than female crabs (n = 1131), but the numbers were not significantly different ($P = 0.32$, $t = 1.03$, d.f. = 16). We caught five times as many green-colored crabs (n = 1921) as red-colored crabs (n = 364) ($P = 0.0004$, $t = 4.73$, d.f. = 13). As is typical of this species (4), males were larger than females in our collections ($P < 0.0001$, $t = 21.447$, d.f. = 2386). Red-colored males (mean = 56 ± 0.593 SE) were larger than green-colored males (mean = 52 ± 0.193 SE; $P < 0.0001$, $t = 5.75$, d.f. = 1187), and red-colored females (mean = 48 ± 0.269 SE) were also larger than green-colored females (mean = 47 ± 0.165 SE; $P = 0.0006$, $t = 3.43$, d.f. = 1094). We found no significant difference in average crab size between the beginning (mean = 49 ± 1.073 SE) and the end (mean = 49 ± 0.215 SE) of the study period. This stability in crab size over time suggests that we did not lose many marks to molting.

About half of the 149 recaptured crabs were trapped at the same site both times (Fig. 1). As the distance from the marking site increased, the number of recaptured crabs decreased: only 5% of the crabs were recaptured 300–400 m upstream or downstream from their original marking site (the extent of the trapping area). There was no significant difference between the numbers of crabs found upstream and those found downstream ($P = 0.37$, $t = 0.97$, d.f. = 6). Three percent crossed from one branch of the creek to the other, either through the mosquito ditch network connecting the two branches (about 150 m of travel), or down to the confluence and back up the other branch (about 300 m).

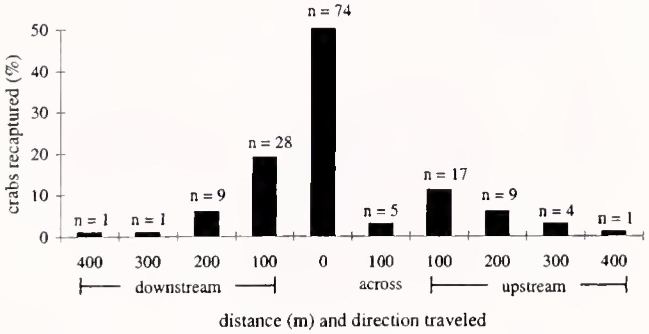

Figure 1. *Distance and direction (upstream, downstream, or across) traveled by recaptured green crabs,* Carcinus maenas, *in a tidal creek in Rowley, Massachusetts.*

Our population density estimate of 5 crabs per m^2 is comparable to previous estimates for green crabs on rocky shores in Wales (4). The results of the catch-per-unit-effort comparison for the six creeks suggest that this value may be a good estimate of green crab populations in the Rowley River.

Green-colored crabs are found throughout the molt cycle, but some crabs become red-colored during prolonged intermolt stages (5, 6). Green-colored crabs are more tolerant of low salinities than are red-colored crabs (6): the green form has been found primarily in the intertidal zone on Welsh shores and the red form primarily in the subtidal zone (7, 8). The dominance of green-colored crabs in our collection may be a result of the large tidal range (>3 m) and narrow subtidal zone in the study creek. McGaw (5) found red-colored males to be larger than green-colored males and hypothesized that this color change may be partly associated with sexual maturity.

The recapture data suggest that green crabs can move at least 400 m upstream or downstream, but that for the most part they remain within a 400-m range during the summer. Frequency of distance traveled was calculated only from crabs recaptured 1 to 3 weeks after each marking period in order to allow marked crabs to remix with the general population of the creek. But we also recaptured several crabs 300–400 m away from their original marking site within 4 days of being marked, indicating that they can move at least 400 m in a matter of days; distance traveled may thus not be directly related to time.

A study of the movement of crabs within the creeks in relation to tidal cycles would expand on previous research showing that these crabs follow tides up and down rocky shorelines in Wales (4, 7, 8). Warman (7) and Crothers (4) suggest that green crabs move offshore in the winter; an investigation of the winter range of green crabs would also add to information on the annual range of individual green crabs. Such research would contribute to the understanding of the role of this invasive species in coastal ecosystems.

This research was funded by the NSF Research Experience for

Undergraduates through the Boston University Marine Program and also by the Plum Island Sound LTER Program. We thank Simon Panall, João Feliciano Salgado, Susan Oleszko, Jaimie Champagne, Nate Tsao, Marc McDonnell, Jeff Hughes, and Jesse Young for their help.

Literature Cited

1. **Ropes, J. W. 1968.** *Fishery Bull. Fish Wildl. Serv. U.S.* **67:** 183–203.
2. **Cohen, A. N., J. T. Carlton, and M. C. Fountain. 1995.** *Mar. Biol.* **122:** 225–237.
3. **Tanner, J. T. 1978.** *Guide to the Study of Animal Populations.* The University of Tennessee Press, Knoxville.
4. **Crothers, J. H. 1967.** *Field Stud.* **1:** 407–434.
5. **McGaw, I. J., M. J. Kaiser, E. Naylor, and R. N. Hughes. 1992.** *J. Zool. Lond.* **228:** 351–359.
6. **Reid, D. G., P. Abello, I. J. McGaw, and E. Naylor. 1989.** Pp. 40–60 in *Phenotypic Responses and Individuality in Aquatic Ectotherms,* J. C. Aldrich, ed. Japaga, Co. Wicklow, Ireland.
7. **Warman, C. G., D. G. Reid, and E. Naylor. 1993.** *J. Mar. Biol. Assoc. U.K.* **73:** 355–364.
8. **Edwards, R. L. 1958.** *J. Anim. Ecol.* **27:** 37–45.

Reference: *Biol. Bull.* **197:** 299–300. (October 1999)

Influence of Marsh Flooding on the Abundance and Growth of *Fundulus heteroclitus* in Salt Marsh Creeks

Sharon Komarow (Earth Systems Program, Stanford University, Stanford, California 94305), Talia Young[1]*, Linda Deegan*[2]*, and Robert Garritt*[2]

Like many other estuarine fish and crustaceans, *Fundulus heteroclitus* (mummichog) regularly makes use of the marsh as a foraging area, nursery habitat, and refuge from predators. Mummichogs are known to follow flooding tides onto the intertidal marsh to forage (1, 2). Through this behavior, they provide an important trophic link between salt marsh and open estuary (3). Previous research indicates that access to the intertidal flooded marsh has significant effects on the growth rate of *F. heteroclitus.* Weisberg and Lotrich (4) showed that foraging exclusively on subtidal food sources was not sufficient to support normal growth rates of mummichogs. Javonillo *et al.* (5) found that mummichogs denied access to the marsh had lower growth rates than those that were allowed entrée to the marsh surface. Both of these studies employed caging techniques on a relatively small scale. Our goal was to examine the importance of marsh flooding to mummichog growth and abundance in a natural environment without enclosures.

Tidal creek flooding onto the marsh determines the vegetation in the area surrounding the creek. *Spartina alterniflora* grows on the marsh adjacent to the creek that floods on every high tide, whereas *S. patens* grows on the higher marsh that floods less frequently. We measured the length from the creek edge to the transition between *S. alterniflora* and *S. patens* at increments along the creek. The mean of these measurements multiplied by the length of the creek was considered the area of marsh accessible to mummichogs at high tides. This area is equivalent to the area of marsh adjacent to the creek covered by *S. alterniflora.* A comparison of the regularly flooded area in the 5 tidal creeks that were part of our study is shown in Figure 1a.

We measured the abundance and growth of *F. heteroclitus* in tidal salt marsh creeks of the Rowley River in the Plum Island Estuary in northeastern Massachusetts (42°44′ N × 70°50′ W). Over 6 weeks, catch-per-unit-effort (CPUE) was measured three times in each of five salt marsh creeks. Ten minnow traps (6.35-mm mesh), spaced evenly in the primary tidal creeks, were set at high tide and retrieved about 5 h later during low tide. In two of the creeks, we measured growth of mummichog young-of-the-year, the life stage in which the most dramatic growth occurs. Four times during the 6 weeks (first three times coincided with CPUE measurements, plus one additional growth measurement), the total lengths of between 275 and 1000 fish from each creek were measured, and length-frequency histograms were constructed. Probability paper was used, according to the method described by Harding (6), to identify the young-of-the-year cohort from the length-frequency histograms. Mean values from each set of measurements were plotted to evaluate growth.

Catch-per-unit-effort measurements indicated that mummichogs tended to be more abundant in creeks with greater areas of frequently flooded marsh (correlation coefficient = 0.83, $P = 0.09$) (Fig. 1b). This relationship suggests that creeks with increased marsh flooding are able to support a larger population of mummichogs by providing greater regularly flooded areas for foraging, or that creeks with increased flooding offer greater refuge from predation. Mummichogs that follow the high tide onto the marsh surface become more exposed to predation by shorebirds, but they gain protection from predation by larger fish, the more likely predator. Although the creeks are very similar, properties other than regularly flooded area—including dimensions, water volume, temperature regime, productivity, and food availability—may affect the abundance of mummichogs in a creek.

The pattern of growth was the same for young-of-the-year mummichogs in Sweeney Creek and Club Head Creek (Fig. 1c). However, the mean total length values of mummichogs from Sweeney Creek were significantly greater than mean total length measurements from Club Head Creek (Complete Randomized Block ANOVA $P < 0.05$). Though statistically significant, the very small mean difference between measurements of 1.25 mm is unlikely to be of ecological significance, especially since the pattern of growth did not differ between the creeks. Unlike in enclosure experiments in which mummichogs were denied access to the marsh (4, 5), all fish in our study could access the marsh, though the extent of this access differed among creeks. Thus, because the lower marsh is accessible at every high tide, differences in regularly flooded accessible marsh area may not be great enough to cause a large difference in mummichog growth.

---

[1] Swarthmore College, Swarthmore, Pennsylvania 19081.

[2] The Ecosystems Center, The Marine Biological Laboratory, Woods Hole, Massachusetts 02543.

This work was funded by NSF Research Experience for Undergraduates through the Boston University Marine Program and the Plum Island Sound Long-term Ecological Research Program. We thank Simon Panall, Nate Tsao, Marc McDonnell, Susan Oleszko, João Salgado, Jaimie Champagne, and Jeff Hughes for their help with the project.

Literature Cited

1. **Butner, A., and B. H. Brattstrom. 1960.** *Copeia* **1960:** 139–141.
2. **Weisberg, S. B., R. Whalen, and V. A. Lotrich. 1981.** *Mar. Biol.* **61:** 243–246.
3. **Kneib, R. T., and A. E. Stiven. 1978.** *J. Exp. Mar. Biol. Ecol.* **31:** 121–140.
4. **Weisberg, S. B., and V. A. Lotrich. 1982.** *Mar. Biol.* **66:** 307–310.
5. **Javonillo, R., L. Deegan, K. Chiaravalle, and J. Hughes. 1997.** *Biol. Bull.* **193:** 288–289.
6. **Harding, J. P. 1949.** *J. Mar. Biol. Assoc. U.K.* **28:** 141–153.

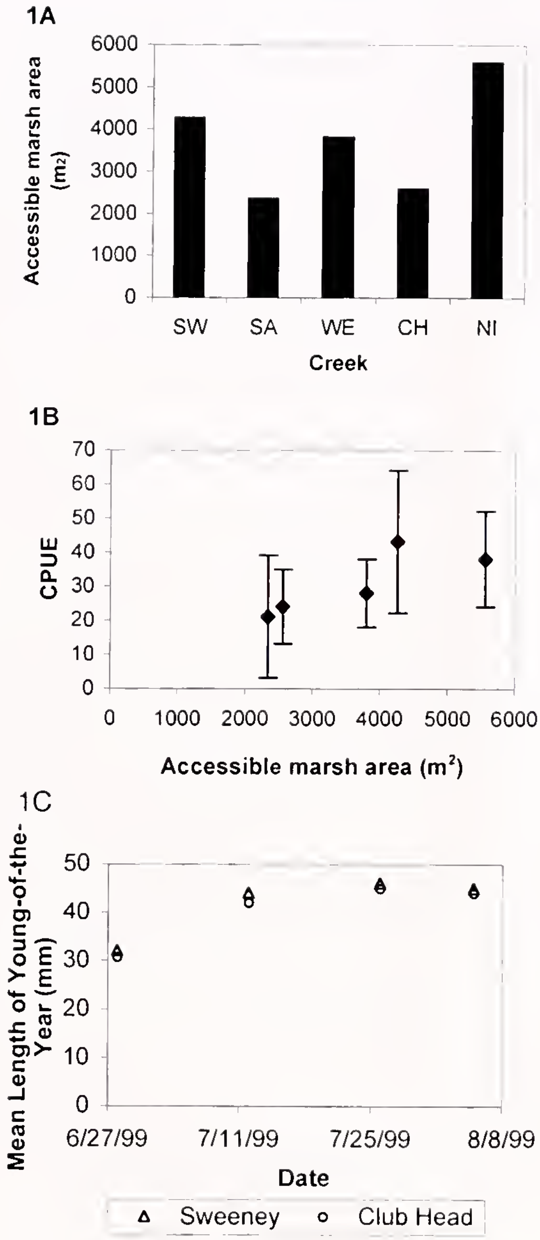

Figure 1. *(A) Regularly flooded accessible marsh area (m^2) by tidal creek, ordered from upstream to downstream: SW, Sweeney Creek; SA, Sand Creek; WE, West Creek; CL, Club Head Creek; and NE, Nelson Island Creek. (B) Mean catch-per-unit-effort (number of fish ± 1 standard error) plotted against regularly flooded accessible marsh area (m^2). (C) Mean total length measurements (mm ± 1 standard error, standard errors all < 0.1) at Sweeney Creek and Club Head Creek plotted against date of measurement.*

Reference: *Biol. Bull.* **197:** 300–302. (October 1999)

Decline of a Horseshoe Crab Population on Cape Cod

Justin W. Widener and Robert B. Barlow (Marine Biological Laboratory, Woods Hole, Massachusetts 02543)

The American horseshoe crab, *Limulus polyphemus*, inhabits coastal estuaries of North America from Northern Maine to Florida, as well as the region around the Yucatan peninsula. Delaware Bay contains the largest known population, but surveys of the New Jersey beaches that border the Delaware Bay show a decline of about 50% in the spawning population since 1990 (ref. 1 and B. L. Swan, pers. comm.). Trawl surveys of Delaware Bay from 1990 to 1997 yielded a 74% decline in crabs caught per tow (2). These declines do not appear to be isolated events; the populations of crabs spawning on the beaches of Cape Cod have also declined. We report here the results of a longitudinal study of the spawning population at Mashnee Dike, Bourne, Cape Cod, Massachusetts. In the 15 years from 1984 to 1999 the population declined more than 80%, and its spawning activity decreased 95%.

We surveyed the horseshoe crab population at Mashnee Dike in parallel with studies of their visually guided behavior (3, 4). We selected Mashnee Dike because its south-facing beach was an active spawning area for horseshoe crabs when we began our studies in the early 1980s, and because no humans inhabit the area bordering the spawning beach (length: ~1 km). Mashnee Dike is under the jurisdiction of the U.S. Army Corps of Engineers, which does not permit alteration or development of the Dike. Each spring animals migrate to the beach from offshore as the moon approaches new and full phases. Maximum migration is coordinated with the higher of the two daily high tides that occurs in the late afternoon and throughout the night (5). To quantify the dynamics of the crabs' migratory behavior we followed a surveying procedure published elsewhere (5). In brief, we mapped out three 10-m^2 quadrats with 10-m spacings along a 50-m transect at the water's edge (longitude: 70° 37′46″ W and latitude 41°46′34″ N). We then counted the number of animals in each quadrat at 30-min intervals for a period of 2 to 3 h as the tide flooded and ebbed. The 10-m spacings of the quadrats, together with the animals' slow movements and the insignificant tidal flow, precluded the crabs being counted twice in an observation period. Summing the data from the three quadrats for an observation period yielded a measure of the density of spawning animals for that period of the tidal cycle. Comparison of the data over the 2- to 3-h tidal cycle revealed the dynamics of the animal's migratory behavior. In general, animal density increases as the tide floods, peaks about 1 h after high tide, and decreases as the tide ebbs. Frequent surveys outside the quadrats during a tidal cycle indicated that the density of animals in the quadrats was representative of that along the appoximately 1 km of spawning beach. On this basis we assume that the maximum density per tidal cycle observed in a spawning season is proportional to the size of the spawning population in the vicinity of Mashnee Dike for that year. The sum of the maximum densities per tidal cycle over an entire spawning season is a measure of the spawning activity for that year.

Figure 1 shows a dramatic decline in the spawning population of horseshoe crabs at Mashnee Dike from 1984 to 1999. We counted a maximum of 247 crabs in the three quadrats near the time of the new moon in late May of 1984. Six years later, in 1990, near the full moon at the beginning of June, the maximum count was 73 crabs. In 1999 the maximum number of crabs was also observed near the time of full moon at the beginning of June, but it was considerably less (total of 42) than those in 1984 and 1990. Taken together the results from 1984 to 1999 reveal an 83% decline in the maximum density/transect/season, implying a comparable decline in the spawning population all along Mashnee Dike. The decline in spawning activity was greater, decreasing from 3171 in 1984 to 736 in 1990 and finally to 148 in 1999—a remarkable 95.3% decline.

The decline in spawning activity at Mashnee Dike accompanied a shortening of the spawning season. In 1984, crabs began spawning on the nighttime high tide of 13 May and were last seen in the transects on 7 July—a total of 56 days. In 1999 the spawning season lasted only 11 days—28 May to 7 June. The 5-fold shortening of the spawning season and concomitant decrease in spawning activity may be related to the decrease in the spawning population. The data shown in Figure 1 are representative of the overall trend we observed of high densities in the early 1980s, intermediate densities from the mid-1980s to the mid-1990s, and low densities in the late 1990s. We have surveyed systematically only the crab population near Mashnee Dike. Because of the decline in this population we transferred our studies of horseshoe crab vision in 1994 to a spawning beach in Stage Harbor (Chatham, Massachusetts). Over the 5-year period, we observed a substantial decrease in the Stage Harbor population, suggesting that the decline of horseshoe crab populations on Cape Cod may be widespread.

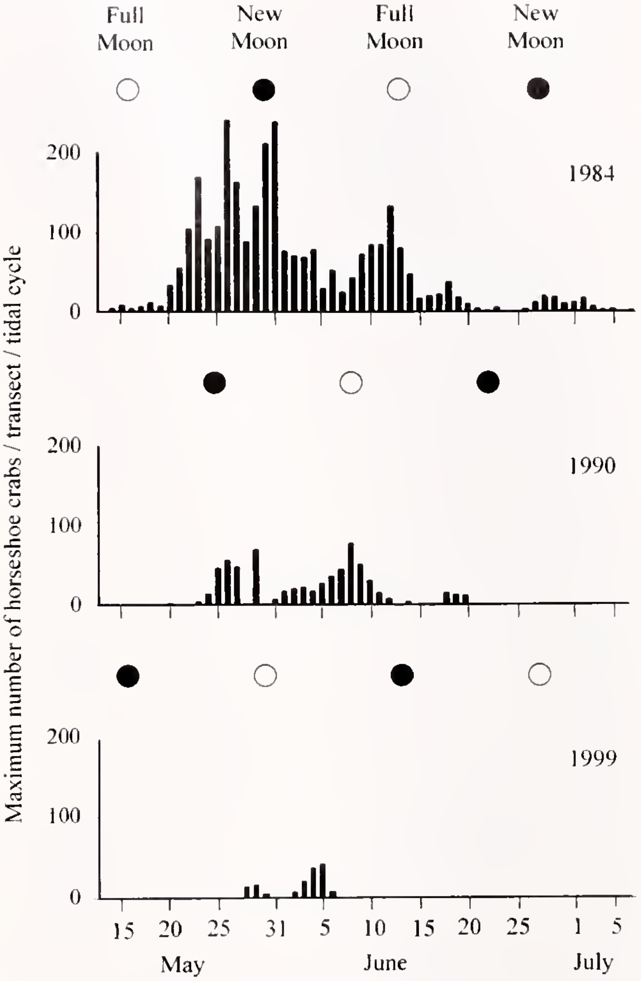

Figure 1. *Maximum number of* Limulus *counted in three 10-m^2 quadrats during the 1984, 1990, and 1999 spawning seasons at Mashnee Dike. The height of each bar gives the maximum number of males and females in a single half-hourly survey each day. The open and filled circles indicate the times of full and new moons. Surveys were not done on 28 and 30 May 1990 because of bad weather. Data were interpolated for these two days to calculate spawning activity. Observation periods were 14 May to 8 July 1984; 19 May to 22 June 1990, and 24 May to 16 June 1999.*

The causes of the declines in the horseshoe crab populations in Delaware Bay, Mashnee Dike, and Stage Harbor are not known. Possibities include loss of habitat, loss of food source, change in water conditions, and increase in predation. Mashnee Dike is an exemplary site, for it has been under the jurisdiction of the U.S.

Army Corps of Engineers since its construction over 50 years ago, and consequently no man-made alteration or development of the beach has occurred. Also no known changes have occurred in the availability of food sources at Mashnee Dike. The crabs are primarily scavengers with a diet of polychaetes, seaweed, nematodes, soft-shell bivalves, and detritus (6). In addition, no changes in chemical or other characteristics of water conditions of Phinney's Harbor have been reported. There is, however, clear evidence of increased predation. Each year since the mid-1980s, fishermen have been observed removing horseshoe crabs from the entire length of the Dike at high tide during the spawning season (R.B. Barlow, unpubl. obs.). On two occasions during the 1990 and 1995 spawning seasons, we succeeded in intercepting some fishermen, purchased the harvested animals (total: 1376), and returned them to their habitat. The yearly harvesting of crabs at the Dike has intensified since the mid-1990s, and activity correlates well with the large decline in the spawning population we observe. Also, the recent decline in the spawning population at Stage Harbor correlates with intensified harvesting in that area. It is not certain that harvesting caused the observed population declines in either area. Note however that the population at Mashnee Dike appears to be a local one. Animals tagged during a spawning season return the following seasons, and pairs of horseshoe crabs (some tagged) have been found during winter scuba dives buried in the bottom of Phinney's Harbor 100 to 300 m offshore (R. B. Barlow, unpubl. obs.). Harvesting large numbers of animals from such a local population would have a significant impact on its size.

Delaware Bay has also experienced increasingly large annual harvests of horseshoe crabs for use as bait in the eel and conch fisheries (7). Expansion of this bait fishery has led to near historic peaks in annual harvests in Delaware Bay (8) concomitant with the decline in population noted above. Although the spawning population in Delaware Bay is the largest on the East Coast, local populations appear to inhabit various beaches along the Bay (B. Swan, personal communication), as they do at Mashnee Dike. In an attempt to preserve the horseshoe crab fishery, the states of Delaware, Maryland, and New Jersey that border Delaware Bay have established regulations for harvesting the animals (9). Virginia, New Hampshire, and South Carolina have also established regulations, with those of South Carolina being the strictest. No regulations exist in Massachusetts.

What is the impact of a declining horseshoe crab population? In Delaware Bay it may have an important effect on the survival of shorebirds that migrate 3000 to 4000 miles from South America to the Arctic. The Bay provides an essential stopover for nourishment and rest for perhaps as many as one million shorebirds (10). Their springtime arrival coincides with the intense spawning activity of horseshoe crabs, and upon landing they devour crab eggs, with some birds consuming more than 100,000 in 2 weeks before continuing on to the Arctic for their own spawning activity (11). There is concern that the current density of crabs in Delaware Bay is not sufficient to provide nourishment for the migratory shorebirds. Indeed, Joan Walsh of the Cape May Research Observatory has been quoted as saying that "the density (of horseshoe crabs) is not great enough to provide food for shorebirds." She also noted that birds are arriving at their Arctic destinations "underweight" (12). The effect of declining spawning populations of horseshoe crabs on Cape Cod is not known.

We thank N. Buelow, S. Gibson, E. Herzog, L. Kass, M. Kelly-Manglapus, J. Marler, M. Parsley, J. Pelletier, M. Powers, and T. Thiele for assistance in transect counts at Mashnee Dike. We also thank the U.S. Army Corps of Engineers for providing access to Mashnee Dike. Study was supported in part by the National Science Foundation and the National Institutes of Mental Health.

Literature Cited

1. **Swan, B. L., W. R. Hall, Jr., and C. N. Shuster, Jr. 1996.** Pages 35–39 in *Proceedings of the Horseshoe Crab Forum: Status of the Resource*, J. Farrell and C. Martin, eds. University of Delaware, Sea Grant Program, Lewes, Delaware.
2. **Atlantic States Marine Fisheries Commission. 1999.** Stock Assessment Report No. 98-01 (Supplement) page 47, Washington, DC.
3. **Barlow, R. B., Jr., L. C. Ireland, and L. Kass. 1982.** *Nature* **296:** 65–66.
4. **Herzog, E. H., M. K. Powers, and R. B. Barlow. 1996.** *Visual Neurosci.* **13:** 31–42.
5. **Barlow, R. B., Jr., M. K. Powers, H. Howard, and L. Kass. 1986.** *Biol. Bull.* **171:** 310–329.
6. **Botton, M. L., and H. H. Haskin. 1984.** *Fish. Bull.* **82**(2): 383–389.
7. **Shuster, C. N., Jr. 1996.** Pages 5–14 in *Proceedings of the Horseshoe Crab Forum: Status of the Resource*, J. Farrell and C. Martin, eds. University of Delaware, Sea Grant Program, Lewes, Delaware.
8. **Loveland, R. E., M. L. Botton, and C. N. Shuster, Jr. 1996.** Pages 15–22 in *Proceedings of the Horseshoe Crab Forum: Status of the Resource*, J. Farrell and C. Martin, eds. University of Delaware, Sea Grant Program, Lewes, Delaware.
9. **Schrading, E., T. O'Connell, S. Michels, and P. Perra. 1998.** Fishery Management Plan for the Horseshoe Crab *Limulus polyphemus. Fisheries Management Report of the Atlantic States Marine Fisheries Commission.* 7–9. Washington, DC.
10. **Clark, K. E., L. J. Niles, and J. Burger. 1993.** *Condor* **95:** 694–705.
11. **Myers, J. P. 1986.** *Nat. Hist.* **95**(5): 68–77.
12. **McDonald, G. G. 1999.** *The Cape Codder.* June 18, 1999, p. 3.

Reference: *Biol. Bull.* **197:** 303–306. (October 1999)

Evaluation of a Reporter Gene System Biomarker for Detecting Contamination in Tropical Marine Sediments

Lisa M. Kerr (Biology Department, University of Massachusetts, 100 Morrissey Blvd., Boston, Massachusetts 02125), Phillip S. Lobel[1]*, and J. Mark Ingoglia*[2]

A major challenge in conducting field assessments of potential ecological impacts is optimizing the number of samples and the costs. This is especially important in light of the growing concern over the presence of persistent organic contaminants, such as PCBs, dioxins, furans, and PAHs in sediments. A reporter gene system (RGS) assay that measures induction of the CYP1A1 gene and transcription of P450 enzyme systems is often used to assess potential toxicity of these compounds in environmental samples (1, 2, 3). RGS has gained acceptance as an inexpensive, rapid method for screening environmental samples for contaminants (4, 5). The RGS approach has been validated in the laboratory with pure compounds, known chemical mixtures, and from field-collected sediments by comparing RGS system response and chemical concentrations (1, 2, 3, 6). Our study differed from other validation studies in two respects: we used field-collected sediments over a wide range of contaminant concentrations and evaluated RGS response to sediment samples containing a mixture of dioxins, furans, and PAHs. With few exceptions, the previous validation studies using field-collected samples used fairly small sample sizes and generally evaluated one chemical group (3, 6). Few studies have compared large numbers of samples containing both PAHs and 2,3,7,8 tetrachlorodibenzo-p-dioxin (TCDD) over the range reported here. The purpose of this study was to determine if there is a high correlation between RGS response and chemistry results from the same samples. If this proves to be the case, the assay could be used to screen large areas at a relatively low cost. Samples exhibiting high responses could be targeted for further characterization using more precise, but costly, GC/MS methods.

Matched sediment samples ($n = 31$) were collected off the northwestern shore of Johnston Island, adjacent to potential sources of PAHs and 2,3,7,8 tetrachlorodibenzo-p-dioxin (TCDD) (Site 1), and at sites farther removed from the potential contaminant sources (Sites 3, 4). To ensure blind analysis of the samples, P450 RGS assays were conducted by MEC Analytical Systems (Carlsbad, California) and Columbia Analytical Services (Vista, California) while chemical analyses were completed by the Toxic Contaminant Research Laboratory at Wright State University (Dayton, Ohio).

The RGS assay used in this study was developed by Anderson *et al.* (1) and detailed methods have been described (1, 7). Induction in the assay is dependent upon the aryl hydrocarbon receptor (AhR) activation pathway. AhR ligands, including planar PCBs, PAHs, and TCDD, bind to AhR, activating it and resulting in its translocation to the nucleus of the cell. In the nucleus, the activated AhR complex binds to the xenobiotic responsive element in the promoter region of the CYP1A1 gene, resulting in its transcription. Compounds that are not AhR ligands, such as metals and pesticides, do not cause induction in the system (1, 7). Briefly, the RGS methodology involves exposing human 101L cells to 10 μl of solvent extracts for 16 hours (1, 5). Sediment extracts were prepared according to EPA method 3540. The cells are stably transfected with a plasmid containing firefly luciferase linked to the human CYP1A1 promoter sequence. This promoter sequence contains 1800 bp of flanking regulatory DNA with three xenobiotic responsive elements (1). Exposure to Ah receptor ligands induces luciferase activity which is quantified with a luminometer (7, 8).

Previous studies have determined that RGS detection limits in sediment are 8 pg/g for dioxin, 63 pg/g for furan, 6.2 to 7500 ng/g for specific PAHs, and 250 ng/g for a mixture of PAHs (7). Solvent blanks were used as negative controls while extracts from sediments spiked with 2 ng/g TCDD were used as positive controls ($n = 6$). From the level of induction generated by each sample, equivalent doses of TCDD or benzo(a)pyrene (BaP) that would result in the observed level of induction were calculated. While the level of induction is the same in each sample, the amount of pure compound (either TCDD or BaP) required to produce the observed induction level differs between the compounds. Equivalent doses for total PAHs and dioxins/furans calculated from RGS induction are designated as "RGS BaPEQ" and "RGS TEQ" respectively.

For the GC/MS analyses, sediments were extracted using EPA Method 3540. PAHs and dioxins/furans were measured using EPA Methods 8270 and 8290. Detection limits were from 0.0638 to 0.777 pg/g for the 17 individual dioxin or furan congeners measured. Total PAHs measured included 14 individual compounds with detection limits ranging from 19.1 to 40.7 ng/g. Toxicity equivalents (TEQs) based on the 17 dioxin and furan congeners measured were calculated using human/mammalian toxic equivalency factors (TEFs; 9). TEQs calculated from the chemical analysis of dioxins and furans are designated as "Chem TEQ." Total PAHs measured by chemical methods are referred to as "Chem PAHs."

Linear regression analysis was used to determine if significant relationships existed between the RGS TEQ and Chem TEQ. Similarly, the relationship between Chem PAH and RGS BaPEQ was determined. Data were log transformed to equalize variances.

There was a significant statistical relationship between Chem TEQ and RGS TEQs ($r^2 = 0.774$; $P < 0.001$) (Fig. 1). However, 41.9% of the points fall outside the 95% confidence intervals. Additionally, there was a significant statistical relationship between Chem PAHs and RGS BaPEQ ($r^2 = 0.564$; $P < 0.001$). In this case, 35.5% of the points fall outside of the 95% confidence intervals. While there was significant covariance between Chem and RGS values, the actual

---

[1] Boston University Marine Program, Marine Biological Laboratory, Woods Hole, Massachusetts 02543.

[2] United States Air Force, Environmental Restoration, Hickam AFB, Hawaii 96853.

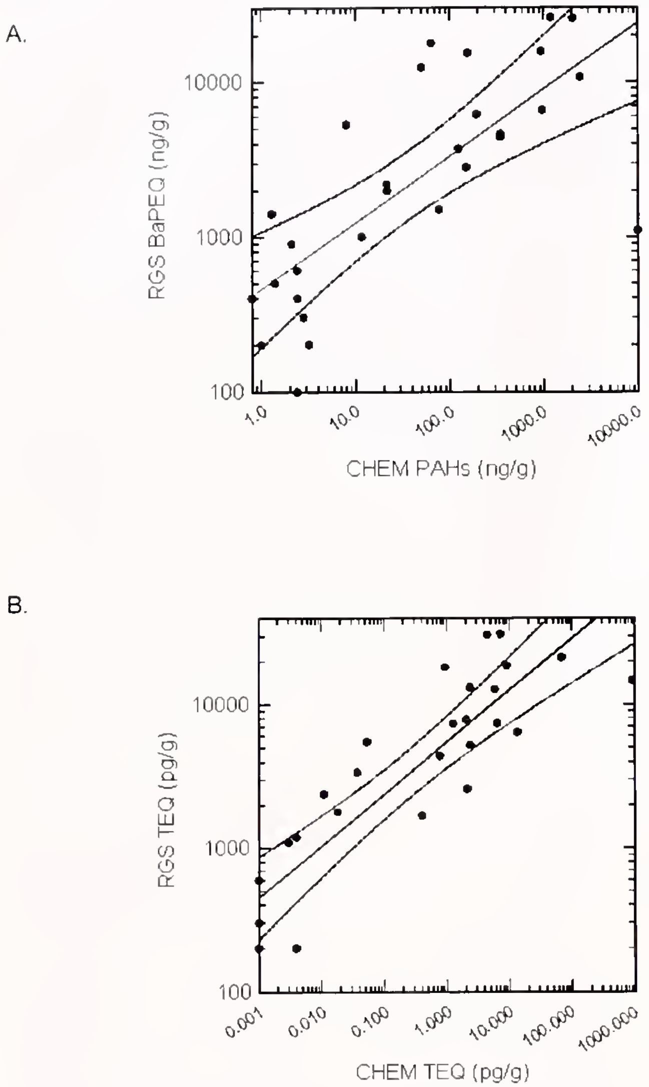

Figure 1. *(A) Comparison of chemically derived total PAH concentration (Chem PAHs) to RGS estimates of benzo(a)pyrene equivalents (RGS BaPEQs)* $r^2 = 0.564$ $P < 0.001$. *(B) Comparison of chemically derived TEQs (Chem TEQ) to P450 RGS estimated TEQs (RGS TEQ)* $r^2 = 0.564$ $P < 0.001$. *Best fit regression lines are shown with 95% confidence intervals.*

magnitude of the values differed. RGS TEQs were 10^2 to 10^4 times higher than Chem TEQs (Table 1). Similarly, RGS BaPEQs were 10 to 10^4 times higher than Chem PAHs.

The levels of induction and the resultant estimates of RGS TEQ and RGS BaPEQ decreased with distance from shore (Table 1). This pattern also held for Chem TEQ and Chem PAHs, with those samples with the highest concentrations being the closest to shore (Site 1). Three samples exceeding ecological screening levels were found closest to shore. One sample exceeded the effects range low (ER-L) screening levels for Chem PAHs, including total PAHs, low and high molecular weight PAHs, and nine individual PAHs (10). Two additional samples from site 1 had contaminant concentrations exceeding ecological screening levels. These samples with Chem TEQs of 68.24 pg/g and 901.27 pg/g exceeded the low and high risk to aquatic life screening values respectively (11).

When using the RGS assay as a screening method, the samples with the highest responses or induction levels might be "chosen" as the samples expected to contain the highest contaminant concentrations. In this study, this was the case, and the three samples with the highest contaminant concentrations would have been detected. However, there are two important points: 1) induction was higher than that of the positive controls (around 100-fold) in eight samples (129- to 316-fold), and 2) the samples with the highest overall induction levels were not necessarily the samples with the highest dioxin or PAH concentrations. Additionally, some samples exhibited significant RGS induction, although very low levels of PAHs, dioxins, or furans were detected. These responses could be considered false positives. A false negative could be identified only if arbitrary limits were set on the number of samples further characterized. For example, if budget constraints limited the number of samples that could be chemically characterized to five samples and we chose to characterize only those samples with the highest RGS response, the sample with the highest concentration of PAHs would not have been detected, resulting in a false negative.

One potential explanation for the variable RGS response in this study is induction by other compounds not measured by GC/MS. Other chemicals that may induce the RGS system include planar PCBs as well as some dioxin congeners not measured in this study. The contribution of PCBs to induction is unlikely since previous sampling events at the same sites found total PCB concentrations below the 10 ng/g RGS detection limit.

Another explanation suggests that in tropical environments, P450 activity is higher in some fishes and may be related to a herbivorous diet (12). This suggests further consideration of the presence of naturally occurring toxins such as ciguatoxins or other allelochemicals potentially inducing the RGS assay or interfering with cell function. Furthermore, coral reef environments may have different sediment characteristics due to physical and chemical factors that may affect bioavailability. The RGS assay detects compounds that may or may not be specifically measured by GC/MS and assesses the synergistic and/or antagonistic effects of the constituents in the mixture.

This study found significant co-variance between Chem TEQ and RGS TEQ as well as between Chem PAHs and RGS BaPEQs. However, there was a high level of variability (more than 35% of values fall outside the 95% CI); and of the samples with the highest RGS response (greater than positive controls), a high percentage (5 of 8) could be identified as false positives. Qualitatively, the RGS assay revealed a contaminant gradient on a scale of hundreds of meters. We conclude that this method is useful as a broad area assessment tool for screening purposes, provided that data are interpreted carefully.

Use of this screening method is substantially complicated by the presence of multiple compounds, as at Johnston Atoll. This may include natural or other anthropogenic compounds that were not chemically measured in the GC/MS analysis. While the response to these various compounds may be complex, the value of the RGS assay is that it gives an integrated and more biologically relevant response than chemistry alone. Additionally, given the expense of GC/MS analysis of dioxin congeners (>$1000/sample), use of the

Table I

Contaminant concentrations in sediment samples from the west end of Johnston Atoll compared to responses generated by the RGS assay

Sample Number	Site	Chem TEQ pg/g	RGS TEQ pg/g	Chem PAH ng/g	RGS BaPEQ ng/g	Induction
030	1[1]	0.01	2400	21.7*	2000	25
064	1	0.95	18200	158.5*	15200	183
074	1	0.40	1700	1.3*	1400	17
076	1	0.02	1800	77.1*	1500	18
086	1	2.04	7800	937.9	6500	79
088	1	7.29	31200	1125.0	26000	316
095	1	0.00	1200	11.6*	1000	12
104	1	13.63	6400	8.0*	5300	64
108	1	0.00	1100	2.1*	900	11
120[a]	1	2.35	13200	9711.0	11000	133
217	1	0.04	3400	151.7*	2800	34
225[b]	1	68.27	21300	64.9*	17700	218
233	1	0.78	4400	124.5*	3700	45
234	1	4.44	30700	1988.0	25600	308
238	1	6.43	7400	41.5	6100	74
242	1	2.38	5200	343.2*	4400	53
248	1	0.05	5500	174.8	4600	55
249	1	1.26	7300	nd	6100	73
254	1	9.13	18700	906.3	15600	188
256[c]	1	901.29	14700	50.5*	12300	147
257	1	5.87	12800	2383	10600	129
307	1	2.14	2600	21.4*	2200	26
013	3[2]	0.00	700	2.4*	600	7
027	3	0.00	600	1.4*	500	6
043	3	0.00	300	2.8*	300	3
118	3	0.00	200	2.4*	100	2
243	3	0.00	200	1.4*	200	2
038	4	0.00	200	3.2*	200	2
124	4	0.00	400	2.4*	400	5
105	4	0.00	200	0.8*	400	2
119	4	0.00	200	nd	200	2
Control[d]		2000.00				79
Control		2000.00				101
Control		2000.00				90
Control		2000.00				77
Control		2000.00				81
Control		2000.00				137

[1] Site 1 is adjacent to the former herbicide orange storage site and burn pits on Johnston Island.
[2] Sites 3 and 4 are across the shipping channel from site 1, approximately 1000 m from shore.
[a] Exceeds screening level for PAHs (Effects Range-Low for total PAHs = 4022 ng/g).
[b] Exceeds low risk screening limit for TCDD (60 pg/g).
[c] Exceeds high risk screening limit for TCDD (100 pg/g).
[d] Positive Controls.
[*] [PAHs] below quantifiable limit.
nd-none detected.

RGS assay ($150/sample) shows potential for possible cost savings through incremental, phased use in combination with GC/MS methods. As site specific complexities and relationships between the two methods and the matrix are further defined, the understanding of and confidence in the RGS results can improve. This can lead to reduced need for GC/MS analyses and increased emphasis on RGS results. Annual long-term monitoring, which may span decades, lends itself to such incremental cost savings through the development of large data sets and cumulative experience gained over time.

This research supported by Army Research Office grant DAAG 55-98-1-0304 for the Johnston Atoll Reef Study.

Literature Cited

1. **Anderson, J. W., S. S. Rossi, R. L. Tukey, T. Vu, and L. C. Quattrochi. 1995.** *Environ. Toxicol. Chem.* 7: 1159–1169.

2. **Murk, A. J., J. Legler, M. S. Denison, J. P. Giesy, C. van de Guchte, and A. Brouwer. 1996.** *Fundam. Appl. Toxicol.* **33:** 149–160.
3. **Jones, J. M., and J. W. Anderson. 1998.** Pp. 1–6 in *Risk, Resource, and Regulatory Issues,* G. B Wickramanayake and R. E. Hinchee, eds. Battelle Press, Columbus, Ohio.
4. **APHA. 1996.** Pp. 24–25 in *Standard Methods for the Examination of Water and Waste Water,* 19th ed. Supplement. American Public Health Association, Washington, DC.
5. **ASTM. 1997.** Pp. 1392–1397 in *Biological Effects and Environmental Fate: Biotechnology; Pesticides. 1997 Annual Book of ASTM Standards.* Vol. 11.05. American Society for Testing and Materials, West Conshohocken, Pennsylvania.
6. **Kim, G. B., J. W. Anderson, K. Bothner, J. Lee, C. Koh, and S. Tanabe. 1997.** *Biomarkers* **2:** 181–188.
7. **Anderson, J. W., K. Bothner, D. Edelman, S. Vincent, T. P. Vu, and R. H. Tukey. 1996.** Pp. 150–168 in *Field Applications of Biomarkers for Agrochemicals and Toxic Substances,* J. Blancato, R. Brown, C. Dary, and M. Saleh, eds. American Chemical Society, Washington, DC.
8. **Jones, J., and J. W. Anderson. 1999.** *Environ. Toxicol. Pharm.* **7:** 19–26.
9. **Van den Berg, M. L. Birnbaum, A. T. C. Bosveld, B. Brunstrom, P. Cook, M. Freely, J. P. Giesey, A. Hanberg, R. Hasegawa, S. W. Kennedy, T. Kubjak, J. C. Larsen, R. X. R. van Leeuwen, A. K. D. Liem, C. Nolt, R. E. Peterson, L. Poellinger, S. Safe, D. Schrenk, D. Tillitt, M. Tysklnd, M. Younes, F. Waern, and T. Zacharewski. 1998.** *Environ. Health Perspect.* **106:** 775–792.
10. **Long, E. R., D. D. MacDonald, S. L. Smith, and F. D. Calder. 1995.** *Environ. Manage.* **19:** 81–97.
11. **U.S. EPA. 1993.** P. xx in *Interim Report on Data and Methods of 2,3,7,8 tetrachlorodibenzo-p-dioxin Risks to Aquatic Life and Associated Wildlife.* EPA-600-R-93-089. Environmental Protection Agency, Washington, DC.
12. **Stegeman, J. J., B. R. Woodin, H. Singh, M. F. Olesiak, and M. Celander. 1997.** *Comp. Biochem. Physiol.* **116C(1):** 61–75.

Reference: *Biol. Bull.* **197:** 307. (October 1999)

Published By Title Only

Kuzirian, Alan, and John Clay
Isolation of K^+ channel containing vesicles from squid giant axons.

Simpson, Tracy, Max M. Burger, and William J. Kuhns
Localization and selectivity of CD44 antigen for a cell population from the marine sponge *Microciona prolifera.*

Yang, Stacy, and Oladele Ogunseitan
Cell swarming and ALAD activity in *Vibrio alginolyticus:* testing an environmental selective pressure hypothesis.

Furlong, Christopher, David Lawrence, and Ivan Valiela
Impact of anthropogenic nitrogen loading on phytoplankton production in Waquoit Bay and Popponessett Bay.

MARINE BIOLOGICAL LABORATORY

WOODS HOLE, MASSACHUSETTS

Substantial financial assistance is available for many programs!

2000 Course Offerings

Modeling of Biological Systems
(March 25 – May 4, 2000)
Director: Robert Silver, Marine Biological Laboratory

Analytical and Quantitative Light Microscopy
(May 4 – May 12, 2000)
Directors: Greenfield Sluder and David Wolf, University of Massachusetts Medical Center, Worcester

Neurobiology & Development of the Leech
(May 6 – June 3, 2000)
Directors: Christie Sahley, Purdue University; and Martin Shankland, University of Texas, Austin

Rapid Electrochemical Measurements in Biological Systems (May 11 – May 16, 2000)
Director: Greg Gerhardt, University of Kentucky

Microinjection Techniques in Cell Biology
(May 16 – May 23, 2000)
Director: Robert Silver, Marine Biological Laboratory

Frontiers in Reproduction: Molecular and Cellular Concepts and Applications (May 22 – July 2, 2000)
Directors: Joan Hunt, University of Kansas Medical Center; Kelly Mayo, Northwestern University; and Gerald Schatten, Oregon Health Sciences University

Medical Informatics – *sponsored by the National Library of Medicine*
(May 28 – June 3, 2000)
Director: Daniel Masys, University of California, San Diego

Biology of Parasitism: Modern Approaches
(June 8 – August 11, 2000)
Directors: Edward Pearce, Cornell University; and Christian Tschudi, Yale University

Microbial Diversity
(June 11 – July 27, 2000)
Directors: Caroline Harwood, University of Iowa; and Alfred Spormann, Stanford University

Neural Systems & Behavior
(June 11 – August 4, 2000)
Directors: Catherine Carr, University of Maryland; and Richard Levine, University of Arizona

Neurobiology
(June 11 – August 12, 2000)
Directors: Donald Faber, Albert Einstein College of Medicine; and Jeff Lichtman, Washington University School of Medicine

Physiology: The Biochemical & Molecular Basis of Cell Signaling (June 11 – July 22, 2000)
Directors: David Garbers, University of Texas Southwestern Medical Center, Dallas; and Randall Reed, Johns Hopkins University School of Medicine

Embryology: Concepts and Techniques in Modern Developmental Biology (June 18 – July 29, 2000)
Directors: Marianne Bronner-Fraser and Scott Fraser, California Institute of Technology

Summer Program in Neuroscience, Ethics, and Survival (SPINES)
(June 10 – July 8, 2000)
Directors: Joe Martinez, University of Texas, San Antonio; and James Townsel, Meharry Medical College

Methods in Computational Neuroscience
(July 30 – August 26, 2000)
Directors: William Bialek and Rob de Ruyter van Steveninck, NEC Research Institute

Workshop on Molecular Evolution
(July 30 – August 11, 2000)
Director: Michael Cummings, Marine Biological Laboratory

Molecular Biology of Aging – *sponsored by the Ellison Medical Foundation*
(August 1 – August 18, 2000)
Directors: Leonard Guarente, Massachusetts Institute of Technology; and Douglas Wallace, Emory University

Molecular Mycology: Current Approaches to Fungal Pathogenesis (August 7 – August 25, 2000)
Directors: Aaron Mitchell, Columbia University; P.T. Magee, University of Minnesota; and John Edwards, Harbor-UCLA Medical Center

Fundamental Issues in Vision Research – *sponsored by the National Eye Institute* (August 13 – August 26, 2000)
Director: David Papermaster, University of Connecticut Health Center

Neural Development & Genetics of Zebrafish
(August 13 – August 25, 2000)
Directors: John Dowling, Harvard University; and Nancy Hopkins, Massachusetts Institute of Technology

Medical Informatics – *sponsored by the National Library of Medicine*
(October 1 – October 7, 2000)
Director: James Cimino, Columbia University

Optical Microscopy and Imaging in the Biomedical Sciences (October 11 – October 19, 2000)
Director: Colin Izzard, State University of New York, Albany

VISIT COURSES.MBL.EDU FOR DETAILS!

For further information, contact:
Carol Hamel, Admissions Coordinator / Marine Biological Laboratory / 7 MBL Street, Woods Hole, MA 02543
email: admissions@mbl.edu / phone: 508-289-7401

MARINE
BIOLOGICAL
LABORATORY
WOODS HOLE, MASSACHUSETTS

[illegible]

VISIT COURSES.MBL.EDU FOR DETAILS

THE

BIOLOGICAL BULLETIN

DECEMBER [illegible]

[illegible]

THE
BIOLOGICAL BULLETIN
DECEMBER 1999

DEC 27 1999

Editor	Michael J. Greenberg	The Whitney Laboratory, University of Florida
Associate Editors	Louis E. Burnett	Grice Marine Biological Laboratory, College of Charleston
	R. Andrew Cameron	California Institute of Technology
	Charles D. Derby	Georgia State University
	Michael LaBarbera	University of Chicago
Section Editor	Shinya Inoué, *Imaging and Microscopy*	Marine Biological Laboratory
Online Editors	James A. Blake, *Keys to Marine Invertebrates of the Woods Hole Region*	ENSR Marine & Coastal Center, Woods Hole
	William D. Cohen, *Marine Models Electronic Record and Compendia*	Hunter College, City University of New York
Editorial Board	Peter B. Armstrong	University of California, Davis
	Ernest S. Chang	Bodega Marine Lab., University of California, Davis
	Thomas H. Dietz	Louisiana State University
	Richard B. Emlet	Oregon Institute of Marine Biology, Univ. of Oregon
	David Epel	Hopkins Marine Station, Stanford University
	Gregory Hinkle	Cereon Genomics, Cambridge, Massachusetts
	Makoto Kobayashi	Hiroshima University of Economics, Japan
	Donal T. Manahan	University of Southern California
	Margaret McFall-Ngai	Kewalo Marine Laboratory, University of Hawaii
	Mark W. Miller	Institute of Neurobiology, University of Puerto Rico
	Tatsuo Motokawa	Tokyo Institute of Technology, Japan
	Yoshitaka Nagahama	National Institute for Basic Biology, Japan
	Sherry D. Painter	Marine Biomed. Inst., Univ. of Texas Medical Branch
	J. Herbert Waite	University of California, Santa Barbara
	Richard K. Zimmer	University of California, Los Angeles
Editorial Office	Pamela Clapp Hinkle	Managing Editor
	Victoria R. Gibson	Staff Editor
	Carol Schachinger	Editorial Associate
	Patricia Burns	Subscription & Advertising Secretary

Published by
MARINE BIOLOGICAL LABORATORY
WOODS HOLE, MASSACHUSETTS

Cover

The polychaete worm *Chaetopterus* is found worldwide in littoral sediments, where it builds and inhabits a U-shaped, parchment-like tube. Seawater is pumped through the tube by "fans"—modified appendages on three adjacent mid-body segments. Microscopic food particles suspended in the seawater current are caught in a mucous net that the worm secretes, deploys, and then (when the net is full) ingests. *Chaetopterus* has highly specialized segments that are grouped in three functionally distinct regions, so the morphology is more complex than that of most annelids. This complexity is evident in the two adults shown in the large photograph on the cover; note that because the worms are designed to fit within the curve of the tube, they curl up when removed from it (anterior is up).

Chaetopterus is well-known for studies of its feeding behavior, its intense luminescence, as well as its development. In particular, this worm is a classic model for the study of early embryogenesis because it can be readily spawned *in vitro* and also cultured through its larval development. As a rule, annelidan segments are generated from a posterior growth zone, arising and developing sequentially, from anterior to posterior. But morphogenesis in *Chaetopterus* does not follow this canonical pattern. Rather, an examination of larval ontogeny—reported by Steve Irvine and his colleagues in this issue (p. 319)—reveals that those segments destined for the mid-body region develop precociously and more rapidly than the anterior segments. This accelerated development (or heterochrony) is not seen in other polychaetes—not even in very closely related families. Thus it must have arisen within the chaetopterid lineage. [Segmental development is shown in the small photographs on the cover; they depict (left to right) an early larval stage (4 days old, 180 μm), a mid-stage larva (about 30 days old, 400 μm), and a newly metamorphosed juvenile (about 60 days old; 1.2 mm).]

Further information on the laboratory culture of *Chaetopterus* larvae and those of related spionidan polychaetes is available in a companion article by S. Q. Irvine and M. Q. Martindale published in the *Marine Models Electronic Record* (MMER) at: www.mbl.edu/html/BB/MMER/IRV/IrvTit.html. In addition, a general review of *Chaetopterus* as a system for studying developmental biology, including methodology and a comprehensive bibliography, is set out by W. R. Eckberg and S. D. Hill (1996) in another MMER paper at: http://www.mbl.edu/html/BB/MMER/ECK/EckTit.html.

Cover design by Beth Liles

CONTENTS

Volume 197, No. 3: December 1999

RESEARCH NOTE

Kelman, Dovi, and Richard B. Emlet
Swimming and buoyancy in ontogenetic stages of the cushion star *Pteraster tesselatus* (Echinodermata: Asteroidea) and their implications for distribution and movement 309

Yusa, Yoichi, and Shigeyuki Yamato
Cropping of sea anemone tentacles by a symbiotic barnacle 315

DEVELOPMENT AND REPRODUCTION

Irvine, Steven Q., Oleg Chaga, and Mark Q. Martindale
Larval ontogenetic stages of *Chaetopterus:* developmental heterochrony in the evolution of chaetopterid polychaetes 319

Degnan, Bernard M., and Craig R. Johnson
Inhibition of settlement and metamorphosis of the ascidian *Herdmania curvata* by non-geniculate coralline algae 332

Kanungo, Jyotshna, Ruth M. Empson, and Howard Rasmussen
Microinjection of an antibody to the Ku protein arrests development in sea urchin embryos 341

NEUROBIOLOGY AND BEHAVIOR

Lindsay, S.M., T.M. Frank, J. Kent, J.C. Partridge, and M.I. Latz
Spectral sensitivity of vision and bioluminescence in the midwater shrimp *Sergestes similis* 348

Ristvey, Andrew, and Steve Rebach
Enhancement of the response of rock crabs, *Cancer irroratus*, to prey odors following feeding experience 361

PHYSIOLOGY

Silverman, Harold, John W. Lynn, Peter G. Beninger, and Thomas H. Dietz
The role of latero-frontal cirri in particle capture by the gills of *Mytilus edulis* 368

Bayne, Brian L., Susanne Svensson, and John A. Nell
The physiological basis for faster growth in the Sydney rock oyster, *Saccostrea commercialis* 377

Siebenaller, Joseph F., and Thomas F. Murray
Hydrostatic pressure alters the time course of GTP[S] binding to G proteins in brain membranes from two congeneric marine fishes 388

CELL BIOLOGY

Lema-Foley, Christine, Kyeng G. Lee, Tchaiko Parris, Zoya Koroleva, Nishal Mohan, Pierre Noailles, and William D. Cohen
Reversible alteration of morphology in an invertebrate erythrocyte: properties of the natural inducer and the cellular response 395

* * *

Index for Volume 197 415

CONTENTS
for Volume 197

No. 1, August 1999

RESEARCH NOTES

Pierce, Sidney K., Timothy K. Maugel, Mary E. Rumpho, Jeffrey J. Hanten, and William L. Mondy
Annual viral expression in a sea slug population: life cycle control and symbiotic chloroplast maintenance . . . 1
Thomas, Florence I.M., Kristen A. Edwards, Toby F. Bolton, Mary A. Sewell, and Jill M. Zande
Mechanical resistance to shear stress: the role of echinoderm egg extracellular layers 7
Rinkevich, B., S. Ben-Yakir, and R. Ben-Yakir
Regeneration of amputated avian bone by a coral skeletal implant 11

ECOLOGY AND EVOLUTION

Miner, Benjamin G., Eric Sanford, Richard R. Strathmann, Bruno Pernet, and Richard B. Emlet
Functional and evolutionary implications of opposed bands, big mouths, and extensive oral ciliation in larval opheliids and echiurids (Annelida). 14
Johnsen, Sönke, Elizabeth J. Balser, Erin C. Fisher, and Edith A. Widder
Bioluminescence in the deep-sea cirrate octopod *Stauroteuthis syrtensis* Verrill (Mollusca: Cephalopoda) 26

NEUROBIOLOGY AND BEHAVIOR

Ganter, Geoffrey K., Ralf Heinrich, Richard P. Bunge, and Edward A. Kravitz
Long-term culture of lobster central ganglia: expression of foreign genes in identified neurons 40
Hanlon, Roger T., Michael R. Maxwell, Nadav Shashar, Ellis R. Loew, and Kim-Laura Boyle
An ethogram of body patterning behavior in the biomedically and commercially valuable squid *Loligo pealei* off Cape Cod, Massachusetts 49
Bushmann, Paul J.
Concurrent signals and behavioral plasticity in blue crab (*Callinectes sapidus* Rathbun) courtship 63

PHYSIOLOGY

Engebretson, Hilary P., and Gisèle Muller-Parker
Translocation of photosynthetic carbon from two algal symbionts to the sea anemone *Anthopleura elegantissima* 72

DEVELOPMENT AND REPRODUCTION

Grabowski, Gregory M., John G. Blackburn, and Eric R. Lacy
Morphology and epithelial ion transport of the alkaline gland in the Atlantic stingray (*Dasyatis sabina*) . . . 82
Krug, Patrick J., and Adriana E. Manzi
Waterborne and surface-associated carbohydrates as settlement cues for larvae of the specialist marine herbivore *Alderia modesta* 94
Chaparro, O.R., R.J. Thompson, and C.J. Emerson
The velar ciliature in the brooded larva of the Chilean oyster *Ostrea chilensis* (Philippi, 1845). 104

* * *

Annual Report of the Marine Biological Laboratory R1

No. 2, October 1999

EDITORIAL

Greenberg, Michael J.
A century of science: *The Biological Bulletin* looks back—and forward 113

IMAGING AND MICROSCOPY

Dailey, Michael, Glen Marrs, Jakob Satz, and Marc Waite
Concepts in Imaging and Microscopy: Exploring biological structure and function with confocal microscopy 115

CONTENTS: VOLUME 197

NEUROBIOLOGY AND BEHAVIOR

Chee, Francis, and Maria Byrne
Development of the larval serotonergic nervous system in the sea star *Patiriella regularis* as revealed by confocal imaging 123

Hartline, D.K., E.J. Buskey, and P.H. Lenz
Rapid jumps and bioluminescence elicited by controlled hydrodynamic stimuli in a mesopelagic copepod, *Pleuromamma xiphias* 132

Harrison, Paul J.H., and David C. Sandeman
Morphology of the nervous system of the barnacle cypris larva (*Balanus amphitrite* Darwin) revealed by light and electron microscopy 144

PHYSIOLOGY

Gainey, Louis F., Jr., Kelly J. Vining, Karen E. Doble, Jennifer M. Waldo, Aurora Candelario-Martinez, and Michael J. Greenberg
An endogenous SCP-related peptide modulates ciliary beating in the gills of a venerid clam, *Mercenaria mercenaria* 159

DEVELOPMENT AND REPRODUCTION

Saigusa, Masayuki, and Hiroshi Iwasaki
Ovigerous-hair stripping substance (OHSS) in an estuarine crab: purification, preliminary characterization, and appearance of the activity in the developing embryos 174

IMMUNOLOGY

Shirae, Maki, Euichi Hirose, and Yasunori Saito
Behavior of hemocytes in the allorejection reaction in two compound ascidians, *Botryllus scalaris* and *Symplegma reptans* 188

ECOLOGY AND EVOLUTION

Skorokhod, Alexander, Vera Gamulin, Dietmar Gundacker, Vadim Kavsan, Isabel M. Müller, and Werner E.G. Müller
Origin of insulin receptor-like tyrosine kinases in marine sponges 198

Crain, Jennifer A.
Functional morphology of prey ingestion by *Placetron wosnessenskii* Schalfeew Zoeae (Crustacea: Anomura: Lithodidae) 207

SHORT REPORTS FROM THE 1999 GENERAL SCIENTIFIC MEETINGS OF THE MARINE BIOLOGICAL LABORATORY

Featured Article

Rome, Lawrence C.
Introduction. Bringing the script to life: the role of muscle in behavior 225

Rome, Lawrence C., Andrei A. Klimov, and Iain S. Young
A new approach for measuring real-time calcium pumping and SR function in muscle fibers 227

Physiology

Malchow, Robert Paul, and David J. Ramsey
Responses of retinal Müller cells to neurotransmitter candidates: a comparative study 229

Clay, John R., and Alan M. Kuzirian
Fluorescence localization of K^+ channels in the membrane of squid giant axons 231

Ruta, Vanessa J., Frederick A. Dodge, and Robert B. Barlow
Evaluation of circadian rhythms in the *Limulus* eye. . . 233

Novales Flamarique, Iñigo, and Ferenc I. Hárosi
Photoreceptor pigments of the blueback herring (*Alosa aestevalis*, Clupeidae) and the Atlantic silverside (*Menidia menidia*, Atherinidae) 235

Hanley, Janice S., Nadav Shashar, Roxanna Smolowitz, William Mebane, and Roger T. Hanlon
Soft-sided tanks improve long-term health of cultured cuttlefish 237

Piscine Neurobiology and Behavior

Zottoli, S.J., F.R. Akanki, N.A. Hiza, D.A. Ho-Sang, Jr., M. Motta, X. Tan, K.M. Watts, and E.-A. Seyfarth
Physiological characterization of supramedullary/dorsal neurons of the cunner, *Tautogolabrus adspersus*. . . . 239

Fay, R.R., and P.L. Edds-Walton
Sharpening of directional auditory input in the descending octaval nucleus of the toadfish, *Opsanus tau*. 240

Kaatz, Ingrid M., and Phillip S. Lobel
Acoustic behavior and reproduction in five species of *Corycoras* catfishes (Callichthyidae) 241

Lobel, Phillip S., and Lisa M. Kerr
Courtship sounds of the Pacific damselfish, *Abudefduf sordidus* (Pomacentridae) 242

Oliver, Steven J., and Elise Watson
Threat-sensitive nest defense in domino damselfish (*Dascyllus albisella*) 244

Price, Nichole N., and Allen F. Mensinger
Predator-prey interactions of juvenile toadfish, *Opsanus tau* 246

Tang, Kathleen Q., Nichole N. Price, Maureen D. O'Neill, Allen F. Mensinger, and Roger T. Hanlon
Temperature effects on first-year growth of cultured oyster toadfish, *Opsanus tau*. 247

Chemoreception and Behavior

Mjos, Katrin, Frank Grasso, and Jelle Atema
Antennule use by the American lobster, *Homarus americanus*, during chemo-orientation in three turbulent odor plumes. 249

Hanna, John P., Frank W. Grasso, and Jelle Atema
Temporal correlation between sensor pairs in different plume positions: A study of concentration information available to the American lobster, *Homarus americanus*, during chemotaxis 250

Zettler, Erik, and Jelle Atema
Chemoreceptor cells as concentration slope detectors: preliminary evidence from the lobster nose . . . 252

Berkey, Cristin, and Jelle Atema
Individual recognition and memory in *Homarus americanus* male-female interactions 253

McLaughlin, Leslie C., Jennifer Walters, Jelle Atema, and Norman Wainwright
Urinary protein concentration in connection with agonistic interactions in *Homarus americanus*. 254

King, Alison J., Shelley A. Adamo, and Roger T. Hanlon
Contact with squid eggs increases agonistic behavior in male squid (*Loligo pealei*) 256

Cell Motility

Bearer, E.L., M.L. Schlief, X.O. Breakefield, D.E. Schuback, T.S. Reese, and J.H. LaVail
Squid axoplasm supports the retrograde axonal transport of herpes simplex virus 257

Gould, Robert, Concetta Freund, Frank Palmer, Pamela E. Knapp, Jeff Huang, Hilary Morrison, and Douglas L. Feinstein
Messenger RNAs for kinesins and a dynein are located in neural processes 259

Fukui, Yoshio, Taro Q.P. Uyeda, Chikako Kitayama, and Shinya Inoué
Migration forces in *Dictyostelium* measured by centrifuge DIC microscopy. 260

Tran, P.T., P. Maddox, F. Chang, and S. Inoué
Dynamic confocal imaging of interphase and mitotic microtubules in the fission yeast, *S. pombe*. 262

Maddox, Paul, Arshad Desai, E.D. Salmon, T.J. Mitchison, Karen Oogema, Tarun Kapoor, Brian Matsumoto, and Shinya Inoué
Dynamic confocal imaging of mitochondria in swimming *Tetrahymena* and of microtubule poleward flux in *Xenopus* extract spindles 263

Wöllert, Torsten, Ana S. DePina, and George M. Langford
Effects of vanadate on actin-dependent vesicle motility in extracts of clam oocytes 265

Cell and Developmental Biology

Billack, Blase, Jeffrey D. Laskin, Michael A. Gallo, and Diane E. Heck
Effects of α-bungarotoxin on development of the sea urchin *Arbacia punctulata*. 267

Silver, Robert B., and Nicole M. Deming
Leukotriene B_4 as calcium agonist for nuclear envelope breakdown: an enzymological survey of endomembranes of mitotic cells 268

Weidner, Earl, and Ann Findley
Extracellular survival of an intracellular parasite (*Spraguea lophii*, Microsporea) 270

Kaltenbach, Jane C., William J. Kuhns, Tracy L. Simpson, and Max M. Burger
Intense concanavalin A staining and apoptosis of peripheral flagellated cells in larvae of the marine sponge *Microciona prolifera:* significance in relation to morphogenesis 271

Comparative Biochemistry

Harrington, John M., and Peter B. Armstrong
A cuticular secretion of the horseshoe crab, *Limulus polyphemus:* a potential anti-fouling agent 274

Asokan, Rengasamy, and Peter B. Armstrong
Cellular mechanisms of hemolysis by the protein limulin, a sialic-acid-specific lectin from the plasma of the American horseshoe crab, *Limulus polyphemus*. 275

Biswas, Chhanda, and Peter B. Armstrong
Identification of a hemolytic activity in the plasma of the gastropod *Busycon canaliculatum* 276

Kuhns, William J., Max M. Burger, and Eva Turley
Hyaluronic acid: a component of the aggregation factor secreted by the marine sponge, *Microciona prolifera*. 277

Popescu, Octavian, Rey Interior, Gradimir Misevic, Max M. Burger, and William J. Kuhns
Biosynthesis of tyrosine O-sulfate by cell proteoglycan from the marine sponge, *Microciona prolifera*. 279

Vasse, Aimee, Alice Child, and Norman Wainwright
Prophenoloxidase is not activated by microbial signals in *Limulus polyphemus* 281

Ogunseitan, O.A., S.L. Yang, and E. Scheinbach
The δ-aminolevulinate dehydratase of marine *Vibrio alginolyticus* is resistant to lead (Pb) 283

Hoskin, Francis C.G., Diane M. Steeves, and John E. Walker
Substituted cyclodextrin as a model for a squid enzyme that hydrolyzes the nerve gas soman 284

Zigman, Seymour, Nancy S. Rafferty, Keen A. Rafferty, and Nathaniel Lewis
Effects of green tea polyphenols on lens photooxidative stress 285

Ecology and Evolution

Mondrup, Thomas
Salinity effects on nutrient dynamics in estuarine sediment investigated by a plug-flux method 287

Pease, Katherine M., L. Claessens, C. Hopkinson, E. Rastetter, J. Vallino, and N. Kilham
Ipswich River nutrient dynamics: preliminary assessment of a simple nitrogen-processing model 289

Wolfe, Felisa L., Kevin D. Kroeger, and Ivan Valiela
Increased lability of estuarine dissolved organic nitrogen from urbanized watersheds 290

Evgenidou, A., A. Konkle, A. D'Ambrosio, A. Corcoran, J. Bowen, E. Brown, D. Corcoran, C. Dearholt, S. Fern, A. Lamb, J. Michalowsky, I. Ruegg, and J. Cebrián
Effects of increased nitrogen loading on the abundance of diatoms and dinoflagellates in estuarine phytoplanktonic communities 292

Cubbage, Andrea, David Lawrence, Gabrielle Tomasky, and Ivan Valiela
Relationship of reproductive output in *Acartia tonsa*, chlorophyll concentration, and land-derived nitrogen loads in estuaries in Waquoit Bay, Massachusetts. 294

Canfield, Susannah, Luc Claessens, Charles Hopkinson Jr., Edward Rastetter, and Joseph Vallino
Long-term effect of municipal water use on the water budget of the Ipswich River Basin 295

Young, Talia, Sharon Komarow, Linda Deegan, and Robert Garritt
Population size and summer home range of the green crab, *Carcinus meanus*, in salt marsh tidal creeks 297

Komarow, Sharon, Talia Young, Linda Deegan, and Robert Garritt
Influence of marsh flooding on the abundance and growth of *Fundulus heteroclitus* in salt marsh creeks . . . 299

Widener, Justin W., and Robert B. Barlow
Decline of a horseshoe crab population on Cape Cod. 300

Kerr, Lisa M., Phillip S. Lobel, and J. Mark Ingoglia
Evaluation of a reporter gene system biomarker for detecting contamination in tropical marine sediments. 303

Oral Presentations

Published by Title Only 307

No. 3, December 1999

RESEARCH NOTE

Kelman, Dovi, and Richard B. Emlet
Swimming and buoyancy in ontogenetic stages of the cushion star *Pteraster tesselatus* (Echinodermata: Asteroidea) and their implications for distribution and movement 309

Yusa, Yoichi, and Shigeyuki Yamato
Cropping of sea anemone tentacles by a symbiotic barnacle. 315

DEVELOPMENT AND REPRODUCTION

Irvine, Steven Q., Oleg Chaga, and Mark Q. Martindale
Larval ontogenetic stages of *Chaetopterus:* developmental heterochrony in the evolution of chaetopterid polychaetes 319

Degnan, Bernard M., and Craig R. Johnson
Inhibition of settlement and metamorphosis of the ascidian *Herdmania curvata* by non-geniculate coralline algae 332

Kanungo, Jyotshna, Ruth M. Empson, and Howard Rasmussen
Microinjection of an antibody to the Ku protein arrests development in sea urchin embryos 341

NEUROBIOLOGY AND BEHAVIOR

Lindsay, S.M., T.M. Frank, J. Kent, J.C. Partridge, and M.I. Latz
Spectral sensitivity of vision and bioluminescence in the midwater shrimp *Sergestes similis* 348

Ristvey, Andrew, and Steve Rebach
Enhancement of the response of rock crabs, *Cancer irroratus*, to prey odors following feeding experience 361

PHYSIOLOGY

Silverman, Harold, John W. Lynn, Peter G. Beninger, and Thomas H. Dietz
The role of latero-frontal cirri in particle capture by the gills of *Mytilus edulis* 368

Bayne, Brian L., Susanne Svensson, and John A. Nell
The physiological basis for faster growth in the Sydney rock oyster, *Saccostrea commercialis*. 377

Siebenaller, Joseph F., and Thomas F. Murray
Hydrostatic pressure alters the time course of GTP[S] binding to G proteins in brain membranes from two congeneric marine fishes. 388

CELL BIOLOGY

Lema-Foley, Christine, Kyeng G. Lee, Tchaiko Parris, Zoya Koroleva, Nishal Mohan, Pierre Noailles, and William D. Cohen
Reversible alteration of morphology in an invertebrate erythrocyte: properties of the natural inducer and the cellular response 395

* * *

Index for Volume 197 415

Notice to Subscribers

2000 SUBSCRIPTION RATES FOR *THE BIOLOGICAL BULLETIN*

	Libraries	**Individuals**
Per year (six issues, two volumes):	$225.00	$95.00
Per volume (three issues):	$112.50	$47.50
Back and single issues: (subject to availability)	$ 40.00	$20.00

For additional information, please contact our subscription manager at the Marine Biological Laboratory, 7 MBL Street, Woods Hole, MA 02543; tel: (508) 289-7402; e-mail: subscriptions@mbl.edu.

Reference: *Biol. Bull.* **197:** 309–314. (December 1999)

Swimming and Buoyancy in Ontogenetic Stages of the Cushion Star *Pteraster tesselatus* (Echinodermata: Asteroidea) and Their Implications for Distribution and Movement

DOVI KELMAN[1] AND RICHARD B. EMLET[2,*]

[1] *Department of Zoology, George S. Wise Faculty of Life Sciences, Tel-Aviv University, Ramat Aviv,*
Tel Aviv 69978, ISRAEL; and [2] *Institute of Marine Biology and Department of Biology,*
University of Oregon, Charleston, Oregon 97420

The eggs of some marine fish (1) and benthic invertebrates such as many corals (2, 3) and lecithotrophic echinoderms (4, 5) are positively buoyant at time of release from the parent, and density increases later in ontogeny. How these eggs and larvae are distributed in the water column and eventually reach suitable habitat for settlement will depend, in part, on their vertical velocity and on the turbulence in the water (i.e., *the eddy diffusivity). For eggs and unhatched stages, vertical velocity is passive and depends on egg or embryonic volume and density relative to the seawater (6, 7). For motile stages, vertical velocity depends on relative density, swimming ability, and behavior of the larvae (8, 9). We have measured the vertical velocity of eggs and larvae of the sea star* Pteraster tesselatus *Ives, which spawns floating eggs (1.1 to 1.5 mm diameter) that develop into nonfeeding larvae and spend several weeks in the plankton before settling to the benthos (10). Because of the simple shapes of eggs and larvae, we used force balance equations for drag and buoyant forces to determine the density of eggs and two larval stages. Initially the eggs were positively buoyant and floated upwards at about 1 mm/s. Even formalin-fixed eggs floated in seawater, so concentrations of light ions were not responsible for the buoyancy. The density of the larvae increased in the first 10 to 11 days, but it varied considerably between the three larval cohorts examined. Ten-day-old larvae that were negatively buoyant swam downward at mean speeds as high as 1.7 mm/s, while positively buoyant larvae of the same age swam upward at about 1 mm/s. These patterns of buoyancy and swimming velocity should initially facilitate dispersion and later promote settlement into subtidal habitats.*

Position in the water column and relative to the sea bottom will determine the amount of advection and the likelihood of encountering suitable habitat for settlement; variation in vertical position between related propagules will increase the spread of siblings or species (9, 11, 12). Predicting the depth distribution of eggs and larvae and other planktonic organisms requires information on their vertical velocity and on the turbulence structure of the water column (6–9). Alternatively, if the vertical velocity and distribution of propagules are known, one can estimate the turbulence structure (6). Many studies examine the density of fish eggs, and some relate this to their vertical distribution (*e.g.*, 6, 7, 13, 14). For larvae of benthic invertebrates, studies on swimming behavior and responses to environmental cues dominate discussions of vertical distribution (see reviews 15–17). With the exception of numerous studies on crustacean meroplankton (*e.g.*, 18, 19), there are few observations on vertical distribution as a function of stage of development or on density of the eggs and larvae of benthic invertebrates. Medeiros-Bergen *et al.* (20) showed that the lecithotrophic larvae of several sea cucumber species, which are released as positively buoyant eggs, can be distributed to depths exceeding 50 m, though they were most common in the upper 20 m of the water column. Young and Cameron (21) measured the rate of rise of positively buoyant eggs of the bathyl echinoid *Phormosoma placenta*, calculated the density of the eggs, and predicted that these embryos would

Received 24 May 1999; accepted 16 August 1999.

* To whom correspondence should be addressed. E-mail: remlet@oregon.uoregon.edu

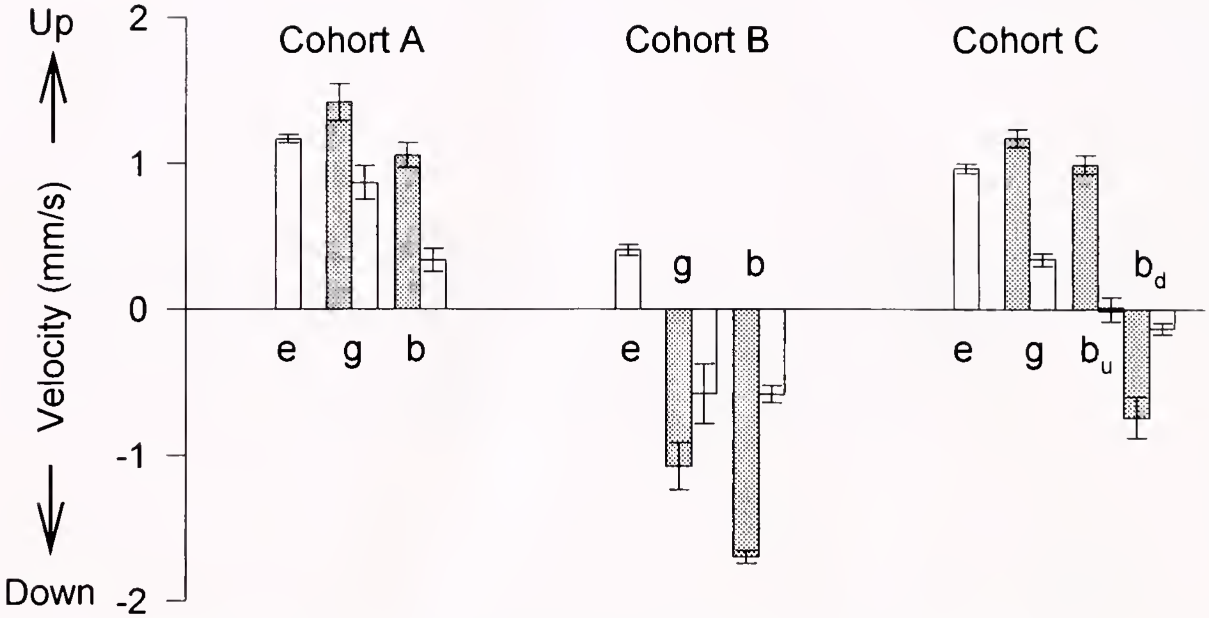

Figure 1. Rising and sinking rates of eggs with jelly coats (e), hatched gastrulae (g), and bilobed larvae (b) from three cohorts of *Pteraster tesselatus*. The open bars represent passive movement of eggs or deciliated larvae, and the shaded bars represent swimming larvae. The value on each bar represents the mean from 10 or 12 eggs, gastrulae, or larvae. Error bars are 1 S.E. b_u, bilobed larvae swimming up; b_d, bilobed larvae swimming down.

We collected adult *Pteraster tesselatus* Ives near San Juan Island, Washington (USA), in May 1998. Adult sea stars were induced to spawn by intracoelomic injection of 2–3 ml of 100 μM 1-methyladenine (4). We collected the spawned eggs from each of three females and washed them in filtered seawater (FSW). Larval stages that we studied were from eggs exposed to sperm at low concentrations. We do not know whether the sperm fertilized the eggs or was necessary for development, as oocytes of this species have been reported to develop without sperm (see Ref. 10).

Vertical speeds were measured in a cylindrical chamber (10 cm in diameter, and 15 cm tall) filled to within 2 cm of the top with 1 liter FSW (salinity, 28‰) and marked with graduations that circled the chamber at 2-cm intervals. The chamber was covered and immersed in an insulated aquarium maintained by a circulating water bath at a temperature of 12.2° (±0.1°C) to minimize convection currents that might affect the movement of the eggs and larvae in the chamber. Positively buoyant eggs and larvae that floated or swam up were introduced to the center of the chamber bottom. Negatively buoyant larvae and those that swam down were released at the surface in the center of the chamber. Rising and sinking times were measured for two successive 2-cm intervals in the middle of the water column where wall effects were minimal. Measurements that differed more than 10% were discarded. The individual was then repositioned at the bottom (or top) and allowed to rise (or sink) again; the new times were recorded. The average time to rise or sink 2 cm was calculated and used to determine speed.

rise into the warmer surface waters where their rate of development would be increased.

Measurement of vertical velocities of invertebrate eggs and swimming larvae is relatively simple and can be used to determine ontogenetic changes in velocity and density as well as to predict distributions of propagules in the field. Measurements on multiple cohorts can reveal variation among offspring from different parents. Among echinoderms, lecithotrophic larval development has evolved repeatedly from planktotrophic larval development (22–24), and many of the lineages with derived, nonfeeding larval development also have large, positively buoyant eggs that have evolved from negatively buoyant ones (5). Shifts in egg and embryonic buoyancy may require functional changes in swimming that are revealed by observations on vertical movement and orientation.

For three cohorts (from separate female parents), we measured the vertical velocities of unfertilized eggs, newly hatched gastrulae (5 d), and older, bilobed larvae (10–11 d). After swimming velocities were measured for individual larvae, they were deciliated in hypertonic seawater and their vertical velocity was measured again and used to determine the density of these stages.

Eggs (with intact jelly coats) always floated up, rising at speeds between 0.2 and 1.3 mm/s. The mean rising rates of eggs were 1.2, 0.4, and 1.0 mm/s for cohorts A, B, and C, respectively (Fig. 1). An ANOVA followed by a multiple comparisons test indicated that the rising rates of eggs were significantly different among cohorts ($F = 135.6$, df 2,27, $P < 0.001$; Tukey HSD test, $p < 0.001$ for all three pairwise comparisons).

Differences in egg rising rates among cohorts were due to differences in egg density and in part to differences in the egg and jelly coat volumes (Fig. 2a). Cohorts had significantly different egg densities (ANOVA, $F = 125.6$, df 2,27, $P < 0.001$; Tukey HSD test, $P < 0.001$ between all three pairwise comparisons). Eggs of cohort A, with the fastest mean rising rate, also had the lowest density (1020.2 kg/m^3); eggs of cohort B, with the slowest rising rate, had the highest density (1021.4 kg/m^3). Comparisons of the egg diameter and jelly coat thickness revealed significant variation among the cohorts in each trait (egg diameter ANOVA, $F = 125.3$, df 2,27, $P < 0.001$; jelly coat ANOVA, $F = 23.02$, df 2,27, $P < 0.001$). However, multiple comparisons (Tukey HSD tests) revealed that cohorts A and B each differed from cohort C in egg diameter ($P < 0.001$) and jelly coat thickness ($P < 0.001$), but A and B were not significantly different from each other in egg diameter ($P = 0.76$) or jelly coat thickness ($P = 0.15$). Thus differences in rising rates between cohorts A and B were due to differences in egg density, whereas differences between cohorts A and C and cohorts B and C were due to both density and dimensions of the eggs. Though eggs of cohort C had an intermediate density, their relatively large diameters and thin jelly coats contributed to their rising rates, which approached those of cohort A.

To determine whether active metabolic concentration of light ions was a possible buoyancy mechanism in the eggs of *Pteraster*, we fixed eggs in 3% formalin in filtered seawater (FSW) for several hours and then transferred them to fresh FSW. Formalin-fixed eggs floated, indicating that their positive buoyancy did not involve the metabolic mechanisms that maintain ion gradients (*e.g.*, 25, 26). Positive buoyancy may also be due to the presence of buoyant lipid reserves. According to Jaeckle (27), lipid content in lecithotrophic eggs of echinoderms ranges between 34% and 50% of total organic weight and is twice that found in planktotrophic eggs. A high lipid content could reduce the densities of the eggs and cause them to float. No data are available on the biochemical composition of *P. tesselatus* eggs and larvae or on the possible importance of lipid content in floating.

For another estimate of egg density, we assumed that the jelly coats were neutrally buoyant in seawater (Fig. 2a). Because the jelly coat has a very high water content, we believe this assumption was reasonable. Furthermore, the jelly coats of eggs of the sand dollar *Dendraster excentricus* are neutrally buoyant (28). The estimated densities of eggs without jelly coats were also significantly different among cohorts (ANOVA, $F = 159.4$, df 2,27, $P < 0.001$; Tukey HSD test, $P < 0.001$ between all three pairwise comparisons). Differences in egg density may be due to variation in biochemical composition and could also reflect variation in egg or maternal nutritional state. The estimated densities of the eggs without jelly coats were lower by 0.4 kg/m^3 (range, 0.7 to 0.2 kg/m^3) than those for the eggs with jelly coats. If the jelly coat is neutrally buoyant, it slows the rising rate of the buoyant egg. We calculated that the mean rising rates of eggs without jelly coats would be 12%, 15%, and 7% faster than those measured for intact eggs of cohorts A, B, and C respectively.

Eggs hatched after 3 to 4 d, and by day 5 swimming gastrulae were either at the water surface or at the bottom of their mesh-bottom culture vessels, depending on the female of origin. Gastrulae in cohorts A and C swam up at mean speeds of 1.4 and 1.2 mm/s respectively. When deciliated, all gastrulae in these cohorts were positively buoyant, rising at mean speeds of 0.9 mm/s (cohort A) and 0.3 mm/s (cohort C). In contrast, all gastrulae of cohort B swam down at a mean speed of 1.1 mm/s; when deciliated, 7 of 10 gastrulae were negatively buoyant and three others were slightly positively buoyant. The mean sinking speed of deciliated gastrulae from cohort B was 0.6 mm/s (see Fig. 1).

Larvae swam up or down, usually along a straight, vertical path, and rotated around their anterior-posterior axes as they swam. Regardless of its direction of vertical motion, a gastrula always had its anterior end up and its posterior end, with blastopore, down. Deciliated gastrulae also showed this orientation whether they rose or sank. This posture was assumed as soon as a swimming gastrula was placed in the stable water column and was maintained, without exception, as long as the larva was moving in the water column. This orientation appeared to result from an uneven distribution of buoyancy, with the anterior end being less dense than the posterior end. Because swimming speeds downward exceeded sinking speeds, the cilia must have produced currents that moved water from the posterior end toward the opposite end. The downward movement was sustained and was not likely to result from the transient reversal of ciliary beat that is known for planktotrophic larvae (29; Emlet, pers. obs.). The consistent and sustained downward swimming by gastrulae of cohort B, with the blastopore leading, indicates that the coordination of their cilia was different from that of negatively buoyant gastrulae that swim up, anterior end first, by moving water from anterior to posterior. This change in ciliary coordination from that typical of planktotrophic species has also been observed in downward-swimming, positively buoyant, lecithotrophic larvae of the echinoids *Heliocidaris erythrogramma* and *Holopneustes purpurascens* (Emlet, pers. obs.).

Larvae developed into a bilobed stage, with a circumferential groove that divided the larval body into anterior and posterior regions. By 10–11 d after fertilization, podia were beginning to form within the circumferential groove, but most larvae were still shaped like prolate spheroids and

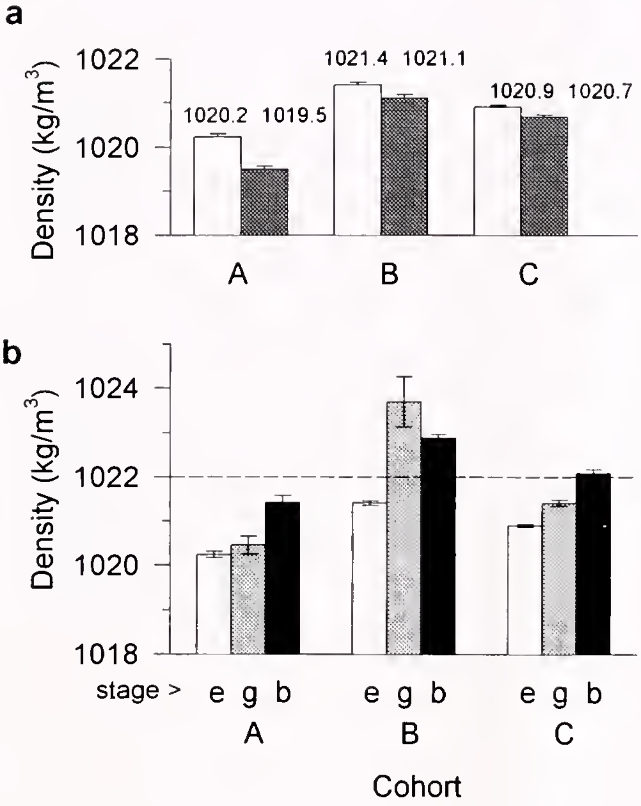

Figure 2. Density of unfertilized eggs (a) and eggs and larvae (b) for three cohorts of *Pteraster tesselatus*. (a) Two estimates of density: open bars are for eggs with jelly coats; dark bars are for eggs only, assuming the jelly to be neutrally buoyant. The value on each bar represents the mean for 10 eggs. Error bars are 1 S.E. (b) Ontogenetic changes in density from eggs and two larval stages for three cohorts. The bars represent the means for eggs with jelly coats (e), hatched gastrulae (g), and bilobed larvae (b). All sample sizes were 10 eggs or 10–12 larvae. Error bars are 1 S.E. The dotted line shows the density of seawater at 12.2°C and 28‰ salinity.

The Reynolds numbers (Re) were ≤ 0.8 for all eggs and < 0.5 for all passively moving larvae, so we used the low-Re equation for terminal velocity and solved for the density of the egg or larva (see *e.g.*, 31, equation 15.11, p. 340). We treated eggs as spheres and larvae as prolate spheroids; in the latter case we included a shape-correction term (see 32). We measured the diameter of each egg and the thickness of the jelly coat on a microscope with a 4× objective, after the egg rising time was measured. A suspension of India ink was added to reveal the edge of the translucent jelly coat. The length and width of gastrulae and larvae at their widest point were measured after larval swimming times were measured. Each larva was then deciliated by placing it in double-strength seawater for 10–15 s, then immediately rinsed three times in normal-strength seawater. This method has been used to collect cilia from echinoderm larvae and does not kill the larva; in fact, cilia are regenerated in a matter of hours (*e.g.*, 33; Emlet, pers. obs.). After the deciliated larvae were equilibrated in seawater at 28‰, we placed them individually in the chamber and measured their passive rising or sinking rates. The seawater in the chamber was at 12.2°C and had a salinity of 28‰; from tables (34) we determined its viscosity to be 0.0013 N s/m^2 and its density to be 1022 kg/m^3.

Sources of error in our calculations of the densities of eggs and larvae include our measurements of dimensions (including jelly coat for eggs) and our assumptions of shape (prolate spheroid or spheres). Measurement errors of 100 μm (7%–10% of egg + jelly diameters) would result in deviations of density of ≤ 0.5 kg/m^3. These errors would be random and should inflate the variation without biasing the means. Our assumption of shape could systematically bias the means through estimates of drag force or volume, but again the magnitude of the error would be about 0.2 kg/m^3. We do not think that any of these biases created erroneous trends in the data.

were not as advanced as the 8-day larva in figure 3 of McEdward (10). The swimming direction and buoyancy of larvae varied among the cohorts (Fig. 1). All larvae of cohort A swam up and were positively buoyant after they were deciliated, and all those of cohort B swam down and were negatively buoyant after they were deciliated. Cohort C was highly variable, with 7 of 12 larvae swimming up and 5 of 12 swimming down. Five of the seven larvae of cohort C that swam up were either positively or neutrally buoyant after being deciliated, whereas all of those that swam down were negatively or neutrally buoyant after being deciliated. The exceptions were two larvae that swam up opposite the direction of their passive motion. Compared to gastrulae, the bilobed larvae swam up at slower speeds or down at higher speeds, reflecting the generally increased density of these later stages (Figs. 1 and 2b). Bilobed larvae showed the same orientation that gastrulae did with larval anterior (adult oral) up and posterior (adult aboral) down regardless of their direction of swimming.

During development, the density of gastrulae and larvae increased relative to that of the eggs, though cohorts varied in the extent and timing of increase (Fig. 2b). Cohorts A and C showed consistent increases in density, with the bilobed larvae of cohort C obtaining a mean density not different from that of seawater (t test, $t = 0.95$, df = 11, $P = 0.362$). In contrast, the mean density of gastrulae of cohort B exceeded that of seawater ($t = 3.0$, df = 9, $P = 0.015$), and some of these individuals had higher densities than any other stages across all cohorts (Fig. 2b).

Differences in density among eggs (without jelly), gastrulae, and bilobed larvae were analyzed separately for each cohort because of significant heterogeneity of variances within cohorts A and B but not cohort C (Cochran's C tests, $P < 0.01$ for cohort A, $P < 0.001$ for cohort B, $P = 0.11$ for cohort C). Cohorts A and C had significantly different densities among all stages. (Cohort A: Kruskal-Wallis test, $H = 21.8$; multiple comparisons with a nonparametric equivalent of the Tukey test (Ref. 30), $P < 0.05$; cohort C: ANOVA, $F = 91.9$ df 2,29, $P < 0.001$; Tukey HSD, $P \leq 0.002$ for all comparisons). Cohort B also had significant differences in density among stages (Kruskal-Wallis test, $H = 19.9$, $P < 0.001$). Nonparametric pairwise comparisons indicated that density differed significantly between eggs and gastrulae ($P < 0.001$), between eggs and bilobed larvae ($P < 0.005$), but not between gastrulae and bilobed larvae ($P > 0.5$).

McEdward (10) observed that eggs and embryos of *P. tesselatus* were positively buoyant until the time close to settlement, when larvae swam near the bottom. The present study confirms that observation for two cohorts, but a third cohort was negatively buoyant soon after hatching. The rising speeds of eggs and the swimming speeds of gastrulae and larvae of *Pteraster* usually exceeded 1 mm/s. Although still slow, these rates are about five times the sinking speeds of planktotrophic eggs and two to three times the swimming speeds of planktotrophic larvae of echinoderms (5). Our measurements showed significant increases in density as development progressed (Fig. 2b), with bilobed larvae approaching or exceeding the density of seawater. Becoming less positively buoyant or negatively buoyant may increase downward swimming speed and assist larvae in the search for suitable settlement habitats.

The mean downward swimming speed of 1.7 mm/s for bilobed larvae of cohort B should allow them to overcome resuspension by turbulent mixing during some parts of the tidal cycle. Gross *et al.* (8) modeled larval settlement in tidally dominated flows found in estuarine and shelf conditions, exploring how larval swimming speed influenced the probability of settlement. For a water depth of 50 m, the model predicted that a doubling of fall velocity from 0.8 to 1.6 mm/s resulted in a 12-fold increase in the probability of contacting the bottom throughout the entire tidal cycle. During periods of weak tidal flows, the model predicted that up to 40% of larvae swimming at 1.6 mm/s could interact with the bottom and possibly settle, while 1% to 4% of those swimming at 0.8 mm/s would be capable of settling (8).

Our studies were conducted at a salinity of 28‰ and a temperature of 12.2°C, conditions typical of the surface waters near San Juan Island, Washington. Though seawater higher in salinity (and hence more dense) is found in other coastal settings, we believe that our results are applicable to these regions as well. Preliminary observations showed that when deciliated larvae of *Pteraster* that were negatively buoyant at 28‰ were placed in water with a salinity of 30‰, they would initially float for a few minutes before sinking at constant speed. A possible explanation is that the osmotic difference resulted in water loss and salt gain by larvae, restoring the relative density of the larvae in seawater. Further studies that vary salinity would be necessary to determine if the absolute magnitude of the differences between the density of the larvae and the seawater are the same when the salinity changes. Other studies (Emlet, unpub. data) of buoyancy and swimming in ontogenetic stages of two echinoids at a salinity of 35‰ found patterns similar to those reported here.

This study has documented ontogenetic changes in buoyancy from positive to either neutral or negative buoyancy and found changes in swimming direction and speed that correlate with buoyancy for one species of sea star with positively buoyant eggs. The eggs and larvae exceeded 1 mm in diameter and departed from the density of seawater by as much as 2.0 kg/m^3. (For comparison, the density of seawater changes by 2 kg/m^3 for each 10°C change in temperature.) Though small, the resulting difference in density caused the eggs and larvae to rise or sink relatively rapidly compared to planktotrophic larvae, and rates of movement were augmented later in development by ciliary swimming. These patterns should initially facilitate dispersion from the site of egg release and then promote settlement. Buoyancy and swimming for specific stages were also found to vary within and between cohorts, which should increase the spread of siblings as well as offspring of conspecifics (12). Finally, the swimming orientation of anterior up, posterior down that was maintained during development suggests that the ciliary coordination of positively buoyant larvae has been changed from that of planktotrophic ancestors.

Acknowledgments

A. O. D. Willows, Director, provided space and facilities at the Friday Harbor Laboratories. We thank R. Strathmann and J. Hoffman for contributing ideas throughout this study and for valuable comments that improved the manuscript. The manuscript was also improved with helpful comments by O. Mokady and anonymous reviewers. Funding was provided by the Friday Harbor Laboratories Marine Science fund (# 63-3972), an Aharon Katzir Foundation travel grant to D.K, and NSF grant OCE-9416590 to R.B.E.

Literature Cited

1. **Craik, J. C. A., and S. M. Harvey. 1987.** The causes of buoyancy in eggs of marine teleosts. *J. Mar. Biol. Assoc. UK* **67:** 169–182.
2. **Harrison, P. L., R. C. Babcock, G. D. Bull, J. K. Oliver, C. C. Wallace, and B. L. Willis. 1984.** Mass spawning in tropical reef corals. *Science* **223:** 1186–1189.
3. **Harrison, P. L., and C. C. Wallace. 1990.** Reproduction, dispersal, and recruitment of scleractinian corals. Pp. 133–207 in *Coral Reefs*, Z. Dubinsky, ed. Elsevier, Amsterdam.
4. **Strathmann, M. F. 1987.** *Reproduction and Development of Marine Invertebrates of the Northern Pacific Coast.* University of Washington Press, Seattle.
5. **Emlet, R. B. 1994.** Body form and patterns of ciliation in nonfeeding larvae of echinoderms: functional solutions to swimming in the plankton? *Am. Zool.* **34:** 570–585.
6. **Sundby, S. 1983.** A one dimensional model for the vertical distribution of pelagic fish eggs in the mixed layer. *Deep-Sea Res.* **30:** 645–661.
7. **Sundby, S. 1997.** Turbulence and ichthyoplankton: influence on vertical distributions and encounter rates. *Sci. Mar.* **61 (Suppl. 1):** 159–176.
8. **Gross, T. F., F. E. Werner, and J. E. Eckman. 1992.** Numerical modeling of larval settlement in turbulent bottom boundary layers. *J. Mar. Res.* **50:** 611–642.
9. **Eckman, J. E., F. E. Werner, and T. F. Gross. 1994.** Modelling some effects of behavior on larval settlement in a turbulent boundary layer. *Deep-Sea Res. II Top. Stud. Oceanogr.* **41:** 185–208.
10. **McEdward, L. R. 1992.** Morphology and development of a unique type of pelagic larvae in the starfish *Pteraster tesselatus* (Echinodermata: Asteroidea). *Biol. Bull.* **182:** 177–187.

11. **Okubo, A. 1980.** *Diffusion and Ecological Problems: Mathematical Models.* Springer-Verlag, Berlin.
12. **Strathmann, R. R. 1974.** The spread of sibling larvae of sedentary marine invertebrates. *Am. Nat.* **108:** 29–44.
13. **Coombs, S. H., C. A. Fosh, and M. A. Keen. 1985.** The buoyancy and vertical distribution of eggs of sprat (*Sprattus sprattus*) and pilchard (*Sardina pilchardus*). *J. Mar. Biol. Assoc. UK* **65:** 461–474.
14. **Bullman, C. M., and J. A. Koslow. 1995.** Development and depth distribution of the eggs of orange roughy, *Holostethus atlanticus* (Pisces: Trachichthyidae). *Mar. Freshw. Res.* **46:** 697–705.
15. **Sulkin, S. D. 1984.** Behavioral basis of depth regulation in the larvae of brachyuran crabs. *Mar. Ecol. Prog. Ser.* **15:** 181–205.
16. **Young, C. M., and F. S. Chia. 1987.** Abundance and distribution of pelagic larvae as influenced by predation, behavior, and hydrographic factors. Pp. 385–463 in *Reproduction of Marine Invertebrates,* Vol. 9, A. C. Giese, J. S. Pearse, and V. B. Pearse, eds. Blackwell Scientific, Palo Alto, California.
17. **Young, C. M. 1995.** Behavior and locomotion during the dispersal phase of larval life. Pp. 247–277 in *Ecology of Marine Invertebrate Larvae,* L. McEdward, ed. CRC Press, Boca Raton, Florida.
18. **Shanks, A. L. 1986.** Vertical migration and cross-shelf dispersal of larval *Cancer* spp. and *Randallia ornata* (Crustacea: Brachyura) off the coast of southern California. *Mar. Biol.* **92:** 189–199.
19. **DeVries, M. C., R. A. Tankersley, R. B. Forward, Jr., W. W. Kirby-Smith, and R. A. Luettich, Jr. 1994.** Abundance of estuarine crab larvae is associated with tidal hydrologic variables. *Mar. Biol.* **118:** 403–413.
20. **Medeiros-Bergen, D. E., R. R. Olson, J. A. Conroy, and T. D. Kocher. 1995.** Distribution of holothurian larvae determined with species-specific genetic probes. *Limnol. Oceanogr.* **40:** 1225–1235.
21. **Young, C. M., and J. L. Cameron. 1987.** Laboratory and *in situ* floating rates of lecithotrophic eggs from the bathyl echinoid *Phormosoma placenta. Deep-Sea Res.* **34:** 1629–1639.
22. **Strathmann, R. R. 1978.** The evolution and loss of feeding larval stages of marine invertebrates. *Evolution* **32:** 894–906.
23. **Emlet, R. B. 1990.** World patterns of developmental mode in echinoid echinoderms. Pp. 329–334 in *Advances in Invertebrate Reproduction* Vol. 5, M. Hoshi and O. Yamashita, eds. Elsevier, Amsterdam.
24. **Wray, G. A. 1995.** Evolution of larvae and developmental modes. Pp. 413–447 in *Ecology of Marine Invertebrate Larvae,* L. McEdward, ed. CRC Press, Boca Raton, Florida.
25. **Lambert, C. C., and G. Lambert. 1978.** Tunicate eggs utilize ammonium ions for floatation. *Science* **200:** 64–65.
26. **Newton, C., and W. T. W. Potts. 1993.** Ionic regulation and buoyancy in some planktonic organisms. *J. Mar. Biol. Assoc. UK* **73:** 15–23.
27. **Jaeckle, W. B. 1995.** Variation in the size, energy content, and composition of invertebrate eggs: correlates to the mode of larval development. Pp. 49–77 in *Ecology of Marine Invertebrate Larvae,* L. McEdward, ed. CRC Press, Boca Raton, Florida.
28. **Podolsky, R. D. 1995.** Consequences of temperature, viscosity, and small size for early life-history processes in the sand dollar *Dendraster excentricus.* Ph.D. dissertation, University of Washington, Seattle.
29. **Strathmann, R. R. 1971.** The feeding behavior of planktotrophic echinoderm larvae: mechanisms, regulation and rates of suspension-feeding. *J. Exp. Mar. Biol. Ecol.* **6:** 109–160.
30. **Zar, J. H. 1984.** *Biostatistical Analysis.* Prentice Hall, Englewood Cliffs, New Jersey.
31. **Vogel, S. 1994.** *Life in Moving Fluids. The Physical Biology of Flow.* Princeton University Press, Princeton.
32. **Happel, J., and Brenner, H. 1986.** *Low Reynolds Number Hydrodynamics.* Martin Nijhoff, Dordrecht, The Netherlands.
33. **Stephens, R. E. 1986.** Isolation of embryonic cilia and sperm flagella. Pp. 217–227 in *Methods in Cell Biology, Vol. 27: Echinoderm Gametes and Embryos,* T. E. Schroeder, ed. Academic Press, Orlando, Florida.
34. **Walton Smith, F. G., and F. A. Kalber, eds. 1974.** *CRC Handbook of Marine Science.* CRC Press, Cleveland, Ohio.

Reference: *Biol. Bull.* **197:** 315–318. (December 1999)

Cropping of Sea Anemone Tentacles by a Symbiotic Barnacle

YOICHI YUSA* AND SHIGEYUKI YAMATO

Seto Marine Biological Laboratory, Kyoto University, Shirahama, Wakayama 649-2211, Japan

As sessile animals, barnacles (Cirripedia: Thoracica) are generally suspension feeders, extending their cirri into the surrounding water to collect food particles (1). Although it has been suggested that some symbiotic barnacles obtain nutrients directly from their hosts, either by absorbing body fluids (2–4) or by rasping the host's tissue (4–6), most of these cases are inferred from their morphology. Direct evidence, such as gut content analysis, has been limited (for an exception, see ref. 5), and no actual feeding on their hosts has been observed. Koleolepas avis *(Hiro, 1931) is a pedunculate barnacle symbiotic with the sea anemone* Calliactis japonica, *which lives on gastropod shells occupied by large hermit crabs (7), mainly* Dardanus arrosor. *Symbiotic relationships between various hermit crabs and sea anemones have been well documented (8), but the relationship between the barnacle and its host sea anemone has been virtually unknown. From February to April 1996, we collected living individuals of* K. avis *from lobster nets landed at Minabe Fishery Port, southwestern Japan (33° 44′ N, 135° 20′ E). On the basis of behavioral observations in the laboratory and analyses of fecal pellets and gut contents, we concluded that this barnacle feeds actively on its host's tentacles.*

The shape of *Koleolepas avis* (Fig. 1) differs from that of typical pedunculate barnacles like *Lepas* spp. in many ways (7). First, *K. avis,* like its two congeners *K. willeyi* Stebbing (9) and *K. tinkeri* Edmondson (10), has a sheath-like structure extending from the base of the peduncle and covering the main body (the attachment disk). Second, at the orifice, *K. avis* has a chitinous, bill-like projection that is developed only in this species. Hiro (7) stated that this projection gives "the cirriped a bird-bill-shape." These two characteristics are reflected in the generic and specific names, respectively ("koleo" means sheath and "avis" means bird). Third, the peduncle is highly distensible, being about three times as long as the length of the capitulum. In addition to these external characteristics, the internal morphology is also distinct. The cirri are short, with sparse setae, and thus unsuitable for filter feeding, and the cutting edge of the mandible is peculiarly serrate (7).

Observations on living individuals showed that the attachment disk of *K. avis* was interposed between the pedal disk of its host anemone and the gastropod shell. Most of the barnacle's main body was retracted into the attachment disk, and only the upper part of the capitulum was visible from outside of the host (Fig. 2A). A rhythmical cirral movement could be seen through the semitransparent capitulum, but otherwise the barnacle usually remained motionless.

When tentacles of the sea anemone touched *K. avis* (presumably its cirri), the capitulum of the barnacle immediately came out from the gap under the host and began to follow the tentacles (Fig. 2B). This tentacle-following behavior lasted 89 ± 122 s (mean ± SD of 46 observations on 10 individuals). During this period, the cirri were widely spread and almost motionless. When the cirri of *K. avis* touched a tentacle of its host again, the barnacle grabbed it with its cirri, pulled part of it into the capitulum, and closed the orifice firmly. At the same time the peduncle shrank and bent frontally (to the direction of the orifice). As a result, the tentacle became pinched by the upper ridge of the bill-like projection of *K. avis* (Fig. 2C). In response to the pinching, the sea anemone contracted its tentacles. Pulled from the both ends, the pinched tentacle tore off (Fig. 2D). This tentacle pulling lasted 109 ± 95 s.

A barnacle cropped a tentacle 1.4 ± 1.4 times a day (mean ± SD of 10 individuals). We did not observe the barnacles eat other parts of the host, nor other possible foods

---

Received 12 April 1999; accepted 28 September 1999.

* Author to whom correspondence should be addressed. Present address: Laboratory of Insect Ecology, Kyushu National Agricultural Experiment Station, Nishigoshi, Kumamoto 861-1192, Japan. E-mail: yusa@knaes.affrc.go.jp

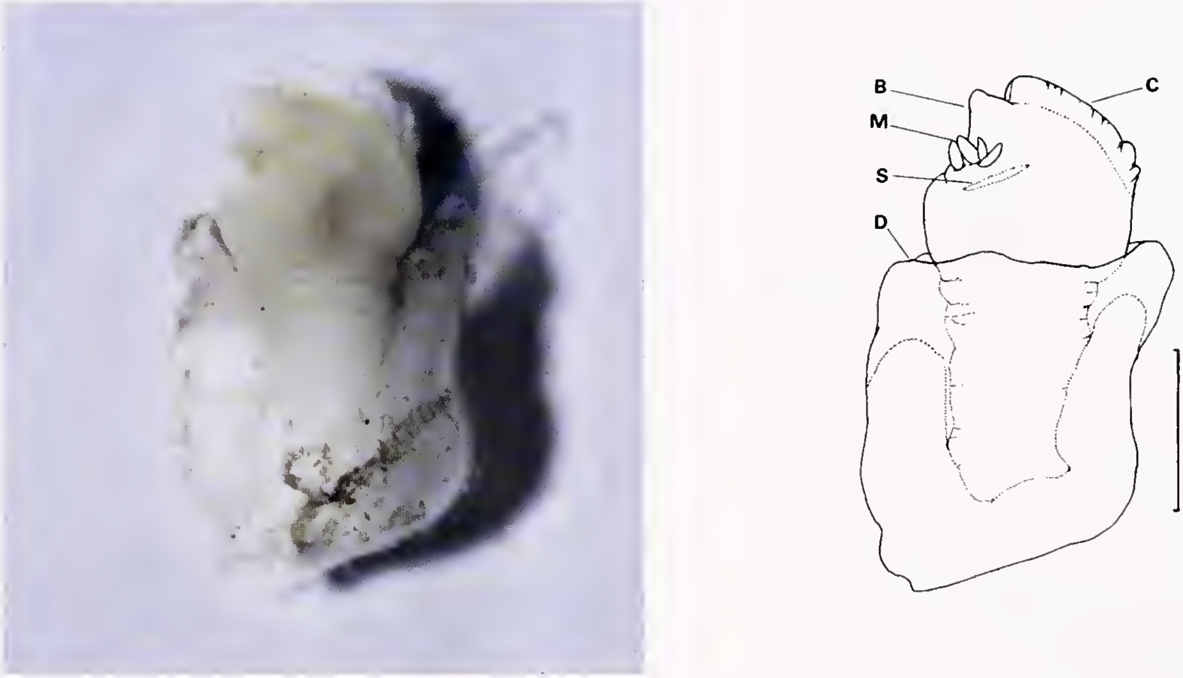

Figure 1. *Koleolepas avis*, viewed from shell side. B, bill-like projection surrounding the orifice; C, crest-like projection; D, attachment disk; M, complemental males (five males, including the one on the other side, are attached to this specimen); S, scutum. Scale bar, 5 mm.

such as living *Artemia* larvae, minced mysids, or commercial fish meal, all of which were readily eaten by *Lepas* spp. (pers. obs.). Fecal pellets of *Koleolepas* were cream white, a color similar to that of its host's tentacles. When observed under a microscope, the pellets were filled with nematocysts. We also found nematocysts in 80% (12/15) of the guts of newly collected barnacles. The guts of the remaining barnacles were almost empty, probably because they could eat little after the snail shells on which they lived were trapped in lobster nets.

The relationship of *K. avis* to the host anemone can be best regarded as parasitic. We did not quantify detrimental effects on the host, mainly because the number of specimens was too small to conduct such a study. However, up to six barnacles per host (pers. obs.) may have some effects on the host, as reported for other parasitic arthropods that feed on their host anemones [a shrimp (11) and a pycnogonid (12)]. Experiments with hermit crabs are necessary to test this assumption, because the presence of hermit crabs may change the frequency with which the barnacles crop anemone tentacles.

Koleolepas avis is the only barnacle known to eat sea anemones, although two other species of barnacles have been reported to eat cnidarian prey (4, 5, 13, 14). Among cnidarian-eating barnacles, *Lepas anserifera* feeds on neustonic medusae as one of many food items (13, 14), whereas *Hoekia monticulariae*, a balanomorph barnacle symbiotic with corals, seems to feed only on its host (4, 5). However, the feeding behavior of *H. monticulariae* is much less active than that of *K. avis:* that balanomorph barnacle is believed to rasp the host's tissue (5) and possibly absorb body fluids of the host coral (4).

The morphological characteristics of *K. avis* are related to the tentacle feeding. First, the bill-like projection of *K. avis* functions like a bill in pinching a long prey. The other two species of *Koleolepas* (the only genus in the family Koleolepadidae) also occur on gastropod shells that are carrying sea anemones and are occupied by hermit crabs (9, 10). However, these species apparently do not have bill-like projections, suggesting that they may have adopted a different feeding habit. Second, the long distensible peduncle is used to follow a tentacle of the sea anemone. Third, the attachment disk allows the peduncle to move freely under the pedal disk of the sea anemone. Finally, its short cirri and peculiar mouth parts are specialized for grabbing and chewing tentacles. A similar specialization is reported in *Hoekia monticulariae*, a coral-eating barnacle: the cirri are strongly reduced and the mandible is modified as a sawlike blade (5).

Whereas tentacle cropping by *K. avis* is a highly unique behavior, it consists of behavioral components common among other pedunculate barnacles: cirral activity, closure of the orifice, elongation and sudden shortening of the peduncle (1). In *K. avis*, the morphology and behavioral components are modified to specialize in cropping the host's tentacles and to live under sea anemones.

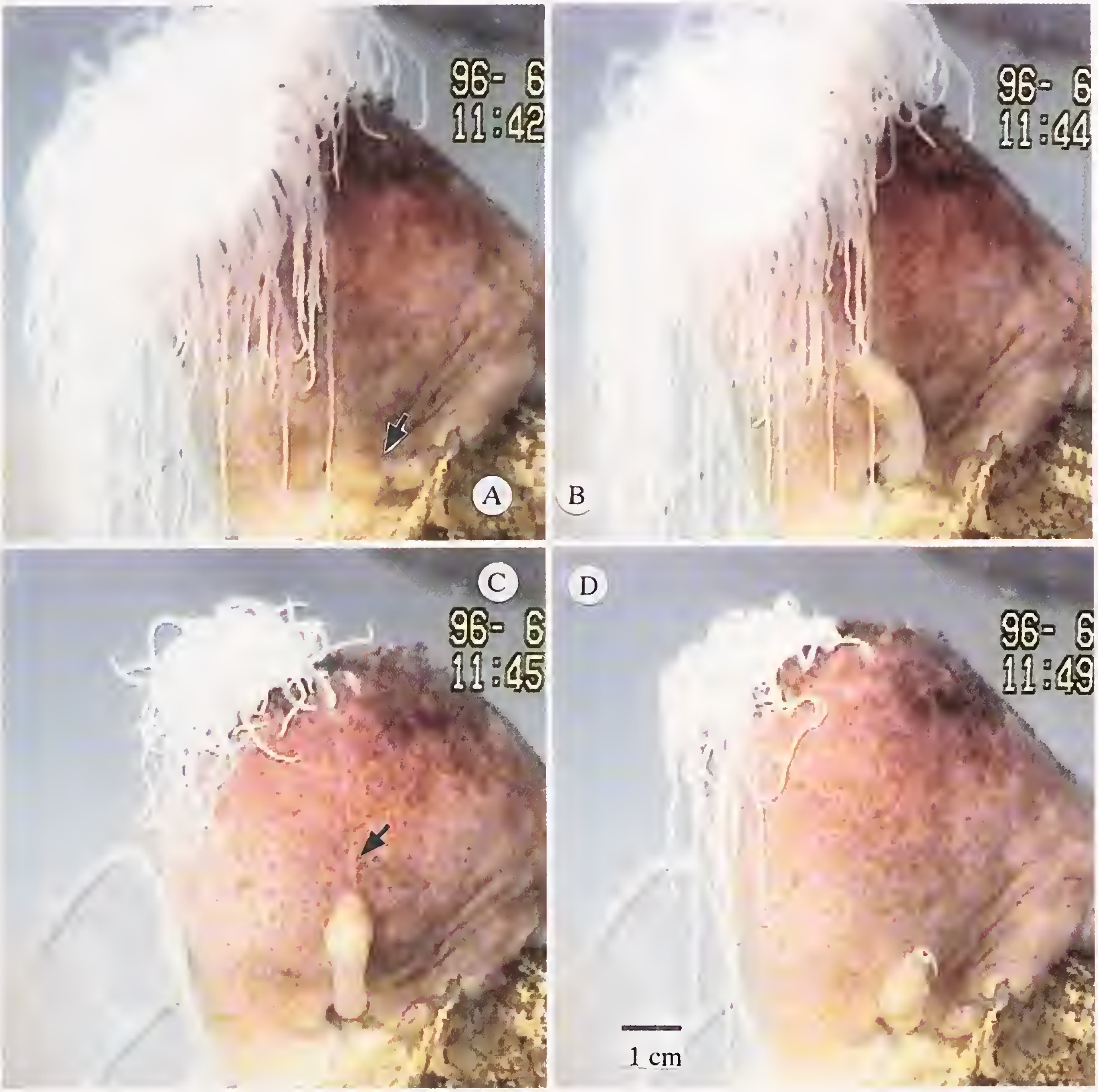

Figure 2. Tentacle cropping behavior by *Koleolepas avis:* (A) Barnacle in resting position (arrow); (B) elongation of the peduncle to follow sea anemone tentacles; (C) pinching a host tentacle (arrow); (D) after cutting off the tentacle, part of which hangs from the orifice of the barnacle. The barnacles and sea anemones were kept in an aquarium with running seawater (symbiotic hermit crabs were removed from the gastropod shells). The sea anemones were fed with minced mysids or commercial fish meal. A fluorescent light (20 W) was used throughout the observations, together with the natural light. The behavior of the barnacles was recorded with a time-lapse video recorder.

Acknowledgments

We thank Masahiro Marumura, Hidetomo Tanase, Taiji Yamamoto, and Mitsuru Ohta for providing the materials; Takashi Wada, Hirotsugu Kiyota, and Tadashi Furuie for facilities to analyze the data; and two anonymous referees for comments on the manuscript.

Literature Cited

1. **Anderson, D. T. 1994.** *Barnacles: Structure, Function, Development and Evolution.* Chapman & Hall, London.
2. **Johnstone, J., and W. E. Frost. 1927.** *Anelasma squalicola* (Lovén): its general morphology. *Rep. Lancashire Sea-Fish. Lab.* **35:** 27–91.
3. **Day, J. H. 1939.** A new cirripede parasite—*Rhizolepas annelidicola* nov. gen. et sp. *Proc. Linn. Soc. Lond.* **51:** 64–79.

4. **Ross, A., and W. A. Newman. 1995.** A coral-eating barnacle, revisited (Cirripedia, Pyrgomatidae). *Contrib. Zool.* **65:** 129–175.
5. **Ross, A., and W. A. Newman. 1969.** A coral-eating barnacle. *Pac. Sci.* **23:** 252–256.
6. **Grygier, M. J., and W. A. Newman. 1991.** A new genus and two new species of Microlepadidae (Cirripedia: Pedunculata) found on western Pacific diadematid echinoids. *Galaxea* **10:** 1–22.
7. **Hiro, F. 1933.** Notes on two interesting pedunculate cirripeds, *Malacolepas conchicola* n. gen. et sp. and *Koleolepas avis* (Hiro), with remarks on their systematic positions. *Mem. Coll. Sci. Kyoto Imp. Univ. Ser. B.* **8:** 233–247 + Pls. 8–9.
8. **Ross, D. M. 1983.** Symbiotic relations. Pp. 163–212 in *The Biology of Crustacea, Vol. 7, Behavior and Ecology.* F. J. Vernberg and W. B. Vernberg, eds. Academic Press, New York.
9. **Stebbing, T. R. R. 1900.** On Crustacea brought by Dr. Willey from the South Seas. Pp. 605–687 + Pls. 64–74 in *Zoological Results Based on Materials from New Britain, New Guinea, Loyalty Islands and Elsewhere, Collected during the Years 1895, 1896 and 1897, Part V.* Cambridge University Press, Cambridge.
10. **Edmondson, C. H. 1951.** Some Central Pacific crustaceans. *Occas. Pap. Bernice P. Bishop Mus.* **20:** 183–243.
11. **Fautin, D. G., C-C Guo, and J-S Hwang. 1995.** Costs and benefits of the symbiosis between the anemoneshrimp *Periclimenes brevicarpalis* and its host *Entacmaea quadricolor. Mar. Ecol. Prog. Ser.* **129:** 77–84.
12. **Mercier, A., and J. F. Hamel. 1994.** Deleterious effects of a pycnogonid on the sea anemone *Bartholomea annulata. Can. J. Zool.* **72:** 1362–1364.
13. **Bieri, R. 1966.** Feeding preferences and rates of the snail, *Ianthina prolongata,* the barnacle, *Lepas anserifera,* the nudibranchs, *Glaucus atlanticus* and *Fiona pinnata,* and the food web in the marine neuston. *Publ. Seto Mar. Biol. Lab.* **14:** 161–170.
14. **Jones, E. C. 1967.** *Lepas anserifera* Linné (Cirripedia: Lepadomorpha) feeding on fish and *Physalia. Crustaceana* **14:** 311–313.

Reference: *Biol. Bull.* **197:** 319–331. (December 1999)

Larval Ontogenetic Stages of *Chaetopterus*: Developmental Heterochrony in the Evolution of Chaetopterid Polychaetes

STEVEN Q. IRVINE[1,*], OLEG CHAGA[2], AND MARK Q. MARTINDALE[1,2,†]

[1] *Committee on Evolutionary Biology, and* [2] *Department of Organismal Biology and Anatomy, University of Chicago, 1027 E. 57th Street, Chicago, Illinois 60637*

Abstract. Seven post-gastrulation larval stages are described for the sedentary polychaete *Chaetopterus*. Analysis of larval anatomy and morphology through ontogeny reveals significant differences in the temporal sequence of segmentation, and in the character of segments formed, from the typical embryological pattern described for other polychaete families, such as nereidids or spionids. When compared in alternative phylogenetic schemes, these differences represent significant developmental heterochrony, among other evolutionary transitions, which has arisen in the chaetopterid lineage. The heterochrony is correlated with the extreme morphological regionalization along the anterior-posterior body axis, a feature that is also characteristic of chaetopterids.

Introduction

The peculiar morphology and lifestyle of the sedentary polychaetes of the genus *Chaetopterus* have long attracted the interest of a range of biologists. *Chaetopterus* is unique among annelids in the degree of morphological differentiation of segments along the body axis. However, the larval ontogeny of representatives of the common North American species complex has never been completely described. This work is meant to be a basis for comparative studies of molecular development in this heteronomously segmented worm. The phylogenetic position of *Chaetopterus* and its implications for variation in developmental programs is also discussed.

Adult chaetopterids live in mucus-lined U-shaped tubes, either partly buried in the sediment or attached to hard objects such as stones or corals. The tubes are usually paperlike, hence the common name *parchment worm*. The worm feeds by pumping seawater through its tube with modified parapodial "fans," catching suspended organisms in a mucous net that it then rolls up, using the accessory feeding organ; sends to the mouth, *via* the mid-dorsal ciliary groove; and ingests (MacGinitie, 1939). The body form and parapodia are highly modified in relation to members of other polychaete families to enable this unique feeding behavior. The chaetopterids have generally been considered to be related to the spioniform families, but their unique and very complex external morphology sets them apart from other polychaetes (Fauchald and Rouse, 1997). The purpose of studying *Chaetopterus* in the present context is as a basis for comparative evolutionary embryology aimed at elucidating the developmental sources of morphological innovation.

The genus *Chaetopterus* is a species complex sometimes mistakenly described as monotypic (Petersen, 1984a, b). The species we have used is that described by Enders (1909) as *Chaetopterus variopedatus*; however, it is different from the type species *C. variopedatus* Renier, 1804. Unfortunately, the type specimen of *C. variopedatus* has been lost, making comparison uncertain (M. E. Petersen, Copenhagen Museum, personal correspondence). We will refer to the animal we describe, commonly available in Woods Hole, Massachusetts and Beaufort, North Carolina, as *Chae-*

Received 28 April 1999; accepted 5 August 1999.

* Current address: Steven Q. Irvine, Department of Cellular, Molecular and Developmental Biology, Yale University, P.O. Box 208103, New Haven, CT 06520-8103. E-mail: sqi2@pantheon.yale.edu

† Current address, and to whom correspondence should be addressed: Mark Q. Martindale, Kewalo Marine Lab, PBRC/Univ. of Hawaii, 41 Ahui St., Honolulu, HI 96813. E-mail: mqmartin@hawaii.edu

topterus. A more definitive name awaits a complete revision of the genus (M. E. Petersen, in preparation).

Chaetopterus was an important model for classical studies of early embryogenesis (Mead, 1897; Lillie, 1906). The accessibility of large numbers of gametes in *Chaetopterus* has made it a model organism for the cell biology and biochemistry of eggs and sperm (*e.g.*, Inoué *et al.*, 1974; Jeffery, 1985; Eckberg and Anderson, 1995). Since the gametes are easily fertilized *in vitro*, *Chaetopterus* lends itself to studies of early cleavage and embryogenesis (*e.g.*, Mead, 1897; Henry, 1986, 1989; Henry and Martindale, 1987).

Several turn-of-the-century papers describe the anatomy and life history of *Chaetopterus* in some detail (Joyeux-Laffuie, 1890; Béraneck, 1894; Enders, 1909). Joyeux-Laffuie established a scheme for numbering segments (not a trivial matter) in the adult worm that has been followed by subsequent authors. Cazaux (1965) has the most complete description of external larval morphology in the literature, although his findings differ from ours in some respects (see below). Bonch-Bruevich and Malakhov (1987) describe the internal anatomy of the 48-h larva on the basis of transmission electron micrography. Detailed early embryogenesis was traced by Mead (1897) and more recently by Malakhov (1984) and Henry (1986) through 72 h of development; this paper thus concentrates on postgastrulation larval ontogeny through metamorphosis. We also present the first photographic documentation of larval ontogeny and propose a scheme for numbering the larval stages. The ontogeny is then analyzed in a phylogenetic context to propose the occurrence of a novel developmental heterochrony in the chaetopterid lineage.

Materials and Methods

Larval culture. Methods for obtaining and fertilizing gametes are described by Henry (1986) and Eckberg and Hill (1996). Specific aspects of methods used in this study are described in Irvine and Martindale (1999a). Larvae through stage L4 were photographed using DIC (differential interference contrast) optics on a Zeiss Axioplan microscope. Later stages were imaged on a Wild M8 stereo microscope using an Optronics DI-750 3-chip CCD camera and digitized with a PDI frame grabber on a Macintosh computer.

Staining and sectioning. Larvae were fixed in 4% formaldehyde in filtered artificial seawater for 30 min., washed, and stored in PTw (phosphate buffered saline + 0.1% Tween-20) at 4°C. They were dehydrated in a 25%, 50%, 70%, and 90% ethanol series and embedded in JB-4 medium (Polysciences) in accordance with the manufacturer's instructions. During the dehydration, some of the animals were stained with 1% alcian blue in 70% ethanol for 20–30 min. Serial sections (4 μm thick) were cut on a Sorvall MT2-B ultramicrotome using diamond knives. Sections were stained with Harris's hematoxylin and 0.1% eosin Y and mounted in 70% glycerol.

β-tubulin RNA probe. A 780-bp fragment of the *β-tubulin* gene was amplified by polymerase chain reaction using degenerate oligonucleotide primers from a larval *Chaetopterus sp.* cDNA library (details available on request). Two primers were used:

b-tub.for: 5′-TGGGCNAARGGNCAYTA
b-tub.rev: 5′-ATNCCYTCNCCNGTRTAC

Amplicon termini were prepared for cloning with T4 DNA polymerase and T4 polynucleotide kinase (New England Biolabs) and ligated into pMOB vector cut with SmaI. The resulting ligation was transformed into *E. coli* by electroporation and sequenced on both strands. The DNA sequence has been deposited in GenBank under accession number AF140551. Sense and antisense digoxygenin-labeled riboprobes were transcribed from the plasmid template using the MegaScript kit (Ambion) according to the manufacturer's instructions, except for nucleotide concentrations. These were 7.5 m*M* GTP, ATP, and CTP, 6.35 m*M* unlabeled UTP, and 1.15 m*M* digoxygenin-11-UTP (Boehringer-Mannheim).

In situ *hybridization.* A detailed protocol is available on request—the following is a brief description of our procedure. Larvae were fixed for 20 min in buffered 4% formaldehyde at 50°C and prepared for hybridization by treatment with chitinase and acetic anhydride. The specimens were then incubated in a detergent solution (1% sodium dodecyl sulfate (SDS); 0.5% Tween-20; 50 m*M* Tris-HCl, pH 7.5; 1 m*M* EDTA, pH 8; 150 m*M* NaCl) for 1 h. Hybridization was done overnight at 65°–69°C with 0.1 μg/ml of digoxygenin-labeled probe in RNA-Hybe buffer (50% formamide; 5× saline sodium citrate, pH 4.5; 1% SDS; 0.1% Tween-20; 50 μg/ml heparin; 50 μg/ml yeast tRNA, 100 μg/ml sonicated salmon sperm DNA). The washed larvae were incubated in alkaline phosphatase conjugated sheep anti-digoxygenin Fab antibody (Boehringer-Mannheim), and the hybridization signal was developed with B-M purple chromogenic substrate (Boehringer-Mannheim), postfixed in 4% formaldehyde for 15 min, and cleared in 70% glycerol.

Results

Adult body plan

The adult worm consists of three functionally distinct body regions called, from anterior to posterior, regions A, B, and C (Crossland, 1904; Bhaud *et al.*, 1994) (Fig. 1). Region A is composed of the morphologically fused presegmental prostomium and peristomium along with the first nine setigers (A1–A9). A setiger is a body segment bearing setae (sometimes spelled *chaetae*). The prostomium bears

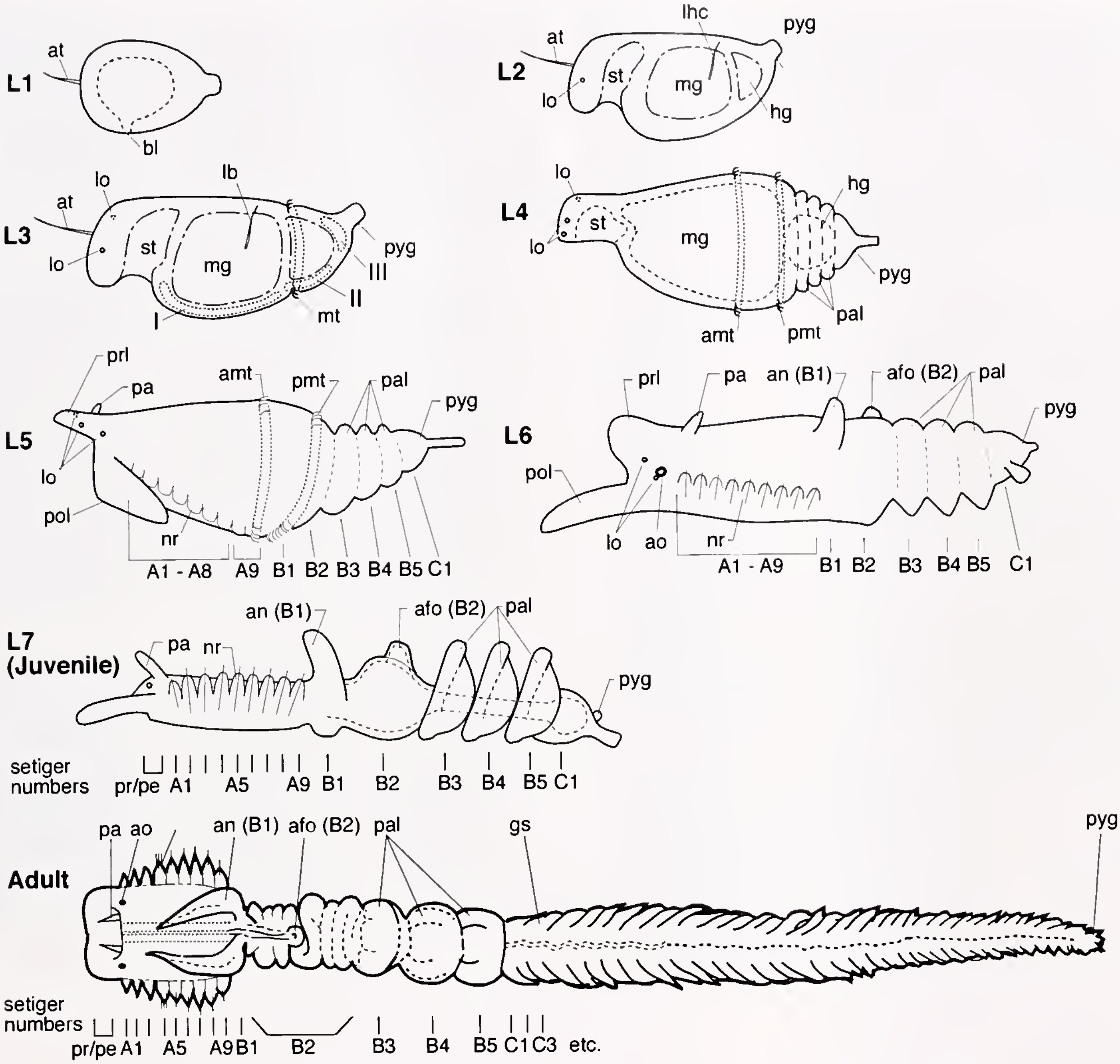
L1
at
bl
L2
at
lhc
pyg
st
mg
lo
hg
L3
at
lo
lb
st
mg
lo
pyg
III
II
I
mt
L4
lo
hg
st
mg
lo
pyg
pal
amt
pmt
L5
prl
pa
amt
pmt
pal
pyg
lo
pol
nr
A1 - A8
A9
B1
B2
B3
B4
B5
C1
L6
prl
pa
an (B1)
afo (B2)
pal
pyg
pol
lo
ao
nr
A1 - A9
B1
B2
B3
B4
B5
C1
L7 (Juvenile)
an (B1)
afo (B2)
pal
pa
nr
pyg
setiger numbers
pr/pe
A1
A5
A9
B1
B2
B3
B4
B5
C1
Adult
pa
ao
an (B1)
afo (B2)
pal
gs
pyg
setiger numbers
pr/pe
A1
A5
A9
B1
B2
B3
B4
B5
C1
C3
etc.

Figure 1. Diagrammatic views of *Chaetopterus* from larval stage L1 through adult, showing relationships between larval and adult structures. Larvae are in lateral view with anterior to the left and ventral towards the bottom of the page; the adult is in dorsal view, anterior to the left. The setiger numbering scheme is correlated below the drawings of stages L5, L6, L7, and the adult. Setiger numbering scheme follows Crossland (1904) and Bhaud *et al.* (1994). I, II, III, anterior, middle, and posterior larval trunk coeloms respectively; afo, accessory feeding organ; amt, anterior mesotroch; an, aliform notopodium; ao, adult ocellus; at, apical tuft; bl, blastopore; gs, gametogenic segments; hg, hindgut; lb, lateral bristle; lhc, lateral hooked cilia; lo, larval ocellus; mg, midgut; mt, mesotroch; nr, notopodial rudiment; pa, palp; pal, palette; pmt, posterior mesotroch; pyg, pygidium.

one pair of lateral ocelli, and the peristomium has a pair of small grooved palps. The setigerous region of region A is flattened dorsoventrally and bears only notopodia—except for setiger A9, which also has neuropodial uncini. Notopodia and neuropodia are the dorsal and ventral rami, respectively, of the parapodia. The notopodium of setiger A4 is modified and bears a bundle of dark spines, although this morphology did not appear in the postmetamorphic stages examined in this study. The slightly convex muscular ventral surface of region A is termed the *plastron*.

The middle tagma, region B, has five specialized segments that enable the peculiar suspension-feeding behavior.

Setiger B1 has dorsally extended aliform notopodia, which secrete and support a mucous net. This net is gathered by the accessory feeding organ of setiger B2, which is located dorsal to a convoluted portion of the gut. From this organ, a ciliated groove on the dorsal midline carries food particles anteriorly to the mouth. Setiger B2 is much longer than other segments, but derives from a single larval segment, as demonstrated below. The posterior three segments of this region consist of highly modified neuropodia forming fans termed *palettes* that pump water through the animal's tube by a metachronal, rhythmic movement (MacGinitie, 1939; Barnes, 1965). Each of the five segments in this middle region has a neuropodial torus bearing uncinal plates. Tori are flattened ridgelike parapodia, and uncini are dentate deeply imbedded setae with platelike bases (Fauchald, 1977).

The posterior tagma (region C) has an indeterminate number of gametogenic segments of a uniform morphology, tapering in size towards the posterior. Each segment bears a crescent-shaped notopodium and bilobed neuropodium. The small pygidium bears two pairs of cirri surrounding the anus.

Larval stages

The following stage-numbering system begins with the earliest pelagic larva. Although embryonic development prior to gastrulation and production of the swimming larva have been described (Malakhov, 1984; Henry, 1986), no complete staging scheme has been previously devised for *Chaetopterus* larvae. Developmental times are postfertilization ages based on laboratory culture at room temperature of 21°–23°C. Sizes listed are in micrometers, anterior-posterior length (excluding apical tuft and posterior papilla) by maximum lateral width (excluding setae). The numbering of segments is as shown in Figure 1.

Stage L1—18–36 hours (Fig. 2a):
Protrochophore
Size: 125 × 100 μm
Ciliary structures: apical tuft present; one pair of lateral hooked cilia; trochal band absent
Ocelli: absent
References: Henry (1986) fig. 3a; Cazaux (1965) plt. 1, fig. 4

The initial swimming gastrula, or protrochophore, is completely ciliated but lacks any trochal band. An apical cilia tuft about 50 μm in length is present. The gut has not achieved its functional form and is still filled with the progeny of the yolky macromeres. A bilateral pair of tufts of diffuse hooked cilia, termed *lateral hooked cilia* (Henry, 1986), form during this stage. At no time is a prototroch typical of early polychaete trochophore larvae formed (Henry, 1986; Eckberg and Hill, 1996).

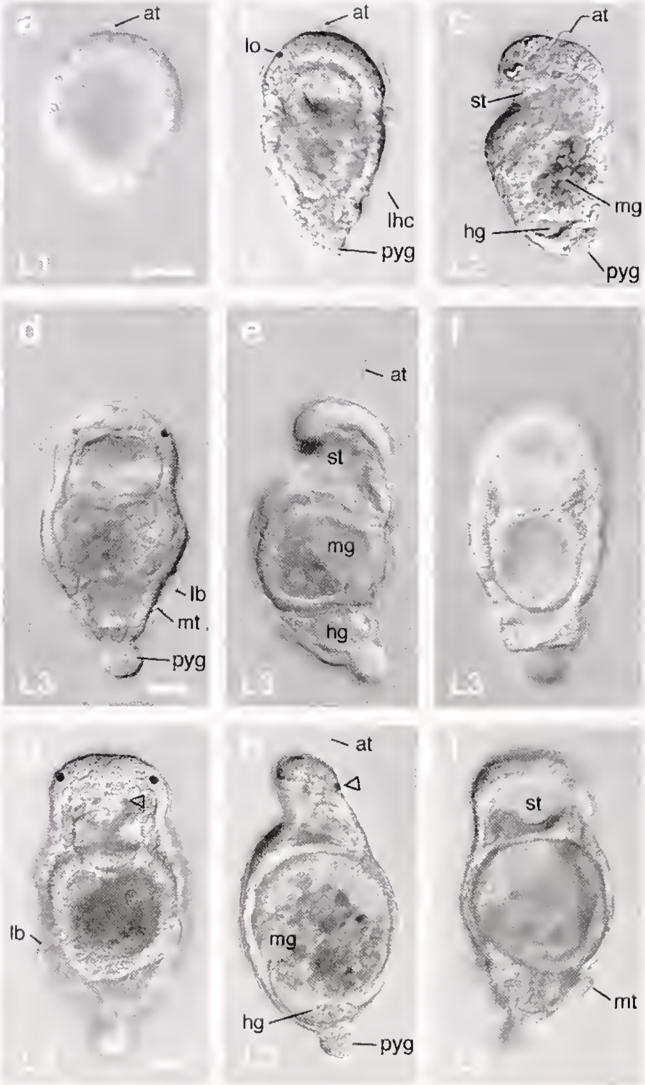

Figure 2. Larvae, stages L1 through L3. Anterior is toward the top of the page in all plates, unless noted. (a) Stage L1 protrochophore at 24 h. (b, c) Stage L2 metatrochophores at 48 h in ventral and left-lateral views respectively. (d–f) Early stage L3 larvae at 4 days in dorsal, lateral, and ventral views respectively. (g–i) Late stage L3 larvae at 18 days in dorsal, left-lateral, and ventral views respectively. Medial pair of eyes is slightly out of focus in (g) and at dorsal surface in (h) (open arrowheads). Unicellular ingested algae are visible in the midgut at all stages. at, apical tuft; hg, hindgut; lb, lateral bristle; lhc, lateral hooked cilia; lo, larval ocellus; mg, midgut; mt, metatroch; pyg, pygidium; st, stomodeum. Scale bars are 50 μm.

Stage L2—36–72 hours (Fig. 2b–e):
Metatrochophore
Size: 180 × 90 μm
Ciliary structures: apical tuft present; one pair of lateral bristles form; trochal band absent

Ocelli: 2; one lateral pair

References: Henry (1986) fig. 3b–c; Bonch-Bruevich and Malakhov (1987) fig. 1

By this stage gastrulation is complete, forming a tripartite gut. A ventrally opening ciliated stomodeum is visible anteriorly. The more medial stomach occupies about half the volume of the larva, and a much smaller intestine is located just anterior to the pygidium. The anus opens dorsally. The gut is functional at this time, as evidenced by algal particles in the stomach. A pair of stiff lateral hooked bristles, composed of hooked cilia, take the place of the lateral hooked cilia (Henry, 1986). A distinct trochal band is not present at this stage.

Stage L3—3–30 days (Fig. 2d–i):

Size: 180–320 × 90–180 μm

Ciliary structures: apical tuft present; mesotroch present; lateral bristles persist

Ocelli: early: 2; one lateral pair; late: 4; one lateral pair and one medial pair

References: early: Cazaux (1965) plt. 2, fig. 5; late: Cazaux (1965) plt. 3, fig. 6; Enders (1909) plt. II, fig. 9

Early period, 3–10 days. In this period the relative size of the stomach enlarges to occupy most of the larva. A more distinct pygidial papilla forms. A distinct trochal band is first visible at the level of the intestine, here referred to as a *mesotroch*, following the terminology of Okada (1957). The lateral bristles of Stage L2 persist.

In histological sections the neuropil of the cerebral ganglion is visible anterior and dorsal to the stomodeal opening (Fig. 3a, b). At this stage other neural tissues were not visible in section, although a ventral nerve network has been reported in slightly younger specimens examined with transmission electron microscopy (Bonch-Bruevich and Malakhov, 1987). The stomodeum itself has three dorsal diverticulae and opens to the stomach through a pharyngeal valve in the midposterior floor of the stomodeal cavity (Fig. 3b). The midgut endoderm consists of relatively large cells, especially at the anteroventral side, whereas the endoderm of the intestine forms a much thinner epithelium. The anus opens from the intestine dorsally, just anterior to the pygidium (not shown).

Mesoderm-lined coelomic compartments are visible anterior to the stomodeum and along the ventral midgut and hindgut (Fig. 3a, b). These observations are consistent with those of Bonch-Bruevich and Malakhov (1987), who report one unpaired preoral coelom and three pairs of trunk coeloms, although we were unable to locate with certainty the boundaries between the trunk cavities.

Identifiable cell types present at this stage include neurons, secretory digestive cells, trochoblasts, and muscle

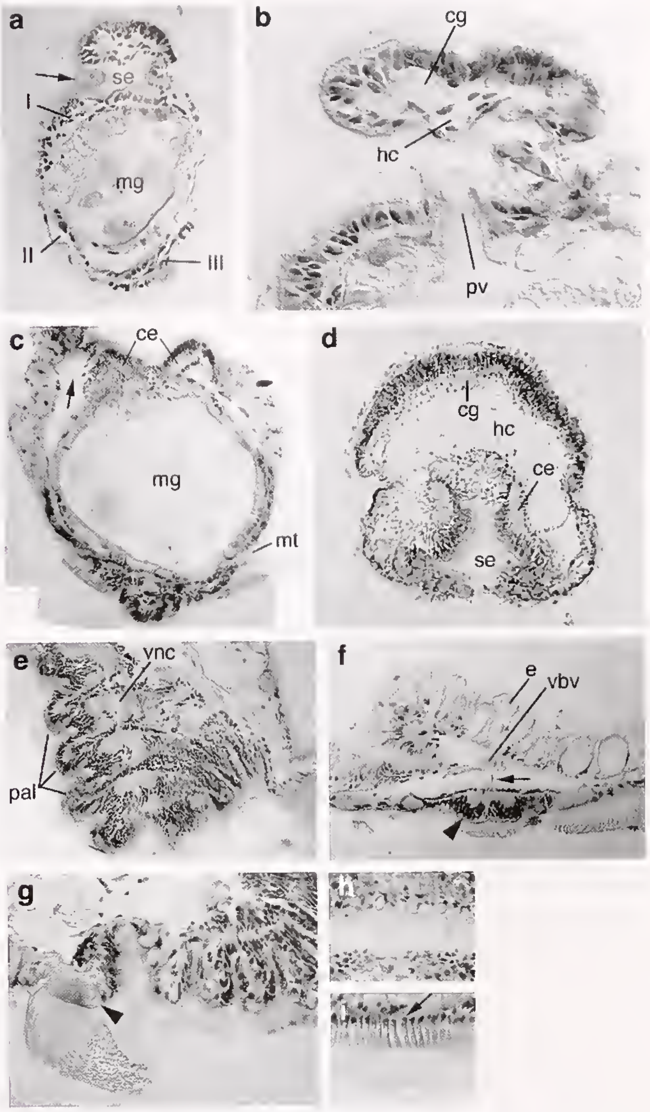

Figure 3. Semithin plastic sections of stages L3 and L4 larvae stained with hematoxylin, eosin, and alcian blue. (a) Early stage L3 larva in sagittal section; ventral is to the left and anterior toward the top of the page, unless noted. Arrow points to algal particle entering stomodeum. Roman numerals denote locations of three trunk coelomic spaces. (b) Higher magnification view of same stage larva as in (a). (c) Oblique frontal section of a late stage L3 larva. Arrow points to an anterior septum dividing one of the region A segments. (d) Oblique transverse section through head of stage L4 larva with dorsal side up. (e) Frontal section through palette rudiments (segments B2–B5). (f) High-magnification view of transverse section through ventral body wall of stage L4 larva midway between the mouth and anterior mesotroch. Arrowhead points to the ventral nerve cord. Arrow indicates the ventral mesentery. (g) Transverse section, with anterior to the left, through posterior metatroch (setiger B2) and palette rudiments (setigers B3–B5). Arrowhead points to trochal cell. (h, i) Sections through trochal bands at stage L4 tangential to body wall. Arrow points to line of basolateral trochal cell nuclei. ce, circumesophogeal connective; cg, neuropil of cerebral ganglion; e, endodermal cell of the midgut; hc, head coelom; mg, midgut; mt, mesotroch; pal, pallette rudiment; pv, pharyngeal valve; se, stomodeum; vbv, ventral blood vessel; vnc, neuropil of ventral nerve cord.

cells. Also visible are light-emitting photocytes ventrolateral to the intestine; these, described by Henry (1989), are functional by stage L2. Staining with alcian blue (not shown) reveals large mucosal cells dorsal and lateral to the stomodeum.

Late period, 11–30 days. This period is morphologically similar to the preceding, the most obvious difference being the addition of a pair of dorsomedial eyes. The stomach becomes still larger relative to the overall body, and the mesotroch widens with it. The pygidial papilla becomes longer and more distinct. The apical tuft is still present along with the lateral bristles, both of which are lost by the end of this stage. These observations correlate well with previous descriptions (Enders, 1909; Cazaux, 1965).

In situ hybridization with a *β-tubulin* riboprobe reveals cells with extensive ciliation in the apical tuft, stomodeum, and mesotroch (Fig. 4a). However, at this stage our probe does not reveal neural elements.

Stage L4—30–60 days (Fig. 5a, b):
Size: approx. mean 600 × 400 μm
Ciliary structures: apical tuft lost; two mesotrochs
Ocelli: 6; 2 pairs lateral, 1 pair medial
References: Cazaux (1965) plt. 4, figs. 7–8; Enders (1909) plt. II, fig. 10

Two major changes from stage L3 are evident in this stage. The first is the appearance of a second trochal band just anterior to the existing mesotroch. The second change is the advent of overt segmentation in the region between the posterior mesotroch and the pygidium. Three distinct annular bulges are visible in this region; as becomes evident in later stages, these are rudiments of setigers B3–B5. The segmental anlage of the anterior 11 setigers are not apparent by visual inspection, but the prospective cell populations of the parapodia are present. This was shown by staining with an anti-Distal-less antibody that recognizes the prospective apical cells of body wall outgrowths (refer to Panganiban *et al.*, 1997). The basic structure of the gut present from stage L2 persists, with the intestine occupying the postmesotrochal segmented region. A second pair of lateral ocelli develop at this stage, making a total of six ocelli in three bilateral pairs.

The central nervous system now has the basic components of the juvenile. The cerebral ganglion forms a disk just beneath the most rostral epidermis (Fig. 3d). The circumesophogeal connectives flank the stomodeum (Fig. 3c, d) and join in the ventral midline at the anterior midgut level (Fig. 3f). The ventral nerve cord (VNC) remains paired as it travels toward the posterior, with numerous commissures connecting the bilateral segmental ganglia. In the overtly segmented posterior region (setigers B3–B5), distinct paired segmental ganglia are visible (Fig. 3e). Late in this stage the two hemilateral cords of the VNC diverge anterior to the mesotrochs. This splitting of the paired nerve cords results in the adult arrangement of the CNS: laterally placed nerve cords in setigers A1–A11 join at setiger B1 and run at the ventral midline more posteriorly (Martin and Anctil, 1984). The lateral divergence of the anterior nerve cord is visible in

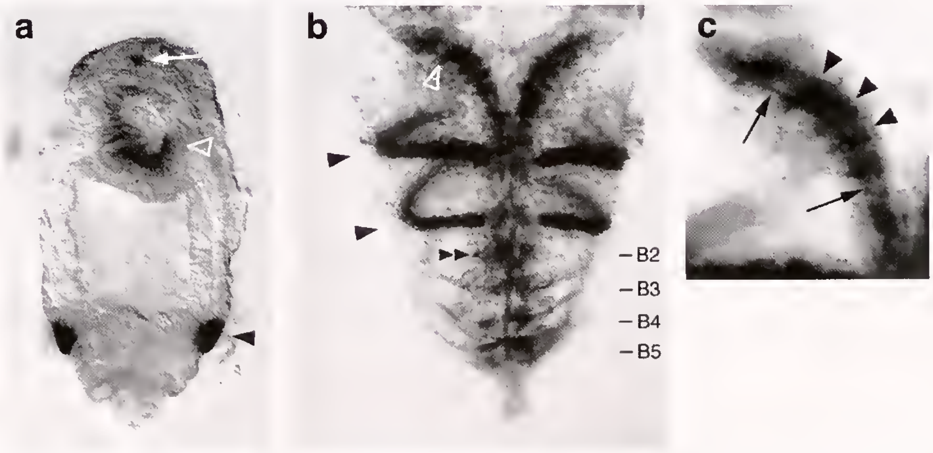

Figure 4. Whole mount *in situ* hybridization to a digoxygenin-labeled antisense *β-tubulin* riboprobe. Anterior is toward the top of the page in each view. (a) Stage L3 larva viewed from the ventral side in optical section. Staining is visible at the base of the apical tuft (arrow), around the posterior stomodeum (open arrowhead), and in the trochoblasts of the mesotroch (arrowhead). (b) Ventral view of a stage L4 larva. The dorsal body wall and head have been dissected open for photography. Strong staining is seen in the trochoblasts of both mesotrochs (arrowheads), and in the anterior (open arrowhead) and posterior (double arrowhead) ventral nerve cord. Setiger numbers of posterior ganglia are labeled on the right. (c) Higher magnification view of anterior ventral nerve cord. The axon tract of the nerve cord (arrows) is visible just subjacent to serially iterated blocks of staining ectodermal cells (arrowheads).

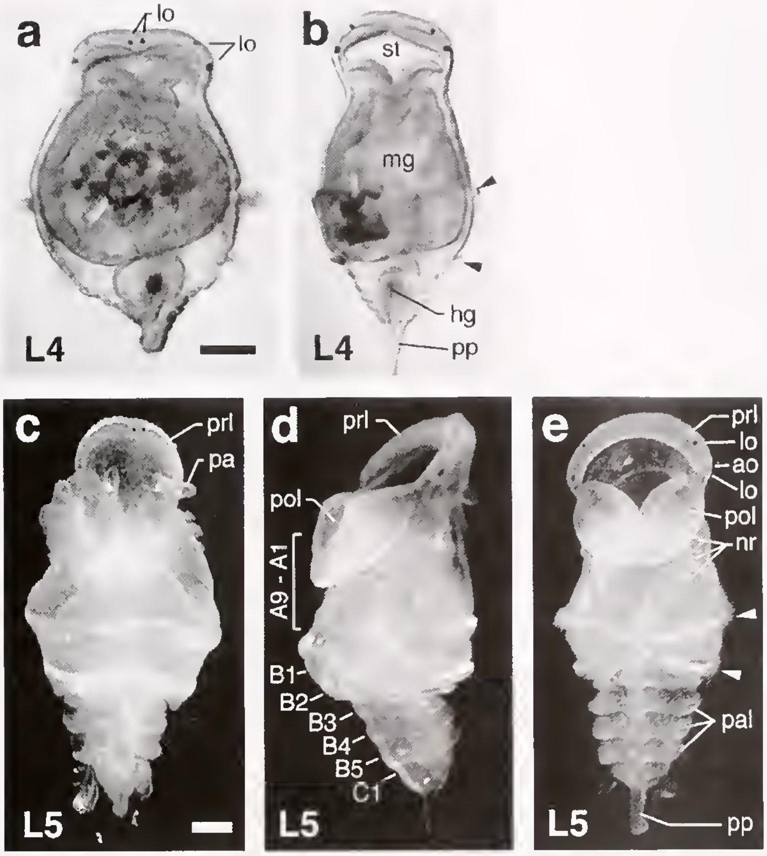

Figure 5. Larvae, stages L4 and L5. Anterior and posterior mesotrochs are marked by arrowheads. (a, b) Stage L4 larvae at 30 days in dorsal and ventral views. (c–e) Stage L5 larvae at 60 days in dorsal, lateral, and ventral views respectively. The locations of adult setiger rudiments are labeled in (d). Note the appearance of the red adult ocelli, visible in (e) along with the persistent larval ocelli. ao, adult ocellus; hg, hindgut; lo, larval ocellus; mg, midgut; nr, notopodial rudiment of setigers A1–A9; pa, palp rudiment; pal, palette rudiment of setigers B3–B5; pol, post-oral lobe; pp, papilla; prl, pre-oral lobe; st, stomodeum. Scale bars are 100 μm.

the expression pattern of β-*tubulin* visualized by *in situ* hybridization (Fig. 4b, c). The fact that *in situ* hybridization to β-*tubulin* transcripts failed to detect a distinct VNC prior to this stage suggests that the VNC had not yet formed.

Segmental boundaries are not distinguishable, by conventional microscopy, anterior to the mesotrochs in any tissue. However, *in situ* hybridization to β-*tubulin* transcripts reveals that reiterated ganglionic cell populations, presumably segmental, are present at this stage (Fig. 4b, c). Bilateral ganglionic cell populations are also visible in the overtly segmented anlagen of setigers B2–B5 (Fig. 4b).

Capacious coelomic cavities with distinct septa surround the larval foregut, as seen in frontal section (Fig. 3c). Transverse sections at the middle of the larva reveal bilateral coelomic cavities, separated by a ventral mesentery, medial to the nerve cord. Between these cavities and the gut, the ventral blood vessel is located at the midline (Fig. 3f).

A particularly distinctive cell type is that of the ciliated cells of the trochal bands. These are large prismatic cells with a uniform granular cytoplasm (Fig. 3g). They are extended along the anterior-posterior axis, and packed regularly in a continuous circumferential ring (Fig. 3h). The cell nuclei are positioned at the basilateral ends of the cells (Fig. 3i).

Stage L5—approx. 60 days (Fig. 5c–e):
Competent to metamorphose
Size: approx. mean 800 × 400 μm
Ciliary structures: apical tuft absent; two mesotrochs
Ocelli: 8; 4 lateral, 2 medial, 2 lateral adult ocelli
References: Cazaux (1965) plt. 5, fig. 10; Enders (1909) plt. II, figs. 11–12

At this stage larvae are competent to metamorphose—in fact, we observed one specimen from this stage that had reached late stage L7 within 6 h after transfer from mass culture to a petri dish with fresh seawater. Specimens from this stage routinely passed completely through metamorphosis overnight, indicating that the rudiments of all juvenile structures are present.

As compared with stage L4, the postoral lobe grows disproportionately with respect to the preoral lobe and folds towards the posterior. Many eosin-reactive secretory cells are visible in section in the epidermis of this organ (Fig. 6b). Appearing at this stage are visible palp and anterior parapodial rudiments. A pair of red adult ocelli appear at the most lateral margin of the preoral lobe. The smaller dark larval ocelli remain throughout the stage. In section, the setal sacs and septation of segments A1–A9 are apparent (Fig. 6a, b). The epidermis in the region of prospective setigers B2–B5 develops deeper infolding, creating distinct annuli anchored at the ventral midline (Figs. 3g, 6b). However, the region around the two mesotrochs has yet to exhibit any segmental character visible either in the exterior morphology or in section. A pair of lateral outgrowths emerge just anterior to the pygidium, which Enders (1909) identifies as the notopodia of segment C1. These bear stout setal sacs (not shown). Based on the locations of ganglia in the B and C regions and the developing parapodia of the A region, it is possible to locate the primordia of the first 15 adult setigers at this stage (Fig. 5d). The identity of the posterior mesotroch with the aliform notopodia of setiger B1 can be inferred from Hox gene expression patterns (Irvine, 1998; Irvine and Martindale, 1999b). Ironically, the longest adult segment, B2, forms from the shortest, most cryptic of the larval setigers.

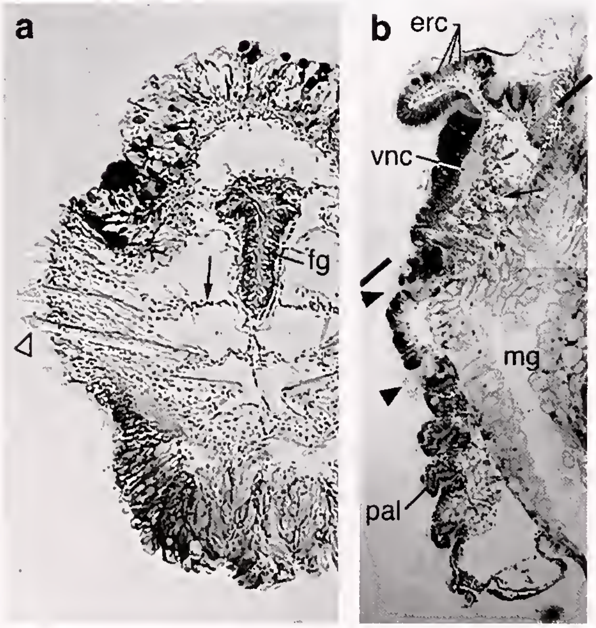

Figure 6. Semithin sections of stage L5 larvae stained as in Figure 7. (a) Oblique transverse section through region A. Dorsal is towards the top of the page. Open arrowhead points to a typical anterior seta. Arrow points to an anterior septum. (b) Parasagittal section with ventral to the left and anterior up, cutting through several anterior setal sacs (arrow) and both mesotrochs (arrowheads). Bars denote approximate plane of section shown in (a). erc, eosin-reactive cells; fg, foregut; mg, midgut; pal, palette rudiment of setiger B2; vnc, axon tract of ventral nerve cord.

The hemilateral cords of the anterior ventral nerve cord have continued to diverge from the ventral midline to approach the ladderlike form of the adult nervous system in setigers A1–A9 (Martin and Anctil, 1984). The basic structure of the nervous system more posteriorly persists, as described for stage L4.

Stage L6—approx. 60 days (Fig. 7a–d):
Mid-metamorphosis
Size: 1–2 mm
Ciliary structures: apical tuft absent; two mesotrochs
Ocelli: 8: 4 lateral, 2 medial, 2 lateral adult ocelli
References: Cazaux (1965) plt. 5, fig. 10; Enders (1909) plt. 11, figs. 11–12

This transitory stage is characterized by the transformation of larval to adult structures (Fig. 1). The prostomium and peristomium form by the retraction of the preoral lobe and the folding rostrally of the postoral lobe. The pair of dorsomedial ocelli disappear during this stage (compare Fig. 7a and 7c). The two larval pairs of lateral ocelli persist, with the adult ocelli roughly coincident with the most ventrolateral pair of larval ocelli. The parapodial rudiments of setigers A1–A9 emerge laterally, correlated with a dorsoventral flattening of region A. The anterior mesotroch degenerates, and the posterior mesotroch becomes incorporated into the aliform notopodia of segment B1, which appear dorsolaterally. This fate is confirmed by *in situ* hybridization to Hox segmental markers (Irvine, 1998; Irvine and Martindale, 1999b). Just caudally, the digestive and accessory feeding organs of setiger B2 appear along the dorsal surface with a swelling of this portion of the larva. The three annular bulges evident at stage L4 expand to take on the shape of the palettes of segments B3–B5. The notopodia of segment C1 continue to project ventrolaterally.

Stage L7—approx. 60 days (Fig. 8a–b):
Juvenile
Size: 2–3 mm
Ocelli: 2 lateral adult ocelli (2 pairs of larval ocelli degenerate)
References: Cazaux (1965) plt. 6, figs. 11–14

At the completion of metamorphosis, the juvenile worm has taken on the general form of the adult for the head and anterior 15 setigers. The most conspicuous change from stage L6 is the extreme extension of the body axis from setigers B1–B5. In addition, the aliform notopodia in setiger B2, the accessory feeding organ in setiger B2, and the palettes in setigers B3–B5 all extend out from the body wall and assume their adult form. The remaining two pairs of larval ocelli degenerate, leaving the larger red adult ocelli. The remainder of the roughly 40 abdominal gametogenic

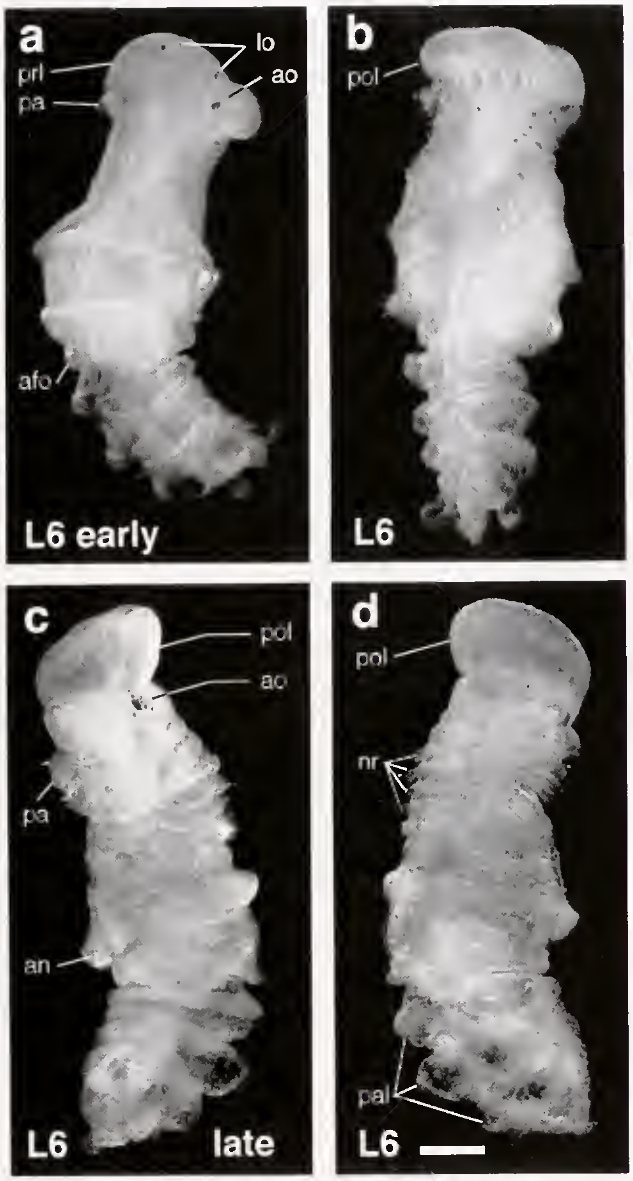

Figure 7. Stage L6 larvae. (a, b) Early stage L6 larva in dorsolateral and ventrolateral views. (c, d) Late stage L6 larva in dorsolateral and ventrolateral views. Note the rotation of the postoral lobe to an anterior-facing direction in comparison with the orientation at stage L5. afo, accessory feeding organ rudiment; an, aliform notopodium rudiment; ao, adult ocellus; lo, larval ocellus; nr, notopodial rudiment of setigers A1–A9; pa, palp rudiment; pal, palette rudiment of setigers B3–B5; pol, postoral lobe; prl, preoral lobe. Scale bar is 100 μm.

segments have yet to be produced. This occurs by interpolation between setiger C1 and the pygidium (Cazaux, 1965).

Tube construction was never observed in these cultures. This is probably because that substrate was never provided, the stage L7 juveniles always being kept in glass or plastic vessels without mud or sand (Irvine and Martindale, 1999a).

Discussion

Developmental variation within the genus Chaetopterus

The genus *Chaetopterus* has several species that show variation in overall adult size, tube morphology, and details of parapodial and setal form. Published descriptions of *Chaetopterus* development differ from our results in some respects. Cazaux's (1965) figure 5 is a drawing of a 48-h larva corresponding in part to our observations. However, our cultures and those described in Henry (1986) do not reach the general morphology depicted until at least 72 h, despite higher culture temperatures. Four other differences are apparent between our results and those in figure 5 of Cazaux (1965): (i) we do not detect trochal bands around the stomodeum; (ii) a distinct intestine is visible, rather than the extension of the posterior stomach shown; (iii) the mesotroch is more posterior in our preparations; (iv) only one pair of laterally placed eyes are visible rather than the two pairs depicted. Since Cazaux's specimens came from the Atlantic coast of France, he may have been observing another species of *Chaetopterus*—neither *C. variopedatus* Renier, 1804, nor *C. variopedatus sensu* Enders, 1909, but possibly *C. valencinii* Quatrefages, 1866 (M. E. Petersen, Copenhagen Museum, pers. comm).

Trochal bands

As mentioned, a circumferential ciliary band appears midway along the anterior-posterior body axis at Stage L3; following Okada (1957), we have termed this band a mesotroch. At Stage L4 another trochal band, which we also call a mesotroch, forms just anterior to the first band. Rouse (1999) characterizes this younger band as a metatroch, following early work of Wilson (1882) that depicts a larva resembling our Stage L3. However, tracing the fate of both these trochal bands ahead in ontogeny reveals that they come to lie well within the segmented trunk of the larva, contrary to the definition of a metatroch as a presegmental structure lying on the peristomium (Rouse, 1999). Thus, rather than a metatroch having evolved within the Chaetopteridae lineage, as concluded in the transformations of the Rouse (1999) analysis, a different type of trochal band arose, not strictly homologous to a metatroch.

Although the *Chaetopterus* mesotrochal bands are not metatrochs, as defined above, they may be homologous to other types of trochal bands at the level of their developmental pathway. Rouse's (1999) analysis indicates that the various types of larval trochal bands can appear and be lost independently in different lineages; *i.e.*, as characters they exhibit a high degree of homoplasy. This finding suggests that trochal bands share a developmental pathway that can be activated at various levels along the anterior-posterior axis.

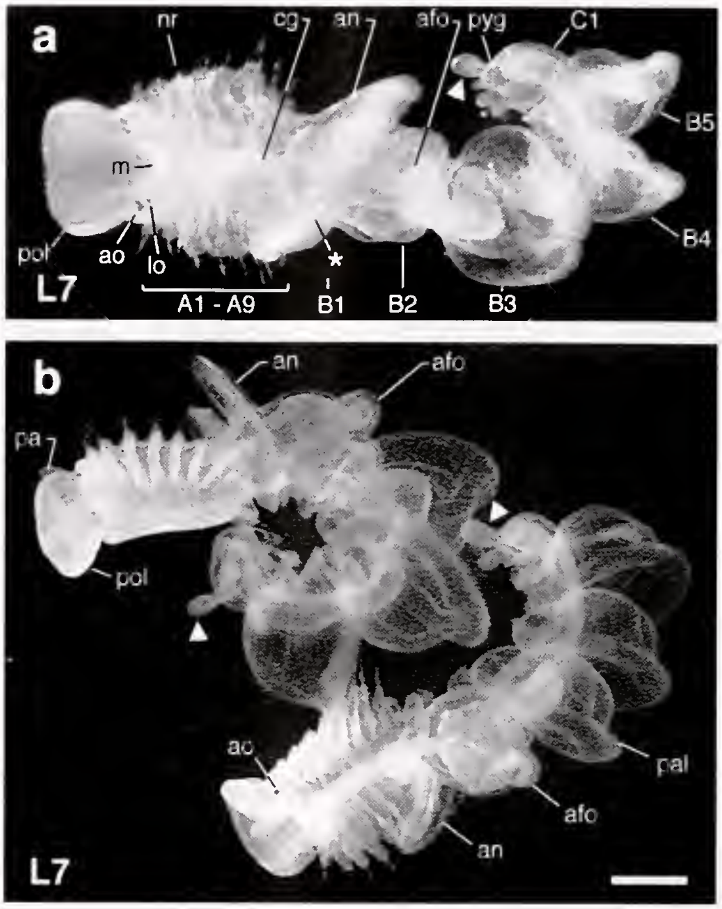

Figure 8. Juvenile worms within 1 day of metamorphosis at about 60 days. Anterior is to the left. (a) Dorsal view. Letters and numbers indicate adult setiger locations. Asterisk denotes the ciliary groove of the aliform notopodium of setiger B1, derived from the posterior mesotroch. Arrowhead points to a parapodium of the first 'abdominal' setiger C1. (b) Two newly metamorphosed specimens. Upper specimen is in ventrolateral view and lower is in dorsolateral view. Arrowheads as in (a) above. afo, accessory feeding organ rudiment; an, aliform notopodium rudiment; ao, adult ocellus; cg, ciliated groove; lo, larval ocellus; m, mouth; nr, notopodial rudiment of setigers A1–A9; pa, palp rudiment; pal, palette rudiment of setigers B3–B5; pol, postoral lobe; pyg, pygidium. Scale bar is 100 μm.

Larval segmentation and relationship to adult body plan

The most commonly described form of larval development in polychaetes is the production of a trochophore larva that adds segments sequentially from a posterior growth zone to produce a nectochaete larva (Okada, 1957; Anderson, 1966). There is some controversy over whether the first three larval segments develop in the same sequential manner as subsequent segments, but in typical cases the demarcation of each of the segmental boundaries is evident in the external form of the larva from a very early stage. *Chaetopterus* represents a distinct departure from this general pattern. The first external signs of segmentation are the rudiments of segments B3–B5 visible at stage L4, at an age of 30 days. At no point does the metatrochophore take on the overtly segmented form of the typical nectochaete larva. However, some incipient segmentation is present before it becomes visible externally. Bonch-Bruevich and Malakhov (1987) describe three trunk coeloms existing at stage L2, which is consistent with our stage L3 sections (Fig. 3a). If we use the trochal bands as landmarks, the anterior trunk coelom ('I' in Fig. 1 stage L3) roughly corresponds with the position of adult segments A1–A9, the middle coelom ('II') with segment B1 or segments B1 and B2, and the posterior coelom ('III') with juvenile segments B3–B5. By stage L4 the segmental character of the ventral nerve ganglia is apparent in *β-tubulin* expression, even though no segmental divisions are visible by conventional microscopy (Fig. 4b, c). Expression of Distal-less protein also reveals segmentally iterated structures, the parapodia of setigers A1–A9, at stage L4, before they are evident morphologically (Panganiban *et al.*, 1997). Our observations never give the impression that these segmental rudiments are produced sequentially, anterior to posterior, from a mesodermal band or bands.

We propose the hypothesis, supported by all the existing data from this and other studies, that the anterior 15 segments in *Chaetopterus* are formed by subdivision of existing anlage, rather than by sequential addition from a growth zone. The segments B1–B5 are formed first, at stage L4, by subdivision of the stage L3 coeloms II and III. Segments A1–A9 form later, at stage L5, by subdivision of the stage L3 coelom I. This hypothesis does not rule out the production of the segmented body elements from a teloblastic growth zone, but does temporally dissociate the production of those elements from their morphogenesis as discrete segmental structures. Other recent work has shown that Hox gene expression begins as early as stage L2 in the putative growth zone (Irvine, 1998; Irvine and Martindale, 1999b; Kevin J. Peterson, pers. comm.). If the Hox genes are acting as segmental specification genes at this stage, this early onset of expression suggests that the delay in the appearance of overt segmentation in *Chaetopterus* is the result of a lengthening of the period between molecular specification of segments and their morphogenesis. Testing the accuracy of this model will require more extensive analysis of intervening stages, possibly using histological sections or cell-labeling techniques.

Even if the correlation of early larval structures with their final segmental products differs from what we have proposed, the timing and nature of segmental differentiation in *Chaetopterus* remain highly diverged relative to the patterns seen in related polychaete families. This is not surprising given the extreme level of adult body plan divergence. What is remarkable is how far back into larval development the changes in segment formation extend.

Phylogenetic position and larval evolution

A consideration of the phylogenetic position of *Chaetopterus* within the Polychaeta can give some insight into the probable ancestral larval form and the evolutionary changes that must have taken place to result in the animal described here. The family Chaetopteridae has generally been allied to the spionid families (Dales, 1962; Fauchald, 1977), to the sabellids, or to both (Fitzhugh, 1989). A cladistic analysis of polychaete relationships by Rouse and Fauchald (1997) presents two alternatives for the position of the Chaetopteridae, depending on the method used to code character states. In the first case (Fig. 9a), which uses presence/absence coding, initial weighting of characters by their dependence on other characters, and sequential weighting based on consistency index, the Chaetopteridae are a sister group to the traditional spionid families (Spionidae, Apistobranchidae, Trochochaetidae, Longosomatidae, Magelonidae, and Poecilochaetidae). This is the topology favored by Rouse and Fauchald, who include the Chaetopteridae in a clade called the Spionida (figs. 70 and 73 in Rouse and Fauchald, 1997). (Examination of other members of the Chaetopteridae, such as *Spiochaetopterus* [Bhaud *et al.*, 1994], makes the spionid connection very clear.) On the other hand, when multi-state characters are used (fig. 71 in Rouse and Fauchald, 1997), the parsimony analysis results in the Chaetopteridae being a sister group to the sabellid families and pogonophorans (Frenulata, Vestimentifera, Sabellariidae, Sabellidae, and Serpulidae; collec-

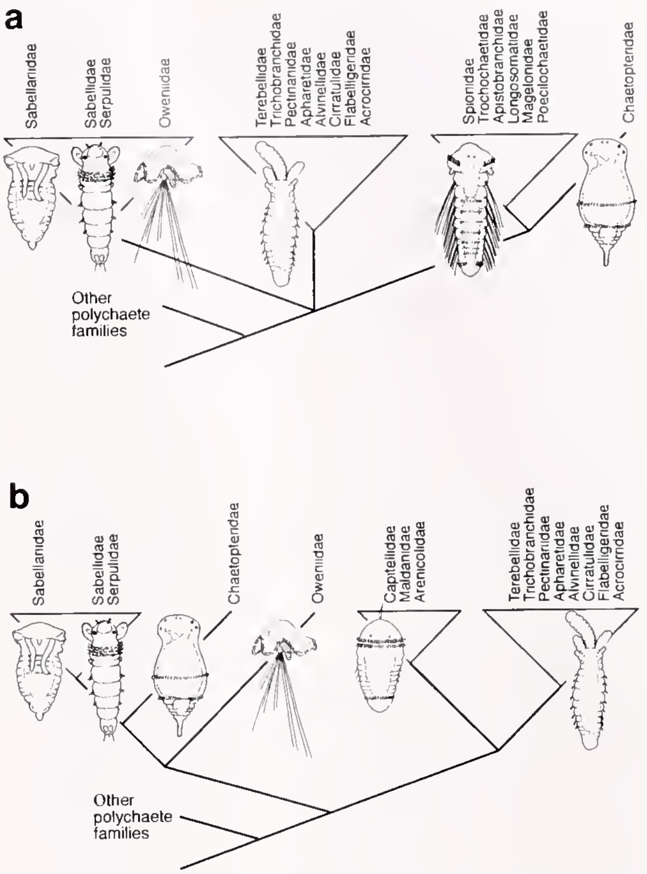
a
Sabellariidae
Sabellidae
Serpulidae
Oweniidae
Terebellidae
Trichobranchidae
Pectinariidae
Apharetidae
Alvinellidae
Cirratulidae
Flabelligeridae
Acrocirridae
Spionidae
Trochochaetidae
Apistobranchidae
Longosomatidae
Magelonidae
Poecilochaetidae
Chaetopteridae
Other polychaete families
b
Sabellariidae
Sabellidae
Serpulidae
Chaetopteridae
Oweniidae
Capitellidae
Maldanidae
Arenicolidae
Terebellidae
Trichobranchidae
Pectinariidae
Apharetidae
Alvinellidae
Cirratulidae
Flabelligeridae
Acrocirridae
Other polychaete families

Figure 9. Two alternative cladograms showing larval form of *Chaetopterus* compared with that of related polychaete families. The cladograms are adapted from Rouse and Fauchald (1997)—(a) from figure 70 and (b) from figure 71. The presence of the Pogonophora in the sabellid clade is omitted from these diagrams. Note that in either cladogram, outgroup taxa to the Chaetopteridae have overtly segmented early larvae, indicating that the chaetopterid larval form and ontogenetic heterochrony are unique to that lineage. Representative larval forms are adapted from the following sources: spionid, *Polydora webster* (Blake, 1969); terebellid, *Ramex californiensis* (Blake, 1991); oweniid, *Owenia fusiformis* (Plate and Husemann, 1997); sabellid, *Megalomma vesiculosum* (Wilson, 1936); sabellariid, *Lygdamis muratis* (Bhaud and Cazaux, 1987); capitellid, *Capitella capitata* (Plate and Husemann, 1997).

tively called the Sabellida) (Fig. 9b). Using weighted presence/absence coding but adding larval characters to the data, a more recent analysis (Rouse, 1999) also allies the Chaetopteridae with an order Sabellida.

In the first case, depicted in Figure 9a, overtly segmented early larvae are common both in the sister group of the chaetopterids, the spionid clade, and in the outgroups, the terebellid and sabellid clades. With the exception of the oweniids, the larvae can be described as variants of a basic nectochaete type (Okada, 1957; Wilson, 1948). Thus, by parsimony, the hypothetical common ancestor of the entire clade depicted would have some type of nectochaete larva. The divergent larval forms of *Owenia* and the Chaetopteridae are autapomorphies of their families in this scheme. Other chaetopterid genera share the basic larval form of *Chaetopterus* (Bhaud and Cazaux, 1987). Within the family there are no larvae with morphology intermediate to a nectochaete type, indicating that the ancestor of extant family members had already developed this modified larval ontogeny.

In the second case, depicted in Fig. 9b, the Chaetopteridae are a sister group to a sabellid clade, and these groups together are a sister group to the Oweniidae. This entire clade is in turn a sister group to a clade consisting of the capitellid and terebellid families. Once again, because of the phylogenetically widespread presence of overtly segmented nectochaete larvae in sister groups and outgroups, the hypothetical common ancestor at the basal node of this cladogram would be some sort of nectochaete.

From the foregoing it follows that, regardless of the phylogenetic scheme favored, the larval ontogeny of *Chaetopterus* is highly modified from a probable nectochaete ancestor. This ancestor developed as an initial trochophore larva forming three larval segments by subdivision of mesodermal bands. Subsequent segments were added sequentially from a pre-pygidial growth zone. In the chaetopterid lineage the following evolutionary changes in ontogeny took place: (1) loss of early body wall segmentation; (2) loss of larval setae; (3) loss of prototroch; (4) gain of one or more mesotrochs; (5) delay in segmentation of anterior trunk; (6) modification of parapodia in region B setigers to form specialized feeding and pumping organs.

Ontogenetic heterochrony

As described above, the temporal pattern of segmentation in *Chaetopterus* is modified from that typical of annelids. This pattern correlates with the regionalization of the adult body plan along the anterior-posterior axis. In the common annelid form, segmental morphology is homonomous, and segments form in a strict anterior-posterior temporal sequence. In many groups, there is a measure of heteronomy in segment form, such as groups of segments bearing branchiae in spionids, or nereidids with differing anterior and posterior parapodial morphology. However, even where this regionalization of adult body plan exists, the segments develop sequentially in the larva. In *Chaetopterus*, on the other hand, each tagma, or body region, develops overt segmentation at a different time. The first segments clearly visible are those of setigers B1–B5 at stage L4; these form the middle tagma of the adult body. Segmentation more anterior, which would be morphologically apparent in a nectochaete larva, is visible at this stage only by the use of molecular markers, such as *β-tubulin* and Distal-less, to show segmental cell populations.

These changes in the temporal pattern of development from the ancestral state can be regarded as ontogenetic heterochrony in an evolutionary sense. In deBeer's terminology (DeBeer, 1958), the structures of setigers B3–B5 exhibit *acceleration* relative to the anterior setigers, while all segments exhibit *deviation* in morphogenesis relative to the ancestral form.

An important question raised by consideration of this case of heterochrony is whether the changes in larval ontogeny in the extant chaetopterids were part of the direct evolutionary transformation leading to the tagmatization of the adult body plan, or if they are secondary modifications of larval development independent of the changes in adult body plan. In the first case, the changes in ontogeny would have to result in the changes in the adult without significant deleterious effect on larval survival, and thus overall fitness. In the second case, it could be that extinct ancestors of *Chaetopterus* evolved the heteronomous body form seen today using the primitive larval developmental program based on sequential anterior-posterior segmentation. After these changes produced the tagmatization of the adult body, the heterochrony in larval ontogeny may have evolved independently either as adaptations to larval ecology or as changes in developmental pathways that may or may not have adaptive value. Further comparative work on the molecular basis of polychaete development may help to distinguish between these scenarios.

Acknowledgments

The authors thank Mary E. Petersen of Copenhagen Museum for extensive discussion and information on chaetopterid systematics. Jonathan Q. Henry was a great help sharing his expertise on rearing larvae, and he, Susan D. Hill, Elaine Seaver, and Michael LaBarbera provided insightful commentaries on earlier versions of the manuscript. S. Q. I. was supported by National Institutes of Health training grant T32HD07136-20, National Science Foundation dissertation improvement grant 9623453, and a Hind's Fund grant from the University of Chicago. M. Q. M. was supported by National Science Foundation grant 9315653.

Literature Cited

Anderson, D. T. 1966. The comparative embryology of the Polychaeta. *Acta Zool.* **47:** 1–42.

Barnes, R. D. 1965. Tube-building and feeding in chaetopterid polychaetes. *Biol. Bull.* **129:** 217–233.

Béraneck, E. 1894. Quelques stades larvaires d'un Chetoptere. *Revue Suisse Zool.* **2:** 377–402.

Bhaud, M. R., and C. P. Cazaux. 1987. Description and identification of polychaete larvae: their implications in current biological problems. *Oceanis* **13:** 595–753.

Bhaud, M., M. C. Lastra, and M. E. Petersen. 1994. Redescription of *Spiochaetopterus solitarius* (Rioja, 1917), with notes on tube structure and comments on the generic status (Polychaeta: Chaetopteridae). *Ophelia* **40:** 115–133.

Blake, J. A. 1969. Reproduction and larval development of *Polydora* from northern New England (Polychaeta: Spionidae). *Ophelia* **7:** 1–63.

Blake, J. A. 1991. Larval development of Polychaeta from the northern California coast. V. *Ramex californiensis* Hartman (Polychaeta: Terebellidae). *Bull. Mar. Sci.* **48:** 448–460.

Bonch-Bruevich, E. V., and V. V. Malakhov. 1987. Organization of early larvae of the polychaete worm *Chaetopterus variopedatus* (Spiomorpha, chaetopteridae). *Dokl. Akad. Nauk. SSSR* **292:** 107–109.

Cazaux, C. 1965. Developpement larvaire de *Chaetopterus variopedatus* (Renier). *Actes Soc. Linnéenne de Bordeaux* **102:** 1–16.

Crossland, C. 1904. The Polychaeta of the Maldive Archipelago from the collections made by J. Stanley Gardiner in 1899. *Proc. Zool. Soc. Lond.* **1:** 270–286.

Dales, R. P. 1962. The polychaete stomodeum and the inter-relationships of the families of Polychaeta. *Proc. Zool. Soc. Lond.* **139:** 389–428.

DeBeer, G. 1958. *Embryos and Ancestors.* Clarendon Press, Oxford.

Eckberg, W. R., and W. A. Anderson. 1995. Cytoskeleton, cellular signals, and cytoplasmic localization in *Chaetopterus* embryos. *Curr. Top. Dev. Biol.* **31:** 5–39.

Eckberg, W. R., and S. D. Hill. 1996. *Chaetopterus*—oocyte maturation, early development and regeneration. *Mar. Mod. Elec. Rec.* [Online]. Available: http://www.mbl.edu/html/BB/MMER/ECK/EckTit.html [1999, July 19].

Enders, H. E. 1909. A study of the life-history and habits of *Chaetopterus variopedatus. J. Morph.* **20:** 479–531.

Fauchald, K. 1977. The polychaete worms. Definitions and keys to the orders, families and genera. *Nat. Hist. Mus. Los Angel. Cty. Sci. Ser.* **28:** 1–188.

Fauchald, K., and G. Rouse. 1997. Polychaete systematics: past and present. *Zool. Scr.* **26:** 71–138.

Fitzhugh, K. 1989. A systematic revision of the Sabellidae-Caobangidae-Sabellongidae complex (Annelida: Polychaeta). *Bull. Am. Mus. Nat. Hist.* **192:** 1–104.

Henry, J. J. 1986. The role of unequal cleavage and the polar lobe in the segregation of developmental potential during first cleavage in the embryo of *Chaetopterus variopedatus. Roux's Arch. Dev. Biol.* **195:** 103–116.

Henry, J. J. 1989. Removal of the polar lobe leads to the formation of functionally deficient photocytes in the annelid *Chaetopterus variopedatus. Roux's Arch. Dev. Biol.* **198:** 129–136.

Henry, J. J., and M. Q. Martindale. 1987. The organizing role of the D quadrant as revealed through the phenomenon of twinning in the polychaete *Chaetopterus variopedatus. Roux's Arch. Dev. Biol.* **196:** 499–510.

Inoué, S., G. G. Borisy, and D. P. Kiehart. 1974. Growth and lability of the *Chaetopterus* oocyte mitotic spindles isolated in the presence of porcine brain tubulin. *J. Cell Biol.* **62:** 175–184.

Irvine, S. Q. 1998. Ontogeny and developmental gene expression in the polychaete *Chaetopterus*: the evolution of developmental patterning. Ph.D. dissertation, University of Chicago, Chicago, IL.

Irvine, S. Q., and M. Q. Martindale. 1999a. Laboratory culture of the larvae of spionidan polychaetes. *Mar. Mod. Elec. Rec.* [Online]. Available: http://www.mbl/html/BB/MMER/IRV/IrvTit.html [1999, November 1].

Irvine, S. Q., and M. Q. Martindale. 1999b. Expression patterns of anterior Hox genes in the polychaete *Chaetopterus*: correlation with morphological boundaries. *Dev. Biol.* (in press).

Jeffery, W. R. 1985. The spatial distribution of maternal mRNA is determined by a cortical cytoskeletal domain in *Chaetopterus* eggs. *Dev. Biol.* **110:** 217–229.

Joyeux-Laffuie, J. 1890. Étude monographique du Chétoptère (*Chaetopterus variopedatus,* Rénier) suivie d'une revision des espèces du genre *Chaetopterus. Arch. Zool. Exp. Gen.* **8:** 245–360.

Lillie, F. R. 1906. Observations and experiments concerning the elementary phenomena of embryonic development in *Chaetopterus. J. Exp. Zool.* **3:** 153–268.

MacGinitie, G. E. 1939. The method of feeding of *Chaetopterus. Biol. Bull.* **77:** 115–118.

Malakhov, V. V. 1984. Embryogenesis of *Chaetopterus variopedatus* (Spiomorpha, Chaetopteridae). *Zool. Zh.* **63:** 656–661.

Martin, N., and M. Anctil. 1984. The nervous system of the tube-worm *Chaetopterus variopedatus* (Polychaeta). *J. Morph.* **181:** 161–173.

Mead, A. D. 1897. The early development of marine annelids. *J. Morph.* **13:** 227–326.

Okada, K. 1957. Annelida. Pp. 192–241 in *Invertebrate Embryology.* M. Kumé and K. Dan, eds. NOLIT, Belgrade.

Panganiban, G., S. M. Irvine, C. Lowe, H. Roehl, L. S. Corley, B. Sherbon, J. K. Grenier, J. F. Fallon, J. Kimble, M. Walker, G. A. Wray, B. J. Swalla, M. Q. Martindale, and S. B. Carroll. 1997. The origin and evolution of animal appendages. *Proc. Natl. Acad. Sci. USA* **94:** 5162–5166.

Petersen, M. E. 1984a. *Chaetopterus variopedatus* (Annelida: Polychaeta): another victim of the "characteristic species" disease. *Am. Zool.* **24:** 64A.

Petersen, M. E. 1984b. *Chaetopterus variopedatus* (Renier) (Annelida: Polychaeta: Chaetopteridae): a species complex. What species are being used at MBL? *Biol. Bull.* **167:** 513.

Plate, S., and E. Husemann. 1997. Identification guide to planktonic polychaete larvae. *Helgol. Wiss. Meeresunters.* **48:** 1–58.

Rouse, G. 1999. Trochophore concepts: ciliary bands and the evolution of larvae in spiralian Metazoa. *Biol. J. Linn. Soc.* **66:** 411–464.

Rouse, G., and K. Fauchald. 1997. Cladistics and polychaetes. *Zool. Scr.* **26:** 139–204.

Wilson, D. P. 1936. The development of the sabellid *Branchiomma vesiculosum. Q. J. Microsc. Sci.* **78:** 543–603.

Wilson, D. P. 1948. The larval development of *Ophelia bicornis* Savigny. *J. Mar. Biol. Assoc. U. K.* **27:** 540–553.

Wilson, E. B. 1882. Observations on the developmental stages of some polychaetous annelids. *Stud. Biol. Lab. Johns Hopkins Univ.* **2:** 271–299.

Reference: *Biol. Bull.* **197:** 332–340. (December 1999)

Inhibition of Settlement and Metamorphosis of the Ascidian *Herdmania curvata* by Non-geniculate Coralline Algae

BERNARD M. DEGNAN[1,*] AND CRAIG R. JOHNSON[2]

[1] *Department of Zoology and Entomology, University of Queensland, Brisbane, Qld 4072, Australia; and*
[2] *Zoology Department, University of Tasmania, GPO Box 252-05, Sandy Bay, Tasmania 7001, Australia*

Abstract. The surfaces of non-geniculate coralline algae (NCA) are known to induce the settlement and metamorphosis of disparate marine taxa. In this study we investigate the responsiveness of larvae of *Herdmania curvata* (Ascidiacea: Stolidobranchia) to three species of NCA (*Neogoniolithon brassica-florida, Hydrolithon onkodes,* and *Lithothamnium prolifer*) that cohabit the slope and crest of Heron Reef, Great Barrier Reef. *H. curvata* larvae were first exposed to these NCA at or within 2 h of hatching, which is 1 to 2 h prior to attaining competence, and then cultured continuously with the NCA for 12 to 14 h. Rates of settlement and metamorphosis of *H. curvata* cultured in laboratory chambers in the presence of the different NCA were significantly lower than spontaneous rates in seawater. The limited settlement in treatments containing NCA were confined entirely to the chamber periphery, and settlement never occurred on the surface of the NCA. The inhibitory effect was dose-dependent and was stronger in *N. brassica-florida* and *H. onkodes* than in *L. prolifer*. Larvae that did not settle in treatments with NCA had rounded anterior trunks and, in extreme cases, kinked tails with rounded and dissociated tail muscle cells. In some individuals, we observed the anterior chemosensory papillae being sloughed off the larval body. Morphological analysis of trunk ectodermal and mesenchymal nuclei of larvae cultured in the presence of the NCA revealed that general necrotic cell death was occurring. Importantly, *H. curvata* larvae that were exposed to NCA could not subsequently be induced to metamorphose in KCl-elevated seawater, whereas larvae not exposed to NCA metamorphosed at high rates in KCl-elevated seawater.

Introduction

Marine invertebrate larvae traverse a complex chemical seascape and can encounter factors that promote or deter settlement and metamorphosis. The unique and sometimes opposite responses of different larvae to chemicals emanating from or on the surface of a particular substratum has been attributed to differences in larval chemosensory capabilities (reviewed in Hadfield, 1986; Hadfield and Pennington, 1990; Morse, 1990, 1993; Pawlik, 1992; Leitz, 1997) and developmental states (Trapido-Rosenthal and Morse, 1986; Degnan and Morse, 1995). At different ages, competent larvae of a given species can respond differentially to a particular inductive cue, either by settling or metamorphosing at different rates (*e.g.*, Coon *et al.*, 1990; Degnan *et al.*, 1995).

Despite the apparent diversity of larval chemosensory systems, disparate marine invertebrate taxa often respond in a similar manner to particular substrata. Bacterial films on both biotic and abiotic substrata induce settlement in a wide range of marine invertebrates (reviewed in Pawlik, 1992; Johnson *et al.*, 1997), although several species are inhibited from settling by bacteria or their products (*e.g.*, Maki *et al.*, 1988, 1992) or show no response to bacteria (*e.g.*, Keough and Ramondi, 1995). In contrast, in most cases the surfaces of sessile marine invertebrates such as sponges, bryozoans, and ascidians either contain inhibitors or do not provide morphogenic cues to induce the settlement of larvae (reviewed in Davis *et al.*, 1989; Pawlik, 1992). A finer scale of analysis reveals greater complexity in larval/substratum interactions. For example, in the case of microbial films,

---

Received 24 February 1999; accepted 22 September 1999.

* Author to whom correspondence should be addressed. E-mail: bdegnan@zoology.uq.edu.au

larvae of some species respond to a variety of bacterial genera (*e.g.*, Fitt *et al.*, 1989), whereas others apparently require particular strains or communities (*e.g.*, Wilson, 1955; Kirchman *et al.*, 1982; see also Johnson and Sutton, 1994). Similarly, a particular strain may induce settlement in some species but not others (Tritar *et al.*, 1992) or even inhibit settlement in some species but promote settlement in others (*cf.* Kirchman *et al.*, 1982; Maki *et al.*, 1990, 1992).

The range of interactions between invertebrate larvae and the surface of non-geniculate coralline algae (NCA) is similar to that exhibited between larvae and microbial films. NCA induce settlement, metamorphosis, or both in a variety of echinoderms (*e.g.*, Rowley, 1989; Johnson *et al.*, 1991), molluscs (*e.g.*, Barnes and Gonor, 1973; Heslinga, 1981; Rumrill and Cameron, 1983; Morse and Morse, 1984; Moss and Tong, 1992), annelids (*e.g.*, Gee and Knight-Jones, 1962; Gee, 1965), and coelenterates (*e.g.*, Harrigan, 1972; Sebens, 1983a, b; Morse *et al.*, 1988), but do not provide a morphogenic signal for several species of tubicolous annelids (*e.g.*, De Silva, 1962; Gee and Knight-Jones, 1962; Jensen and Morse, 1984). Among species whose larvae are induced by NCA, the specificity of the interaction covers a spectrum from species that manifest specificity for a particular species of NCA (Gee and Knight-Jones, 1962; Gee, 1965; Johnson *et al.*, 1991), to those requiring contact with any of a variety of NCA (Morse *et al.*, 1988), to those requiring a cue from NCA or any of a variety of other substrata (Harrigan, 1972; Heslinga, 1981; Hahn, 1989).

In this study we investigate the responsiveness of larvae of the tropical solitary ascidian *Herdmania curvata* (previously known as *H. momus* "Heron Reef" or *H. momus* forma *curvata;* see Degnan and Lavin, 1995) to three species of NCA, *viz. Neogoniolithon brassica-florida* (previously known as *N. foslei*), *Hydrolithon onkodes* (previously known as *Pololithon onkodes*), and *Lithothamnium prolifer. H. curvata* and these NCA inhabit the slope and crest of reefs along the Great Barrier Reef. Since larval ontogeny and the cellular basis of morphological change are understood in solitary ascidians to a greater extent than in most marine invertebrates (reviewed in Satoh, 1994), and the developmental and morphogenetic processes that regulate the attainment of competence, settlement, and metamorphosis have been documented in *H. curvata* and other ascidians (Cloney, 1982; Torrence and Cloney, 1983; Degnan *et al.*, 1996, 1997; Eri *et al.*, 1999), this tropical ascidian is a useful model for investigating the inductive and inhibitory activities of various substrata. Settlement and metamorphosis can be induced rapidly in *H. curvata* by a range of artificial and natural cues, with most competent larvae initiating metamorphosis within 1 h of contact with the inductive signal (Degnan *et al.*, 1997). In addition, *H. curvata* larvae spontaneously settle and metamorphose in axenic cultures at a slower rate, such that up to 80% will be settled within 24 h of hatching. This "spontaneous" settlement and metamorphosis facilitates the analysis of inhibition of these processes.

Here we demonstrate that all three species of NCA inhibit settlement and metamorphosis of *H. curvata* in the laboratory. In the presence of the algae, settlement rates were much less than rates of spontaneous settlement in the absence of the NCA, and the limited settlement in the presence of NCA was confined to the periphery of the culture chamber and never occurred on the surface of the plant. Morphological analysis of larvae cultured in the presence of the NCA revealed that the NCA were toxic to the larvae, resulting in necrotic cell death and sloughing of the anterior chemosensory papillae. This toxic inhibition prevents these larvae from subsequently responding to a strong artificial inductive cue (40 m*M* KCl-elevated seawater; Degnan *et al.*, 1997). This result contrasts with that observed for some echinoderm larvae, which are readily induced to settle and metamorphose on contact with some of these NCA species (Johnson *et al.*, 1991; Johnson and Sutton, 1994).

Materials and Methods

Collection, maintenance, and cultivation of Herdmania curvata *and coralline algae*

Gravid *Herdmania curvata* and pieces of the non-geniculate coralline algae (NCA) *Neogoniolithon brassica-florida, Hydrolithon onkodes,* and *Lithothamnium prolifer* were collected from the reef crest and slope of Heron Reef, Great Barrier Reef, Australia (23° 27′ S; 151° 55′ E), and maintained separately in flowing, ambient seawater on site. NCA were collected by chiselling the algae from the surface of coral rubble.

H. curvata eggs were fertilized by pooling the gametes from at least three individuals into 0.2-μm-filtered seawater (FSW), and embryos were cultured in FSW as described in Degnan *et al.* (1996). Thin (1–2 mm) shards of NCA were prepared by chipping away most of the coral rubble from underneath the algae. Only shards free of macroscopic fouling organisms were used in the experiments.

Settlement experiments

Three experimental designs were used to examine the settlement response of *H. curvata* to the NCA: (1) larvae were presented with all species of NCA simultaneously (the "choice" experiment); (2) larvae had access to only a single species of NCA (the "no choice" experiment); and (3) a "no choice" design in which a dose-dependent response was examined.

Choice experiment. A variable number of small shards of each species of NCA (total epithallial area of *ca.* 1.5–3 cm^2 for each species) were placed in the center of 100-mm-diameter polycarbonate chambers containing 200 ml of seawater. Shards of each species were arranged so that the epithallial surfaces faced both upwards and downwards. *H. curvata* embryos were mass cultured in FSW at 24°C until hatching, which is about 10 h after fertilization (Degnan *et al.*, 1996); newly hatched larvae require another 3–4 h of development to attain competence (Degnan *et al.*, 1997). Pre-competent *H. curvata* larvae (10–12 h old) were transferred from the mass culture to chambers (mean number of larvae *ca.* 130 per chamber) containing NCA and incubated at the ambient water temperature (22°–24°C) for 12–14 h. For controls, larvae were added to chambers containing seawater only. The experiment was repeated on consecutive days with different batches of larvae. Since the results of the two experiments were similar, data were combined for presentation, yielding a total of 15 replicate chambers of each of the NCA and control treatments.

After incubation, the NCA were removed from the chamber, placed in a shallow dish containing seawater, and inspected microscopically for settled *H. curvata* on the epithallial and rubble surfaces. The seawater in the chamber was filtered through a 60-μm mesh, and the chamber was gently washed with an additional 100 ml of seawater, which was also filtered. The chamber and the mesh were inspected and scored for larvae, settled postlarvae, and unsettled postlarvae (*i.e.*, larvae that underwent metamorphosis but not settlement).

After being scored, specimens of *H. curvata* were either inspected microscopically, fixed for histological analysis, or artificially induced to metamorphose (see below). Light microscopy was performed on living individuals with an Olympus BH-2 light microscope fitted with Nomarski optics; photomicrographs were obtained on an Olympus C-35AD-2 camera attached to this microscope.

No choice experiment. This experiment was conducted similarly to the choice experiment outlined above except that each chamber contained only a single species of NCA. The mean number of pre-competent larvae added to each chamber was 110, and there were 10 replicate chambers of each treatment containing NCA, and 9 replicate controls containing seawater but no NCA.

Dose-dependency (no choice): To determine the nature of any dose-dependency in the response to NCA, larvae were added to polycarbonate tissue culture vessels (35-mm diameter ×10-mm depth) containing 5 ml of seawater and either a single small, medium, or large (surface area of base of chamber respectively 5%–15%, 25%–35%, and 50%–75%) shard of NCA. Each chamber contained a single species of NCA, and about 30 newly hatched larvae (*i.e.*, 3 h before development of competence) were added to each. There were 6 replicate chambers per treatment, to give a total of 3 species NCA × 3 size classes × 6 replicates = 54 chambers containing NCA, and 6 control chambers containing larvae but no NCA, to yield a total of 60 chambers in the experiment.

After 12–14 h of incubation, the following categories of larvae were scored: settled on NCA (epithallus), settled on the rubble surface, settled on the sides of the chamber, metamorphosed but not settled, and neither metamorphosed nor settled. Larvae that had not yet metamorphosed or settled in chambers containing large shards of *L. prolifer* and the smallest shards of *N. brassica-florida* and *H. onkode* were transferred to 40 m*M* KCl-elevated FSW (see below).

Artificial induction of metamorphosis

To determine whether *H. curvata* larvae were competent to metamorphose after exposure to the NCA, we transferred 20 larvae that had been in the presence of large shards of *L. prolifer*, small shards of *H. onkodes* or *N. brassica-florida*, or seawater to new sterile 35-mm polycarbonate chambers containing 5 ml of 40 m*M* KCl-elevated FSW; this was performed in triplicate for each treatment (*i.e.*, 20 larvae × 3 replicates), and all larvae were derived from the same fertilization. KCl-elevated FSW is normally a potent artificial inducer of metamorphosis (Degnan *et al.*, 1997). Because most larvae that were previously exposed to seawater had metamorphosed by the time of the transfer, additional cultures were established as described in the above section to ensure that 60 larvae were transferred. Untreated control larvae were also transferred to FSW to control for the transfer process (an additional 60 larvae).

At 1-h intervals after transferral of larvae, each chamber was scanned to record the number of larvae that were undergoing metamorphosis. *H. curvata* larvae were considered to have initiated metamorphosis when the tail was at least 50% resorbed (Degnan *et al.*, 1996, 1997).

Histology and microscopy

Larvae that had been cultured in seawater or in the presence of the NCA were fixed in 4% (w/v) paraformaldehyde in 100 m*M* Hepes (pH 6.9), 2 m*M* $MgSO_4$, 1 m*M* EGTA for at least 3 h and stained with 2 mg/ml propidium iodide for 1 h as described in Hinman and Degnan (1998). Larvae were examined on a BioRad 600 laser confocal scanning microscope, exciting samples with 488-nm laser light and monitoring emission at 515 nm.

Statistics

Since there was no settlement on the epithallial surface of any NCA in the choice and no choice experiments, settlement rates on the chamber sides only were compared among NCA and control treatments with one-way Model I ANOVA. Similarly, in the dose-dependent experiment, there was little (if any) settlement on NCA surfaces; therefore, total settlement (on NCA and the plastic sides of chambers) was compared among the different "doses" (= size classes, 3 levels) and species (3 levels) using Model I two-way ANOVA. For this experiment the proportion of larvae neither settled nor metamorphosed and the proportion metamorphosed but not settled were analyzed in separate Model I two-way ANOVAs. All *a posteriori* multiple range tests used Tukey's HSD criteria ($P = 0.05$).

For all analyses, the relationship between group means and standard deviations was examined to determine the appropriate transformation (if any) to stabilize variances (Draper and Smith, 1991). Transformations are expressed in terms of the untransformed variate Y. All analyses were undertaken using the SAS/STAT software package (version 6.12, SAS Institute Inc., Cary, NC).

Results

Settlement and metamorphosis of Herdmania curvata *are inhibited by non-geniculate coralline algae*

Responses of *Herdmania curvata* larvae to NCA were similar in experiments in which larvae had access to all three NCA species simultaneously (choice experiment; Fig. 1A), and those in which larvae were presented with only a single species (no choice experiment; Fig. 1B). In control cultures containing seawater only, the majority of larvae (60.8% ±SE = 4.4% and 51.1% ±SE = 4.6% in the choice and no choice trials respectively) had settled and metamorphosed on the bottom of the plastic chamber 11–13 h after attaining competence (~14–16 h after hatching; Figs. 1A, 1B). These larvae were metamorphosing normally; *i.e.*, tail muscle cells were in the process of being degraded, ampullae and the postlarval tunic were forming, and the endodermal primordia had turned and commenced morphogenesis. Larvae that had not settled or metamorphosed were also normal and possessed extended sensory papillae.

In contrast, in treatments containing NCA the majority of larvae (*ca.* 80%) neither settled nor metamorphosed (Fig. 1), no postlarvae settled on the epithallial surface of any of the NCA, and the low levels of settlement (*ca.* 20%) that did occur were confined wholly to the periphery of the plastic chambers. Although we did not quantify larval behavior during the experiment, we did observe some larvae directly contacting the NCA, and we noted that larvae exhibited their usual weak and irregular swimming behavior. Although early metamorphosis appeared normal for *H. curvata* settled on the plastic in the presence of NCA (*i.e.*, larval tail resorption, papillae retraction, and initiation of the programmed degradation of muscle myofibrils appeared normal), metamorphosis was abnormal in that postlarvae did not develop ampullae or undergo the rotation of the endodermal primordium (see Degnan *et al.*, 1996, 1997). Most of the unsettled *H. curvata* larvae appeared abnormal (see below).

By exposing larvae to different quantities of NCA, significant differences were observed in larval responses to the different coralline species, and to different quantities of any given species (Fig. 2). For a given amount of NCA, larval settlement was consistently (and often significantly) greater in the presence of *Lithothamnium prolifer* than either of the other species. Larvae showed greatest sensitivity to *Neogoniolithon brassica-florida*, and the inhibitory effect increased dramatically when the percentage of the base of the settlement chamber that was covered with shards increased from small (5%–15% coverage) to medium (25%–35% coverage). Of these treatments, normal metamorphosis occurred only in *H. curvata* cultured in the presence of small and medium shards of *L. prolifer*. Overall, the inhibitory effect on larval settlement was ranked *N. brassica-florida* > *Hydrolithon onkodes* > *L. prolifer*.

Non-geniculate coralline algae cause sloughing of larval sensory papillae and necrotic cell death

Unlike normal 14–16 h posthatch larvae, which have extended papillae, larvae cultured in the presence of NCA had rounded trunks and lacked papillae (Fig. 3). Normal larvae were evident only in the treatment containing small and medium shards of *L. prolifer* (Fig. 2A). Microscopic inspection of larvae revealed that all three NCA species appeared to induce this same effect on larval morphology, although the amount of NCA required to affect larval morphology differed (Fig. 2A). For these reasons, only the effects of *L. prolifer*, the least potent of the NCA, on *H. curvata* larvae were documented further.

Large shards of *L. prolifer* (Fig. 2A) induced a range of changes in *H. curvata* larval morphology that appeared to be related but differed in severity. Slightly abnormal larvae had normal axial structures (notochord, neural tube, and muscle) and trunk structures (sensory vesicle containing otolith and ocellus, and endoderm rudiment) but lacked projecting papillae and had a slightly rounded trunk (Fig. 3C, D). Some of these larvae still had papillae associated with them; however, the papillae were no longer attached to the anterior trunk and appeared to be in the process of being sloughed off (Fig. 3E). In the most severely altered larvae, the trunk was small and rounded, the tail was kinked, and the muscle cells had lost integrity and their usual columnar shape (Fig. 3F). Between these extremes of NCA-induced abnormalities was a continuum of morphological defects.

To determine whether the inhibitory factor or factors associated with *L. prolifer* or the other NCA were inducing general cell death, we investigated the structure of the nuclei of larvae that exhibited an intermediate abnormal morphology (*i.e.*, rounded trunk, straight tail with slightly rounded muscle cells). Nuclei were stained with propidium iodide and analyzed by laser scanning confocal microscopy. Optical sections were taken through the trunk epidermis and mesenchyme of normal and abnormal larvae, and compared. In both tissues, the nuclei of larvae exposed to *L. prolifer* were larger than those of normal larvae (Fig. 4). Mesenchymal nuclei of normal larvae were circular (diameters between 3.5 and 4.3 μm) and appeared granular when stained

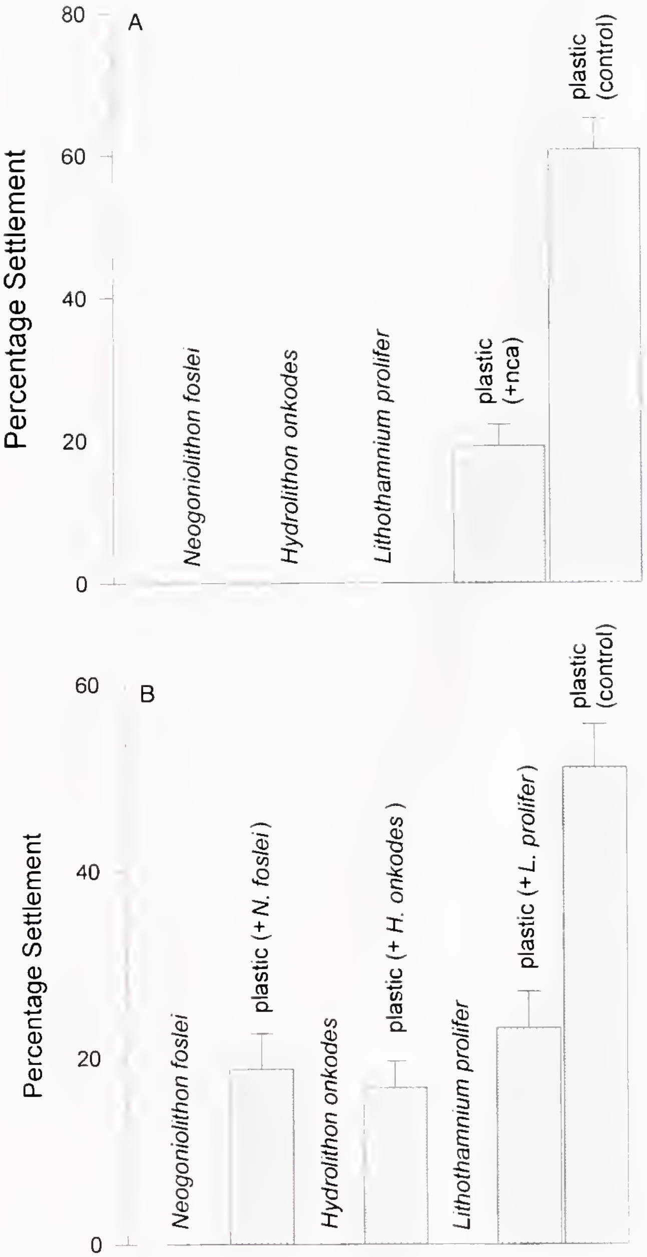

Figure 1. Inhibition of *Herdmania curvata* settlement by non-geniculate coralline algae (NCA). Results are mean percentage settlement (+SE) of *H. curvata* larvae on three species of NCA (*Neogoniolithon brassica-florida, Hydrolithon onkodes, Lithothamnium prolifer*), on the sides of settlement chambers containing NCA, and on the sides of chambers in the control treatment (seawater only). (A) "Choice" experiment in which larvae were presented with all species of NCA simultaneously. No larvae settled on any NCA, and settlement rates on the sides of settlement chambers were significantly lower in chambers containing NCA ($n = 15$) than in control chambers ($n = 15$) containing seawater only (one-way ANOVA, $F(1, 28) = 61.7$, $P < 0.0001$, no transformation required). (B) "No choice" experiment in which larvae were exposed to only a single species of NCA. No larvae settled on any NCA, and settlement rates on the sides of settlement chambers were significantly lower in chambers containing NCA ($n = 10$) than in control chambers ($n = 9$) containing seawater only (one-way ANOVA, $F(3, 35) = 16.9$, $P < 0.0001$, no transformation required). Settlement rates on the sides of chambers did not differ among NCA treatments [Tukey's groupings at $P = 0.05$: control > (*N. brassica-florida* = *H. onkodes* = *L. prolifer*)].

with propidium iodide (Fig. 4A). The mesenchymal nuclei of larvae cultured with *L. prolifer* were oval, larger (4.3–7.1 μm), and more diffusely stained with propidium iodide (Fig. 4B). Normal epidermal nuclei were similar in appearance to normal mesenchymal nuclei (Fig. 4C). Larvae exposed to *L. prolifer* had irregularly shaped epidermal nuclei that stained intensely with propidium iodide and were about the same size as normal nuclei (Fig. 4D). There was additional, non-nuclear staining of these epidermal cells.

Metamorphosis cannot occur in larvae previously exposed to non-geniculate coralline algae

To determine whether the effect of the NCA on *H. curvata* larvae was transient, we transferred larvae that were cultured with either *H. onkodes, N. brassica-florida* or *L. prolifer* into culture chambers containing 40 m*M* KCl-elevated FSW. Because the larvae exhibited a range of abnormalities, we transferred only those showing slight abnormalities (*i.e.,* lost papillae and rounded trunk; *e.g.,* Fig. 3C, D). Larvae from the same fertilization batch that were not exposed to NCA and had not metamorphosed in the plastic chambers acted as controls and were transferred to the KCl-elevated FSW or FSW. We monitored and scored the number of larvae that had initiated metamorphosis (*i.e.,* began tail resorption) every hour for 3 h. Although most of the untreated larvae in both FSW and KCl-elevated FSW began metamorphosing over this period, only 2 of a total of 180 larvae previously exposed to any one of the algae initiated metamorphosis (Fig. 5). Analysis of these cultures after 24 h revealed that control larvae were metamorphosing normally and that larvae previously cultured with NCA had not metamorphosed and died. The two postlarvae previously exposed as larvae to the NCA were also dead after 24 h.

Discussion

Most competent *Herdmania curvata* larvae will normally settle and metamorphose in seawater, FSW, and FSW with antibiotics within 24 h of hatching (Degnan *et al.,* 1997; unpub. data). The percentage of larvae that will spontaneously settle varies between cohorts, with those cultured in unfiltered seawater generally settling at a greater rate than those cultured in FSW. To assess the extent of any inhibitory effects of NCA on larval settlement and metamorphosis, we cultured the larvae and NCA in unfiltered seawater. The high percentage of larvae that settled in chambers containing seawater demonstrated that *H. curvata* will settle spontaneously under these culture conditions. The significant reduction in settlement rates of larvae cultured in the presence of the different NCA demonstrates that these algae are inhibiting settlement in this tropical ascidian.

H. curvata larvae respond differentially to a range of epifloral and faunal substrata associated with the cryptic

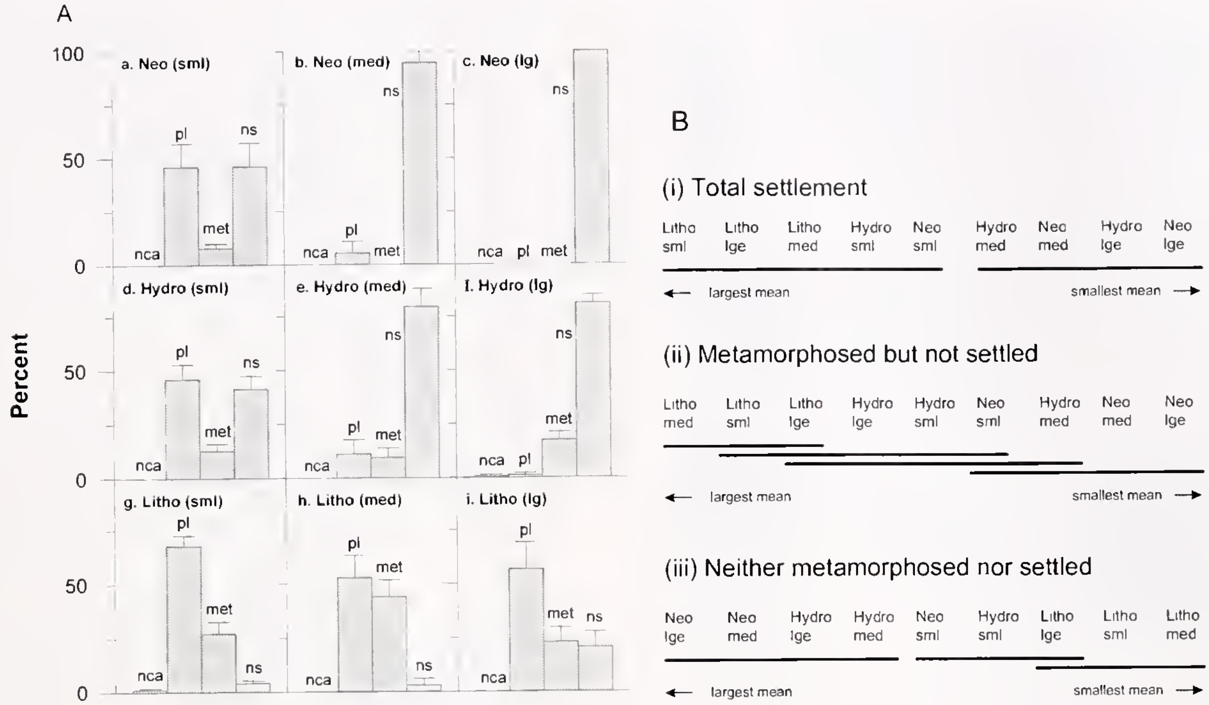

Figure 2. Dose-dependence of inhibitory effect of non-geniculate coralline algae on settlement and metamorphosis of *Herdmania curvata* in a "no-choice" experiment. (A) Mean response (+SE) of *H. curvata* larvae in the presence of small, medium, and large (= "sml," "med," "lge," respectively) shards of the NCA *Neogoniolithon brassica-florida* (= "Neo"), *Hydrolithon onkodes* (= "Hydro"), and *Lithothamnium prolifer* (= "Litho"). "nca" = settlement and metamorphosis on NCA shards; "pl" = settlement and metamorphosis on the sides of the plastic settlement chambers; "met" = larvae metamorphosed but not settled, and "ns" = larvae neither settled or metamorphosed; $n = 6$ for all treatments. Greatest total settlement occurred in controls (68.72% ± SE = 5.11; not shown on figure). Tukey groupings ($P = 0.05$) indicated settlement in controls was significantly greater than in treatments containing medium- and large-sized shards of *N. brassica-florida* and *H. onkodes* (one-way ANOVA, $F(9, 50) = 15.05$, $P < 0.0001$, transformation $\gamma^{0.553}$). The pattern of settlement in control chambers ($n = 6$) containing seawater only (not shown) was not significantly different from the treatment containing small shards of *L. prolifer* (panel g). (B) Tukey groupings following detection of significant interaction between NCA species and size of shard (= "dose") for total larvae settled, larvae metamorphosed but not settled, and larvae neither settled nor metamorphosed (two-way ANOVA, species × size interaction: total larvae settled and metamorphosed, $F(4, 45) = 3.31$, $P = 0.018$, transformation $\gamma^{0.553}$; larvae metamorphosed but not settled, $F(4, 45) = 5.02$, $P = 0.002$, transformation = arcsin $\sqrt{\gamma}$; larvae not settled or metamorphosed, $F(4, 45) = 4.96$, $P = 0.002$, no transformation required). These results show that the inhibitory effect of *N. brassica-florida* and *H. onkodes* on larval settlement and metamorphosis was greater than that of *L. prolifer*, and that the dose-response relationship was significantly steeper for *N. brassica-florida* and *H. onkodes* than for *L. prolifer*.

community of the reef crest and slope of the Great Barrier Reef: metamorphosis is induced by some substrata and not induced or inhibited by others in the laboratory. Manual removal of the larval trunk anterior of the otolith and ocellus prevents the posterior part of the larva from being induced to metamorphose with KCl-elevated FSW or natural inducers (Degnan *et al.*, 1997), suggesting that responsiveness to inductive substrata in *H. curvata* is mediated by the chemosensory papillae and an anterior signaling center. The *Hemps* gene, which encodes a protein with a putative secretion signal sequence and epidermal growth factor (EGF)-like repeats, is expressed in this region and has been shown to regulate the induction of metamorphosis (Arnold *et al.*, 1997; Eri *et al.*, 1999). The NCA investigated in this study (*Neogoniolithon brassica-florida, Hydrolithon onkodes*, and *Lithothamnium prolifer*) appear to be toxic to *H. curvata* larvae, inhibiting settlement on the surface of the algae, significantly lowering the level of spontaneous settlement, and preventing the future ability of larvae to respond to inductive cues. Trunk ectodermal and mesenchymal nuclei of larvae cultured in the presence of *L. prolifer* were bloated and irregular in shape respectively, both features of necrotic cell death (Kerr and Harmon, 1991). Induced morphogenetic changes during normal metamorphosis do not include this form of cell death (see Degnan *et al.*, 1996, 1997; Hinman and Degnan, 1998). *H. curvata* larvae that were

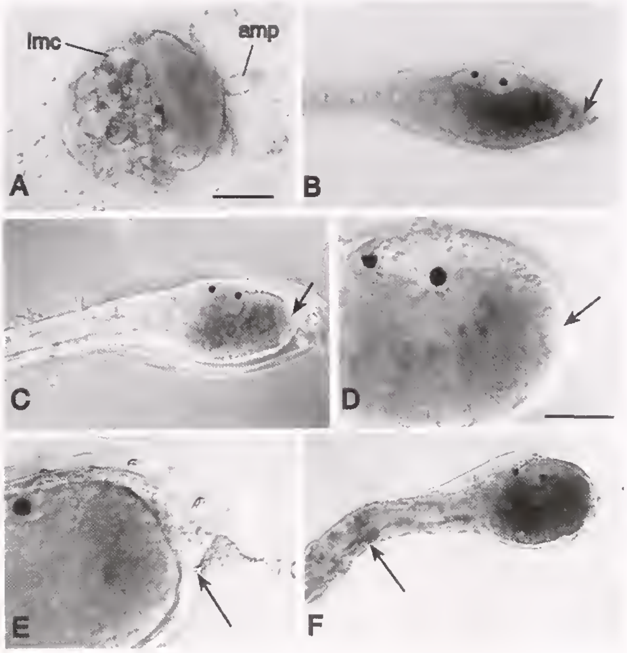

Figure 3. The effect of *Lithothamnium prolifer* on normal development and larval structures of *Herdmania curvata*. Larval anterior is to the right in all micrographs. (A) A normal postlarva approximately 12 h after initiating metamorphosis; degenerating larval muscle cells (lmc) and projecting ampullae (amp) are evident. (B) Normal tadpole larva with sensory papillae (arrow). (C–F) Larvae cultured with *L. prolifer*. (C, D) Larva with a rounded trunk and no papillae; arrows point to region where papillae are normally located. (E) Larva in the process of shedding a papilla (arrow). (F) Larva with rounded trunk, no papillae, kinked tail, and necrosing muscle cells (arrow). Scale bars: A, B, C, F, 100 μm); D, E, 50 μm.

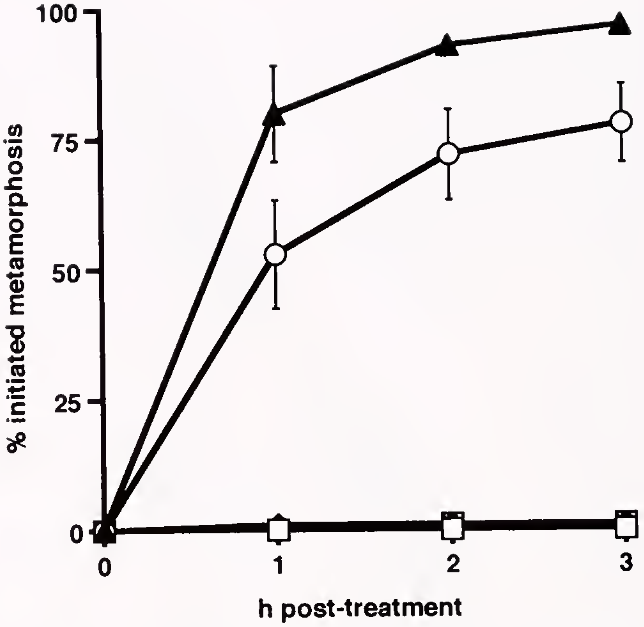

Figure 5. Percentage of *Herdmania curvata* larvae metamorphosing when treated with 40 m*M* KCl-elevated FSW. Prior to treatment with KCl-elevated FSW, larvae were cultured either in FSW, or in the presence of *Neogoniolithon brassica-florida*, *Hydrolithon onkodes*, or *Lithothamnium prolifer* for 12–14 h. Filled triangles, larvae cultured in seawater and then transferred to KCl-elevated FSW; open circles, larvae cultured in seawater and then transferred to FSW; open squares, larvae exposed to *Neogoniolithon brassica-florida* and then transferred to KCl-elevated FSW; diamonds (hidden behind open squares), larvae exposed to *Hydrolithon onkodes* and then transferred to KCl-elevated FSW; half-filled squares (hidden behind open squares), larvae exposed to *Lithothamnium prolifer* and then transferred to KCl-elevated FSW. Data are means (±SE).

cultured with NCA and had not settled lacked papillae and had rounded anterior trunks. In some of the least morphologically disturbed individuals, the palps were observed being sloughed from the trunk of the larva, suggesting that the toxic effect of the NCA upon the larva first disables the chemosensory and primary signaling system. *Hemps* is expressed in the papillae and the papillae-associated tissue (PAT) which is located in the anterior epidermis between the three papillae and consists of about 5 cells (Eri *et al.*, 1999). In the vicinity of the sloughed papillae are individual cells that may have been part of PAT (Fig. 3E). Secretion of the Hemps protein is essential for the induction and progression of metamorphosis (Eri *et al.*, 1999). It is possible that PAT cells are exuded precociously in larvae exposed to NCA, disrupting the Hemps signaling system. *H. curvata* larvae do not have the ability to regenerate these papillae nor regain the ability to respond to artificial (Fig. 5) or natural cues (data not shown). The global toxic effect of the NCA upon *H. curvata* larvae is demonstrated by the high percentage of death within 24 h of larvae being cultured with NCA. Experimental inhibition of papillae morphogenesis by ecotopic application of retinoic acid results in a very similar phenotype to larvae cultured with NCA; however, metamorphosis is not inhibited (Hinman and Degnan, 1998). Toxicity is not limited to the larvae—individuals that

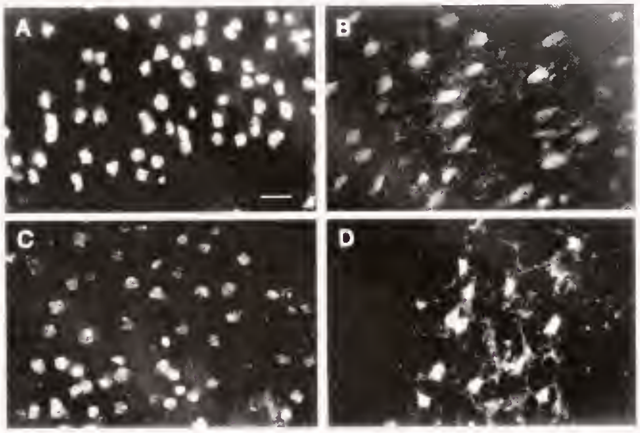

Figure 4. Degeneration of the nuclei of *Herdmania curvata* larvae cultured in the presence of *Lithothamnium prolifer*. Confocal micrographs of nuclei stained with propidium iodide. (A) Normal larval trunk mesenchyme (trunk ventral cells; Satoh, 1996). (B) Trunk mesenchyme of larva exposed to *L. prolifer*. (C) Normal larval trunk epidermis. (D) Trunk epidermis of larva exposed to *L. prolifer*. Scale bar, 10 μm.

did settle and initiate metamorphosis in these assays did not complete metamorphosis and died within 24 h (data not shown).

The inhibitory signals produced by these NCA appear to be taxa specific. Importantly, under similar laboratory conditions, we have induced normal settlement and metamorphosis of an asteroid (with *L. prolifer;* Johnson *et al.*, 1991; Johnson and Sutton, 1994) and observed that coral and mollusc larvae are not affected by these algae under identical assay conditions (unpub. data). Given that the effect of each of the NCA species on *H. curvata* larval morphology was very similar (*i.e.*, all induced rounded trunks and sometimes kinked tails and dissociated muscle cells), a similar inhibitory factor may be being produced by all three species of NCA. We did not determine whether the inhibitors were produced by the NCA or by surface-associated bacteria or microalgae.

Although it is well established that NCA provide morphogenic cues for larvae of a variety of marine invertebrates, but do not induce settlement or metamorphosis in others (see Introduction), this report demonstrates toxic inhibition of settlement and metamorphosis of an invertebrate by NCA. The distinction between the simple absence of a morphogenic cue and inhibition is important. Although larvae will not settle and metamorphose in either case, if the initial contact is with a substratum that simply lacks an inductive cue, the larva can continue to search and may subsequently receive the appropriate stimulus to settle and metamorphose. These NCA are apparently not toxic to other larvae, since some coral and mollusc larvae swim in the assay chambers and behave normally for several days without settling (unpub. data). Importantly, the ability of *H. curvata* larvae to undergo high rates of "spontaneous" settlement and metamorphosis in seawater (Degnan *et al.*, 1997) or when exposed to a potent inducer (KCl) allows us to determine whether a substratum is actually inhibiting settlement and metamorphosis or is merely not providing a morphogenic cue. If the ascidian larva contacts an inhibitory substratum—in this case three species of NCA—then lower (or zero) rates of settlement or metamorphosis will be detected, even when the larvae are subsequently exposed to a potent inducer (KCl). In contrast, because many larvae do not readily undergo spontaneous metamorphosis (*e.g.*, the mollusc and coral used in the unpublished assays), it is not possible to determine whether the NCA are inhibiting settlement by means of a nontoxic pathway or are simply having no effect on the larvae.

If the inhibitory effect reported here occurs in nature as it does in the laboratory, then given extensive cover of NCA in the preferred habitat of *H. curvata* (shallow water on the reef crest), this interaction is likely to have a large effect in determining the small-scale distribution of *H. curvata*. Although the inhibitory effect is evident when larvae are prevented from contacting the surface of the NCA (unpub. data), indicating that the inhibitors can be released from the surface, it is likely that the inhibitors would operate on a microscopic scale because of dilution to noneffective concentrations a short distance from the NCA. The inability of NCA to induce settlement and metamorphosis in *H. curvata* is consistent with a general pattern that NCA induce settlement and metamorphosis in motile species whose feeding activities reduce fouling of the plant surface, and in sessile species that provide preferred habitat for NCA, but not in sessile species that potentially grow to smother and kill NCA (C. R. Johnson, unpub. manuscript).

Acknowledgments

We thank the Vision, Touch and Hearing Centre for use of their confocal microscope facilities, Colin McQueen for his help with confocal microscopy, Veronica Hinman for kindly providing some of the confocal micrographs, the staff of the Heron Island Research Station for their assistance in maintenance of animals, and two anonymous reviewers for their valuable comments. This work was supported by Australian Research Council grants to BMD and CRJ.

Literature Cited

Arnold, J. M., R. Eri, B. M. Degnan, and M. F. Lavin. 1997. A novel gene containing multiple EGF-like motifs transiently expressed in the papillae of the ascidian tadpole larva. *Dev. Dyn.* **210:** 264–273.

Barnes, J. R., and J. J. Gonor. 1973. The larval settling response of the lined chiton *Tonicella lineata*. *Mar. Biol.* **20:** 259–264.

Cloney, R. A. 1982. Ascidian larvae and events of metamorphosis. *Am. Zool.* **22:** 817–826.

Coon, S. L., W. K. Fitt, and D. B. Bonar. 1990. Competence and delay of metamorphosis in the Pacific oyster *Crassostrea gigas*. *Mar. Biol.* **106:** 379–387.

Davis, A. R., N. M. Targett, O. J. McConnell, and C. M. Young. 1989. Epibiosis of marine algae and benthic invertebrates: natural products chemistry and other mechanisms inhibiting settlement and overgrowth. *Bioorg. Mar. Chem.* **3:** 85–114.

Degnan, B. M., and M. F. Lavin. 1995. Highly repetitive DNA sequences provide evidence for a lack of gene flow between morphological forms of *Herdmania momus*. *Mar. Biol.* **124:** 293–299.

Degnan, B. M., and D. E. Morse. 1995. Developmental and morphogenetic gene regulation in *Haliotis rufescens* larvae at metamorphosis. *Am. Zool.* **35:** 391–398.

Degnan, B. M., J. C. Groppe, and D. E. Morse. 1995. Chymotrypsin mRNA expression in digestive gland amoebocytes: cell specification occurs prior to metamorphosis and gut morphogenesis in the gastropod *Haliotis rufescens*. *Roux's Arch. Dev. Biol.* **205:** 97–101.

Degnan, B. M., P. Rohde, and M. F. Lavin. 1996. Normal development and embryonic gene activity of the ascidian *Herdmania momus*. *Mar. Freshw. Res.* **47:** 543–551.

Degnan, B. M., D. Souter, S. M. Degnan, and S. C. Long. 1997. Induction of metamorphosis with potassium ions requires development of competence and an anterior signalling center in the ascidian *Herdmania momus*. *Dev. Genes Evol.* **206:** 370–376.

De Silva, P. H. D. H. 1962. Experiments on choice of substrate by *Spirorbis* larvae (Serpulidae). *J. Exp. Biol.* **39:** 483–490.

Draper, N. R., and H. Smith. 1991. *Applied Regression Analysis.* Wiley, New York. 709 pp.

Eri, R., J. M. Arnold, V. F. Hinman, K. M. Green, M. K. Jones, B. M. Degnan, and M. F. Lavin. 1999. Hemps, a novel EGF-like protein, plays a central role in ascidian metamorphosis. *Development* **126** (in press).

Fitt, W. K., M. P. Labare, W. C. Fuqua, M. Walch, S. L. Coon, D. B. Bonar, R. R. Colwell, and R. M. Weiner. 1989. Factors influencing bacterial production of inducers of settlement behaviour of larvae of the oyster *Crassostrea gigas. Microb. Ecol.* **17:** 287–298.

Gee, J. M. 1965. Chemical stimulation of settlement in larvae of *Spirorbis rupestris* (Serpulidae). *Anim. Behav.* **13:** 181–186.

Gee, J. M., and E. W. Knight-Jones. 1962. The morphology and larval behaviour of a new species of *Spirorbis* (Serpulidae). *J. Mar. Biol. Assoc. UK* **42:** 641–654.

Hadfield, M. G. 1986. Settlement and recruitment of marine invertebrates: a perspective and some proposals. *Bull. Mar. Sci.* **39:** 418–425.

Hadfield, M. G., and J. T. Pennington. 1990. Nature of metamorphic signal and its internal transduction in larvae of the nudibranch *Phestilla sibogae. Bull. Mar. Sci.* **46:** 455–464.

Hahn, K. O. 1989. Induction of settlement in competent abalone larvae. Pp. 101–112 in *Handbook of Culture of Abalone and Other Marine Gastropods,* K. O. Hahn, ed. CRC Press, Florida.

Harrigan, J. F. 1972. Behavior of the planula larva of the scleractinian coral *Pocillopora damicornis* (L.). *Am. Zool.* **12:** 723.

Heslinga, G. A. 1981. Larval development, settlement and metamorphosis of the tropical gastropod *Trochus niloticus. Malacologia* **20:** 349–357.

Hinman, V. F., and B. M. Degnan. 1998. Retinoic acid disrupts ectodermal and endodermal development in ascidian larvae and postlarvae. *Dev. Genes Evol.* **208:** 336–345.

Jensen, R. A., and D. E. Morse. 1984. Intraspecific facilitation of larval recruitment: gregarious settlement of the polychaete *Phragmatopoma californica* (Fewkes). *J. Exp. Mar. Biol. Ecol.* **83:** 107–126.

Johnson, C. R., and D. C. Sutton. 1994. Bacteria on the surface of crustose coralline algae induce metamorphosis of crown-of-thorns starfish. *Mar. Biol.* **120:** 305–310.

Johnson, C. R., D. C. Sutton, R. R. Olson, and R. Giddins. 1991. Settlement of crown-of-thorns starfish: role of bacteria on surfaces of crustose coralline algae and a hypothesis for deepwater recruitment. *Mar. Ecol. Prog. Ser.* **71:** 143–162.

Johnson, C. R., T. E. Lewis, D. S. Nichols, and B. M. Degnan. 1997. Bacterial induction of settlement and metamorphosis in marine invertebrates. *Proc. 8th Int. Coral Reef Symp.* **2:** 1219–1224.

Keough, M. J., and P. T. Raimondi. 1995. Responses of settling invertebrate larvae to bioorganic films: effects of different types of films. *J. Exp. Mar. Biol. Ecol.* **185:** 235–253.

Kerr, J. F. R., and B. V. Harmon. 1991. Definition and incidence of apoptosis: an historical perspective. Pp. 5–30 in *Apoptosis. The Molecular Basis of Cell Death,* L. D. Tomei and F. O. Cope, eds. Cold Spring Harbor Laboratory Press, Cold Spring Harbor, New York.

Kirchman, D., S. Graham, D. Reish, and R. Mitchell. 1982. Bacteria induce settlement and metamorphosis of *Janua* (Dexiospira) *brasiliensis* Grube (Polychaeta: Spiorbidae). *J. Exp. Mar. Biol. Ecol.* **56:** 153–163.

Leitz, T. 1997. Induction of settlement and metamorphosis of cnidarian larvae: signals and signal transduction. *Invertebr. Reprod. Dev.* **31:** 109–122.

Maki, J. S., D. Rittschof, J. D. Costlow, and R. Mitchell. 1988. Inhibition of attachment of larval barnacles, *Balanus amphitrite,* by bacterial surface films. *Mar. Biol.* **97:** 199–206.

Maki, J. S., D. Rittschof, M. O. Samuelsson, U. Szewzyk, A. B. Yule, S. Kjelleberg, J. D. Costlow, and R. Mitchell. 1990. Effect of marine bacteria and their exopolymers on the attachment of barnacle cypris larvae. *Bull. Mar. Sci.* **46:** 499–511.

Maki, J. S., D. Rittschof, and R. Mitchell. 1992. Inhibition of larval barnacle attachment to bacterial films: an investigation of physical properties. *Microb. Ecol.* **23:** 97–106.

Morse, A. N. C., and D. E. Morse. 1984. Recruitment and metamorphosis of *Haliotis* larvae induced by molecules uniquely available at the surfaces of the crustose red algae. *J. Exp. Mar. Biol. Ecol.* **75:** 191–215.

Morse, D. E. 1990. Recent progress in larval settlement and metamorphosis: closing the gap between molecular biology and ecology. *Bull. Mar. Sci.* **46:** 465–483.

Morse, D. E. 1993. Signalling in planktonic larvae. *Nature* **363:** 406.

Morse, D. E., N. Hooker, A. N. C. Morse, and R. A. Jensen. 1988. Control of larval metamorphosis and recruitment in sympatric agariciid corals. *J. Exp. Mar. Biol. Ecol.* **116:** 193–217.

Moss, G. A., and L. J. Tong. 1992. Effect of stage of larval development on the settlement of the abalone, *Haliotis iris. NZ J. Mar. Freshwater Res.* **26:** 69–73.

Pawlik, J. R. 1992. Chemical ecology of the settlement of benthic marine invertebrates. *Oceanogr. Mar. Biol. Annu. Rev.* **30:** 273–335.

Rowley, R. J. 1989. Settlement and recruitment of sea urchins (*Strongylocentrotus* spp.) in a sea-urchin barren ground and a kelp bed: are populations regulated by settlement or post-settlement processes? *Mar. Biol.* **100:** 485–494.

Rumrill, S. S., and R. A. Cameron. 1983. Effects of gamma-aminobutyric acid on the settlement of larvae of the black chiton *Katharina tunicata. Mar. Biol.* **72:** 243–247.

Satoh, N. 1994. *Developmental Biology of Ascidians.* Cambridge University Press, Cambridge. 234 pp.

Sebens, K. P. 1983a. Settlement and metamorphosis of a temperate soft-coral larva (*Alcyonium siderium* Verrill): induction by crustose algae. *Biol. Bull.* **165:** 286–304.

Sebens, K. P. 1983b. The larval and juvenile ecology of the temperate octocoral *Alcyonium siderium* Verrill. I. Substratum selection by benthic larvae. *J. Exp. Mar. Biol. Ecol.* **71:** 73–89.

Torrence, S. A., and R. A. Cloney. 1983. Ascidian larval nervous system: primary sensory neurons in adhesive papillae. *Zoomorphology* **102:** 111–123.

Trapido-Rosenthal, H. G., and D. E. Morse. 1986. Availability of chemosensory receptors is down regulated by habituation of larvae to a morphometric signal. *Proc. Natl. Acad. Sci. USA* **83:** 7658–7662.

Tritar, S., D. Prieur, and R. Weiner. 1992. Effects of bacterial films on the settlement of the oysters, *Crassostrea gigas* (Thunberg, 1793) and *Ostrea edulis,* Linnaeus, 1750 and the scallop *Pecten maximus* (Linnaeus, 1758). *J. Shellfish Res.* **11:** 325–330.

Wilson, D. P. 1955. The role of micro-organisms in the settlement of *Ophelia bicornis* Savigny. *J. Mar. Biol. Assoc. UK* **34:** 531–543.

Reference: *Biol. Bull.* **197:** 341–347. (December 1999)

Microinjection of an Antibody to the Ku Protein Arrests Development in Sea Urchin Embryos

JYOTSHNA KANUNGO[1,2], RUTH M. EMPSON[3], AND HOWARD RASMUSSEN[1,2,*]

[1] *Institute of Molecular Medicine and Genetics, Medical College of Georgia, Augusta, Georgia 30912, and* [2] *Marine Biological Laboratory, Woods Hole, Massachusetts 02543;* [3] *University Department of Pharmacology, University of Oxford, Oxford, OX1 3QT, UK*

Abstract. Ku is the regulatory subunit of the DNA-dependent protein kinase (DNA-PK). This enzyme plays a role in DNA repair, recombination, and transcription. It is composed of a large catalytic subunit (p460), and a regulatory heterodimer, the Ku protein, which consists of 86-kDa and 70-kDa subunits. These various components of the enzyme have been found in both eggs and embryos of the sea urchin. When variable amounts of a specific monoclonal antibody to the Ku protein (Ku 162) were injected into one cell of a 2-cell embryo of *Lytechinus pictus,* they caused a dose-dependent developmental arrest of the injected cell. The non-injected cell continued to develop normally. In contrast, injection of an antibody (N3H10) raised against the 70-kDa subunit of the Ku protein had no effect on development when injected into 2-cell-stage embryos. Co-injection of purified DNA-PK with the antibody reversed the antibody-mediated inhibition of development. In the fertilized egg and during the early stages of development, the DNA-PK was localized largely in the cytoplasm, but in later developmental stages, it assumed a nuclear location. On the basis of these results, we postulate that the injection of the Ku antibody either prevents the translocation of the DNA-PK into the nucleus or interferes with its enzymatic activity either in the nucleus or in the cytoplasm. In either case, the results suggest that DNA-PK plays an important role in regulating the early stages of embryogenesis in this primitive organism.

Introduction

The DNA-dependent protein kinase, DNA-PK, was first detected in the nuclei of mammalian cells (Walker *et al.*, 1985; Carter *et al.*, 1990). Studies in the last several years have provided evidence that this enzyme is involved in DNA repair, and in the activation of specific transcription factors (reviewed by Anderson and Lees-Miller, 1992; Weaver, 1995). It may also be involved in regulating DNA synthesis (Brush *et al.*, 1994), Ku-associated ATP-dependent helicase activity (Tuteja *et al.*, 1994), and DNA-dependent ATPase activity (Vishwanatha and Baril, 1990; Cao *et al.*, 1994). The enzyme consists of a large catalytic subunit, p460, and a heterodimeric regulatory component, the Ku protein. The latter consists of subunits of 86 and 70 kDa (Anderson, 1993; Gottlieb and Jackson, 1993). The Ku protein possesses a DNA-binding domain, and enzymatic activity is thought to be induced when this domain binds double-stranded DNA, (ds)DNA (Anderson and Lees-Miller, 1992; Dvir *et al.*, 1992; Anderson, 1993; Gottlieb and Jackson, 1993). However, the catalytic subunit of DNA-PK can be activated by another DNA-binding protein, heat shock transcription factor 1 (Peterson *et al.*, 1995). Additional complexity of control may be involved in its catalytic function, because the p86 subunit of Ku is a somatostatin receptor protein that can regulate the activity of protein phosphatase 2A (Le Romancer *et al.*, 1994). In addition, it has recently been reported that in cultured mammalian cells, a significant amount of the Ku protein is present in the cytoplasmic portion of the cell (Fewell and Kuff, 1996). These findings have led to the proposal that one or both of the Ku subunits may function in ways other than through the activation of nuclear DNA-PK, or that DNA-PK can be activated by factors other than (ds)DNA and function to regulate events in the cytoplasmic domain.

More recent work has shown that the enzyme is present in lower organisms, and particularly in the oocytes, eggs, and embryos of several marine invertebrates (Walker *et al.*, 1985; Kanungo *et al.*, 1996a, b) as well as in mice, frogs, and

Received 24 March 1999; accepted 16 August 1999.

* Author to whom correspondence should be addressed. E-mail: hrassmus@mail.mcg.edu

Drosophila (Finnie *et al.*, 1995). Thus, DNA-PK may have one or more evolutionarily conserved functions. Transgenic mice that are deficient in the Ku 86 subunit exhibit severe combined immunodeficiency (Nussenzweig *et al.*, 1996; Zhu *et al.*, 1996). Such mice are considerably smaller (40%–80%) than their normal littermates, and cultured cells derived from these mice display variable degrees of delay in cell cycle progression (Nussenzweig *et al.*, 1996).

That high concentrations of DNA-PK exist in the eggs of sea urchins (Kanungo *et al.*, 1996a, b) and frogs (Kanungo *et al.*, 1997) raises the interesting possibility that this enzyme may also play a regulatory role in early embryogenesis in these species. To explore this possibility, we initially undertook studies of DNA-PK localization and activation before and after fertilization of the eggs of *Arbacia punctulata*, the purple sea urchin. The unfertilized egg of this organism contains considerable amounts of both Ku and p460, as measured by western analysis, and by immunocytochemistry (Kanungo *et al.*, 1996b). These enzyme subunits are located largely, if not entirely, in the cytoplasmic compartment of the egg. Nonetheless, in the unfertilized egg, the DNA-PK cannot be activated by the addition of (ds)DNA to cytoplasmic extracts; *i.e.*, the enzyme is present in the cytoplasm in some cryptic form (Kanungo *et al.*, 1996b). Within minutes of fertilization, and without evidence of new protein synthesis, the enzyme is still in the cytoplasmic fraction, but can now be activated when (ds)DNA is added to this fraction. Of equal interest is that, if one coats Protein A Sepharose (PAS) beads with a specific monoclonal antibody to the Ku protein, Ku 162, and then uses these beads to isolate the Ku proteins from the cytoplasmic extracts of fertilized eggs, the beads bind the holoenzyme, and in this bound form the enzyme is active in the absence of (ds)DNA.

As the fertilized egg develops, there is a progressive shift of the various protein components of DNA-PK from a cytoplasmic to a nuclear location within the cell (Kanungo *et al.*, 1996b). The enzyme is located exclusively in the nuclear domain from the blastula stage onward, but in embryos at the 2- and 4-cell stages the enzymatic activity remains largely in the cytoplasm (Kanungo *et al.*, 1996a, b). In this report, we demonstrate that microinjection of the antibody, Ku 162, into one cell of a 2-cell embryo of *Lytechinus pictus*, the white sea urchin, inhibits the further development of the injected cell, but has no effect on the non-injected cell. This species, rather than *Arbacia punctulata*, was employed in the present experiments because the microinjection experiments were more easily performed in its embryos.

Materials and Methods

Collection of eggs and embryos. Male and female *Lytechinus pictus* were obtained from the Marine Resources Department of the Marine Biological Laboratory, Woods Hole, Massachusetts. Shedding of eggs and sperm was induced by injecting 0.5 ml of 0.5 *M* potassium chloride into the coelom. Batches of eggs were inseminated by mixing them with diluted sperm. Embryos were collected at scheduled times.

Kinase assay. Cytoplasmic extracts from the 2-cell embryos of *L. pictus* were prepared following the procedures already described (Ballinger *et al.*, 1984; Kanungo *et al.*, 1996a). Twenty-five units of purified human DNA-PK (Promega) or extracts prepared from *L. pictus* 2-cell embryos (from 250 embryos) was added to the antibody-coated PAS beads (Pharmacia) in a 500-μl volume made up by kinase assay buffer, and incubation was carried out at 4°C with constant mixing for 2 h. The PAS beads were washed six times with kinase assay buffer. The assay consisted of 12 μl of kinase assay buffer containing DTT (dithiothreitol) at a final concentration of 1 m*M*, 200 μ*M* of peptide substrate (EPPLSQEAFADLWKK) (Anderson, 1993), 2 m*M* of $MgCl_2$, 130 m*M* of ATP, and 10 μCi of gamma-[32P]ATP (3000 Ci/mmol) (NEN, Du Pont). The assay was carried out at 25°C for 30 min and stopped by adding glacial acetic acid to a final concentration of 30%. The reaction product was spotted onto p81 phosphocellulose discs (Whatman). Several washes with 15% acetic acid following a 30-min wash with 30% acetic acid were carried out. The discs were finally washed for 5 min in acetone, air-dried, and the uptake of radioactivity was assessed by scintillation counting. The counts obtained from the control beads, not coated with any IgG but treated with either the purified human DNA-PK or extracts of *L. pictus* embryos, were used as a means of measuring nonspecific background radioactivity. These values were subtracted from the counts obtained from reactions using mouse IgG- and Ku 162-coated PAS beads.

Immunoprecipitation. DNA-PK holoenzyme was immunoprecipitated with PAS beads that had been coated with the Ku antibody as follows: PAS beads were pre-swollen in kinase assay buffer (50 m*M* HEPES, pH 7.4; 10 m*M* EGTA, 40 m*M* NaCl, 100 m*M* potassium acetate, 8.5 m*M* $CaCl_2$, 2.29 m*M* $MgCl_2$, 277 m*M* glycerol). Two micrograms of preimmune mouse IgG or of a monoclonal antibody to human Ku (Ku 162) that recognizes a conformational epitope of the Ku protein (Neomarkers, CA) was added to a 10-μl packed volume of PAS beads. After 1 2-h incubation at 4°C with constant mixing, the beads were washed four times with kinase assay buffer.

Immunoblotting. The immunoprecipitates from PAS beads were eluted by boiling in SDS-PAGE sample buffer and resolved on a 7.5% SDS-PAGE column (Laemmli, 1974). Duplicate gels were run. One was employed to prepare autoradiographs. The proteins from the other gel were transferred to nitrocellulose membrane and immunoblotted (Towbin *et al.*, 1979) with anti-p460 antibody as previously described (Kanungo *et al.*, 1996b).

Preparation of antibodies for microinjection. The IgG antibodies (Ku 162 and N3H10) and the control IgGs were used for the microinjection experiments (Wang *et al.*, 1993). They were a generous gifts from Dr. Westley Reeves of the University of North Carolina, Chapel Hill. Antibodies against RNAP II were obtained from Promega, and preimmune mouse IgG was purified using a Pierce immunoglobulin purification kit (Cat # 44667). The purified IgGs were dialyzed against Ca^{2+}-, Mg^{2+}-free PBS (Silver, 1986) and concentrated to 3 μg/μl. The antibody-enzyme complex was prepared using 6 μg of Ku 162 antibody and 10 μg of purified human DNA-PK (Promega) and incubated on ice with intermittent mixing for 2 h. The mixed aliquot was diluted to 1 ml with Ca^{2+}-, Mg^{2+}-free PBS, then dialyzed (4 × 2 liters) overnight. The dialyzed antibody-enzyme complex was collected and concentrated using an Amicon filter concentration unit. The final concentration was brought back to the original volume of the antibody solution used (10 μl), giving a final concentration of 600 ng/μl Ku 162 and 1000 ng/μl DNA-PK.

Microinjection. Specimens of *L. pictus* were obtained from Marinus Inc. (Long Beach, CA). To induce a female to shed eggs, about 0.5 ml of 0.5 *M* KCl was injected into the intracoelomic cavity. The eggs were then passed through an 80-μM diameter Nitex membrane to remove the jelly that surrounded them and washed once in Ca^{2+}-containing seawater. A 0.5-ml sample of eggs was placed onto a glass coverslip previously coated with poly-L-lysine, and the eggs were exposed to sperm. Low densities of activated sperm (1/40,000 dilution of dry collected sperm) were used to prevent the occurrence of polyspermy. If fertilization proceeded with an efficiency of at least 90%, we continued the experiment. After fertilization, the dishes were covered and left at 17°–19°C for 1 h, at which time the embryos begin first division. Solutions of antibodies that had been dialyzed and concentrated to known protein concentrations (3 μg/μl in the pipette, estimated as a final amount of 15×10^{-12} g in the cell) were microinjected into one cell of the 2-cell-stage embryo shortly after first cleavage and before aster formation of the second cleavage. We typically injected 1%–2% of the volume of the embryo. An occasional embryo was damaged by the microinjection procedure; such clearly damaged embryos were discarded. The injected embryos were again covered and remained on the microscope stage for a further 2 h; we then determined the incidence of continued or arrested division. In most experiments, digital images of the eggs were recorded using either an integrating cooled CCD camera (Hamamatsu, USA) or an intensified CCD camera (Photonics Science, Robertsbridge, UK). The camera was attached either to a Metamorph (Universal Imaging, USA) system controlled by a Pentium PC or an Ionvision (Improvision, Coventry, UK) system run by a Macintosh. In all experiments we used the uninjected cell as an internal control.

Immunocytochemistry. Embryos at the 2-cell stage immediately after antibody injection were fixed in 3% formaldehyde (Kanungo *et al.*, 1996b) and processed for indirect immunofluorescence by incubating with fluorescein conjugated anti-mouse IgG (Sigma Cat # F 0257). Embryos were then whole-mounted onto glass coverslips and viewed with epifluorescence and appropriate filters using a Zeiss 135 inverted microscope (Zeiss, Oberkochen, Germany). Pictures were recorded using a cooled CCD camera and collected digitally with Metamorph (Universal Imaging, West Chester, PA). The DNA of some of the injected cells arrested as a consequence of Ku 162 administration were counter-stained with a DNA stain, Hoechst 3342 (0.001 mg/ml, Molecular Probes, Oregon) to determine the structure of the DNA, and specifically to answer the question of whether the failure of these cells to undergo cell division could be due to the induction of apoptosis as a result of the antibody.

Results and Discussion

To determine whether DNA-PK plays a unique role during early embryogenesis, we microinjected two anti-Ku antibodies, both raised against human Ku, into one cell of 2-cell embryos, and examined their effects on subsequent development. For technical reasons, we employed *Lytechinus pictus* in these studies rather than *Arbacia punctulata*. Hence, it was necessary to demonstrate that the fertilized eggs and early embryos of this species would express DNA-PK, and that this enzyme could be activated by the same means as those employed in the *Arbacia*. The first monoclonal antibody against the Ku protein, Ku 162, is an IgG that recognizes a conformational epitope on the Ku heterodimer. It has been used successfully to immunodeplete the DNA-PK activity from *Xenopus* oocytes (Kanungo *et al.*, 1997). When PAS beads are coated with this antibody, the enzyme in cytoplasmic extracts of *L. pictus* 2-cell embryos associates with the beads and is catalytically active in the absence of (ds)DNA (Fig. 1A). This antibody could not be employed in western analysis because it detects the Ku heterodimer, but neither of its subunits. However, a western blot of the proteins eluted from the PAS beads after labeling with [^{32}P]-gamma ATP shows that the interacting catalytic subunit of DNA-PK (p460) is present and can undergo autophosphorylation (Fig. 1B). An immunoblot of the immunoprecipitates made with a monoclonal antibody raised against the human p460 shows that a polypeptide identical to p460 is co-immunoprecipitated by Ku 162 antibody from the cytoplasmic extracts prepared from 2-cell embryos of *L. pictus* (Fig. 1B, lanes 5 and 6).

Based on these results, initial experiments were carried out to determine the effect of the injection of the antibody, Ku 162, or purified DNA-PK, into one cell of a 2-cell embryo. The injection protocol is illustrated in Figure 2A. A concentration of Ku 162 was chosen (2.5 pg) that completely arrested cell division in about one-half of the injected cells in 2-cell embryos 1 h after fertilization ($n = 17$). At that time, most of the uninjected embryos were at the 16/32 cell stage of development. On the other hand, further progression of the injected cell was completely arrested in one-half of the embryos ($n = 17$) injected with 2.5 pg of Ku 162 (Fig. 2B). Some cells were injected with a standard, but not maximally effective, concentration of purified DNA-PK either in the presence or absence of Ku 162. Injection of purified DNA-PK (the holoenzyme) alone had no effect on the development of the injected cells ($n = 12$, data not shown). However, when the holoenzyme was co-injected with Ku 162, the normal Ku 162-dependent inhibition of cell development was overcome, and 90% ($n = 10$) of the co-injected cells developed normally (Fig. 2C). In other cells, injection of either 0.5 *M* KCl ($n = 13$) or anti-RNA polymerase II antibody (Promega) ($n = 15$) had no effect on the ability of the antibody, Ku 162, to induce developmental arrest.

The further effects of the antibody, Ku 162, on embryonic cell development were analyzed in several ways: serial dilutions of Ku 162 were used to construct a dose-response curve; the effect of the second antibody, N3H10, was determined; and that of preimmune mouse IgG was examined. In addition, the possibility that Ku 162 was inhibiting cell division by causing cell necrosis or apoptosis was evaluated.

As shown in Figure 3A, the injection of standard aliquots of serially diluted Ku 162 antibody solution into one cell of a 2-cell embryo produced two effects on cell development. First, the number of cells that are completely arrested decreased as the amount of injected Ku 162 decreased (Fig. 3A, B, C). Second, at the highest concentration of Ku 162 (5 pg/cell) the development of all injected cells ($n = 21$) was completely arrested at the single-cell stage (Fig. 3A). The injection of 2.5 pg/cell of the Ku 162 antibody completely arrested development of 40% of the cells ($n = 18$) (Fig. 3A, right), and the remaining 60% of injected cells ($n = 17$) displayed variable rates of development (Fig. 3B, left). The injection of 1 pg of Ku 162 had no discernible effect on 50% of cells; *i.e.*, there was no evidence of developmental arrest (Fig. 3C, left). In this case, only 10% of cells showed a complete inhibition of cell division, and 40% displayed variable degrees of retarded development (Fig. 3C, right). To determine if Ku 162 antibody acts by inhibiting cell division, and not by causing cell necrosis or apoptosis, a number of the cells of embryos ($n = 12$) that displayed complete arrest were counter-stained with Hoechst 33342. Evidence of apoptosis was not seen in any of the arrested cells (Fig. 3A, right).

In contrast to the results with the Ku antibody 162, injection of comparable amounts of N3H10, a Ku antibody directed against the 70-kDa subunit of Ku, had no apparent effect on the development of the injected cell of a 2-stage

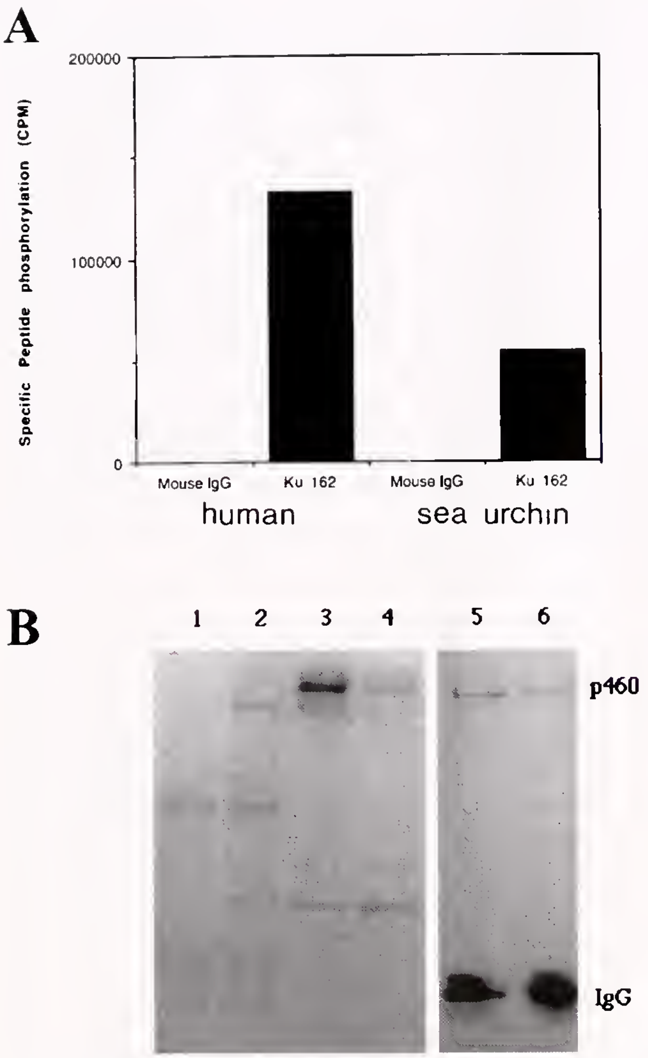

Figure 1. (A) DNA-PK activity of immunoprecipitates of human purified DNA-PK, and of the cytoplasmic extracts of 2-cell embryos of *Lytechinus pictus*. The DNA-PK assay was performed on washed PAS beads coated with the Ku 162 antibody. Reactions for a single experiment were run in duplicate. A representative assay (of five assays) is shown. Note that specific peptide phosphorylation activity is present in immunoprecipitates of cytoplasmic extracts of the sea urchin embryo. The activity from 250 embryos was a little less than half of that obtained from the immunoprecipitates of 25 units of purified human DNA-PK. PAS beads coated with preimmune mouse IgG did not immunoprecipitate any DNA-PK activity. (B) Autoradiograph of proteins recovered from the PAS beads coated with the Ku 162 antibody (lanes 1–4) showing autophosphorylated p460. Preimmune mouse IgG immunoprecipitated no labeled protein from purified human DNA-PK (lane 1) or from cytoplasmic extracts prepared from the two-cell-stage embryos of *L. pictus* (lane 2). The autophosphorylated DNA-PK catalytic subunit (p460) was present in Ku 162 immunoprecipitates of the human enzyme (lane 3), and it was present in Ku 162 immunoprecipitates of cytoplasmic extracts from 2-cell embryos of *L. pictus* (lane 4). Immunoblots of proteins eluted from lanes 3 and 4 are shown in lanes 5 and 6. The p460 polypeptide, eluted from Ku 162 immunoprecipitates of purified human DNA-PK on the immunoblot, was recognized by a monoclonal antibody, mAb 42-26 (Carter *et al.*, 1990) against human p460 (lane 5); a similar protein, from the Ku 162 immunoprecipitates of cytoplasmic extracts of *L. pictus* 2-cell embryos, was also recognized by this antibody (lane 6).

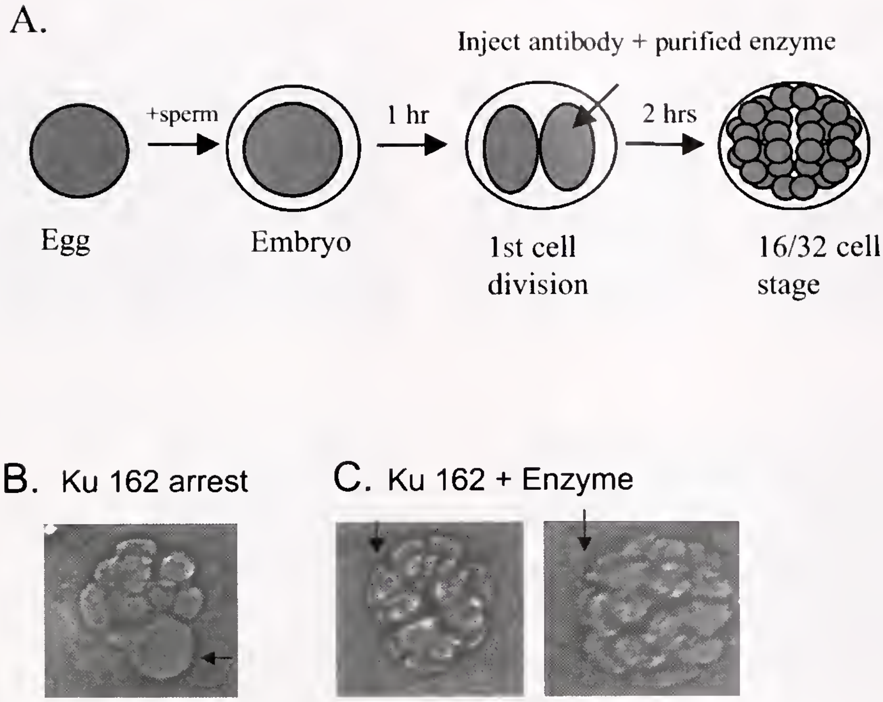

Figure 2. The effect of the antibody, Ku 162, with or without the simultaneous injection of the DNA-PK holoenzyme, on the ability of the injected cell in a 2-cell embryo of *Lytechinus pictus*. Injected cells are identified with an arrow. (A) A diagram of the experimental protocol. (B) The injection of the Ku 162 antibody (2.5 pg/cell) into one cell of a 2-cell embryo caused complete arrest of cell division in the injected cell, but not in the non-injected cell. (C) Two cells, one in each of a 2-cell stage embryo, microinjected simultaneously with Ku 162 antibody (2.5 pg/cell) and purified DNA-PK holoenzyme (4 pg/cell). In neither embryo was arrest or delay of cell division seen in the injected cells, or in the uninjected cells.

embryo (n = 15). It is of interest that one of the subunits (Ku 86) of Ku, but not the other (Ku 70), affected the postfertilization cleavage in sea urchin. This differential function specific to Ku 86 is consistent with the observation that potential functions of DNA-PK, such as X-ray sensitivity, is restored by Ku 86 even when Ku 70 is absent (Smider *et al.*, 1994; Taccioli *et al.*, 1994). An obvious question is whether these two Ku antibodies have different effects on the activity of DNA-PK. On the one hand, we have found that Ku N3H10, when put on PAS beads, is incapable of immunoprecipitating DNA-PK in an active form. What is not yet clear is whether either antibody inhibits DNA-PK *in situ* or in cytoplasmic extracts of sea urchin embryos. Attempts to address this question by using cytoplasmic extracts have proven difficult for several technical reasons, so at present we have no answer.

The present results show that a sufficient concentration of an antibody specific against the Ku heterodimer, Ku 162, when injected into the cytoplasm of one cell of a two-cell sea urchin embryo, completely blocked later cell divisions of the injected cell (Fig. 3). The simultaneous injection of the holoenzyme rescued the injected cells from developmental arrest (Fig. 3C). At intermediate doses, the effects of the Ku 162 antibody were attenuated; *i.e.*, the number of cells completely arrested was reduced, and a number of cells were delayed, but not completely arrested, in their development (Fig. 2B, C). Although the simultaneous injection of the holoenzyme rescued the cells injected with Ku 162 from developmental arrest, injection of the holoenzyme itself had no consistent effect. In these rescue experiments, however, the purified holoenzyme, which is quite labile, appears to be acting as an antigen rather than as an active enzyme. In this light, the lack of effect when the holoenzyme is injected should not be taken as evidence that endogenous active enzyme has no effect on cell cycle progression. Additional experiments will be needed to test this issue in a critical fashion.

An inhibition of mitosis in sand dollar embryos follows the microinjection of antibodies against the calcium transport enzyme of muscle (Silver, 1986). And a similar inhibition occurs in sea urchin embryos after the microinjection of antibodies against kinesin-like proteins (Wright *et al.*, 1993), the mitotic calcium transport system (Hafner and Petzelt, 1987), or a 62-kDa mitotic apparatus protein (Dinsmore and Sloboda, 1989). On the other hand, a controlled translocation of other nuclear enzymes, like DNA polymerase (Loeb *et al.*, 1970), from cytoplasmic stores to the nucleus occurs during sea urchin embryogenesis. Recently,

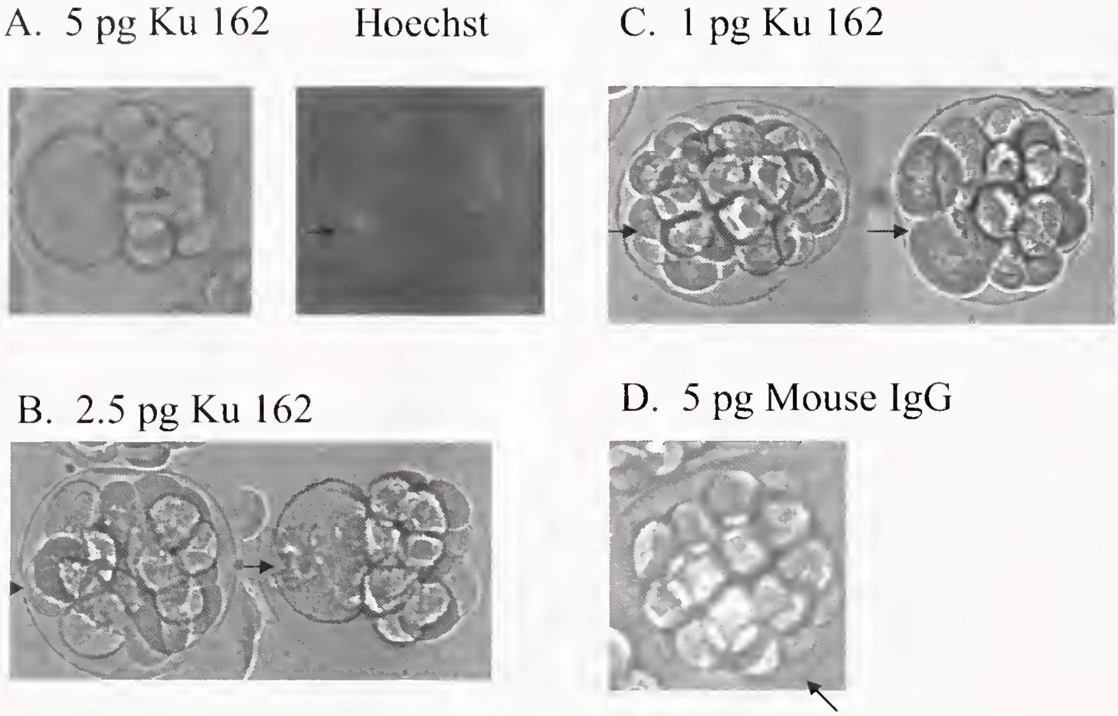

Figure 3. The dose-response effects of the Ku 162 antibody on the arrest of cell division in one cell of a 2-cell stage embryo of *Lytechinus pictus.* (A) When 5 pg/cell of the Ku 162 antibody was microinjected into one cell of a 2-cell embryo, the further development of the injected cells was completely inhibited (left). Shown is an injected cell (arrow) that persists as a single cell, whereas the non-injected cell of the 2-cell stage embryo has undergone further cell divisions. Also shown (right) is an embryo in which Ku 162 had arrested development of the injected cell, and the cell was then labeled with the DNA stain Hoechst 33342. In all arrested cells tested, the DNA could be seen as a single entity (arrow). (B) The injection of 2.5 pg of Ku 162 antibody (see arrow) led to complete arrest in some injected cells (right), whereas the remaining displayed variable rates of cell division. Typical embryos with complete inhibition of cell developmental arrest (right), and partial development arrest (left) are shown. (C) At the lowest concentration of Ku 162, 1 pg/cell, nearly half of the embryos displayed normal rates of cell division (left), 10% displayed complete arrest, and the remainder displayed variable rates of development (right). (D) The effect of preimmune mouse IgG on development. One cell of the 2-cell embryo was injected with 5 pg of preimmune mouse IgG. Of 23 embryos injected with IgG, 23 went on to divide normally. A representative picture of one such cell is shown. The arrow indicates the location of the injected cell.

it has been reported that the catalytic activity of DNA-PK does not require Ku (Yaneva *et al.*, 1997; Hammerstein and Chu, 1998). The simplest hypothesis to account for our result is that the Ku 162 antibody interferes with a temporally controlled transport of DNA-PK from a cytoplasmic store to the nucleus as development proceeds. Alternatively, this antibody may inhibit the activity of the enzyme in either a nuclear or a cytoplasmic location. In any case, our results suggest that Ku plays an important role in the control of cell cycle events during early embryogenesis.

Acknowledgments

We thank Westley Reeves for the generous gift of the Ku antibodies used in these studies and Timothy Carter for the anti-p460 antibody. We thank Judith Venuti, Richard Cameron, and John Hardin for helpful discussions, Krishna Patel for help with some of the experiments, and Rudi Rottenfusser and Ivan Burba of Carl Zeiss, Inc., for their generous help in providing microscopic facilities that allowed this work to be performed. Support was provided by NIH grant DK-19813-20 to H. R. and by funds from the Medical College of Georgia; R.M.E. is supported by the Wellcome Trust.

Literature Cited

Anderson, C. W. 1993. DNA damage and the DNA-activated protein kinase. *Trends Biochem. Sci.* **18:** 433–437.

Anderson, C. W., and S. P. Lees-Miller. 1992. The nuclear serine/threonine protein kinase DNA-PK. *CRC Crit. Rev. Eukaryotic Gene Expression* **2:** 283–314.

Ballinger, D. G., S. J. Bray, and T. Hunt. 1984. Studies of the kinetics and ionic requirements for the phosphorylation of ribosomal protein S6 after fertilization of *Arbacia punctulata* eggs. *Dev. Biol.* **101:** 192–200.

Brush, G. S., C. W. Anderson, and T. J. Kelly. 1994. The DNA-activated protein kinase is required for the phosphorylation of replication protein A during simian virus 40 DNA replication. *Proc. Natl. Acad. Sci. USA* **91:** 12520–12524.

Cao, Q. P., S. Pitt, J. Leszyk, and E. F. Baril. 1994. DNA-dependent ATPase from HeLa cells is related to human Ku autoantigen. *Biochemistry* **33:** 8548–8557.

Carter, T., I. Vancurova, I. Sun, W. Lou, and S. Deleon. 1990. A DNA-activated protein kinase from HeLa cell nuclei. *Mol. Cell. Biol.* **10:** 6460–6471.

Dinsmore, J. H., and R. D. Sloboda. 1989. Microinjection of antibodies to a 62 kD mitotic apparatus protein arrests mitosis in dividing sea urchin embryos. *Cell* **57:** 127–134.

Dvir, A., S. R. Peterson, M. W. Knuth, H. Lu, and W. S. Dynan. 1992. Ku autoantigen is the regulatory component of a template-associated protein kinase that phosphorylates RNA polymerase II. *Proc. Natl. Acad. Sci. USA* **89:** 11920–11924.

Fewell, J. W., and E. L. Kuff. 1996. Intracellular redistribution of Ku immunoreactivity in response to cell-cell contact and growth modulating components in the medium. *J. Cell Sci.* **109:** 1937–1946.

Finnie, N. J., T. M. Gottlieb, T. Blunt, P. A. Jeggo, and S. P. Jackson. 1995. DNA dependent protein kinase activity is absent in xrs-6 cells: implications for site-specific recombination and DNA double-strand break repair. *Proc. Natl. Acad. Sci. USA* **92:** 320–324.

Gottlieb, T. M., and S. P. Jackson. 1993. The DNA-dependent protein kinase: requirement for DNA ends and association with Ku antigen. *Cell* **72:** 131–142.

Hafner, M., and C. Petzelt. 1987. Inhibition of mitosis by an antibody to the mitotic calcium transport system. *Nature* **330:** 264–266.

Hammerstein, O., and G. Chu. 1998. DNA-dependent protein kinase: DNA binding and activation in the absence of Ku. *Proc. Natl. Acad. Sci. USA* **95:** 525–530.

Kanungo, J., B. Calhoun, Y. Takeda, J. A. Hardin, and H. Rasmussen. 1996a. Gradual loss of a DNA-inducible protein kinase activity from the cytoplasmic extracts of *Arbacia* embryos. *Biol. Bull.* **191:** 281–282.

Kanungo, J., J. A. Walker, D. Woodrum, J. A. Hardin, and H. Rasmussen. 1996b. A DNA-inducible kinase activity undergoes a change in cellular localization during development in *Arbacia*. *Biol. Bull.* **191:** 283–284.

Kanungo, J., R. S. Cameron, Y. Takeda, and J. A. Hardin. 1997. DNA-dependent protein phosphorylation activity in *Xenopus* is coupled to a Ku-like protein. *Biol. Bull.* **193:** 147–152.

Laemmli, U. K. 1974. Cleavage of structural proteins during the assembly of the head of bacteriophage T4. *Nature* **227:** 680–685.

Le Romancer, M. L., F. Reyl-Desmars, Y. Cherifi, C. Pigeon, S. Bottari, O. Meyer, and M. J. M. Lewin. 1994. The 86-kDa subunit of autoantigen Ku is a somatostatin receptor regulating protein phosphatase-2A activity. *J. Biol. Chem.* **269:** 17464–17468.

Loeb, L. A., B. Fansler, R. Williams, and D. Mazia. 1970. Sea urchin nuclear DNA polymerase. I. Localization in nuclei during rapid DNA synthesis. *Biochim. Biophys. Acta* **217:** 50–55.

Nussenzweig, A., C. Chen, V. D. C. Soares, M. Sanchez, K. Sokol, M. C. Nussenzweig, and G. C. Li. 1996. Requirement for Ku80 in growth and immunoglobulin V(D)J recombination. *Nature* **382:** 551–555.

Peterson, S., A. Kurimasa, M. Oshimura, W. S. Dynan, E. M. Bradbury, and D. J. Chen. 1995. Loss of the catalytic subunit of the DNA-dependent protein kinase in DNA double-strand-break-repair mutant mammalian cells. *Proc. Natl. Acad. Sci. USA* **92:** 2934–2938.

Silver, R. B. 1986. Mitosis in sand dollar embryos is inhibited by antibodies directed against the calcium transport enzyme of muscle. *Proc. Natl. Acad. Sci. USA* **83:** 4302–4306.

Smider, V., W. K. Rathmell, M. R. Lieber, and G. Chu. 1994. Restoration of X-ray resistance and V(D)J recombination in mutant cells by Ku cDNA. *Science* **266:** 288–291.

Taccioli, G. E., T. M. Gottlieb, T. Blunt, A. Priestley, J. Demengeot, A. R. Lehman, F. W. Alt, S. P. Jackson, and P. A. Jeggo. 1994. Ku80: product of the XRCC5 gene and its role in DNA repair and V(D)J recombination. *Science* **265:** 1442–1445.

Towbin, H., T. Staehelin, and J. Gordon. 1979. Electrophoretic transfer of proteins from polyacrylamide gels to nitrocellulose sheets: procedure and some applications. *Proc. Natl. Acad. Sci. USA* **76:** 457–460.

Tuteja, N., R. Tuteja, A. Ochem, P. Taneja, N. W. Huang, A. Simoncsits, S. Susik, K. Rahman, L. Marusik, J. Chen, J. Zhang, S. Wang, and A. Falaschi. 1994. Human DNA helicase II: a novel DNA unwinding enzyme identified as Ku autoantigen. *EMBO J.* **13:** 4991–5001.

Vishwanatha, J. K., and E. F. Baril. 1990. Single-stranded-DNA-dependent ATPase from HeLa cells that stimulates DNA polymerase alpha-primase activity: purification and characterization of the ATPase. *Biochemistry* **29:** 8753–8759.

Walker, A. I., T. Hunt, R. J. Jackson, and C. W. Anderson. 1985. Double-stranded DNA induces the phosphorylation of several proteins including the 90,000 mol. wt. heat-shock protein in animal cell extracts. *EMBO J.* **4:** 139–145.

Wang, J., C. H. Chou, J. Blankson, M. Satoh, M. W. Knuth, R. A. Eisenberg, D. S. Pisetsky, and W. H. Reeves. 1993. Murine monoclonal antibodies specific for conserved and non-conserved antigenic determinants of the human and murine Ku antigens. *Mol. Biol. Rep.* **18:** 15–28.

Weaver, D. T. 1995. What to do to an end: DNA double-strand-break repair. *Trends Genet.* **11:** 388–392.

Wright, B. D., M. Terasaki, and J. M. Scholey. 1993. Roles of kinesin and kinesin-like proteins in sea urchin embryonic cell division: evaluation using antibody microinjection. *J. Cell. Biol.* **123:** 681–689.

Yaneva, M., T. Kowalewski, and M. R. Lieber. 1997. Interaction of DNA-dependent protein kinase with DNA and with Ku: biochemical and atomic-force microscopy studies. *EMBO J.* **16:** 5098–5112.

Zhu, C., M. A. Bogue, D-S. Lim, P. Hasty, and D. B. Roth. 1996. Ku86-deficient mice exhibit severe combined immunodeficiency and defective processing of V(D)J recombination intermediates. *Cell* **86:** 379–389.

Reference: *Biol. Bull.* **197:** 348–360. (December 1999)

Spectral Sensitivity of Vision and Bioluminescence in the Midwater Shrimp *Sergestes similis*

S. M. LINDSAY[1,*], T. M. FRANK[2], J. KENT[3], J. C. PARTRIDGE[3], AND M. I. LATZ[1]

[1] *Marine Biology Research Division, Scripps Institution of Oceanography, University of California San Diego, La Jolla, California;* [2] *Harbor Branch Oceanographic Institution, Ft. Pierce, Florida; and* [3] *School of Biological Sciences, University of Bristol, United Kingdom*

Abstract. In the oceanic midwater environment, many fish, squid, and shrimp use luminescent countershading to remain cryptic to silhouette-scanning predators. The midwater penaeid shrimp, *Sergestes similis* Hansen, responds to downward-directed light with a dim bioluminescence that dynamically matches the spectral radiance of oceanic downwelling light at depth. Although the sensory basis of luminescent countershading behavior is visual, the relationship between visual and behavioral sensitivity is poorly understood. In this study, visual spectral sensitivity, based on microspectrophotometry and electrophysiological measurements of photoreceptor response, is directly compared to the behavioral spectral efficiency of luminescent countershading. Microspectrophotometric measurements on single photoreceptors revealed only a single visual pigment with peak absorbance at 495 nm in the blue-green region of the spectrum. The peak electrophysiological spectral sensitivity of dark-adapted eyes was centered at about 500 nm. The spectral efficiency of luminescent countershading showed a broad peak from 480 to 520 nm. Both electrophysiological and behavioral data closely matched the normalized spectral absorptance curve of a rhodopsin with λ_{max} = 495 nm, when rhabdom length and photopigment specific absorbance were considered. The close coupling between visual spectral sensitivity and the spectral efficiency of luminescent countershading attests to the importance of bioluminescence as a camouflage strategy in this species.

Introduction

In terrestrial, aquatic, and aerial environments, vision is central to many predator-prey interactions. Thus, camouflage (crypsis) is a common method of predator avoidance used by a wide variety of invertebrates and vertebrates. The oceanic midwater environment offers few structural refuges from predation. Visual predators commonly search for prey silhouetted against dim downwelling irradiance. Camouflage strategies adopted by midwater animals include transparency, reflective camouflage, and photophore-mediated counterillumination (reviewed by McFall-Ngai, 1990). For example, some animals such as gelatinous zooplankton have a refractive index similar to that of seawater, making them optically transparent (Chapman, 1976). Many fish use reflective camouflage to blend with the optical environment by simulating the angular distribution of oceanic light (Denton, 1970). Finally, animals may produce downward-directed bioluminescence, disrupting or minimizing their silhouette (Clarke, 1963; Herring, 1982; Young, 1983); this behavior is termed luminescent countershading or counterillumination.

For luminescent countershading to be effective, the optical properties of the bioluminescence must match those of the optical environment. Laboratory studies have demonstrated that the angular distribution, intensity, and spectral emission of luminescent countershading from many midwater animals match those of oceanic downwelling irradiance (reviewed by Young, 1983). Under certain conditions, some squid modify the spectral emission of their bioluminescence, presumably to match diel changes in the spectral composition of downwelling light (Young *et al.*, 1980).

The optical properties of the oceanic midwater environment derive from downwelling light and bioluminescence, and the relative importance of these components varies with

Received 15 December 1998; accepted 23 September 1999.

* Present address: School of Marine Sciences, University of Maine, Orono, ME 04469-5741; E-mail: slindsay@maine.edu

time of day, depth, and distance from the source of light. Far-field illumination consists of diffuse, dim downwelling light that decreases exponentially with depth and has an irradiance spectrum centered on 475 nm (Jerlov, 1968). Near-field illumination consists mainly of bioluminescence, manifested as point sources of light with emission spectra peaking primarily between 460 and 490 nm, depending on species (Herring, 1983; Widder *et al.*, 1983; Latz *et al.*, 1988). Deep-sea and midwater animals have well-developed eyes with unique adaptations for dealing with the *in situ* light conditions they encounter. Specialized features include large or tubular eyes (squids and fishes: Bowmaker, 1976; Locket, 1977), yellow-pigmented lenses that increase the contrast between bioluminescence and downwelling light (fishes: Muntz, 1976), rod-dominated retinae in fishes for greater light sensitivity (Bowmaker, 1976), and visual pigments with blue-shifted (470–490 nm) absorption maxima (fishes: Partridge *et al.*, 1989; Douglas *et al.*, 1995; cephalopods: Kito *et al.*, 1993; crustaceans: references in Frank and Case, 1988). These adaptations attest to the importance of bioluminescence and vision in the deep sea.

Thus there may be a close link between visual spectral sensitivity and the spectral efficiency of luminescent countershading (*i.e.*, behavioral spectral sensitivity) if luminescent countershading is to be a successful means of camouflage. In the simplest case, the visual system, bioluminescence emission, and oceanic downwelling light will all operate in the same spectral range. This hypothesis has never been tested, largely due to the difficulty in obtaining quantifiable behavioral data from midwater and deep-sea animals. Typically, these organisms survive for very short periods when brought to the surface, and controlled experimental studies of meaningful behaviors have been difficult to achieve. Studies by Land (1992) and Frank and Widder (1994a,b) are the only investigations of visually mediated swimming responses by midwater and deep-sea crustaceans under environmentally relevant illumination levels. The only examination of the spectral efficiency of bioluminescence in a marine organism was performed by Kay (1965) with the euphausiid crustacean, *Meganyctiphanes norvegica*, although the intensity of the photoflash stimulus employed was considerably brighter than *in situ* levels experienced by the animal.

The present study investigates visual and behavioral sensitivity in the bioluminescent penaeid shrimp, *Sergestes similis*, a common member of the midwater community in the northeast Pacific Ocean. Bioluminescence in *S. similis* originates from modified portions of the hepatopancreas, called organs of Pesta, which produce ventrally directed light. Previous laboratory studies indicate that the emitted light is consistent with a camouflage function. Bioluminescence is tuned to the optical properties of the midwater environment, matching the spectral distribution (Widder *et al.*, 1983), irradiance (Warner *et al.*, 1979), and angular distribution (Latz and Case, 1982) of downwelling oceanic light. In addition, ventrally directed dim glowing is produced only when a downward-directed light stimulus is present and is extinguished within seconds of the cessation of the stimulus (Warner *et al.*, 1979; Latz and Case, 1992).

Luminescent countershading in *Sergestes similis* is clearly dependent on vision; covering the eyes reversibly abolishes the response (Warner *et al.*, 1979). Shrimp that are completely dark adapted are initially unresponsive to light, but continued light exposure induces bioluminescence after a latency of several minutes, reaching maximum intensity about 20 min later (Latz and Case, 1992). Once luminescence is induced, responses exhibit the typical fast kinetics of luminescent countershading observed in squid and fishes; luminescence increases within several seconds of light stimulation and reaches maximum intensity in approximately 30 s (Latz and Case, 1992). Thereafter, the lack of eye shine suggests that the eyes are light adapted when luminescent countershading occurs.

In the present study, behavioral and physiological approaches were used to characterize the link between vision and luminescent countershading behavior in *Sergestes similis*. Results demonstrate a close coupling between visual spectral sensitivity and the spectral efficiency of luminescent countershading, further supporting the hypothesized role of bioluminescence in camouflaging this species.

Materials and Methods

Collection of animals and tissue

Adult specimens of *Sergestes similis* Hansen were collected at night from depths of 55 to 300 m in the San Diego Trough (8 Dec 1996, 12 Jun 1997, and 25 Jun 1997), the San Clemente Basin (10 Aug 1997), both near San Diego, California, USA, and in the Santa Barbara Basin (28 Sep 1997 and 24 Oct 1997), near Santa Barbara, California, during cruises of the *RV R.G. Sproul*. Animals were collected using a modified Tucker trawl with a closing light-proof cod end (after Childress *et al.*, 1977). The cod end was closed at depth and animals were brought to the surface and sorted in 5°C seawater under dim red light. Animals were placed in light-proof containers filled with chilled seawater and transported to the shore laboratory, where they were maintained in constant darkness in aquaria with flow-through, 5 μm filtered seawater at a temperature of 10°C. All experiments were performed within one week of collection; only actively swimming specimens were used for testing. Animals were not fed, and except for brief exposure to dim red light during handling, they remained in constant darkness.

For electroretinogram studies, animals collected on 8 Dec 1996 from the San Diego Trough were shipped in light-tight containers to the Harbor Branch Oceanographic Institution

(HBOI), Fort Pierce, Florida. At HBOI, shrimp were maintained in chilled (10°C) filtered seawater in constant darkness.

For microspectrophotometry experiments, adult *S. similis* were collected off the coast of southern California during a cruise of the *RV New Horizon* between 12 May and 26 May 1996 using similar equipment and methods (see Kent, 1997). Eyes were removed and cryopreserved for subsequent microspectrophotometry, which was carried out at the University of Bristol, UK. Eyes were orientated in plastic wells filled with cryomount (Tissue Tek, OCT Compound, Miles Inc., USA) and rapidly frozen with fluorocarbon spray (Cryospray 22, Bright Instrument Co., UK). Frozen blocks were individually sealed in plastic bags to avoid desiccation, placed in light-tight aluminum tubes, and maintained at −70°C until sectioned for microspectrophotometry.

Microspectrophotometry (MSP) experiments

Frozen eyes from adult *Sergestes similis* were sectioned using a cryostat and cut sections (average thickness 14 μm) were transferred to a 22 × 50 mm No. 1 coverslip, mounted in Tropic Marin™ artificial seawater, covered with a 19 mm diameter No. 1 coverslip, and sealed with a ring of silicone grease. Sectioning proceeded from the region of the cornea most distal to the eyestalk towards the center of the eye.

Visual pigment absorption was measured with a single beam, wavelength scanning, computer-controlled microspectrophotometer described by Hart *et al.*, (1998). For invertebrate MSP, the instrument was modified by the incorporation of a high intensity substage lamp that was used for photoconversion of the visual pigment in the rhodopsin (R) state to the metarhodopsin (M) state using red light, and for the photobleaching of R and M mixtures to photoproducts of non-physiological importance using actinic white light exposure. This protocol is fully described by Kent (1997) and follows the methods of Cronin and Goldsmith (1982).

Initial "baseline" scans were first made from 350 to 750 nm at 1-nm intervals in a tissue-free area of the cell preparation and then followed by several "sample" scans from rhabdomeric tissue. Sample scans were first made from an unexposed rhabdom which was then exposed to red light (wavelength of cut-on *ca.* 610 nm) for approximately 20 s to photoconvert the rhodopsin pigment to a stable R/M mixture, after which the rhabdom was re-scanned. The tissue was then photobleached by an exposure of approximately 30 min to white light and re-measured. Difference spectra between these data sets were calculated, from which the absorption spectra of the M and R pigments in the rhabdom were determined by the method of Cronin and Goldsmith (1982) as further developed by Kent (1997). In brief, visual pigment templates (Stavenga *et al.*, 1993; Palacios *et al.*, 1996) were fitted to the measured difference spectra to provide estimates of the λ_{max} of R and M pigments (Partridge and De Grip, 1991; Hart *et al.*, 1998). The fraction of R in the photo-steady state resulting from the red light exposure was estimated by comparing the integrated absorbances of the two templates to the red light. This fraction was then subtracted from the R/M mixture in the photo-steady state and a new template fitted to provide a better estimate of the λ_{max} of the M pigment. This traditional analytical method assumes that all the visual pigment in the initial measurements made from the rhabdom was in the form of R. The use of iterative template fitting methods developed by Kent (1997) attempted to avoid the need for this assumption, and provided estimates of the proportion of M in the initial measurements and the λ_{max} values of R and M.

Electroretinogram experiments

Specimens used for electrophysiological recordings were mounted under dim red light in a holder and suspended in a chamber filled with chilled (10°C) seawater. This arrangement allowed for enough pleopod movement to maintain respiratory currents across the gills. The electroretinogram (ERG), which is the summed mass responses from a large number of photoreceptor cells, was recorded with a 10 μm tip metal microelectrode (F. Haer & Co.) placed subcorneally under dim red light. The reference electrode was placed in the other eye, which was covered with black Vaseline to block out light, and a silver-chloride electrode grounded the water bath. Signals were amplified with an Xcell-3 Microelectrode amplifier (F. Haer & Co.), equipped with a high impedance probe to eliminate electrode polarization problems. Low frequency filters were set to minimal filtering (0.01–1 Hz) to minimize distortion due to AC amplification. Monochromatic test flashes were provided by a tungsten light source, coupled to a grating monochromator (Instruments SA) with 1 mm slits in place, and delivered to the eye through one branch of a bifurcated light pipe. The light pipe was placed 3 mm away from the eye, providing illumination which covered the whole eye. Flash duration of 100 ms was controlled by a Uniblitz shutter (Model VS14S) under computer control using LabView software (National Instruments, Inc.). Irradiance was controlled with a neutral density wheel under computer control, calibrated in units of photons $cm^{-2} s^{-1}$ with a UDT Optometer (Model S370) and a radiometric probe placed 3 mm from the tip of the light guide. The adapting light source for chromatic adaptation experiments was an incandescent light filtered with a 400 nm or 480 nm broadband filter (Melles Griot). The adapting light was delivered to the eye through the other branch of the bifurcated light guide, ensuring that both the adapting and test lights were acting on the same group of photoreceptor cells. Data were instantaneously analyzed for peak to peak response height using a program written in LabView, digitized and stored to disk for later analysis.

The eye was stimulated with 100 ms test flashes of monochromatic light adjusted for irradiance until either a 100 or 200 μV criterion response was obtained at each wavelength tested. To ensure that the eye remained in the same state of dark adaptation during the experiment, the response to a flash of standard wavelength and irradiance was tested periodically throughout the experiment. Spectral sensitivity curves were generated based on the inverse of the irradiance required to produce the criterion response at each wavelength. Absorptance spectra were constructed from visual pigment templates (Stavenga *et al.*, 1993).

Behavioral sensitivity experiments

Because *Sergestes similis* produces bioluminescence only in the presence of a light stimulus, a chopped light source was used to avoid detection of the stimulus illumination by the light detector (see below). Bioluminescence was measured in the brief dark intervals when the stimulus was off, similar to the methods of Warner *et al.* (1979) and Latz and Case (1992). Illumination from a Dolan-Jenner model 180 tungsten-halogen source was conducted through an optical fiber bundle to an Optometrics model DMC1 monochromator and then through another optical fiber bundle to a JML Optical electro-mechanical shutter that controlled the timing of the "on" and "off" transitions of the stimulus. The stimulus light was chopped at 80 Hz using an Oriel variable frequency chopper, attenuated by neutral density filters to control light intensity, and diffused by a single layer of glassine paper before entering the test chamber. Because the critical flicker-fusion rate at such low irradiances is <60 Hz for marine crustaceans (Waterman, 1961; Frank, 1999), the test animal perceived the chopped stimulus light as continuous.

For testing, specimens were loosely restrained by a clear acrylic clamp around the cephalothorax and placed in a sealed, clear acrylic chamber (1.75 × 2.5 × 10 cm) filled with 10–11°C seawater. The clamp allowed free movement of pleopods and other appendages, yet prevented the specimen from shifting position. Throughout an experiment, seawater chilled to 11–12°C by a Fisher Scientific model 1016S recirculating chiller was recirculated through the chamber at a rate of 100 ml min^{-1} using a Masterflex peristaltic pump. The specimen chamber was placed in the center of the light collection chamber, which consisted of a 25 cm diameter Labsphere integrating sphere. The advantage of an integrating chamber is that the measurement of emitted light is minimally affected by photophore or animal position. Bioluminescence was detected by a Burle model 8850 photon-counting photomultiplier operating at −1790 V, after passing through a second optical chopper operating at 80 Hz but synchronized 180° out of phase with the stimulus light chopper by means of a Scitec Instruments synchronizer. Thus, the photomultiplier measured only the bioluminescence produced by the test specimen and not the stimulus light. The photomultiplier signal was processed by a Pacific Instruments amplifier/discriminator; square wave pulses were sent to a Newport Instruments model P6000A frequency to voltage converter. The resulting voltage was measured using a Data Translation model 2801 data acquisition board mounted in a personal computer. Data acquisition, real-time display, and storage were controlled by a data collection program programmed using Data Translation DTVEE software. Bioluminescence and photodiode levels were continuously acquired at 2 Hz. Voltages were subsequently converted to photon values based on a photometric calibration of the photomultiplier using 1 ml of Cyalume® chemiluminescent liquid and a calibrated Quantalum 2000 photometer. Bioluminescence in units of photons m^{-2} s^{-1} was obtained by dividing photon flux (photons s^{-1}) by the cross-sectional area of the ventral surface of the organs of Pesta for an adult shrimp of size 14 mm carapace length (Latz, 1983).

To measure stimulus intensity, a Graseby Optronics model 260 calibrated sensor head was mounted in the integrating sphere in the same position as the specimen chamber. Light levels measured in watts with a Graseby Optronics model S370 Optometer were converted to irradiance units of photons m^{-2} s^{-1}.

Quantum sensitivity. To determine the threshold level of light that prompts luminescent countershading by *Sergestes similis,* bioluminescence produced by induced animals in response to various intensities of light was measured. To induce luminescent countershading, dark-adapted animals were exposed to a standard light stimulus (490 nm, 2.24 × 10^{13} photons m^{-2} s^{-1}) for 25 min (Latz and Case, 1992); wavelength and irradiance settings were chosen based on preliminary experiments. After induction, shrimp were exposed to a series of test stimuli as follows: 60 s darkness, 60 s test stimulus, 60 s darkness, 5 or 10 min standard stimulus (490 nm, 2.24 × 10^{13} photons m^{-2} s^{-1}), repeating this pattern with new test stimuli until all irradiances were tested, typically within 2 h. The purpose of the standard stimulus was to maintain shrimp in the light-adapted induced state for luminescent countershading so that their bioluminescence responses to the test stimuli would show fast kinetics representative of luminescent countershading (Latz and Case, 1992). In addition, the responses to the standard stimulus were used to monitor the condition of the animal, and, if necessary, correct for changes in animals' responsiveness over time (see data correction below). The duration of the standard stimulus was determined by the return to the level of bioluminescence measured during the initial induction. Typically, this occurred within 5 min, but occasionally, after the dimmest irradiance test stimuli, 10 min of the standard stimulus was required. Test stimuli of

490 nm light were used at the following irradiance levels (in units of photons $m^{-2} s^{-1}$): 2.22×10^{11}, 3.45×10^{11}, 6.41×10^{11}, 3.95×10^{12}, 1.01×10^{13}, 2.24×10^{13}, 3.40×10^{13}, 3.87×10^{13}, 4.98×10^{13}, 7.65×10^{13}, 9.72×10^{13}.

Spectral sensitivity. To measure the spectral efficiency of luminescent countershading, dark-adapted animals were first exposed to a 490-nm stimulus (at 2.24×10^{13} photons $m^{-2} s^{-1}$) for 25 min to induce counterillumination. Animals were then exposed to light stimuli at 20-nm increments from 400 to 640 nm, following the general protocol described above: 60 s darkness, 60 s test wavelength stimulus, 60 s darkness, 5 or 10 min of the standard illumination to maintain the induced countershading state. This process was repeated for each wavelength tested. The average duration of a complete trial was 3 h. The order of test wavelengths was randomized. Because shrimp eyes operate as photon counters, and the total number of photons in a given stimulus is a function of both light intensity and wavelength, stimulus irradiance was adjusted at each wavelength using neutral density filters to obtain equal photon irradiance levels at each wavelength. Even so, there were slight variations in stimulus irradiance levels, which ranged from 1.16×10^{13} photons $m^{-2} s^{-1}$ at 400 nm to 2.52×10^{13} photons $m^{-2} s^{-1}$ at 620 nm. Bioluminescence data were subsequently corrected as detailed below to reflect a standard irradiance of 1.20×10^{13} photons $m^{-2} s^{-1}$. Mean bioluminescence was based on the last 20 s of each 60-s test stimulus, and the last 4 min for the standard 5–10-min illumination.

Data correction. Because the test stimuli in the spectral sensitivity experiments varied slightly in intensity, all data were corrected to reflect the intensity of bioluminescence at each wavelength based on a stimulus irradiance of 1.20×10^{13} photons $m^{-2} s^{-1}$. Data collected in the quantum sensitivity experiments were used to model the correlation between bioluminescence intensity and stimulus intensity at 490 nm. One of two regression equations (for either San Diego or Santa Barbara collected specimens) was used to calculate (1) the predicted bioluminescence at 1.20×10^{13} photons $m^{-2} s^{-1}$, and (2) the predicted bioluminescence at the irradiance level measured for each test wavelength stimulus. Dividing (1) by (2) gave a proportional correction factor that was multiplied by the bioluminescence value at each test wavelength. Because not enough specimens were available to empirically derive the relationship between stimulus intensity and bioluminescence intensity at every wavelength tested, the assumption was made that quantum sensitivity did not change with stimulus wavelength, so that the relationship observed at 490 nm holds for the other wavelengths. This assumption of univariance is supported by the visual sensitivity and MSP experiments which demonstrated that only a single visual pigment is present.

The correction for variable stimulus intensity also assumes that the observed relationship between bioluminescence intensity and stimulus intensity holds at all levels of light adaptation or for changes in specimen responsiveness due to fatigue. This is an important assumption because in 4 of 9 spectral efficiency experiments, bioluminescence intensity showed slight but significant decreases over the course of the experiment. Nevertheless, in all cases the bioluminescent responses to test stimuli showed the characteristic fast kinetics indicative of the induced counterillumination condition (Latz and Case, 1992). In those 4 specimens demonstrating a decrease in the standard response at 490 nm, a correction factor for each data point for each of these individuals was determined based on a linear regression describing the intensity of bioluminescence in response to the standard stimuli as a function of time.

The effects of these corrections are shown for a single individual (Fig. 1). Responses were corrected for a standard stimulus irradiance of 1.20×10^{13} photons $m^{-2} s^{-1}$ as shown in the following example. For this individual, the relationship between bioluminescence irradiance (in original units of volts s^{-1}) and stimulus irradiance at 490 nm (the standard stimulus wavelength) is best described by the equation: bioluminescence $= 3.66 \times 10^{-6} * \text{irradiance}^{0.391}$ ($r^2 = 0.40$, $F = 20.03$, d.f. $= 1,31$, $P = 0.0001$). Using this regression equation, the predicted bioluminescence at an irradiance of 1.20×10^{13} photons $m^{-2} s^{-1}$ is 0.4805 volts s^{-1}. For a test wavelength of 400 nm, the measured stimulus irradiance was 1.28×10^{13} photons $m^{-2} s^{-1}$. The predicted bioluminescence (using the regression equation) for a 490 nm stimulus at this irradiance level is 0.4924 volts s^{-1}, giving a correction factor of 0.976 (0.4805/0.4924). Thus, for a 490-nm stimulus, bioluminescence intensity at 1.20×10^{13} photons $m^{-2} s^{-1}$ is 0.976 times that at 1.28×10^{13} photons $m^{-2} s^{-1}$. Making the important assumption that quantum sensitivity does not change with stimulus wavelength, the bioluminescence value measured at 400 nm is multiplied by 0.976 to reflect the response to a "standard"

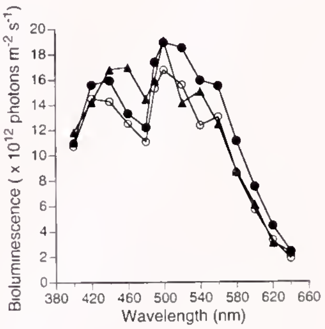

Figure 1. Correction of spectral efficiency data for a single specimen of *Sergestes similis.* Uncorrected data (solid circles) were corrected for variations in stimulus intensity (open circles) and for both stimulus intensity and temporal decrease in responsiveness (closed triangles). Refer to Materials and Methods for details on data correction.

stimulus of 1.20×10^{13} photons $m^{-2} s^{-1}$. This correction was made in turn for each stimulus wavelength.

Data from this individual were also corrected for a decrease in responsiveness, because the least-squares linear regression between bioluminescence intensity (in volts s^{-1}) and the order of presentation of the 490 nm standard stimulus showed a slight but significant decay in response according to the following equation: bioluminescence = −0.022 * (order of presentation) + 0.887 ($r^2 = 0.72$, F = 36.35, d.f. = 1,15, $P < 0.0001$). Because the response to 490 nm standard stimuli was somewhat variable over time, this regression equation is the best description of the general decay in response. The decay correction factor was calculated based on time of stimulus presentation by first calculating the predicted bioluminescence at a given stimulus time using the previous equation, and then dividing that result by the bioluminescence measured at the first 490 nm standard stimulus. For example, bioluminescence in response to the fifth 490 nm standard stimulus was calculated to be 0.7771 using this regression equation. Dividing this value by the value for the first standard stimulus (0.7857) gives a decay correction factor of 0.989. Making similar calculations for the order of presentation of each test wavelength stimulus, the bioluminescence value for each test stimulus was divided by the appropriate decay correction factor. The decay correction assumes that the effects were equivalent at all wavelengths tested. Following corrections for stimulus intensity and response decay, all bioluminescence data were converted from units of volts s^{-1} to photons $m^{-2} s^{-1}$ as previously described, based on the photometric calibration of the photomultiplier and the cross-sectional area of the ventral surface of the organs of Pesta for an adult shrimp of size 14 mm carapace length (Latz, 1983). To directly compare visual and behavioral spectral sensitivity, irradiance values from the electrophysiological experiments and bioluminescence values from the behavioral experiments were normalized for each individual.

Results

Microspectrophotometry (MSP)

Spectral absorbance, based on MSP measurements of five sections of rhabdomeric tissue from a single individual, was unimodal with maximum absorbance in the blue-green (Fig. 2A). Assuming that the initial scans were uncontaminated with metarhodopsin (M) pigment, template fitting to the difference spectra (Fig. 2B) indicated a rhodopsin (R) pigment with a λ_{max} of 492 nm. The template best-fitting the R/M mixture after red light exposure yields a λ_{max} of 485 nm. This value was corrected to allow for the residue of R in the R/M mixture to give a best estimate of the M pigment λ_{max} of 484 nm, and an M/R extinction ratio (at the respective λ_{max} values) of 1.333. Iterative template-fitting methods (Kent, 1997) suggest, however, that the fraction of M in the initial measurements may have been as high as 15% and, after correction for this contamination, the R and M λ_{max} values can be revised to 495 nm and 484 nm, respectively, with a M/R extinction ratio of 1.406.

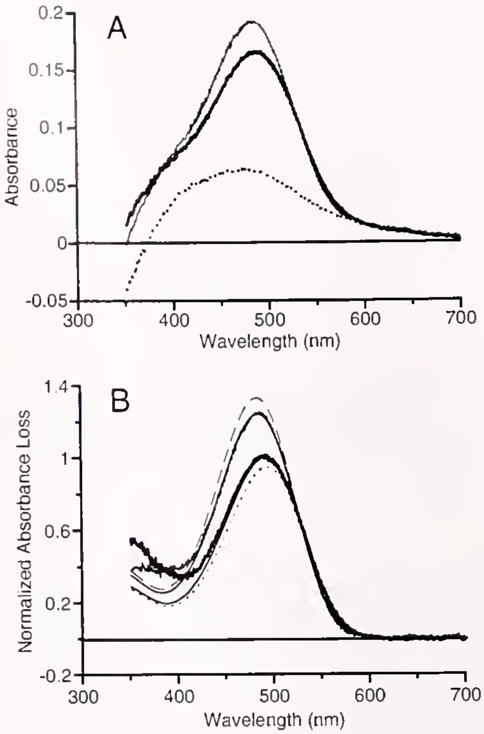

Figure 2. Spectral absorbance based on microspectrophotometry of five sections of rhabdomeric tissue from the retina of *Sergestes similis*. (A) Averaged absorbance spectra; bold trace shows the initial absorbance, light trace shows the absorbance following saturating red light illumination, dashed trace shows the absorbance following photobleaching with bright white light. For display, spectra have been standardized to an absorbance of zero at 730 nm, the limit of the spectral scan. (B) Averaged difference spectra for photobleaching of the rhabdom from its initial state [bold; derived from bold trace minus dotted trace in (A)] and for the photobleaching of the rhabdom from its steady state R/M mixture following saturating red light [light; derived from light trace minus dotted trace in (A)]. Specific absorbances at the λ_{max} for these absorbance spectra were 0.0078 μm^{-1} and 0.0094 μm^{-1}, respectively. Smooth solid traces are best-fit templates (Stavenga *et al.*, 1993) with λ_{max} values of 492 nm and 485 nm, respectively. The dashed line is the estimated metarhodopsin absorbance spectrum (λ_{max} = 484 nm) resulting from the correction for the residual M in the R/M mixture difference spectrum (light trace), and the absorbance spectrum of the rhodopsin (dotted; λ_{max} = 495 nm), after correcting for contaminating M in the initial scan (bold).

Visual sensitivity of the eye (ERG)

The electrophysiologically determined visual spectral sensitivity of dark-adapted specimens of *Sergestes similis* indicated that the sensitivity maximum was centered at approximately 500 nm in the blue-green region of the spectrum (Fig. 3). Both blue (480 nm) and near-UV (400 nm) chromatic adaptation uniformly depressed the sensitivity

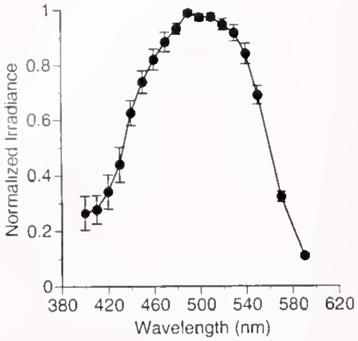

Figure 3. Visual spectral sensitivity of *Sergestes similis* based on electroretinogram (ERG) measurements. Sensitivity, based on the inverse of the irradiance required to elicit a 100 or 200 μV response, showed a broad maximum centered around 500 nm. Symbols represent means ± SE for 6 specimens.

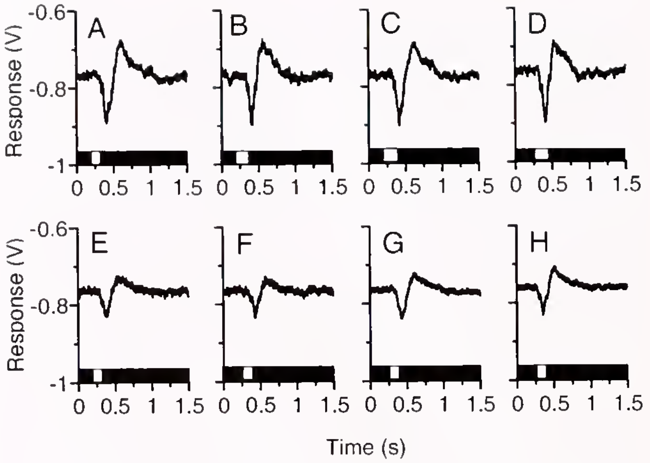

Figure 5. Effect of chromatic adaptation on the ERG waveform of *Sergestes similis*. Dark bars indicate light stimulus off; white bars indicate light stimulus on. (A–D) 200 μV responses measured in one specimen. (E–H) 100 μV responses measured in another specimen. Response to a 430 nm stimulus for the (A) dark-adapted condition and (B) after 400 nm light adaptation. Response to a 530 nm stimulus for the (C) dark-adapted condition and (D) after 400 nm light adaptation. Response to a 430 nm stimulus for the (E) dark-adapted condition and (F) after 480 nm light adaptation. Response to a 530 nm stimulus for the (G) dark-adapted eye and (H) after 480 nm light adaptation.

curve across the spectrum (Fig. 4), and had no effect on ERG waveform (Fig. 5). These results are consistent with those of the MSP study indicating that only a single visual pigment is present.

Behavioral sensitivity

The magnitude of luminescent countershading by *S. similis* depended on the level of stimulus irradiance (Fig. 6). A behavioral threshold occurred at approximately 2–3 × 10^{12} photons $m^{-2} s^{-1}$ (Fig. 7). At lower stimulus irradiances, light levels were near background as measured in an empty chamber. At higher stimulus irradiances, bioluminescence increased as the 0.35 power of irradiance according to a power law (log-log) regression ($r^2 = 0.61$). Thus the increase in bioluminescence by *S. similis* did not match the increase in stimulus irradiance.

The magnitude of bioluminescence varied according to stimulus wavelength (Fig. 8). After correcting the data to reflect a standard irradiance of 1.20 × 10^{13} photons $m^{-2} s^{-1}$, and when necessary, for temporal decreases in responsiveness, the mean spectral efficiency curve for luminescent countershading showed a broad peak between 480 and 540 nm (Fig. 9) in the blue-green region of the visible spectrum. The wavelength dependence of the spectral efficiency was not symmetrical. Bioluminescence decreased dramatically approaching the red wavelengths and was negligible above 600 nm, while an intermediate response still occurred in the near-UV at 400 nm. A comparison of the mean data for all 9 specimens tested showed that the corrected data fell within the 95% confidence limits of the original data.

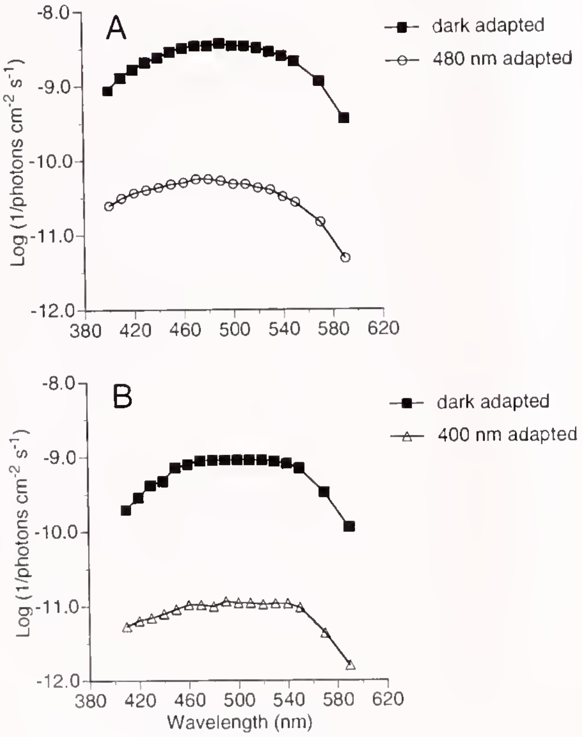

Figure 4. Effect of chromatic adaptation on the spectral sensitivity of *Sergestes similis*. Illumination of the eyes with (A) 480 nm, and (B) 400 nm light uniformly depressed spectral sensitivity across the spectrum compared to the response of dark-adapted eyes.

Discussion

In the midwater shrimp, *Sergestes similis*, there is a close similarity between visual and behavioral photon and spectral sensitivities. The microspectrophotometry results indi-

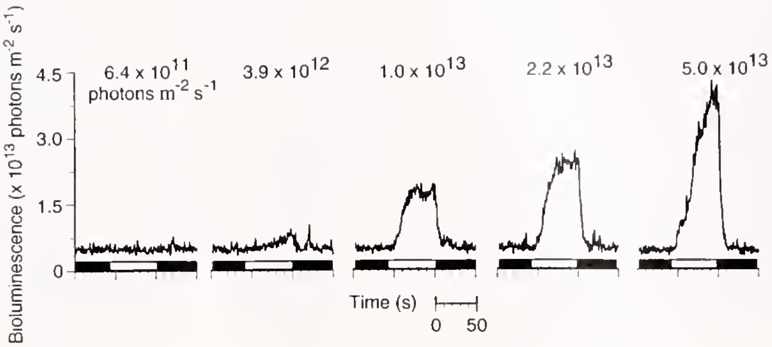

Figure 6. Representative bioluminescent responses by a single specimen of *Sergestes similis* to increasing stimulus irradiance. Bioluminescence was first induced using a 490 nm stimulus of intermediate intensity, then the specimen was presented with 60-s stimuli from a range of intensities, all at 490 nm. The line represents the level of bioluminescence versus time. Dark bars indicate stimulus light off; white bars indicate stimulus light on. Values above graphs are stimulus intensities.

cated that *S. similis* possesses a single visual pigment with maximum absorbance around 495 nm. Such data can be used to calculate the spectral sensitivity of a photoreceptor containing this visual pigment by first calculating the spectral absorptance of an axially illuminated rhabdom. To do this, two additional pieces of information are required: rhabdom length and the specific absorbance (*i.e.*, absorbance μm^{-1}) of the visual pigment in the photoreceptor. Rhabdom lengths vary somewhat with eye size, but by sectioning the aldehyde preserved eyes of *S. similis*, rhabdom lengths were found to range from 128 to 161 μm for shrimps with carapace lengths of 11.8 to 14.2 mm (T. Frank, unpublished data). For the specimens used in the ERG experiments, which ranged in size from 10.3 to 13.5 mm carapace length, the estimated upper and lower bounds for rhabdom lengths in these animals were approximately 120 to 150 μm, with a mean of approximately 135 μm. This value is similar to that reported by Hiller-Adams *et al.* (1988) for the sergestid *Sergia tenuiremis.* MSP measurements of specific absorbance for *S. similis* suggest a specific absorbance of 0.0074 μm^{-1} (Kent, 1997) although this is significantly lower that the value of 0.01 μm^{-1} reported by Cronin and Frank (1996) in *Systellaspis debilis,* but only slightly lower than the value of 0.008 μm^{-1} reported as being 'typical' of crustacean photoreceptors (*e.g.*, Cronin and Goldsmith, 1982). At wavelengths greater than the peak absorbance (495 nm), the spectral absorptance closely matches spectral sensitivity data from ERG measurements and the spectral efficiency curve of luminescent countershading (Fig. 10). Using maximum or minimum values instead of mean rhabdom length has little effect on spectral absorptance, while increasing specific absorbance to levels more typical of crustacean photoreceptors leads to a better fit between the different data sets at long wavelengths. At short wavelengths, however, there is significant divergence which probably cannot be attributed to the photosensitivity spectrum of the rhodopsin departing from the absorptance spectrum at short wavelengths, although data on this subject are limited (Dartnall, 1972). It is more likely that the effective spectral sensitivity of the eye is affected by intraocular, pre-retinal filters which selectively filter short wavelength light (Goldsmith, 1978; reviewed by Fein and Szuts, 1982).

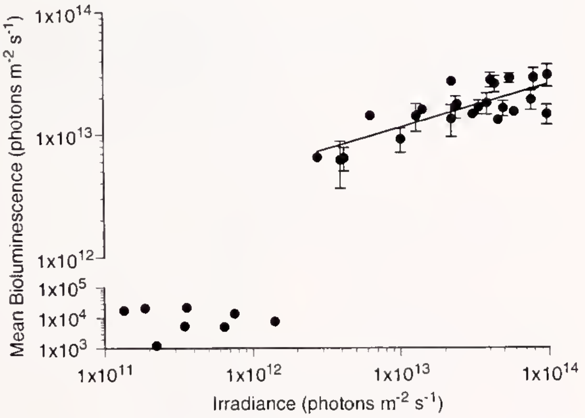

Figure 7. Effect of light intensity on average maximum bioluminescence produced by *Sergestes similis.* All stimuli were at a wavelength of 490 nm. The magnitude of bioluminescence measured during the last 20 s of each 60-s test stimulus was averaged for each individual. Ten specimens were tested; means ± SE are shown. Responses for stimulus irradiance $> 2 \times 10^{12}$ photons m^{-2} s^{-1} were best described by the power law (log-log) equation $y = (1.87 \times 10^{6})x^{0.35}$ ($r^2 = 0.61$). At lower stimulus irradiance values, light levels were near background. Note the separate scale for above-threshold bioluminescence.

Electrophysiological measurements using the electroretinogram (ERG), corresponding to the summed mass response of a large number of photoreceptor cells to a light stimulus, were performed to determine the behaviorally relevant spectral sensitivity of *S. similis.* While this technique provides a more comprehensive assessment of the visual spectral sensitivity of an organism than do measure-

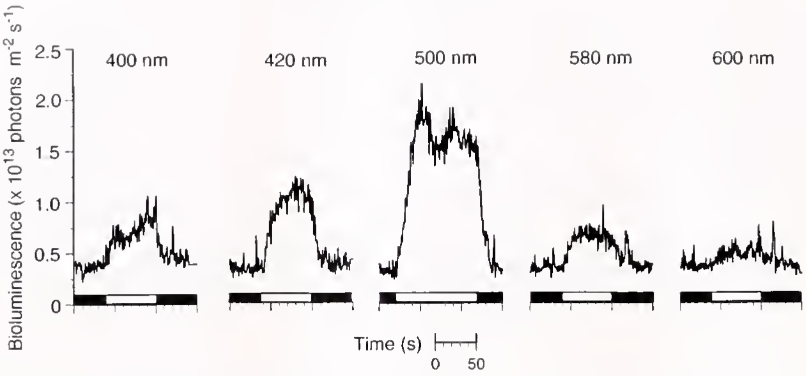

Figure 8. Representative bioluminescent responses by a single specimen of *Sergestes similis* to different wavelengths of light. Bioluminescence was first induced using a 490 nm stimulus of intermediate intensity, then the specimen was presented with 60 s stimuli at various wavelengths, at approximately equal irradiance of 1.5 × 10^{13} photons m^{-2} s^{-1}. Bars as for Figure 5.

ments from single photoreceptors (reviewed by Goldsmith, 1986), ERG results do not reflect the amount of higher order processing of visual input, nor the behavioral response to visual stimuli. Thus the behavioral studies of luminescent countershading extend the physiological assessment, resulting in a comprehensive description of the organism's sensory and behavioral response to ecologically relevant light stimulation.

Luminescent countershading by *S. similis* occurred over a relatively narrow range of irradiance. A behavioral threshold occurred at approximately 3 × 10^{12} photons m^{-2} s^{-1}, as lower irradiance levels resulted in minimal levels of bioluminescence which were not significantly different from background. This illumination level may represent the minimum irradiance causing light adaptation of the eye, which appears to be required for luminescent countershading (Latz and Case, 1992). Under ideal conditions, bioluminescence should exactly match stimulus irradiance. As discussed by Young *et al.* (1980), differences in geometry between stimulus and response as well as calibration assumptions make direct comparisons difficult, although relative changes should still be valid. In the present study, the range of stimulus irradiance tested was less than two orders of magnitude. Within this range, bioluminescence increased with stimulus irradiance according to a power law (log-log) regression as found by Young *et al.* (1980) for midwater squid and fish. However, the magnitude of the increase in bioluminescence did not match the magnitude of the increase in stimulus irradiance. Other counterilluminating animals may not precisely match changes in the stimulus irradiance (Young *et al.*, 1980), yet they exhibit a better match over a larger dynamic illumination range for luminescent countershading than did *S. similis* in the present study.

In *Sergestes similis*, behavioral spectral efficiency was similar to visual spectral sensitivity. A survey of species for which behavioral and physiological spectral sensitivity data are available (Table 1) suggests that behavioral spectral

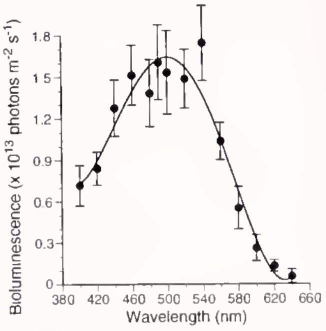

Figure 9. Behavioral spectral sensitivity of *Sergestes similis* based on the bioluminescence spectral efficiency, corrected for a stimulus irradiance of 1.2 × 10^{13} photons m^{-2} s^{-1} (see text). Symbols represent means ± SE for 9 specimens; the curve is a fourth degree polynomial function fitted to the data, where $y = 6.1 \times 10^4x^4 - 1.2 \times 10^8x^3 + 9.2 \times 10^{10}x^2 - 3.0 \times 10^{13}x + 3.6 \times 10^{15}$.

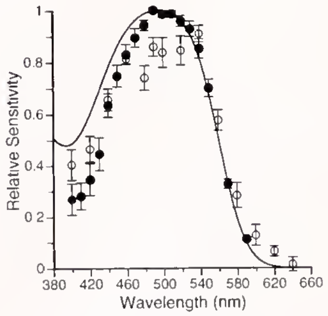

Figure 10. Comparison of relative visual and behavioral spectral sensitivity of *Sergestes similis*. Symbols represent means ± SE. Both the normalized ERG sensitivity (solid circles) and normalized bioluminescence spectral efficiency (open circles) coincide well at long wavelengths with the calculated spectral absorbance (solid line) of a rhodopsin with peak absorbance at 495 nm, a rhabdom axial length of 135 μm and a specific absorbance of 0.0074 μm^{-1}.

Table I

Comparison of behavioral and visual spectral sensitivities of several species

Species	Behavioral λ_{max} (nm)	Behavior assayed	Visual λ_{max} (nm)*	Photopigment absorption λ_{max} (nm)	References
Bioluminescent					
Photinus pyralis (Firefly)	565	Female BL flash in response to simulated male BL flash	565	Rhodopsin, 545; screening pigment, 517 (MSP)	Worthy and Lall, 1996
Photinus scintillans (Firefly)	575	Initiation of BL flashing, horizontal light stimulus	Approx. 435, approx. 575, possibly 360	2 receptors with near-UV and yellow peak sensitivity; screening pigment, 525 (MSP)	Lall, 1993 Lall *et al.*, 1988
	360, 425	Initiation of BL flashing, vertical light stimulus			
Meganyctiphanes norvegica (euphausiid crustacean)	Broad peak from 470–490	Number of individuals producing BL in response to photoflash	490	488 (MSP)	Kay, 1965 Denys and Brown, 1982 Frank, unpubl. data
Sergestes similis (penaeid shrimp)	Broad peak from 480–540	Magnitude of bioluminescence	500	Rhodopsin, 495 (MPS)	Present study
Non-bioluminescent					
Nautilus pompilius (cephalopod mollusc)	470	Positive phototaxis	NA	Rhodopsin based, 467 (PE)	Muntz, 1986, 1987
Clupea harengus (herring)	510–520	Feeding, phototaxis, barrier perception	NA	500 (PE)	Blaxter, 1964
Gadus morhua (cod)	460–520 and 550 (dark adapted) 400–470 (light adapted)	Heart rate, using cardiac conditioning protocol	490 (dark adapted) 490 and 550–590 (light adapted)	NA	Anthony and Hawkins, 1983
Hyalomma dromedarii (tick)	380 and 480–520	Positive phototaxis	470, weak secondary max in UV	NA	Kaltenrieder *et al.*, 1989
Amblyomma variegatum (tick)	480–520	Positive phototaxis	470	NA	Kaltenrieder *et al.*, 1989
Hyla cinerea (treefrog)	430 and 500	Optomotor response	NA	Two pigments: 435 and 503	King *et al.*, 1993

In most examples, data are drawn from several sources rather than from a single comprehensive study. Studies were limited to those that measured sensitivity in response to a broad spectrum of wavelength stimuli. Maximum absorbance by photopigments was determined by microspectrophotometry (MSP) or pigment extraction (PE). BL = bioluminescence/bioluminescent, ERG = electroretinogram, NA = not available or unknown.

* Visual λ_{max} based on ERG data except for Worthy and Lall (1996), where it is based on both ERG data and intracellular retinal recordings.

Table II

Relative behavioral and visual sensitivities to near-UV versus blue-green light for bioluminescent deep-sea crustaceans possessing a single visual pigment

Species	Visual Spectral Sensitivity Maximum (nm)	Relative Visual Sensitivity (400 nm/500 nm)	Relative Behavioral Sensitivity (400 nm/500 nm)
Acanthephyra curtirostris	510	0.24	0.18
Acanthephyra smithi	510	0.30	0.16
Notostomus gibbosus	490	0.24	0.10
Sergestes similis	500	0.27	0.48

For species except *Sergestes similis*, behavioral sensitivity was defined as the reciprocal of the irradiance required to elicit a simple movement behavior for 400 nm or 500 nm stimuli (Frank and Widder, 1996). For *S. similis*, behavioral sensitivity was based on the standardized magnitude of bioluminescence. For all species, visual sensitivity was based on electroretinogram (ERG) measurements (data from present study and Frank and Case, 1988).

sensitivity tends to be somewhat broader than that measured electrophysiologically, though the behavioral maxima are similar to maxima in visual sensitivity and photopigment absorption. Douglas and Hawryshyn (1990) noted that behavioral measurements of spectral sensitivity in fish varied with method, with some behaviors, such as the tail-flip response, being activated only by certain wavelength stimuli. Behavioral sensitivity also may depend on the type of stimulus applied. For example, the initiation of bioluminescent flashing by the firefly, *Photinus scintillans*, has different spectral sensitivity maxima for horizontal and vertical light stimuli (Table I; Lall, 1993). These different sensitivities appear to be associated with different classes of photoreceptors. Similarly, multiple peaks in behavioral sensitivity in the tree frog *Hyla cinerea* (King *et al.*, 1993) and the tick *Hyalomma dromedarii* (Kaltenrieder *et al.*, 1989) correspond to peak sensitivities of different classes of photoreceptors in these animals (Table I).

Sergestes similis shows somewhat greater behavioral sensitivity in the near-UV compared to several other species of deep-sea decapods that have single visual pigments and similar ERG-measured visual sensitivities (Table II; Frank and Widder, 1996). This difference may be a reflection of the different behaviors assayed (*i.e.*, luminescent countershading versus movement behaviors) and their ecological context. The ecological significance of sensitivity to near-UV and UV light remains unknown. The intensity of downwelling irradiance at mesopelagic depths, calculated utilizing attenuation coefficients measured in the epipelagic zone, may be sufficient to be visually detected (Frank and Widder, 1996). High UV visual sensitivity may aid in luminescent countershading where the strategy is to match the downwelling irradiance field. Alternatively, UV sensitivity may play a role in regulating the diurnal vertical migrations of *S. similis* and other vertically migrating crustaceans (Forward, 1988).

The present study is the first to measure the complete spectral efficiency of behavior in a deep-sea animal using ecologically relevant light stimuli. Previously, Kay (1965) measured peak behavioral spectral sensitivity of 470–490 nm in the euphausiid, *Meganyctiphanes norvegica*, based on the number of individuals responding to bright photoflash stimulation. The peak in spectral efficiency corresponds to the visual pigment absorbance maximum at 488 nm determined by MSP (Denys and Brown, 1982) and to the peak visual sensitivity of 490 nm measured by electroretinogram (Frank and Widder, in press). As with *S. similis*, both visual and behavioral peaks for *M. norvegica* lie in the blue-green region of the visible spectrum. Even though it has long been suggested that bioluminescence by euphausiid crustaceans may serve as camouflage (Herring and Locket, 1978), to date there has been no direct demonstration that dim bioluminescence appropriate for luminescent countershading is produced by euphausiids in response to environmentally relevant light cues.

The response thresholds for light-induced behaviors of three species of deep-sea caridean shrimp with single visual pigments occurs at approximately $0.4–4 \times 10^{11}$ photons $m^{-2} s^{-1}$ at 500 nm (Frank and Widder, 1994b). Because the eyes of the caridean shrimp were in the dark-adapted state, it is expected that the response threshold for *S. similis* bioluminescence would occur at higher illumination levels because of the apparent need for the eyes to be light-adapted for the initiation of luminescent countershading (Latz and Case, 1992). The *S. similis* response threshold of $2–3 \times 10^{12}$ photons $m^{-2} s^{-1}$ at 490 nm for the light-adapted eye suggests that the absolute visual sensitivity of *S. similis* is similar to that for the caridean shrimp.

Sergestes similis and other midwater animals inhabit daytime depths where dim downwelling light is sufficient to silhouette their opaque body structures, making them potentially more detectable by predators. Previous studies have demonstrated that the spectral emission (Widder *et al.*, 1983), angular distribution (Latz and Case, 1982) and irradiance of bioluminescence (Warner *et al.*, 1979) of *S. similis* are consistent with a camouflage function. The results of the present study show that the behavioral sensitivity of bioluminescence is also appropriate for camouflage, based on the daytime optical environment encountered by this species. In the northeast Pacific, *S. similis* inhabits daytime depths of approximately 200–700 m (*e.g.*, Clarke, 1966; Pearcy *et al.*, 1977). The apparent behavioral threshold for luminescent countershading at approximately 3×10^{12} photons $m^{-2} s^{-1}$ (for a 490 nm light stimulus) would be reached at a daytime depth of approximately 350 m in the coastal waters off San Diego (Kampa, 1960). Therefore, ambient light levels at the depths inhabited by *S. similis* would be sufficient to induce and maintain luminescent countershading.

The control of luminescent countershading in *S. similis* represents a simple case, where the visual system, bioluminescence emission, and oceanic downwelling light all operate in the same spectral range. There are other cases where these simple conditions do not hold. All vertically migrating animals including *S. similis* experience diel changes in their optical environment. However, animals such as the squid *Abralia*, which is able to modify the spectral emission of bioluminescence (Young and Mencher, 1980), must coordinate the adjustable spectral emission of its bioluminescence with diel changes in the spectral distribution of downwelling light in order for luminescent countershading to be effective. Animals with multiple visual pigments, such as the oplophorid shrimp *Systellaspis debilis* (Frank and Case, 1988), may use only one of their photoreceptor classes to drive luminescent countershading. In these more complex cases, the relationship between visual sensitivity and behavioral spectral efficiency promises to offer an intriguing insight into the coordination of luminescent camouflage behavior in midwater animals.

Acknowledgments

The authors thank the captains, crews, and resident marine technicians of the *RV Robert Gordon Sproul* and the *RV New Horizon* for assistance with animal collections, as well as numerous volunteers from the Scripps Institution of Oceanography and the Birch Aquarium at Scripps. In addition, we thank J. Childress for generously inviting one of us (J.K.) to participate on his research cruise on the *RV New Horizon*. C. Andon, D. Hutchinson, and D. Kelley assisted with data collection and analysis. We greatly appreciate the comments of two anonymous reviewers. This work was funded by NSF grant IBN96-01069 to M.I.L., NSF grant OCE-9313972 to T.M.F. and E.A. Widder, NERC grant GR3/9329 to J.C.P., and a NERC CASE studentship GT4/93/3/A to J.K. Harbor Branch Oceanographic Institution Contribution #1269.

Literature Cited

Anthony, P. D., and A. D. Hawkins. 1983. Spectral sensitivity of the cod, *Gadus morhua* L. *Mar. Behav. Physiol.* **10:** 145–166.

Blaxter, J. H. S. 1964. Spectral sensitivity of the herring, *Clupea harengus* L. *J. Exp. Biol.* **41:** 155–162.

Bowmaker, J. K. 1976. Vision in pelagic animals. Pp. 430–479 in *Adaptation to Environment: Essays on the Physiology of Marine Animals*, R. C. Newell, ed. Butterworth, London.

Chapman, G. 1976. Reflections on transparency. Pp. 491–499 in *Coelenterate Ecology and Behavior*, G. O. Mackie, ed. Plenum Press, New York.

Childress, J. J., A. T. Barnes, L. B. Quetin, and B. H. Robison. 1977. Thermally protecting cod ends for the recovery of living deep-sea animals. *Deep-Sea Res.* **25:** 419–422.

Clarke, W. D. 1963. Function of bioluminescence in mesopelagic organisms. *Nature* **198:** 1244–1246.

Clarke, W. D. 1966. Bathyphotometric studies of the light regime of organisms of the deep scattering layers. *AEC Res. Devel. Rep.* **UC-48:** 1–47.

Cronin, T. W., and T. M. Frank. 1996. A short-wavelength photoreceptor class in a deep-sea shrimp. *Proc. R. Soc. Lond. B.* **263:** 861–865.

Cronin, T. W., and T. H. Goldsmith. 1982. Quantum efficiency and photosensitivity of the rhodopsin metarhodopsin conversion in the crayfish photoreceptors. *Photochem. Photobiol.* **36:** 447–454.

Dartnall, H. J. A. 1972. Photosensitivity. Pp. 122–145 in *Handbook of Sensory Physiology, Vol. VII/1. Photochemistry of Vision.* H. J. A. Dartnall, ed. Springer-Verlag, Berlin.

Denton, E. J. 1970. On the organization of reflecting surfaces in some marine animals. *Phil. Trans. Roy. Soc. B* **258:** 285–313.

Denys, C. J., and P. K. Brown. 1982. The rhodopsins of *Euphausia superba* and *Meganyctiphanes norvegica* (Crustacea, Euphausiacea). *J. Gen. Physiol.* **80:** 451–472.

Douglas, R. H., and C. W. Hawryshyn. 1990. Behavioral studies of fish vision: an analysis of visual capabilities. Pp. 373–418 in *The Visual System of Fish*, R. H. Douglas and M. B. A. Djamgoz, eds. Chapman and Hall, London.

Douglas, R. H., J. C. Partridge, and A. J. Hope. 1995. Visual and lenticular pigments in the eyes of demersal deep-sea fishes. *J. Comp. Physiol. A.* **177:** 111–122.

Fein, A., and E. Z. Szuts. 1982. *Photoreceptors: Their Role in Vision.* Cambridge University Press, Cambridge.

Forward, R. B., Jr. 1988. Diel vertical migration: zooplankton photobiology and behavior. *Oceanogr. Mar. Biol. Annu. Rev.* **26:** 361–393.

Frank, T. M. 1999. Comparative study of temporal resolution in the visual systems of mesopelagic crustaceans. *Biol. Bull.* **196:** 137–144.

Frank, T. M., and J. F. Case. 1988. Visual spectral sensitivities of bioluminescent deep-sea crustaceans. *Biol. Bull.* **175:** 261–273.

Frank, T. M., and E. A. Widder. 1994a. Evidence for behavioral sensitivity to near-UV light in the deep-sea crustacean *Systellapsis debilis*. *Mar. Biol.* **118:** 279–284.

Frank, T. M., and E. A. Widder. 1994b. Comparative study of behavioral-sensitivity thresholds to near-UV and blue-green light in deep-sea crustaceans. *Mar. Biol.* **121:** 229–235.

Frank, T. M., and E. A. Widder. 1996. UV light in the deep-sea: *in situ* measurements of the downwelling irradiance in relation to the visual threshold sensitivity of UV-sensitive crustaceans. *Mar. Freshw. Behav. Physiol.* **27:** 189–197.

Frank T. M., and E. A. Widder. A comparative study of the spectral sensitivities of mesopelagic crustaceans. *J. Comp. Physiol. A.* (In press).

Goldsmith, T. H. 1978. The effects of screening pigments on the spectral sensitivity of some Crustacea with scotopic (superposition) eyes. *Vision Res.* **18:** 475–482.

Goldsmith, T. H. 1986. Interpreting trans-retinal recordings of spectral sensitivity. *J. Comp. Physiol.* **159:** 481–487.

Hart, N. S., J. C. Partridge, and I. C. Cuthill. 1998. Visual pigments, oil droplets and cone photoreceptor distribution in the European starling (*Sturnus vulgaris*). *J. Exp. Biol.* **201:** 1433–1446.

Herring, P. J. 1982. Aspects of bioluminescence of fishes. *Oceanogr. Mar. Biol. Annu. Rev.* **20:** 415–470.

Herring, P. J. 1983. The spectral characteristics of luminous marine organisms. *Proc. R. Soc. Lond.* **220:** 183–217.

Herring, P. J., and N. A. Locket. 1978. The luminescence and photophores of euphausiid crustaceans. *J. Zool.* **186:** 431–462.

Hiller-Adams, P., E. A. Widder, and J. F. Case. 1988. The visual pigments of four deep-sea crustacean species. *J. Comp. Physiol.* **163A:** 63–72.

Jerlov, N. G. 1968. *Optical Oceanography.* Elsevier, Amsterdam.

Kaltenrieder, M., T. Labhart, and E. Hess. 1989. Spectral sensitivity, absolute threshold, and visual field of two tick species, *Hyalomma dromedarii* and *Amblyomma variegatum. J. Comp. Physiol. A.* **165:** 155–164.

Kampa, E. M. 1960. Daylight penetration measurements in three oceans. *Intl. Union Geodesy and Geophysics Monographie* **10:** 91–95.

Kay, R. H. 1965. Light-stimulated and light-inhibited bioluminescence of the euphausiid *Meganyctiphanes norvegica* (G.O. Sars). *Proc. Roy. Soc. (B)* **162:** 365–386.

Kent, J. 1997. The visual pigments of deep-sea crustaceans. Ph.D. Thesis, University of Bristol.

King, R. B., J. K. Douglass, J. B. Phillips, and C. L. Baube. 1993. Scotopic spectral sensitivity of the optomotor response in the green treefrog *Hyla cinerea. J. Exp. Zool.* **267:** 40–46.

Kito, Y., K. Narita, M. Seidou, M. Michiniomae, K. Yoshihara, J. C. Partridge, and P. J. Herring. 1993. A blue sensitive visual pigment based on 4-hydroxyretinal is found widely in mesopelagic cephalopods. Pp. 123–127 in *Structures and Functions of Retinal Proteins,* Vol. 221, J. L. Rigaud, ed. John Libbey Eurotext, Paris.

Lall, A. B. 1993. Action spectra for the initiation of bioluminescent flashing activity in males of twilight-active firefly *Photinus scintillans* (Coleoptera: Lampyridae). *J. Insect Physiol.* **39:** 123–127.

Lall, A. B., G. K. Strother, T. W. Cronin, and H. H. Seliger. 1988. Modification of spectral sensitivities by screening pigments in the compound eyes of twilight-active fireflies (Coleoptera: Lampyridae). *J. Comp. Physiol. A* **162:** 23–33.

Land, M. F. 1992. Locomotion and visual behavior of mid-water crustaceans. *J. Mar. Biol. Assoc. U.K.* **72:** 41–60.

Latz, M. I. 1983. Control of bioluminescence in the midwater shrimp, *Sergestes similis.* Ph.D. Dissertation. University of California, Santa Barbara. 175 pp.

Latz, M. I., and J. F. Case. 1982. Light organ and eyestalk compensation to body tilt in the luminescent midwater shrimp, *Sergestes similis. J. Exp. Biol.* **98:** 83–104.

Latz, M. I., and J. F. Case. 1992. Slow photic and chemical induction of bioluminescence in the midwater shrimp, *Sergestes similis* Hansen. *Biol. Bull.* **182:** 391–400.

Latz, M. I., T. M. Frank, and J. F. Case. 1988. Spectral composition of bioluminescence of epipelagic organisms from the Sargasso Sea. *Mar. Biol.* **98:** 441–446.

Locket, N. A. 1977. Adaptations to the deep sea environment. Pp. 68–192 in *Handbook of Sensory Physiology,* Vol. VII/5, F. Crescitelli, ed. Springer-Verlag, Berlin.

McFall-Ngai, M. J. 1990. Crypsis in the pelagic environment. *Am. Zool.* **30:** 175–188.

Muntz, W. R. A. 1976. On yellow lenses in mesopelagic organisms. *J. Mar. Biol. Assoc. U.K.* **56:** 963–976.

Muntz, W. R. A. 1986. The spectral sensitivity of *Nautilus pompilius. J. Exp. Biol.* **126:** 513–517.

Muntz, W. R. A. 1987. Visual behavior and visual sensitivity of *Nautilus pompilius.* Pp. 231–244 in *Nautilus: The Biology and Paleobiology of a Living Fossil,* W. B. Saunders and N. H. Landman, eds. Plenum Press, New York.

Palacios, A. G., T. H. Goldsmith, and G. D. Bernard. 1996. Sensitivity of cone from a cyprinid fish (*Danio aequipinnatus*) to ultraviolet and visible light. *Visual Neurosci.* **13:** 411–421.

Partridge, J. C., and W. J. De Grip. 1991. A new template for rhodopsin (vitamin A1 based) visual pigments. *Vision Res.* **31:** 619–630.

Partridge, J. C., J. Shand, S. N. Archer, J. N. Lythgoe, and W. A. H. M. van Groningen-Luyben. 1989. Interspecific variations in the visual pigments of deep-sea fishes. *J. Comp. Physiol. A.* **164:** 513–529.

Pearcy, W. G., E. E. Krygier, R. Mesecar, and F. Ramsey. 1977. Vertical distribution and migration of oceanic micronekton off Oregon. *Deep-Sea Res.* **24:** 223–245.

Stavenga, D. G., R. P. Smits, and B. J. Hoenders. 1993. Simple exponential functions describing the absorbance bands of visual pigment spectra. *Vision Res.* **33:** 1011–1017.

Warner, J. A., M. I. Latz, and J. F. Case. 1979. Cryptic bioluminescence in a midwater shrimp. *Science* **203:** 1109–1110.

Waterman, T. H. 1961. Light sensitivity and vision. Pp. 1–64 in *The Physiology of Crustacea. Vol. II. Sense Organs, Integration, and Behavior,* T. H. Waterman, ed. Academic Press, New York.

Widder, E. A., M. I. Latz, and J. F. Case. 1983. Marine bioluminescence spectra measured with an optical multichannel detection system. *Biol. Bull.* **165:** 791–810.

Worthy, K. M., and A. B. Lall. 1996. Action spectra of the bioluminescence response in firefly *Photinus pyralis* females (Coleoptera, Lampridae). *Soc. Neurosci. Abstr.* **22(1–3):** 1145.

Young, R. E. 1983. Oceanic bioluminescence: an overview of general functions. *Bull. Mar. Sci.* **33:** 829–845.

Young, R. E., and F. M. Mencher. 1980. Bioluminescence in mesopelagic squid: diel color change during counterillumination. *Science* **208:** 1286–1288.

Young, R. E., E. M. Kampa, S. D. Maynard, F. M. Mencher, and C. F. E. Roper. 1980. Counterillumination and the upper depth limits of midwater animals. *Deep-Sea Res.* **27A:** 671–691.

Reference: *Biol. Bull.* **197:** 361–367. (December 1999)

Enhancement of the Response of Rock Crabs, *Cancer irroratus,* to Prey Odors following Feeding Experience

ANDREW RISTVEY[1] AND STEVE REBACH*

Department of Natural Sciences, University of Maryland Eastern Shore, Princess Anne, Maryland 21853

Abstract. The rock crab, *Cancer irroratus* Say, uses chemically mediated learning in the search for food. Rock crabs are opportunistic benthic predators and scavengers. Observations indicate that although they eat a variety of items, they are more sensitive to, and prefer, odors of food items that they have been eating. We found that *C. irroratus* is more responsive to a familiar food source than to an unfamiliar one and can distinguish between the odors of two different prey after being fed one species for an extended time. Initial preferences for two mytilid bivalves, *Mytilus edulis* and *Geukensia demissa,* were determined in a Y-maze. Crabs were then fed only one of the mussel species for 28 days and retested, using sequential and simultaneous presentations, for their responses to familiar and unfamiliar prey odors. Crabs increased their responses to familiar prey odors, but not to unfamiliar odors. In foraging tests, crabs ate *M. edulis* more often regardless of the species to which they had been familiarized.

Introduction

A search image can be defined as a perceptual filtering mechanism learned from experience. It may be only a transitory improvement in perceptual ability, but this selective attention can increase the possibility of stimulus detection (Bond and Riley, 1991). In foraging behavior selective attention results in certain prey characteristics being discriminated by a predator, facilitating more efficient foraging. Search images increase accuracy and decrease response time because the predator requires less information about the prey and becomes more efficient in locating it (Lawrence, 1985a).

Search images, originally postulated for visual stimuli (Croze, 1970; Pietrewicz and Kamil, 1979; Lawrence, 1985a, b) could also be associated with chemical stimuli (Atema *et al.*, 1980; Atema and Derby, 1981; Derby and Atema, 1981). In the aquatic environment, especially in the absence of light, chemical signals may be the best cues for information about the surrounding environment. Organic molecules are part of the ambient milieu, and an organism must sift out extraneous "noise" to find the information needed for foraging, predator avoidance, and mating (Zimmer-Faust, 1991).

Chemosensory cues play a major role in agonistic (Karavanich and Atema, 1998), sexual (Gleeson, 1980), host-finding (Atema and Derby, 1981), and foraging (Pearson and Olla, 1977) behaviors in crustaceans. Experience influences an animal's response to those cues. Derby and Atema (1981) demonstrated that after lobsters (*Homarus americanus*) fed on a specific prey, their sensitivity to that prey odor increased, and they developed a preference for that particular prey. The rocky shore gastropod *Nucella lamellosa* can discriminate between predatory and nonpredatory crab effluents (Marko and Palmer, 1991), and the nudibranch *Aeolidia papillosa* can distinguish between odors from a learned prey anemone and five other possible prey anemones (Hall *et al.*, 1982). Yellowfin tuna (*Thunnus albacares*) became more sensitive to specific fish odors after feeding on that prey for a period of time, but lost their sensitivity after a few weeks without reinforcement (Atema *et al.*, 1980). In predatorily naïve postlarval lobsters, responses to metabolites of *Cancer irroratus* and *Mytilus edulis* (normal lobster prey) were lower than in field-collected adult lobsters that may have had experience with those prey (Daniel and Bayer, 1987a). When naïve lobsters were fed amphipods or clams, those fed amphipods developed stronger responses to amphipod and not to clam metabolites, but those fed clams did not develop strong responses to either prey (Daniel and

---

Received 19 August 1998; accepted 2 September 1999.

[1] Present address: 10470 Longwoods Rd., Easton, Maryland 21601.

* Author to whom correspondence should be addressed. E-mail: srebach@umes-bird.umd.edu.

Bayer, 1987b). In theory, search images need to be reinforced (Atema *et al.*, 1980; Atema and Derby, 1981), and their strength may vary with experience and with the availability and palatability of the food (Gendron, 1986).

Many studies have tested the role of chemoreception in foraging, but few have centered on search images. We examined search images and foraging behavior in the rock crab *C. irroratus* preying on the bivalve mussels *Geukensia* and *Mytilus.* These two groups of mussels occur in the range of *C. irroratus,* are frequently taken as prey items (Stehlik, 1993), and have similar physical characteristics. *Mytilus* is found on hard substrates in the tidal zone, and individuals located close to shore are known to be eaten by rock crabs (Drummond-Davis *et al.*, 1982; Stehlik, 1993). *Geukensia* is found in soft substrates in tight clumps attached to marsh grasses, and is less likely to be encountered by a crab. No data are available on innate prey preferences in *C. irroratus.*

Using effluents from these two species, we examined changes in the responsiveness and sensitivity of crabs to prey. Chemoreceptors on various body parts appear to influence behaviors such as walking, searching, and dactyl grasping, and these actions are dependent upon the concentration of the stimulus (Derby and Atema, 1982). The position and movements of these structures are good indicators of the sensitivity to food odors (Derby and Atema, 1981). We determined a baseline response for rock crabs, familiarized them with a single prey, and retested them to determine if there were acquired or changed responses to familiar and unfamiliar odors.

Materials and Methods

Rock crabs were collected by local watermen using traps off the coast of Delaware and Maryland and by the investigators at Chincoteague on Assateague Island, Virginia. Ribbed mussels, *Geukensia demissa,* between 2 and 6 cm, were collected from salt marsh environments in Girdletree, Maryland, and Chincoteague, Virginia. Blue mussels, *Mytilus edulis,* between 2 and 6 cm, were collected on the rock jetty at the Ocean City, Maryland inlet.

Maintenance conditions

A recirculating, biologically filtered saltwater system was used for tests. The water temperature was 11° ± 3°C, the salinity was 32 to 35 ppt, and the photoperiod was 12 h light:12 h dark. Crabs were kept in 40-l tanks (50 × 25 cm), two per tank, with an acrylic plastic divider separating them to prevent aggression and to enable staggered feeding. They were acclimated to laboratory conditions for 1–2 weeks and fed a diet of squid (*Loligo* sp.) every other day. Mussels were housed in an isolated 80-l tank equipped with a power filter. Fresh mussels were collected every week. The water in the mussel tank was kept at 15° ± 2°C and the salinity at 33 to 34 ppt.

The Y-maze

Crabs were tested in a 92 × 33 × 20 cm acrylic plastic Y-maze containing 55 to 60 l of salt water. A piece of acrylic divided the top 50 cm of the maze into two arms (see Fig. 1, Rebach, 1996). A dual-head MasterFlex peristaltic pump (Cole-Parmer #7553.20) delivered liquids through plastic tubing to a 2.5-cm hole in either arm of the Y-maze at the rate of about 0.33 l min^{-1}. A concentration gradient was established, with the odor becoming more dilute at the drain located at the base of the maze. In dye trials using methylene blue, the average dilution at the base of the maze was determined by spectrophotometer to be 13.6% that of the original concentration. These trials indicated that odor reached the crab within 3 min, with little mixing. In preliminary trials, crabs responded to odor within a few minutes of its reaching them. Each test lasted 10 min during which the observer recorded, from a blind, crab location in the maze and behaviors exhibited.

Mussel effluent

Mussel effluent was produced daily by placing live mussels (equivalent to 10 g soft tissue l^{-1}) in seawater for 10 h (Derby and Atema, 1981). Mussels were checked weekly for reproductive condition to ensure that effluents would be consistent in character.

Behaviors

We adapted methods used by Derby and Atema (1981) for tests of chemoreceptive sensitivity and measured changes in behavior in the Y-maze that reflected changes in sensitivity. An approach to the source of the effluent was defined as a high-sensitivity behavior. Low sensitivity was characterized by the following behaviors:

1. Chela raise—claws lifted beyond normal position.
2. Antennule burst—flicking rate increased suddenly.
3. Antennule wipe—antennules groomed, usually with third maxillipeds. May occur in bouts. Wipes occurring within 5 s of each other were considered to be one wipe.
4. Maxilliped wave—third maxillipeds moved slowly back and forth without touching one another.
5. Maxilliped wipe—third maxillipeds rubbed against each other within a 5-s period.
6. Shift—body position changed.
7. Body raise—body raised up on dactyls.
8. Fanning—rapid movement of second maxillipeds along with third maxillipeds opened widely to expose mouth parts.

An approach was scored when a crab crossed a line 8 cm from the inlet flow at the end of an arm of the Y-maze before a 10-min run was completed. Crabs began the experiment at the base of the maze. If an approach did not occur during a test run, the low-sensitivity behaviors were used for scoring. In every run, each occurrence of a behavior other than an approach was counted as one unit (Derby and Atema, 1981). Totals for each crab were then averaged to determine a mean frequency. The higher the value, the more sensitive the crab was, or had become, to the prey odor. Scores were obtained for each crab tested before and after training was complete.

Initial response to mussel effluent

Sixteen crabs were fasted for 24 h and then tested. In control tests, seawater was used on both sides of the Y-maze. Each crab was allowed to acclimate in the maze for 8–12 h and then tested with effluent and a seawater control. This was repeated for the other mussel species about 10 h later. Initial response tests were completed within 24 days.

Familiarization with a specific mussel odor

After testing crabs for their initial response, training began. Eight crabs were fed *Geukensia* and eight *Mytilus* for a period of 28 days. Crabs were fed whole mussels *ad libitum* during the training period. The average number of mussels eaten each day was recorded.

Response to odors in sequential presentation after familiarization

Familiarized crabs were retested as in the first experiment. The tests began with a post-familiarization seawater control using seawater in both arms of the Y-maze. Responses to the two prey effluents (familiar and unfamiliar) were recorded based on sequential presentation; each prey odor was tested against a seawater control. Approaches were recorded when they occurred; if no approach occurred, low-sensitivity behaviors were scored.

Response to odors in simultaneous presentation after familiarization

Familiarized crabs were retested for preference between the two effluents. Odors were presented simultaneously without a seawater control. Distinguishing which odor elicited heightened behavioral responses was not possible in this test, so only approaches were scored.

Influence of experience on mussel selection

A foraging test was performed using live prey in 40-l tanks. Five equal-sized mussels of each species were randomly positioned in the tank and buried to about 66% of their length in a calcite substrate to make them tactually cryptic. Crabs were allowed to forage for 12 h, and each test was videotaped. The total number of mussels handled and the species handled first, eaten first, or rejected after being handled were recorded. Mussel shells were marked with small spots of white epoxy to make them easier to see during videotape analysis.

Analysis of data

Initial scores for responses to seawater, the *Mytilus* and *Geukensia* effluents, and the sequential presentation test results were compared using the Friedman test (Systat 8.0, SPSS Inc., Chicago, Illinois). Responses to familiar and unfamiliar odors for each familiarization group were compared with the Wilcoxon signed rank tests. (Systat 8.0). Differences between means were determined with Bonferroni post hoc analysis (Systat 8.0). Mussel selection data from the foraging test was analyzed using a Wilcoxon signed rank test, a Mann-Whitney test with tied ranks, and a chi-square 2 × 2 contingency table (Zar, 1984).

Results

Behavioral observations

Crabs responded to effluents within 2 to 3 min. Those that did not approach responded by displaying lower sensitivity behaviors. Typically, crabs flicked their antennules slowly or intermittently, with occasional bursts, before odors reached them. A burst, with maxilliped or antennule wipes, occurred when the effluent reached the crab. Within 5 min, chela waves and raises occurred, and crabs began to move. Antennule flicks pointed in the direction of movement. These behaviors continued until tests were concluded.

In a typical approach, the initial behavior was similar to that of a non-approach. At about 5 min, crabs began walking towards the effluent. Upon reaching the end of the maze, they often grabbed the inflow hole with their chelae. In some simultaneous presentation tests, crabs entered one arm of the maze, turned back, and then proceeded down the other side, through which the familiar effluent flowed.

Initial response to mussel effluent

Figure 1 shows the responses of 16 crabs to mussel effluent before the crabs were familiarized with other mussel species. The Friedman test revealed no differences between the responses to the seawater control and to the *Mytilus* or *Geukensia* effluents ($P > 0.05$, Table 1).

Familiarization with mussel odor

Familiarization periods began after initial responses were obtained. Crabs were fed their assigned species of mussel *ad libitum*. At first, crabs consumed 6 to 8 mussels a day, although within 4 weeks this decreased to 2 to 3 mussels a day, especially those fed *Geukensia*. During familiarization, crabs exhibited periods of increased activity. Usual behav-

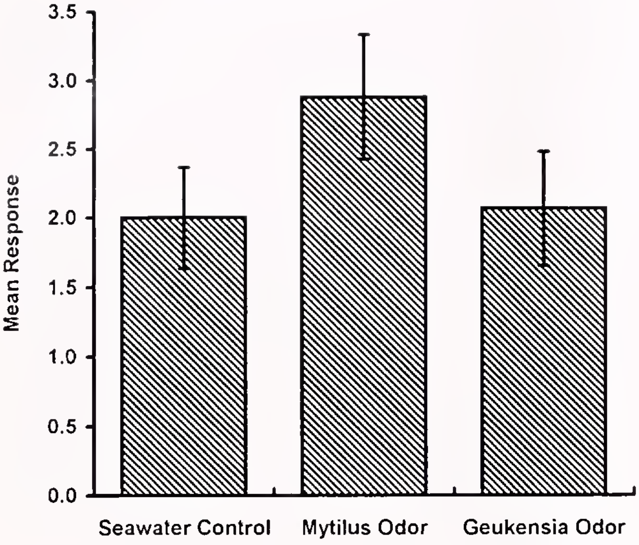

Figure 1. Comparison of mean (±SEM) frequencies for the initial tests for responses to odor. No differences were found between responses to odors.

iors consisted of climbing tank walls, eating, and resting with intermittent antennule flicking.

Response to odors in sequential presentation after familiarization

Two crabs, fed with blue mussel, made approaches to their familiar effluent. One crab, fed with ribbed mussel, died during the familiarization period; another crab, fed with blue mussel, stopped eating 3 weeks into the training period. Activity scores from the remaining 12 crabs were analyzed for increases in sensitivity to familiar prey odor. A Friedman test determined that responses were significantly different ($P < 0.01$, Table I) to pre-familiarization seawater, post-familiarization seawater, unfamiliar mussel effluent, and familiar effluent (Fig. 2). Bonferroni post hoc analysis demonstrated that the response to familiar effluent was significantly greater than to all of the other water samples and effluents ($P < 0.01$). No other significant differences were found (Table I).

Figure 3 shows the responses of crabs familiarized with *Mytilus* or with *Geukensia* to familiar and unfamiliar odors. Wilcoxon signed ranks tests determined that responses differed to familiar and unfamiliar odors for both familiarization groups ($P < 0.05$, Table I). Bonferroni post hoc comparison determined that each familiarization group could detect the difference between the odors that were familiar and the odors that were unfamiliar to their training groups ($P < 0.01$, Table I). There was no difference in the response of each of the familiarization groups in their ability to distinguish their own familiar or their own unfamiliar odors ($P > 0.05$).

Response to odors in simultaneous presentation after familiarization

Of the 8 crabs familiarized with *Mytilus*, 4 approached familiar prey effluent; of the 8 familiarized with *Geukensia*,

Table I

Responses to effluents

Odors compared	Method of comparison	*n*	*P* value
Initial odors	Friedman statistic (Fig. 1)	16, 16, 16	>0.05
Pre-familiarization and post-familiarization seawater, familiar and unfamiliar mussel effluents	Friedman statistic (Fig. 2)	12, 12, 12, 12	<0.01
familiar *vs.* unfamiliar effluents	Bonferroni test (Fig. 2)	12, 12	<0.01
familiar effluent *vs.* post-familiarization seawater	Bonferroni test (Fig. 2)	12, 12	<0.01
familiar effluent *vs.* pre-familiarization seawater	Bonferroni test (Fig. 2)	12, 12	<0.01
unfamiliar effluent *vs.* pre-familiarization seawater	Bonferroni test (Fig. 2)	12, 12	>0.05
unfamiliar effluent *vs.* post-familiarization seawater	Bonferroni test (Fig. 2)	12, 12	>0.05
Familiar and unfamiliar odors–familiarized w/ *Mytilus*	Wilcoxon signed ranks test (Fig. 3)	5	<0.05
Familiar and unfamiliar odors–familiarized w/*Geukensia*	Wilcoxon signed ranks test (Fig. 3)	7	<0.05
familiar *vs.* unfamiliar odors–familiarized w/ *Mytilus*,	Bonferroni test (Fig. 3)	5, 5	<0.01
familiar *vs.* unfamiliar odors–familiarized w/*Geukensia*	Bonferroni test (Fig. 3)	7, 7	<0.01
unfamiliar odor–familiarized w/*Geukensia* *vs.* unfamiliar odor–familiarized w/ *Mytilus*	Bonferroni test (Fig. 3)	7, 5	>0.05
familiar odor–familiarized w/*Geukensia* *vs.* familiar odor–familiarized w/ *Mytilus*	Bonferroni test (Fig. 3)	7, 5	>0.05
Mytilus eaten *vs.* *Geukensia* eaten	Wilcoxon signed ranks test	14	<0.05
Mytilus rejected *vs.* *Geukensia* rejected	Wilcoxon signed ranks test	9	>0.05
No. mussels eaten–familiarized on *Mytilus* or *Geukensia*	Mann-Whitney tied ranks (Fig. 4)	7, 7	>0.05
No. mussels rejected–familiarized on *Mytilus* or *Geukensia*	Mann-Whitney tied ranks (Fig. 4)	7, 7	>0.05
Species eaten *vs.* familiarization species	2 × 2 chi-square (Fig. 4)	14	>0.05
Species rejected *vs.* familiarization species	2 × 2 chi-square (Fig. 4)	14	>0.05

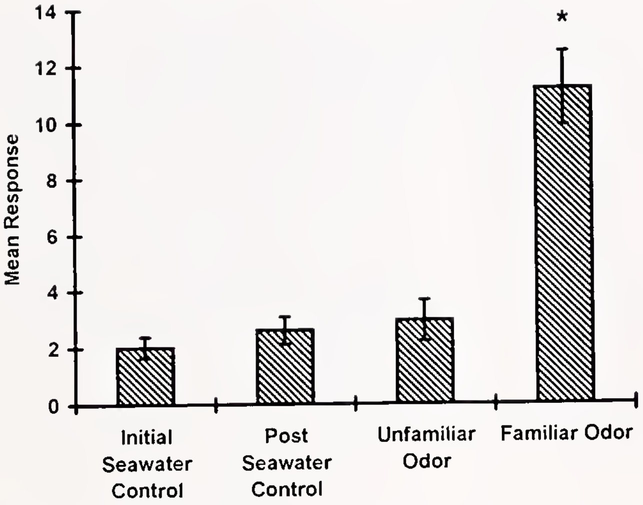

Figure 2. Comparison of mean (±SEM) frequencies of initial and post-familiarization control tests, and tests of familiar and unfamiliar odors after familiarization. No differences were found between responses to seawater controls and unfamiliar odors, but responses to familiar odors were significantly greater than to unfamiliar odors and controls (as indicated by an asterisk).

1 approached unfamiliar effluent. These tests failed to yield significant responses because only approaches were scored. The 11 crabs that did not approach during the simultaneous presentation exhibited increased sensitivity, as in the sequential tests. These crabs began to search soon after the odor reached them; they raised chela and walked upcurrent and downcurrent, but they failed to make an approach. Low-sensitivity scoring could not be used because it would not have been possible to determine which odor was influencing the behavior.

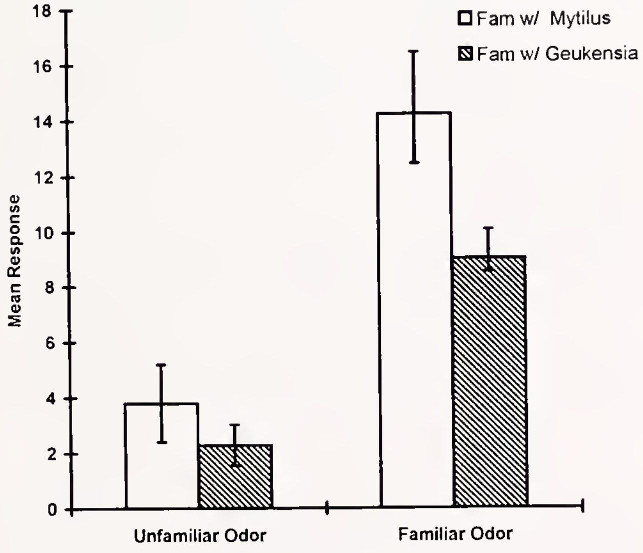

Figure 3. Comparison of mean (±SEM) frequencies between familiarization groups. No differences were found in unfamiliar odor responses between familiarization groups. Differences were found in familiar odor responses. Abbreviations: Fam w/ *Mytilus* = Familiarized with *M. edulis;* Fam w/ *Geukensia* = Familiarized with *G. demissa.*

Influence of experience on prey selection

Within 15 min of being placed in the tanks, crabs probed the calcite substrate with their dactyls, attempted to climb tank walls, or walked around. During this period, all crabs touched and moved both species of mussels.

More *Mytilus* (45) were eaten than *Geukensia* (19), but about the same number of mussels of both species were rejected (*Mytilus,* 13; *Geukensia,* 14). A Wilcoxon signed ranks test determined that, overall—regardless of familiarization group—significantly more *Mytilus* were eaten than *Geukensia* ($P < 0.05$), but there was no difference in numbers of *Mytilus* or *Geukensia* rejected ($P > 0.05$) (Table I).

Figure 4 compares the species of prey eaten and rejected by crabs in the two familiarization groups. Crabs familiar with *Geukensia* cumulatively ate 21 *Mytilus* and 5 *Geukensia,* and rejected 11 *Mytilus* and 11 *Geukensia.* Crabs familiar with *Mytilus* ate 24 *Mytilus* and 14 *Geukensia,* and rejected 2 *Mytilus* and 3 *Geukensia.* In all cases, *Mytilus* was handled first and eaten first. Both groups of crabs handled about the same number of mussels (43 for *Mytilus*-familiarized crabs and 48 for *Geukensia*-familiarized crabs).

A Mann-Whitney test with tied ranks determined that there was no significant difference in total mussels, regardless of species, eaten ($P > 0.05$) or rejected ($P > 0.05$), between crabs familiarized with *Mytilus* and crabs familiarized with *Geukensia* (Table I).

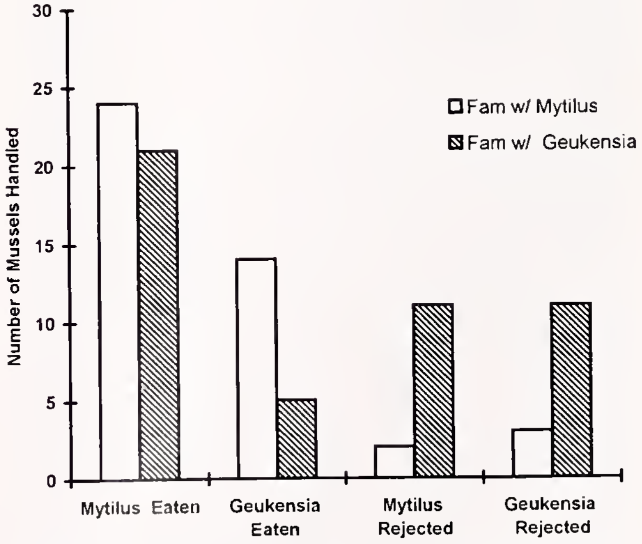

Figure 4. Comparison of total number of prey eaten and rejected by crabs familiarized with *Mytilus* and *Geukensia.* No differences were found in ratios. Abbreviations: Same as in Figure 3.

A chi-square analysis of a 2 × 2 contingency table determined that the ratio of *Mytilus* to *Geukensia* eaten was not different ($P > 0.05$), nor was there a difference between the ratio of mussel species rejected ($P > 0.05$) for each of the familiarization groups (Table I). Regardless of the mussel species that the crabs were familiar with, they ate and rejected the same proportion of mussel species.

Discussion

Our results show that, in the absence of recent experience, *Cancer irroratus* did not strongly respond to the effluent of either *Mytilus edulis* or *Geukensia demissa.* Exposure to one prey type increased the sensitivity of the crabs to that prey's odor, and responsiveness increased with experience. The results of the sequential presentation tests indicated a significantly increased sensitivity towards familiarized prey. Scores of low-sensitivity behaviors were higher for familiar effluents than for unfamiliar effluents. However, the simultaneous presentations could not distinguish the responses to the two odors because it was not possible to determine which odor was eliciting the heightened behaviors.

Crabs did not often approach the effluent source in either the sequential or simultaneous tests. These results may be misleading since crabs did react to the odors. The use of prey effluents instead of live prey can influence observed behaviors, because the lack of reinforcement with actual prey may have been responsible for the observed decreases in response.

It is also possible that the concentrations of stimulatory compounds may have been below the thresholds necessary to initiate search or approach. The amino acids glycine, taurine, glutamate, serine, and threonine have been found to be the most stimulatory in feeding assays in several species of *Cancer* (Case, 1964; Allen *et al.*, 1975). These amino acids may have been present at low concentrations in test-mussel metabolites. *Palaemonetes pugio,* a grass shrimp, specifically recognizes various foods by qualitative and quantitative differences in combinations of low molecular weight substances intrinsic to those foods (Carr, 1978).

Concentrations that elicited antennular responses may have been too low for activation of approaches and feeding behaviors. Rebach *et al.* (1990) found antennular sensitivity for mussel extract in *C. irroratus* to be as low as 10^{-10} g l^{-1}. Pearson *et al.* (1979) found similar sensitivities for littleneck clam extract in *C. magister.* Both of those studies used tissue extracts, whereas this study used prey rinse (body odor) from intact animals. The threshold to elicit feeding is 10^5 higher than the arousal threshold in rock crabs (Rebach *et al.*, 1990) and 10^{10} to 10^{17} times higher in blue crab (*Callinectes sapidus;* Ache, 1982). Arousal thresholds are found at concentrations of picograms (10^{-12} g) per liter, search behavior thresholds at micrograms (10^{-6} g) per liter, and handling and ingestion of food at milligrams (10^{-3} g) per liter (McLeese, 1973; Mackie, 1973; Pearson and Olla, 1977; Ache, 1982). The effluents used in this study did not often direct the crabs' responses towards familiar effluents, but did arouse them. We may therefore infer that these effluents had concentrations between 10^{-12} and 10^{-3} g l^{-1}.

The stomach contents of rock crabs indicate that they are opportunistic feeders (Drummond-Davis *et al.*, 1982). An assortment of algae, polychaetes, gastropods, mussels, and bits of hermit crabs and other crustaceans are typically consumed. It is possible that nutritional needs were not being met by a diet restricted to a single food for an extended time, and the crabs may have lost interest in familiarized prey. Again, feeding reinforcements were absent and may have counteracted the effects of training.

In the foraging tests, tactile and visual cues were introduced by the use of living prey rather than effluents. Both groups of familiarized crabs ate and rejected similar numbers of mussels, and there was no difference in the ratios of *Mytilus* to *Geukensia* eaten and rejected. However, even though crabs encountered both species of mussels, they handled *Mytilus* first, ate *Mytilus* first, and consumed more *Mytilus* than *Geukensia* regardless of familiarization group. Since crabs walked over both species before selecting any prey, both species should have had an equal chance to be handled. *Geukensia* has a heavier shell than *Mytilus,* possibly making it more difficult to open, but this did not account for the crabs' preference, because equal numbers of both species were rejected. Metabolites from both species were present in the test tank. As soon as a mussel was eaten, freshly killed prey odors would have filled the tank, possibly decreasing the importance of odor in choosing the next prey, and other cues may have become more important.

If crabs use more than one sensory cue in prey choice, a hierarchy may exist for all sensory functions in determining prey selection. Maynard and Sallee (1970) found that chemotactile stimulation of lobster dactyls overrode antennular stimulation. Our tests were run in the light to permit videotaping, so visual cues might have played a role in prey selection. *Geukensia* was difficult to see against the mottled calcite, whereas the blue-black colored *Mytilus* contrasted well with the background. Arthropod compound eyes are adept at discerning contrasts (Evans, 1984). *Mytilus* may have been visually less cryptic and thus more susceptible to predation.

The crabs were more likely to have been in contact with *Mytilus* than with *Geukensia* before they were caught, and might have retained their sensitivity for that species. Alternatively, *Mytilus* may have been easier to open, or may have simply tasted better than *Geukensia.* Lobsters are also able to detect differences between two closely related mussels—in this case *Mytilus* and *Modiolus*—and showed increased sensitivity with experience and training (Derby and

Atema, 1981). Atema *et al.* (1980) found qualitative differences in the amino acid content of live prey rinses. The foraging study supported the differences found in sensitivities between crabs familiarized with *Mytilus* and crabs familiarized with *Geukensia*. However, *Mytilus* appeared to be more attractive than *Geukensia* when crabs were given a choice between live prey.

The responses of crabs to mussel odors before and after experience with those mussels indicated that familiarization increased sensitivity towards a prey item. Whether this resulted in the formation of a chemosensory search image or a species-specific preference is not clear. However, recognition and remembrance of familiar prey odors facilitates the location of suitable prey in a benthic habitat where few other cues are available.

Acknowledgments

We thank D. French, C. Loshon, and V. Kennedy for their advice and assistance, E. Layman, M. Ailes, and D. Birkett for their help and support. We also thank two anonymous reviewers for their helpful suggestions and thoughtful commentary. AR submitted parts of this manuscript in partial fulfillment of the MS degree at UMES. This research was partially supported by NSF Grant # RII-8704054. This is Contribution No. 30 from the Crustacean Research in Ecology and Mariculture (CREAM) Institute of the University of Maryland Eastern Shore.

Literature Cited

Ache, B. 1982. Thermoreception and chemoreception. Pages 369–398 in *The Biology of Crustacea*, Vol. 3. H. L. Atwood and D. C. Sandeman, eds. Academic Press, New York.

Allen, W., E. Frederick, and R. Wong. 1975. Experiments on the development of artificial bait for the dungeness crab, *Cancer magister* (Dana). *Sea Grant Rep.* HSU-SG7, *Humboldt State Univ.*, Arcata, California.

Atema, J., and C. Derby. 1981. Ethological evidence for search images in predatory behavior. Pages 395–400 in *Advanced Physiological Sciences*, Vol. 16. *Sensory Functions*. E. Graystyan and P. Molnar, eds. Pergamon Press, New York.

Atema, J., K. Holland, and W. Ikehara. 1980. Olfactory responses of yellowfin tuna (*Thunnus albacares*) to prey odors: chemical search image. *J. Chem. Ecol.* **6:** 457–465.

Bond, A. B., and D. A. Riley. 1991. Searching image in the pigeon: a test of three hypothetical mechanisms. *Ethology* **87:** 203–224.

Carr, W. E. S. 1978. Chemoreception in the shrimp, *Palaemonetes pugio:* the role of amino acids and betaine in elicitation of a feeding response by extracts. *Comp. Biochem. Physiol.* **61:** 127–131.

Case, J. 1964. Adequate stimulus of certain *Cancer* dactyl chemoreceptors. *Am. Zool.* **4:** 276–277.

Croze, H. J. 1970. Searching image in carrion crows. *Z. Tierpsychol.* Suppl. **5:** 1–85.

Daniel, P. C., and R. C. Bayer. 1987a. Attraction of predatorily naïve postlarval lobster to extracts of metabolites of common prey: *Mytilus edulis, Mya arenaria, Cancer irroratus*, and *Asterias vulgaris*. *J. Chem. Ecol.* **13:** 1201–1216.

Daniel, P. C., and R. C. Bayer. 1987b. Development of chemically mediated prey-search response in postlarval lobsters (*Homarus americanus*) through feeding experience. *J. Chem. Ecol.* **13:** 1217–1233.

Derby, C. D., and J. Atema. 1981. Selective improvement in responses to prey odors by the lobster, *Homarus americanus*, following feeding experience. *J. Chem. Ecol.* **7:** 1073–1080.

Derby, C. D., and J. Atema. 1982. Chemosensitivity of the walking legs of the lobster, *Homarus americanus:* neurophysiological response spectrum and thresholds. *J. Exp. Biol.* **98:** 303–315.

Drummond-Davis, N. C., K. H. Mann, and R. A. Pottle. 1982. Some estimates of population density and feeding habits in the rock crab, *Cancer irroratus*, in a kelp bed in Nova Scotia. *Can. J. Fish. Aquat. Sci.* **39:** 636–639.

Evans, H. E. 1984. *Insect Biology: A Textbook of Entomology*. Addison-Wesley, Reading, Massachusetts. 436 pages.

Gendron, R. P. 1986. Searching for cryptic prey: evidence for optimal search rates and the formation of search images in quail. *Anim. Behav.* **34:** 898–912.

Gleeson, R. E. 1980. Pheromone communication in the reproductive behavior of the blue crab, *Callinectes sapidus*. *Mar. Behav. Physiol.* **7:** 119–134.

Hall, S. J., C. D. Todd, and A. D. Gordon. 1982. The influence of ingestive conditioning on the prey species selection in *Aeolidia papillosa* (Mollusca: Nudibranchia). *J. Chem. Ecol.* **51:** 907–921.

Karavanich, C., and J. Atema. 1998. Olfactory recognition of urine signals in dominance fights between male lobster, *Homarus americanus*. *Behaviour* **135:** 719–730.

Lawrence, E. S. 1985a. Evidence for search image in blackbirds (*Turdus merula* L.): short-term learning. *Anim. Behav.* **33:** 929–937.

Lawrence, E. S. 1985b. Evidence for search image in blackbirds (*Turdus merula* L.): long-term learning. *Anim. Behav.* **33:** 1301–1309.

Mackie, A. 1973. The chemical basis of food detection in the lobster, *Homarus gammarus*. *Mar. Biol.* **21:** 103–108.

Marko, P. B., and R. Palmer. 1991. Responses of a rocky shore gastropod to the effluents of predatory and non-predatory crabs: avoidance and attraction. *Biol. Bull.* **181:** 363–370.

Maynard, D. M., and A. Sallee. 1970. Disturbance of feeding behavior in the spiny lobster, *Panulirus argus*, following bilateral ablation of the *medulla terminallis*. *Z. Vgl. Physiol.* **66:** 123–140.

McLeese, D. 1973. Olfactory responses of lobsters (*Homarus americanus*) to solution from prey species and to seawater extracts and chemical fractions of fish muscle and effects of antennule ablation. *Mar. Behav. Physiol.* **2:** 237–249.

Pearson, W. H., and B. L. Olla. 1977. Chemoreception in the blue crab, *Callinectes sapidus*. *Biol. Bull.* **153:** 346–54.

Pearson, W. H., P. C. Sugarman, D. L. Woodruff, and B. L. Olla. 1979. Thresholds for detection and feeding behavior in the Dungeness crab, *Cancer magister*. *J. Exp. Mar. Biol. Ecol.* **39:** 65–78.

Pietrewicz, A. T., and A. C. Kamil. 1979. Search image formation in the blue jay (*Cyanocitta cristata*). *Science* **204:** 1332–1333.

Rebach, S. 1996. The role of odor in prey recognition by rock crabs, *Cancer irroratus* Say. *J. Chem. Ecol.* **22:** 2197–2207.

Rebach, S., D. P. French, F. C. Von Staden, M. Wilber, and V. E. Byrd. 1990. Antennular sensitivity of the rock crab *Cancer irroratus* to food substances. *J. Crustac. Biol.* **10:** 213–217.

Stehlik, L. L. 1993. Diets of the brachyuran crabs *Cancer irroratus, C. borealis*, and *Ovalipes ocellatus* in the New York Bight. *J. Crustac. Biol.* **13:** 723–735.

Zar, J. H. 1984. *Biostatistical Analysis*. Prentice Hall, Englewood Cliffs, New Jersey. 718 pages.

Zimmer-Faust, R. K. 1991. Chemical signal-to-noise detection by spiny lobsters. *Biol. Bull.* **181:** 419–426.

Reference: *Biol. Bull.* **197:** 368–376. (December 1999)

The Role of Latero-Frontal Cirri in Particle Capture by the Gills of *Mytilus edulis*

HAROLD SILVERMAN[1], JOHN W. LYNN, PETER G. BENINGER*, AND THOMAS H. DIETZ

Department of Biological Sciences, Louisiana State University, Baton Rouge, Louisiana 70803; and
** Département de Biologie, Faculté des Sciences, Université de Nantes, 2 rue de la Houssinière,*
44322 Nantes Cedex, France

Abstract. In this study we examined the mechanism of particle capture in *Mytilus edulis*, using radioactive-label clearance studies, progressive fixation, and scanning electron microscopy to visualize in detail the cirri and their range of motion. Confocal laser scanning microscopy was used to observe the interaction of cirri with 1 μm fluorescent latex particles on live strips of control and serotonin-treated isolated gill tissue. The gills of *M. edulis* possess large, complex latero-frontal cirri composed of 18–26 pairs of cilia. Particles that were intercepted by the cirri were transferred to the water current on the frontal surface of the filament where they were propelled toward the ventral particle groove. Clearance studies demonstrated that *M. edulis* removed *Escherichia coli* from 5°C seawater bathing medium at 4.9 ml g^{-1} dry tissue min^{-1}. When the gills were exposed to 10^{-3} *M* serotonin, the latero-frontal cirri stopped moving and became fixed in a flexed position that partially blocked the frontal surface of the filament. Clearance studies demonstrated that removal of *E. coli* from the seawater bathing medium was reduced 90% to 0.5 ml g^{-1} dry tissue min^{-1} when 10^{-3} *M* serotonin was present. These data demonstrated that for small particles (< 2 μm) in the near field, movement of cirri was essential for successful capture either by direct contact or with water acting as a hydromechanical coupler.

Introduction

Considerable progress in understanding particle processing mechanisms in suspension-feeding bivalves has been made in recent years (Beninger *et al.*, 1993, 1997; Jørgensen, 1990; Ward *et al.*, 1998b). Investigations have focused on various components of the feeding sequence: capture–transport–selection–ingestion. However, the actual mechanism(s) of particle capture remains difficult to determine.

A number of components are important in understanding the mechanism of particle capture. Fluid mechanics has been used to describe both the delivery of particles to the gill filaments and their movement on the gill (Jørgensen, 1983; Nielsen *et al.*, 1993; Ward *et al.*, 1998a; Riisgård and Larsen, 2000). The potential interaction of particles with a structure on the gill would be an equally important component to understanding the mechanisms leading to particle capture events. Generally, suspension feeding bivalves can capture particles over a wide range of sizes from 10^{-1} μm to 10^{2} μm, with most showing efficient clearance of particles in the range of a few to tens of μm (Møhlenberg and Riisgård, 1978; Ten Winkel and Davids, 1982; Sprung and Rose, 1988). The mechanisms used to capture particles at the extremes of the size range may differ, because the behavior in fluid would change depending on particle density and geometry.

To observe the actual particle capture event, one needs to be able to resolve both the particle and the cellular organelles that are involved with the capture. To date, Riisgård and his colleagues have used isolated preparations and constructed half filament models to analyze particle movements close to the filaments of *Mytilus edulis* (Nielsen *et al.*, 1993; Riisgård *et al.*, 1996). Their observations indicate that particles can be directed to the frontal surface of gill filaments by direct interception of particles by latero-frontal cirri. They have extended these observations by determining the path as particles approach the gill filaments, *in vivo*, using a side-mounted microscopic preparation (Riisgård and Larsen, 2000).

Silverman *et al.*, (1996, 2000) and Beninger *et al.*, (1997) have examined gill strips using confocal laser scanning

Received 3 June 1999; accepted 5 October 1999.

[1] To whom correspondence should be addressed. E-mail: cxsilv@lsu.edu

microscopy (CLSM). The disadvantages of this system are that the observations are made on gill strips that are isolated; normal fluid flow is altered; and normal neural or hormonal cues are modified or missing. However, the advantages of this system include magnification, resolution, tunable depth of focus, and preselection of a gill strip where all cilia are in motion as confirmed by observation before adding particles. The near-field events of particle interaction with cirri are not altered by isolation procedures. The only bivalve investigated to date using this technique is *Dreissena polymorpha*, a species with a homorhabdic eulamellibranch gill type (Silverman *et al.*, 1996). In this freshwater bivalve, the latero-frontal cirri direct particles from the water onto the frontal surface of the gill filaments, where the particles were transported to the ventral particle groove by the frontal cilia.

Mytilus edulis, a marine bivalve species often used for a variety of particle capture studies, has a homorhabdic filibranch gill type. It also has latero-frontal cirri and a ventral particle groove (Atkins, 1937; Owen, 1974; Owen and McCrae, 1976). The organization and structure of latero-frontal cirri in *M. edulis* have been extensively described (Moore, 1971; Owen, 1974; Owen and McCrae, 1976; Jones *et al.*, 1990). The cirri are large, complex structures composed of two ciliary plates; each plate consists of between 18 and 26 fused cilia that are hinged at the base (Owen, 1974). The tips of the cilia are free and oriented at an angle, suggesting a "paddle" or "filtering" structure (Riisgård *et al.*, 1996). Capture and retention studies have shown that *M. edulis* can intercept particles down to 1 μm with retention efficiencies of approximately 50% (Møhlenberg and Riisgård, 1978). Using a video microscope to observe single isolated gill filaments, Riisgård *et al.*, (1996) showed that the latero-frontal cirri of *M. edulis* can intercept relatively large (7 μm) particles. However, the exact sequence of particle-cirrus interaction was not readily resolvable.

In the present study we examined small particle capture by live gill strips using confocal microscopy and high-speed video recording. This approach enabled us to document in detail particle-cirrus interactions in the marine bivalve, *Mytilus edulis*. We reported some of the preliminary data recently in a brief commentary (Silverman *et al.*, 2000).

Material and Methods

Animals

Observations were made on *Mytilus edulis* individuals collected at low tide in Chamcook Harbour (Passamaquoddy Bay, Bay of Fundy, Canada) and on animals purchased from the Marine Biological Laboratory (Woods Hole, Massachusetts). The specimens were flown on moist icepacks to the Life Sciences Microscopy Facility at Louisiana State University. Specimens from Canada were stored for 1–2 days at 4°C in seawater-soaked towels prior to dissection and observation. Specimens from Woods Hole were maintained in the laboratory for several months in artificial seawater (Chambers and de Armendi, 1979) at 4°–6°C and fed algae weekly until used.

Confocal laser scanning microscopy

In larger specimens ($\geq$ 30 mm anterior-posterior shell length), the posterior extremity of the gill was used for CLSM preparations, because the demibranchs are thinnest and shortest in this region, while still presenting the typical gill architecture. This preparation facilitated the observation of 4–5 mm wide strips of gill extending from the gill arch to the ventral particle groove. Strips from the posterior extremity of each demibranch were removed using microsurgical instruments, and placed in isosmotic (1060 mosm) seawater on a microscope slide lined with Nitex screen (125 μm mesh). This screen allowed cilia-generated water currents to flow on both sides of the demibranch, and mechanical disturbance of the gill was avoided by supporting the coverslip above the preparation with silicone vacuum lubricant posts at each corner. For larger animals with thicker gills, we also observed single isolated filaments. For specimens $<$ 30 mm, the gill was sufficiently small and thin to allow any region to be used. We observed the gills of more than 40 specimens (range of shell length = 18–81 mm) during this study.

The preparations were observed using the CLSM technique previously described (Silverman *et al.*, 1996). The gills were examined with a Noran Instruments confocal system attached to a Nikon Optiphot microscope with a 40× fluor lens (NA 1.3). The laser wavelength was set at 529 nm with an FITC barrier filter in the return image path. Reflected channel images were acquired (laser scan and image digitization $<$ 1 μs/frame) and sequentially stored at 120 frames s^{-1} ($\sim$ 8 ms between frames). Images were captured and analyzed using the Odyssey InterVision (Noran) software on a Silicon Graphics Indy computer. Images were not altered except to adjust the contrast.

Fluorescent beads of 0.7 μm or 1.0 μm diameter were added to the preparations to track particle motion in cilia-generated water currents and particle transport on the ciliated epithelia. Gill preparations were oriented such that beads could be added under the coverslip in the dorsal region of the strip and subsequently moved from dorsal to ventral. Particle velocities were determined after observing the movement of individual fluorescent beads over known distances and times.

Scanning electron microscopy

To examine the spatial relationships of cirri and cilia, gill tissue was prepared for scanning electron microscopy using a progressive fixation technique that allowed the arrest of cilia at all stages of their beat cycles. Small mussels were placed in containers with enough seawater ($\sim$ 20–30 ml) to cover the shells. They were left undisturbed until their siphons were clearly visible. Drops of 2% OsO_4 (1–2 ml) were slowly added near the edge of the container; the specimen was left intact for 20 min. The posterior adductor muscle was then cut and the animal exposed to fixative for another 40 min. In a few cases, the adductor muscle was carefully cut before OsO_4, was added, with total exposure to osmium in the bath being 30 min. The mussels were then rinsed in seawater and fixed for an hour in 2% glutaraldehyde in seawater. After fixation, the gill was removed, dehydrated in a graded ethanol series, critical-point dried, and sputter-coated with gold-palladium. Specimens were mounted on stubs and visualized with a Cambridge Scanning Electron Microscope. Some gills were removed and photographed before and after fixation, and again after critical-point drying to monitor tissue shrinkage.

Bacterial clearance

Clearance of ^{35}S-labeled *Escherichia coli* from the bathing medium was quantified with an adaptation of the method of Riisgård (1988) as described previously (Silverman *et al.*, 1995, 1997). Mussels (< 30 mm shell length) were placed in individual test tubes containing 20 ml aerated artificial seawater (5°C) with or without 10^{-3} *M* serotonin for 15 min. Radiolabeled bacteria were added to each tube after the mussels opened their siphons, and after 1 min equilibration, four samples (100 μl) were collected at 10-min intervals. The reduction of bathing medium radioactivity followed first order kinetics, and the clearance was expressed as ml g^{-1} dry tissue min^{-1}. Data are expressed as the mean ± one standard error with the number of animals in parentheses.

Results

Cirral structure

Progressive fixation stopped the cirri and cilia in various stages of their beat cycle. The cirri position varied from being arched over the frontal surface of a gill filament to extending into the interfilament space (Fig. 1). Adjacent cirri on a filament were arrested during fixation in a staggered pattern, such that neighboring cirri were not in the same position relative to the frontal surface (Fig. 1). The CLSM time series micrographs (Figs. 3–6) are of filaments in the same orientation as in Figure 1. Confocal images of a cirrus beat cycle indicated that during the power stroke the cirrus bent over the frontal surface into a flexed position (Fig. 2D). On recovery it returned to an extended position perpendicular to the apical surface of the latero-frontal cirrus cell (Fig. 2A, I). The body of the cirrus beat as a single unit; a complete beat required the cirral body to pivot at its base in addition to moving through the ciliary waveform (Fig. 2). The cirrus moved out of the plane of focus during the flexion, but as the free ciliary tips were moving out of view they were clearly resolvable (Fig. 2E). The high rate of capture of each image (< 1 μs) minimized blurring due to the movement of the cirrus (Fig. 2E). The cirral beat averaged 7.9 ± 0.4 Hz ($n = 6$).

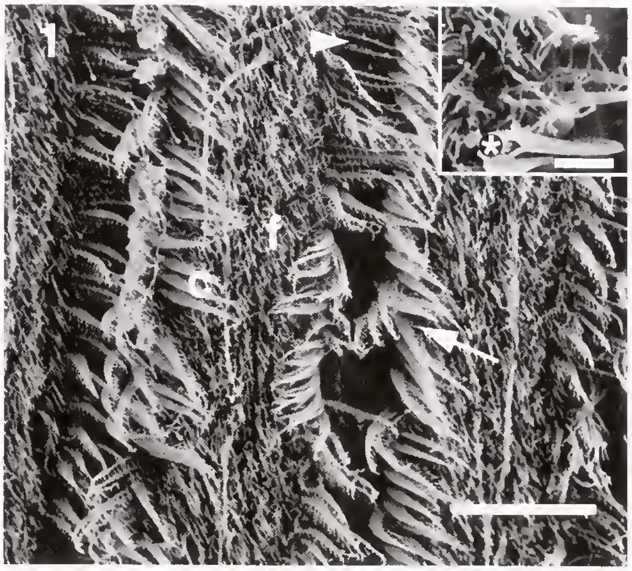

Figure 1. Scanning electron micrograph of gill filaments from *Mytilus edulis* treated to allow fixation of cirri during the beat cycle. Cirri flex during their power stroke moving over the frontal surface (f) of the filament. Cirri are in the extended position (arrowhead) in the interfilament space, and in the flexed position (c) with their free tips bent over the frontal surface. Adjacent cirri on a filament were stopped at different stages of a beat cycle (arrow). The inset of a higher magnification indicates that the free ciliary tips associated with the two ciliary plates of a cirrus angle away from the body of the cirrus to give a 'V' like appearance (*). Bar = 25 μm; inset bar = 5 μm.

Cirral interaction with particles

Particles interacted with moving cirri in several different ways but usually were (i) swept onto the frontal surface of the filaments and entrained into the frontal water current (Fig. 3). Fluorescent particles (1 μm) entering the interfilament space were captured within the 2.2–2.8 μm wide "V" of the free ciliary tips of the cirrus and moved toward the frontal surface as the cirrus beat from the extended into the flexed position. In most cases, particles interacting with a cirrus were moved directly into the frontal current and transported at 307 ± 36 $\mu m\ s^{-1}$, $n = 4$ (Figs. 3, 4) toward the ventral particle groove.

Three additional types of particle interaction with a beating cirrus were observed. (ii) During flexion of the cirrus the particle may be deposited at the edge of the frontal surface without being immediately transported. Subsequent cirral movement positioned the particle into the frontal surface current (Fig. 4). (iii) Some particles remained between the cirral plates and moved with the cirrus for multiple beat cycles (Fig. 5). These particles were finally incorporated into the frontal flow after several cirral beat cycles. The particles that moved with the cirral extension away from the

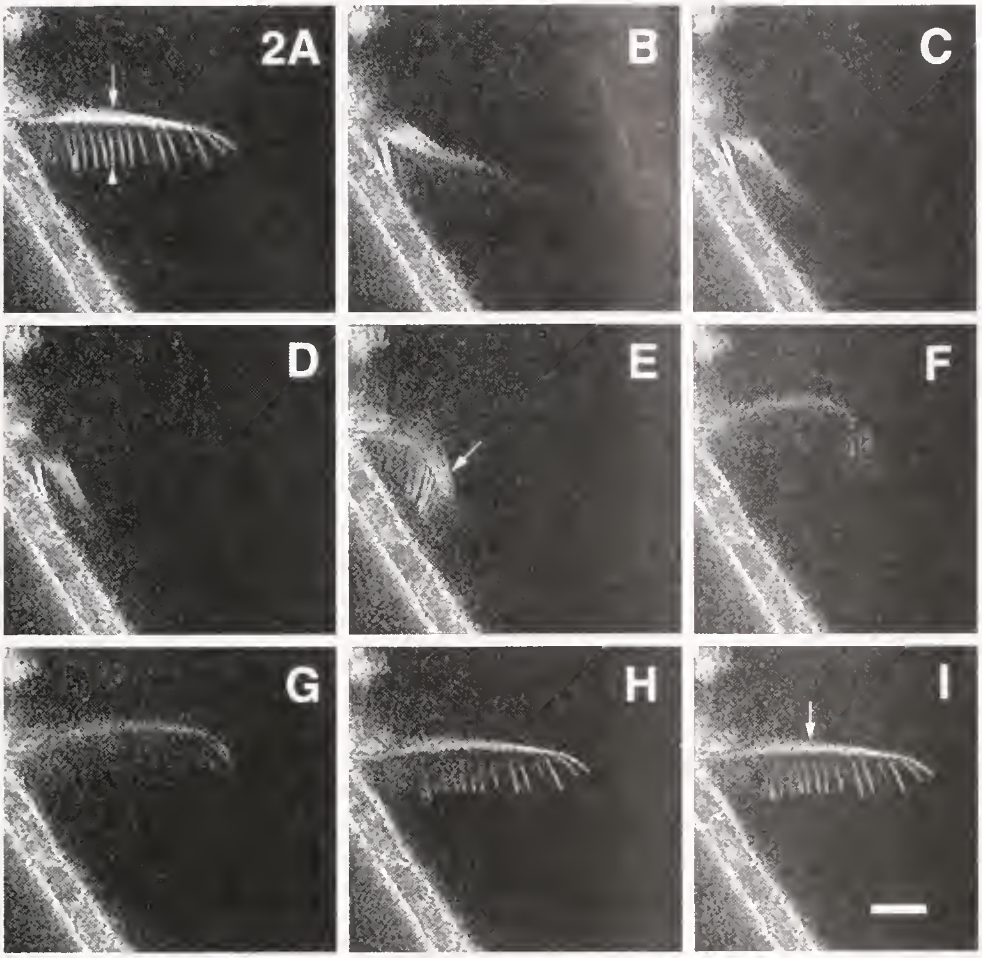

Figure 2. A series of confocal video images (120 frames s^{-1}) of a single cirrus from an *in vitro* gill strip of *Mytilus edulis.* The time between each frame shown in this series is 25 ms. The focal plane of the video is slightly off the perpendicular to the dorso-ventral axis of the filament. The parallel bright lines flank the lateral surface of the filament. Thus, the beat of the cirral tip is toward the frontal surface of the filament that lies to the right and into the background, at a right angle to the visible lateral surface of the filament. The resolution of individual ciliary tips (arrowhead) on one side of the cirrus (one cirral plate) is clear. The bending (power stroke) in A–D moves the plane of the ciliary tips toward the frontal surface of the filament. Images in frames E–I represent the recovery stroke. The total time taken for this beat cycle was ~200 ms (beat frequency ~ 5 Hz). The arrow identifies the midpoint of the cirrus. Bar = 4 μm.

frontal surface suggest that there was intimate contact, either directly or within a few tenths of a μm, from a cirrus (Fig. 5). (iv) Finally, on rare occasions the particle did not reappear, indicating it became dislodged from the cirrus in the interfilament space (not shown).

Particle entrainment in the frontal surface current of the gill was observed both in association with mucus rafts (Beninger *et al.*, 1993, 1997) and in the absence of any visible mucus rafts (Figs. 3, 4). Indeed, we have observed filaments where two particles were being transported, but at different velocities. One moving particle can overtake another particle on the frontal surface (Fig. 6). Such events indicate independent transport of the two particles along the frontal surface, and would suggest that they were not moving in a single mucus raft, or not at the same height above the epithelium. Quick-time videos used to construct Figures 3–6 are archived in the electronic data base of *The Biological Bulletin* at www.mbl.edu/html/BB/VIDEO/BB.video.html.

Serotonin effects on cirral position and clearance of Escherichia coli

Progressive fixation (as described above) revealed that the cirri in the serotonin-treated animals were arrested in the flexed position, occluding most of the frontal surfaces of the gill filament (Fig. 7). The amount of frontal surface covered by the cirri is somewhat exaggerated in this figure because the fixation caused 44 ± 3% (n = 4) shrinkage. From our CLSM observations in some sections of the gill, both frontal and lateral cilia continued to beat in the presence of 10^{-3} *M*

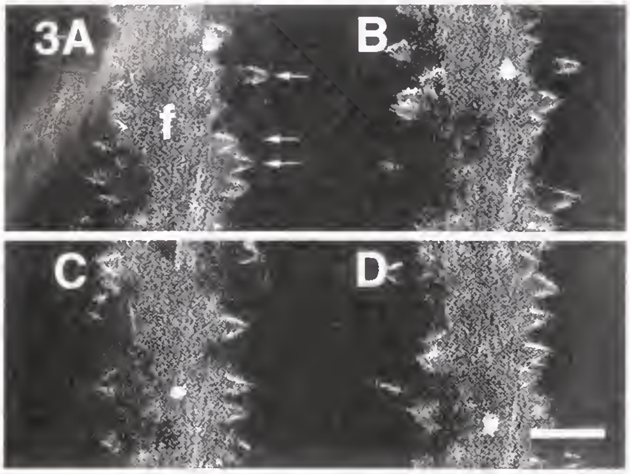

Figure 3. A confocal microscopy time series of the frontal surface of an *in vitro* gill filament from *Mytilus edulis*. Dorsal is at the top of each image and ventral toward the bottom. The time elapsed between each successive frame is 33 ms. Cirral tips are visible as 'V' structures (arrows). The cirri beat in and out of the plane of the image and the 'V's are the tips of the cirri as they flex over the frontal surface on each side of the filament. One cirrus directed a 1-μm fluorescent latex particle onto the edge of the filament from the right interfilament space (A; bright spot at top right). The particle was entrained in the frontal water current and moved ventrally down the frontal surface (B). The particle was transported on the frontal surface of the filament (C and D) moving 20 μm in 100 ms by frame D. Bar = 10 μm.

serotonin. This was also evident in some areas of gill that were fixed for scanning microscopy. This motion is inferred in the wave-like pattern formed by the tips of lateral cilia (Fig. 7). Although the fixation was not instantaneous, the positions of the lateral cilia tips are suggestive of a synchronized or metachronal motion (Fig. 7).

To assess particle capture in the absence of movement by latero-frontal cirri, cirral motion was arrested by adding 10^{-3} *M* serotonin to the seawater bathing medium (Jorgensen, 1983; Ward *et al.*, 1998a). Clearance (ml g^{-1} dry tissue min^{-1}) of ^{35}S-labeled *E. coli* by *M. edulis* in 5°C seawater was 4.92 ± 0.43 ($n = 3$) for controls (130 ± 12 mg dry tissue) compared to 0.51 ± 0.18 ($n = 3$) for treated animals (142 ± 26 mg dry tissue). Clearance of bacteria from control mussels displayed first order kinetics with 21 min required to remove 50% of the label (Fig. 8). The serotonin-treated mussels also displayed first order kinetics, but experienced an 89.6% reduction in the rate of removal of bacteria from the seawater.

Discussion

The movement of an individual cirrus on a living strip of *Mytilus edulis* gill can be observed at high resolution using confocal laser scanning microscopy (CLSM). The beat cycle is similar to that described for the cirri of *Dreissena polymorpha* (Silverman *et al.*, 1996). In the flexed position the tips of the cirri are located over the frontal surface of the gill filament, whereas in the extended position they project into the interfilament space at the level of the latero-frontal cells from which they originate.

Confocal microscopy permits resolution of individual cirri and, depending on reflectance and light scattering, includes their individual ciliary tips. The lateral (x–y plane) resolution (about 0.2 μm) of CLSM, the enhanced rate of sequential image acquisition (~ 8 ms/frame), and high speed of capture of individual images (< 1 μs) enabled observation of the interaction of 1-μm particles with latero-frontal cirri. Although particles were seen to be directed

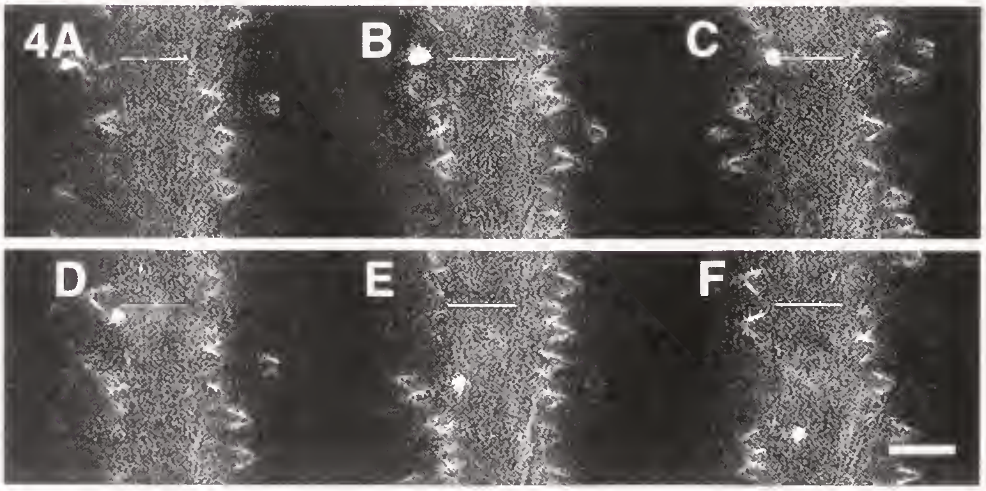

Figure 4. A confocal microscopy time series of an *in vitro Mytilus edulis* gill filament. A 1-μm fluorescent particle (bright spot under the letter A) interacted with a cirrus and was moved toward, but not onto, the frontal surface of the filament (A–C). On the next contact with a cirrus, the particle was moved into the frontal surface water current and transported rapidly (D–F). The reference line marks the initial location of the particle in all of the images. The elapsed time of the series was 125 ms. Bar = 10 μm.

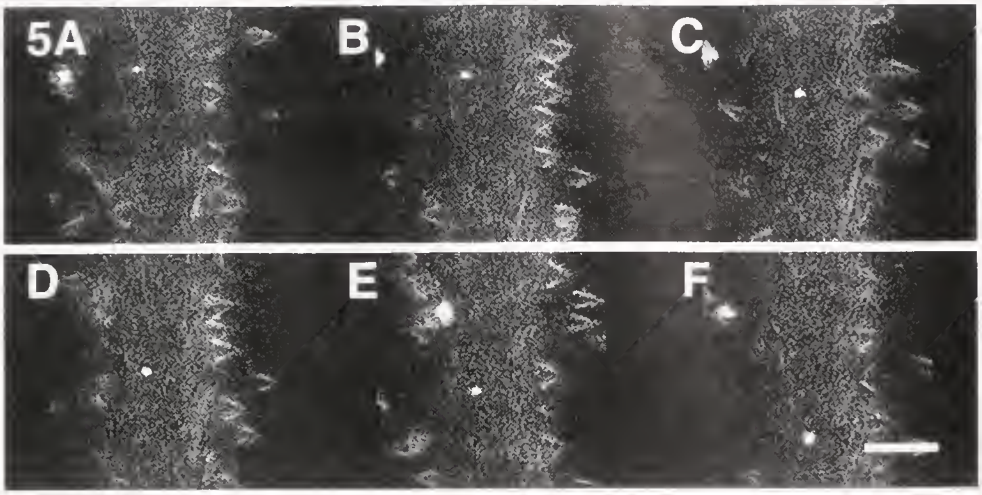

Figure 5. A confocal microscopy time series of an *in vitro Mytilus edulis* gill filament. A fluorescent particle moved rapidly down the center of the filament (A–F) in 125 ms. A second particle was associated with a cirrus (A; upper left) whose ciliary tips were partially out of the plane of focus. As the cirrus continued to move back toward the extended position in the left interfilament space, the particle was drawn back with the cirrus (B–C) until it moved out of the plane of focus in D. It reappeared in E–F as the cirrus moved into its flexed position over the frontal surface of the filament. Bar = 10 μm.

onto the frontal surface during the power stroke of a cirrus, we could not determine whether the interaction was direct or if water acted as a mechanical coupler between the cirrus and particle (Riisgård *et al.*, 1996). However, the close interaction (herein defined as within a few tenths of μm) of the beating cirrus with the particle is responsible for the movement of many particles to the frontal surface of the filament where particles subsequently move in the frontal water flow. Under the experimental conditions described here for *M. edulis*, the particles can be moved to the frontal surface of the filaments even when no mucus is visible or onto visible mucus rafts that are observed to be moving along the frontal surface (Beninger *et al.*, 1997). In both cases, transport of particles along the frontal surface averaged about 307 μm s^{-1}, and was similar to previously reported rates (Jones *et al.*, 1990; Ward *et al.*, 1991, 1993; Nielsen *et al.*, 1993).

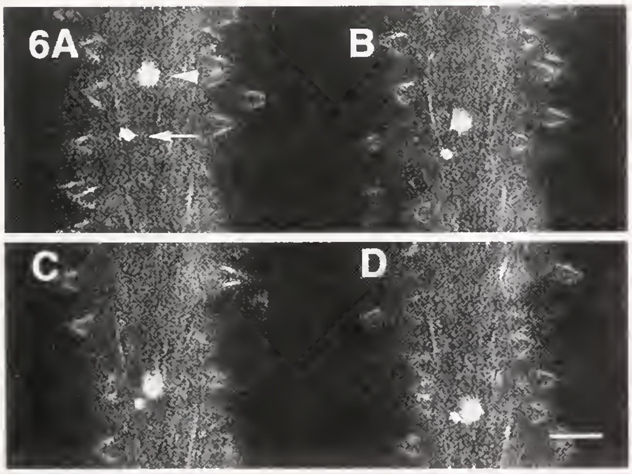

Figure 6. A confocal microscopy time series (25 ms between each image) of an *in vitro Mytilus edulis* gill filament showing that transport of particles along a filament can occur at different rates. In these images two particles moved along the frontal surface of the filament. The larger particle (arrowhead) moved at 750 μm s^{-1}, while the velocity of the smaller particle (arrow) was 350 μm s^{-1}. Bar = 10 μm.

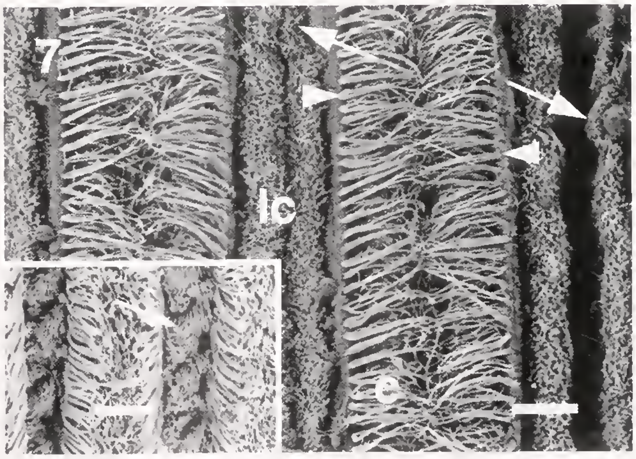

Figure 7. A scanning electron micrograph of two filaments from a *Mytilus edulis* gill treated with 10^{-3} *M* serotonin. The space between these fixed filaments was larger than that observed in Figure 1 (20 μm, *versus* the 15 μm). Visible in the enlarged interfilament space are the tips of the underlying lateral cilia (lc), whose origins from two adjacent filaments are easily discernible. The arrows indicate areas where the lateral cilia were fixed in the various phases of beat associated with the metachronal wave form (inset, lower magnification). The cirri (c) in these preparations are stopped over the frontal surface of the filament, occluding much of the frontal surface. Each cirrus is composed of pairs (arrowheads) of cirral plates containing 18–26 cilia. Bar = 10 μm, inset bar = 20 μm.

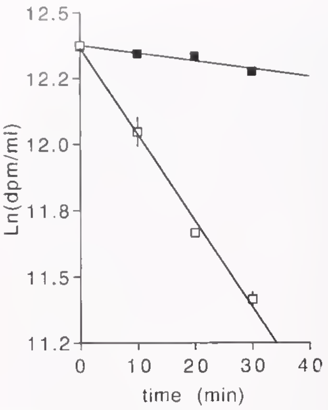

Figure 8. Time-dependent removal of *Escherichia coli* from 5°C seawater by *Mytilus edulis* controls (open square) or treated with 10^{-3} *M* serotonin (filled square). Each point represents the mean ± SEM for 3 animals (SEM smaller than the symbols are not visible). The regression equation for the control mussels was: $Y = -0.033X + 12.365$, $r^2 = 0.994$, and treated: $Y = -0.003X + 12.376$, $r^2 = 0.908$.

The role of these ciliary organelles in particle capture associated with suspension feeding has been controversial. Early workers including Atkins (1937) and Dral (1967) suggested that cirri were important as "mechanical" filters or traps that moved particles onto the frontal surface of the gill filament for subsequent transport. Support for this view is gained from the differential particle capture in bivalve species with cirri of different sizes (Owen and McCrae, 1976; Møhlenberg and Riisgård, 1978; Jørgensen *et al.*, 1984). McHenery and Birkbeck (1985) suggested that *Escherichia coli* were captured more effectively by marine bivalves with larger cirri than by those with small or no latero-frontal cirri. A similar relationship between cirral size and particle capture has been reported for several freshwater bivalves (Silverman *et al.*, 1995, 1997; Tankersley, 1996).

The observations of particle/cirral interactions described here extend the observations of Riisgård *et al.*, (1996). These earlier observations were based on traditional light microscopic lenses immersed in water (theoretical maximum resolution approximately 0.5 μm) to observe particle interaction with cirri in isolated *M. edulis* gills. Their isolated gill preparation contained 10^{-7} *M* serotonin to stimulate ciliary activity and were positioned to maintain the normal interfilament gap (40 μm) at the level of the lateral ciliated cells. The greater resolution of CLSM provides more structural detail, and the high image capture speed (< 1 μs) and recording speed (120 frames s^{-1}) allow better visualization of particle interaction with the cirri. The confocal images indicate that the cirrus was responsible for the movement of 1 μm particles onto the frontal surface of the gill filament. The similarity of the results between these two studies, where different methods were used, supports the accuracy of information gained from both studies.

While observation of cirral/particle interactions with the CLSM provides evidence for the role of cirri in the particle capture process, it does not provide the information under the normal water flow conditions expected *in vivo.* Ward and his colleagues have provided endoscopic videos (1998a, b) that permit observation of dye streams and the motion of relatively large particles (7 μm) as they move within the pallial cavity toward the gill of a living *M. edulis.* Ward *et al.* (1998a) indicate that particles approach the gill at a low angle (less than 30°) and are either captured by the filament or bounce until they are subsequently captured. Observing these endoscopic videos, it appears that there is a nonrandom location of the particles interacting at or near the edge of the filament. These near-field interactions probably represent interception by the cirri, rather than particle capture by the frontal water flow (Ward *et al.*, 1998a). The endoscopic observations are valuable to describe flows and gross movements of particle approach to the filaments. The variable resolution and relatively low magnification limit the observations that are necessary to identify precise mechanism(s) of interaction between filament organelles and individual particles. Thus, it is not possible to determine the distances separating particles from the structures on the gill filament. Despite the particular limitations of both the confocal and the endoscopic observational approaches, the data obtained from each appear to be complementary and suggest the importance of both cirral interaction (near-field) and water flow (far-field) for particle capture in this species. These data also are complementary to those obtained by Riisgård and his colleagues (1996, 2000) demonstrating cirral interaction with particles in various isolated preparations and also in young undisturbed mussels.

Although most reports indicate that isolated *M. edulis* gills must be stimulated by 10^{-7} *M* serotonin to maintain ciliary activities, we have found that sections of isolated gills commonly have beating cilia. We selected preparations where latero-frontal cirri, and frontal and lateral cilia were all beating. The beat frequency of the cirri (8 Hz) and the patterns of motion were similar to the 4–9 Hz observed by Dral (1967) in young mussels *in vivo.* He noted that intact *M. edulis* displayed a diverse repertoire of ciliary activity, including spontaneous arrest. While Dral (1967) highlights a beat cycle that places adjacent cirri offset by ½ beat cycle, he points out that there are many other relationships between adjacent cirri that would not be detected with the methods used. The data presented in this study also are consistent with the recent *in vivo* observations of Riisgård and Larsen (2000) and with the modeling done by Riisgård and colleagues based on isolated filament preparations (Nielsen *et al.*, 1993; Riisgård *et al.*, 1996). Indeed, the observations made here are consistent with the calculations of Silvester and Sleigh (1984) who suggest that latero-frontal cirri can act as "sieves," although perhaps more water moves around rather than through the cirrus (Riisgård *et al.*, 1996).

The finding of an 83% reduction in particle capture in *Mytilus edulis* after serotonin is used to block cirral movement (Ward *et al.*, 1998a) also is consistent with the previous results of Jørgensen (1983), who showed that cirral movement was critical to particle capture. The reduction in particle capture efficiency after serotonin administration has been ascribed to a breakdown in cirral-generated water currents (Ward *et al.*, 1998a). However, the data of the present study provide an alternate explanation. The observations of the present study confirm that the cirri of treated specimens are arrested in the flexed position (Jørgensen, 1975, 1983), eliminating direct cirri particle interaction while the frontal and lateral cilia continue to beat. Furthermore, the positions of the arrested cirri physically block particles from approaching the frontal surface following serotonin treatment. Bacterial clearance was reduced 90% under these conditions. On occasion we have noted that cirral beating may be spontaneously arrested. Dral (1967) also noted that ciliary organelles on *in vivo* mussel gills would spontaneously become motionless. Fluorescent particles moving in the frontal water current were observed to "fall" occasionally or be deflected from the frontal surface (Nielsen *et al.*, 1993; unpub. obs. in *D. polymorpha*). Thus, cirral activity is important for both particle capture and, perhaps, keeping particles entrained in the frontal water current.

In addition to the cirral arrest, serotonin also caused gill musculature to relax in preparations (Jørgensen, 1983; Medler and Silverman, 1997), which can increase the interfilament distance. In modeling particle-capture mechanisms, the dimensions of gill structures (ostial size, interfilament space, filament size, cirral size), rate of ciliary beat, and ambient hydrostatic pressure are all critical components (Silvester and Sleigh, 1984; Famme *et al.*, 1986; Grünbaum *et al.*, 1998). Riisgård and Larsen (2000) point out that the calculations based on *in vitro* gill dimensions must at least match intact clearance values, microscopic measurements on intact tissues, and particle transport rates, if such calculations are to accurately predict mechanism. Many of these components are neither fixed nor necessarily uniform across a gill at any particular time (Medler and Silverman, 1997; Medler *et al.*, 1999).

We cannot determine whether the particle-delivery mechanism involves direct particle contact with the cirri. However, at the observed proximity of the particle with the cirrus (< 1 μm), the question of 'hydromechanical' *versus* 'mechanical' becomes irrelevant, as any intervening water is essentially a mechanical coupler. Evidence for this reasoning comes from particles that were not successfully moved to the frontal surface on the first cirral interaction. Many of these particles were drawn back with the cirrus as it moved toward the extended position (Figs. 4, 5). These particles appeared to reside within the space (2.2–2.8 μm) between the free tips of the two ciliary plates making up the cirrus. The particle (1 μm in diameter) could be physically wedged between the plates, moving within the water being drawn back by the cirrus during its extension, or by cohesive contact with the plates. The amount of water that might be moving with the cirri is small according to the model of Riisgård *et al.* (1996). In addition, their model indicates that particles can make contact with the cirral plate. The mechanism for particle capture is close interaction with the cirrus, and at low Reynolds numbers, hydromechanical and mechanical are essentially the same, and consistent with the confocal observations made in this study.

Both the eulamellibranch, *Dreissena polymorpha* and the filibranch *Mytilus edulis* species have homorhabdic gills and complex cirri, and capture small particles in the near-field when cirral movements cause particles to be deflected onto the frontal surface. The cirri stop the particles and then transfer them to the frontal flow (Riisgård *et al.*, 1996; Beninger *et al.*, 1997; Riisgård and Larsen, 2000; this study). The environment of the transfer is non-steady state, low Reynolds number (Grünbaum *et al.*, 1998). Predicting exact particle movements without actually observing them is difficult (Shimeta and Jumars, 1991). Far-field observations are possible using endoscopy that situate particle capture in intact specimens near the latero-frontal cirri (Ward *et al.*, 1998a). Near-field interactions are visible with CLSM (Silverman *et al.*, 1996; this study). These observations, together with microscopic observations on single filaments or isolated gills (Nielsen *et al.*, 1993; Riisgård *et al.*, 1996), and studies using *in vivo* preparations (Dral, 1967; Riisgård and Larsen, 2000) all demonstrate the importance of cirri and their direct interaction with particles during the capture process.

Acknowledgments

This project was supported by Louisiana State University Sea Grant Program NA46RG0096 R/ZMM-5. We thank Julie Cherry, Ron Bouchard, Paul Bruce, and Chris Thibodaux for technical assistance. This research was aided by the M. D. Socolofsky Microscopy Facility. Additional video images may be viewed at http://www.biology.lsu.edu/research.

Literature Cited

Atkins, D. 1937. On the ciliary mechanisms and interrelationships of lamellibranchs. II. Sorting devices on the gills. *Q. J. Microsc. Sci.* **79:** 339–373.

Beninger, P. G., S. St-Jean, Y. Poussart, and J. E. Ward. 1993. Gill function and mucocyte distribution in *Placopecten magellanicus* and *Mytilus edulis* (Mollusca: Bivalvia): the role of mucus in particle transport. *Mar. Ecol. Prog. Ser.* **98:** 275–282.

Beninger, P. G., J. W. Lynn, T. H. Dietz, and H. Silverman. 1997. Mucociliary transport in living tissue: the two-layer model confirmed in the mussel *Mytilus edulis* L. *Biol. Bull.* **193:** 4–7.

Chambers, E. L., and J. de Armendi. 1979. Membrane potential, action potential and activation potential of eggs of the sea urchin, *Lytechinus variegatus*. *Exp. Cell Res.* **122:** 203–218.

Dral, A. D. G. 1967. The movements of the latero-frontal cilia and the mechanism of particle retention in the mussel (*Mytilus edulis* L.). *Neth. J. Sea Res.* **3:** 391–422.

Famme, P., H. U. Riisgård, and C. B. Jorgensen. 1986. On direct measurement of pumping rates in the mussel *Mytilus edulis. Mar. Biol.* **92:** 323–327.

Grünbaum, D., D. Eyre, and A. Fogelson. 1998. Functional geometry of ciliated tentacular arrays in active suspension feeders. *J. Exp. Biol.* **201:** 2575–2589.

Jones, H. D., O. G. Richards, and S. Hutchinson. 1990. The role of ctenidial abfrontal cilia in water pumping in *Mytilus edulis* L. *J. Exp. Mar. Biol. Ecol.* **143:** 15–26.

Jorgensen, C. B. 1975. On gill function in the mussel *Mytilus edulis* L. *Ophelia* **13:** 187–232.

Jorgensen, C. B. 1983. Fluid mechanical aspects of suspension feeding. *Mar. Ecol. Prog. Ser.* **11:** 89–103.

Jorgensen, C. B. 1990. *Bivalve Filter Feeding: Hydrodynamics, Bioenergetics, Physiology and Ecology.* Olsen and Olsen Press, Fredensborg, Denmark.

Jorgensen, C. B., T. Kiørboe, F. Møhlenberg, and H. U. Riisgård. 1984. Ciliary and mucus-net filter feeding, with special reference to fluid mechanical characteristics. *Mar. Ecol. Prog. Ser.* **15:** 283–292.

McHenery, J. G., and T. H. Birkbeck. 1985. Uptake and processing of cultured microorganisms by bivalves. *J. Exp. Mar. Biol. Ecol.* **90:** 145–163.

Medler, S., and H. Silverman. 1997. Functional organization of intrinsic gill muscles in zebra mussels, *Dreissena polymorpha* (Mollusca: Bivalvia), and response to transmitters *in vitro. Invertebr. Biol.* **116:** 200–212.

Medler, S., C. C. Thompson, T. H. Dietz, and H. Silverman. 1999. Ionic effects on intrinsic gill muscles in the freshwater bivalve, *Dreissena polymorpha. Comp. Biochem. Physiol. A.* **122:** 163–172.

Møhlenberg, F., and H. U. Riisgård. 1978. Efficiency of particle retention in 13 species of suspension feeding bivalves. *Ophelia* **17:** 239–246.

Moore, H. J. 1971. The structure of the latero-frontal cirri on the gills of certain lamellibranch molluscs and their role in suspension feeding. *Mar. Biol.* **11:** 23–27.

Nielsen, N. F., P. S. Larsen, H. U. Riisgård, C. B. Jorgensen. 1993. Fluid motion and particle retention in the gill of *Mytilus edulis:* video recordings and numerical modelling. *Mar. Biol.* **116:** 61–71.

Owen, G. 1974. Studies on the gill of *Mytilus edulis:* the eu-latero-frontal cirri. *Proc. R. Soc. Lond. B.* **187:** 83–91.

Owen, G., and J. M. McCrae. 1976. Further studies on the latero-frontal tracts of bivalves. *Proc. R. Soc. Lond. B.* **194:** 527–544.

Riisgård, H. U. 1988. Efficiency of particle retention and filtration rate in 6 species of Northeast American bivalves. *Mar. Ecol. Prog. Ser.* **45:** 217–223.

Riisgård, H. U., and P. S. Larsen. 2000. A comment on experimental techniques for studying particle capture in filter-feeding bivalves. *Limnol. Oceanogr.* (In press).

Riisgård, H. U., P. S. Larsen, and N. F. Nielsen. 1996. Particle capture in the mussel *Mytilus edulis:* the role of latero-frontal cirri. *Mar. Biol.* **127:** 259–266.

Shimeta, J., and P. A. Jumars. 1991. Physical mechanisms and rates of particle capture by suspension-feeders. *Oceanogr. Mar. Biol. Annu. Rev.* **29:** 191–257.

Silverman, H., E. C. Achberger, J. W. Lynn, and T. H. Dietz. 1995. Filtration and utilization of laboratory-cultured bacteria by *Dreissena polymorpha, Corbicula fluminea,* and *Carunculina texasensis. Biol. Bull.* **189:** 308–319.

Silverman, H., J. W. Lynn, and T. H. Dietz. 1996. Particle capture by the gills of *Dreissena polymorpha:* structure and function of latero-frontal cirri. *Biol. Bull.* **191:** 42–54.

Silverman, H., S. J. Nichols, J. S. Cherry, E. Achberger, J. W. Lynn, and T. H. Dietz. 1997. Clearance of laboratory-cultured bacteria by freshwater bivalves: differences between lentic and lotic unionids. *Can. J. Zool.* **75:** 1857–1866.

Silverman, H., J. W. Lynn, and T. H. Dietz. 2000. *In vitro* studies of particle capture and transport in suspension-feeding bivalves. *Limnol. Oceanogr.* (In press).

Silvester, N. R., and M. A. Sleigh. 1984. Hydrodynamic aspects of particle capture by *Mytilus. J. Mar. Biol. Assoc. UK* **64:** 859–879.

Sprung, M., and U. Rose. 1988. Influence of food size and food quantity on the feeding of the mussel *Dreissena polymorpha. Oecologia* **77:** 526–532.

Tankersley, R. A. 1996. Multipurpose gills: effect of larval brooding on the feeding physiology of freshwater unionid mussels. *Invertebr. Biol.* **115:** 243–255.

Ten Winkel, E. H., and C. Davids. 1982. Food selection by *Dreissena polymorpha* Pallas (Mollusca: Bivalvia). *Freshwater Biol.* **12:** 553–558.

Ward, J. E., P. G. Beninger, B. A. MacDonald, and R. J. Thompson. 1991. Direct observations of feeding structures and mechanisms in bivalve molluscs using endoscopic examination and video image analysis. *Mar. Biol.* **111:** 287–291.

Ward, J. E., B. A. MacDonald, R. J. Thompson, and P. G. Beninger. 1993. Mechanisms of suspension feeding in bivalves: resolution of current controversies by means of endoscopy. *Limnol. Oceanogr.* **38:** 265–272.

Ward, J. E., L. P. Sanford, R. I. E. Newell, and B. A. MacDonald. 1998a. An new explanation of particle capture in suspension-feeding bivalve molluscs. *Limnol. Oceanogr.* **43:** 741–752.

Ward, J. E., J. S. Levinton, S. E. Shumway, and T. Cucci. 1998b. Particle sorting in bivalves: *in vivo* determination of the pallial organs of selection. *Mar. Biol.* **131:** 283–292.

Reference: *Biol. Bull.* **197:** 377–387. (December 1999)

The Physiological Basis for Faster Growth in the Sydney Rock Oyster, *Saccostrea commercialis*

BRIAN L. BAYNE[1,*], SUSANNE SVENSSON[1,2] AND JOHN A. NELL[3]

[1] *Centre for Research on Ecological Impacts of Coastal Cities, Marine Ecology Laboratories A11, University of Sydney, NSW 2006, Australia;* [2] *Department of Zoophysiology, University of Göteborg, Medicinaregatan 18, 413 90 Göteborg, Sweden; and* [3] *NSW Fisheries, Port Stephens Research Centre, Taylors Beach, NSW 2316, Australia*

Abstract. Sydney rock oysters were sampled from a mass selection experiment for growth (the "selected" category) and from a control ("not selected") population and held in the laboratory at three ration levels. We evaluated three models to explain faster rates of growth by selected oysters. Selection resulted in oysters feeding at up to twice the rate and with greater metabolic efficiency than controls. A field experiment confirmed that selection leads to faster rates of feeding across a wide range of food concentrations. Selected oysters also grew more efficiently, at a smaller cost of growth (C_g): mean values for C_g were 0.43 $J \cdot J^{-1}$ in selected individuals and 0.81 $J \cdot J^{-1}$ in the controls. In contrast, oysters in both categories showed similar metabolic rates at maintenance, *i.e.*, at a ration supporting zero growth. There was no evidence that differential energy allocation affected the balance between total metabolic requirements above and below zero net energy balance. By experimenting with selected and control oysters of different sizes and ages, then standardizing the data for size, we found no effects of age on the differences due to selection. Faster-growing oysters feed more rapidly; invest more energy per joule ingested; show a higher net growth efficiency; and are able to allocate less energy per unit of tissue growth, than slower-growing individuals.

Introduction

The physiological processes that constitute growth are of fundamental interest. A striking feature of growth in nature is its variability amongst individuals, which is a result of the effects of exogenous and endogenous factors. Of the various endogenous factors involved, genotypic composition may play a significant part.

Genetic properties may affect growth in various ways (Koehn, 1991), including correlations between growth rate and genetic heterozygosity (Mitton and Grant, 1984; Zouros *et al.*, 1988; Britten, 1996). For marine bivalve molluscs in particular, presumed interactions between genotype and growth are of particular interest in aquaculture (Newkirk, 1980), and the selective breeding of oysters has often succeeded in increasing average rates of growth (see review by Sheridan, 1997).

Analysis of the bioenergetics of growth is useful in studies seeking to link phenotypic variability in growth to genetic causes. This approach involves the dissection of growth into its component processes, as represented by the "balanced energy equation" of Winberg (1956; see review by Wieser, 1994). For example, Present and Conover (1992) have described how genetically based latitudinal differences in the growth rate of the fish *Menidia menidia* were due to differences in both food consumption rates and somatic growth efficiency. In this present study, we set out to identify physiological mechanisms to explain observed variability in growth in oysters. We postulated three ways by which an individual animal may increase its rate of growth above that of other individuals, when held in the same environmental conditions. Though not fully independent nor mutually exclusive, these are sufficiently different in both underlying mechanisms and likely ecological consequences to act as useful alternative models to explain variability in growth rate among individuals. We then evaluated these models by comparing oysters artificially selected for faster growth with control, "not-selected," oysters.

Received 16 December 1998; accepted 29 September 1999.

* To whom correspondence should be addressed. E-mail: blb@bio.usyd.edu.au

First, in the *increased acquisition* model, an individual may obtain more food per unit time by feeding more rapidly than others, so increasing its metabolizable energy intake (Present and Conover, 1992; Rist *et al.*, 1997; De Moed *et al.*, 1998). This may be evaluated by comparing a variety of traits of feeding behavior (Bayne *et al.*, 1999) and relating the results to rates of growth. We tested the hypothesis that, under similar conditions of ration (quantity and quality), oysters selected for faster growth will have faster rates of ingestion than do control (not-selected) oysters.

Second, in the *modified allocation* model, faster growth may be the result of greater proportional allocation of energy to growth at the expense of other energy-demanding processes, such as body maintenance (Wieser, 1989). We evaluated one aspect of this model by estimating the metabolic rate of selected and not-selected oysters at maintenance, when growth is neither negative nor positive, to test the hypothesis that selected oysters would show reduced maintenance rates.

Finally, in the *metabolic efficiency* model, faster growth may result from a higher growth efficiency (Present and Conover, 1992) from reduced metabolic costs of growth (Wieser, 1994), or from a combination of the two. This model was evaluated in two ways. Firstly, net somatic growth efficiency, defined as the proportion of metabolizable energy intake allocated to growth, was determined. Secondly, by measuring metabolic rates at different rates of growth, we tested the hypothesis that reduced costs of growth correlate, amongst individuals, with increased growth rate.

We used the Sydney rock oyster, *Saccostrea commercialis* (Iredale and Roughley). The New South Wales Fisheries Research Centre at Port Stephens, Australia, established a mass selection program for these oysters in 1990 (Nell *et al.*, 1996). Four selected lines were established for faster growth, and these have been bred in alternate years since. After one generation of selection, Nell *et al.*, (1996) found that oysters from two of the lines were heavier than oysters from two control lines. After two generations, their weight was 18% greater than controls (Nell *et al.*, 1998). Oysters from the third generation of selection (referred to in Nell *et al.*, 1998, as the "loose 2" selection line) were used in the present study and compared with control oysters. The experiment was designed to test hypotheses derived from the three models discussed above and to identify the physiological characteristics that may explain enhanced growth in the selected lines.

Materials and Methods

Material and general procedures

Oysters were provided by the NSW Fisheries Laboratory at Port Stephens. The selected oysters were as described above. Controls were from a commercial oyster farm and are referred to as "not-selected." These oysters were grown under identical conditions to the selected oysters, within Nelson Bay, New South Wales, though they were from a natural larval settlement and not cultured as larvae within the hatchery, as were the selected individuals. Within each category, we distinguished one group of "small" and one group of "large" oysters (Table I). The selected oysters were 23 months old. The ages of the not-selected oysters were not known with certainty, but the "not-selected, small (NSS)" individuals are considered to be of similar age to the "selected, large (SL)" individuals, though of smaller size, and of similar age and size to the "selected, small (SS)" oysters. The "not-selected, large (NSL)" oysters are thought to be about 6 months older than the selected, large oysters.

Table I

Mean (±SD; n = 12) shell heights (cm) and whole weights (shell plus flesh, grams) of oysters in the four experimental categories

Category	Shell height	Whole weight
Selected, Large	7.93 ± 0.33^a	52.95 ± 1.05^c
Not selected, Large	7.89 ± 0.47^a	49.66 ± 2.40^c
Selected, Small	6.37 ± 0.32^b	38.40 ± 3.87^d
Not selected, Small	6.54 ± 0.36^b	36.96 ± 2.84^d

Values sharing superscripted letters are not significantly different.

Twelve oysters from each experimental category (Table I) were tagged for individual identification and held in the water-table of a research aquarium of recirculating seawater in Sydney. The aquarium contained 600 l of water, of which 33% was replaced every 7 days. Water temperature was controlled at 20 ± 5°C and salinity at 33 ± 1.5‰.

The laboratory experiment was as follows:

- *20 January to 8 February 1998 (20 days).* No supplementary food added; physiological measurements made from 28 January to 5 February and labeled the "field" condition.
- *9 February to 4 March (24 days).* Food added to make up the "middle ration" condition; measurements made from 23 February to 2 March.
- *5 March to 18 March (14 days).* Food added to comprise the "high ration" condition; measurements made 12 to 18 March.
- *19 March to 9 April (22 days).* No food added; the "low ration" condition; measurements made from 6 to 10 April, after 16-20 days without food.

Rations

The food was unicelled algae *Isochrysis galbana* (strain T-ISO) and *Chaetoceros gracilis*, supplied as algal pastes by Reed Mariculture Inc., California. Individual pastes were combined in the proportion 3 parts T-ISO to 7 parts *C.*

gracilis, and the cells were suspended in seawater in a feeding reservoir at the desired concentration (Table II). The cells were dosed to the oysters by peristaltic pump, from 0930 to 1530 daily (middle ration) and 0930 to 1630 (high ration). Cell concentrations in the trays were monitored frequently with a particle size analyzer (Coulter Counter model Z1). Samples of cells from the feeding reservoir were weighed after drying overnight at 80°C, and then measured for nitrogen content (by Leco CHN analyser).

Physiological measurements

All oysters were measured for clearance rate, absorption efficiency, rate of oxygen consumption, and rate of ammonia-nitrogen excretion, at each ration level. Following preliminary studies, care was taken not to use the same individuals in any two measurements without at least 24 h of recovery from the stress of handling.

Clearance rate (CR). Clearance rate is a measure of the volume of water cleared of algal cells per hour. When pseudofeces (that is, material cleared from suspension but not ingested) are not produced (as in this experiment), the rate of ingestion of food is calculated as CR × [food concentration].

Oysters were placed individually in 1-l beakers in water from the feeding trays and left undisturbed in a water bath for 30 min. A beaker without an oyster was used as the blank control. The water was gently aerated using Pasteur pipettes coupled to a compressed air supply. About 600 ml of the water was then siphoned off and replaced with seawater containing algal cells at a concentration equivalent to the experimental ration. A 10-ml sample was taken after 10 min and then at 10-min intervals for a further 40 min. Cell concentrations were measured with a particle size analyzer (Coulter Counter model Z1).

For data analysis, a check was first made for linearity (ln cell concentration plotted over time), then clearance rate as liters per hour was calculated according to Coughlan (1969):

$$\mathrm{CR} = ([\ln C_0\text{-}\ln C_1] \cdot \mathrm{Vol}/t)\text{-Blank},$$

where C_0 and C_1 are concentrations of cells at the beginning and end of incubation time t, Vol is the volume of water in the beaker, and Blank is the change in cell concentration in the blank control beaker.

Table II

Maximal concentrations of cells (T-ISO + C. gracilis) *and total particulate matter (TPM) in the oyster trays for each of the experimental rations*

Ration	Maximal cell conc:10^3 ml^{-1}	Maximal TPM. mg · l^{-1} [="Peak rations"]	% body weight ingested · d^{-1}
Low	2.9 ± 0.9	0.07 ± 0.02	—
Middle	44.0 ± 1.9	0.59 ± 0.02	0.87 ± 0.37
High	90.9 ± 5.3	1.07 ± 0.07	2.41 ± 1.58

TPM is based on a conversion from cell numbers (10^6 cells = 0.013 ± 0.003 mg dry mass). The "% body weight ingested" is calculated from mean ingestion rates across the four experimental categories, as presented later in the Results section. All values are means ± SD.

Absorption efficiency (AE). Absorption efficiency measures the efficiency with which ingested organic material is absorbed by the animal. When multiplied by the ingestion rate, AE estimates absorption rate (milligrams of organic matter per hour).

Samples of feces were collected from the beakers in which the oysters were held for CR measurements. It proved impossible to collect enough material for analysis by individual; rather, samples were pooled according to category, at each of the middle and high ration levels. Food cells were sampled at the same time. Samples were filtered onto ashed, preweighed, GF/C filters, washed with 0.9% ammonium formate, dried overnight at 80°C, weighed, ashed for 4 h at 450°C, and weighed again. AE was estimated according to Conover (1966):

$$\mathrm{AE} = F - E/[(1 - E) \cdot F],$$

where F and E are the ratios of ash-free dry weight to dry weight of the food and feces, respectively.

Oxygen consumption (VO_2). Oxygen consumption is an indirect measure of the metabolic rate, or rate of energy expenditure, by the animal.

Oysters were placed individually in airtight flasks of ~500 ml volume, on a perforated base that allowed stirring of the water by magnetic stirrers. Each flask was fitted with a Strathkelvin oxygen electrode to record the rate of decline of dissolved oxygen in the flasks. The flasks were also fitted with two 5-ml syringes, one containing algal cells, the other empty as a compensation chamber. After 30 min at constant temperature in a water bath, the algal cells were injected into the flask to achieve a cell concentration equivalent to that measured in the feeding trays (middle and high ration levels only). The rate of oxygen consumption was then recorded for a further 60–90 min. For each set of measurements of five oysters, one flask was used as a blank control.

The rate of oxygen consumption, as milliliters of oxygen per hour, was calculated as:

$$\mathrm{VO}_2 = ([O_{2t1} - O_{2t2}] \cdot \mathrm{Vol}/t) - \mathrm{Blank},$$

where O_{2t1} and O_{2t2} are oxygen concentrations (milliliters per liter) at least 30-min apart; Vol is the volume of water in the flask; t is the time in hours, and Blank is the change of oxygen concentration in the blank control respirometer.

Excretion rate (VNH_4–N). This is the rate at which nitrogen is excreted as ammonia. Oysters were placed individually in 1 l of filtered seawater and left undisturbed for 3 h. Beakers without oysters served as blank controls. Concentrations of ammonia were measured using the phenol-hypochlorite method of Solorzano (1969); a full set of standards was analyzed for each experimental run. Rates of excretion, as milligrams of ammonia-nitrogen per hour, were calculated as:

$$VNH_4 - N = (\mathrm{Conc}_{\mathrm{exptl}} - \mathrm{Conc}_{\mathrm{control}}) \cdot \mathrm{Vol}/t,$$

where $\mathrm{Conc}_{\mathrm{exptl}}$ and $\mathrm{Conc}_{\mathrm{control}}$ are ammonia concentrations in experimental and control beakers, respectively, Vol is the volume of water in the beaker, and t is the incubation time (3 h).

Oxygen:nitrogen ratio. The ratio, in molar equivalents, of oxygen consumed to nitrogen excreted serves as an index of catabolic substrate (Bayne and Newell, 1983), and was calculated to evaluate whether the oysters in the different growth and size categories were utilizing different biochemical substrates, a difference which might then explain other observed metabolic differences.

Growth. The 12 oysters in each experimental category were weighed (shell plus flesh) at the beginning (Table 1) and end of the experiment. Growth was calculated by subtraction and related to the period spent at high ration (14 days) to convert to a daily rate. At the end of the experiment, the oysters were shucked and dry flesh weights determined after drying overnight at 80°C.

Due to uncoupling in the growth of shell and tissue in bivalves (Hilbish, 1986; Lewis and Cerrato, 1997) conversions of total weight to weight of tissue, using a constant conversion factor, must be made with caution. For this study, we derived such conversion factors for each individual at the end of the experiment. Given the relatively short duration of the experiment, we considered it appropriate to use these factors to estimate equivalent dry flesh weight at the start, and so to estimate growth also as milligrams of dry tissue per day.

Converting rates to a standard body size

This conversion was based on allometric relationships between dry flesh weight and the measured physiological rates, following Bayne and Newell (1983):

$$V_{\mathrm{stand}} = (W_{\mathrm{stand}}/W_{\mathrm{meas}})^{\beta} \cdot V_{\mathrm{meas}},$$

where V_{stand} and W_{stand} are the standardized rate and dry flesh weight, respectively; V_{meas} and W_{meas} are the rate and dry flesh weight as measured; and β is the allometric exponent in the equation describing physiological rate as a function of body size.

Estimates of β were derived for clearance and respiration rates across all experimental categories from the "field condition" measurements. The exponent for excretion rate is based on a separate sample of oysters (Svensson, unpublished). The exponent for growth was determined from rates of growth calculated (see above) for the high ration condition. The values were as follows:

$$\text{Clearance rate: } \beta = 0.641 \pm 0.113 (n = 32)$$
$$\text{Oxygen consumption rate: } \beta = 0.536 \pm 0.107 (n = 25)$$
$$\text{Excretion rate: } \beta = 0.772 \pm 0.156 (n = 50)$$
$$\text{Growth rate: } \beta = 1.96 \pm 0.58 (n = 45).$$

As measured over all categories ($n = 48$), the mean dry flesh weight of the experimental oysters at the end of the experiment was 0.920 ± 0.243 g. W_{stand} was set at 1.0 g.

Field measurements

Rates of ingestion were measured in the field on two occasions, as a test of the hypothesis that results of the laboratory experiment on feeding rates, and in the context of a model of energy acquisition, would be repeated under the more natural conditions of food availability. Selected and not-selected oysters of similar size (64.0 ± 3.35 g and 62.7 ± 2.86 g whole weight, respectively) were held overnight in wide-mesh bags at the mouth of the Karuah River as it enters the Port Stephens estuary, on 9–10 September and 3–5 November, 1998. This is an area used for cultivating oysters. The selected oysters were from the same mass selection as those used in the laboratory. During the field measurements, water temperatures were 19.1 ± 1.9°C (over both months) and salinities were 28.2 ± 1.9‰ (September) and 32.5 ± 8.3‰ (November). Total particulate matter in suspension was 8.0 ± 2.3 and 29.3 ± 5.8 $\mathrm{mg \cdot l^{-1}}$ in September and November, respectively.

The oysters were placed individually in specially designed trays (36 × 16 × 8 cm, with a sill at one end to reduce turbulent flow) at flow rates of 450 ± 15 $\mathrm{ml \cdot min^{-1}}$ of water pumped directly from the river. After 1 h all biodeposits were removed from the trays and the oysters left undisturbed for a further 30 or 60 min. Feces and pseudofeces were then collected quantitatively, together with samples of suspended particulate matter, and filtered onto ashed and weighed GF/C filters. The filters were dried overnight at 80°C, weighed, ashed at 450°C for 4 h, and weighed again. The results were used to calculate rates of filtration and ingestion by the "biodeposition" method as described by Iglesias *et al.* (1998) and Bayne *et al.* (1999).

Statistical analysis

The results of the laboratory experiment were analyzed in three stages, using SYSTAT 6.0 (Wilkinson, 1996).

1. For each ration condition the physiological measurements, standardized to an animal size of 1 g dry flesh weight, were analyzed as a two-way ANOVA with "selection" (*i.e.*, selected or not-selected) and "size"

(large or small) as the main effects. In all cases the "selection × size" interaction was not significant.

2. Given the "repeated measures" nature of the experimental design, a different approach was taken to analyze the data across rations. Three groups of four individuals were first selected at random from each category (selection and size). These were then allocated, again at random, to one of the three ration levels. A three-way ANOVA was then done, with "selection," "size," and "ration" as the main effects. Where both "selection" and "ration" showed significant effect, a regression analysis was performed, with ration as the independent variable, to compare oysters from the different categories.
3. Finally, data for each individual oyster over the three ration levels were analyzed by linear regression, and comparisons between categories were made on the basis of the average "within category" values for the slope and intercept in the fitted equations. These regressions were for three data points only, per individual; only those for which the level of significance in the analysis was $P < 0.10$ were used for comparisons.

The results of the measurements in the field were analyzed by two-sample *t* test with pooled variance.

Results

Laboratory experiment

Ration levels. The cell concentrations in the feeding trays (Table II) were converted to equivalent dry mass using the constant 0.013 mg per 10^6 cells, and to nitrogen content using 5.6% N by weight. "Peak rations" are the levels recorded between 1100 and either 1500 (low and middle ration) or 1600 (high ration), and are the concentrations applied during the physiological measurements (except excretion rates, which were measured in filtered seawater). Peak rations were as follows: low ration, 0.074 ± 0.018; middle ration, 0.593 ± 0.024; high ration, 1.071 ± 0.068 $\mathrm{mg \cdot l^{-1}}$.

Clearance and ingestion rates. These were measured for the middle and high ration levels only (Table III). Differences due to size alone, following standardization to 1 g dry flesh weight, were significant only for ingestion rates at the middle ration. This result indicates that the effects of age on feeding rates were not greatly significant overall. The effects of selection were greater, particularly at high ration, where the selected, large oysters had significantly faster rates of clearance and ingestion than the not-selected, large and not-selected, small oysters.

When the original ingestion rates (*i.e.*, before standardizing them to 1 g dry flesh weight) were converted to percentages of body weight (as dry mass in milligrams), significant differences among categories were evident (Fig. 1; high ration). Selected oysters at both middle and high ration levels had faster relative ingestion rates than the not-selected oysters, with no significant differences between large and small oysters. For example, at the middle ration, SL oysters ingested 1.14 ± 0.47 $\%\mathrm{bw} \cdot \mathrm{d}^{-1}$, compared with 0.80 ± 0.22 $\%\mathrm{bw} \cdot \mathrm{d}^{-1}$ for NSL individuals; the values for SS and NSS oysters were 0.88 ± 0.44 and 0.68 ± 0.33 $\%\mathrm{bw} \cdot \mathrm{d}^{-1}$, respectively (see Fig. 1 for the high ration data).

Absorption efficiency. There were no significant differences due either to selection or to size. Values were all between 0.66 and 0.78 (mean 0.71 ± 0.06), with slightly lower values at high than at middle ration ($P < 0.05$).

Rates of oxygen consumption. Differences among categories (Table IVA) were significant ($P < 0.05$) only for size effects at the middle ration, where the $\mathrm{VO_2}$ was higher for the NSL oysters than for the NSS oysters.

Differences between selected, large, and not-selected, large, and between selected, small, and not-selected, small, oysters were not significant at any of the ration levels.

The effects of ration on rates of oxygen consumption, however, were highly significant for all categories, with

Table III

Clearance rates (CR: $l \cdot h^{-1}$) and ingestion rates (IR: $mg \cdot h^{-1}$) for oysters in each of four experimental categories, at two rations

	CR		IR	
Category	Middle ration	High ration	Middle ration	High ration
Selected, Large	2.53 ± 0.28	3.10 ± 0.37	10.36 ± 1.13	23.59 ± 2.74
Not selected, Large	2.12 ± 0.18	2.05 ± 0.29	8.59 ± 0.73	16.42 ± 2.14
Selected, Small	2.07 ± 0.25	3.00 ± 0.34	8.45 ± 1.04	23.54 ± 2.32
Not selected, Small	1.65 ± 0.22	2.01 ± 0.29	6.73 ± 0.88	15.09 ± 2.16
P for selection	<0.01	<0.01	ns	<0.005
P for size	ns	ns	<0.05	ns

Values are means ± SE, for weight-standardized data; $n = 12$ per category. The results of an analysis of variance are shown as the relevant probability, *P*, comparing selected with not-selected, and large with small oysters; ns signifies $P > 0.05$.

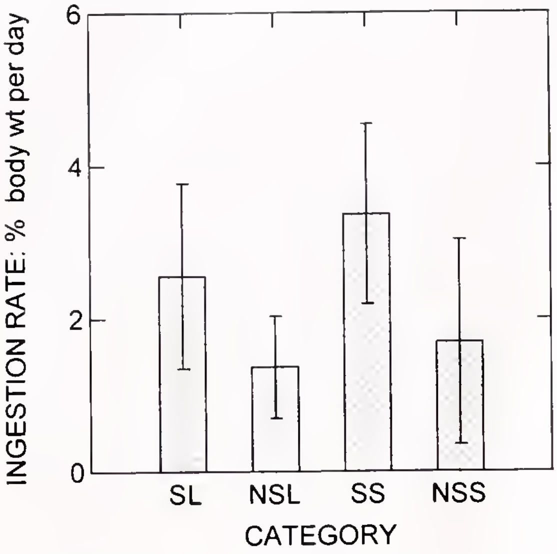

Figure 1. Rates of ingestion (not standardized for differences in body weight), as percent of dry body weight per day, by oysters in the four experimental categories at high ration; means ± SD. The categories are SL, Selected, large; NSL, Not-selected, large; SS, Selected, small; NSS, Not-selected, small.

respiration rate increasing as ingested ration increased. Oxygen consumption rates were converted to energy equivalents as 20.1 $J \cdot ml\ O_2^{-1}$ (Gnaiger, 1983), and ingestion rates converted as 26.5 $J \cdot mg^{-1}$ (Widdows and Hawkins, 1989). The energy ingested per unit of energy respired was then calculated.

At the middle ration, differences in this efficiency measure between categories were not significant; the overall mean value was 0.83 ± 0.38 joule ingested per joule respired, which indicates a ration level below the maintenance requirement. At the high ration, average energy ingested per unit respiration was higher (1.53 ± 0.55 $J \cdot J^{-1}$), with significant differences due to selection ($P < 0.01$). Selected oysters (large and small: 1.86 ± 0.78 $J \cdot J^{-1}$) were more efficient in this respect than the not-selected oysters (1.20 ± 0.55 $J \cdot J^{-1}$).

This conclusion was confirmed by the analysis of data for individuals. For each oyster, a regression analysis was made of respiratory energy loss, R ($J \cdot d^{-1}$), as a function of ingested ration, IR ($J \cdot d^{-1}$). Figure 2 shows the means and standard deviations of the fitted slopes, grouped by category. Categories SL and NSL ($P < 0.02$), and SS and NSS ($P < 0.001$) were significantly different. Differences between size categories (SL *vs.* SS and NSL *vs.* NSS), however, were not significant. On average, selected oysters respired 0.24 J for every joule ingested, across ration levels, compared with 0.45 J by the not-selected oysters.

Excretion rates. At all ration levels, selected oysters excreted more ammonia than the not-selected oysters (Table

Table IV

Metabolic measurements for oysters in four experimental categories at low, middle, and high ration levels

	Ration		
Category	Low ration	Middle ration	High ration
		A. Oxygen consumption rate (VO_2): $ml\ O_2 \cdot h^{-1}$*	
Selected, Large	0.408 ± 0.080	0.591 ± 0.138	0.738 ± 0.218
Not selected, Large	0.391 ± 0.105	0.662 ± 0.148	0.701 ± 0.180
Selected, Small	0.363 ± 0.074	0.538 ± 0.126	0.614 ± 0.150
Not selected, small	0.333 ± 0.061	0.514 ± 0.096	0.631 ± 0.110
P for selection	ns	ns	ns
P for size	ns	<0.05	ns
		B. Excretion rate ($VNH_4 \cdot N$): $\mu g\ NH_4 \cdot h^{-1}$*	
Selected, Large	25.0 ± 4.6	28.7 ± 4.1	27.4 ± 3.4
Not selected, Large	18.5 ± 2.8	19.9 ± 2.7	17.1 ± 2.5
Selected, Small	22.9 ± 4.3	25.4 ± 3.5	31.9 ± 4.6
Not selected, small	8.9 ± 1.2	18.1 ± 2.5	25.2 ± 4.5
P for selection	<0.05	<0.05	<0.05
P for size	ns	ns	ns
		C. Scope for growth (SFG): $J \cdot g^{-1} \cdot d^{-1}$	
Selected, Large	−212 ± 11	−76 ± 23	87 ± 29
Not selected, Large	−199 ± 15	−154 ± 17	−33 ± 31
Selected, Small	−175 ± 10	−122 ± 28	154 ± 47
Not selected, small	−160 ± 8	−106 ± 25	−33 ± 26
P for selection	ns	ns	<0.001
P for size	ns	ns	ns

Values are means ± SE; $n = 12$ per category. The results of an analysis of variance are shown as the relevant probability, P, comparing selected with not-selected, and large with small oysters; ns signifies $P > 0.05$.

* Values represent weight-standardized data.

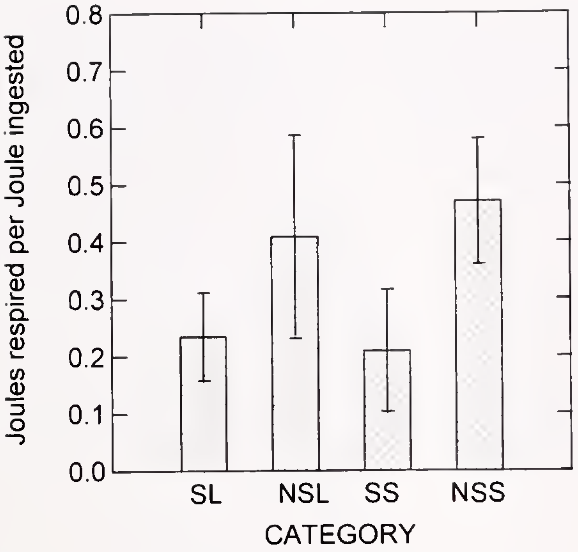

Figure 2. Energy respired ($J \cdot d^{-1}$) per unit of ingested energy ($J \cdot d^{-1}$) by oysters in the four experimental categories; means ± SD. The four categories are SL, Selected, large; NSL, Not-selected, large; SS, Selected, small; NSS, Not-selected, small.

IVB). Size (age) effects were not significant. Only for the small oysters was there a suggestion of excretion rates increasing with increased rates of ingestion.

At the middle ration, excretion rates were fast relative to ingested nitrogen (1.50 ± 1.13 mg excreted $\cdot$ mg^{-1} ingested, across all categories), indicating that this ration was well below the maintenance requirement for nitrogen, as it was also for energy (see above). At high ration, on average, 56% of ingested nitrogen was lost in excretion.

Oxygen:nitrogen ratio. Analysis of variance indicated no significant effects of either growth category or ration on the O:N ratio. Mean ratios for selected and not-selected individuals were 59.8 ± 7.0 and 66.6 ± 7.3, respectively.

Scope for growth (SFG) and maintenance metabolic rate. SFG was calculated as the difference between metabolizable energy intake (ingested ration × absorption efficiency) and the sum of respiratory and excretory energy losses. At low ration, SFG is assumed equal to the summed energy losses (*i.e.*, there was no significant energy intake). There were no significant differences between either selection or size categories at this ration. Similarly, at the middle ration (Table IVC), where the SFG was negative in all cases (*i.e.*, metabolizable energy intake was below the maintenance requirement), there was no significant effect of selection or size overall.

At high ration, however, the SFG was high and positive for selected oysters (both large and small) and negative for not-selected oysters, a highly significant difference (Table IVC; $P < 0.001$). Differences due to size (age) in these weight-standardized data were not statistically significant.

The maintenance metabolic rate (R_{maint}; joules per day) is the rate expressed when growth is neither positive nor negative. This was estimated by plotting R as a function of the SFG (Fig. 3); the intercept at zero growth indicates the metabolic rate at maintenance. Linear regression analysis was applied to all individuals, and the slopes and intercepts were compared by analysis of variance (Table V). Data from eight individuals (2, 3, 2, and 1 in the SL, NSL, SS, and NSS categories, respectively) were rejected as not meeting the chosen level of significance ($P < 0.10$).

There was no significant effect of selection on the estimated maintenance metabolic rate (mean = 308 ± 19 $J \cdot d^{-1}$). Size, however, did have a significant effect; maintenance rate was 337 ± 19 $J \cdot d^{-1}$ for large oysters and 278 ± 19 $J \cdot d^{-1}$ for small oysters.

Regression analysis demonstrated a significant linear relation, over all individual oysters, between intercepts and slopes from the individual regressions of R *vs.* SFG. Therefore, to confirm the absence of any significant differences in estimated R_{maint} due to selection, a separate statistical test was performed. Individual oysters were ranked for R_{maint}, and the two selection categories were compared by the Mann-Whitney U test. The result was not statistically significant, $0.10 > P > 0.05$, over 34 cases.

Growth, the costs of growth, and growth efficiency. Rates of growth, standardized to 1 g dry flesh weight, were derived for the 14 days spent at high ration, from measures of whole weight (shell plus flesh). Growth in selected oysters was faster than in the not-selected oysters (Table V).

The data for growth in whole weight were converted to equivalents in growth of dry tissue weight using total/dry

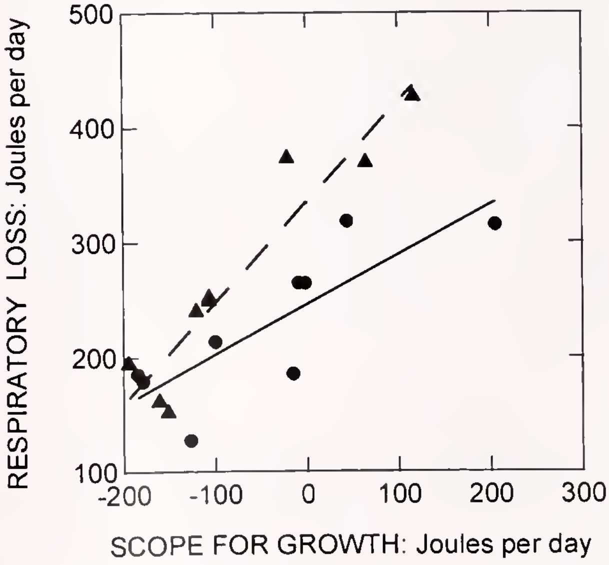

Figure 3. Respiratory energy loss ($J \cdot d^{-1}$) at different levels of scope for growth ($J \cdot d^{-1}$) in three oysters from each of two categories: selected, large (circles) and not-selected, large (triangles). Fitted regression lines are shown. The intercepts at zero scope for growth represent energy losses at maintenance (R_{maint}).

Table V

Rates of growth and growth efficiency at high ration, the estimated costs of growth and maintenance metabolic rate (R_{maint}), *for oysters in each of four experimental categories*

Category	Growth at high ration: mg total weight · d^{-1}	Growth efficiency	Cost of growth: J · J^{-1}	Maintenance metabolic rate: J · d^{-1}
Selected, Large	71.4 ± 4.6	0.26 ± 0.03	0.48 ± 0.07	313.1 ± 23.2
Not selected, Large	58.8 ± 6.2	0.16 ± 0.02	0.75 ± 0.14	361.6 ± 25.8
Selected, Small	63.9 ± 5.0	0.29 ± 0.03	0.35 ± 0.07	248.4 ± 16.4
Not selected, Small	52.0 ± 3.7	0.25 ± 0.03	0.85 ± 0.15	308.9 ± 32.2
P for selection	<0.01	<0.05	<0.05	ns
P for size	ns	<0.05	ns	<0.05

Values are means ± SE for n = 12 per category (growth and growth efficiency) and n = 10, 9, 10, and 11 for categories SL, NSL, SS, and NSS, respectively (costs of growth and R_{maint}). Growth values are for shell + flesh. Growth efficiency is for tissue growth as a proportion of metabolizable energy intake. The costs of growth and maintenance metabolic rate are estimated as described in the text. The results of an analysis of variance are shown as the relevant probability, *P*, comparing selected with not-selected, and large with small oysters; ns signifies $P > 0.05$.

tissue conversion factors for each individual. When values for metabolic rate associated with growth (R_{grow}, in units of joules per day), calculated as $R - R_{maint}$, are plotted against these estimates of tissue growth in energy units, the slope of the regression provides an estimate of the cost of growth, *i.e.*, R_{grow} per unit tissue growth (joules per joule). This analysis yields (see Table V) 0.43 ± 0.19 J · J^{-1} for the selected oysters (categories 1 and 3 together) and 0.81 ± 0.26 J · J^{-1} for the not-selected oysters (categories 2 and 4). These estimates are significantly different ($P < 0.01$).

Growth efficiency was calculated as metabolizable energy intake/tissue growth, both in units of joules per day, for high ration (Table V). The effects of both selection ($P < 0.05$) and size ($P < 0.05$) were significant. Over all categories of selection and size, growth efficiency was low, 0.24 ± 0.04.

Field measurements

Selected oysters (n = 17) had significantly faster rates of both filtration and ingestion than not-selected oysters (n = 21) on both occasions in the field (September and November; Table VI). Rates were faster in November, when concentrations of suspended particulate material were higher (TPM, 29.3 ± 5.8 mg · l^{-1} compared to 8.0 ± 2.3 in September; particulate organic matter, POM, 4.0 ± 1.5 mg · l^{-1} compared to 1.6 ± 0.4 in September). The ratios of ingestion rates for selected:not-selected oysters were 2.70 for September and 2.06 for November.

Discussion

The rock oysters (*Saccostrea commercialis*) used in this experiment were taken from the third generation of a mass selection program (the "selected" categories) and from a control ("not-selected") population from the same location in the Port Stephens estuary, Australia. At a ration level that peaked daily at 1.1 mg total particulate matter per liter (the "high ration" level), the selected oysters grew, on average, 22% faster than the not-selected oysters. This accords with Newkirk and Haley (1982) for selection for growth in *Ostrea edulis* (23% gain over controls), Paynter and Dimichele (1990) for *Crassostrea virginica* (24%-28% gain), and Toro *et al.* (1994) for *Ostrea chilensis* (13%-33% gain). It also accords with assessment of the Port Stephens selection study itself, where an 18% improvement in growth rate was recorded after two generations (Nell *et al.*, 1998).

The molar ratio of oxygen consumed to nitrogen excreted was calculated to evaluate whether the two groups of selected and not-selected (=control) oysters were catabolizing

Table VI

Filtration and ingestion rates of oysters measured on two occasions in the field at Karuah, New South Wales

Category	Filtration: mg · h^{-1}		Ingestion: mg · h^{-1}	
	September	November	September	November
Selected	20.2 ± 1.6	70.3 ± 17.7	2.7 ± 0.3	16.1 ± 3.0
Not selected	13.3 ± 1.4	22.3 ± 5.4	1.0 ± 0.2	7.8 ± 1.4
P comparing categories.	<0.005	<0.05	<0.001	<0.01

Values are means ± SE for n = 16 (September) and n = 22 (November). *P* values are the result of t tests comparing categories.

different energy substrates at the time of the experiment. Such differences might indicate different physiological states in the two growth categories, which would render more detailed metabolic comparisons complex. There was, however, no significant difference in the O:N ratios ($P > 0.05$), in spite of differences in rates of excretion, suggesting that selection for growth did not shift the normal seasonal pattern of metabolism significantly in these oysters.

Until we know more about nitrogen metabolism in this species, we cannot fully interpret the observed differences in excretion rates. However, the selected oysters both fed more quickly and excreted nitrogen at a higher rate than the control individuals. This is not unexpected, but more information on the relationship between ingested and excreted nitrogen is needed before these observations can be set in context with selection for growth.

We proposed three models to explain the observed differences in rates of growth: faster growing individuals may feed more rapidly; they may reduce their maintenance energy requirement; or they may grow more efficiently than slower growing individuals. The results of the laboratory experiment supported the first and third, but not the second, of these models. Further, by experimenting with different sizes (and therefore ages) of oysters, but correcting the measurements according to observed size/rate relationships, we demonstrated that age was not a significant factor in explaining most of the observed differences between individuals. The exceptions were estimated maintenance metabolic rate, which increased with age, and growth efficiency, which declined with age.

Oysters from the selected line had faster clearance rates (volume of water cleared of food cells per hour) than control, not-selected oysters. This was reflected in a 44% increase in ingestion rates at the greatest ration. Because of a similarity across experimental categories in the efficiency with which these cells were absorbed in the gut, an identical difference in metabolizable energy intake was observed. In experiments with hybrid and inbred lines of Pacific oysters (*Crassostrea gigas*), Bayne *et al.* (1999) recorded faster clearance rates by hybrids in three out of four comparisons, consistent with observed differences in growth rate. Genetically based differences in feeding behavior are an important component of differences in rates of growth among individual oysters.

A similar difference between selected and not-selected oysters was observed in the field experiment, in which a different technique for measuring feeding behavior was used (the biodeposition method in the field, in contrast to direct cell counts in the laboratory), and the concentration of food was significantly greater (8.00 ± 2.28 and 29.3 ± 5.8 in the field, compared with a maximum of 1.07 ± 0.07 mg $\cdot$ l^{-1} in the laboratory). Under these conditions the differences between the two experimental categories of oyster were actually more marked than in the laboratory. This finding lends general support to the "energy acquisition" model and demonstrates that the inferred genetic component of variability in feeding behavior supports faster growth, both under natural circumstances in the field and in the laboratory.

Feeding rates were not only faster in selected oysters, they were also more metabolically efficient. Feeding is not itself energetically expensive in bivalve molluscs, although the total costs of feeding and digestion plus absorption may account for up to 20% of total metabolic rate (Hawkins and Bayne, 1992). Feeding rates may increase significantly without seriously compromising net energy yield. The rock oysters selected for growth achieved a greater gain of energy per unit of energy lost in metabolism than did control oysters. The actual mechanisms of feeding that are responsible for these differences remain unknown. We presume, however, that increasing rate of ingestion as a mechanism for increasing gross energy yield will be limited eventually by decreased gut passage time, which ultimately limits maximum absorption efficiency (Bayne *et al.,* 1989).

Our second model, which we call the energy allocation model, was not supported by the results of the experiment. The estimated rate of metabolism at maintenance varied between 250 and 360 joules per day, standardized for oysters of 1 g dry flesh weight, and it increased with age but not with selection. An average of 308 $J \cdot d^{-1}$ is equivalent to a maintenance requirement for metabolizable energy intake of ~1.4% of body weight per day. This is similar to published values for other bivalves of similar size (reviewed by Bayne and Newell, 1983) and accords with our conclusion that the middle ration level in the laboratory was insufficient to meet the requirements for maintenance of these oysters. Increased maintenance costs with age have commonly been reported for other bivalves (review by Griffiths and Griffiths, 1987).

Studies with blue mussels, *Mytilus edulis,* by Hawkins *et al.* (1986) and Bayne and Hawkins (1997), and with rainbow trout, *Oncorhynchus mykiss,* by McCarthy *et al.* (1994), have demonstrated how reduced rates of protein turnover contribute to reduced metabolic costs and higher rates of growth. These processes appear to be genotype dependent, and they support the concept of differential energy allocation (Wieser, 1989) as a means of increasing growth. In our experiments, differences in maintenance metabolic rate between fast- and slow-growing oysters were not statistically significant. This result merits further research, however. For example, the data (Table V) show a tendency towards higher maintenance metabolic rates in the not-selected oysters, particularly among the smaller size categories, but with high variance. In similar experiments with Pacific oysters, *Crassostrea gigas* (Bayne, in press), we have observed significant differences in R_{maint} among individuals, which correlated with differences in growth rate. The energy allocation model remains a possibility in

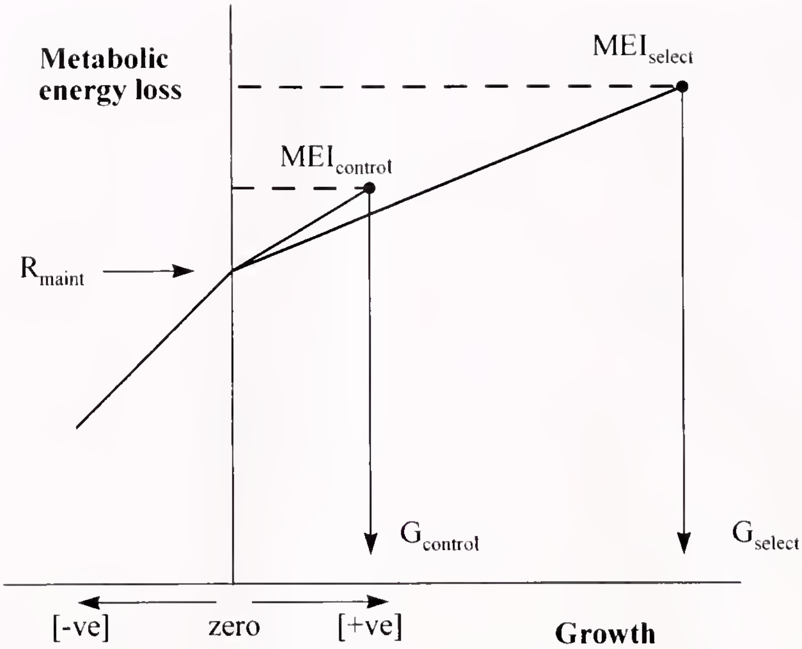

Figure 4. A qualitative illustration of the main findings of this study. Metabolic energy loss is plotted as a function of growth for oysters selected for fast growth, and for control oysters. Below the maintenance requirement, where growth is negative, there is no difference in metabolic expenditure due to selection; the maintenance metabolic demand (R_{maint}) is the same for both experimental categories. However, selected oysters achieve a higher metabolizable energy intake (MEI) than the controls and express a lower cost of growth. The net result is an increased growth rate and a higher growth efficiency (G_{select} *vs.* $G_{control}$). Differences due to selection have been exaggerated for illustration purposes.

the general case, therefore, although not supported directly by these data on *Saccostrea.*

Our third model concerned growth and metabolic efficiency. This was evaluated by estimating both the costs of growth and net growth efficiency in selected and not-selected oysters. The results supported the hypothesis that selected oysters would show a lower cost of growth (0.43 $J \cdot J^{-1}$) than control oysters (0.81 $J \cdot J^{-1}$). Both values are high compared with published values (Wieser, 1994; average for "ectothermic metazoans" of 0.30 $J \cdot J^{-1}$), possibly reflecting a relatively poor-quality diet and slow overall rates of growth. Nevertheless, the differences due to selection, and the lack of significant differences due to age, are evident. Clearly, selection for growth in this species, as in others (Bayne and Hawkins, 1997), involves selection for reduced costs of growth.

Selected and not-selected oysters also differed in growth efficiency measured as the proportion of metabolizable energy intake utilized in tissue growth. This efficiency was low in all cases—for example, 0.28 ± 0.09 and 0.21 ± 0.08 for selected and not-selected oysters, respectively. The results do, however, support the hypothesis that selected oysters utilize a higher proportion of absorbed ration for growth, and do so at a reduced cost of growth relative to the controls.

In summary (Fig. 4), our experiments indicate that mass selection for growth in the rock oyster resulted in individuals that had a greater intake of metabolizable energy by virtue of faster (and more metabolically efficient) feeding, and were able to use this intake more efficiently for growth. Selected and control oysters did not differ in their energetic costs at maintenance. The field experiment confirmed that selected oysters fed more rapidly than the controls. The challenge now is to analyze in more detail the feeding behavior and the metabolic processes that contribute to the costs of growth and to link these processes more directly to observed individual differences in genotype.

Acknowledgments

We are grateful to Shannon Long, who helped with many aspects of this work, and to Shannon and Alison Phillips for their work in the field. Graham Housefield provided invaluable support throughout the project. The research was supported by a grant from the Australian Research Council to the Special Research Centre on Ecological Impacts of Coastal Cities. Susanne Svensson was supported by the Foundation for Strategic Environmental Research, Sweden (Sucozoma Project, DNR 95005). The manuscript benefited significantly from the comments of Gee Chapman and Tony Underwood.

Literature Cited

Bayne, B. L., and A. J. S. Hawkins. 1997. Protein metabolism, the costs of growth, and genomic heterozygosity: experiments with the mussel *Mytilus galloprovincialis* Lmk. *Physiol. Zool.* **70:** 391-402.

Bayne, B. L., and R. C. Newell. 1983. Physiological energetics of marine molluscs. Pp. 407-515 in *The Mollusca, Vol. 4, Physiology, Part 1.* A. S. M. Saleuddin, and K. M. Wilbur, Eds. Academic Press, New York.

Bayne, B. L., A. J. S. Hawkins, E. Navarro, and I. P. Iglesias. 1989. Effects of seston concentration on feeding, digestion and growth in the mussel *Mytilus edulis. Mar. Ecol. Prog. Ser.* **55:** 47-54.

Bayne, B. L., D. Hedgecock, D. McGoldrick, and R. Rees. 1999. Feeding behaviour and metabolic efficiency contribute to growth heterosis in Pacific oysters [*Crassostrea gigas* (Thunberg)]. *J. Exp. Mar. Biol. Ecol.* **233:** 115-130.

Britten, H. B. 1996. Meta-analyses of the association between multilocus heterozygosity and fitness. *Evolution* **50:** 2158-2164.

Conover, R. J. 1966. Assimilation of organic matter by zooplankton. *Limnol. Oceanogr.* **11:** 338-345.

Coughlan, J. 1969. The estimation of filtering rate from the clearance of suspensions. *Mar. Biol.* **2:** 356-368.

De Moed, G. H., G. De Jong, and W. S. Scharloo. 1998. The energetics of growth in *Drosophila melanogaster:* effect of temperature and food conditions. *Neth. J. Zool.* **48:** 168-188.

Gnaiger, E. 1983. Calculation of energetic and biochemical equivalents of respiratory oxygen consumption. Pp. 337-345 in *Polarographic Oxygen Sensors.* E. Gnaiger and H. Forstner, eds. Springer-Verlag, Berlin.

Griffiths, C. L., and R. J. Griffiths. 1987. Bivalvia. Pp 1-88 in *Animal Energetics, Vol. 2: Bivalvia Through Reptilia.* T. J. Pandian and F. J. Vernberg, eds. Academic Press, New York.

Hawkins, A. J. S., and B. L. Bayne. 1992. Physiological processes, and the regulation of production. Pp. 171-222 in *The Mussel* Mytilus: *Ecology, Physiology, Genetics and Culture.* E. Gosling, ed. Elsevier, Amsterdam.

Hawkins, A. J. S., B. L. Bayne, and A. J. Day. 1986. Protein turnover, physiological energetics and heterozygosity in the blue mussel *Mytilus edulis:* the basis of variable age-specific growth. *Proc. R. Soc. Lond.* **229B:** 161-176.

Hilbish, T. J. 1986. Growth trajectories of shell and soft tissue in bivalves: seasonal variation in *Mytilus edulis* L. *J. Exp. Mar. Biol. Ecol.* **96:** 103-113.

Iglesias, J. I. P., M. B. Urrutia, E. Navarro, and I. Ibarrola. 1998. Measuring feeding and absorption in suspension-feeding bivalves: an appraisal of the biodeposition method. *J. Exp. Mar. Biol. Ecol.* **219:** 71-86.

Koehn, R. K. 1991. The cost of enzyme synthesis in the genetics of energy balance and physiological performance. *Biol. J. Linn. Soc.* **44:** 231-247.

Lewis, D. E., and R. M. Cerrato. 1997. Growth uncoupling and the relationship between shell growth and metabolism in the soft shell clam *Mya arenaria. Mar. Ecol. Prog. Ser.* **158:** 177-189.

McCarthy, I. D., D. F. Houlihan, and C. G. Carter. 1994. Individual variation in protein turnover and growth efficiency in rainbow trout, *Oncorhynchus mykiss* (Walbaum). *Proc. R. Soc. Lond. B.* **257:** 141-147.

Mitton, J. B., and M. C. Grant. 1984. Associations among protein heterozygosity, growth rate and developmental homeostasis. *Annu. Rev. Ecol. Syst.* **15:** 479-499.

Nell, J. A., A. K. Sheridan, and I. R. Smith. 1996. Progress in a Sydney rock oyster, *Saccostrea commercialis* (Iredale and Roughley), breeding program. *Aquaculture* **144:** 295-302.

Nell, J. A., I. R. Smith, and A. K. Sheridan. 1998. Third generation evaluation of Sydney rock oyster *Saccostrea commercialis* (Iredale and Roughley) breeding lines. *Aquaculture* **170:** 195-203.

Newkirk, G. F. 1980. Review of the genetics and the potential for selective breeding of commercially important bivalves. *Aquaculture* **19:** 209-228.

Newkirk, G. F., and L. E. Haley. 1982. Progress in selection for growth rate in the European oyster *Ostrea edulis. Mar. Ecol. Prog. Ser.* **10:** 77-79.

Paynter, K. T., and L. Dimichele. 1990. Growth of tray-cultured oysters (*Crassostrea virginica* Gmelin) in Chesapeake Bay. *Aquaculture* **87:** 280-297.

Present, T. M. C., and D. O. Conover. 1992. Physiological basis of latitudinal growth differences in *Menidia menidia:* variation in consumption or efficiency? *Funct. Ecol.* **6:** 23-31.

Rist, L., R. D. Semlitsch, H. Hotz, and H.-U. Reyer. 1997. Feeding behaviour, food consumption, and growth efficiency of hemiclonal and parental tadpoles of the *Rana esculenta* complex. *Funct. Ecol.* **11:** 735-742.

Sheridan, A. K. 1997. Genetic improvement of oyster production—a critique. *Aquaculture* **153:** 165-179.

Solorzano, L. 1969. Determination of ammonia in natural waters by the phenolhypochlorite method. *Limnol. Oceanogr.* **14:** 799-801.

Toro, J. E., P. Aguila, and A. M. Vergara. 1994. Spatial variation in response to selection for live weight and shell length from data on individually tagged Chilean native oysters (*Ostrea chilensis* Philipi, 1845). *Aquaculture* **146:** 27-36.

Widdows, J., and A. J. S. Hawkins. 1989. Partitioning of rate of heat dissipation by *Mytilus edulis* into maintenance, feeding and growth components. *Physiol. Zool.* **62:** 764-784.

Wieser, W. 1989. Energy allocation by addition and by compensation: an old principle revisited. Pp. 98-105 in *Energy Transformation in Cells and Animals.* W. Wieser and E. Gnaiger, eds. Thieme Verlag, Stuttgart.

Wieser, W. 1994. Cost of growth in cells and organisms: general rules and comparative aspects. *Biol. Rev.* **68:** 1-33.

Wilkinson, L. 1996. *SYSTAT 6.0 for Windows.* SYSTAT, Evanston, IL.

Winberg, G. C. 1956. Rate of metabolism and food requirements in fishes (In Russian). *Translation Series Fisheries Research Board of Canada* **194.** 253 pp.

Zouros, E., M. Romero-Dorey, and A. L. Mallet. 1988. Heterozygosity and growth in marine bivalves: further data and possible explanations. *Evolution* **42:** 1332-1341.

Reference: *Biol. Bull.* **197:** 388–394. (December 1999)

Hydrostatic Pressure Alters the Time Course of GTP[S] Binding to G Proteins in Brain Membranes from Two Congeneric Marine Fishes

JOSEPH F. SIEBENALLER[1,*] AND THOMAS F. MURRAY[2]

[1] *Department of Biological Sciences, Louisiana State University, Baton Rouge, Louisiana 70803; and*
[2] *Department of Physiology and Pharmacology, University of Georgia College of Veterinary Medicine, Athens, Georgia 30602*

Abstract. The effects of hydrostatic pressure on the receptor-stimulated exchange of guanosine triphosphate (GTP) for guanosine diphosphate (GDP) on the α subunit of G proteins were studied in two congeneric marine teleost fishes that differ in their depths of distribution. The poorly hydrolyzable GTP analog [^{35}S]guanosine 5′-[γ-thio]triphosphate ([^{35}S]GTP[S]) was used to monitor the modulation of signal transduction by the A_1 adenosine receptor agonist N^6-R-(phenylisopropyl)adenosine (R-PIA) in brain membranes of the scorpaenids *Sebastolobus alascanus* and *S. altivelis.* The maximal binding (B_{max}) and dissociation constant (K_d) values, determined from equilibrium binding isotherms at atmospheric pressure (5°C), were similar in the two species. The B_{max} values for these species are much lower than literature values for mammalian brain tissue (25°C); however, the K_d values of the teleost and mammalian G proteins are similar. The EC_{50} values for the A_1 adenosine receptor agonist R-PIA were similar in the two species. Hydrostatic pressure of 204 atm altered the binding of [^{35}S]GTP[S]; basal [^{35}S]GTP[S] binding decreased 25%. The A_1 adenosine receptor agonist R-PIA and the muscarinic cholinergic receptor agonist carbamyl choline stimulated [^{35}S]GTP[S] binding at 1 and 204 atm. At atmospheric pressure the half-time ($t_{1/2}$) of [^{35}S]GTP[S] binding differed between the two species. The GTP[S] on rate (k_{on}) is larger in the shallower-living *S. alascanus.* Increased hydrostatic pressure altered the time course, decreasing the $t_{1/2}$ in both species. The pressures that elicit this change in the time course differ between the species. However, interpolating over the range of *in situ* pressures the species experience, the values are similar in the two species. The guanyl nucleotide binding properties of the G protein α subunits appear to be conserved at the environmental temperatures and pressures the species experience.

Introduction

The high hydrostatic pressures characteristic of the deep ocean significantly influence guanine-nucleotide-binding protein (G protein)-coupled signal transduction systems (Siebenaller and Murray, 1995). Because of the large number and ubiquity of G protein-coupled signaling complexes, the effects of pressure on such systems will have an important role in shaping the evolution of signal transduction systems in marine species and may play a part in determining the bathymetric distribution of species.

G proteins couple a diverse superfamily of cell surface receptor proteins, characterized by seven membrane-spanning regions, to a variety of effector elements, such as adenylyl cyclase, ion channels, and phospholipases (Spiegel *et al.,* 1994). The subunits of the heterotrimeric G proteins are designated α, β, and γ. The classes of G proteins, such as G_i and G_s, which inhibit and stimulate adenylyl cyclase, respectively, and G_o, a common G protein in brain tissue that may be coupled to Ca^{++} channels and phospholipase C, are defined by the α subunit type (Gilman, 1994).

Receptors with bound agonist interact with heterotrimeric G proteins, promoting the binding of GTP in exchange for GDP on the α subunit. The binding of GTP evokes a conformational change that results in the dissociation of the G protein into $\alpha \cdot$ GTP and a $\beta\gamma$ dimer (Coleman *et al.,* 1994; Wall *et al.,* 1995). The activated $\alpha \cdot$ GTP subunit and the $\beta\gamma$ dimer interact with the target enzyme or ion channel. Signaling is terminated by the hydrolysis of bound GTP by

---

Received 16 June 1998; accepted 8 September 1999.

* To whom correspondence should be addressed. E-mail: zojose@unix1.sncc.lsu.edu

the intrinsic GTPase activity of the α subunit and the subsequent reassociation of the α and $\beta\gamma$ subunits (Gilman, 1994; Mixon *et al.*, 1995).

Guanyl nucleotide binding is important in the pressure-sensitivity of signal transduction (Murray and Siebenaller, 1993; Siebenaller and Murray, 1994a, b). The present study was designed to test the hypothesis that alteration of guanyl nucleotide binding contributes to the perturbation of transmembrane signaling by hydrostatic pressure. To directly examine one of the initial steps of G protein activation, the binding of GTP, we used the GTP analog guanosine 5′-[γ-thio]triphosphate (GTP[S]). This analog is not hydrolyzed by the GTPase activity of the G protein α subunit (Wieland and Jakobs, 1994). The effects of pressure on the activation of G proteins were studied by measuring the binding of [^{35}S]GTP[S] to the G protein α subunit. The binding of this analog of GTP reflects the GDP-GTP exchange reaction, which is stimulated by receptor agonists.

We have used the A_1 adenosine-G_i-adenylyl cyclase signaling complex as a representative G protein-coupled receptor system to study the influence of environmental factors (Murray and Siebenaller, 1987; Siebenaller and Murray, 1988, 1990, 1995). This system was chosen because it is amenable to the use of frozen tissues, and because of the array of pharmacological tools available to probe the system (Siebenaller and Murray, 1994c). This receptor is found in brain tissue of vertebrates but has not been detected in central nervous tissue of the arthropods or molluscs tested (Siebenaller and Murray, 1986). Adenosine is a potent physiologic regulator with central nervous, cardiac, and peripheral effects (Bruns, 1990; Palmer and Stiles, 1995; Sundin and Nilsson, 1996). Agonist occupation of the A_1 adenosine receptor results in the negative modulation of adenylyl cyclase (Daly *et al.*, 1981).

We have focused on the A_1 adenosine-G_i-adenylyl cyclase signaling complex in brain tissue of two closely related scorpaenid fish species. These fishes have been employed as a model system to study adaptation to hydrostatic pressure. The congeners *Sebastolobus alascanus* and *S. altivelis*, co-occur geographically (Miller and Lea, 1976; Lauth *et al.*, 1997), are genetically close (Siebenaller, 1978), have similar life histories (Moser, 1974), and experience similar temperatures (Hubbs, 1926; Siebenaller, 1984); but they have different patterns of depth distribution (Hubbs, 1926; Siebenaller and Somero, 1978; Wakefield and Smith, 1990; Lauth *et al.*, 1997) and hence encounter different hydrostatic pressures. Pressure increases 1 atm (= 101,325 Pa = 1 bar) for every 10-m depth increase in the ocean (Saunders and Fofonoff, 1976). Demersal *S. alascanus* adults are commonly found between 100 and 850 m and have a maximum reported depth of 1524 m; *S. altivelis* adults have a maximum reported depth of 1755 m and are common between 305 and 1755 m (Orr *et al.*, 1998; Lauth *et al.*, 1997). Although the depth ranges of the adults of these species overlap, *S. altivelis* is always more common at greater depths (Hubbs, 1926; Siebenaller and Somero, 1978; Pearcy *et al.*, 1982; Wakefield and Smith, 1990; Lauth *et al.*, 1997). These species have been a sensitive model with which to discern fine-scale adaptations to pressure without the potentially confounding effects of phylogenetic distance or other environmental variables (Siebenaller, 1987; Siebenaller and Somero, 1989).

To test the hypothesis that increased hydrostatic pressure alters guanyl nucleotide binding and thus contributes to the perturbation of G protein-coupled signaling, we have studied the binding of [^{35}S]GTP[S] to the G protein α subunit in response to the A_1 adenosine receptor agonist N^6 (R-phenylisopropyl)adenosine (R-PIA). The binding of [^{35}S]GTP[S] is a direct measure of the GDP-GTP exchange reaction, which is stimulated by R-PIA.

Materials and Methods

Specimens

Demersal adult specimens of *Sebastolobus* were collected using a 40-ft semiballoon otter trawl on cruises of the R/V *Wecoma* off the coast of Oregon. *S. alascanus* was collected at depths of 380 to 415 m; *S. altivelis* was collected from 600 to 1030 m. The collecting sites were at 45° 21.6′ N, 124° 29.6′ W and 45° 30.9′ N, 124° 48.8′ W. Brain tissue was dissected and frozen in liquid N_2 at sea. Tissues were transported to the laboratory on dry ice and maintained at −80°C until used.

Preparation of brain membranes

Brains from several individuals were pooled, and the tissue was homogenized in 100 volumes (volume to weight) of 50 m*M* Tris-HCl, pH 7.4 at 5°C, using a Dounce tissue homogenizer (Pestle A). The sample was centrifuged for 10 min at 27000 × *g* (0–4°C). The pellet was resuspended in 100 volumes of buffer and centrifuged. The pellet was resuspended in 100 volumes of buffer and adenosine deaminase was added to 7.5 units (measured at 25°C) per milliliter. The sample was incubated at 18°C for 30 min, chilled on ice, and centrifuged for 10 min. The pellet was resuspended in 50 volumes of buffer and brought to 7.5 units of adenosine deaminase per milliliter and used in the assays. Adenosine deaminase is included in the incubations to remove endogenous adenosine (see Siebenaller and Murray, 1994c).

Protein determination

Protein was determined using the method of Lowry *et al.* (1951). Samples were solubilized in 0.5 *M* NaOH. Bovine serum albumin (Sigma Chemical Co., St. Louis, MO) was used as the standard.

Binding of [^{35}S]GTP[S] to membranes

The binding of the GTP analog [^{35}S]GTP[S] to membranes was assayed following the methods described by Lorenzen *et al.* (1993) and Wieland and Jakobs (1994). Binding at atmospheric pressure was determined in a volume of 100 μl. The assay mixture contained 50 m*M* Tris HCl, pH 7.4 at the assay temperature of 5°C, 1 m*M* EDTA, 5 m*M* magnesium acetate, 10 μ*M* GDP, 1 m*M* dithiothreitol, 100 m*M* NaCl, 5 mg bovine serum albumin per milliliter, 2.5 units (at 25°C) of adenosine deaminase per milliliter, and approximately 100,000 disintegrations per min (dpm) [^{35}S]GTP[S] (0.3 to 0.5 n*M*). Other additions are as indicated. Approximately 13 to 28 μg of membrane protein was used per tube. The assay was terminated by filtration under vacuum on a Brandel (Gaithersburg, MD) model M-24R cell harvester using Schleicher and Schuell Inc. (Keene, NH) number 32 glass fiber filters. The filters were then rinsed with four 4-ml washes of ice-cold 50 m*M* Tris HCl, pH 7.4 at 5°C, 5 m*M* $MgCl_2$ to remove unbound [^{35}S]GTP[S]. Filter disks were placed into counting vials to which 9 ml of Biocount scintillation fluid (Research Products International Corp., Mount Prospect, IL) was added. Filter-bound radioactivity was determined by scintillation spectrometry (Beckman Instruments, Fullerton, CA, model LS6000IC) following overnight extraction at room temperature. The amount of radioligand bound was less than 10% of the total added in all experiments. Specific binding was defined as total binding minus binding occurring in the presence of 10 μ*M* unlabeled GTP[S]. Nonspecific binding was approximately 1% of the total binding at 0.3 n*M* [^{35}S]GTP[S].

Assays at elevated pressure

The procedures used for assays at elevated pressure were as described by Siebenaller *et al.* (1991). Briefly, samples were sealed in polyethylene tubing and incubated in high-pressure vessels that were kept in a refrigerated water bath at 5°C. The pressure vessels are modeled after those of Zobell and Oppenheimer (1950); the pump and gauges used are as described by Hennessey and Siebenaller (1985). A volume of 200 μl was used for the pressure incubations. A 100-μl aliquot was taken, and the assay was terminated by filtration under vacuum onto a Schleicher and Schuell number 32 glass fiber filter supported on a Hoefer Scientific (San Francisco, CA) single filter holder. The sample was then treated as described above.

All assays were at 5°C to approximate the body temperatures of the two species (Siebenaller and Somero, 1978; Siebenaller and Murray, 1988). Tris was used as the buffer because of the low sensitivity of its pK_a to pressure (Kauzmann *et al.*, 1962). Experiments with both species were conducted in parallel each day. There were no differences in ligand binding between samples incubated in test tubes and samples sealed in tubing and incubated at atmospheric pressure.

Reagents

[^{35}S]guanosine 5′-[γ-thio]triphosphate ([^{35}S]GTP[S], 1332.0 Ci/mmol) was from DuPont NEN (Boston, MA). N^6(R-phenylisopropyl)adenosine (R-PIA) was from Research Biochemicals, Inc. (Natick, MA). Adenosine deaminase (Sigma, type VI) and all other chemicals were from Sigma Chemical Co. (St. Louis, MO). Water was processed with a four-bowl Milli-Q purification system to a resistivity of 10 to 18 MΩ-cm (Millipore, Bedford, MA).

Data analysis

Data were fit using nonlinear regression analyses. [^{35}S]GTP[S] equilibrium binding isotherms were analyzed using AccuFit Saturation-Two Site (Lundeen and Gordon, 1986; Beckman Instruments). Other experiments were analyzed using Prism (version 2.01, GraphPad Software, Inc., San Diego, CA). Comparisons were made using Student's *t* test or analysis of variance with a Tukey-Kramer multiple comparisons test (Sokal and Rohlf, 1995; BIOMstat, version 3.2, Applied Biostatistics, Inc., Setauket, NY, and GraphPad Instat, version 3.00). The *n* values reported represent determinations using different membrane preparations.

Pseudo-first-order association kinetics of the interaction of [^{35}S]GTP[S] and the G proteins were fit to a one-phase exponential association equation:

$$Y = Y_{max}(1 - e^{-kt})$$

where Y is ligand bound, Y_{max} is the maximal binding at the concentration of [^{35}S]GTP[S] used, t is time (min), and k is the observed rate constant. At $t_{1/2}$, when t equals 0.6932/k, $Y = 0.5\ Y_{max}$. The observed rate constant is a function of the on (k_{on}) and off (k_{off}) rates and the concentration of [^{35}S]GTP[S]:

$$k = k_{on}[[^{35}S]GTP[S]] + k_{off}$$

Equilibrium binding was analyzed using the equation:

$$Y = (B_{max} \cdot X)/(K_d + X)$$

where Y represents the specific binding, B_{max} is the maximal specific binding, X is the concentration of free ligand and K_d is the apparent dissociation constant. The K_d is determined by the off and on rates:

$$K_d = k_{off}/k_{on}$$

The fits of the data were also tested against a two-site model, but the two-site model did not statistically improve the fit of the data ($P > 0.05$), based on a partial F test (Hoyer *et al.*, 1984).

Results

High-affinity binding sites for [^{35}S]GTP[S] were characterized in equilibrium saturation experiments at 5°C and atmospheric pressure, using concentrations of [^{35}S]GTP[S] up to 13.5 nM. Incubations were carried out for 3 h. The binding capacities and binding affinities of brain membrane preparations of the two species were identical (B_{max}, $P = 0.27$; K_d, $P = 0.88$; Table I).

The IC (inhibitory concentration)$_{50}$ values for GDP were determined at atmospheric pressure using 0.3 nM [^{35}S]GTP[S]. The values were 20.66 ± 19.23 μM for *S. alascanus* and 27.60 ± 26.24 μM for *S. altivelis* (mean ± SE, three independent determinations for each species). The IC$_{50}$ values do not differ between the two species ($P > 0.05$).

The EC (effective concentration)$_{50}$ values for R-PIA stimulation of [^{35}S]GTP[S] binding at atmospheric pressure were determined using 0.3 nM [^{35}S]GTP[S] in the standard assay mixture. The values were 40.92 ± 17.45 nM for *S. alascanus* and 67.04 ± 47.70 nM for *S. altivelis* (mean ± SE, three independent determinations for each species). The values do not differ between the species ($P = 0.63$). [^{35}S]GTP[S] binding was maximally stimulated by 3 μM R-PIA. Increased concentrations of R-PIA (10 μM and 100 μM) did not increase the maximal binding of [^{35}S]GTP[S]. For assays of agonist-stimulated [^{35}S]GTP[S] binding, 10 μM R-PIA was used.

The effects of 204 atm pressure on the stimulation of [^{35}S]GTP[S] binding by the A_1 adenosine receptor agonist R-PIA and the muscarinic cholinergic receptor agonist carbamyl choline (carbachol) were examined in 3-h incubations (Fig. 1). Increased pressure inhibited basal [^{35}S]GTP[S] binding about 25% in both species. At 204 atm, both 10 μM RPIA and 100 μM carbachol increased [^{35}S]GTP[S] binding over the basal binding at 204 atm. For these agonists, the percent stimulation was similar in both species.

The time course of the association of [^{35}S]GTP[S] with G proteins was determined at atmospheric pressure (Fig. 2). The time course differed between the *Sebastolobus* species. At atmospheric pressure, brain membrane preparations from *S. altivelis* had $t_{1/2}$ values for binding of [^{35}S]GTP[S] that were significantly higher than for *S. alascanus*. The values determined from the pseudo-first-order association kinetics are given in Table II. The on rate of GTP[S] (k_{on}), calculated from k and the K_d value, is larger in brain membranes of *S. alascanus* than of *S. altivelis* ($2.606 \times 10^7\ M^{-1}\ \text{min}^{-1}$ and $1.630 \times 10^7\ M^{-1}\ \text{min}^{-1}$, respectively).

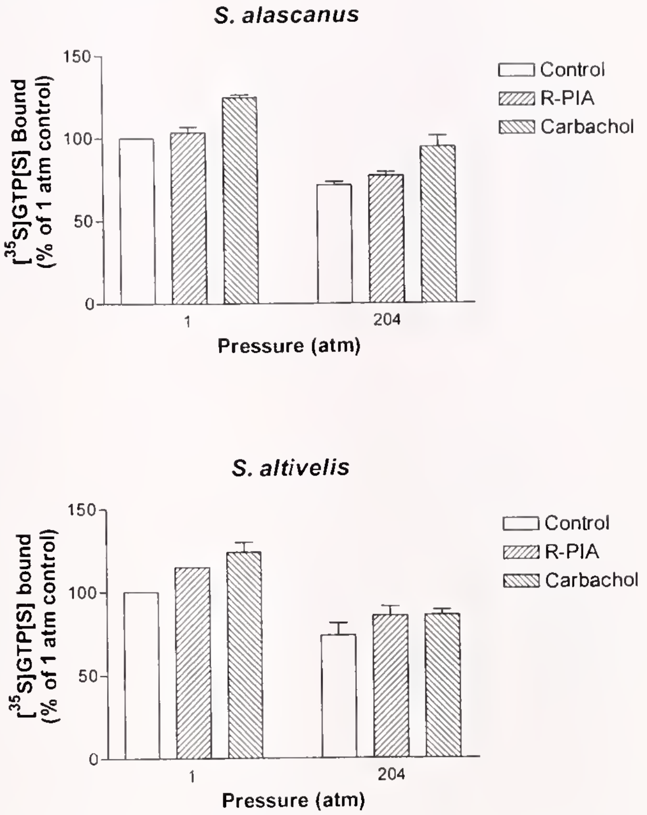

Figure 1. The effects of hydrostatic pressure on the binding of [^{35}S]GTP[S] to brain membrane preparations of *Sebastolobus alascanus* (upper) and *S. altivelis* (lower). [^{35}S]GTP[S] binding is normalized to the atmospheric pressure basal value (no added agonist). The agonists RPIA (10 μM) and carbamyl choline (100 μM) were used. Standard errors are shown. The values represent determinations on five membrane preparations for each species. Increased pressure decreased [^{35}S]GTP[S] binding ($P < 0.05$).

Table I

B_{max} and K_d determinations from [^{35}S]GTP[S] equilibrium binding isotherms at 5°C and atmospheric pressure in the absence of other added guanyl nucleotides

Species	B_{max} (pmol/mg)	K_d (nM)
S. alascanus	1.49 ± 0.25	0.41 ± 0.10
S. altivelis	1.15 ± 0.10	0.43 ± 0.07

Mean ± SE of three independent determinations for each species. The values were identical in the two species: B_{max}, $P = 0.27$; K_d, $P = 0.88$.

In both species the $t_{1/2}$ values were sensitive to increased hydrostatic pressure (Table II). Increased pressure decreased the $t_{1/2}$ values in *S. altivelis* from 58 min at atmospheric pressure to about 36 min. This value was the same at both 204 and 408 atm and was indistinguishable from values seen in *S. alascanus* brain membranes at 1 and 204 atm. In preparations of *S. alascanus* brain membrane, 204 atm did not alter the $t_{1/2}$ value; 408 atm significantly decreased the $t_{1/2}$ value to 13.50 min, less than half the atmospheric pressure value.

Discussion

The observation that signal transduction is sensitive to hydrostatic pressure is of general significance for organisms

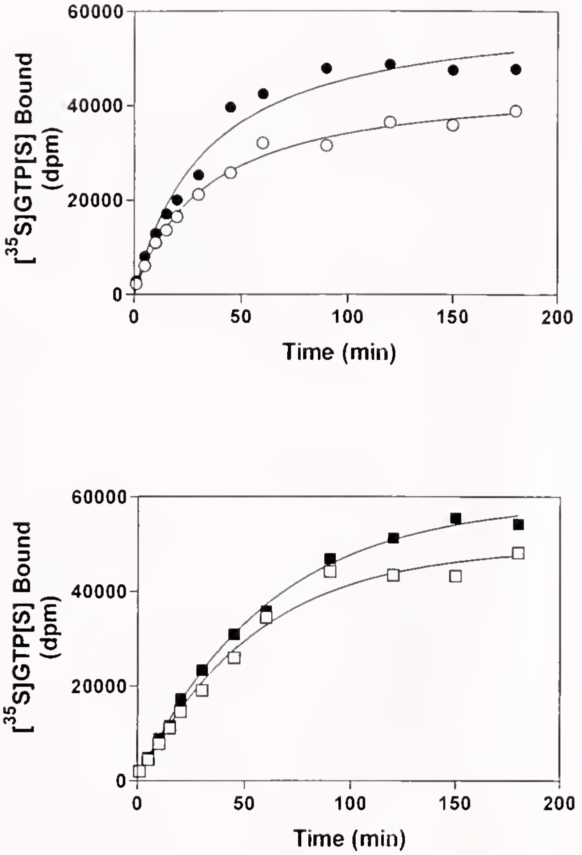

Figure 2. Time course of $[^{35}S]GTP[S]$ binding determined at atmospheric pressure (5°C), in the absence (open symbols) and presence (filled symbols) of 10 μM R-PIA. Upper panel: *Sebastolobus alascanus.* Lower panel: *S. altivelis.* Each point is the mean of three determinations. The standard errors are smaller than the symbols.

colonizing the deep ocean because of the large number of G protein-coupled transmembrane signaling systems (Siebenaller and Murray, 1995). Among the loci of pressure perturbation in these pathways, the intrinsic GTPase activities of the G protein α subunits are affected by increased pressure (Siebenaller and Murray, 1994a). In brain membranes of the congeneric *Sebastolobus* species, increased pressure (340 atm) decreased the apparent K_m of GTP about 10% and increased V_{max} values. Thus, increased pressure stimulates the high-affinity GTPase activity of G protein α subunits and may perturb transmembrane signal transduction by prematurely terminating signaling. The exchange of GTP for GDP is thought to be the rate-limiting step of the GTPase reaction (Higashijima *et al.,* 1987). The present study examined this exchange reaction. Increased pressure can alter this exchange and differentially affects the process in brain membranes of the *Sebastolobus* species.

At atmospheric pressure, the GTP-GDP exchange occurs at different rates in the two species. The $t_{1/2}$ values, which are determined by the on (k_{on}) and off (k_{off}) rates of GTP[S] and the concentration of $[^{35}S]GTP[S]$ used, differ between the two species. The exchange occurs faster in *S. alascanus* brain membranes (Fig. 2, Table I). The on rate in *S. alascanus* is $2.606 \times 10^7\ M^{-1}\ \text{min}^{-1}$, in contrast to the k_{on} value of $1.630 \times 10^7\ M^{-1}\ \text{min}^{-1}$ in brain membranes of *S. altivelis.* These different rates of GTP binding may reflect differences in the coupling of G proteins and receptors in the *Sebastolobus* species. A number of lines of evidence, including studies of A_1 adenosine receptor agonist binding (Murray and Siebenaller, 1987; Siebenaller and Murray, 1988) and studies using pertussis toxin to probe G protein-receptor interactions (Murray and Siebenaller, 1993; Siebenaller and Murray, 1994b), indicate that in *S. alascanus* brain membranes, a higher fraction of receptors are more closely coupled to G proteins than in *S. altivelis.* The tighter receptor-G protein coupling results in a larger fraction of coupled receptors in *S. alascanus,* which would promote the dissociation of GDP, facilitating $[^{35}S]GTP[S]$ binding to the unliganded guanyl nucleotide binding site on the α subunit of G proteins coupled to receptors. This would be less likely in *S. altivelis* brain membranes because the uncoupled pop-

Table II

Comparison of half-time ($t_{1/2}$) *and the binding rate constant* (k) *of* $[^{35}S]GTP[S]$ *determined at three pressures and 5°C, in the presence of 10* μM *R-PIA*

Species	Pressure (atm)		
	1	204	408
S. alascanus			
$t_{1/2}$ (min) ± SE (*n*)	37.47 ± 2.37 (4)	44.34 ± 7.46 (5)	13.36 ± 2.14 (4)
k (min^{-1})	0.0185	0.0156	0.0519
S. altivelis			
$t_{1/2}$ (min) ±SE (*n*)	58.06 ± 7.75 (4)	35.52 ± 2.84 (5)	35.75 ± 2.77 (4)
k (min^{-1})	0.0119	0.0195	0.0194

n = the number of determinations on different membrane preparations. Pseudo-first-order association kinetics of the interaction of $[^{35}S]GTP[S]$ and the G proteins were determined from a one-phase exponential association equation. For *S. alascanus,* the $t_{1/2}$ value at 408 atm differs significantly from those at 204 atm ($P < 0.01$) and 1 atm ($P < 0.05$); the values at 1 atm and 204 atm do not differ ($P > 0.05$). For *S. altivelis* the $t_{1/2}$ value at 1 atm differs from those at 204 atm ($P < 0.05$) and 408 atm ($P < 0.05$); the values at 204 atm and 408 atm do not differ ($P > 0.05$).

ulation of G proteins appears to be largely GDP-liganded (Murray and Siebenaller, 1993).

The bulk phospholipid and fatty acid compositions of the brain membranes of the *Sebastolobus* species are the same (Siebenaller *et al.*, 1991). The ordering effects of increased pressure on membrane acyl chain organization (Cossins and Macdonald, 1989) would be expected to also be the same. The difference in coupling efficiency at atmospheric pressure between the species may reflect the need for conformational flexibility and mobility in the membranes at the environmental pressures the species experience (Murray and Siebenaller, 1993). The coupling of receptors to G proteins depends on membrane fluidity (Houslay *et al.*, 1980, 1981; Casadó *et al.*, 1992). The effect of pressure on the time course of GTP binding in the *Sebastolobus* species supports this interpretation.

Increased pressure increases the observed binding constant (decreased $t_{1/2}$) of [^{35}S]GTP[S], and the pressure sensitivities of the observed binding rate constants (k) of the two species differ (Table I). In *S. altivelis*, the heightened rate of GTP binding may result from increased pressure raising the proportion of G proteins accessible to [^{35}S]GTP[S] binding. Alteration of the localization of signal transduction complexes in the plasma membrane (Huang *et al.*, 1997) or alteration of the interacting pool of subunits (Figler *et al.*, 1997) may contribute to the change in the rate of guanine nucleotide exchange.

Because the $t_{1/2}$ and observed k values depend on the concentration of GTP, values *in vivo* will differ from those reported here. However, it is clear that the pressure effects on the observed binding constant, k (Table II), reflect changes in the binding constants, k_{on} and k_{off}, that are independent of the GTP concentration. Of note is the observation that the k values of the species are similar over the range of *in situ* pressures that the species experience. At the typical habitat pressures of *S. alascanus* (10 to 85 atm), the k value, calculated from the mean of the 1 and 204 atm values, which do not differ, is approximately 0.0171. Over the range of 30.5 to 177.5 atm, the k values for *S. altivelis*, obtained by interpolation, are 0.0128 to 0.0180. These k values were calculated from a plot of the replicates of ln k versus 1 and 204 atm pressure. This assumes that the change in k is due to a pressure-independent volume change. If the pressure effect diminishes at higher pressures, as suggested by the fact that the 204 and 408 atm values are the same in *S. altivelis*, our interpolation underestimates how close the values are for the two species. Nonetheless, at their respective depths of occurrence, the binding rates are more similar than apparent from a comparison at atmospheric pressure. Thus the guanyl nucleotide binding properties of the α subunits appear to be conserved at their habitat pressures.

As seen previously (Siebenaller *et al.*, 1991; Siebenaller and Murray, 1994a), increased pressure decreases the efficacy of agonists (Fig. 1). The maximal binding (B_{max}) values (Table I) for A_1 adenosine receptor agonist stimulated-[^{35}S]GTP[S] binding in *Sebastolobus* brain membranes at 5°C are about 70-fold lower than the B_{max} value (25°C) in bovine brain membranes (Lorenzen *et al.*, 1993). However, the K_d values (Table I) of the mammalian and teleost species are similar. This observation is consistent with the conservation of binding parameters, and is similar to the pattern observed for enzymes and receptors at their environmental temperatures (*e.g.*, Yancey and Somero, 1978; Yancey and Siebenaller, 1987; Siebenaller and Murray, 1988) and pressures (*e.g.*, Siebenaller, 1987). Maintaining the affinity and selectivity of ligand binding under environmental temperatures and pressures maintains the regulatory and catalytic functions of enzymes (see Hochachka and Somero, 1984) and the selectivity and sensitivity of receptors (Siebenaller and Murray, 1988).

The effects of pressure make it clear that evolutionary adaptation of transmembrane signal transduction complexes is a major challenge for organisms colonizing the deep ocean. The extent of such adaptations for other receptor systems—for example, receptors coupled to G_s—and for receptors in deeper occurring species remain to be determined.

Acknowledgments

This work was funded by NSF grant IBN-9407205. We thank the crew and scientific parties of the R/V *Wecoma* cruises.

Literature Cited

Bruns, R. F. 1990. Adenosine receptors: roles and pharmacology. *Ann. N. Y. Acad. Sci.* **603:** 211–226.

Casadó, V., J. Mallol, E. I. Canela, R. Franco, and C. Lluis. 1992. Modulation of adenosine agonist [^{3}H]N^6-(R)-phenylisopropyladenosine binding to pig brain cortical membranes by changes of membrane fluidity and of medium physicochemical characteristics. *Eur. J. Pharmacol. Mol. Pharmacol.* **225:** 7–14.

Coleman, D. E., A. M. Berghuis, E. Lee, M. E. Linder, A. G. Gilman, and S. R. Sprang. 1994. Structures of the active conformations of $G_{i\alpha1}$ and the mechanism of GTP hydrolysis. *Science* **265:** 1405–1412.

Cossins, A. R., and A. G. Macdonald. 1989. The adaptations of biological membranes to temperature and pressure: fish from the deep and cold. *J. Bioenerg. Biomembr.* **21:** 115–135.

Daly, J. W., R. F. Bruns, and S. H. Snyder. 1981. Adenosine receptors in the central nervous system: relationship to the central action of methylxanthines. *Life Sci.* **28:** 2083–2097.

Figler, R. A., M. A. Lindorfer, S. G. Graber, J. C. Garrison, and J. Linden. 1997. Reconstitution of bovine A_1 adenosine receptors and G proteins in phospholipid vesicles: $\beta\gamma$-subunit composition influences guanine nucleotide exchange and agonist binding. *Biochemistry* **36:** 16288–16299.

Gilman, A. G. 1994. G proteins and regulation of adenylate cyclase (Nobel Lecture). *Angew. Chem. Int. Ed. Engl.* **34:** 1406–1419.

Hennessey, J. P., Jr., and J. F. Siebenaller. 1985. Pressure inactivation of tetrameric lactate dehydrogenase homologues of confamilial deep-living fishes. *J. Comp. Physiol.* **155:** 647–652.

Higashijima, T., K. M. Ferguson, M. D. Smigel, and A. G. Gilman. 1987. The effect of GTP and Mg^{2+} on the GTPase activity and the fluorescent properties of G_o. *J. Biol. Chem.* **262:** 757–761.

Hochachka, P. W., and G. N. Somero. 1984. *Biochemical Adaptation.* Princeton University Press, Princeton, New Jersey.

Houslay, M. D., I. Dipple, and R. F. Elliott. 1980. Guanosine 5′-triphosphate and guanosine 5′[$\beta\gamma$-imido]phosphate effect a collision coupling mechanism between the glucagon receptor and catalytic unit of adenylate cyclase. *Biochem. J.* **186:** 649–658.

Houslay, M. D., I. Dipple, and L. M. Gordon. 1981. Phenobarbital selectively modulates the glucagon-stimulated activity of adenylate cyclase by depressing the lipid phase separation occurring in the outer half of the bilayer of liver plasma membranes. *Biochem. J.* **197:** 675–681.

Huang, C., J. R. Hepler, L. T. Chen, A. G. Gilman, R. G. W. Anderson, and S. M. Mumby. 1997. Organization of G proteins and adenylyl cyclase at the plasma membrane. *Mol. Biol. Cell* **8:** 2365–2378.

Hubbs, C. L. 1926. The supposed intergradation of two species of *Sebastolobus* (a genus of scorpaenoid fishes) of western America. *Am. Mus. Novit.* **216:** 1–9.

Kauzmann, W., A. Bodanszky, and J. Rasper. 1962. Volume changes in protein reactions. II. Comparison of ionization reactions in proteins and small molecules. *J. Am. Chem. Soc.* **84:** 1777–1788.

Lauth, R. R., M. E. Wilkins, and P. A. Ramore, Jr. 1997. Results of trawl surveys of groundfish resources of the West Coast upper continental slope from 1989 to 1993. U.S. Department of Commerce, NOAA Technical Memorandum NMFS-AFSC-79, 342 pp.

Lorenzen, A., M. Fuss, H. Vogt, and U. Schwabe. 1993. Measurement of guanine nucleotide-binding protein activation by A_1 adenosine receptor agonists in bovine brain membranes: stimulation of guanosine-5′-O-(3-[^{35}S]thio)triphosphate binding. *Mol. Pharmacol.* **44:** 115–123.

Lowry, O. H., N. J. Rosebrough, A. L. Farr, and R. J. Randall. 1951. Protein measurement with the Folin phenol reagent. *J. Biol. Chem.* **193:** 265–275.

Lundeen, J. E., and J. H. Gordon. 1986. Computer analysis of binding data. Pp. 31–49 in *Receptor Binding in Drug Research,* R. A. O'Brien, ed. Marcel Dekker, New York.

Miller, D. J., and R. N. Lea. 1976. *Guide to the Coastal Marine Fishes of California,* California Department of Fish and Game, Sacramento.

Mixon, M. B., E. Lee, D. E. Coleman, A. M. Berghuis, A. G. Gilman, and S. R. Sprang. 1995. Tertiary and quaternary structural changes in $G_{i\alpha 1}$ induced by GTP hydrolysis. *Science* **270:** 954–960.

Moser, H. G. 1974. Development and distribution of juveniles of *Sebastolobus* (Pisces: Family Scorpaenidae). *U.S. Natl. Mar. Fish. Serv. Fish. Bull.* **72:** 865–884.

Murray, T. F., and J. F. Siebenaller. 1987. Comparison of the binding properties of A_1 adenosine receptors in brain membranes of two congeneric marine fishes living at different depths. *J. Comp. Physiol. B* **157:** 267–277.

Murray, T. F., and J. F. Siebenaller. 1993. Differential susceptibility of guanine nucleotide-binding proteins to pertussis toxin-catalyzed ADP-ribosylation in brain membranes of two congeneric marine fishes. *Biol. Bull.* **185:** 346–354.

Orr, J. W., M. A. Brown, and D. C. Baker. 1998. Guide to rockfishes (Scorpaenidae) of the genera *Sebastes, Sebastolobus,* and *Adelosebastes* of the Northeast Pacific Ocean. U.S. Department of Commerce, NOAA Technical Memorandum NMFS-AFSC-95, 46 pp.

Palmer, T. M., and G. L. Stiles. 1995. Neurotransmitter receptors. VII. Adenosine receptors. *Neuropharmacology* **34:** 683–694.

Pearcy, W. G., D. L. Stein, and R. S. Carney. 1982. The deep-sea benthic fish fauna of the northeastern Pacific Ocean on Cascadia and Tufts Abyssal Plains and adjoining continental slopes. *Biol. Oceanogr.* **1:** 375–428.

Saunders, P. M., and N. P. Fofonoff. 1976. Conversion of pressure to depth in the ocean. *Deep-Sea Res.* **23:** 109–111.

Siebenaller, J. F. 1978. Genetic variability in deep-sea fishes of the genus *Sebastolobus.* Pp. 95–122 in *Marine Organisms,* B. Battaglia and J. Beardmore, eds. Plenum Press, New York.

Siebenaller, J. F. 1984. Pressure-adaptive differences in NAD-dependent dehydrogenases of congeneric marine fishes living at different depths. *J. Comp. Physiol.* **154:** 443–448.

Siebenaller, J. F. 1987. Biochemical adaptation in deep-sea animals. Pp. 33–48 in *Current Perspectives in High Pressure Biology,* H. W. Jannasch, A. M. Zimmerman, and R. E. Marquis, eds. Academic Press, London.

Siebenaller, J. F., and T. F. Murray. 1986. Phylogenetic distribution of [^{3}H]cyclohexyladenosine binding sites in nervous tissue. *Biochem. Biophys. Res. Commun.* **137:** 182–189.

Siebenaller, J. F., and T. F. Murray. 1988. Evolutionary temperature adaptation of agonist binding to the A_1 adenosine receptor. *Biol. Bull.* **175:** 410–416.

Siebenaller, J. F., and T. F. Murray. 1990. A_1 adenosine receptor modulation of adenylyl cyclase of a deep-living teleost fish, *Antimora rostrata. Biol. Bull.* **178:** 65–73.

Siebenaller, J. F., and T. F. Murray. 1994a. The effects of hydrostatic pressure on the low-K_m GTPase in brain membranes from two congeneric marine fishes. *J. Comp. Physiol. B* **163:** 626–632.

Siebenaller, J. F., and T. F. Murray. 1994b. The effects of hydrostatic pressure on pertussis toxin-catalyzed ribosylation of guanine nucleotide-binding proteins from two congeneric marine fishes. *Comp. Biochem. Physiol.* **108B:** 423–430.

Siebenaller, J. F., and T. F. Murray. 1994c. Membrane preparation and receptor assays-adenosine. Pp. 475–484 in *Biochemistry and Molecular Biology of Fishes,* Vol. 3, P. W. Hochachka and T. P. Mommsen, eds. Elsevier, Amsterdam.

Siebenaller, J. F., and T. F. Murray. 1995. The effects of pressure on G protein-coupled signal transduction. Pp. 147–174 in *Biochemistry and Molecular Biology of Fishes,* Vol. 5, P. W. Hochachka and T. P. Mommsen, eds. Elsevier, Amsterdam.

Siebenaller, J. F., and G. N. Somero. 1978. Pressure adaptive differences in lactate dehydrogenases of congeneric fishes living at different depths. *Science* **201:** 255–257.

Siebenaller, J. F., A. F. Hagar, and T. F. Murray. 1991. The effects of hydrostatic pressure on A_1 adenosine receptor signal transduction in brain membranes of two congeneric marine fishes. *J. Exp. Biol.* **159:** 23–43.

Sokal, R. R., and F. J. Rohlf. 1995. *Biometry,* 3rd ed. W. H. Freeman, New York. 887 pp.

Spiegel, A. M., T. L. Z. Jones, W. F. Simonds, and L. S. Weinstein. 1994. *G Proteins.* R. G. Landes, Austin, Texas. 144 pp.

Sundin, L., and G. E. Nilsson. 1996. Branchial and systemic roles of adenosine receptors in rainbow trout: an *in vivo* microscopy study. *Am. J. Physiol.* **271:** (*Regulatory Integrative Comp. Physiol.* **40**): R661–R669.

Wakefield, W. W., and K. L. Smith, Jr. 1990. Ontogenetic vertical migration in *Sebastolobus altivelis* as a mechanism for transport of particulate organic matter at continental slope depths. *Limnol. Oceanogr.* **35:** 1314–1328.

Wall, M. A., D. E. Coleman, E. Lee, J. A. Iñiguez-Lluhi, B. A. Posner, A. G. Gilman, and S. R. Sprang. 1995. The structure of the G protein heterotrimer $G_{i\alpha 1}\beta_1\gamma_2$. *Cell* **83:** 1047–1058.

Wieland, T., and K. H. Jakobs. 1994. Measurement of receptor-stimulated guanosine 5′-O-(γ-thio)triphosphate binding by G proteins. *Methods Enzymol.* **237:** 3–13.

Yancey, P. H., and J. F. Siebenaller. 1987. Coenzyme binding ability of homologs of M_4-lactate dehydrogenase in temperature adaptation. *Biochim. Biophys. Acta* **924:** 483–491.

Yancey, P. H., and G. N. Somero. 1978. Temperature dependence of intracellular pH: its role in the conservation of pyruvate apparent K_m values of vertebrate lactate dehydrogenases. *J. Comp. Physiol.* **125:** 129–134.

Zobell, C. E., and C. H. Oppenheimer. 1950. Some effects of hydrostatic pressure on the multiplication and morphology of marine bacteria. *J. Bacteriol.* **60:** 771–778.

Reference: *Biol. Bull.* **197:** 395–405. (December 1999)

Reversible Alteration of Morphology in an Invertebrate Erythrocyte: Properties of the Natural Inducer and the Cellular Response

CHRISTINE LEMA-FOLEY, KYENG G. LEE, TCHAIKO PARRIS, ZOYA KOROLEVA,
NISHAL MOHAN, PIERRE NOAILLES, AND WILLIAM D. COHEN*

Department of Biological Sciences, Hunter College of CUNY, 695 Park Ave., New York, New York 10021; and Marine Biological Laboratory, Woods Hole, Massachusetts 02543

Abstract. The normal shape of the erythrocytes of the bivalves known as *blood clams* is maintained by a marginal band (MB) of microtubules. When hemolymph (or "blood") is withdrawn from the animal, its erythrocytes change, within minutes, from the normal smooth-surfaced, flattened ellipsoids (N-cells) to spheroids with folded surfaces (X-cells). This alteration can be prevented by rapidly diluting the hemolymph with physiological medium, yielding N-cells for use in studying the transformation to X-cells. Bioassays showed that shape transformation was induced by a hemolymph activity (H_x) and was a function, in part, of cell responsiveness to this activity. Eventually the shape of the cells spontaneously returned to normal, at a rate dependent upon the concentration of the cells and of H_x; recovery was correlated with loss of H_x. The X-cells contained an intact but highly deformed MB, but this was not the effector of the transformation. Erythrocytes made to lack MBs still changed shape, although they did not recover as completely as did the MB-containing controls. When clams were cooled before hemolymph was withdrawn, the concentration of H_x was reduced. H_x was retained after dialysis of hemolymph, and initial filtration and chromatography indicated that its M_r was greater than 500,000. Shape transformation was blocked by EGTA, by serine protease inhibitors, and by sodium azide; the last indicates ATP-dependence. Although the mechanism responsible for shape transformation remains to be determined, the data suggest that the change is triggered by a coagulation-related activity in response to the removal of hemolymph from the animal.

Introduction

The nucleated erythrocytes of non-mammalian vertebrates are useful for studying the role of cytoskeletal elements in cellular morphogenesis and cell-shape maintenance. When mature, these cells are characteristically flattened ellipsoids or discoids with a nuclear bulge. Their cytoskeletal system contains a marginal band (MB), composed principally of microtubules, enclosed within the membrane skeleton (MS) in the plane of flattening, and in at least some species, intermediate filaments link sites on the MS to the MS or nucleus. The morphology of these cells is relatively stable and is maintained by the MB against potentially deforming mechanical or osmotic forces (Joseph-Silverstein and Cohen, 1984, 1985; Cohen, 1991). Certain invertebrates also have hemoglobin-bearing nucleated erythrocytes (Ratcliffe and Rowley, 1981; Cohen and Nemhauser, 1985), and in some cases these cells change morphologically when they are removed from the animal (*e.g.*, Terwilliger *et al.*, 1985). Erythrocyte-containing species include bivalves of the genera *Anadara* and *Noetia*. The cytoskeletal system of their red cells resembles that of non-mammalian vertebrates but, unlike the latter, it also includes a functional centrosome associated with the MB (Cohen and Nemhauser, 1980; Nemhauser *et al.*, 1983). Most importantly for the present work, the shape of the erythrocytes changes drastically—from normal flattened ellipsoids ("N-cells") to wrinkled spheroids ("X-cells")—in hemolymph samples from these and related species (Sullivan, 1961; Cohen *et al.*, 1985). We have found that this transformation is induced by a hemolymph activity, and that, surprisingly, it eventually reverses spontaneously, so that the cells return to a near-normal shape ("R-cells";

Received 23 April 1999; accepted 13 August 1999.

* To whom correspondence should be addressed. E-mail: cohen@genectr.hunter.cuny.edu

Dadacay *et al.*, 1996). This is the only natural, reversible morphological change in non-mammalian erythrocytes of which we are aware, and it offers an opportunity to analyze the interplay between extracellular factors and cytoskeletal elements in maintaining cellular shape. We present here experimental work that defines major properties of the natural inducing factors and of the cellular response in this system.

Materials and Methods

Experimental material

Specimens of *Noetia ponderosa* (the "ponderous ark") were obtained from Terry Bros. Co. (Willis Wharf, VA) and were maintained in a refrigerated seawater tank at about 17°C or in the running natural seawater system at the Marine Biological Laboratory. Blood from the mantle cavity or foot muscle was drawn using syringes with 22- or 27-gauge needles, or was obtained by cutting muscle during clam sacrifice. Shape-transforming activity in the whole blood, as measured by the percentage of X-cells present, was recorded 5 or 10 min after blood was obtained, when it was typically maximal. Because we occasionally found clams in which activity was very low, we adopted an activity of 85% or greater as the minimal level for subsequent experimental use.

To obtain N-cells (cells of normal morphology that had not undergone transformation), blood was immediately diluted a minimum of 1:200 into "physiological medium" consisting of MBL formula artificial seawater (Cohen, 1997) containing 0.5 m*M* NaH_2PO_4 at pH 7.2, in which cells retained normal shape. In a few experiments, marine molluscan Ringer's solution (MMo-1; Cohen, 1997), a similar medium also containing 0.5 m*M* NaH_2PO_4 at pH 7.2, was employed with the same results. The resulting suspension was centrifuged (2000 rpm, 3 min, Beckman Accuspin at 17°C), yielding an erythrocyte pellet overlaid by a thin layer of white cells and trapped erythrocytes. This layer was removed by aspiration, and the cells were washed two or three times by centrifugation in about 5 times the original blood volume of physiological medium. Washed erythrocytes were resuspended to the original blood volume and hematocrit was measured to determine cell concentration by volume. N-cells were ready for use after final adjustment to a concentration of 1% by volume and inspection with phase contrast microscopy to verify normal shape.

Bioassay of shape transforming activity

Cell-free hemolymph was obtained as the supernate after a 3-min microfuge centrifugation of whole blood. As noted previously (Dadacay *et al.*, 1996), the shape-transforming activity (H_x) of cell-free hemolymph was stable with freezing, permitting storage of hemolymph at −20°C or −80°C until use. The basic bioassay consisted of suspending N-cells in normal or experimentally treated cell-free hemolymph ($t = 0$), incubating at 21°–23°C (room temperature), then counting samples under phase contrast to determine the percentage of X-cells present after 5 min and at subsequent time points. Samples were either counted rapidly, to avoid appearance of morphology-distorting "glass effects," or were fixed in physiological medium containing 8% formaldehyde before counting. In each sample (*i.e.*, per data point), 200 or more cells were counted in non-selected fields. Unless otherwise specified, cell-free hemolymph was diluted with physiological medium just prior to use, such that the X-cell concentration reached 90% or more within 5–10 min, and reversal to less than 10% X-cells occurred in 1–2 h.

Experiments involving bioassays were performed a minimum of three times using material from different clams, unless otherwise noted; each data point records a specific cell count, and the data presented are representative.

Preparation of erythrocytes with and without marginal bands

Erythrocytes were pre-incubated with either no inhibitor (dimethyl sulfoxide [DMSO] solvent only), 10 μg/ml nocodazole, or 20 μM taxol (Sigma Chemical Co., St. Louis, MO) for 30 min at room temp. (22°–24°C) and subsequently incubated at 0°C for 3 h. These cell suspensions (still containing inhibitors) were then rewarmed for 30 min at room temperature (22°–24°C), and the presence or absence of MBs was ascertained by phase-contrast examination of cytoskeletons produced in Triton lysis medium. Triton lysis medium consisted of 100 m*M* piperazine-*N,N'*-bis(ethanesulfonic acid) [PIPES buffer], 5 m*M* ethylene glycol-bis-(β-aminoethyl ether) *N,N'*-tetraacetic acid [EGTA], 1 m*M* $MgCl_2$, pH 6.8 (=PEM), containing 0.4% Triton X-100 (Cohen and Nemhauser, 1980, 1985; Joseph-Silverstein and Cohen, 1984). MBs were observed in taxol-treated or untreated cells, but were not present in nocodazole-treated cells (Joseph-Silverstein and Cohen, 1984, 1985).

Microscopy

Cells for morphological examination were either unfixed or fixed immediately (<30 s) by dilution into physiological medium containing 4%–8% formaldehyde. Cells were examined and images recorded using a Zeiss phase contrast microscope equipped in most instances with a DAGE NC-70 video camera, Hamamatsu Argus-10 video image processor, and video printer.

For fluorescence microscopy, living cells suspended in physiological medium were first trapped within fibrin clots as described previously (Lee *et al.*, 1998; see also Forer and Behnke, 1972). Briefly, 1 volume of cell suspension was mixed with 4 volumes of the same medium containing

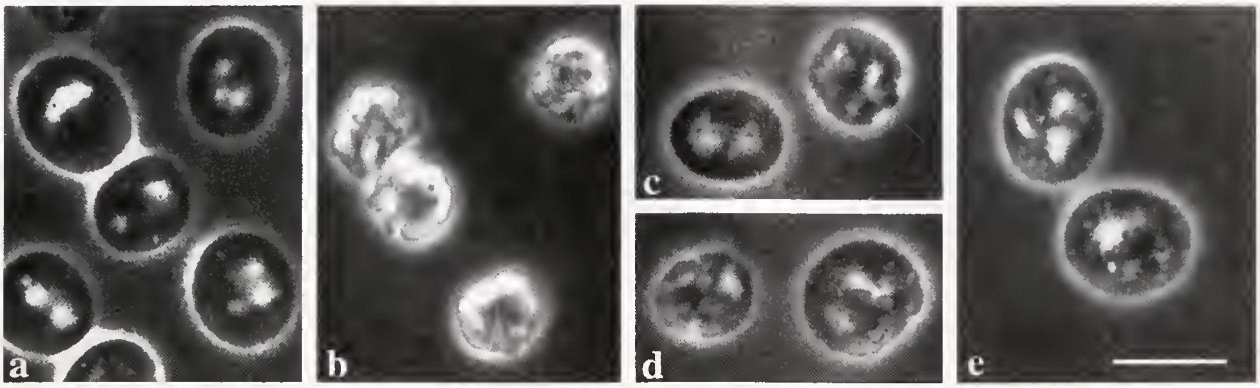

Figure 1. Light micrographs of *Noetia ponderosa* erythrocytes before and after shape transformation. (a) Normal erythrocytes (N-cells), flattened and slightly ellipsoidal; (b) shape-transformed erythrocytes (X-cells), appearing refractile, lumpy, and spheroidal at this level of resolution; (c, d) examples of shape-transformed erythrocytes at different stages during recovery; (e) cells of essentially normal shape post-recovery. Video-enhanced phase contrast microscopy; bar = 10 μm.

10 mg/ml fibrinogen (Sigma F-8630). Thrombin (Sigma T-4648) was added to 1 U/ml to produce a firm clot in about 10 min; within this time window, 5- to 25-μl samples were spread inside plastic rings adhering to coverslips. Cytoskeletons were produced by immersing coverslips bearing fibrin-trapped cells in Triton lysis medium (see above) for 1 min, followed by fixation in PEM containing 8% formaldehyde. In some cases, 4% formaldehyde was included in the lysis medium for additional stabilization. This was followed by PBS washes and incubation with a 50:50 mix of monoclonal anti-α- and anti-β-tubulin (Sigma T-9026, T-4026), using secondary FITC goat anti-mouse IgG F(ab$'$)$_2$ (Sigma F-8521). Fibrin-trapped specimens were examined using epifluorescence and confocal fluorescence microscopy. Controls lacking primary antibody or phalloidin exhibited little background fluorescence.

For scanning electron microscopy, cells were fixed for 1 h in 16% formaldehyde in 0.5 *M* KH_2PO_4, pH 6.8, at 21°–23°C (room temperature); dehydrated in ethanol to 70%; incubated on acid-cleaned polylysine-coated coverslips; dehydrated to 100% ethanol; and critical-point dried (Tousimis Samdri-780A). Coverslips were mounted on stubs with double-sided tape and sputter coated with Au/Pd (Tousimis Samsputter 2A), with silver paste added for conductivity.

Hemolymph dialysis, filtration, and chromatography

Hemolymph samples were dialyzed overnight at 0°C against physiological medium in dialysis tubing with a molecular weight cutoff of about 12,000; control samples were similarly treated except that the dialysis medium was omitted. Hemolymph fractions were obtained by centrifugation through Centricon concentrators (Amicon Inc.) of various molecular weight cutoffs (10,000–500,000), and by chromatography on Sephadex G-200SF and Sephacryl 400HR columns. The protein content of the fractions was assayed by the Bradford method (Bradford, 1976), and fractions were bioassayed for H_x as described above.

Results

Cell morphology

As observed by video-enhanced phase contrast of fixed samples, normal erythrocytes ("N-cells") were flattened ellipsoids when initially removed from the animal (Fig. 1a). Upon incubation in cell-free hemolymph under our standard assay conditions, most N-cells were transformed to an irregular spheroidal shape (X-cells) within 5–10 min (Fig. 1b), with a lag of several minutes, but eventually recovered normal or near-normal shape ("R-cells"; Fig. 1c–e).

More detailed views of cell morphology were obtained by scanning electron microscopy. Surveys at lower magnifications verified the light microscopic observations (Fig. 2). At higher magnifications it was clear that N-cells were relatively smooth-surfaced (Fig. 3a, b), whereas the surface of X-cells was thrown into large folds (Fig. 3c, d).

Shape transformation: time course and general features

In undiluted hemolymph, recovery of most of the erythrocyte population typically required many hours. In hemolymph diluted in the range of ½ to ⅕ with physiological medium, time spent in the fully transformed state was progressively reduced. A typical time course for shape transformation and recovery in diluted hemolymph is presented in Figure 4, and a comparison of cell response to undiluted and diluted hemolymph is shown in Fig. 5. The rate of shape reversal was positively correlated with erythrocyte concentration (Fig. 6).

Shape transformation was not triggered by a change in hemolymph pH, nor could it be mimicked by simple

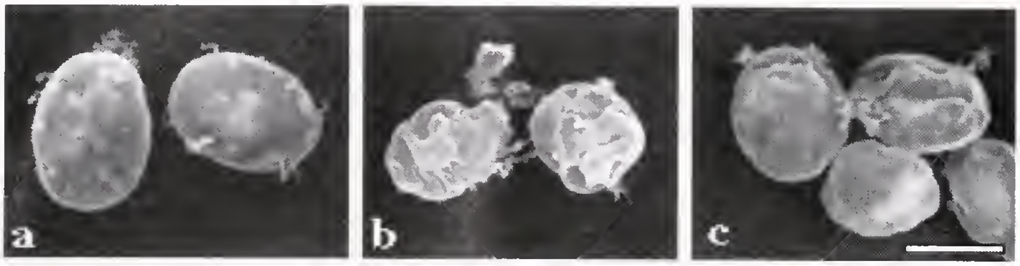

Figure 2. Survey view of *Noetia ponderosa* erythrocytes. (a) Normal cells, flattened and ellipsoidal; (b) shape-transformed erythrocytes; (c) erythrocytes during recovery. Scanning electron microscopy; bar = 10 μm.

changes of pH in the medium. Cells were found to be morphologically stable over a tested pH range of 6.6–7.5 in physiological medium, and the pH of native cell-free hemolymph remained stable at about 6.7 as measured before and after shape transformation.

Cell responsiveness

The percentage of cells that changed shape was markedly lower in native blood samples from certain clams. To test whether this was due to variable H_x or to variable cell

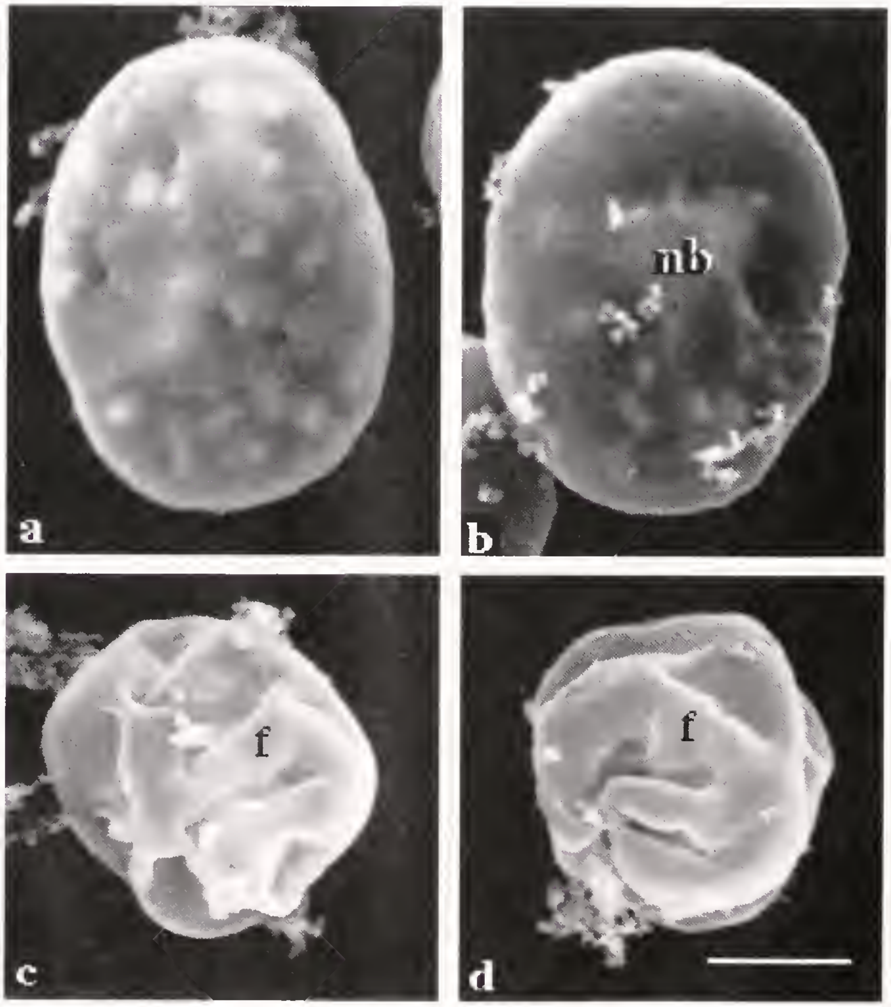

Figure 3. Higher magnification view of two cells in Figure 2, plus two additional examples: (a, b) Normal erythrocytes, flattened and ellipsoidal (nb = nuclear bulge); (b) shape-transformed erythrocytes, with "lumpiness" resolved as extensive surface folding. Scanning electron microscopy; bar = 10 μm.

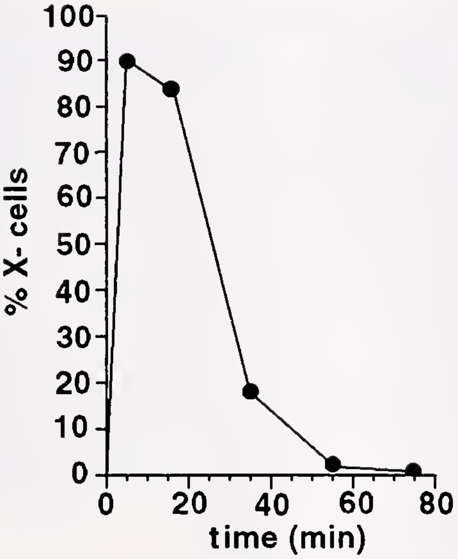

Figure 4. Typical time-course of cell-shape transformation and recovery in diluted hemolymph. The percentage of X-cells rose to >90% within 5 min, held at >80% for ~15 min, and declined to near zero by 60 min.

responsiveness to H_x, N-cells and hemolymph were prepared from clams exhibiting high and low levels of native shape transformation respectively, and cells and hemolymph were mixed in all four combinations. The results (Fig. 7) show that H_x was high in all hemolymphs, but that erythrocytes of two different clams can vary greatly in their responsiveness to hemolymph from the same clam.

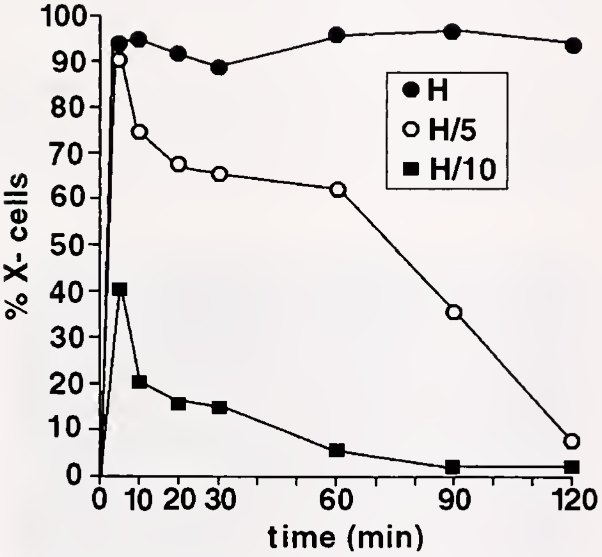

Figure 5. Effect of hemolymph dilution on cell-shape transformation and recovery. H = undiluted hemolymph; H/5 and H/10 = hemolymph diluted 1:5 and 1:10 with physiological saline, respectively. Note that <50% of the cells responded in H/10. In experiments such as this using undiluted hemolymph, reversal to <10% X-cells was frequently not observed for 6 or more hours.

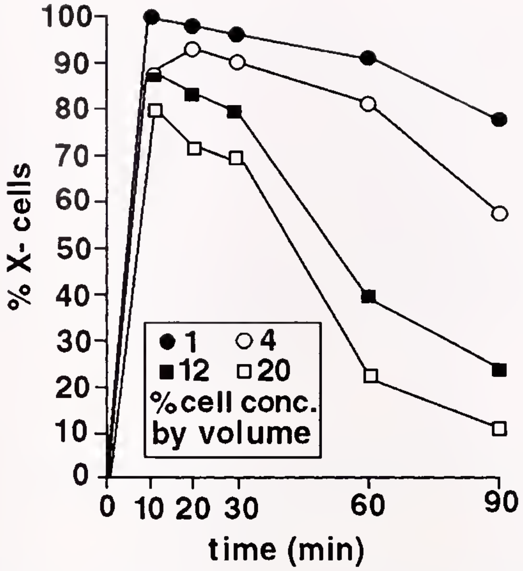

Figure 6. Effect of cell concentration on cell-shape transformation and recovery (undiluted hemolymph). At the standard cell concentration (1%) the percentage of shape transformation was maximal, with only modest subsequent reversal. At higher cell concentrations the peak percentage of X-cells was reduced, and reversal rate was progressively greater.

Post-recovery cell responsiveness and depletion of Hx

Cells that had recovered normal shape (R-cells) were able to undergo a second transformation to X-cells, comparable to that of controls, when transferred into fresh hemolymph

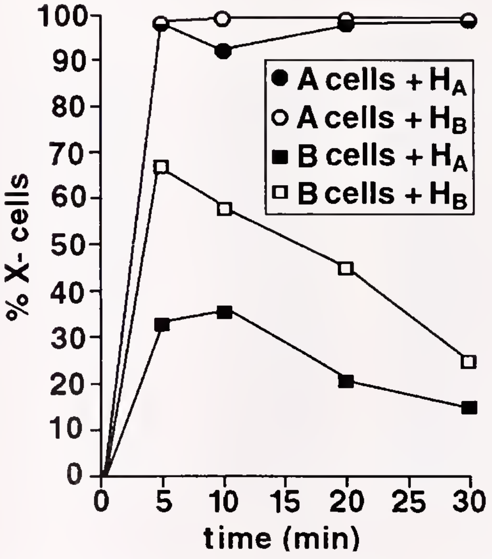

Figure 7. Dependence of shape transformation on cellular factors. Cells and cell-free hemolymph (H) were obtained from two clams (A and B), and all four mixtures were made as indicated. Clam A cells yielded >90% X-cells within 5 min and maintained that activity independent of hemolymph source, whereas clam B cells showed submaximal activity independent of hemolymph source.

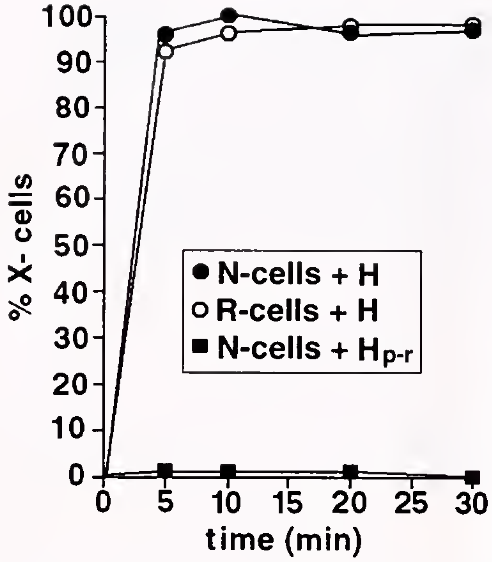

Figure 8. Assay for hemolymph activity (H_x) following cell-shape transformation and recovery, and test of capacity of recovered cells (C_R) to undergo a second transformation. Upon recovery, R-cells reincubated with fresh hemolymph again underwent shape transformation, whereas reincubation of fresh N-cells in the "post-reversal" cell-free hemolymph (H_{p-r}) showed that it lacked H_x.

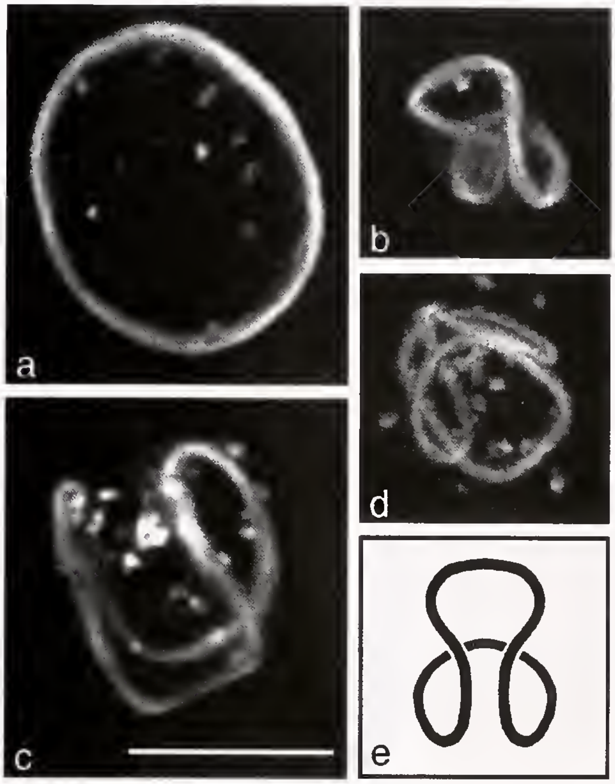

Figure 9. Marginal bands (MBs) of microtubules as revealed by anti-tubulin immunofluorescence. (a) N-cell cytoskeleton; (b–d) X-cell cytoskeletons. N-cell MBs were typically ellipsoids, sometimes twisted into figure-8s. X-cell MBs were essentially intact, but assumed highly convoluted shapes without apparent breakage. A diagram of the basic MB deformation pattern observed in many X-cells (*e.g.*, b, c) is given in (e); some twist patterns were more complex, however (*e.g.*, d). Fluorescence microscopy; bar = 10 μm.

(Fig. 8, open circles). However, the converse was not true: N-cells incubated in hemolymph in which other cells had previously undergone shape transformation and recovery either remained normal or exhibited only partial transformation and very rapid recovery, indicating depletion of H_x (Fig. 8, squares).

Cytoskeletal structure and function

As revealed by indirect anti-tubulin immunofluorescence, the MB was still present and continuous in the cytoskeletons of shape-transformed cells, but its shape was highly convoluted compared to that of normal cells (Fig. 9). To test whether the MB was a primary effector of shape transformation, erythrocytes with and without MBs were prepared by temperature cycling in the presence of inhibitors of disassembly (taxol) or reassembly (nocodazole). Similarly cycled controls (DMSO solvent only) contained completely or partially reassembled MBs. Bioassays in diluted hemolymph produced more than 96% X-cells in all three preparations within 10 min, and reversal after 3 h.

One major difference was noted in cells lacking MBs, however: many of the major transformation-induced surface indentations were not eliminated during reversal (Fig. 10).

Shape transformation inhibitors

Heating hemolymph in a boiling water bath, followed by cooling and bioassay, showed H_x to be heat-labile. In three experiments in which controls showed very high initial activity (99% at 10 min), samples heated for 20 min exhibited initial residual activity of 75%–95%, but recovery of cell shape began after only about 20 min. By 60 min, experimentals had 0%–15% X-cells, whereas controls still

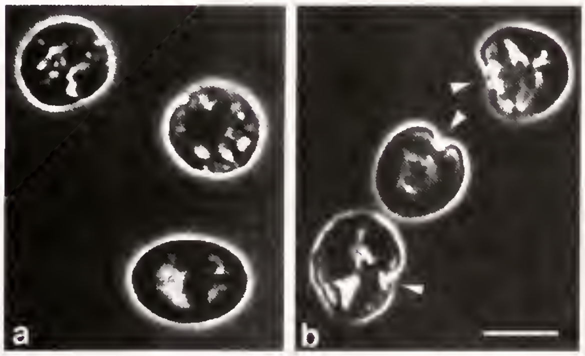

Figure 10. Shape reversal in cells containing or lacking MBs. (a) MB-containing cells; only minor post-reversal surface deformations were observed; (b) cells lacking MBs; major surface indentations were retained post-reversal. Video-enhanced phase contrast microscopy; bar = 10 μm.

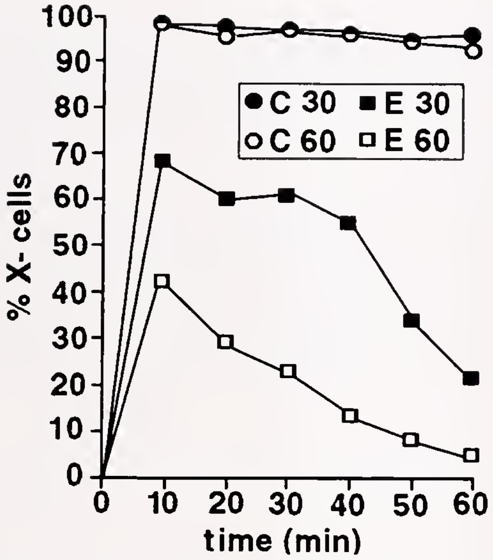

Figure 11. Effect of sodium azide on shape transformation and recovery. N-cells were incubated for 30 or 60 min in 3 m*M* sodium azide in physiological medium (=experimentals E30 and E60) or in physiological medium alone (=controls C30 and C60) prior to assay. Azide pre-incubation markedly reduced the percentage of X-cells and accelerated shape reversal, with greater effect for the 60-min period. Controls maintained >90% X-cells throughout.

had 95%–99%. In two additional experiments, controls with 90%–93% initial activity retained 80%–90% after 30 min, whereas experimentals heated for 10 min had only 5%–6% X-cells initially, and less than 2% in 30 min.

Bioassays were conducted with various potential biochemical inhibitors added to hemolymph prior to the addition of N-cells. Shape transformation was completely inhibited by 10 m*M* (or greater) EGTA, as reported previously (Dadacay *et al.*, 1996); at a given concentration, EDTA was less effective. The protease inhibitors initially surveyed were antipain, aprotinin, bestatin, chymostatin, leupeptin, aminoethylbenzenesulfonyl fluoride (AEBSF), and phosphoramidon. As assayed after a 10-min exposure, only chymostatin and AEBSF were effective, at 18% and 7% X-cells, respectively (*vs.* 91% for controls). AEBSF produced complete inhibition at 3 mg/ml (12 m*M*) and above, and an excess (5 mg/ml) was typically employed in other experiments.

ATP-dependence of shape transformation was tested by pre-incubation of N-cells in physiological medium containing 3 m*M* sodium azide for either 30 min or 60 min, followed by a wash, prior to mixing cells and cell-free hemolymph. Controls were similarly incubated, except without azide. As shown in Figure 11, the percentage of cells undergoing shape transformation was markedly reduced and shape reversal accelerated in both cases compared to controls, with the longer period of ATP depletion having the greater effect.

Activity sequence

The inhibitor studies indicated that shape transformation involved a calcium-activated step and a proteolytic activity, but in what sequence did they occur? To answer this question, N-cells were mixed with hemolymph at $t = 0$, and inhibitors were added at subsequent time intervals (Fig. 12). EGTA was found to be effective only if present initially ($t = 0$); in contrast, AEBSF was effective initially and was at least partially effective at later time points. Importantly, when added at $t = 5$ min and 10 min, AEBSF induced some shape reversal, whereas EGTA did not.

Triggering of transformation activity

Shape transformation was apparently triggered during the removal of blood and thus might be a response to wounding. Three pairs of clams were used to test this hypothesis: physiological responsiveness was reduced by pre-cooling clams to 1°C, and tissue trauma was minimized by removing blood through a very fine (28-ga) syringe needle. The activity of hemolymph obtained using both variables together (assayed using N-cells from a non-cooled clam) was reduced to about 50% of that of hemolymph obtained from the same clam after re-warming and sacrifice by slashing muscle (Fig. 13). Activity reduction of lesser extent was also observed when each variable was tested separately (low temp. *vs.* normal; fine needle *vs.* sacrifice; not shown).

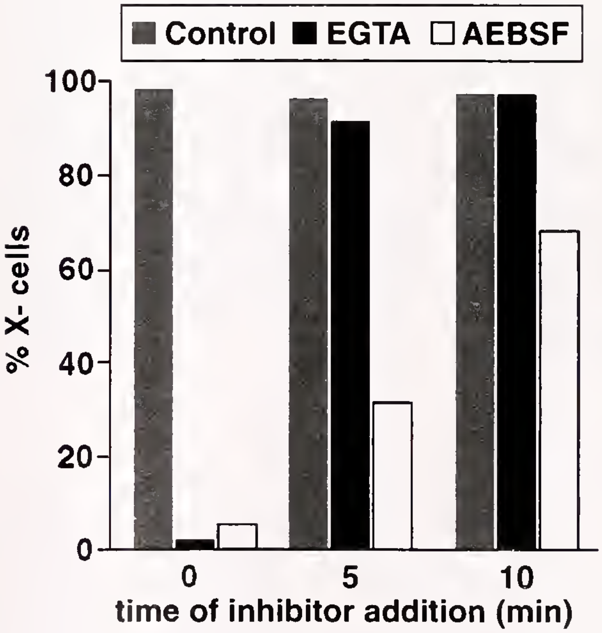

Figure 12. Effect of addition of EGTA and AEBSF at various times after exposure of N-cells to hemolymph. The percentage of X-cells was determined 5 min after the addition of inhibitor (final concentrations: 20 m*M* EGTA, 5 mg/ml AEBSF). EGTA was effective only when present initially, whereas AEBSF was still partially effective when added later.

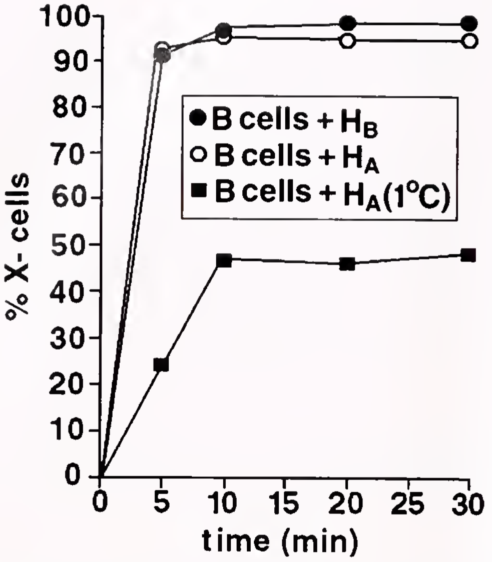

Figure 13. Tissue trauma as a possible factor in H_x level. Two preparations of cell-free hemolymph were made from clam A: $H_{A(1°C)}$ was obtained *via* syringe after pre-cooling clam A to 1°C, and H_A from the same clam was obtained by cutting muscle after 3 h of rewarming. N-cells (C_B) and cell-free hemolymph for control bioassay were obtained from clam B. Three mixtures were made as indicated, with $H_{A(1°C)}$ exhibiting less than half the activity of H_A.

Dialysis and initial fractionation of hemolymph

Active hemolymph was dialyzed for 12 h against physiological medium at 0°C, with a molecular weight cutoff of about 12,000. Control hemolymph was similarly treated except that the dialysis sac was simply kept moist. Bioassay with fresh N-cells showed that both samples exhibited excellent activity, with the experimental comparable to the control except for an extended activation lag (Fig. 14). Centrifugation through filters with different molecular weight cutoffs (Centricon) indicated that the M_r for H_x is greater than 500,000, and chromatogaphy on Sephadex G-200SF confirmed that H_x moved together with the blue dextran marker, indicating the M_r to be greater than 250,000.

Discussion

Shape transformation and recovery

The results show that shape transformation occurs in response to an activity (H_x) in the cell-free hemolymph, and that the extent of response is a property of the erythrocyte population. In typical assays, more than 90% of cells were responsive to H_x, but individual cells, as well as cells from certain clams, varied in both responsiveness and rate of recovery. Variability was particularly clear at high hemolymph dilutions (*e.g.*, Fig. 5, H/10), in which only a fraction of the erythrocytes responded. This was verified by experiments using erythrocytes from clams with high *vs.* low percentages of transformation, in which the variable response was attributable to cells rather than hemolymph (Fig. 7). In addition, recovery during a typical time course (*e.g.*, Figs. 4–6) was not synchronous, indicating a range of cell sensitivity to H_x.

Cells that had undergone shape transformation and recovery (R-cells) retained the capacity to change shape a second time (Fig. 8). In contrast, hemolymph assayed after removal of R-cells was depleted of H_x, and thus the recovery phenomenon is correlated with loss of H_x. The increased rate of recovery with increasing cell concentrations (Fig. 6) is consistent with increased cell-induced loss of H_x.

Biochemical activities involved in shape transformation

Shape transformation was markedly inhibited by EGTA, with EDTA less effective, indicating that the process is Ca^{++}-activated. Transformation was also greatly reduced by preheating of hemolymph and blocked by the serine protease inhibitors AEBSF and chymostatin. Both EGTA and AEBSF were effective when present at $t = 0$ (mixing of N-cells and hemolymph), but only AEBSF was effective when added later (Fig. 12). Thus, the initial step is presumed to be Ca^{++}-activated, resulting in a hemolymph proteolytic activity for which Ca^{++} is no longer required.

One relatively simple hypothesis is that a proteolytic product maintains cell shape transformation, and that cells recover when the proteolytic activity ceases and product concentration falls. This is at least partly supported by the observation that addition of AEBSF produces considerable reduction in the percentage of X-cells present (Fig. 12)

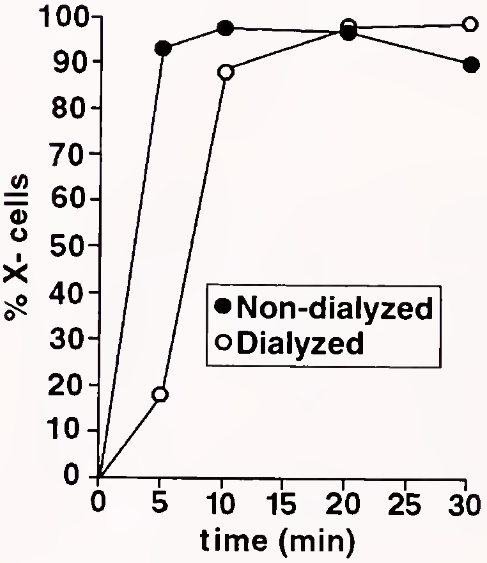

Figure 14. Activity of cell-free hemolymph after dialysis. Non-dialyzed and dialyzed hemolymph reached comparable X-cell levels, with the latter exhibiting a longer lag period.

compared to controls. With time, the X-cells presumably inhibit this proteolytic activity or exhaust its product, accounting for the loss of transforming activity in post-recovery hemolymph.

Mechanism of shape transformation and recovery

ATP-depletion by pre-incubating the erythrocytes with azide inhibits shape transformation in most of the cell population, showing that it is an active phenomenon. Three hypotheses for an active shape-transformation mechanism are (a) alteration of MB shape by a microtubule-motor protein system, (b) contraction of a cell-surface–associated actomyosin system, and (c) reduction of cell volume by an osmotic pump system. Each is considered here in relation to the data.

(a) Microtubule-motor protein mechanism: MB function. Transformation of cell shape, as well as initiation of shape reversal, takes place in the presence or absence of the MB; thus, the MB is not the primary effector, and this mechanism can be ruled out. However, the MB is needed to return to completely normal cell shape (Fig. 10), a finding consistent with previous studies showing that the MB is required for the erythrocytes of dogfish and blood clams to resist deformation caused by mechanical and osmotic stress (Joseph-Silverstein and Cohen, 1984, 1985).

Whereas normally the MB of the blood clam erythrocyte appears to deform the MS and maintain its shape (Joseph-Silverstein and Cohen, 1985), the mechanism at work here generates sufficient force to produce substantial secondary deformation of the MB (Fig. 9b–d). Such deformation without breakage demonstrates that the MB has remarkable flexibility, as expected for shape-maintenance function. The contours assumed by many of these deformed MBs appear to be twisted variations of a "baseball seam" model, in which a spheroidal shape is accommodated by an initially planar ellipse folding back on itself (Fig. 9e). The complete cell-shape recovery observed in the presence of azide is compatible with non-ATP-requiring, mechanical MB function in response to deformation.

(b) Cell-surface–associated actomyosin contraction mechanism. The entire X-cell surface has a folded appearance, and thus the underlying membrane skeleton (MS) is a potential cytoskeletal effector. We have observed previously that F-actin is prominently associated with the *Noetia* erythrocyte MS (Lee *et al.*, 1998), but the presence of myosin has not yet been demonstrated in these cells. Myosin resembling that of platelets has, however, been identified in mammalian erythrocytes (Fowler *et al.*, 1985). It can form bipolar filaments (myosin II class) and is believed to participate in contractile activity associated with the erythrocyte membrane (Fowler, 1986; Pasternack and Racusen, 1989; der Terrossian *et al.*, 1994). Thus there is sufficient precedent for serious consideration of such a mechanism in blood clam erythrocytes.

(c) Active reduction of cell volume by osmotic efflux. The appearance of shape-transformed cells (Fig. 3) is compatible with osmotic distortion, and osmotic mechanisms are attractive in being potentially readily reversible. However, if an osmotic mechanism is at work here, it cannot be a simple phenomenon attributable to use of physiological media or other experimental manipulations. First, the native shape of these red cells is flattened and ellipsoidal, as shown previously by immediate fixation of blood samples (Cohen and Nemhauser, 1986); when the "blood" is diluted immediately and extensively with our physiological media, the cells retain their native shape indefinitely. Second, both the shape change and recovery occur in the clam's own hemolymph without any experimental manipulation whatever. Third, hemolymph diluted tenfold with physiological medium in which N-cells are osmotically stable still induces complete shape change in some cells of the population. Fourth, freshly added N-cells are morphologically stable in hemolymph in which cells have undergone the complete cycle of transformation and recovery (Fig. 8). Finally, the effect cannot be mimicked by suspension of N-cells in hyperosmotic media, as reported earlier (Dadacay *et al.*, 1996); N-cells get thinner in such media, but retain their flattened ellipsoidal shape.

It is quite possible, however, that the shape transformation involves a more complex osmotic mechanism, such as one in which an external signal triggers hyperactivity of an active efflux system that produces and maintains excessive volume loss until reversal. Amende and Pierce (1980a) have shown that hypo-osmotically stressed *Noetia* red cells reduce their volume to normal levels by a mechanism involving active efflux of taurine and other amino acids. Like the shape transformation reported here, this osmoregulatory mechanism is activated by Ca^{++} and inhibited by ATP depletion (Amende and Pierce, 1980b; Pierce and Maugel, 1985; Pierce *et al.*, 1989). Thus it is possible that activation of the same system in N-cells by some other means could further reduce cell volume. We have not reported hematocrit volume measurements in this paper, however, because we believe that differences in the packing of N-cells—smooth-surfaced, flattened ellipsoids—and X-cells—spheroids with highly folded surfaces—make such data highly unreliable. Studies of this mechanism will require more sophisticated volume measurements.

Triggering of erythrocyte shape transformation

The hemolymph of this and closely related molluscan species (*Anadara ovalis, A. transversa*) does not undergo complete *in vitro* clotting in the classic sense, but microscopy of whole-blood samples shows that white hemocytes begin to aggregate shortly after the blood is obtained. In other molluscs (oysters, mussels), hemocytes have been shown to aggregate at wound sites and plug them (Sparks and Morado, 1988), and eventual spontaneous disaggregation has also been observed in oysters under certain conditions (Bang, 1961; Feng, 1965, 1988). The act of obtaining hemolymph by syringe or by tissue cutting may initiate similar wound-repair mechanisms in blood clams, with elevation of Ca^{++} by entry of seawater a possible trigger. Erythrocyte shape transformation might then be a secondary effect triggered and maintained by a local mechanism of wound repair, with recovery advantageous for affected erythrocytes that move away from the site and enter the general circulation.

The data are consistent with the idea that the mechanism for triggering shape alteration is analogous to that of vertebrate blood clotting, in which Ca^{++} is required for early activation steps, serine protease activity yields fibrin, and generation of plasmin causes clot dissolution (reversal). The analogy is not necessarily superficial, as serine proteases are involved in clotting cascades in certain other invertebrates (*e.g., Limulus;* Bergner *et al.,* 1997). Though not the focus of present work, initial characterization of molecular species participating in H_x showed retention of activity in dialyzed cell-free hemolymph, indicating that components of relatively low molecular mass ($<$12,000 Da) were not involved. H_x was present in fractions produced by column chromatography and centrifugal filtration that respectively indicate M_r values of more than 250,000 and more than 500,000 for critical components. Their identification should provide further insight into the signals triggering this morphogenetic alteration, as well as into the effector mechanism.

Acknowledgments

We thank L. Kerr (MBL) for preparation of critical-point-dried SEM samples, and L. Bonacci, K. Brown, A-V. Dadacay, F. Harrow, and J. Huerta (Hunter College) for additional technical contributions. Student support from the Hunter College Howard Hughes Undergrad. Biology Program, NIGMS-MBRS GM08176-18, NIGMS-MARC GM07823-18, and the NSF-REU program, as well as research support from PSC-CUNY 668201 and NSF 9808368, is gratefully acknowledged.

Literature Cited

Amende, L. M., and S. K. Pierce. 1980a. Cellular volume regulation in salinity stressed mollusks: the response of *Noetia ponderosa* (Arcidae) red blood cells to osmotic variation. *J. Comp. Physiol.* **138:** 283–289.

Amende, L. M., and S. K. Pierce. 1980b. Free amino acid mediated volume regulation of isolated *Noetia ponderosa* red cells: control by Ca2+ and ATP. *J. Comp. Physiol.* **138:** 291–298.

Bang, F. B. 1961. Reaction to injury in the oyster (*Crassostrea virginica*). *Biol. Bull.* **121:** 57–68.

Bergner A., T. Muta, S. Iwanaga, H. G. Beisel, R. Delotto, and W. Bode. 1997. Horseshoe crab coagulogen is an invertebrate protein with a nerve growth factor-like domain. *Biol. Chem.* **378:** 283–287.

Bradford, M. M. 1976. A rapid and sensitive method for the quantitation of microgram quantities of protein utilizing the principle of protein-dye binding. *Anal. Biochem.* **72:** 248–254.

Cohen, W. D. 1991. The cytoskeletal system of nucleated erythrocytes. *Int. Rev. Cytol.* **130:** 37–83.

Cohen, W. D., ed. 1997. *Compendium of Physiological Solutions. Biol. Bull. Comp.* [Online] Biological Bulletin Publications, Marine Biological Laboratory, Woods Hole, MA. Available: http://www.mbl.edu/html/BB/COMPENDIUM/Comp-TabCont.html. [1999, April 12].

Cohen, W. D., and I. Nemhauser. 1980. Association of centrioles with the marginal band of a molluscan erythrocyte. *J. Cell. Biol.* **86:** 286–291.

Cohen, W. D., and I. Nemhauser. 1985. Marginal bands and the cytoskeleton in blood cells of marine invertebrates. Pp. 1–49 in *Blood Cells of Marine Invertebrates.* W. D. Cohen, ed. Alan R. Liss, New York.

Cohen, W. D., P. B. Armstrong, J. Levin, R. L. Ornberg, I. Nemhauser, K. T. Edds, N. B. Terwilliger, R. C. Terwilliger, and S. K. Pierce. 1985. Blood cells of marine invertebrates: a practical guide. Pp. 251–279 in *Blood Cells of Marine Invertebrates,* W. D. Cohen, ed. Alan R. Liss, New York.

Dadacay, A-V. M., J. C. Huerta, C. J. Theiner, S. Swarnakar, and W. D. Cohen. 1996. Reversible alteration of molluscan erythrocyte morphology by a natural hemolymph activity. *Biol. Bull.* **191:** 276–277.

der Terrossian, E., C. Deprette, I. Lebhar, and R. Cassoly. 1994. Purification and characterization of erythrocyte caldesmon. Hypothesis for an actin-linked regulation of a contractile activity in the red blood cell membrane. *Eur. J. Biochem.* **219:** 503–511.

Feng, S. Y. 1965. Heart rate and leucocyte circulation in *Crassostrea virginica.* (Gmelin). *Biol. Bull.* **128:** 198–210.

Feng, S. Y. 1988. Cellular defense mechanisms of oysters and mussels. *Am. Fish. Soc. Spec. Publ.* **18:** 153–168.

Forer, A., and O. Behnke. 1972. An actin-like component in spermatocytes of a crane fly (*Nephrotoma suturalis* Loew). I. The spindle. *Chromosoma* **39:** 145–173.

Fowler, V. M. 1986. An actomyosin contractile mechanism for erythrocyte shape transformations. *J. Cell. Biochem.* **31:** 1–9.

Fowler, V. M., J. Q. Davis, and V. Bennett. 1985. Human erythrocyte myosin: identification and purification. *J. Cell Biol.* **100:** 47–55.

Joseph-Silverstein, J., and W. D. Cohen. 1984. The cytoskeletal system of nucleated erythrocytes. III. Marginal band function in mature cells. *J. Cell. Biol.* **98:** 2118–2125.

Joseph-Silverstein, J., and W. D. Cohen. 1985. Role of the marginal band in an invertebrate erythrocyte: evidence for a universal mechanical function. *Can. J. Biochem. Cell Biol.* **63:** 621–630.

Lee, K. G., N. Mohan, Z. Koroleva, L-F. Huang, and W. D. Cohen. 1998. Fluorescence localization of cytoskeletal proteins in fibrin-trapped cells. *Biol. Bull.* **195:** 211–212.

Nemhauser, I., J. Joseph-Silverstein, and W. D. Cohen. 1983. Centrioles as microtubule organizing centers for marginal bands of molluscan erythrocytes. *J. Cell. Biol.* **96:** 979–989.

Pasternack, G. R., and R. H. Racusen. 1989. Erythrocyte protein 4.1 binds and regulates myosin. *Proc. Natl. Acad. Sci. U.S.A.* **186:** 9712–9716.

Pierce, S. K., and T. Maugel. 1985. A comparison of the water-regulating responses of bivalve and polychaete red cells to osmotic stresses. Pp. 167–189 in *Blood Cells of Marine Invertebrates.* W. D. Cohen, ed. Alan R. Liss, New York.

Pierce, S. K., A. D. Politis, D. H. Cronkite, L. M. Rowland, and

L. H. Smith, Jr. 1989. Evidence of calmodulin involvement in cell volume recovery following hypo-osmotic stress. *Cell Calcium.* **10:** 159–169.

Ratcliffe, N. A., and A. F. Rowley, eds. 1981. *Invertebrate Blood Cells,* Vols. 1 and 2. Academic Press, London.

Sparks, A. K., and J. F. Morado. 1988. Inflammation and wound repair in bivalve molluscs. *Am. Fish. Soc. Spec. Pub.* **18:** 139–152.

Sullivan, G. E. 1961. Functional morphology, microanatomy, and histology of the "Sydney cockle," *Anadora trapezia* (Deshayes) (Lamellibranchia: Arcidae). *Aust. J. Zool.* **9:** 219–257.

Terwilliger, N. B., R. C. Terwilliger, and E. Schahtach. 1985. Intracellular respiratory proteins of sipuncula, echiura, and annelida. Pp. 193–225 in *Blood Cells of Marine Invertebrates.* W. D. Cohen, ed. Alan R. Liss, New York.

INDEX

A

A century of science: *The Biological Bulletin* looks back—and forward, 113
A cuticular secretion of the horseshoe crab, *Limulus polyphemus*: a potential anti-fouling agent, 274
A new approach for measuring real-time calcium pumping and SR function in muscle fibers, 227
Acartia tonsa, reproductive output, 294
Acetylcholine, 267
Acoustic behavior and reproduction in five species of *Corycoras* catfishes (Callichthyidae), 241
Acoustics, underwater, 241
Active factor, 174
Adamo, Shelley A., see Alison J. King, 256
Aggression, 256
Akanki, F. R., see S. J. Zottoli, 239
Alkaline gland, 82
Allelochemicals, 332
Allorejection, 188
Amazonian fish, 241
δ-aminolevulinate dehydratase, 283
An endogenous SCP-related peptide modulates ciliary beating in the gills of a venerid clam, *Mercenaria mercenaria*, 159
An ethogram of body patterning behavior in the biomedically and commercially valuable squid *Loligo pealei* off Cape Cod, Massachusetts, 49
Annelida, 14
Annual Report of the Marine Biological Laboratory, v. 197(1), R1
Annual viral expression in a sea slug population: life cycle control and symbiotic chloroplast maintenance, 1
Antennule use by the American lobster, *Homarus americanus*, during chemo-orientation in three turbulent odor plumes, 249
Anthopleura elegantissima, 72
Anti-fouling, 274
Apoptosis, 271
Armstrong, Peter B., see John M. Harrington, 274; Rengasamy Asokan, 275; Chhanda Biswas, 276
Ascidian, 188
Asokan, Rengasamy, and Peter B. Armstrong, Cellular mechanisms of hemolysis by the protein limulin, a sialic-acid-specific lectin from the plasma of the American horseshoe crab, *Limulus polyphemus*, 275
Astrocyte, 115
Atema, Jelle, see Katrin Mjos, 249; John P. Hanna, 250; Erik Zettler, 252; Cristin Berkey, 253; Leslie C. McLaughlin, 254
Avian fracture, 11

B

Bacteria, marine, 283
Balser, Elizabeth J., see Sönke Johnsen, 26
Barlow, Robert B., see Vanessa J. Ruta, 233; Justin W. Widener, 300
Barnacle, 144
Bayne, Brian L., Susanne Svensson, and John A. Nell, The physiological basis for faster growth in the Sydney rock oyster, *Saccostrea commercialis*, 377
Bearer, E. L., M. L. Schlief, X. O. Breakefield, D. E. Schuback, T. S. Reese, and J. H. LaVail, Squid axoplasm supports the retrograde axonal transport of herpes simplex virus, 257
Behavior, 49, 225
  courtship, 63
  feeding, 207, 315, 361, 377
Behavior of hemocytes in the allorejection reaction in two compound ascidians, *Botryllus scalaris* and *Symplegma reptans*, 188
Behavioral plasticity, 63
Ben-Yakir, R., see B. Rinkevich, 11
Ben-Yakir, S., see B. Rinkevich, 11
Beninger, Peter G., see Harold Silverman, 008
Berkey, Cristin, and Jelle Atema, Individual recognition and memory in *Homarus americanus* male-female interactions, 253
Billack, Blase, Jeffrey D. Laskin, Michael A. Gallo, and Diane E. Heck, Effects of α-bungarotoxin on development of the sea urchin *Arbacia punctulata*, 267
Bioacoustics, 241, 242
Bioenergetics, 377
Bioluminescence, 26, 132, 348
Bioluminescence in the deep-sea cirrate octopod *Stauroteuthis syrtensis* Verrill (Mollusca: Cephalopoda), 26
Biosynthesis of tyrosine O-sulfate by cell proteoglycan from the marine sponge, *Microciona prolifera*, 279
Biswas, Chhanda, and Peter B. Armstrong, Identification of a hemolytic activity in the plasma of the gastropod *Busycon canaliculatum*, 276
Bivalve feeding, 368
Blackburn, John G., see Gregory M. Grabowski, 82
Blood clam, 395
Body coloration, 49
Bolton, Toby F., see Florence I. M. Thomas, 7
Botryllus scalaris, 188
Bowen, J., see A. Evgenidou, 292
Boyle, Kim-Laura, see Roger T. Hanlon, 49
Brain slice, 115
Breakefield, X. O., see E. L. Bearer, 257
Bringing the script to life: the role of muscle in behavior, 225
Brooding, 104
Brown, E., see A. Evgenidou, 292
Bunge, Richard P., see Geoffrey K. Ganter, 40
Buoyancy, 309
Burger, Max M., see Jane C. Kaltenbach, 271; William J. Kuhns, 277; Octavian Popescu, 279
Bushmann, Paul J., Concurrent signals and behavioral plasticity in blue crab (*Callinectes sapidus* Rathbun) courtship, 63
Buskey, E. J., see D. K. Hartline, 132
Byrne, Maria, see Francis Chee, 123

C

Calcium, 115, 227, 229, 268
Calliactis japonica, 315
Camouflage, 348
Cancer irroratus, 361
Candelario-Martinez, Aurora, see Louis F. Gainey, Jr., 159
Canfield, Susannah, Luc Claessens, Charles Hopkinson Jr., Edward Rastetter, and Joseph Vallino, Long-term effect of municipal water use on the water budget of the Ipswich River Basin, 295
Carbohydrates, 94
Carbon translocation, 72
Carcinus meanus, 297
Cebrián, J., see A. Evgenidou, 292
Cell morphology, 395
Cell shape transformation, 395
Cellular mechanisms of hemolysis by the protein limulin, a sialic-acid-specific lectin from the plasma of the American horseshoe crab, *Limulus polyphemus*, 275

Central nervous system, 240
Centrifuge microscopy, 260
Cephalopod, 26, 256
Chaga, Oleg, see Steven Q. Irvine, 319
Chapparo, O. R., R. J. Thompson, and C. J. Emerson, The velar ciliature in the brooded larva of the Chilean oyster *Ostrea chilensis* (Philippi, 1845), 104
Chee, Francis, and Maria Byrne, Development of the larval serotonergic nervous system in the sea star *Patiriella regularis* as revealed by confocal imaging, 123
Chemical cues, 94
Chemo-orientation turbulence, 249, 250
Chemoreceptor cells as concentration slope detectors: preliminary evidence from the lobster nose, 252
Chemoreceptor filter properties, 252
Chemoreception, 361
Chemotaxis, 250
Child, Alice, see Aimee Vasse, 281
Cilia
  bands, 14
  beating, 159
  in feeding, 14
  velar, 104
Circadian rhythms, 233
Cirri, 008
Claessens, Luc, see Katherine M. Pease, 289; Susannah Canfield, 295
Clam, 159
Clay, John R., and Alan M. Kuzirian, Fluorescence localization of K+ channels in the membrane of squid giant axons, 231
Cohen, William D., see Christine Lema-Foley, 395
Colony specificity, 188
Columba livia, 11
Communication, 49
Concentration slope detectors, 252
Concepts in Imaging and Microscopy: Exploring biological structure and function with confocal microscopy, 115
Concurrent signals and behavioral plasticity in blue crab (*Callinectes sapidus* Rathbun) courtship, 63
Confocal microscopy, 115, 262, 263
Contact with squid eggs increases agonistic behavior in male squid (*Loligo pealei*), 256
Copepod, 132
Coral reef, 303
Coral reef fish, 242
Coralline algae, 332
Corcoran, A., see A. Evgenidou, 292
Corcoran, D., see A. Evgenidou, 292
Countershading, 348
Courtship, 63
Courtship sounds of the Pacific damselfish, *Abudefduf sordidus* (Pomacentridae), 242
Crab, 63, 174, 361
Crain, Jennifer A., Functional morphology of prey ingestion by *Placetron wosnessenskii* Schalfeew zoeae (Crustacea: Anomura: Lithodidae), 207
Cropping of sea anemone tentacles by a symbiotic barnacle, 315
Crustacea, 144, 348, 361
Cubbage, Andrea, David Lawrence, Gabrielle Tomasky, and Ivan Valiela, Relationship of reproductive output in *Acartia tonsa*, chlorophyll concentration, and land-derived nitrogen loads in estuaries of Waquoit Bay, Massachusetts, 294
Cyclodextrin, 284
Cyprid, 144
Cytochrome P450, 303

D

D'Ambrosio, A., see A. Evgenidou, 292
Dailey, Michael, Glen Marrs, Jakob Satz, and Marc Waite, Concepts in Imaging and Microscopy: Exploring biological structure and function with confocal microscopy, 115
Damselfish, 242, 244
Dearholt, C., see A. Evgenidou, 292
Decline of a horseshoe crab population on Cape Cod, 300
Deegan, Linda, see Talia Young, 297; Sharon Komarow, 299
Deep sea, 26, 348
Defense mechanism, 281
Degnan, Bernard M., and Craig R. Johnson, Inhibition of settlement and metamorphosis of the ascidian *Herdmania curvata* by non-geniculate coralline algae, 332
Deming, Nicole M., see Robert B. Silver, 268
Density, 309
DePina, Ana S., see Torsten Wöllert, 265
Desai, Arshad, see Paul Maddox, 263
Development, 123, 267, 319, 341
Development of the larval serotonergic nervous system in the sea star *Patiriella regularis* as revealed by confocal imaging, 123
Diatom, 292
Dictyostelium, 260
Dietz, Thomas H., see Harold Silverman, 368
Dinoflagellate, 292
Dioxin, 303
Disease, 237
Displays, 49
DNA-PK in development, 341
Doble, Karen E., see Louis F. Gainey, Jr., 159
Dodge, Frederick A., see Vanessa J. Ruta, 233
Dorsal cell, 239
Dynamic confocal imaging of interphase and mitotic microtubules in the fission yeast, *S. pombe*, 262
Dynamic confocal imaging of mitochondria in swimming *Tetrahymena* and of microtubule poleward flux in *Xenopus* extract spindles, 263
Dynein, 259

E

Echinoid, life history, 7
Echiuridae, 14
Edds-Walton, P. L., see R. R. Fay, 240
Edwards, Kristin A., see Florence I. M. Thomas, 7
Effects of α-bungarotoxin on development of the sea urchin *Arbacia punctulata*, 267
Effects of green tea polyphenols on lens photooxidative stress, 285
Effects of increased nitrogen loading on the abundance of diatoms and dinoflagellates in estuarine phytoplanktonic communities, 292
Effects of vanadate on actin-dependent vesicle motility in extracts of clam oocytes, 265
Elasmobranch, 82
Electrophysiology, 82
Electroretinogram, 348
Ellipsosomes, 235
Elysia, 1
Emerson, C. J., see Benjamin G. Miner, 14; O. R. Chaparro, 104; Dovi Kelman, 309
Empson, Ruth M., see Jyotshna Kanungo, 341
Endosymbiosis, 1
Engebretson, Hilary P., and Giséle Muller-Parker, Translocation of photosynthetic carbon from two algal symbionts to the sea anemone *Anthopleura elegantissima*, 72
Enhancement of the response of rock crabs, *Cancer irroratus*, to prey odors following feeding experience, 361
Epidermal growth factor, 198
Erythrocyte, 395
Escape behavior kinematics, 132
Ethogram, 49
Eutrophication, 290
Evaluation of a reporter gene system biomarker for detecting contamination in tropical marine sediments, 303
Evaluation of circadian rhythms in the *Limulus* eye, 233
Evgenidou, A., A. Konkle, A. D'Ambrosio, A. Corcoran, J. Bowen, E. Brown, D. Corcoran, C. Dearholt, S. Fern, A. Lamb, J. Michalowsky, I. Ruegg, and J. Cebrian, Effects of increased nitrogen

loading on the abundance of diatoms and dinoflagellates in estuarine phytoplanktonic communities, 292
Evolution, 26, 198, 319
Extracellular survival of an intracellular parasite (*Spraguea lophii*, Microsporea), 270

F

Fay, R. R., and P. L. Edds-Walton, Sharpening of directional auditory input in the descending octaval nucleus of the toadfish, *Opsanus tau*, 240
Feeding, 207
  barnacle, 315
  bivalve, 368
Feinstein, Douglas L., see Robert Gould, 259
Fern, S., see A. Evgenidou, 292
Fertilization, 7
Findley, Ann, see Earl Weidner, 270
Fish
  Amazonian, 241
  Coral reef, 242
Fisher, Erin C., see Sönke Johnsen, 26
Fluorescence localization of K+ channels in the membrane of squid giant axons, 231
Fluorescence speckle microscopy, 263
Foraging, 361
Frank, T. M., see S. M. Lindsay, 348
Freund, Concetta, see Robert Gould, 259
Fukui, Yoshio, Taro Q. P. Uyeda, Chikako Kitayama, and Shinya Inoué, Migration forces in *Dictyostelium* measured by centrifuge DIC microscopy, 260
Functional and evolutionary implications of opposed bands, big mouths, and extensive oral ciliation in larval opheliids and echiurids (Annelida), 14
Functional morphology, 207
Functional morphology of prey ingestion by *Placetron wosnessenskii* Schalfeew zoeae (Crustacea: Anomura: Lithodidae), 207

G

G proteins, 388
Gainey, Louis F., Jr., Kelly J. Vining, Karen E. Doble, Jennifer M. Waldo, Aurora Candelario-Martinez, and Michael J. Greenberg, An endogenous SCP-related peptide modulates ciliary beating in the gills of a venerid clam, *Mercenaria mercenaria*, 159
β-galactosidase, 40
Gallo, Michael A., see Blase Billack, 267
Gamete properties, 7
Gamulin, Vera, see Alexander Skorokhod, 198
Ganter, Geoffrey K., Ralf Heinrich, Richard P. Bunge, and Edward A. Kravitz, Long-term culture of lobster central ganglia: expression of foreign genes in identified neurons, 40
Garritt, Robert, see Talia Young, 297; Sharon Komarow, 299
GFP-tubulin, 262
Glial cells,
Glutathione S-transferase, 268
Gould, Robert, Concetta Freund, Frank Palmer, Pamela E. Knapp, Jeff Huang, Hilary Morrison, and Douglas L. Feinstein: Messenger mRNAs for kinesins and a dynein are located in neural processes, 259
Grabowski, Gregory M., John G. Blackburn, and Eric R. Lacy, Morphology and epithelial ion transport of the alkaline gland in the Atlantic stingray (*Dasyatis sabina*), 82
Grasso, Frank, see Katrin Mjos, 249; John P. Hanna, 250
Green crab, 297
Green tea polyphenols, 285
Green-fluorescent protein, 40
Greenberg, Michael J., A century of science: *The Biological Bulletin* looks back—and forward, 113
Greenberg, Michael J., see Louis F. Gainey, Jr., 159
Growth, 377
Gundacker, Dietmar, see Alexander Skorokhod, 198

H

Hanley, Janice S., Nadav Shashar, Roxanna Smolowitz, William Mebane, and Roger T. Hanlon, Soft-sided tanks improve long-term health of cultured cuttlefish, 237
Hanlon, Roger T., Michael R. Maxwell, Nadav Shashar, Ellis R. Loew, and Kim-Laura Boyle, An ethogram of body patterning behavior in the biomedically and commercially valuable squid *Loligo pealei* off Cape Cod, Massachusetts, 49
Hanlon, Roger T., see Janice S. Hanley, 237; Kathleen Q. Tang, 247; Alison J. King, 256
Hanna, John P., Frank W. Grasso, and Jelle Atema, Temporal correlation between sensor pairs in different plume positions: a study of concentration information available to the American lobster, *Homarus americanus*, during chemotaxis, 250
Hanten, Jeffrey J., see Sidney K. Pierce, 1
Hárosi, Ferenc I., see Iñigo Novales Flamarique, 235
Harrington, John M., and Peter B. Armstrong, A cuticular secretion of the horseshoe crab, *Limulus polyphemus*: a potential anti-fouling agent, 274
Harrison, Paul J. H., and David C. Sandeman, Morphology of the nervous system of the barnacle cypris larva (*Balanus amphitrite* Darwin) revealed by light and electron microscopy, 144
Hartline, D. K., E. J. Buskey, and P. H. Lenz, Rapid jumps and bioluminescence elicited by controlled hydrodynamic stimuli in a mesopelagic copepod, *Pleuromamma xiphias*, 132
Hatching, crab, 174
Hearing, 240
Heck, Diane E., see Blase Billack, 267
Heinrich, Ralf, see Geoffrey K. Ganter, 40
Hemocyanin, 276
Hemocytes, 188
Hemolysis, 275, 276
Herpes virus, 257
Hippocampus, 115
Hirose, Euichi, see Maki Shirae, 188
Hiza, N. A., see S. J. Zottoli, 239
Ho-Sang, D. A. Jr., see S. J. Zottoli, 239
Homarus americanus, 249, 252, 253, 254
Hopkinson, Charles Jr., see Katherine M. Pease, 289; Susannah Canfield, 295
Hoskin, Francis C. G., Diane M. Steeves, and John E. Walker, Substituted cyclodextrin as a model for a squid enzyme that hydrolyzes the nerve gas soman, 284
5-HT neurogenesis, 123
Huang, Jeff, see Robert Gould, 259
Hyaluronic acid, 277
Hyaluronic acid: a component of the aggregation factor secreted by the marine sponge, *Microciona prolifera*, 277
Hyaluronic acid binding protein, 277
Hydrostatic pressure, 388
Hydrostatic pressure alters the time course of GTP[S] binding to G proteins in brain membranes from two congeneric marine fishes, 388

I

Identification of a hemolytic activity in the plasma of the gastropod *Busycon canaliculatum*, 276
Identified neurons, 40
Immunity, 274
Immunocytochemistry, 231
Increased lability of estuarine dissolved organic nitrogen from urbanized watersheds, 290
Individual recognition, 253, 254
Individual recognition and memory in *Homarus americanus* male-female interactions, 253

Influence of marsh flooding on the abundance and growth of *Fundulus heteroclitus* in salt marsh creeks, 299

Ingestion, 207

Ingoglia, Mark J., see Lisa M. Kerr, 303

Inhibition of settlement and metamorphosis of the ascidian *Herdmania curvata* by non-geniculate coralline algae, 332

Inoué, Shinya, see Yoshio Fukui, 260; P. T. Tran, 262; Paul Maddox, 263

Insulin receptor-like tyrosine kinase, 198

Intense concanavalin A staining and apoptosis of peripheral flagellated cells in larvae of the marine sponge *Microciona prolifera*: significance in relation to morphogenesis, 271

Interior, Rey, see Octavian Popescu, 279

Internal fixation, 11

Invertebrate
  reproduction, 7
  larvae, 207

Ion channels, 231

Ipswich River, 289, 295

Ipswich River nutrient dynamics: preliminary assessment of a simple nitrogen-processing model, 289

Irvine, Steven Q., Oleg Chaga, and Mark Q. Martindale, Larval ontogenetic stages of *Chaetopterus*: developmental heterochrony in the evolution of chaetopterid polychaetes, 319

Iwasaki, Hiroshi, see Masayuki Saigusa, 174

J

Johnsen, Sönke, Elizabeth J. Balser, Erin C. Fisher, and Edith A. Widder, Bioluminescence in the deep-sea cirrate octopod *Stauroteuthis syrtensis* Verrill (Mollusca: Cephalopoda), 26

Johnson, Craig R., see Bernard M. Degnan, 332

Johnston atoll, 242

K

Kaatz, Ingrid M., and Phillip S. Lobel, Acoustic behavior and reproduction in five species of *Corycoras* catfishes (Callichthyidae), 241

Kaltenbach, Jane C., William J. Kuhns, Tracy L. Simpson, and Max M. Burger, Intense concanavalin A staining and apoptosis of peripheral flagellated cells in larvae of the marine sponge *Microciona prolifera*: significance in relation to morphogenesis, 271

Kanungo, Jyotshna, Ruth M. Empson, and Howard Rasmussen, Microinjection of an antibody to the Ku protein arrests development in sea urchin embryos, 341

Kapoor, Tarun, see Paul Maddox, 263

Kavsan, Vadim, see Alexander Skorokhod, 198

Kelman, Dovi, and Richard B. Emlet, Swimming and buoyancy in ontogenetic stages of the cushion star *Pteraster tesselatus* (Echinodermata: Asteroidea) and their implications for distribution and movement, 309

Kent, J., see S. M. Lindsay, 348

Kerr, Lisa M., Phillip S. Lobel, and J. Mark Ingoglia, Evaluation of a reporter gene system biomarker for detecting contamination in tropical marine sediments, 303

Kerr, Lisa M., see Phillip S. Lobel, 242

Kilham, N., see Katherine M. Pease, 289

Kinesin, 259

King, Alison J., Shelley A. Adamo, and Roger T. Hanlon, Contact with squid eggs increases agonistic behavior in male squid (*Loligo pealei*), 256

Kitayama, Chikako, see Yoshio Fukui, 260

Klimov, Andrei A., see Lawrence C. Rome, 227

Knapp, Pamela E., see Robert Gould, 259

Koleolepas avis, 315

Komarow, Sharon, Talia Young, Linda Deegan, and Robert Garritt, Influence of marsh flooding on the abundance and growth of *Fundulus heteroclitus* in salt marsh creeks, 299

Komarow, Sharon, see Talia Young, 297

Konkle, A., see A. Evgenidou, 292

Koroleva, Zoya, see Christine Lema-Foley, 395

Kravitz, Edward A., see Geoffrey K. Ganter, 40

Kroeger, Kevin D., see Felisa L. Wolfe, 290

Krug, Patrick J., and Adriana E. Manzi, Waterborne and surface-associated carbohydrates as settlement cues for larvae of the specialist marine herbivore *Alderia modesta*, 94

Ku antigen, 341

Kuhns, William J., Max M. Burger, and Eva Turley, Hyaluronic acid: a component of the aggregation factor secreted by the marine sponge, *Microciona prolifera*, 277

Kuhns, William J., see Jane C. Kaltenbach, 271; Octavian Popescu, 279

Kuzirian, Alan M., see John R. Clay, 231

L

Lability, 290

Lacy, Eric R., see Gregory M. Grabowski, 82

Lamb, A., see A. Evgenidou, 292

Langford, George M., see Torsten Wöllert, 265

Larva, 104, 123, 207, 309
  cypris, 144
  feeding, 14
  nonfeeding, 309
  settlement, 94

Larval ecology, 207

Larval ontogenetic stages of *Chaetopterus*: developmental heterochrony in the evolution of chaetopterid polychaetes, 319

Laskin, Jeffrey D., see Blase Billack, 267

Lateral inhibition, 233

Latz , M. I., see S. M. Lindsay, 348

LaVail, J. H., see E. L. Bearer, 257

Lawrence, David, see Andrea Cubbage, 294

Lead (Pb), 283

Lectin staining, 271

Lee, Kyeng G., see Christine Lema-Foley, 395

Lema-Foley, Christine, Kyeng G. Lee, Tchaiko Parris, Zoya Koroleva, Nishal Mohan, Pierre Noailles, and William D. Cohen, Reversible alteration of morphology in an invertebrate erythrocyte: properties of the natural inducer and the cellular response, 395

Lens, 285

Lenz, P. H., see D. K. Hartline, 132

Leukotriene B4, 268

Leukotriene B4 as calcium agonist for nuclear envelope breakdown: an enzymological survey of endomembranes of mitotic cells, 268

Lewis, Nathaniel, see Seymour Zigman, 285

Life cycle, 1

Life history, 7

Limulin, 275

Limulus, 233, 274, 275, 300

Lindsay, S. M., T. M. Frank, J. Kent, J. C. Partridge, and M. I. Latz, Spectral sensitivity of vision and bioluminescence in the midwater shrimp *Sergestes similis*, 348

Lobel, Phillip S., and Lisa M. Kerr, Courtship sounds of the Pacific damselfish, *Abudefduf sordidus* (Pomacentridae), 242

Lobel, Phillip S., see Ingrid M. Kaatz, 241; Lisa M. Kerr, 303

Lobster, 40, 249, 252, 253, 254
  chemo-orientation, 249

Loew, Ellis R., see Roger T. Hanlon, 49

Loligo pealei, 49

Long-term culture of lobster central ganglia: expression of foreign genes in identified neurons, 40

Long-term effect of municipal water use on the water budget of the Ipswich River Basin, 295

Lynn, John W., see Harold Silverman, 008

M

Maddox, Paul, Arshad Desai, E. D. Salmon, T. J. Mitchison, Karen Oogema, Tarun Kapoor, Brian Matsumoto, and Shinya Inoué, Dynamic confocal imaging of mitochondria in swimming *Tetrahymena* and of microtubule poleward flux in *Xenopus* extract spindles, 263

Maddox, P., see P. T. Tran, 262
Malchow, Robert Paul, and David J. Ramsey, Responses of retinal Müller cells to neurotransmitter candidates: a comparative study, 229
Manzi, Adriana E., see Patrick J. Krug, 94
Marginal band, 395
Mariculture, 237
Marrs, Glen, see Michael Dailey, 115
Marsh flooding, 299
Martindale, Mark Q., see Steven Q. Irvine, 319
Mating
  behavior, 300
  systems, 256
Matsumoto, Brian, see Paul Maddox, 263
Maugel, Timothy K., see Sidney K. Pierce, 1
Maxwell, Michael R., see Roger T. Hanlon, 49
McLaughlin, Leslie C., Jennifer Walters, Jelle Atema, and Norman Wainwright, Urinary protein concentration in connection with agonistic interactions in *Homarus americanus*, 254
Mebane, William, see Janice S. Hanley, 237
Mechanical resistance to shear stress: the role of echinoderm egg extracellular layers, 7
Mechanosensory thresholds, 132
Memory, 253
Mensinger, Allen F., see Nichole N. Price, 246, Kathleen Q. Tang, 247
Mercenaria mercenaria, 159
Messenger mRNAs for kinesins and a dynein are located in neural processes, 259
Metabolic efficiency, 377
Metamorphosis, 94
Michalowsky, J., see A. Evgenidou, 292
Microciona prolifera, 277, 279
Microglia, 115
Microinjection of an antibody to the Ku protein arrests development in sea urchin embryos, 341
Microspectrophotometry, 348
Microsporidian, 270
Microtubule, 262, 263
Migration forces, 260
Miner, Benjamin G., Eric Sanford, Richard R. Strathmann, Bruno Pernet, and Richard B. Emlet, Functional and evolutionary implications of opposed bands, big mouths, and extensive oral ciliation in larval opheliids and echiurids (Annelida), 14
Misevic, Gradimir, see Octavian Popescu, 279
Mitchison, T. J., see Paul Maddox, 263
Mjos, Katrin, Frank Grasso, and Jelle Atema, Antennule use by the American lobster, *Homarus americanus*, during chemo-orientation in three turbulent odor plumes, 249
Mohan, Nishal, see Christine Lema-Foley, 395
Mollusc, 276
Mondrup, Thomas, Salinity effects on nutrient dynamics in estuarine sediments investigated by a plug-flux method, 287
Mondy, William L., see Sidney K. Pierce, 1
Morphology, 82, 144, 319
Morphology and epithelial ion transport of the alkaline gland in the Atlantic stingray (*Dasyatis sabina*), 82
Morphology of the nervous system of the barnacle cypris larva (*Balanus amphitrite* Darwin) revealed by light and electron microscopy, 144
Morrison, Hilary, see Robert Gould, 259
Morula cell, 188
Motta, M., see S. J. Zottoli, 239
Müller, Isabel M., see Alexander Skorokhod, 198
Müller, Werner E. G., see Alexander Skorokhod, 198
Muller-Parker, Giséle, see Hilary P. Engebretson, 72
Mummichog, 299
Murray, Thomas F., see Joseph F. Siebenaller, 388
Muscle, 225, 227
Mussel, 008
Myosin-dependent vesicle transport, 265
Mytilus edulis, 008

N

Natural population, 300
Necrosis, 332
Nell, John A., see Brian L. Bayne, 377
Nerve gas, 284
Nervous system, 144
Neurogenesis, 123
Neuron, 115
  identifiable, 239
  supramedullary, 239
Neuropeptides, 159
Nitrogen
  cycling, 287, 289
  dissolved organic, 290
  land-derived, 294
  model, 289
Noailles, Pierre, see Christine Lema-Foley, 395
Noetia ponderosa, 395
Novales Flamarique, Iñigo, and Ferenc I. Hárosi, Photoreceptor pigments of the blueback herring (*Alosa aestevalis*, Clupeidae) and the Atlantic silverside (*Menidia menidia*, Atherinidae), 235
Nuclear envelope breakdown, 268
Nutrient loading, 292

O

O'Neill, Maureen D., see Kathleen Q. Tang, 247
Octopus, 26
Odor, 361
Ogunseitan, O. A., S. L. Yang, and E. Scheinbach, The δ-aminolevulinate dehydratase of marine *Vibrio alginolyticus* is resistant to lead (Pb), 283
Oligodendrocyte, 259
Oliver, Steven J., and Elise Watson, Threat-sensitive nest defense in domino damselfish (*Dascyllus albisella*), 244
Oogema, Karen, see Paul Maddox, 263
Opheliidae, 14
Opisthobranch, 94
Organ culture, 40
Origin of insulin receptor-like tyrosine kinases in marine sponges, 198
Ostrea chilensis, 104
Ovigerous-hair stripping substance (OHSS) in an estuarine crab: purification, preliminary characterization, and appearance of the activity in the developing embryos, 174
Oyster, 104, 377

P

Palmer, Frank, see Robert Gould, 259
Parasitism, 315
Parris, Tchaiko, see Christine Lema-Foley, 395
Particle capture, 368
Partridge, J. C., see S. M. Lindsay, 348
Patiriella regularis, 123
Paul, Robert, see Robert Paul Malchow, 229
Pease, Katherine M., L. Claessens, C. Hopkinson, E. Rastetter, J. Vallino, and N. Kilham, Ipswich River nutrient dynamics: preliminary assessment of a simple nitrogen-processing model, 289
Pentose phosphate pathway, 268
Pernet, Bruno, see Benjamin G. Miner, 14
Phospholipase A2, 268
Photo-oxidation, 285
Photoreceptor pigments of the blueback herring (*Alosa aestevalis*, Clupeidae) and the Atlantic silverside (*Menidia menidia*, Atherinidae), 235
Physiological characterization of supramedullary/dorsal neurons of the cunner, *Tautogolabrus adspersus*, 239
Physiology, 377
Phytoplankton biomass, 294
Pierce, Sidney K., Timothy K. Maugel, Mary E. Rumpho, Jeffrey J. Hanten, and William L. Mondy, Annual viral expression in a sea

slug population: life cycle control and symbiotic chloroplast maintenance, 1
Polarization, 49
Polychaete, 14, 319
Polyclonal antibody, 174
Pomacentrid, 244
Popescu, Octavian, Rey Interior, Gradimir Misevic, Max M. Burger, and William J. Kuhns, Biosynthesis of tyrosine O-sulfate by cell proteoglycan from the marine sponge, *Microciona prolifera*, 279
Population size and summer home range of the green crab, *Carcinus maenus*, in salt marsh tidal creeks, 297
Predation, 246, 361
Predator-prey interactions of juvenile toadfish, *Opsanus tau*, 246
Price, Nichole N., and Allen F. Mensinger, Predator-prey interactions of juvenile toadfish, *Opsanus tau*, 246
Price, Nichole N., see Kathleen Q. Tang, 247
Prophenoloxidase, 281
Prophenoloxidase is not activated by microbial signals in *Limulus polyphemus*, 281
Protein tyrosine phosphatase, in clam oocyte extracts, 265
Purification, 174

R

Rafferty, Keen A., see Seymour Zigman, 285
Rafferty, Nancy S., see Seymour Zigman, 285
Ramsey, David J., see Robert Paul Malchow, 229
Rapid jumps and bioluminescence elicited by controlled hydrodynamic stimuli in a mesopelagic copepod, *Pleuromamma xiphias*, 132
Rasmussen, Howard, see Jyotshna Kanungo, 341
Rastetter, Edward, see Katherine M. Pease, 289; Susannah Canfield, 295
Real-time confocal system, 263
Rebach, Steve, see Andrew Ristvey, 361
Reese, T. S., see E. L. Bearer, 257
Regeneration of amputated avian bone by a coral skeletal implant, 11
Relationship of reproductive output in *Acartia tonsa*, chlorophyll concentration, and land-derived nitrogen loads in estuaries of Waquoit Bay, Massachusetts, 294
Reproduction, 82
Response latency, 233
Responses of retinal Müller cells to neurotransmitter candidates: a comparative study, 229
Retina, 229
Retrograde axonal transport, 257
Retrovirus, 1
Reversible alteration of morphology in an invertebrate erythrocyte: properties of the natural inducer and the cellular response, 395
Rinkevich, B., S. Ben-Yakir, and R. Ben-Yakir, Regeneration of amputated avian bone by a coral skeletal implant, 11
Ristvey, Andrew, and Steve Rebach, Enhancement of the response of rock crabs, *Cancer irroratus*, to prey odors following feeding experience, 361
RNA-injection, 40
Rock crab, 361
Rome, Lawrence C., Andrei A. Klimov, and Iain S. Young, A new approach for measuring real-time calcium pumping and SR function in muscle fibers, 227
Rome, Lawrence C., Bringing the script to life: the role of muscle in behavior, 225
Ruegg, I., see A. Evgenidou, 292
Rumpho, Mary E., see Sidney K. Pierce, 1
Ruta, Vanessa J., Frederick A. Dodge, and Robert B. Barlow, Evaluation of circadian rhythms in the *Limulus* eye, 233

S

Saigusa, Masayuki, and Hiroshi Iwasaki, Ovigerous-hair stripping substance (OHSS) in an estuarine crab: purification, preliminary characterization, and appearance of the activity in the developing embryos, 174
Saito, Yasunori, see Maki Shirae, 188
Salinity, 287
Salinity effects on nutrient dynamics in estuarine sediments investigated by a plug-flux method, 287
Salmon, E. D., see Paul Maddox, 263
Salt marsh, 297, 299
Sandeman, David C., see Paul J. H. Harrison, 144
Sanford, Eric, see Benjamin G. Miner, 14
Sarcoplasmic reticulum, 227
Satz, Jakob, see Michael Dailey, 115
Scheinbach, E., see O. A. Ogunseitan, 283
Schlief, M. L., see E. L. Bearer, 257
Schuback, D. E., see E. L. Bearer, 257
Sea anemone, 72
Sea slug, 1
Sea star, 123, 309
Search image, 361
Sebastolobus
  alascanus, 388
  altivelis, 388
Sediment, 287
Sepia, 237
Sergestes, 348
Settlement, ascidian, 332
Sewell, Mary A., see Florence I. M. Thomas, 7
Seyfarth, E.-A., see S. J. Zottoli, 239
Sharpening of directional auditory input in the descending octaval nucleus of the toadfish, *Opsanus tau*, 240
Shashar, Nadav, see Roger T. Hanlon, 49; Janice S. Hanley, 237
Shirae, Maki, Euichi Hirose, and Yasunori Saito, Behavior of hemocytes in the allorejection reaction in two compound ascidians, *Botryllus scalaris* and *Symplegma reptans*, 188
Shrimp, 348
Siebenaller, Joseph F., and Thomas F. Murray, Hydrostatic pressure alters the time course of GTP[S] binding to G proteins in brain membranes from two congeneric marine fishes, 388
Signaling, 49, 63
Silver, Robert B., and Nicole M. Deming, Leukotriene B4 as calcium agonist for nuclear envelope breakdown: an enzymological survey of endomembranes of mitotic cells, 268
Silverman, Harold, John W. Lynn, Peter G. Beninger, and Thomas H. Dietz, The role of latero-frontal cirri in particle capture by the gills of *Mytilus edulis*, 368
Simpson, Tracy L., see Jane C. Kaltenbach, 271
Skeleton, 11
Skorokhod, Alexander, Vera Gamulin, Dietmar Gundacker, Vadim Kavsan, Isabel M. Müller, and Werner E. G. Müller, Origin of insulin receptor-like tyrosine kinases in marine sponges, 198
Smolowitz, Roxanna, see Janice S. Hanley, 237
Soft-sided tanks improve long-term health of cultured cuttlefish, 237
Soman, 284
Sound source localization, 240
Spawning, 7
Spectral sensitivity of vision and bioluminescence in the midwater shrimp *Sergestes similis*, 348
Sperm, 82
Sponge, 198, 271, 277, 279
Sporoplasm, 270
Squid, 49, 256
  axons, 231, 257
Squid axoplasm supports the retrograde axonal transport of herpes simplex virus, 257
Steeves, Diane M., see Francis C. G. Hoskin, 284
Stingray, 82
Strathmann, Richard R., see Benjamin G. Miner, 14
Stylophora pistillata, 11
Substituted cyclodextrin as a model for a squid enzyme that hydrolyzes the nerve gas soman, 284
Summer home range, 297
Supramedullary neurons, 239
Svensson, Susanne, see Brian L. Bayne, 377
Swimbladder, 225

Swimming, 309

Swimming and buoyancy in ontogenetic stages of the cushion star *Pteraster tesselatus* (Echinodermata: Asteroidea) and their implications for distribution and movement, 309

Symbiosis, 1, 72, 315

Symplegma reptans, 188

T

Tan, X., see S. J. Zottoli, 239

Tang, Kathleen Q., Nichole N. Price, Maureen D. O'Neill, Allen F. Mensinger, and Roger T. Hanlon, Temperature effects on first-year growth of cultured oyster toadfish, *Opsanus tau*, 247

Teleost, 246

Temperature effects on first-year growth of cultured oyster toadfish, *Opsanus tau*, 247

Temporal correlation between sensor pairs in different plume positions: a study of concentration information available to the American lobster, *Homarus americanus*, during chemotaxis, 250

Territoriality, interspecific, 244

The δ-aminolevulinate dehydratase of marine *Vibrio alginolyticus* is resistant to lead (Pb), 283

The physiological basis for faster growth in the Sydney rock oyster, *Saccostrea commercialis*, 377

The role of latero-frontal cirri in particle capture by the gills of *Mytilus edulis*, 368

The velar ciliature in the brooded larva of the Chilean oyster *Ostrea chilensis* (Philippi, 1845), 104

Thomas, Florence I. M., Kristin A. Edwards, Toby F. Bolton, Mary A. Sewell, and Jill M. Zande, Mechanical resistance to shear stress: the role of echinoderm egg extracellular layers, 7

Thompson, R. J., see O. R. Chaparro, 104

Threat-sensitive nest defense in domino damselfish (*Dascyllus albisella*), 244

Time-lapse, 115

Toadfish, 225, 227, 240, 246, 247

Tomasky, Gabrielle, see Andrea Cubbage, 294

Tran, P. T., P. Maddox, and S. Inoué, Dynamic confocal imaging of interphase and mitotic microtubules in the fission yeast, *S. pombe*, 262

Translocation of photosynthetic carbon from two algal symbionts to the sea anemone *Anthopleura elegantissima*, 72

Trochophore, 14

Turley, Eva, see William J. Kuhns, 277

Tyrosine O-sulfate, 279

Tyrosine sulfation substrates, 279

U

Ultrastructure, 144

Urchin, 267

Urinary protein, 254

Urinary protein concentration in connection with agonistic interactions in *Homarus americanus*, 254

Uyeda, Taro Q. P., see Yoshio Fukui, 260

V

Valiela, Ivan, see Felisa L. Wolfe, 290; Andrea Cubbage, 294

Vallino, Joseph, see Katherine M. Pease, 289; Susannah Canfield, 295

Vanadate, 265

Vasse, Aimee, Alice Child, and Norman Wainwright, Prophenoloxidase is not activated by microbial signals in *Limulus polyphemus*, 281

Veliger, 104

Velum, 104

Vining, Kelly J., see Louis F. Gainey, Jr., 159

Vision, 235

Visual pigment, 235, 348

W

Wainwright, Norman, see Leslie C. McLaughlin, 254; Aimee Vasse, 281

Waite, Marc, see Michael Dailey, 115

Waldo, Jennifer M., see Louis F. Gainey, Jr., 159

Walker, John E., see Francis C. G. Hoskin, 284

Walters, Jennifer, see Leslie C. McLaughlin, 254

Water budget, 295

Waterborne and surface-associated carbohydrates as settlement cues for larvae of the specialist marine herbivore *Alderia modesta*, 94

Watson, Elise, see Steven J. Oliver, 244

Watts, K. M., see S. J. Zottoli, 239

Weidner, Earl, and Ann Findley, The extracellular survival of an intracellular parasite (*Spraguea lophii*, Microsporea), 270

Widder, Edith A., see Sönke Johnsen, 26

Widener, Justin W., and Robert B. Barlow, Decline of a horseshoe crab population on Cape Cod, 300

Wolfe, Felisa L., Kevin D. Kroeger, and Ivan Valiela, Increased lability of estuarine dissolved organic nitrogen from urbanized watersheds, 290

Wöllert, Torsten, Ana S. DePina, and George M. Langford, The effects of vanadate on actin-dependent vesicle motility in extracts of clam oocytes, 265

Y

Yamato, Shigeyuki, see Yoichi Yusa, 315

Yang, S. L., see O. A. Ogunseitan, 283

Young, Iain S., see Lawrence C. Rome, 227

Young, Talia, Sharon Komarow, Linda Deegan, and Robert Garritt, Population size and summer home range of the green crab, *Carcinus maenus*, in salt marsh tidal creeks, 297

Young, Talia, see Sharon Komarow, 299

Yusa, Yoichi, and Shigeyuki Yamato, Cropping of sea anemone tentacles by a symbiotic barnacle, 315

Z

Zande, Jill M., see Florence I. M. Thomas, 7

Zettler, Erik, and Jelle Atema, Chemoreceptor cells as concentration slope detectors: preliminary evidence from the lobster nose, 252

Zigman, Seymour, Nancy S. Rafferty, Keen A. Rafferty, and Nathaniel Lewis, Effects of green tea polyphenols on lens photooxidative stress, 285

Zoochlorellae, 72

Zooxanthellae, 72

Zottoli, S. J., F. R. Akanki, N. A. Hiza, D. A. Ho-Sang, Jr., M. Motta, X. Tan, K. M. Watts, and E.-A. Seyfarth, Physiological characterization of supramedullary/dorsal neurons of the cunner, *Tautogolabrus adspersus*, 239

4326 51

MBL/WHOI LIBRARY
WH 1B35 Q